



NOT TO
CIRCULATE

261

X
4

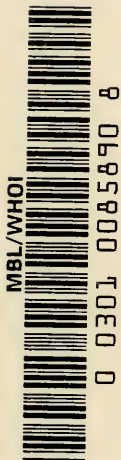
6

27 June 66

26 May 67

WOODS HOLE
OCEANOGRAPHIC INSTITUTION
REFERENCE Room

LABORATORY
BOOK COLLECTION



WOODS HOLE OCEANOGRAPHIC INSTITUTION
REFERENCE LIBRARY

Giff, ONR, Geophysics Branch
Aug. 1961

PHYSICAL OCEANOGRAPHY

Volume I
of
PHYSICAL
OCEANOGRAPHY

by

ALBERT DEFANT

Dr. phil., Dr. rer.nat., h.c.

EMERITUS PROFESSOR OF METEOROLOGY AND GEOPHYSICS

at the

UNIVERSITY OF INNSBRUCK

HONORARY PROFESSOR OF OCEANOGRAPHY

at the

UNIVERSITY OF HAMBURG

and at the

FREE UNIVERSITY, BERLIN

PERGAMON PRESS

NEW YORK · OXFORD · LONDON · PARIS

1961

PERGAMON PRESS INC.
122 East 55th Street, New York 22, N.Y.
P.O. Box 47715, Los Angeles, California

PERGAMON PRESS LTD.
Headington Hill Hall, Oxford
4 & 5 Fitzroy Square, London W.1.

PERGAMON PRESS S.A.R.L.
24 Rue des Écoles, Paris Ve

PERGAMON PRESS G.m.b.H
Kaiserstrasse 75, Frankfurt am Main

COPYRIGHT

©

1961

PERGAMON PRESS LTD.

LIBRARY OF CONGRESS CARD NUMBER 59-6845

Printed in Great Britain by Page Bros. (Norwich) Ltd.

Contents

PART I

	Page
PREFACE	ix
INTRODUCTION	xiii
I. THE OCEAN	1
A. The horizontal extent and the structure of the ocean	1
1. Introduction, vertical structure of the total Earth	1
2. The horizontal extent of the ocean and its boundaries	1
3. Sea level and its variations. Chart datum	5
B. The three-dimensional structure of the ocean	10
1. Methods of recording deep-sea data	10
2. The general morphology of the sea bottom	10
3. Special characteristics of sea-bottom topography	18
4. Arrangement of the general bottom topography of the individual oceans	27
II. THE SEA-WATER AND ITS PHYSICAL AND CHEMICAL PROPERTIES	32
1. Collecting oceanographic samples	32
2. Temperature determination for all layers of the ocean	34
3. Salinity and its determination	36
4. The density of sea-water and its dependence on temperature, salinity and pressure	41
5. Vapour pressure, freezing point, boiling point and osmotic pressure of sea-water	44
6. Other physical properties of sea water	48
7. The optical properties of sea water	51
8. The chemistry of the sea	64
III. TEMPERATURE IN THE OCEAN, THE THREE-DIMENSIONAL TEMPERATURE DISTRIBUTION AND ITS VARIATION IN TIME	88
1. Heat sources, heat exchange and heat budget in the ocean	88
2. Heat transport in the sea: absorption, conduction, thermo-haline and dynamic convection (turbulence)	94
3. Diurnal and annual variation of the temperature in the ocean	109
4. The vertical distribution of temperature in the ocean	117
5. Temperature distribution in horizontal and vertical sections	140
6. Mean vertically integrated temperature for individual oceans in zonal rings	153
IV. THE SALINITY OF THE OCEAN, ITS VARIATION IN OCEANIC SPACE AND IN TIME	154
1. Periodic and aperiodic variations of salinity	154
2. The horizontal distribution of surface salinity	161
3. The vertical distribution of salinity (in vertical profiles and sections)	165
4. The horizontal distribution of salinity at particular depths	179
5. Salinity in adjacent seas and sea straits	181

	Page
V. THE DENSITY OF WATER MASSES IN THE OCEAN, VERTICAL AND HORIZONTAL DENSITY DISTRIBUTION AND ITS STABILITY	185
1. Diurnal and annual variations at the surface	185
2. Density distribution at the surface of the ocean	187
3. Vertical density distribution and horizontal charts for different depths	187
4. Potential density and isentropic analysis	192
5. The vertical equilibrium in the ocean and stability	195
6. The distribution of stability in the Atlantic Ocean	198
VI. THE [TS]-RELATIONSHIP AND ITS CONNECTION WITH MIXING PROCESSES AND LARGE WATER MASSES	202
1. Temperature as a function of salinity and large water masses	202
2. Practical significance of the [TS]-curve	203
3. The [TS]-curve and the mixing of water masses	204
4. Further examples of the [TS]-relationship	210
5. The water masses of the oceans	216
VII. EVAPORATION FROM THE SURFACE OF THE SEA AND THE WATER BUDGET OF THE EARTH	219
1. Introduction	219
2. Direct measurement of the evaporation on board ship and methods for obtaining corresponding values for the sea surface	220
3. Meridional distribution of evaporation over the whole ocean and its determination from energy considerations	223
4. Geophysical aspects of evaporation problem	226
5. The water budget of the earth	231
6. Energy budget between ocean and atmosphere for different oceans and oceanic regions	236
VIII. ICE IN THE SEA	243
1. Formation and terminology of sea ice	243
2. Physical and chemical properties of sea ice	245
3. Ice conditions and their seasonal and aperiodic variations in Arctic and Antarctic regions	257
4. Land ice in the sea	271
5. Effect of Polar-ice conditions on the atmospheric and oceanic circulation	279
BIBLIOGRAPHY	285

PART II

DYNAMICAL OCEANOGRAPHY

INTRODUCTION	299
IX. THE GEOPHYSICAL STRUCTURE OF THE SEA	301
1. Introduction	301
2. The distribution of gravity and gravity potential	301
3. The field of mass	303
4. The pressure field and its relationship to the mass fields; solenoids	304
5. The dynamical method of preparation of oceanographic data	309

	Page
X. FORCES AND THEIR RELATIONSHIP TO THE STRUCTURE OF THE OCEAN	312
1. External, internal and secondary forces	312
2. The basic hydrodynamic equations	320
3. The continuity equation and the boundary-surface conditions	323
4. Potential flow, the Bernoulli equation, impulse and the impulse form of the hydrodynamic equations	325
5. Circulation and vorticity	329
XI. THE OCEAN AT REST (STATICS OF THE OCEAN)	337
1. The basic static equation and the conditions for static equilibrium	337
2. Quasi-static equilibrium and its importance in the dynamic evaluation of oceanographic observations	338
3. Disturbances and re-establishment of static equilibrium	339
XII. THE REPRESENTATION OF OCEANIC MOVEMENTS AND KINEMATICS	342
1. Methods of observation and measurement of oceanographic currents	342
2. The current field and its representation	356
3. Special cases of current fields near land and at the boundaries of water masses (compensation currents)	370
4. Divergence of the current field and the continuity equation	374
5. The Knudsen relations	379
XIII. GENERAL THEORY OF OCEAN CURRENTS IN A HOMOGENEOUS SEA	382
1. Introduction	382
2. Steady currents in a homogeneous sea without friction	383
3. Eddy viscosity (turbulent friction) in ocean currents	387
4. Steady currents in a homogeneous ocean under the action of external forces	398
5. Ice drift	436
6. Inertia currents	441
XIV. WATER BODIES AND STATIONARY CURRENT CONDITIONS AT BOUNDARY SURFACES	451
1. Water bodies and the boundary surface between them	451
2. Stable discontinuity surfaces	453
3. Stable stratification of water masses	458
4. Up-and down-gliding surfaces: pulsations of stationary vortices	469
XV. OCEAN CURRENTS IN A NON-HOMOGENEOUS OCEAN	476
1. Introduction	476
2. Relationships between current and density fields in a horizontal plane. The law of parallel fields	476
3. Horizontal steady currents in a stratified ocean	479
4. Ekman's theory of density currents including friction	482
5. Oceanographic applications of Bjerknes's circulation theorem	486
6. The "reference-level" for the conversion of the relative topography of the pressure surfaces into the absolute one	492
7. Remarks about the observational material necessary for a dynamic computation and critical discussion of the procedure	504
8. The determination of water transport in density currents	508

	Page
XVI. CURRENTS IN A STRAIT	513
1. Water stratification and water movements in sea straits	513
2. Theory of currents in sea straits	517
3. Ocean currents in individual sea straits	523
4. External influences (bottom topography, tides) on the oceanographic conditions in sea straits	534
5. Processes in estuaries (river mouths)	538
XVII. EFFECT OF WIND ON THE MASS FIELD AND ON THE DENSITY CURRENT	544
1. A limited and stratified sea	544
2. General conditions in the open ocean	547
3. General relationships between wind and currents	550
4. Velocity computations of oceanic surface currents in the equatorial regions from wind data	552
XVIII. BASIC PRINCIPLES OF THE GENERAL OCEANIC CIRCULATION	556
1. Introduction	556
2. Oceanic sea surface currents	557
3. Currents caused by excess of precipitation and run-off over evaporation	572
4. The thermo-haline circulation	574
5. Wind effects and the current system in a hydrographic circular vortex	576
6. The influence of meridionally oriented coasts on the oceanic circulation	579
XIX. THE TROPOSPHERIC CIRCULATION	592
1. The position and structure of the oceanic troposphere	592
2. The tropospheric circulation of the tropical and subtropical oceans	594
3. Other currents of the oceanic troposphere	606
4. Upwelling phenomena	643
5. Processes at the polar boundary of the subtropical convergence region	656
XX. THE STRATOSPHERIC CIRCULATION	661
1. Introduction	661
2. Polar currents of the northern hemisphere	662
3. The processes which occur at the Antarctic convergence zone	669
4. Dynamics of the Antarctic circumpolar current	673
5. The Sub-Antarctic intermediate current	675
6. The Polar bottom current	680
7. The deep currents in the middle part of the oceanic stratosphere of individual oceans	683
8. A survey of the water transports in the individual layers of the Atlantic Ocean	688
9. The effect of the subtropical adjacent sea on the deep sea circulation	690
XXI. THE MAIN FEATURES OF THE GENERAL OCEANIC CIRCULATION AND THEIR PHYSICAL EXPLORATION	694
1. The oceanic circulation in the Atlantic	694
2. Summary of present individual theories and the prospects of a comprehensive theory of the general circulation including the deep layers	696
3. Model experiments on stationary planetary flow patterns	701
4. The transient response of an ocean to a variable wind stress	702
BIBLIOGRAPHY	708
AUTHOR INDEX	721
SUBJECT INDEX	725

Preface

OCEANOGRAPHY, the science of the ocean, has undergone a rather rapid development during the last decades tending from a more descriptive science towards one working according to exact mathematic-physical principles as applied in the natural sciences. Oceanography can be subdivided into two fundamentally different parts: (1) The "biology of the oceans" and (2) the "physical oceanography". For the first, physical oceanography can be looked upon as the scientific foundation, since the biology of the oceans dealing with conditions and forms of life of all the living beings existing in the oceans requires an exact knowledge of the environmental medium for these beings. Physical oceanography in itself is a subpart of geophysical science. This book involves physical oceanography only, the scientific progress of which has been especially fast during the last 50 years owing to technical improvement of the working methods used on oceanographic research vessels and also to the extensive widening of our physical and chemical views about the phenomena occurring in the sea.

The start of the manuscript work of this book goes rather far back, to the time when the scientific results of the German Atlantic Expedition on the research vessel *Meteor* 1925–1927 were almost completed. However, these first compilations took a considerable time and served as the basis of extensive oceanographic lectures at the Institute and Museum of Oceanography (Meereskunde) at the University of Berlin (1925–1945), assembled together in book form. The book was completed in its first form at the end of the Second World War (1945). Of course, at the time, it was impossible to achieve a publication of the work. Consequently the first manuscript has been rearranged several times and has, on these occasions, been revised rather extensively and completed according to the momentary state of oceanographic research. From one point of view this circumstance may be looked upon as an advantage for the presentation, but from the other as a drawback for the internal uniformity of the book, since it was unavoidable sometimes to present some subjects shorter and others longer than needed. However, a compromise was always tried and found.

More recently (1957), after some failures to achieve publication of the book, two institutions took interest: On the one hand the Deutsche Forschungsgemeinschaft in Bonn, Germany, proposed a generous fund for a publishing house, Dietrich-Reimer, Adrews & Steiner, Berlin. On the other hand the Woods Hole Oceanographic Institution, U.S.A. which by way of the Office of Naval Research, U.S. Navy, arranged with the Pergamon Press, Oxford (Capt. I. R. Maxwell) the publication of the book in the English language. There were many reasons favouring a publication in the English language. Certainly international oceanographic science was hoped to be better served because of the larger audience possible.

It was doubtful, besides, if the large funds necessary for publication could have been raised from the German side.

These circumstances required a translation of the German text into English. Before approaching this large task, the work had again to be revised completely and brought

up-to-date. This time-taking job was done at the International Institute of Meteorology in Stockholm, thanks to a kind invitation by the late Prof. C. G. Rossby shortly before his untimely death. It remains a pleasure and self-evident duty to express my gratitude towards the present director of the Institute, Docent Dr. B. Bolin, as well as towards his closer co-workers, for their interest, and for all the Institute facilities at my disposal, whereby my work benefited greatly. During my six-month stay in Stockholm the first volume of the book was translated (Physics of the Ocean, Statics and Dynamics of Ocean Currents) (translator Ing. H. E. Knoll, Stockholm), while the second volume (Waves, Tides and Related Phenomena) already drafted years ago was translated by Dr. Louis Lek, La Jolla, California. I express my thanks to both translators for the trouble they undertook. As modes of expression differ among languages it is natural that the detailed refinements of the originally German formulation and presentation naturally suffered to some extent, but I hope that a still representative version of the contents has satisfactorily been achieved. All this, however, could not have been completed had not my son *Prof. Fr. Defant*, on leave from the weather service and the University of Innsbruck, Austria, been present at the Stockholm Institute, engaged in investigations on the General Circulation of the Atmosphere. He also devoted his time to my work, especially concerning detailed revisions of the translations and the completion of the large amount of illustrations. For this troublesome work, which for him also meant loss of time, I am especially grateful.

The printing of this textbook would have been doubtful had not the Office of Naval Research, in the first place (Dr. Atkins and Mr. G. Lill, Office of Naval Research, Wash. D.C.), generously sponsored the undertaking, at the same time conceding to my wishes with regard to its publication. Furthermore, I wish to thank Commander C. Palmer of the U.S. Navy, at present with the International Institute, Stockholm, for additional help.

The publishing has been done by Pergamon Press, Oxford, in its well-known and outstanding manner, and I express my gratitude in the first place to the publisher, Captain I. R. Maxwell. Also to Mr. Buchanan my heartfelt thanks and appreciation for the excellent drafting of the numerous illustrations.

Physical Oceanography consists of two volumes, each having two sub-parts. The first part of Volume I deals with the spatial, material and energetical characteristics of the water envelope of the earth, as well as with the evaporation problem and the ice in the sea. For this reason it specially involves the physical and chemical properties of sea-water, the spatial distributions of the oceanographic elements in the total oceanic space and its periodic as well as aperiodic changes. The second part of Volume I concerns the various modes of motion of sea-water in the form of ocean-currents (dynamic oceanography). Finally, Volume II is devoted to periodic movements of the water masses (waves, tides and related phenomena). The individual problems of physical oceanography are discussed in as much detail and supported as far as possible by appropriate examples and references to existing compilations of observational data. The scientific progress of the last decades has been considered almost completely, not only with regard to the observational facts, but also concerning the theoretical treatment and explanation of the observed phenomena. The oceanographic literature has been considered in its entirety to the end of May 1957. Extensive reference lists are

provided at the end of each sub-chapter concerning the literature sources used and can be considered as unique in their completeness.

A presentation of instruments and apparatus in use in oceanographic research, their technical function and instrumental theory, was not intended to be included in the textbook. Since the different nations engaged in oceanographic research mostly use their own instruments and apparatus, it would be rather difficult in the frame of such a textbook to deal with all instruments and explain their function. I believed this to be unnecessary since much has already been summarized by authoritative institutions and also because a detailed textbook on oceanographic instrumentation has been commissioned from the international side.

The contents of the book formed the basis, as already mentioned, for my lectures on physical oceanography held at the University of Berlin Institute and Museum for Oceanography (1927-1942); later on, until 1953, they were the basis for my lectures held at the University of Innsbruck, Austria, Institute for Meteorology and Geophysics and, after my retirement, lectures at the University of Hamburg and the Free University of Berlin, where I was invited as an honorary professor.

The internal structure of the text resembles the old text of the well-known and, in its time, excellent *Handbook of Oceanography* by O. Krümmel (E. Engelhorn, Stuttgart, Vol. I, 1907, Vol. II, 1911). This two-volume work is outdated in all of its parts and had to be replaced in time by a completely revised modern text corresponding to our present knowledge of the oceans. In one respect the text under consideration differs fundamentally from Krümmel's book since no attempt was made to deal in the present book with historical and older work about oceanic phenomena and with attempts to explain them in such minuteness of detail. Most of Krümmel's material, as will be understood, deserves at present only historical interest and would have been for my book only unnecessary ballast. The reader who has a special historical interest may therefore be referred to the text of Krümmel.

Being fully aware that not all the chapters of my work will perhaps be quite to the taste of my oceanographic colleagues, I have always tried to present everything which may still be of value for the further development of oceanography. I may best speed this book to the reader with the words, splendid due to their simplicity, of the great Newton:

"Ut omnia candide legantur, defectus in materiam tam difficile non tam reprehendantur, quam novis lectorum conatibus investigentur, benigne suppleantur, enixe rogo."

"I heartily beg that what I have here done may be read with forbearance; and that my labours in a subject so difficult may be examined, not so much with the view to censure, as to remedy their defects."

"Mögen Mängel in einer so schwierigen Materie den Leser weniger zum Tadel als zu neuen Versuchen und gefälliger Ergänzung veranlassen! Um das bitte ich denselben recht dringend."

A. DEFANT

Innsbruck,
March 1960

Introduction

OCEANOGRAPHY is the branch of science concerned with the oceans and the phenomena occurring therein. It is a part of the sciences dealing with the Earth, and in so far as it gives a qualitative description of phenomena it belongs to the geographical sciences. It uses methods essentially similar to those of the other geographical sciences and its aim is the same as that of general geography, the classification of the different material and energy characteristics of the phenomena found with precise definitions into different categories and the systematic inter-relation of these. Regional geography groups all locally co-existing and interacting phenomena on the basis of a common area of occurrence which may be of greater or lesser extent. From the geographical point of view there is thus a *general* and a *regional* oceanography both using principally statistical and descriptive methods.

The rapid progress of the exact sciences in recent times has led to an increasingly rapid transition from a geographic to a geophysical treatment of the problems of oceanography. This has given rise to a *quantitative* conception of oceanographic phenomena based on physical-mathematical principles. In this respect oceanography is a branch of *geophysics* and is recognized as an independent science comparable with meteorology (the physics of the atmosphere) and with geophysics in its more restricted sense (the physics of the Earth).

The history of the development of oceanography into a science is essentially the same as that of other scientific disciplines, although it is still at a comparatively early stage. Like all the other sciences its facts are obtained by observation. Initially these observations were made only of phenomena and conditions in the immediate neighbourhood of continental coasts or islands. Conditions in the open sea were for long indefinite and uncertain, and furthermore things that were new, exceptional or spectacular, were much more interesting than normal everyday phenomena. As knowledge increased men ceased to be content to recognise conditions and changes immediately around them; they also sought after insight into the nature of phenomena occurring all over the Earth. Men penetrated out into the vast stretches of the seas and there gradually developed a conception of the ocean. The bold voyages of seamen gradually clarified ideas of the figure of the Earth and the confirmation of its spherical shape showed the finiteness of the oceans.

Systematic order in the collection of ships' observations and the increased accuracy obtainable by the use of instruments came only after the beginning of the nineteenth century. The regular navigation of the seas necessary for the expansion of trade and commerce rapidly increased the knowledge of surface conditions which was recorded in thousands of *ships' journals* of merchant marine ships. At the suggestion of the American naval officer and oceanographer Matthew Fontaine Maury (1806–73) an agreement was reached in 1853 at an international conference in Brussels on the form and content of these journals, and this was supplemented by an international conference

in London in 1873. These important observations were collected in the records of hydrographic offices or of central meteorological offices and scientifically correlated. Records of temperature, salinity and currents at the surface, of tides and of the meteorological conditions over the sea were compiled, and the rapid development and the safety of navigation can be attributed not least to this detailed knowledge of surface conditions.

However, ships' journals of merchant marine ships are not sufficient to give a broad comprehension of oceanographic phenomena. Maritime traffic is interested only in the fastest crossing between the continents and the observations recorded in ships' journals are confined very largely to certain routes, usually those that are as short as possible, while the remoter parts of the oceans have been left untouched. In many cases, however, phenomena occurring in these areas are important for a correct scientific assessment and the comprehension of ocean phenomena in general. A knowledge of conditions at the surface and beneath it covering the whole oceanic space is necessary for the further development of oceanography.

These considerations have led to the *oceanographic expeditions* that have contributed so much to the science of the seas. The task of deep-sea expeditions is first and foremost to determine the shape of the sea bottom and to measure as accurately as possible the physical-chemical conditions of sea water between the bottom and the surface. Of major importance are the horizontal and vertical variations of the oceanographic factors: temperature, salinity and dissolved gases. Variations in the first of these indicate the variations in density and the latter ones allow a correlation with marine biology which requires a knowledge of the environment of marine life.

In addition to this more statistical knowledge of the physical-chemical structure of the sea it is also desirable to know something about the circulation of water masses. It is obvious that the internal circulation of the ocean must be related to the oceanic structure. Because the driving force for the oceanic circulation lies partly in the movement of the air over the ocean surface and partly in regional differences between masses of water (or differences of density of the masses) due to differences in temperature and salinity. If conditions in the oceans are steady there will be an inverse relationship between the circulation and the thermo-haline structure. The earliest method used to deduce the circulation system was based on such a correlation, using an accurate survey of the thermo-haline structure. The determination of the movements of water masses, the forces causing them and their seasonal variations in time as well as local variations and transports are the main problem of modern oceanography.

During the development of oceanography the character of oceanic expeditions has undergone a transformation. The first expeditions were naturally only attempts to clarify conditions and to overcome experimental difficulties on board the research ships. The major deep-sea expeditions at the end of the nineteenth century and at the beginning of the twentieth laid the foundations of modern oceanography. At first they investigated only a section through the ocean, that is, along the route of the ship. The results were based on discontinuous sampling and rarely reached to the sea bottom. This method did not allow any three-dimensional conception of oceanic phenomena.

Progress in oceanographic technique on board research vessels and modern developments in the recording and interpretation of results have made it possible since the First World War to carry out *systematic investigation* of the ocean, not along one

or two sections but using a narrow spaced net-work of stations over the whole of a water mass from the surface to the sea bottom. This was the logical development of the first voyages of research ships progressing from straightforward discovery to systematic exploration of a whole ocean along a carefully prepared plan. After some minor research voyages of this type by Norwegian oceanographers came the first major expedition for the systematic survey of a whole ocean, the German Atlantic Expedition of the "Meteor" 1925-7 (DEFANT, 1928).

Large expeditions such as this that give a deeper insight into the geographic variation of the oceanographic factors over the entire ocean are essential for an extensive view of the phenomena occurring in the oceans. The closer the network of stations the more accurate such a survey will be, but the establishment of the closest possible network is capable of only partial fulfilment. The work of the research ships can be intensified only with difficulty to get a more rapid sequence of stations and there are difficulties in the interpretation of the data recorded. The treatment of the results of a survey of a whole ocean is based on the assumption that conditions in the ocean are *steady*. However, this is only approximately true. Conditions in the water mass in an ocean are on the whole *quasi-stationary* provided that they are not examined in too great detail. Only in this case one is justified in concluding that the movements of water masses from the thermo-haline structure, and the results of all the major ocean surveys that have been made, have shown that this correlation of the physical-chemical conditions can be relied upon for the general interpretation of the prevailing currents in the ocean. This, however, gives a view of *average* conditions only. The dynamics of the processes in detail are more complicated, as the somewhat rough idea of the widely spaced network of oceanographic stations shows.

This, together with more recent theoretical considerations, has led to the conclusion that a closer study of the *dynamics of the currents* in the ocean cannot be based on the observations of a rather wide-spaced network of oceanographic stations. It will require closely knit, preferable *synoptic* observations which can be obtained only by collaboration between several research ships. Apart from these more specialized surveys of oceanographic problems the older type of oceanographic survey remains indispensable, although modern oceanographic research will change to an increasingly synoptic concept of oceanographic phenomena. The last international joint survey in the Gulf Stream area north of the Azores during the early summer of 1938 (DEFANT and HELLAND-HANSEN, 1939) marked the beginning of this type of joint investigation. Probably the largest synoptic oceanographic survey has been the *Operation Cabot* of the U.S. Hydrographic Office, 6-23 June 1950, which investigated the Gulf Stream area between Cape Hatteras and the Grand Banks of Newfoundland using six ships (FUGLISTER and WORTHINGTON, 1951).

This book is concerned with *physical oceanography*. It describes the three-dimensional structure and movements, material and energy characteristics of the hydrosphere. Furthermore, the physical and chemical properties of sea-water, the regional variations in the oceanographic factors and their periodic variations are dealt with. It also describes the different types of ocean currents (ocean dynamics), and finally the periodic movements of the water in waves, tides and related phenomena (dynamics

of periodic phenomena). The contents of this book are therefore concerned only *with general geography, chemistry, physics and the dynamics of the sea*. However, outside the scope of this book lies marine biology which is concerned with the organic life of the oceans (plankton and fishes) which reacts not only to the external environment but also to stimuli and incentives of non-physical origin.

PART 1

Chapter I

The Ocean

A. THE HORIZONTAL EXTENT AND THE STRUCTURE OF THE OCEAN

1. Introduction, Vertical Structure of the Total Earth

THE total Earth system can be subdivided into three parts. The solid rock forms the *Lithosphere* and is the solid core on which the other two layers rest. If the rock layer was freed from all its characteristic irregularities it would be in the geodetic sense "flat" (a simple rotational ellipsoid). The water forming the layer next in density, the *Hydrosphere*, would cover as a single ocean the entire surface of the Earth. This is not the case. The lithosphere is very uneven, and large depressions and elevations disturb its regular shape. There is not sufficient water to cover all these irregularities entirely, but it fills the depressions between the continental plateaus and leaves uncovered the upper parts as continents. This outlines the form of the lithosphere and gives the Earth its characteristic appearance.

The third major part of the total Earth, the *Atmosphere*, lies as a gaseous envelope above the hydrosphere and touches the lithosphere only over the continents. It should be remembered that this is in fact exceptional, occurring over little more than a quarter of the surface of the Earth. Normally, the lithosphere, the hydrosphere and the atmosphere are arranged one above the other with the different strata of each layer arranged in order of density by the force of gravity. This is a necessary condition for the static stability of the three parts of the total Earth.

The transition from one layer to another is finite and rather abrupt. The water masses of the ocean are bounded by two main surfaces (Fig. 1, DEFANT, 1940).

(a) The interface between the lithosphere and the hydrosphere is the *sea bottom*: across it there is a density change from approximately 2.5 to 1.06 g/cm³. The investigation of the morphology of the sea bottom is one of the main tasks of oceanography.

(b) The interface between the ocean and the atmosphere is the *sea surface*; here the density change is from about 1.03 to 0.0013 g/cm³. All phenomena affecting both, ocean as well as atmosphere, take their origin from this surface. An accurate knowledge of its form is of the greatest importance to oceanography.

The water masses of the ocean lie entirely within these surfaces, forming a single continuous mass. All the energy absorbed by the ocean or given off by it must pass through these boundaries, and this energy entering or leaving the ocean is the basic cause of all the phenomena and changes of state in the water mass.

2. The Horizontal Extent of the Ocean and its Boundaries

The incomplete covering of the surface of the Earth by the ocean separates it into

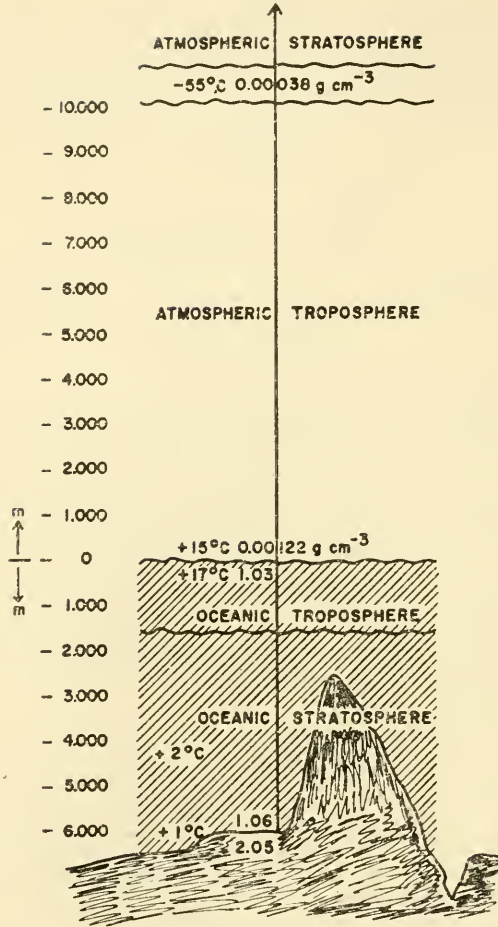


FIG. 1. Diagrammatic representation of the main boundary surfaces in the structure of the Earth and the density changes at each. The figures at the right are the heights or depths in metres above or below sea level.

land and sea. The coastal limits of the continents projecting above the surface of the ocean are known almost everywhere with satisfactory accuracy. It is only in the polar regions where vast areas of land are buried under ice that it is difficult to determine accurately the limits between continent and sea. These uncertainties have recently been considerably reduced, however. Apart from this reservation, of the 510.01 million km^2 of the Earth's surface not less than 361.1 million km^2 is ocean and only 148.9 million km^2 is land (KOSSINNA, 1921). The ratio of land to sea is 1 : 2.43 or 29.20 relative to 70.80%. The uncertainty in these values is not more than a few hundredths. The Earth's surface is thus mostly oceanic. Similar relationships hold for the Northern and Southern Hemispheres taken separately: in the Northern Hemisphere 60.7% water, 39.3% land; in the Southern Hemisphere 80.9% water, 19.1% land. Water still predominates in the Northern Hemisphere, while in the Southern Hemisphere land is very markedly in the minority. A great circle can be drawn dividing the surface of the

Earth into a land and a water hemisphere, one containing the largest possible land area and the other containing the largest possible water area. The pole of the land hemisphere lies at 47.25° N., 2.5° W. near the mouth of the Loire, and this hemisphere contains 52.17% sea and 47.3% land, corresponding to a ratio of 1 : 0.90; the water area is still slightly greater than that of the land. The centre of the water hemisphere lies at 47.25° S., 177.5° E., south-east of New Zealand, and this hemisphere contains 90.5% water and 9.5% land corresponding to a ratio of 1 : 0.11; slightly less than 10% is land. For many phenomena affecting the Earth as a whole this division into land and marine sides is of some importance.

The distribution of land and water areas given in percentage is very irregular and apparently completely asymmetric. Table 1 gives the percentages of land and sea in zones of 5° of latitude.

Table 1. *Distribution of sea and land for zones of 5° of latitude*
(In per cent, according to E. KOSSINNA, 1921)

Latitude zone	Northern Hemisphere		Southern Hemisphere	
	Water	Land	Water	Land
90-85°	100.0	0.0	0.0	100.0
85-80°	85.2	12.8	0.0	100.0
80-75°	77.1	22.9	10.7	89.3
75-70°	65.5	34.5	38.6	61.4
70-65°	28.7	71.3	79.5	20.5
65-60°	31.2	69.8	99.7	0.3
60-55°	45.0	55.0	99.9	0.1
55-50°	40.7	59.4	98.5	1.5
50-45°	43.8	56.2	97.5	2.5
45-40°	51.2	48.8	96.4	3.6
40-35°	56.8	43.2	93.4	6.6
35-30°	57.7	42.3	84.2	15.8
30-25°	59.6	40.4	78.4	21.6
25-20°	65.2	34.8	75.4	24.6
20-15°	70.8	29.2	76.4	23.6
15-10°	76.5	23.5	79.6	20.4
10-5°	75.7	24.3	76.9	23.1
5-0°	78.6	21.4	75.9	24.1
90-0°	66.66	39.34	80.92	19.08

90° N.-90° S. { total ocean 361.059 × 10⁶ km², 70.80%
total continents 148.892 × 10⁶ km², 29.20%

The thin dotted lines in Fig. 2 for 50% and 25% land show that land predominates only in two places, between 70° and 45° N. across the Eurasian and North American continents and at about 70° S. in the region of the Antarctic continent. In the Southern Hemisphere, with the exception of the polar area, the land is nowhere more than 25% of the total area. Between 55° and 65° S. the ocean forms a continuous belt around the Earth, a fact which is of fundamental importance for many oceanographic phenomena.

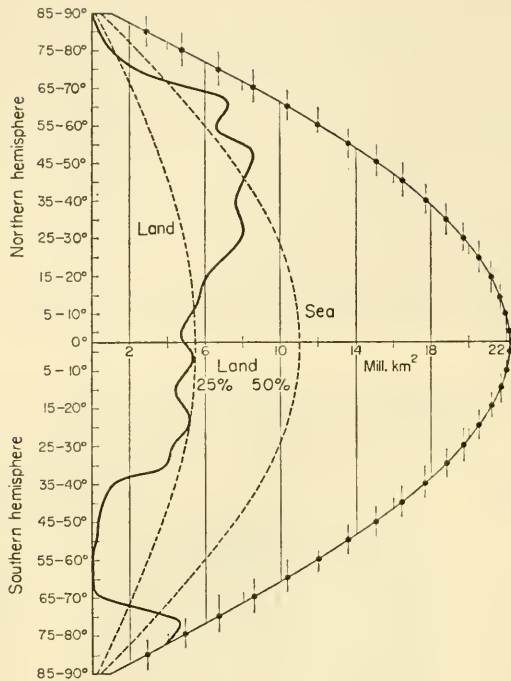


FIG. 2. Percentage distribution of water and land areas in five degree zones.

The arrangement of the continents outlines the irregular distribution of the sea. The sea fills the depressions between the continents as far as its volume allows. On closer inspection a division into three major oceans can be recognized: *the Atlantic, the Pacific and the Indian Ocean*. They are all connected with each other, forming a continuous ocean belt in the higher latitudes of the Southern Hemisphere. This can be seen very clearly on Steinbauer's star projection centred on the south pole. Here the Atlantic and the Indian Oceans appear as very large and extended bays radiating out from the circumpolar Southern Ocean (Fig. 3).

The main boundaries of the three oceans are fixed in the first place by the continents. Conventional boundaries are necessary only to the south of Australia, South America and Africa where distinct morphological boundaries are missing. These have been fixed by international agreement (INTERN. HYDROGR. BUREAU, MONACO, 1937; WÜST, 1939).

The three major oceans are subdivided by the continental coast lines which in some places are remarkably irregular. There is a particularly marked contrast between the open ocean and the seas enclosed between mainland and groups of islands. The sea areas which are separated from the ocean and project to a greater or lesser extent into the continents are denoted *adjacent seas*, and according to the degree of separation from the open ocean they may be either *marginal* or *mediterranean* seas. The demarcation from the ocean is usually topographical. The more important adjacent seas are listed in Table 4 (see p. 17), together with the area, the mean and maximum depths of the

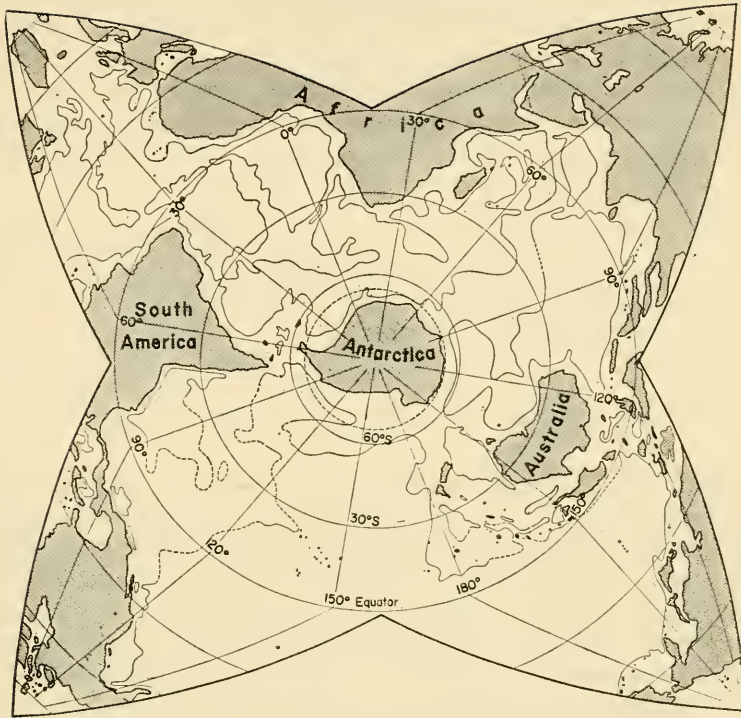


FIG. 3. Steinhauser star projection to show the distribution of oceans and continents.

three major oceans (with and without adjacent seas) as well as for the marginal and mediterranean seas (KOSSINNA, 1921; LANDOLT-BÖRNSTEIN, 1952, article by Dietrich, p. 460).

3. Sea-level and its Variations. Chart Datum

The surface of the ocean which forms the boundary between the ocean and the atmosphere is in a physical sense a *free boundary* that may assume different forms at different times under the influence of various internal and external forces. This boundary surface is called the "sea-level". If the Earth was covered entirely by a homogeneous ocean unaffected by atmospheric phenomena such as winds and atmospheric pressure or the tidal forces of the sun and the moon, then there would be only a single force acting on the sea: *gravity*. In the equilibrium state there can be no component of the force of gravity along the surface of the sea and the direction of the force of gravity must be perpendicular to the surface. This "ideal" sea-level is thus a *geopotential* surface or a *gravitational equipotential* surface. If minor variations in the force of gravity due to the irregular distribution of the mass of the outer crust of the Earth are disregarded, the ideal sea-level will coincide with the surface of a *rotational ellipsoid*. Even if the sea does not cover the entire Earth, the ideal sea-level will correspond to the surface of this rotational ellipsoid. When the small irregularities in gravitational force due to the irregular mass distribution of the Earth crust are taken into account,

the sea-level as a geopotential surface will no longer have the same simple ellipsoidal form but will show little variations to either side. This irregularly shaped surface is called in the theory of the Earth figure the "geoid". The geoid can be regarded as displaced from the surface of the rotational ellipsoid by the distortions of the continental masses. The geoid rises on passing from the sea towards the continents and falls on passing towards the sea again. Figure 4 illustrates the undulations of the geoid around

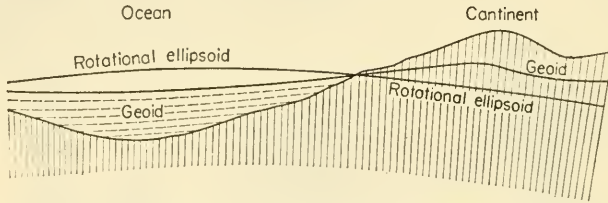


FIG. 4. Undulations of the geoid about the rotational ellipsoid.

the rotational ellipsoid. The ideal sea-level (geoid) lies below the rotational ellipsoid in sea areas and above it in land areas. The magnitude of these deviations depends on the magnitude of the gravitational anomalies in the upper crust of the Earth. It was at first thought from theoretical considerations that the undulations of the geoid must be rather large. However, it was found that due to the almost perfect *isostatic adjustment* of the masses of the outer crust (hydrostatic equilibrium), these remain rather small and amount to not more than ± 100 m. The forces that cause *periodic* variations of the actual sea-level from the geoid were mentioned above. Amongst these are the forces due to the attraction of the sun and the moon which produce the tides in the ocean and the tangential force of the wind on the surface of the sea which causes ordinary sea waves. Both of these effects on the sea-level initiate waves that can be considered as oscillations to either side of a *mean sea-level*. It can be fixed at any coastal station by continuous observation of the water level, because the influence of the tides can be excluded if full-yearly observations are available while the effect of the ordinary wave motions disappears in a daily mean of observations.

Other forces affecting the ideal sea-level may cause long lasting displacements of the actual sea-level from the geoid. If these forces are *steady* the corresponding displacements will also be steady and give a static equilibrium state. Also in the case of slowly changing forces the time will be sufficient for the sea-level to follow the changes. If, however, there are rapid changes in the intensity of the force the situation will be more complicated and an oscillation may develop depending on the size of the water masses involved.

An important source of steady displacements of this kind from the ideal sea-level is the effect of barometric pressure. The ocean reacts to *steady* changes in the atmospheric pressure on the surface like an enormous water barometer: as the atmospheric pressure rises the sea-level will fall below the geoid, as the atmospheric pressure falls it will rise above it. When conditions are stationary there can be no pressure difference between two points at the same level within the ocean. The pressure at a depth h_0 below ideal sea-level in a homogeneous sea of density ρ_0 will be

$$p = p_0 + g\rho_0(h_0 + \xi_0),$$

where p_0 is the air pressure at the surface, g is the gravitational acceleration and ξ_0 is the deviation of the surface from ideal sea-level. At another place it will be

$$p = p_1 + g\rho_1(h_0 + \xi_1).$$

The pressure difference between the two places will then be

$$\Delta p = -g(\rho_0 - \rho_1)h_0 - g(\rho_0\xi_0 - \rho_1\xi_1). \quad (\text{I.1})$$

For a completely homogeneous sea ($\rho_0 = \rho_1$) the relative deviation of the sea-level from the geoid will be

$$\Delta\xi = -\frac{1}{g\rho} \cdot \Delta p. \quad (\text{I.2})$$

If the average density for sea-water is taken as 1.028 then

$$\left. \begin{aligned} \Delta\xi \text{ in dynamical cm} &= -0.973\Delta p; (\Delta p \text{ in mbar}), \\ \Delta\xi \text{ in cm} &= -0.993\Delta p; (\Delta p \text{ in mbar}). \end{aligned} \right\} \quad (\text{I.3})$$

The numerical factor in the last equation will be 1.326 when Δp is expressed in mm Hg, because 1 millibar (mbar) corresponds to 0.75 mm Hg.

For a *steady* difference in air pressure the displacement of the sea-level from the geoid in cm will be 0.993 times the local variation in atmospheric pressure measured in mbar, in the opposite direction. From a knowledge of the steady pressure distribution at sea-level the deviation from ideal sea-level can easily be found. In January the barometric pressure in the high-pressure cell near the Azores is about 1020 mbar, in the Icelandic low-pressure area it is about 990 mbar. It can therefore be expected that the sea-level in the area of the Irming Sea will be about 30 cm higher than at the Azores. Comparisons between changes in barometric pressure and changes in sea-level made at polar stations, where the ice covering allows them to be followed more easily, have shown satisfactory agreement between observed and calculated values of sea-level (HESSEN, 1931; WEGENER, 1924).

Other effects due to the inhomogeneity of the water in the ocean and to the currents associated with it, and also to phenomena caused by the blocking of ocean currents at continental coasts (water level rise, Anstau) are harder to deal with. All these aperiodic stationary deviations of the actual sea-level from the ideal are included in the concept of the *physical sea-level*. This physical sea-level is, under steady conditions, the true boundary between the ocean and the atmosphere.

The methods used to fix the position of the physical sea-level relative to the surface of the geoid will be described later (Part II). The effect by itself of different distributions of density in different water masses within the ocean can be found using equation (I.1). Assuming the barometric pressure being the same at both stations ($\Delta p = 0$) it follows approximately

$$\Delta\xi = \frac{\rho_0 - \rho_1}{\rho} h_0,$$

where h_0 is the depth at which the pressure difference within the water mass vanishes. For a density difference of 10^{-3} and a water volume of 100 m vertical extent, the

lighter of the water masses must be 10 cm higher than the heavier. If the density difference changes with the depth the above equation will include the integral of

$$\int \frac{\rho_0 - \rho_1}{\rho} dz$$

taken from the surface to the depth h .

For practical purposes the mean water level is determined at coastal stations by a tide gauge. Calculation of a mean value will eliminate the periodic factors (tides and waves) but other factors will remain; in the first place the aperiodic changes in meteorological factors such as the wind, barometric pressure, precipitation and evaporation that can only be eliminated by taking a mean value over a number of years. However, even this mean value cannot be taken as invariable. It will reflect secular (long period) changes in meteorological factors and also slow deformations of the Earth and slow changes in the total water mass of the oceans. For comparison and inter-relation of mean sea-levels fixed at different places along a coast, precision levelling between these points is essential. This must be taken over land and be independent of the conditions in the sea in order to show whether the mean sea-levels are in one and the same or in different niveaus. On the subject of precision levelling along the Baltic coast (1896-8) see WESTPHAL (1900), along the east coast of North America see ANVERS (1927) and BOWIE (1936), and on the interpretation of these see DIETRICH (1937).

Sea-level at almost all coastal stations shows clearly an annual period which is related principally to wind conditions along the adjacent sea coast; thus the sea-level at Aden is connected with the monsoon in the Arabian Sea (KRÜMMEL, 1907), while in Japanese waters the annual changes in barometric pressure and in density of the water are of greater influence (NOMITSU and OKAMOTO, 1927). On the annual variation in the sea-level along the Baltic coast see HAHN and RIETSCHEL (1938), and BERGSTEN (1917). Along the coasts of those seas where there are strong tides the determination of mean sea-level is more complicated since the effect of the tides has first to be eliminated. This is best done by subtracting the mean tide level calculated by means of the harmonic tide constant from the actual change in water level as shown by the tide gauge. The remaining part is the aperiodic deviation in water level (in addition possibly free-oscillations of water masses) which must be related to meteorological factors (MARMER, 1927). If this ideal method is not possible the mid-point of each tide can be found by taking an average of hourly readings over a full tide period and it can be assumed that this value is reasonably free from any cosmic influence. An investigation of this type has been carried out for the German Bay (North Sea) by LEVERKINCK (1915).

The changes in sea-level recorded on a tide gauge can also be simulated by a rise or a fall of the land on which the gauge stands. Movements of the coast line forming the boundary between land and sea may be compounded of two movements, those of the water and those of the land (PENCK, 1934). As the ocean may be compared with a large vessel filled with water, changes in the water surface may arise through changes in the volume of water in the ocean or by alteration of either its size or the position of the water surface in the vessel. All changes in sea-level that affect the entire ocean surface in the same direction are termed, following SUESS (1888), *eustatic*. This includes two very slow changes: the *nomie* and the *juvenile* motion. The first is due to the slow erosion of the land that lifts the sea bottom, the second is due to the continuous

addition of juvenile water from the interior of the Earth by volcanic and thermal activity.

According to Penck, about 12 km^3 of solid material are carried into the sea annually and this would raise the level of the sea by about 33 mm in a thousand years. This nomic movement will continue as long as there is land that can be eroded. When this final state of erosion has been reached the sea-level will have risen about 250 m higher than it is at the present time. The juvenile increase in the level of the sea amounts, according to Penck, to not more than about 2.8 mm in 1000 years or barely one-twelfth of the nomic. It will continue as long as volcanic activity on the Earth persists.

A faster change than either of these eustatic movements is that due to the melting of glaciers. During the ice ages there was approximately 40 million km^3 more ice covering the land than there is at the present time. This melted during a period of 10,000 to 20,000 years and raised the surface of the sea by 100 m or by 5–10 m in 1000 years (RAMSAY, 1939; PENCK, 1933). Melting of the present-day ice of glaciers covering the land ($22.2 \text{ million km}^3$) would raise the sea-level by 55 m. The level of the ocean varied during the ice ages over a maximum range of 155 m.

The movements of the solid crust of the Earth may be of either *tectonic* or *volcanic* origin or they may be due to *isostatic* elevation or subsidence of single parts of the crust. The first may be accompanied by considerable local changes in a short time.

Chart datum. Sea charts showing depths at different places give a picture of the topography of the sea bottom. These depths are not calculated from sea-level (as a reference level) but from a so-called chart datum. This has been done for purely practical reasons concerned with navigation. Chart datum on English and German charts is that of mean low-water springs; on French charts it is the level of the local

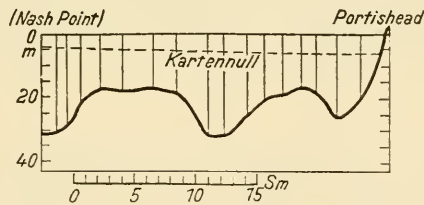


FIG. 5. Mean sea level and chart datum in the main shipping route in the Bristol Channel.

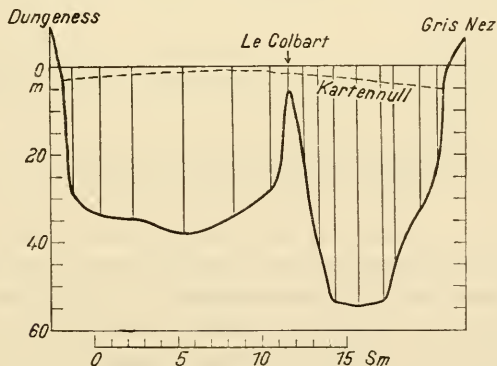


FIG. 6. Mean sea level and chart datum in the straits of Dover.

lowest low water and on American charts it is the level of local mean low water. Only the sea charts of tideless mediterranean seas relate their depths to mean sea-level (e.g. the Baltic). Chart datum is nowhere the same as normal datum (*NN*) for cartographical surveys on land but is generally lower. Since the tidal range varies from one coastal station to another the chart datum forms an undulating surface which in general falls as it approaches a coast. This fall is greatest in funnel-shaped bays where the tidal range rapidly increases towards the inner end. On the open sea there are only small differences between chart datum and mean sea-level.

Chart datum must be taken into consideration in more accurate hydrographic calculations. RAVERSTEIN (1886) first pointed out the importance of chart datum and prepared two charts of a part of the English Channel. One of these showed isobaths according to the sea chart (calculated from chart datum), and the other showed isobaths calculated from the surface of the geoid. These charts demonstrate clearly the importance of considering a reference level. Figures 5 and 6 show two profiles of the differences between mean sea-level and chart datum for a longitudinal section along the Bristol Channel and for a cross-section of the Straits of Dover. For further information on the often very complex question of chart datum see especially HORN (1944).

B. THE THREE-DIMENSIONAL STRUCTURE OF THE OCEAN

1. Methods of Recording Deep-sea Data

The safety of shipping in coastal waters requires an accurate topographical survey to considerably greater depths than the 12 m draught of the biggest ships, usually down to 200 m. This is about the maximum depth at which soundings can be made with any accuracy using a hand lead line. Soundings taken in this way can also be used to measure the depth of water under a vessel anchored in shallow water and hence to

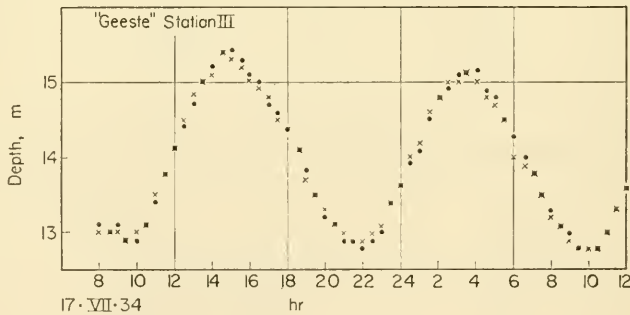


FIG. 7. Tides determined by sounding from an anchored ship
($\phi = 53^{\circ} 55.9' N$, $\lambda = 7^{\circ} 52.2' E$).

determine the range of the tide at that point. This is the simplest method of determining the tidal range at a distance from the coast in adjacent seas that are not too deep and along the continental shelves. The hemp lead line should have a piano wire trace at the upper and lower ends. Soundings of this type can, with some practice, be determined to within ± 5 cm even for wave motion. Figure 7 gives an example of a tidal cycle measured in this way at a station in the southern North Sea.

Soundings at depths greater than 200 m cannot easily be made with a hemp line by hand since the weight of the line and lead is too great and it is difficult to feel the contact with the bottom. The measurement of greater depths is extremely difficult and it took several decades of experimental work before deep-sea soundings could be made reliably at any point in the ocean.

The measurement of the depth of the sea (STAHLBERG, 1920) is the determination of the perpendicular distance between the surface and the sea bottom. At great depths this is difficult because: (1) the bottom contact is not easy to detect, and (2) hauling in the increased sounding weight is very laborious unless it is done by machine. Two conditions are necessary for a reliable deep-sea sounding: (1) the use of a thin steel wire in place of the hemp line used previously, and (2) the release of the sounding weight on contact with the sea bottom.

The wire sounding method used at great depths will not be described in detail here since it is essentially a technical question. Further details can be found in technical handbooks [see especially PRATJE (1952), and *Oceanographic Instrumentation* (Report of conference, Rancho Santa Fe, California, 21–23 June 1952)].

The development of echo sounding has revolutionized the investigation of sea-bottom topography; wire soundings could never have been made in such large numbers nor have given such good results for the rapid and precise elucidation of conditions at the bottom of the ocean, and centuries would have been needed to get the results that can be obtained without difficulty in a few years by echo sounding. The basic principle of echo sounding is very simple; it measures the time required for a sound wave to travel from the bottom of a vessel (the sea surface) to the sea bed and back. The returning wave can be detected as an echo and amplified. To calculate the depth, knowing the speed of sound in sea water, it is only necessary to determine the time from emission of the sound until the echo is detected—the echo time. If the time is t , the speed of sound in water v and the depth of the sea h , then

$$h = \frac{1}{2}vt.$$

Echo sounding makes it possible to sense the bottom of the sea accurately and to ascertain its actual topography. A vessel equipped with echo sounding can fix the depth of the sea without loss of time while moving at full speed. Scientifically, sonic sounding is of value only when: (1) it is combined with an accurate determination of the position of the vessel which in general should not be determined less accurately than ± 1 nautical mile and (2) when the mean velocity of the sound emitted by the echo sounding apparatus is known in addition to the echo distance. Only then is it possible to convert the value obtained to the true depth. The enormously increasing number of echo soundings requires the establishment of an international office to correct and unify the mass of data and to chart it after critical interpretation. This would give results of great utility both scientifically and for the improvement of the sea charts of all nations (DEFANT, 1938).

Echo sounding has only one disadvantage compared with wire sounding; it cannot be combined with the collection of bottom samples which are necessary to ascertain the nature of the bottom sediments. If these are needed wire sounding is indispensable. However, it is possible with more modern types of echo sounding equipment to draw some conclusions about the nature and thickness of the bottom sediments from the

appearance of the echo in the receiver. The structure and form of the returning wave is dependent on the nature of the reflecting surface. If the oscillatory form of the reflected wave can be ascertained in the receiver it is possible to decide whether the bottom is rock, sand, mud, or other material. It is very frequently found that the echo is split into broader or narrower bands which are clearly connected with the different layers in the bottom sediment (mud or rock). The echo sounder thus gives a preliminary idea of the nature of the bottom and often the thickness of the soft upper sediment. This was first mentioned by STOCKS (1935). For further details reference may be made to EWING, CRARY and RUTHERFORD (1917), BULLARD (1938) and EWING and VINE (1938). Another method of studying the structure and thickness of the deep sea sediments has recently been developed by WEIBULL (1947). Very good results were obtained with this by the Swedish "Albatross" Expedition (PETTERSSON 1946).

Indirect depth determination with an unprotected reversing thermometer. RUPPIN (1906, 1912) first suggested the use of the difference between protected and unprotected reversing thermometers for the measurement of the depth at which the reversing frame or the water sampler on which the thermometers are mounted is reversed. The usefulness of the method has been shown by the investigations which he carried out at depths up to 100 m and by those of VON PERLEWITZ at up to 1000 m. BRENECKE (1921) on the "Deutschland" Expedition of 1911-12 made valuable use of it, and it was used systematically for the first time on the "Meteor" Expedition of 1925-7 (WÜST, 1932). In both wire sounding and in oceanographic serial observations there is always a wire angle of greater or lesser magnitude and it is therefore extremely valuable to have a method available which allows a reduction of the temperature and salinity values to true depth or which ascertains a determination of depth independent of the wire angle.

For the construction and function of the reversing thermometer, the corrections applied and the accuracy of the depths obtained [see particularly Oceanographic Instrumentation (Report of conference, Rancho Santa Fe, California, 21-23 June 1952, p. 55)].

2. The General Morphology of the Sea Bottom

The topography of the bottom of an ocean or part of an ocean can be conveniently shown on a depth chart on which all available soundings are recorded after critical interpretation. The reliefs of the sea bottom can be shown by drawing lines of equal depth (isobaths) at fixed intervals. Constructing the isobaths between separate soundings is essentially a question of interpolation which is considerably facilitated if the soundings are distributed as evenly as possible over the whole area. This condition is unfortunately very rarely satisfied, even less so after the introduction of sonic sounding. Apart from the more sporadic distribution of earlier wire soundings there is now a greater concentration of soundings along isolated lines of echo soundings resulting in an extremely uneven distribution of depths and, while some parts are extremely well surveyed, there are very large areas with only single soundings. The task of preparing isobaths for an entire ocean has thus become more difficult than before the introduction of echo sounding.

The construction of the isobaths for an ocean area depends on subjective considerations; the lines must of course be fitted to the soundings, but the available points

usually allow considerable elbow-room for the use of ideas and speculations on the bottom topography afforded by other knowledge (for example, geological). In particular, the construction of the isobaths requires good use of oceanographic viewpoints. The distribution of temperature and salinity at the sea bottom and in the water immediately above it are dependent on the bottom topography and often allow greater accuracy than is possible from the records of depths alone, for example in the determination of depths on saddle points or the position of cross-ridges and others. Indicators such as these of the course of the isobaths are always valuable and deserve full attention. In this connection, see especially STOCKS and WÜST (1935) in the addenda to the chart of the Atlantic Ocean in the "Meteor" volumes.

Good charts are not available at the present time for all the oceans and adjacent seas; it is to be expected that there will be considerable improvement here in the future. Apart from the older depth charts in the Sailing Directions for single oceans and charts produced by single expeditions the following may be noted:

- (1) *The Carte Générale Bathymétrique des Océans*, scale 1 : 10 million, produced by the Hydrographic Bureau in Monaco; 16 sheets on Mercator projection; second edition, 1911–30, third edition from 1935.
- (2) The ocean chart published by GROLL (1912) in which all depths available up to that time were interpreted in a uniform way and used for careful construction of the isobaths; equal-area projection on a scale of 1 : 40 million.
- (3) The chart of the total Atlantic Ocean on the records of the "Meteor"; a general chart, 1 : 20 million on the Lambert equal-area azimuthal projection with isobaths at 500 m intervals (STOCKS and WÜST, 1935). In addition to this there is a basic chart of oceanic soundings on a scale of 1 : 5 million in 13 sheets (4 sheets published, STOCKS, 1937) showing all the critically checked soundings in this ocean.
- (4) A more recent chart of the Indian and Pacific Oceans has been given by SCHOTT (1935) on an equal-area projection, on a scale of 1 : 60 million, with the nature of the bottom topography of these oceans indicated with sufficient accuracy.
- (5) An excellent chart of the sea bottom topography of East-Indian Seas was constructed by VAN RIEL (1934) and was published in the scientific results of the "W. Snellius" Expedition.

For more recent charts of parts of the oceans and adjacent seas, see the sections on the special morphology of these areas. The charts accompanying this book (Plate 1) give a summary of what is known of the main features of bottom topography of the oceans. Much of the knowledge obtained by more recent expeditions by echo sounding has been taken into consideration here, in so far as the small scale will allow. In these charts the isobaths are drawn for every 1000 m and the 200 m isobath has been shown where the scale permits to show the limits of the continental shelf. The coloration of the depth-intervals gives a clear picture of the general bottom topography in spite of the confusion of lines at some points. In order to make the characteristic bottom configurations such as deep-sea basins, troughs and ridges and of the cross-ridges, deep-sea canyons and other forms which may occur, more visible, a somewhat *schematic* chart has been prepared and is reproduced in Plate 2 (DEFANT, 1947). All the important peculiarities of bottom topography of the ocean have been indicated by letters and numbers.

The first scientific interpretation of the topographical chart of the ocean bottom taken in conjunction with a contour map of the land areas of the Earth was a general investigation of the *relationships of heights and depths* on the surface of the Earth crust. This was a purely statistical analysis of the variations of the surface of the solid crust about an average value, the mean crust level. If the whole of the solid crust of the Earth were levelled off to give a single solid sphere, the mean level of the solid surface would be 2440 m below the present sea-level. The level of the sea itself would then be about 260 m above the present level, that is, the solid crust would be covered by a layer of water 2700 m thick (KOSSINNA, 1921). It would be expected that the frequency of occurrence of individual heights and depths was entirely random. The mean crust level (taking the present sea-level as zero: -2440 m) should occur most frequently, and the frequencies of individual heights and depths around this should form a probability curve. In these *chance* cavities the water would collect as oceans and the formation of the oceans would then offer no problems, since they would obviously form in the deepest depressions of the crust.

The statistical distribution of the heights and depths of the Earth crust has, however, led to the striking result that the frequency in no way approaches a Gaussian-probability curve. On the contrary, there are two height-intervals which occur with high frequency while the other, less frequent, intervals group themselves around these *two culmination points* as two probability curves (Fig. 8, Table 2).

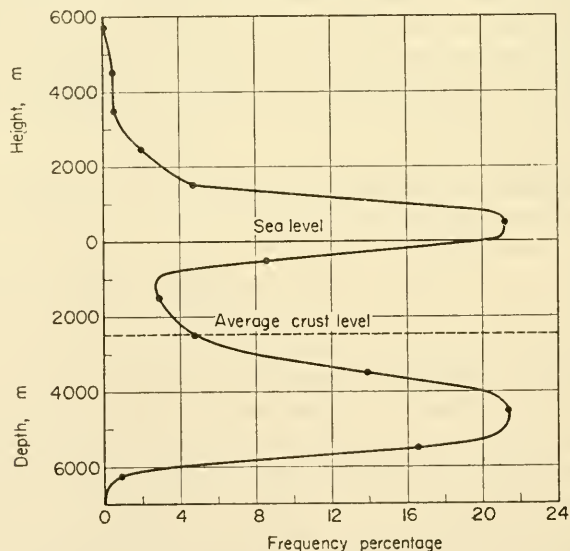


FIG. 8. Frequency distribution of different height and depth intervals over the entire surface of the Earth.

The two maximal frequencies lie at the height-interval of 0–1000 m and at a depth interval of 4000–5000 m; nearly 45% of the entire surface of the Earth falls within these two intervals, while only 10% falls on the other eleven steps. It is especially noticeable that the mean crust level of -2440 m (depth interval -2000 m to -3000 m) occurs infrequently, and is indeed very near the minimum between the two maxima.

Table 2. Frequency and areas of individual height- and depth-intervals of the earth crust
(According to KOSSINNA, 1921)

Interval (m)	Areas (10 ⁶ km ²)	Per cent	Interval (m)	Areas (10 ⁹ km ²)	Per cent
> 5000	0.5	0.1	> 5000	0.5	0.1
4000-5000	2.5	0.5	> 4000	3	0.6
3000-4000	3	0.6	> 3000	6	1.2
2000-3000	10	2.0	> 2000	16	3.2
1000-2000	24	4.7	> 1000	40	7.9
1000-500	27	5.3	> 500	67	13.2
500-200	33	6.5	> 200	100	19.7
200-0	48	9.4	> 0	148	28.1
0- -200	28.5	5.6	> -200	176.5	33.7
- 200- -1000	15.5	3.0	> -1000	192	36.7
-1000- -2000	15	2.9	> -2000	207	39.6
-2000- -3000	24.5	4.8	> -3000	231.5	44.4
-3000- -4000	71	13.9	> -4000	301.5	58.3
-4000- -5000	119	23.3	> -5000	421.5	81.6
-5000- -6000	84	16.5	> -6000	505.5	98.1
> -6000	4.5	0.9	> -10,000	510.0	100.0

The position of the two maxima can be fixed more closely by investigation of denser intervals. It is apparent that one maximum falls within the interval 0-200 m and the other within the depth interval 4600-4800 m. The structure of the crust thus includes *two special areas*: (1) a *land area* with a height of 100 m to 200 m, and (2) a *sea area* at a depth of about 4700 m. These two areas together include almost 65% of the entire surface of the Earth. These relationships can also be shown in another way in the "Hypsographic curve for the surface of the Earth" (Fig. 9) which depends on the areas in each separate height- and depth-interval over the surface of the Earth.

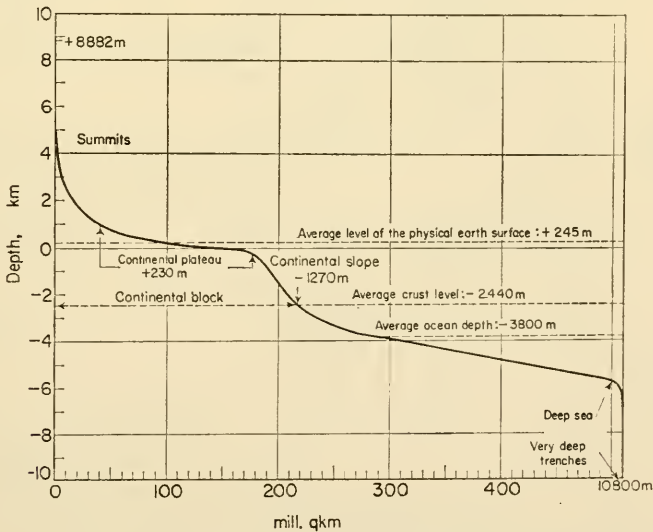


FIG. 9. Hypsographic curve for the surface of the Earth.

This shows a stepwise form and is divided by four inflection points into five parts which may be regarded as natural regions of the land and of the sea:

- (1) *Summits*. All land above 1000 m (approx. 40 million km², mean height 2040 m, maximum height: Mount Everest 8882 m)
- (2) *Continental plateaus*. Land below 1000 m and the continental shelf to -200 m (approx. 136 million km², mean height 230 m)
- (3) *Continental slope*. From the edge of the shelf at -200 m to mean crust level -2440 m (approx. 39 million km², mean depth 1270 m)
- (4) *Deep-sea bottom*. Sea bottom from -2440 to -5750 m (approx. 284 million km², mean depth 4420 m)
- (5) *Deep-sea depressions and trenches*. Below -5750 m (approx. 11 million km², mean depth 6100 m, greatest depth: "Emden" deep in the Philippines trench 10,800 m).

This marked distribution into high and low areas divides the surface of the Earth into: (1) a high continental block which includes all land areas, the adjacent and parts of the marginal seas and the continental shelf and projects about 3100 m above the mean crust level, and (2) the *deep sea* which lies in basins in the Earth's crust whose bottom is about 2000 m below the mean crust level. The division of the Earth's crust between the continental block and the deep sea is shown in the summary in Table 3 and is illustrated schematically in Fig. 10. These show clearly the sharp division between the two parts: the continental block and the deep sea; the continental slope

Table 3

OCEANS					
			per cent	per cent of total Earth surface	
$361.1 \times 10^6 \text{ km}^2$ 70.8% of the Earth surface	<i>Adjacent and mediterranean seas:</i> $40.0 \times 10^6 \text{ km}^2$ 7.9% of Earth surface	Shelf	43.7	3.5	
		Continental slope	31.8	2.5	
		Deep sea	24.5	1.9	
					7.9
	<i>Oceans:</i> $321.1 \times 10^6 \text{ km}^2$ 62.9% of Earth surface	Shelf	2.7	1.7	
		Continental slope	4.8	3.0	
Deep sea		92.5	58.2		
				62.9	
CONTINENTS					
$148.9 \times 10^6 \text{ km}^2$ 29.2% of the Earth surface	—	—	—	29.2	
				Total	
				100.0	
Total deep sea: 60.1%; Continental plateau (continents plus shelf): 34.4%; Continental slope: 5.5%				100.0	

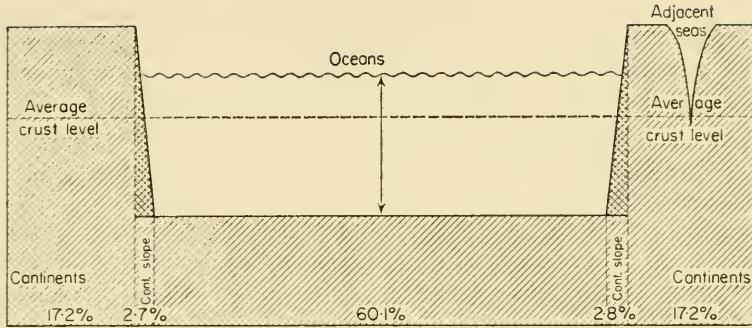


FIG. 10. Schematic representation of the Earth's crust by a continental block and a deep sea.

Table 4. Area, volume and mean depth of oceans and seas

(For Atlantic Ocean according to STOCKS 1938, otherwise according to KOSSINNA 1921)

Body	Area (10 ⁶ km ²)	Volume (10 ⁶ km ³)	Mean depth (m)	Greatest depth (m)
Atlantic Ocean	106.198	353.498	3331	8526 [†]
Indian Ocean	74.917	291.945	3897	7450 [‡]
Pacific Ocean	179.679	723.699	4028	10,800 [§]
<i>Atlantic Ocean</i> (excluding adjacent seas)	82.216	318.078	3868	8526
Arctic Mediterranean	14.057	21.453	1526	5180 [?]
American Mediterranean	4.311	9.373	2174	6269
Mediterranean Sea and Black Sea	2.969	4.318	1458	4404
Baltic Sea	0.422	0.023	55	463
Hudson Bay	1.232	0.158	128	229
North Sea	0.575	0.054	94	665
English Channel and Irish Sea	0.178	0.010	58	263
Gulf of St Lawrence	0.238	0.030	127	549
<i>Indian Ocean</i> (excluding adjacent seas)	73.443	291.030	3963	7450
Red Sea	0.438	0.215	491	2359
Persian Gulf	0.239	0.006	25	84
Andaman Sea	0.798	0.694	870	4177
<i>Pacific Ocean</i> (excluding adjacent seas)	165.246	707.555	4282	10,800
Asiatic Mediterranean	8.143	9.873	1212	6504
Bering Sea	2.268	3.259	1437	4273
Okhotsk Sea	1.528	1.279	838	3374
Japan Sea	1.008	1.361	1350	3712
East China Sea	1.249	0.235	188	2377
Gulf of California	0.162	0.123	813	2274
Bass Strait	0.075	0.005	70	—
<i>All oceans</i> (including adjacent seas)	361.059	1370.323	3795	—

[†] Puerto Rico trough north of Puerto Rico.

[‡] Java trench, south of Java.

[§] Philippines trench north-east of Mindanao ("Emden" depth).

^{||} Mariana trench, about 11° N., 143° E. Gr. greatest depth 10,363 m (according to CARRUTHERS and SAWFORD, 1952).

includes not more than 6% of the surface of the Earth, and this percentage is being decreased rather than increased by the results of echo sounding. These figures emphasize that the deep-sea basins are *not just chance depressions in the crust of the Earth*. This division of the structure of the Earth is one of the most important of geophysical phenomena and requires a special explanation that must be very closely connected with the history of the Earth.

Charting the sea bottom by means of isobaths and measurement of the areas of the different depth-intervals makes it possible to calculate the volume of *each ocean* and of the total ocean. The quotient of the volume and the surface area gives the mean depth. The volume of the ocean (including all the adjacent seas) amounts to 1370.6 million km³ and the mean depth is therefore around 3800 ± 100 m. The volume and mean depth can also be worked out for parts of the ocean and for the adjacent seas: the values for most areas according to Kossinna are given in Table 4. The Atlantic, Indian and Pacific Oceans have the mean depths 3930, 3960 and 4280 m respectively. These figures are not very different; the mean deviation is little more than 4%. In addition to this general agreement, the figures for the depth-intervals in all three oceans, as shown in Table 5, demonstrate a very similar morphological structure of the Earth crust. This is further proof of a uniform structure in different parts and an indication that the existence of the two favoured levels of the Earth's crust represented by the continents and the deep-sea bottom is a universal phenomenon prevailing over all parts of the Earth's crust. If the average density of sea water, taking the compressibility into account, is as 1.037, the total mass of the ocean will be $1.42 \times 10^{18} = 1.42$ trillion tons which is only 1/4200 part of the mass of the Earth.

Table 5. Morphological structure of the three oceans (excluding mediterranean seas). Areas of the different depth-intervals given in percentage of the total Earth surface (Atlantic Ocean according to STOCKS 1938; otherwise according to KOSSINNA 1921)

Depth-interval in km	0-0.2	0.2-1	1-2	2-3	3-4	4-5	5-6	6-7	7	Sum
Atlantic Ocean	5.8	3.8	3.7	7.5	21.3	33.9	23.3	0.7	0.3	100.0
Indian Ocean	3.2	2.7	3.1	7.4	24.4	38.9	19.9	0.4	—	100.0
Pacific Ocean	1.7	2.2	3.4	5.0	19.1	37.7	28.8	1.8	0.3	100.0
All oceans	3.1	2.8	3.4	6.2	20.1	36.6	26.2	1.2	0.1	100.0

3. Special Characteristics of Sea-bottom Topography

The larger and smaller oceans and parts of the oceans are usually considered as more or less extended volumes sunk into the solid crust of the Earth. From this one is guided to assume that the sea bottom taken as a whole is concave inward. In reality this is so only in exceptional cases; in general the sea bottom arches upward and follows the surface of a sphere with a somewhat larger radius than that of the surface of the Earth.

Expressed in another way the radius of curvature of the sea bottom points towards the centre of the Earth almost all the time and differs little from the radius of curvature of the Earth. If large areas are considered, really concave basins occur very infrequently and are limited to the margins of the deep ocean trenches, to crater-shaped basins and especially to individual adjacent seas. Bathymetric charts of the

ocean bottom, based on a few wire soundings, gave rise earlier to an impression of a certain smoothness and evenness of the sea bottom. Especially the bottom slope between two sounding points was ascertained and in most cases was found to be less than the smallest deviation from horizontal that the human eye can still detect. (a slope of 1 : 200 or a slope angle of $0^{\circ} 17'$). Actually, values found in this way showed very few vertical divisions over wide stretches of the ocean. This very smooth seabottom topography has, however, been shown by the much closer values given by echo sounding to be at least partly a misapprehension caused by the small number of wire soundings. Without doubt the sea bottom on the whole and especially away from areas where orogenetic and volcanic forces are active is *on a small scale* far more smooth and even than the surface of the land. The effects of the atmosphere, weathering and erosion by running water which all contribute to the variety of small forms which occur on land surfaces are of course all absent. However, echo-sounding profiles at close intervals very often show considerable bottom irregularity. All echo-sounding profiles so far obtained are similar in this respect. The morphological interpretation must be made with the greatest caution since for greater clarity the results are usually shown with a strongly exaggerated vertical scale. Some vertical distortion is, however, essential when the profile extends over such great distances in order to show the details of the sea bottom clearly. Figures 11 and 12 show the "Meteor" profile

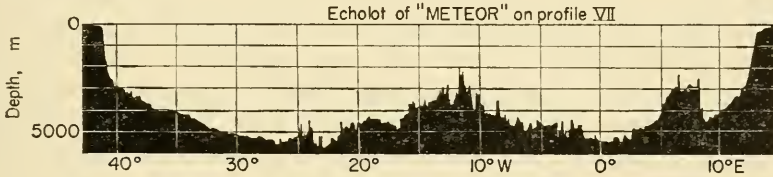


FIG. 11. Echo sounding profile across the South Atlantic obtained by the "Meteor" at 23° S. (profile VII: $21^{\circ}25'$ – 24° S.); with 180-fold enlargement of the vertical scale and disregarding the curvature of the Earth.

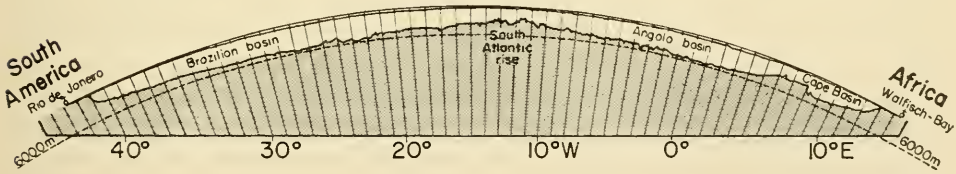


FIG. 12. The same echo sounding profile as in Fig. 11 taking the curvature of the Earth into account. Upper curve: vertical enlargement 1:3; lower curve: 1:30 (according to Stocks).

VII ($21^{\circ}25'$ – 24° S.) in two different forms (according to STOCKS, 1936). The upper diagram shows the echo-sounding profile along a line from Rio de Janeiro to Whalefish Bay with a 180-fold magnification of the vertical scale and without taking the curvature of the Earth into consideration. In the lower profile, on the same horizontal scale, the curvature of the Earth at latitude 23° has been taken into account; the outer arc is the surface of the sea, and below this the upper curve shows the sea bottom with a vertical exaggeration of 3 : 1 while the lower curve shows the sea bottom with a vertical exaggeration of 1 : 30. The details of bottom topography and changes of slope are still easily recognizable on the curve with a 30-fold vertical exaggeration and

are closer to reality than that in the upper diagram. A quantitative reading of differences in height is, however, hardly possible here, and with a vertical magnification of only $\times 3$ the thickness of the thinnest lines on the diagram is significant. The appearance of prominent features such as the Whalefish ridge can scarcely be seen and any qualitative differentiation into areas of greater or lesser irregularity is hardly possible. Magnification of the vertical scale is thus necessary from the topographical point of view, but must be used with appropriate caution.

No accurate numerical evaluation of the echo-sounding profile, in order to fix the degree of bottom irregularity in different parts of the ocean, has yet been made. The superficial appearance of most of these profiles shows that the bottom relief varies from one area to another, and care is needed in making generalizations as these soundings give more and more detail. In most cases there is a relatively smooth bottom profile in the broad extended deep-sea basins and considerably greater irregularity over the central ridges and over the rises that separate the broad basins; considerable elevations above the mean surface of an area occur frequently in the vicinity of great depths and depressions so that extreme variations in depth are very often situated close together.

Only certain especially characteristic forms of the commonly occurring typical bottom features will be discussed here. Stretching out to sea from the edge of the land there is first the *beach* which at high water is part of the sea bottom and, at low water, is part of the land. This amphibious part of the Earth's surface according to the estimate of SCHOTT has an area of 1.6 million km² or about 0.4% of the ocean area. Outside this the ledge-like rim appears, sometimes narrow, sometimes broad, but rarely completely absent, and is called the *continental shelf*. From the boundary between the land and the sea the sea bottom, except along coastal cliffs, slopes gently down at a slight angle, at the most 1–1.5°. This angle gradually increases and near the 200 m isobath it changes abruptly to the steeper gradient of the continental slope. The mean slope angle is about 3° here but in isolated cases it may be appreciably larger (6–10° or more). The edge of the shelf is normally at a depth of between 100 m and 200 m, but in some cases it appears only at a depth of 400–500 m. The continental shelf is seldom a uniform surface. It is very frequently broken by canyons, furrows and troughs, and shows clearly the effects of the more intense movements of the water because of the shallow depth (ocean and tidal currents). These effects of the action of the ocean are not found everywhere; in some places the sea bottom has clearly been formed during the ice ages by glacial action and has the character of a drumlin landscape as in the Irish Sea, for instance, between Ireland and Scotland.

The continental shelf can usually be regarded as a part of the continental block which has been flooded by the sea, and its formation and topography are partly the product of the separation of the continents through accumulation and partly due to the erosion of the coast by wave action (PENCK, 1934). Up to the present time no detailed investigation of the extent of the continental shelf has been made. Usually the 200 m isobath is taken as the outer limit of the shelf and the area of the shelf within this is usually designated as "bathymetric". In his statistics of the ocean depth Kossinna has listed these areas for each continent (Table 6). The bathymetric shelf extends over an area of 27.5 million km² or 7.6% of the area of the ocean; Wagner has given the value 30.6 and Kegel has given 29.5 million km². The mean depth of the

shelf has been estimated by Kossinna as less than 100 m and is probably between 50 m and 70 m.

Table 6. The shelf-areas (0–200 m) of the continents and oceans respectively (10^6 km^2 , according to KOSSINNA, 1921)

Continents	Areas	Oceans (excluding mediterranean seas)	Mediterranean seas
Europa	3.11	Atlantic Ocean 4.59	of the Atlantic Ocean 9.52
Asia	9.38	Indian Ocean 2.37	of the Indian Ocean 0.80
Africa	1.28	Pacific Ocean 2.89	of the Pacific Ocean 7.32
Australia	2.70		
North America	6.74	Sum 9.85	Sum 17.64
South America	2.42		
Antarctic	0.36		
Sum	25.99 + rather distant islands 1.50	Sum $27.49 \times 10^6 \text{ km}^2$, 7.6% of the sea surface	

The shelf near the continental slope, often at a considerable distance from the coast, shows remarkable *canyon-like troughs* stretching over the bottom of the shelf and the adjacent continental slope. While previously only a few of these remarkable structures were known it has been shown recently, especially by the work of the United States Coast and Geodetic Survey, that they are of wide occurrence. Their topography can be rapidly and accurately determined by echo sounding. They were first thought to be drowned, sunken valleys, but it has been shown that they probably have a different origin. Two trough forms are found: submarine valleys in areas which have at some time been strongly glaciated (for instance around Iceland) and submarine canyons in regions which have remained unglaciated. The latter are usually found only at the edge of the shelf in the area of transition to the continental slope; these reach large depths (2000–3000 m) and often have little apparent connection with the topography of the neighbouring coastal area. Several series of these submarine canyons have been found and accurately charted: on the continental shelf and the edge of the shelf along the North American coast north of Cape Hatteras among which is the long-known submarine valley of the Hudson mouth (Fig. 13), along the coast of California and along the coast of Washington and Vancouver Island (SMITH, 1939). Individual submarine valleys are known along the east coast of Korea, along both coasts of Japan and on the eastern and southern coasts of Formosa. Submarine valleys frequently occur at the mouths of large rivers, such as the Ganges, the Indus (Fig. 14), the Congo (Fig. 15), the Ogowe and the Niger. They are also present in different parts of the European and American mediterranean seas. Some parts of the continental shelf are free from these canyons, for example the North American coast south of Cape Hatteras or the eastern coast of Asia south of the Yellow Sea. A summary of the distribution of canyons in all oceans and the possible nature of their origin was recently given by SHEPARD (1948).

The walls of these submarine canyons are usually very steep on both sides, often with a slope of $5\text{--}10^\circ$ and sometimes $20\text{--}35^\circ$ or even more. These canyon walls must be made of hard rock since thick layers of soft loose sediments could not be

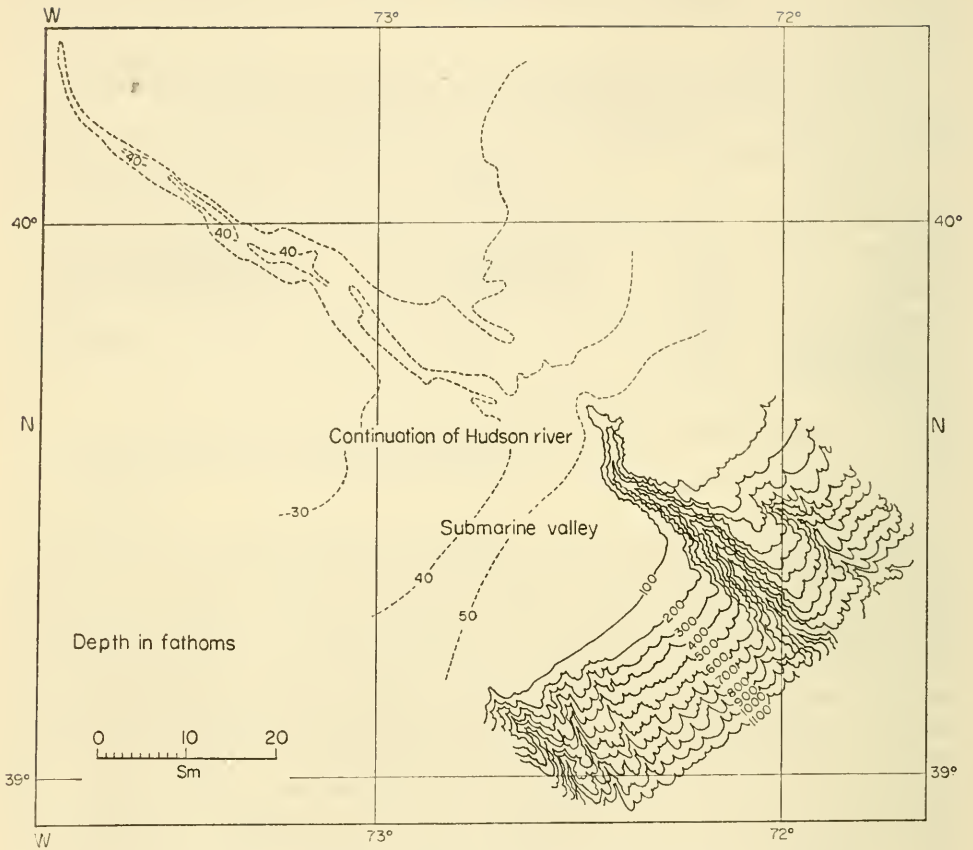


FIG. 13. Submarine valley off the mouth of the Hudson (according to Smith).

expected to remain at such steep angles for any length of time without collapsing. Nor can it be supposed that they have been washed out of thick soft bottom sediments since they would then hardly be permanent. On the other hand, they appear definitely to be quite young formations that have been formed only in recent times; they appear, at least in part, to be connected with earthquakes, tectonic breaks and fissures. For a description of the morphology of these canyons see especially the work of SHEPARD and his collaborators (1933, 1938); concerning their probable origin see particularly DALY (1936) and KUENEN (1938); reference might also be made to the interesting work of COOPER and VAUX (1949), of KULLENBERG (1954), HECSON, ERICSON and EWIN (1954). They have been discussed from the purely geological standpoint by JESSEN (1943), and a survey has been given by KAEHNE (1941).

Turning to the *general form of the deep sea bottom* it is immediately obvious that the rises and ridges that divide the ocean are features of such enormous size that they could scarcely occur on the land. The most prominent of these features is the Atlantic Ridge that extends from Iceland through the Azores, Ascension and Tristan da Cunha to Bouvet Island and resembles an enormous mountain range 20,000 km

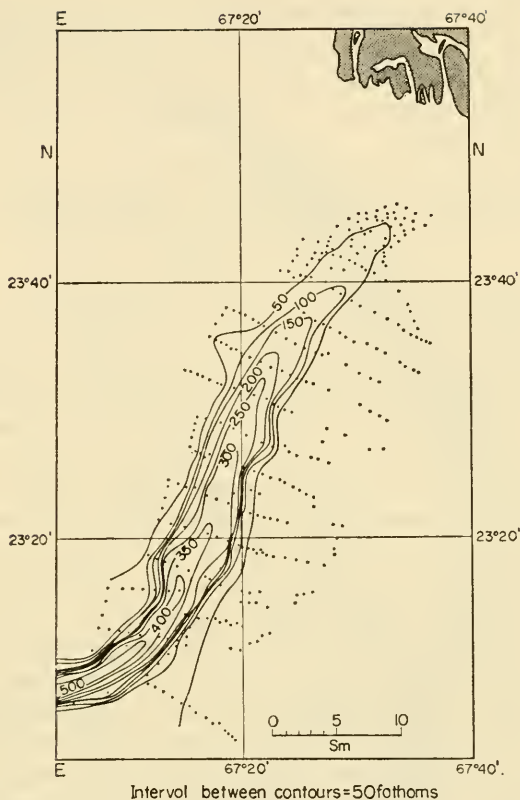


FIG. 14. Submarine valley off the mouth of the Indus.

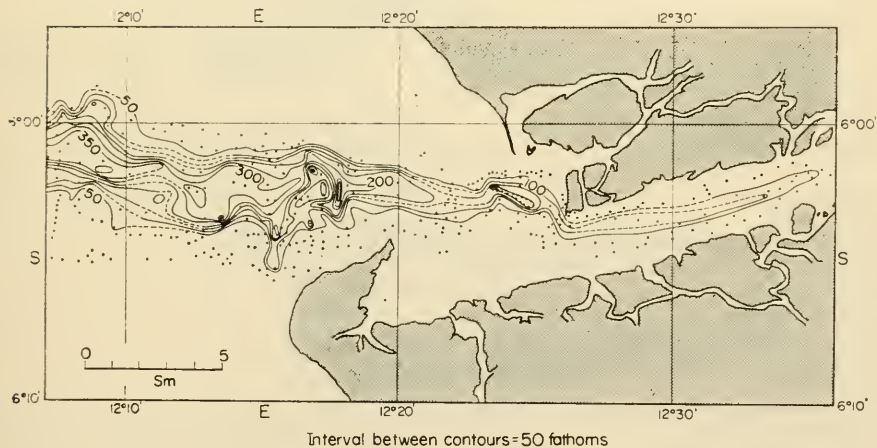


FIG. 15. Submarine valley of the Congo.

long. It divides the Atlantic Ocean into two parts: the eastern and the western Atlantic troughs. These two elongated depressions are further divided into basins by transverse ridges. The peculiar relief features of the Atlantic Ridge which forms the axis of the Atlantic and runs roughly parallel to the continental coast on both sides is regarded by many as the beginning of a mountain fold, but it could also be the rump of an old one (KOSSMAT, 1931).

The Indian Ocean shows a similar division. Here also there is an Indian Ocean Ridge dividing it into an eastern and a western half, though these two halves appear to be less subdivided. The Pacific Ocean, on the other hand, is largely a single basin (see p. 29).

Amongst the most prominent features of the oceanic bottom topography are the narrow elongated arcs of marginal deeps that lie near the surrounding mountain chains (or island chains) of the Pacific basin and contain the greatest ocean depths. These remarkable depressions are confined exclusively to the margins of the Pacific Ocean; they can also be found in the Sunda arc in the eastern Indian Ocean, in the Caribbean, in the middle Atlantic Basin and in the south Sandwich marginal deep in the western part of the South Atlantic. They are usually termed "deep-sea trenches" or "troughs". This has reference only in a morphological sense and not to its origin. They are very closely connected with folding processes in the earth's crust, and to some extent are the counterpart of the mountain chains of the land, and have a related origin. As an example, the Mariana marginal deep is shown in Fig. 16 both on an isobathic chart and in a profile perpendicular to its longitudinal extension (SIGEMATSU, 1933). Its topographical form is typical of all well-developed marginal deeps. On the side towards the land, towards the submarine ridge which runs alongside the deep and is always of mountainous character, the slope is steep, on the ocean side of the deep the slope is more gentle. On the landward side the angle of the slope may be as much as 20° or more; according to Schott the mean value for a large number of Pacific deeps is 6.3°. They are always long and narrow.

Table 7. The most important trenches
(With reference to soundings up to 1954)

	Greatest depth (m)		Greatest depth (m)
<i>North Pacific Ocean</i>		<i>East Pacific Ocean</i>	
Alaska-Aleutian Trench	7679	Chile-Peru Trough	7634
		Atacama Trench	6867
		Arica Trench	5342
<i>West Pacific Ocean</i>		South Mexico Trough	5121
Japan Trench		Manzanillo Trench	4867
(Kurillen, Hokkaido, East-Hondo)	10,554	California Trench	
Bonin Trench	9156	<i>East Indian Ocean</i>	
Mariana Trench	10,897	Sunda Trough	7455
Ryu-Kyu Trench	7507		5664
Philippines Mindanao Trench	10,497	Andamana Trough	5257
Yap Trench	7141	<i>Atlantic Ocean</i>	
Palau Trench	8138	Puerto Rico Trough	9219
Bougainville-New Britain Trench	9140	Cayman Trough	7200
New Hebrides Trench	7570	South Sandwich Trench	8264
Tonga-Kermadec Trench	10,633		

Table 7 gives a list of the marginal deeps and the greatest depths that have so far been measured in each. Without doubt these marginal deeps contain the deepest fissures in the Earth's crust, and in their neighbourhood are the greatest vertical differences in height that are to be found within a short horizontal distance on the Earth's crust.

The marginal deeps are conspicuously associated with the volcanic belt which stretches along the landward side (on island chains or submarine ridges) parallel with the line of deep-sea trenches and with the earthquake belt which is also present in the immediate neighbourhood of the trenches, especially on the landward side. This connection with seismic and volcanic activity is always present and indicates a causative connection between these phenomena. Another phenomenon closely associated with the marginal deeps is the strong negative gravitational anomaly occurring along a very narrow line. The investigations of VENING-MEINESZ (1932, 1934) on the gravitational field in the East Indies and later the investigation of HESS (1938) in the West Indies have clarified this connection. The belt of abnormal gravity does not coincide exactly with the line of deep-sea trenches, but is displaced towards the adjacent mountain ridge. There exists in all cases a parallelism with the deep-sea trenches, but the relationship to the topography is more complicated than this. In the Philippine trench the line of negative anomaly lies directly underneath the trench (see Fig. 17) but it is

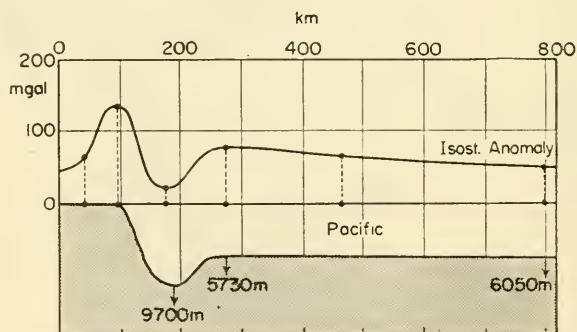


FIG. 17. Gravity profile over the Philippine Trench at Surigao (isostatic anomaly; observed values indicated by black dots; the bottom profile shown schematically with a vertical enlargement by 1:15) (according to Vening-Meinesz).

weak, although the trench is particularly deep; in the Java trench the gravitation anomaly is very pronounced but lies at the side of the trench (Fig. 18). Since a line of negative gravitational anomaly is present wherever there is a deep-sea trench, there must undoubtedly be some connection between the two phenomena. This is also indicated by the relationship of seismic activity and the distribution of volcanoes mentioned above. For the explanation of this relationship, see especially VENING-MEINESZ (1940).

In addition to the deep-sea trenches there are also the differently shaped, nearly circular depressions. It cannot yet be decided whether these should be regarded as deformed marginal deeps but those between the Sunda Islands, the Moluccas, and the Philippines (Celebes, Sulu, Banda and other deeps) occur in close connection with the

East Indian negative gravitational anomaly. There are similar shaped deeps in the European Mediterranean, in the Gulf of Mexico and in other places, though not of the same depth or extent. Amongst these may be reckoned the comparatively small but very deep Romanche deep which divides the mid-Atlantic Ridge in two, at about 18–19° W. on the equator. The corresponding lowering of the mid-Atlantic ridge is as low as 4500–4800 m. The great significance of this deep connection between the eastern and the western troughs for the hydrographic structure of the water masses of

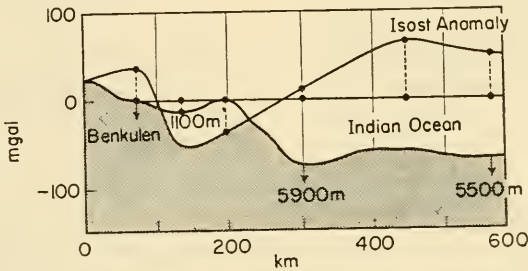


FIG. 18. Gravity profile from Benkulen (Sumatra) towards the Indian Ocean (see Fig. 17).

the eastern trough will be discussed later (see Chap. III, 5, b). The greatest depth measured in the Romanche deep is 7230 m. A bathymetric chart of the area has been given by STOCKS and WÜST (1935).

While the slope of the deep-sea bottom is in general slight and only reaches larger values at the continental slope, occasionally very steep gradients occur near islands, submarine banks and reefs. As on land there has often been major volcanic activity on the sea bottom, partly in extended zones associated with the deep-sea trenches and partly more widely spread. The steepest slopes are always those of the purely oceanic islands which are all of volcanic origin; these slopes are of the same order of magnitude as those of land volcanoes. The slope of the island St Helena, for example, over short distances is as much as 38–40° and the Atlantic island St Paul has slopes of 62°.

In numerous cases the volcanic forces have been insufficient to build an island cone up to the surface. They form submarine peaks, whose summits may still be some hundreds of metres below the surface and seldom come up to normal anchorage depths. These submarine volcanic cones were only occasionally found by wire sounding, which allows them to be quickly and accurately charted. In this connection there might be mentioned the surveys of the area of the Bogoslov volcano (Bering Sea) by the United States Coast and Geodetic Survey (SMITH, 1937) and the survey of the "Altair" peak (DEFANT, 1939).

4. Arrangement of the General Bottom Topography of the Individual Oceans

For an elucidation and abbreviation of the following discussion Plate 2 is presented, and it shows all the main characteristic features of sea-bottom topography in a clear manner. For each ocean there is a list of the principal features which have been designated by letters and numbers on the plate. The capital letters show the deep-sea basins (troughs) in succession for each ocean, the small letters denote the ridges and rises that separate these basins, and the numbers indicate the deep-sea trenches.

(a) Atlantic Ocean

<i>Deep-sea basins</i>	<i>Ridges and rises</i>
A North America Basin	a North and South Atlantic Ridge
B Brazil Basin	b Rio Grande Rise
C Argentina Basin	c Whalefish Ridge
D Cape Verde Basin	d Atlantic Indian Ridge
E Sierra Leone Basin	e Guinea Rise
F Guinea Basin	f Sierra Leone Rise
G Angola Basin	
H Cape Basin	
J Agulhas Basin	<i>Deep-sea trenches and troughs</i>
K Atlantic–Antarctic Basin	1 Cayman Trough
L South Antilles Basin	2 Puerto Rico Trough
	3 South Sandwich Trench
	4 Romanche Trench

The topography of the Atlantic Ocean bottom is characterized by its division into East and West Atlantic Troughs by the Atlantic Ridge. This ridge begins at Iceland; from the Iceland shelf it runs south-westward as the narrow Reykjanaes Ridge whose bottom form was fixed by the soundings of the "Meteor" (Bathymetric chart by DEFANT, 1930, 1931, 1936). At 51° N. the ridge broadens out somewhat towards the west (Telegraph Plateau), and then runs into the Azores Plateau which can be regarded as a great extension of the central ridge to the east and south-east. The ridge then narrows and remains at a depth of 2500–3500 m and apart from St Paul Island supports no islands as far as the equator. At 7–8° N. 36° W. there is a gap which reaches to a depth of 4400 m. The greatest gap is, however, on the equator near the Romanche Trench (see p. 27). South of this the ridge is broad and rounded and carries the islands Ascension (height 860 m), Tristan da Cunha (2329 m), Gough (1335 m) and Bouvet (935 m). St. Helena belongs to a minor ridge farther to the east. These extended minor ridges are peculiar to the section of the ridge between 0° and 20° S. The South Atlantic Ridge is connected west of Bouvet Island by the Atlantic Indian Ridge to the Crozet and Kerguelen Ridges of the Indian Ocean. The Atlantic Ridge extends over 20,300 km and is by far the longest underwater mountain system on the Earth.

The Eastern and the Western Atlantic Basins are further divided by transverse ridges. An outline of the main division is shown in Plate 2 where the geographical arrangement of the basins is particularly clearly shown. A special characteristic of the Atlantic Ocean is that it is completely closed in the north towards the Arctic Sea and the Norwegian Sea below a depth of about 500 m. This has far-reaching oceanographic consequences. In contrast to this nearly complete blocking of the deeper layers to the north, the Atlantic in the south is completely open down to great depths to the Atlantic–Antarctic Basin.

There are topographical differences between the eastern and the western troughs that have a considerable effect on the oceanographic structure. The transverse ridges are not as well developed in the western trough as in the eastern, and particularly the Rio Grande Ridge, which is somewhat better developed, has deep openings that permit continuous communication from the Atlantic–Antarctic Basin through the Argentina Basin, the Brazil Basin and the Guiana Basin to the North America Basin below 4000 m. In the eastern trough, on the other hand, the Whalefish Ridge, which

separates the Cape Basin from the Angola Basin, forms a continuous diagonal transverse barrier. It rises steeply from a depth of 5000–5500 m to only 964 m, forming an unbroken submarine wall connecting the mid-Atlantic Ridge between Tristan da Cunha and Gough Island with the broad shelf of the African mainland. All the other ridges in the east Atlantic trough have openings that reach below 4000 m.

(b) *Indian Ocean*

<i>Deep-sea Basins</i>		<i>Ridges and rises</i>	
A	Arabian Basin	a	Bengal Ridge
B	Somali Basin	b	Carlsberg Ridge
C	Madagascar Basin	c	Diego Garcia Bank
D	Agulhas Basin	d	Central Indian Ridge
E	South-west Indian Antarctic Basin	e	Mascarene Ridge
F	South-east Indian Antarctic Basin	f	Atlantic-Indian transverse Ridge
G	South Australian Basin	g	Crozet Ridge
H	India–Australia Basin	h	Kerguelen–Gaussberg Ridge
		i	Macquarie Ridge
<i>Deep-sea trenches</i>			
1	Sunda Trench		
2	Nicobar Trench		

It is only in more recent times that it has been found that the Indian Ocean is also divided into two large troughs by a central ridge. This central ridge runs north-westward from the Kerguelen–Gaussberg Ridge, gradually narrowing, then through the elevation around the volcanic islands of New Amsterdam and St Paul in the section between the 20° and 0°, where it reaches its highest elevation. Here it carries the shallow waters and banks of the Saya da Malha and the Nazareth Bank. Two outlying ridges run out from this point, one to the north-west to the Seychelles and the Amirantes, and the other to the south-west, here it carries the islands of Mauritius and Reunion. In this middle section the ridge stretches over more than 10° of latitude. From here it splits into two parts running towards the north. The eastern part carries the Chagos Islands and runs up through the Maldives and the Laccadives, gaining a connection to the south-west Indian shelf. The western part, which was first mapped by the Danish “Dana” Expedition (Carlsberg Ridge), is much narrower and not as high. This Indian Ridge is also of enormous length and runs from the South Arabian Sea to the edge of Antarctica at Kaiser Wilhelm Land (Wüst, 1934).

(c) *Pacific Ocean*

<i>Deep-sea basins</i>		<i>Deep-sea trenches</i>	
A	Central Pacific Basin	1	Aleutian Trench
B	Philippines Basin	2	Kurile Trench
C	Caroline Basin	3	Japan Trench
D	Coral Basin	4	Bonin Trench
E	Fiji Basin	5	Mariana Trench
F	Tasman Basin	6	Japan Trench
G	South Pacific Basin	7	Philippines Trench
H	Berlinghausen Basin	8	Riukiu Trench
J	Peru–Chile Basin	9	Bougainville–New Britain Trench
K	Californian Basin	10	New Hebrides Trench
L	Banda Sea	11	Tonga Trench
M	Celebes Sea	12	Kermadec Trench
N	North China Sea	13	Chile Trench
		14	Peru (Atacama) Trench
		15	Californian Trench

Ridges and rises

- a Bonin Ridge
- b Eastern Pacific longitudinal Ridge
- c South Pacific transverse Ridge
- d Macquarie Ridge
- e Fanning Ridge
- f Hawaii Ridge
- g Fiji Ridge
- h New Hebrides Ridge

As has already been mentioned above (see p. 24), the deep-sea trenches that are a major characteristic of the Pacific Ocean are marginal, that is, they occur around the rim of the ocean, either near the coast or beside outlying island chains. The main part of the ocean forms a vast deep-sea basin that, judged by the rather sparse soundings available, is not as strongly subdivided as the Atlantic and the Indian Oceans. The western, and especially the north-western open Pacific Ocean, contains the greatest continuous extension of the sea bottom below 5000 m and wide areas have a depth even greater than 6000 m. The eastern and south-eastern parts are less deep. Soundings have confirmed the deep-sea division, apparent from the individual chains of islands, along a direction from north-west to south-east. In the central part of the ocean, especially to the south, there are groups of islands that are not associated with deep-sea trenches and that occur in clusters. It was earlier supposed that these were on top of plateaus or ridges at no great depths. More recent soundings have shown, however, that this is not the case; only islands that are very close have any submarine connection, and the others usually rise separately as volcanic cones from very great depths and form a very characteristic topographical feature of the South Pacific.

(d) Mediterranean and Adjacent Seas

The Atlantic Ocean is connected with the greatest number of mediterranean seas, which have also greatest extent. These are the Arctic Sea, which can also be regarded as a continuation of the open ocean across the Greenland-Iceland-Faroes Ridge, and the American and European mediterranean seas.

The North Polar Sea, also known as the Arctic Mediterranean, includes: (1) the North Polar Basin surrounded by the seas of the flat shelf of Northern Europe and Northern Asia (Barents Sea, Karelian Sea, West Siberian Sea, Nordenskjöld Sea, the East Siberian Sea and the Tjuktjen Sea) and of North America (Beaufort Sea and the large number of sea straits in the North American archipelago); (2) the European North Sea south of the Spitzbergen Ridge (depth 1750 m); and (3) the Baffin Sea. The total area amounts to 14.06 million km².

The European North Sea is divided by a ridge at a depth of about 2400 m, running from Iceland through Jan Mayen to the Bear island into two basins; the southern Norwegian deep and the northern Greenland deep, both with a depth of over 3000 m. For the bottom topography of the North Polar Basin see WÜST (1941).

The American Mediterranean is divided by the coastal orography and by the bottom topography into three areas: the Mexico Basin (1.602 million km²), the Yucatan Basin (0.760 million km²), and the Caribbean Basin (1.948 million km²) with a total area of 4.310 million km². A new bathymetric chart has been prepared by STOCKS

(1938) taking into account numerous recent soundings. The Caribbean Basin is itself further subdivided by two north-south ridges the Beata and the Aves Ridges into three parts: the Magdalena Basin in the west, the Venezuela Basin in the middle and the Aves Basin in the east.

The general form of the bottom topography of the whole of the American mediterranean basins shows considerable regional differences that can be explained by their different origins (see DIETRICH, 1937, 1939). All three basins are to a large extent cut off from the Atlantic Ocean; this is of decisive importance for the question of renewal of the deep water of the individual basins. The Gulf of Mexico is connected with the free ocean only through the Florida Straits (sill depth 800 m) and with the Yucatan Basin through the Yucatan Channel (sill depth 1600 m). The Yucatan Basin and the Caribbean Sea are connected over the Jamaica Ridge with a sill depth of not more than 1400 m. The Yucatan Basin has a single connection with the Atlantic Ocean, the Windward Passage between Haiti and Cuba with a sill depth of about 1600 m. The Caribbean Sea is connected with the open ocean by several gaps between the West Indian Islands, the deepest of these are the Mona, the Jungfern and the Anegada Passages, which are the only ones concerned in the renewal of the deep water of this mediterranean sea. Their sill depths are 1600-1620 m and 1780-1800 m, respectively.

The European Mediterranean Sea. This falls into two clearly separated main divisions, the Western Mediterranean from the Straits of Gibraltar (sill depth 320 m) to the Sicilian Ridge (sill depth 324 m), and the Eastern Mediterranean. To the latter are connected the Adriatic Sea and the Aegean Sea which in turn is connected through the Dardanelles (sill depth 57 m) with the Sea of Marmora and further, through the Bosphorus (sill depth 37 m) with the Black Sea. A modern bathymetric chart for the European Mediterranean has been given by STOCKS (1938). The Western Mediterranean is separated by a ridge running from Tunis through Sardinia, Corsica and Elba to the Italian mainland into two basins: the Balearic Basin in the west and the Tyrrhenian Basin to the east (greatest depth 3731 m). The Eastern Mediterranean goes down to considerable depths (more than 4000 m) especially in the Ionian Basin; the greatest depth is 4715 m south-west of Cape Matapan.

Of the smaller mediterranean seas around the Atlantic, the Baltic and the Hudson Bay may be mentioned, but will not be described further since they have largely the character of shelf seas. The mediterranean seas of the other oceans are also of the same type except for the *Red Sea* which is an elongated canyon-like trough with depths of more than 2000 m and forming a real trench between the coastal strips of the Arabian and Egyptian plateaus. Its outlet in the south is the Strait of Bab el Mandeb with a sill depth of about 150 m. The Persian Gulf is a shelf sea with depth less than 100 m (STOCKS, 1944).

Chapter II

The Sea-water and its Physical and Chemical Properties

1. Collecting Oceanographic Samples

THE ocean basins are filled with a liquid that is essentially the same as rain water formed by the condensation of water vapour. An accurate knowledge of the different contents of sea-water is indispensable in order to be able to learn something of the geophysical-chemical structure of the ocean. This knowledge of the structure must be derived from samples collected at oceanographic stations. It cannot be limited to the surface layers of the sea but must include all layers down to the sea bottom and must be based on a network of observation stations placed as systematically as possible. The precise determination of the spatial distribution of the oceanographic factors is a major achievement of modern oceanography and its observational technique.

Collecting samples from the surface of the sea offers no real difficulties, or at the most only those that can be overcome by simple means. The collection of unobjectionable and homogeneous material of definite origin from deep layers of the sea is, however, not easy and it has required the work of several decades to overcome the difficulties. The differences in the oceanographic factors (such as temperature and salinity) at deeper levels become continuously smaller both in horizontal and vertical direction; the accuracy of measurements at great depths must therefore be increased, and it has only been possible by the use of modern analytical techniques to do this with the degree of accuracy needed to follow small local variations.

Almost all the properties of sea-water, apart from the temperature, can be determined if genuine samples of water are available from each particular depth, because these properties show no appreciable alteration when the sample is brought from the deep sea to the surface. The temperature of the water must, however, be determined at the place and at the depth from which the water sample was taken (*in situ*).

To collect oceanographic data at a station it is necessary to lower a thermometer in order to measure the temperature at different depths, and to bring back genuine samples of water from these depths in sampling bottles. The work at such an oceanographic station is done with a series-machine so-called because it is usually used for series observations, that is, the sampling bottles and thermometers are lowered at the same time to predetermined depths and a series of samples is collected and brought back together with temperature measurements. More recently, specially built machines have been used for this, but sounding winches or hydrographic winches were used previously. The oceanographic series machine and its operation on board ship will not be described here, but details are given "*Meteor*" *Work*, 4, No. 1 (WÜST, BÖHNECKE and MEYER, 1932, Berlin).

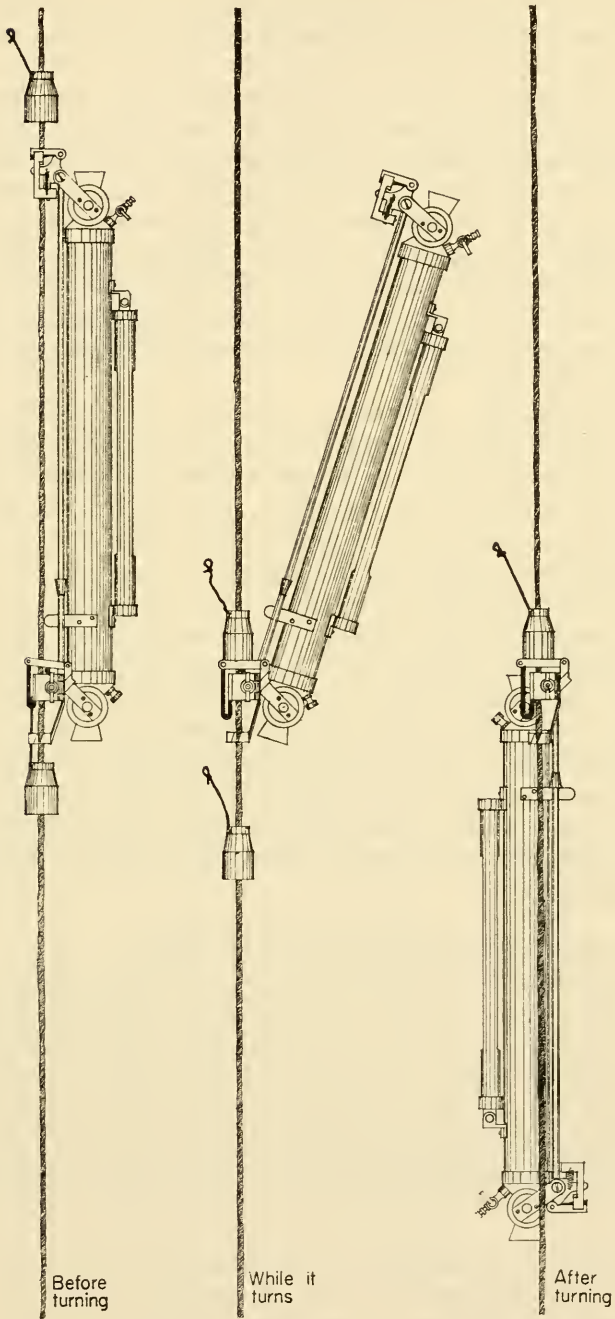


FIG. 19. Water bottle used on the "Meteor" Expedition and method of operation.

Sampling bottles and thermometers are the most important of the instruments used at an oceanographic station. To be suitable for series observations the sampling bottle must be as light as possible; while still having sufficient capacity, it must allow free circulation of water and it must function and close reliably. There are many different models of sampling bottles. They are all lowered open, allowing the water to pass through freely as the bottle sinks and are closed automatically for hauling to the surface. The most successful design is that of Nansen with two plug valves. The series water bottle used by the "Meteor" Expedition 1925-27 was constructed on the same principles but was a little larger and had a number of minor improvements. This water bottle and its function is illustrated in Fig. 19 (WÜST, 1932). It had a capacity of 1250 cm³, weighed 4.4 kg (with thermometer frame approx. 5 kg) and had an overall length of 75 cm. Among the older designs may be mentioned that of EKMAN (1905) with improvements by KNUDSEN (1923) and a special 4 l. water bottle ("Meteor" Report, 4, No. 1, 1932).

Small 100-200 cm³ bottles of ordinary green glass are suitable for storage of water samples (for chlorine titration and analysis) since they have been found by the investigations of Helland-Hansen and Nansen to have very slight solubility; they are fitted with a patent stopper with a porcelain head carrying the sample number. Before use the bottles must be boiled, cleaned with chromic acid-sulphuric mixture, rinsed with distilled water and very carefully dried.

A definitive programme has been worked out for the work required at each oceanographic station and this has been found to be very successful as, for instance, during the "Meteor" Expedition 1925-27, and has been described in Vol. 4, No. 1 of the "Meteor" Report. It is worth mentioning particularly that a machine and an observations schedule containing everything of importance in the working programme for the series should be kept for each oceanographic station. Very often the results of an oceanographic series depend on the careful compilation of the machine and observations schedules. Apparently unimportant details may become important later during the interpretation of the observations and can contribute to the uniformity and homogeneity of the observations.

2. Temperature Determination for all Layers of the Ocean

The determination of the temperature of the surface layer of the sea offers little difficulty. A sample taken from water collected in an ordinary bucket, lowered into the sea for a short time while the vessel is under way, is put immediately in a shady place and its temperature is taken with a sensitive thermometer while at the same time it is kept stirred. The water sample must be drawn from as far forward as possible (on steam ships forward of the condenser exhaust). See LUMBY (1927) on the measurement of surface temperatures and the collection of suitable water samples. New surface sampling bottles have been designed by SUND (1931) and improved by SCHUMACHER (1938).

The determination of the temperature of the deeper layers of the sea is considerably more difficult, and this also needed the work of almost a decade to reach an accuracy suitable for scientific requirements. In the upper layers temperatures correct to 0.1°C are usually sufficient, but in the deep layers the variations both horizontally and vertically are usually so small that an accuracy of 0.01°C is needed to get some idea of

the spatial variations in temperature. This accuracy is also necessary for the calculation of densities accurate to the fifth decimal place. Deep-sea thermometers are thus extremely accurate and sensitive instruments which cannot be handled skilfully just by anyone.

An ordinary thermometer suspended freely in the water will not show the correct temperature since the pressure of the water will compress the thermometer bulb and force the mercury to a higher level. It is therefore necessary to protect the thermometer against the water pressure by enclosing it in a thick-walled glass tube. The part of the tube surrounding the thermometer bulb is filled with mercury to improve the heat transfer between the water and the bulb. Since the temperature usually decreases with depth the instrument first used was a maximum and minimum thermometer constructed by Six and adapted for deep-sea use, and this was the classical instrument used on the "Challenger" and the "Gazelle" Expeditions. Since 1874 the *reversing thermometer*, first produced commercially by the firm Negretti and Zambra, has been used instead, and with numerous modifications is still used at the present time as the standard instrument for oceanographic temperature recording. This is a thermometer with the capillary considerably constricted a little above the mercury bulb, so that the mercury thread will break at this point when the thermometer is turned through 180° and slide down to the other end of the capillary. The higher the temperature when the thermometer is reversed the longer the mercury thread that is broken off. This thread gives a direct reading of the temperature at that time when read against a scale running in the reverse direction with appropriate corrections. The accuracy of the thermometer is very dependent on the shape of the constriction. It must, of course, be made so that the mercury thread always breaks at the same point and it must be designed so that further mercury cannot follow the thread if the thermometer passes subsequently through a warmer layer of water. All the initial difficulties were overcome by the work of Richter (of the firm Richter & Wiese, Berlin) so that the reversing thermometer is now a true precision instrument. The shape of the constricted part of the capillary is shown in Fig. 20. Further details are given in the "Meteor" Report, 4, No 1, by BÖHNECKE (1932), and in "Oceanographic Instrumentation" (*Rep. Conf. Rancho Santa Fe, Calif.* 21-23 June 1952, p. 55).

In use the reversing thermometer is enclosed in a suitable holder (a brass tube) which is attached directly to a reversing sampling bottle or to a frame which can be reversed at the desired depth (reversing frame, propeller frame).

The reversing thermometer does not show the true temperature (*in situ*) directly since it will have been brought back to the surface through layers of water at different temperatures. After removal from the sampling bottle on deck it is placed immediately in a water bath and allowed to adjust to the water temperature before it is read. To show the temperature of the water bath every reversing thermometer is fitted with a normal auxiliary thermometer. To correct the reading to the temperature *in situ* a small correction given by the formula

$$C = \frac{(T' - t)(T' + V_0)}{6100} \left[1 + \frac{(T' - t)(T' + V_0)}{6100} \right]$$

must be applied. In this equation T' is the uncorrected reading of the reversing thermometer, t the reading of the auxiliary thermometer (bath temperature), V_0 is the

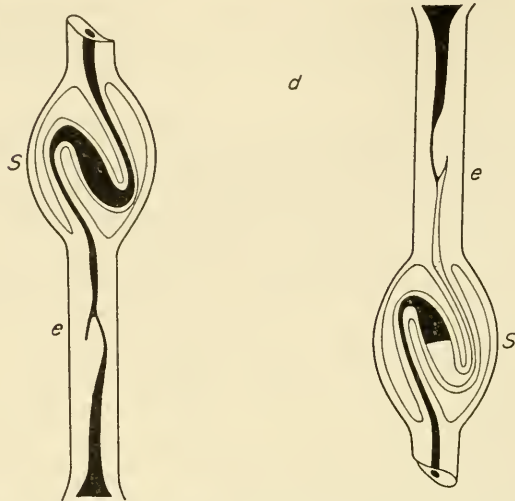


FIG. 20. Reversing thermometer (with visible constriction).

volume of the small bulb and the capillary of the main thermometer until 0°C and expressed in degree units on the capillary scale, $1/6100 = \beta$ being the coefficient of expansion of mercury. The corrections given by the formula are listed in tables to allow quick accurate working (SCHUMACHER, 1923, 1933; HIDAKA, 1933; GEISSLER, 1934). KALLE (1953) has given a simple graphical method for the determination of the corrections (C). A calibration correction has to be added to the corrected reading of the thermometer.

By very careful attention to all the factors involved (continual checking of the reversing apparatus, accurate readings using a magnifying glass, checking the zero point, proper correction) the mean error in the temperature determination can be kept down to, on the average, $\pm 0.01^{\circ}\text{C}$. This method gives the temperature at single points in the ocean and is of considerable use in series observations at oceanographic stations. For a special purpose, however, it may be desirable to have a continuous record of the temperature at a fixed depth or to obtain quick successive readings of the temperature in a particular layer. A thermograph is usually used for the first purpose (at coastal stations or for continuous recording of the temperature at the surface of the sea from a moving vessel). For greater depths different types of electrical resistance thermometers have been designed but they have not yet proved very satisfactory in use. For a rapid survey of the upper 150 m of the sea or for a continuous registration of the vertical temperature gradient of this upper layer to about 200 m, SPILHAUS (1938, 1940) has developed and tested a bathythermograph. This has proved successful and offers considerable advantages where rapid changes of temperature can be expected. For greater depths MOSBY (1940) has designed a "thermosounder" that has given useful results.

3. Salinity and its Determination

One of the most important properties of water is its ability to dissolve a very large number of solids and gases without chemically reacting with them. As a consequence

of this property all the water on the earth is more or less impure, that is it contains in addition to chemically linked hydrogen and oxygen (H_2O) a number of other substances in varying amounts. If the salt content, the salinity, were defined as the weight of all the salts dissolved in a kg of sea-water this would provide to be the simplest numerical specification of the amount of dissolved salts in the water. Unfortunately it is rather difficult to measure this definite quantity since, when sea-water is evaporated to dryness and heated to red heat to remove the last traces of water, some hydrogen chloride, carbon dioxide and a small amount of hydrogen bromide are also lost. This loss is not easily compensated with sufficient accuracy by adding a corresponding correction. At the suggestion of FORCH, SORENSEN and KNUDSEN (1902) the salinity has been defined as the total amount of solid material in grammes contained in 1 kg of sea-water when all the bromine and iodine have been replaced by the equivalent amount of chlorine, all the carbonate converted to oxide and all organic matter has been completely oxidized. The salinity defined in this way can be determined with great accuracy and can thus serve as a basis for the investigation of the relationship between any single component and the total salinity.

Sea-water is a dilute solution of a mixture of salts; in such an aqueous solution salts, acids and bases are more or less completely electrolytically dissociated (Arrhenius and van't Hoff). The chemical compounds precipitated on evaporation of such solution are in solution split into atoms or groups of atoms with an electric charge, either positive (cations) or negative (anions). The electrical charges balance exactly so that the solution remains electrically neutral. The constituents of this mixture of salts are therefore listed as their ions. Table 8 shows the composition of a typical sample of sea-water with a salinity of 34.40‰.

Table 8. The principal constituents of sea-water
(34.40‰ salinity)

Cations	g/kg	mmole/kg	percent- age of <i>S</i>	Anions	g/kg	mmole/kg	percent- age of <i>S</i>
Sodium	10.47	455.0	30.4	Chloride	18.97	535.1	55.2
Potassium	0.38	9.7	1.1	Bromide	0.065	0.81	0.2
Magnesium	1.28	52.5	3.7	Sulphate	2.65	27.6	7.7
Calcium	0.41	10.2	1.2	Bicarbonate	0.14	2.35	0.4
Strontium	0.013	0.15	0.05	Borate	0.027	0.44	0.08

It was formerly customary to give the constituents of sea-water in terms of the compounds that were precipitated on evaporation. DITTMAR (1884) has given the figures shown in Table 9 as the mean of seventy-seven very complete analyses of sea-water samples made by the "Challenger" Expedition; they have been calculated on the basis of a salinity of 35 g of salts in 1 kg of sea-water.

In the open ocean the total concentration of salinity varies between moderate limits, usually between about 33 and 38‰ depending in the first place on the climate (precipitation, evaporation and in polar regions ice melting). In coastal areas where there is a considerable inflow of fresh water from rivers and from ground water the salinity may have a considerably lower value. Especially in the almost closed adjacent seas of higher latitudes (such as the Baltic) with low evaporation, a considerable

Table 9. The salts obtained from sea-water
(Calculated as 35 g of salts per kg)

Salt	weight in g/kg sea-water	Percentage of total salts
Sodium chloride (NaCl)	27.213	77.758
Magnesium chloride (MgCl)	3.807	10.878
Magnesium sulphate (MgSO ₄)	1.658	4.737
Calcium sulphate (CaSO ₄)	1.260	3.600
Potassium sulphate (K ₂ SO ₄)	0.863	2.465
Calcium carbonate† (CaCO ₃)	0.123	0.345
Magnesium bromide (MgBr ₂)	0.076	0.217
Total	35.000	100.000

† Includes all the other salts present in trace amounts.

inflow of fresh water and precipitation on the surface may have a low salinity (8–5‰) and at the inner ends mostly only brackish water with 1‰ or even lower. The highest salinities are to be found, on the other hand, in the subtropical adjacent seas with almost no inflow of fresh water, no precipitation and strong evaporation as, for instance, in the Red Sea and in the Persian Gulf which at the inner ends have maximum salinities of almost 40‰.

While the salinity is always liable to show some variations the proportion of the different ions in sea-water is remarkably constant. This constancy which is of considerable oceanographic importance is only further confirmed by all carefully made analyses. Accurate chemical analysis of the samples collected by the “Challenger” Expedition from almost all parts, and depths of the ocean demonstrated this constant proportion between the individual constituents and more recent investigations as shown in Table 10 have led to the same results.

Table 10. Analysis of the salt content of sea-water (percentages)

(DITTMAR, 1884; MAKIN 1898; WHEELER, 1910)

No. of samples	77	22	5
Cl	55.29	55.18	55.29
Br	0.19	0.13	—
SO ₄	7.69	7.91	7.56
CO ₃	0.31	0.21	0.37
K	1.11	1.11	1.14
Na	30.59	30.26	30.76
Ca	1.20	1.24	1.22
Mg	3.72	3.90	3.70

The mean ratio Mg : Cl is 0.0682 and for SO₄ : Cl the ratio is 0.1397. The most recent analyses by Matthews, Thompson, and others, have given a value of 0.6802 (with limits of 0.6785 and 0.6814) for the first ratio and 0.1395 (with limits of 0.1387 and 0.1403) for the second. Using very accurate analyses calcium and bicarbonate

show sometimes smaller variations from the above-mentioned general proportionality (not more than 1%) which are due to biological processes (precipitation of calcium carbonate), to the solution of calcium carbonate from sea bottom and in coastal areas to the inflow of river water (containing calcium carbonate).

The very constant proportions of the ions present in sea-water allow chlorine to be used as a measure of the salinity of a sample of sea-water. This was done many years ago by FORCHHAMMER (1859, 1865) and later by KNUDSEN (1902), from a very careful examination between 2.69 and 40.18‰, derived the simple equation

$$S = 0.030 + 1.8050 \text{ Cl},$$

which is now used generally for the calculation of the salinity (S) from the chlorine content. This salinity is that given in the definition above. It is a little smaller than the actual salt content (by about 0.14‰) but since it is the differences in salinity that are important this has very little significance.

The most convenient method for the determination of salinity is that of MOHR (1956) in which the sample is titrated with silver nitrate with a calcium chromate solution as indicator; this is also suitable for use on board ship. This chemical method gives a relatively fast and accurate determination of the chlorine in sea water, and the salinity can be calculated from this value using the equation given above. This method is the usual method used at the present time in practical oceanography (see especially MEYER (1932) for the practical details of the titration and the necessary working routine).

The chlorine titration is only a relative determination, and to find the absolute value it is necessary to standardize the solution used for titration against the "Normal water" introduced by KNUDSEN (1903, 1925); this standardization very largely eliminates the effect of the subjective assessment of the colour of the indicator. Normal water is sea-water kept in sealed glass tubes of which the chlorine content has been very accurately determined, formerly by the central laboratory of the International Hydrographic Institute in Copenhagen, and at the present time by the Woods Hole Oceanographic Institution. The difference between the value obtained by titration of the normal water and that marked on the tube gives the total error in the titration. KNUDSEN (1901) has prepared hydrographic tables for the comparison of chlorine determinations of sea-water with different salinities with the chlorine determination made on normal water.

If the average salinity of the ocean is taken as 35‰ then calculation gives the total amount of salt in the ocean as 4.84×10^{16} tons; this corresponds to a volume of 21.8 million km³ which, spread evenly over the sea (361 million km²), would be a layer of salt 60 m thick.

In addition to the substances already mentioned, sea-water also contains traces of a large number of elements which are of little importance for oceanography, though they are probably important in the metabolism of marine organisms. The determination of the concentrations of these elements presents very great analytical difficulties and the older determinations must be treated with great caution. Table 11 shows a more recent list of the elements present in the sea according to KALLE (1945), which is based on a similar one given earlier by WATERBERG (1938). In many cases the figures given represent only the order of magnitude of the concentration of an element. Of

the elements that are present in somewhat greater concentration may be mentioned iron, copper and gold. Iron is present in extremely small quantities and sea-water is probably one of the naturally occurring materials poorest in iron. The importance of copper can be seen from its occurrence in place of iron in the blood pigments of many marine animals (hæmocyanin). The occurrence of gold in sea-water at one time aroused particular interest since, according to older determinations, the isolation of gold from sea-water was technically promising. These older determinations have, however, been shown by the results of HABER (1928) and JAENICKE (1935) to be incorrect, and the gold found came largely from the reagents used, from the air and from the glass of the apparatus. The gold content of sea-water found by analysis of the samples collected on the "Meteor" Expedition was only 4×10^{-9} g/kg of sea-water, a concentration which would be of no technical use.

Table 11. Concentrations of the trace elements present in sea-water in milligrams per cubic metre

(According to KALLE, 1945)

Fluorine	1400	Selenium	4
Silica	1000	Uranium	2
Nitrogen (NO ⁻ , NO ₂ ⁻ , NH ₃)	1000	Caesium	2
Rubidium	200	Molybdenum	0.7
Aluminium	120	Cerium	0.4
Lithium	70	Thorium	0.4
Phosphorus	60	Vanadium	0.3
Barium	54	Yttrium	0.3
Iron	50(2)	Lanthanum	0.3
Iodine	50	Silver	0.3
Arsenic	15	Nickel	0.1
Copper	5	Scandium	0.04
Manganese	5	Mercury	0.03
Zinc	5	Gold	0.004
		Radium	0.000001

The radioactivity of sea-water has been accurately investigated in recent times, and detailed examinations have been made principally by PETERSSON (1937, 1938), and THOMPSON and his collaborators (1932). According to these investigations the radium content of sea-water with a salinity of 35‰ varied between 0.04 and 0.2×10^{-12} ‰ (or between 0.04 and 0.2 billionth parts of a gramme per litre); 0.07×10^{-12} ‰ radium can be taken as mean value. Deep water has a uranium content of $1.5-2 \times 10^{-6}$ ‰; surface water has a somewhat lower value. The thorium content is less than 0.5×10^{-6} ‰.

Since the radium content of sea-water is 10,000 times less than that of rocks of the Earth crust, it is extremely small and corresponds to only 10% of the amount that would be in equilibrium with the uranium content. According to the view of PETERSSON, this remarkable deficiency of radium in the sea can be attributed to the very rapid precipitation of the iron carried into the sea, almost entirely as ferric hydroxide. In the precipitation the thorium and its isotope ionium that immediately precedes radium in the disintegration series are co-precipitated. The ionium produced from the uranium in solution in the sea is thus steadily removed by precipitation of the iron.

Only that part of the element remaining in solution disintegrates to give radium and its disintegration products in the sea (see also HESS, 1918).

4. The Density of Sea-water and its Dependence on Temperature, Salinity and Pressure

The density ρ of a material is the mass of a unit volume [g cm^{-3}]. Frequently the specific weight is given instead of the density; this is defined as the quotient of two densities ρ/ρ_w , where ρ is the density of the substance in question and ρ_w is the density of distilled water at a fixed temperature. The specific weight is thus a dimensionless quantity. In the CGS system the density and the specific gravity are numerically equal if distilled water at 4°C is taken as the comparison liquid.

Due to its salt content sea-water is heavier (more dense) than pure water. The density is always fairly close to 1 and varies depending on the salinity S , the temperature t and the pressure p between narrow limits; for example, at the surface of the open ocean between 1.02750 and 1.02100. For oceanographic purposes it is necessary to know the density correctly to at least 5 decimal places. For simplicity instead of using ρ it is customary to use a density value σ derived from the equation $\sigma = (\rho - 1) \times 10^3$; for instance instead of $\rho = 1.02754$, $\sigma = 27.54$ is used. Very often the reciprocal of the density $1/\rho = v$, the specific volume [$\text{cm}^3 \text{g}^{-1}$] is used. This also is required correct to the fifth decimal place and for simplicity and convenience only the last three figures are given according to the equation $\alpha = (v - 0.97) \times 10^5$. For example when $v = 0.97320$, $\alpha = 320$.

The dependence of the density and the specific volume on the temperature, the salinity and the pressure were first investigated at the beginning of this century (1899) by an international commission headed by KNUDSEN (1902, 1903). The relationship of the density at 0°C and atmospheric pressure at sea-level to the chlorinity is given by

$$\sigma_0 = -0.069 + 1.4708 \text{ Cl} - 0.001570 \text{ Cl}^2 + 0.0000398 \text{ Cl}^3.$$

This equation is valid for chlorinities between 1.47362 and 22.2306.

The dependence of the density of sea-water on the temperature requires a knowledge of the thermal expansion of sea-water. The thermal expansion coefficient determined in the laboratory shows that the density has a pronounced dependence on the temperature; at atmospheric pressure (sea surface) is given by $\sigma_t = \sigma_0 - D$. D is a very complicated function of σ_0 and of the temperature t and has been given to the fifth place in Knudsen's hydrographic tables (1901). SCHUMACHER (1922) has also given graphical tables, and further tables for the determination of the density of sea-water under normal pressure have been given by MATTHEWS (1932) and THORADE and KALLE (1940). These tables show that an increase of 0.01% in the salinity gives an approximate increase in the density (σ_t) of 8 units in the third decimal place. The increase is about the same for all temperatures and salinities. For low and high temperatures the density change is very different and depends also somewhat on the salinity. Figure 21 (HELLAND-HANSEN, 1911-12) shows the effect of variations in temperature on the densities of distilled water and of sea-water with salinity 35% . From the relationship between temperature and density the *temperature of maximum density* can be determined for different salinities. This is also given with somewhat less accuracy by the equation

$$t_{\max} = 3.95 - 0.266\sigma_0.$$

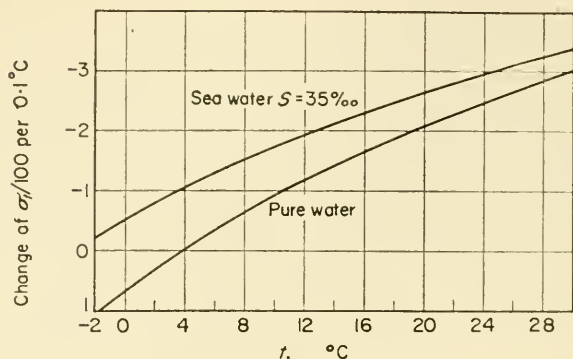


FIG. 21. Effect of changes in temperature on the density of pure water and of sea water at 35‰ salinity.

Thus for different salinities, where

S in ‰	=	0	10	20	25	30	35	40
σ_{\max}	=	0.00	8.18	16.07	20.10	24.15	28.22	32.32
t_{\max} in °C	=	3.947	1.860	-0.310	-1.398	-2.473	-3.524	-4.510

Since water is compressible, though only slightly, the density depends on the pressure. In the deeper parts of the ocean the pressures are enormous and have a considerable effect on the density of the water. The change in unit volume of a material per pressure unit is termed its compressibility coefficient μ . If the pressure unit is taken as 1 bar ($= 10^6$ dynes/cm²) then the compressibility coefficient of sea-water is of the order of magnitude of 450×10^{-7} ; it increases somewhat with increasing pressure, increasing salinity and increasing temperature and its extreme values lie somewhere between the limits 510 and 390×10^{-7} . EKMAN (1908) derived a precise empirical formula for the effect of pressure on the density that takes into consideration the changes in the compressibility coefficient with salinity and temperature (see LANDHOLT-BÖRNSTEIN, 1952; DIETRICH, p. 484). This gives the density of sea-water for a given salinity, given temperature and a fixed pressure and thus gives the density *in situ* $\sigma_{s,t,p}$ of a water sample directly from σ_t .

BJERKNES and SANDSTRÖM (1910) have presented complete tables to allow the specific volume anomaly or the density to be quickly found from the basic values for a homogeneous sea at 0°C and with 35‰ S for depths down to 10,000 m or pressures of 10,000 decibars. HESSELBERG and SVERDRUP (1915) have given a method by which the vertical variations in density can be calculated in a fairly simple way from the temperature and the salinity. This simplification is due largely to the elimination of part of the work by starting in the first place from the value for σ_t . If only the anomaly is required, the tables prepared by SVERDRUP (1933), which are still further simplified and which give more accurate results, can be used. In general the relation $\alpha_{s,t,p} = \alpha_{35,0,0} + \delta$ can be used where δ is the specific volume anomaly. δ is the sum of three terms: $\delta = \Delta_{s,t} + \delta_{s,p} + \delta_{t,p}$. As shown by the indices the first term depends on the temperature and the salinity, the others depend on the pressure and on one of the other two factors each.

Since

$$\alpha_{s, t, 0} = \alpha_{35, 0, 0} + \Delta_{s, t} = 1 + \frac{\delta_t \times 10^{-3}}{1 + \sigma_t \times 10^{-3}}$$

and

$$\alpha_{35, 0, 0} = 0.97264,$$

then

$$\Delta_{s, t} = 0.02736 - \frac{\sigma_t \times 10^{-3}}{1 + \sigma_t \times 10^{-3}}.$$

The values of the three terms $\Delta_{s,t}$, $\delta_{s,p}$ and $\delta_{t,p}$ can be given in short tables from which the anomaly can be found correct to five decimal places. The same accuracy can be obtained by accurate graphical methods or with the ingenious slide rule of SUND (1929).

The usual method for determining the density in oceanography is by calculation from the temperature, the salinity and the pressure. The physical methods of determining density such as the hydrostatic weighing and the pycnometer are unsuited for oceanographic purposes, but the hydrometer has however often been utilized in oceanography. Some very troublesome sources of error present with the ordinary stem hydrometer have been discussed in detail by KRÜMMEL (1900), BUCHANAN (1884) and NANSEN (1900). They originate from insufficient attention to temperature differences between the instrument and the water sample and within the water sample itself, the variable wetting of the instrument (traces of oil on the surface), the air content of the water sample and not least to the variable capillary rise of the water in the stem of the instrument which is often difficult to allow for. With proper use this instrument gives values for σ_t correct to two units in the second decimal place. NANSEN (1900) avoided the errors due to varying surface tension at the stem by using a "hydrometer of total immersion" in which the float is balanced in the water sample by the addition of suitable weights. This method gives σ_t correct to the third decimal place (SVERDRUP, 1929). Since work with small weights is inconvenient on board ship O. and H. PETERSSON (1929), used a different method of loading a float hydrometer which is very simple and requires no handling of the float. A fine chain is suspended from the float (chain hydrometer) so that the length of chain supported above the bottom is a measure of the density.

Another method for the direct determination of the density which has been used in older investigations (Pulfrich refractometer) utilizes the difference in refractive index of the water sample from that of distilled water. This is measured either by the *Hallwach method* or by interferometry. The first method was used by KRÜMMEL (1889) on the "Plankton" Expedition and later in 1892 by Drygalski on the Greenland Expedition. The interference method is more sensitive, although it requires suitable laboratory work to give the desired accuracy. (Askania Interferometer, BEIN, HIRSEKORN and MÖLLER, 1933, 1935). This interference method has been developed to give greater precision and will give the density to the third decimal place in σ_t .

As well as the optical refractivity it is also possible to use the electrical conductivity for the determination of densities. This method has several times been recommended but has seldom actually been used. A survey of these experiments has been given by BEIN (1936). An instrument suitable for routine use was first developed by the Bureau of Standards in Washington (THURAS, 1918; WENNER, 1930). It was in continual use by vessels of the Ice Patrol in the North Atlantic Ocean from 1921 and was used by the

oceanographic vessel "Carnegie". Experience with this "saline tester" was not very encouraging and the accuracy attained was, in spite of the greatest precautions, not entirely satisfactory.

5. Vapour Pressure, Freezing Point, Boiling Point and Osmotic Pressure of Sea-water

Sea-water is a "dilute" solution and has the properties of such a solution. Due to the low concentration of the dissolved material these will in several respects approach those of the pure solvent, i.e. of pure water. It was shown quite early that the vapour pressure p of a dilute solution is always less than the vapour pressure p_0 of the pure solvent and that the elevation of the boiling point is accompanied by a depression of freezing point. As shown by Raoult and van't Hoff the relative lowering in vapour pressure is independent of the nature of the material in solution and of the temperature of the solution, and is proportional to the amount of dissolved material in solution in the solvent. For a solution of n moles of a substance in N_0 moles of a solvent:

$$\frac{p_0 - p}{p_0} = \frac{n}{N_0}$$

Figure 22 shows the different phase states for pure water and for sea-water; it illustrates more clearly the relationship between the three well-known properties of dilute solutions mentioned above. The curve $G'S'$ showing the lowering of vapour pressure is always lower than the vapour-pressure curve for pure water by the amount of the

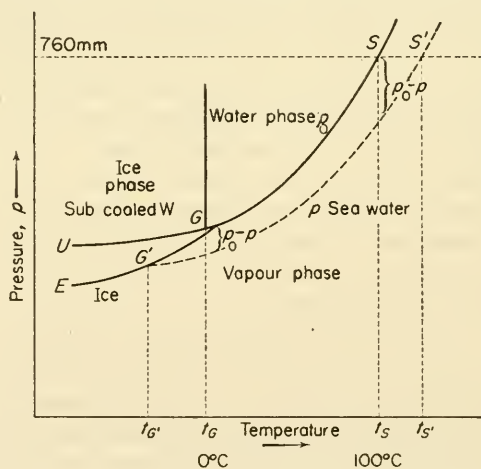


FIG. 22. Phase states for pure water and for sea-water (schematic).

depression $p_0 - p$. Since for a given concentration $(p_0 - p)/p_0$ is constant, this depression increases with increasing pressure and therefore also with increasing temperature. The p_0 -curve for pure water cuts the line for a pressure of 760 mm Hg at the point S ; this is the boiling point of pure water for which the corresponding temperature $t_s = 100^\circ\text{C}$. The vapour-pressure curve for sea-water cuts this isobar first at S' and this boiling point corresponds to a temperature $t_{s'}$ which is higher than t_s . The elevation of boiling point Δt_s of sea-water of a given concentration is given by $\Delta t_s = t_{s'} - t_s$.

The depression of freezing point by a dissolved substance can also be inferred from this diagram. The intersection G of the solid and liquid phases (the triple point) corresponds to a temperature of 0.0075°C . At 760 mm Hg the freezing point t_G of pure water is 0°C and is fixed by the position of the intersection of the melting-point curve GT with the 760 mm isobar. It is the temperature at which the two phases (water and ice) have the same vapour pressure, and therefore are in equilibrium with each other. On the other hand, the freezing point of sea-water is at the intersection G' of the vapour pressure curve for sea-water and that for ice; at this point the vapour pressures over sea-water and over ice are the same. This corresponds at 760 mm Hg to the freezing point of sea-water $t_{G'}$ which is lower than t_G . The freezing-point depression for sea-water is given by $\Delta t_G = t_{G'} - t_G$.

From this diagram it can immediately be deduced that both quantities Δt_G and Δt_s are larger the larger the value of $p_0 - p$ of the relative lowering of vapour pressure $\Delta p_0/p$, that is the larger the concentration of the solution of the salinity. Quantitatively it has been shown experimentally and theoretically that for low concentrations the elevation of the boiling point and the depression of the boiling point are both proportional to the concentration. In dilute solutions of substances termed in physical chemistry "strong electrolytes", amongst which sea-water is included, it is found that the electrolytic dissociation of the molecules is equivalent to an apparently larger molecular concentration so that the simple proportionality no longer holds. The accurate determination of saturated vapour pressures and of boiling points is experimentally difficult and has been described in detail. The freezing point has been determined by Hansen on eleven samples of sea-water, and by KNUDSEN (1903), using determination of the constants, and the following empirical equation has been found

$$t_G = -0.0086 - 0.064633 \sigma_0 - 0.0001055 \sigma_0^2$$

This gives freezing temperatures correct to $\pm 0.003^{\circ}$.

Table 12. Freezing point and osmotic pressure of sea-water

Salinity (%)	5	10	15	20	25	30	35	40
Freezing point ($^{\circ}\text{C}$)	-0.267	-0.534	-0.802	-1.074	-1.349	-1.627	-1.910	-2.196
Density (σ_0)	3.96	8.00	12.02	16.07	20.10	24.14	28.21	32.27
Osmotic pressure (atmos.)	3.23	6.44	9.69	12.98	16.32	19.67	23.12	26.59

Table 12 shows related values of salinities, freezing point t_s , the density of sea-water at this temperature and also the osmotic pressure (see later, p. 48). For the relative lowering of vapour pressure WITTING (1908) has given the equation

$$\Delta p/p_0 = 0.538 \times 10^{-3} S;$$

the elevation of boiling point can as a first approximation be obtained from

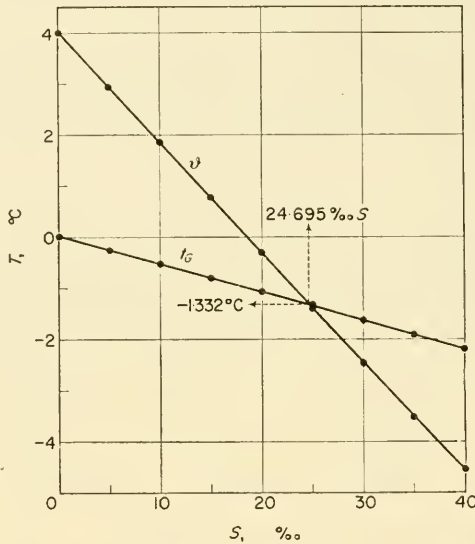
$$\Delta t_s = 0.0158S.$$

Table 13 gives related values for the elevation of boiling point and the lowering of vapour pressure at boiling point (at 760 mm Hg).

Table 13. Elevation of boiling point and lowering of vapour pressure in sea-water

Salinity, ‰	5	10	15	20	25	30	35	40
Δt_b (°C)	0.05	0.16	0.23	0.31	0.39	0.47	0.56	0.64
Δp in mm Hg at 760 mm Hg	2.13	4.23	6.45	8.47	10.73	12.97	15.23	17.55

A comparison of the temperature of the freezing point t_G , that of maximum density ϑ and their corresponding densities at different salinities is of some interest. Figure 23 shows the change in these temperatures with increasing salinity. The temperature of

FIG. 23. Dependence of freezing temperature t_G on the salinity S .

maximum density decreases with increasing salinity more rapidly than the temperature of the freezing point. At a salinity of 24.695‰ ($\sigma_0 = 19.839$) both temperatures are the same and

$$\vartheta = t_G = -1.332^\circ\text{C} \quad \text{and} \quad \sigma_\vartheta = \sigma_{t_G} = 19.852.$$

Reference might be made here to an oceanographic use of this (HELLAND-HANSEN, 1911–12). Suppose a surface layer of a sea area is homo-haline with a salinity less than 24.695‰ and that its surface is subject to strong cooling in winter. This cooling will increase the density of the surface water, and as a consequence a vertical convection must occur and will continue until the whole homo-haline surface layer reaches the temperature of maximum density. It will then cease. The surface only will now be cooled further by radiation until it reaches the freezing point and ice begins to form. This will increase the salinity, and convection will again be set up and will be maintained by the double effect of the increase in salinity and the decrease of temperature. These conditions may occur, for example, in the Baltic. The homo-haline surface layer with $S = 10\text{‰}$ during the winter cools and the vertical convection continues until the

temperature reaches $+1.86^\circ$. The whole layer then has the maximum density $\sigma_\theta = 8.18$. If cooling proceeds further the temperature falls *only at the surface* until this reaches the freezing point $t_G = -0.53^\circ$, where $\sigma_{t_G} = 8.00$, while the remainder of the water mass remains at $+1.86^\circ$ and $\sigma_{t_G} = 8.18$. On further loss of heat ice is formed and the density is raised by the liberation of salt until it reaches 8.18 when convection starts again and continues as long as ice continues to form.

If, on the other hand, the surface layer has a salinity greater than 24.695% then the vertical convection continues until the whole layer reaches the temperature of the freezing point and proceeds further without interruption as long as fresh ice continues to form. The difference between the two densities σ_{t_G} and σ_θ is, however, not large. As shown in Fig. 24 these differences are largest at salinities of $6-7\%$ and very small between 20% and 35% .

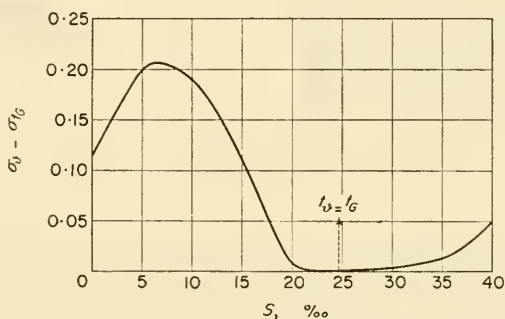


FIG. 24. Density at the freezing temperature and maximum density of sea water as a function of salinity.

Two adjacent water masses of different salinity will not, as far as their salinity is concerned, be in equilibrium. In solutions of different concentrations in contact in this way the material dissolved in the water will move from the region of higher concentration to that of lower concentration, that is, in the direction of the concentration gradient. Known as *molecular diffusion*, it follows the same laws as thermal conductivity. If the salinity gradient is $-(dS/dx) \times 10^{-3}$, where S is given in ‰, there will, by diffusion, pass in unit time (sec) through unit area at right angles to the direction of the gradient (1 cm^2) an amount of salt M_s given by $M_s = -\kappa(dS/dx) \times 10^{-3}$ where κ is the molecular diffusion coefficient with the dimensions ($\text{g cm}^{-1} \text{ sec}^{-1}$). The change with time in a given distribution of salinity follows from the differential equation $\partial S/\partial t = \kappa(\partial^2 S/\partial x^2)$ where κ is a constant independent of the time and the distance (Fickian-diffusion equation). The diffusion coefficient for sea-water is very small ($0.0189 \text{ g cm}^{-1} \text{ sec}^{-1}$ at 35%), molecular diffusion thus proceeds extremely slowly, and long periods are needed to eliminate larger differences in salinity by pure molecular diffusion. In this respect diffusion is quite analogous to thermal conductivity.

Osmotic pressure is a phenomenon that is closely related to the properties of dilute solutions described above. It is of very considerable importance for the biology of living organisms in the sea. If a tank II (see Fig. 25) filled with sea-water of salinity

$S\%$ is separated from a tank I containing distilled water by a semi-permeable membrane M which is permeable only for water and not for the substances in solution, water will pass from tank I through the membrane M into tank II which contains the the salt solution, and as a result the pressure in the tank II will rise. The sea-water could be said to draw the pure water through the membrane. This process will continue until the excess pressure in II exceeds that in I by a fixed value P . This excess pressure at which the system is in equilibrium is termed the osmotic pressure. According to physical chemistry it has been shown (see NERNST, *Theoretische Chemie*, 4th ed. 1903,

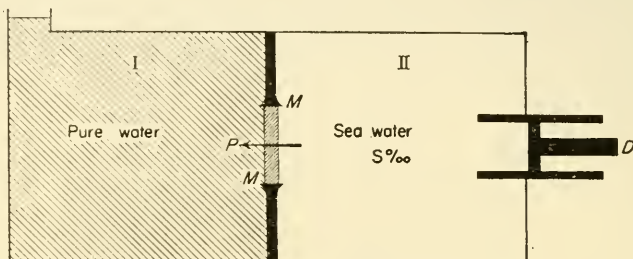


FIG. 25. For explanation of the osmotic pressure.

p. 157) that there is a relationship between the osmotic pressure and the depression of freezing point which for sea-water at 0° takes the form $P = -12.4\Delta t G$. STENIUS (1904; see also THOMPSON, 1932) found the proportionality value 12.08 atm for the constant in this equation. For other temperatures P_0 must be multiplied by $(1 + 0.00367t)$. Table 12 gives values for the osmotic pressure at 0° according to Stenius.

The size of the osmotic pressure gives an idea of its biological importance. Organisms that live in the water are usually covered by a skin that is partly permeable to water. They live in osmotic equilibrium with their environment. If one of these organisms is placed in water of lesser salinity, water will pass in through its skin into its body; if the salinity is higher, water will be removed. Both processes, if they occur to any extent, are unfavourable to the life of the organism since the capacity of adaptation is fixed within narrow limits.

6. Other Physical Properties of Sea-water

Other properties of sea-water that are also of importance in oceanography and should be briefly mentioned are the heat capacity and the thermal conductivity, the surface tension and the internal viscosity.

(a) The heat capacity of the specific heat of a body is the number of calories required to heat 1 g of the material through 1°C . The specific heat of pure water is dependent on the temperature and shows a minimum of 0.947 at 34°C . It rises more rapidly towards lower than towards higher temperatures and at 18°C it is 0.999 .

A series of experimental determinations of the effect of the salinity was made by THOULET and CHEVALLIER (1899) and their results have been utilized by Krümmel to prepare the figures shown in Table 14. The experimental value for the specific heat of sea-water c_p is less than would be expected from the amount of salt in solution.

Table 14. The specific heat of sea-water at 17.5°

Salinity (‰)	0	5	10	15	20	25	30	35	40
c_p	1.000	0.982	0.968	0.958	0.951	0.945	0.939	0.932	0.926

The dependence of c_p for sea-water on the temperature has not yet been closely investigated, but presumably it is of the same form as that for pure water. Figure 26 shows the effect of temperature on c_p for pure water and for sea-water with 35‰ S . The dependence of c_p on the pressure p can be found using well known thermodynamic

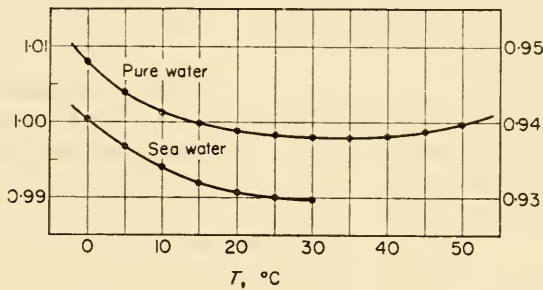


FIG. 26. Specific heat for pure water and for sea water at 35‰ salinity.

principles (EKMAN, 1914). If the pressure p is taken in decibars, and the density of the water is ρ , the absolute temperature T , the coefficient of thermal expansion β , and J is the mechanical equivalent of heat (4.1863×10^7 ergs/cal or dyn cm/cal), then

$$\frac{\partial c_p}{\partial p} = - 10^5 \frac{T}{\rho J} \left(\frac{\partial \beta}{\partial t} + \beta^2 \right).$$

Ekman has calculated the value of c_p for atmospheric pressure and for pressures from $p = 2000$ to $p = 10,000$ decibars, corresponding to depths of about 2000 to 10,000 m (Table 15). At great depths c_p differs appreciably from 1 and this must be taken into account in accurate theoretical calculations.

Table 15. Specific heat of sea-water at different pressures when $\sigma = 28$ (34.8‰)

Temperature (°C)	-2	0	5	10	15	20
Pressure in dbar						
0	0.942	0.941	0.938	0.935	0.933	0.932
1000	0.933	0.933	0.930	0.929	0.928	0.927
2000	0.925	0.925	0.924	0.923	0.922	0.921
3000	0.910	0.912	0.913	0.913	0.913	—
6000	0.898	0.901	0.904	—	—	—
8000	—	0.892	0.896	—	—	—

The relationship $\kappa = c_p/c_v$ is also of interest. The specific heat/constant volume c_v is a little less than c_p . From thermodynamics the equation

$$c_p = c_v + \beta^2 \frac{T}{\rho \mu J}$$

can be derived, where μ is the cubic compressibility. For sea-water where $\sigma_0 = 28$ (34.84‰ *S*) at temperatures of 0° and 30°C respectively, $\beta = 15 \times 10^{-6}$ and 334×10^{-6} grad⁻¹ and $\mu = 46.59 \times 10^{-12}$ and 42.07×10^{-12} dyn⁻¹ cm². From this it can be found that $\kappa = 1.0004$ and 1.0207 for 0°C and 30°C respectively. At greater depths μ is smaller and there κ is larger than at the surface.

(b) The thermal conductivity coefficient λ is defined by the equation

$$Q = -\lambda(\partial\vartheta/\partial x),$$

where Q (cal/sec) is the amount of heat passing through 1 cm² at right angles to the flow and $d\vartheta$ (°C) is the change in temperature along a distance dx (cm) in the direction of flow. λ thus has the dimensions (cal cm⁻¹ sec⁻¹ grad⁻¹). For pure water $\lambda = 0.001325 + 4 \times 10^{-6}t$.

λ has not been determined directly for sea-water; as a first approximation, according to Weber's rule, the ratio of the thermal conductivities of two substances is the same as that of the thermal capacities of equal volumes. This gives the values shown in Table 16 for the coefficient of thermal conductivity for different salinities.

Table 16. Coefficient of thermal conductivity at different salinities

Salinity (‰)	0	10	20	30	35	40
Thermal conductivity coefficient ($\times 10^{-3}$)	1.400	1.367	1.353	1.346	1.341	1.337

For oceanic water (35‰ *S*) the thermal conductivity coefficient is about 4.2% less than for pure water. The *temperature conductivity coefficient* is the quantity $\alpha = \lambda/(\rho c_p)$ and has the dimensions (cm² sec⁻¹). For sea-water ρc_p is not very different from 1 and the numerical difference between λ and α is slight.

(c) In fluids with motion there is a shear stress between every layer in the direction of flow and the adjacent parallel layer, and this shearing stress is proportional to the velocity gradient perpendicular to the direction of flow, that is

$$\tau = -\mu \frac{\partial v}{\partial z}.$$

The proportionality factor μ is a measure of viscosity or inner (molecular) friction (g cm⁻¹ sec⁻¹). For many flow phenomena there occurs the coefficient $\nu = \mu/\rho$, the kinematic viscosity (cm² sec⁻¹). These frictional coefficients decrease rapidly with increasing temperature. For pure water, the values shown in Table 17 are obtained. According to the investigations of KRÜMMEL and RUPPIN (1905) viscosity increases very little with salinity; at 0°C by 3.9 or 5.2% for 25‰ *S* and 35‰ *S* respectively and at 30°C by 6.1 or 8.2%. The effect of pressure appears to be negligible.

Table 17. Viscosity coefficients for pure water
(g cm⁻¹ sec⁻¹)

Temperature (°C)	0	10	20	30	40
μ	0.0179	0.0131	0.0100	0.0080	0.0065

The magnitude of the molecular viscosity was earlier attributed some importance in the biological and dynamic processes in the sea, but it has since been recognized that processes in oceanic currents are always turbulent and the coefficient of turbulent viscosity is considerably larger than the coefficient of molecular viscosity. This has very much reduced the importance of the latter.

(d) *Surface tension.* KRÜMMEL (1907) investigated the dependence of the surface tension on the temperature and the salinity; it decreases with rising temperature and with decreasing salinity. FLEMING and REVELLE (1939) have taken more recent values to derive the equation

$$\text{surface tension in dyn/cm}^2 = 75.64 - 0.144t + 0.0399 Cl.$$

Impurities in the water always lead to a considerable reduction and this must be taken into consideration for surface waters of the sea.

7. The Optical Properties of Sea-water

(a) The Extinction of Incoming Radiation

Parallel radiation entering a layer of sea-water is gradually weakened in three ways:

- (1) By absorption by the pure sea-water.
- (2) By scattering by the pure sea-water.
- (3) By scattering, diffraction and reflection by suspended particles in the water (impurity of sea-water).

The last two factors do not change the form of the energy but divert a part of the radiation from its original direction. A beam of radiation of wavelength λ passing through a distance dx in water is reduced in intensity by an amount dI which is proportional to the intensity and to the distance dx travelled through the water, so that $dI = -\kappa I dx$. κ the extinction coefficient (cm^{-1}) is dependent on the wavelength λ . If the intensity of the radiation is I_0 when $x = 0$, then for a distance x

$$I = I_0 e^{-\kappa x}.$$

The reduction in intensity of the radiation is often characterized in practice by the extinction E for a layer of thickness 1 m and is given as a percentage of the incident radiation

$$E = 100 \left(1 - \frac{I}{I_0} \right).$$

The transmission D may also be used, and gives the percentage of the incident radiation passing through a layer of fixed thickness

$$D = 100 \frac{I}{I_0} = 100 e^{-\kappa x}.$$

Detailed measurements have been made of the extinction coefficient for water over the whole spectral region from 0.186μ in the ultraviolet to 8.5μ in the infra-red. The spread of 2-3% in the values obtained in different series of measurements are largely due to the difficulty of preparing "pure water". DIETRICH (1939) has given a comparison of the older measurements of ASCHKINAS (1895) and more recent values by KREUSLER (1901), SAWYER (1931) and COLLINS (1925, 1933) from which the values shown in Table 18 have been abstracted.

Table 18. Absorption coefficient κ (cm^{-1}) for pure sea-water

Wavelength		Wavelength		Wavelength		Wavelength	
λ in μ	κ	λ in μ	κ	λ in μ	κ	λ in μ	κ
0.20	0.00899	0.70	0.0084	1.30	1.50	2.00	85
0.30	0.00151	0.80	0.0240	1.40	16.0	2.10	39
0.31	0.0084	0.90	0.0655	1.50	19.4	2.30	24
0.40	0.00072	1.00	0.397	1.60	8.0	2.40	42
0.50	0.00016	1.10	0.203	1.70	7.3	2.50	85
0.60	0.00125	1.20	1.232	1.90	73	2.60	100

0.2–0.3 μ according to KREUSLER (1901), 0.31–0.60 μ according to SAWYER (1931) and from 0.7 μ according to COLLINS (1933).

Figure 27 shows the spectral range from 0.186 μ to 2.65 μ . From about 0.48 μ towards the red end of the spectrum and beyond, the absorption coefficient increases strongly and continuously. According to the measurements of Aschkinas, weaker absorption bands follow stronger bands between 2.86 μ and 3.27 μ , and at 6.7 μ where there is almost complete extinction of the radiation. The absorption depends slightly on the

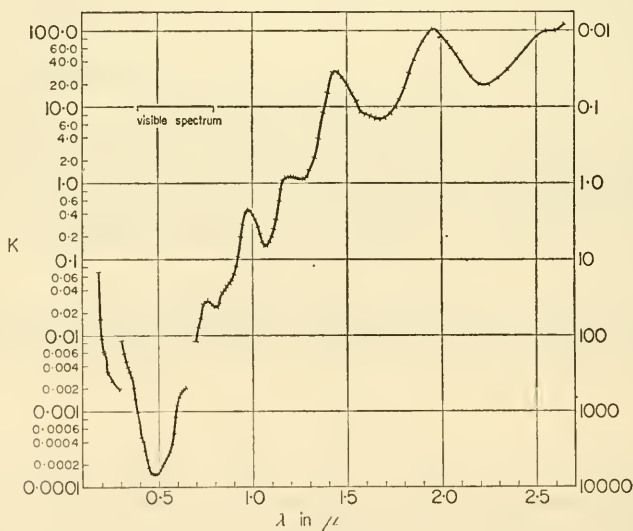


FIG. 27. Absorption coefficient for pure water (pure sea water for parallel radiation (wavelength range 0.186–2.65 μ) (From 0.2 to 0.3 μ according to Kreusler; from 0.31 to 0.60 μ according to Sawyer; from 0.70 μ on . . . according to Collins).

temperature and an effect of the salinity has been found but from the summary given by Dietrich it can be seen that the absorption in pure sea-water is almost the same as in pure fresh water.

The extinction coefficient κ takes account of the effects of both scattering and absorption. The scattering of light in a turbid medium is caused by reflection and diffraction of the incident light by the small particles suspended in the medium. If the size

of these particles is very small compared with the wavelength of light and if the concentration is not too large, the scattering is due to pure diffraction following Rayleigh's law; according to this the reduction in intensity of the incident light is inversely proportional to the fourth power of the wavelength. Amongst the phenomena due to scattering is included that known as the *Tyndall effect*, where a beam of light passing through a turbid medium produces a more or less intensive illumination of those portions in the medium affected by light. This is due to reflection and scattering of the light by the suspended particles. Since the shorter wavelengths are more strongly scattered, the Tyndall-light is bluish. The water molecules themselves can be regarded as scattering particles. Thereby one thought to explain also the blue colour of the scattered light in pure water. However, it has later been recognized that a direct scattering by the water molecules can hardly occur since there are too many compressed into a small space and the distances between them are too small relative to their diameter. According to the theory of Smoluchowski irregular molecular movements give rise to an optical inhomogeneity (streaks; Schlieren) of very small dimensions and are therefore responsible for the scattering of light.

Table 19. The energy distribution in the spectrum of sunlight after passing through water layers of different thickness

Wave-length (μ)	Thickness of the water layer								
	0	0.01 mm	0.1 mm	1 mm	1 cm	10 cm	1 m	10 m	100 m
0.2-0.6	237	237	237	237	237	236	229	172	14
0.6-0.9	360	360	360	359	353	305	129	9	—
0.9-1.2	179	179	178	172	123	8	—	—	—
1.2-1.5	87	86	82	63	17	—	—	—	—
1.5-1.8	80	78	64	27	—	—	—	—	—
1.8-2.1	25	23	11	—	—	—	—	—	—
2.1-2.4	25	24	19	1	—	—	—	—	—
2.4-2.7	7	6	2	—	—	—	—	—	—
2.7-3.0	0.4	0.2	—	—	—	—	—	—	—
Total	1000.0	993.7	952.1	859.4	730.2	549.3	358.1	181.5	13.9

The only natural parallel radiation occurring in the upper surface of the sea is direct sunlight. On passing through water the spectrum of sunlight undergoes great changes. SCHMIDT (1908), on the basis of the extinction values of Aschkinas and values according to Langley for the distribution of radiation energy from the sun on the surface of the sea, has calculated the spectrum of the sunlight at different depths and obtained the values given in Table 19 for water layers of different thickness; the total radiation from the sun incident on the surface of the sea is taken as 1000 (Fig. 28). The total extinction for different layer-thickness is given in Table 20. The reduction in intensity of sunlight after passing through very thin layers of water is quite considerable. For a layer 1 cm thick, wavelengths $>1.5 \mu$ are completely eliminated and the spectrum extends only to 0.9μ . For layers 100 m thick the remaining energy has fallen to less than 1.5%.

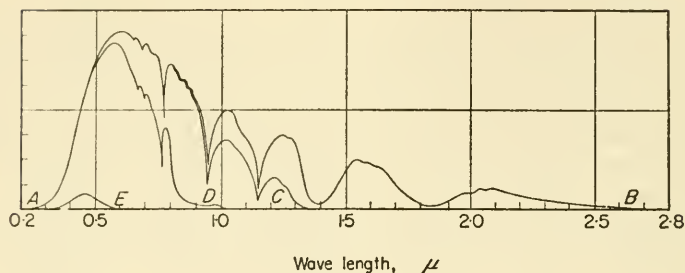


FIG. 28. Energy distribution in solar radiation after passing through water layers of different thickness (according to Schmidt). A-B, at the water surface; A-C, after passing through 1 cm of water; A-D, after passing through 100 m of water; A-E, after passing through 100 m of water.

Table 20. Extinction values for sunlight passing through sea-water

Down to a depth of	0.01 mm	0.1 mm	1 mm	1 cm	10 cm	1 m	10 m	100 m
Extinction in per cent	0.6	4.8	14.1	27.0	45.1	64.1	81.8	98.6

The extinction coefficients in Table 18 are valid only for pure sea-water. The water of the sea is, however, not optically pure, and always contains more or less large amounts of suspended organic and inorganic particles. The intensity of the light passing through the water is still further reduced by scattering on these particles as well as by the ordinary extinction. It may be so strong that the actual absorption, especially in the presence of very small particles Rayleigh's law applies, but for larger particles the scattering is almost independent on the wavelength. It depends primarily on that part of the total surface influenced by the sun radiation of all the individual particles present in a unit volume. Scattering by large particles is then no longer colour selective (PERNTER, 1901).

The reduction in the intensity of radiation in the sea under natural conditions has, for the first time, recently been subjected to more accurate investigation, because of its special biological interest (see especially JERLOV, 1951; JOSEPH, 1952). These measurements have been made principally with photo-electric cells which have a sensitivity extending over a considerable range of wavelengths, while the extinction coefficients mentioned above were measured by spectrophotometric methods. The results are thus only comparable after appropriate corrections. The most detailed measurements have been made on lakes (SAUBERER and RUTTNER, 1941); measurements in the sea which are of greater interest in the present connection are rather few in number. The extinction coefficient applies to the solar radiation and the diffuse sky radiation taken together. When radiation passes through water it undergoes a progressive alteration both qualitatively and quantitatively. The long wave and short wave parts of the spectrum are filtered out almost at once so that the light soon takes on a bluish-green or blue colour. With a greater degree of optical impurity the effect of the scattering is less colour selective; the remaining light is more greenish, or with strong turbidity even yellowish green (PETERSSON, 1936). At the same time the light

undergoes a progressive change in direction since the most oblique light is diminished most while the diffuse light formed by scattering increases continuously.

The first light measurements on the open sea were made by POOLE and AITKINS (1924). Detailed measurements have been made more recently by CLARKE (1933, 1936, 1938) and by CLARKE and OSTER (1935); (see also UTTERBACK 1936). For an example Figs. 29 and 30 show the percentage reduction in intensity of light in different parts of the spectrum for the surface layers of the Sargasso Sea and of the Gulf of Maine.

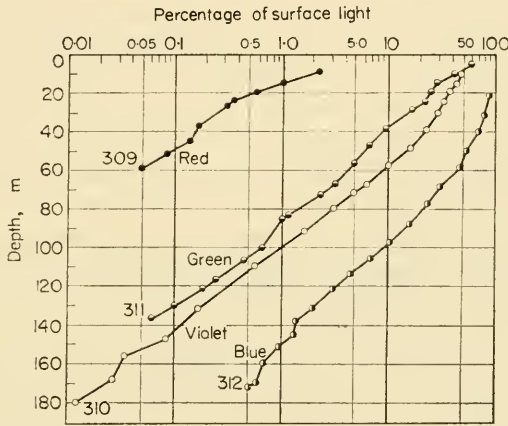


FIG. 29. Decrease in the intensity of light in the Sargasso Sea for different spectral ranges as a percentage of the intensity at the surface (according to Oster and Clarke).

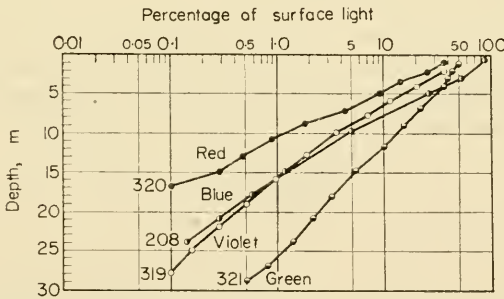


FIG. 30. Decrease in the intensity of light in the Gulf of Maine for different spectral ranges, as a percentage of the surface intensity (according to Oster and Clarke).

As a striking feature the extinction curve is almost linear with depth so that within the spectral region investigated the extinction coefficient is almost constant and is independent of the depth. The violet and the blue are most strongly affected by the turbidity, the red is least affected.

The extinction coefficient for shelf and coastal water is considerably larger than for ocean water, approximately two to three times larger or even more. Its size represents only the order of magnitude of the coefficient since these types of water show large variations both in time and locality. Swedish light measurements, which have been

made, principally by the Oceanographic Institute in Göteborg (Pettersson), since 1933 in fiords, in the Skagerrak, in the Kattegat, and in the Baltic have given similar results, but they also show a particularly strong dependence of the reduction in intensity of the light near to the thermocline (discontinuity in vertical density distribution). This intensification of the extinction is undoubtedly due to an enrichment of suspended particles at such layers. This enrichment shows considerable local differences and causes strong variations in the extinction coefficient. If the scattering and the absorption due to the suspended particles is removed by filtering the water samples there remains a selective absorption which must be due to strongly absorbing humic material dissolved in the water. This "yellow material" must be an organic metabolic product, either from the land or from the remains of decomposed plankton. The turbidity of the water can now be determined continuously from a moving ship by the self-recording transparency meter (JOSEPH, 1950, 1952) and the results can be used in suitable cases to determine the origin of a water mass since the extinction value provides a persistent characteristic (DIETRICH, 1953; JOSEPH, 1953; JERLOV, 1953; see also WYRTKI, 1950). The distribution of particles in suspension can be studied with the Tyndall-meter which measures the intensity of the scattered light produced from a parallel beam of light, by comparison with the known intensity of an illuminated glass filter using a Pulfrich photo-meter. This apparatus can also be used for the measurement of the scattering from suspended and dissolved material in especially transparent ocean water, corresponding measurements of this type have been made by JERLOV (1953) in the three oceans during the "Albatross" Expedition.

(b) Refraction and Reflection of Radiation

Parallel radiation incident on the surface of the water will be partly reflected and in part will enter the water. The angle of reflection will be the same as the angle of incidence but the ratio of the intensities of the incident and the reflected beam will be dependent on the angle of incidence of the original radiation itself. Radiation entering the reflecting medium undergoes a change of direction on passing through the surface, and the angle of this refracted beam is given by the equation

$$\frac{\sin i}{\sin r} = n,$$

where i is the angle of incidence, r is the angle of refraction and n is known as the refractive index. For air and pure water it is almost exactly 1.333338 or $\sim 4/3$. That is, in water which is optically denser the beam is refracted towards the perpendicular (Fig. 31). The refractive index for a ray passing from the water into air is $1/n \simeq 0.75$. If the angle of incidence of radiation passing from the water into air increases, the angle i will increase faster than the angle r until finally the value of i reaches 90° ; the outgoing ray then passes along the surface of the water. This occurs when $r = 48.5^\circ = R$ (see Fig. 31). If r increases still further, radiation cannot enter the air but is reflected entirely within the water; R is known as the critical angle for *total reflection*.

SORET and SARASIN (1889) have measured the refractive index of mediterranean water (approx. 37‰ S) for various wavelengths and compared these values with those for pure water. Table 21 shows the results. The dependence on salinity is, however, sufficiently large for use in the optical determination of salinity (refractometer);

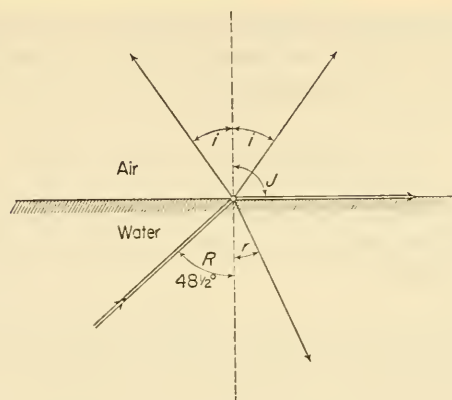


FIG. 31. Reflection and refraction of radiation at the interface between air and water.

Table 21. Values of the refractive index for sea-water and for pure water (After SORET and SARASIN, 1889)

Fraunhofer line	λ in μ	Pure H ₂ O $t = 20^\circ\text{C}$	Sea-water 37‰		Sea-water-pure water 20°C
			20°C	10°C	
C	0.6563	1.33120	1.33816	1.33906	0.00696
D	0.5896	1.33305	1.34011	1.33092	0.00706
F	0.4861	1.33718	1.34437	1.34518	0.00719
h	0.4102	1.34234	1.34973	1.35064	0.00739

besides this it is much stronger dependent on the temperature. More recent investigations on the dependence of the refractive index of sea-water on the temperature and salinity have been carried out by BEIN (1935) at the Physikalisch Technische Reichsanstalt in Berlin. Table 22 shows the deviation of the refractive index of sea-water n_s from the refractive index for pure water, $n_w = 1.333338$ (at 15°C , $\lambda = 587, 6 \text{ m}\mu$) at different temperatures and salinities. The dependence on the wavelengths of the light used is not as large and only has to be taken into consideration for more accurate treatment.

Table 22. Variation of the refractive index $(n_s - n_w) \times 10^6$ with temperature and salinity (According to BEIN, 1935)

$t^\circ\text{C}$ \diagdown $S\text{‰}$	0	10	20	30	35	40
20	4001	3814	3697	3621	3594	3571
25	4989	4759	4617	4524	4491	4463
30	5977	5708	5538	5429	5390	5357
35	6966	6657	6463	6337	6292	6254
40	7956	7610	7391	7250	7199	7157

The relationship between the intensities of the incident and the reflected radiation is expressed by Fresnel's law. If J is the intensity of the incident radiation and R that of the reflected radiation, the relationship between them is given by

$$\frac{R}{J} = \frac{1}{2} \left[\frac{\sin^2(i - r)}{\sin^2(i + r)} + \frac{\text{tg}^2(i - r)}{\text{tg}^2(i + r)} \right].$$

If $J = 100$ and $n = 1.333$ this gives the values shown in Table 23. If the angle of incidence is 0° , only 2% of the radiation is reflected and almost the whole of the energy penetrates through the surface.

Table 23. Reflected radiation R and refracted radiation D for different angles of incidence i of radiation on a water surface ($J = 100$, $n = 1.333$)

i	0°	10°	20°	30°	40°	50°	60°	70°	80°	100°
r	0°	$7^\circ 29'$	$14^\circ 52'$	$22^\circ 02'$	$28^\circ 50'$	$35^\circ 05'$	$40^\circ 31'$	$44^\circ 49'$	$47^\circ 38'$	$48^\circ 35'$
R	2.0	2.1	2.1	2.1	2.5	3.4	6.0	13.4	34.8	100.0
D	98.0	97.9	97.9	97.9	97.9	96.6	94.0	86.6	65.2	0.0

With increasing angle of incidence the reflected energy increases only slowly up to about $i = 60^\circ$ and thereafter very rapidly. The larger the angle of incidence the more is reflected, at 70° more than 13%, at 80° more than 35%. This is shown in Fig. 32. The rays coming from the upper left incident on the surface are split into reflected and

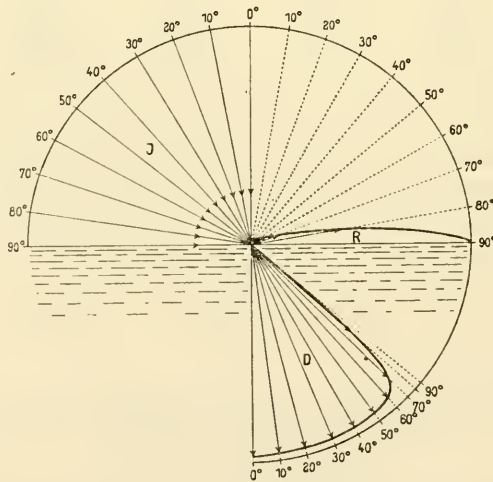


FIG. 32. Graphical representation of the proportions of reflected and transmitted radiation incident on the surface of water at different angles. For each ray incident from the upper left with an intensity of 100 there will be a reflected ray and a ray transmitted into the water.

Both are represented by vectors which give the intensity and the direction of the ray.

entrant rays; the incident rays have an intensity of 100 and the vectors marked on the diagram correspond in intensity and direction to the reflected and entrant rays. Larger values for the reflected energy only occur with obliquely incident light and especially in that range, where the entrant radiation falls to very low values. It can be seen that

the direct incident radiation coming from a whole quadrant is concentrated into a fairly narrow beam range from 0° to 48.5° , while at angles of incidence more than 65° the intensity of the entrant radiation is rather small. SCHMIDT (1908) showed by actinometric measurements at the surface of pure water that the same conditions apply for the total solar radiation as for the D line of sodium ($n = 1.333$). More recent measurements by POOLE and ATKINS (1926) and by WHITNEY (1938), as well as by Ångström (1925) using the pyranometer, show that the theoretical values for reflection are also obtained essentially in practice. However, the reflection is more or less strongly increased by waves on the surface of the water; it may be increased in this way by more than 50% (LAUSCHER, 1944).

(c) *The Behaviour of the Water Surface for Diffuse Incoming and Outgoing Radiation*

As well as the direct sunlight, which may be regarded as unilateral parallel radiation, there is also a general diffuse radiation for which conditions relative to the sea surface are rather different. The diffuse radiation on the surface of sea includes: (1) *diffuse sky light* (daylight) which is essentially short-wave radiation (between 0.38μ and 0.75μ) and is only present in the day time; and (2) the *long-wave radiation* from the atmosphere which is long-wave (maxima at 7.5μ and 12.5μ), and is present both day and night. Each single beam of the diffuse radiation that is incident on the surface of the water at an angle i is partly reflected following Fresnel's law and is thus subject to a corresponding reflection loss as shown by the values given in Table 23. Since the diffuse radiation comes from all directions and the radiation with a greater angle of incidence is more strongly reflected, it is necessary to find the sum of the losses for each angle of incidence in order to determine the total loss by reflection. The calculation of this total from the values $r(i)$ given in Table 23 gives the reflection losses (for $n = 1.333$) as 0.660, that is 6.6% of the diffuse radiation is reflected from the surface of the water. Considering the refractive index to be slightly different for different parts of the spectrum this value varies between 5% and 10%.

Mention should also be made here of the properties of water as a *source of radiation* (SCHMIDT, 1915). Since the extinction coefficient of water for long-wave radiation is particularly large and the thermal radiation from the surface of the sea contains only longer wavelengths (around 10μ) it can be expected from *Kirchhoff's* law that as a source of radiation water would behave as a black body. Nevertheless, water radiates less than a surface of the same temperature since each beam coming from the interior of the water mass will suffer a reflection loss at the surface which will reduce the intensity of the total from the surface outgoing radiation (Fig. 33).

In addition to this reflection loss the intensity of the radiation suffers a further decrease since in passing through the surface to the air it must spread out into a larger space. The radiation from water within a space angle of $2 \times 48^\circ 35' = 97^\circ 2'$ is spread out over a full 180° . If this is taken into account (SCHMIDT, 1916) it is found that for a temperature range of 0 – 20°C the outgoing radiation from a water surface is about 9–10% less than that from a black surface. Since the radiation from a black body according to the *Stefan-Boltzmann* law is given by $E = \sigma T^4$ where $\sigma = 1.374 \times 10^{-12}$ cal cm^{-2} sec^{-1} grad^{-4} the radiation from a flat water surface will be given by $A = 0.904\sigma T^4$. Ångström has found experimentally that for long-wave radiation the efficiency of emission of sea-water is 96% of that of a black body. The constant in the above equation should therefore be not very different from 0.95 for the temperature range

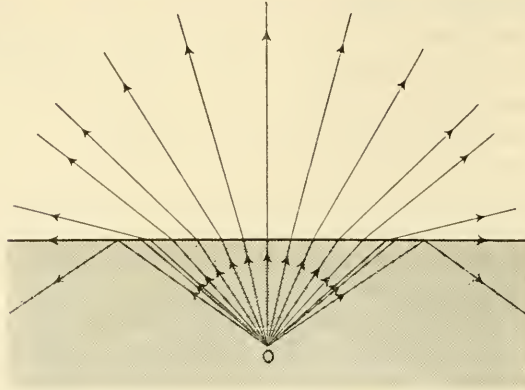


FIG. 33. Back radiation from the interior of the sea towards the water surface.

concerned. LAUSCHER (1944) has obtained the same result in another way and found the value 0.9535 for the constant. FALKENBERG (1928) has made similar calculations and has found the somewhat lower value 0.937 for this constant.

(d) *The Colour of Sea-water*

The colour of sea-water in the scientific sense is taken to include all those colour phenomena which arise because of the optical properties of sea-water and the substances dissolved and suspended in it. The colour of the sea can vary widely and may assume any shade from a yellowish green to the deepest blue. To observe the colour of the sea undisturbed by external reflections it is best to look through a tube which is blackened inside, dipped in the water. The colour can be determined by comparison with standard colours or by spectrophotometry. KALLE (1938) has designed a special colour measurement tube in which the colour of the sea can be determined with a comparator. In practice, the colour is for preference determined with standard colours, using the *Forel-Ule* scale. Accurate colour determinations in the open sea are by no means frequent and have been made almost only by oceanographic expeditions. The largest part of the surface of the ocean is blue (*Forel* 1 and 2), particularly, the regions within the tropics and subtropics, while the green colour is prevalent in coastal areas and shallow seas, especially in adjacent seas and polar regions. In the Atlantic Ocean (SCHOTT, 1942) there is a certain symmetry in the distribution of colour. From 15° to 35° N. and from 10° to 30° S. it is a deep blue. The purest and richest colour is in the central parts of these areas, roughly from the Bermudas to near Madeira and off the Brazilian coast till St. Helena. In the Benguela current, generally in areas of upwelling, for example off the West African coast in the north and off the south-west African coast in the south the sea-water has a more greenish colour. In the Southern Hemisphere a tongue of greenish blue water runs from this coast of South Africa far up to the north between 0° and 10° S. (up to St. Paul Island).

The higher latitudes in both hemispheres are always discoloured. Greenish blue predominates north of 40° N. and gradually changes to green. The waters of the English Channel, the North Sea and the Baltic are of the same colour. In the Southern

Hemisphere the colder water of the Falkland current and the oceans areas around Bouvet Island are mostly greenish blue to green.

An explanation of the colour of pure sea-water must be sought, in the first place, in the optical properties of sea-water. The Bunsen theory ascribed the blue colour of the sea to the combined effects of the spectral absorption of pure sea-water and reflection by the particles suspended in the water (absorption theory). The light entering the water (direct sunlight and diffuse radiation from the sky) will be weakened least in the blue by absorption. Down into the deeper layers the light becomes more and more blue. This relative concentration of blue is further increased in the light reflected from small particles and passing back to the surface, the light returning through the surface is thus blue. Against this absorption theory, Soret has set a diffraction theory according to which the explanation of the blue colour of the sea is analogous to that of the blue colour of the sky and is due to the scattering of light in the water. RAMANATHAN (1923) has attempted to prove by experiment and theoretical investigation that pure sea-water should show an indigo blue colour by molecular dispersion and by selective absorption, and that small amounts of suspended matter have little effect on the colour. According to the theoretical investigations of GANS (1924), the colour is due principally to diffraction of higher orders (see also LAUSCHER, 1947).

A third possible explanation for the widely occurring greenish colour was advanced by WITTSTEIN (1860) and later by SPRING (1886, 1898) in the so-called "solution theory". In this, blue was regarded as the actual colour of the water and all variations were due to different substances dissolved in the water. This effect was ascribed principally to organic humus materials that in increasing concentration made the water first green, then yellowish green and finally, in extreme cases, brown.

It was first pointed out by KALLE (1938, 1939) that the physiology of colour vision must play a large part in the explanation of the colour assumed by the sea and must be taken into consideration. According to the Young-Helmholtz theory of colour vision, the human eye has three groups of colour-sensitive elements (cones), each of which is sensitive to one of the three primary colours, red, blue and green. The stimulation of two or all three of these groups at the same time gives the impression of a mixed colour. Every different colour impression is produced by a definite ratio in the strength of the stimulation of the three different types of cones. A "colour triangle" (Fig. 34) can be used to represent diagrammatically all possible colour impressions. The three corners of the triangle represent the total (100%) stimulation of only one group of receptors—red, green or blue. At every point on the triangle the sum of the oblique co-ordinates of the point is always 100%, and these co-ordinates represent the percentage composition of the mixed colour characterized by that point. The point W = white which, by definition, is composed of a mixture of $33\frac{1}{3}\%$ of each of the three primary colours lies at the centre of gravity of the triangle. All tones of the same colour lie along a straight line that runs radially from the white point; the nearer a point on such a line lies to one of the sides of the triangle the more saturated is the colour it represents. The position of the spectral colours within the triangle is shown by the curve marked on the diagram. Since the spectral colours are the most saturated colours possible in nature, all colours found in nature must lie on the area within the spectral curve and the line joining its two end-points.

In the light of the consequences of this theory, Kalle has investigated the effects

of selective absorption and selective scattering and also of the interaction of these two processes on the colour of the sea. These results are summarized in Fig. 35 which shows a part of the colour triangle and the spectral curve. The absorption colour of sea-water lies on a curve running from the white point and approaching concave

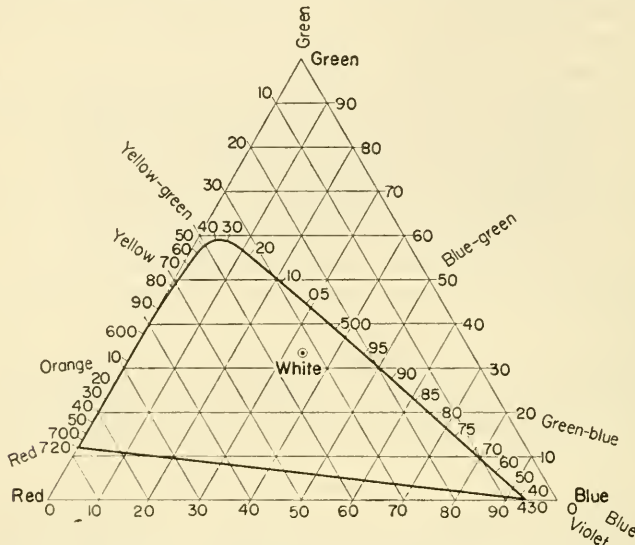


FIG. 34. Colour triangle of the Young-Helmholtz colour theory and spectral curve.

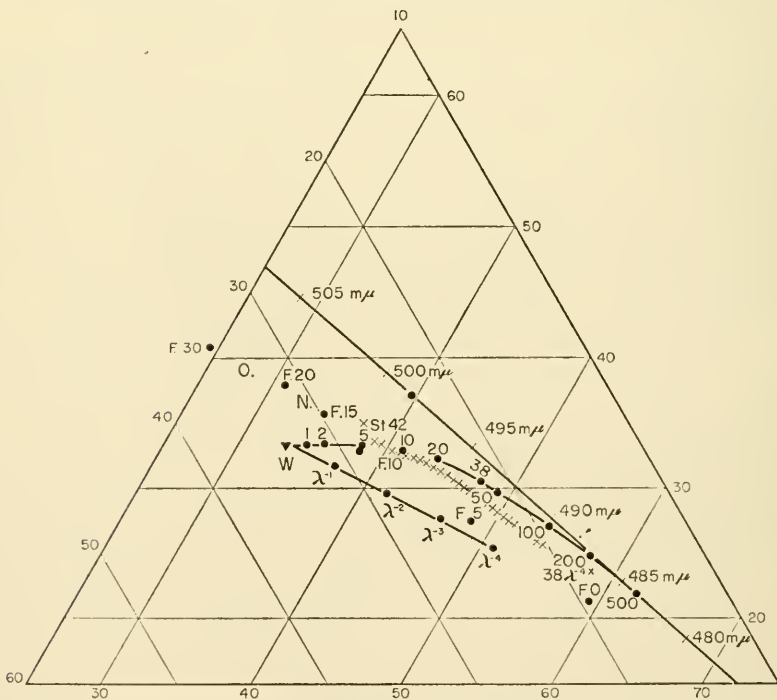


FIG. 35. Part of the colour triangle showing colour points for sea-water colour.

downwards the spectral curve asymptotically. With layers of increasing thickness the increasing saturation of the colour gives a slow displacement towards the blue, while at the same time the brightness of the colour decreases rapidly so that only a relatively thin surface layer is concerned in the colour of the sea. According to Kalle, the result is a colour with a wavelength approaching $492\text{ m}\mu$, a somewhat greenish blue, corresponding to a light path of 38 m. This shows immediately that the deep blue colour of the Sargasso Sea cannot be explained in this way. If selective scattering of the different colours is taken into account the colour curve lies further towards shorter wavelengths. As far as the colour is concerned the most important point on this curve approaches that corresponding to a 50 m thick layer where the colour value is $485\text{ m}\mu$. This value agrees fairly well with the colour of the Sargasso Sea, especially if the higher order scattering which would give a further slight displacement towards shorter wavelengths is taken into account. The absorption and the scattering of light are thus responsible for the blue colour of the tropical and subtropical areas of the ocean and they are reinforced by the greater brightness of the sunlight and of the diffuse light from the sky and by the almost completely pure sea-water of these areas.

For water masses that are not so pure and contain large numbers of suspended particles (mostly plankton), as is usually the case in higher latitudes, the depth from which the selective scattering is reflected is less, and the colour gradually reverts to a value of $495\text{ m}\mu$. This would be more or less the longest wavelength for the colour of the sea if only absorption and scattering were involved during its formation. Other causes are, however, required to explain the greenish colours of longer wavelength than $495\text{ m}\mu$ that are also of frequent occurrence in the open ocean. Investigation has shown that these are due to coloration caused by yellowish substances dissolved in the water. These substances appear to be related to humus and are apparently to be regarded as products of phytoplankton metabolism. They displace the colour of the water towards the green especially in water masses such as in the English Channel and in the North Sea where values of $498\text{ m}\mu$ to $505\text{ m}\mu$ may occur. In coastal regions further humus material carried by fresh water flowing into the sea from rivers is added to the more oceanic yellow material and causes a further displacement towards yellow-brown colours. In addition to these yellow substances there may also be fluorescence phenomena in the seas as Ramanathan, and later Kalle, believed; these would give a further displacement towards the green but the extent to which such factors are present is not yet certain.

A qualitative survey of the contribution of each single factor to the colour of the sea has been given by Kalle in Fig. 36. In the clearest water and with a depth of visibility of 50–60 m, selective scattering plays to a very large extent the principal part. If cloudiness due to the presence of plankton occurs, the depth of visibility gradually decreases and the natural absorptive colour of water which tends towards a greenish shade begins to predominate. At the same time small amounts of yellowish substances may be formed as the colour tends more and more towards green. With the increasing turbidity the yellow material becomes more and more important until finally, at very small depths of visibility, the discoloration is due to the natural colour of the material causing the turbidity. Very close to the coast the natural colour of the bottom begins to show through the shallow water, and the colour of the water is clearly altered towards this.

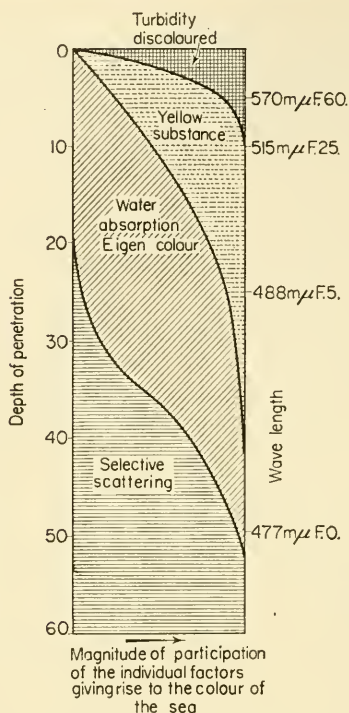


FIG. 36. Quantitative representation of the contribution of the individual factors giving rise to the colour of the sea (according to Kalle).

8. The Chemistry of the Sea

In general, liquids have the property of absorbing gases with which they are in contact to give a solution of the gas in the liquid. The solubility of the gas in the liquid is not unlimited, but usually fairly soon reaches a limit; the liquid is then saturated. According to Henry's law the amount of gas dissolved in a saturated solution is proportional to the pressure of the gas in contact with the liquid. If the liquid is in contact with a mixture of gases then each separate gas is absorbed according to its partial pressure. When the liquid is completely at rest the process of solution depends on the process of diffusion, and thus requires time for the pressure of the gas in the liquid to come to the same pressure as the gas outside it. In nature, the wave motions, turbulent currents and convections can accelerate considerably the uptake of gas by the liquid. By the gas content of a sample of water is understood the amount of gas in the water expressed in volume units (ml/litre) at NTP (0°C and standard pressure of 760 mm Hg). The actual gas content may of course differ more or less from the amount present when saturated.

Besides, by this *absolute* definition the gas content may also be characterized by the ratio of actual content to that by saturation. It is then specified by the *relative gas content* which is expressed in per cent of the amount required for saturation. The absorption coefficient is taken as that volume of gas which can be absorbed by unit volume of liquid at a given temperature and standard pressure.

If the solution process is limited to purely physical absorption the absorbed gas does not enter into chemical combination with the water; the situation is then fairly simple. It is, however, possible for the gas to combine chemically with the liquid. Both possibilities occur in the atmosphere-ocean system. Oxygen, nitrogen and the rare gases obey the pure physical absorption; carbon dioxide, on the other hand, follows the second possibility since it reacts both with the water itself and in part also with the salts dissolved in it. (For chemistry of sea waters see especially HARVEY, 1955.)

(a) *Oxygen, Nitrogen and Hydrogen Sulphide Contents of Sea-water*

The composition of the air absorbed by pure water can be calculated from the absorption coefficients of the gases present in the atmosphere and is shown in Table 24 for 0° and 30°C. It is different from that of atmospheric air since the absorption coefficient of the individual gases is very different. In atmospheric air the ratio of oxygen to nitrogen is 21 : 78 or about 1 : 4, but in the air dissolved in water at 0°C it is 35 : 62, and at 30°C 33 : 64 or about 1 : 2. The air dissolved in water is thus twice as rich in oxygen as atmospheric air, but it should not be forgotten that while a litre of air contains 210 ml of oxygen, a litre of water saturated with air contains only about 10 ml.

Table 24. *Distribution of atmospheric gases at saturation dissolved in sea-water*

	Oxygen	Nitrogen	Argon	Carbon dioxide	Total
ml./l. { 0°C	10·31	18·11	0·54	0·51	29·47
{ 30°C	5·60	10·74	0·30	0·20	16·84
In ‰ { 0°C	35·0	61·5	1·8	1·7	100·0
{ 30°C	33·2	63·8	1·8	1·2	100·0

The solubility of gases in water is very strongly dependent on the temperature and falls off rapidly as the temperature rises. The sea-water as a dilute salt solution shows also a dependence on the salinity and the absorption coefficients fall with increasing salinity. FOX (1905, 1907, 1909) has carried out extensive research on this subject, and RAKESTRAW and EMMEL (1937, 1938) have made further investigations. Table 25 shows saturation volumes at different temperatures and salinities for oxygen and nitrogen. The weights present in mg can be obtained by multiplying the figures for oxygen by 1·4292 and those for nitrogen by 1·2542. If oxygen-nitrogen ratios O_2/N_2 for different temperatures and salinities are worked out, it can be seen that there is little variation; the dependence on salinity is small; with temperature it falls off slightly.

For chemical methods of determining the oxygen and nitrogen contents of a sample of sea-water see *Report of "Meteor" Expedition, 3* or "Oceanographic Instrumentation. Chemical Measurements" (CARRIT, *Nat. Acad. Sci. Nat. Res. Coun.*, no. 309, pp. 166-85, 1952).

At the surface of the sea, in contact with the atmosphere, there is ample oxygen and nitrogen available and it would be expected that the upper layers of the ocean were saturated with both gases. This is generally the case, especially for nitrogen which is

Table 25. Saturation values for oxygen and for nitrogen in sea-water in millilitres per litre for a dry standard atmosphere

Temp. (°C)	Oxygen salinity (‰)					Nitrogen salinity (‰)				
	20	25	30	35	40	20	25	30	35	40
- 2	9.50	9.16	8.82	8.47	8.12	—	—	—	—	—
0	9.01	8.68	8.36	8.03	7.71	16.02	15.46	14.90	14.34	13.78
5	7.94	7.67	7.40	7.13	6.86	14.08	13.62	13.17	12.72	12.27
10	7.10	6.86	6.63	6.40	6.17	12.74	12.32	11.92	11.51	11.10
15	6.43	6.23	6.04	5.84	5.64	11.57	11.20	10.84	10.48	10.11
20	5.88	5.70	5.53	5.35	5.18	10.53	10.21	9.91	9.61	9.30
25	5.40	5.21	5.03	4.93	4.77	9.69	9.42	9.16	8.88	8.62
30	4.96	4.80	4.65	4.50	4.35	—	—	—	—	—

less reactive than oxygen and is biologically inert. Water samples from different depths show mostly only minor deviations in nitrogen content from the saturation values. This could be used to draw conclusions about the origin of deep layers and about the vertical and horizontal displacements that they have undergone since their last contact with the atmosphere, but since very few nitrogen determinations have been made in the open ocean the method has so far been of little use. In any case, care would be required in the interpretation of such results since super-saturation or incomplete saturation may be due to other causes: to subsequent heating and cooling, to the mixture of saturated water masses at different temperatures which always leads to small super-saturation, to variations in atmospheric pressure and to the production of nitrogen by bacteria that decomposes nitrite or nitrate. Since the equalization of existing differences in saturation always proceeds slowly these deviations will be conserved for a long time and can simulate water movements that would otherwise be quite impossible.

The oxygen is also for the most part in equilibrium between the air and water at the surface of the sea, but the deviations are more frequent and more marked than for nitrogen. Besides the causes of more physical factors mentioned above (temperature and pressure alterations, mixing, etc.), there are also biological factors which cause variations. The respirations of plants and animals produces carbon dioxide and uses up oxygen. Animals, however, obtain their essential carbon compounds from ingested organic material, while plants, on the other hand, obtain it by the assimilation of carbon dioxide. This is converted with the help of sunlight into organic substances and oxygen, which is set free, raising the oxygen content of the water.

The oxygen in sea-water is consumed not only by the respiration of living organisms but also by the bacterial oxidation of dead organic matter and of organic compounds in solution. This oxygen consumption is proportional to the rate of oxidation, which is in the first place dependent on the temperature and also on the amount and nature of the organic material present.

In the assimilation layer (the upper layer of the sea), usually down to the thermocline (rapid density change in the vertical) conditions are rather complicated due to the mutual interaction of the different factors. Oxygen is being steadily absorbed from

the atmosphere and produced by photosynthesis. Usually this addition is not exceeded by removal of the respiration of the organisms present and by the oxidation of dead material. Super-saturation by oxygen is thus quite possible and is occasionally found. The surface layer is generally, however, the layer which is nearest to equilibrium with the air. In the deeper layers of the ocean, below the assimilation layer, the oxygen is provided almost exclusively by transport of the water from the surface by vertical and horizontal movements. On the trajectories which the water particles perform there is a continuous progressive consumption of oxygen so that the oxygen supply in deeper layers depends either on the distance covered since the water mass left the surface or on the speed with which it moved. A stationary state is only possible when the supply of oxygen by renewal of the water mass and the oxygen consumption are in equilibrium. Estimation of the oxygen distribution in the deeper layers of the ocean, especially of the vertical and horizontal differences in saturation, until very recently gave only the "age" of the water mass, i.e. the time since it left the surface layers. After that some clarification had been obtained of conditions for similar processes in lakes, the chemical-biological processes of oxygen depletion in the sea were further elucidated by SEIWELL (1937, 1938), SVERDRUP (1938) and WATTENBERG (1938). The last one has discussed in detail the relevant chemical-biological factors in the "*Meteor*" Report and has pointed out its great importance for a proper understanding of the distribution of oxygen in the ocean.

This distribution within the ocean shows that the explanation given can account qualitatively for the oxygen producing and consuming factors mentioned above. The maximum oxygen content is always found in the surface layers; in this skin layer mixing by the wind and the waves and the turbulence due to ocean currents gives a more or less even distribution that normally differs little from equilibrium with the atmosphere. The lower limit of this oxygen-rich layer, which coincides with the assimilation layer, follows essentially the thermocline in the general oceanic structure. At this transition layer, when it is strongly developed as is always the case in lower latitudes, the oxygen content falls to a minimum. According to the geographical position of the part of the ocean and the range of the annual convection at that point the depth of this minimum varies between 100 and 1500 m. This oxygen-poor intermediate layer is the most prominent feature of the oxygen distribution of the ocean in middle and low latitudes. Below this minimum layer there is always oxygen-rich water with up to 70–90% saturation. As is explained later, this oxygen content of the deep-sea circulation of the oceans originates from the major convection areas of the subpolar and polar regions of the ocean where the water masses in the surface layers can sink to great depths, and from there also fill the depths at middle and lower latitudes. In spite of the long path travelled by these water masses there is little depletion because of the low temperature and the small amount of organic material present, and the oxygen content shows only a slight decrease. Figure 37 shows as an example the vertical distribution of oxygen at about 10° S. in the South Atlantic; the vertical variation of density is also shown and the density transition can be clearly seen. The right-hand side of the figure shows the vertical changes in percentage oxygen saturation and in density σ_t at a station in the North Atlantic near Greenland in the area where, according to a view expressed by NANSEN (1912), the North Atlantic deep water is formed and sinks during the late autumn and winter. The almost constant value of the density down to

below 2000 m and the high oxygen content proves the possible presence of convection descending to great depths and the considerable ventilation it would give.

The renewal of the deeper water layers has a major effect on the oxygen distribution in them. If renewal did not occur oxygen depletion processes would in time reduce the oxygen content until it would be finally zero. It is to be expected that enclosed, stagnating water masses will always have a very low oxygen content when their thermo-haline structure prevents the thermal circulation from the surface reaching the bottom. If the surface layer density is so low that it does not become heavy enough when the temperature decreases in the autumn and winter in order to change places with the

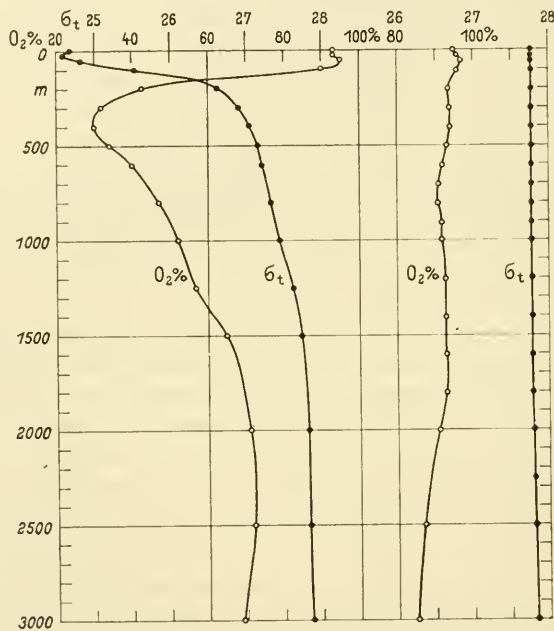


FIG. 37. Left: Vertical distribution of oxygen and density at about 10° S. in the South Atlantic (according to the values of the "Meteor" Expedition). Right: the same for "Meteor" station 122 (Greenland, $\phi = 55^{\circ} 3' N.$, $\lambda = 44^{\circ} 46' W.$).

more saline deeper layers thus carrying oxygen to the layers beneath, the oxygen content of the deep stagnating layers may fall to zero, especially when a lateral addition of fresh water, due to the orographic conditions, is hindered or completely missing. In this case hydrogen sulphide will be formed either by the decomposition of proteins or by the reduction of sulphate by the carbon compounds of organic material under the action of certain bacteria. The classic example of these conditions is the *Black Sea*, where the water from about 200 m down to the greatest depths contains considerable amounts of free hydrogen sulphide and thus forms a "Kingdom of the Dead" from which all life has disappeared and where the organic world is represented only by the lowest forms of plant life (SCHOKALSKI, 1924; NIKITIN, 1927; NEUMANN, 1942, 1944). The thermo-haline structure of the Black Sea is indicated in Fig. 38 which shows the vertical distribution of temperature, salinity, density, oxygen content and

hydrogen sulphide content at three stations in July in different places in the eastern part of the Black Sea (NEUMANN, 1943). The station P.M. 298 lies in the southern part, the station P.M. 308 lies in the northern part of the central eastern basin near an area with little current, and the station P.M. 303 lies south-west of Sochum in the area of the strong current along the Caucasian coast.

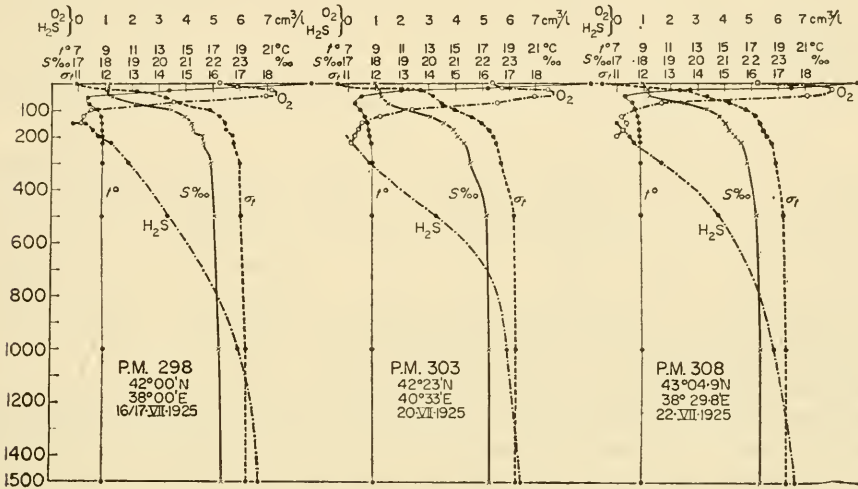


FIG. 38. Vertical structure of the water masses in the eastern part of the Black Sea. (Sept. 1925 stations: P.M. 298, 303, 308; temperature, salinity, density, oxygen content and sulphur content.)

The vertical structure of the Black Sea is characterized by two layers. The upper layer shows a very rapid increase of density with depth and usually extends down to about 200 m. After a sharp bend in the σ_t -curve the density changes little with depth. The boundary between these two layers coincides approximately with the upper limit of the hydrogen sulphide; its depth varies from place to place depending on the dynamics of the currents prevailing. The upper layer (the troposphere) is divided in summer at a depth of about 50–70 m by a definite temperature minimum at 6.5°–7.5°C. This surface zone has a constant salinity and shows a pronounced vertical thermal convection; it is well ventilated and has a rich oxygen supply from the atmosphere and also from plant assimilatory activity. In the lower part of the surface layer the oxygen falls off rapidly with depth and finally disappears, and in places is replaced by hydrogen sulphide. The oxygen of these upper layers comes partly from above and partly from horizontal advection but the latter effect is limited to the immediate vicinity of the Bosphorus.

The whole of the layer from below the oxygen zone down to the bottom at about 2000 m has an almost constant temperature, about 8.8–9.0°C; the slight increase from 300 m is largely an adiabatic effect. The principal characteristic of this lower water is the hydrogen sulphide content which increases down to the bottom (see Table 26).

Similar conditions, though on a smaller scale, are shown by several Norwegian fiords where in most cases there is a considerable depth, a fresh-water influx at the

Table 26. Average vertical distribution of *t*, *S* and Hydrogen Sulphide in the Black Sea

Depth (m)	0	100	200	300	500	1000	1500	2000
Temp. (°C)	13·80	7·95	8·69	8·80	8·83	8·93	—	9·00
Potential temp. (°C)	—	7·94	8·67	8·76	8·77	8·81	—	8·75
Salinity (‰)	—	20·36	21·35	21·73	22·09	22·24	22·31	22·34
H ₂ S content ml/l. (standard pressure and °C)	0·0	0·0	0·45	1·42	3·45	5·55	6·09	6·24

inner end and access to the open ocean only over a bar or a very shallow sill. They have recently been reviewed in detail by MÜNSTER (1936). Of 30 fiords on the western and southern coasts, 16 showed hydrogen sulphide in the bottom layers; the other 14 had very low oxygen values varying between 0·22 and 5·47 ml/l. The ventilation of the deeper layers depends in the first place on the sill depth and the width of the passage to the free ocean. In some fiords changes in the hydrogen sulphide content were found which must be due to the addition of ocean water.

The formation of hydrogen sulphide is only possible in closed or very poorly ventilated deep basins. The *Baltic* which has a much lesser depth than the Black Sea shows very similar hydrographic conditions, although the deep water in the Baltic is renewed occasionally by the spasmodic entry of masses of North Sea water (WATTENBERG, 1941) so that it is only in stagnant periods that the oxygen content is depleted by the respiration of animals and by the oxidation of organic material in the water and on the bottom. Table 27 shows typical conditions at a summer station in the middle of the Baltic.

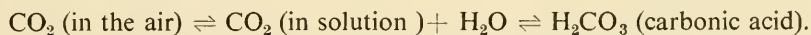
Table 27. *Gotland Basin* (57°24' N., 19°52' E.); "Skagerrack" Station Alf. 96, 31 July, 1922

Depth (m)	Temp. (°C)	<i>S</i> ‰	Density σ_t	Oxygen		Free CO ₂ ml/l.
				ml/l.	‰ satur.	
0	15·52	6·64	4·19	6·78	101	0·23
20	10·60	7·27	4·37	7·64	103	0·28
30	4·15	7·36	5·91	—	—	—
40	2·95	7·63	6·14	8·74	99	0·64
60	2·20	7·92	6·35	7·86	87	0·83
80	4·05	10·42	8·34	3·72	44	2·9
100	4·35	10·90	8·70	3·62	43	2·7
150	4·55	12·59	10·04	3·72	45	2·4
209	4·60	12·81	10·21	2·45	30	3·3

The temperature minimum caused by winter cooling is at 60 m depth. The oxygen content falls from the well-ventilated upper layer with 7–8 ml/l. to less than 2 ml/l. a little above the bottom where it reaches only 30% of saturation. The carbon dioxide content here is 3·3 ml/l., which is eight times the normal concentration (SCHULZ, 1924).

(b) The Carbon Dioxide Cycle in the Ocean and its Relationship to the Atmosphere

Unlike nitrogen and oxygen, the carbon dioxide in the sea is present not only in solution but also in considerably larger amounts chemically combined as salts. Conditions are thus much more complicated, and the situation has only been clarified in recent times by Buch and McClendon using modern dissociation theory. Fundamentally one realized by this that the free and the combined carbon dioxide in solution are not independent of each other, but according to the law of mass action are in chemical equilibrium with each other. The combinations occurring can be represented by the following equations:



The carbonic acid splits partially into its ions according to:



which can dissociate further by:



All these forms derived from carbon dioxide are present in sea-water principally as carbonate and bicarbonate ions, and only to a lesser extent in the free state. Equilibrium exists between these forms, the carbonate and the bicarbonate ions, free carbon dioxide and the hydrogen ion, and it will be discussed later. The reasons are now understood for the long time needed in oceanographic research to obtain suitable accuracy in the determination of the carbon dioxide in solution in sea-water.

Free carbon dioxide and carbon dioxide pressure. The solubility of carbon dioxide in sea-water is relatively large, almost thirty times that of nitrogen. Fox investigated its dependence on the temperature and on the chlorine content of NaCl solutions, and corresponding measurements have been made by Krogh for sea-water. On this basis of these investigations BUCH and collaborators (1932) WATTENBERG, (1936) prepared tables showing the dependence of the solubility of carbon dioxide in sodium chloride (NaCl) solutions on the temperature and the salinity. Table 28 shows a condensed extract from these tables. The solubility of carbon dioxide decreases considerably with increasing temperature and salinity. One litre of sea-water at 0° and 35.19‰ S, when in equilibrium with the atmosphere (partial pressure of carbon dioxide 0.0003

Table 28. Solubility of carbon dioxide in sodium chloride (NaCl) solution in millilitres per litre at a carbon dioxide pressure of 1 atm.

$t^\circ\text{C}$ $S_{\text{‰}}$	-2	0	5	10	15	20	25	30
0	1890	1713	1424	1194	1019	878	759	665
20	1708	1554	1291	1088	932	808	702	617
30	1622	1479	1228	1038	890	774	674	594
32	1605	1464	1215	1028	882	768	669	590
34	1588	1449	1203	1018	874	761	663	585
36	1572	1435	1191	1009	866	755	658	581
40	1540	1406	1167	990	850	742	648	572

atmosphere) contains 0.42 ml/l. of free carbon dioxide, which is very little. In water in the uppermost layer of the open ocean the carbon dioxide content is usually not far from the equilibrium value with the atmosphere.

According to Krogh's measurements in the North Atlantic the value for the carbon dioxide pressure varies between 1.55×10^{-4} and 2.9×10^{-4} . According to Brennecke's values in the Weddell Sea ("Deutschland" Expedition) the carbon dioxide pressure was higher than that in the atmosphere. Carbon dioxide in solution comes only slowly to equilibrium with the atmosphere. Detailed investigations along this line have been made by BUCH (1917), in the waters around Finland, by SCHULZ (1923) in the Baltic, by WATTENBERG (1933) on the "Meteor" Expedition (1925-7 principally between Africa and South America), by DEACON (1934) especially in the Arctic and Antarctic regions and finally by BUCH (1939, 1939a) in the North Atlantic and on a cruise in the Arctic. All these measurements of the carbon dioxide pressure show variations around the equilibrium position, sometimes the pressure in the water is higher than in the atmosphere and at other times it is lower. These variations, however, are small as in the course of the long time which has been available, sea and atmosphere have come into a mutual adjustment. WATTENBERG (1936), from the observations available, arrived at the following conclusions (Fig. 39):

(1) There are limited areas of the sea where the carbon dioxide pressure of the water is definitely greater than that of the air; these are principally places where rising water currents bring water rich in carbon dioxide to the surface from intermediate layers rich in carbon dioxide (west coasts of North and South Africa and of North and South America).

(2) In other places there are, however, large areas where the carbon dioxide pressure is somewhat less than the normal partial pressure of the atmosphere. These occur especially in temperate and cold zones during the spring and summer, when rich plant plankton is actively assimilating. There may be pronounced annual changes here in the carbon dioxide pressure at the surface of the sea: a strong reduction in spring at the beginning of diatom development and a gradual rise in autumn when dead organisms start to decompose. See p. 77 for the distribution of carbon dioxide in deep water and at the sea bottom.

Total carbonic acid. If the sea was neutral it would contain little carbon dioxide. Sea-water is in fact alkaline and has a total carbon dioxide content that is much greater than would be concluded from the carbon dioxide pressure. By far the largest part is chemically combined in the sea salt.

The total amount of carbon dioxide present depends on the one hand on the carbon dioxide pressure and on the other on the amount of base available for combination with the carbon dioxide which is termed the *alkalinity*. Since the carbon dioxide pressure is small, there is an almost linear relationship between the total amount of carbon dioxide present and the alkalinity, and thus also the salinity since the alkalinity is dependent very largely on this. Thus BUCH (1914) for the Pojowick under average conditions found the relationship

$$A = 0.07 + 1.00 \text{ CO}_2 \quad \text{and} \quad \text{CO}_2 = 0.32 - 0.173S$$

where CO_2 is expressed in millimoles/litre and A in milliequivalents. Similar relationships were also derived for the Gulf of Finland and the Gulf of Bothnia.

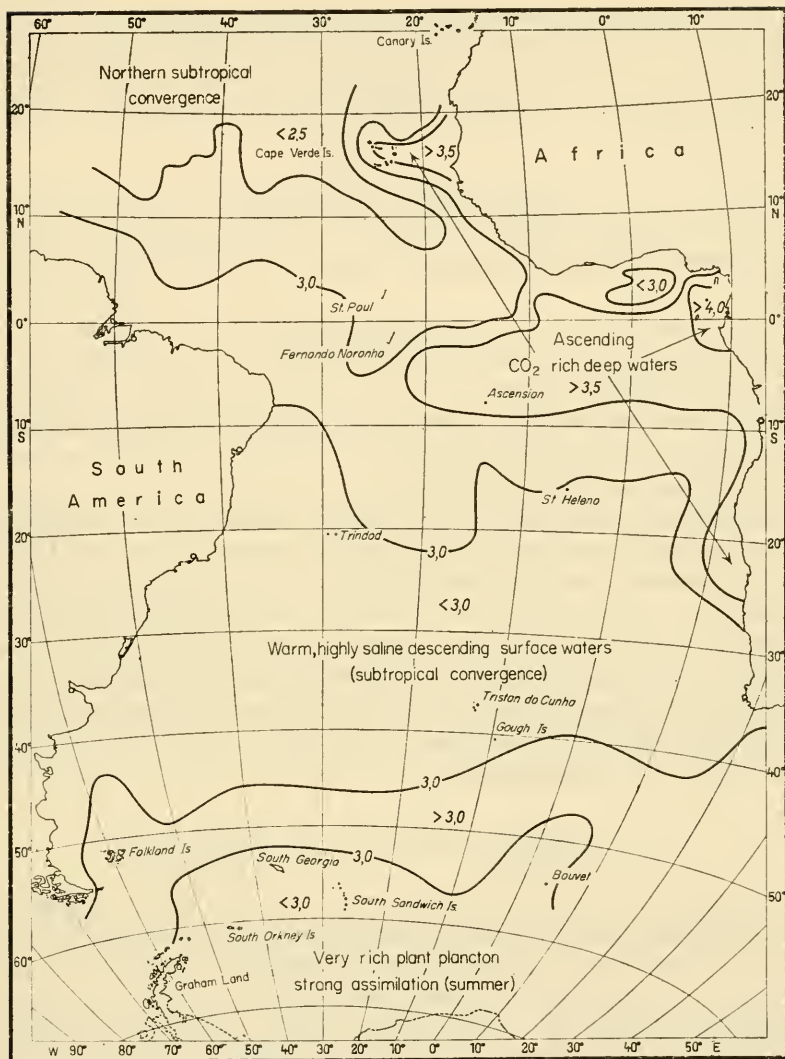


FIG. 39. Distribution of carbon dioxide pressure (given in 10^{-4} atm.) at the surface of the South Atlantic (according to Wattenberg).

In the open ocean the average value for total free carbon dioxide is usually between 45 and 55 ml/l. Ruppin has found for the middle North Sea 45.9 for the Beltsea 36.7 and for the southern part of the Baltic 31.9, while BRENNER (1909) found values between 46 and 55 in the Atlantic and in the Indian Ocean and between 45 and 59 in the Antarctic Ocean. In the North Sea KNUDSEN (1899, "Ingolf" Expedition) found lower values, between 34.1 and 46.6 ml/l.

Alkalinity. In sea-water the sum of the cations of bases (Na^+ , K^+ , Mg^{2+} , Ca^{2+}), is always a little greater than the sum of the anions of strong acids (SO_4^{2-} , Cl^- , Br^-). This excess of base is known as the "alkaline reserve"; it gives sea-water an alkaline

reaction and is very largely present in the form of carbonates and bicarbonates. Since Tornøe, it is also known as the "alkalinity", a term which is also used for the hydrogen-ion concentration. To avoid confusion the sum of the carbonate and bicarbonate ions is termed in oceanography (following Buch) the "titration alkalinity". This is expressed in the equation

$$A = 2[\text{CO}_3^{2-}] + [\text{HCO}_3^-],$$

and can be found by simple titration with hydrochloric acid (WATTENBERG, 1933; see also 1930).

The alkaline reserve in sea-water is largely combined with carbonic acid, but a smaller part is also combined with other acids the most important of which is boric acid. Sea-water of 35‰ *S* contains 4.7 mg/l. of boric acid (BUCH, 1933). The last anomalies in the carbon dioxide system of sea-water have only been eliminated by taking this acid into consideration since it and its ions are definitely concerned in the equilibrium despite their small concentration.

Since the individual constituents of the salt in sea-water are in almost constant ratio to one another, it would be expected that the amount of base available for the formation of carbonate and bicarbonate, that is the titration alkalinity, would be directly dependent on the salinity. This is the case. The dependence between the two was first shown by HAMBERG (1885) and the investigation by Brennecke of the surface samples collected on the "Deutschland" Expedition gave the relationship between them as $A = 0.06779S$ (according to SCHULZ, 1921). Later investigations have shown that for the open ocean the dependence of alkalinity on the salinity is given with sufficient accuracy by the relationship

$$A = 0.068S\text{‰} = 0.123 \text{ Cl (in milliequivalents).}$$

This simple proportionality does not apply to the sea-water of the marginal and adjacent seas as has been shown by RUPPIN and BUCH; these variations appear to be due to the inflow of fresh water from the land. The North Sea and the Baltic, especially in coastal areas, show alkalinity values that are higher than would correspond to the salinity (addition of carbonate in river water). Similar conditions are found in the Gulf of Bothnia, the Gulf of Finland and in the Adriatic.

Carbonate at the sea bottom passing into solution has the same effect as the addition of carbonate from the land. The investigations of the "Challenger" Expedition clearly indicated that the water immediately above the sea bottom was more alkaline than that at the surface or in the middle layers (DITTMAR, 1884; BRENNKE, 1921). The more accurate alkalinity determinations of the "Meteor" Expedition 1925-7 showed definitely that the specific alkalinity (the ratio of alkalinity to chlorinity, $A : \text{Cl}$) almost always increased near the sea bottom. This increase can only be explained by calcium carbonate from the bottom sediments going into solution (see p. 85).

Hydrogen-ion concentration. Pure water dissociates according to the equation



H^+ is the positively charged hydrogen ion and OH^- is the negatively charged hydroxyl ion. The law of mass action gives the equation

$$\frac{[H^+] \cdot [OH^-]}{[H_2O]} = K_w,$$

where the square brackets indicate concentrations in mols per litre. The concentration of pure water $[H_2O]$ is approximately the same for all dilute aqueous solutions such as sea-water. Since $[H_2O]$ is constant for a given temperature it can be included with the constant K_w so that

$$[H^+] \cdot [OH^-] = K_w.$$

At 18° , 25° and $50^\circ C$ K_w has the values 0.61×10^{-14} , 1.0×10^{-14} and 5.4×10^{-14} respectively. The concentration of either of the ions can be calculated if that of the other is known. Solutions where $[H^+] > [OH^-]$ are acid and where $[H^+] < [OH^-]$ are alkaline; in neutral solutions the two concentrations are equal. The character of the solution is thus specified completely by $[H^+]$. In pure neutral water at $25^\circ C$ $[H^+] = [OH^-] = \sqrt{K_w} = 10^{-7}$. The hydrogen ion concentration of a solution is usually not given as $[H^+]$ but as the quantity $-\log [H^+] = \text{pH}$. For pure water at $25^\circ C$ the pH is thus 7.0.

Carbon dioxide system in sea-water. There is an equilibrium between the different chemical species derived from carbon dioxide that are present in sea-water and this must follow the law of mass action. As for every electrolyte there is a reciprocal relationship between the concentrations of the undissociated substance and those of its ions. For the first and second dissociations of carbonic acid

$$\frac{[H^+] \cdot [HCO_3^-]}{[H_2CO_3]} = K_1 \quad \text{and} \quad \frac{[H^+] \cdot [CO_3^{2-}]}{[HCO_3^-]} = K_2.$$

To these equations can be added the equation for the titration alkalinity

$$2[CO_3^{2-}] + [HCO_3^-] = A.$$

Since the dissociation constants K_1 and K_2 are known, these three equations contain four unknown quantities

$$[H^+]; [HCO_3^-]; [CO_3^{2-}] \quad \text{and} \quad [H_2CO_3].$$

If one of these can be determined, for instance the $\text{pH} = (-\log [H^+])$ then the other three can be calculated.

The dissociation constants for carbonic acid in pure water ($18^\circ C$) are

$$K_1 = 3.06 \times 10^{-7} \quad \text{and} \quad K_2 = 5 \times 10^{-11}.$$

In sea-water the values of these dissociation constants are different because of the effect of the considerable amounts of other ions present in sea-water. The ions of the neutral salts such as Na^+ , K^+ , Mg^{2+} , SO_4^{2-} also affect the carbon dioxide equilibrium but not

in proportion to the total amount present: according to the theory of interionic forces developed by Milner, Bjerrum, Debye and Huckel, amongst others, only a small fraction is involved. This fraction of the total concentration is termed the "activity"; the equilibrium thus involves not the total concentrations of the different ions, for instance $[H^+]$ but the activities, in this case $f_1[H^+]$, where f is the "activity coefficient" and the above equations are replaced by others where the factors on the left-hand side are multiplied by the activity coefficients f_1, f_2, f_3 and f_4 . The constants K_1 and K_2 remain unchanged; they are termed "activity constants". However, instead of taking the effect of the neutral salts directly into consideration it can be allowed for by its effect on the dissociation constant; the apparent dissociation constants K'_1 and K'_2 are termed the "concentration constants". At the suggestion of the International Council for Oceanography Research they have been determined by BUCH and co-workers (1932) WATTENBERG, (1936). Table 29 gives numerical values for $-\log K'_1$ and $-\log K'_2$ for different temperatures and salinities (see also BUCH, 1951).

The calculation of the concentration of the individual forms of carbon dioxide in sea-water (free carbon dioxide, carbon dioxide pressure, carbonate and bicarbonate

Table 29. Values of the first and second dissociation constants of carbonic acid in sea-water at different temperatures and salinities

S‰	$-\log K'_1$				$-\log K'_2$			
	0°C	10°C	20°C	30°C	0°C	10°C	20°C	30°C
0	6.66	6.57	6.49	6.43	10.56	10.56	10.45	10.34
10	6.32	6.23	6.16	6.11	9.59	9.46	9.35	9.24
15	6.29	6.20	6.12	6.07	9.47	9.34	9.23	9.12
25	6.23	6.14	6.06	6.00	9.32	9.20	9.09	8.98
35	6.19	6.10	6.02	5.95	9.24	9.12	9.00	8.80

ions and total carbon dioxide) is now a simple calculation if the hydrogen-ion concentration, the pH, is measured directly and the titration alkalinity is found from the salinity using the relationship given on page 74. This calculation can be shortened considerably if the carbon dioxide pressure and the total carbon dioxide are tabulated or plotted graphically for the most frequently occurring values of salinity, temperature and pH.

The relationship between pH and the concentrations of free carbon dioxide, carbonate and bicarbonate can be shown clearly in a diagram (Fig. 40), where the percentage of each form is given as a function of the hydrogen-ion concentration. The S-shaped curves separate these factors in such a way that for any value of the pH the composition of the total carbon dioxide present is given along the ordinate. The curves for sea-water are drawn with full lines, the curves for pure water with dashed lines; the first is displaced towards lower pH-values. The presence of neutral salts in sea-water displaces the equilibrium towards the acid side because the apparent dissociation constant increases. It can be seen that at very low pH-values there is almost only free carbon dioxide present, as the pH rises the concentration of bicarbonate increases and reaches a maximum at $pH = 7.5$; the carbonate ion becomes important only at higher pH-values. The two vertical lines in Fig. 40 show the normal range of the pH

in the open ocean. It comes within the range where all three factors: HCO_3 , CO_3^{2-} and free CO_2 are present in measurable amounts, although bicarbonate predominates considerably.

The above values for the apparent dissociation constants are for water at a pressure of one atmosphere. If the pressure is increased the constant also increases since the pressure strengthens the dissociation both of the carbon dioxide and of the neutral

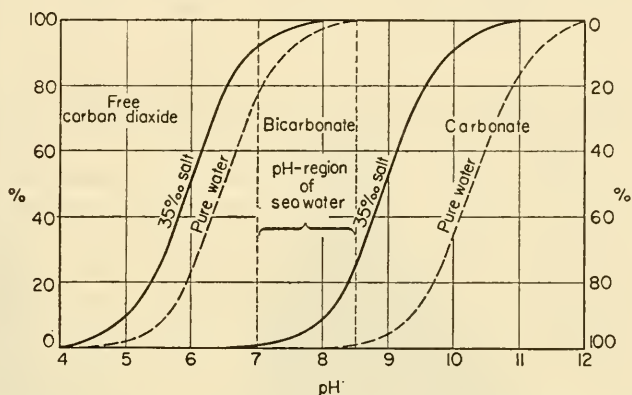


FIG. 40. Percentage distribution of the three forms of carbon dioxide (free carbon dioxide, bicarbonate, carbonate) in pure water and in sea water as a function of pH (according to Buch).

salts. This dependence implies, as shown in Table 30, that water displaced from the surface downwards to great depths will be more acidic, and inversely that of a sample brought from a definite depth with a collecting bottle will as a consequence of the decrease of pressure show a higher pH (be more alkaline).

Table 30. Dependence of the concentration constants for carbon dioxide CO_2 on the hydrostatic pressure

Depth in m	0	2000	4000	6000	8000	10,000
K'_1	1.0	1.26	1.58	2.00	2.45	$3.02 \times K'_1$
K'_2	1.0	1.10	1.20	1.32	1.41	$1.55 \times K'_2$

} at 0 m

Wattenberg gives the example shown in Table 31 of this effect. This pressure effect has a practical significance in processes involving the hydrogen-ion concentration such as the life of deep-sea organisms and the solubility of calcium carbonate at the sea bottom.

Carbon dioxide in the deep layers of the ocean. The work of the "Meteor" Expedition 1925-7 gave the first reasonably good information on the distribution of carbon dioxide in the deep layers of the sea. The essential results have been summarized by WATTENBERG (1936). For the most part there is an approximate equilibrium at the surface of the sea between the partial pressures of carbon dioxide in the sea and in the

Table 31. Variations of pH with depth at constant carbon dioxide content due to the change in pressure

(After WATTENBERG, 1936)

Depth (m)	0	2000	4000	6000	8000	10,000
pH	7.80	7.75	7.70	7.65	7.60	7.55
	8.00	7.95	7.91	7.87	7.82	7.78
	8.20	8.16	8.12	8.08	8.04	8.00

atmosphere (see p. 72). Down to 50 m there is a slight reduction in the carbon dioxide content due to the assimilatory activities of the phytoplankton. Then follows a thin layer where the effects of assimilation and respiration are in balance. Beneath this layer the carbon dioxide pressure rises until it reaches a pronounced maximum at a depth of 500–1500 m (intermediate layer) depending on the latitude; it then falls off again, at first steeply and finally in the deeper layers approaches the values found at the surface. This carbon dioxide inversion (see Fig. 41) is accompanied by a change in the pH which is almost the exact mirror image. Figure 42, which shows the carbon dioxide pressures along a cross-section through the subtropical South Atlantic, illustrates how clearly marked these changes are. According to Wattenberg, these pronounced variations in the carbon dioxide distribution are due principally to the following factors:

(1) The strong renewal of the deep water of the oceanic stratosphere by water masses of polar and subpolar origin which sink during the late autumn and winter in

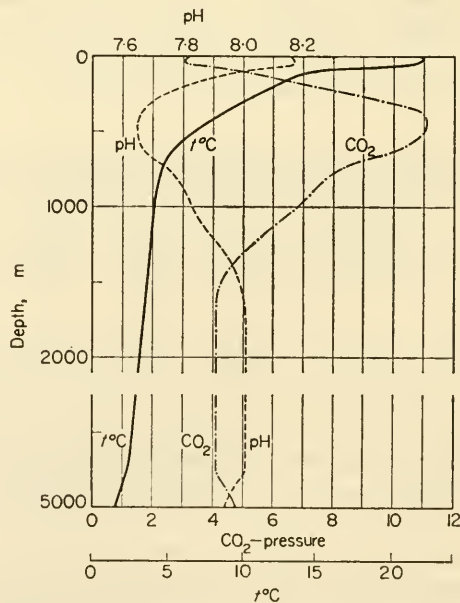


FIG. 41. Vertical distribution of the carbon dioxide pressure P_{CO_2} (10^{-4} atm), the hydrogen concentration pH and the temperature in middle latitudes of the Atlantic (according to Wattenberg).

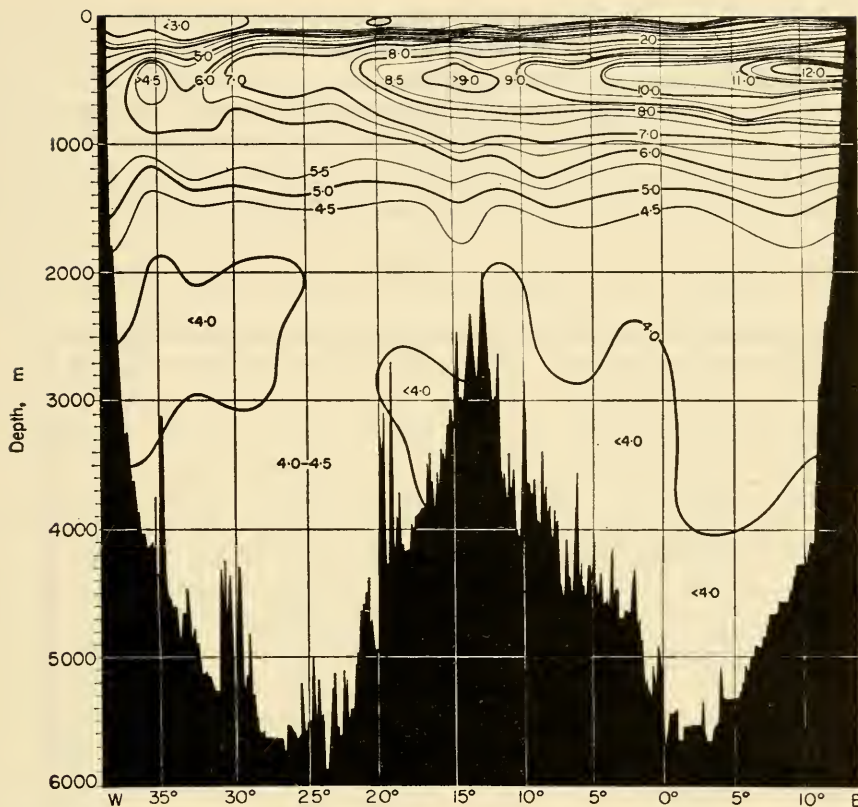


FIG. 42. Carbon dioxide pressure cross-section through the subtropical part of the South Atlantic (8.5° – 13° S., profile VIII from the "Meteor" Expedition; given in 10^{-4} atm).

higher latitudes and reduce the carbon dioxide content of the water at middle depths (2000–4000 m).

(2) The decomposition of dead organisms that takes place principally in the upper layers beneath the transition layer. In shallow seas dead organisms reach the bottom before decomposition is complete and the carbon dioxide pressure thus increases down to this depth. In the deeper layers of the major oceans decomposition occurs largely in the upper layers and the carbon dioxide pressure then decreases with further increase in depth.

(3) The respiration and oxidation processes that produce carbon dioxide proceed more rapidly at the higher temperatures in shallow depths than at greater depths where the temperature is lower.

All three factors combine to bring about the observed distribution, although a stationary state can naturally only occur when the addition and the consumption of carbon dioxide are in equilibrium. However, for quantitative considerations of this type there is as yet no numerical estimate of the effect of the different processes.

In the last hundred metres immediately above the sea bottom there is a more or less large increase in the carbon dioxide content above the almost constant value of the

deeper layers (see Fig. 41). This apparently almost universal phenomenon may be due partly to the slower renewal of the water in the layer next to the bottom and partly to the gradual decomposition of material, not easily oxidizable, which with the shells and skeletal parts of organisms forms the sediments of the bottom and makes possible the formation of carbon dioxide in the bottom layer. This bottom layer with a definite increase is particularly well developed and sharply separated from the upper layers in the western half of the South Atlantic in the area of Antarctic bottom water (see Fig. 43).

The carbon dioxide system between the ocean and the atmosphere (BUCH, 1942). The state of equilibrium at the surface of the sea between the ocean and the atmosphere



FIG. 43. Distribution of carbon dioxide pressure (10^{-4} atm) at the sea bottom (below 4000 m) (according to Wattenberg).

does not extend over the whole surface. More recent investigations have shown that measurable variations occur, though they tend towards equilibrium. To investigate more closely the direction of variations in the carbon dioxide content of the atmosphere from equilibrium with that of the sea, and the mutual interaction of the two, it is necessary to know: (1) the nature of the factors causing changes in the carbon dioxide content in both spaces; (2) the distribution of the carbon dioxide in both media when equilibrium has been finally established; and (3) the duration of the exchange process leading to a new equilibrium and, dependent on that, the extent to which the sea and the atmosphere come into contact enabling equalization of the differences between them.

As far as the first point is concerned, the principal source of the changes in the carbon dioxide content appear to lie in the atmosphere. GOLDSCHMIDT (1934) has given a general carbon dioxide budget for the atmosphere and the sea which is of fundamental importance for the present problem. Table 32 shows the amounts of carbon dioxide in γ ($=0.001$ mg) per cm^2 of the total surface of the Earth entering or leaving the atmosphere and the sea annually. "Juvenile" carbon dioxide enters the atmosphere from volcanoes, fumaroles and carbonated spring water. The value given in Table 32 is the order of magnitude of the steady supply that would give the total amount released during the course of geological history. In more recent times there has been a particularly large increase in the amount of carbon dioxide entering the atmosphere due to the steadily growing combustion of coal and oil by man.

Compared with this large addition of carbon dioxide the amount removed from the cycle by weathering processes and by the formation of carboniferous sediments is very small. All these processes are, however, greatly exceeded by the amounts of carbon dioxide involved in the biological processes of assimilation and respiration. These two processes appear very largely to balance each other. The combustion of coal by man can, however, as shown in Table 32, produce in time a measurable change in the carbon dioxide contents of the atmosphere and the ocean, in spite of its small annual effectiveness.

Table 32. Annual budget of carbon dioxide per square centimetre of the Earth's surface

(After GOLDSCHMIDT, 1934)

Supply by	{	juvenile CO_2	3-6 γ
		industrial combustion of coal and oil	800 γ
		respiration and decomposition	Approx. 40,000 γ
Consumption by	{	photosynthesis	Approx. 40,000 γ
		weathering processes	3-4 γ
		the formation of carboniferous sediments	0.3-2 γ

The addition of 0.0008 g/ cm^2 over a period of 35 years (1900-35) would give an increase in the carbon dioxide content of the atmosphere of 0.028 g/ cm^2 provided that all this carbon dioxide remained in the atmosphere. A more recent and somewhat more detailed presentation of the carbon dioxide cycle in the atmosphere, the hydrosphere and the lithosphere has been given by LETTAU (1954) and is shown in Fig. 43a. This gives detailed information on the individual parts of these interchanges and shows

that compared with the long cycles of water H₂O, there are only short vertical cycles. This is a consequence of the non-existence of a liquid carbon dioxide phase. According to RANKAMA and SAHAMA (1950) the total mass of the carbon dioxide in the atmosphere is 23×10^{17} g.

It should be emphasized that the existence of a pressure difference in the carbon dioxide cycle between the atmosphere and the ocean will always lead to an interchange

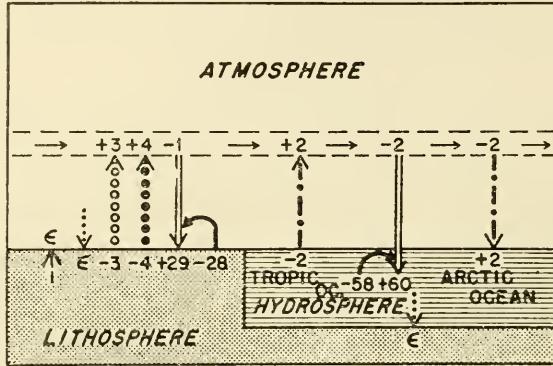


FIG. 43a. Schematic diagram of the carbon dioxide cycles in the atmosphere, the hydrosphere and the lithosphere. 100 relative units = 16×10^{16} g CO₂ per year or 0.032 g cm⁻² years⁻¹. Note that biological processes are dominant, particularly those of marine life. Balances: atmosphere + 9 - 5 = 4; lithosphere + 29 - 35 = -6; hydrosphere + 62 - 60 = 2; total + 100 - 100 = 0. The atmosphere gains $0.04 \times 16 \times 10^{16} = 0.64 \times 10^{16}$ g per year or 3.2×10^{17} g in 50 years which corresponds to 14% of the estimated total CO₂ amount of 23×10^{17} g present in the entire atmosphere.

- > , Release from rocks;> , Deposition in sediments and minerals;
 - oooo> , Forest and prairie fires;> , Combustion of coal and oil;
 - ↪ , Respiration; ==> , Assimilation; -.-> , Flux following CO₂ tension differences in the sea; ε = value smaller than 0.5 rel units
- (Lettau, 1954).

between the two media that will cease only when equilibrium is established. Schlösing, in laboratory investigations, has clarified these exchange phenomena and shown that the sea always has a levelling effect on pressure differences that occur between the atmosphere and the sea. Since the sea has a carbon dioxide content several times greater than that of the atmosphere it suppresses fluctuations in the atmospheric carbon dioxide content and it tends to hold the atmospheric carbon dioxide at a constant value. In this respect the sea acts as a "regulator" of the carbon dioxide content, opposing changes in the content of this gas in the atmosphere. Nevertheless, recent investigations have shown that the variations in carbon dioxide content in both the ocean and the atmosphere are of the same order of magnitude. The sea in acting as a damper thus undergoes the same variations as the atmosphere, and under these conditions it is not easy to decide which is the "regulator" and which is the passive part. When changes occur and a new equilibrium is established, the sea of course takes up a much larger amount of carbon dioxide than the atmosphere. According to Table 32 the annual production of carbon dioxide amounts to about 0.0008 g/cm² of the Earth's surface. The amount of carbon dioxide already present in the atmosphere amounts to about 0.4 g/cm². If the whole of the carbon dioxide produced remained

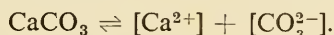
in the atmosphere the present carbon dioxide content would be doubled in 500 years. In actual fact if there is a pressure difference between the ocean and the atmosphere the sea takes up carbon dioxide until this difference vanishes. BUCH (1939) has calculated that if the ocean and the atmosphere are always in equilibrium then five-sixths of the carbon dioxide produced is absorbed by the sea while only one-sixth remains finally in the atmosphere. Thus, if the sea absorbs the industrial carbon dioxide so rapidly that equilibrium is always maintained, then its present content would double at first in 3000 years.

However, some time is needed to reach a new equilibrium and this is probably not reached as quickly as is customarily assumed. The cause could lie in the very slow vertical circulation within the ocean. In a short time only a very thin contact layer can interchange with the atmosphere. The equilibrium time for the whole volume of the ocean should certainly be more than several thousand years, and it must also be remembered that the initial pressure differences are very small and at first rise only slowly. According to the investigations of Buch in the North Atlantic in summer 1935 and in the sub-arctic regions in summer 1936, this part of the ocean and of course the corresponding region in the Southern Hemisphere appear to be the only areas where over long periods carbon dioxide is absorbed from the air in water masses which, by convective sinking in the autumn and winter, convey it to the rest of the ocean. Only in these layers is a rapid renewal of the surface water to be expected and these are thus the principal sites of equilibration in the carbon dioxide interchange between the ocean and the atmosphere (see also BUCH, 1948).

At the present time insight into the dynamics of these processes is rather inadequate due to the scarcity of carbon dioxide pressure determinations. Extensive systematically collected series observations are needed for a better understanding of these phenomena. A more accurate investigation of the distribution of carbon dioxide in an adjacent sea (the Baltic) has been described by BUCH (1945).

(c) Calcium Carbonate in the Sea

The solubility of calcium carbonate in water increases with the carbon dioxide content. This can be explained chemically as follows: calcium carbonate in solution is almost completely dissociated into Ca^{2+} and CO_3^{2-} ions according to the equation



Since the concentration of undissociated calcium carbonate is very small and, if the sea-water is saturated, must be constant, the solubility product is given in a first approximation by

$$[\text{Ca}^{2+}] \cdot [\text{CO}_3^{2-}] = K'_s.$$

In the carbon dioxide equilibrium shown on p. 75 most of the hydrogen ions present combine with the carbonate ions to form bicarbonate ions since the bicarbonate ion, HCO_3^- , is dissociated only to a small extent. This alters the calcium carbonate equilibrium, and calcium carbonate will thus go into solution until $[\text{Ca}^{2+}]$ increases sufficiently to satisfy the equilibrium equation. The equilibrium thus depends on the concentrations of all the ions, H^+ , HCO_3^- , CO_3^{2-} and Ca^{2+} involved (WATTENBERG, 1933, 1936).

As well as the concentration of free carbon dioxide there are other factors also that affect the solubility and, while they are not so important, they must still be taken into consideration. The first of these is the concentration of Ca^{2+} derived not from the dissolved calcium carbonate but from the calcium sulphate and calcium chloride, that is, the excess of calcium ions above that corresponding to the combined carbon dioxide. These calcium ions, by the law of mass action, reduce the solubility of the calcium carbonate. An additional factor affecting the situation is the increase in the solubility product due to the presence of neutral salts in the same way as for carbon dioxide. Table 33 shows that the constant K'_3 is a hundred times greater in sea-water than in pure water.

The solubility constant depends not only on the salinity but also on the temperature and, unlike most salts, decreases with increasing temperature. The pressure (at constant carbon dioxide pressure) also has a considerable effect on the solubility of calcium carbonate, but it is not yet certain how large this effect is. The factors affecting the solubility of calcium carbonate in sea-water thus fall into two groups: (1) those that increase the solubility such as increasing carbon dioxide concentration, salinity and hydrostatic pressure; (2) those that decrease the solubility such as increasing temperature and calcium concentration. The values for solubility given in Table 34 show that in sea-water these factors more or less compensate each other so that there are no major differences from the solubility in pure water.

Table 33. *Dependence of the solubility product, K'_3 , for calcium carbonate on the salinity and temperature*

(After WATTENBERG, 1936)

	S in ‰ (at 20°C)				Temp. in °C (at 35 ‰ S)			
	0	10	25	35	0	10	20	30
K'_3	0.5	22	48	62×10^{-8}	8.3	7.4	6.2	4.4×10^{-7}

The calcium carbonate content can be found by determination of the alkalinity which varies in direct proportion to the variations (in milliequivalents/litre) in calcium carbonate. Since the variations in calcium content are not very large it is necessary to determine the alkalinity very carefully (WATTENBERG, 1930).

Table 34. *Solubility of calcium carbonate (CaCO_3) in milligrams per litre in sea-water (35‰) for different temperatures and carbon dioxide pressures (in 10^{-4} atm)*

(After WATTENBERG, 1936)

$t^\circ\text{C}$	$p_{\text{CO}_2} \times 10^4$				
	1	2	3	5	10
0	60	75	80	100	135
10	45	60	65	78	105
20	35	45	50	60	83
30	25	35	35	45	60

The mean vertical distribution of calcium carbonate in the Atlantic between 20° N. and 20° S. is shown in Fig. 44 from the results of 236 determinations made during the "Meteor" Expedition. The variations in calcium carbonate content can be divided into two groups: (1) *Those due to differences in the total salinity*—the alkalinity and therefore the calcium carbonate both increase with increasing salinity;

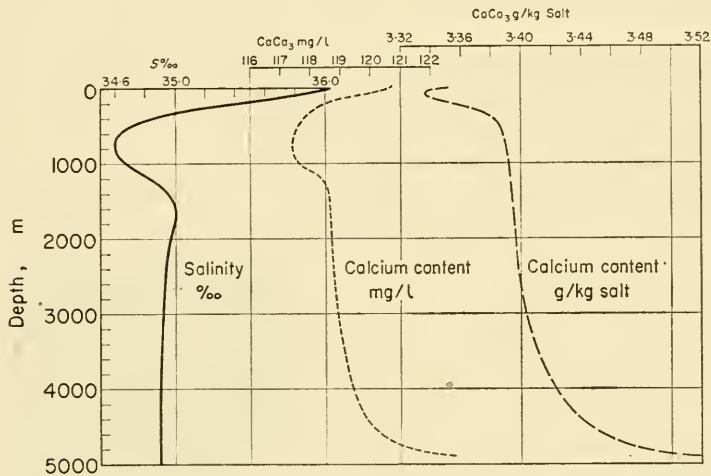


FIG. 44. Mean vertical distribution of salinity ($S^{0/00}$, calcium carbonate (mg per litre of water) and calcium hydroxide (in g per kg of salts). The last curve gives a measure of the deviation of the calcium hydroxide content from proportionality with the salt respective to chlorine contents.

(2) *Those caused by chemical and biological changes.* To show the last more clearly the calcium content is given not in terms of unit volume of water but in unit weight of salt; these are therefore expressed in g CaCO_3 per kg of salt or as per mill (‰). This then shows the variations in the calcium carbonate content of sea-water from proportionality with the salinity or the chlorinity. These are particularly important; they are furthest from normal at two places: (1) in the surface layers close to the atmosphere; (2) in the layer immediately above the sea bottom. The relatively small calcium carbonate content of the very surface layer must be attributed to consumption by plankton, while the sharp increase at the sea bottom must be due to calcium carbonate dissolving from the sediments at the bottom.

The normal calcium content of the water in the open ocean can be taken as about 3.40 g CaCO_3 per kg of salt. The depletion of calcium carbonate in the surface layer is about 2% and the enrichment at about 50 m above the bottom is about 4%. Special measurements would be needed to determine whether there is a further increase nearer the bottom. The maximum value in the bottom water is not the same everywhere. It appears to be larger the greater the depth of the bottom, as is shown in Table 35 (WATTENBERG, 1931).

At depths of 3000 m this increase begins at about 300 m above the bottom, at 4000 m depths at 600 m and at 5000 m depths at about 1000 m. There are two factors involved in producing this apparently stationary state: (1) the continuous upward flux of the calcium carbonate content as specified above; and (2) the advective transport

Table 35

Bottom depth in metres	2000	3000	4000	5000
CaCO ₃ -content in g/kg salt of the deep water (at 50 m above the bottom)	3.398	3.448	3.500	3.525

of more or less calciferous water by the bottom currents. Approximate calculations made by WATTENBERG (1935) have given an intensity for bottom currents which agrees well with that deduced from oceanographic factors.

The surface and bottom waters show regional differences, while the intermediate water masses of the ocean show practically the same calcium carbonate content

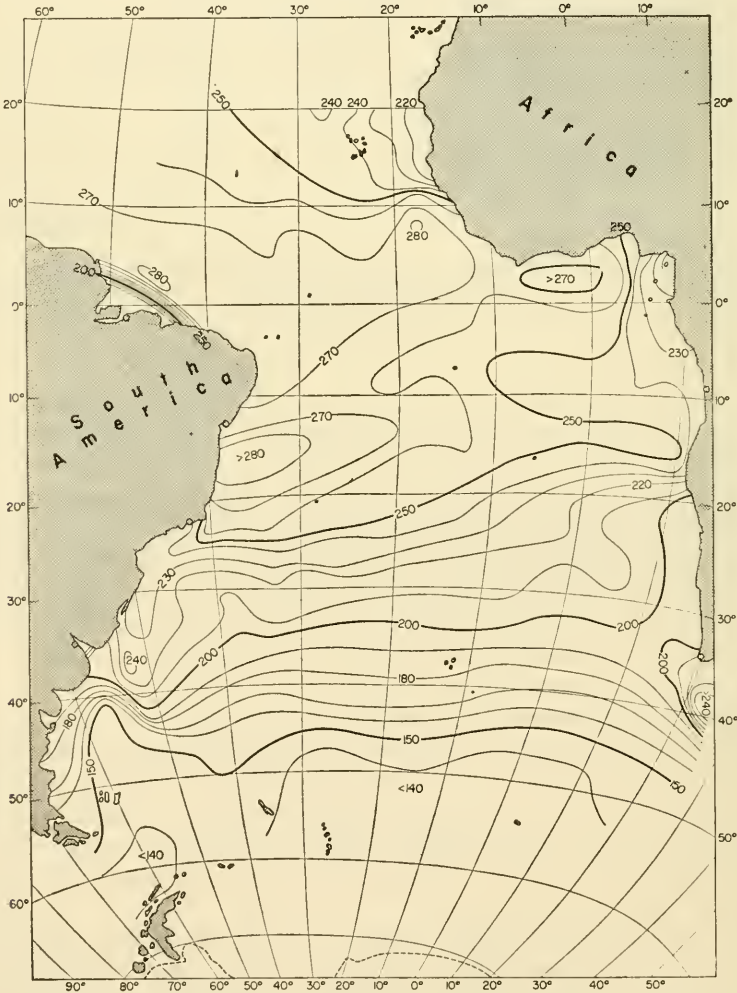


FIG. 45. Chart of the calcium percentage saturation of the surface water in the Atlantic Ocean (CaCO₃) (according to Wattenberg).

throughout. In the polar and subpolar regions the surface minimum is largely absent because of the winter convection which eliminates the minor depletion of calcium carbonate by the few calcium-carbonate-consuming organisms during the brief summer. In low latitudes, on the other hand, the depletion of calcium carbonate is particularly pronounced due to the isolation of the upper layer by the thermocline in the tropics. The regional differences in the bottom layers are shown principally by the degree of saturation with calcium carbonate.

The degree of saturation of sea-water by calcium carbonate in solution is found by comparison of the actual content with the solubility of the water *in situ*. Calculation of the degree of saturation shows that the *surface water* in equilibrium with the atmosphere is *supersaturated with calcium carbonate* at all temperatures found. In the tropics and the subtropics the supersaturation is very large and the water may contain up to three times more calcium carbonate than that corresponding to the equilibrium value; Fig. 45 shows the percentage saturation with calcium carbonate in the surface water of the Atlantic. The large supersaturation in low latitudes shows very clearly; only the presence of this supersaturation allows an equilibrium between the addition of calcium in river water and its consumption by various organisms and sometimes by spontaneous inorganic precipitation at the bottom. It can be readily understood that the production of calcium by various organisms is facilitated and favoured by this supersaturation.

Beneath the thermocline in low latitudes the saturation value falls rapidly with increasing carbon dioxide pressure to below 100% and reaches a minimum in the intermediate layers; in places the saturation may fall to less than 92%. While there are no large differences in the deep water below 1500 m (degree of saturation 98–100%) the bottom water in the Atlantic Ocean differs somewhat in saturation just as it also differs in carbon dioxide content.

Calcium is also involved in a closed cycle. In the upper layers of the sea there is a strong withdrawal of calcium carbonate, partly by biological processes associated with calcium using animals and plants and partly by inorganic precipitation.

Compensation is performed at the sea surface by the supply of calcium due to river water and at the sea bottom by solution from the bottom sediments. Without an accurate quantitative estimation of the individual components in the cycle it is impossible to state whether supply or consumption predominates, or whether the present condition of considerable supersaturation at the surface of the sea is a stationary state.

Chapter III

Temperature in the Ocean, the Three-dimensional Temperature Distribution and its Variation in Time

1. Heat Sources, Heat Exchange and Heat Budget in the Ocean

ALL changes of state in the liquid and gaseous envelopes of the Earth are due basically to energy changes. Energy is very largely supplied from outside the Earth, principally from the sun which provides an inexhaustible source of radiant energy for the Earth. There is a constant inflow of energy from the sun and a constant outgoing radiation from the Earth into space. The Earth does not retain the energy supplied to it but returns all except a vanishingly small part to outer space in the same form (radiation) in which it received it. The possibility of life on the Earth and all changes of state on the Earth depend not so much on the inflow of solar energy as on the enormous supply of entropy involved in the conversion of the high-temperature radiation from the sun to the low-temperature radiation from the Earth.

These considerations lead to the concept of a stationary state as far as the heat energy of the Earth, taken as a whole, is concerned. This constancy in heat energy can be confirmed for the solid part of the Earth and for the atmosphere, and it can be expected that it holds as a close approximation for the energy budget of the oceans. There are, of course, small variations with time in the temperature of the ocean, but these can be taken as variations around a *mean* value which remains essentially unchanged.

Heat budget of the ocean. In this quasi-stationary state all the supply in energy is balanced by equally large losses of energy. The most important factors are the radiation, the interchange of sensible heat with the atmosphere above the sea and evaporation from the surface of the sea or the condensation of atmospheric water vapour. Other minor sources of heat that may be mentioned besides the above stated ones are listed in Table 36.

The order of magnitude of the heat amounts involved in each of these processes varies considerably. The largest is certainly the heat absorbed from solar and sky radiation which is the principal factor in the heat budget of the very upper layers of the sea. At its upper limit the Earth atmosphere obtains per cm^2 by normal incidence an energy of 1.94 g cal/min (solar constant). The entire surface of the Earth receives per cm^2 on the average 0.485 g cal/min or during the entire day 700 g cal/ cm^2 . This incoming radiation from the sun is largely short wave. Its intensity is decreased on passing through the atmosphere so that only 43%, that is 0.21 g cal $\text{cm}^{-2} \text{min}^{-1}$

Table 36.

<i>Heat sources</i>	<i>Heat losses</i>
1. Absorption of solar and sky radiation Q_s	1. Radiation from the sea surface Q_b
2. Convection of sensible heat from atmosphere to sea	2. Convection of sensible heat from sea to atmosphere Q_h
3. Conduction of heat through the sea bottom from the interior of the earth	3. Evaporation from the sea surface Q_e
4. Conversion of kinetic energy into heat	
5. Heat produced by chemical and biological processes	
6. Condensation of water vapour on the sea surface	
7. Radioactive disintegration in the sea-water	

reaches the surface of the sea. Of this, 27% is direct solar radiation and 16% is diffuse radiation from the sky (sky light). From the other sources listed in Table 36 those with a comparatively smaller effectiveness can be neglected. The sources listed under item 2 for heat gain and loss can be added giving one source. The same applies to item 6 (heat gain) and item 3 (heat loss).

The heat obtained from the interior of the Earth is about 50–80 g cal/cm² per year or on the average about 10×10^{-5} g cal/cm² min. The heat supplied from the interior of the Earth has recently been measured directly for the deep-sea basins of the Pacific Ocean by REVELLE and MAXWELL (1952) and for the Atlantic Ocean by BULLARD (1954). These measurements gave in agreement the value 6.2×10^{-5} g cal/cm² min which corresponds to the value for the continents. Compared with the heat from solar radiation this is unimportant; it probably causes only small local variations in the thermal structure of deeper, enclosed stagnating water (see Chap. III, 4 d).

The kinetic energy which the sea obtains by the tangential action of the wind on the sea surface and by the dissipation of tidal energy by turbulent friction and which will be transformed into heat gives only a very small heat contribution. The energy imparted by the winds amounts scarcely to a ten-thousandth part of the solar and sky radiation energy and can therefore be neglected. Also the tidal energy dissipated by turbulence is only of any appreciable influence in shallow waters. For example, Taylor found the value of 1050 g cal/cm² per year = 0.002 g cal/cm² min for the Irish Sea (see Vol, II, Chap. XV, 3). If this heat could accumulate in the Irish Sea for a whole year the temperature rise would be only 0.2°C. The item 5 in Table 36 has no significance in the general budget of the sea and only requires to be taken into consideration where there are local concentrations of plant life. The disintegration of radioactive material in sea-water will afford barely 4×10^{-3} g cal/cm² min. Under these conditions the heat budget of the ocean requires the following equation

$$Q_s - Q_b - Q_h - Q_e = 0.$$

For particular parts of the sea and for short intervals of time it may also be necessary to take into consideration the heat carried by ocean currents, or by mixing processes into or out of the oceanic region under consideration and also the heat which causes over short periods of time changes in water temperature. The above equation is, however, sufficient for the ocean as a whole. The individual terms will now be discussed in some detail.

(a) *Direct Solar Radiation*

Of the solar constant I_0 is 1.94 g-cal cm⁻² min⁻¹ one horizontal cm² at the surface of the Earth obtains for a zenith distance z of the sun (altitude $h = 90^\circ - z$) and due to the angle of incidence and the reduction in intensity due to the atmospheric absorption only the intensity

$$I = I_0 e^{-Ta \sec z \cos z}.$$

Sec z is the relative thickness of the air through which the radiation passes (equals 1 for an atmosphere pressure of 760 mm Hg with the sun at zenith; equal to 2 when the sun is at an altitude of 30°). $e^{-Ta} = q$ is the transmission coefficient and q has under normal conditions a value between 0.6 and 0.7, $a = 0.128 - 0.054 \log \sec z$ and T is the "turbidity factor". If z and T are known then the direct solar radiation incident per cm² on a horizontal surface can be calculated directly for any altitude of the sun.

Part of the solar energy reaching the sea surface will be reflected there. This part depends on the angle of incidence, that means from the zenith distance of the sun. SCHMIDT (1915) has calculated that due to the compensatory effects of solar radiation, which decreases with increasing zenith distance and of the simultaneously increasing reflection the intensity of the reflected radiation for approximate calculations can be put as $R = 0.010 - 0.013I_0$. By using the known total amounts of heat received by 1 cm² of the Earth's surface by direct solar radiation with an average value of the transmission coefficient, and by knowing the reflection loss at the sea surface, it is possible to calculate the amount of energy obtained by 1 cm² of the sea surface in one day. Table 37 gives the mean daily total sum for a year for $q = 0.6 - 0.7$. The figures show that even assuming a continuously clear sky the equator receives barely one-half and the pole only a fifth of the solar radiation incident on the upper atmosphere. When the transmission coefficient is 0.6 the entire surface of the Earth receives only 44% of the theoretical amount of heat. This value will be still further reduced by the presence of clouds. If the cloudiness is w (as a fraction of the visible sky) then the radiation actually reaching the surface of the sea is only

$$S_2 = (1 - w) S_1,$$

where S_1 is the value given in Table 37.

Table 37. Mean total daily sums of direct solar radiation on a free water surface (g cal/cm² day¹). ($J_0 = 1.94$ g cal/cm² min¹)

Latitude	0°	10°	20°	30°	40°	50°	60°	70°	80°	90°
$q = 0.6$	402	392	365	322	270	211	155	105	74	60
$q = 0.7$	493	481	452	402	341	274	206	146	109	94

Since the radiation on the surface of the ocean is difficult to measure and only few determinations have been made, MOSBY (1936) has given an empirical equation for the mean monthly and annual values of the radiation incident per cm^2 on a horizontal surface for given values of the mean altitude of the sun and of the mean cloudiness

$$Q_s = k\bar{h}(1 - 0.071\bar{w}); \text{ g cal cm}^{-2} \text{ min}^{-1}.$$

The bars indicate mean values and k is a factor which depends on the turbidity of the atmosphere; at the equator it is 0.023, at 40° latitude 0.024 and at 70° latitude 0.027.

(b) Diffuse Sky Radiation

During the day the surface of the Earth also receives general scattered short-wave radiation from the atmosphere and also direct solar radiation reflected from clouds. Estimates based on the direct measurement of total radiation (direct + diffuse radiation) show that in general the average value of the diffuse sky radiation for the whole Earth and for a cloudless sky amounts to about 56% of the total radiation on the upper limit of the atmosphere. If we take this value as an average for all latitudes, for a cloudiness w , the direct radiation S_2 will be increased by diffuse radiation amounting to $0.56w \cdot S_1$. At the surface of the water this more or less generally scattered radiation will suffer a reflection loss of 6.6%. The fraction of diffuse radiation from the sky entering the water is thus given by $D = 0.52w \cdot S_1$.

(c) Long-wave Radiation of the Atmosphere

The effective back-radiation R_0 is the difference between the radiation according to the Stefan-Boltzmann law ($E = \sigma T^4$) and the long-wave radiation of the atmosphere and depends, for a cloudless sky, on the absolute temperature T of the lowest layer of the atmosphere and on the water-vapour pressure in this layer (e in mm Hg) (ÅNGSTRÖM, 1936). The effect of clouds is shown in a reduction of the effective back-radiation and can be calculated if the cloudiness is given. With this equation it is possible to calculate numerically the longwave radiation of the atmosphere for a given temperature, water-vapour pressure and mean cloudiness. The effective back-radiation can be measured directly, but such measurements have only seldom been made over the sea. Ångström has derived an empirical formula which has been given by Möller in the following form

$$Q_{\text{eff}} = \sigma T^4 [1 - (0.210 + 0.174 \times 10^{-0.055} e_0)(1 - 0.675\bar{w})],$$

where σ is the Stefan-Boltzmann radiation constant, T is the absolute temperature, R_{e_0} is the vapour pressure above the surface of the sea and \bar{w} —as before—is the mean cloudiness.

For the surface of the sea it can be rearranged to give

$$Q_b = 0.954\sigma T^4 - \sigma T^4 [(0.210 + 0.174 \times 10^{-0.055} e_0)(1 - 0.765\bar{w})].$$

Since, as shown by LAUSCHER (1944), the radiation from a plane water surface is decreased by 6.6% by back-reflection (see p. 60). The effective radiation is the first loss in the heat balance (see Table 36, item 1 (heat loss)).

(d) *Evaporation* (see Chapter VII).

A further debit item is the heat lost by evaporation. The amount of heat involved can be easily found from the mean zonal values for evaporation (WÜST, 1922), since for the evaporation of 1 mm of water from 1 cm² of a water surface 60.65 g cal are needed.

(e) *Convection* (heat exchange between the ocean and the atmosphere)

Little is known of the transfer of heat from water to air by convection. From the approximate calculations of ÄNGSTRÖM (1920) it can be concluded that for a difference in temperature of 1°C between the water and the air (air temperature measured 60 cm above the surface) the mean heat transfer by convection is between 0.01 and 0.03 g cal/cm⁻² min⁻¹. For the mean temperature difference between the water surface and the air which has been measured more accurately for the Atlantic Ocean (KUHLEBRODT, 1938 *a, b*) the convective flux amounts on the average to about 0.014 g cal/cm⁻² min⁻¹ or the average heat loss from the surface of the sea results to about 20 g cal/cm⁻² per day. In warmer climates this value will be increased up to about 0.030 g cal/cm⁻² min⁻¹ which is about 45–50 g cal/cm⁻² per day. These values are only rough estimates of this heat loss which is too large to be neglected in the heat budget of the ocean.

The heat transport by convection follows from the equation

$$Q_h = -c_p A \left(\frac{d\vartheta}{dz} + \gamma \right),$$

where c_p is the specific heat of the air at constant pressure, A the turbulent exchange coefficient (eddy conductivity), $-d\vartheta/dz$ is the vertical temperature gradient of the air above the water (positive since the temperature decreases with height) and γ is the adiabatic lapse rate. $c_p A$ replaces the thermal conductivity coefficient (see p. 50); γ can be neglected in the above equation since it is much smaller than $d\vartheta/dz$. For stationary conditions, that is with constant heat flux through a horizontal unit surface, the temperature changes rapidly with height near to the sea surface and there A is very small. For larger distances A increases and the temperature decreases so that $A(d\vartheta/dz)$ can remain constant.

If the surface of the sea is warmer than the air above, the air is heated from below. The vertical stratification of the air is then unstable and as the air turbulence increases the vertical heat transport becomes large. If the vertical temperature differences are large this can lead to intensive atmospheric disturbances. On the other hand, heat is transported from the atmosphere to the sea when the water is colder than the air above, but the heat transferred by this process is not very large since it stabilizes the air. The exchange A is then small and if the vertical stability is sufficiently large, turbulence of the air and the corresponding downward heat flux then ceases.

If mean values for the heat gain and loss, described in the above discussion, are calculated for different latitudes, a heat budget for the ocean surface can be drawn up as shown in Table 38.

Table 38. Heat budget of the total ocean (g cal/cm² day¹)

Latitude	0°	10°	20°	30°	40°	50°	60°	70°	80°	90°
Heat gain										
Direct solar radiation after allowing for cloudiness	202	255	267	233	171	107	80	58	44	39
Diffuse radiation	166	129	106	99	98	95	73	54	41	36
Total heat gain	368	384	373	332	269	202	153	112	85	75
Heat loss										
Effective back-radiation	118	134	144	143	133	116	121	126	131	137
Evaporation heat	164	170	176	160	125	78	36	13	6	0
Convection	45	45	40	35	20	20	20	20	20	20
Total heat loss	327	349	360	338	278	214	177	159	157	157
Gains-losses	+41	+35	+13	-6	-9	-12	-24	-47	-72	-82

In this heat budget it has been tacitly assumed that the heat exchange through the ocean surface occurs independently for each separate latitude belt. Therefore no meridional heat exchange (by ocean currents and by horizontal mixing) was allowed to occur.

The differences between heat gain and heat loss show that for lower latitudes northward, until about 25° N. the gain in solar energy is greater than the loss, while between about 45° latitude and the poles the back-radiation is dominating because only a small consumption of heat occurs due to evaporation and convection. The excess of the large tropical and subtropical area is, however, roughly equalled by the deficiency of the higher latitudes so that, when the effect of meridional heat transport is taken into account, it can be seen that with reasonable accuracy there is a heat equilibrium for the entire ocean.

This meridional heat transport is largely due to the turbulent motion in the ocean currents through lateral mixing (in meridional direction) (see Chap. III, 2e). If the eddy coefficient of lateral mixing is denoted by A_y (g cm⁻¹ sec⁻¹), the meridional temperature gradient by $d\vartheta/dy$, then the heat W carried towards the north through a unit vertical area is given by the equation

$$W = -c_p A_y \frac{d\vartheta}{dy}$$

The amount of heat transferred from south to north across latitude 25° is given in Table 38 and it can be calculated from these values that for turbulence effective down to a depth of 1000 m an amount W of heat, which is approx. 1 g cal cm⁻¹ sec⁻¹, will be transferred through a vertical area of 1 cm². The mean horizontal temperature gradient at 25° latitude is about -4°C per 10° of latitude which is -3.6×10^{-8} deg/cm. The above equation thus gives $A_y \simeq 3 \times 10^7$ g cm⁻¹ sec⁻¹. This calculation for A_y is naturally a very rough one, but it gives a value for the lateral eddy coefficient which corresponds rather well to more accurate other determinations. It

is, however, certain that lateral mixing in ocean currents is a factor of considerable importance for the horizontal distribution of the heat in the ocean and thus plays an important role in the heat budget.

2. Heat Transport in the Sea: Absorption, Conduction, Thermo-haline and Dynamic Convection (Turbulence)

The previous section gave an outline of the average heat amounts reaching the uppermost layer of the ocean; the question of what happens to this energy shall now be considered. First of all, it can be expected that the radiation energy absorbed will manifest itself as a rise in temperature.

(a) Temperature Change Caused by the Absorption of Radiation

The almost complete absorption of the solar radiation (direct and diffuse), and also of the long-wave radiation of the atmosphere in the uppermost layers of the sea, must cause large daily and annual variations in temperature if this heat is not conducted in some way to the deeper layers. As given in Table 37, middle latitudes receive about $300 \text{ g cal/cm}^{-2}$ per day from direct and diffuse solar radiation. 120 g cal of it would be required for the evaporation of about 2 mm of water so that there would remain approximately 180 g cal for heating the water mass and for producing a daily temperature cycle. Of this amount the uppermost layer of 10 cm thickness absorbs about 81 g cal, according to Table 20, while the top meter absorbs 115 g cal per day.

Table 39.

	Fore-noon	After-noon	Night	Total
Heat gain by absorption	+61	+20	0	+81
Heat loss by radiation	-20	-20	-41	-81
Diurnal variation	+41	0	-41	0

Under stationary conditions this energy gain must be re-radiated during daytime by the water. The partition between day (incident and back-radiation) and night (back-radiation) for the 10 cm layer will be roughly as shown in Table 39. The rise in temperature of the top 10 cm of water, during the forenoon until the temperature maximum, is caused by the absorption of 41 g cal, while the rise for the top meter (100 cm³ of water) is derived from the absorption of 57 g cal; these amounts correspond to a temperature range of 4.1° and 0.57°C . Therefore, the diurnal temperature changes in the surface layer of the sea (and in lakes) may remain very small and are much less than that of the land and the air immediately above it. During the summer half of the year the gain during the day is greater than the loss during the night and heat is accumulated in the uppermost layer.

These considerations raise the question of a possible radiational equilibrium within the uppermost layers of the sea; only in this way can there be an appreciable absorption of radiation. In layers that are not too thick, water is somewhat more transparent for short wave than for long wave radiation (see p. 52). Since the absorption

coefficient is different for different wavelengths, water cannot be considered as a grey radiator (EMDEN, 1913). It is, however, only for grey radiation that the final state of the radiation equilibrium is an isothermal state, in which every layer absorbs just as much energy as it gives off so that the temperature remains constant. For these reasons an isothermal top layer (thin homogeneous layer of uniform density) thus cannot be in radiational equilibrium with the solar radiation (direct and diffuse) (see DEFANT, 1936).

(b) Thermal Conductivity

If there exists a vertical temperature gradient in the water, then heat will be transferred from warmer to colder locations by the process of ordinary heat conduction. There is a constant tendency towards equalization of temperature differences, and this heat transport disappears only when there is a fully isothermal state. The question of interest here is the speed of this process. From theoretical physics it can be shown that the change of temperature with time for a temperature gradient $d\vartheta/dz$ is given by the differential equation

$$\frac{d\vartheta}{dt} = \frac{\lambda}{c_p \rho} \frac{\partial^2 \vartheta}{\partial z^2}$$

In case of a horizontal (along x -axis) movement (velocity u) in the water

$$\frac{d\vartheta}{dt} = \frac{\partial \vartheta}{\partial t} + u \frac{\partial \vartheta}{\partial x}$$

where $\partial\vartheta/\partial t$ is the local change of temperature with time. For no horizontal motion ($u = 0$) the equation for the thermal conductivity takes the form

$$\frac{\partial \vartheta}{\partial t} = \frac{\lambda}{c_p \rho} \frac{\partial^2 \vartheta}{\partial z^2}$$

The solution of this equation (see, for example, RIEMANN-WEBER, 1910) for different boundary conditions provides the answer to important questions concerning the temperature distribution in the sea. It is, for example, of interest to know how fast a temperature change at the surface travels downwards within the water mass by thermal conductivity. The numerical evaluation of the corresponding solution gives for different depths the time required by the disturbance to reduce magnitude to half of its surface value (half value-time). For a thermal conductivity

$$a = \lambda/c_p \rho = 1.309 \times 10^{-3} \text{ cm}^2/\text{sec}$$

one obtains the following values (Table 40). Millions of years would be required for a temperature change at the surface of the sea to reach the larger ocean depths. These values show in the clearest possible way the unimportance of thermal conductivity for oceanographic phenomena, since there are other processes which give a much faster propagation of temperature changes down to the ocean interior.

Table 40. Downward progression of a sudden temperature change in the sea by thermal conductivity (time needed to reach the half value of the surface disturbance)

Depth (m)	1	10	50	100	500	1000	3000	9000
Time (years)	$\frac{1}{4}$	27	665	2660	66,500	$\frac{1}{4}$ mill.	$2\frac{1}{4}$ mill.	9 mill.

Only in the absence of any more rapid processes could the lower temperature of the deep sea be taken, as was previously assumed, as evidence of a much lower former temperature at the surface of the ocean (ice ages). Periodic changes of temperature at the surface of the sea will be transmitted to the deeper layers and cause a periodic change there also. The theory of conductivity shows that when the surface change has the simple form

$$\vartheta_0 = a_0 \cos \frac{2\pi}{T} t$$

it will have at a depth z the form

$$\vartheta_z = a_0 e^{-\alpha z} \cos \left(\frac{2\pi}{T} t - \alpha z \right),$$

where $\alpha = \sqrt{(\pi/aT)} = \sqrt{(c_p \rho \pi / \lambda T)}$ and T is the period of the oscillation. The amplitude of the change in temperature decreases according to the e -function and at the same time there is a phase shift. For the diurnal variation in temperature the amplitude at the surface is reduced to 1% at a depth of 28 cm and the extremes at this depth have already been shifted by three-quarters of the period (18 h). The corresponding values for the annual variation are 5 m with here also a phase change of three-quarters of the period (268 days). The general effect of molecular thermal conductivity confines both these periodic changes to the very uppermost layers of the sea.

(c) *Thermo-haline Convection*

A much more rapid process than molecular thermal conductivity is the vertical displacement of small quanta of water which occurs when a small part of a water mass is heavier than the water underneath it. To restore the disturbed equilibrium the heavier water tends to sink and the lighter to rise. Associated with these forced vertical movements of small water quanta there is also a transport of the characteristic properties of sea-water in vertical direction which leads to an equalization of any vertical differences in these properties which may be present (see p. 195).

This has a rather important effect on the state of the deep water layers. An increase in the weight of small water particles at the surface may be caused either by an increase in salinity due to evaporation or by the formation of ice or it may be due to cooling. If the temperature of a small water particle falls, its specific volume also decreases as long as the salinity is greater than 24.7‰ (see p. 46). In a volume of water with a horizontal cross-section of 1 cm² and a height of h cm the temperature change $\Delta\vartheta$ due to a removal of an amount of heat ΔQ is given by

$$\Delta\vartheta = \frac{\Delta Q}{c_p h}.$$

If a layer of water of ϵ mm thickness evaporates from the top of such a column of water with S ‰ salinity then the increase in salinity when evenly distributed over the column of water is given with sufficient accuracy by

$$\Delta S_\epsilon = \frac{S}{10h} \epsilon.$$

If at the top of a similar column an ice layer of e cm thickness is formed with a salt

content S_e , smaller than S , then, as a first approximation the corresponding increase in salinity is given by

$$\Delta S_e = \frac{0.9e(S - S_e)}{h}.$$

If the ice contains no salt ($S_e = 0$) then

$$\Delta S_e = \frac{0.9e}{h} S.$$

In these quantities ΔQ , ΔS_e and ΔS_e (heat loss, salinity increase by evaporation and by ice formation) lies the primary cause of every thermo-haline convection. In lower latitudes where there are only small variations in the temperature the heat loss is outweighed by the effect of evaporation; in temperate latitudes the heat loss by radiation is the decisive factor, while in polar regions, in addition to these processes, the increase in salinity due to the formation of ice is also effective.

Only very small changes in the specific volume are needed to initiate convection in the uppermost surface layer since the resistance to be overcome is not large, a hundredth ‰ salinity or a hundredth degree centigrade is sufficient.

The range of effectiveness of convection depends entirely on the vertical density distribution in the water mass in which it occurs. For a given surface disturbance it can only extend down to that depth at which the displaced quantum of surface water reaches, water having the same specific volume. If there is a rapid decrease in the specific volume, then the convection will cease in the upper layers; this is liable to occur particularly at the density transition layer (thermocline) which acts as a *barrier layer* and confines the thermo-haline convection to the top layer of the sea (thin homogeneous layer of uniform density). On the other hand, a randomly initiated disturbance of any size at the surface leads to convection which extends in a *homogeneous* water mass down to the bottom. The range of effectiveness of convection is a maximum only when the density disturbance of the sinking water quantum is retained while it sinks. If, as is to be expected, it mixes with the surrounding water the disturbance will be rapidly decreased and the depth of influence of convection will be correspondingly less. The larger the density difference between the sinking water and its surroundings the more rapidly the difference between them will be diminished and the greater the reduction in the depth of the convection layer.

When the sea has a normal stable structure (tropics, subtropics and temperate latitudes) the nocturnal convection before sunrise will extend to a depth of 10 or 20 m. The seasonal convection processes, caused by prolonged cooling during the autumn and the winter, will extend to greater depths, normally to about 300 m. The convection is developed to its greatest extent in polar and subpolar latitudes, where it is assisted by a very uniform temperature and salinity distribution. The question for the primary cause initiating these major convection processes, which are of decisive importance for the deep-sea circulation of the ocean, has been the subject of a controversy that is still not without interest. The initiation and maintenance of the vertical convection in higher latitudes could be due to the cooling of the upper layers by radiation, or it could be due principally to contact with melting ice. PETERSSON (1904) supported the strong cooling effect of the ice that is so plentiful in these latitudes, while NANSEN (1912) favoured the direct cooling of the surface layer by outgoing

radiation. This controversy was settled by important and interesting experiments in the sense of Nansen's reasoning. He suggested that the winter convection in parts of the Norwegian Sea and of the North Atlantic (south and south-east of Greenland and in the Irminger Sea) could reach very great depths because of the almost uniform density structure of the sea, so that the autumn and winter cooling thus continued almost to the bottom. This should therefore be the place where the uniform North Atlantic Deep Water was formed. The observations of the winter cruises of the "Meteor" in the Iceland-Greenland waters during 1929-35 have shown that these views of Nansen were correct. The cause of this convection is certainly the radiation of the surface layer during the late autumn and early winter.

In the North Polar Basin conditions are somewhat different. The very large rivers of Asia and North America bring large amounts of fresh water into this basin and these overlay the saline water that flows into the deeper layers from the Atlantic Ocean. Any deep-reaching convection is scarcely possible here, cooling is limited to the surface layer and is correspondingly stronger. The melting of ice in the spring and summer sets up a barrier against the denser water masses in the deeper layers so that the summer heating does not penetrate far.

Characteristic examples of a convection that extends to great depths, and can be attributed primarily to an increase in the salinity of the surface layer caused by strong evaporation, are found in the Mediterranean Sea and in the Red Sea. The low precipitation, the small amount of river water flowing in, and the high rate of evaporation raise the salinity of the surface layers especially in the summer, though at this time only a limited convection occurs, since the increase in density is largely offset by the effect of the summer heating. However, in the autumn and winter a well-developed convection is set up due to the lowering of the temperature of the surface water and reaches to great depths because of the uniformity of the vertical structure of the deeper layers.

The accurate mathematical treatment of thermo-haline convection processes is not easy. It can be attempted in the following way (DEFANT, 1949). To begin one considers two thin layers of thickness h_1 and h_2 , temperature ϑ_1 and ϑ_2 , salinity S_1 and S_2 and density ρ_1 and ρ_2 . A disturbance introduced in the entire upper layer so that $\rho_1 = \rho_2$ will cause mixing of the two layers h_1 and h_2 by convection and the final result will be the layer $h_1 + h_2$ of density ρ_2 . If the disturbance in the upper layer is assumed to be due entirely to a reduction in the temperature of the upper layer by $\vartheta_1 - \Delta\vartheta_1$ then the final temperature at the end of convection results to

$$\frac{(\vartheta_1 - \Delta\vartheta_1)h_1 + \vartheta_2h_2}{h_1 + h_2} = \vartheta_{1,2} - \frac{h_1}{h_{1,2}}\Delta\vartheta_1,$$

when the mean temperature that would be obtained by simple mixing of the initial water masses is given by

$$\vartheta_{1,2} = \frac{\vartheta_1 h_1 + \vartheta_2 h_2}{h_1 + h_2}.$$

The final salinity after ceasing of convection is given by

$$S_{1,2} = \frac{S_1 h_1 + S_2 h_2}{h_1 + h_2}$$

and corresponds to the salinity obtained on simple mixing.

If the disturbance in the upper layer is due to an increase in the salinity by ΔS_1 , then the final temperature and salinity are

$$\vartheta_{1,2} \text{ and } S_{1,2} + \frac{h_1}{h_{1,2}} \Delta S_1.$$

A disturbance in the second layer can in the same way be passed on to a third and from this to a fourth and so on while at the same time its intensity decreases continually. If the disturbance in the layer $h_1 + h_2$ is due to a temperature decrease of $\Delta \vartheta_{1,2}$ then progression of the convection to the third layer in an analogous way gives the temperature and salinity at the end of the convection process as

$$\vartheta_{1,2,3} - \frac{h_1 \Delta \vartheta_1 + h_{1,2} \Delta \vartheta_{1,2}}{h_{1,2,3}} \text{ and } S_{1,2,3}.$$

If the disturbance is due to an increase in the salinity of $\Delta S_{1,2}$ then the temperature and salinity are

$$\vartheta_{1,2,3} \text{ and } S_{1,2,3} + \frac{h_1 \Delta S_1 + h_{1,2} \Delta S_{1,2}}{h_{1,2,3}}.$$

The simplest way of calculating $\Delta \vartheta$ and ΔS is to use a $[TS]$ -diagram (see Chap. VI). In Fig. 46 the thin lines are lines of equal density (isopycnals). The point A shows the values

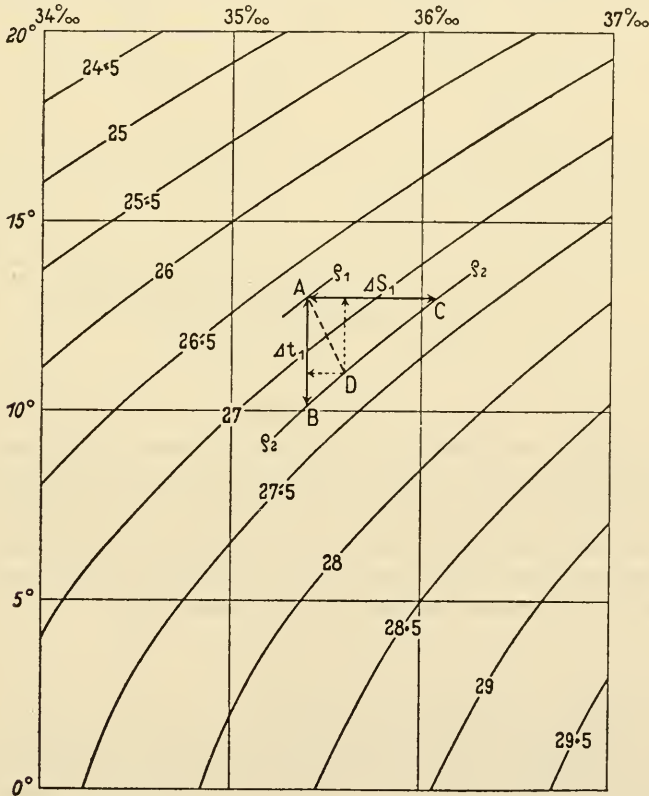


FIG. 46. $[TS]$ -diagram for the determination of degree of disturbance during the initiation of convection processes in the sea.

of ϑ and S of the upper layer h_1 . The density ρ_2 of the second layer h_2 corresponds to the isopycnal that passes through the points B and C . Since the density of the upper layer must be equal to the density of the lower layer, as must be the case at the end of the mixing by convection, then either the temperature must decrease by $AB = -\Delta\vartheta_1$ if the salinity is constant, or the salinity must increase by $AC = \Delta S_1$ if the temperature is constant. A convenient connection of the point A with a point D on the isopycnal ρ_2 , between B and C , gives the value of the disturbance for the temperature and the salinity if both are present at the same time. The determination of magnitude of the disturbances from the $[TS]$ -diagram in this way offers little difficulty.

A simple schematic diagram gives a convenient representation of the results of convective mixing. Figure 47 shows the normal vertical distributions of ϑ and S and of

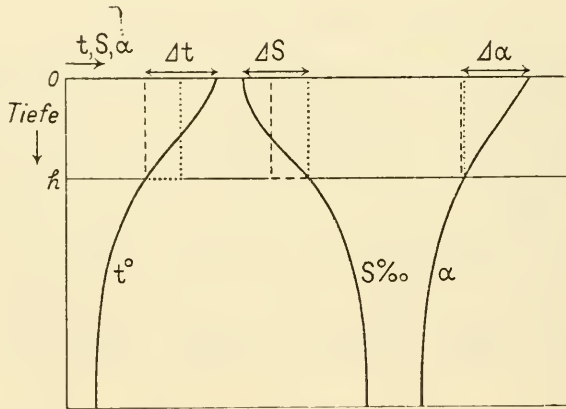


FIG. 47. Change in the thermo-haline structure of the sea produced by convection processes.

the specific volume α ; they represent the conditions before the mixing of the upper layers by a convection extending only to a depth h . If the convective disturbance is entirely due to a reduction in ϑ (by radiation) then the state of the upper layer at the end of the convection process is characterized by the broken straight line; if, on the other hand, the convection disturbance is entirely due to an increase in salinity the dotted straight line shows the final state. It can be seen that the convection levels out any differences in the vertical gradient for the different factors.

(d) *Dynamic Convection* (forced vertical mixing)

While thermo-haline convection is produced by external sources of disturbance and continues as long as these disturbances remain, dynamic convection depends on the forced mixing of superimposed layers of water embedded in a turbulent current. The disordered eddying flow of larger quanta of water within such a current causes a continuous mixing of the water mass in both vertical and horizontal directions. This mixing

process affects not only the vertical distribution of velocity within the current, but also plays a considerable role for the distribution of the properties of the water mass. The importance of such a mixing process, due to turbulent flow in a water mass, was realized much earlier in oceanography than in meteorology. GEHRKE (1909, 1912) was the first to show that the mixing of the water masses in an ocean current must give rise to a vertical transfer of heat. He found that this vertical heat transfer is proportional to the product of the specific heat and the vertical temperature gradient, so that it corresponds to the ordinary equation for the molecular thermal conductivity, but with a coefficient which is dependent on the intensity of mixing and is considerably larger than the coefficient for molecular thermal conductivity. Gehrke termed this a "coefficient of turbulent mixing"; it has the dimensions $[\text{cm}^2 \text{sec}^{-1}]$. Following Gehrke, JACOBSEN (1913, 1915, 1918), in particular, has dealt in detail with the "apparent" thermal conductivity and with the "apparent" diffusion which are connected with turbulent processes. He pointed out that for all the processes initiated by the mixing of the properties of the water (temperature, salinity and the content in sea-water of other dissolved and suspended materials and of organisms) the turbulent mixing coefficient should be the same and should be dependent only on the intensity of the turbulence in the current. Through the turbulence also the flow momentum (impulse of the current) is affected by the "mixing" process, i.e. a vertical equalization that manifests itself in the turbulent (apparent) viscosity. Already Jacobsen has put forward the view that in the transfer of the small quanta of water from layer to layer within the turbulent flow produces an immediate and complete equalization of the momentum; however, complete equalization of the properties of the water does not necessarily follow. This would imply that the "intensity of mixing" of the momentum (turbulent viscosity coefficient) must always be larger than that of, for example, the temperature or the salinity (apparent thermal conductivity coefficient, apparent diffusion coefficient). These views of Jacobsen appear to be confirmed by the quantitative determination of these coefficients.

Following these investigations which gave a deep insight into the nature and efficiency of turbulent flow, SCHMIDT (1917, 1917*a*, 1925) and TAYLOR (1915, 1918, 1922), at about the same time, carried out extensive work on turbulent flow and on the phenomena connected with it, which has had a wide utility for the explanation of several oceanographic phenomena. These started from the basic approach that due to the random movement of individual small quanta of water in a turbulent flow there is not only an equalization of the momentum in the direction of the largest velocity gradient, but that every property can be transferred to an adjacent mass in the direction of its largest gradient. The simplest derivation of the most important and fundamental equation for the interchange of properties within a turbulent flow has been given by Schmidt. Consider a horizontal unit area (1 cm^2) in such a horizontal flow, whereby the vertical direction z is counted positive upwards and negative downwards of it (the zero point ($z = 0$) lies in the surface itself). Due to the turbulence of the flow there will pass through this unit area a mass of water m_u upwards and a mass m_d downwards. Since, however, there is on the average a displacement of the water only in a horizontal direction it follows that over a long period of time $\Sigma m_u = \Sigma m_d$. Every small quantum of water will, however, carry its properties with it during its turbulent displacement. If one of these properties is designated by s (for instance the

salinity) and s is a function of z only, then at the unit surface as a first approximation

$$s = s_f + \frac{\partial s}{\partial z} z,$$

where s_f is the value in the surface where $z = 0$. Every small particle of water passing through the surface from below will take with it an amount $m_u s_u$, while those from above will carry an amount $m_d s_d$. The final exchange flux S through the unit surface upwards can be expressed as the difference

$$S = \Sigma m_u s_u - \Sigma m_d s_d,$$

whereby the summation has to be taken for all the small particles moving upwards and downwards through the surface. Now

$$s_u = s_f + \frac{\partial s}{\partial z} z_u \quad \text{and} \quad s_d = s_f + \frac{\partial s}{\partial z} z_d,$$

where the values of z_u are all negative and the values of z_d are all positive. This gives

$$S = (\Sigma m_u z_u - \Sigma m_d z_d) \frac{\partial s}{\partial z}.$$

Considering the different signs of z , the quantity in brackets gives a negative sum $-\Sigma m |z|$, where every small mass m of water moving through the surface is now multiplied by the initial absolute distance $|z|$ from the unit surface. This sum depends *only* on the state of turbulence of the flow. Schmidt has called it the "Austausch (exchange) coefficient" η . It has the dimensions $\text{g cm}^{-1} \text{sec}^{-1}$. The basic equation for the exchange is thus

$$S = -\eta \frac{\partial s}{\partial z}.$$

The most important exchange quantities involved in oceanographic turbulent transfer processes are: heat-temperature, salt-salinity, gas amount-gas content, number of organisms-organism content. The flow momentum-flow speed also follows this law (see later).

It appears that the assumption that every small quantum of water starts from its initial position with a property s corresponding to the *mean* vertical distribution at that point does not entirely accord with the actual conditions. Only for the pair flow momentum-velocity does there appear to be a complete and immediate equalization of the velocity differences. For all other properties a correction must be applied to the above basic equation. ERTEL (1942) has attempted to take these circumstances into account, and obtained the equation

$$S = -\eta(1 - 2n) \frac{\partial s}{\partial z} = -A \frac{\partial s}{\partial z}.$$

Thereby, it was assumed that a small particle of water passing through the unit surface is not immediately mixed completely with the surrounding water but is mixed in the proportion 1 : n . For the velocity in a turbulent flow, n would be equal to zero and the exchange coefficient A for the property s (eddy conductivity and eddy diffusivity) would then be less than the eddy viscosity coefficient η . Determinations of A and η also verify this. Table 41 gives list of such determinations measured in currents in different parts of the oceans.

It can be seen that η is of the order of 100–200 or more while A is of the order of 5–40, on the average about $20 \text{ g cm}^{-1} \text{ sec}^{-1}$. The ratio η/A is of the order 5–20. Taking an average value of about 10, then $A/\eta = 1-2n$, $n = 0.45$, that means that the small quanta of water in random movement are mixed with the surrounding water only to the extent of about 45% of their mass and accordingly the temperature and salinity, for example, tend towards the values of their surroundings at this rate. This value is not unreasonable considering the difficulty of mixing water of different densities and the constant tendency for water masses of different densities to separate again.

The exchange equation applied to the pair heat-temperature has the same form as that for the molecular thermal conductivity (p. 50), except that the thermal conductivity coefficient $a = (\lambda/c_p\rho)$ is replaced by the quantity $c_p A$ (specific heat \times exchange coefficient). The exchange coefficient A is of course not constant and will vary from layer to layer. Taking a mean value of about $20 \text{ g cm}^{-1} \text{ sec}^{-1}$, then since c_p is approximately equal to 1, $c_p A$ will be about 15,000 times greater than a . The molecular thermal conductivity is thus of no importance compared with the eddy conductivity (dynamical convection). The thermal conductivity equation for turbulent heat transport is therefore

$$\frac{\partial \vartheta}{\partial t} = \frac{A}{\rho} \frac{\partial^2 \vartheta}{\partial z^2},$$

where A is assumed to be independent of the depth. If this is not the case the equation is

$$\frac{\partial \vartheta}{\partial t} = \frac{1}{\rho} \frac{\partial}{\partial z} \left(A \frac{\partial \vartheta}{\partial z} \right).$$

Temperature changes at the surface will be transmitted much more rapidly by turbulent thermal conductivity down to the deep-ocean layers. For the process of molecular heat conductivity surface disturbances were shown to require a half-value time of some millions of years (see Table 40), however, for conductivity it would take only some hundreds of years according to Table 42. Indeed, in the upper layers surface changes will penetrate downwards by turbulent action remarkably rapidly; only a few days are required to spread completely through the layer down to 50 m. Periodic changes will of course reach deeper. For values for A of 20 and $100 \text{ g cm}^{-1} \text{ sec}^{-1}$ the amplitude of a diurnal variation will decrease to 1/100 of its value at the surface in 34 and 75 m, respectively. For the annual variation the corresponding values are 644, 1440 m, respectively. This corresponds better with the values given by temperature observations.

(e) *Horizontal Convection and Lateral Mixing*

The dynamic convection discussed in the preceding section applies only to mixing of water masses in a vertical direction moving in a horizontal turbulent flow. In addition to this vertical mixing process there will also be a mixing process, largely

Table 41. *Coefficients of eddy conductivity, eddy diffusivity and eddy viscosity*

Coefficient	Current or oceanic region	Depth of layer (m)	Magnitude (g cm ⁻¹ sec ⁻¹)	Reference
Eddy conductivity and diffusivity from temperature and salinity measurements, <i>A</i>	Philippine Trench	5000-9788	2.0-3.2	Schmidt, 1917
	Algerian Coast	0- 20	35-40	Schmidt, 1917
	Mediterranean	0- 28	42	Schmidt, 1917
	California Current	0- 200	30-40	McEwen, 1919
	Caspian Sea	0- 100	1- 3	Stockman, 1936
	Barents Sea	—	4-14	Subov, 1938
	Bay of Biscay	0- 100	2-16	Fjeldstad, 1933
	Equatorial Atlantic Ocean	0- 50	320	Defant, 1932
	Randesfjord	0- 15	0.1-0.4	Jacobsen, 1913
	Schultz Grund	0- 25	0.04-0.74	Jacobsen, 1913
	Kuroshio	0- 200	30-80	Sverdrup-Staff, 1942
	Kuroshio	0- 400	7-90	Suda, 1936
	Southern Atlantic Ocean	400-1400	5-10	Defant, 1936
	Arctic Ocean	200- 400	20-50	Sverdrup, 1933
	Caribbean Sea	500- 700	2.8	Seiwell, 1938
	South Atlantic Ocean	3000-Bottom	4	Defant, 1936
	South Atlantic Ocean	Near Bottom	4	Wattenberg, 1935
	Eddy viscosity η	Wind currents	Surface layer	1.02w ³ (w < 6 m/sec)
Wind currents		Surface layer	4.3w ² (w > 6 m/sec)	Ekman, 1905
North Siberian Shelf		0-60 (tide)	75-260	Sverdrup, 1926
North Siberian Shelf		0-60 (tide)	10-400	Fjeldstad, 1936
North Siberian Shelf		0-22	$385\left(\frac{z+0.1}{2z+1}\right)^3$	Fjeldstad, 1929
Schultz Grund		0-15	1.9-3.8	Jacobsen, 1913
Caspian Sea		0-100	0-224	Stockman, 1936
Kuroshio		0-200	680-7500	Suda, 1936
Japan Sea	0-200	150-1460	Suda, 1936	

Table 42. *Advance of a sudden temperature change penetrating into the sea by thermal turbulent conductivity (half value time of surface disturbance)*

Depth (m)	1	10	50	100	500	1000	3000	6000
Time when $A/\rho = 20 \text{ cm}^2/\text{sec}$	9 min	15 h	16 days	64 days	4.4 years	17.4 years	185 years	624 years
Time when $A/\rho = 100 \text{ cm}^2/\text{sec}$	1.8 min	3 h	3 days	13 days	320 days	3½ years	37 years	125 years

effective in the *horizontal* direction caused by currents moving side by side carrying small masses of water at greater or lesser velocity and by eddies of varying size with vertical axes, that is, by the lateral turbulence in the flow.

In the horizontal direction the disturbances are of greater dimensions than in the vertical direction, particularly those due to atmospheric effects (wind, squalls and rapid changes of pressure), which affect the surface layer of the sea and to some extent the deeper layers also. Disturbances due to coastal and bottom topography are also able to produce turbulence in an horizontal direction with turbulence elements which must obviously develop on a much larger scale than the vertical turbulence. The corresponding exchange coefficient will be much larger than for vertical mixing. In a certain sense there is an analogy with the large-scale lateral turbulence in the atmosphere which is also quasi-horizontal (isentropic). In this case the coefficient is on the average of the order of $10^8 \text{ g cm}^{-1} \text{ sec}^{-1}$ as compared with an average value of 50–100 of ordinary vertical turbulence. That lateral large-scale turbulence is also important in oceanic phenomena was first pointed out by DEFANT (1926), who determined the order of magnitude of this exchange coefficient as about 5×10^7 . Later, WITTING (1933) discussed both vertical mixing and lateral mixing, and has attempted the determination of the exchange coefficient by large-scale coloration experiments. ROSSBY and co-workers (1936) have clearly shown that there occurs in the ocean, as in the atmosphere, a lateral mixing of this type along the isotropic surfaces, which is essentially in the ocean the same as along the σ_t -surface. PARR (1938) has shown the large effect of this lateral mixing on the distribution of temperature and salinity in the water masses around Newfoundland; SVERDRUP and FLEMING (1941) have found the same effect in the coastal water off California and STOMMEL (1950) has determined the lateral mixing coefficient A/ρ in the Gulf Stream to be $2.3 \times 10^8 \text{ cm}^2/\text{sec}$.

For a given horizontal gradient in any of the properties of a mass of water the horizontal convection will play a large part in the long-period equalization of this gradient. This presupposes a transport of the property along the direction of the gradient. Furthermore, if a small mass of water has a property s (for instance, temperature) present in amount S (for instance, heat), then the horizontal transport of S across the horizontal turbulent flow in the direction n is as before, $S_n = -A_n(\partial s/\partial n)$. A_n is now the horizontal exchange coefficient. Its order of magnitude is several times larger than that of the coefficient for vertical mixing A_z . Since, in general, the vertical gradient of a water property (such as temperature, salinity) $\partial s/\partial z$ is considerably larger than that in the horizontal direction $\partial s/\partial n$, the horizontal transport S_n may still be of the same order as the vertical transport S_z , since in the above equation the product of the two quantities is essential. This appears to be the case in reality so that lateral mixing is no less important than the vertical.

Consider a volume element dx, dy, dz through which there is a turbulent flow with velocity components u, v, w ; the exchange coefficients in the three directions A_x, A_y, A_z . Then, for the individual change with time in the property s the following equation will apply

$$\frac{ds}{dt} = \frac{\partial s}{\partial t} + u \frac{\partial s}{\partial x} + v \frac{\partial s}{\partial y} + w \frac{\partial s}{\partial z} = \frac{1}{\rho} \left\{ \frac{\partial}{\partial x} \left(A_x \frac{\partial s}{\partial x} \right) + \frac{\partial}{\partial y} \left(A_y \frac{\partial s}{\partial y} \right) + \frac{\partial}{\partial z} \left(A_z \frac{\partial s}{\partial z} \right) \right\}.$$

If the x -axis is taken as the direction of the turbulent flow (positive in the flow

direction) ($v = w = 0$), then stationary conditions in the distribution of the property s in the volume element ($\partial s / \partial t = 0$) are only possible if the equation

$$A_x \frac{\partial^2 s}{\partial x^2} + A_y \frac{\partial^2 s}{\partial y^2} + A_z \frac{\partial^2 s}{\partial z^2} - \rho u \frac{\partial s}{\partial x} = 0$$

is satisfied, where A_x , A_y and A_z are taken as constants. From this general equation can be derived more special cases:

$$A_z \frac{\partial^2 s}{\partial z^2} - \rho u \frac{\partial s}{\partial x} = 0 \quad (a)$$

if there is vertical mixing only ($A_x = A_y = 0$);

$$A_y \frac{\partial^2 s}{\partial y^2} - \rho u \frac{\partial s}{\partial x} = 0 \quad (b)$$

if there is transverse mixing (in a horizontal direction normal to the flow) ($A_x = A_z = 0$);

$$A_x \frac{\partial^2 s}{\partial x^2} + A_y \frac{\partial^2 s}{\partial y^2} + A_z \frac{\partial^2 s}{\partial z^2} = 0 \quad (c)$$

if there is mixing in all directions but no average water transport in the x -direction ($u = 0$).

Cases (a) and (b) are mathematically identical but solely the vertical and horizontal directions are interchanged. A solution for the equations (a) and (b) has been given by DEFANT (1929)

$$s = s_0 + m e^{-\alpha z} \cos \frac{\pi}{2l} z \quad \text{and} \quad \alpha = \frac{\pi^2}{4l^2} \frac{A_z}{\rho u}.$$

For case (b), the co-ordinate z is replaced by the co-ordinate y . The distribution of the property s along the homogeneous turbulent flow has been found to be tongue-shaped if the s -content initially has a maximum value at the centre of the flow (at $x = 0$, $s = s_0 + m \cos (\pi/2l)z$).

This is also the case when the velocity is the same over the whole transverse cross-section. Figure 48 gives an example of the course of the s -lines for $A/\rho = 4 \text{ cm}^2/\text{sec}$, $u = 10 \text{ cm}/\text{sec}$ and $l = 2 \times 10^4 \text{ cm}$. The further the cross-section is taken from the initial section ($x = 0$) the lesser are the horizontal and vertical differences in s . By the extension of the above solution to different initial conditions for $x = 0$ (THORADE, 1931) it became evident that neither the tongue-form of the distribution of the property s nor the distribution of the velocity u in the cross-section is considerably affected. In addition, the initial distribution of s at $x = 0$ has equally little effect. The tongue-form of the s -curves is always re-established in a short time and is very largely a consequence of the turbulent mixing. This is shown particularly well in Fig. 48a, which shows the distribution of the property s in the case where the velocity is constant across the transverse section, and initially for $x = 0$ the property s is constant within the distance $2l$ ($s = 100$), while outside of this range there is no content of s in the water ($s = 0$). In the flow a tongue-shaped distribution of s is produced immediately. This

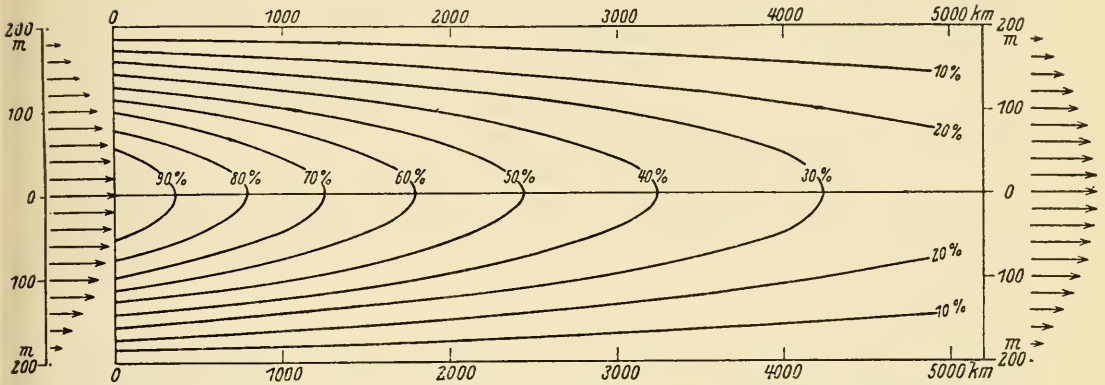


FIG. 48. Formation of a tongue-shaped distribution in a property of sea water by advection and mixing (turbulence).

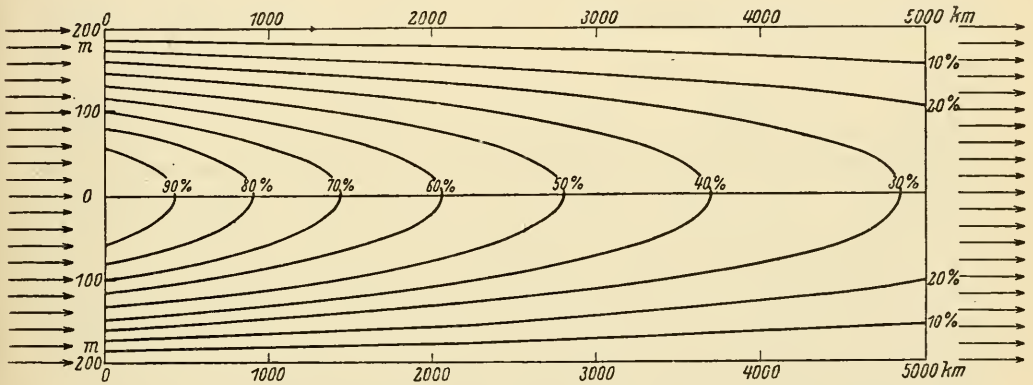


FIG. 48a. Tongue form produced by turbulent mixing at constant flow velocity shown in a cross-section (tongue of S -content for a steady current, which attains a constant S -content in its total cross-section when it enters into a second water type.)

case corresponds to the conditions present in the spreading of a current of water of high salinity penetrating into a body of water of lower salinity.

In the horizontal and vertical distribution of the temperature and salinity over a large space in the ocean there are often found cases where the isolines have a tongue-form. This distribution allows the numerical determination of the relationship between the exchange and the velocity of the flow, that is, of the quantity $A/\rho u$ provided that this is imposed by exchange processes. Such calculations are fairly numerous: they have been made, for instance, by DEFANT (1936) for the subantarctic intermediate current and for the Antarctic bottom current in the South Atlantic ($A_z/\rho u = 1 - 10$ which for $u = 1-5$ cm/sec gives A_z as about $0.5-10$ g cm⁻¹,sec⁻¹); by MONTGOMERY (1939) for the equatorial counter current in the Atlantic (maximum value for A_z 0.4 g cm⁻¹,sec⁻¹, for A_y 4×10^7 g cm⁻¹,sec⁻¹); by SVERDRUP and FLEMING (1941) for the coastal water off California at 200 and 400 m depths ($A_x/\rho = 2 \times 10^6$ cm²/sec) and by Seiwel for the distribution of temperature and salinity in the Caribbean Sea (A_x/ρ larger than 10^6 cm²/sec). Recently DEFANT (1955) in an investigation of the

spreading of the Mediterranean water into the North Atlantic found a horizontal exchange coefficient of $5.5 \times 10^7 \text{ cm}^2/\text{sec}$.

There is no doubt that the exchange coefficients for lateral mixing A_x and A_y are about a million times larger than that for vertical mixing. The lateral mixing has thus, despite the low values of the horizontal gradients for the different properties of sea-water, at least the same importance as the vertical exchange. It can, however, be stressed that the nature and inner mechanism of these two exchange processes are different; the vertical mixing is small-scale, the lateral operates over a large space. It may be expected that they are related to different ranges in the total turbulence spectrum (see Chap. XIII, 3).

The third special case is for mixing operating in all directions but without any displacement of water in a particular direction; it shows therefore the effect of mixing alone *unaffected by advection*. In the two-dimensional case (x - and z -directions) the solution takes the form (SVERDRUP, 1940)

$$s = s_0 + m \frac{\cosh [\alpha(h - z)]}{\cosh [\alpha h]} \sin \frac{\pi}{2l} x, \quad \text{whereby} \quad \frac{A_x}{A_z} = \frac{4l^2}{\pi^2} \alpha^2.$$

For $z = 0$, that is at the surface of the sea, the distribution of a property s is $s = s_0 + m \sin (\pi/2l)x$.

Selecting, for example, $h = 4 \text{ km}$, $s_0 = 0$, $m = 5$ and $A_x/A_z = 6 \times 10^6$, then $\alpha = 0.384$ and Fig. 49 gives the distribution of s in an ocean of a horizontal extent

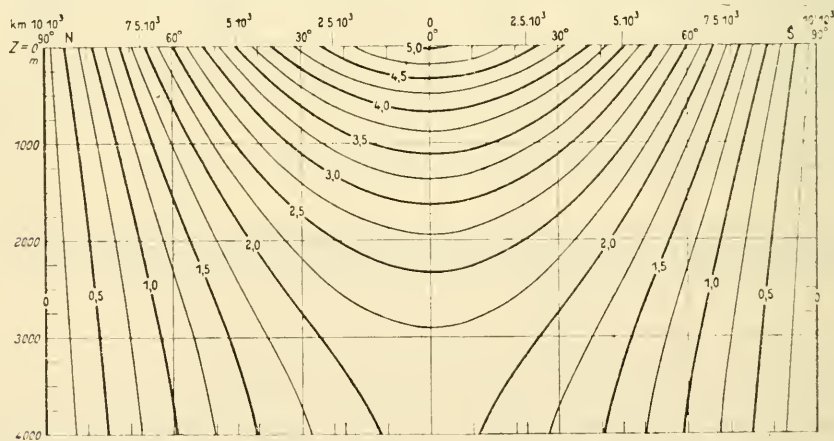


FIG. 49. Distribution of a property "s" in the total ocean due to mixing alone (according to Sverdrup).

$2l = 20,000 \text{ km}$. In this case it would reach from pole to pole. The abscissa in Fig. 49 is therefore divided into meridional degrees from 90° N . to 90° S . For a persistent maximum accumulation of the property s at the surface of the sea in equatorial regions, the effect of mixing *alone* would in the stationary state force a distribution of s in ocean space shown by curves of equal s in this representation. For a persistent temperature difference at the sea surface along a meridian, essentially the same as that produced by the combined effect of the solar and back-radiation, the effect of a mixing process acting alone over the entire ocean would give a vertical temperature distribution such as that shown by the isotherms in Fig. 49. The temperature decreases

everywhere with increasing depth, most rapidly at the equator and least at the poles. This case will be considered later in connection with the actual temperature distribution in the deep ocean (see p. 123).

Another solution for the third special case is

$$s = s_0 + m e^{-\beta z} \cos \frac{\pi}{2l} z \quad \text{with} \quad \beta = \frac{\pi}{2l} \sqrt{\frac{A_z}{A_x}}.$$

Obviously the solution of this distribution of s is identical with that of the first case on p. 106 if β is put equal to α , that is if

$$\frac{A'_z}{u} = \frac{2l}{\pi} \sqrt{\frac{A_z}{A_x}}.$$

This means that in a vertical cross-section a tongue-shaped distribution of s can be equally well regarded as the effect of a horizontal advection with velocity u in the direction of the tongue and as a vertical turbulence with an exchange coefficient A'_z , or as the sole effect of pure mixing in horizontal and vertical directions without any advection. See Vol. I, Part II, Chap. XIII, 3, for a theoretical discussion of turbulent mixing in ocean currents.

3. Diurnal and Annual Variation of the Temperature in the Ocean

The daily variations in temperature at the surface of large bodies of water (lakes and seas) are confined within narrow limits as was mentioned previously. In lakes, away from the shore, there may be diurnal variations exceeding 2 °C. They decrease rapidly with depth so that at 4–6 m they may be not more than 0.1 °C (see particularly the investigations by HOMEN (1913) in Lake Logo (Finland). Some idea of the diurnal temperature variation (of the air and the water) is afforded by the investigation of MERZ (1911) in the Gulf of Trieste (an enclosed basin, relatively close to the land). The amplitude of the water temperature was 0.87 °C, for the air it was 3.1 °C, which is considerably more. For a discussion of the diurnal and annual variations of the surface temperature in a shallow water especially in the North Sea and in the Baltic, see DIETRICH (1953).

(a) The Diurnal Temperature Variation in the Open Sea

The diurnal variations of temperature in the open sea are even smaller than in lakes; usually smaller than 0.4 °C and can rise at the most to about 1 °C in calm and fair weather. The most accurate measurements of the daily temperature variation in the open sea are obtained at anchor stations (fixed location). Four equatorial stations between 12.5° N. and 4° S. of the “Meteor” Expedition in the Atlantic Ocean (DEFANT, 1932) gave the following values (Table 43).

Table 43. Mean daily temperature variation from four “Meteor” anchor stations

Local time (hours)	0	2	4	6	8	10	12	14	16	18	20	22	Amplitude
Δt (°C)	-7	-10	-12*	-10	-8	-1	+11	+19†	+15	+7	-1	-5	31

* Minimum; † Maximum

Latitude	12¼° N.	4° N.-4° S.	8°-14° S.	21½° S.	Mean
Diurnal variation					
At the surface (°C)	0.19	0.40	0.23	0.16	0.25
At 50 m depth (°C)	0.034	0.056	<0.05	(0.09)	(0.04)

The diurnal temperature variations always decrease towards higher latitudes; the maximum occurs at 14.00 h and the minimum at 04.00-05.00 h. The diurnal course corresponds almost exactly to a pure sine curve. KUHNBRODT (1938) obtained the same results from a study of the daily temperature records of the "Meteor" Expedition by the elimination of the effect of changes in position of the vessel. The average daily amplitude for all areas of the South Atlantic amounts to only 0.26 °C. This value, which was obtained by averaging all days without any selection, is somewhat smaller than the value obtained by WEGEMANN (1920) from the "Challenger" observations and by MEINARDUS (1929) from the "Gauss" observations.

The heating of the sea surface begins soon after sunrise due to the absorption of solar radiation in the uppermost layer of the water, but the largest part of the added heat is used for the evaporation of water (about two-thirds) and only a small part remains for a temperature rise. The temperature thus rises only slowly to the maximum at 14.00 h. After sunset the temperature fall continues due to outgoing radiation.

There are very few measurements of the depth to which the diurnal temperature variation penetrates. The only information for 50 m depth is given by the hourly observations at the anchor stations. However, for these depths near the thermocline the influence of tides through the associated vertical currents (internal tide waves) cannot be entirely excluded. Table 43 contains some values for the diurnal temperature variation at 50 m depth showing that for these depths the amplitude is less than 0.05 °C. Aimé has made measurements of the diurnal temperature variation at different depths off the Algerian coast. It is, however, not entirely certain that all the observed changes can be attributed to the diurnal cycle; however, if this assumption is made it is found that the nocturnal cooling at 14 m is one-fifth of the surface amplitude and that the heating during the day, which is three to four times stronger than the nocturnal cooling, falls to a tenth at 28 m. SCHMIDT (1925) calculated from this decrease of temperature the vertical exchange coefficient as 35-40 g cm⁻¹ sec⁻¹. The observations of Knott on the "Pola" Expedition in the eastern Mediterranean show a decrease in the amplitude to a tenth at 29 m, which corresponds to an exchange coefficient of 42 g cm⁻¹ sec⁻¹. Since the ocean covers more than two-thirds of the surface of the Earth it can be said that over much the largest part of the surface the diurnal temperature variations remains less than half a degree. Therefore, the considerably greater diurnal temperature variations of the continents play only a minor part in the total heat budget for the Earth.

(b) *The Annual Temperature Variation*

Changes in temperature over longer periods can be investigated in two different ways. They can be recorded as "individual" temperature changes in a water mass which is followed in its course in the ocean; they are then described by reference to "oceanographic" co-ordinates. On the other hand, they can be followed at fixed

points and are then referred to "geographic" co-ordinates. These last changes are more complicated, since they are a combination of thermal changes within an individual water mass and of changes caused by the displacement of different water bodies (ocean currents).†

For most parts of the ocean the annual displacements of the currents are known and most of the major annual changes in these areas can be ascribed to these. The seasonal displacements of the Gulf Stream system and the Labrador Current in the region of the Grand Banks of Newfoundland are well known. The large annual temperature variations in this region of the sea are associated with these displacements. Similar conditions are found off the Norwegian coast where the seasonal displacements of the coastal current and the Atlantic current cause pronounced seasonal variations in temperature and salinity.

For smaller areas the annual temperature variation at the sea surface can be derived only from a statistical evaluation of ship's observations and for the deeper layers from series observations made by oceanographic expeditions. Averaging the values that fall for different parts of the year into one, two or more degree squares gives mean temperatures for these subsections of the year with sufficient accuracy, provided there is a reasonable number of observations available. This of course gives only values related to "geographic" co-ordinates. Such a rough statistical method can only be used with some reliability for the sea surface.

All the available data on surface temperature in the Atlantic Ocean have been collected and studied by BÖHNECKE (1936) and presented in a comprehensive form. For the Indian and Pacific Oceans a less complete presentation has been given by SCHOTT (1942). These show that there is an absolute minimum in the annual variation of surface temperature of all oceans in the tropics where over extended areas, especially in the Indian and Pacific Oceans, this variation is less than 1°C. There is also a secondary minimum in the Southern Hemisphere everywhere in the water encircling the Antarctic continent which also shows values less than 1°C. In the Northern Hemisphere there is a decrease in the annual temperature variation in the Norwegian Sea and the variation becomes gradually smaller towards the north; this is true also for the North Pacific, but the northward decrease is slower. The maximum annual temperature variation always occurs in the subtropical high-pressure belt where, near to the Bermudas and near the Azores, the maximum value is greater than 8°C. This region is connected with that showing the absolute maximum surface temperature variation

† The individual change in temperature $d\vartheta/dt$ in a given unit mass is caused by the addition or abstraction of a given quantity of heat Q . This quantity Q is due to the absorption of radiation, to back-radiation, to thermal conductivity, to evaporation and to mixing and others. If the local distribution and that with time of these properties is given along the path followed by the unit mass of water then the "individual" variation in temperature $d\vartheta/dt$ can be found. If the "local" temperature change $\partial\vartheta/\partial t$ is required for a fixed point occupied successively by different masses of water, then for a given flow (velocity u) in the direction n the following equation is valid:

$$\frac{d\vartheta}{dt} = \frac{\partial\vartheta}{\partial t} + u \frac{\partial\vartheta}{\partial n} = \frac{1}{c_p} Q.$$

The advection term $u(\partial\vartheta/\partial x)$, which includes the effects of the transport and the displacement of different masses of water at different temperatures in the direction n , thus plays an important role for the assessment of the local temperature change $\partial\vartheta/\partial t$.

(larger than 15 °C) off the coast of North America and in the region of the Newfoundland Banks. There, as already mentioned, the annual variation in temperature is caused by the fluctuating seasonal movements of ocean currents. Similar conditions occur in the North Pacific; the absolute maxima of more than 20°C in the Yellow Sea, and in the Sea of Japan, are associated with a zone of maximum annual amplitude (greater than 9°C) extending from Japan eastward towards the east coast of North America. In the Southern Hemisphere the subtropical maxima of temperature variations are of a smaller extension. The annual temperature range is also large (8–10°C) in the areas of cold water upwelling (off western Africa in the Northern and Southern Hemispheres and off California) in accordance with the seasonal variations in these phenomena.

The geographical distribution of the annual temperature variation at the sea surface is not difficult to explain. In the tropics the small amplitude is due in the first place to the constant high altitude of the sun throughout the whole year and also to the relatively high cloudiness, so that there are only small annual variations in the incoming radiation. In the subtropics the absorption of solar radiation has a much greater influence on the development of a marked annual temperature variation because of the already larger seasonal changes in the zenith distance of the sun, and also because of the stronger effect of back-radiation due to the low cloudiness prevalent in these areas. With increasing latitude the incoming radiation becomes less effective and the autumn and winter convection, which is able to penetrate down to greater depths here, still further reduces the annual amplitude of the temperature variation until it reaches a minimum in the polar regions. Table 44 shows mean annual variations in temperature for equatorial, temperate and high latitudes, by the use of the mean temperatures for zones of 10° latitude given by BÖHNECKE (1938). In the equatorial zone there are two maxima at the time of the equinoxes. In the subtropics the maximum occurs in September and March, respectively, and in the extra-tropical regions in August and February, respectively. The minimum values in the first area occur in March and August respectively, and in the latter, in February and September, respectively.

Table 44. Annual variation in the water temperature at the sea surface in the Atlantic
(Deviation from annual mean 0·1°C)

Latitude	Jan.	Feb.	Mar.	Apr.	May	June	July	Aug.	Sept.	Oct.	Nov.	Dec.	Annual variation
50°–70° N.	–16	–21*	–13	–17	–11	+2	+15	+26†	+13	+6	–5	–6	4·7°
10°–50° N.	–23	–29	–30*	–24	–12	+9	+28	+38†	+34	+19	0	–14	6·8°
20°N.–20°S.	+1·5	+2·5	+7	+8·5†	+6	0	–5	–8*	–6	–2	–0·5	+1	1·7°
20°–50° S.	+19	+27†	+23	+15	+4	–8	–15	–20	–23*	–18	–8	+7	5·0°
70°N.–60°S.	–1	–1	0	–3	–5*	–1	0	+4	+2	+2	–1	+1	0·9°

* Minimum; † Maximum

In general the surface temperature minimum is retarded about two to three months after the sun reaches its lowest height; the maximum is retarded also by about the

same. A comparison of the oceanic and continental annual temperature variations is given in Table 45.

Table 45. Annual temperature variations (°C)

Latitude	Equator	10°	20°	30°	40°	50°
Oceans	2.3	2.4	3.6	5.9	7.5	5.6
Continents	(1.3)	3.3	7.2	10.2	14.0	24.4*

* Only Northern Hemisphere

Figure 50 shows isopleths for the annual surface temperature variations in the Atlantic. It can be seen at once, that there is a narrow zone just north of the equator, where there is a six-monthly temperature variation so that over the whole of the tropics the amplitude of the annual temperature variation remains very small and that the middle latitudes between 30° and 50° show a maximum which decreases towards the pole, especially in the Southern Hemisphere.

The annual temperature variation is transmitted to the deeper layers beneath the surface by the effect of convection and turbulence, with a corresponding reduction in amplitude and a retardation of the extremes, until it finally disappears. However, the annual displacements of water masses can also simulate an annual temperature variation, which is then not due to the total production and expenditure rates of heat at that point, but to others at more distant parts of the sea. Our present knowledge of these phenomena is still very poor. To obtain the exact annual temperature variation at deeper layers it is necessary, because of the small number of observations

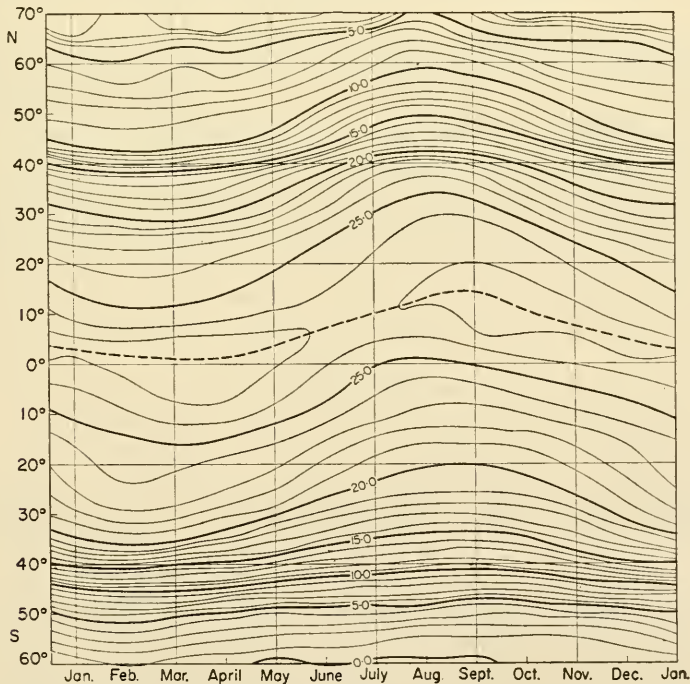


FIG. 50. Isopleths of surface temperature in the Atlantic Ocean.

available, to eliminate aperiodic changes. This elimination is done by the "temperature anomaly" method given by HELLAND-HANSEN (1930). According to the mean $[TS]$ -diagram (see Chap. VI, 3) there is normally, for every value of the salinity in the water mass under consideration, a definite mean temperature ϑ . If an observation (ϑ_1, S) is obtained in this area, then the difference $\vartheta_1 - \vartheta$ is termed the "temperature anomaly" of this observation. Experience shows that the temperature anomalies in a given set of data is of a *considerably smaller scatter* than the original values and that the aperiodic change of it has very largely been eliminated. The annual temperature variation in particular is shown much better than by the original values.

By these methods Helland-Hansen has worked out the annual temperature variation for the water layer down to 200 m depth for three ocean areas in the North Atlantic. Figure 51 gives the results for the Bay of Biscay (area B) for the surface, as well as for

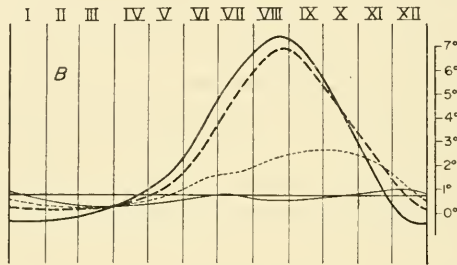


FIG. 51. Annual temperature variation in the water layer down to 100 m depth in the Bay of Biscay (area B) (according to Helland-Hansen).

the depths of 25, 50 and 100 m. Table 46 presents the time of occurrence of the maxima and minima in this area and in the area between Portugal, Morocco and Madeira and also gives the amplitude at different depths. The amplitude at 25 m is still quite considerable and not very much smaller than the surface amplitude. However, lower down it decreases more rapidly and at 200 m the annual variation is more or less insignificant. The shape of the curve is almost the same in both areas and quite characteristic. In late autumn and in winter the surface water cools rapidly and the resulting convection also involves the deeper layers in this cooling. Thus, the vertical temperature gradient decreases continuously and becomes almost zero in spring. Heating now raises rather rapidly the temperature of the uppermost 25 m layer.

Table 46. Annual temperature variation in the Bay of Biscay (B) and in the area between Portugal, Morocco and Madeira (C)

Depth (m)	Area B			Area C		
	Min.	Max.	Variation (°C)	Min.	Max.	Variation (°C)
0	Jan.	Aug.	7.7	Feb.	Sept.	5.3
25	Feb.	Aug.-Sept.	6.8	Feb.	Sept.	4.7
50	Mar.	Sept.-Oct.	2.4	Mar.	Oct.	1.4
100	Mar.	Dec.	0.7	Mar.-Apr.	Nov.	0.9
200	—	—	0.3	—	—	0.25

This effect may still be noted down to 50 or 100 m, but the heating process is interrupted in June and only reappears later at 50 m. The reason for this remarkable phenomena can be seen in the circumstance that turbulence due to the wind affects the greater depths in spring, while the water mass processes an indifferent or weakly stable stratification, so that surface heat can penetrate still to depths below 50 m. The rapid temperature rise of the surface layers soon builds up such a strong temperature gradient that turbulence is unable to prove a match for the created strong vertical stability of the water masses and the turbulent transport of heat therefore ceases. The upper layer is heated further by continued incoming radiation, and because of mixing becomes almost isothermal while the lower layers remain cold. The temperature in these layers rises again. Only when the density gradient is destroyed in the autumn can the effect of mixing and convection again extend to deeper layers. Only then can further heat be carried to the layer beneath the thermocline (DEFANT, 1936a).

In places where the ocean currents are subjected to considerable displacements, in both direction and strength during the year, the annual temperature variation can be considerably affected down to great depths by these current displacements. A typical example for this is the annual temperature variation in Monterey Bay, California (SKOGSBERG, 1936). Here there are three different periods in the annual variation: the period of the Davidson Current from the middle of November to the middle of February, when the temperature varies only slightly with depth down to almost 100 m; then follows a period of upwelling water from the middle of February to the end of July with low temperatures and stronger stratification; while from the middle of July to the middle of November the Californian Current prevails and the temperature variation shows normal oceanic conditions.

On the other hand, the temperature variation in the Kuroshio south of Japan (KOENUMA, 1939) shows almost exactly the same conditions as in the Bay of Biscay which was mentioned above.

FJELDSTAD (1933) has attempted to use the observations of Helland-Hansen in area B to calculate the eddy conductivity coefficient from the changes in the annual temperature variation with depth. He developed the annual temperature variation in the individual depths into harmonic series, and obtained in that way the values a_n and α_n as the amplitude and phase of the n th term of the series. Fjeldstad then showed that

$$\frac{A}{\rho} = \frac{n\sigma}{a_n^2 (\partial\alpha_n/\partial z)} \int_z^h a_n^2 dz,$$

where $\sigma = 2\pi/T$, T is the annual period and h is the depth at which the amplitude vanishes. A better representation of the observations can only be achieved by assuming a seasonal variation of the eddy conductivity coefficient. The mean value at the surface is $16 \text{ g cm}^{-1} \text{ sec}^{-1}$, at 25 m it is $3 \text{ g cm}^{-1} \text{ sec}^{-1}$ and at 100 m the annual mean is only 3, in summer 0.5 and in winter 5.5.

The same method has been applied by SVERDRUP (1940) to values for the Kuroshio which in this case appears to be permissible, since the advective effects are outweighed by radiation and the eddy conductivity. In the Kuroshio area, where the strength of the current is large and the turbulence correspondingly high, the annual temperature

variation penetrates almost to 300 m depth with an eddy coefficient of about $70 \text{ g cm}^{-1} \text{ sec}^{-1}$ at the surface, 30 and 27 at 50 m, and 200 m, respectively.

For a selection of 1 and 2 degree squares in the area between the Faroes and the Bay of Biscay, NEUMANN (1940, unpublished manuscript) using simple statistical methods has derived the annual temperature variation for 20, 40 and 100 m and has obtained rather similar results. The effect of stratification on heat transport in the deeper layers of a water mass also appears in lakes in the same way as described above and the annual temperature variation can be explained only under consideration of these processes. In shallow seas (Shelf seas) it is possible to study more accurately the penetration of heat and especially the effect of turbulence generated by the wind, and also to investigate the eddy viscosity caused by strong tidal currents at the sea bottom. Recently DIETRICH (1950, 1953, 1954) has given an instructive example of the various possibilities by the use of isopleths of temperature in vertical cross-sections in different shelf waters which illustrates the conditions present in the best possible way. Figure 51a shows the annual variation of temperature and salinity from the surface to the bottom.

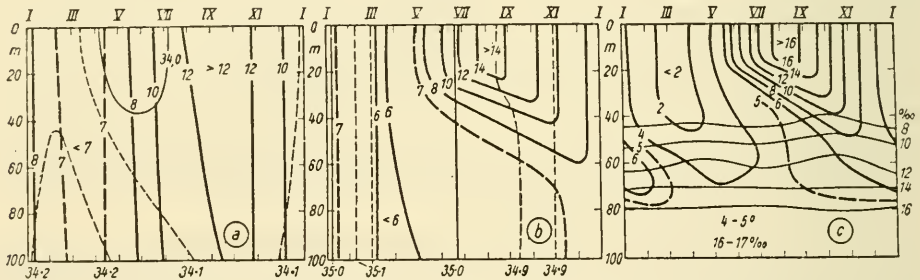


FIG. 51a. Example of annual temperature and salinity variations from the surface down to the bottom (according to Dietrich). *a*, Irish Sea, North-Channel; *b*, Central North Sea; *c*, Baltic, Bornholm deep.

(*a*) In the Irish Sea, north channel, with strong tidal currents where even in summer a thermocline cannot form and the strong turbulence evens out the annual temperature variation in the whole mass of water from the surface to the bottom (extremely strong heat transport from the surface downwards due to turbulence).

(*b*) In the middle of the North Sea where the weak tidal current has little effect. The formation of a thermocline prevents the development of a more pronounced annual temperature variation beneath it.

(*c*) In the Bornholm deep in the Baltic, no noticeable tidal current and a strong increase in salinity with depth (strong density stratification during the whole year) so that the lower layer is isolated and shows no annual temperature variation. See p. 115 and MUNK and ANDERSON (1948 on the theory of the thermocline).

The *annual heat budget* of a limited water mass can also be calculated without difficulty if sufficient observational data are available. A number of calculations of this type have been made for lakes and similar calculations have been carried out for more or less enclosed seas. According to O. PETTERSSON (1896) the Baltic gives off $137\cdot500 \text{ kg cal/m}^2$ from August to November and a further $385\cdot500$ up to March, in total about $523\cdot000$

kg cal/m². The annual heat budget for the Ionian Sea has been calculated by HANN (1906, 1908) as about 371,000 kg cal/m²; for the sea south of Cyprus he found 426,000, for the Bay of Naples 432,000 and for the Black Sea 482,000 kg cal/m². In the polar regions the annual heat budget is much smaller. MALMGREN (1927) has made corresponding calculations for the North Polar Basin; he estimated that the atmosphere received 68,000 kg cal/m² from the sea annually. This mean annual value was obtained from the difference between the loss of 76,700 kg cal/m² from September to April and a gain of 8,700 kg cal/m² from June to August. See DEITRICH (1950) for a discussion of the annual variation of heat content in the English Channel.

4. The Vertical Distribution of Temperature in the Ocean

Figure 52 shows the vertical temperature distribution for a series of oceanographic stations along a meridional cross-section through the middle and central parts of the Atlantic. The general and common characteristics of the vertical temperature distribu-

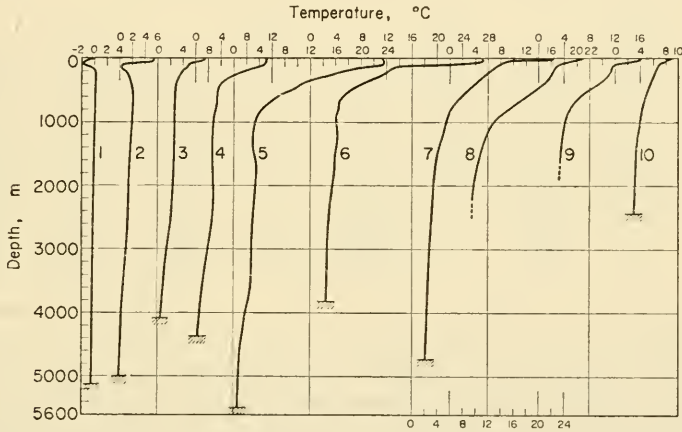


FIG. 52. Vertical temperature distribution at a series of stations along a meridian in the Atlantic Ocean:

1. "Will. Scoreby" 554	63° 20' S. 17° 23' W.	5143 m	5. ii. 1931
2. "Meteor" 58	48° 30' S. 30° 0' W.	4989 m	7.8. x. 1925
3. "Meteor" 83	32° 9' S. 25° 4' W.	4506 m	29. xi. 1925
4. "Meteor" 170	22° 39' S. 27° 55' W.	5454 m	9. vii. 1926
5. "Meteor" 191	9° 7' S. 2° 2' W.	4533 m	9/10. ix. 26
6. "Meteor" 212	0° 36' N. 29° 12' W.	3773 m	19. x. 1926
7. "Meteor" 283	17° 53' N. 39° 19' W.	5748 m	22/23. iii. 1927
8. "Dana" 1376	33° 42' N. 36° 16' W.		10. vi. 1922
9. "Armauer Hansen" 17	58° 0' N. 11° 0' W.	1860 m	29. vii. 1913
10. "Fram" 29	78° 1' N. 9° 10' E.	1075 m	22. vii. 1910

tion thereby stand out clearly. Conditions in the other oceans are also essentially the same. The typical curve for the vertical temperature distribution in the open ocean is *anorthic*, that is it shows a decrease of temperature with increasing depth, though this decrease is not uniform. In latitudes between about 45° S. and 45° N. the thermal

stratification of the sea is characterized by two principal layers. The upper layer extends from the surface down to about 600–1000 m and is termed the *oceanic troposphere*; its uppermost part down to about 100 m is subject to the direct influence of the atmosphere. This is the layer of diurnal and annual convections originating at the surface and it shows the strongest mixing due to the effects of the wind and waves; it can be designated as the *layer of surface disturbances*. The troposphere shows the strongest temperature decrease with depth and in low and middle latitudes forms an upper warm layer of water overlying the cold water masses underneath and separated from them by a more or less sharply marked thermocline.

Table 47. Mean vertical temperature ($^{\circ}\text{C}$) distribution in the three oceans between 40°N . and 40°S .

Depth (m)	Atlantic Ocean		Indian Ocean		Pacific Ocean		Mean	
	ϑ°	$\Delta\vartheta^{\circ}/$ 100 m	ϑ°	$\Delta\vartheta^{\circ}/$ 100 m	ϑ°	$\Delta\vartheta^{\circ}/$ 100 m	ϑ°	$\Delta\vartheta^{\circ}/$ 100 m
0	20.0		22.2		21.8		21.3	
100	17.8	2.2	18.9	3.3	18.7	3.1	18.5	2.8
200	13.4	4.4†	14.3	4.7†	14.3	4.4†	14.0	4.5†
400	9.9	1.8	11.0	1.6	9.0	2.6	10.0	2.0
600	7.0	1.5	8.7	1.2	6.4	1.2	7.4	1.3
800	5.6	0.7	6.9	0.9	5.1	0.65	5.9	0.75
1000	4.9	0.35	5.5	0.7	4.3	0.4	4.9	0.5
1200	4.5	0.20	4.7	0.4	3.5	0.4	4.2	0.35
1600	3.9	0.15	3.4	0.3	2.6	0.2	3.3	0.22
2000	3.4	0.12	2.8	0.15	2.15	0.1	2.8	0.12
3000	2.6	0.08	1.9	0.09	1.7	0.05	2.1	0.07
4000	1.8	0.08	1.6	0.03	1.45	0.03	1.6	0.05

† Maximum

The lower part of the thermal stratification is the oceanic *stratosphere* which extends from the bottom of the troposphere (thermocline) down to the sea bottom; to it belong the major water masses of the deep sea which are characterized by the very small changes in temperature both in horizontal and vertical direction. Table 47 presents the mean vertical temperature distribution in the three oceans for latitudes between 40°N . and 40°S . and also the vertical temperature gradient at each depth in degrees per 100 m. The approximate limits between the zone of disturbance, troposphere and stratosphere are indicated in Fig. 53. This twofold subdivision in the thermal structure of the ocean is limited to the tropical and subtropical parts of the ocean. As is shown in Fig. 52 the troposphere becomes less well developed towards higher latitudes and the stratosphere comes closer to the sea's surface. In the subarctic and subantarctic regions (polewards of the oceanic polar front, see Chap. XIX) the troposphere disappears and the cold-water masses of the stratosphere extend generally to the surface. The water masses of the troposphere lie on top of and are embedded in the cold-water mass of the stratosphere in tropical and subtropical areas, but thin out and disappear in higher northern and southern latitudes.

Because of the decrease of salinity with depth it can be expected, just for reasons of stability, that the temperature must also decrease with depth. Solar radiation is converted into heat in the upper layers and from here the heat spreads rapidly downwards.

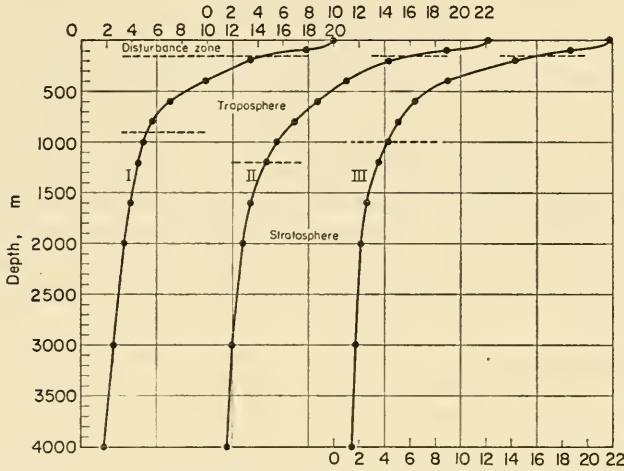


FIG. 53. Mean vertical temperature distribution in the three oceans.

The temperature distribution of the ocean must be regarded as quasi-stationary and this leads to the deduction that the vertical temperature distribution is a phenomenon closely connected with the oceanic circulation. Assuming that there was no motion in the very deep ocean this vertical temperature distribution could not be understood. HUMBOLDT (1816) emphasized at an early date that the low temperature at great depths in the tropical ocean can only be explained by assuming an equatorward flux of cold-water masses originating in high latitudes.

(a) The Oceanic Troposphere

In general, the troposphere shows a well-developed subdivision into three parts. In the top layer the vertical differences in temperature and salinity are very small—so frequently that this top layer can be regarded as homogeneous. Its thickness is seldom greater than 100 m. In the Atlantic an isothermal surface layer (temperature gradient $<0.015^{\circ}/m$) is present only in the region between about 35° S. and 25° N. polewards from these limits the isothermal stratification is slowly destroyed and the effect of the seasons begins to predominate (disturbance zone). Table 48 presents mean

Table 48. The quasi-isothermal top layer in the Atlantic Ocean

Total no. of stations	6	3	3	6	6	3
Mean geographical position	24° S. 16° W.	15° S. 15° W.	9° S. 17° W.	0° S. 22° W.	8° N. 23° W.	18° N. 36° W.
Depth (m)	Temp. (°C)					
0	20.36	24.10	24.40	26.50	25.80	22.78
25	20.32	24.44	24.36	26.43	25.82	22.86
50	20.38	24.45	24.28	26.28	25.43	22.91
75	20.37	23.46	23.79	22.77	24.55	22.65
100	20.30	20.65	20.32	17.02	19.77	22.50
150	17.72	17.10	14.60	13.42	12.98	20.22

conditions at several stations in the central part of the Atlantic. In the subtropics (30° – 20° S. and 20° – 25° N.) the isothermal layer extends down to about 100 m, but is more shallow in the tropics and in regions close to the equator (in the west about 75 m and in mid-latitudes 50 m or less). Off the African coast, especially in the Gulf of Guinea, the thickness decreases to 25 m or less, and in the regions with cold water upwelling it is entirely absent. Underneath the top layer there is a strong temperature decrease that continues, gradually weakening, down to the lower limit of the troposphere. The maximum of vertical temperature gradient (*thermocline*) is generally found between 100 and 200 m, with a mean value of nearly 5°C per 100 m. The meridional variation of the depth of thermocline is shown in Table 49 (Fig. 54).

Table 49. Meridional variation of the depth of thermocline in the Atlantic Ocean
(Mean values for the entire ocean)

Latitude	20° S.	15°	10°	5° S.	0°	2.5° N.	5°	10°	15°	20°	25° N.
Depth (m)	141†	121	108	77	69*	83†	81	53*	89	160	195*

* Minimum; † Maximum

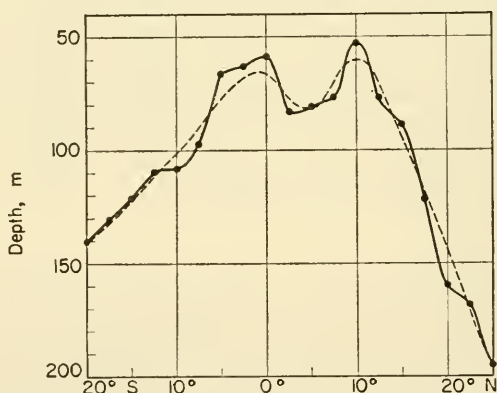


FIG. 54. Meridional distribution of the depth of thermocline in the Atlantic.

The thermocline rises steadily from a depth of 150 m in the subtropics to minimum values in the equatorial regions. Approaching the equator from the Southern Hemisphere a minimum of about 70 m is reached directly at the equator; however, coming from the north the minimum (about 55 m) already shows in 10° N. Between these two highest locations the thermocline drops about 15–20 m to a deeper level (approx. 80 m) at 2.5° N. These changes in level are rather characteristic for the entire width of the ocean and due to dynamical reasons are associated with the zonal oceanic circulation of the equatorial water masses (see Chap. XVIII and XIX). The intensity of the thermocline is greatest in the equatorial areas, where it has a mean value greater than $0.4^{\circ}\text{C}/\text{m}$. An actual transition layer (temperature gradient $>0.1^{\circ}\text{C}/\text{m}$) properly speaking only occurs between 15° N. and 15° S.; on either side of this belt the gradient falls rapidly to $0.05^{\circ}\text{C}/\text{m}$ or lower and the transition layer shows only as an intensification of the vertical temperature gradient.

Table 50. Heat transport downwards assuming a temperature gradient of 1°C/100 m

Vertical exchange coefficient (A_z g cm ⁻¹ sec ⁻¹)	20	10	5	2.5	1
Heat amount (g cal cm ⁻² day ⁻¹)	172	86	43	21.5	8.6

Beneath the thermocline from about 200–300 m the water masses of the subtroposphere are remarkably constant in their nature and geographical distribution. The vertical temperature gradient in these waters rapidly decreases with depth and gradually changes its magnitude into that of the stratosphere. Considerable amounts of heat are transported by dynamic convection through the layer immediately beneath the almost isothermal top layer to the layer below. Table 50 gives an idea of the quantities of heat involved; it assumes a mean temperature gradient of 1°C/100 m. These amounts of heat are surprisingly high. Even for small values of A_z the downward heat flux amounts to 10–40 g cal cm⁻¹ day⁻¹. Since there is always a temperature gradient, this raises the very natural question of where all this heat goes to. In the lower layers of the troposphere the temperature gradient is again smaller and therefore the downward heat flux becomes smaller again in the middle layers of the troposphere; the accumulation of heat in these layers should soon destroy the vertical temperature gradient and thus also the thermocline. It must therefore be true that the vertical temperature gradient in the troposphere can only be maintained if the lateral influx of colder water compensates the flow of heat from above and indeed the heat from above and the horizontal advection must compensate each other exactly. The vertical temperature distribution in the troposphere is thus maintained in a stationary state by the *oceanic circulation* (DEFANT, 1930).

The cause for formation of the thermocline below an almost isothermal top layer in the tropics and the subtropics is therefore as follows: The top layer is certainly more or less in thermal equilibrium with the atmosphere above. The lower temperatures of the lower subtroposphere and of the stratosphere are essentially of polar origin; as they flow towards the equator these water masses mix with warmer water and thereby gain heat, but are continually renewed and are thus kept at a relatively low temperature. It would be expected that the difference between the high temperature at the top and the low temperature of the deeper layers would give rise to a roughly linear vertical temperature gradient in the middle layer; instead a homogeneous top layer is formed and the transition to the lower temperatures of the subtroposphere takes place abruptly in a well-developed *transition layer* (thermocline).

The explanation of this thermal stratification in the tropics and the subtropics lies in the same circumstances that give rise to the summer transition layer in lakes as well as in the ocean. The turbulence induced by the wind and the waves will slowly transport the heat from the upper layers downwards and the temperature differences thus formed will work their way down into deeper and deeper layers. However, further rise in temperature in the top layers will also increase the vertical density gradient. The downward transfer of heat from above by turbulence will cease when the increase in vertical stability diminishes the intensity of the turbulence. If the vertical density gradient is very strong the turbulence of the flow cannot overcome the great stability of the stratification and a transfer of heat to a deeper level through the thermocline can no longer occur. In the top layer the turbulence leads finally to a complete

equalization of temperature thus forming an upper isothermal top layer. Beneath this, at a definite constant level, lies the thermocline, which acts as a *barrier for all turbulent processes*. The important point in the explanation of the formation of tropical and subtropical thermoclines is the exclusion of turbulence and their consequences in a fixed depth due to the increase of the vertical density gradient above a critical value. The condition for the reduction and final elimination of the turbulence in a non-laminar flow is that the dimensionless quantity (Richardson number):

$$\frac{(g/\rho)(\delta\rho/\partial z)}{(\partial u/\partial z)^2} > \frac{A_B}{A_T}.$$

In this relation u is the basic velocity of the turbulent flow, A_B is the exchange coefficient for the flow momentum (apparent viscosity) and A_T is the exchange coefficient for density differences (temperature and salinity). In the ocean the ratio between these two quantities is between about 5 and 20 (see p. 103). In the thermocline of the equatorial region of the Atlantic the quantity $\delta\rho/\partial z$ is of the order of 5×10^{-4} for a vertical interval of 20 m. In drift currents $\partial u/\partial z$ can be taken as about 10 cm/sec for every 20 m. The left-hand side of the above inequality is thus 100, which is considerably more than the value of the right-hand side. With such a stratification the turbulence in a current cannot be maintained (DEFANT, 1936).

The basis of the theory for the formation of the thermocline has been given by MUNK and ANDERSON (1948). They have shown that the sharp transition between the top layer with mixing and the thermocline can be explained theoretically on the assumption that the eddy coefficients are a function of the vertical stability and of the wind shear. This theory gives a value for the depth of the thermocline that is somewhat too small but it is of the correct order of magnitude. This depth depends on the wind velocity, on the latitude, on the heat flux and on the [TS]-relation in that order. This theory undoubtedly penetrates deeply into the important processes that control this phenomenon but it does not yet completely satisfy all points. Experimental investigation and systematically planned observations would very probably improve the basis of the theory.

(b) *The Oceanic Stratosphere*

The vertical temperature differences in the very deep layer of the oceanic stratosphere are small. Here also the distribution is almost everywhere anothermic; however, the temperature gradient at depths below 1000 m falls rapidly to values less than 0.4°C per 100 m, at 2000 m it is at the most 0.1°C and at 3000 m and below it is barely $0.05^\circ\text{C}/100$ m. Departures from this anothermic distribution are found only in the Western Atlantic (Brazilian and Argentinian basins) and in the south-western Indian Ocean where at a depth of 1300–1600 m there is a very weakly marked temperature *inversion*, a phenomenon of particular importance for the oceanic circulation of these oceanic spaces. Table 51 shows particularly well-developed inversions at some "Meteor" stations. Inversions such as these occur only rarely in the eastern half of the South Atlantic and are very weak. They appear to be due to long-term changes associated with aperiodic variations in intensity of the deep-sea circulation (MERZ, 1922; WÜST, 1936, 1948).

Table 51. Temperature inversions in the western Atlantic (°C)

"Meteor" station	Depth (m)							
	800	900	1000	1200	1400	1600	1800	2000
170: 22.6° S., 27.9° W.	4.55	3.91	3.53	3.05	3.02	3.465†	3.45	3.30
158: 15.9° S., 30.0° W.	4.03	3.70	3.605	3.79†	3.78	3.55	3.34	3.14
201: 9.5° S., 30.0° W.	4.125	3.91	3.79	3.97	4.13†	3.86	3.54	3.31

† Maximum

Also in a horizontal direction the temperature differences in the stratosphere are small. The temperature distribution here must certainly be due to the stratospheric circulation which starts from the locations where the stratosphere extends up to the surface, that is in the polar and subpolar regions where it is in direct contact with the atmosphere. The water masses that sink in these places, where the major convection processes (see p. 97) originate, spread out very largely in a quasi-horizontal direction towards the equator to fill up the greater part of the space underneath the troposphere of the tropics and subtropics, and are thereby subjected to considerable lateral mixing at the same time.

SVERDRUP (1938) has pointed out that the stratospheric temperature distribution can be mainly explained on the assumption that there is extensive lateral and vertical mixing of the water masses. This mixing takes place along the isopycnic surfaces that rise towards the surface in the polar and subpolar parts of the oceans. Figure 55 shows that the temperature distribution in a meridional cross-section through the Atlantic below 1000 m can be interpreted roughly as due to the effects of this lateral and vertical mixing; the theoretical isotherms calculated from the equation on p. 108 taking $A_x : A_y$ as 6×10^6 follow a similar course than the observed isotherms. The temperature distribution in the Atlantic asymmetric to the equator is partly due to the effects of an inflow of warm water from the Mediterranean and partly due to the strong cooling effect of the Antarctic. It cannot be doubted that mixing along the isopycnic surfaces in the oceanic stratosphere is of very considerable importance in the distribution of the oceanographic elements.

(c) *Adiabatic Temperature Changes and Potential Temperature*

Since sea-water is compressible, although only slightly, the pressure changes undergone by a small mass of water in the ocean must be accompanied by adiabatic changes in temperature which can be significant for oceanographic problems. NANSEN (1900, 1902) first drew attention to the thermal effects of the compressibility of sea-water. If a mass of water is raised from a given depth to a shallower one, will be subjected to less pressure and will expand, performing work against the external pressure, and the water will be cooled by a definite amount. Analogous conditions will apply for a water mass which sinks; its temperature will increase. Since the compressibility of water is not large these temperature changes will remain only in limits; however, since the vertical temperature gradient in the deeper layers is extremely small, these *adiabatic effects* must be taken into account.

The adiabatic temperature change $\delta\theta$ for a displacement from a depth h_1 to a depth

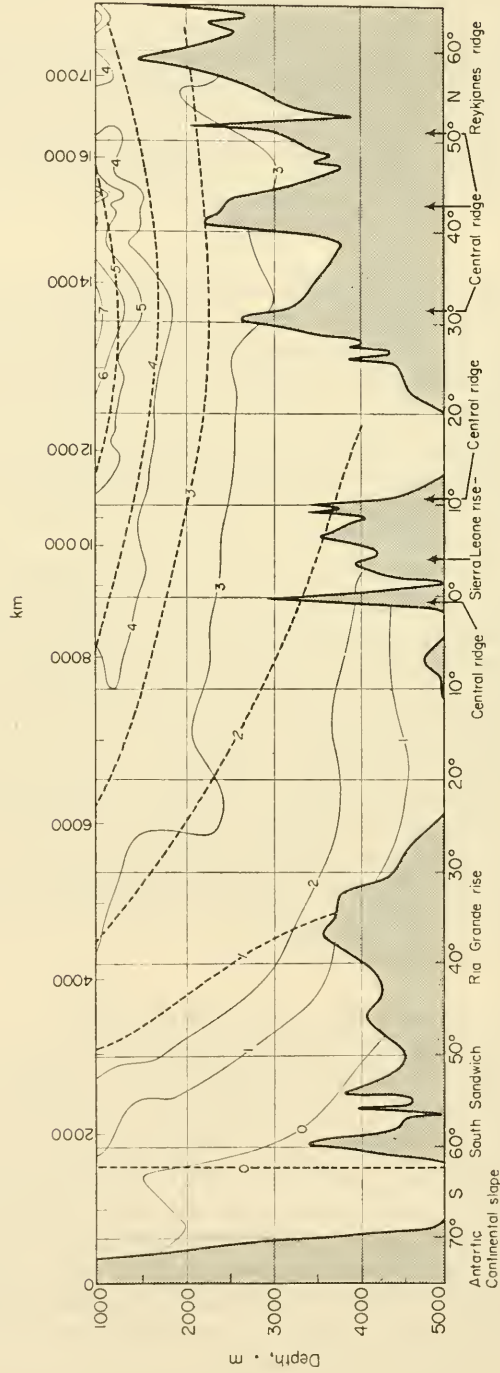


FIG. 55. Longitudinal temperature section through the Atlantic Ocean below 1000 m and the effect of lateral and vertical mixing (according to Sverdrup). Thin lines: actual temperature distribution. Broken lines: theoretical temperature distribution.

h_2 can be calculated using a formula derived from the energy principle by Lord Kelvin† which in c.g.s.-units take the form:

$$\delta \vartheta = \int_{h_1}^{h_2} \frac{T \alpha^* g}{c_p J} dz,$$

where T is the absolute temperature of the water, α^* is its coefficient of thermal expansion, c_p is the specific heat at constant pressure, g is the gravitational acceleration and J is the mechanical equivalent of heat (4.1863×10^7 erg/cal).

The adiabatic temperature change $\delta \vartheta$ for a displacement from a depth h_1 to a depth h_2 is thus dependent on the coefficient of thermal expansion and on the specific heat of sea-water, which are both effectively dependent on the temperature, the salinity and the pressure (see p. 49).

After solving the above equation, EKMAN (1914) has presented numerical values which allow an easy determination of the adiabatic effects for sea-water. HELLAND-HANSEN (1930) later prepared from these values tables giving directly the adiabatic heating and cooling in sea-water of $\sigma_0 = 28.0$ (corresponding to a salinity of 34.85‰) when raised from a given depth to the surface with a given temperature; a further table gives the adiabatic temperature change for the upper 100 m for salinities between 30.0‰ and 38.0‰. With these tables or the corresponding diagrams, any adiabatic change can be determined without difficulty. Table 52 is extracted from these tables.

Example: at a depth of 9788 m (Philippine Trench) a temperature of 2.60°C was measured and a density $\sigma = 28$. What would be the temperature of the water for an adiabatic ascent to the surface? Table 52 gives, by interpolation, a T -change at 2.60° of -1.137°C for 9000 m; for 10,000 m the change would be -1.319° and this for 9788 m -1.280°C . If the water at 9788 m rises to the surface there will be an adiabatic temperature change from 2.60°C to 1.32°C.

The temperature of a water mass after being moved adiabatically to the surface is known as the *potential temperature*. It is given by $\theta = \vartheta + \delta \vartheta$. If the vertical stratification of the sea were such that the salinity were constant, so that the density would only depend on the temperature, then the equilibrium state of the sea could be shown by the vertical distribution of the potential temperature in the same way as in the atmosphere. Complete mixing of the water masses in vertical direction would eliminate

† This above equation can be derived without difficulty from the first and second laws of thermodynamics. If the state of a body is defined as a function of the temperature T and the pressure p , then

$$dQ = c_p dT - \frac{T}{J} \frac{\partial \alpha}{\partial T} dp.$$

Taking the definition of the coefficient of thermal expansion (see p. 48) as

$$\frac{1}{\alpha} \frac{\partial \alpha}{\partial T} = \alpha^*$$

and the static equation as $dp = g \rho dz$ then for an adiabatic process ($dQ = 0$) with $\rho_\alpha = 1$ and $J\vartheta = JT$

$$\delta \vartheta = \frac{T \alpha^* g}{c_p J} dz$$

or for the interval from $h_1 - h_2$ the above formula is derived.

Table 52. (A) *Adiabatic cooling (in 0.01°C) resulting from an ascent of a water particle of temperature ϑ_m up to the sea surface ($\sigma = 28.0$; $S = 34.85\%$)*

Depth (m)	ϑ_m (°C)						
	-2	0	2	4	6	8	10
1000	2.6	4.4	6.2	7.8	9.5	11.0	12.4
2000	7.2	10.7	14.1	17.2	20.4	23.3	26.2
3000	13.6	18.7	23.6	28.2	32.7	37.1	41.2
4000	21.7	28.4	34.7	40.6	46.3	51.9	57.2
6000	42.8	52.2	61.1	69.4	—	—	—
8000	—	81.5	92.5	102.7	—	—	—
10,000	—	115.7	128.3	140.2	—	—	—

(B) *Adiabatic temperature change (in 0.01°C) for the upper 1000 m at different salinities*

$S\%$	ϑ (°C)					
	0	4	8	12	16	20
30	3.5	7.0	10.3	13.2	16.1	18.9
32	3.9	7.3	10.6	13.5	16.4	19.1
34	4.3	7.7	10.9	13.8	16.6	19.3
36	4.7	8.1	11.2	14.1	16.9	19.6
38	5.1	8.4	11.6	14.4	17.2	19.8

all temperature differences except those due to adiabatic effects. The temperature of each depth would be fixed by purely adiabatic displacements of water from the surface or from the bottom to the given depth and in that way the vertical distribution of temperature would remain invariable. In this case a mass of water from the surface would be subjected neither to a force upwards nor to a force downwards, but would always be in equilibrium with its surroundings (*indifferent equilibrium*). In a vertical direction the potential temperature within it would be constant. The vertical distribution of temperature in such a case for some initial values at the sea surface is shown in Table 53. In neutral equilibrium there is thus a slight increase of temperature with depth which does not reach a temperature of 1.5°C in the 10 km depth.

Table 53. *Vertical temperature distribution of indifferent equilibrium*

Potential temperature (°C)	Depths (km)							
	0	1	2	3	4	5	7	9
0	0.00	0.045	0.109	0.192	0.293	0.412	0.698	1.044
5	5.00	5.087	5.191	5.312	5.448	—	—	—
10	10.00	10.125	10.265	10.419	10.587	—	—	—

If the vertical temperature gradient is greater than the adiabatic, i.e. if the potential temperature calculated from the temperature *in situ* increases with increasing depth,

then the equilibrium state is *unstable* in the vertical. If a small water mass in such a thermal stratification is displaced downwards, it will remain colder than its surroundings in spite of adiabatic heating, and it will be forced down further and further from its initial position. If it is displaced upwards then it will remain warmer than the surroundings and will therefore continue to rise. If, on the other hand, the vertical temperature gradient is less than the adiabatic, particularly if the temperature decreases with depth, then the potential temperature will also decrease with depth and the stratification is *stable*.

Table 54. Vertical distribution of potential temperature ($^{\circ}\text{C}$) below 3000 m for several stations in the western and eastern troughs of the Atlantic Ocean

Depth (m)	Western trough			Eastern trough		
	Argentina Basin Met. 56 48.4° S., 42.6° W.	Brazil Basin Met. 249 5.0° S., 26.4° W.	North America Basin Dana 1356 30.0° N., 59.6° W.	Antarctic Basin Met. 129 58.9° S., 4.9° E.	Cape Basin Met. 77 34.0° S., 3.0° E.	Cape Verde Basin Met. 264 10.2° N., 26.6° W.
3000	+1.40	+2.44	+2.66	-0.60	+2.07	+2.46
3500	+0.96	+2.28	+2.32	-0.73	+1.73	+2.22
4000	+0.33	+1.66	+2.03	-0.82	+0.94	+2.06
4500	-0.05	+0.48	+1.85	-0.85	+0.68	+1.92
5000	-0.27	(+0.25)	+1.66	-0.86	+0.60	+1.84
5500	-0.27	—	+1.61	-0.88	—	+1.77

The vertical temperature distribution present in the ocean is such that the stratification, in so far as it depends on the temperature, is stable. In the oceanic troposphere the temperature decrease is so large that, in spite of the vertical decrease in salinity, the equilibrium state remains quite stable. In the upper layers of the stratosphere the stratification is still stable, however, it becomes continuously less stable with increasing depth. Table 54 shows the vertical distribution of the potential temperature below 3000 m for several stations in the eastern and western troughs of the Atlantic Ocean which show these conditions rather clearly. The same is usually also found in the open sea of the Indian and Pacific Oceans.

At very great depths, below about 4500 m, especially in the more or less extended deep-sea basins, the vertical temperature distribution approaches the adiabatic and may even exceed it a little, so that there is an indifferent stratification at great depths or sometimes it may even be slightly unstable. It is principally in the deep-sea trenches of the Pacific and Indian Oceans that this occurs. In these there is nearly always temperature increase, but it seldom exceeds the adiabatic gradient and if it does then only by very little. Such a condition of indifferent stability is formed only when there is an almost complete separation of the water mass from the surrounding waters. More or less fully enclosed deep inland seas such as the individual basins of the European Mediterranean and the North Polar Basin show this phenomenon to a marked degree in their deeper parts. The classic example of conditions in a deep-sea trench is the vertical temperature distribution in the Philippine Trench (SCHOTT, 1914; SCHULZ, 1917; WÜST, 1937; VAN RIEL, 1934; SCHUBERT, 1931). According to

more recent calculations from the observations made in this trench there is no instability in the deepest layers as was previously supposed. Table 55 presents the data obtained in this case.

Table 55. *Vertical temperature distribution in the Philippine Trench: "Will. Snellius" Exp., Stat. 262 (9° 40.5' N., 126° 50.5' E.)*

Depth (m)	1455	1970	2470	2970	3470	3970	4450	5450	6450	7450	8450	10035
Temperature (°C)	3.205	2.27	1.825	1.66	1.585*	1.595	1.64	1.78	1.925	2.075	2.23	2.475
Potential temp. (°C)	3.095	2.13	1.65	1.44	1.31	1.26	1.25	1.26†	1.25	1.24	1.22	1.16
Change over 500 m (0.1°C)	-9.4	-4.8	-2.1	-1.3	-0.5	-0.1	+0.05	-0.05	-0.05	-0.05	-0.05	-0.1
Salinity (‰)	34.58	0.605	0.64	0.66	0.67	0.67	0.67	0.67	0.67	0.685	0.695	0.67

* Minimum; † Maximum

Between 3500 and 10,035 m with almost constant salinity there is an increase in temperature from 1.58 to 2.47°C, an increase of 0.89°C; this increase is, however, less than the adiabatic one; the stratification is thus still stable but very close to the indifferent equilibrium. At a level of 5500 m there exists a small anomaly because a thin layer of water, with a warmer potential temperature (1.26°C), is situated underneath another layer with a colder potential temperature (1.25°C). The difference is, however, only small. The stratification here is thus very close to a vertically unstable state. However, if the salinity would decrease only a little more with depth the weakly stable temperature stratification could be changed by the salinity into an indifferent or even into a slightly unstable one.

It was at first supposed that the almost adiabatic or slightly superadiabatic temperature gradient, in the deep-sea trenches and the deep troughs of the major oceans, was due to a heat gain from the solid Earth. The heat transferred from the interior of the Earth to the lowermost water layer per second is

$$Q = -2.1 \times 10^{-6} \text{ g cal/cm}^2 \quad (\text{see p. 88}).$$

This heat amount would accumulate in the layer very close to the sea bottom, until such a temperature gradient is formed that the incoming heat per unit time would equalize the heat transfer to the layers above. If the water mass were to be completely motionless, then according to the calculations of SCHMIDT (1925), the stationary temperature gradient would be determined by the heat entering the layer from the Earth and by the coefficient of thermal conductivity, so that in this case there would be a temperature decrease away from the bottom of 1.5°C in 10 m.

$$\frac{d\vartheta}{dz} = \frac{2.1 \times 10^{-6}}{1.4 \times 10^{-3}} = 1.5 \times 10^{-3} \text{ } ^\circ\text{C/cm}.$$

Thus, in a deep-sea trench below 5000 m the temperature should rise linearly due to the heat transferred from the Earth to the water, and at the bottom (10,000 m) would be over 700°C. Since this does not occur it must be concluded that even the deepest

layers are not at complete rest, and that due to the exchange produced by turbulent motions in these layers the heat is more rapidly dissipated than by normal conductivity. An exchange of about $4 \text{ g cm}^{-1} \text{ sec}^{-1}$ would be sufficient to account for the observed slightly superadiabatic temperature gradient. This appears, however, not entirely conclusive. Even when the water masses in these more or less enclosed deep-sea troughs and trenches do not participate in the general horizontal circulation of the deep sea and can therefore be regarded as motionless in horizontal direction, there may still occur *vertical convection currents* produced by the continuous influx of heat from the Earth which will carry this heat to the layers above. Such a convection will be effective if there is the smallest vertical instability. Once such instability exists in the bottom layer there will be a steady interchange of small water quanta rising and sinking, and this convectational circulation will be maintained by the steady inflow of heat through the sea bottom. In the water masses above an adiabatic temperature gradient will be established; a gradient greater than the adiabatic can, however, form only in the very bottom layer, though even here it will be scarcely possible to detect it by physical measurement. It is required here in order to maintain the vertical circulation against the internal viscosity. This might be the cause that the water masses of the deep-sea trenches and the deep basins in the ocean show a vertical stratification approximating closely indifferent equilibrium state.

(d) The Vertical Temperature Distribution in Adjacent Seas

While a steady decrease in temperature with increasing depth is characteristic for the open oceans, in adjacent seas connected with the open ocean over shallow sills the temperature below a certain depth is almost constant no matter how deep they may be. The adjacent seas can be divided into two groups according to their temperature stratification: the first includes all those adjacent seas where the surface water in winter cools to a temperature which is lower than that of the open ocean at the greatest depth at which they are in communication (*sill depths*). Provided there is an almost homo-haline structure in these adjacent seas, the autumn and winter convection causes the cooled surface water to sink to the bottom, and the deeps in these adjacent seas are thus filled with water masses at approximately the lowest surface temperature occurring during the coldest month of the year. The deep layers in this show roughly the winter temperature of the region concerned, provided the convection is not prevented from reaching the greatest depths by irregularities in the thermo-haline structure of the surface layers, for instance, by a layer of low salinity.

Examples of this type of adjacent sea are the Red Sea and the European Mediterranean. In the first case, in the Straits of Bab-el-Mandeb (north of Perim island), the sill depth is 150 m; in the second, in the Straits of Gibraltar, about 350 m. In the Mediterranean during the summer there is a pronounced anothermal stratification in the upper layers, while depths below about 300–400 m are essentially homo-thermal. Towards the end of the winter this homo-thermal state extends upwards to the surface. The temperature of this deep layer is thus about $12.9\text{--}13.2^\circ\text{C}$ in the Balearic Basin and in the Tyrrhenian Basin, and about $13.6\text{--}13.9^\circ\text{C}$ in the Ionian Basin and in the eastern basin near the Syrian coast. The northern Adriatic Sea shows values near to 12°C . These temperatures are all in good agreement with the winter temperatures in these regions (Table 56).

Table 56. *Vertical distribution of temperature and salinity in the European Mediterranean*

Depth (m)	Tyrrhenian Sea "Dana" 4119 (30.v.1930) 40° 13' N., 12° 6' E., 3400 m		Ionian Sea "Thor" 144 (23.vii.1910) 34° 31' N., 18° 40' E.; 3340 m	
	T (°C)	S (‰)	T (°C)	S (‰)
0	20.0	37.72	26.05	38.49
25	17.36	37.80	22.50	38.13
50	14.79	38.00	17.28	38.26
100	13.81	38.30	15.40	38.35
150	14.09	38.50	14.66	38.64
200	14.12	38.60	14.41	38.78
400	14.13	38.69	13.96	38.77
600	13.76	38.61	13.76	38.72
1000	13.19	38.49	13.58	38.66
1500	13.06	38.46	13.55	38.64
2000	13.04	38.44	13.56	38.64
3000	13.21	38.41		
Bottom (3200 m)	13.30	38.42	Bottom (3000 m) 13.69	38.64

During the autumn and winter the deep water forms at the surface and is carried by the convection to the deep basins. This is not influenced through the Straits of Gibraltar, since the bottom current through the straits carries water out from the Mediterranean and the influence of the upper current on salinity and temperature does not reach very far to the east.

Conditions in the Red Sea are similar (see Table 57, RIEL, 1932).

Table 57. *Vertical distribution of temperature and salinity in the Red Sea and in the Gulf of Aden. "Will. Snellius" Exp., April 1929*

Depth (m)	Red Sea St. 18 15° 52' N., 44° 43' E.		Straits of Bab-el-Mandeb St. 19 13° 27' N., 42° 51' E.		Gulf of Aden St. 20 12° 55' N., 45° 48' E.	
	T (°C)	S (‰)	T (°C)	S (‰)	T (°C)	S (‰)
0	26.70	37.07	27.60	36.12	28.80	36.25
25	26.10	37.11	27.41	36.33	—	—
50	25.99	37.42	27.28	36.36	25.36	36.05
100	22.51	40.27	24.53	38.57	22.70	35.87
150	21.94	40.46			18.12	35.52
250	21.66	40.57			14.76	35.45
500	21.59	40.61	125 m	39.98	14.89	35.36
600	21.58	40.57			—	—
700	21.60	40.60			13.50	35.24
900	21.63	40.60	Bottom 135 m		12.51	35.22
1000	21.66	40.60			10.26	35.88
	Bottom 1030 m					

Below about 300 m down to the greatest depths it is filled with a water mass at a temperature between 21.5°C and 21.6°C. The deep water has its origin at the surface in the northern half of this sea, where in March and April the water temperature is 21.5°C combined with salinity values of 40.5–40.7‰ increased by evaporation. The currents present definitely exclude any influence from conditions outside the open straits in the south.

With this group can be included the temperature distribution in the deeper layers in the Norwegian Sea (from 1000 to 3500 m approximately homo-thermal, –0.8 to –1.3°C and 34.9‰). Presumably this water mass must be formed at the surface to the north of Jan Mayen.

The second group of adjacent seas belongs exclusively to the warmer zones, where the surface temperature during the whole year is so high that the temperature at the sill depth is the determining factor for the thermal structure of the sea below the sill depths. Only oceanic water has access in this case to the deeper layers below sill depth. The sinking of oceanic water into the enclosed space produces a potential temperature extending to the bottom, that is determined by the potential temperature of the open ocean at the level of the sill. This phenomenon is in many cases so marked that inversely the sill depth can often be deduced from the vertical temperature distribution in the adjacent sea.

A characteristic example of this second group is the quasi-homo-thermal structure of the water masses in the Australian–Asiatic deep-sea basins beneath the depths of the sills over which they are connected with the Pacific Ocean or with the neighbouring basins. An accurate and detailed investigation of these conditions based on the observations made by the “Willebrod Snellius” Expedition has been made by RIEL (1934), Table 58.

Table 58. Vertical distribution of temperature and salinity in the Australian–Asiatic Basins (“Will. Snellius” Exp.)

Depth (m)	Sulu Sea 7° N., 120° E., Sept. 1929		Celebes Sea 3° N., 121° E., Sept. 1929		Banda Sea 7° S., 128° E., Apr. 1930	
	T (°C)	S (‰)	T (°C)	S (‰)	T (°C)	S (‰)
0	27.8	33.46	28.4	34.22	28.4	33.48
50	27.75	33.59	27.33	34.33	27.07	34.20
100	24.26	34.32	24.41	34.68	21.42	34.52
150	18.66	34.40	20.44	34.81	17.46	34.60
200	15.25	34.48	17.26	34.70	13.71	34.56
400	11.50	34.50	8.99	34.42	8.83	34.57
600	10.53	34.47	6.90	34.52	6.62	34.55
800	10.15	34.45	5.54	34.52	5.71	34.59
1000	10.08	34.46	4.49	34.55	4.70	34.59
1500	10.09	34.47	3.78	34.58	3.71	34.59
2000	10.14	34.47	3.61	34.57	3.24	34.61
3000	10.28	34.46	3.60	34.58	3.06	34.61
4000	—	—	3.72	34.59	—	—
Bottom	10.42	34.45	3.77	34.59	3.10	34.61
	Bottom 3950 m		Bottom 4773 m		Bottom 3308 m	

The Sulu Sea between Borneo and the Philippines is connected in the north with the Pacific through a sill with a maximum depth of about 400 m. Below this depth the vertical temperature gradient becomes very small and down to the greatest depth at approximately 5580 m the temperature remains almost constant (minimum 10.07°C at 1225 m, rising to 10.42°C at the bottom). The deep basin of the Celebes (greatest depth 6220 m) has an almost constant temperature below 1400 m (sill depth at 1400 m in the Kawio Strait). The broad Banda Basin has a sill depth of 3130 m and in the northern part shows a temperature minimum of 3.04°C at 2990 m, in the southern part 3.06°C at 2720 m.

Similar conditions are also present in the American Mediterranean. The main morphological structure consists of three major basins: the Gulf of Mexico, the Yucatan Basin with the Cayman Trench and the Caribbean Basin (PARR, 1932, 1937, 1938; see also, DIETRICH, 1937, 1939). Table 59 shows the vertical distribution of temperature and salinity at three stations in the three major basins of this adjacent sea. Figure 56 shows several characteristic vertical temperature distributions for four adjacent seas.

Table 59. Vertical distribution of temperature and salinity in the American Mediterranean

Depth (m)	Gulf of Mexico "Mabel Taylor" 1104 25.8° N., 92.5° W., 17 Apr. 1932		Cayman Trench "Atlantis" 1570 19.3° N., 77.5° W., 24 Apr. 1933		Caribbean Sea "Atlantis" 1509 14.0° N., 68.6° W., 23 Mar. 1933	
	T (°C)	S (‰)	T (°C)	S (‰)	T (°C)	S (‰)
0	22.94	36.16	27.32	35.99	26.08	36.38
50	21.90	36.12	27.07	36.02	26.01	36.28
100	19.30	36.31	25.08	36.04	24.97	36.68
150	16.00	36.18	22.86	36.66	21.86	36.80
200	13.40 ₅	35.70 ₅	20.35	36.67	18.15	36.35
400	7.99	34.96	15.25	36.06	10.90	35.25
600	5.77	34.87	10.61	35.31	7.71	34.82
800	4.94	34.92	7.04	34.94	6.10	34.75
1000	4.54	34.93	5.14	34.90	5.18	34.84
1500	4.16	34.97	4.26	34.97	4.20	34.96
2000	4.16	34.97	4.14	34.99	4.08	34.96
3000	4.23	34.96 ₅	4.09	34.99	4.13	34.96
4000	—	—	4.20	34.97	4.25	34.96
5000	—	—	4.34	34.97	—	—
Bottom depth	> 3000 m		5373 m		4892 m	

The question of the origin and renewal of the deep water in individual basins from different sides has been discussed on the basis of the modern oceanographic data collected by the "Atlantis" Expedition in the spring of 1933 and 1934 in the Caribbean, and by the "Mabel Taylor" Expedition in 1932 in the Gulf of Mexico. There are only two passages through the Antilles that are important for the conditions in the deep layers of the American Mediterranean: the Windward Passage between Cuba and Haiti (sill depth at 1600 m), and the Anegada-Virgin Passage (sill depths at

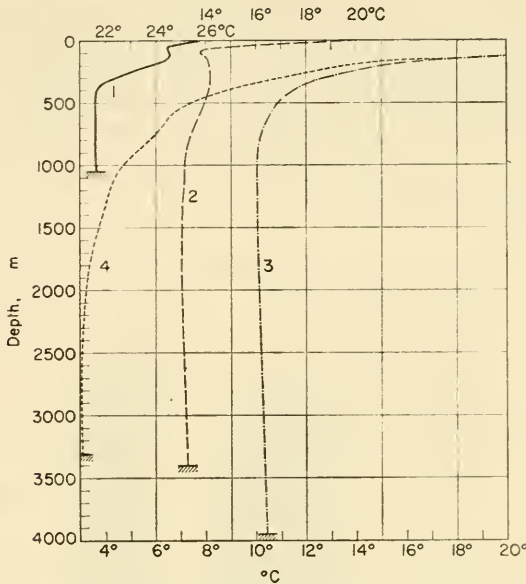


FIG. 56. Vertical distributions of temperature for four adjacent seas.

1780–1800 m and at 1600–1620 m) between the Virgin Islands and the northern Lesser Antilles. The Caribbean and Yucatan Basins show similar and almost constant values for the temperature and salinity below sill depth, and it is not easy using these values to determine the sources of the water in each basin. This was even more difficult using the older observations. However, an unequivocal solution was reached only on the basis of the vertical oxygen distribution. Having the same potential temperature (Yucatan Basin 3.79–3.81°C, Caribbean Basin 3.81–3.83°C) the water in the Windward Passage contains more oxygen than that of the Anegada Passage. Since the mean oxygen content at 2500 m (ml/l.) in the Caribbean Basin is about 5.0, in the Yucatan Basin about 5.5–6.0 and in the Gulf of Mexico about 5.0, it follows that the renewal by transport through the Windward Passage and that in the Caribbean Sea is determined by that of the Anegada–Virgin Passage. The depth of the two sills can be deduced very reliably, as shown by Dietrich, from the potential temperatures. Earlier determinations based on the observed temperatures recorded *in situ* resulted in much too large a depth. The potential temperature along a cross-section through the Anegada–Virgin Passage is shown in Fig. 56a.

The renewal of the deep water in the Gulf of Mexico is more simple to decide. Since the transport through the Florida Straits with a rather shallow sill depth of about 600 m is not likely to be of great influence, the renewal must come from the Yucatan Basin through the Yucatan Strait (sill depth 1600 m).

(e) *Vertical Temperature Distribution in Adjacent Seas at Higher Latitudes and in the Polar Regions; Autumn and Winter Convection and Ice Formation*

The basic condition for the formation of a quasi-homo-thermal state in adjacent seas is the presence of an approximately constant salinity at all depths below the sill

depth. If this condition is not satisfied the convection processes in the autumn and winter will not be able to extend to the bottom. The consequence of this limitation of the convection to a surface layer of greater or lesser thickness is a *dichothermal* temperature stratification during the warmer period of the year. There is a colder intermediate layer situated between a warmer upper and a warmer lower layer, which can be interpreted as the remainder of the convective flux extending to this depth during the cold period of the year.

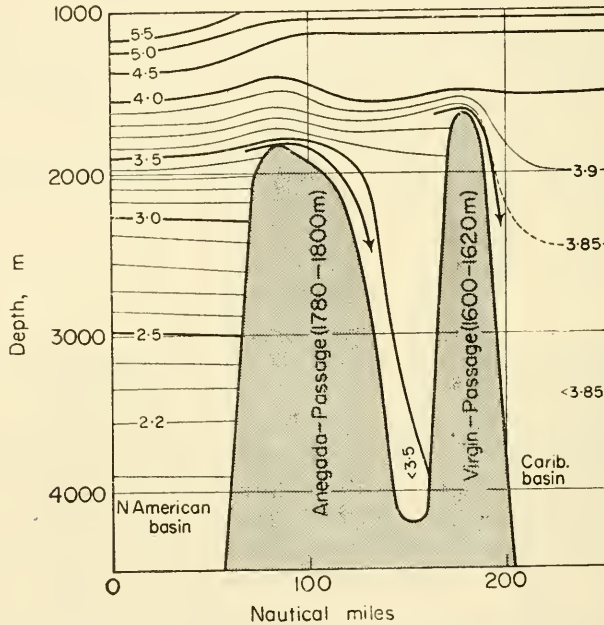


FIG. 56a. Vertical distribution of the potential temperature beneath 1000 m over a vertical section through the North American Basin, the Aneгада-Virgin Passage and in to the Caribbean Basin (according to Dietrich). Vertical enlargement by 1:1500.

This *cold intermediate layer* is typical of the whole of the open Baltic Sea during the summer. The approximately homo-haline top layer heated by solar radiation extends down to about 30–50 m depth; underneath a depth of 50–80 m there is a core of relatively cold water with a temperature of 2–3°C, while still further down to the bottom the temperature gradually rises to 4–5°C. This cold intermediate layer results from cooling of the surface water during winter. The temperature distribution of the top layer during this time shows an almost isothermal state due to mixing by turbulence and convection, whereby at the same time the temperature at the surface may fall to near or slightly below the freezing point (see Fig. 51a, c; p. 116). Similar conditions can be found in the Black Sea. For further detail see SKORZOW and NIKITIN (1927) and especially a monograph on conditions in the Black Sea by NEUMANN (1944).

During the summer the water masses in the polar waters may also show a similar temperature distribution in the upper 100–150 m. Conditions in this layer at the end

of the winter can be represented by the curve shown in Fig. 57. The winter cooling reaches down to a depth h_w . The heating during spring and summer initially affects only the uppermost layer and penetrates very slowly downwards to lower layers. During the summer it reaches to a depth h_s and the vertical distribution can then be

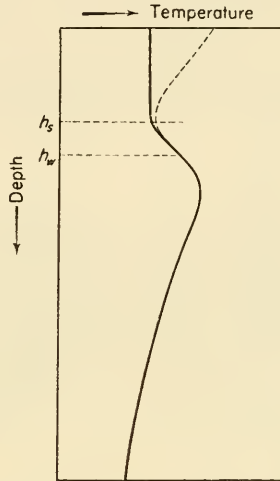


FIG. 57. Development of the vertical temperature distribution in the polar seas.

represented by the broken curve. The formation of a cold intermediate zone is clearly shown; it is *not* in a stationary state, but is gradually weakened by continuous heating from above and by mixing with the warmer water masses above and below, and may even disappear towards the end of summer to be reformed the following winter.

Table 60. The cold intermediate layer in the polar waters

Depth (m)	Barents Sea "Poseidon" 15 2 Aug. 1927; 214 m 75.2° N., 26.0° E.		Cape Farewell "Utekor" 43 9 Aug. 1930; 173 m 59.6° N., 44.0° W.		Baffin Bay "Godthaab" 50 13 July 1928; 215 m 69.7° N., 57.4° W.		Labrador Current "Marion" 1251 11 July 1931; >200m 54.6° N., 53.5° W.	
	T (°C)	S (‰)	T (°C)	S (‰)	T (°C)	S (‰)	T (°C)	S (‰)
0	+2.49	30.30	+0.49	32.35	+4.10	33.35	+3.85	32.26
10	+1.19	32.00	+0.63	32.69	+3.60	33.37	—	—
25	0.00	34.16	+0.98	32.90	+0.64	33.40	+0.01	33.05
50	-0.79	34.74	-0.79	33.08	-1.60	33.68	-1.19	33.27
75	-0.79	34.83	-0.81	33.31	-1.56	33.75	-0.72	33.69
100	-0.07	34.88	+1.12	33.71	-0.91	33.86	-0.24	34.00
150	+0.26	34.94	+2.82	34.14	+0.65	34.13	+0.51	34.21
175	+0.47	34.96			+1.20	34.29	—	—
200	+0.56	34.96			—	—	+1.36	34.47
			165 m +2.02 34.16					
	213 m +0.61 34.96							

The cold intermediate layer is particularly pronounced and lasts longest at the edge of pack ice and polar ice. Table 60 presents several examples. Figure 58 shows the temperature along a longitudinal cross-section through the northern Barents Sea (74° – 77° N., 19° – 38° E.) along the pack ice limit in August 1927 according to series observations made by the "Poseidon" (SCHULZ and WULF, 1929). From west to east exists a layer of increasing thickness of cold winter water at a depth between 20–100 m, while above this there is a layer heated by solar radiation, partly also melt water. With distance from the ice limit this cold intermediate layer weakens and is gradually eliminated by mixing. This cold intermediate layer forms the core of the cold ice carrying currents around Greenland, in Baffin Bay and in the Labrador current (DEFANT, 1936).

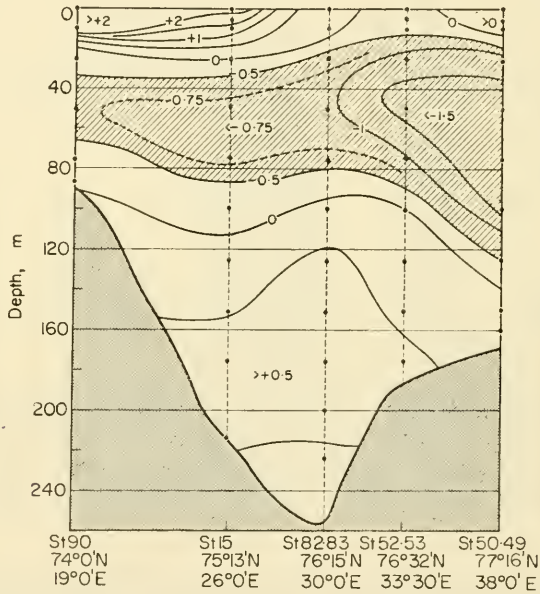


FIG. 58. Longitudinal temperature section in the northern Barents Sea (74° – 77° N., 19° – 38° E.) along the drift-ice limit (August 1927).

The thermal structure of the Polar Sea in the layer beneath the top layer, in contrast to the cold intermediate layer, is determined by the deep circulation of the polar water. In the European North Polar Basin between 250 m and 750 m underneath the cold top layer, a relatively warm intermediate layer of water of Atlantic origin is introduced with a temperature of about $0.5^{\circ}C$ (maximum of $2.0^{\circ}C$). Its salinity, 34.94 – 34.96% , shows its Atlantic origin clearly. Underneath this layer spreads cold deep and bottom water that reaches its lowest temperature of $-0.83^{\circ}C$ to $-0.87^{\circ}C$ between 2000 m and 3000 m (WÜST, 1941, 1942). In high latitudes of the Southern Hemisphere there is generally a similar vertical temperature distribution in all the oceans as shown in Table 61.

Some numerical values were given previously for the annual heat exchange in adjacent seas and in more or less enclosed parts of the ocean (see p. 116). The method used for this can also be applied, as mentioned on p. 98, to the special case of the

Table 61. Vertical distribution of temperature and salinity in high latitudes of the Southern Hemisphere

Depth (m)	Atlantic Ocean "Will. Scoresby" 554 5 Feb. 1931; 5143 m 63.3° S., 17.4° W.		Indian Ocean "Gauss" 26 March 1903; 3397 m 65.3° S., 80.5° E.		Pacific Ocean "Discovery" II 13 Jan. 1931; 3098 m 66.2° S., 71.8° W.	
	T (°C)	S (‰)	T (°C)	S (‰)	T (°C)	S (‰)
0	-0.20	33.96	-1.82	33.69	+1.21	33.71
50	-1.75	34.46	-1.5	33.69	-1.54	34.06
100	-1.80	34.42	-1.6	34.35	-0.90	34.25
150	-0.35	34.51	-1.6	34.33	+0.30	34.43
200	+0.22	34.60	-1.6	34.30	1.43	34.58
400	0.37†	34.63	+0.05	34.48	1.65†	34.70
600	0.37	34.68	1.05	34.61	1.53	34.72
800	0.29	34.68	0.90	34.62	1.42	34.72
1000	0.20	34.67	0.75	34.63	1.25	34.72
1500	0.00	34.65	0.15	34.60	0.88	34.72
2000	-0.14	34.66	0.0	34.58	0.62	34.71
3000	-0.32	34.63			0.38	34.70
4000	-0.46	34.64	3397 m -0.25 34.58		—	—

† Maximum

heat exchange at single stations. For polar stations it affords some idea not only of the heat amounts involved in such a winter convection, but also of readiness for ice formation at the surface of the sea which finally occurs after the temperature has been reduced to the freezing point due to convection. These conditions can be illustrated by an example recorded by station 888 of the "Andrey Perwoswanny" ("Murman" Expedition) on 6 August 1903 at 71° 5' N. and 49° 0' E. in the south-eastern part of the Barents Sea (BREITFUSS, 1906). Table 62 gives the oceanographic conditions down to a depth of 120 m, with mean values of the temperature and the density in each layer. Layer 1 is in direct contact with the atmosphere and is exposed to all the disturbances proceeding from it.

Table 62. "Andrey Perwoswanny" St. 888; 6 Aug. 1903 (71.1° N., 49.0° E.; 126 m)

Depth (m)	T (°C)	S (‰)	Layer (m)	Thick-ness (m)	T (°C)	S (‰)	Specific volume
0	2.84	33.96	—	—	—	—	—
5	2.78	34.04	0-5	5	2.71	34.00	359
10	4.55	34.33	5-10	5	3.665	34.18 ₅	352
15	4.64	34.33	10-15	5	4.595	34.33	352
20	3.85	34.33	15-20	5	4.245	34.33	347
30	0.07	34.45	20-30	10	1.96	34.39	322
40	-1.12	34.56	30-40	10	-0.525	34.50 ₅	300
50	-1.35	34.63	40-50	10	-1.235	34.59 ₅	291
75	-0.65	34.72	50-75	25	-1.00	34.67 ₅	285
100	-0.41	34.74	75-100	25	-0.53	34.73	282
120	-1.13	34.81	100-120	20	-0.77	34.77 ₅	277

At the beginning of the winter convection the temperature in this layer falls while the salinity remains constant. When the specific volume of the first layer becomes the same as that of the second there will be complete mixing of the two layers by convection; the resultant layer will have the mean specific volume of the second layer, given in Table 62 as 352, while the salinity will be the mean of the original salinities, that is 34.09‰. This specific volume and salinity correspond on the [TS]-diagram to

Table 63. *Heat available from convection and the readiness for ice formation at St. 888 "Andrey Perwoswanny".*

Layer	Thick-ness of the af-fected layer	Before mixing		After mixing		$\Delta t(^{\circ}\text{C})$	q_k (kg cal)	S(‰)	e (cm)	q_e (kg cal)	$\Sigma q_k + q_e$ (kg cal)	Σe (cm)	
		T(^{\circ}\text{C})	S(‰)	spec. vol.	T(^{\circ}\text{C})								S(‰)
1-2	10	3.187	34.092	352	2.85	34.092	-0.34	0.34	—	—	0.34	0	
1-3	15	3.43	34.17	351	3.45	34.17	+0.02	-0.03	—	—	0.31	0	
1-4	20	3.65	34.23	347	3.37	34.23	-0.28	0.56	—	—	0.57	0	
1-5	30	2.90	34.32	322	1.25	34.32	-1.65	4.95	—	—	5.82	0	
1-6	40	0.81	34.39	300	-1.80	34.44	-2.61	10.42	0.05	7.0	16.74	7.0	
1-7	50	-1.69	34.49	291	-1.80	34.55	-0.11	0.56	0.06	10.1	0.73	18.04	17.1
1-8	75	-1.53	34.61	285	-1.80	34.64	-0.27	2.00	0.03	7.2	0.53	20.57	24.3
1-9	100	-1.49	34.67	282	-1.80	34.675	-0.32	3.18	0.001	0.3	0.02	23.78	24.6
1-10	120	-1.63	34.69	277	-1.80	34.74	-0.17	2.06	0.05	17.6	1.27	28.10	42.2

a temperature of 2.85°C. Since the mean temperature of the two layers before mixing was 3.19°C the convection process has been accompanied by a temperature fall of 0.34°C and the amount of heat q_k given off from the surface will be 0.34 kg cal/cm² by the equation on p. 96. Taking the third layer into consideration, it is now possible to calculate the amount of heat to be removed from the two initial layers before the third layer enters into the convection process with the two layers already mixed and so on. Table 63 shows the final result of the mixing in each successive layer by convection. However, the process proceeds in this way *only* until the sixth layer has been included. After the inclusion of this layer the specific volume of all the layers cannot reach the expected value of 300 even if the entire column of water has already been cooled to the freezing point of salt water (-1.8°C). At this depth the convection due to reduction of the temperature ceases. In reality, however, after the temperature has reached the freezing point ice begins to form at the surface and this causes an increase in the mean salinity of the water column. From the [TS]-diagram it follows that the salinity must increase by 0.125‰ for the specific volume to reach 300. From this increase in salinity it is possible to calculate, using the equation on p. 96, the amount of ice that must be formed to raise the salinity by this amount. The formation of ice releases heat to the atmosphere; this is given by $q_e = 7.2 (e/100)$, if e cm of ice are formed. The quantity of heat given off during the course of the convection process down to and including the sixth layer is thus given by $q_k + q_e$ which is 17.4 kg cal/cm².

As long as the convection extends only to layer 5, i.e. to a depth of 30 m, there is no readiness for formation of ice in the water found at station 888. However, when the convection includes deeper layers it increases rapidly and when the convection extends to the bottom it requires a layer of ice 63 cm thick.

This method presented above (DEFANT, 1949) is of course a little rough and not

very precise and affords only an approximation to the time required for such convection processes, but it does give a *criterion of the readiness for ice formation* in polar waters. This advantage shows clearly when evaluating an oceanographic cross-section from this aspect. Figure 59 shows such a section from the Murmansk coast (69° N., 36° E.) in an E.N.E.-direction almost to Novaya Zembla in the southern Barents Sea, based on measurements made by the "Murmansk" Expedition 1903.

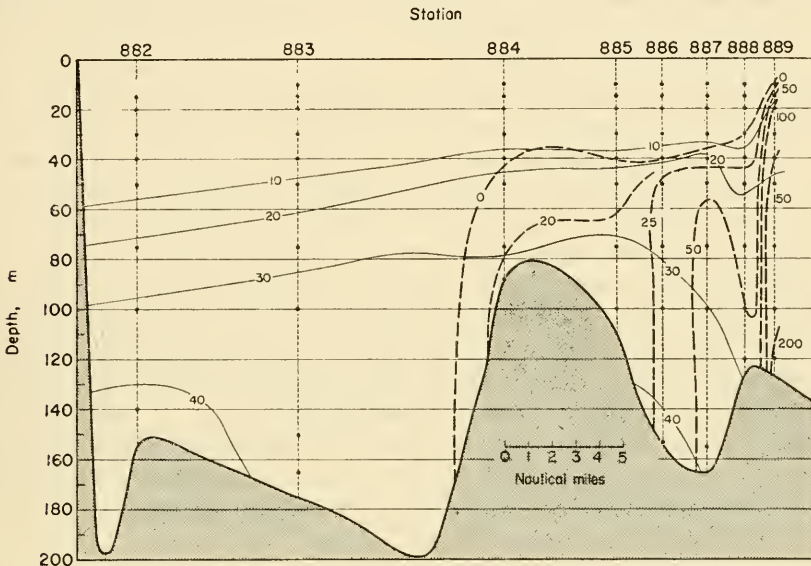


FIG. 59. Section in the Barents Sea from the Murmansk coast (69° N. 36° E) north-east to nearly Novaya Zembla.

These observations were made a little before the beginning of the convection period. The full lines show the heat in kg cal/cm² transmitted to the atmosphere from the sea surface when the convection process extends to the corresponding depth. From the Murmansk coast to about 42° E., where warm Atlantic water reaches to considerable depth, conditions are uniform and there is no readiness for ice formation even when the entire water mass down to the bottom is affected by the convection. East of the centre of the Barents Sea towards Novaya Zembla the readiness for ice formation increases considerably and while the amount of ice that can form is at first not very large it reaches at the easternmost station 889 the respectable thickness of 1.5 m or more.

ZUBOV (1938) has developed, as it seems, a similar method for the determination of ice potential in the ocean, without putting it into practice. He and SIMPSON (1954) have again dealt with the same problem of predicting ice formation and growth and in addition have derived new formulae for computing ice growth in terms of known or predicted oceanographic and meteorological data. The method was used to forecast the general features of the ice distribution in the Baffin Bay–Davis Strait area for the season 1952–3. The methods for ice potential calculation have proved in practice to give a reasonable answer for open seas, and for inshore areas where local variations in the physical properties of the water are not large. In harbours and areas where run

off is important, changes in salinity and density are too rapid to give correct forecast values.

The forecast of ice growth based on the ice potential can only be used during the period when ice thickness is increasing. No theory has been given which accounts for the decreasing ice thickness during the break-up period. A mathematical theory for this period is still needed.

The warm intermediate layer to be found at 250–750 m depth over the whole of the North Polar Basin is of an advective nature. Its thickness depends on this, i.e. on the strength of the oceanic circulation. It is thus not surprising that it shows strong aperiodic variations especially in its upper boundary against the cold intermediate layer. These variations may be as wide as 50–100 m and it is known that at the beginning of this century this upper limit was at a depth of 150–200 m in the northern Barents Sea and in the North Polar Sea. Since then it has risen to a depth of 75–100 m due to the general climatic warming up of the Arctic, and in recent times the oceanic circulation has undoubtedly increased in strength (WÜST, 1942; WEICKMANN, 1942). There has been a strong increase both in the amount of ice transported into the Greenland Sea from the central Arctic and in the transport of warmer, more saline Atlantic water directed into the Arctic basin. Thus, since the “Fram” Expedition 1893–6, the temperature of the warm intermediate layer of Atlantic water has risen noticeably, as has been clearly shown by the observations of the “Sedow” Expedition 1937–40. It is not impossible that a systematic study of these phenomena might show a close correlation between the aperiodic variations of the boundary between the cold and the warmer intermediate layers in the North Polar Sea and the variations in the strength of the Atlantic oceanic circulation.

5. Temperature Distribution in Horizontal and Vertical Sections

The temperatures found at an oceanic station show the vertical temperature distribution at that point, but only horizontal or vertical sections will give a two-dimensional picture and thereby lead a step further towards a spatial conception of the temperature distribution in the sea. A chart of the temperature distribution in the Atlantic was first given by MAURY in 1852 as a supplement to his charts of the winds and currents in the Atlantic. The reliability of such horizontal temperature charts—just as for vertical sections along fixed lines—depends on the amount of data available and on its more or less uniform distribution over the entire section. The isotherms are interpolated linearly between values given by observations, although it is known that the *linear* interpolation does not always correspond to reality. However, the otherwise sparse data leave too much freedom to the imagination of the analyst and the resultant chart may soon be further from actual conditions than is tolerable.

At the present time there are several recent temperature charts available covering the entire ocean surface. The most comprehensive presentation of surface temperature conditions in the Atlantic has been given by BÖHNECKE (1936) in the “*Meteor*” Report. The same report also gives isothermal charts for different main levels in the Atlantic; WÜST (1936). A selection of surface charts and such for individual depths has been given by SCHOTT (1935, 1942) for the Atlantic, the Indian and the Pacific Oceans. Recent surface charts have been published by the National Hydrographic Office in Washington (1948), *World Atlas of Sea Surface Temperatures*.

(a) Mean Sea Surface Temperature

It seems to be unnecessary to give a detailed description of the graphical distribution of surface temperature here. Reference is made to Plate 2a and b; this chart will give a better conception of the actual conditions to the reader than the most accurate description. It might be useful, however, to mention the main features of the temperature distribution.

KRÜMMEL (1907) and BÖHNECKE (1936) have derived from the mean values for 10° zones the values shown in Table 64 for the mean surface temperatures of the oceans.

Table 64. Mean surface temperature of the oceans (°C)

Zone	Atlantic Ocean	Indian Ocean	Pacific Ocean	Mean for all oceans
90° N.–80° S.	16.9	17.0	19.1	17.4

The mean annual sea surface temperature of 17.4°C thus exceeds the mean annual surface temperature of the air near the ground (land and sea) given by Hann, 14.4°C, by a full 3°C. There is thus a considerable difference in temperature between the hydrosphere and the atmosphere at the sea surface interface. Table 65 presents the mean annual temperatures for the three oceans and for the entire ocean surface separately for 10° zones.

Table 65. Mean annual sea surface temperature for 10° zones (°C)

Latitude	Northern Hemisphere				Southern Hemisphere			
	Atlantic Ocean	Indian Ocean	Pacific Ocean	Mean for all oceans	Atlantic Ocean	Indian Ocean	Pacific Ocean	Mean for all oceans
0–10°	26.6	27.9	27.2	27.3	25.2	27.4	26.0	26.4
10–20°	25.8	27.2	26.4	26.5	23.1	25.9	25.1	25.1
20–30°	24.1	26.1	23.4	23.7	21.1	22.5	21.5	21.7
30–40°	20.4	—	18.6	18.4	16.8	17.0	17.0	17.0
40–50°	13.4	—	10.0	11.0	8.6	8.7	11.2	9.8
50–60°	8.7	—	5.7	6.1	1.8	1.6	5.0	3.0
60–70°	5.6	—	—	3.1	(–1.3)	–1.5	–1.3	–1.4
70–80°	—	—	—	–1.0	(–1.7)	–1.7	–1.7	–1.7
80–90°	—	—	—	–1.7	—	—	—	—
	0°–90°				0°–80°			
	20.1	27.5	22.2	19.2	14.1	15.2	16.8	16.0

It can be seen from this table that the Pacific is the warmest ocean and the Atlantic is the coldest. This is partly a consequence of the configuration of the three oceans; the Pacific Ocean is more of a tropical ocean because three-fifths of its total surface lie between 30° N. and 30° S. The Atlantic, on the other hand, is rather narrow just in the tropics. The Tables also show that in the sea (as in the atmosphere) the

thermal equator is displaced towards the north so that the temperature maximum lies in annual average at 7° N. The large contrast between the Northern and the Southern Hemisphere in sea surface temperature is particularly noticeable; in the Northern Hemisphere this temperature is on the average about 2°C warmer in all latitudes. It is especially pronounced in the Atlantic where between 50° and 60° N. the difference is almost 7°C. This is due to the system of currents in the North Atlantic Ocean and especially due to the general coastal configuration of the North Atlantic which separates the water masses of the North Polar Basin, so that its cooling effect only shows to a small extent in the North Atlantic. Analogous separation occurs in the North Pacific. In the Southern Hemisphere, on the other hand, the three oceans are fully exposed to the influence of the Antarctic. A further factor intensifying the temperature differences in the Atlantic is the projection of the South American continent out to Cape San Roque in a latitude of 7° S. which deflects a considerable part of the Southern Hemisphere tropical water across the equator into the Northern Hemisphere.

The warmest part of the tropical ocean is a long belt with a temperature between 28°C and 29°C extending from the central Indian Ocean at about 60° E. through Australian Asiatic waters to about 175° E. in the western Pacific. The western half in the tropics is warmer than the eastern half and this circumstance is one of the most important features of the temperature distribution in the Pacific. All the other oceanographic factors are influenced in that way. In addition to this large area at a temperature above 28°C there is also a part of the Red Sea and a small isolated area off the south-west coast of Central America where the temperature rises above 28°C. The total oceanic area with a temperature higher than 28°C amounts to 21.6 million km² of 6% of the total ocean surface. In the Atlantic, areas with the mean annual temperature above 28°C are entirely missing.

Table 66. Area (in million square kilometres) with mean annual temperature above 25 and above 20°C

	Atlantic Ocean	Indian Ocean	Pacific Ocean	Mediterranean seas	Total area	In per cent of the total ocean surface
> 25°	18	28	66	14	126	35
> 20°	41	38	97	16	191	53

Table 66 shows total areas with mean annual surface temperatures above 25 and 20°C; the warm parts of the oceans are really of enormous horizontal extent. More than half of the entire ocean surface is warmer than 20°C and of this 50% more than two-thirds has a mean annual temperature above 25°C. The oceans over much of their surface are decidedly warm. The coldest parts of the ocean are at -1.7°C (close to freezing point of salt water) in the North Polar Basin and in the circumpolar Antarctic waters.

Referring to the general distribution of the isotherms at the sea surface the following points may be mentioned:

(1) The isotherms tend to be arranged zonally, especially in higher southern latitudes in all three oceans, where they almost parallel the latitude circles. This is due to the homogeneous climatic conditions over this almost exclusively oceanic area.

(2) The major equatorial ocean currents to a large extent run from east to west. At east coasts of the continents they diverge and the isotherms do the same. The western sides of the oceans are thus appreciably warmer than the eastern sides. These differences are particularly pronounced in the Atlantic; here in temperate and higher latitudes this difference between east and west is actually reversed, and from about 35° N. the east is appreciably warmer than the west. However, this phenomenon does not occur in the Southern Hemisphere. Again, the major current system at the sea surface can be considered to be the cause of different behaviour of both hemispheres. The horizontal advection of water with a different temperature produces almost stationary contrasts in temperature between the eastern and western side of the ocean. In addition the distribution of land and sea and in some regions local oceanographic-meteorological phenomena, such as upwelling water, and piling up ("Anstau"), influence the temperature distribution.

(3) There is another phenomenon apparent on the chart which is not clearly shown in the Southern Hemisphere because of the sparsity of the observations, although it has long been recognized in the Northern Hemisphere. This is the *uneven, stepwise* change in temperature towards higher latitudes. Already Fig. 50 (see p. 113) shows clearly this phenomenon, as it appears in the Atlantic. In both the Northern and the Southern Hemisphere there is an increase in the meridional temperature gradient in the zone between 40° and 50° which, during the year, is displaced towards and away from the poles following the movements of the sun. The concentration of the isotherms into a narrow belt between the Gulf Stream and the Labrador Current and between the Atlantic water and the Greenland Current is quite obvious. This boundary is called, in analogy with the atmospheric polar front, the "oceanic polar front" which indicates the position of the Arctic convergence where the two different types of water are brought into close contact. Its southern continuation along the east coast of North America has long been known as the "cold wall". This discontinuity appears in the chart of mean values because the aperiodic displacements of the ocean currents are confirmed within narrow limits. Accurate information about this sharp discontinuity has only been obtained from numerous thermographic recordings made by shipping across the whole system of currents off the east coast of North America (CHURCH, 1937; SPILLHAUS, 1940). Figure 60 shows the most important of the results obtained by analysis of these recordings. The coastal water with a slowly increasing temperature eastwards borders the warm belt of water in the Gulf Stream which is barely 50 km wide. Towards the east the Gulf Stream is separated almost as sharply by a rapid fall of temperature from the water of the Sargasso Sea, where the temperature rises again slowly towards the east and south-east.

The "band" character of the Gulf Stream does not show very clearly in the horizontal temperature charts, since the temperature is recorded at one or two degree squares which completely blurs this phenomenon, and the strong aperiodic displacements of the discontinuity along the right-hand side of the band (looking downstream) contribute to this blurring when mean values are taken. The observations are also not strictly synoptic but are only obtained with differing time.

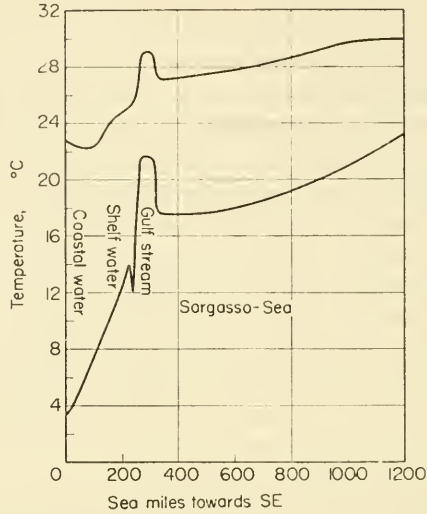


FIG. 60. Surface temperature distribution in the western North Atlantic (in the area of the Gulf Stream) from repeated temperature recordings made along shipping routes (according to Church).

In the western part of the North Pacific there is also a similar phenomenon at the boundary between the warm Kuroshio and the cold Oyashio where arctic water and subtropical water come advectively in close contact.

Due to the lack of data it was for a long time impossible to determine the position of this discontinuity in the circumpolar water in the Southern Hemisphere. MEINARDUS (1923) first showed its presence from observations made in the southern Indian Ocean. Its position in the Atlantic was deduced later from the current charts and it was recognized as the line of convergence between the oceanic west wind drift and the Antarctic water (DEFANT, 1928). It runs from about 48° W. to well out into the Indian Ocean (80° E.) between latitudes of 50° and 48° S. and then gradually turns southwards to about 62° S. at Drake's Passage.

(4) A second temperature discontinuity which is sometimes more sharply marked, though it can still only be detected on continuous recordings, lies where the subtropical water meets the subarctic water of the oceanic west wind drift (*subtropical convergence*). The frontal discontinuity in the region of the subtropical convergence shows large local meridional displacements and is therefore completely smoothed in mean temperature charts. Figure 61 shows two thermograph recordings given by DEACON (1938) that were taken on passing through the subtropical convergence and the Antarctic convergence (*oceanic polar front*). They show clearly the character of frontal discontinuity of this dynamically important phenomenon.

(5) A useful aid in comparing temperature conditions in the oceans, especially in a zonal direction, are charts with lines of equal deviation from the normal value characteristic for each latitude. Such isonamalic charts show which parts of the ocean are cold and which are warm relative to a normal latitude. In the Atlantic the heat surplus from the Gulf of Mexico across the North Atlantic to the Norwegian Sea as far as

Spitzbergen is particularly noticeable. This warm zone is associated with the Gulf Stream. There are negative anomalies showing the advection of polar water in the east Greenland Sea and the Labrador Sea down to Newfoundland. The Moroccan and the south-west African areas of upwelling water also show negative anomalies, and the eastern side of the Atlantic south of 35° N. is colder than the west side. A similar phenomenon also appears in the South Atlantic. The Pacific generally shows a similar subdivision, with the western half decidedly warmer and the eastern half too cold.

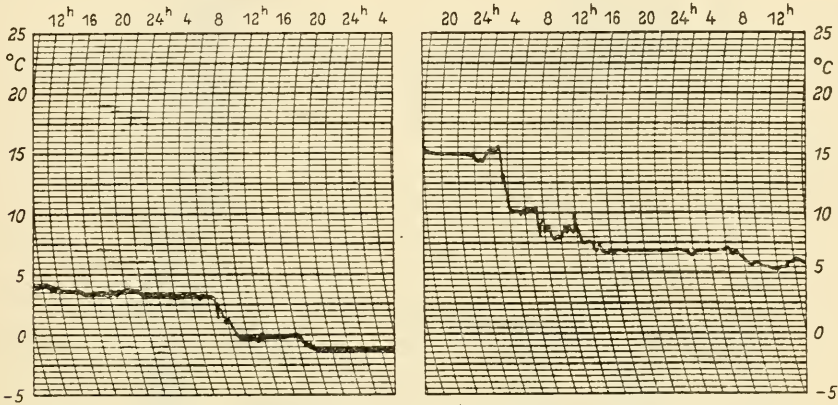
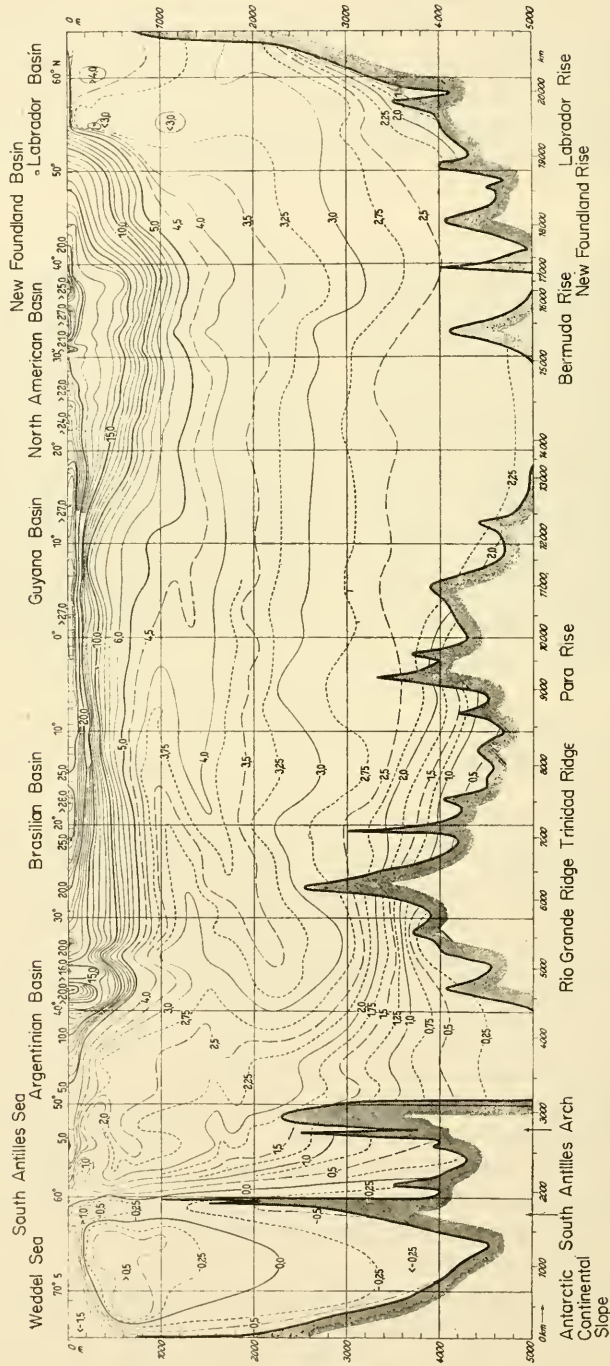


FIG. 61. Thermograph recordings made passing through the subtropical and antarctic convergences (according to Deacon).

(b) Horizontal Temperature Distribution at Different Depths and Vertical Temperature Sections

The horizontal temperature distribution remains similar to that at the surface down to a depth of at the most 50–75 m and then changes rapidly. It was already shown in Table 48 that the thickness of the top layer (*disturbance layer*) is least in the equatorial areas and this is where the cold water masses of the subtroposphere come closest to the surface. It is thus to be expected that horizontal temperature charts, even for shallow depths, will show a band of cold water embedded between the warm-water masses of the subtropics which becomes greater in width with increasing depths. This can be seen on horizontal temperature charts at 200 m intervals both for the Atlantic and also on charts for the other oceans. The subtropical warm-water areas of both hemispheres are thus separated by a cooler equatorial zone almost 30° wide and are limited polewards by two cold-water areas in higher latitudes. In the layers between 400 and 800 m the highest temperatures are always found on the *western* side of the oceans, particularly in the Atlantic. This is a dynamic consequence of the stationary distribution of the currents at these depths.

The chart for a depth of 800 m shows already the *asymmetry* typical for the temperature distribution in the deep layer of the Atlantic, which is due to the cold sub-antarctic intermediate current in the south and to the influence of the Gulf Stream and the inflow of Mediterranean warm water in the north. This asymmetry dominates the temperature distribution down to depths of more than 3000 m. The influence



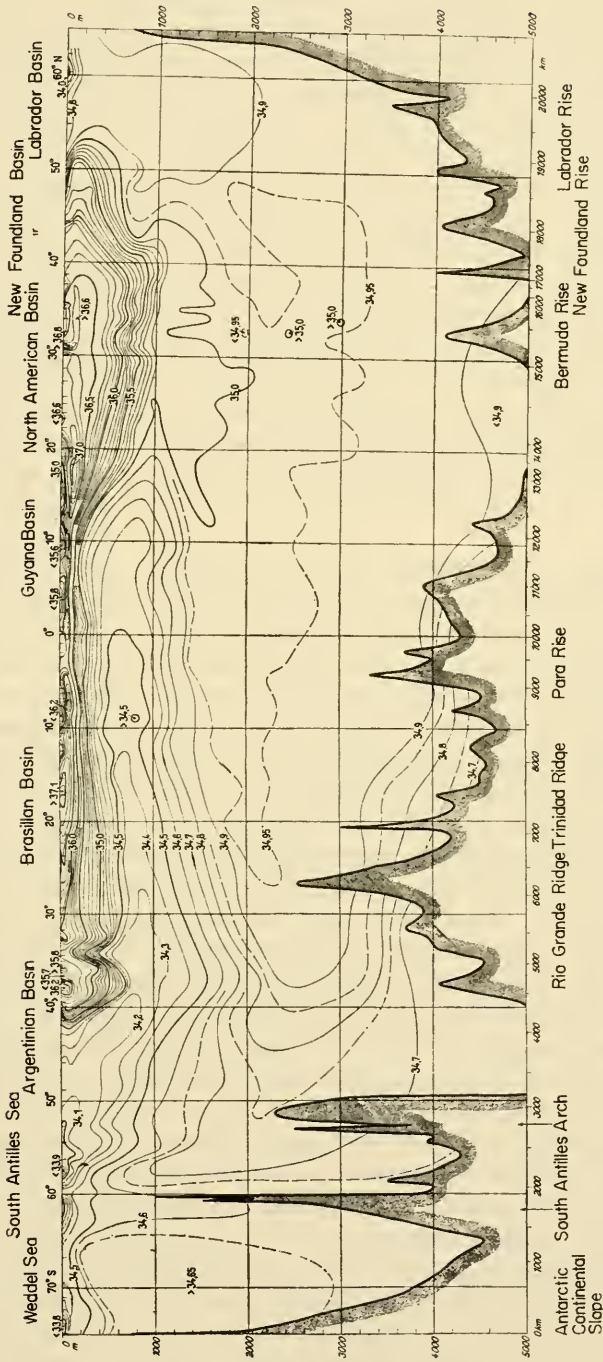


FIG. 62. Longitudinal temperature section (p. 146) and salinity section (p. 147) through the Western Trough of the Atlantic (according to Wüst).

of the Gulf Stream extends down to about 3000 m and that of the Mediterranean water down to 2000 m, so that there is always a considerable heat surplus even at these great depths in the North Atlantic. Below 3000 m the cold Antarctic bottom water first appears and at deeper levels spreads northward with slowly increasing temperature. There are insufficient systematic data available for the Indian and Pacific Oceans below 2000 m to allow any reasonably accurate description of the horizontal temperature distribution in the deeper layers.

The importance of horizontal charts of the distribution of temperature and other oceanographic factors, as a geographic aid to the comprehension of the distribution of these factors throughout the ocean, has in the past been somewhat overestimated. Oceanic processes never, or very rarely, occur along horizontal planes or are quasi-horizontally arranged. Because the three-dimensional field of oceanic elements is *arbitrarily intersected* by horizontal planes, connected phenomena will therefore be cut by such planes. They are thus, for example, quite insufficient for following water movements in the depths of the oceans. The same is equally true for the study of atmospheric phenomena. Before these were deduced in other ways it was difficult to interpret the arrangement of the isotherms in horizontal sections. In all cases vertical cross-sections must also be used to clarify the three-dimensional field of any oceanographic element.

Vertical temperature sections can be taken in any direction and thus can give a far better idea of the thermal stratification of a water mass than a horizontal chart. It is, of course, best and most convenient to take the vertical section either along the axis of major spreading of the water mass in the ocean concerned or across it.

At the present time there are several such longitudinal or transverse vertical sections (relative to the direction of flow) for all three oceans, showing temperature, salinity and in part also the oxygen content. Those for the Indian Ocean (MÖLLER, 1929; CLOWES and DEACON, 1935) and for the Pacific Ocean (WÜST, 1929; SVERDRUP, 1942, 1945; SCHOTT, 1942) are less accurate because of the smaller number of stations than those for the Atlantic Ocean (WÜST, DEFANT, 1936). It is neither possible nor appropriate to describe and interpret these vertical sections individually. An interpretation can only suitably be given in conjunction with the phenomena of the oceanic circulation in the deeper layers. Figure 62 shows, as an example, a longitudinal section along the western side of the Atlantic giving temperatures and salinities (after WÜST, 1928). This runs from 75° S. near the area of formation of the Antarctic bottom water, through the Weddell Sea and the South Antilles Sea, along the western side of the West Atlantic Trough to the Newfoundland Banks through the Labrador Basin to the Davis Ridge. There is a vertical distortion of the section by a factor 1 : 1300. This section is quite typical of all sections through the Atlantic Ocean and shows the important characteristics of the meridional vertical temperature distribution: the two large warm-water accumulations in the subtropical troposphere of both hemispheres, the approach of the cold-water mass in the equatorial subtroposphere towards the surface, the concentration of the isotherms at the polar limits of the troposphere between 40° and 50° S. and 45°–55° N., and the oceanic polar fronts. This western section also shows at about 1000 m an intrusion of colder water from 55° S. towards the north as a tongue-shaped bulge on the isotherms which is visible even across the equator. In a central section this is only weakly developed, in an eastern section it is

not visible at all. It is caused by the intrusion of subantarctic intermediate water and represents the same phenomenon as the isothermal layer or actual inversion in the vertical distribution which was mentioned previously (see p. 123). South of 55° S. the oceanic space all around the Antarctic is filled down to the greatest depths with cold Antarctic water. The isotherms here steeply descend from the surface to 2500–3000 m, clearly showing the extension of this cold-water type northward along the deep basins that open to the south.

This, like all other longitudinal sections, shows the considerable asymmetry in the temperature distribution of the oceans. As previously mentioned this asymmetry is caused by topographic conditions of the Atlantic, which allow only a spreading of the cold heavy Antarctic bottom water towards the north. This is, of course, also the case in the Indian Ocean but not entirely so in the Pacific where, although only to a small extent, there is an Arctic component from the Okhotsk Sea to be taken into account. The meridional temperature contrast between high-southern and high-northern latitudes, which is especially well shown in the Atlantic and can also be seen in the Pacific Ocean, is the main cause of the deep-sea circulation of these oceans and also gives rise to their asymmetry relative to the equator.

(c) *Bottom Temperatures in the Three Oceans*

The question of the origin and the spreading of the lowermost layer of bottom water in the oceans was raised at a very early stage in the development of oceanography—much earlier than the problems dealing with the oceanic circulation of the middle layers. This was due to the existence of a greater amount of data for the bottom layer than for the middle and deep layers, since bottom temperatures were measured from cable-laying ships as well as from research vessels. The low temperatures found in the bottom layers clearly indicated at an early stage a polar origin of the bottom water and formed the main basis for the assumption of a deep-sea circulation. An historical account of the exploration of the nature of the bottom water has been made by WÜST (1936), who has also given a description and comparison of the movements of the bottom water spreading out into the three oceans based on a critical inspection of all the available data (WÜST, 1938). Plate 4 gives a chart of bottom temperatures on the deep-sea basins. The course of the isotherms is much more certain in the Atlantic than in the other incompletely explored oceans. The temperatures given are *potential* temperatures in order to give a clear picture of the spreading of bottom water influenced by the relatively large irregularities of the bottom topography. Table 67 gives mean values for 10° latitude zones in the three oceans and for the total ocean. In general, there is a continuous rise in the bottom temperature to be seen from high southern latitudes across the equator as far as to temperate northern latitudes.

The maximum temperature that can be taken as the boundary between Arctic and Antarctic influences at the bottom is situated rather asymmetrically at 40° N. in the Atlantic and at 30° N. in the Pacific. In almost all latitudes the coldest bottom water is found in the Indian Ocean. The coldest water is in the deepest depressions in the Atlantic South Polar Basin; the cold pole with -0.92°C lies at the western edge of the Weddell Sea, where according to BRENNKE (1921) and DEACON (1937) that thermo-haline stratification in the autumn and early winter exists, which permits the ice-cold shelf water to sink by convection along the continental slope down

to the ocean bottom. From here this cold heavy water spreads out in general towards the east within the Antarctic circumpolar Ocean to form the source of the meridional northward outflow along the deep-sea troughs of the Ocean. It is still uncertain whether there are other regions of bottom-water formation in the Antarctic, but that in the Weddell Sea is in any case the most important and the most intense one.

In each ocean the Antarctic bottom water spreads out both in zonal and meridional direction according to the bottom topography. There are seven cold streams of bottom water spreading out along the seven major longitudinal troughs of the oceans towards the north. These are listed in Table 68.

Table 67. Mean zonal distribution of bottom potential temperature (°C) in the deep sea (> 4000 m); mean for each latitude circle.

(After Wüst 1938)

Latitude	Atlantic Ocean	Indian Ocean	Pacific Ocean	All oceans
S. 70°	-0.71	—	-0.15*	-0.43*
60	-0.87*	-0.54*	0.06	-0.42
50	-0.33	-0.25	0.49	0.12
40	0.17	0.36	0.67	0.44
30	1.00	0.53	0.84	0.76
20	1.04	0.61	1.03	0.90
S. 10°	1.19	0.86	1.03	1.01
0	1.32	0.93	1.06	1.07
N. 10	1.66	1.16†	1.08	1.20
20	1.89	—	1.08	1.32
30	1.83	—	1.10†	1.33†
40	1.95†	—	1.00	1.32
N. 50°	1.81	—	1.06	1.22
Strongest meridional difference	2.82	1.70	1.25	1.76

* Minimum; † Maximum

Table 68. Initial temperatures and northward extent of the cold Antarctic bottom water

Deep-sea Trough	Initial temp. (°C) at 55° S.	Northern extent of cold water tongue (potential temp. 1.0°C)	
		To lat.	To cross ridge
1. West Atlantic	-0.8	8° N.	Para Rise
2. East Atlantic	-0.7	22° S.	Whalefish Ridge
3. West Indian	-0.6	10° N.	Carlsberg Ridge
4. East Indian	-0.3	5° N.	—
5. Western Pacific (Tasman Basin)	0.2	24° S.	Coral Rise
6. Central Pacific	0.4	25° N.	Hawaii Rise (?)
7. Eastern Pacific (South Polar Basin)	0.0	37° S.	Eastern Rise (?)

The distance to which each of these streams extend in each meridionally-oriented trough is very largely dependent:

(1) on the morphological form of the trough, on whether there are deep passages through cross-ridges or whether the stream can flow over any rises, and

(2) on the kind of water mass spreading above the cold bottom water towards the equator. It combines and interchanges with this and shows much stronger conservatism in its character of Antarctic water the lesser the influence of the water above. The most extended is the central Pacific cold stream which, due to the favourable topography and partly also because of the absence of deep warm currents in the North Pacific, reaches as far as 25° N. Also, in the Indian Ocean, the cold-water currents on both sides of the central ridge extend almost to the northern limit of the ocean. The most impressive one of these streams is, however, the west Atlantic cold water spreading where the Antarctic water penetrates through gaps from deep-sea basin to deep-sea basin as far as the Para Rise at 8° N., and finally warms up by mixing with the relatively warm North Atlantic deep water and flows into the North American Basin. In the East Atlantic Trough the Whalefish Ridge completely prevents further extension north and there is therefore a large difference in the temperature of the bottom water on the north and south sides of this cross-barrier. The bottom layers of the Atlantic Eastern Trough *north* of the Whalefish Ridge are formed by colder West Atlantic bottom water flowing in through deep gaps in the central parts of the Middle Atlantic Ridge at 0° latitude (Romanche Deep) and at 10° N. There are cross-rises also in the eastern and western deep-sea troughs of the Pacific that prevent the northward extension of Antarctic water beyond 22° and 37° S., respectively.

There is very little bottom water of *Arctic* origin. The most productive source is probably the outflow from the Okhotsk Sea which extends southwards as a cold stream, with an initial temperature of less than 0.6°C about 15° N. In the Atlantic deep-sea troughs there are indications of bottom water at less than 1.8° between 53° and 45° N. which is probably of subarctic origin.

A detailed investigation of the horizontal spreading of the Antarctic bottom water in the Atlantic has been made by Wüst (1936). Figure 63 shows the potential temperature along a quasi-meridional section through the Western and Eastern Troughs below 3000 m. In the western section the bottom water is separated from the water mass above by a marked discontinuity in the vertical temperature (and salinity) distribution. It descends from south to north with a gradient of about 20 m in 100 km and follows the bottom topography closely. Such influences on the temperature (and salinity) are recognized as far north as 40° N., 16,500 km away from the origin of the stream at the rim of the South Polar Basin.

The eastern quasi-meridional section is rather different. The barrier due to the Whalefish Ridge shows even more prominently here and the effect of the local inflow of Antarctic–West Atlantic water through the Romanche Trench is also clearly visible. From here and from the saddle at about 10° N. the bottom water spreads north and south in the eastern Atlantic Basin. The increase in temperature and salinity along the core of spreading of the relatively shallow bottom water is due to mixing processes with the warmer North Atlantic deep water above, comparatively of larger vertical extent. The distribution of temperature and salinity in the bottom water can be regarded as *stationary* and this can only happen when advection and mixing are in

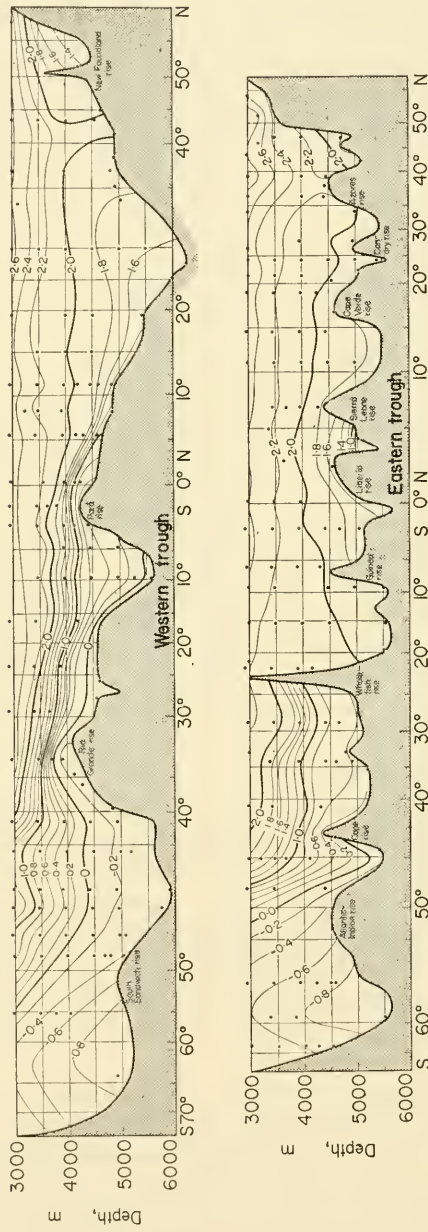


FIG. 63. Vertical distribution of potential temperature in deep and bottom water along longitudinal sections through the Atlantic Ocean (according to Wüst). (a) Longitudinal section through the Western Trough. (b) Longitudinal section through the Eastern Trough. The difference in spreading of the cold antarctic bottom current in the two troughs can be seen very clearly.

balance. From the distribution of these factors the ratio of the vertical exchange A_z to the velocity u of the spreading can be calculated (DEFANT, 1936). The value of A_z/u is between 2 and 3 over the transverse rises and between 5 and 6 in the troughs, with a maximum value of 10. Because this ratio as a first approximation is proportional to the Prandtl mixing length (see Chap. XIII) and this length is more suited for the characterization of a turbulent flow than A_z the above result therefore means that the mixing length is greater in the troughs than over the rises. In the core of this flow for a narrowing of the gap and corresponding increase in the velocity the mixing is somewhat reduced (more laminar flow), while in basins, on the other hand, the contrary occurs (velocity-decrease, stronger mixing).

6. Mean Vertically Integrated Temperature for Individual Oceans in Zonal Rings

Calculations of mean temperatures of parts of the sea, or of particular zones of latitude or for the total ocean, are of course only of statistical value. KRÜMMEL (1907) determined the values of some of these mean temperatures on the basis of the horizontal charts then available; Table 69. The mean temperature of the total ocean of 3.8°C appears very low especially compared with the surface value of 17.4°C. The decisive factor is the very large water masses of the oceanic stratosphere and the comparatively shallow oceanic troposphere. The mean values for 10° latitude zones show again the marked decrease of about 5°C between the equator and higher latitudes, but the differences between 40° N. and 30° S. remain, in general, small. This is also true for differences in the values for the three oceans.

Table 69. Mean vertical integrated temperatures °C for different oceans and the total ocean
(According to KRÜMMEL 1907)

Zone of latitude	Northern Hemisphere				Southern Hemisphere			
	Atlantic Ocean	Indian Ocean	Pacific Ocean	All oceans	Atlantic Ocean	Indian Ocean	Pacific Ocean	All oceans
0-10°	5.0	5.8	4.5	4.9	4.4	5.2	4.6	4.7
10-20°	5.1	7.4	4.1	4.8	4.2	4.8	4.7	4.7
20-30°	5.8	10.3	3.8	4.7	4.7	4.8	4.5	4.6
30-40°	6.1	—	3.1	4.5	3.7	4.2	4.1	4.0
40-50°	5.1	—	2.4	3.2	2.1	2.6	3.0	2.8
50-60°	3.8	—	2.3	2.8	0.6	0.8	1.4	1.0
60-70°	4.4	—	—	2.2	-0.2	-0.2	0.4	0.0
70-80°	—	—	—	(-0.6)	-0.2	-0.2	0.3	0.1
80-90°	—	—	—	(-0.9)	—	—	—	—
0-90° (resp. 80°)	5.3 ₅	6.5 ₇	3.6 ₆	4.3 ₄	2.9 ₉	3.4 ₄	3.7 ₂	3.4 ₇
90° N.- 80° S.	4.0 ₂	3.8 ₂	3.7 ₃	—	—	—	—	—

On the whole, the mean temperature of 3.8°C for the entire ocean makes a rather cold environment for the living organisms in it, however, they are mainly concentrated in the upper warmer layers.

Chapter IV

The Salinity of the Ocean, its Variation in Oceanic Space and in Time

1. Periodic and Aperiodic Variations of Salinity

If tidal effects are disregarded the most obvious periodic changes in salinity to be taken into account are the diurnal and annual variations. There is little data on daily variations. The diurnal variation of evaporation must give rise to a similar change in the salinity but it can have only little signification. Apart from the small diurnal variation in evaporation, the variations in salinity will be further diminished by the vertical convection set up immediately in the homogeneous top layer by increased salinity at the surface. The effect of an increase in salinity by a high evaporation rate will thus spread very rapidly over a large water mass and will scarcely be detectable.

The true salinity variation uninfluenced by other factors can only be shown by observations made at an oceanographic anchor station, and in this case also all stations that showed any appreciable vertical salinity gradient should be left out of account. At such stations the vertical displacements of water by the tides cause variations in salinity with a tidal period which are usually several times greater than the normal diurnal variations. A small diurnal variation can only be clearly shown in an almost completely homo-haline top layer. Five "Meteor" anchor stations between 21° S. and 4° N. gave the mean diurnal variation shown in Table 70.

The second column of the table shows the diurnal salinity variation as hourly values taken over three days at the "Altair" anchor station (44.5° N., 34° W.); see Fig. 64. The range is very small and amounts to less than half of 1/100 part ‰; there is a broad flat minimum during night time until sunrise after which the salinity rises, slowly at first and then rapidly, to a pronounced maximum in the late afternoon and falls off just as rapidly to the night values. Physically the process can be regarded as the effect of a positive transient source of salt at the surface, the surface amplitude of the effect being somewhat modified by vertical exchange with the layers underneath. The variation proceeds so regularly that despite its small amplitude it deserves more attention than it has hitherto received. VISSER (1928) deduced a value for the mean diurnal variation of the surface salinity by analysis of the observations of the "William Snellius" Expedition; this is similar to that found in the Atlantic: minimum at 04.00 h, maximum at about 17.00 h; but the amplitude was almost twice as large probably due to climatic conditions in the area.

Knowledge of the annual salinity variation is also rather meagre. BÖHNECKE (1936) has prepared charts showing surface salinities for each month in the North Atlantic and seasonal means of salinity for the total Atlantic which allow the annual

salinity variations to be found; these are supplemented by a chart showing mean annual amplitudes. Over the major part of the open ocean surface away from coastal areas the annual range in salinity in middle latitudes is less than 0.5‰, usually less than 0.25‰. A zone with more than 0.5‰ and a core with more than 1‰ and occasionally over 1.5‰ extends right across the Atlantic from South America to Africa between 5° and 15° N. and includes the area of the equatorial counter current. There is a further region with values greater than 0.5‰ and several cores about 1‰ in the Gulf Stream region until the south-east of the Newfoundland banks. Otherwise the maxima of annual variation are found in coastal areas especially off the mouths of the larger rivers (Amazon, La Plata, and the inner part of the Gulf of Guinea) with large seasonal variations in fresh-water inflow or in polar areas with seasonal melting of the

Table 70. Diurnal salinity variation

Time (hours)	Five "Meteor" stations 2.1° S.-4° N.	"Altair" anchor-station 44.5° N.-34.0° W.; 3 days
1	35.468	35.800*
3	35.466	35.866
5	35.464*	35.887
7	35.464	35.876
9	35.466	35.882
11	35.470	35.889
13	35.480	35.885
15	35.490	35.893
17	35.540†	35.913†
19	35.486	35.900
21	35.474	35.883
23	35.466	35.879
Range	0.042	0.040

* Minimum; † Maximum

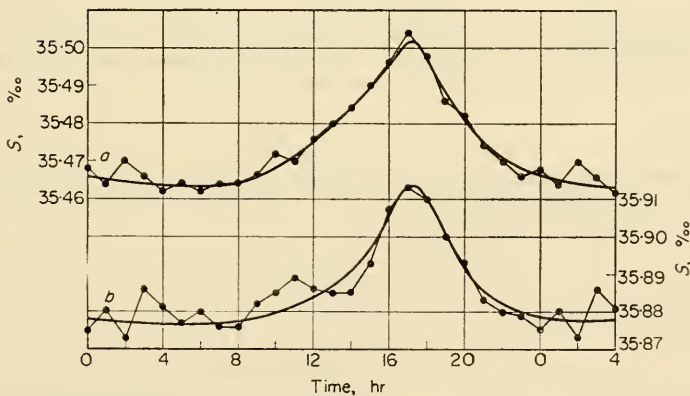


FIG. 64. Diurnal salinity variation. Above: the mean of five "Meteor" anchor stations between 21° S. and 4° N. in the Atlantic Ocean. Below: the mean for three days at the Altair anchor station (44.5° N., 34° W.).

ice (especially around Greenland, Tierra del Fuego and similar places). A special investigation of the annual salinity variation in the open North Atlantic has been made by SMED (1943).

NEUMANN (1938) has made a detailed investigation of the annual temperature and salinity variations over twelve five-degree squares for part of the Gulf Stream region between Newfoundland and about 25° W. (north and north-west of the Azores). These variations are presented graphically in detail in Fig. 65. It shows a rapid decrease

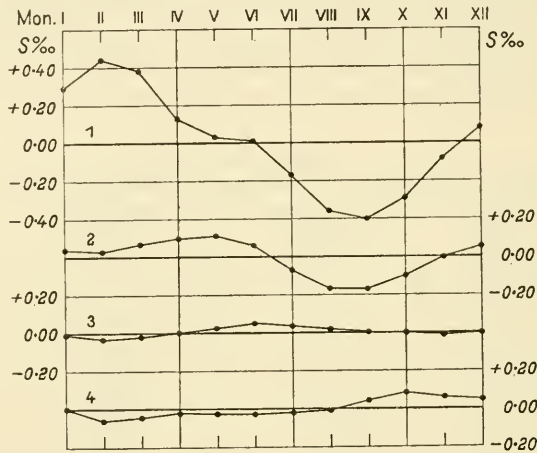


FIG. 65. Annual salinity variations in the North Atlantic between the Newfoundland Banks and the Azores (according to Neumann).

in the annual amplitude and a displacement of the maximum on moving from the west to the east and south-east away from the Newfoundland Banks, where the large annual change in salinity is due in the first place to seasonal changes in the inflow of salt with the Labrador Current. This area is the starting point of an annual disturbance that spreads out to the east and south-east and gradually diminishes in intensity due to mixing. This phenomenon can be treated theoretically† and comparison with ob-

† The differential equation governing the process requires that the local change $\partial s/\partial t$ of salinity with time and the change by horizontal salinity advection $u(\partial s/\partial x)$ should be exactly balanced by the change in salinity due to mixing $(A_y/\rho)(\partial^2 s/\partial y^2)$ so that

$$\frac{\partial s}{\partial t} + u \frac{\partial s}{\partial x} = \frac{A_y}{\rho} \frac{\partial^2 s}{\partial y^2}$$

The boundary condition for a linear increase in salinity from $y = -m$ to $y = +m$ on which is superimposed a periodic disturbance at $x = 0$ with a maximum amplitude at the zero point and vanishing at $y = \pm m$ may be formulated as

$$s_{x=0} = M + Ny + C \cos \frac{\pi y}{2m} \cos \frac{2\pi t}{T}$$

Then a general solution can be given in the form

$$s = M + Ny + C \exp \left[-\frac{\pi^2 A_y}{4m^2 \rho u} \right] \cos \frac{\pi y}{2m} \cos \left[\frac{2\pi}{T} \left(t - \frac{x}{u} \right) \right]$$

This solution gives a salinity distribution that varies with time in the region from $+m$ to $-m$ as a function of distance and time. The intensity of the disturbance decreases in the direction of flow according to a power of e -function.

served values leads to a maximum lateral exchange coefficient of $4.9 \times 10^8 \text{ g cm}^{-1} \text{ sec}^{-1}$ which in view of the intense mixing in the Gulf Stream is of an order of magnitude in good agreement with this coefficient (see p. 105).

From the extensive data available for the Australian-Asiatic Mediterranean (largely from the "William Snellius" Expedition) VISSER (1928) has determined the annual temperature and salinity variations and has discussed them in detail. The rather large annual variations here (more than 2.5‰) are also mainly produced by advection. Table 70a gives, as an example, some values for the eastern Java Sea. While the temperature shows the equatorial double wave with maxima in April and December and minima in January and August, the salinity shows only a single main maximum in September and single minimum in May. These phenomena are due to the monsoon change and the associated changes in advection. During the east monsoon cold saline water flows in from the east (May to August) and the salinity rises; it remains almost constant during the monsoon change (September to November) and falls from December to February, while the west monsoon carries water of lower salinity in from western Java Sea.

Table 70a. Annual temperature and salinity variations in the eastern Java Sea

	Jan.	Feb.	Mar.	Apr.	May	June	July	Aug.	Sept.	Oct.	Nov.	Dec.	Annual range
Temp. (°C) 26° plus:	1.88*	1.96	2.25	2.66†	2.41	1.79	1.05	0.74*	0.95	1.99	2.44	2.47†	1.92
Salinity (‰) 31 plus:	0.71	0.84	1.38	(0.88)	0.39*	(1.24)	2.10	2.73	2.98†	2.57	2.56	(1.64)	2.59

* Minimum; † Maximum; () Approximate values

In the interval between the monsoons from March to May the changes are only small. It is obvious that here also the advection of water masses of different salinities is the principal factor involved.

In the Polar regions the annual salinity and temperature variations may be due not only to the effects of advection but also to ice formation and melting thereby producing large amplitudes. The annual salinity variation may be increased to as much as 25‰ or more, but this occurs *only* in a very thin top layer; the layers underneath show only a small annual variation with a maximum in winter and a minimum in summer. This small annual variation can be regarded as a consequence of ice formation. Table 71 shows, as an example, conditions in the homogeneous top layer of the east Siberian Sea from November 1922 to October 1923.

SVERDRUP (1929) pointed out that between February and the end of May there was an increase of 0.47‰ in the salinity of the layer below the top layer. If this is assumed to be due to ice formation, and the ice formed is assumed to have a salinity of 5‰, then the increase observed corresponds to an ice layer 67 cm thick which is in agreement with actual measurement of ice thickness. The salinity decrease between May and August is about 0.55‰, corresponding to the melting of 87 cm of ice which is also in agreement with the observed values.

Footnote continued from opposite page

Knowing the amplitude of the variation in the region of the flow the quantity $A_y/\rho u$ can be calculated and knowing ρ and u a numerical value of the lateral exchange coefficient A_y can be found (see p. 106. *et seq.*).

Table 71. Monthly mean values for *T* and *S* in the homogeneous top layer in the East Siberian Sea, Nov. 1922–Oct. 1923

	Depth (m)	1922		1923			
		Nov.	Dec.	Jan.	Feb.	Mar.	Apr.
Temp. °C	0	−1.63*	−1.61	−1.60	−1.57	−1.58	−1.57
	10–30	−1.61 ₂	−1.62 ₆	−1.59 ₃	−1.59 ₀	−1.60 ₀	−1.60 ₅
Salinity (‰)	0	29.45	29.56	28.99	29.21	29.28	29.49
	10–30	29.50	29.50	29.23	29.20	29.36	29.46

	Depth (m)	1923						Annual range
		May	June	July	Aug.	Sept.	Oct.	
Temp. °C	0	−1.58	−0.98	0.80†	0.47	−0.21	−0.35	2.43
	10–30	−1.62 ₀ *	−1.58 ₇	−1.55 ₂	−1.48 ₆ †	−1.49 ₈	−1.52 ₄	0.13 ₄
Salinity (‰)	0	29.67†	29.25	24.70	23.58*	24.79	27.57	6.09
	10–30	29.67	29.71†	29.61	29.14	28.74	28.56	1.15

* Minimum; † Maximum

The annual variation in the surface salinity in an adjacent sea depends very largely on whether it has a humid climate with a large inflow of fresh water from rivers and from precipitation, or whether it is in an arid climate with little fresh-water gain but with a high evaporation rate. The latter type of adjacent seas with high salinities show only a small annual variation, since the evaporation has very little effect on the surface salinity; in the first type, on the other hand, the annual range may reach relatively large values. The annual surface salinity variation at the Adlergrund light-ship in the south-western part of the Baltic is presented as an example (NEUMANN, 1938) (Mean monthly values for the period 1926–35) in Table 72.

Table 72. Annual surface salinity variation at the Adlergrund light-ship (Baltic Sea) and total fresh-water inflow into the Baltic

	Jan.	Feb.	Mar.	Apr.	May	June	July	Aug.	Sept.	Oct.	Nov.	Dec.	Mean	Range
Salinity (‰) Variation	7.51	7.52†	7.50	7.45	7.39	7.30	7.31*	7.31	7.32	7.36	7.41	7.48	7.41	0.21
Inflow (km ³ /month)	23.1	26.8	34.4	59.8	84.2†	71.0	48.0	41.2	30.2	26.4	23.5	22.8*	40.09	61.4

* Minimum; † Maximum

These values follow almost exactly a pure sine curve

$$S = 7.41 + 0.103 \sin \left(\frac{2\pi}{T} t + 66.8 \right) + 0.006 \sin \left(\frac{4\pi}{T} t + 15.4^\circ \right),$$

with a maximum in January–February and a minimum in July–August. The most important factor affecting the amount of salinity in the Baltic is the inflow of fresh

water from rivers and from precipitation. There is therefore a very close correlation between the two phenomena if one applies a readily explicable phase difference of about two months. GEHRKE (1910) has already pointed out that this phase difference becomes smaller and smaller approaching the coast from the open sea. Similar conditions are found in the eastern part of the Baltic (GRANQUIST, 1938).

Of the occasional disturbances in the surface salinity occurring only for very short time due to the influence of external agencies, probably the most interesting is that caused by precipitation. It is to be expected that heavy precipitation of long duration will reduce the salinity. However, this reduction, first affecting the surface, will extend when precipitation continues down to deeper and deeper layers beneath the surface due to turbulent mixing. After the cessation of the precipitation there is a continued equalization of the salinity change by these turbulent processes that gradually eliminates the disturbances. Some data are found in the literature (KRÜMMEL 1907) on the relationship between precipitation and simultaneous and subsequent decreases in salinity, but these observations have been made from moving vessels and therefore do not permit an unequivocal quantitative determination of the effect of dilution by precipitation. NEUMANN (1940) has given some more recent results on the determination of salinity before, during, and after rain. Figure 66 shows three sets of observation made by the research vessel "Carimaré" of the surface salinity given as deviations ($1/100\%$) of the value at the time of the rain. In total agreement with each other all three cases show minimum salinity at the time and at the end of the rain. After the rain the salinity rose, at first rapidly and then more and more slowly to the value

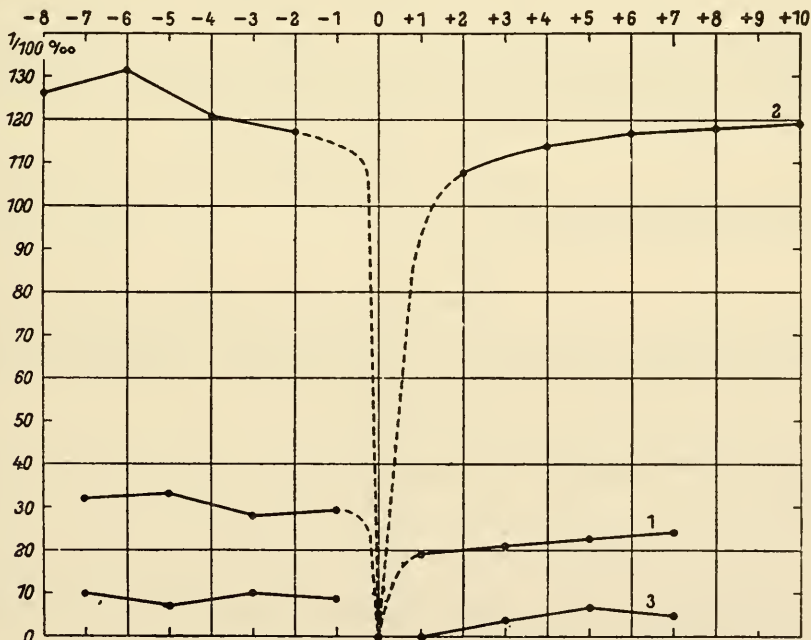


FIG. 66. Changes in surface salinity due to precipitation (according to the observations of the research vessel "Carimaré"). The zero point on the abscissa corresponds to: in case 1 (6-7 June, 1938 at 17.00 h); in case 2 (8 June, 1938 at 04.00 h); in case 3 (16 June, 1938 at 02.00 h).

present before the disturbance produced by rainfall, so that 2–3 h after the rain had ceased the salinity values did not differ from the value before the rain by more than 0.05–0.10‰.

A quantitative treatment of these processes has been given by DEFANT and ERTEL (1939). The rain water falling on the surface can be regarded physically as a salinity sink at the surface ($z = 0$) that consumes a quantity of salt $-\Sigma$ per unit time and unit area; this corresponds to an intensity in the salinity flux $-A_z(\partial s/\partial z)$ immediately at the sea surface $z = 0$ (A_z is the vertical exchange coefficient, s is the amount of salt in unit mass, z is counted positive downwards). This reduction in salinity extends downwards into deeper layers by mixing during the precipitation period according to the exchange equation

$$\frac{\partial s}{\partial t} = \frac{A}{\rho} \frac{\partial^2 s}{\partial z^2}.$$

At the start of precipitation ($t = 0$) the salinity should be uniform ($s = s_0$). Σ will be dependent on the intensity of precipitation and on the time t and therefore for a duration T of precipitation

$$\Sigma(t) > 0 \quad \text{for} \quad 0 \leq t \leq T$$

while at the end of precipitation

$$\Sigma(t) = 0 \quad \text{for} \quad t \geq T.$$

At large depths the disturbance will vanish so that for $z = \infty$ and for any time $s = s^*$. Solution of the problem for the given boundary conditions will give a complete answer for the entire process not only for the sea surface but also for all the layers underneath the surface. The simplest case is that where for the total duration T of precipitation Σ is constant for $0 \leq t \leq T$, while after the rainfall $\Sigma = 0$ for $t \geq T$.

In this case the solution for the total precipitation time T is

$$s = s^* - \left(\frac{2\Sigma}{\sqrt{(\rho\pi A)}} \right) \sqrt{t}$$

and when precipitation has ceased

$$s = s^* - \left(\frac{2\Sigma}{\sqrt{(\rho\pi A)}} \right) [\sqrt{t} - \sqrt{(t - T)}].$$

The maximum salinity disturbance q will reach by the end of the precipitation a value

$$q = \frac{2\Sigma \sqrt{T}}{\sqrt{(\rho\pi A)}}.$$

The salinity disturbance at the sea surface during the precipitation will follow the equation

$$s^* - s = q \sqrt{\frac{t}{T}} \quad \text{for} \quad (0 \leq t \leq T).$$

At the end of rain ($t = T$) q reaches a maximum value and then the disturbance decreases according to the formula

$$s^* - s = q \left[\sqrt{\frac{t}{T}} - \sqrt{\left(\frac{T}{t} - 1\right)} \right] \quad \text{for} \quad (t \geq T).$$

The change in time of a salinity disturbance at the surface of the sea caused by precipitation has the form shown in Fig. 67. Case 2 on Fig. 66 corresponds completely to the theoretical solution as far as the observations allow a comparison. For the time t required to reduce a salinity disturbance produced in a time T to a fraction q by turbulence alone the above equation gives

$$\text{for } q = \frac{1}{2} \quad \frac{1}{4} \quad \frac{1}{10},$$

$$t = 0.56 T \quad 3.52 T \quad 24.95 T.$$

Thus a salinity disturbance produced by precipitation lasting one hour would fall to one-tenth of its maximum value in about a day. Therefore, heavy rain can have an appreciable effect on surface salinity and in a discussion of frequent rainfall this circumstance deserves considerable attention.

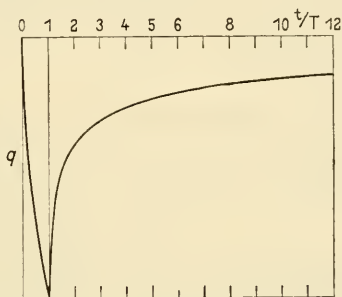


FIG. 67. Change in time in salinity due to precipitation at the surface according to the theory.

In addition to the precipitation, the melting of icebergs which have drifted into warm water can appreciably reduce the salinity in the remote and in the close surrounding waters. This process operates much more slowly than the precipitation but no data for investigation are as yet available.

The physical process should not be so very different except that the limited extent of an iceberg will confine it to a smaller space and it will thus have to be considered in three dimensions.

2. The Horizontal Distribution of Surface Salinity

The most detailed charts for the Atlantic Ocean are those prepared by BÖHNECKE (1936) based on all the available data. More recent charts for all the oceans have been given by SCHOTT (1928, and in improved form 1934); corresponding charts are also given in his geography of the Indian and Pacific Oceans (1935). Plate 5 shows such a chart on an equal area projection. The salinity of the open ocean varies between less than 33‰ in the north-eastern Pacific and a little more than 37‰ in the horse latitudes of the North Atlantic. The range of variations is little more than 5‰. All three oceans have zones of maximum salinity in the subtropics with maxima of more than 37.25‰ in the North Atlantic and the South Atlantic. In the open northern Indian Ocean the Arabian Gulf has maximum salinity values of more than 36.5‰ in sharp contrast with the low salinity of the Bay of Bengal. In the southern Indian Ocean towards Australia there is a subtropical oval region with a maximum salinity of more than 36.0‰.

In the Pacific the zonally oriented cores of maximum salinity lie between 30° and 20° N. with somewhat more than 35.6‰ and between 15° and 25° S. with about 35.6‰. Between the areas of the subtropical salinity maxima there is a belt of low salinity for all three oceans located in correspondence with the region of the equatorial counter currents.

On the polar side of the subtropical maxima in salinity there is a rapid decrease in salinity which is particularly pronounced in the Southern Hemisphere in all three oceans as far as the southern oceanic Polar Front (45°–50° S.). On the polar side of this the salinity remains everywhere a little less than 34‰ especially in the area of the Antarctic pack ice and drift ice. In the North Atlantic, due to the effect of the Gulf Stream and the Atlantic Current, there is a sharp difference between the eastern and western sides. In the eastern part there is only a slow decrease in salinity towards the north; in the western part shows a belt of low salinity (less than 32‰) associated with the Greenland and the Labrador Current which borders with a strong salinity gradient the warm, more saline Atlantic water.

Table 73. Factors increasing or decreasing the surface salinity.

Increasing	Decreasing
E = evaporation	P = precipitation
J_i = ice formation	I_m = ice melting
C^+ = surface circulation (advection of more saline water)	C^- = surface circulation (advection of less saline water)
M^+ = mixing with more saline deep water (turbulence and convection)	M^- = mixing with less saline deep water (turbulence and convection)
L = Solution of salt deposits (Gulf of Suez, Suez Canal, Gulf of Akaba)	R = Inflow of fresh water from the land (rivers, glaciers, icebergs) (run off).

Table 73 shows the factors listed by WÜST (1936), which increase or decrease the salinity at the surface of the ocean. For a stationary distribution of salinity the effect of all these factors at any point must balance. An analysis of the horizontal distribution of salinity in this way is not yet possible at the present time. However, if only the mean meridional distribution in the space between 40° N. and 50° S. is considered the above factors are considerably reduced so that a good correlation equation of the form

$$S = f(E - P, C, M)$$

could be expected. At first attempts have been made to determine the dependence of the salinity on the quantity $(E - P)$ from the available data. Recent calculations of this type have been made by WÜST (1930, 1936). Table 74 gives values of S , T and σ_t separately for the three oceans and for the total ocean. Values for $E - P$ are given later on in Table 87 (see Chap. VII, 3). Figure 68 shows the close relationship between the distributions of S and $(E - P)$. It has been found by accurate analysis that the correlation equation $S = f(E - P)$ for the entire ocean is linear:

$$70^\circ \text{ N.} - 10^\circ \text{ N.: } S = 34.47 + 0.0150 (E - P) \pm 0.11\text{‰},$$

$$60^\circ \text{ S.} - 10^\circ \text{ N.: } S = 34.92 + 0.0137 (E - P) \pm 0.09\text{‰}.$$

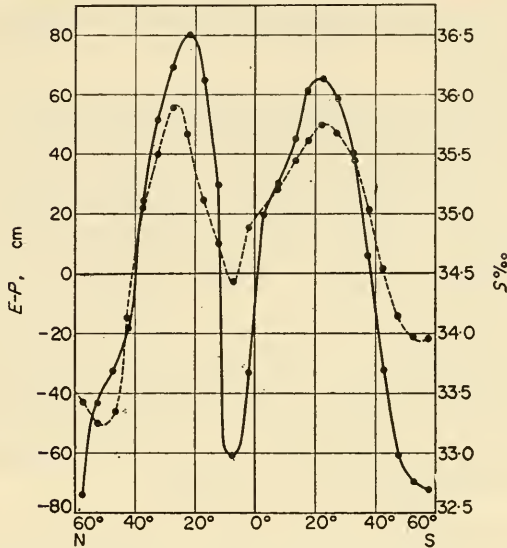


FIG. 68. Mean meridional distribution of evaporation–precipitation ($E-P$) and surface salinity for the entire ocean (according to Wüst, 1954).

Table 74. Mean values of salinity, temperature and density for 5° latitude zones for each ocean and for the total ocean including adjacent seas (Wüst, 1954)

Zone	Atlantic Ocean			Indian Ocean			Pacific Ocean			Mean for all oceans		
	° lat.	S(‰)	T(°C)	σ_t	S(‰)	T(°C)	σ_t	S(‰)	T(°C)	σ_t	S(‰)	T(°C)
N. 70–65	(33.5)	2.1*	(26.79)†	—	—	—	(30.0)*	(-0.6)*	(24.12)	(33.4)	(2.1)*	(2671)†
65–60	(32.45)*	(4.4)	(25.73)	—	—	—	(32.0)	(0.8)	(25.67)	(32.35)	(3.7)	(25.73)*
60–55	32.90	6.6	25.83	—	—	—	32.37	3.6	25.76†	32.66	5.2	25.84
55–50	34.56	8.8	26.82†	—	—	—	32.63	5.8	25.74	33.41	7.0	26.19†
50–45	34.80	11.4	26.53	—	—	—	32.98	7.7	25.74	33.69	9.2	26.08
45–40	34.90	14.9	25.94	—	—	—	33.53	11.8	25.51	34.14	13.2	25.70
40–35	36.47	19.3	26.08	—	—	—	33.98	16.2	24.93	35.11	17.6	25.48
35–30	36.91†	21.5	25.89	—	—	—	34.49	19.8	24.45	35.50	20.5	25.03
30–25	36.75	23.5	25.13	(39.57)†	25.6*	26.63†	34.95†	22.0	24.20	35.76†	22.7	24.62
25–20	36.74	24.8	24.74	36.92	26.2	24.44	34.90	24.4	23.47	35.6	24.6	23.98
20–15	36.22	25.7	24.04	35.27	26.8	23.00	34.61	26.0	22.76	35.14	26.0	23.16
15–10	35.90	26.2	23.67	35.13	27.5	22.67	34.29	27.0	22.14	34.76	26.9	22.59
10–5	35.18	26.7†	22.98	35.12	27.6	22.63	34.04*	27.5†	21.85*	34.43*	27.4†	22.18*
5–0	35.01*	26.6	22.87*	35.07*	27.8†	22.49*	34.54	27.4	22.27	34.73	27.2	22.47
N. 70–0‡	35.45	18.87	25.11	35.38	27.18	22.90	34.17	21.46	23.51	34.71	21.06	24.01
S. 0–5	35.65	25.5†	23.69*	35.01	27.6†	22.55	34.91	27.0†	22.67*	35.07	26.9†	22.85*
5–10	36.04	25.0	24.14	34.83	27.3	22.51*	35.20	26.6	23.01	35.25	26.5	23.09
10–15	36.65	23.9	24.94	34.62*	26.7	22.58	35.45	26.0	23.39	35.42	25.8	23.42
15–20	36.66†	22.7	25.26	34.93	25.3	23.22	35.65	24.9	23.88	35.62	24.6	23.96
20–25	36.34	21.7	25.34	35.34	23.4	24.09	35.70†	23.3	24.39	35.74†	23.0	24.51
25–30	35.98	20.6	25.37	35.69	21.2	24.98	35.53	21.2	24.86	35.68	21.1	24.99
30–35	35.53	18.4	25.59	35.81†	18.4	25.81	35.17	18.7	25.24	35.46	18.5	25.52
35–40	34.97	15.4	25.65	35.43	15.4	26.24	34.73	15.8	25.60	35.04	15.6	25.89
40–45	34.42	11.0	26.34	34.66	11.2	26.49	34.51	12.8	26.07	34.54	11.8	26.29
45–50	34.07	6.6	26.76	34.07	6.3	26.80	34.24	9.6	26.48	34.14	7.7	26.58
50–55	33.87	3.0	27.01	33.85	2.9	27.00	34.12	6.6	26.80	33.96	4.4	26.94
55–60	(33.88)*	(0.5)*	(27.19)†	33.88	(0.7)*	27.18†	(34.02)*	(3.2)*	(27.11)†	(33.94)	(1.7)*	(27.18)†
S. 0–60‡	35.31	16.07	25.63	34.84	16.08	25.08	35.03	19.64	24.65	35.03	17.99	24.99

* Minimum; † Maximum; ‡ Without polar zones; () Approximate values.

For the individual oceans the deviations from a linear form are larger and Wüst was able to show that these were due in the first place to mixing of the surface layers with the layers underneath.

This linear dependence although unequivocal cannot be taken as a casual physical relationship. This is readily seen, since if the surface salinity in an area was dependent only on the difference evaporation-precipitation the constant excess of evaporation (for always positive $E - P$) would cause it to rise continuously and a linear correlation could not be maintained. The simple linear dependence is only a part of the generally applicable equation $S = f(E - P, C, M)$ and to this equation adds the varying effect of advection and mixing (DEFANT, 1931). This influence enters into the above equation partly in the coefficient of the $(E - P)$ term and partly in the first term which represents primarily the effect of vertical mixing. If surface water of salinity S is mixed with water of constant salinity S_0 then the change of salinity due to mixing will be proportional to $S_0 - S$. The change of salinity due to processes of evaporation and precipitation will be proportional to $E - P$. Under stationary conditions the local change in surface salinity will be zero. Thus

$$\frac{\partial S}{\partial t} = a(S - S_0) + b(E - P) \quad \text{or} \quad S = S_0 + k(E - P).$$

As shown above, this formula has been confirmed empirically and this mixing in general proceeds with water masses of mean salinities of either 34.47‰ or 34.92‰. These values are mean values for the salinity at 400–800 m (subpolar intermediate water). The fact that the value S_0 is somewhat different for the individual oceans, as Wüst has shown, proves the correctness of this assumption. The North Atlantic north of 20° N. possesses a markedly high salinity which can be explained by the absence of the weakly saline subantarctic intermediate water at a depth of 600–800 m. The deep-reaching effect of the Gulf Stream and the strong inflow from the Mediterranean exert by mixing a noticeable effect on the surface layer. Conditions in the North Pacific are just the opposite. In contrast to the North Atlantic there is in the North Pacific a well-developed subarctic intermediate current at 600–800 m, which has its origin in the cold adjacent seas with a low salinity in the north-western Pacific Ocean. The strong negative anomaly in the North Pacific is certainly associated with this, because subtropical and adjacent seas are missing and therefore no inflow of water with high salinity can occur. The South Atlantic and the South Pacific with no adjacent seas and well-developed subantarctic intermediate water show similar but almost normal conditions. The difference $E - P$ is, however, always of decisive importance, and since it is closely related to the general atmospheric circulation it is clearly understood that the general outlines of the mean surface salinity must be controlled by the atmospheric circulation.

Returning to the horizontal charts, an understanding of all the salinity details in these charts involves not only the vertical mixing process with the layers underneath, but also all the other factors influencing the surface salinity distribution. It is, however, the oceanic and the atmospheric circulation that determine the details of the horizontal distribution of salinity. The factors “solution of salt deposits” and “inflow of fresh water” play no particularly far-reaching part although the last factor (R) of Table 73 has some importance in coastal regions.

3. The Vertical Distribution of Salinity (in Vertical Profiles and Sections)

(a) General Conditions

An increase of salinity with depth is not a necessary condition for vertical stability in the ocean, since in general the temperature decreases so rapidly that static stability is assured. In actual fact the highest values of the salinity in the individual oceans are found at the surface or in the uppermost layers and usually a decrease of salinity downwards. Figure 69 shows the vertical distribution of salinity down to 4000 m for the same station as in Fig. 52. From 40° N. to 50° S., i.e., in the troposphere, S decreases rapidly below a more or less homo-haline surface layer of varying thickness. The strong

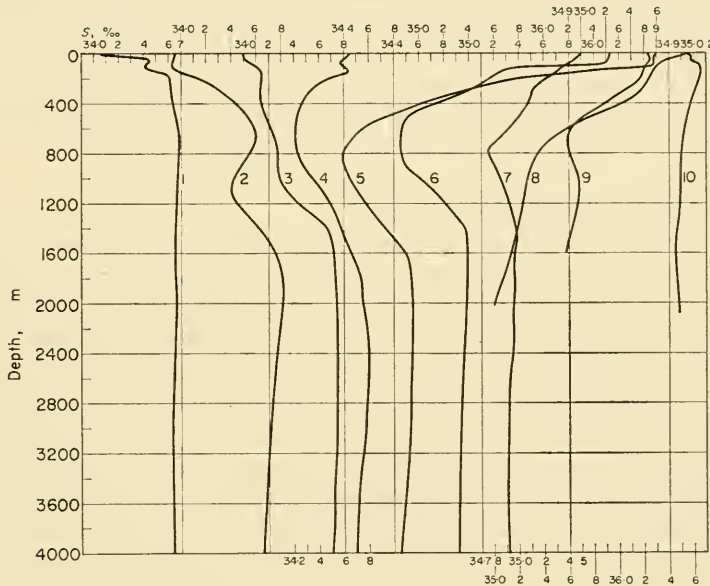


FIG. 69. Vertical salinity curves for a series of oceanographic stations along a meridional section through the Atlantic (corresponding vertical temperature curves are shown in Fig. 52).

Footnote from opposite page

† This is demonstrated by the low salinity of the adjacent seas with a strong freshwater inflow (such as the Black Sea and the Baltic a.o.) and can also be seen in coastal areas where there is a large fresh-water inflow. The effect of these frequently turbid river waters is often found surprisingly far out at sea. Charts of the mouths of the major rivers (Amazon, Congo, Tajo, La Plata) usually contain a limited area in which the lighter water shows at the surface on top of the heavier sea-water; but this is usually only the case in a thin layer and already in the wake of a ship the sea-water of much more blue colour may be brought to the surface. An investigation of the mixing of the lighter river water and the heavier sea-water at the mouth of a large river would be of some interest. The Suez Canal shows the great effect on the salinity of solution of a salt deposit, in this case at the bottom of the great Bitter Lake which is connected by the canal with the Mediterranean and with the Gulf of Suez. Water of lower salinity flows in from both sides and causes a progressive dissolution of the salt deposit and maintains in that way the high salinity of the water above at 50‰ at the surface and 56‰ at the bottom (about 10 m depth). Since the canal was first built (1869) when the water depth was 7.56 m dissolution of the salty canal bottom has increased the depth here linearly to give a depth in 1921 of 11.7 m. At the same time the salinity of 68‰ in 1872 had fallen to about 52‰ by 1924. The available and, in parts, sparse data on the distribution of salinity in the Suez Canal and on the currents caused by it have been dealt with by WÜST (1934, 1935) in two interesting papers.

decrease in temperature in these layers is thus associated with a strong decrease in the salinity. This extends down to about 800 m where the salinity reaches a minimum of 34.3–34.9‰. There is then a second increase to about 34.8–34.9‰ at about 1600–2000 m and then a further slow decrease is generally observed down to the bottom. The inversion in salinity at 800–1000 m becomes weaker and weaker towards higher northern and southern latitudes, and from the polar fronts of both hemispheres towards the poles it is entirely missing; the vertical differences are then small with usually a slight increase in salinity if fresh water has not been added to the surface layers by the melting of ice, but this becomes weaker and weaker towards the poles. In contrast to this vertical distribution generally found, the North Atlantic shows a pronounced peculiarity in middle latitudes which can be seen at some of the stations in Fig. 69. The intermediate salinity minimum at about 800 m is missing here, and from the core of upper layer of high salinity situated in middle latitudes the salinity decreases almost uniformly down to the bottom. There is thus a marked asymmetry between North and South Atlantic vertical distributions of salinity.

(b) The Salinity of the Oceanic Troposphere

The vertical distribution of salinity in the troposphere layers of the subtropics and the tropics is worth a somewhat more detailed description. It has, of course, been investigated more closely in the Atlantic (DEFANT, 1936). Almost all stations in the tropics and subtropics show a nearly *homo-haline top layer*. Its thickness is not the same as that of the thermal top layer but is usually somewhat smaller. In many cases just below the quasi-isothermal top layer, however, still in the upper part of the thermocline, there is a more or less well-developed *salinity maximum*. This maximum is one of the most characteristic phenomena of the vertical salinity distribution of the upper troposphere. Figure 70 shows an example of this. The "Meteor" 256 station shows the maximum particularly well developed; in a thin layer from about 50 m the salinity rises from about 36.1 to 37.0‰ and then falls again to the previous value. It is worth noting that the salinity maximum appears there where the first drop in temperature occurs beneath the isothermal surface layer and not at about the maximum temperature gradient of the thermocline (see Fig. 71). The salinity maximum thus extends just *above* the thermocline, but does not fully coincide with the density transition layer, the position of which is in turn fixed by the high salinity value. Careful investigation of this salinity maximum in the tropical and subtropical regions of the Atlantic has shown that it is almost always present. Starting from the extensive subtropical accumulation of very saline water (at about 25° S. and at about 30° N.), where in a top layer down to the thermocline a homo-haline structure is found, a thin layer of maximum salinity spreads out northward in the Southern Hemisphere and southwards in the Northern immediately above or directly inside the thermocline. This spreading occurs below the upper part of the top layer, in which salinity decreases in both hemispheres towards the equator.

From this it can be concluded that the layer of the salinity maximum is formed from the lowermost parts of the subtropical high salinity water by currents flowing towards the equator. It thus represents the *intrusion of highly saline water* under the surface layers of lower salinity of the equatorial regions and forms a part of the upper tropospheric circulation.

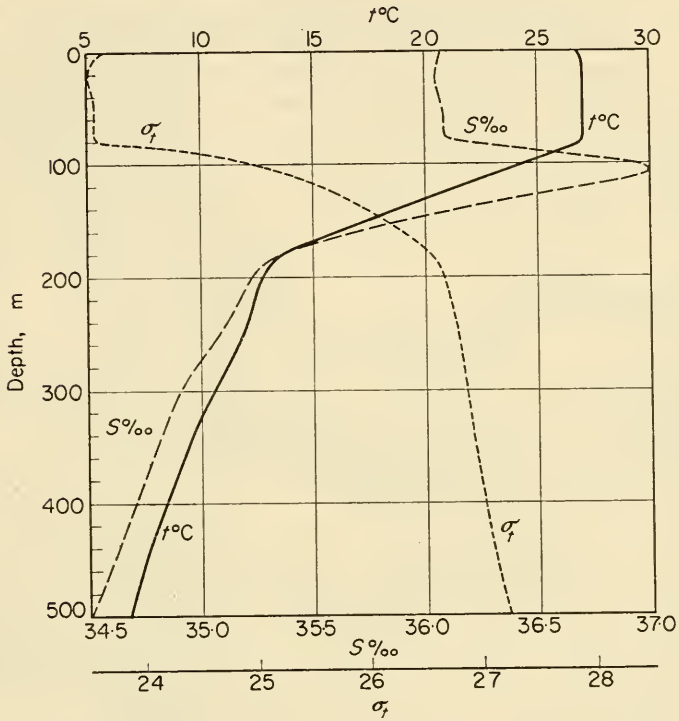


FIG. 70. Vertical temperature, salinity and density curves for the troposphere at "Meteor" Stn. 256 ($\phi = 2.4^{\circ}\text{ S.}$, $\lambda = 39.3^{\circ}\text{ W.}$).

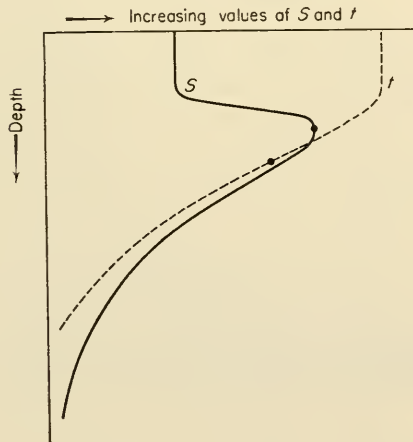


FIG. 71. Position of the tropospheric salinity maximum relative to that of the thermocline (schematic).

While the entire area between the belts of subtropical highly saline water in the Northern and the Southern Hemisphere show these salinity maxima, just above or inside the thermocline *two belts without maxima* stand out sharply; one between 10° and 15° N. and extending from 45° W. eastwards to the African continent and a second, but more narrow belt, between 2° S. and 3° S. and extending from 30° to 10°, which is particularly well developed in the central part of the Atlantic Ocean (see Fig. 72). These two belts without salinity maxima more or less mark the southern

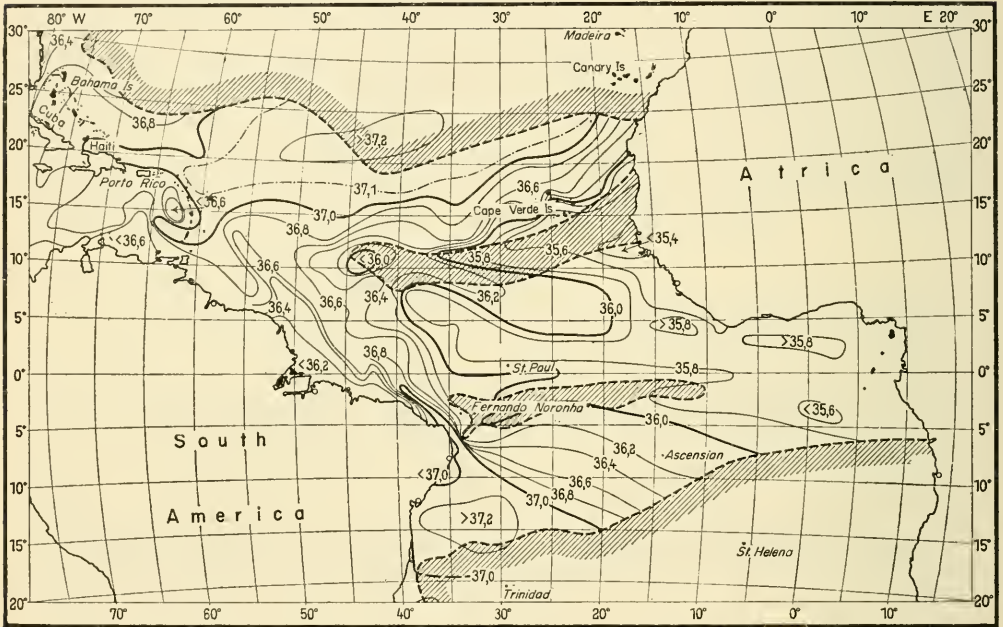


FIG. 72. Distribution of salinity in the tropospheric salinity maximum in the subtropic and tropics of the Atlantic.

and northern limit, respectively, of the subtropical water masses spreading towards the equator. Between these two belts from about 7° N. to the equator the maximum appears again and may be very pronounced. This is the region of the Equatorial Countercurrent which is fed at a depth of 80–100 m from regions west of 35°–40° W., which are situated outside the area with no maximum. The salinity maxima of the tropics and the subtropics are thus very closely connected with the tropospheric circulation in these areas. The best illustration of the formation, extent and intensity of this very pronounced thin layer of high salinity lying between low salinity layers (above and below) is given by a vertical cross-section along the core of the Equatorial Countercurrent and the Guinea Current in the Atlantic Ocean. This section is shown in Fig. 73. It starts in the central Atlantic at about 18° N., 37° W., proceeds southwards to 10° N., 38° W. and then along the core of the Equatorial Countercurrent, finally reaching the inner Gulf of Guinea. The layer of maximum salinity spreads southward from the homo-haline top layer of the subtropical North Atlantic below the low salinity surface layer towards equatorial latitudes. If the 35.5‰ isohaline is

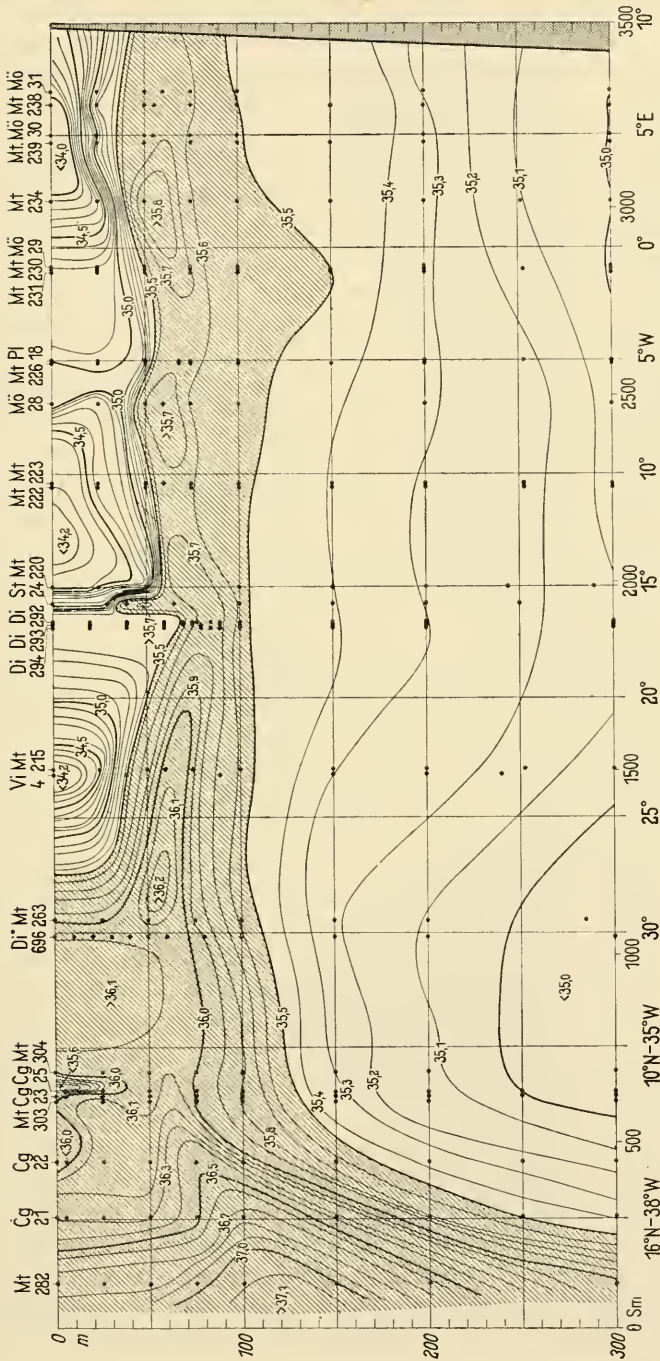


FIG. 73. Vertical salinity section along the Equatorial Counter Current and the Guinea Current in the Atlantic. (In the central Atlantic running from 18° N., 37° W. to 10° N. 38° W. then along the main axes of these currents.)

taken as the upper and lower limit of the layer with maximum salinity it has an average vertical thickness of only 50 m; it stays about the same thickness over its long course to well within the Gulf of Guinea, and the salinity of the core layer changes very little after it has lost its tongue-like form along the first half of its route. A comparison of the salinity section with a corresponding density section shows that the position of the salinity maximum along the greater part of the cross-section coincides with the strongest vertical concentration in the density field. The very saline water thus extends in a thin layer along the *thermocline* itself. The spreading in this layer is caused by advection and turbulence but the latter factor must be of very little effectiveness, because of the almost unchanged character in this remarkably thin layer over such large distances. It must be supposed that above and below the thermocline the transport of water with maximum salinity is accompanied by strong mixing with the water above and below, but that in the thermocline itself the stability strongly suppresses turbulence, so that the almost horizontal spreading takes the character of a *laminar* flow. This has been confirmed by calculations of the vertical exchange coefficient in the area of the Equatorial Countercurrent by MONTGOMERY (1939), who found $A_z = 0.4 \text{ g cm}^{-1} \text{ sec}^{-1}$ along the axis of the Countercurrent. Since lateral mixing was neglected in these calculations the value found will be a maximum value; the true one must approach rather closely the molecular diffusion coefficient for salt in water (0.011). As mentioned above, the spreading must therefore be of laminar character. However, in horizontal direction lateral mixing is very effective and the lateral exchange coefficient A_y reaches the value of $4 \times 10^7 \text{ g cm}^{-1} \text{ sec}^{-1}$, generally found.

From the deep-reaching accumulations of warm and saline water in the subtropics there is not only a flow of this water towards the equator but also towards the poles in somewhat deeper layers. Thus at depths only a little below the upper layer, and the almost homo-haline top layer which shows decreasing salinity towards the pole, there is a secondary maximum in the vertical distribution of the salinity. In the Southern Hemisphere this poleward flow of highly saline water occurs first at a depth of 100 m, but descending to a depth of 150 m or more, and continues on over a very broad front across the entire ocean; however, the energy of this outflow is soon dissipated and the maxima disappear due to mixing. In the Northern Hemisphere this maximum is associated with the Gulf Stream and its continuation (the Atlantic Current) and it can be followed across the entire Atlantic Ocean into the Norwegian Sea and further polewards. Figure 74 shows a longitudinal salinity section given by SCHOTT (1942) through the Atlantic Current from the Wyville-Thomson Ridge past the Shetland Islands as far as Spitzbergen. The Atlantic water soon descends underneath the cold and low saline polar water of the surface layer. Although the salinity maximum is decreased by mixing it can still be traced in the North Polar Basin and into the Barents Sea. Its occurrence here was discussed in connection with the description of the vertical temperature distribution in the North Polar Basin (see p. 133). An interesting and, from the point of view of the method used, important study of this spreading of Atlantic water ($\vartheta = 10.2^\circ$, $S = 35.45\%$) in the northern part of the North Sea, in the Norwegian Sea and in the Barents Sea and its mixing with the surrounding water ($\vartheta = 2.5^\circ$, $S = 34.90\%$) made by JACOBSEN (1943) should specially be mentioned here.

From our knowledge of the tropospheric salinity maxima of the Pacific and the

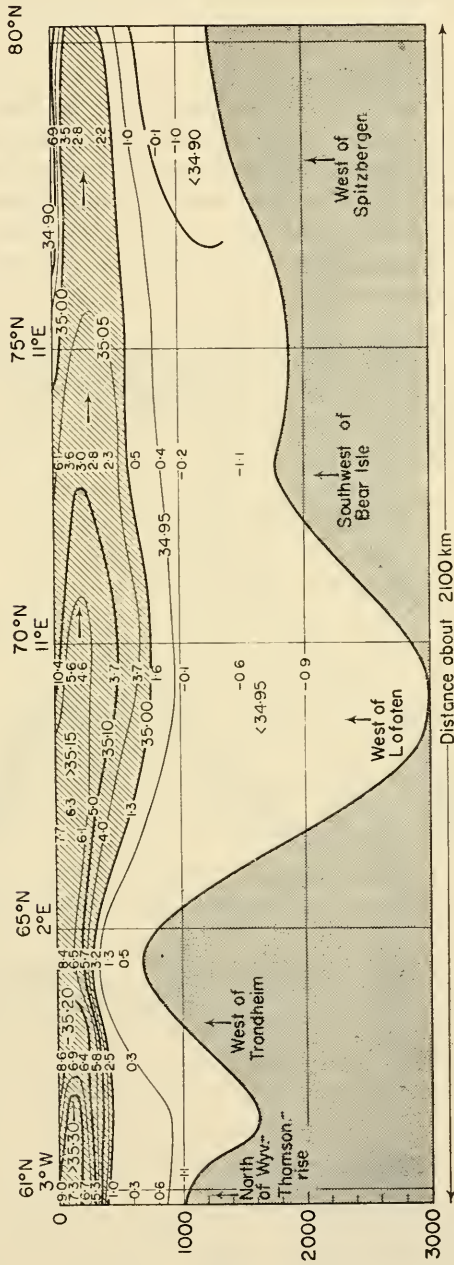


FIG. 74. Longitudinal salinity profile along the core of the Atlantic Current from The Wyville Thompson Ridge, over the Shetland Islands to west of Spitzbergen (according to Schott).

Indian Oceans, we know their formation and spreading are still very pure. The much stronger intensity of this phenomenon in the Pacific Ocean has been shown by several recent oceanographic stations but detailed information about their extent is still lacking.

(c) *The Salinity of the Stratosphere*

The vertical salinity distribution in the stratosphere of the three oceans can best be discussed by means of longitudinal sections through the Atlantic, the Indian Ocean and the Pacific. The longitudinal section through the Atlantic Ocean is that given by WÜST (1936) through the Western Trough from the Weddell Sea to Davis Strait (see Fig. 62). In the Indian Ocean a central section (Fig. 75) from the Antarctic to the southern tip of India has been selected (MÖLLER, 1929); the Pacific Ocean is characterized by a vertical section through its eastern half (Fig. 76). In the northern part this section

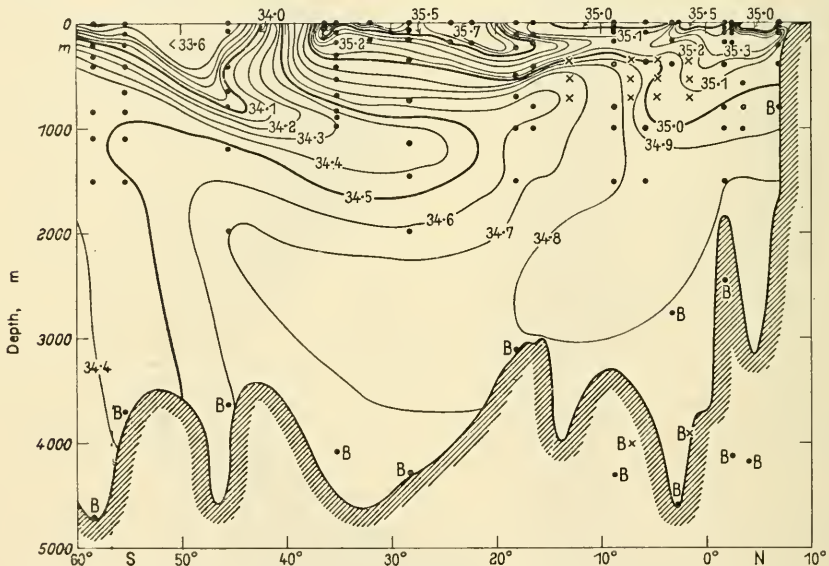


FIG. 75. Longitudinal salinity section through the central part of the Indian Ocean.

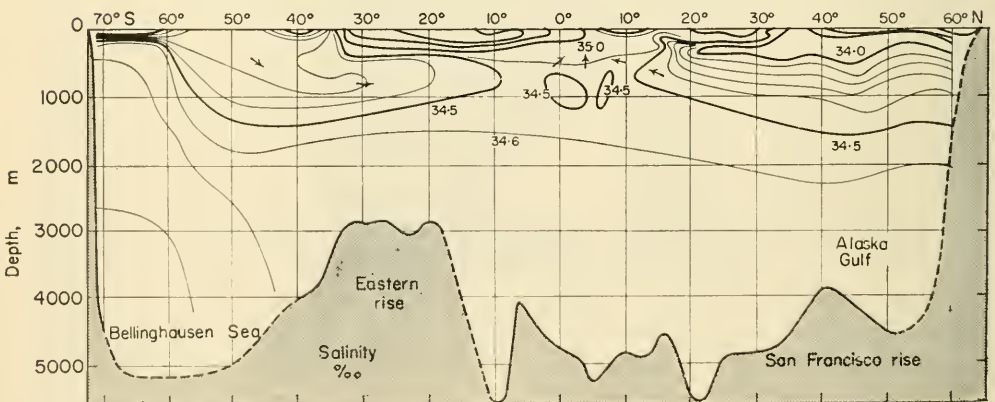


FIG. 76. Longitudinal salinity section through the central part of the Pacific Ocean.

is based on the "Carnegie" observations (Sverdrup) and south of 40° S. on the "Discovery" observations (DEACON, 1937). Longitudinal sections through the western and central parts of the Pacific Ocean have been given also by WÜST (1929).

(d) *Subpolar Intermediate Water*

At 800–1000 m there is a characteristic low salinity zone extending across almost the entire ocean though not always equally well developed. In the south it begins always just south of the oceanic polar front where this special water mass sinks rapidly from the surface to a depth of 800 m and spreads out from here with decreasing vertical thickness and decreasing salinity in its core into the *Atlantic* across the equator to about 20° N. It can still be traced north of here until it joins the deep and saline water accumulations of the subtropics. There is little to be seen from an Arctic counterpart to this *subantarctic intermediate* water. Only in the western section weak indications of such arctic intermediate water may be found as far as the Newfoundland rise.

Also in the Indian Ocean this intermediate water is found everywhere underneath the high saline water mass south of the subtropics as an intrusion of low saline water with its core somewhat deeper than in the *Atlantic* (approx. 1000–1200 m). In the *Pacific* tongues of low saline polar water spread out below the high saline troposphere almost to the equator, from both north and south. The Antarctic branch of low saline water forms just south of the oceanic polar front at 50°–60° S.; the arctic branch formed in the area of the Okhotsk Sea is weaker; in the western and central parts of the Pacific Ocean it can be followed to about 10° N. It is completely absent in the whole of the eastern part of the Pacific and there is thus an asymmetry in the salinity distribution similar to that in the *Atlantic Ocean*.

The vertical thickness of the subantarctic intermediate water is about the same in all the three oceans (about 600 m) and it is separated from the troposphere above by a sharp salinity (and density) transition layer. It is of particular interest that the intermediate water is found with the same characteristics and thickness across the entire transverse section of the ocean, especially in the *Atlantic*. Evidence for this is given in Fig. 77 which gives a cross-section of salinity through the *Atlantic* at about 22° S. This uniformity of this water across the total cross-section can be regarded as a consequence of strong lateral mixing which leads to an equalization of all existing major horizontal salinity differences.

A detailed investigation of conditions in the subantarctic intermediate water and its meridional spreading in the *Atlantic* has been given by DEFANT (1936). The vertical salinity distribution in successive cross-sections normal to the main direction of spreading is best characterized by the dimensionless quantity $(s_0 - s)/(s_0 - s_m)$, where s_0 ($=34.85\%$) is the salinity which the subantarctic intermediate water takes on by continuous mixing with the surrounding water and s_m ($=34.19\%$) is the salinity of the subantarctic intermediate water in its region of origin before spreading out towards the north. The quantity $(s_0 - s_m)$ corresponds to a potential difference present between the two oppositely moving types of water which is finally eliminated by mixing. Determination of this quantity in cross-sections, 500 km apart from each other, for the core layer (salinity minimum) and for several layers above and below this core allows of construction of lines of equal values of the quantity $(s_0 - s)/(s_0 - s_m)$ expressed in percentage of intermediate water. These lines then illustrate the mixing process

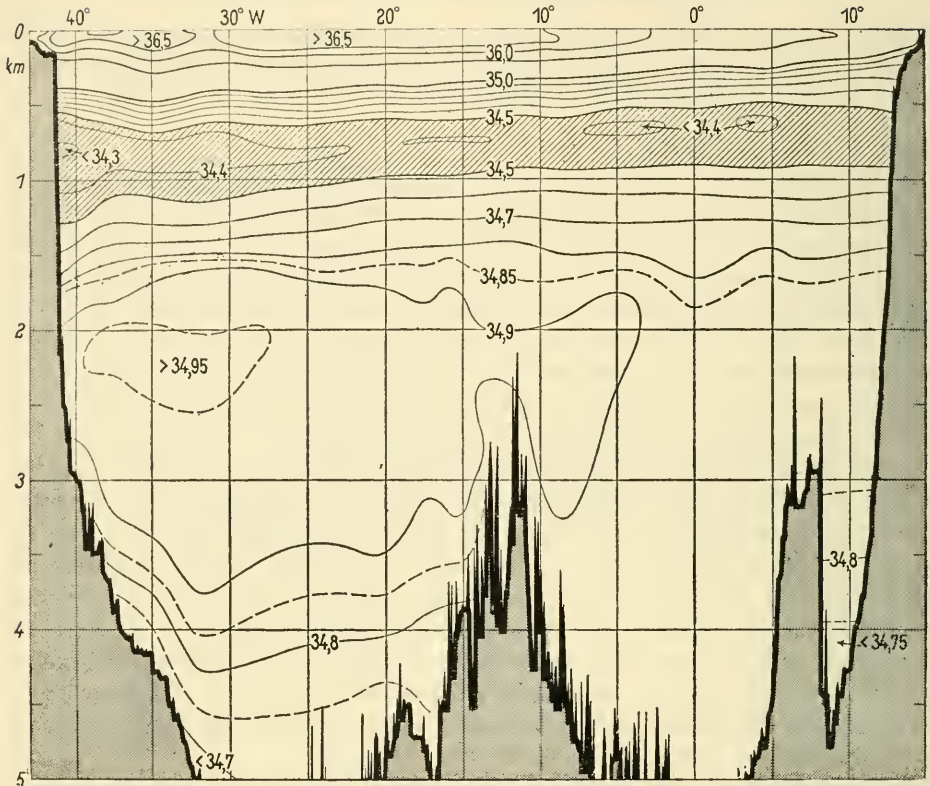


FIG. 77. Cross-section of salinity through the Atlantic Ocean at about 23° S (profile VII at 24°-21°-25° S., of the "Meteor" Expedition).

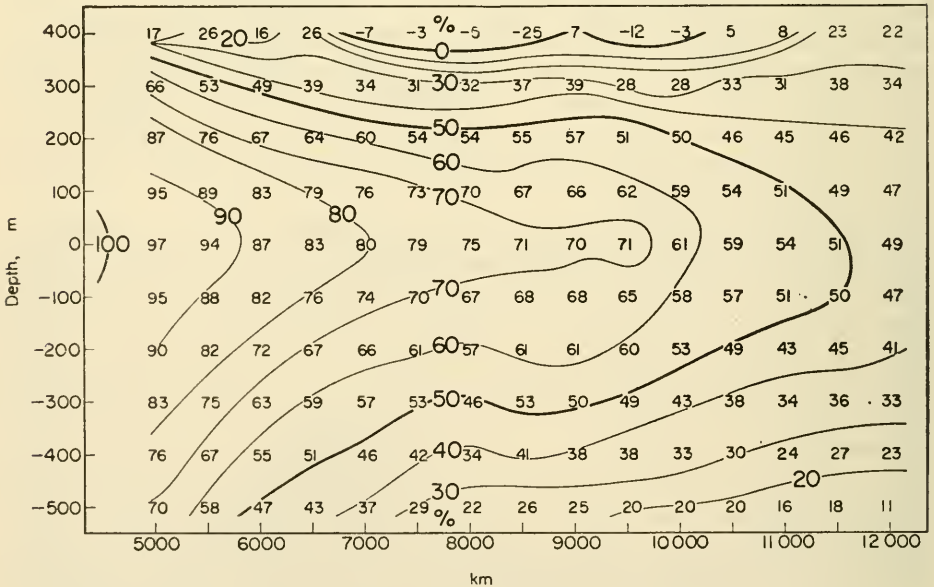


FIG. 78. Percentage of subantarctic intermediate water in the core layer of this water type the western side of the Atlantic. (Distribution of the quantity $(s_0 - s)/(s_0 - s_m)$ in per cent.)

along the entire spreading area for the entire western section through the Atlantic Ocean (Fig. 78). This distribution has a clear similarity to that presented in Fig. 48 which shows the radial and turbulent spread of a particular water mass into surrounding waters. This distribution also corresponds to the processes of spreading in a so-called "jet" (Freistrah) (PRANDTL, 1926; TOLMEIN, 1926; RUDEN, 1933). Figure 79

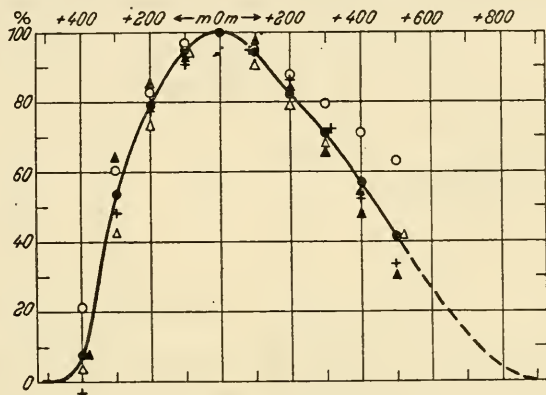


FIG. 79. Distribution of salinity relative to the minimum in the core layer of the subantarctic intermediate water along the western side of the Atlantic for different vertical cross sections.

shows for each cross-section the distribution of salinity *relative* to the minimum in the core and shows that the general distribution is the same for all cross-sections and that the processes involved must be essentially the same, geometrically and mechanically, as in a "jet".

An accurate knowledge of the salinity values throughout the entire region of the subantarctic intermediate water allows the vertical distribution of the quantity $A/\rho u$ to be calculated from the equation on p. 106 for all cross-sections.

A rough calculation shows at once that vertical mixing and advection are able to maintain the tongue-formed salinity distribution *stationary* in the subantarctic intermediate current. The vertical salinity distribution at a distance of 8000 km from the zero point of the western section (about 13° S.) is as follows

	+300	+200	+100	core	-100	-200	-300	-400 (m)
salinity in %	34.71	0.54	0.42	0.38*	0.44	0.52	0.60	0.69
vertical gradient (per 100 m)	-0.17	-0.12	-0.04	+0.06	+0.08	+0.08	+0.08	+0.09

Considering a vertical water column of 1 cm² base between +250 and -250 m the inflow of salt into the column from above and below is shown in Fig. 80, taking $A = 4 \text{ g cm}^{-1} \text{ sec}^{-1}$. The salt gain in the entire volume ($5 \times 10^4 \text{ cm}^3$) thus amounts to $1.00 \times 10^{-7} \text{ g/sec}$ or 8.64 mg/day. Without an advective outflux this continuous gain of salt would soon eliminate the salinity minimum of the subantarctic intermediate water. Through the left-hand (southern) boundary of the water column (with an area of $5 \times 10^4 \text{ cm}^2$) there enters an amount of salt of $5 \times 10^4 \times u \cdot s \times 10^{-3} \text{ g}$, where u

is the velocity of the horizontal advection. At the right-hand (northern) boundary there is at the same time an outflow of $5 \times 10^4 \times u \cdot s_1 \times 10^{-3}$ g of salt from the entire volume so that the loss of salt in g/sec will be $50u(s_1 - s)$. For a stationary salinity distribution this loss must be compensated by a gain due to mixing, that is by 1.0×10^{-7} g/sec. Taking u equal to 5 cm/sec, this is only possible for a horizontal salinity gradient of $(s_1 - s) = 4 \times 10^{-10}$ ‰/cm in the current. The salinity at 7000 km

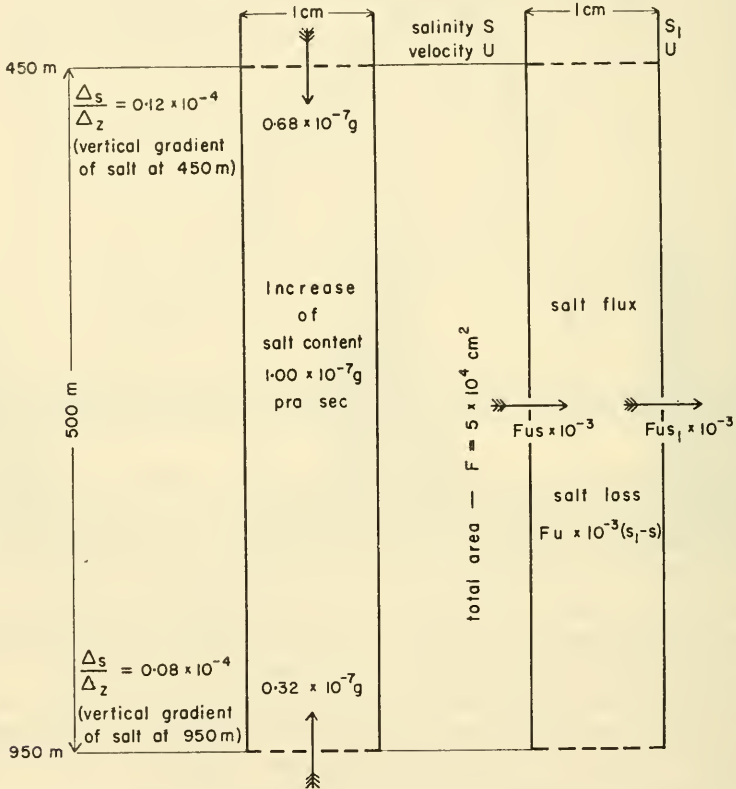


FIG. 80. Salinity exchange and advection. For $u = 5$ cm/sec results salinity gain = salinity loss: $5 \times 10^4 \times 5 \times 10^{-3} (s_1 - s) = 2.41 \times 10^{-7}$ or $(s_1 - s) = 0.97 \times 10^{-9}$ ‰ per centimetre.

distance in the core of subantarctic intermediate water is 34.34‰, at 9000 km, however, 34.42‰, so that according to the observed values there is a salinity gradient of 0.08 ‰ for the 2000 km = 2×10^8 cm. This gives exactly the value derived above of 4×10^{-10} ‰/cm. The vertical and horizontal salinity distribution in the subantarctic intermediate current at this point can thus remain stationary with values of $4 \text{ g cm}^{-1} \text{ sec}^{-1}$ for A and 5 cm/sec for u . The ratio

$$A/\rho u = \frac{4}{5} = 0.8 \text{ cm/sec}$$

satisfies therefore the condition of a stationary state of the phenomenon in time. It is fairly easy to see that the above calculation gives only the quantity $A/\rho u$ and not the absolute value of the individual quantities.

Using the above mentioned relationship the quantity $A/\rho u$ can be determined numerically for every point more accurately than in the rough calculation made here by deliberately selecting a large water column.

Table 75. Mean values for $A/\rho u$ for transverse sections (normal to the direction of spreading) through the subantarctic intermediate water in the Atlantic

Position of sections	Vertical distance from the core (m)							Mean depth of the core (m)
	+300	+200	+100	0	-100	-200	-300	
37°-30° S.	3.5	2.0	1.3	1.0	1.2	1.7	2.4	850
27°-21° S.	2.8	1.7	1.0	0.7	1.6	3.0	3.0	800
25°-12° S.	2.4	1.4	0.8	0.4	1.3	3.2	3.9	725
3° S.-2° N.	(2.2)	1.4	1.1	0.9	1.2	2.2	3.2	700
4°-8° N.	(2.3)	1.7	1.7	1.0	1.6	2.4	3.4	625
Mean	2.64	1.64	1.12	0.82	1.38	2.50	3.18	740

Table 75 shows that the vertical distribution of $A/\rho u$ scarcely changes along the entire region of spreading: $A/\rho u$ is least at the core of the spreading water (on the average 0.82) and rises steadily both above and below with the distance from the core to large values (about 3). If the distance from the core axis is denoted by z , then $A/\rho u = f(z)$.

When l is the Prandtl mixing length

$$A = \rho l^2 \frac{\partial u}{\partial z}$$

and therefore

$$f(z) = \frac{l^2}{u} \frac{\partial u}{\partial z}$$

Integrating this equation for constant l from the core ($z = 0$), to a distance b above and below the core then, since $\partial u/\partial z$ is always negative,

$$\int_0^b f(z) dz = -l^2 \ln \frac{u}{u_0},$$

where u_0 and u are the values of u in the core and at a distance b from the core. The value of the left-hand side can be found from Table 75 and this gives, knowing l , the ratio of u/u_0 as a function of the vertical distribution and thus also of the quantity A/A_0 , where A_0 and A are the exchange coefficients in the core itself and at a distance b from it. The constancy of l can be tested on the plausible assumption that the velocity of the current within a distance of ± 300 m from the core falls to a low value; over a wide region l is almost constant with a value of about 150 cm. The results of the calculation are shown in Fig. 81. The relative distribution of velocity over a transverse section has a striking similarity to that distribution found *experimentally* in turbulent spreading processes in a "jet". This justifies the conclusion that the spread of the subantarctic intermediate water in the Atlantic northwards, along the boundary between the oceanic stratosphere and the troposphere, is very probably a process that

is largely equivalent to the phenomena in a "jet" (Freistrah) at some distance from the nozzle (Düse). The distribution of A/A_0 in transverse section is also quite characteristic. The maximum appears in the lower part of the spreading layer (150 m beneath the core); below this the ratio falls rapidly, but above only slowly. This striking distribution of the exchange coefficients can be readily explained by the different stability conditions above and below the core.

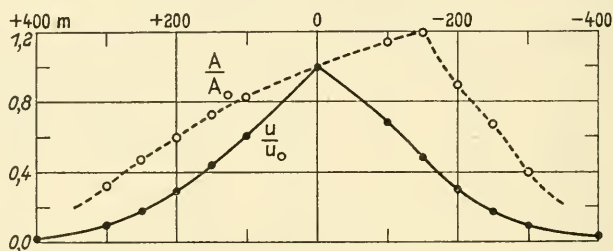


FIG. 81. Relative distribution of the exchange coefficients, A/A_0 and the current velocity, u/u_0 along a cross-section through the subantarctic intermediate water along the western side of the Atlantic.

(a) *Salinity of the deep water below 1500 m.* In the deep layers of the Atlantic the salinity increases slowly from the Antarctic regions across the equator as far as the deep-reaching, warm and high saline water of the northern subtropics (20° – 40° N.); from here towards the north it decreases slowly in the upper layers. However, in the deeper layers the increase to about 20° – 40° N. is much less. The asymmetry of the salinity distribution shown so strongly in the subantarctic intermediate water is also present in the deeper layers but not to the same extent. This contrast is due in the first place to the strong accumulations of saline water in the subtropics, but in these layers it is also reinforced by the inflow of highly saline water from the Mediterranean through the Straits of Gibraltar. Everywhere in this area there exists a well-defined maximum in the vertical salinity distribution at 1300 m (at about 20° N.) lowering to 2500 m (at 35° S.) that must be attributed to the spreading of the Mediterranean water. This effect of inflow from the European Mediterranean can be seen particularly on the salinity chart for 1000 m depth. The spread of this type of water will be discussed in greater detail later on (Vol. I, part 2, Chap. XVI, 3).

The nature of the water *beneath* the upper part of the stratosphere in the Atlantic indicates an area of formation in higher northern latitudes (north of 50° N.) in the Western Trough. Here it is formed at the surface during the late autumn and early winter, sinks by thermo-haline convection to great depths and spreads out more or less horizontally below 2000–2500 m to fill the lower part of the stratosphere. The high oxygen content which characterizes this water type will be discussed later in connection with the oceanic circulation (see Vol. I, part 2, Chap. XX, 7).

A similar contrast between the higher latitudes of both hemispheres is also present in oceanic stratosphere of the *Indian Ocean*. Here it is due in the first place to the inflow of highly saline water from the Red Sea. Coming from the Straits of Bab-el-Mandeb (see p. 182 and Fig. 84), it sinks to about 1000 m, mixes with less saline water in the Gulf of

Aden and from here extends southwards beneath the Antarctic intermediate water at a depth of 1500–2000 m as a tongue of highly saline water. This salinity maximum shows very clearly throughout the western and central parts of the Indian Ocean.

In the *Pacific* the few observations that have been made below 1500 m show a remarkably uniform vertical and horizontal salinity distribution at all latitudes. Its average value is about 34.65–34.68‰, but it is nowhere connected with the equally high values in salinity of the surface layers. There is no tropical or subtropical adjacent sea acting as a source for saline water for the Pacific stratosphere like the Mediterranean does for the Atlantic one or the Red Sea for the Indian Ocean stratosphere. It must therefore be supposed as pointed out by SVERDRUP (1931), that the Pacific deep water below about 1500 m depth for which there is no area of formation in the Pacific itself must be formed in the Indian Ocean or even in the Atlantic. Water masses from these two oceans must be carried to the east by the Antarctic circumpolar ocean current and then spread northward in form of current branches to fill the deep basins of the Pacific.

(β) *The salinity of the bottom layers.* The salinity of the deepest layers shows also the same characteristic distribution already known from the bottom temperatures. In the Atlantic Ocean (WÜST, 1936) it varies between 34.62 and 34.92‰ in the most northern parts; this is explicable from conditions of formation of the bottom water. The deepest parts of the Antarctic regions are filled with Antarctic bottom water with a salinity of 34.67–34.69‰, formed at the continental slope of the Weddell Sea (see p. 149). Above this the Antarctic deep water is found at 5000–4000 m with 34.62–34.66‰ that feeds the Antarctic bottom currents of the Eastern and Western Troughs. The isohalines of meridional sections demonstrate a clear conformity with the bottom profile and show the penetration of the water across the Equator in the Western Trough and the Eastern Trough as far as the Whalefish ridge. Figure 82 gives meridional salinity sections through the Western and Eastern Troughs of the Atlantic which show how the spreading of the bottom water is reflected in the distribution of the salinity in the same way as in the distribution of potential temperature (see p. 152) deduced previously.

A typical *Arctic bottom water* cannot be recognized from the salinity distribution though traces of it can be detected in the Labrador Basin north of the Newfoundland Rise (WÜST, 1943). Our knowledge of the salinity of the bottom water of the other two oceans is still pure due to a lack of systematic salinity data.

4. The Horizontal Distribution of Salinity at Particular Depths

Horizontal charts of salinity distribution are so far available only for the Atlantic: they are given for instance in the "*Meteor*" *Report* for depths of 200–800 m at 200 m intervals, for depths of 1000–2000 m at 250 m intervals and for depths of 2000–4000 m at 500 m intervals. Plate 6 shows charts for 400 m and 1000 m depths. It is clear that these charts do not give other information than the longitudinal and transverse sections. The charts down to 800 m, of which the 400 m chart is given as an example, all show essentially the surface salinity distribution; only the horizontal differences become smaller with increasing depth. Of the two extensive regions with salinity maxima in the subtropics the northern is the larger. The highest values appear,

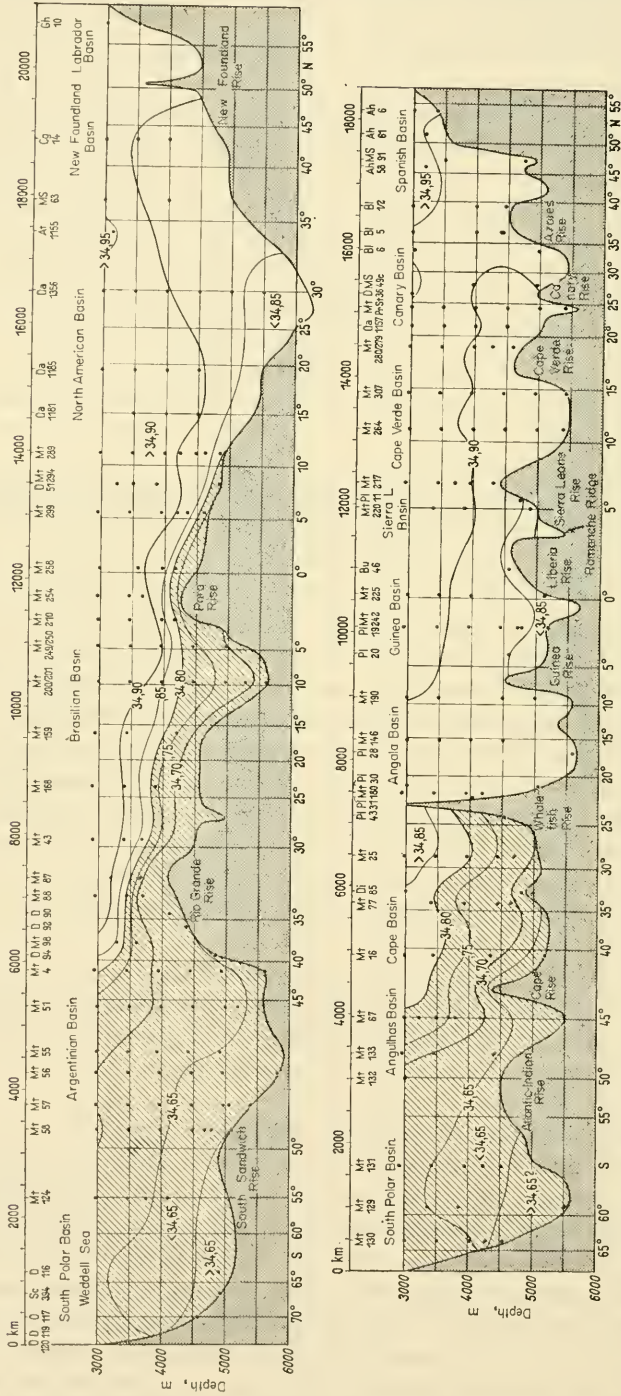


Fig. 82. Longitudinal salinity section in the bottom water (below 3000 m) in the Western and Eastern Atlantic Troughs (according to Wüst; for temperature distribution see Fig. 63).

however, not in the central part of the Sargasso sea but are displaced in the peripheral parts towards the west, partly on the right hand (north) side of the North Equatorial Current (especially at 200 m) and partly on the right-hand side of the Gulf Stream (especially at 400 m, but still visible at 1000 m). This distribution is a dynamic effect of the currents which cause an enormous water transport.

Below 600 m the influence of the high salinity inflow from the European Mediterranean begins to appear and extends already at 800 m to 40° W. It remains the principal phenomenon in all charts down to almost 2000 m and the remarkable asymmetry between the North and the South Atlantic shows particularly clearly here.

Below 2500 m the horizontal salinity differences already become very small though there is still a noticeable salinity gradient from north to south. South of 40° S. more pronounced differences in salinity reappear which indicate the increasing influence of the Antarctic deep and bottom water.

5. Salinity in Adjacent Seas and Sea Straits

In discussing the temperature distribution in adjacent seas (see p. 129) it was already emphasized that beneath the sill depth in all the adjacent seas there is an almost constant salinity; in the adjacent seas without winter convection it is identical with the salinity of the open ocean at the sill depth off the passage; in the adjacent seas with a winter convection, on the other hand, it is identical with the surface salinity at the time of the thermo-haline mixing (see Tables 56–66).

When there are relatively large differences between the water masses of the free ocean and those of the adjacent sea, the equilibration movements in the more or less narrow sea straits connecting them show rather striking conditions which deserve particular attention. The interchange of water between the European Mediterranean and the Atlantic is a consequence of currents through the *Straits of Gibraltar*, which carry water at the surface and in the uppermost layers into the Mediterranean towards the east, but in the deeper layers beneath towards west. Corresponding conditions are also found in the Straits of Bab-el-Mandeb, but in other sea straits the thermo-haline structure imposes reversed flow conditions. In the *Dardanelles* and the *Bosporus*, Aegean water flows into the Black Sea in the lower layers, while the flow into Mediterranean occurs in the upper layers.

Similar conditions also prevail in the connecting straits between the North Sea and the Baltic, where North Sea water enters through the Öresund and the Great and Little Belts along the bottom, while contrary the surface water flows out of the Baltic. All these water transports are associated with considerable changes in temperature and salinity. It could hardly be expected that these processes should be stationary ones. In fact they are turbulent and occur in pushes and therefore cause extremely large variations in both factors that they can only be investigated and understood with the aid of synoptic surveys. The available summarizing descriptions of the distribution of the different oceanic factors in such straits should thus be interpreted with some caution.

Figure 83 shows the distribution of temperature and salinity according to SCHOTT (1928) through the Straits of Gibraltar for the transitional period from spring to summer when average conditions prevail in the currents. The isohalines of the longitudinal section show clearly that the highly saline Mediterranean water, for which,

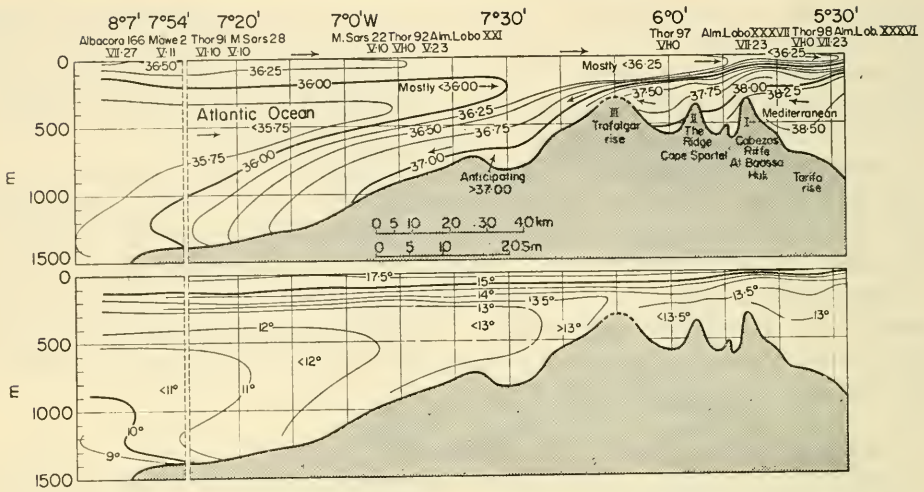


FIG. 83. Temperature and salinity distribution through the Straits of Gibraltar at the transition from spring to summer (mean conditions, according to Schott).

due to mixing, a slowly westwards decreasing salinity with the surrounding water is characteristic, sinks beneath the weakly saline Atlantic water below about 300 to 400 m. The temperature distribution shows identical conditions. This water continues to sink to about 1000–1200 m off the Spanish Bay, and from here it spreads out into the Atlantic as a more or less horizontal layer of highly saline water. The distribution within the strait shows strong seasonal variation: at the end of the winter the contrasts are reinforced, at the end of the summer they are weakened, but there is always a continuous outflow of water with a high salinity from the Mediterranean into the Atlantic and the submarine ridge never forms a barrier to the Mediterranean water as BUEN attempted to show (1927).

Conditions in the Straits of Bab-el-Mandeb are rather similar (SCHOTT, 1929). The highly saline deep water of the Red Sea (S 37‰) flows over the sill at 150 m depth north of the strait of Perim into the Gulf of Aden (Fig. 84). It sinks here to 500–1000 m and then spreads out horizontally at such a depth, in which the density of the sinking water becomes equal to that of the surrounding water.

Also the transition from the higher salinity of the North Sea (about 32‰) to the lower salinity of the Baltic (about 7‰) is not at all continuous, as one might easily be misled by studying mean charts only, but usually occurs rapidly, mostly in two steps (WATTENBERG, 1941). The first rapid change occurs near the boundary between Skagerrak and Kattegatt and changes its position very little in time; the second much sharper change has a more variable position between the southern edge of the Kattegatt through the Great and Little Belts to the rises leading to the actual Baltic (Darsser and Drogen Rises). These jumps in salinity have all the properties of true *hydrographic fronts*. They separate three water types: North Sea, Kattegatt and Baltic water. Figure 85 shows the distribution of the surface salinity from the Skagerrak to the Baltic in three different cases, and illustrates clearly the typical distribution at the fronts. The latter are not, however, stationary in location but *move around* continually

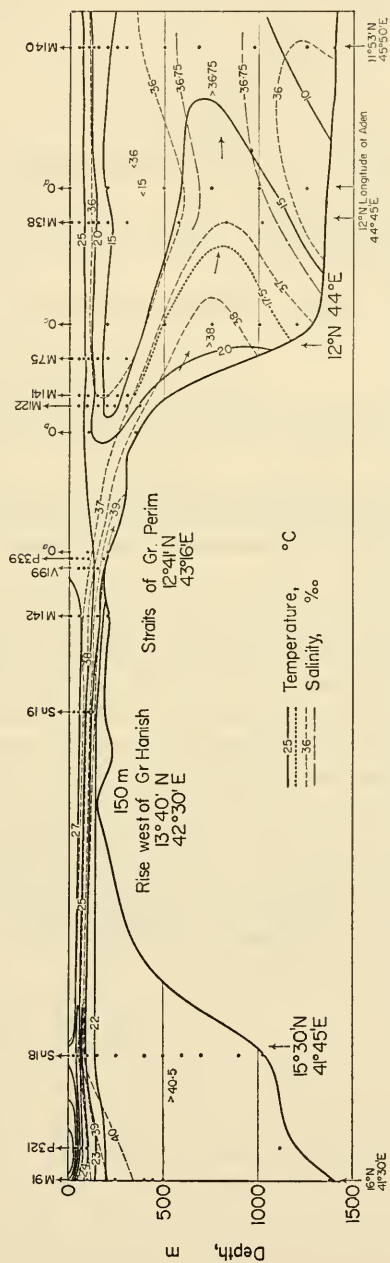


FIG. 84. Temperature and salinity distribution through the Straits of Bab el Mandeb.

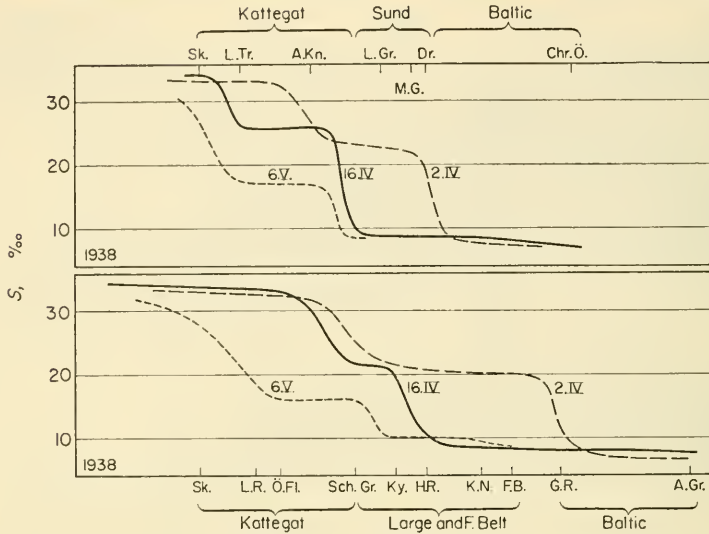


FIG. 85. Changes in surface salinity between the North Sea and the Baltic (from the Skagerrak into the Baltic) in three cases (according to the individual values recorded on 2 and 16 April and 16 May 1938, according to Wattenberg).

often at considerable speed in one or the opposite direction, and these displacements are then associated with jump-like changes in T and S at any given point.

In the sea straits so far discussed the equalization currents are superimposed (one above the other) and the water movements occur along a boundary surface sloping in the direction of the strait. This superposition of the two types of water appears to be causally associated with the *narrow width* of these straits. If this surpasses a certain value then the interchange of the different waters no longer takes place through currents flowing one above the other, but rather side by side in the strait, whereby the boundary surface now slopes transverse or normal to the main longitudinal axis of the strait. This type of water interchange is apparently present in the straits between the White Sea and the Barents Sea (TIMONOFF 1925), see Vol. I, Chap. XVI, p. 1-3 for a discussion of the dynamics of this process.

Chapter V

The Density of Water Masses in the Ocean, Vertical and Horizontal Density Distribution and its Stability

1. Diurnal and Annual Variations at the Surface

THE diurnal and annual variations are uniquely determined by that of the temperature and salinity. Since the diurnal temperature variation is essentially parallel with that of salinity, the effects of both factors on the density partly cancel each other out, and apart from the fact that they are both small anyway, the diurnal surface-density variation is thus a rather insignificant phenomenon. In general, the aperiodic changes in density during the day are so large that they completely mask the regular diurnal variation. At anchor stations the average diurnal variation in density, taken as the average over several days, is of the order of 0.05–0.1 in σ_t (Table 76).

Table 76. Diurnal density (σ_t) variation at the ocean surface (Atlantic Ocean)

Anchor stations	Hours												Diurnal variation	
		1	3	5	7	9	11	13	15	17	19	21		23
"Meteor" 5° S.–5° N.	22+	0.75	0.75	0.76†	0.76	0.74	0.71	0.67	0.65*	0.69	0.71	0.73	0.74	0.11
"Altair" 44.5° N., 34° W.	26+	0.19	0.19	0.19	0.20	0.21†	0.21†	0.18	0.17	0.16*	0.16	0.16	0.17	0.06

* Minimum; † Maximum

The maximum occurs in the morning or in the forenoon; the density then falls, probably due to the rising temperature—and in spite of the increasing salinity—to a minimum in the afternoon; the amplitude is everywhere very small.

The annual density variation is much larger and its amplitude usually is of the order of 1.00 and 2.00 in σ_t depending on whether the annual variation in the temperature is parallel or inverse to the corresponding salinity variation. The annual density variation can be conveniently presented by plotting the monthly values on a $[TS]$ -diagram. This has the advantage of providing a visual impression of the variations in temperature and salinity, and also in density. For annual variations in T and S , following pure sine curves, the annual variation in density will be shown on such a diagram as a straight line if the annual variations of the two factors run either parallel or inverse. If the amplitudes are normalized (choosing scales of equal length for T and S in the diagram) then the straight line will be at an angle of 45° with the temperature axis, but for inverse

variations of T and S (phase difference of 6 months) it will be at an angle of 135° . For a phase difference of three months the density values will lie either clockwise or anticlockwise around a circle. This method has been used by NEUMANN (1940) for a close investigation of the annual density variation in the area of the Gulf Stream north of the Azores. Figure 86 shows such annual density variations for some five-

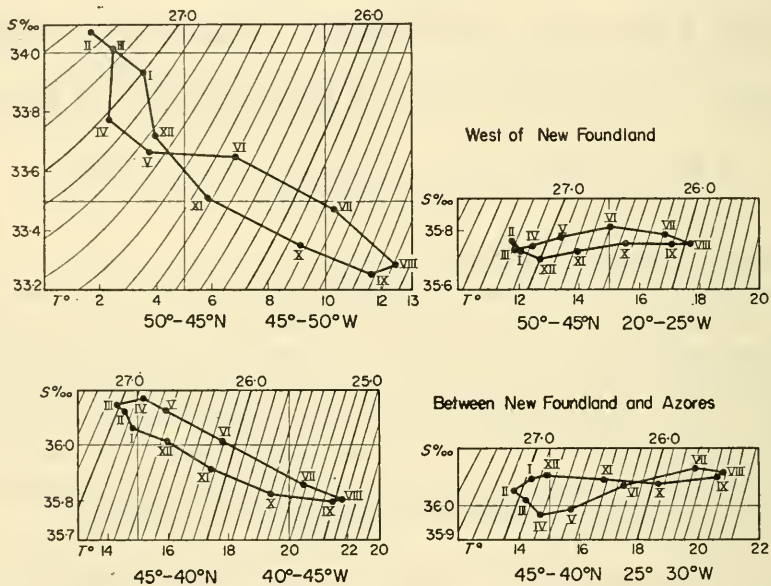


FIG. 86. Annual density variation at the surface of the sea in the area of the Gulf Stream north-west of the Azores (according to Neumann).

degree squares according to the above method. The amplitude is largest ($\Delta\sigma_t = 2.09$) at the boundaries of the Gulf Stream and the Labrador Current, then decreases to the east and south-east to only $1.5-1$ in σ_t . The maximum occurs in late winter (February–March) and the minimum without exception in August. In the western squares the densities lie almost on a straight line inclined at an angle of 135° to the temperature axis. The more or less sinusoidal annual variations in T and S show therefore a phase difference of about six months.

Similar investigations for other oceanic regions are entirely missing. BÖHNECKE (1936) has given a chart showing the annual variations in surface density over the entire Atlantic. As may be seen from this chart in the large areas of the North and the South Equatorial Currents the annual variation in σ_t is generally less than 1.0 . It rises locally above 1.5 only at the boundary between the North Equatorial Current and the Equatorial Counter Current (about 10° N.). In the tropics and the subtropics the annual variation is on the whole large only in those areas, where there exists a large annual variation in salinity (mouth of the Amazon, Gulf of Guinea, region with upwelling water east of Cape Verde Island). In higher latitudes the annual density variation remains, in general, also between 1.0 and 1.5 , only falling below 1.0 north of

50° N.; however, in regions close to the coasts seasonal displacements of different types of water also cause large annual density variations (>2.0).

2. Density Distribution at the Surface of the Ocean

It is very characteristic of the density distribution at the surface of the ocean that in spite of the extended strong salinity maximum in middle latitudes there is a rather regular increase of density from the equatorial regions towards the poles in all oceans. This already points towards a decisive influence of the temperature. Figure 86 shows the distribution of density at the surface of the Atlantic Ocean according to BÖHNECKE (1936). This picture illustrates the meridional increase from about 23.0 at 7°–8° N. to a value somewhat larger than 27.0 in higher latitudes mentioned above. Table 77 gives mean values for successive latitude zones of 5 degrees width. The increase is not entirely uniform in all these zones; the regions of subtropical convergence stand out as zones with a smaller density gradient and this gradient becomes larger again only near the oceanic polar fronts. Beyond the extensive areas of maximum density in subpolar and polar regions of maximum density the surface density seems again somewhat to decrease.

Table 77. Mean meridional density distribution in the Atlantic (σ_t)

Latitude	0°	10°	20°	30°	40°	50°	60°	70°
Northern Hemisphere	23.50	23.28*	24.48	25.44	25.90	26.69	27.25†	26.61
Southern Hemisphere	23.50*	24.53	25.31	25.42	26.06	26.75	27.15†	26.93

* Minimum; † Maximum

For the Indian and the Pacific Oceans the surface density charts of SCHOTT (1935) give only summer conditions for each hemisphere. These charts show essentially the same basic features as in the Atlantic. In the northern Indian Ocean only, conditions are somewhat complicated due to the large annual variations in salinity. The large differences in density between the Bay of Bengal with values of 22.0–18.0 and the Arabian Sea with an increase to 23.0 or even to 24.0 should particularly be mentioned.

3. Vertical Density Distribution and Horizontal Charts for Different Depths

The density is equally expressed by the quantity σ_t for the deeper layers. In this quantity the effect of pressure acting on the water mass is not taken into consideration and it refers therefore to zero sea pressure. As a rough approximation, σ_t can be taken as the density which would occur in a water mass after displacement of the mass with its *in situ* temperature and salinity from the depth to the surface (potential density); thereby only the adiabatic temperature effect remains out of consideration.

For a study of the vertical density stratification of the ocean it is necessary to go back to the values of the density or the specific volume *in situ*. Table 78 contains values for a standard sea at 0°C and 35‰ salinity, the vertical distribution of the density $\sigma_{s,t,p}$ and of the specific volume $\alpha_{s,t,p}$, and the corrections which must be applied to these $\alpha_{s,t,p}$ to obtain the distribution at 35‰ for 10° and 20°C, respectively, or at 0°C for 32.5 and 37.5‰, respectively.

Table 78. *Density and specific volume for different s, t, p ($\sigma_{s, t, p}$ and $\alpha_{s, t, p}$)*

Depth (m) Pressure in dbar	Density $\sigma_{s, t, p}$ ($^{\circ}\text{C}$, 35‰)	Specific vol. $\alpha_{s, t, p}$ ($^{\circ}\text{C}$, 35‰)	35‰		0°C	
			10°C	20°C	32.5‰	37.5‰
0	28.13	0.97264	+109 + 0 × 10 ⁻⁵	+318 + 0 × 10 ⁻⁵	-191 - 0 × 10 ⁻⁵	+190 + 0 × 10 ⁻⁴
25	28.23	253	+ 0	+ 1	- 0	+ 0
50	28.36	242	+ 1	+ 2	- 0	+ 0
100	28.61	219	+ 2	+ 3	- 0	+ 0
200	29.08	174	+ 4	+ 7	- 1	+ 1
300	29.56	129	+ 7	+ 11	- 1	+ 1
400	30.03	084	+ 9	+ 14	- 1	+ 1
500	30.50	040	+ 11	+ 17	- 2	+ 2
1000	32.85	0.96819	+ 21	+ 34	- 4	+ 4
2000	37.52	388	+ 41	+ 66	- 7	+ 7
3000	41.09	0.95970	+ 60	—	- 11	+ 11
4000	46.40	566	+ 77	—	- 14	+ 14
5000	50.72	173	—	—	- 17	+ 17

This type of presentation was chosen in order to allow differences from the values for standard ocean to stand out. The correction terms enclosed by rectangles refer to the quantities already considered during the determination of σ_t and α_t . It is obvious that these are the main correction terms. It is, however, generally customary to judge the vertical density stratification from the σ_t -values. This will also be done here and the more correct $\sigma_{s, t, p}$ and $\alpha_{s, t, p}$ will be considered again later.

From stability considerations it is to be expected that the values of σ_t will increase with depth. Apart from the surface layer down to about 50–100 m, this is always the case. In the tropics and subtropics the increase is characterized by a *transition layer* which begins just beneath the top layer, rising to a maximum gradient, then slowly changing towards the deeper layers to a much smaller gradient. Towards higher latitudes the intensity of the transition layer decreases more and more and beyond 35° N. and S. it becomes of no significance. In the Atlantic, for example, it can then scarcely be regarded as a transition layer. In these regions the vertical density gradient decreases steadily from the surface value downwards. In polar and subpolar regions the density gradient from the surface layer down to the sea bottom becomes minimal. Figure 87 shows the vertical distribution of σ_t for some stations for which the T - and S -distributions were given already in Figs. 52 and 69.

In the uppermost layer a small increase in the σ_t -values with depth can occasionally be noted (see the first three stations of Fig. 87). This does not, however, necessarily mean that the vertical density stratification of these water masses is unstable. Because reduction of the σ_t -values to the more correct $\sigma_{s, t, p}$ may remove these small differences as happens in the three cases in Fig. 87. There still remains, however, a large number of stations where there is undoubtedly a state of weak instability (see Chap. V, 6).

A better insight into the nature of the vertical σ_t -distribution through the entire ocean is given by constructing longitudinal sections. Wüst has prepared sections of this type for the Atlantic, indeed he chooses the same sections as for T and S (see Fig. 62, p. 146 and 147). Figure 88 presents the σ_t -section along the Western Trough of the Atlantic; the others show in principle the same picture. Although at the surface there is a general slow increase of density, from the equatorial zone towards high southern and northern latitudes, already at 100 m depth and below a different distribution is

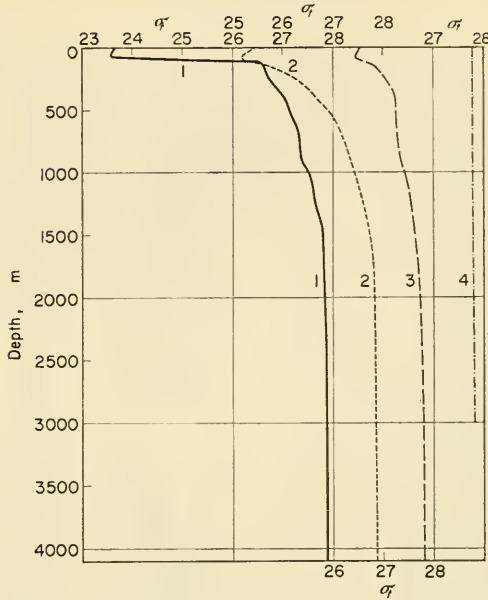


FIG. 87. Vertical distribution of the density σ_t at some oceanographic stations in the Atlantic:

1. "Meteor" 254 2° 27' S. 34° 57' W.
2. "Meteor" 170 22° 39' S. 27° 55' W.
3. "Meteor" 8 41° 39' S. 30° 06' W.
4. "Meteor"
Greenland 122 55° 03' N. 44° 46' W.

found that resembles more closely that of the temperature at these depths. In the subtropics of each hemisphere the lighter water extends down to great depths while in the equatorial zone the heavier waters of the deeper layers extend higher upwards to just below the strongly developed density transition layer. This gives rise to a horizontal density gradient from the equatorial zone towards the two subtropical regions, that is opposite to the surface gradient. This gradient remains unchanged in direction, though becoming weaker and weaker down to about 2000 m below which the meridional density differences are usually rather small. In all the vertical sections there is, however, a weak density gradient from high northern latitudes across the equator to as far as 40–50° S. which is connected with the oceanic circulation of the deeper layers.

It is readily understood that *horizontal charts* of σ_t -values show in principle the same picture. A comparison of such charts with charts of the relative topography of the isobaric surfaces (HELLAND-HANSEN and NANSEN, 1926) demonstrate that the course of the isopycnals on the horizontal charts is in essential agreement with that of the dynamic isobaths. The horizontal circulation of the water masses can thus be deduced approximately from the horizontal distribution of the σ_t -values. In that way stream lines for the *relative water flow* are obtained (i.e., with reference to the lower layers). Arrows showing the direction of flow are thus often inserted on the isolines on isopycnic charts of the upper layers to indicate the currents. These are subject to the

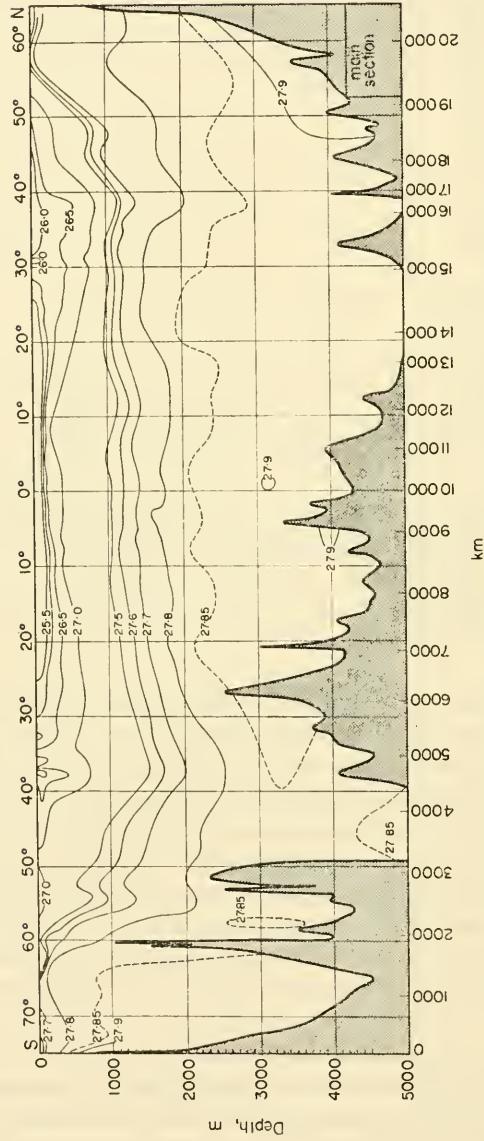


FIG. 88. Longitudinal density section along the Western Trough of the Atlantic (corresponding temperature-salinity section see Fig. 62).

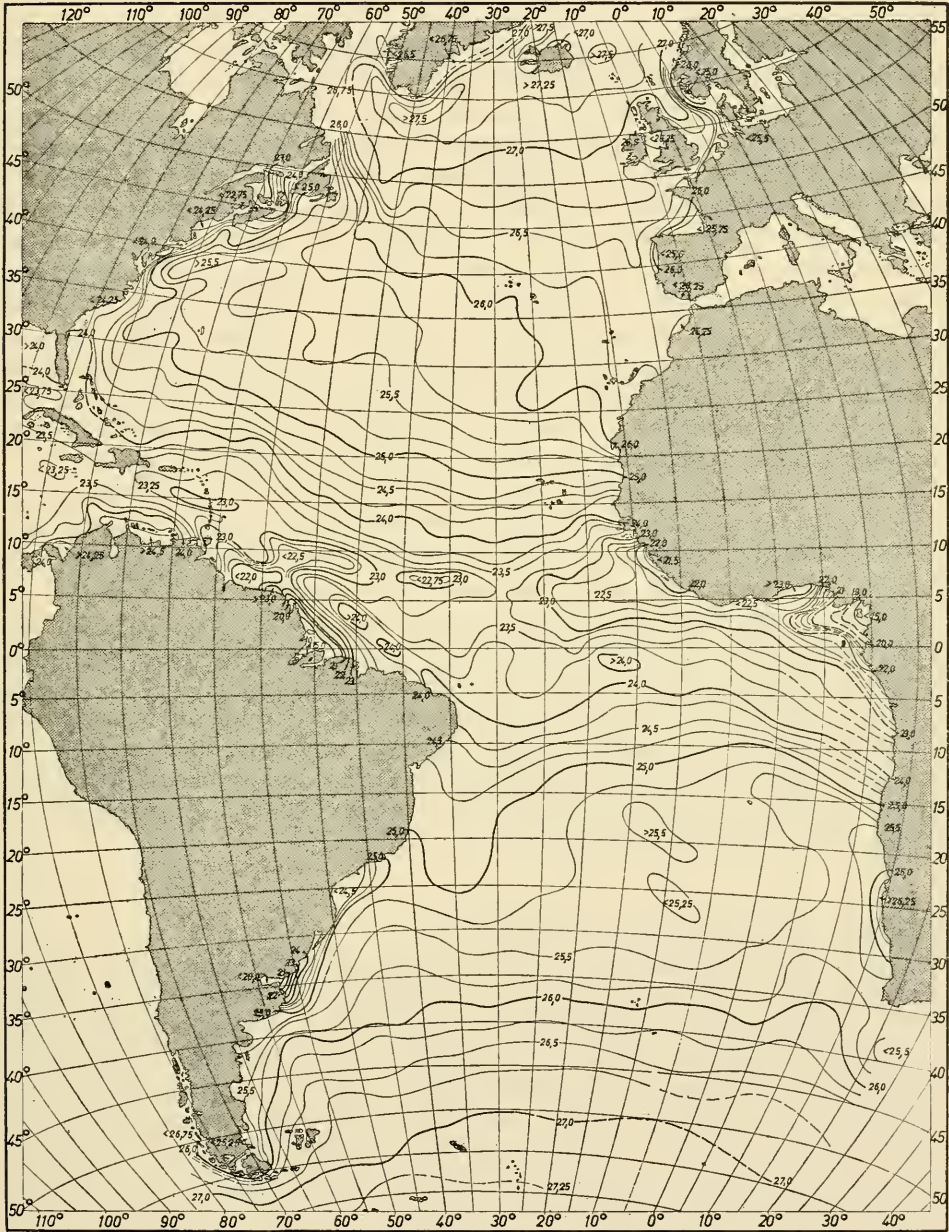


FIG. 89. Density of sea water σ_t at the surface of the Atlantic (according to Böhnecke).

rule that in the Northern Hemisphere the higher density values are found to the left of the direction of flow, while in the Southern Hemisphere they are found to the right (see Fig. 89).

Horizontal charts of the density for 400 and 1500 m in the Atlantic Ocean have been given in Plate 7 to supplement the above brief remarks. The first chart shows the Gulf Stream system very clearly by the strong concentration of the isopycnals into a narrow belt running from the Gulf of Mexico through the Florida Straits to the Newfoundland Banks and beyond to the north-east. Compared with this very large horizontal density gradient, that connected with the equatorial currents is only very small. In the Gulf Stream region the 400 m chart indicates another phenomenon that is characteristic of stronger gradient currents and is apparently missing in pictures of the surface current. On the right-hand side of the Gulf Stream some isopycnals deviate outward and turn into a south or south-west direction, opposite to the direction of the narrow band surrounding a strong longish density maximum at the right-hand side of the current core. These backward-turning isopycnals indicate the presence of a *countercurrent* to the right (to the east) of the Gulf Stream which is of considerable importance for the dynamics of this ocean current near the American coast.

In the Southern Hemisphere the isopycnals are strongly concentrated in the regions of the Agulhas Current, the Brazil Current and the Falkland Current. In addition, a steady rise of density exists in the Southern Hemisphere extending around the entire southern ocean which is associated with the broad circumpolar West Wind Drift of the higher southern latitudes. All density charts down to 800 m show very much the same picture, though the density gradient becomes gradually smaller and the density maxima of the subtropics are thereby somewhat displaced towards the poles. At first, a different distribution begins to appear below 1000 m, which dominates in the 1500 m chart. This is the density gradient from high northern latitudes to the minimum zone between 35° and 40° S. This north to south density gradient becomes less and less pronounced with increasing depth and below 4000 m the horizontal density differences become already very small.

4. Potential Density and Isentropic Analysis

In earlier times potential density was considered a significant property on which to form an opinion about the state of vertical equilibrium of oceanic stratification. As already stated (see p. 188) potential density is calculated from the *in situ* salinity and the potential temperature. Since the latter differs only at great depths from the *in situ* temperature and then by only a few tenths of a degree centigrade, the difference between σ_θ and σ_t remains very small and is almost insignificant as shown in Table 79. It thus makes little difference whether the vertical density distribution is judged by means of the customary σ_t or of the more correct σ_θ . The potential density has recently become of greater interest due to the introduction of the method of *isentropic analysis*. In meteorology, the investigation of the distribution of individual meteorological elements on surfaces of equal entropy has been modernized and this has led to appreciable success. PARR (1938, 1938*a*) has studied the spreading of oceanic water types in a similar way by following the changes in salinity and temperature on surfaces of equal density σ_t .

Table 79. Density σ_t and potential density σ_θ at "Meteor" station 310 (19.3° N., 25.0° W.)

Depth (m)	Temp. (°C)	Salinity (‰)	σ_t (density)	σ_θ (potential density)	$\sigma_\theta - \sigma_t$ (difference)
0	21.45	36.69	25.68	25.68	0.00
25	21.35	.65	.68	.68	.00
50	20.27	.77	26.05	26.05	.00
75	20.01	.79 ₅	.14	.14	.00
100	19.53	.75	.24	.25	.01
200	15.83	.11	.65	.66	.01
300	13.63	35.74	.84	.85	.01
400	11.69	.44	27.00	27.01	.01
500	10.58	.36	.16	.17	.01
600	9.03	.14	.24	.25	.01
800	7.00	34.94	.39	.40	.01
1000	6.04	.96	.53	.54	.01
1500	4.50	35.03	.77	.79	.02
2000	3.55	34.96 ₅	.82	.84	.02
3000	2.83	.93	.87	.89	.02
4000	2.43	.885	.87	.90	.03

Atmospheric isentropic analysis requires an investigation of conditions on a surface of constant entropy. In the atmosphere, provided there is no condensation, these surfaces are identical with surfaces of constant potential temperature and also with surfaces of constant potential density. For oceanic water the relationships between entropy, potential temperature and potential density are not so straightforward as for atmospheric air and in particular, under normal conditions the surfaces of constant entropy, constant potential temperature and constant potential density in the sea are not identical sets of surfaces. It can easily be understood that especially the surfaces of equal potential temperature are not identical with surfaces of equal potential density by considering the complete dependence of the latter on the locally varying salinity which plays only a minor role in the calculation of the potential temperature. Thus for an investigation of the spreading of the water masses neither one of these surfaces can be favoured, since each satisfies certain conditions which seem to be necessary for such considerations, but are not sufficient to give any of the two methods a special preference. It is thus equally incorrect to denote the method of using surfaces of equal potential density as reference surfaces as "isentropic" method because they have nothing to do with entropy which for sea-water is difficult to define.

Since there is, as previously pointed out, very little difference between the potential density σ_θ and the density σ_t (down to a pressure of 1000 decibars or a depth of 1000 m), instead of strictly "isentropic analysis" simply the distribution of the oceanographic factors on surfaces of constant σ_t has been studied. The method is thus quite simple in practice, but its usefulness is rather limited if one considers strictly its proper limits of applicability, and it offers little advantage over the "core layer" method and other similar methods which will be discussed later. The displacement of water masses

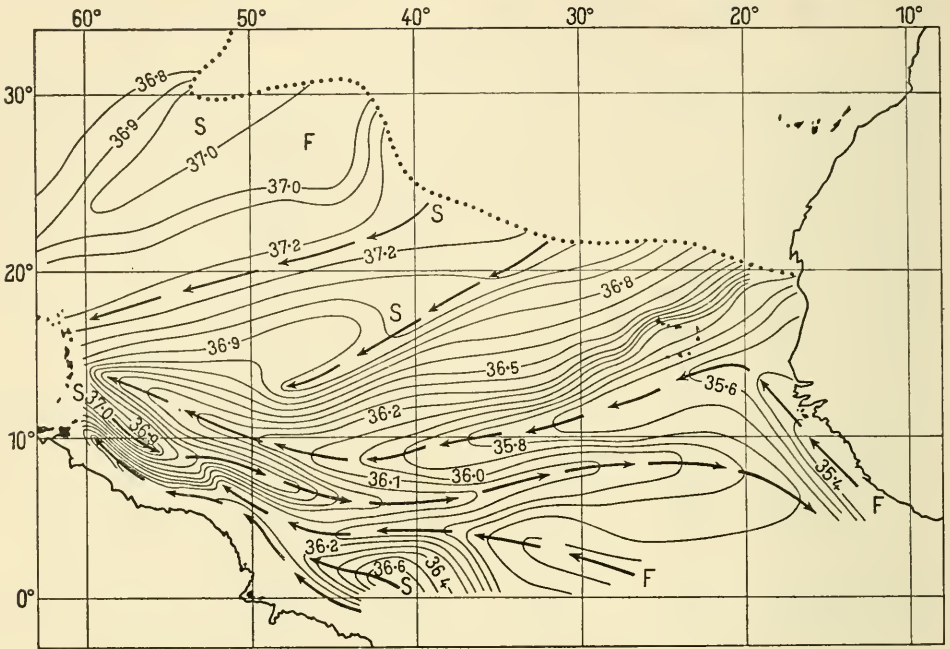


FIG. 90. Salinity distribution on the $25.5 \sigma_t$ -surface in the north-east Atlantic between 0° and about 30° N. (according to Montgomery) (only decimals have been entered as salinity values).

within such an isopycnic surface must by definition proceed without changes in the potential density and thus without changes in the potential temperature and the salinity (or in the oxygen content also). If the distribution of the temperature and the salinity (or of the oxygen content) pictured on such a surface show signs of change, these *must* be due to mixing, and it is therefore possible to investigate these more closely and to follow the main direction of flow and the spreading of different water types by means of isolines.

Thereby it was assumed that the mixing in such "isentropic" surfaces occurs predominantly in horizontal direction (that is in the direction of the surface) and to a much smaller extent in vertical direction (normal to the surface). This assumption is not entirely justifiable and may be satisfied only in cases where the σ_t -surface runs just within the density transition layer, since here the exchange coefficient in vertical direction is strongly reduced due to the great stability of the vertical stratification, and lateral exchange is thus very much favoured. Outside the density transition layer, however, there is no reason to assume that the effect of vertical mixing is less important than that of lateral mixing, especially as the reduced magnitude of the vertical exchange coefficient is compensated for by rather pronounced vertical gradients of the oceanographic factors, as was seen earlier.

MONTGOMERY (1938) has applied this method to determine the oceanic circulation of the upper layers of the southern North Atlantic. The results of this investigation will be discussed later in connection with the dynamics of ocean currents; here only the method for the use of the σ_t -chart will be presented. Figure 90 gives an example of such

an "isentropic" chart for the salinity distribution at the $25.5 \sigma_t$ -surface in the North Atlantic between 0° and 30° N. This surface intersects the sea surface at the dotted line and south of this it lies mostly at a depth of between 75 and 125 m. The arrows show the main direction of spreading of the highly saline (*S*) and low saline (*F*) water according to Montgomery. The arrows pointing in the west-east-direction show the Equatorial Countercurrent and correspond to actual flow. Only the east-west-arrows in the low-salinity tongue between the Equatorial Current and the southern branch of the north Equatorial Current and those directed from south to north off the West African coast may have little relation to actual currents; the first low-salinity tongue represents the salinity minimum between the intrusions of highly saline water to the north and the south, the latter minima are due to upwelling water off the West African coast.

5. The Vertical Equilibrium in the Ocean and Stability

The use of the potential temperature θ , or the potential density σ_θ , as criteria for the equilibrium conditions in the sea is only correct if the salinity is constant everywhere. Under these conditions the equilibrium is stable, indifferent (neutral) or unstable according to whether $d\sigma_\theta/dz \gtrless 0$. Correct equilibrium conditions can be derived in the following way: a small mass of water displaced from a level z by a vertical distance Δz towards the surface comes to a density ρ , while the surrounding water at this point has a density ρ' . This displaced water quantum will then be subject to a vertical acceleration proportional to $\rho - \rho'$. If the difference is positive then the displaced water mass will be subject to a downward force tending to move it back to its previous position; the equilibrium is then said to be *stable*; if the difference is negative then it is subject to an upward force tending to displace it further and further away from its new position—the equilibrium is then *unstable*. If, after a displacement, it always has the same density as the surrounding water then the equilibrium is indifferent (*neutral*). The difference $\rho - \rho'$ per unit length is thus a measure of the state of equilibrium. HESSELBERG (1918) therefore denoted the expression $E = \delta\rho/dz$ as "stability", where $\delta\rho/dz$ is the individual change in density (in contrast to $d\rho/dz$ which gives the geometric change in ρ with height). For positive values of E the stratification is stable and is not altered by vertical displacement of individual small water quanta. For negative values of E the stratification is unstable and the slightest disturbance is sufficient to cause a new adjustment in stratification (EKMAN, 1920). Between layers with positive and negative stability there is always a surface with $E = 0$. A small mass of water on displacement to the side where E is positive is always driven back to the surface, but a displacement to the side where E is negative removes it more and more from that surface.

HESSELBERG and SVERDRUP (1914, see also, SCHULZ, 1917) have given a simple method for the calculation of the quantity E . If a small water quantum at a depth z at point a (Fig. 91) is subject to a pressure p and has a salinity s and a temperature ϑ , at a depth $z + dz$, the corresponding values are $p + dp$, $s + ds$ and $\vartheta + d\vartheta$. If the water quantum is displaced near to point a , it will be subject to the pressure p and it will retain a salinity $s + ds$, but its temperature will change due to adiabatic expansion

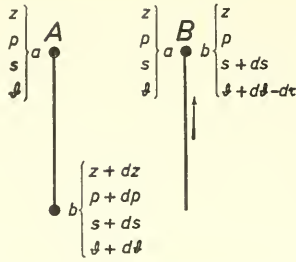


FIG. 91. Calculation of stability.

by $d\tau$ so that its temperature becomes $\vartheta + d\vartheta - d\tau$. The density difference between points b and a will thus be

$$\rho_{p, s+ds, \vartheta+d\vartheta-d\tau} - \rho_{p, s, \vartheta} = \frac{\partial \rho}{\partial s} ds + \frac{\partial \rho}{\partial \vartheta} (d\vartheta - d\tau).$$

The stability E is then given by the expression:

$$E = \left[\frac{\partial \rho}{\partial s} \frac{ds}{dz} + \frac{\partial \rho}{\partial \vartheta} \left(\frac{d\vartheta}{dz} - \frac{d\tau}{dz} \right) \right].$$

The geometrical changes in salinity and temperature ds/dz and $d\vartheta/dz$ for the depth z at a give station can thus be determined from the given values of T and S , and the temperature gradient $\partial\tau/\partial z$ as well as $\partial\rho/\partial s$ and $\partial\rho/\partial\vartheta$ can be found from hydrographic tables.

If the salinity is constant in vertical direction ($ds/dz = 0$) then

$$E = \frac{\partial \rho}{\partial \vartheta} \left(\frac{d\vartheta}{dz} - \frac{d\tau}{dz} \right) = \frac{d\sigma_\theta}{dz}.$$

This is in agreement with the previously given equilibrium condition for the potential temperature. For a given vertical change in salinity its effect on E is so large that it cannot be ignored.

“Meteor” St. 310 (see Table 79) has been selected as an example for the vertical stability distribution; the E distribution is given in Table 80.

In the top layer down to 25 m there is a very weak negative stability and just below the top layer E rises to very large values. This is the density transition layer where the stratification of the water is extremely stable. Underneath the stability decreases somewhat to assume a value of about 100 at the boundary between the oceanic troposphere and the stratosphere. It then decreases steadily approaching neutral equilibrium in the greatest ocean depths. All tropical and subtropical stations show similar conditions. Towards polar latitudes the large positive values of E in the upper layers disappear and are replaced by a more uniform, however, not especially large stability; only the surface layer can be disturbed to any extent by changes from season to season.

The vertical stability at great depths in the deep-sea trenches is of particular interest. Since in these the salinity is very largely constant the vertical stability conditions can be estimated fairly accurately from the potential temperature (see p. 127). According

Table 80. Stability in the Atlantic ($10^8 \times E$)

Depth (m)	"Meteor" St. 310	All "Meteor" stations	Depth (m)	"Meteor" St. 310	All "Meteor" stations
0-25	-6	—	900-1000	75	63
25-50	1541	—	1000-1200	57	59
50-75	360	—	1200-1400	63	48
75-100	377	—	1400-1600	43	35
100-150	343	—	1600-1800	17	24
			1800-2000	16	18.1
150-200	514	—			
200-300	219	202	2000-2250	13	12.6
300-400	168	151	2250-2500	9.5	10.4
400-500	152	120	2500-3000	8.6	8.2
			3000-3500	7.3	7.9
500-600	113	102	3500-4000	3.6	8.4
600-700	108	75			
700-800	74	70	4000-4500	—	8.6
800-900	92	65	4500-5000	—	3.3

to the observations made by the "Snellius" Expedition (SCHUBERT, 1931) the Philippine Trench shows the values of $E \times 10^8$ given in Table 81.

POLLAK (1954) has given a different definition for the stability which has some advantages in many cases. It gives somewhat different values for E , but differences remain in the limits.

Table 81. Vertical stability ($10^8 \times E$) in the Philippine Trench according to the observations of the "Snellius" Expedition

Depth interval	3500-4000	4000-4500	4500-5500	5500-6500	6500-7500	7500-8500	8500-10,030
$10^8 \times E$	+1.2	+0.8	-0.3	+0.5	+0.7	+0.2	+0.8

It may also be of interest to deal with another equation for the vertical stability which shows clearly the difference of the E -values from the vertical density gradient $d\sigma_t/dz$ which has often been used previously as a measure of stability. The density $\rho_{s,\theta,p}$ *in situ* is calculated from hydrographic tables by applying three correction terms to the value

$$\rho_{s,\theta,0} = 1 + 10^{-3} \sigma_\theta.$$

The first of these ϵ_p depends only on the pressure p , the second $\epsilon_{s,p}$ depends on the salinity and the pressure and the third $\epsilon_{\theta,p}$ depends on temperature and pressure.

Then

$$\rho_{s,\theta,p} = 1 + [\sigma_\theta + \epsilon_p + \epsilon_{s,p} + \epsilon_{\theta,p}]$$

and

$$\rho_{s+d_s, \theta+d_\theta-d\tau, p} = 1 + \left[\sigma_{\theta+d_\theta} + \epsilon_p + \epsilon_{s+d_s,p} + \epsilon_{\theta+d_\theta, p} - \frac{\partial \rho}{\partial \theta} d\tau \right].$$

From these equations one obtains

$$\delta\rho = d\sigma_\theta + \frac{\delta\epsilon_{s,p}}{\partial s} ds + \frac{\partial\epsilon_{\theta,p}}{\partial\vartheta} d\vartheta - \frac{\partial\rho}{\partial\tau} d\tau$$

and thus

$$E = \frac{d\sigma_\theta}{dz} + \frac{\partial\epsilon_{s,p}}{\partial s} \frac{ds}{dz} + \frac{\partial\epsilon_{\theta,p}}{\partial\vartheta} \frac{d\vartheta}{dz} - \frac{\partial\rho}{\partial\tau} \frac{d\tau}{dz}.$$

In this expression for E the first term is usually the main one and the others are only correction terms; the second term shows the effect of changes in salinity, the third shows the effect of changes in temperature on the compressibility while the fourth allows for the adiabatic temperature effect. Estimation of the order of magnitude of these terms shows that they cannot be neglected; the effect of the temperature difference on the compressibility must already be taken into consideration for depths below 100 m; in deeper layers also the adiabatic effect is of the same order of magnitude as the first term. In general only the effect of changes in salinity is mostly small. The quantity $d\sigma_\theta/dz$ for itself thus cannot give a very precise measure of the stability.

6. The Distribution of Stability in the Atlantic Ocean

SCHUBERT (1935) has carried out a detailed examination of stability conditions in the Atlantic Ocean—in particular of regional stability differences in vertical sections and on horizontal charts. Table 80 also gives mean values of E for the entire ocean calculated as means of all “Meteor” stations; the surface layer down to 200 m, i.e. the zone of disturbance, has been omitted. Of the many irregularities in the vertical distribution at individual stations, only two remain in the mean values, the most important being that at 1000 m. This is a definite intermediate stability maximum. From the location of this rather strong interruption, or sometimes even reversal, of the normal decrease of stability downwards, the decrease in stability is considerably larger than before. This irregularity is present at about the same depth throughout the total ocean in temperate and tropical latitudes, and is connected with the subantarctic intermediate water. Its basic cause is the reversal in the salinity gradient.

There is another secondary maximum imposed on the regular decrease of the E -values at a depth of 2000–4000 m. In contrast to the more sudden change at 1000 m a weak and more gradual increase in stability is characteristic.

In the regional variability of the stability in particular, a strong decrease towards higher latitudes stands out. The higher values of E disappear already beyond 50° latitude; the greater uniformity and lower values indicate that only in higher latitudes do favourable conditions for vertical displacements of water exist. Solely by this, higher latitudes become the principal regions of origin for the deep-sea circulation of the oceanic stratosphere.

Characteristic stability conditions are found in the top layer down to 100 m or occasionally to 200 m where frequently *negative* values occur. Apart from cases in the upper 25 m, where they are very frequent, these negative stabilities were formerly regarded as due to observational errors (especially in the salinity). However, variations of 0.01‰ are in fact quite sufficient to explain them (HELLAND-HANSEN, 1910).

Observations of more recent expeditions have shown that negative stabilities extending down at the most to about 250 m are of such a frequent occurrence, that they are difficult to account for by observational errors alone. For example, in ninety-five cases with E greater than -100 the observational errors must be 0.04% in δ or 1°C in temperature. There is, however, further confirmation of the reality of this phenomenon. This comes from the occurrence of negative values throughout the *entire* layer, and the fact that mostly a pronounced regional distribution of stations with negative values of E is found which would scarcely be possible if random observational errors would have been made. In the Atlantic, for example, there is an extended area with negative values of E in the entire open ocean from 50°S . to 20°N . The highest negative values (< -200) fall within a latitudinal zone between 15° and 20°S . and there is probably a corresponding zone also in the North Atlantic approximately between 20° and 30°N .

This instability in the top layer in tropical and subtropical areas must be due to the effectiveness of evaporation. The increase in salinity and the decrease of the temperature at the surface leads to an increase in density and to a reduction in stability. Solely incoming radiation during day time works in the opposite direction, which compensates the density increase by a corresponding rise in temperature, but during night time when incoming radiation is missing and evaporation continues, the density increase will predominate and negative stability values can persist for a considerable time as long as the intensity of evaporation is sufficient. It is, however, a rather peculiar phenomenon that a vertically unstable stratification can be maintained for a longer time over such an extended area in the top layer in spite of convection and mixing.

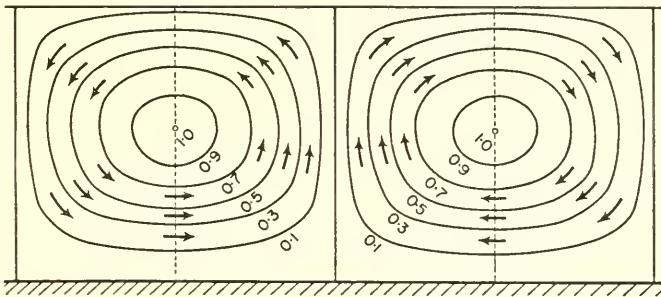


FIG. 92. Circulation in a convection cell according to Bénard.

Perhaps a possible explanation lies in the “convection cells”, first observed and investigated experimentally by BÉNARD (1901). He was able to show that when a relatively thin layer of a liquid with volatile components was cooled by evaporation, the entire mass of the liquid divided into a number of cells. In each of these the liquid rises in the centre, diverges in the upper part of the cell and descends again in the outer parts as shown schematically in Fig. 92. The diameter of the cells corresponds to about three or four times that of the thickness of the liquid layer. Instability in the

stratification is associated with such convection cells and is maintained by the circulation. RAYLEIGH (1916) and JEFFREYS (1928) investigated such a Bénard cell theoretically and showed that there could be an equilibrium state with an upper layer of greater density on top of a lower one with smaller density if the vertical density difference between the upper and the lower layer was less than a certain limiting value given by the inequality

$$\frac{\rho' - \rho}{\rho} < \frac{27\pi^4 \kappa \nu}{4gh^3},$$

where κ is the molecular thermal conductivity coefficient, ν is the kinetic viscosity coefficient and h is the thickness of the liquid layer. The unstable density difference is largest in the upper part of the layer; as long as the loss of heat by evaporation tends to maintain the unstable stratification the circulation will continue. It will, however, cease immediately as soon as the evaporation ceases. If there is a steady current in any direction in such a liquid the convection cells resolve into long bands with a corresponding transverse circulation.

It is not impossible that the existence and maintenance of density instability in the top layer of the ocean has something to do with such phenomena. However, in order to simulate conditions actually found in the ocean, the influence of radiation and evaporation and especially that of the eddy conductivity and eddy viscosity must be taken into account in the above inequality, instead of the molecular thermal conductivity and the molecular viscosity. For a layer 25–50 m thick resting on top of a transition layer with a stable stratification, the above inequality will give a value for $(\rho' - \rho)$ of the order of magnitude of the observed negative stabilities. By the effect of the circulation a mechanical instability is thus changed into a *dynamic* stability.

In more recent times the theory of convection cells has been considerably advanced and has been discussed in detail in a symposium on the problems of boundary layers and convection cells in the *Section of Oceanography and Meteorology* of the New York Academy of Sciences, 1942. STOMMEL (1947) has presented a summary of the theory of convection cells which should especially be mentioned. NEUMANN (1948) has paid special attention to cell convection in the sea and has shown that indifferent (neutral) stratification occurs only when

$$E = - \frac{A_0}{\rho g} \frac{A^2}{h^4},$$

where A_0 is a dimensionless quantity of the order of 1.1×10^3 in the ocean, A is the vertical exchange coefficient and h is the thickness of the layer. This equation follows directly from that given by Rayleigh if the above-mentioned change from molecular into turbulent conditions is introduced. The greater the thickness of the layer h and the smaller the exchange coefficient A , the smaller is the decrease in density with depth that is still compatible with static equilibrium. Convection starts only when denser water is situated on top of lighter and when A in the above equation exceeds the critical value 1100.

At the "Meteor" anchor station 385 ($16^\circ 48.3' N.$, $46^\circ 17.1' W.$; second continuation of the German North Atlantic Expedition, February 1938) it was found, as a

mean of sixty series of observations, that the water at the sea surface was always appreciably denser (heavier) than that at 6 m depth and even at 15 m depth the water was still specifically lighter than at the surface. Taking $A = 100 \text{ g cm}^{-1} \text{ sec}^{-1}$ and $h = 500 \text{ cm}$, then $E = -16 \times 10^{-1}$; this means that convection is initiated in this layer at this value and not at $E = 0$. If the turbulence becomes stronger the critical value of E increases rapidly and strong density gradients are required for any start of convectional motion.

The long lines of foam often observed on the surface of the sea can be regarded as "convection rolls" formed by a combination of a strong current in a single direction, and circulations in convection cells in the above sense. Their frequent occurrence is an indication that regular formations of Bénard convection cells occur in the sea.

Chapter VI

The [TS]-relationship and its Connection with Mixing Processes and Large Water Masses

1. Temperature as a Function of Salinity and Large Water Masses

TEMPERATURE and salinity vary with the depth h or the pressure p , and an investigation of the vertical distribution of these factors is based mainly on a graphical representation of the variation of these quantities with depth h . In this way it is almost unconsciously assumed that these factors (temperature and salinity) are independent of each other. This is, however, not the case. Assuming salinity as a function of temperature or plotting it against temperature in a system of co-ordinates (temperature as ordinate, the salinity as abscissa) the points for each depth are not distributed at random over the diagram but fall on a definite, more or less smooth curve. It is found that for oceanic regions with uniform oceanographic and special climatic, as well as undisturbed flow conditions, the [TS]-relationship is quite characteristic. A given temperature corresponds to a given salinity regardless of the depth. The practical significance of this [TS]-relationship was first pointed out by HELLAND-HANSEN (1918) and since then it has become increasingly important. Any given water type, a *water mass*, formed continuously in a particular oceanic area for any kind of conditions is characterized by a definite temperature and a definite salinity. If this water mass is *homogeneous* then the oceanographic factors in it are constant and it can be represented on a [TS]-diagram by a *single point*. If this water mass is moved in any direction without altering its physical-chemical structure the point does not change its position on the diagram. However, under influence of certain processes, for instance mixing, radiation or evaporation, the water mass loses its homogeneity and the position of the point in the co-ordinate system is changed. Such changes occur especially in the top layer (down to 200 m), where climatic conditions are able to produce continuous "disturbances" in the normal state. Beneath the top layer with disturbances, however, conditions in the ocean are *quasi-stationary* and thus every station has its characteristic [TS]-curve which for that special station remains largely *invariable*. This constancy is, however, not only true for each individual station but applies also in a somewhat wider sense to more or less larger oceanic spaces. *Standard curves* can thus be constructed for different regions and conclusions can be drawn about the origin and spreading of a water mass from the deviations of the values at a particular station from those of the standard curves.

Figure 93 shows an example of such a [TS]-curve for "Meteor" station 171 in the central part of the South Atlantic. Its shape is characteristic for the entire South Atlantic from 40° S. to beyond 10° N. Its constancy over such a large area expresses well the strong *conservatism of vertical stratification* which is of course necessary under stationary conditions. If, in addition, lines of equal density σ_t (isopycnals) are also included in the same diagram, as was done in Fig. 93, a rather instructive although not completely correct representation of the stability of vertical stratification is obtained. If

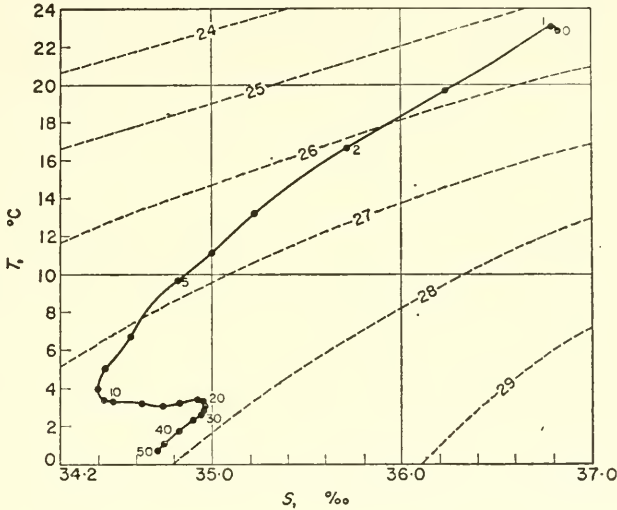


FIG. 93. [TS]-curve for "Meteor" St. 171 (22° 1.5' S. 23° 47.0' W.) in the central part of the South Atlantic (the thin dashed curves are the isopycnals σ_t).

the [TS]-curve of a certain layer runs approximately parallel to the isopycnals the stability in the layer is only small but if the [TS]-curve cuts the isopycnals at a wide angle the stability is larger. For greater accuracy the [TS]-curve must be constructed by using potential temperatures, but the differences in most cases remain small.

As with temperature, so can any other property of sea-water be combined with the salinity in exactly the same way. Such a combination was made in particular with the oxygen content in order to see how changes in the oxygen content affect the temperature and salinity conditions, which determine the water mass.

2. Practical Significance of the [TS]-curve

The [TS]-curve offers advantages in the scientific preparation of oceanographic data and is used to detect errors and to make it homogeneous. If the value for a particular depth at an oceanographic station does not fall on the simple, regular and usually smooth [TS]-curve it can be confidently assumed that there is an observational error or a fault in calculation (for examples see MERZ, 1925). The [TS]-curve is thus a reliable criterion of the accuracy and homogeneity of a set of data. Since curves for neighbouring stations are similar all values can be checked immediately, but a faulty

observation can also thereby be replaced by an approximate, rather more correct value. Only in this way is it possible to perform an objective and satisfactory "interpolation" of oceanographic values in order to fill gaps (missing data) in the observational material.

3. The [TS]-curve and the Mixing of Water Masses

If two homogeneous water masses are mixed in any given proportion, the mixture will have a definite [TS]-curve. Each of the two homogeneous water masses is characterized by the two points, 1 (s_1, ϑ_1) and 2 (s_2, ϑ_2), in the co-ordinate system. proceeds in the ordinary way; if two masses are mixed in the ratio $m_1 : m_2$ then the mixing final temperature and salinity of the mixture will be given by

$$\vartheta = \frac{m_1\vartheta_1 + m_2\vartheta_2}{m_1 + m_2}; \quad s = \frac{m_1s_1 + m_2s_2}{m_1 + m_2}.$$

An example is presented in Fig. 94 where a homogeneous water mass U ($10^\circ, 35\%$) from 100 m to 500 m depth is situated above a second mass Z ($5^\circ, 34.5\%$) which extends down to a depth of 900 m (DEFANT and WÜST, 1930). These two homogeneous water masses are represented in the [TS]-diagram by the two points U and Z . The boundary surface at 500 m depth, which is initially a sharp physical discontinuity surface, gradually disappears due to mixing. Different stages of this destruction of the discontinuity is shown on the left-hand side of Fig. 94 (DEFANT, 1929). It is obvious that, whatever the ratio of mixing of the two water masses may be, the mixture will be represented on the diagram only by points lying between U and Z . However, the graphical construction shows that all points of the mixture must be situated on the *straight line* from U to Z and that only the depth changes on this line according to the intensity of mixing. This is readily shown theoretically (DEFANT, 1935). It can also be demonstrated that the distance of any point along the straight line from the two end-points (representing the two original water types) is inversely proportional to the ratio of mixing, the result of which is the mixed water type at the point in question. It is thus simple to determine from the position of a point relative to the end-points U and Z in Fig. 94 to what degree (in percentage) the final mixed water mass under consideration is composed of each of the original water types.

The case where three water types are mixed is illustrated in Fig. 95. The three types are:

Water mass ..	U	Z	T
Layer thickness (m)	100-500	500-1000	1000-1500
Temperature ($^\circ\text{C}$)	10	5	5
Salinity (‰) ..	35.0	34.5	35.0

The thermal boundary surface at 500 m disappears in the same way as in the previous case. The salinity boundary surface does the same up to the time when the intermediate water mass Z becomes involved in its total height in the mixing process and in that way is slowly destroyed at its core. An advanced stage of this is shown in the

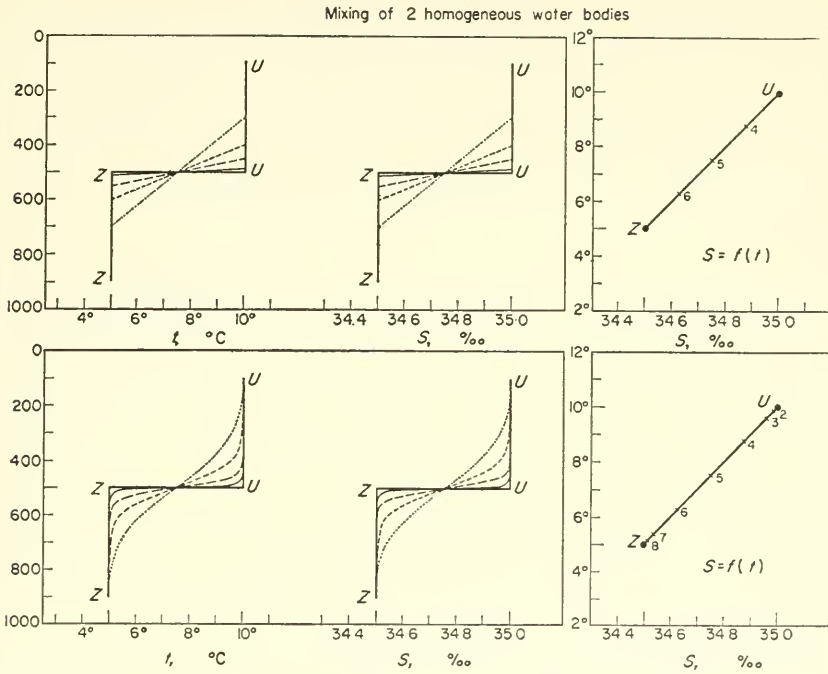


FIG. 94. Mixing of two homogeneous water masses and the resulting [TS]-relationship.

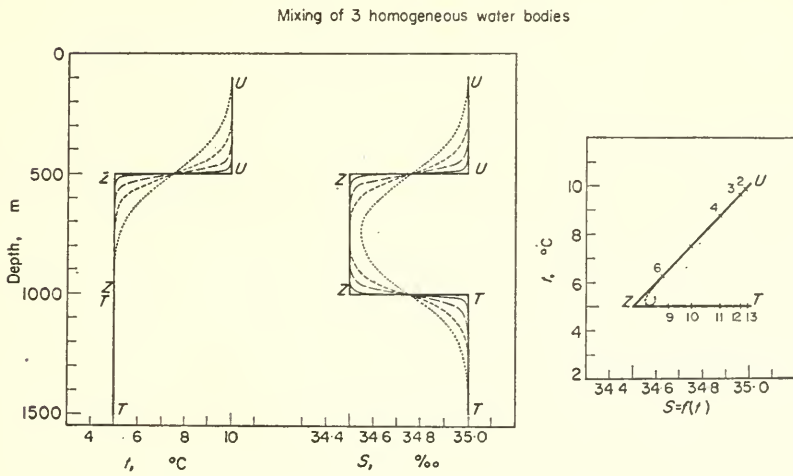


FIG. 95. Mixing of three homogeneous water masses.

S-distribution by the dotted line. In the [TS]-diagram the mixing of the three water types is represented by the *broken* line *UTZ*, but the point *Z* remains on this [TS]-curve only as long as the core of the intermediate water is not involved in mixing with the water masses *U* and *T*. When this happens the *Z*-point moves into the acute angle and the [TS]-curve no longer has a peak point at *Z* but becomes rounded there. The reversal point and the concentration of the depth marks around it shows the core of the intermediate water already affected by mixing, but even at this advanced stage the mixing of the three water masses can be represented by a curve *UZT* made up of two straight lines.

Analysis of actual [TS]-curves of the oceans show essentially these main theoretical characteristics; they are remarkably constant over large oceanic regions, they have characteristic reversal points associated with the cores of the individual water types and large parts of these curves often show a surprising approach to a straight line. In these cases the [TS]-curves allow a precise determination of the depth, temperature and salinity of the water masses, which finally combine and form individual water types in the deep layers and they also allow the percentage of the individual components to be found at all intermediate stages.

In the foregoing discussion it has so far been assumed only that mixing proceeds according to the usual mixing rules; the magnitude of the exchange coefficients is not involved. The percentages of the original component-waters before mixing give no information on this point. For obtaining a connection with the [TS]-curve the basic equation given on p. 106

$$A_z \frac{\partial^2 s}{\partial z^2} - \rho u \frac{\partial s}{\partial x} = 0$$

is required. This implies that in order to secure a *stationary state* the vertical exchange and the horizontal advection must completely balance. By choosing for the origin of the *x*-coordinate (pointing positively in the direction of movement of the water mass under consideration in a longitudinal section) that point where the water mass 1 is still pure, then the salinity at a distance *x* will be *s_x* and at a distance *x* + Δ*x* will be *s_{x+Δx}* and one obtains with sufficient accuracy:

$$s_{x+\Delta x} = s_x + \frac{\partial s}{\partial x} \Delta x = s_x + \frac{A_z}{\rho u} \frac{\partial^2 s}{\partial z^2} \Delta x.$$

If *s_x* is formed from *s₁* and *s₂* in the proportion *m₁* and *m₂* of water masses 1 and 2 and *s_{x+Δx}* in the proportion *m₁ - Δ*m** and *m₂ + Δ*m**, then using the mixing rule the above equation transforms to

$$\frac{(s_2 - s_1)\Delta m}{m_1 + m_2} = \frac{A_z}{\rho u} \frac{\partial^2 s}{\partial z^2} \Delta x.$$

If now *m₁ + m₂* is replaced by the distance *D* of points 1 and 2 on the [TS]-curve and Δ*m* by the distance Δ*D* of the point (*s* + Δ*s*; *ϑ* + Δ*ϑ*) from the point (*s*, *ϑ*), then

$$\frac{A_z}{\rho u} = \frac{s_2 - s_1}{D} \frac{\Delta D}{\Delta x} \frac{1}{(\partial^2 s / \partial z^2)}.$$

This formula allows the value at any point along the line of spreading of a water type to be calculated from the [TS]-curve if the vertical distribution of salinity (or of temperature) is known. In the special case of a tongue-like spreading s is given with sufficient accuracy by the simple form (see p. 106, *et seq.*)

$$s = s_0 + f(x) \cos \frac{\pi}{2l} z.$$

Then

$$\frac{\partial^2 s}{\partial z^2} = \frac{\pi^2}{4l^2} (s - s_0),$$

and for the core layer ($z = 0$)

$$\frac{\partial^2 s}{\partial z^2} = \frac{\pi^2}{4l^2} f(x).$$

Because

$$f(1) = s_0 - s_1 \quad \text{and} \quad f(2) = s_0 - s_2,$$

and therefore

$$s_2 - s_1 = f(1) - f(2)$$

we obtain

$$\frac{A_*}{\rho u} = \frac{4l^2}{\pi^2 D} \frac{f(1) - f(2)}{f(x)} \frac{\Delta D}{\Delta x}.$$

The application of this equation to the core layer of the subantarctic intermediate water along the western section in the Atlantic gives values for between 0.6 and 1.1 which is in rather good agreement with those determined by other methods. However, this method, using the [TS]-relationship, also gives only the ratio between vertical exchange and velocity.

An interesting method that also uses the [TS]-relationship and allows a deeper insight into the process of mixing has been given by JACOBSEN (1927). Consider a vertical column of water with cross-section of 1 cm^2 . From this column we consider two cubes (volume 1 cm^3) at A ($z = 0$) and also at a point B at a distance z beneath A . In the course of a mixing process, which should follow the laws valid for diffusion and occurs within the total column which we assume at rest, there will be an exchange of $q \text{ cm}^3$ of water in the time of t sec between the two cubes. If the displacement of the water quanta during the mixing process follows a Maxwellian distribution then

$$q = ke^{-\alpha^2 z}.$$

Since there is no increase in mass in the entire water column the integral of qdz from $-\infty$ to $+\infty$ must be equal to 1. This gives $\alpha^2 = \pi k^2$. The amount of salt in cube B is $\rho s \times 10^{-3}$, where the salinity s is given in per thousand and the increase in salt amount in a small time dt according to the exchange equation is

$$\rho \Delta s = A dt \frac{d^2 s}{dz^2}.$$

Corresponding relationships with s_0 and Δs_0 applies to cube A . The salinity ($s_0 + \Delta s_0$) in the cube after a time t is the sum of the salt amount originally present and the

208 [TS]-relationship and Connection with Mixing Processes and Large Water Masses
 salt increase due to the exchange of water quanta by mixing and is thus

$$\rho(s_0 + \Delta s_0) \times 10^{-3} = \int_{-\infty}^{+\infty} \rho s \times 10^{-3} q ds.$$

Putting with sufficient accuracy

$$s = s_0 + \left(\frac{ds}{dz}\right)_0 z + \frac{1}{2} \left(\frac{d^2s}{dz^2}\right)_0 z^2,$$

and using the above expression for q gives for the point A ($z = 0$)

$$k = \left(4\pi \frac{A}{\rho} t\right)^{-\frac{3}{2}}.$$

Then k is expressed in terms of the exchange coefficient A . The [TS]-relationship for the water column under consideration is presented in Fig. 96. At the reversal point A , $z = 0$ and the depth marks $+1, +2, +3, \dots$, and $-1, -2, -3, \dots$, respectively, correspond to the centre points of water cubes of 1 cm^3 ; the cube at A is thus the zero cube. The circle with a radius R ($AO = R$) approximates closely to the [TS]-curve at the point A . For the part of the curve under consideration the depth marks are so situated that the arc between each pair of depth marks always corresponds to the same angle α in point O . It is necessary to find the co-ordinates (temperature and salinity) after t sec of the zero cube initially at A . Two points M and N at vertical distances z and $z + dz$ cut out a volume element of $dz \text{ cm}^3$ of water. According to the previous discussion a quantity of water qdz is transferred from this element to the zero cube in t seconds. The same quantity of water qdz is also transferred from the symmetrically situated volume element $M'N'$ in the same time. These two quantities of water mix, and according to the mixing rule the mixture $2qdz$ corresponds on the [TS]-diagram to the small interval BC which is situated on the radius of curvature AO . It is determined by the distance

$$AB = r = R - R \cos(\alpha z) = \frac{1}{2} R \alpha^2 z^2$$

and

$$BC = dr = \frac{1}{2} \alpha^2 z^2 dR.$$

The water masses entering the zero cube during time t are not only transferred from the two cubes MN and $M'N'$, but also from all other cubes above and below, and it is easily understood that the T and S values for all these water masses must lie on the radius AO . Mixing of all these differential quantities gives the co-ordinates of the zero cube after t sec. Its position on the [TS]-diagram will be fixed by the distance Z along AO . According to the mixing rule this must be given by

$$Z = \int_0^R \int_0^\infty 2q dr dz.$$

One therefore obtains

$$Z = \frac{A}{\rho} R \alpha^2 t.$$

On the other hand, the chord drawn through Z perpendicular to AO intercepts an arc on the [TS]-curve with a centre angle ha (the depth marks at the end-points of the chord are $+\frac{1}{2}h$ and $-\frac{1}{2}h$) and

$$Z = R - R \cos \left(\frac{1}{2}ha\right) + \frac{1}{8} R a^2 h^2.$$

Comparison of the two values for Z finally leads to an exchange coefficient

$$A = \frac{\rho h^2}{8t}.$$

This equation can be used for the numerical determination of A if the [TS]-curve for a water column has been found by observation for successive times. In Fig. 97 I

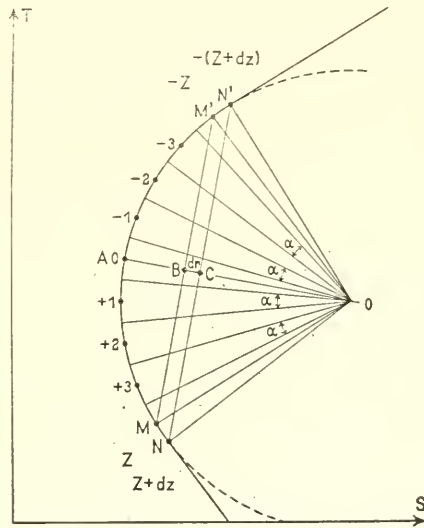


FIG. 96. Calculation of exchange coefficients by the method of Jacobsen.

denotes the initial distribution which is followed by distribution II after t seconds. It shows the changes that have taken place in the water column during time t . The points are depth marks for the determination of h . The tangent at A cuts the [TS]-curve I at the depth marks h_1 and h_2 ; the size of h is thus $h_1 - h_2$. The equation then allows calculation of the exchange coefficient A if t is known.

The Jacobsen method applies almost only to oceanic regions which are practically motionless and in which the gradual disappearance of a disturbance in the vertical structure due to vertical mixing can be determined by successive measurements. An application to *stationary water displacements* is possible using the principle that *phenomena occurring one after the other in time* can be replaced by *others occurring side by side in space*. Then the [TS]-diagrams I and II in Fig. 97 represent two successive stations at a distance L in the direction of water displacement. If u is the velocity of this displacement then $L = ut$ and from the above relation one obtains $A/\rho u = h^2/8L$. It can be seen that this method again gives only the ratio A/u .

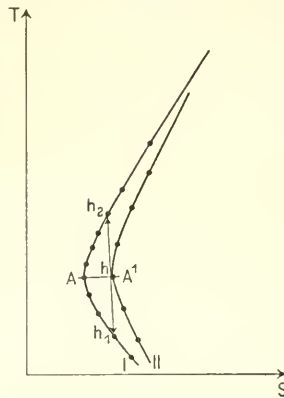


FIG. 97. [TS]-relationship in a water column at successive times.

4. Further Examples of the [TS]-Relationship

Extensive use has been made of the [TS]-relationship in oceanographic investigations of different oceanic regions. A detailed discussion of these investigations belongs to the individual sections on special oceanography and would be out of place here. The attention of the reader will therefore at present be directed more to the method used rather than to the phenomena characteristic for different parts of the ocean.

A most intensive analysis of the [TS]-curves for a single ocean was first made by JACOBSEN (1929) on the data collected by the "Dana" Expedition. He divided the North Atlantic into twenty-four areas with approximately uniform conditions, and he derived *mean* characteristic [TS]-curves for these areas, using then these curves to give an interpretation of the formation of the stratification by mixing of the five principal water types. A homogeneous set of data for the preparation of [TS]-curves for the South Atlantic as far as 10° N. has been provided by the "Meteor" Expedition. Figure 98 presents [TS]-curves for the West Atlantic Trough as an example for meridional changes. In this region extending over more than 44° of latitude (almost 5000 km) the thermo-haline structure follows the same law almost without exceptions. It is in principle fixed by five water masses U , Z , T , B_N and B_S and corresponding mixing curves. Basic values are given in Table 82.

Five points on the diagram characterize each of these water masses together with straight lines joining them, on which the mixed water masses must lie. The variations of the actual [TS]-curves from these ideal curves of pure mixing are surprisingly small, especially when there is a sufficient mass of water in the cores. This is usually the case, though for the subantarctic intermediate water as it progresses from south to north the [TS]-curve moves farther and farther into the angle between UZ and ZT , as is required by theory, showing that in this comparatively thin layer of water the core is also involved in the mixing process. This case can be used to calculate the ratio $A/\rho u$ for the spreading of the sub-antarctic intermediate water by applying the Jacobsen method (DEFANT, 1954). Figure 99 shows [TS]-curves at four successive oceanographic stations from south to north in the Western Trough of the South

Table 82. Water masses of the South Atlantic between 33° S. and 11° N.

		Temp. (°C)	Salinity (‰)
Antarctic components	Subantarctic intermediate water	Z	3.25
	Antarctic bottom water	B_s	0.4
North Atlantic components	North Atlantic deep water	T	4.0
	North Atlantic bottom water	B_N	2.5
Beneath the disturbed top layer approx. 100–200 m	Subtropical lower water	U	18.0

Atlantic but solely for 400–1400 m depth. The values for L and h in the Jacobsen equation on p. 210 can be obtained immediately from the curves and in that way Table 82a is obtained.

The mean value of $A/\rho u$ is 0.74 and for $u = 10$ cm/sec the quantity A is 7.4 cm²/sec which is in good agreement with values determined by use of other methods. A

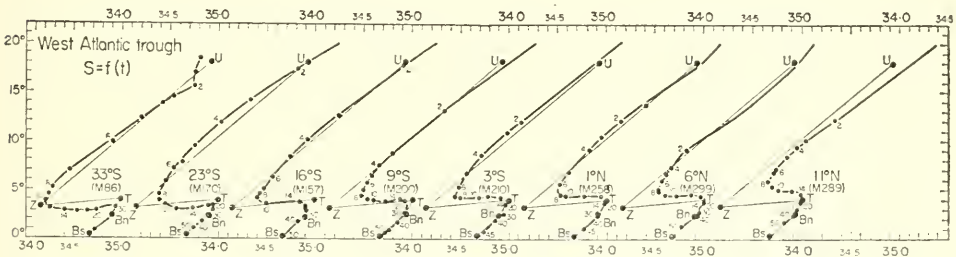


FIG. 98. [TS]-curves for a series of stations along the Western Trough of the Atlantic.

Table 82a. Determination of $A/\rho u$ by means of the JACOBSEN method

Station pair (St. no.)	L (km)	h (m)	$A/\rho u$ (cm)
160–202	600	215	0.96
160–297	3050	380	0.59
160–290	4150	485	0.71
202–297	2450	350	0.625
202–290	3550	510	0.92
297–290	1100	220	0.55

considerably more detailed treatment of problems briefly outlined here has been given by Wüst (1936) using this data and applying the so-called "core-layer method". The characteristic properties of a water mass are retained in the core layer and an analysis of changes in the core layers is therefore of decisive importance for an investigation of the spreading of a water type. The most difficult and essential part of such an investigation is the accurate determination of the core layer of each water type at each station from the vertical distribution of the different oceanic factors. A single factor will not necessarily be best for the characterization of the core layer. Thus salinity was found to be the most suitable indicator for the subantarctic intermediate water and also for the upper North Atlantic deep water which gets in the North Atlantic a continuous supply from mediterranean water, while the potential temperature is used for antarctic bottom water and oxygen content for Lower Deep Water (intermediate maxima in oxygen content). The spreading of a water type can be found by following the appropriate indicator. The subantarctic Intermediate Water can be taken as an example, to show the use of the "core layer method"; here the intermediate salinity minimum between 50° S. and 20° N. is an excellent indicator. The depth of this minimum and its salinity, temperature and oxygen content can be evaluated from the vertical curves of all stations. This water type sinks as shown by the analysis at the southern oceanic Polar front. The 100 m depth line runs parallel to and immediately to the north of it, and from here the depth of the core layer is shown by the isobath on Fig. 100. From 45° S. to 39° S. the core lowers continuously and rapidly from 100 m down to 800 m and reaches its greatest depth on the average at about 900 m between 37° S and 30° S. It then rises to about 800 m, falling again to 900 m or more north of 10° N. A chart of the S distribution shows that rapid lowering of the core goes parallel with a rapid rise in salinity from 33.9‰ to 34.2‰ ; beyond this region the meri-

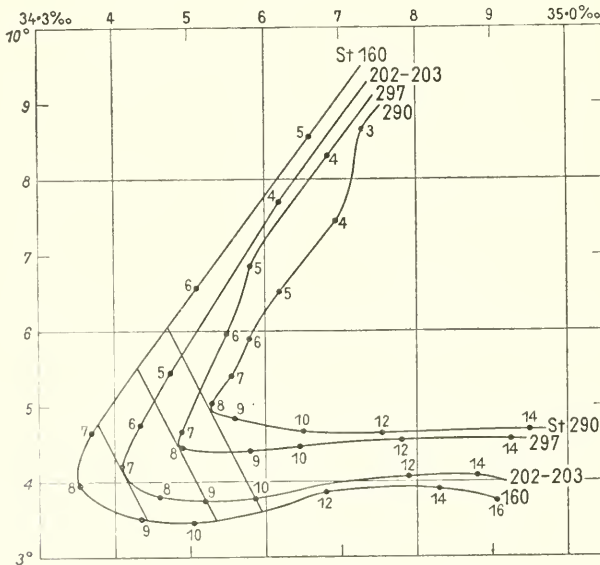


Fig. 99. [TS]-curves for four "Meteor" stations along a western longitudinal section in the Atlantic in the area of the subantarctic intermediate water (the figures give depths in 100 m-units).

dional increase in salinity is less, reaching 34.5‰ at the equator, and from there to 20° N. the increase is again more rapid (up to 34.9‰). According to the distribution of the isohalines, stronger mixing occurs at the western edge of the ocean. [TS]-relations of the core layer for the western and eastern parts of the ocean are approximately the same for the two halves of the ocean so that a standard curve can be prepared for the entire area where this water type (Fig. 101) is found. The point Z_p represents the mean properties of the unadulterated water in the area of formation near the oceanic Polar front and the last traces of this water type are found at point O . Dividing the interval between Z_p and O into 100 parts allows the determination of

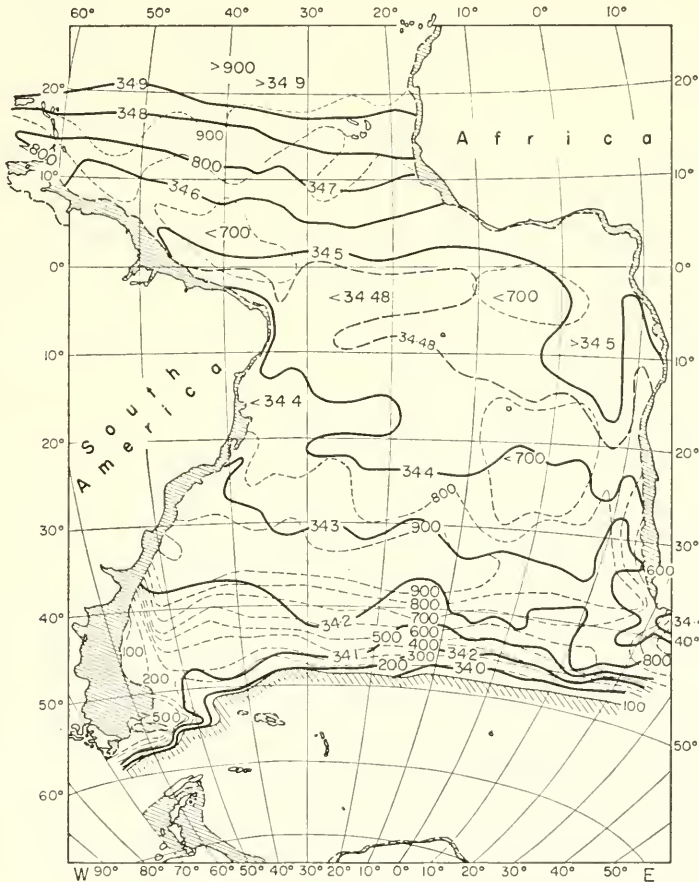


FIG. 100. Salinity (‰) and depth (metres) of the core layer of the subantarctic intermediate water in the Atlantic (according to Wüst).

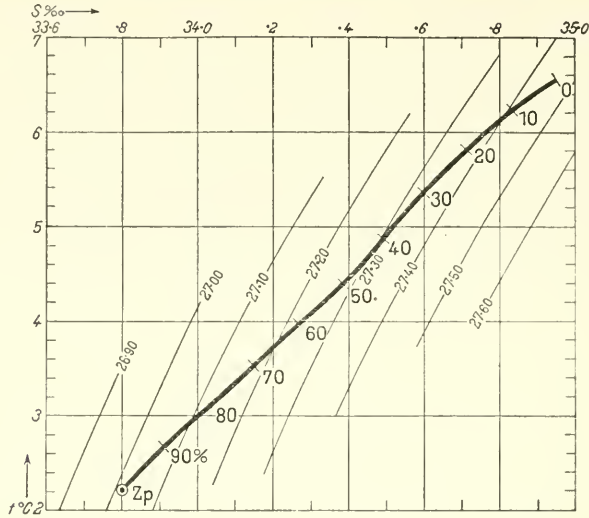


FIG. 101. Standard curve of the [TS]-relationship for the entire area of the core layer of the subantarctic intermediate water in the Atlantic.

the percentage influence of each individual component at any point in the spreading area. From these percentages for all stations a chart can be made with lines of equal percentages of subantarctic water to give a quantitative representation of the spreading, the gradual mixing and the final disappearance of this type of water (Fig. 102). Between 45° and 40° S. the subantarctic component of the intermediate water is still about 7%; the 50% line runs from South Africa to Cape San Roque and the 40% line extends from here in a narrow tongue along the continental slope to 9° N. The principal direction of spread is shown by arrows on Fig. 102.

Wüst has investigated in a similar way the other water types important in the thermo-haline structure of the Atlantic, and by making a numerical estimate of their spread from the [TS]-relations in the core layers. He thereby obtained a quantitative measure of the mixing of these water types.

A further example of the use of the [TS]-diagram in the study of the spreading of a water type is the *equivalent thickness-method* of JACOBSEN (1943); he applied this method in practice to investigate the penetration of Atlantic water through the Faroes-Shetland gap into the Norwegian Sea, the northern part of the North Sea and into the Barents Sea. This water type is characterized by values $\vartheta = 10.2^{\circ}\text{C}$ and $S = 35.45\text{‰}$. The water mass at any point in this area is formed by a mixture of pure Atlantic water with other water types. If it were possible to separate pure Atlantic water from the other types it would have at any point a definite thickness which Jacobsen called the "equivalent thickness" of Atlantic water. At any station this thickness can be found from the [TS]-relation in the following way: Fig. 103 shows the [TS]-diagram at a "Hjort" station on 1 May, 1935 at 63.0° N., 3.8° E. The [TS]-curve approximates the observed points rather closely.

The dashed straight line connects the points of the mixing components A (10.2°C , 34.5‰) and P (2.5°C , 34.90‰). The distance AP is divided into ten equal intervals and indicates the individual share of the two components. The section of the curve

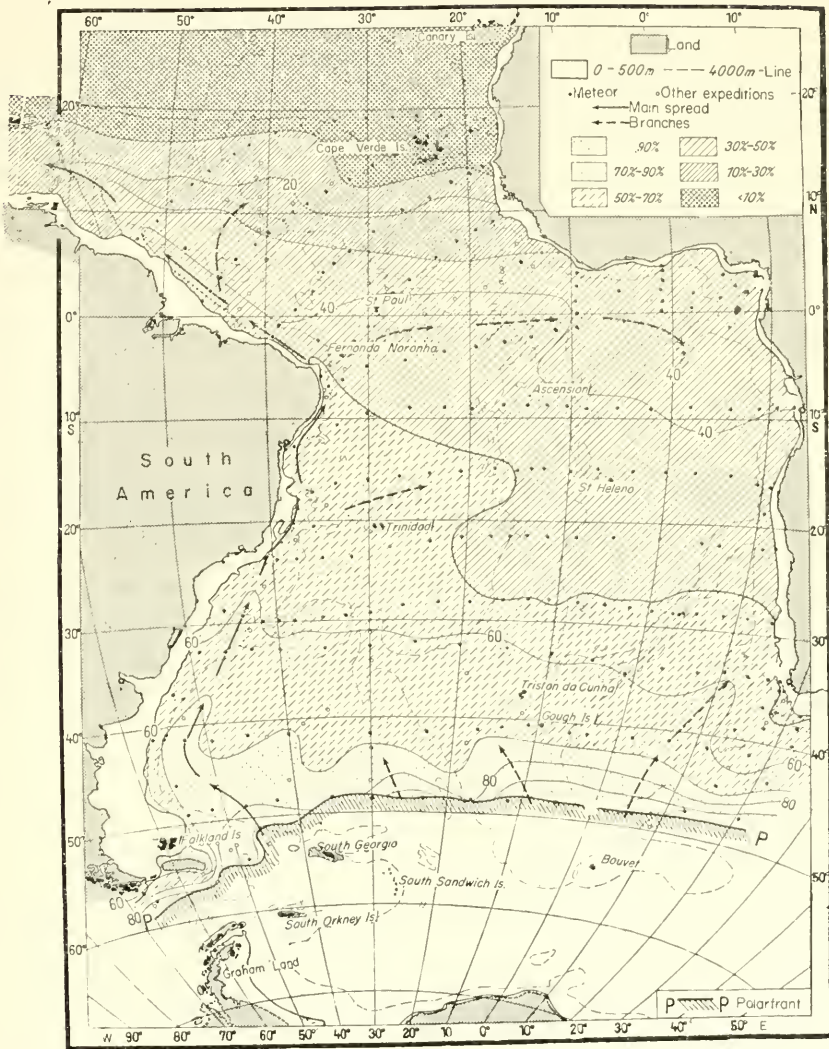


FIG. 102. Spreading of the subantarctic intermediate water represented by lines of equal percentage content of this water type (according to Wüst). The full arrows indicate the main course of the water spreading and the dashed arrows indicate the (more turbulent) side branches of it.

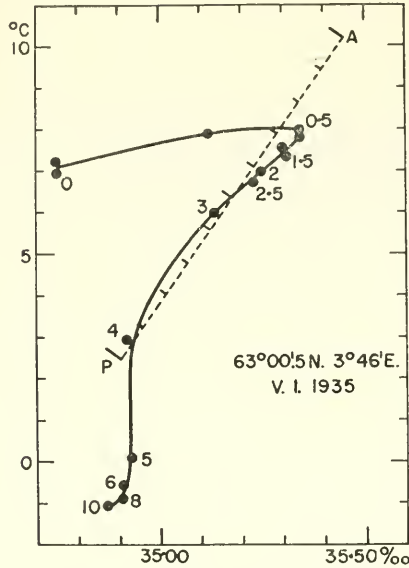


FIG. 103. Calculation of the equivalent thickness of Atlantic water type according to Jacobsen for the "J. Hjort"-Station 1 May 1935 (63° 0' N., 3° 08' E.).

50–100 m follows the straight line *AP* rather well and therefore shows that the water masses of this layer are composed principally of these two components. For different depths the participation of the Atlantic water in the vertical stratification of the ocean at this station can directly be read from the diagram. The following values are obtained:

Depth in m	50	150	200	250	300	400	410
Participation of component <i>A</i>	0.73	0.67	0.60	0.57	0.43	0.04	0.01

The equivalent thickness of Atlantic Ocean water at this station is then computed in the following way:

$$\frac{1}{2}(0.73 \times 50 + 0.70 \times 100 + 0.64 \times 50 + 0.58 \times 50 + 0.50 \times 50 + 0.24 \times 100 + 0.02 \times 10) = 108 \text{ m}$$

The resulting thickness is a measure of the amount of Atlantic water which participated in the formation of the water column at this station. A geographical distribution of the equivalent thicknesses over the entire spreading region of Atlantic water in the Norwegian Sea and in the Barents Sea is a rather good representation of the effect of the Atlantic current and of the heat carried by this current towards the north, and also allows a quantitative evaluation.

5. The Water Masses of the Oceans

An accurate analysis of the [TS]-relation in different parts of the oceans leads to a closer classification of the water types of which the ocean is made up. By a somewhat

schematic treatment it is possible to derive from the complicated forms of the [TS]-relations graphical representations of the characteristic water types of each ocean that give a good insight into the thermal and haline structure of the sea. This also assists in a clarification of the formation, spreading and mixing of the individual water types and thus facilitates a quantitative description of the oceanic circulation of the deep and bottom layers. Table 83 summarizes the characteristic water types of the three oceans and indicates the temperature and salinity ranges in them. These limiting values for temperature and salinity must naturally only be looked upon as a rather crude measure to demonstrate in what extreme limits oceanographic factors may vary.

Table 83. Water masses of the Atlantic Ocean

North Atlantic	Temp. (°C)	Salinity (‰)	South Atlantic	Temp. (°C)	Salinity (‰)
1. North Polar water	-1 to +2	34.9	1. South Atlantic central water	+5 to +16	34.3-35.6
2. Subarctic water	+3 to +5	34.7-34.9	2. Antarctic intermediate water	+3 to +5	34.1-34.6
3. North Atlantic central water	+4 to +17	35.1-36.2	3. Subantarctic water	+3 to +9	33.8-34.5
4. North Atlantic deep water	+3 to +4	34.9-35.0	4. Antarctic circumpolar water	+0.5 to +2.5	34.7-34.8
5. North Atlantic bottom water	+1 to +3	34.8-34.9	5. South Atlantic deep and bottom water	0 to +2	34.5-34.9
6. Mediterranean water	+6 to +10	35.3-36.4	6. Antarctic bottom water	-0.4	34.66

Water masses of the Indian Ocean

	Temp. (°C)	Salinity (‰)
1. Equatorial water	4-16	34.8-35.2
2. Indian central water	6-15	34.5-35.4
3. Antarctic intermediate water	2-6	34.4-34.7
4. Subantarctic water	2-8	34.1-34.6
5. Indian Ocean deep and antarctic circumpolar water	0.5-2	34.7-34.75
6. Red Sea water	9	35.5

Water masses of the Pacific Ocean

North Pacific	Temp. (°C)	Salinity (‰)	South Pacific	Temp. (°C)	Salinity (‰)
1. Subarctic water	2-10	33.5-34.4	1. Eastern South Pacific water	9-16	34.3-35.1
2. Pacific equatorial water	6-16	34.5-35.2	2. Western South Pacific water	7-16	34.5-35.5
3. Eastern North Pacific water	10-16	34.0-34.6	3. Antarctic Intermediate water	4-7	34.3-34.5
4. Western North Pacific water	7-16	34.1-34.6	4. Subantarctic water	3-7	34.1-34.6
5. Arctic Intermediate water	6-10	34.0-34.1	5. Pacific deep water and Antarctic circumpolar water	(-1)-3	34.6-34.7
6. Pacific deep water and Arctic circumpolar water	(-1)-3	34.6-34.7			

The central water at 500–800 m in each of the three oceans forms the principal mass which always has a structure with an almost linear [TS]-relation and thus manifests its normal mixing in both horizontal and vertical directions. Underneath, and separated from it by the Antarctic intermediate water, the deep and bottom waters are found in the Southern Hemisphere which have a remarkably similar structure in all three oceans. In the Northern Hemisphere the Atlantic is blocked off from the Arctic Sea and has little or no Arctic intermediate water, but the Pacific Ocean, on the other hand, definitely shows this water and thus this ocean is of a more symmetrical structure. The North Atlantic and the Indian Ocean show a strongly increased salinity in the layers between 800 and 2000 m due to the inflow of warm saline water from the Mediterranean and the Red Sea. These effects are quite strong and are evidenced even in the southern parts of these oceans. There are no corresponding disturbances in the Pacific Ocean. On careful examination of Table 83 one cannot fail to regard the striking similarity of the thermo-haline structure of the oceans with astonishment. There can be no doubt that this is a consequence of an analogous oceanic circulation driven and maintained by the same forces.

Chapter VII

Evaporation from the Surface of the Sea and the Water Budget of the Earth

1. Introduction

ONE of the most important problems with which both meteorology and oceanography is concerned is the water budget of the Earth. It can be assumed with a very considerable degree of probability that the cycle through which the water passes is closed. This follows, if a sufficiently long period is taken into consideration, from the constancy of the amount of water on the earth and from the absence of processes which could alter, and especially decrease, the total amount of water present. A *stationary* water cycle requires that the amount of water passing through any particular part of this cycle (as either liquid, solid or vapour) should not vary with time, and particularly that the amount of water entering the cycle by evaporation from the ocean is returned to it. In that way there is never any permanent gain or loss of water from any point of the cycle.

For a *quantitative* assessment of the water cycle on the Earth it is necessary to make a numerical estimate of the amount of water circulating through it. This can be done either at the place where water reaches the surface of the Earth from the atmosphere (precipitation), or where water leaves the Earth's surface in form of water vapour (evaporation). In both cases the numerical basis necessary for an estimate must be obtained from observations. On the continents the amount of water vapour precipitated from the atmosphere can be determined with sufficient accuracy by direct measurement of the precipitation, and this quantity can be determined more accurately the denser the network of rainfall measuring stations. The determination of the mean precipitation amount over the sea is, on the other hand, very difficult and is never precise because of uncertainties in the measurement of precipitation on boardship. On the other hand, the accurate determination of the amount of *mean* evaporation on the continents is accompanied by considerable difficulty while the direct determination of the evaporation from the oceans seems possible and can be made more easily because of the more uniform conditions at this surface, however, in practice critical examination is still needed. These circumstances give particular importance to the question of the magnitude of evaporation amount from different regions of the oceans.

2. Direct Measurement of the Evaporation on Board Ship and Methods for Obtaining Corresponding Values for the Sea Surface

The evaporation from the surface of the ocean can only be measured from ships under way and this involves—probably even more than in direct measurements ashore—a number of sources of error that require special attention. Evaporation differs from other meteorological factors such as barometric pressure, temperature, wind, and cloudiness, in that the apparatus used to measure it is able to exert a very considerable influence on the observed values. This greatly increases the difficulty of getting reliable and useful results, because the values obtained are always only *relative values* which give correct *absolute values* only after the application of suitable *corrections*.

Measurements on board a moving ship are made by using a vessel filled with sea-water and hung in a cardan suspension. MOHN (1883) used a volumetric method of determining the amount of water evaporated at a given moment. The loss in weight due to evaporation of the cylindrical evaporation vessel was replaced by refilling it with fresh water to bring it back to a zero mark; the evaporation height could thus be determined. A more accurate and reliable method is the determination of evaporation by observing the *change in salinity* which occurs in the evaporating water as a consequence of evaporation. Following a suggestion of Penck, a cylindrical glass vessel is used which has a cross-section of 288 cm² and a volume of 2400 cm³; it is filled with sea water and placed within a white-painted or nickel-plated mantle that protects the vessel against direct radiation. Chlorine titration before and after the evaporation period gives the increase in salinity and allows a very accurate determination of the evaporation. The mean error in a single measurement is seldom more than 3%; it derives from the uncertainties of the salinity determination and in refilling the vessel, while the diminution in volume during the observation can be disregarded.

Denoting with g_1 and g_2 the weights of the sea-water at the beginning and at the end of the evaporation time, with g_e and g_w those of evaporated water and of pure water and finally with g_s that of the salt at the beginning of the evaporation, then

$$g_1 = g_w + g_s \quad \text{and} \quad g_2 = (g_w - g_e) + g_s.$$

The salinity at the beginning and at the end of the measurement is then

$$s_1 = 10^3 \times \frac{g_s}{g_w + g_s} \quad \text{and} \quad s_2 = 10^3 \times \frac{g_s}{(g_w - g_e) + g_s}.$$

If ρ is the specific weight (density) of sea-water at the beginning of the measurement and J is the volume of the evaporated water amount from the vessel, it follows that, from the above relations,

$$g_2 = g_1 \frac{s_1}{s_2} \quad \text{and} \quad g_e = \rho J \frac{s_2 - s_1}{s_2}.$$

If ρ is the specific weight (density) of distilled water at the mean temperature t_w at the time of the measurement and o is the area of the evaporating surface, then the evaporation height becomes

$$h_e = \frac{J}{o} \frac{\rho}{\bar{\rho}} \frac{s_2 - s_1}{s_2}.$$

If $30\% < s < 40\%$ and $-2^\circ\text{C} < t_w < 30^\circ\text{C}$, then with sufficient accuracy $\rho/\bar{\rho} = 1.027$ and with the above values for o and J

$$h_e = 88.3 \frac{s_2 - s_1}{s_2}.$$

For mean conditions the accuracy of h_e is 3.4%, which is quite sufficient. If systematic errors in the measurement are avoided (such as spray from the sea, water drips, and inflow of ash, etc.), the difficulty at the present day is not in getting comparable measurements of evaporation but in the correction of the values in order to obtain sea surface values. The value required is not the evaporation height in a vessel *on board* but the considerably different values at the surface *of the sea*. For this it is necessary to know: (1) the factors on which in the most general case the magnitude of the evaporation depends; and also (2) the differences between these factors in the vessel on board the ship and at the free sea surface. For an answer to these questions it is thus essential, during long-term series of observations on board ship, to perform special additional measurements; for instance, of the temperature of the surface of the water in the evaporation vessel, etc., in addition to the self-evident meteorological observations on board. Measurements of the evaporation in this way have not been made very often. They were first carried out by WÜST (1920, see also SCHMIDT, 1921) in a fundamental investigation, and these values after critical interpretation were used to derive more correct average zonal values of the evaporation at the surface of the ocean. From all the formulae which have been used many times to calculate the effect of the meteorological factors, the best is the expanded Dalton evaporation formula in the form:

$$h_e = cf(u)(1 + at)(0.98e_s - e_a).$$

e_s is the height of water evaporated in 12 or 24 h, c is a constant and $f(u)$ takes into account the effect of wind velocity. The last two expressions in brackets, which were termed the "evaporation potential p " by MARVIN (1909), take into account the effect of the air temperature t and of the difference between the saturation pressure of water vapour at the temperature of the evaporating water e_s and the water-vapour pressure in the air e_a . The factor 0.98 takes into account the effect of salinity which hinders evaporation. As it is known if $30\% < s < 50\%$ at the sea surface then e_s can be put equal to $0.98e_s$ in the atmosphere whereby the evaporation is almost independent of the salinity.

From reliable measurements on board a moving ship single values of the quotient e_s/p can be computed and can be related with the motion of the air at the time of measurement, which is identical to the actual wind measured on board the moving ship. A conversion of the evaporation measured on a moving ship into that which was measured at deck height with an evaporation vessel at rest and at the true wind speed over the sea can be done with sufficient accuracy.

For correction of the true evaporation obtained from the instrument on board ship to that at the surface of the sea, i.e. of the free ocean, Wüst used the gradient of the *meteorological factors* between the evaporation vessel and the sea surface. A basis for estimating the gradients of air temperature, humidity and wind speed immediately above the sea surface was obtained from observations in the Baltic Sea (September

1919). The mean values of the gradients used by Wüst are, however, obtained from relatively few observations but appear, as confirmed by later observations, to be of the correct order of magnitude (SHOULEIKIN, 1928, MONTGOMERY, 1936-7/8, BRUCH 1940).

The total reduction factor for a conversion of this kind amounts to

$$k = 0.48 \pm 0.08.$$

It is seen that the *actual evaporation at the surface of the sea is on the average somewhat less than half of the true evaporation measured by an evaporation vessel on board ship.*

In this way Wüst obtained for the North Atlantic, for example, the following mean evaporation heights (Table 84) for average meteorological conditions.

Table 84. Evaporation in the Atlantic

Climatic regions	Latitude	Mean wind speed (km/h)	Mean vessel evaporation according to Wüst		Mean evaporation at the sea surface	
			mm/day	cm/year	According to Wüst	According to Lütgens
					cm/year	cm/year
Variable winds	50°-40° N.	30	4.0	146	66	95
Subtropical region	40°-30° N.	24	5.8	212	95	160
North-east Trade	30°-8° N.	24	7.8	285	128	240
Doldrums	8°-3° N.	10	5.5	201	91	115
South-east Trades	3° N.-20° S.	22	7.3	267	120	225
Subtropical region	20°-40° S.	20	5.8	212	95	175
Variable winds	40°-55° S.	28	2.8	102	47	100

This table also gives some idea of the values measured by an evaporation vessel in different climatic zones and of the meridional distribution of the evaporation amounts over the Atlantic Ocean. The last column on the right gives values obtained by LÜTGENS (1911) from his excellent measurements of evaporation; due to unsuitable correction, however, the latitudinal differences are overestimated, especially the evaporation amount in the trade regions, relative to that in the doldrums. The total procedure of a direct reduction of the observed evaporation on board a moving ship suggested by Wüst was later again controlled by CHERUBIM (1931), and he found, after application of some refined but not very important corrections, a reduction factor of 0.54 which, however, he multiplied by 1.08 in order to account for the influence of the motion of the sea giving the final value 0.583. This latter increase in the size of the correction factor by about 8% for the motion of the sea, for which there was no observational evidence, was regarded by WÜST (1936) as unsuitable since there were other factors, some acting in an opposite direction which had not been taken into account and of which the magnitude was equally unknown. The uncertainties of the direct correction are certainly rather large but if the value obtained by Cherubim is taken as a maximum and that obtained by Wüst as a minimum then a mean of 0.53 can be taken at the present time as the most probable correction factor.

3. Meridional Distribution of Evaporation over the Whole Ocean and its Determination from Energy Considerations

The mean values of the true evaporation for different parts of the ocean which can be regarded as the direct result of observations have been used by Wüst to give values for latitude zones of 10° width in the Atlantic and for the total ocean. These depend on interpolation and in part on extrapolation and can thus be considered only as a first approximation. The values recalculated with a correction factor $k = 0.53$ are given in Table 85. The zonal variations in evaporation, with pronounced maxima in the trade wind regions and a low value in the doldrums, are less pronounced in the figures for the total ocean than in those for the Atlantic alone. Due to the relatively large proportion of the Polar Sea with a low evaporation the mean value for the Atlantic is less than that for the total ocean. The *mean evaporation for the total ocean* found in this way is 93 cm/year or 2.54 mm/day. The limits of error for this mean value and for the zonal values are about $\pm 12\%$.

Table 85. Zonal distribution of evaporation in the Atlantic and for the total ocean (According to Wüst. (Correction factor $k = 0.53$.)

Zone	Atlantic (cm/year)	Total ocean (mean over all oceans) (cm/year)
80°–70° N.	8	8
70°–60° N.	12	13
60°–50° N.	44	44
50°–40° N.	78	78
40°–30° N.	107	107
30°–20° N.	138	130
20°–10° N.	146	133
10°–0° N.	107	112
0°–10° S.	141	125
10°–20° S.	138	133
20°–30° S.	125	125
30°–40° S.	99	99
40°–50° S.	65	65
50°–60° S.	26	26
60°–70° S.	8	8
Mean	91	93

The mean evaporation of the total ocean can also be determined by another method, suggested by SCHMIDT (1915). It has already been shown in Chapter III/1 (see p. 88), in discussing the heat budget, that evaporation is one of the most important items (loss) in the heat budget of the sea. From a comparison of the amounts of heat involved in the heat budget for the world ocean the maximum heat amount available for evaporation can be estimated.

Denoting the mean annual energy gain of the total ocean surface due to sun and sky radiation by Q_s , the energy loss due to outgoing radiation from the ocean to the

atmosphere with Q_b , the loss by evaporation with Q_e , and the loss by convection (turbulent heat conduction) with Q_h , then for a stationary state $Q_s = Q_b + Q_e + Q_h$. Introducing $R = Q_h/Q_e$ and $E = Q_e/L$, where L is 585 cal/g, the latent heat of evaporation of water, into the basic equation for the heat budget of the ocean (see p. 89) then

$$E = \frac{Q_s - Q_b}{L(1 + R)}.$$

If the radiation terms $Q_s - Q_b$ and R are known it is possible to calculate the evaporation. Schmidt carried out this calculation using, however, $R' = Q_e/(Q_s - Q_b)$ instead of R , and determined R' from general considerations as about 0.70. This gives a mean correction factor k for evaporation measurements on board ship, and he found $k = 0.43$ as the most probable value. For the extreme case $Q_h = 0$ (disregarding all convective processes) KLEINSCHMIDT (1921) found an upper value for k of 0.61. The good agreement with the value of Wüst of 0.48 is remarkable. ÅNGSTRÖM (1920) showed that Schmidt's estimate gave too large a value for R . From measurements and energy considerations he concluded that the value of R is only 0.1, which means that of the total gain in energy $Q_s - Q_b$, only 10% will be given off to the atmosphere by convection and approximately 90% used for evaporation.

The method of Schmidt has been carried further by MOSBY (1936), who attempted in particular to remove the uncertainty in the determination of the incoming radiation Q_s by the use of an empirical formula (see p. 91). The values for Q_s , thus obtained, are given in Table 86.

Table 86. Heat budget for the ocean.

(According to Mosby (g cal cm⁻² min⁻¹))

Latitude	$Q_s - Q_b$	Areas of the zones in million km ²
70°-60° N.	0.040	5.3
60°-50° N.	65	11.0
50°-40° N.	93	15.0
40°-30° N.	125	20.8
30°-20° N.	150	25.1
20°-10° N.	167	31.5
10°-0° N.	171	34.0
0°-10° S.	175	33.6
10°-20° S.	171	33.3
20°-30° S.	150	30.9
30°-40° S.	129	32.2
40°-50° S.	097	30.5
50°-60° S.	067	25.4
60°-70° S.	0.041	17.1

The mean value between 70° N. and 70° S., taking into consideration the ocean area of the separate zones, is estimated to 0.132 g cal cm⁻² min⁻¹. Since on average for the entire ocean advective processes are assumed to be of no importance, this is the *average* amount of heat available for evaporation and convection. However, Mosby

could give only an estimated value for the heat contribution to be ascribed to convective processes, which was based principally on Ångström's investigation. This quantity was finally assumed to be about one-tenth of the heat available for evaporation, so that a heat amount of about $0.119 \text{ g cal cm}^{-2} \text{ min}^{-1}$ must be available for evaporation. The estimation of the convectonal flow discussed on p. 92 led to a value of about $20 \text{ g cal cm}^{-2} \text{ day}^{-1}$, i.e., about $0.014 \text{ g cal cm}^{-2} \text{ min}^{-1}$. The agreement with the value assumed by Mosby is rather good, but this estimate applies only to temperate latitudes and the value should be increased for warmer climates to $0.030 \text{ g cal cm}^{-2} \text{ min}^{-1}$. Choosing a *mean* value of about $0.022 \text{ g cal cm}^{-2} \text{ min}^{-1}$, then the amount of heat available for evaporation will be $0.111 \text{ g cal cm}^{-2} \text{ min}^{-1}$. Since the evaporation of 1 cm^3 of water requires approximately 590 g/cal this latter value gives a *mean evaporation of 97 cm a year*, while Mosby's value is 106 cm a year . The accuracy here is also scarcely more than 10%. These values are in good agreement and within the limits of uncertainty of the value derived by Wüst.

Another possibility for determining the value of R was pointed out by BOWEN (1926). For identical eddy coefficients for the diffusion of water vapour and the turbulent conductivity of heat, the upward flux of the latent energy of water vapour and heat are given by

$$Q_e = -L \frac{0.621}{p} A \frac{de}{dz} \quad \text{and} \quad Q_h = -c_p A \frac{d\vartheta}{dz}$$

(see p. 92 concerning the latter equation).

From these equations it follows that

$$R = \frac{Q_h}{Q_e} = \frac{c_p p}{0.621 L} \frac{d\vartheta/dz}{de/dz}.$$

Putting $p = 1000 \text{ mb}$ and $L = 585$ and replacing the differentials by corresponding finite differences the Bowen ratio is obtained:

$$R = 0.64 \frac{\vartheta_s - \vartheta_a}{e_s - e_a}$$

where ϑ_s and ϑ_a denote the temperatures of water and air and e_s is the maximum vapour pressure of water at temperature ϑ_s and e_a is the actual vapour pressure in the air. JACOBS (1942, 1943) has determined the dependence of the Bowen ratio on latitude in the North Atlantic and the North Pacific and found that R decreases with latitude. The following values were found as the mean for both oceans:

Latitude (° N.)	70-60	60-50	50-40	40-30	30-20	20-10	10-0
R	0.45	0.31	0.21	0.15	0.11	0.10	0.10

The northward increase is an effect of the continents from which the cold air flows out over the warm sea in the winter. In the Southern Hemisphere this effect is missing so that R may increase only to about 0.25 at 70° S .

By making proper use of all observations and methods which were more or less independent on each other, WÜST (1954) has evaluated a mean meridional distribution

of evaporation. These mean annual evaporation amounts together with mean annual values of precipitations are contained in Table 87.

Table 87. Mean values of precipitation, evaporation and the difference between them ($E - P$) for the entire ocean (including adjacent seas)
(According to WÜST, 1954)

Zone in degrees	Precipitation cm/year	Evaporation cm/year	Evaporation-Precipitation cm/year
70-65 N.	34	12	-22
65-60 N.	65	20	-45
60-55 N.	77	34	-43
55-50 N.	105	55	-50‡
50-45 N.	112†	66	-46
45-40 N.	102	84	-18
40-35 N.	86	108	22
35-30 N.	74	125	51
30-25 N.	63	132	69
25-20 N.	57‡	137†	80†
20-15 N.	70	135	65
15-10 N.	103	132	29
10-5 N.	187†	126	-61‡
5-0	146	113‡	-33
70-0 N. §	101.0	110.6	9.6
0-5 S.	105‡	125	20
5-10 S.	109†	137	28
10-15 S.	94	139†	45
15-20 S.	76	137	61
20-25 S.	68	133	65†
25-30 S.	65‡	123	58
30-35 S.	70	110	40
35-40 S.	90	96	6
40-45 S.	110	78	-32
45-50 S.	117†	56	-61
50-55 S.	109	39	-70
55-60 S.	84	12‡	-72‡
0-60 S. §	91.45	102.1	10.7

† Maxima; ‡ Minima; § Excluding polar zones

4. Geophysical Aspects of Evaporation Problem

Evaporation is a physical process that takes place at the boundary surface between water and the air above it and depends on the conditions both in the water and in the air in the immediate vicinity of the surface. The formula showing the dependence of the evaporation height occurring in a certain time on the meteorological factors is usually given in the form

$$h_h = f_1(p) \times f_2(T) \times f_3(u) \times (e_s - e_a),$$

where each term represents the effect of one of the meteorological elements (p the pressure, T the absolute temperature, u the wind speed); e_s is the maximum vapour

pressure corresponding to temperature and salinity of water, e_a is the vapour pressure in the air. Different expressions have been chosen for the functions f_1 , f_2 and f_3 and a formula of this type is given on p. 220 which shows the dependence of observed evaporation on the prevailing meteorological conditions and with a suitable choice of constants gives satisfactory values. However, it can hardly be assumed that such an evaporation formula which is a product of different functions could give a correct and causative description of the actual *physical process* of evaporation; it is rather to be expected that such a formula would be of the form

$$h_e = f(p, T, u) (e_s - e_a),$$

where the function f is probably a complicated function of the meteorological factors.

According to the results of research in turbulence, the transport of the water vapour continuously formed at the sea surface into the air immediately above it proceeds by turbulent exchange; the magnitude of this exchange depends on the roughness of the evaporating surface which in turn also depends on the velocity of the air over the water. SVERDRUP (1936, 1937-8, 1951) was the first to attempt to clarify the problem as to how the evaporation process operates at the surface of the sea with a well-defined roughness under the influence of the turbulent exchange. His ideas are based on two circumstances which are essential for a solution of this problem:

(1) Immediately above the water surface a thin boundary layer exists in which the water vapour transport proceeds only by ordinary (molecular) diffusion.

(2) Above this boundary layer the water vapour transport proceeds through the turbulent *exchange A* in form of random movements of the air particles (turbulence).

The exchange A (according to laboratory experiments) is a linear function of the height above the water surface and depends on the roughness of the water surface. The latter is described by the *roughness parameter* z_0 , and according to the results of Rossby about the increase of wind velocity with height z_0 is considered constant immediately above the sea surface ($z_0 = 0.6$ cm). This is valid for weak to moderately strong winds. Correspondingly,

$$A = \rho k_0 (z - z_0) \sqrt{\frac{\tau}{\rho}},$$

where τ is the tangential force (stress) of the wind, ρ is the density of the air and k_0 is the Kármán constant with a value of 0.38-0.40 (see Vol. I, Pt. 2).

The thickness of the boundary layer immediately above the water surface depends on the wind velocity. The layer itself can hardly be regarded as invariably composed of the same air particles. Since the turbulent eddies will sometimes penetrate down to and into the boundary layer, it must clearly be understood that this layer occasionally disappears completely; however, after some time it will always be re-formed so that a mean thickness of this layer can be introduced.

In addition to the theoretical case built up on the basis of these ideas Sverdrup also discussed a second possibility where the water surface was assumed to be "smooth" and the transport of water vapour away from the sea, due to turbulence, starts from the sea surface itself. Observations seem to favour the first case with a diffusion layer and turbulent transport above, and therefore only this case will now be dealt with.

For the exchange coefficient A we may write

$$A = \rho k_0 (z - z_0) u_*,$$

if the so-called "friction velocity" is introduced according to Kármán:

$$u_* = \sqrt{\frac{\tau}{\rho}}.$$

The values for z_0 and u_* follow from measurements of the wind over the surface and depend on the character of this surface.

In the turbulent layer the water vapour transport E (expressed in $\text{g cm}^{-2} \text{sec}^{-1}$) directed upwards is due to the turbulent exchange process and is given by

$$E = -A \frac{dq}{dz},$$

where q is the specific humidity which decreases upwards. q may be replaced in this formula by the vapour pressure e according to the well-known formula

$$q = \frac{0.623}{p - e} e,$$

and one obtains with sufficient accuracy

$$E = -\frac{0.623}{p} A \frac{de}{dz}.$$

The process of evaporation must be regarded as *stationary* ($E = \text{constant}$), so that with the above value for A , if c is a constant,

$$\frac{de}{dz} = -\frac{c}{(z + z_0)}.$$

Denoting the value of e at the lower boundary of the turbulent layer or at the upper limit of the diffusion layer (thickness d , $z = d$) with e_d , then integration gives

$$e_z = e_d - c \ln \frac{z + z_0}{d + z_0}.$$

On the other hand, the quantity E was found to be

$$E = -\frac{0.623}{p} \rho k_0 u_* (z + z_0) \frac{dz}{de} = \frac{0.623}{p} \rho k_0 u_* c.$$

The transport of water vapour through the diffusion layer is given by the equation

$$E' = \delta \frac{e_s - e_d}{d},$$

where δ is the diffusion coefficient of water vapour in the boundary layer with reference to vapour pressure. At the boundary of the two layers the water vapour transport is steady so that the necessary condition

$$z = d, \quad E = E'$$

must be satisfied. Considering, in addition,

$$\delta = \kappa \frac{0.623}{p} \rho,$$

where κ is the diffusion coefficient in cm^2/sec then the thickness of the diffusion layer is given by

$$d = \frac{\kappa}{k_0 u_*} \left[\frac{e_s - e_z}{c} - \ln \frac{z + z_0}{d + z_0} \right]$$

and for a roughness parameter z_0

$$u_* = \sqrt{\frac{\tau}{\rho}} = \frac{k_0}{\ln\{(z + z_0)/z_0\}} \quad u_z = \frac{0.165}{\log\{(z + z_0)/z_0\}} u_z,$$

where u_z is the wind velocity at a height z . Finally, the evaporation E is thus obtained from the above formula

$$E = \frac{\delta u_*}{\frac{\kappa}{k_0} \ln \frac{z + z_0}{d + z_0} + u_* d} (e_s - e_z).$$

If the thickness of the diffusion layer is known then the evaporation E can be calculated, if we observe: (1) the wind velocity at a height above the surface of the water, by means of which u_* is found; (2) the temperature and the relative humidity at this height, wherewith e_z is known; (3) the salinity, from which e_s can be determined. Only observations can give information on the thickness of the layer d . For this Sverdrup used the values determined by MONTGOMERY (1940) on board the research vessel "Atlantis", wheriby $z_0 = 0.6 \text{ cm}$ was assumed. Table 88 contains this calculation.

Table 88. Values of the friction velocity u_* , the evaporation E and the thickness of the diffusion layer d for a rough water surface ($z_0 = 0.6 \text{ cm}$)

(According to observations of the research vessel "Atlantis")

Observation group	u_* (cm, sec)	$10^6 E$ ($\text{g cm}^{-2} \text{ sec}^{-1}$)	$10^6 E$ $e_{u_*} - e_{0.6\text{cm}}$	d (cm)
b_1	13.2	1.06	0.30	0.28
a_1	14.3	1.34	0.34	0.22
c_1	17.0	1.98	0.30	0.33
d	18.7	2.86	0.33	0.31
g	24.8	5.15	0.39	0.29
f	25.3	4.64	0.45	0.23
a_3	25.6	5.82	0.53	0.16
c_2	29.2	8.49	0.74	0.09
e	29.2	5.68	0.70	0.10
h	36.3	6.98	0.80	0.10

The value of d decreases with increasing wind velocity, and Fig. 103a shows that as a rough approximation d increases linearly with $1/u_*$. With suitable weighting of each group Sverdrup obtained $d = 4.12/u_*$.

Unfortunately, there are no simultaneous measurements of evaporation available to allow a close test of the theory. Sverdrup with these values of d and using the meridional distribution of temperature, relative humidity and wind velocity at the surface of the Atlantic, calculated the meridional distribution of evaporation and compared this theoretical distribution with the zonal values obtained by Wüst, applying the

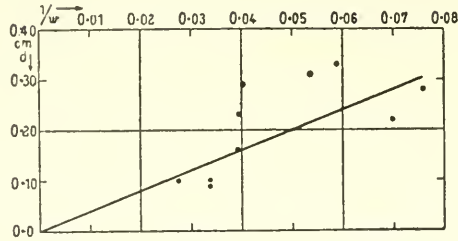


FIG. 103a. Relationship between the thickness of the diffusion layer (d) and the reciprocal of the shearing-stress velocity ($1/u^*$).

correction method to the direct measurements of the evaporation on board ships. Taking, according to the preceding section, the mean annual evaporation height for the Atlantic as 100 cm then the values given by Wüst, and shown in Table 89 having a mean evaporation of 83 cm, must be multiplied by the factor 1.22 (they have to be divided by 293 if values in mm/day are needed).

Table 89. *Values of evaporation for zonal regions of the Atlantic found by calculation from the meteorological data and from observations of evaporation*

Latitudinal zone	Temperature (°C)		Relative humidity (%)	e_s † (mb)	e (mb)	u (m/sec)	Evaporation (mm/day)	
	Water	Air					Calculated	Observed
50°–40° N.	10.8	10.5	82	12.74	10.10	8.4	2.3	2.2
40°–30° N.	18.3	17.2	80	20.64	15.73	6.7	3.3	3.2
30°–8° N.	25.4	24.9	76	31.82	24.92	6.7	5.2	4.3
8°–3° N.	27.4	26.8	83	35.80	29.26	2.8	1.9	3.0
3° N.–20° S.	25.8	25.7	78	32.62	25.80	6.1	4.1	4.0
20°–40° S.	19.5	18.3	80	22.25	16.85	5.6	3.2	3.2
40°–55° S.	9.9	8.7	82	12.00	9.26	7.8	2.2	1.6

† Taking into account the factor 0.98 as the effect of salinity

Table 89 presents this calculation, and a comparison between calculated and observed E values. Figure 104 shows the results graphically. The agreement between the observed and the calculated values is rather good, and in any case considerably better than in the second case treated by Sverdrup for a smooth surface without any diffusion layer. This agreement shows that the theory of a diffusion-layer with a thickness decreasing with increasing wind velocity and with a turbulent layer above it with a roughness parameter $z_0 = 0.6$ cm is capable of explaining the evaporation at the surface of the sea. However, all the assumptions so far are based on very few observations, so that further support by systematic measurements would be extremely desirable. The evaporation formula on p. 228 shows in any case that the dependence of the evaporation on the meteorological conditions in the atmosphere above it is more complicated than was assumed in previous relationships, and that deeper insight into these phenomena can only be obtained by a geophysical analysis of the evaporation process.

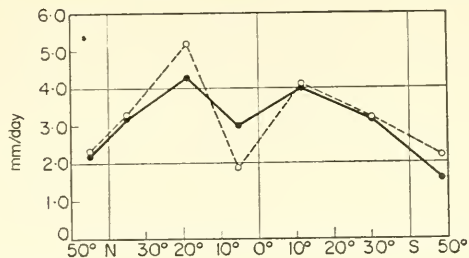


FIG. 104. Calculated and observed values of evaporation in successive latitudinal zones of the Atlantic (according to Wüst).

The formula given above for E can be changed into a more practical form. Expressing e in mm and u in m/sec and putting $p = 1000$ mb and $z = 10$ m then E in mm/24 h will be given by

$$E = K_{10}(e_s - e_{10}) u_{10}.$$

K_{10} lies between 0.12 and 0.19. This simple formula is quite remarkable since it is based solely on theoretical considerations. The theory of evaporation discussed above involves a hydrodynamically smooth surface with a laminar boundary layer (molecular diffusion of water vapour) with a turbulent layer of air above it. The evaporation from the water surface can also be calculated for other different stratifications of the layer of air above the water and there can be obtained the general equation

$$E = \rho \kappa_0 \gamma \Gamma_a (e_s - e_a) u_a,$$

where κ_0 is the Kármán constant, γ is the frictional coefficient and Γ is the Montgomery evaporation factor. The latter depends on the structure of the lowermost layer of air, on the wind velocity and on the stability and nature of the boundary layer. The observations of Montgomery seem to indicate a sharp increase in Γ at $u = 6.5$ m/sec for $a = 6$ m, while lower values for Γ are found for lower wind velocities. In this case, the water surface is smooth and has a laminar boundary layer above it. Turbulence only becomes effective with higher wind velocities and increases the evaporation rate. Only further observation can show whether this transition is gradual or sudden. On this subject see Vol. I, Pt. 2, and especially MUNK (1947).

5. The Water Budget of the Earth

The source of atmospheric water vapour is to be found in the first place in the evaporation of water at the surface of the ocean; the evaporation of water from the continents taking only a secondary place. In so far as the water vapour formed over the surface of the ocean remains there, condenses to clouds and returns as precipitation, it is referred to as a *minor water cycle*. Part of the oceanic water vapour is, however, carried by air currents inland over the continents and together with water vapour originating from the land gives rise to precipitation over the land. If this water is not evaporated again and returned directly to the atmosphere, it will be returned to the sea by streams, rivers and ground water (run off), and closes in that way the major water cycle.

Since the total amount of water on the Earth from a more general view-point can be considered a constant, seven items enter into the total water budget, which for a stationary state must be related with each other according to a strict principle of dependence.

These seven items are the following:

- E_0 the mean annual evaporation amount from the oceans;
- E_c the mean annual evaporation amount from the continents;
- P_0 the mean annual precipitation amount over the oceans;
- P_c the mean annual precipitation over the continents;
- W_0 the annual amount of water vapour in the atmosphere above the sea passing over to the continents;
- W_c the annual amount of water vapour in the atmosphere above the land passing over to the sea;

R The annual outflow of water in rivers, etc., into the sea (run off).

The constancy of total water in all oceans requires that the total mean annual inflow of water into the oceans $P_0 + R$ must be balanced by the total amount of water removed E_0 ; the constancy of the water on the land requires that the water gained by the land P_c must be equal to the water lost $E_c + R$; and finally the constancy of the atmospheric water vapour over the oceans and over the continents requires that

$$E_0 - W_0 + W_c = P_0,$$

and

$$E_c + W_0 - W_c = P_c.$$

From this it follows that the annual outflow of river water and other water into the ocean (total run off) must be exactly equal to the difference between the amount of water vapour in the atmosphere passing from the sea into the land and that passing from the land out over the sea. Thus, the following formulation for the balance of the budget of the water cycle on the Earth is obtained, which are known as the basic "Brückner" equations for the water balance of the Earth (BRÜCKNER, 1905; FISCHER, 1925).

These basic equations can also be derived, as has been shown by DEFANT and ERTEL (1943), from the continuity considerations of the total water content of the atmosphere in a closed and more general form. The amount of water contained in a unit volume of atmospheric air consists, on the one hand, of the dry air (density: ρ_a g/cm³) and of the amount of water vapour (density: ρ_w), and on the other hand, of the amount κ (g/cm³) of the condensed water vapour in liquid or solid form. Changes in the amount (ρ_w) of water vapour in unit volume and unit time can occur locally:

- (1) By the convergence (negative divergence) — $\text{div}(\rho_w \mathbf{w})$ of the convective flow $\rho_w \mathbf{w}$ of water vapour.
- (2) By the convergence of the turbulent flux — $\text{div} \mathfrak{S}$. The turbulent flux is given by $\mathfrak{S} = -A \text{ grad } q$, where A is the exchange coefficient (g cm⁻¹ sec⁻¹) of the specific humidity $q = (0.623/p)e$.
- (3) By evaporation of a definite amount of condensate or by condensation of a definite amount of water vapour, respectively:

$$\pm m [\text{g cm}^{-3} \text{ sec}^{-1}].$$

This quantity m represents the internal turnover of water in unit volume per unit time and is positive if more condensate evaporates than water vapour condenses, but negative if more water vapour condenses than condensate evaporates.

The continuity equation for water vapour is thus

$$\frac{\partial \rho_w}{\partial t} + \text{div}(\rho_w \mathbf{w}) + \text{div} \mathfrak{S} = +m.$$

Local changes in the condensate κ in a unit volume in unit time can occur in two ways:

(1) By the evaporation of a definite amount of condensate or by condensation of a definite amount of water vapour respectively. If more condenses than evaporates, then according to the above argument this change is $+m$; however, in the opposite case, $-m$.

(2) The water content in a unit volume (liquid or solid) can also change if, for instance, part of it is removed as precipitation or is advected by air currents to other levels. For each point in space this movement of condensate can be considered a *condensate flow* which can be described by a vector \mathfrak{R} . The absolute value $|\mathfrak{R}|$ is the amount of condensate which passes in unit time through a unit area of a surface perpendicular to the direction of movement of the condensate. At the point where there is no condensate or if the condensate shows no movement then $|\mathfrak{R}| = 0$. The flux of condensate through a unit surface along the normal μ is $\mathfrak{R}_n = \mathfrak{R}_\mu$, and in particular, for $z = 0$

$$\mathfrak{R}_n = -\mathfrak{R}_z = N$$

gives the precipitation amount per unit area and unit time at the surface of the Earth ($z = 0$). The change of κ due to such processes of condensate movement is then given simply by the convergence $-\text{div} \mathfrak{R}$ of the condensate flux.

The *condensate continuity equation* is then

$$\frac{\partial \kappa}{\partial t} = -\text{div} \mathfrak{R} - m.$$

Adding the two continuity equations for water vapour and condensate gives the *continuity equation for the total water content* finally in the form

$$\frac{\partial(\rho_w \mathbf{w} + \kappa)}{\partial t} + \text{div}(\rho_w \mathbf{w} + \mathfrak{S} + \mathfrak{R}) = 0.$$

For a *stationary*, average state in the atmosphere this equation reduces to

$$\text{div}(\rho_w \mathbf{w} + \mathfrak{S} + \mathfrak{R}) = 0.$$

Imagine now a vertical surface of control B , which parallels the coasts of a (not necessarily continuous) continent and reaches upwards to the upper limit of the atmosphere. Considering a surface element dB with a horizontal normal n directed towards the interior of the continent (landwards). Then, integrating the above equation over the total volume between the surface of control B , the surface of the Earth and the

upper limit of the atmosphere, it follows, according to the Gaussian integral law,* that for the total column of air over the land

$$-\iint_B (\rho_w w + \mathfrak{E}) dB - \iint_L \mathfrak{E}_z dL - \iint_L \mathfrak{R}_z dL = 0,$$

where dL is an element of the land surface L ; the two terms of the first integral vanish for the land surface and the upper limit of the atmosphere since at these extreme limiting surfaces either ρ_w or w will be equal to 0 or A will be 0; for the two other integrals the amounts passing through the control surface B disappear. Now, the mean precipitation amount per unit time on the continent is

$$P_c = - \iint_L \mathfrak{R}_z dL = \iint_L P dL,$$

and the mean evaporation amount over the continent is

$$E_c = \iint_L \mathfrak{E}_z dL.$$

Finally, the water vapour flux through the surface B towards the land is

$$W_0 - W_c = \iint_B (\rho_w w + \mathfrak{E})_n dB.$$

The condition of a stationary state thus gives one of the basic Brückner equations as

$$E_c - P_c + (W_0 - W_c) = 0.$$

If, on the other hand, the integration is taken over the total ocean, one obtains in the same way [the inwards (oceanwards) directed horizontal normal of dB is now $-n$] the second basic Brückner equation

$$P_0 + E_0 + (W_0 - W_c) = 0.$$

Integration of the continuity equation over the entire atmosphere above the surface ($C + O$) gives

$$P_c + P_0 = E_c - E_0,$$

which can, of course, also be obtained by subtraction of the first two equations.

The basic equations for the water budget of the Earth involve five quantities; a knowledge of three is sufficient to evaluate the others numerically. In general, it does not matter which of them we presume as known and which we want to obtain. However, the accuracy with which the different quantities can be determined from the available observations is not the same for each. The precipitation over the sea can be estimated only with difficulty. For that purpose in wide regions of the oceans only the rain density (the mean precipitation amount for a single rain day) and the rain frequency (the average number of days with precipitation) are available from ships'

* The *Gaussian* integral law states that the volume integral of a volume V with a surface A taken over $\text{div } a$ is equal to the negative surface integral of a_n taken over the entire surface A , where n is the normal to A directed towards the interior, so that

$$\iiint_V \text{div } a dV = - \iint_A a_n dA.$$

observations, and the product of these quantities gives only an approximate idea of the annual precipitation amount. In addition to these observations there are also available precipitation records in coastal areas or from islands, but these are often strongly affected by local topography so that there is usually a greater precipitation amount than over the neighbouring oceanic regions. Therefore, the utmost critical inspection and caution is needed in the use of records of coastal and island precipitation for the construction of isohyets for the oceans. However, with suitable allowances, better numerical estimates can be made of the evaporation over the sea so that the mean evaporation amount allows in return an estimate of the precipitation amount over the oceans.

The reverse applies on the land; here the determination of the mean evaporation involves almost insuperable difficulties, but a dense network of precipitation stations can give the mean precipitation with suitable accuracy. In this way a complete picture of the water budget of the sea, the land and of the total Earth can be obtained. Such a summary however, does not give absolutely correct annual values since the accuracy of each item in the water budget is not very great. It is thus of more importance to enclose the different values within the most narrow limits possible so that the individual values either support or exclude each other, in order to obtain maximum probability. Table 90 summarizes the essential characteristics of the water budget of the Earth.

Table 90. Most probable water budget of the Earth

	Precipitation		Evaporation		Outflow (–) and inflow (+)	
	10 ³ km ³ /year	cm/year	10 ³ km ³ /year	cm/year	10 ³ km ³ /year	cm/year
Ocean	324	90	361	100	+37	+10
Continent	99	67	62	42	–37	–25
Entire Earth	423	83	423	83	—	—

The following points may be noted. The figures for precipitation are based on those obtained by MEINARDUS (1934) from a most detailed investigation of the distribution of precipitation over the Earth based on the precipitation charts for the oceans prepared by Schott. The values for the land were taken directly. For the sea a correction was applied based on the criticisms made by WÜST (1936) of these charts. Meinardus found a total precipitation over the oceans of $411.6 \times 10^3 \text{ km}^3$ which corresponds to a mean annual rainfall of 114 cm/year. The mean precipitation over the oceans would thus be 1.7 times greater than over the land (67 cm/year), which can hardly correspond to actual conditions. No doubt too much consideration of island and coastal precipitation must have appreciably raised the precipitation amount over the oceans. Calculation of the precipitation over the sea from the total evaporation over the sea of 100 cm/year = $361 \times 10^3 \text{ km}^3/\text{year}$ and the inflow from the land (FRITSCHÉ, 1906) of $37.1 \times 10^3 \text{ km}^3/\text{year}$ gives a correction factor of 0.79 for correcting the rainfall at coastal and insular stations to values for the undisturbed sea surface. The coastal and insular values are thus on the average raised by about 20% by the effects

of topography above the values for the open ocean. This probably is not too far from the actual conditions.

For the entire Earth, according to recent calculations (REICHEL, 1952), the mean annual precipitation is about 86 cm/year, which under stationary conditions is balanced by an equally large evaporation amount. Therefore the average evaporation amount for the whole Earth amounts to 2.37 mm water per day. An interesting graphical representation of the total hydrologic cycle has been given by LETTAU (1954), and is shown in Fig. 105. It gives detailed information on all aspects of this cycle.

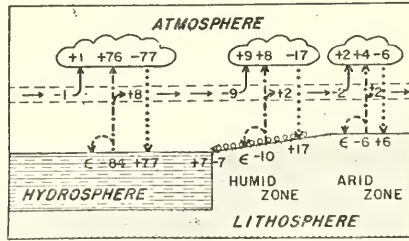
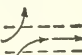


FIG. 105. Schematic diagram of the hydrologic cycle. 100 relative units = $85.7 \text{ g cm}^{-2} \text{ year}^{-1}$ or 857 mm global annual mean of precipitation (according to Lettau, 1954).

1 — — — ►, Evaporation; 2 ····►, Precipitation; 3 — — —▷, Dew deposit;

4 ○ ○ ○ ○ ○▷, Run off; , Removal from and addition to horizontal advection

of water vapour; 6 € = values smaller than 0.5 rel. units.

6. Energy Budget between Ocean and Atmosphere for Different Oceans and Oceanic Regions

The heat turnover between the total ocean and the total atmosphere has already been discussed in previous chapters. It is also of considerable interest to know the energy budget between the ocean and the atmosphere for the individual oceans and for different parts of the ocean, since on this depend the effects of the sea on the atmosphere above it or, in turn, the influences of the atmosphere on the sea. Such investigations, in spite of their importance, have only recently been made and indeed have been carried out almost exclusively by JACOBS (1942, 1943, 1951*a, b*) and ALBRECHT (1949, 1951). These investigations are based on the calculation of the evaporation from the formula on p. 230 using the differences $\vartheta_s - \vartheta_a$ and $e_s - e_a$ derived from climatological charts of the oceans. Doubts about these latter values have been expressed by DIETRICH (1950), but it appears that any errors that may have been introduced in this way are not systematic but may vary from one region of the sea to another and should, at least in part, cancel out. Calculations of this type have been made especially for the North Atlantic and the North Pacific, for which the climatic charts are more reliable. Such calculations of course give only a rough estimate but they serve, however, to give an approximately quantitative idea of the interplay between ocean and atmosphere. At first the most important is the pure heat gain by the radiation turnover $Q_s - Q_b$, whereby Q_s is the absorption of solar and sky radiation and Q_b is the radiation loss from the sea surface.

Figure 106 shows the geographical distribution according to SVERDRUP (1943) of the annual surplus of radiation penetrating the water surface. Over the whole year the oceans have everywhere a gain of heat from radiation, but north of 25° N . this gain decreases rapidly with latitude, therefore from 10° to 45° N . it is smaller on the eastern

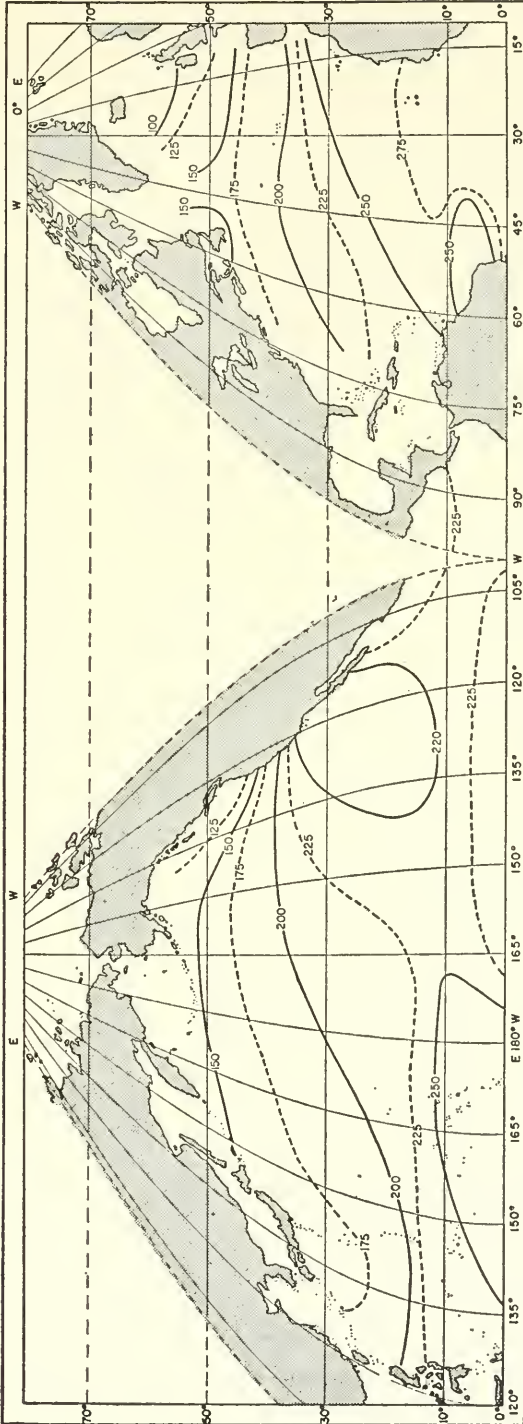


FIG. 106. Net annual surplus of radiation penetrating the water surface ($\text{g cal}^{-2} \text{ day}^{-1}$) (according to Sverdrup, 1943).

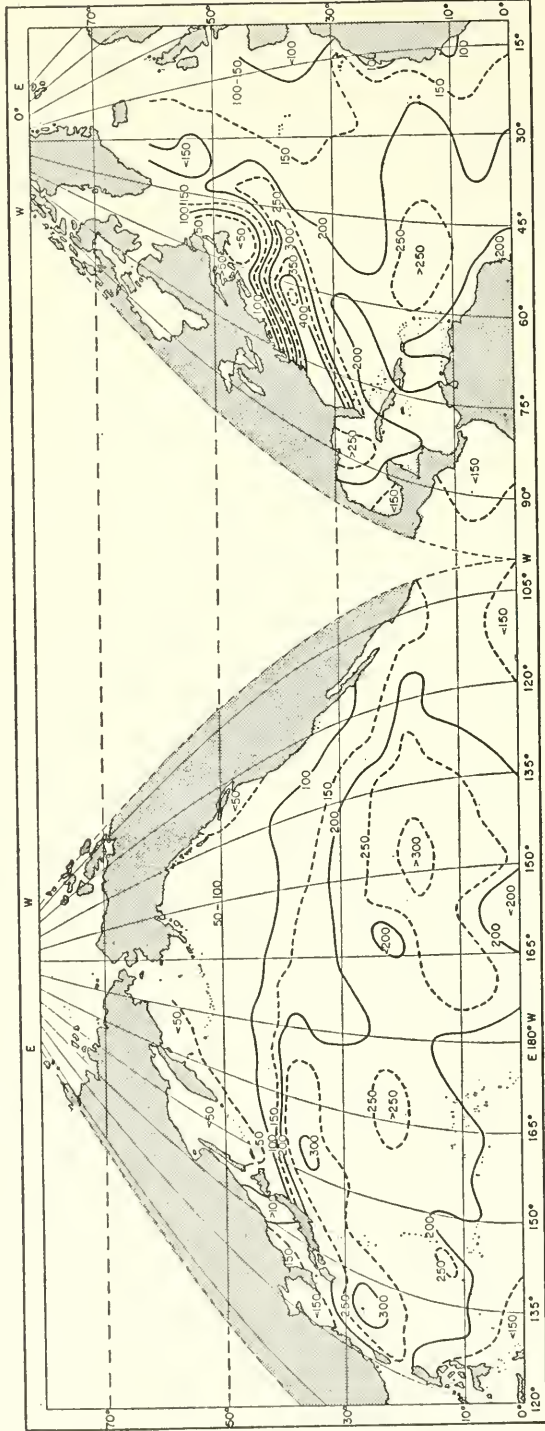


Fig. 107. Mean annual values of the rate of energy loss from the sea surface by evaporation: Q_e ($\text{g cal cm}^{-2} \text{ day}^{-1}$).

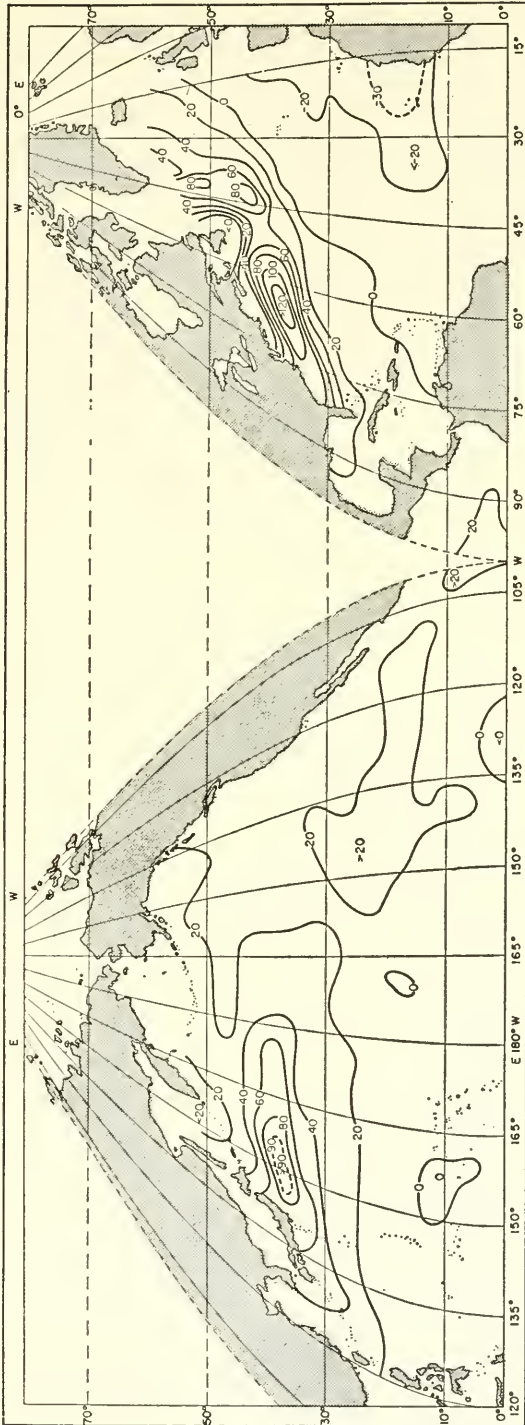


FIG. 108. Mean annual values of the rate of exchange of sensible heat between ocean and atmosphere Q_s ($\text{g cal cm}^{-2} \text{ day}^{-1}$).

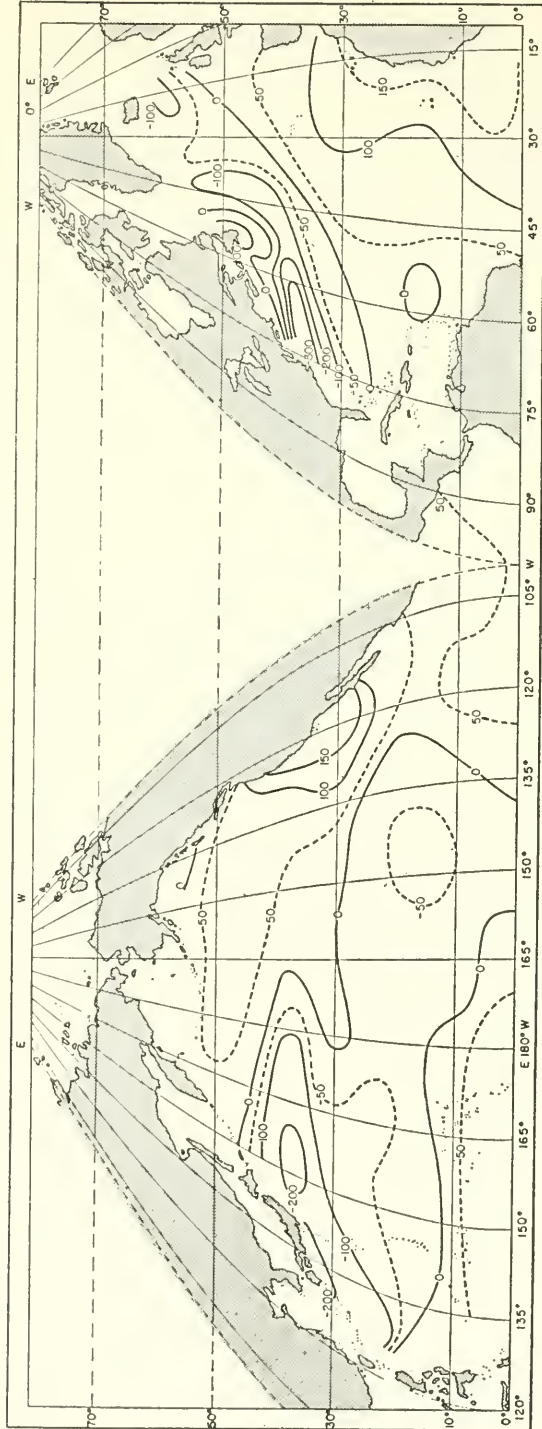


FIG. 109. Total annual energy surplus received by the ocean Q_e ($\text{g cal cm}^{-2} \text{ day}^{-1}$).

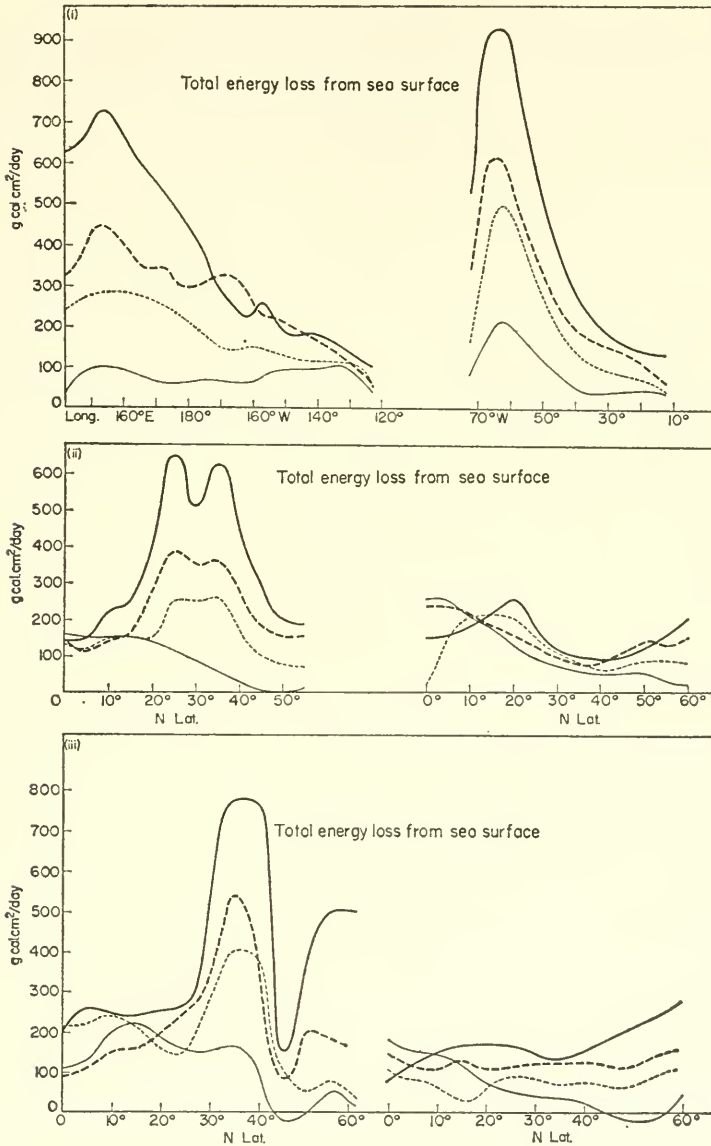


FIG. 110. Energy interchange between the sea surface and the atmosphere at different seasons of the year (1) between 35° and 40° N. in the Pacific and Atlantic Oceans; left side: North Pacific Ocean, right side: North Atlantic Ocean. (2) along the western (left side) and eastern (right side) sides of the North Pacific Ocean; (3) along the western (left side) and eastern (right side) sides of the North Atlantic.

- Dec. Jan. Feb.
- - - Mar. Apr. May
- - - - Jun. Jul. Aug.
- · - · - Sep. Oct. Nov.

side of continents than on the western side. This is mainly due to differences in cloudiness.

The annual heat loss by evaporation, Q_e , according to JACOBS (1951) is given in Fig. 107. Evaporation is particularly large in the western parts of the two oceans, where the currents carry warm water northward (Gulf Stream and Kuroshio). It is, however, less in the eastern parts where there are cold currents flowing southward. The extreme seasons show considerable quantitative differences in evaporation. In middle and higher latitudes the evaporation is large in winter and small in summer, but conditions may be rather complicated on the western sides of the oceans where in winter cold air is advected out from the continents over the warmer sea.

The heat loss Q_h of sensible heat by convection is shown in Fig. 108 for the same oceans. Also one notices here a distinct increase on the western sides of the oceans which is of the same type as in the distribution of Q_e . In the over-all distribution of energy given off from the sea as heat, the values for the evaporation predominate and set the basic pattern. With respect to seasonal changes also the behaviour of both loss items is rather similar. The sum $-Q_a = (Q_e + Q_h)$ gives a final value for the total heat turnover as far as it applies to a current-free ocean. If currents are present then the equation $Q_v = Q_r - Q_a$ must apply, where Q_v is the energy surplus which is obtained by each cm^2 of the surface under influence of a complete heat exchange with the atmosphere. This energy surplus, when positive, is carried away from the water mass under consideration by currents and mixing processes and represents that part of the radiational gain Q_r which is stored in the water. A negative surplus implies that energy is supplied to the water mass by currents and mixing processes which then is dissipated by the excess in radiation into the atmosphere (SVERDRUP, 1945). Figure 109 shows the total energy surplus of the oceanic water ($\text{g cal cm}^{-2} \text{ day}^{-1}$), and shows that in the water of larger ocean surfaces, especially in middle and lower latitudes along and near to the western coasts of continents, some energy is stored in the water while enormous amounts of energy are dissipated (lost by the ocean) in the Gulf Stream and Kuroshio systems. Thus, to a very noticeable extent, the areas in which large amounts of energy are available to the atmosphere are localized in definitive oceanic regions. Comparison of Figs. 109 and 107 clearly shows that the pattern of *total energy exchange* corresponds to that of *evaporation*. In order to recognize the seasonal variations in the energy turnover, it is of advantage to compare these quantities along definite latitudes or meridians along the eastern and the western sides of the oceans respectively. This can be seen from Fig. 110. The first diagram shows a marked contrast between western and the eastern sides of the oceans. A narrow band representing the energy loss appears along with the Gulf Stream in the North Atlantic, while a corresponding and more broad band is connected with the Kurishio. This is understandable from the direction of the two currents in the zone between 35° N and 40° N . The contrast of the two sides of the ocean in a meridional direction is shown in the other two diagrams. Along the western sides at all times of the year, except in summer, the largest amounts of energy are given off between 25° N . and 40° N to 50° N . Along the eastern sides there is a winter minimum in these latitudes. These energy transports are undoubtedly of decisive importance for the climatic conditions in the effected regions and form the basis of the study of the inter-relation between ocean and atmosphere.

Chapter VIII

Ice in the Sea

EXTENSIVE icefields cover the polar seas. The outer boundaries where the ice borders upon the warmer surrounding waters of lower latitudes are subjected to a constant change due to the freezing and melting process. They may take a wide variety of forms depending on the given external conditions. A plastic and lively description of the magic of the polar ice world has been given by WEYPRECHT (1879). Besides the so-called *sea ice*, formed by the freezing of sea-water, other floating ice is introduced to the sea from the neighbouring land by the great rivers (*river ice*), and in addition *icebergs* from the glaciers reach the sea. Floating river ice is comparatively unimportant, except in coastal Siberian and North American waters, therefore; sea ice and icebergs dominate ice conditions in the Arctic and the Antarctic, and may be carried by ocean currents to warmer oceanic regions. This ice drift prolongs the existence of the winter ice barrier in the polar regions into spring and summer, and is thus of considerable importance for navigation.

1. Formation and Terminology of Sea Ice

Ice crystals are formed in the water either on crystallization nuclei, which are the smallest possible particles of organic or inorganic origin that are always present, or at an aggregation of several molecules which meet each other grouped more or less by chance giving a configuration favourable for crystal formation (NERNST, 1909). It appears that the triplex molecules are decisively engaged in the first phase of ice formation. Besides the crystallization nuclei, *supercooling* of the water is also necessary. The greater the purity of the water and the less disturbed it is, the more supercooling is needed. In natural waters there are always sufficient crystallization nuclei present, and the water is usually in movement so that a very small degree of supercooling of only some hundredths of a degree Celsius is required to initiate ice formation. However, supercooling has to be continuous for the formation of ice crystals.

Since the formation of ice releases a latent heat of 80 g cal/g, for a change of water into ice heat must be continually removed by an amount greater than the latent heat. The more intensive the cooling and the less disturbed the water, the smaller are the ice crystals so formed, which show a needle-like structure. If the water is in movement then the forming ice particles lose this needle-like character, looking then like flat plates with irregular rounded edges, about 2–4 cm long, 0.5–1 cm wide and 0.1–1 mm thick. They usually accumulate and form muddy clumps.

The dependence of the freezing point on the salinity is discussed on p. 45. Only *pure* water is involved in the actual freezing process. Part of the salt content of the water is separated during the formation of the ice and, as a more or less concentrated salt solution, fills the small separating layers between the ice crystals which themselves

consist of pure water. As the ice crystals grow they withdraw pure water from this enclosed salt solution, which thus becomes more concentrated and of more specific weight; it gradually percolates out between the ice crystals and increases the salinity of the surrounding water. This diffusion process beneath a forming ice layer is presumably the reason why the crystal plates in sea-water are always oriented perpendicular to the freezing surface, while in fresh water they are parallel to it. The arrangement of the crystal plates is in similar groups and they are oriented approximately parallel, relative to each other, so that the structure of simple sea ice is fibrous; therefore the fracture surfaces of the ice lumps appear perpendicular to the surface of the ice layer.

The classification and terminology of ice formation and ice forms can be made according to different viewpoints; unfortunately there is still no uniform terminology. DRYGALSKI (1930) has given a completely general classification of ice forms based on genetic relationships. The two main forms of ice are *shelf ice* and *sea ice*. Shelf ice represents a transitional stage between the forms of ice occurring on the land and those found at sea. It lies along the coast over the continental shelf and is for the most part a mixture of sea ice and land ice (coastal snow ice). Shelf ice reaches its greatest thickness and extent around the Antarctic; a typical example of this type is that found along the northern coast of Grant Land which is known as palaeocrystalline ice (Ureis). Other forms of Arctic shelf ice are found along the east coast of Greenland (WEGENER, 1902, "floating land ice"). In sea ice there occurs a gradual change of the ice crystals to pap ice (ice mud, ice slush); in calm weather and at low temperatures it freezes together to a hard layer of ice up to 5 cm thick and forms, especially at the surface, a weakly saline top layer. In a rough sea and at still lower temperatures small sheets of ice are formed which grow rapidly and assume a plate-shaped form with upwards bulging edges (pancake ice). The individual plates have a diameter of 0.5–1 m, with a maximum of about 3 m. In calm weather pancake ice and ice slush freezes together to form a solid layer of *young ice* with a thickness of between 5 and 20 cm, having a greenish blue colour; the surface is wet and still rather plastic. Further growth gives *sheet ice*, often forming large lumps which are broken and piled up by pressure forming *pack ice*.

A detailed terminology of ice forms has been given by MAURSTAD (1935; see also ZUKRIEGEL, 1935). Sea ice is divided according to age into two groups: *winter ice* (including young ice) and *polar ice*. The first is not more than one year old, still relatively soft and plastic, and usually occurs in the form of ice lumps. Polar ice, on the other hand, is mostly two or more years old, contains little salt and is therefore hard. Due to ice pressure it soon takes the form of pack ice.

With reference to its position and movement Maurstad distinguishes between *solid ice* and *drift ice*. The first is found for the most part in bays, fiords and above shallow waters. Also winter ice, as long as undisturbed, may remain stationary during the entire winter; however, it is usually broken up by long open cracks and drifts away. Drift ice can take all forms and reaches its greatest extent in the drifting ice fields of polar ice in the Arctic.

In spring and summer, under influence of the increasing solar and sky radiation and the warm winds, the winter ice begins to melt. The volume of the salt solution enclosed in the ice increases and the inner structure of the pure ice crystals is weakened.

The ice melts in this way from the interior outwards and becomes "putrid". The surface takes on the appearance of a honeycomb (cells), and the entire mass of ice soaks through down to a considerable depth. In contrast to the ice formed from pure water, sea ice has no definite melting temperature, but begins to melt as soon as the temperature starts to rise. Putrid ice breaks up easily, exposing a much larger surface to the effects of solar radiation and to warmer sea-water in which it is floating. Most of the winter ice melts in summer, but a large part still remains, especially along the edge of the Siberian Shelf, that survives the summer and then becomes polar ice and in consequence is exposed to a strong annual melting cycle.

2. Physical and Chemical Properties of Sea Ice

(a) *The Salinity of Sea Ice*

The salinity of sea ice is defined as that quantity of solid matter (in g) remaining after evaporation of 1000 g of melted sea ice. The limitation that was found essential in the definition of the salinity of sea-water (see p. 36) thus also applies here. The essential difference between the salinity of sea-water and that of sea ice is that the first is a rather conservative property of sea-water; while the second, in strict contrast, is a very rapid changing quantity for each single piece of ice. Nevertheless, the salinity of a sample of ice shows only minor variations. This has been shown by the numerous analyses made by the "Maud" Expedition, 1918-25 (MALMGREN, 1927). As has been noticed by all polar expeditions the surface of young ice is covered by a surface salt solution, which remains liquid even for low temperatures and keeps the surface of the ice continuously wet. For very low temperatures only this layer also freezes, giving a mixture of ice and salt crystals which isolate themselves in form of snow-white clusters.

Beneath the surface a part of the salt solution remains enclosed between the ice crystals and determines the salinity of the sea ice. Its amount depends on the processes going on during the ice formation, specifically on three factors: (1) on the salinity of sea-water from which the sea ice was formed; (2) on the rapidity of ice formation; and (3) on the age of the ice. Referring to the first, the salinity of sea ice is less than that of sea-water, since the part of the salt solution between the ice crystals is always

Table 91

Air temperature (°C)	-16	-28	-30	-40
Salinity of young ice (‰)	5.64	8.01	8.77	10.16

Table 92

Ice thickness below the ice surface (cm)	0	6	13	25	45	82	95
Salinity (‰)	6.74	5.28	5.31	(3.84)	4.37	3.48	3.17

able to escape. In the analyses of young ice samples made during the "Maud" Expedition the salinity of sea ice reached a maximum value of 14.59‰, but usually the salinity of sea ice was between 3 and 8‰. Referring now to the rapidity of ice formation it

shows that the faster the ice is formed (at lower temperatures) the less salt solution can escape and the higher therefore the salinity of sea ice (Table 91). Since ice is formed more slowly in the deeper layers than at the surface some dependence on depth can also be expected. For a young ice layer that began to freeze in November 1924, Malmgren found in April 1925 the values shown in Table 92. Referring finally to the age of the ice, the older the ice the smaller its salinity. The salt solution leaks through continuously and this process is accelerated by changes in temperature. Blocks of ice lifted by the pressure of the ice become almost completely salt-free in the summer by this process of deconcentration, and can be used after melting for drinking water.

The changes in salinity in winter ice occurring during the course of a year have been summarized by Malmgren in a diagram given in Fig. 111. The ice formed in October gradually increases in thickness, and initially the salinity decreases from the surface downwards. Corresponding to their age the middle layers have the lowest salinity,

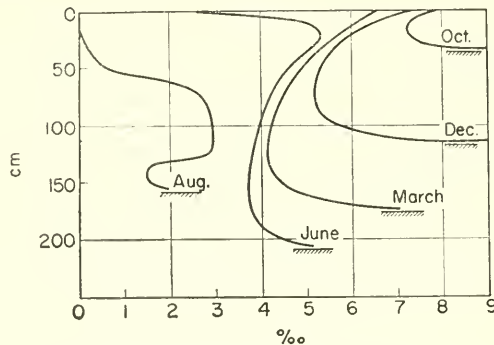


FIG. 111. Salinity changes in winter ice during the course of the year (schematic, according to Malmgren).

but at the lower surface of the ice layer the salinity again increases since the water freezes here from below. This is due to melt water sinking below the ice layer and freezing again immediately due to temperatures below freezing point (about -1.6°C).

In a dilute aqueous solution freezing proceeds with the formation of pure ice only until the eutectic point is reached, the concentration of the solution increasing at the same time. This critical point depends on the salts dissolved in the water. When sea-water freezes the separation of the salts dissolved in the water begins only at -8.2°C . For sea-water the situation is simplified only in so far as: (1) all types of water have the same salt composition; and (2) ice is always the first substance to freeze out. In consequence, no matter how great the salinity, the freezing process always proceeds in the same way. For a given temperature the concentration and the composition of the salt solution is to a close approximation the same for all types of sea-water, regardless of their original salinity (Malmgren). If τ_s is the freezing temperature of 1 g of sea-water of salinity S , then for a temperature τ between τ_s and -8.2°C only pure ice will separate out according to the above discussion, and at this temperature there will be a_τ g of pure ice and $(1 + a_\tau)$ g of salt solution. If the salinity of the salt solution is S_τ , then necessarily

$$(1 + a_\tau)S_\tau = S.$$

For sea-water of salinity S' there will be a similar relationship

$$(1 + a_{\tau'})S_{\tau'} = S'$$

Since $S_{\tau} = S_{\tau'}$ it follows

$$\frac{S}{1 - a_{\tau}} = \frac{S'}{1 - a_{\tau'}} = \text{const.},$$

that means, the amount of salt solution per gramme is proportional to the salinity of the sea-water from which the ice has been formed. The first substance which begins to separate at temperature below -8.2°C is sodium sulphate (Na_2SO_4). However, the chlorine is retained since its separation begins only at -23°C . This selective separation process during freezing changes the composition of the salts in the sea-water (RINGER, 1906; see also O. PETTERSSON, 1883). Thus in the polar seas sulphate is expected to be steadily withdrawn by the freezing process from the sea-water which thus becomes enriched in chloride. On the other hand, in areas where the ice carried away by the ocean currents melts sodium sulphate goes again into solution and the sea-water should show a surplus in SO_3 .

MALMGREN and SVERDRUP (1929) have found that deviations of this type from normal behaviour are only very slight, and thus there occurs no selective process on a large extent during ice formation in nature. On the other hand, the investigations of Liakionoff, according to WIESE (1938), have shown that in the Barents Sea both in sea ice, as well as in melt water, there is a deficit of chloride and a surplus of sulphate (SO_3). Further investigation is required to settle this point.

(b) Density and Porosity of Sea Ice

The density of pure ice at 0°C is 0.91676, while the density of water at the same temperature is 0.999867. The density of sea ice which is free of air bubbles increases with its salinity. If it increases at the same rate as the density of sea-water increases with salinity, the density of sea ice is expected to increase by about 0.0008 for every 1‰ in salinity. The density of sea ice free of air bubbles and with a salinity of 15‰ would thus be about 0.9296. The first precise determinations of the density of sea ice were made by MAKAROFF (1901) by extensive measurements of the mean height h and the mean depth d (above and below the sea surface) of freely floating ice floes. If σ_t is the density of the sea-water then the density of the sea ice is given by

$$\rho_i = \frac{d}{h + d} (1 + 10^{-3}\sigma_t).$$

This gives a mean value for the entire floe. Makaroff's measurements apply only to summer floes of drift ice and give reliable values only for regular floes without any snow cover. These observations gave results between 0.96 and 0.85. These large variations are due to the considerable amounts of air and water which may be present in sea ice. The greatest effect is that due to air bubbles enclosed in the ice, which can be of a twofold origin. One part originates already during the ice formation, due to a separation of gases dissolved in the sea-water which cannot always escape from the cells between the ice crystals. Thus the gas bubbles will be more numerous and larger the faster the rate of freezing of the ice. The upper parts of freshly frozen ice thus usually contain more air than the lower parts.

A second source of air-bubble formation is the penetration of air during the melting process (HAMBERG, 1895). In the upper part of a mass of ice which begins to melt from the inside the rise in temperature first widens the small intermediate spaces containing the salt solution. As the ice particles melt their volume decreases and empty spaces are formed into which air is pressed in due to the atmospheric pressure. These spaces finally become so enlarged that the melt water, together with the salt solution, can flow out and finally they are replaced entirely by air. The originally pure and clear ice thus becomes a porous mass penetrated by a number of air channels. On top the drift ice floes in the summer thus always appear white simulating a snow cover. The lower parts below the water surface are still cold and hard (solid). They do not melt from the inside and show, at first, only very little porosity. However, when the ice disintegrates more and more and still drifts in sea-water, the temperature of which is above freezing point, the already existing empty spaces become filled with water and the ice density increases rapidly.

The air enclosed in sea ice, according to Hamberg, has an oxygen content greater than that of atmospheric air but less than that of the air mixture absorbed by sea-water (24–26% as compared with 20.95 for atmospheric air and 34.6 for sea-water at 0°C and 35‰ salinity).

The most accurate determinations of the density of sea ice *in situ* have been made by MALMGREN (1927) on the "Maud" Expedition. These were made by determination of the loss of weight of a piece of ice on immersion in petroleum of specific weight p_t . If the weight of the ice sample in air is G and in petroleum g grammes then the density is given by

$$\rho_i = \frac{G}{G - g} p_t.$$

Table 93. Density of sea ice
(According to Malmgren ("Maud" Expedition))

Sample No.	Time	$t(^{\circ}\text{C})$	Salinity (‰)	Depth of sample (cm)	Density (g/cm ³)
1–7 ¹	Jan.–Mar.	–26.4 –29.0 –22.0	9.1 14.6 3.6	— 132 2	0.919 Max. 0.924 Min. 0.914
8 and 8a ²	Feb.	–24.0	0.0	2	0.921
9 ³	Feb.	–29.0	1.9	2	0.918
10 ⁴	Mar.	–22.4	4.7	5	0.911
11 ⁵	Mar.	–27.0	0.0	8	0.857
12 ⁶	May	–6.2	—	2	0.885
13 and 14 ⁶	May	–6.2	—	65	0.892

¹ Young ice partly broken open.

² Young ice from a freshwater pool on a thick old ice floe.

³ Young ice frozen in autumn from low salinity water.

⁴ Thick broken young ice some time exposed to the sun.

⁵ Top peak of ice exposed to sun ("gesommert").

⁶ Sample of old ice at the place of temperature measurement.

Petroleum is particularly suitable as an immersion liquid because it cannot penetrate into the small air-filled channels of the ice pieces. The results of these determinations are summarized in Table 93. The conspicuous result is the very small variation in the density of young ice, in spite of the strongly varying salinity of the samples and of the equally variable depth from which they were taken, as well as of the changing thickness of the floes. The smallest values (0.914 and 0.916) were given by two thin and highly saline young ice floes which had been formed at very low temperatures. The rapid freezing must of course have trapped a large number of air bubbles, probably more than normal. The uniformity of the values between autumn and winter disappears gradually in spring as melting becomes more and more effective. There is a progressive fall in density in late spring, and this decrease becomes stronger as the disintegration of the ice proceeds during the summer. Values less than 0.90 show by the large number of enclosed air bubbles that the ice must have been exposed to the sun ("gesommert"). The lowest value in density was found at the top peak of a large floe. During the preceding summer the salinity in this ice had been completely removed, and in winter the melting water of it could be used for drinking water.

(c) *Thermal Properties of Sea Ice and the Temperature in the Interior of Ice Flow*

It is characteristic of sea ice that its thermal properties such as specific heat, latent heat of melting and thermal expansion behave quite abnormally. During investigations of the heat expansion of sea ice PETERSSON (1883) found that highly saline sea ice expanded with decreasing temperature down to -20°C , though for ice of lower salinity this temperature was considerably higher. Malmgren showed by investigations during the "Maud" Expedition that Krümmels' assumption, that this was due to the salt solution enclosed in the ice, was correct. This abnormal behaviour relative to the specific heat, latent heat of melting and thermal expansion is thus also a consequence of the formation and melting of pure ice occurring in the interior of sea ice. At a temperature τ , 1 g of sea ice of salinity 1‰ will contain a_{τ} g of pure ice and $(1 - a_{\tau})$ g of salt solution. If the specific heat of sea ice at the temperature τ is c_{τ} then this quantity of ice for a temperature change $d\tau$ will require a quantity of heat $c_{\tau}d\tau$. It is made up essentially of: (1) the rise in temperature $a_{\tau}cd\tau$ of pure ice (with specific heat c); (2) the rise in temperature of the salt solution $(1 - a_{\tau})\kappa d\tau$ (with specific heat κ); and (3) the heat $\lambda_{\tau}da_{\tau}$ required to melt da_{τ} g of ice (with latent heat of melting λ_{τ}). This gives the equation

$$c_{\tau} = a_{\tau}c + (1 - a_{\tau})\kappa + \lambda_{\tau} \frac{da_{\tau}}{d\tau}.$$

Since the second term is small and as a first approximation $a_{\tau} = 1$ then

$$c_{\tau} = c + \lambda_{\tau} \frac{da_{\tau}}{d\tau}.$$

For sea ice of salinity S ‰ the variable amount of ice is Sda_{τ} and therefore one obtains for it the relation:

$$c_{\tau} = c + S\lambda_{\tau} \frac{da_{\tau}}{d\tau}.$$

According to p. 247 if S_τ is the salinity of the salt solution

$$(1 - a_\tau)S_\tau = 1,$$

so that

$$\frac{da_\tau}{d\tau} = \frac{1}{S_\tau^2} \frac{dS_\tau}{d\tau},$$

and

$$c_\tau = c + \lambda_\tau \frac{S}{S_\tau^2} \frac{dS_\tau}{dt}.$$

According to the investigations of PETERSSON (1878) $\lambda_\tau = 80 + 0.5\tau$. The factor of λ_τ can be calculated from investigations made by Ringer, so it is therefore possible to evaluate the above equation for different temperatures and salinities (Table 94).

Table 94. The specific heat of sea ice

(According to Malmgren)

Temp.(°C)	-2	-4	-6	-8	-10	-12	-14	-16	-18	-20	-22	
S‰	2	2.57	1.00	0.73	0.63	0.57	0.55	0.54	0.53	0.53	0.52	0.52
	4	4.63	1.50	0.96	0.76	0.64	0.59	0.57	0.57	0.56	0.55	0.54
	6	6.70	1.99	1.20	0.88	0.71	0.64	0.61	0.60	0.58	0.57	0.56
	8	8.76	2.49	1.43	1.01	0.78	0.68	0.64	0.64	0.61	0.60	0.58
	10	10.83	2.99	1.66	1.14	0.85	0.73	0.68	0.67	0.64	0.62	0.60
	15	16.01	4.24	2.24	1.46	1.02	0.85	0.77	0.76	0.71	0.68	0.65

Malmgren has also determined the specific heat of ice samples experimentally, and has obtained values in excellent agreement with the theoretical. At higher temperatures the heat capacity of sea ice is quite high, at -2°C and 15‰ salinity it reaches 16.0 g cal. These high values can be explained either by melting or freezing of large amounts of pure ice in the salt cells of the ice at temperatures close to freezing point and for temperature changes of about 1°C , which is accompanied by release or uptake of large amounts of heat from the latent heat of melting. For sea ice the specific heat and the latent heat of melting are properties closely related to each other.

The dependence of the *latent heat of melting* on temperature and salinity can also be calculated theoretically from S_τ , the salinity of the ice, and τ_s , the freezing temperature of sea-water of salinity S . If τ is close to zero, the latent heat of melting for pure ice will be constant between τ and τ_s and will be 80 g cal. The amount of heat required to melt 1 g of sea ice will be made up of: (1) the heat = $80[1 - S(1 - a_\tau)]$ required to melt pure ice; and (2) the heat required to raise the temperature of the pure ice and the salt solution from τ to τ_s . Since the specific heat of pure water is 0.5 this quantity of heat will be approximately $0.5(\tau_s - \tau)a_\tau$. The latent heat of melting of sea ice will thus be given by

$$U = 80 \left(1 - \frac{S}{S_\tau} \right) + 0.5(\tau_s - \tau)$$

Table 95. Latent heat of melting of sea ice

Salinity (‰)	0	2	4	6	8	10	15
Temp. $\left\{ \begin{array}{l} -1.0^{\circ}\text{C} \\ -2.0^{\circ}\text{C} \end{array} \right.$	80	72	63	55	46	37	16
	81	77	72	68	63	59	19

Table 95 shows values for different salinities and for temperatures equal to 1° and -2°C .

The *coefficient of thermal expansion* can be calculated in a similar way; it is made up of the coefficient of thermal expansion of pure water ($\alpha = 1.7 \times 10^{-4}$) and a term which depends on the amount of ice forming or melting due to the change in temperature in 1 cm^3 of sea ice. Since the freezing of 1 g of water at τ° is accompanied by an increase in volume of $\gamma_{\tau} = 0.091$, the coefficient of thermal expansion of sea ice will, according to the above discussion, be given by

$$u_{\tau} = \alpha - S\gamma_{\tau} \frac{da_{\tau}}{d\tau} = \alpha - \gamma_{\tau} \frac{S}{S_{\tau}^2} \frac{dS_{\tau}}{d\tau}.$$

Table 96. Coefficient of thermal expansion of sea ice ($u_{\tau} \times 10^4$)
(According to Malmgren)

Temp. ($^{\circ}\text{C}$)	-2	-4	-6	-8	-10	-12	-14	-16	-18	-20	-22	
Salinity ‰	2	-22.10	-4.12	-1.06	0.16	0.83	1.13	1.23	1.27	1.33	1.38	1.44
	4	-45.89	-9.92	-3.81	-1.37	-0.02	0.56	0.78	0.85	0.96	1.07	1.18
	6	-69.67	-15.73	-6.55	-2.90	-0.88	0.00	0.33	0.43	0.60	0.76	0.93
	8	-93.46	-21.53	-9.30	-4.43	-1.73	-0.57	-0.13	0.02	0.23	0.45	0.67
	10	-117.25	-27.34	-12.05	-5.95	-2.59	-1.13	-0.59	-0.40	-0.13	0.14	0.42
15	-176.72	-41.85	-18.92	-9.78	-4.73	-2.54	-1.72	-1.45	-1.03	-0.63	-0.22	

From this equation Malmgren has calculated the values given in Table 96, and experimental determinations of u_{τ} , on samples of natural ice have fully confirmed the theoretical values. There is an essential difference between u_{τ} for sea ice and freshwater ice.

Pure ice always expands with increasing temperature; sea ice expands only to a lesser extent, and then only at very low temperatures and low salinities. Thus the second term in the above equation becomes unimportant. At higher temperatures and salinities the second term predominates; this means that the ice volume increases with decreasing temperature and at very low temperatures and high salinities this increase may be considerable.

Extensive series of *temperature recordings* at different depths in sea ice (ice floes) have been made by the "Fram" Expedition 1893-6 and the "Maud" Expedition 1918-25. The latter were obtained by using electrical resistance thermometers and are much more reliable. Table 97 gives monthly means for five depths down to 2 m for every month during which the snow cover at the place of measurement was left undisturbed.

The annual temperature variation at all depths can be approximated closely by a simple sine curve of the form

$$\tau_m = M + a \sin \left(\frac{2\pi}{12} t + \alpha \right),$$

and the result of this analysis, given in the last lines of Table 97, shows how regular is the annual temperature wave, with a decrease in amplitude and a phase shift in the

Table 97. Annual temperature variation at different depths in sea ice
(According to the values of the "Maud" Expedition, North Siberian Shelf)

Depth (m)	0.00	0.25	0.75	1.25	2.00
Jan.	-28.0	-24.1	-18.9	-14.0	-6.5
Feb.	-30.9	-26.9	-21.3	-16.3	-8.5
Mar.	-29.1	-26.0	-21.0	-16.5	-9.6
Apr.	-21.6	-20.1	-17.3	-14.4	-9.4
May	-7.4	-8.6	-9.3	-9.2	-7.4
June	-1.5	-3.0	-4.1	-4.5	-3.8
July	-0.0	-0.1	-1.3	-1.7	-1.8
Aug.	-0.0	-0.0	-0.8	-1.1	-1.2
Sept.	-4.7	-1.3	-0.9	-1.1	-1.3
Oct.	-12.3	-7.6	-3.3	-1.6	-1.4
Nov.	-23.0	-17.8	-11.9	-7.1	-2.4
Dec.	-29.9	-24.4	-17.7	-12.2	-4.6
Mean <i>M</i>	-15.70	-13.32	-10.65	-8.31	-4.82
<i>a</i> (°C)	16.82	14.60	11.17	8.36	4.40
<i>a</i> (degrees)	259.6	250.9	240.9	230.7	210.4

extremes, penetrating into the ice (Fig. 112). In both series of recordings there is good agreement in the upper layers of ice down to about 1.5 m, but this is not true at greater depths. The "Fram" values are too low, probably due to the observational method using bar-thermometers. The decrease in the annual amplitude with depth shows the same. According to the "Maud" values the annual variation disappears at a depth of 2.9 m. At a depth of 2.8 m the temperature of sea-water underneath the ice floe reaches -1.6°C and remains constant throughout the whole year. At the side underneath an ice floe, the thickness of which varies on the average as seen from Table 97, the amplitude of the annual temperature variation thus falls to zero.

Fundamental investigations on the *thermal conductivity of ice* have also been made by Malmgren. STEFAN (1890) found a thermal conductivity coefficient $k = 4.3 \times 10^{-3}$ from theoretical investigation of the process of ice formation, but this value can only apply for freshly formed pure ice. Later MOHN (1900) attempted to compute the thermal conductivity coefficient from the decrease in the annual temperature variation and from the retardation of the extremes with depth in ice floes. However, these methods cannot give reliable values since the theory is valid only for infinite thickness, while the thickness of sea ice is small and the lower side of a floe remains almost always at a temperature of -1.6°C . Correct values of k can be determined, according to Malmgren, from the temperature gradient and its change with time at different depths. Assuming a cylinder with a vertical axis through an ice floe, then definite amounts of heat will enter the cylinder through its upper surface in t sec. If the ice floe is of sufficient horizontal extent no heat will pass through the vertical wall of the cylinder and the heat flux will only occur normal to the surface of the ice floe. If the heat content of the cylinder for a given time remains constant then $k_1 G_1 = k_2 G_2$, where k_1 , k_2 and

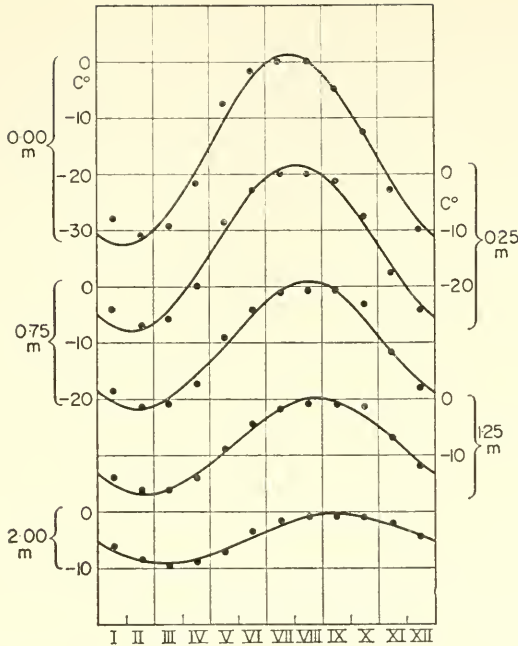


FIG. 112. Annual temperature variation at different depths in sea ice.

G_1 , G_2 are the thermal conductivity coefficients and the temperature gradients at the upper and the lower surface of the cylinder. However, if the mean temperature changes from τ_1 to τ_2 , then the following relation holds:

$$(k_1 G_1 - k_2 G_2)t = hc\sigma(\tau_1 - \tau_2),$$

where h is the height of the cylinder, c the mean specific heat and σ the mean density. From observations of temperature in ice it is possible to find cases where the mean temperature of a layer is constant for a certain time, and cases where it undergoes large rapid changes. The above equation can then be used to calculate k_1 and k_2 . Table 98 shows numerical values for k determined for the winter periods 1922-3 and 1923-4. They are of the same order of magnitude as the mean values obtained by Stefan but have a marked dependence on the depth (Fig. 113).

Table 98. Thermal conductivity of sea ice at different depths
(According to Malmgren)

Depth (m)	0	25	60 and 75 resp.	125
Winter { 1922-3	2.4	3.6	4.0	4.2×10^{-3}
1923-4	1.7	3.3	4.5	5.0×10^{-3}

There is a rapid decrease in the thermal conductivity in the top layers of sea ice which must be due to the numerous air bubbles in these layers (density about 0.88).

Deeper in the ice the thermal conductivity approaches a limiting value of 5.0×10^{-3} which corresponds to the value obtained for clear freshwater ice without air bubbles.

Malmgren's determination of the physical constants of sea ice are of considerable importance in questions of the heat balance in polar regions, since they allow the determination of the amount of heat gained by the surface of the ice in polar regions and

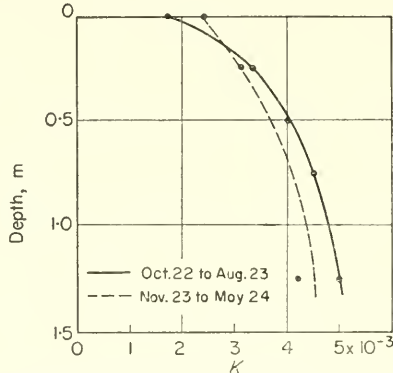


FIG. 113. Changes in thermal conductivity in sea ice with depth.

thus also by the atmosphere immediately above it from the water below. For the greater part of the year the water underneath is warmer than the ice cover and the air above it, and therefore there is a continuous flux of heat upwards. Such a calculation can be made with the temperature observations of the "Maud" over a period of a year. The total amount of heat passing through the different depth-levels in a year amounts on the average to 6800 g cal/cm^2 and should be the same for all levels. This amount of heat is released to the atmosphere above the ice year after year. In the cold season of the year when the temperature gradient is several times larger this flux of heat is greater; in summer it may even be reversed but is then never very large. Taking a depth of 0.75 m as representative for the entire layer of ice, the amount of heat, $W_{0.75}$ passing through this level per cm^2 and month can be calculated, knowing the temperature gradient for each month during the colder season of the year. Part of this heat serves to raise the temperature of the 0.75 m thick surface layer. If the temperature difference between the beginning and the end of the month is $\Delta\tau$ then the heat gained by the atmosphere during that month is

$$W_a = W_{0.75} - 75c\sigma\Delta\tau = W_{0.75} - 34.4\Delta\tau.$$

The values calculated by Malmgren using this equation for the months from September 1923 to April 1924 show that during the cold season of the year the atmosphere receives the very large amount of $76,700 \text{ kg cal/cm}^2$, which is sufficient to melt 96 cm of ice. However, large as this may appear, it is only a ninth part of the heat that the European Mediterranean, for example, provides to the atmosphere ($676,000 \text{ kg cal/m}^2$). However, in the polar regions its effect is none the less still important. During the cold part of the year there is a thin layer of cold air over the Polar Sea, extending to a height of about 150 m (SVERDRUP, 1926). This layer of air has such a stable stratification that it mixes only to a very small extent with the air above. The heat from below is thus imparted almost entirely to this layer and prevents a decrease of the

temperature to very low values. The increase in temperature per day due to the flow of heat W_a from below can be found from the mean height of this cold atmospheric surface layer. As Malmgren showed, this heat is quite large and it is obviously this source of heat that prevents an intensive cooling of the atmosphere above the North Polar basin. The temperature can thus never reach the low values found in central Siberia or central Greenland, where this heat source is not available.

(d) *The Mechanical Properties of Sea Ice*

The continuous formation of ice by freezing is counter-balanced by very effective processes that reform and destroy the ice fields. The mechanical properties of ice (elasticity, plasticity and resistance against deformation, bending and compression) are of the greatest importance in the interplay between these processes. Large ice surfaces seldom remain unchanged for longer periods. They are broken up rapidly from the edges, by the combined action of the wind, waves and periodic tidal currents, and in a short time become separate ice floes. With the aid of strong winds they are piled up by the large horizontal pressures and pushed one above the other. The resultant mass, when finally covered with snow, cemented together and built up into several layers, is pack ice. Pressure and tensions are common in the polar regions (especially in the Arctic). Gaps and open spaces may exist for a short time but are rapidly covered over by young ice which again re-unites the whole mass. These pressures are not due to the effect of the wind alone, because often the wind only influences far-off regions, thereby subsequently causing pressures in the Arctic (distant effect); they are often due to rapid temperature changes at the surface of the ice. Since the under-side of an ice floe is always at the temperature of the water (near freezing point) there will be tensions and stresses in the floe. Figure 114 shows schematically the cracks and fissures formed when the stresses due to thermal expansion at the surface exceed the elastic limit. In the same way thermal contraction at the surface forms in an

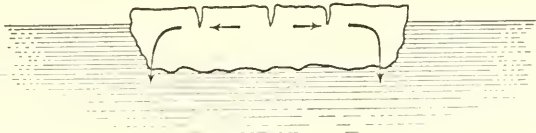


FIG. 114. Changes in an ice floe due to thermally induced expansion.

analogous manner cracks at the lower side. The cracks on the upper surface of the floe soon fill with snow and melt water and those in the bottom surface fill with ice due to the rapid freezing of sea water in contact with the cold ice. There is thus a continuous formation of ice. The ice-covered regions in the Antarctic are not basins surrounded by land, and therefore ice pressures occur less often and are considerably weaker. The humps, hummocks and ridges of piled-up floes, known by the Siberian name *toross*, which are sometimes up to 5 m or more in height are much less common in the Antarctic pack ice; instead the action of pressure often forms folds and flexures.

The mechanical properties of ice, like its other properties, depend on the temperature and salinity, but due to the multiplicity of ice forms and conditions these determine only the order of magnitude, and there may be considerable variations caused by the

special structure of an ice floe and its past history. The most important of the mechanical properties is the elasticity, which is characterized by Young's modulus E and the modulus of rigidity μ . Ice is of course composed of ice crystals and its elasticity is not the same in all stress directions. An ice crystal can be regarded as built up of a large number of thin platelets at right angles to the crystal axis. Deformation at right angles to this axis meets a much smaller resistance than one in the direction of the axis. The different values for Young's modulus shown by different natural samples are probably due to this. Few direct determinations have been made of the elasticity constants for sea ice, but they have been determined more often for fresh water ice by a variety of different methods. The more reliable values for the modulus of elasticity E are those of Reusch, which give 23, 632 kg/cm². Its variability with the position of the crystal axis relative to the axis of force has also been determined, giving between 18, 200 and 38, 300 kg/cm². E increases with decreasing temperature.

A more accurate determination of these constants can probably be made indirectly by measurement of the velocity of elastic waves in the ice, and a large number of determinations of this type have been made. EWING, GRAY and THORNE (1934) measured this velocity in thin ice rods and found the following values for the elasticity constants:

Young's modulus E	Rigidity modulus μ	Poisson constant σ
9.17×10^{10} dyn/cm ²	3.36×10^{10} dyn/cm ²	0.365

Seismic measurements of the thickness of the ice on alpine glaciers and in Greenland (BROCKAMP and MOTHES, 1930) have given

$$E = 6.82 \times 10^{10} \text{ dyn/cm}^2; \quad \mu = 2.51 \times 10^{10} \text{ dyn/cm}^2; \quad \sigma = 0.361.$$

Considering the difference between experimental and natural conditions these values agree quite well. The elastic limit in ice is not large; for river ice Weinberg found 0.57 kg/cm²; for granular glacier ice Hess found 0.09 kg/cm². The plastic limit is, of course, much higher.

The strength of ice of different origins provides a more useful comparison than the above numerical values and has been used by Makaroff. His measurements show clearly that freshwater ice is of much greater strength than sea ice and that an increasing salinity in the water in which it is formed and a higher temperature, makes the sea ice less resistant. WEINBERG (1907) investigated the strength of a large number of sea-ice samples and found that the values obtained usually increased with decreasing temperature; compared with the values at -3°C there were increases of 20%, 35% and 45% at -10° , -20° and -30°C respectively.

Investigations of the deformation of ice under the effect of continuous pressure have been made by Andrews, and especially by ROYEN (1922). From their results, it is worth mentioning that the plastic deformation of ice under the influence of continuous pressure can be expressed by the equation

$$\epsilon = \kappa \frac{p\sqrt[3]{T}}{1 - \tau},$$

where p is the pressure (load) in kg/cm², T is the duration of this pressure in hours, τ is the mean temperature of the ice and κ is a constant characteristic for each sample and

varies within the limits 6×10^{-7} and 9×10^{-4} . These investigations showed the considerable effect of the temperature on the hardness of the ice. The strength of ice is very important in calculating the loads that can be put upon it. The following empirical data may be given based on experience: freshwater ice 4 cm thick will carry a man, from 10–12 cm thick a galloping horse, from 15 cm thick a heavy-loaded truck, and over 45 cm thick a railway train. This question is also of importance for aircraft landing on ice. Moskatov (see "Die Naturverhältnisse des Sibirischen Seeweges" ("Conditions along the Siberian Sea route"), *Oberkom. Kriegsmarine*, Berlin 1949, p. 84) has given the following table for the minimum safety thickness of freshwater ice for aircraft landings:

Aircraft weight (tons)	2	5	10	15	20
Minimum thickness (cm)	15	24	32	39	45

The strength of sea ice, and that of salt-free ice formed from sea ice due to a decaying process of several years is considerably less than that of freshwater ice. To carry the same load the ice in the centre of the Arctic basin must be two to three times thicker.

3. Ice Conditions and their Seasonal and Aperiodic Variations in Arctic and Antarctic Regions

(a) Ice Conditions of both Polar Caps

In the Northern Hemisphere sea ice is largely confined to the Arctic Mediterranean, the central basin of which is always covered by it. Figure 115 shows the general outlines of mean ice coverage in summer and winter (BÜDEL, 1943, 1950). September is the time of minimum extension in ice cover, and the ice is limited to the inner part of the North Polar Basin, which at that time is most remote from the warm land masses. This ice lasts throughout the summer and then extends again enormously during the winter. Except in the area of Gulf Stream water it reaches everywhere to the northern coasts of the continents and extends as long tongues of pack ice along the eastern coasts of Greenland and Labrador. To this winter ice then adds the one-year-old winter ice of the adjacent seas. In winter, of the total area of the North Polar Basin (11.6 million km²) on an average 8.7 million km², (or 75%) are covered by ice. If the pole were surrounded by land with a circular area of 2.9 million km² then the above mentioned ice-coverage would extend southward everywhere to the 72.7° parallel (thus everywhere 17.3° lat. distance from the pole).

In the Southern Hemisphere, where the Antarctic land mass surrounds the South-pole with a total area of 14.8 million km², the ice-coverage is 29.0 million km² and for an even distribution would then reach northward to the 55.8° parallel. These figures show the strong contrast in ice conditions between the two polar regions. The ice covers 3.35% of the total Northern Hemisphere, but 11.30% of the total Southern Hemisphere.

In the Southern Hemisphere (see Fig. 116) the ice extends uniformly around the central Antarctic continent, enclosing it on all sides, and the symmetric circumpolar arrangement of the ocean surface and the ocean currents fix zonal drift ice limits



FIG. 115. Average extent of sea ice (mean drift ice limit) in the Northern Hemisphere for summer and winter:

AVERAGE DISTRIBUTION OF

- Polar ice coverage closed in summer (about beginning of September)
- ⊗ Broken polar ice coverage in summer (about beginning of September)
- ▲▲ Southernmost iceberg limit in summer (May to September)
- ⊘ Closed polar ice coverage in winter (March to April)
- ⊙ Broken polar ice coverage in winter (March to April)
- △△ Southernmost iceberg limit in winter (October to March)
- //// Closed ice on inland seas and lakes in winter (February to March)
- ⊙ Broken ice on inland seas and lakes in winter (February to March)

without any large meridional irregularities. In the Northern Hemisphere, on the other hand, the continents and the eccentric position of the large polar icelands confine the ice field on all sides, and allow warm ocean currents to enter at only one gate, between Iceland and Scandinavia where the warm Atlantic current pushes the limits of drift ice back to the northern coast of Spitzbergen and into the inner parts of the Barents Sea.

Referring to the special regional distribution of the three different types of ice (polar ice, pack ice and solid ice) the central area of the North Polar ice consists always of pure polar ice (SMITH, 1931); it is 3–3.5 m thick at the end of the winter and 2–2.5 m thick at the end of the summer. It covers about 70% of the entire Polar Basin, i.e. 5.2 million km². It is usually a continuous layer, but especially towards the edges it is split up by ice pressure into large ice fields and ice floes. This large polar ice cap is closely confined to the 1000–800 m isobath and has a more or less elliptical shape lying much nearer to the continental coast and coastal islands on the Greenland–North American side than towards the coast between Spitzbergen and Alaska where the broad Siberian Shelf lies between. The centre of the polar cap is often called the “pole of inaccessibility” and is situated about 400 nautical miles north of Alaska.

The maintenance of this polar ice cap represents a state of equilibrium with the total annual growth. The total gain consists at first of an addition of ice from the surrounding pack ice zone due to freezing at the bottom layers of ice floes, secondly of snow falls on the ice surface and the re-freezing of open spaces. The ice loss is caused by

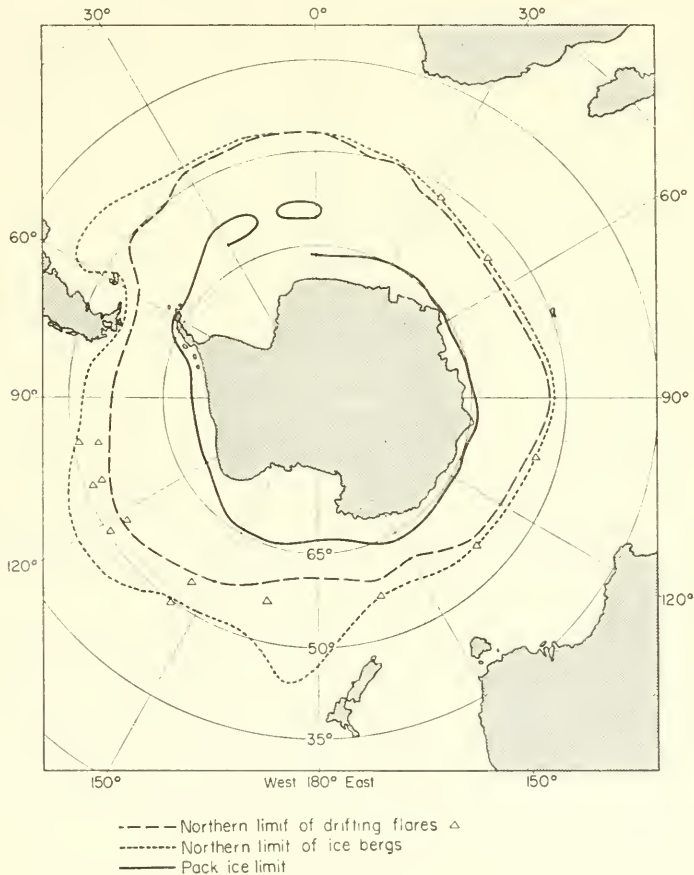


FIG. 116. Average extent of sea ice in the Southern Hemisphere; the dotted line . . . gives the mean northern iceberg limit, the continuous line — gives the northern limit of pack ice and the broken line - - - the northern limit of drift ice.

evaporation, melting and the southward drift of ice away from the edges. It can reasonably be assumed that the equilibrium is of a quasi-stationary nature.

Our knowledge of the movements of the polar ice is largely obtained from the drift of vessels beset in, i.e. frozen into, the ice. These show that, at least in the western half of the polar ice cap, there is an east-west drift; on the North American side there appears to be a drift in the opposite direction so that in the North Polar Basin there is a general anticyclonic ice drift. North of Greenland and Grant's Land, however, the drift is directed towards the area between Greenland and Spitzbergen. The speed of the ice drift to the north of Franz Josef Land and towards Spitzbergen is about 1 nautical mile a day; the "Sedow" found values twice as great; the "Maud" found values between 0.6 and 3.2 nautical miles a day; the "drifting polar station" found at first, near the pole about 4 nautical miles a day and then, after a decrease to 2-4 nautical miles a day, a further increase to 5-6 off the Greenland coast. Similar values have also been found by means of drifting buoys which have been laid out recently inside the North Polar basin by the Russians.

The *pack ice zone* is continuous with the polar ice zone and covers about 25% of the North Polar Basin; in summer it usually forms the southern limit of the drift ice fields, here broken up by kilometre-long channels. The part over deep water proceeds with the motion of the ice drift though probably at a lower speed, but in shallow waters (over the shelf) its movement is towards the east. As a consequence of this opposite movement, the ice fields in the intermediate areas are very much broken up and large, and sometimes navigable, fracture zones appear (termed "polynya" by Russian research workers). The main fracture zones run north of Spitzbergen, Franz-Josef Land, Severnaya Semlja the New Siberian Islands and Wrangel Island. They are particularly well marked to the north of these islands and may occur even in winter during persistent south-easterly and southerly winds. The pack ice penetrates extremely far southwards into the North Atlantic in two places; (1) along the east coast of Greenland until Cape Farewell and around it; (2) along the eastern coast of North America from Baffin Bay southwards in the Labrador current as far as the Grand Banks of Newfoundland. These ice currents carry not only pack ice from the North Polar Basin but also winter ice and solid ice from the Greenland Sea and from the northern part of the Baffin Sea. In both outflows there is an outer zone of drifting ice floes, a middle zone of more compact ice with occasional channels running through it and finally an inner core of solid ice joining the solid ice along the coast. Smith gives the following data (Table 99) for these two ice currents.

The pack ice zone is bordered by a zone of *solid ice* which transforms into the land in coastal areas. During the winter in both Northern Siberia and in the North American Archipelago it covers all channels, bays and fiords, etc., and these only become free of ice again in summer. In coastal areas the solid ice at the beginning of the summer contains earthy material (stones and shells) picked up by freezing of ice of the sea bottom melting out in summer; the surface of the ice is then often brownish (TRANSCHÉ, 1928).

In the Antarctic (DRYGALSKI, 1921) floe ice occurs only outside a certain broad belt containing icebergs and the remains of icebergs. This belt extends for the most part to about 60° S. but reaches farther north near the Falkland Islands and South Georgia and past 50° S. only near Bouvet Island. The ice floes are frequently found in large

Table 99

Ice current	From	To	Distance (nautical miles)	Mean speed (nautical miles/day)	Total drift time of a single ice field from origin to end given in months
East Greenland ice	75° N., 0° W.	62° N., 51° W.	1850	7.5	8½
East American ice (Baffin and Labrador ice)	74° N., 70° W.	45° N., 49° W.	1950	12.5	5½

groups, sometimes associated with icebergs which were formerly frozen into them. South of 64° S. begins the continuous drift ice which is held together by the westward directed currents which tend to the south due to the influence of the Coriolis force. Icebergs are more frequent here and have the table-form characteristic of the Antarctic. The ice masses are driven together partly by the wind, but the ice pressure is not as strong here as in the Arctic. The belt of drift ice extends to the edge of the continental shelf.

In the shelf zone over the shallow waters the ice is a mixture of floating ice floes and icebergs which form here and accumulate. The whole mass is held together by the larger icebergs stranded in shallow water. Superficially the shelf ice appears as a flattened, smooth, rounded ice-surface because of the frequent snow storms, but if the upper parts of the ice is broken off by the wind, the solid ice layers stand out more clearly; these have been termed *blue ice* by Drygalski on account of their colour. This permanent region of shelf ice between the drift ice and the coast completely surrounds the coast and obliterates the actual coast-line. This is the main cause of the uncertain charting of the Antarctic continent.

There are only a few approximate estimates of the budget of ice transport of the total polar regions. KRÜMMEL (1907, p. 515) gave the following approximate summary for the Northern Hemisphere: between Spitzbergen and Greenland the main carrier of outflowing sea ice is the East Greenland Current. It has a width of about 500 km, and according to Makaroff in summer and winter about 76% of its surface is covered with ice floes and pack ice. Taking the mean velocity of the current as about 10 nautical miles a day and the average thickness of the ice as 5 m then the annual volume of ice carried out from the central Polar Basin by the East Greenland Current will be 12,700 km³. This is about one-third of the total pack ice and polar ice in the entire North Polar Basin. Another stream of ice floes comes from Baffin Bay. This has a width of 200 km when leaving Davis Strait and on the same basis as before will carry somewhat more than 5000 km³ a year. If, furthermore, the drift ice entering the Barents Sea is estimated as 2000 km³, there must be a total annual flow of about 20,000 km³ of ice to be melted in the northern part of the North Atlantic each year.

(b) Seasonal Displacements of the Ice Limits

The inner part of the North Polar Basin is covered by polar ice throughout the year and changes appear only at the edges in the outer ice zone, especially near land areas.

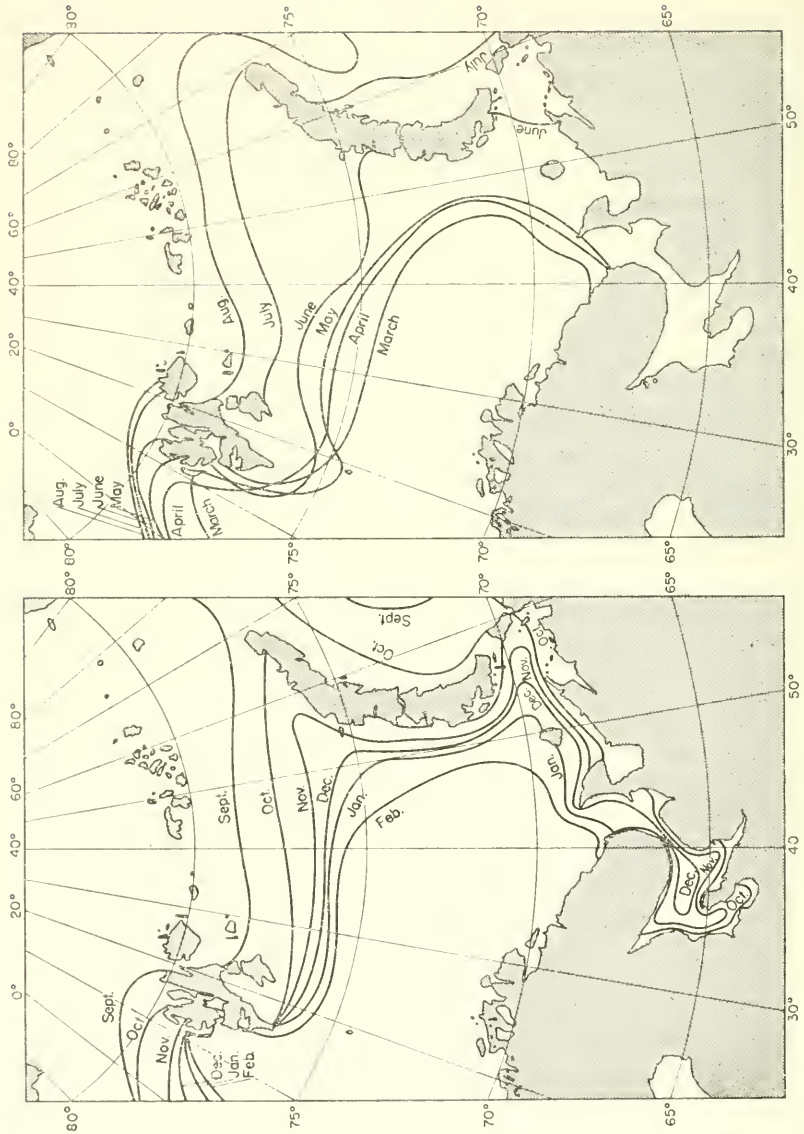


FIG. 117. Average ice limits in the Barents Sea for each month (1929-38).

The solid ice of the coastal shelf shows particularly a pronounced annual variation since it melts away almost completely during summer and re-forms again during the autumn. The North European and Siberian Shelf areas thus show large seasonal displacements in the ice limits. In the eastern part of the Siberian sea-way east of Novaya Zembla and remote from the influence of the North Atlantic current the distribution of ice, even in the summer months, may change so rapidly and so much that it is difficult to give exact mean ice limits for individual months (see *Atlas der Deutschen Seewarte*, 1942; BÜDEL, 1950; NUSSER, 1952).

In the Barents Sea, which is particularly influenced by the Atlantic Current, the seasonal displacements of the ice limit are very large. The two small charts in Fig. 117 present the mean ice limits as separate monthly means for a 10-year period from 1929 to 1938. One of them (March to August) shows the retreat of the ice limit in spring and summer, and the other (September to February) shows its advance in autumn and winter. During this period from 1929 to 1938 ice conditions were particularly favourable and this should be borne in mind.

The monthly limits of the ice along the eastern coast of Greenland, in the Davis Strait, in the Baffin Bay and along the east coast of North America as far as the Grand Banks of Newfoundland are almost entirely within the region of influence of the two great polar currents, the East Greenland Current and the Labrador Current. Figure 118 shows two charts, again for the period of retreat (March to September) and advance (September to February) (see also *Atlas der Deutschen Seewarte*, 1940, means for the years 1929–38). The east coast of Greenland is blocked for almost the whole year by a belt of ice varying strongly with latitude; this coast is only free of ice in the

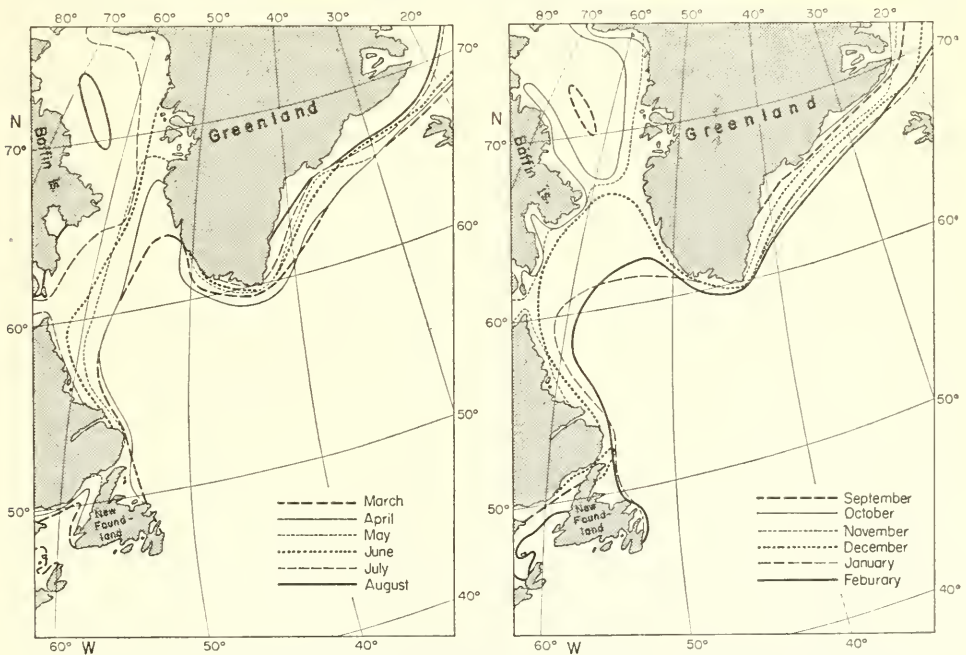


FIG. 118. Average ice limit along the eastern coast of Greenland, in Davis Strait and Baffin Bay, and along the east coast of North America for each month (1929–38).

southernmost parts in ice-poor years and frequently, even in the summer, there is a broad belt of drift ice off the south-west coast (Julinaachaab), although the fiords are completely ice-free.

Iceland is usually entirely ice-free, but during steady northerly winds ice may be driven against the north-west coast, drifting then along the northern coast towards the east where, in unfavourable years, this ice may be united with the drift ice moving towards the south-east in the East Iceland Current. The north coast of Iceland is then partly or entirely blocked by the ice. The probability of ice occurrence off the coast of Iceland is not small, as Table 100 shows (MEINARDUS, 1906; BROOKS and QUENNEL, 1928). The maximum ice season around Iceland is in early spring (March and April). At this time ice is observed about every second year off the coast and usually remains there nearly a full month.

Table 100. Frequency and persistence of ice occurrence around Iceland 1801-1900

Month	Jan.	Feb.	Mar.	Apr.	May	June	July	Aug.	Sept.	Oct.	Nov.	Dec.
Probability of ice in (%)	24	28	42	53	56†	43	22	14	4	1	3	5
Average duration given in % of each month	14	20	31	42	46†	28	18	9	1	1	1	1

† Maximum

The entrance into the Davis Strait and into Baffin Bay is completely blocked from October to November; however, beginning in April the eastern part of the northern Baffin Sea becomes ice-free in the east. In the central parts an ice-free area forms already in May, growing in extent during the following month and joining with the open water on the eastern side during July. This phenomenon is due to currents carrying warmer Atlantic water into the Baffin Bay weakening and breaking up the ice fields from beneath. Another further peculiarity is the formation of the "middle pack" a mass of ice surrounded by open water that still occurs in the western part of Baffin Bay during August and September.

The drift of pack ice along the coasts of Labrador and Newfoundland begins in late autumn (October and November), and reaches the northern parts of the Grand Banks of Newfoundland in January or, at the latest, in February. The ice fields reach their greatest extent, though not their greatest intensity, during April and the ice limit then begins to retreat. Figure 119, according to HUNTSMAN (1930), presents the extent of the pack ice south of Newfoundland and shows clearly the position of the main ice-fields relative to the Labrador current system and to the Gulf Stream flowing farther south.

MECKING (1906, 1907) made a detailed investigation of the dependence of the ice drift from the Baffin Bay on currents and weather. Table 101 shows mean values for a period of 18 years of the monthly amount of ice presented as a percentage of the annual amount of ice in the area of the Grand Banks of Newfoundland.

The season with ice fields lasts from January to about the middle of July; then it ends rapidly in August, when rapid melting due to higher air and water temperatures occurs. The secondary maximum in May is due to the icebergs, which are also at a maximum at this time (Fig. 120).

Table 101. Mean monthly ice amounts (as a percentage of the mean annual ice) for the Newfoundland Grand Banks

Month	Jan.	Feb.	Mar.	Apr.	May	June	July	Aug.	Sept.	Oct.	Nov.	Dec.
Drift ice or ice fields	9	37†	18	13	14‡	5	2	1	0	0	0	0

(† Max., ‡ secondary Max.)

In the Pacific Ocean, sea ice is limited to the north-western marginal seas; Bering Sea, the Okhotsk Sea and the Sea of Japan. The ice limits for the periods of advance (November to March) and retreat (March to July) are shown in Fig. 121. In the north the Bering Sea is connected through the Bering Strait with the Tschuktschen Sea where ice is plentiful. The mean annual duration of ice here is about 270 days, and the

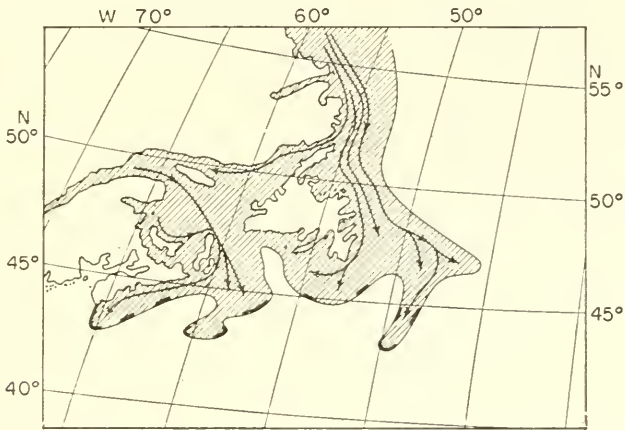


FIG. 119. Chart of the distribution of pack ice south of Newfoundland (according to Huntsman). The short thick lines show the position of the ice fields at the time of maximum ice extent.

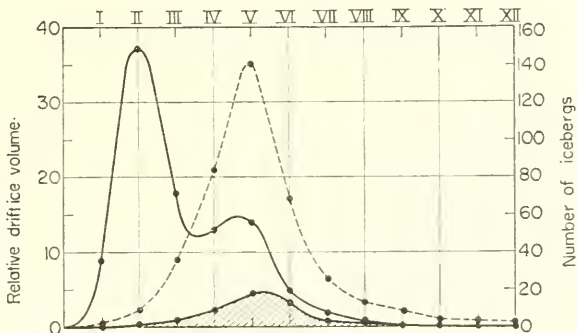


FIG. 120. Annual ice variation in the area of the Newfoundland Banks. The full curve shows the relative volume of drift ice normally present south of Newfoundland; the dashed curve shows the mean number of icebergs present south of Newfoundland and in the western Atlantic. The lower curve gives the mean number of icebergs south of the Grand Banks.

strait is only completely ice-free from July to the end of September (HEGEMANN, 1890; SCHULZ, 1911). To the south and south-west of the Lorenz Island along the east coast of Asia the ice season is still very long; in the Tartar Gulf (between the continent and Sakhalin, 52° N.) it lasts through half the year and in the Gulf of Vladivostok (43° N.) 3 months. The climatic conditions of the neighbouring continent with its monsoon-like winds blowing off the land carry a strong continental type of climate well out over the ocean, and even in spring when the land already warms up, the cold ocean currents along the coast prevent the break-up of the ice. Ice is still present in the inner parts of the Okhotsk Sea in May and the last only disappears in

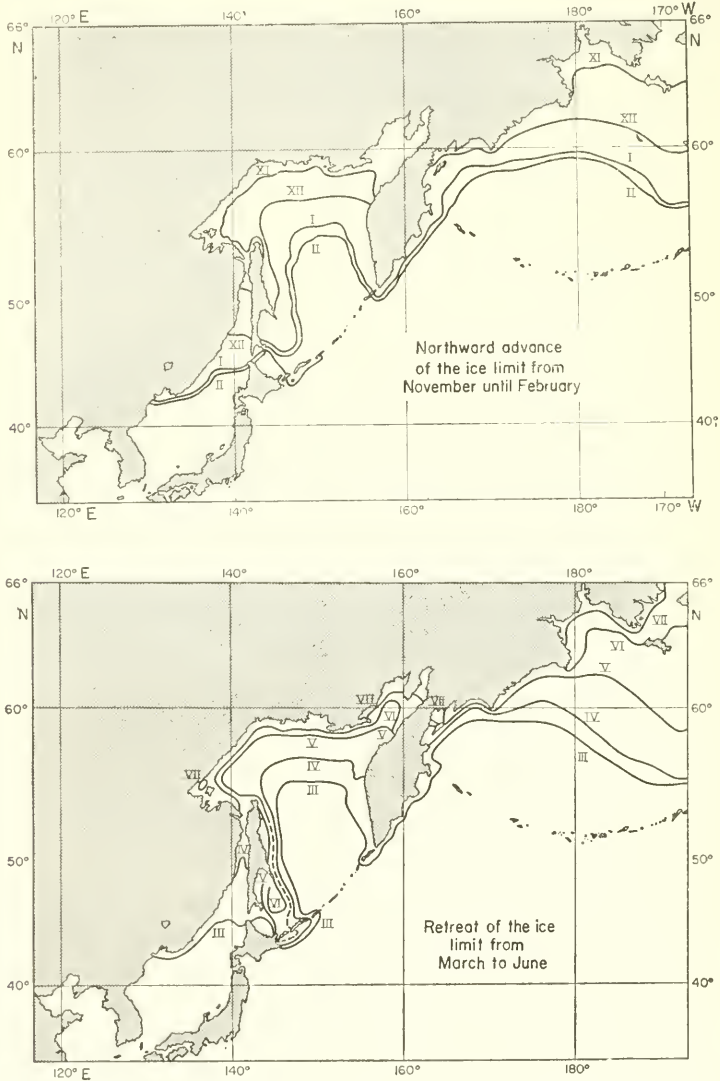


FIG. 121. Ice limits for the months from October to July in the north-western adjacent seas of the Pacific Ocean.

July. At the end of October, and during the first half of November, ice formation begins again along the northern coast. Conditions here are quite different from those along the east coast of North America and Greenland since the ice masses in these adjacent seas of eastern Asia are always of local origin, and are not reinforced by Arctic pack ice and icebergs as in the East Greenland and Labrador Currents.

Knowledge of the annual variations of the ice coverage in the ocean surrounding the *Antarctic* is still very poor. The ice limits in each month have only been known with some accuracy since the intensification of whaling. The pack ice limits in the Antarctic between 40° W. and 110° E. have been given by HANSEN (1934) for the 4 years from 1929 to 1934 (Fig. 122). In the area east of South Georgia to about 20° E. the

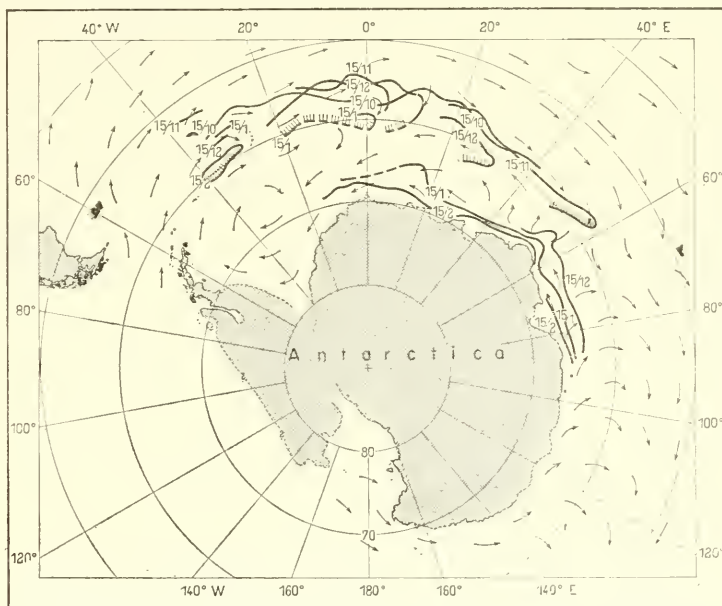


FIG. 122. Pack ice limits in the antarctic region between 40° W., and 110° E., for the whaling season 1930-1 (according to Hansen).

ice extends to a latitude of about 55° S. at the beginning of November. Deviations from this value in the course of the year are small. East of 20° E. the limit trends more and more to the south. As the season advances this outer pack ice retreats slowly towards the south, and by December whaling ships can penetrate it and reach open water at about 60° S. There is then usually no pack ice until the inner pack ice coast is reached.

These two ice zones, the inner drifting westwards and the outer eastwards, are characteristic for the whole region from the Weddell Sea as far as $20-30^{\circ}$ E. They are about 7° lat. apart. There is no such subdivision in the ice drifts east of Enderby Land. The outer pack ice zone melts very rapidly, especially if it is broken up in a number of places into large drifting ice masses. In the region of the Antarctic Ocean from Enderby Island and Balleny Island the ice limit retreats steadily during the melting period; the oceanic currents directed northward (equatorward) in 60° S. carry the ice floes in the same direction whereupon they rapidly disperse and melt.

(c) Aperiodic Variations in the Polar Ice Conditions

It is not surprising that a natural phenomenon such as the polar ice coverage depending on such a large number of different factors should show large aperiodic variations. In addition to their scientific interest these variations are of considerable practical importance for life and commerce in the polar regions. Statistics of the changes in ice coverage in the polar seas do not go very far back.

Following a resolution of the seventh international meeting of geographers, Berlin, 1899, the Royal Danish Meteorological Institute has published since 1894 an annual ice-record for the Arctic, and these annual reports are now the most important source of data of this type. However, knowledge of the extent and movement of the ice is confined mostly to shipping routes and fishing areas. The available data are thus inhomogeneous and incomplete. However, more accurate observations of the polar zones from the air will probably lead in the future to further progress, especially also because of the increasing military interest.

Variations in the ice conditions of polar and subpolar regions do not proceed everywhere in the same way; because they appear to be due, in the first place, to variations in the atmospheric and oceanic circulation, both of which regionally cause quite different effects. Somewhat more detailed investigations of these aperiodic variations have been made for the oceanic regions around Iceland, Davis Strait and Newfoundland and also, in part, for the Barents Sea.

MEINARDUS (1906) has examined the duration and the intensity of ice in the area around Iceland for the years 1800 to 1904. Figure 123 shows that Iceland is situated on

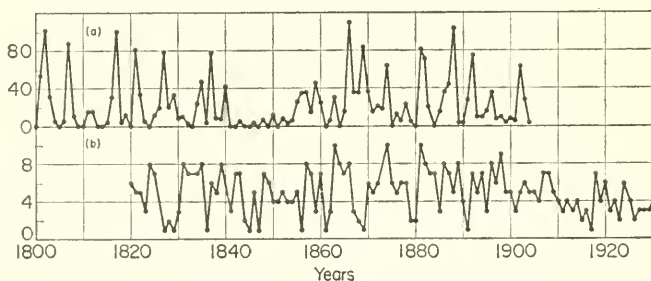


FIG. 123. (a) Character of the ice-years around Iceland for the period 1800–1904 (according to Meinardus). (b) Numbers of ice-character for the Davis Strait region for the period 1820–1930 (according to Speersneider).

the edge of the East Greenland Current and the North Iceland Current; these ice-bearing currents often cause the occurrence of severe "ice-years". Ice-rich years recur rather regularly and there has been a very noticeable ice minimum during the 'forties and the beginning of the following decade in the nineteenth century. There appears to be a 4-to 5-year cycle governing the recurrence of ice-rich years; this is shown quite clearly in Table 102, which gives mean values based on a $4\frac{1}{2}$ -year cycle, beginning always with a maximum for the period 1880–1904. An accurate determination by periodograms gave the period of the cycle as 4.76 years. However, the great variability of the phenomenon does not allow reliable ice-prognoses since the correlation coefficient of a value with the following fourth and fifth values is only -0.04 and 0.06 respectively.

Table 102. Severity of ice years around Iceland for a $4\frac{1}{2}$ -year cycle

Period	Before max. (years)					Max. 0	After max. (years)				
	5	4	3	2	1		1	2	3	4	5
1808-1854	34†	24	12‡	15	19	35§	16	11	7‡	26	27
1854-1904	31	36†	18	14‡	28	44§	36	13‡	24	33†	28
Ice-rich years (≥ 46)	4	5†	2	2‡	3	8§	4	1‡	2	4†	4

§ Main maximum; † Secondary maximum; ‡ Minimum

WIESE (1922) found a very high correlation coefficient ($r = -0.83 \pm 0.05$) for the period 1887-1930 between the autumn temperature in north-west Siberia and the ice volume $4\frac{1}{2}$ years later in the East Greenland Current; lower temperatures are followed by more ice and vice versa. This relationship is reasonable since $4\frac{1}{2}$ years is about the time required for ice to travel from the Siberian coast to the Greenland Sea. By comparison of variations in the meteorological elements and secular changes in ice drift Meinardus was able to show a close relationship with the intensity of the atmospheric circulation. The variations in occurrence of arctic ice in the north-west Atlantic have been investigated in a series of papers by MECKING (1907, 1939). A series of observations covering more than 100 years in the Davis Strait have been presented in the form of "ice character numbers" by SPEERSCHNEIDER (1931) who reduced them on a ten step scale (Table 103 and Fig. 123 series *b*).

Table 103. Drift ice in Davis Strait from 1820 to 1930 (ice-character numbers reduced on a scale from 1 to 10)

Year	0	1	2	3	4	5	6	7	8	9
1820	6	5	5	3	8	7	4	1	2	1
1830	3	8	7	7	7	8	1	6	5	8
1840	5	3	7	7	2	1	5	1	7	6
1850	4	4	5	4	4	5	1	8	7	3
1860	7	1	3	10	8	7	8	3	2	1
1870	6	5	6	8	10	6	5	6	6	2
1880	2	10	8	7	7	3	8	7	5	8
1890	4	1	7	5	7	3	8	6	9	5
1900	5	3	5	6	5	5	4	7	7	5
1910	4	3	4	3	4	2	3	1	7	4
1920	6	3	4	2	6	4	2	3	3	3

Comparison with the values for Iceland shows little similarity. Severe ice years in one area appear rather to correspond to ice-poor years in the others and vice versa, a relationship which had previously been pointed out by SCHOTT (1904) correlating the

pack-ice occurrence off Newfoundland and that off eastern Greenland. The Davis Strait values over a series of nine sunspot periods show, however, that the ice amount in the Davis Strait follows the sunspot cycle with a lag of 2 years rather well (Fig. 124).

The fluctuations in the pack ice in the area of the Newfoundland Banks are of course directly connected with those in Davis Strait. They also parallel exactly the fluctuations in icebergs in the same area. This is shown by the high correlation factor of

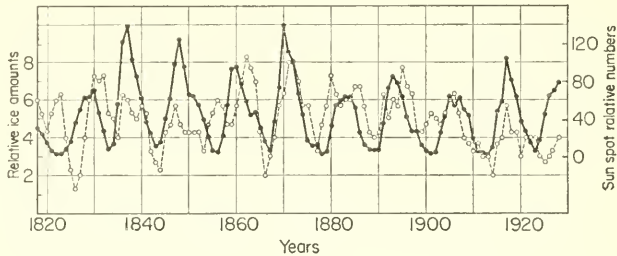


FIG. 124. Relative sunspot numbers and smoothed values for the amount of ice in Davis Strait. (The latter is displaced two years to the left relative to the sunspot curve (9 full periods) (full line: sunspot number, dashed line: amount of ice).)

$+0.86$ between the number of icebergs south of Newfoundland (48° N.) and the pack ice off Newfoundland valid from February until May (47 years, SMITH, 1926-7).

For the Barents Sea particularly good ice statistics are available for areas in which ice-measurements have been made by the Danish Institute during the years 1896-1916 (Nautik-Meteorol. Aarbog 1916). WIESE (1924) has used these in a study of the relationship between the occurrence of ice and variations in the atmospheric circulation. He was able to show that the ice intensity in this sea from May to June depends largely on the distribution of atmospheric pressure over the Norwegian Sea during the period from January to the end of April and that a larger (smaller) atmospheric pressure gradient directed from south-east to north-west between the Norwegian coast and the axis of the low-pressure trough over the Norwegian Sea causes a decrease (increase) in the ice coverage of the Barents Sea. By calculations from the regression equations with the factors affecting the ice coverage, it is possible to obtain reliable ice prognoses for this area.

A very strong aperiodic change in the Arctic has been in progress since 1918. Since the summer of that year there has been a general retreat of the ice limit, and at the same time a warming up of the entire Arctic (WEICKMANN, 1942). This can be seen best from the mean position of the ice limit from April to August in the two periods 1898-1922 (25-year mean) and 1929-38 (10-year mean) (Fig. 125). The especially favourable conditions during the second period are very noticeable when compared with those for the 25-year mean which can be regarded as normal. Bear Island, for example, is normally still surrounded by ice in April and partly also in May. During this second period it was ice-free during all months, and although the northern part of Novaya Zembla is almost never ice-free the ice limit receded during the second period almost to the northern tip in July and during August was only a little south of Franz Josef Land and Wiese Island.

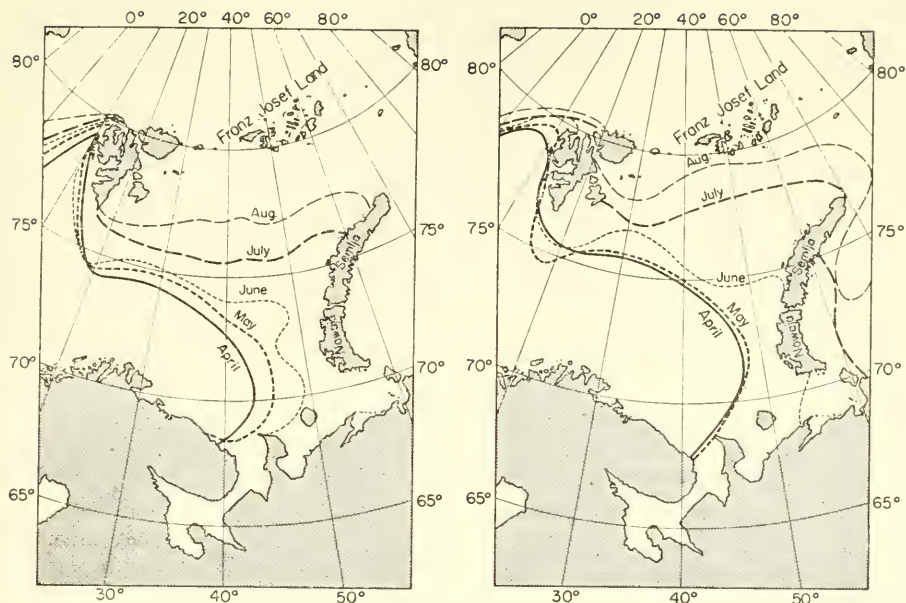


FIG. 125. Mean position of the ice limit from April to August in the Barents Sea for the period 1898–1922 (25-year mean, normal period) and for the period 1929–38 (10-year mean, warm period).

4. Land Ice in the Sea

(a) Glaciation in Polar Areas

In the polar regions the climatic snow-line lies so low that under the prevailing orographic conditions the glacial endings of the ice streams reach the sea and spread into the ocean. The coverage of polar regions by glaciers was given by Hess and is shown in Table 104.

Table 104. Glaciation in the polar regions

	Area in 1000 km ²
Northern Hemisphere	
Greenland including islands	1896
Spitzberger	58
Franz Josef Land	17
Novaya Zembla	15
Severnoja Zembla	45
North American islands	100
Total	2131
Southern Hemisphere	
Antarctica	13,000

In the Northern Hemisphere the overwhelming part of the total glaciation is on Greenland where only 0.325 million km² of its total area of 2.16 million km² is ice-free. Glaciers flow out from all sides from the inland ice and a large number of them

reach the sea in a broad front. The part played by the other Arctic islands in the production of icebergs is quite insignificant; only very few of the ice streams of the other islands reach the sea as calving glaciers, and even these produce only small icebergs.

In Greenland the inland ice reaches the sea through more or less narrow fiords which act as funnels collecting the converging streams of inland ice, but in the Southern Hemisphere the inland ice reaches the sea in an open front. At the edge of the Antarctic the snow-line is everywhere in or below the sea-level. Here the ice takes the form of an *ice barrier* which in the Ross Sea, for example, is about 750 km long and has a mean height of 36 m, but sometimes exceeds 50 m. Enormous icebergs break away continually from the edge of the inland ice cover, and though at first often trapped in the shelf ice, they are carried away with it later on or melt completely in their place.

(b) The Productivity of Glaciers Calving into the Sea in the Arctic

Statistics of iceberg production by glaciers calving into individual oceanic regions are rather poor; reasonably reliable figures can only be given for very few ice streams. SMITH (1931) has attempted to give such a preliminary survey for the Arctic. In the Eurasian Arctic there are only a small number of glaciers producing icebergs. In Spitzbergen, probably the Negri glacier in the Storfjord; the east coast of North-east Land has some calving glaciers as has the completely glaciated Franz Josef Land. But the number of icebergs produced, which are seldom large, is not known and is presumably small. The productivity of Novaya Zembla and Severnaya Zembla is equally not known, but is probably also very small. The few icebergs which are formed at the islands of the Siberian Shelf move mostly to the west and increase somewhat the number from the East Greenland icebergs. Smith estimated the number of icebergs produced annually in the north-east sector of the polar Atlantic ocean as about 600, which is only about 4% of the annual supply of icebergs from Greenland.

Smith believed that the productivity of the eastern Greenland glaciers was somewhat less than that of the west coast (7500 icebergs per year). There is, however, the important difference that in the east most of the icebergs are retained in narrow fiords and are prevented by the solid ice-barrier of the East Greenland Current from drifting southwards. Their importance to the Atlantic is therefore slight; about twenty to thirty a year reach Cape Farewell and then drift northwards with the West Greenland Current. They reach Davis Strait in a collapsing state. The iceberg survey of the "Marion" Expedition during the summer of 1928 found only seventeen icebergs off the south-west coast of Greenland; a very small number compared with the enormous amount that were found in Disko Bay to the north. On the western side of Baffin Bay only Ellesmere Land with two large ice caps shows any extended inland ice. About sixty glaciers reach the sea as calving glaciers, but according to Smith the productivity is not very large (about 1500 icebergs a year). The major source of icebergs is in the great glaciers of West Greenland from Cape Alexander to Disko Bay. The main part, from the North-east Bay as far as Disko Bay has more than 100 calving glaciers, the twelve largest and most productive ones alone producing more than 5400 icebergs a year. The most important of this group, the Jacobshavener Glacier calves about 1350 icebergs a year into Disko Bay. Not all of these reach the open sea immediately—on the contrary most are trapped in the fiords for longer periods. In the summer of

1928 the "Marion" Expedition found that all the icebergs produced during the previous 3-4 years (about 4000 to 6000) were accumulated in the Eisfjord. They were all released from their ice chains during favourable weather at once. Then they arrived all together in Baffin Bay and drifted slowly to the south.

Table 105. Production of icebergs in different regions on the Arctic

	Annual contribution
North-eastern sector of Atlantic	
Islands on the European-Asiatic side	600
East Greenland	7500
From those arriving at Cape Farewell and passing in the East Greenland Current	20-30
North-western sector of Atlantic	
Eastern North America	150
North Greenland	150
Cape Alexander to Cape York	300
Cape York to Svarten Huk	1500
North-east Bay to Disko Bay	5400
Total	7500

Table 105 is a summary given by Smith of iceberg production in the Arctic. This estimate gives a total annual contribution from Baffin Bay of 7500 icebergs, of which 70% come from North-east and Disko Bays. The table gives only a rough idea of the ice amount available in Baffin Bay. Direct estimates of the ice outflow from the Greenland Inland ice by measurement of the speeds of the different glaciers along the western side of the island still differ widely. DE QUERVAIN and MERCANTON (1925) estimated this ice flow as being between 10 km³ and 100 km³ a year. Assuming an average size of a large iceberg to be about 1.5 million m³ and assuming, further, that on calving about one-third of the ice forms icebergs and two-thirds gives debris and smaller pieces, then the total mass of ice released on calving is about 4.5 million m³. About 7500 such calvings per year gives approximately 35 km³ of ice. This value lies within the above limits. HELLAND (1876) found values of 5.8 km³ and 2.3 km³ for the annual ice supply from the Jakobshaven and the Torsukatak Glaciers. DRYGALSKI (1897) found 13.5 km³ for the large Karajak Glacier. According to these figures about 2-6 million m³ of ice are broken off in an average calving of a medium sized glacier; from this about one-third is used for production of icebergs.

(c) Calving, Size, Shape and Destruction of an Iceberg

Careful observation of iceberg calving at the eastern Greenland glaciers led Drygalski to distinguish according to the size of the icebergs formed between three types of calving. The third one proceeds almost continually over several days; small blocks of ice break away from the face of the glacier and fall into the sea, often in such large amounts that the surface is covered with these broken pieces far out into the fiord. In the second type, large masses are suddenly released in the water from the lower

part of the glacier and rise as icebergs to the surface; this leaves the edge of the glacier unchanged. The largest icebergs are produced by the first type: under the influence of the further continuous supply in ice mass the glacier pushes out into the sea for 200–300 m depending on the morphology of the fiord bottom (“fore part of glacier”). The fiord water slowly penetrates into the projecting ice mass and, due to buoyant forces, the forehead of the glacier gets lifted until it finally breaks off. Calving usually occurs exactly there where the depth of the fiord has increased to such a rate that the forward pushing ice-tongue loses contact with the sea bottom and starts floating. In addition to the increasing buoyancy, lifting due to the tides may also upset the equilibrium in the glacier tongue. Presumably the formation of icebergs proceeds in the same way in the Antarctic; however, the process there is of much larger dimension and produces enormous flat-topped icebergs.

The direct production of icebergs proceeds at about the same rate throughout the year, but the number of icebergs reaching the open sea depends on the nature of the fiord and more especially on the season of the year. In winter the fiords are frozen and the icebergs are trapped. They are released with the coming of summer, all within a short time and mostly all at once, and they then drift away. This gives rise to the so-called “iceberg swarms” which often occur in Baffin Bay and Davis Strait.

The shape of icebergs is remarkably variable: the pure-chance forms after calving are remodelled by the action of sea waves and by melting above and below the water; classification of these different forms is thus rather pointless. The height of icebergs varies widely, but the largest are of course found in the area where they are formed. Measurements made by Drygalski on eighty-seven icebergs frozen into the sea ice in the East Greenland fiords gave the results shown in Table 106.

Table 106

Height (m)	20–30	30–40	40–50	50–60	60–70	70–80	80–90	90–100	100
Number	7	6	12	10	12	10	4	4	1

The height decreases rapidly after their formation. The highest iceberg measured by the International Ice Patrol Service south of Newfoundland was 80 m high; it was flat-topped and 517 m long. Its volume was estimated as about 25.5 million m³. According to Smith, the icebergs in the Davis Strait have an average volume of 1.5 million m³; those of the Newfoundland Banks between 0.1 and 0.15 million m³; they are about 30 m high. The “depth of immersion” of an iceberg depends on the specific weight of glacier ice. Since icebergs contain a large percentage of air and numerous cracks and holes this depth does *not correspond* to that calculated solely from the specific weight. For mean densities of 0.8997 for the ice and 1.02690 for polar water, flat-topped icebergs will have one-eighth of their volume above the surface of the sea and seven-eighths will lie below the surface, but the shape of an iceberg has a considerable effect on the depth to which immerses. Smith has made a summary of direct measurements and has found that for the most peculiarly-shaped icebergs of the north-western Atlantic the ratio is 1 : 3. The flat-topped Antarctic icebergs immerse to greater depths.

The *destruction of icebergs* proceeds by calving, melting and erosion. Icebergs are often rapidly decreased in size by the breaking away of large and smaller pieces of ice. This may change the equilibrium of an iceberg so that it capsizes or rolls over. In cold water the melting process goes on mainly at the water line of icebergs (by the formation of holes). Melting increases greatly when they drift into warm water (e.g. south of the Newfoundland Banks in mixed water or in the warm Gulf Stream). Destruction from above is due to melt water running down the sides of the iceberg, by erosion and the action of the waves and rain. According to measurements made by Drygalski in North-east Bay, an iceberg in the summer months may lose from 3 to 4 m in 7 days. Between Greenland and Newfoundland the ice mass may decrease to an eighth, corresponding to a daily loss of 1.8 m a day. In the same time the height decreases by a half.

(d) Iceberg Drift in the Arctic and Antarctic

Icebergs in the open sea are subject to the eroding action of winds and currents. These effects are dependent: (1) on the ratio of the masses of ice above and below the water; (2) on the strength and duration of the wind; and (3) on the velocity and direction of the currents. MECKING (1906) has emphasized the great importance of the wind and currents for iceberg drift in Baffin Bay. The coastal current plays the decisive part and the wind determines the course of the icebergs only when this current is weak. The continuous off-shore wind along the coast of western Greenland in the summer thereby determines the number of icebergs reaching the Labrador current and thus the number of icebergs off Newfoundland in the following spring.

The International Ice Patrol Service, in order to determine the influence of the factors mentioned above on the course of the icebergs, has followed the drift of a large number in the area of the Newfoundland Banks and has recorded the meteorological and oceanographic conditions at the same time and SMITH (1931) has discussed this data in detail. The effect of the wind was made up of two parts: (1) the direct force of the wind exerted on the exposed surface of the iceberg above the water; and (2) the movement of the floating iceberg with the wind drift set up in the top layer of the water. For the latter influence it must be kept in mind that for a steady state the wind drift at the surface of the sea is deflected by 45° to the right of the wind direction (Northern Hemisphere). This deflection increases with depth and a mean deflection of 72° can be assumed for the upper 50 m. For the two cases of (a) deep-immersing larger icebergs and (b) smaller icebergs with immersion ratios of 1 : 1 and 1 : 2 average conditions of the effects of these two forces are given in Table 107 (Fig. 126).

The drift speed of larger, deeper-immersing icebergs with a deflection of 40° to the right of the wind is less than that of smaller icebergs of lesser depth of immersion for which the wind force and the force due to wind drift act more closely together. In this case the deflection from the direction of the wind is only 20° . For more accurate information on the distribution of icebergs in different parts of the sea it is necessary to make a survey of the existing iceberg accumulations. The International Ice Patrol Service carried out a systematic investigation of this type with the patrol boat "Marion" and at the same time the research ship "Godthaab" (RIIS CARSTENSEN,

Table 107. Direct wind force and force due to wind drift on icebergs (According to Smith.) *a*, deep-immersing large icebergs; *b*, smaller icebergs).

Wind velocity Beaufort	Direct wind force in the wind direction (km/day)	Wind drift, deflection 70° to the right of wind (km/day)	Resultant icebergs drift	
			Speed (km/day)	Direction, to the right of wind direction
<i>a</i> { 4-5 6-7	2.6	3.2	4.5	40°
	4.0	4.8	6.9	40°
<i>b</i> { 4-5 6-7	8.8	4.0	10.8	18°
	13.7	6.0	16.4	21°

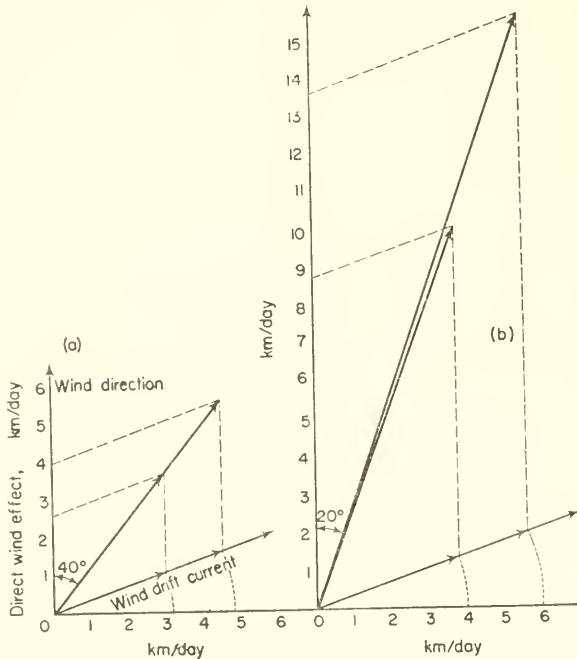


FIG. 126. Diagram of the forces affecting the drift of icebergs (according to Smith), (a) Effect of wind on large icebergs; (b) Effect of wind on small icebergs.

1929, 1936) made an oceanographic survey in Baffin Bay. Figure 127 shows the distribution of icebergs in the Davis Strait and the Labrador Sea during the summer of that year. The few icebergs along the south-west coast of Greenland are from the East Greenland Current. Most of the icebergs are carried southwards by the cold Labrador Current which runs close to the coast. The central parts of Davis Strait and the Labrador Sea are almost completely free of icebergs. The Labrador Current along the coast thus forms the channel along which the icebergs pass towards Newfoundland. The track of the icebergs, especially to the east and south of Newfoundland, has been

accurately fixed by tracking numerous icebergs with the patrol ships. The main iceberg track as shown by these detailed surveys is shown in Fig. 128. An increased frequency is to be expected along the eastern slope of the Newfoundland Banks where the Labrador Current turns towards the west and its cold and weakly saline water mixes along the southern side of the current in large eddies with the warm and highly saline water of the Gulf Stream. A careful study of these eddies by the Ice Patrol vessels has

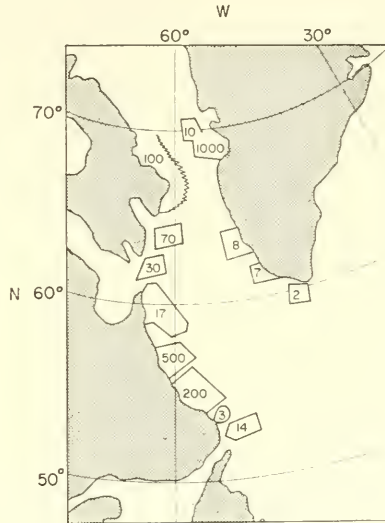


FIG. 127. Extent and distribution of icebergs in Davis Strait and the Labrador-Sea in the summer of 1928 according to the "Marion" Survey.

been made and thereby an explanation was found for the continuing presence of icebergs in this part of the sea, since the eddies keep the icebergs quasi-stationary. Occasionally individual icebergs withstand the destructive effects of the warm Atlantic water and reach much further south than usual. The most southerly position so far recorded was $30^{\circ} 20' N.$ and $62^{\circ} 32' W.$ near the Bermudas for an iceberg about 9 m long, 5 m broad and 1 m above the water, which was sighted by the "Baxtergate" on 5 June, 1926.

Knowledge of iceberg drift in the polar seas of the Southern Hemisphere is very scanty. The approximate northern limit of drifting icebergs is shown in Fig. 122. It is, of course, far north of the northern limit of drifting ice floes since the compact mass of a large iceberg can better withstand the destructive action of warm water and air. It must be assumed that here also winds and currents must be the factors that determine the drift of an iceberg. In some individual cases a relationship to the course of low-pressure areas has been demonstrated, but in view of the irregularities of the latter a strict relationship is hardly to be expected (MECKING, 1932).

Icebergs are especially important in the *Falklands area* where they are sometimes carried, accompanied by drift ice, far to the north in large numbers. They have been sighted as far north as $42^{\circ} S.$ and in 1906 even reached as far as $37^{\circ} S.$ ($59^{\circ} W.$). The aperiodic variations in the occurrence of ice appear to be particularly large here. In

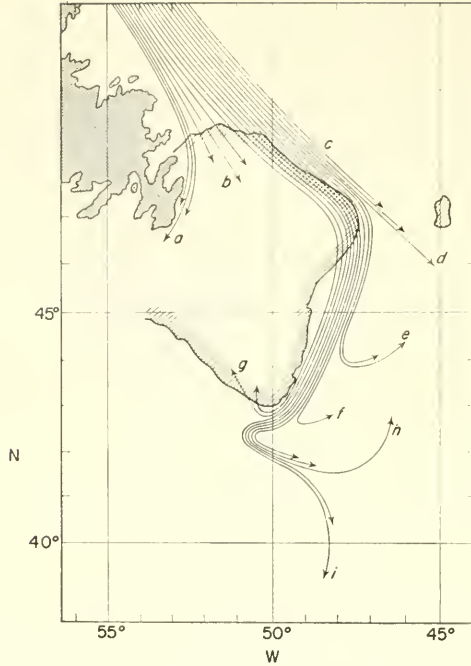


FIG. 128. Main iceberg tracks off Newfoundland and the Grand Banks.

the years 1891, 1892, 1893 and 1906 a remarkable accumulation of icebergs appeared in the area south of Cape Horn and northward of the *Falkland Islands* as far as 40° S. They occurred mainly along the edge of the shelf; farther to the west they were completely absent. They are trapped and melt rapidly inside the numerous eddies along the boundary between the Falklands Current and the Brazil Current in a similar way to those south of the Newfoundland Banks.

(e) *Seasonal and Aperiodic Variations in Iceberg Frequency off Newfoundland*

Surveillance of the distribution of icebergs in the area of the Newfoundland Banks since 1900 has given the mean annual iceberg frequency and its variation from month to month shown by the data in Table 108 for Newfoundland (south of 48° N.) and for the area south of the Grand Banks.

Table 108. Mean annual variation in iceberg frequency (a) off Newfoundland south of 48° N. and (b) south of the Grand Banks

(For the period from 1900-26)

Month	Jan.	Feb.	Mar.	Apr.	May	June	July	Aug.	Sept.	Oct.	Nov.	Dec.	Total
(a)	3	10	36	83	130	68	25	13	9	4	3	2	386
(b)	0	1	4	9	18	13	3	2	1	0	0	0	51

The iceberg season usually lasts from 15 March to 15 July, but the number of icebergs decreases rapidly after the middle of June (see Fig. 117). From the middle of July to the following spring the area south of the Grand Banks is almost free of icebergs. The variations in iceberg frequency from year to year are very large. South of 48° N. there were in 1929 a total of 1351 icebergs, in 1924 only eleven. An accurate monthly record of these values is available starting from 1900. Together with the previous data compiled by Mecking there is now a complete series of records available, covering a period of 50 years for the iceberg frequency off Newfoundland. This is shown graphically in Fig. 129. With these more or less homogeneous data it is possible

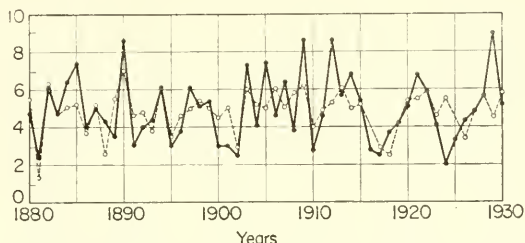


FIG. 129. Character of the iceberg-years from 1880 to 1930 off Newfoundland (ten step-scale, according to Smith).

to investigate with some hope for success the causes of the aperiodic variations in numbers of icebergs. In the first place there appears to be a correlation between the atmospheric pressure gradient from Iceland to Greenland-North America a few months previously and the iceberg maximum off Newfoundland. Determination of the air pressure anomaly for the North Atlantic for the months December to March during 6 years of low iceberg frequency, in this case with a total of 275 icebergs, and for the same months in 5 years with a high iceberg frequency with a total of 774 showed completely opposite conditions (Fig. 130). A weak Icelandic low pressure area during the spring and the autumn with a weak pressure gradient over Baffin Bay and Davis Strait seems to be followed by the low-frequency iceberg years. During iceberg-rich years, on the other hand, the Icelandic low-pressure area is intensified and the strong pressure gradient to the west is accompanied by strong air movements and stronger wind drift in the iceberg area along the North American coast. Smith has also tried a quantitative determination of this relationship using the correlation method, and has obtained a prognostically valuable formula. An increase in the iceberg frequency in the north-western Atlantic is thus accompanied by an intensification of the atmospheric circulation in the polar areas which corresponds to an increase in the outflow of polar air and of the arctic water towards the south. These relationships of course take into account only the meteorological effects and not the possible fluctuations in the production of icebergs by the western Greenland glaciers. At the present time it is not possible to make an estimate of these.

5. Effect of Polar-Ice Conditions on the Atmospheric and Oceanic Circulation

The total annual ice outflow along the whole of the west coast of Greenland has been estimated by Smith as between 42 and 63 km^3 (see p. 272); the American coast

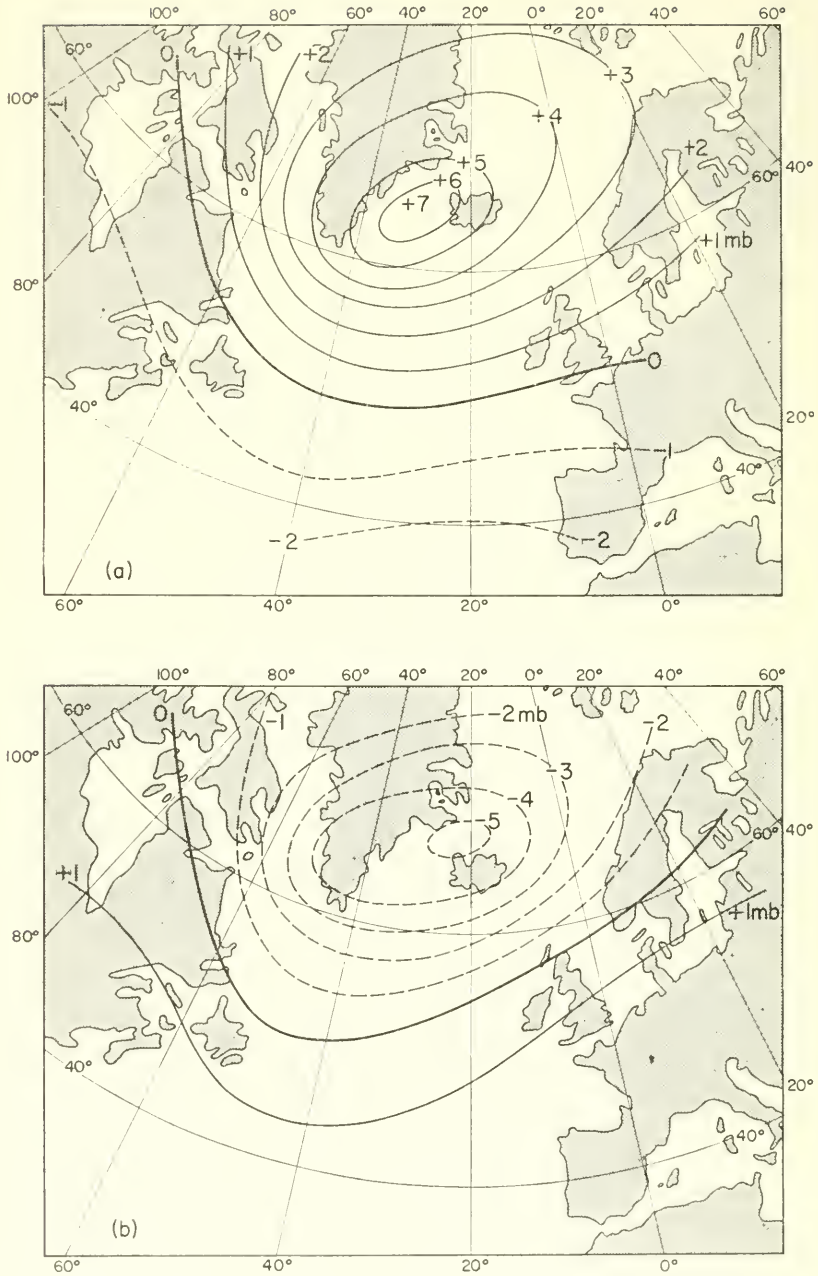


FIG. 130. Iceberg frequency off Newfoundland and atmospheric pressure anomaly over the North Atlantic.

adds only about 1.9 km^3 . This is the *amount of land ice* that exists in Baffin Bay on a yearly average and drifts southward to melt in Davis Strait, along the Labrador coast and in the Newfoundland area. The *amount of sea ice* melting during one year can be calculated from the average area covered by pack ice and drift ice. Smith has made an estimate of this kind based on reliable data collected by the Ice Patrol cruises. The bases of this are contained in Fig. 131 which also shows the areas which stand in question; the most important are the shelf areas where the ice-covered area is about 1.6 million km^2 . Taking the mean thickness of drift and pack ice as about 1.8 m, the total amount of sea ice will be about 3000 km^3 . In contrast to this, the land ice amounts to only 44–65 km^3 , so that of the average annual amount of ice melting in the north-west Atlantic only between a hundredth and a two-hundredth part comes from icebergs. This is vanishingly small (see Fig. 131). This comparison shows that the amount of pack ice and drift ice is the decisive factor. If for any oceanographic or meteorological problem a consideration of the effects of ice destruction in the north-west Atlantic—which vary considerably from year to year—is needed, it is thus not justifiable to compare it with variations in the ice frequency, as has often erroneously been done.

In dealing previously with convection processes (see p. 97) two possibilities were discussed for the initiation of such a process, which are of the greatest importance to the thermal structure of the middle and bottom layers of the oceans. It was assumed by Pettersson that the necessary heat loss of the upper water layers was mainly due to the melting of ice in polar and subpolar oceanic regions. However, laboratory experiments by Nansen showed that this hypothesis was untenable. For the special case of the conditions in the north-west Atlantic it is possible, using the values given by Smith to determine directly the amount of heat which is required for the observed yearly melting of pack ice and drift ice and therefore is not available for heating the ocean and the atmosphere. This can be compared, as has been done by Smith, with the amount of heat supplied during the summer by solar and sky radiation which is required for the increase in temperature of the upper 150 m layer of water (the average depth to which the increase reaches downwards into the sea). From the numbers given in Fig. 131 it can be seen that the mean summer increase in the temperature of the water masses in this area (down to 150 m) is about 1.2°C . It can also be calculated that the annual melting of pack ice and drift ice in the same area is sufficient to decrease the temperature of the layer down to 150 m depth by 0.6°C . Thus in the north-western part of the North Atlantic the water is cooled by the melting of the ice by only about half of the amount of the summer increase in temperature due to the absorption of solar and sky radiation. Dynamic treatment of the oceanographic data of the “Marion” and “Godthaab” Expeditions permits the calculation of the amount of the heat deficit at the Newfoundland Banks due to the continuous supply of cold polar water by the Labrador Current. Comparison of this heat reduction with that due to ice melting shows that the latter accounts for only 10% of the cooling effect of the Labrador Current. The dominant factor in the cooling of the water masses of the northern part of the North Atlantic is thus neither the melting of icebergs nor of the pack ice and drift ice, but much more the continuous advective supply of polar water which the Labrador Current carries southwards towards the warm water of the Gulf Stream.

The “Meteor” cruise in Icelandic and Greenland waters have given the same

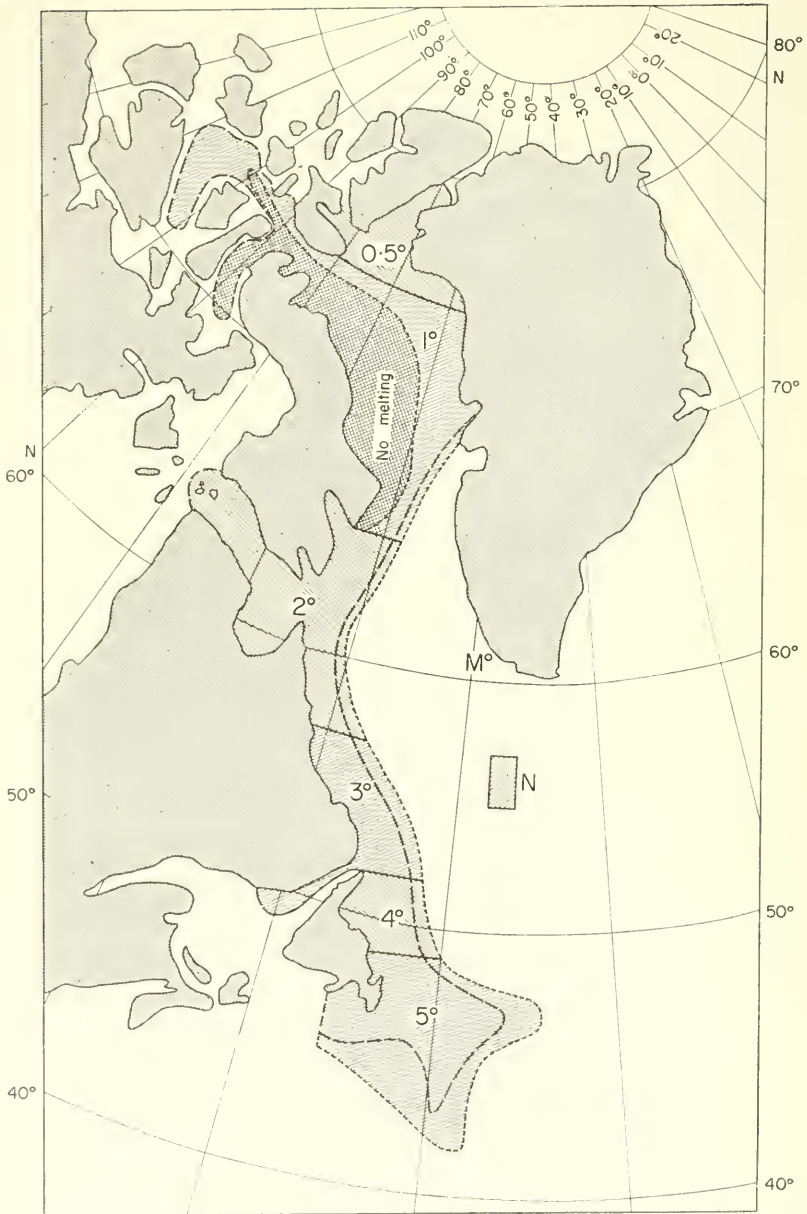


FIG. 131. A quantitative representation of a number of comparisons between ice-melting effects and related phenomena. The shaded area bounded by the full line in the normal pack-ice area. The dotted line marks the mixing zone. The entire melting area, with a uniform thickness of 150 metres is divided into six parts; in summer the southernmost is heated an average of 5°F, and the northernmost only 0.5°F. The spot "M" off Cape Farewell represents the annual crop of glacial ice expressed in the same scale as the pack ice and as one large berg. The shaded area "N" represents the total annual discharge of glacial ice into Baffin Bay, expressed on the same scale and in terms of pack ice 6 ft thick.

results (DEFANT, 1933). The formation of the East Greenland Current and the maintenance of its polar character as far as Cape Farewell is not due to melting processes; its Arctic nature is mainly acquired from its direct connection with the North Polar Basin causing a continuous supply of polar water and from the climatic conditions maintained over Greenland by the inland ice. This advective supply of Arctic water from areas where the effect of solar radiation is very small is the determining factor, and sea ice and icebergs are only accessory phenomena.

A marked effect of the ice masses of the polar seas on the atmospheric circulation has been assumed by many prominent meteorologists. HILDEBRANDSSON (1914) especially has attempted to show that the cause of the secular variations in meteorological factors is to be seen in the aperiodic variations in the amount of polar ice. More recent data from later investigations has lent support to this hypothesis, but a definite proof is difficult. Both phenomena are not independent of each other, so that it is reasonable to assume, of course, a mutual interaction between the ice conditions and the atmospheric circulation; it is not easy to separate cause and effect (WIESE, 1924). Conditions are probably such that variations in the atmospheric circulation change the equilibrium conditions in the polar reservoirs of cold air. Years with weaker circulation favour an increase in the thickness of the cold air masses in the polar regions. This increases the atmospheric pressure in the polar region and correspondingly winds and currents become stronger, which causes a greater extension of the polar ice towards the south. The increased ice surface in turn increases the air pressure; the atmospheric pressure anomaly thus acquires a certain permanence, and due to this mutual reinforcement the effect may last a long time. The atmospheric pressure in the polar areas is thus a very sensitive indicator of the general condition of the atmosphere. Since, however, the atmospheric pressure conditions in these regions is reflected in the ice conditions, the distribution of ice in the polar seas can be taken as a measure of the variations in the general atmospheric circulation, provided sufficiently accurate information is available.

The major variations in the atmospheric circulation usually extend throughout the entire atmosphere over the whole Earth, both in the Northern and Southern

Table 109. Parallelism between changes in ice conditions of the north and south polar regions

Shown by the relation between ice conditions from March to May at the South Orkney Isles (years with close or open ice) and corresponding deviations of the ice coverage in May to August from an average value of the period 1896-1916 in the Barents Sea

South-Orkney-Isles Character of ice conditions for March to May	Barents Sea deviations of the ice coverage (in 1000 km ²) for May to August from an average value of the period 1896-1916					
Close ice {	1903	1909	1910	1911	1912	(above average)
	+88	+102	+17	+97	+176	
Open ice {	1904	1905	1906	1907	1908	(below average)
	-158	-165	-61	-130	-121	

Hemisphere. Thus, for example, it has been shown with sufficient certainty that there is a high positive correlation between the atmospheric pressure pulsations in the North Polar regions and those in the South Polar regions. If this connection is real, certain parallelism would be expected between the variations in ice conditions in the Arctic and in the Antarctic. To test this assumption Wiese has compared 10-year records of ice conditions at the South Orkney Islands from 1903 to 1912 (MOSSMAN, 1923) between March and May, with the area of ice in the Barents Sea between May and August in the same years. The results are given in Table 109 and show the existence of a positive correlation.

It is obvious that such a relationship between Arctic and Antarctic ice conditions can only be investigated by means of the indirect method of an investigation of variations in the general circulation of the entire atmosphere; it shows, however, the great scientific and practical importance of a continuous systematic observational check on ice conditions in the polar regions.

Bibliography

- ÅNGSTRÖM, A. (1920). Applications of heat radiation measurements to the problems of the evaporation from lakes and the heat convection at their surfaces. *Geog. Ann., Stockh.* 2, 237-51; also *Met. Z.* 1918, p. 90.
- ÅNGSTRÖM, A. (1925). The albedo of various surfaces of ground. *Geog. Ann., Stockh.* 7.
- ÅNGSTRÖM, A. (1936). *Sat. Met.-Hydr. Anstalt, Stockh.*, Uppsaler. no. 8.
- ALBRECHT, F. (1949). Über die Wärme- und Wasserbilanz der Erde. *Ann. Met., Hamburg* 2, 129.
- ALBRECHT, F. (1951). Monatskarten des Niederschlags und Monatskarten der Verdunstung und des Wasserhaushaltes des Indischen und Stillen Ozeans. *Ber. dtsh. Wetterdienstes U.S.-Zone*, no. 29.
- AVERS, H. G. (1927). A study of the variation of mean sea-level from a level surface. *Bull. Amer. Geophys. Un., Trans., Nat. Res. Coun.*, no. 61, Washington, D.C.
- BEIN, W., HIRSEKORN, H. G. and MÖLLER, L. (1933). Neue Konstantenbestimmungen des Meerwassers *J. Cons. int. Explor. Mer.*, v. 8/1.
- BEIN, W., HIRSEKORN, H. G. and MÖLLER, L. (1935). Konstantenbestimmungen des Meerwassers und Ergebnisse über Wasserkörper. *Veröff. Inst. Meeresk. Univ., Berl.*, N.F. Reihe A, Heft 28 Berlin.
- BÉNARD, H. (1901). *Ann. Phys., Chem., Paris* 23.
- BERGSTEN, E. (1931). The annual fluctuation of the sea-water stage on the coast of Skandinavia and Denmark. *Geogr. Ann., Stockh.* p. 197.
- BJERKNES, V. and SANDSTRÖM, J. W. (1910). *Statik der Atmosphäre und Hydrosphäre. Braunschweig* 1912. Tabellenband.
- BÖHNECKE, G. (1932). "Meteor" *Werk* 4, no. 1, Berlin. Die Temperaturmessungen an der Oberfläche und in der Tiefe.
- BÖHNECKE, G. (1936, 1938). Temperatur, Salzgehalt und Dichte an der Oberfläche des Atl. Ozeans. "Meteor" *Werk* 5, Berlin.
- BÖHNECKE, G. (1936). Atlas zu: Temp., Salzg. und Dichte an der Oberfläche des Atl. Ozeans. "Meteor" *Werk* 5, Atlas, Berlin.
- BOWEN, J. S. (1920). The ratio of heat losses by conduction and by evaporation from any water surface. *Phys. Rev.* 27, 779-87.
- BOWIE, W. (1936). The place of geodesy in geophysical research. *Bull. Amer. Geophys. Un., Trans., Nat. Res. Coun.*
- BREITFUSS, L. L. (1906). *Wiss. "Murman"-Exp. Ber. über die Tätigkeit pro 1903.* Petersburg.
- BRENNECKE, W. (1909). *Ozeanographie im "Planet" Werk* 1906/07 3. Berlin.
- BRENNECKE, W. (1921). Die ozeanographischen Arbeiten der Deutschen Antarktischen Expedition 1911-12. *Arch. dtsh. Seewarte, Hamburg.*
- BROCKAMP, B. and MOTHES, H. (1930). Seism Untersuchungen am Pasterzen Gletscher. *Z. Geophys.*, 6.
- BROOKS, C. E. P. and QUENNEL, W. A. (1928). The influence of arctic ice u.s.w. *Geophys. Mem.* 5, no. 41. London: Meteor. Off.
- BRÜCKNER, E. (1905). Die Bilanz des Kreislaufes des Wassers auf der Erde. *Geogr. Z.*
- BRUCH, H. (1940). Die vertikale Verteilung von Windgeschwindigkeit und Temperatur in den untersten Metern über der Wasseroberfläche. *Veröff. Inst. Meeresk. Univ. Berl.*, N.F. Reihe A, Heft 38.
- BUCH, K. (1917). Über die Alkalität, Wasserstoffionenkonzentration, Kohlensäure und Kohlensäuretenion im Wasser der Finnland umgebenden Meere. Diss. Helsingfors.
- BUCH, K. (1933). Der Borsäuregehalt des Meerwassers und seine Bedeutung bei der Berechnung des Kohlensäuresystems im Meerwasser. *Rapp. Proc. Verb.* 85, Copenhagen.
- BUCH, K. (1939). Beobachtungen über Kohelnsäuregleichgewicht u.s.w. im Nordatlantischen Ozean. *Acta Acad. Aboensis, Math. Phys.* 11/9.
- BUCH, K. (1939a). Kohlensäure in Atmosphäre und Meer an der Grenze zum Arktikum. *Acta Acad. Aboensis. Math. Phys.* 11/12.
- BUCH, K. (1942). Kohlensäure in Atmosphäre und Meer. *Ann. Hydr. Mar. Met.*, p. 193.
- BUCH, K. (1945). Kolsyrejämvikten i Baltiska Havet. *Fennia* 68, no. 5, 1-208. Helsingfors.

- BUCH, K. (1948). Der Kohlendioxydgehalt der Luft als Indikator der meteorologischen Luftqualität. *Geophysica*, no. 3, 63–79. Geophys. Soc. Finland, Helsinki.
- BUCH, K. (1951). Das Kohlensäure-Gleichgewichtssystem im Meerwasser. Kritische Durchsicht und Neuberechnung der Konstituenten. *Havsforsk. Inst. Skr.* no 151, 1–18. Helsinki.
- BUCH, K., HARVEY, H. W., WATTERBERG, H. and GRIPENBERG, St. (1932). Über das Kohlensäure-system im Meerwasser. *Rapp. Cons. Explor. Mer.* 79, Copenhagen.
- BUCHANAN, J. Y. (1884). "Challenger" Report. *Physics and Chemistry* 1, Kap. II.
- BÜDEL, J. (1943). Das Luftbild im Dienste der Eisforschung und Eiserkundung. *Z. ges. Erdkunde z Ber.*
- BÜDEL, J. (1950). Atlas Im Eisverhaltrisse das Nordatlantischen Ozeans und Übersichtskarten des Eisverhältnisse des Nord- und Südpolargebietes. *Dtsch. Hydrog. Inst.*, no. 2335, Hamburg.
- BUEN DE, R. (1927). Resultats des investigations espagnoles dans de detroit de Gibraltar. *Rapp. Cons. Explor. Mer.* Copenhagen.
- BULLARD, G. (1938). *Proc. Geol. Soc. Camb.*, p. 46.
- BULLARD, E. C. (1954). The flow of heat through the floor of the Atlantic Ocean. *Proc. Roy. Soc. A*, 222.
- CARRUTHERS, N. and SAWFORD, A. L. (1952). *Nature, Lond.* 169, 601.
- CHERUBIM, R. (1931). Über die Verdunstungsmessungen auf See. *Ann. Hydr. Mar. Met.* 59.
- CHURCH, PH. E. (1932). Surface temperature of the Gulf Stream and its bordering waters. *Geogr. Rev.* 22, 286.
- CHURCH, PH. E. (1937). Temperatures of the western North Atlantic from thermograph records. *Ass. Oceanogr. Phys. Publ. Sci.* no. 4, p. 1. Liverpool
- CLARKE, G. L. (1933). Observations on the penetration of daylight in Mid-Atlantic and coastal waters. *Biol. Bull.*, Woods Hole 65.
- CLARKE, G. L. (1936). Light penetration in Western North Atlantic and its application to biological problems. *Rapp. Cons. Explor. Mer.* 101/2, no. 3. Copenhagen.
- CLARKE, G. L. (1938). Light penetration on the Carribean Sea and in the Gulf of Mexico. *J. Mar. Res.* 1.
- CLARKE, G. L. and OSTER, H. R. (1935). The penetration of the sea green and violet component of the daylight into Atlantic Waters. *Ju. Opt. Soc. Amer.* 25, 611.
- CLOWES, A. J. and DEACON, G. E. R. (1935). The deep-water circulation of the Indian Ocean, *Nature, Lond.*, 135, 936–8.
- COOPER, L. H. N. and VAUX, D. (1949). Cascading over the continental slope of water from the Celtic Sea. *J. Mar. Biol. Ass. U.K.* 28, 719–50.
- DALY, R. A. (1936). Origin of submarine "canyons". *Amer. J. Sci.* p. 401.
- DEACON, G. E. R. (1934). Carbon dioxide in arctic and antarctic sea. *Discovery Invest. Nature* 56.
- DEACON, G. E. R. (1937). The hydrology of the southern ocean. "Discovery" Rep. 15, Cambridge.
- DEACON, G. E. R. (1938). A general account of the hydrology of the South Atlantic Ocean. "Discovery" Rep. 7, p. 190. Cambridge.
- DEFANT, A. (1926). Die Austauschgrösse der atmosphärischen und ozeanischen Zirkulation. *Ann. Hydr. u Mar. Met.* p. 12.
- DEFANT, A. (1928). Die systematisch Erforschung des Weltmeeres. *Z. Ges. Erdkunde, Berl.* (Jubiläum-Sonderband), 1928.
- DEFANT, A. (1929). Stabile Lagerung ozeanischer Wasserkörper u. dazu gehörige Stromsysteme. *Veröff. Inst. Meeresk. Univ., Berl.*, N.F. Reihe A, Heft 19.
- DEFANT, A. (1930). Die vertikale Verteilung von Temperatur und Salzgehalt im Weltmeer. *Z. Ges. Erdkunde, Berl.*, p. 28.
- DEFANT, A. (1930). Berichte über die ozeanographischen Untersuchungen des "Meteor" in der Dänemarkstrasse und in der Irmingersee. *S.B. preuss. Akad. Wiss.* (1930, 1931, 1936).
- DEFANT, A. (1931). Physik des Meeres. *Wien-Harns Handb. Exp. Physik* 25, no. 2. Leipzig.
- DEFANT, A. (1932). Ergebnisse der Strom- und Serienmessungen auf den Ankerstationen. "Meteor" Werk 7, p. 250. Berlin.
- DEFANT, A. (1932). Die Gezeiten und inneren Gezeitenwellen des Atl. Ozeans. "Meteor" Werk 7, p. 318.
- DEFANT, A. (1933). Eisberge und Eisbergsicherungsdienst im Nordatlantischen Ozean. *Das Meer in volkstüml. Darstellungen*, 1 (Polarbuch). Berlin.
- DEFANT, A. (1936). Die Troposphäre des Atlantischen Ozeans. "Meteor" Werk 6, no. 1. Berlin.
- DEFANT, A. (1936). Ausbreitungs- und Vermischungsvorgänge im Antarktischen Bodenstrom und im subantarktischen Zwischenwasser. "Meteor" Werk 6, no. 2, p. 55.
- DEFANT, A. (1936). Entstehung und Erhaltung der troposphärischen Sprungschicht. *Z. Geophysik.*, p. 281.

- DEFANT, A. (1936). Ber. d. ozeanogr. Unters. des Vermess. Schiffes "Meteor" in der Dänemarkstrasse und in der Irmingersee. III. *Ber. Sitz. Akad. Wiss. Berl. Math.-Naturw. Kl.* 19.
- DEFANT, A. (1939). Vorschlag betreffs einer Fortführung der "Grundkarte der ozeanischen Lotungen des Atlantischen Ozeane" und Ausdehnung dieser Arbeit auch auf die anderen Ozeane. *Ass. Oceanogr. Phys. Abstract and Comm.*, Washington, D.C., September.
- DEFANT, A. (1939). Die "Altair-Kuppe". *Abh. preuss. Akad. Wiss. Berl.*, no. 5.
- DEFANT, A. (1940). Ozean und Atmosphäre. In "Das Meer in volkstümlichen Darstellungen". 8, Berlin.
- DEFANT, A. (1949). Konvektion und Eisbereitschaft in polaren Eismeeeren. *Geogr. Ann., Stockh.*
- DEFANT, A. (1954). Turbulenz und Vermischung im Meer. *Dtsch. Hydrogr. Z.* 7, Heft 1-2, 1-14.
- DEFANT, A. (1955). Die Ausbreitung des Mittelmeerwassers im Nordatlantischen Ozean. *Papers in Marine Biology and Oceanography*, pp. 465-70. Pergamon Press, London.
- DEFANT, A. and WÜST, G. (1930). Die Mischung von Wasserkörpern im System $s = f(t)$. *Rapp. Cons. Explor. Mer.* 64. Copenhagen.
- DEFANT, A. and ERTEL, H. (1939). Durch Niederschlag verursachte Störungen des Salzgehaltes im Ozean und deren Ausgleich durch Turbulenz. *Abh. preuss. Akad. Wiss.*, Berl., no. 10.
- DEFANT, A. and HELLAND-HANSEN, BJ. (1939). Bericht über die ozeanographischen Untersuchungen im zentralen und östlichen Teil des Nordatlantischen Ozeans im Frühsommer 1938 (Internationale Golfstrom-Expedition). *Abh. preuss. Akad. Wiss.*, Berl. (Phys.-Math. Kl.), no. 5.
- DEFANT, A. and ERTEL, H. (1943). Grundgleichungen des Wasserhaushaltes in der Atmosphäre und die Berechnung der mittleren Austauschkoefizienten der spezifischen Feuchtigkeit aus der Niederschlagsmenge. *Ann. Hydr. Mar. Met.* Bd. 71 S. 269.
- DEVAPUTRA, D., THOMPSON, TH. C. and UTTERBACK, C. L. (1932). The radioactivity of sea-water. *J. Conseil.* 7, no. 3. Copenhagen.
- DIETRICH, G. (1937). Die Lage der Meeresoberfläche im Druckfeld von Ozean und Atmosphäre. Mit besonderer Berücksichtigung des westlichen Nordatlantischen Ozeans und des Golfes von Mexico. *Veröff. Inst. Meeresk. Univ., Berl.*, N.F. Reiche A. Heft. 33.
- DIETRICH, G. (1937). Fragen der Grossformen und her Herkunft des Tiefenwassers im Amerikanischen Mittelmeer. *Ann. Hydr. Mar. Met.* p. 345.
- DIETRICH, G. (1939). Die Absorption der Strahlung im reinen Wasser und im reinen Meerwasser. *Ann. Hydr. Mar. Met.* p. 411.
- DIETRICH, G. (1939). Das Amerikanische Mittelmeer. *Z. Ges. Erdkunde, Berl.* p. 108.
- DIETRICH, G. (1950). Über systematische Fehler in den beobachteten Wasser- und Lufttemperaturen auf dem Meere und über ihre Auswirkung auf die Bestimmung des Wärmeumsatzes zwischen Ozean und Atmosphäre. *Dtsch. Hydrogr. Z.* 3, 314.
- DIETRICH, G. (1950). Elemente des jährlichen Ganges der Oberflächentemperatur in der Nord- und Ostsee und den angrenzenden Gewässern. *Dtsch. Hydrogr. Z.* 6, 1953.
- DIETRICH, G. (1950). Die anomale Jahresschwankung des Wärmeinhaltes im Englischen Kanal, ihre Ursachen und Auswirkungen. *Dtsch. Hydrogr. Z.* 3.
- DIETRICH, G. (1953). Verteilung, Ausbreitung und Vermischung der Wasserkörper in der südwestlichen Nordsee. "Gauss"-Fahrt Febr./März 1952. *Ber. dtsch. Wiss. Komm. Meeresforschung*, 13, no. 2, 104-129, 1953.
- DIETRICH, G. (1954). Einfluss der Gezeitenstromturbulenz auf die hydrographische Schichtung in der Nordsee. *Arch. Met. Geophys. Bioklimat.* A. 7 (Festschrift A. Defant). Wien.
- DITTMAR, C. (1884). "Challenger" Report: Physics and Chemistry. 1, pp. 189, 204.
- DRYGALSKI, V. E. (1897). Grönland Expedition *Ges. Erdkunde Berl.*, 1891-3.
- DRYGALSKI, V. E. (1921). Das Eis der Antarktis und der subantarktischen Meere. *Dtsch. Südpolar-Exp.* 1901-3. 1, no. 4, Berlin.
- DRYGALSKI, V. E. (1930). Die Gliederung der Eisformen. *Petern. Geogr. Mittl.*, Erghft. 209.
- EKMAN, V. W. (1905). On the use of insulated water-bottles and reserving thermometers. *Publ. Circ.* no. 23, p. 27. Copenhagen.
- EKMAN, V. W. (1905). On the influence of the earth's rotation on ocean currents. *Ark. Met. Astr. Fys. Vet. Akad., Stockh.*, 1905-06, 2.
- EKMAN, V. W. (1908). Die Zusammendrückbarkeit des Meerwassers u.s.w. *Publ. Circ.* no. 49. Copenhagen.
- EKMAN, V. W. (1914). Der adiabatische Temperaturgradient. *Ann. Hydr. Mat. Met.* p. 340.
- EKMAN, V. W. (1920). Über den Begriff der stabilen Schichtung. *Met. Z.* p. 22.
- ERTEL, H. (1942). Der vertikale Turbulenzstrom in der Atmosphäre. *Met. Z.* p. 250.
- MCEWEN, G. F. (1919). Ocean temperatures, their relation to solar radiations and oceanic circulation. *Misc. Studies in Agric. and Biol. Publ. Univ. Scripps Inst. Biol. Res., Calif.* p. 335.
- EWING, M., CARY, A. P. and RUTHERFORD, H. M. (1917). *Bull. Amer. Geol. Soc.*

- EWING, M. and VINE, A. (1938). *Trans. Amer. Geophys. Un.* p. 248.
- EWING, M., CRAY, A. P. and THORNE, A. M. (1934). Propagation of elastic waves in ice. *Physics*, 5, New York.
- FALKENBERG, G. (1928). Absorptionskonstanten einiger meteorologisch wichtiger Körper für infrarote Wärmestrahlung. *Met. Z.* p. 334.
- FISCHER, K. (1925). Die Grundgleichungen des Wasserhaushaltes eines Flussgebietes. *Zentralblatt der Bauverwaltung.* p. 209. Berlin.
- FJELDSTAD, J. E. (1929). Ein Beitrag zur Theorie der winderzeugten Meeresströmungen. *Gerl. Beitr. Geophys.* 23,
- FJELDSTAD, J. E. (1933). Die Wärmeleitung im Meer. *Geofys. Publ.* 10, 20. Oslo.
- FJELDSTAD, J. E. (1936). Results of tidal observations. Norw. North Polar-Exp. with the "Maud" 1918-25. *Sci. Res.* 4, 88.
- FLEMING, R. H. and REVELLE, R. (1939). Physical processes in the ocean. In *Recent Marine Sediments. A Symposium*, p. 736. (Parker, D. Trask, ed.) Amer. Ass. Petroleum Geol, Tulsa, Okla.
- FORCH, C., KNUDSEN, M. and SÖRENSEN, S. P. L. (1902). Berichte über die Konstantenbestimmungen zur Aufstellung der hydrogr. Tabellen. *D. Kgl. Danske vidensk. Selsk. Skrifter*, 6. Raekke, *Naturvid. og Math. Afd.* 12, no. 1, 151.
- FÖYN, E., KARLIK, B., PETTERSSON, H. and RONA, E. (1939). The radioactivity of seawater. *Medd. Oceanogr. Inst. Göteborg* 2,
- FOX, CH. (1905). On the determination of the atmospheric gases dissolved in sea water, *Publ. Circ.*, no 21. Copenhagen.
- FOX, CH. J. J. (1907). On the coefficients of absorption of the atmospheric gases in distilled water and sea water. Part 1. Nitrogen and oxygen. *Publ. Circ.* no. 41. Copenhagen.
- FOX, CH. J. J. (1909). On the coefficients of absorption of nitrogen and oxygen in distilled water and sea water and of atmospheric carbonic acid in sea water. *Trans. Faraday Soc.* 5, 68.
- FRITSCHKE, E. (1906). Niederschlag, Abfluss und Verdunstung auf den Landflächen. Diss. Halle.
- GANS, R. (1924). Die Farbe des Meeres. *Ann. Phys.* 75.
- GEHRKE, J. (1909). Beitrag zur Hydrographie des Finnischen Meerbusens. *Finn. Hydrobiol. Unters.* 3. Helsingfors.
- GEHRKE, J. (1912). On vertikale Vaermströmme i Havet. Grundtrækkene af Blandings-processernes teori. Diss. Kopenhagen.
- GEHRKE, J. (1910). Beiträge zur Hydrographie des Ostsee-Bassins. *Publ. Circ.* no. 52. Copenhagen.
- GESSLER, H. (1934). Zur Korrektionsformel für die Richter'schen Kippthermometer. *Ann. Hydr. Mar. Met.* p. 378.
- GOLDSCHMIDT, V. M. (1934). Drei Vorträge über Geochemie. *Geol. Fören. Stockh., Forhandl.* 56.
- GRANQUIST, G. (1938). Zur Kenntnis der Temperatur und des Salzgehaltes des Baltischen Meeres an den Küsten Finnlands. *Habilitationsschr. Univ. Helsinki.*
- GROLL, M. (1912). Tiefenkarte der Ozeane. *Veröff. Inst. Meeres., Berl., N.F. Reihe A. Heft. 2.*
- HABER, F. (1928). Das Gold im Meer. *Z. Ges. Erdkunde, Berl., Verh. ozeanogr. Konf. in Berlin, Mai 1928, Ergh.* 3.
- HAHN, A. and RIETSCHEL, E. (1938). Langjährige Wasserstandbeobachtungen in der Ostsee. 6. *Balt. Hydrol. Konferenz, Berlin 1938, Hauptber.* 13.
- HAMBERG, A. (1885). Hydrogr. Kem. Jak. Hagelser under den Svenska Exp. till Grönland 1883. *Bih. till. K. svensk. vet. Akad. Handl.* 10, no. 3. Stockholm.
- HAMBERG, A. (1895). Studien über Meereis und Gletschereis. *Bih. till. K. Sven. vet. Akad. Handl.* 21, no. 2. Stockholm.
- HANN, J. (1906). Über den jährlichen Wärmeumsatz in Binnenmeeren. *Met. Z.* p. 377.
- HANN, J. (1908). Das Problem der vertikalen Temperaturverteilung im östlichen Mittelmeer. *Met. Z.* p. 215.
- HANSEN, H. E. (1934). Limits of the pack-ice in the Antarctic in the area between 40° W. and 110° E. *Hvalrådets Skrifter*, no. 9. Univ. Biolog. Labor. Oslo.
- HEEZEN, B. C., ERICSON, D. B. and EWING, M. (1954). Further evidence for a turbidity current following the 1929 Grand Banks earthquake. *Deep Sea Res.* 1.
- HEGEMANN, F. (1890). Eis und Strom im Bering-Meer. *Ann. Hydr. Mar. Met.* p. 427.
- HELLAND, A. (1876). Om de isfyldte Fjorde og de glaciæle Dannelser i Nordgrönland. *Arch. Math. Naturvid., Christiania.*
- HELLAND-HANSEN, BJ. (1911-12). The ocean waters. *Intern. Rev. ges. Hydrol. Hydrogr.* 3 (*Hydrogr. Suppl.*), p. 81.
- HELLAND-HANSEN, BJ. (1918). Nogen hydrografisk metoder. *Förh. ved. skand. Naturf. Juli 1916*, p. 357. Oslo.

- HELLAND-HANSEN, BJ. (1930). Physical oceanography and meteorology. *Rep. sci. Res. "Michael Sars" North Atl. Deep-sea Exp.* 1910. Part I.
- HELLAND-HANSEN, BJ. and NANSEN, FR. (1926). The eastern North Atlantic. *Geophys. Publ.* 4, no. 2. Oslo.
- HESS, H. H. (1938). Gravity anomalies and island arc structure with particular reference to the West Indies. *Proc. Amer. Phil. Soc.* 79, Philadelphia.
- HESS, V. F. (1918). Über die Verteilung der radioaktiven Substanzen in und über dem Meer. *Sitzb. Wiener Akad. Wiss.* 127. Wien.
- HESELBERG, TH. (1918). Über die Stabilitätsverhältnisse bei vertikalen Verschiebungen in der Atmosphäre und im Meer. *Ann. Hydr. Mar. Met.* p. 118.
- HESELBERG, TH. and SVERDRUP, H. U. (1914-15). Die Stabilitätsverhältnisse des Seewassers bei vertikalen Verschiebungen. *Bergens Mus. Aarb.* 1914-15.
- HESELBERG, TH. and SVERDRUP, H. U. (1915). Beitrag zur Berechnung der Druck- u. Massenverteilung im Meer. *Bergens Mus. Aarb.* 1914-15, no. 14. Bergen.
- HESSEN, K. (1931). Gezeiten- und Strombeobachtungen auf der Winterstation der "Gauss" 1902-3. *Deutsche Südpolar Exp.* 7, 561. Berlin.
- HIDAKA, K. (1932). Über die neue Korrekionsformel zur Umkippthermometerablesung. *Mem. Imp. Mar. Obs. Kobe* 5 no. 1.
- HILDEBRANDSSON, H. H. (1914). Quelques recherches sur les centres d'action de l'atmosphère. *K. svenska Vetenskapsakad. Handl.* 45, 1909, 51, 1914.
- HORN, W. (1944). Das Seekartennull. *Mittl. Chefhydr. Dienstes, OKM, Amtsgr. Nautik.* Berlin.
- HUMBOLDT, A. v. (1816). *Relation Historique*, 1, 144. also: *Klassiker der Geographie*, 2, Reihe, p. 12.
- HUNTSMAN, A. G. (1930). Arctic ice on our eastern coast. *Bull. Biol. Board of Canada*, no. 13. Toronto.
- JACOBS, W. C. (1942). On the energy exchange between sea and atmosphere. *J. Mar. Res.* 5, 37-66.
- JACOBS, W. C. (1943). Sources of atmospheric heat and moisture over the North Pacific and North Atlantic. *Ann. N.Y. Acad. Sci.* 44, 19-40.
- JACOBS, W. C. (1951a). The energy exchange between sea and atmosphere and some of its consequences. *Bull. Scripps. Instr. Oceanogr.*
- JACOBS, W. C. (1951b). Large-scale aspects of energy transformation over the oceans. *Comp. Met. Amer. Met. Soc.* pp. 1051-70. Boston, Mass.
- JACOBSEN, J. P. (1913). Beitrag zur Hydrographie der Dänischen Gewässer. *Medd. komm. Havunders. Ser. Hydr.* 2, no. 2, p. 94. Copenhagen.
- JACOBSEN, J. P. (1915). Hydrogr. Invest. in Faeroe waters. *Ibid.*, no. 4. Copenhagen.
- JACOBSEN, J. P. (1918). Hydrogr. Untersuchungen in Randsfjord. *Ibid.*, no. 7, Copenhagen.
- JACOBSEN, J. P. (1927). Eine graphische Methode zur Bestimmung des Vermischungskoeffizienten im Meer. *Gerl. Beitr. Geophys.* 16.
- JACOBSEN, J. P. (1929). Contribution to the hydrography of the North-Atlantic. *The Dana Exp.* 1921-22. Copenhagen.
- JACOBSEN, J. P. (1943). The Atlantic current through the Faroese-Shetland-Channel and its influence on the hydrographic conditions in the northern part of the North Sea, the Norwegian Sea and the Barents Sea. *Rapp. Cons. Explor. Mer.* 112. Copenhagen.
- JAENICKE, J. (1935). Habers Untersuchungen über das Gold im Meer. *Naturwissenschaften.*
- JEFFREYS, H. (1928). Some cases of instability in fluid motion. *Proc. Roy. Soc. A*, 118, 195-208.
- JERLOV, N. G. (1951). Optical studies of ocean water. *Rep. Swedish Deep-Sea Exp.* 3, no 1, Göteborg.
- JERLOV, N. G. (1953). Influence of suspended and dissolved matter on transparency of sea water. *Tellus* 5, no. 1, 59-65.
- JERLOV, N. G. (1953). Particle distribution in the ocean. *Rep. Swedish Deep Sea Exp.* 3, no. 3. Göteborg.
- JESSEN, O. (1943). Die Randschwellen der Kontinente. *Erg. Hf. 241 zu Peterm. Geogr. Mittlg.*, p. 169.
- JOSEPH, J. (1950). Durchsichtigkeitsregistrierungen als ozeanographische Untersuchungsmethode. *Dtsch. Hydrogr. Z.* 3, 69-77. Hamburg.
- JOSEPH, J. (1952). *Meeresoptik, in Landolt-Börnstein, Zahlenwerte und Funktionen u.s.w.* 3, Berlin.
- JOSEPH, J. (1953). Die Trübungsverhältnisse in der südwestlichen Nordsee, während der "Gauss"-Fahrt Febr./März 1952. *Ber. dtsch. Wiss. Komm. Meeresforsch.* 13, 93-103.
- INTERNATIONAL HYDROGRAPHIC BUREAU (1937). Limites des Océans et des Mers. *Special Publ.* no. 23, July 1937.
- KAEHNE, K. (1941). Die Erforschung der unterseeischen Täler. *Naturwissenschaften* p. 303.
- KALLE, K. (1938). Zum Problem des Meersfarbe. *Ann. Hydr. Mar. Met.* p. 1.
- KALLE, K. (1939). Die Farbe des Meeres. *Rapp. Cons. Explor. Mer* 109, 98. Copenhagen.
- KALLE, K. (1945). Der Stoffhaushalt des Meeres. *Prob. Kosm. Physik.* 23, 2th ed. Leipzig.

- KALLE, K. (1953). Fluchtentafeln zur Bestimmung der Temperaturkorrekturwerte beim Arbeiten mit Kippthermometern. *Dtsch. Hydrogr. Z.* 6.
- KLEINSCHMIDT, E. (1921). Die Verdunstung auf ausgedehnten Wasserflächen. *Met. Z. S.* 205.
- KNUDSEN, M. (1899). *Hydrography in Danish "Ingolf" Exp.* 1, no. 2. Copenhagen.
- KNUDSEN, M. (1901). *Hydrographic tables. G.E.C. Gad.* Copenhagen 1901.
- KNUDSEN, M. (1903). On the standard water used in the hydrographic research until July 1903. *Publ. Circ.* no. 2. Copenhagen.
- KNUDSEN, M. (1903). Wissenschaftliche Meeresuntersuchungen. *Herausgeg. von der Komm. zur Untersuchung der D. Meere.* 2. Kiel.
- KNUDSEN, M. (1903). Gefrierpunkttabellen für Meerwasser. *Publ. Circ.* no. 5. Copenhagen.
- KNUDSEN, M. (1923). Some new oceanographical instruments. *Publ. Circ.* no. 77, p. 9. Copenhagen.
- KNUDSEN, M. (1925). L'emploi de l'eau normal dans l'oceanographie. *Publ. Cir.* no. 87. Copenhagen.
- KOENUMA, K. (1939). On the hydrography of southwestern part of the North Pacific and the Kuroshio. *Imp. Mar. Obs., Mem.* 7, 41–114. Kobe.
- KOSSINA, E. (1921). Die Tiefen des Weltmeeres. *Veröff. Inst. Meeresk., Univ., Berl.,* Heft 9.
- KOSSMAT, F. (1931). Das Erdbild und seine Veränderungen. *Handb. Exp. Phys.* 25, 2. Teil, Leipzig.
- KRÜMMEL, O. (1900). *Wiss. Meeresuntersuchungen der Kieler Komm.* 5, 25.
- KRÜMMEL, O. (1907). *Handbuch der Ozeanographie*, 1. 2. Aufl. pp. 411, 526. Stuttgart.
- KRÜMMEL, O. and RUPPIN, E. (1905). *Wiss. Meeresuntersuchungen der Kieler Komm.* 9, 29. Kiel.
- KUENEN, PH. H. (1938). Onderseesche Canyons. *Tdsch. nederl. gen. Amst.* p. 861.
- KUHLBRODT, E. (1938a). Der tägliche Gang der meteorologischen Elemente. "*Meteor*" *Werk* 14, 203. Berlin.
- KUHLBRODT, E. (1938b). Kritik der Lufttemperatur-Bertimmung auf See: Grösse der Temperaturdifferenz Wasser-Luft auf der Atlantischen Ozean. *Ann. Hydr. Mar. Met.* 64.
- KULLENBERG, B. (1954): Remarks on the Grand Banks turbidity current. *Deep Sea Res.* 1
- LANDOLT-BÖRNSTEIN (1952). *Zahlenwerte und Funktionen u.s.w.* 6th ed. 3, 426–541. (Contributions by G. Dietrich, J. Joseph, K. Kalle, W. Hansen, W. Horn, F. Nusser.) Berlin. Springer.
- LAUSCHER, F. (1944). Sonnen- und Himmelsstrahlung im Meer und in Gewässern. *Handbuch der Geophysik* 7, Kap. 12, 723–63. Berlin 1944.
- LAUSCHER, F. (1947). Zur Strahlungstheorie der Hydrosphäre. *S.B. Akad. Wiss. Wien, (Math.-Naturw. Kl., Abt. IIa)* 155, 281–308. Wien.
- LEE, O. S. and SIMPSON, L. S. (1954). A practical method of predicting sea ice formation and growth. *U.S. Hydr. Off. Wash. D.L. Tech. Rep.* Sept. 1–27.
- LETTAU, H. (1954). A study of the mass, momentum and energy budget of the atmosphere. *Arch. Met. Geophys. Bioklim.* 7, 131–53. Wien.
- LEVERKINCK, (1915). Über den Einfluß des Windes auf die Gezeiten, unter Berücksichtigung Wilhelmshavens und der Deutschen Bucht. *Veröff. Obs. Wilhelmshaven.* Berlin.
- LÜTGENS, R. (1911). Ergebnisse einer ozeanographischen Forschungsreise in den Atlantischen und südöstlichen Stillen Ozean. *Arch. dtsch Seewarte*, Bd. 34, no. 1. Hamburg.
- LUMBY, J. R. (1927). The surface sampler, an apparatus for the collection of samples from the sea surface from ships in motion. *J. Conseil.* 2. Copenhagen.
- MAKAROFF, (1901). *Jermak waljedach*, pp. 395, 414. Petersburg.
- MAKIN, C. J. S. (1898). *Chem. News*, 77, p. 155.
- MALMGREN, F. (1927). On the properties of sea-ice, *Norw. North Pol. Exp. "Maud"* (1918–25, *Sci. Res.*) 1. no. 5.
- MARMER, H. A. (1927). Tidal datum planes, Washington D.C., U.S. *Spec. Publ. Coast and Geod. Surv.*, no. 135, 142 pp.
- MARVIN, C. F. (1909). A proposed new formula for evaporation. *Mon. Weath. Rev., Wash.*, p. 57.
- MATTHEWS, D. J. (1932). Tables of the determination of density of sea water under normal pressure (σ_t). *Cons. perm. pour l'expl. la mer.* Copenhagen.
- MAURSTAD, A. (1935). Atlas of sea ice. *Gepfys. Publ.* 10, no. 10. Oslo.
- MECKING, L. (1906). Die Eistrift aus dem Bereich der Baffinbai beherrscht von Strom und Wetter. *Veröff. Inst. Meeresk., Univ., Berl.,* Heft 7. Berlin.
- MECKING, L. (1907). Die Treibeiserscheinungen bei Neufundland in ihrer Abhängigkeit von Witterungsverhältnissen. *Ann. Hydr. Mar. Met.* pp. 348, 396.
- MECKING, L. (1932). Die antarktischen Treibeisgrenzen und ihre Beziehung zur Zyklonenwanderung. *Ann. Hydr. Mar. Met.*, p. 225.
- MECKING, L. (1939). Die Periodizität der Eisbedeckung in der Davis-Strasse. *Ann. Hydr. Mar. Met.* p. 23.
- MEINARDUS, W. (1906). Periodische Schwankungen der Eistrift bei Island. *Ann. Hydr. Mar. Met.* pp. 148, 227, 278.

- MEINARDUS, W. (1923). Deutsche Südpolar Exp. 1901–03. *Ergebnisse der Seefahrt der "Gauss"*, 3, 1. pp. 501, 531.
- MEINARDUS, W. (1934). Die Niederschlagsverteilung auf der Erde. *Meteor. Z.* Bd. 51, p. 345.
- MERZ, A. (1911). Hydr. Untersuchungen im Golf von Triest. *Denkschr. Wien. Akad. p. Wiss.* 87. Wien.
- MERZ, A. (1922). Temperaturschichtung und Vertikalzirkulation im Südatl. Ozean nach den "Chalenger" und "Gazelle" Beobachtungen. *Z.d. Ges. Erkunde.* Berlin.
- MERZ, A. (1925). Die Deutsche Atl. Expedition auf dem Forschungs- und Vermessungsschiff "Meteor". *I. Ber. Sitzber. preuss. Akad. Wiss.* 31. Berlin.
- MEYER, H. H. F. (1932). "Meteor" Werk 4, no. 1, 262. Berlin. Die Chlortitrierung.
- MÖLLER, L. (1929). Die Zirkulation des Indischen Ozeans auf Grund von Temperatur- und Salzgehaltstiefenmessungen und Oberflächenstrombeobachtungen. *Veröff. Inst. Meeresk., Univ., Berl., N.F. Reihe A.* Heft. 21.
- MOHN H. (1883). *Den Norske nordhavs Exp.* 1876–78. Vol. II. *Meteorologi*, S. 135 ff. Christiania.
- MOHN, H. (1900). The Norw. North Polar Exp. 1893–6. *Sci. Res. Christiania.*
- MONTGOMERY, R. B. (1938). Circulation in upper layers of southern North Atlantic deduced with use of isentropic analysis. *Pap. Phys. Oceanogr and Meteor. Mass. Inst. Tech. and Woods Hole Oceanogr. Inst.* 6, no. 2, Cambridge, Mass.
- MONTGOMERY, R. B. (1939). Ein Versuch, den vertikalen und seitlichen Austausch in der Tiefe der Sprungschichte im äquatorialen Atl. Ozean zu bestimmen. *Ann. Hydr. Mar. Met.* p. 242
- MONTGOMERY, R. H. (1940). Observations of vertical humidity distribution above the ocean surface and their relation in evaporation. *Pap. Phys. Oceanogr. Meteor. Mass. Inst. Tech. and Woods Hole Oceanogr. Inst.* 7, no. 4, pp. 30.
- MOSBY, H. (1936). Verdunstung und Strahlung auf dem Meere. *Ann. Hydr. Mar. Met.* Bd. 64.
- MOSBY, H. (1940). An oceanographic thermo-sounder. *Un. Géod. Géophys. Intern. Ass. Oceanography Phys. Proc. Verb.* no. 3, 190.
- MOSSMANN, R. (1923). On Indian monsoon rainfall in relation to South American Weather 1875–1914. *Mem. Ind. Met. Dep.* 23. Calcutta.
- MÜNSTER STRÖM, K. (1936). Land-locked waters. Hydrography and bottom deposits in badly-ventilated Norwegian Fjords with remarks upon sedimentation under anaerobic conditions. *Skr. Norske Vidensk. Akad. Oslo, Math.-Naturv.* Kl. no. 7.
- MUNK, W. H. (1947). A critical wind speed for air-sea boundary processes *J. Mar. Res.* 6, no. 3; or *Contr. Scripps Instn Oceanogr., N.S.* no. 349.
- MUNK, W. H. and ANDERSON, E. R. (1948). Notes on a theory of the thermocline. *J. Mar. Res.* 7.
- NANSEN, F. (1900). On hydrometers and the surface tension of liquids. The Norw. North Polar Exp. 1893–96. *Sci. Res.* 3, 10.
- NANSEN, F. (1900). Some oceanogr. results of the Exp. with "Michael Sars" 1900. *Nyt Mag. Naturvid. Kristiania.*
- NANSEN, F. (1902). Oceanography of the north polar basin. The Norw. North Polar Exp. 1893–96. *Sci. Res.* 3. Christiania.
- NANSEN, F. (1912). Das Bodenwasser und die Abkühlung des Meeres. *Int. Rev. ges. Hydrobiol. Hydrogr.* 5, Suppl.
- NERNST, E. (1909). *Theoretische Chemie.* 6. Aufl. p. 247. Stuttgart.
- NEUMANN, G. (1938). Zur Frage des jährl. Ganges des Oberflächensalzgehaltes bei Adlergrund-Feuerschiff. 6. *Balt. Hydrol. Konf. Lübeck*, Aug. 1938. Berlin.
- NEUMANN, G. (1940). Die ozeanogr. Verhältnisse an der Meeresoberfläche im Golfstromsektor nördlich und nordwestlich der Azoren. Aus den wiss. Ergbn. der intern. Golfstromunternehmung 1938. *Ann. Hydr. Mar. Met. Beiheft.*
- NEUMANN, G. (1943). Über den Aufbau und die Frage der Tiefenzirkulation des Schwarzen Meeres. *Ann. Hydr. Mar. Met.* pp. 1, 164.
- NEUMANN, G. (1942). Die absolute Topographie des phys. Meeresniveaus des Schwarzen Meeres. *Ann. Hydr. Mar. Met.* p. 265.
- NEUMANN, G. (1944). Das Schwarze Meer. *Z. Ges. Erdkunde.* Berlin.
- NIKITIN, W. N. (1927). L'Océanographie de la Mer Noire d'après les explorations hydrogr. russes. *Ann. Geogr.* no. 203. Paris.
- NOMITSU, T. and OKAMOTO, M. (1927). The causes of the annual variation of the mean sea-level along Japan's Coast. *Mem. Coll. Sci. Kyoto, Imp. Univ.* 10, no. 3. Kyoto.
- NUSSER, F. (1952). Das Vorkommen von Meereis um den antarktischen Kontinent zur Zeit des südlichen Hochsommers. Auf der Eisübersichtskarte no. 19. *Dtsch. Hydrogr. Inst.* Hamburg.
- PARR, A. E. (1935). Report on hydrogr. Observations in the Gulf of Mexico and adjacent straits. "Mabel Taylor"-Exp. 1932. *Bull. Bingham Oceanogr. Coll.* 5, New Haven.

- PARR, A. E. (1937, 1938). A contribution to the hydrography of the Carribean and Cayman seas. *Bull. Bingham Oceanogr. Coll.* 4, 1937; and 5, 4, 1938. New Haven.
- PARR, A. E. (1938) Isopicnic analysis of current flow by means of identifying properties *J. Mar. Res.* 1, no. 4.
- PARR, A. E. (1938a). Further observations on the hydrography of the eastern Carribean and adjacent Atlantic water. *Bull. Bingham Oceanogr. Coll.* 6.
- PENCK, A. (1933). Eustatische Bewegungen des Meeresspiegels während der Eiszeit. *Geogr. Z.*, Heft. 6.
- PENCK, A. (1934). Theorie der Bewegung der Strandlinie. *S.B. preuss. Akad. Wiss.* 19. Berlin.
- PERNTER, J. M. (1901). Über die Polarstation des Lichtes in trüben Medien und des Himmelslichtes mit Rücksicht auf die Erklärung der blauen Farbe des Himmels. *Denkschr. Wiener Akad. Wiss.* 73. Wien (Jubelband d. Zentralanstalt f. Met. in Wien.)
- PETTERSSON, H. (1936). Das Licht im Meer. *Bioklim. Beiblätter Met. Z.* 3, p. 1.
- PETTERSSON, H. (1937). Das Verhältnis Thorium zu Uran in den Gesteinen und im Meer. *Anz. Akad. Wiss. Wien*, p. 127. Wien.
- PETTERSSON, H. (1938). Die radioaktiven Elemente im Meer. *Rapp. Cons. Explor. Mer.* 57. Copenhagen.
- PETTERSSON, H. (1946). Oceanographic work in the Mediterranean. *Geogr. J.* 1907. p. 163.
- PETTERSSON, O. (1878). *Ofersigt af Kgl. Vet. Akad. Förh.* 1878, no. 2, Stockholm.
- PETTERSSON, O. (1883). On the properties of water and ice. "*Vega*" *Exp. Vetenskap. Jakttagelser* 2, 301. Stockholm.
- PETTERSSON, O. (1896). Über die Beziehungen zwischen hydrogr. u. meteor. Phänomenen. *Met. Z.* p. 285.
- PETTERSSON, O. (1904). On the influence of ice-melting up oceanic circulation. *Geogr. J.* 24, 285.
- PETTERSSON, O. and H. (1929). Methods for determination of the density and salinity of sea water. *Svensk. Hydr.-Biol. Komm. Skrift.*, N.S., *Hydrografi*, no. 3, p. 1.
- POLLAK, M. J. (1954). Static stability parameters in oceanography. *J. Mar. Res.* 13, 101-12.
- POOLE, H. H. and ATKINS, W. R. G. (1926). On the penetration of light in to seawater. *J. Mar. Biol. Ass. U.K.* 14.
- POOLE, H. H. and ATKINS, W. R. G. (1929). Photo-electric measurements of submarine illumination throughout the year. *J. Mar. Biol. Ass. U.K.* 16, 297.
- PRANDTL, L. (1926). Über ausgebildete Turbulenz. *Verh. Int. Kongr. Tech. Mechanik. Zürich* (Sept.).
- PRATJE, O. (1952). Die Erfahrungen bei der Gewinnung von rezenten, marinen Sedimenten in den letzten 25 Jahren. *Mitt Geogr. Ges. Hamburg* 50, 118-97.
- DE QUERVAIN, A. and MERCANTON, P. L. (1925). Rés. scient. del' Exp. suisse an Greenland 1912-13. *Medd. om Grönland* 51. Copenhagen.
- RAKESTRAW, N. W. and EMMEL, V. M. (1937). The determination of dissolved nitrogen in water. *Ind. Engng Chem. (Anal. ed.)* 9, 344.
- RAKESTRAW, N. W. and EMMEL, V. M. (1938). Solubility of nitrogen and argon in seawater. *J. Phys. Chem.* 42, 1211.
- RAMATHAN, K. R. (1923). On the colour of the sea. *Phil. Mag.* 46, 1923.
- RAMSAY, W. (1930). Changes of sea-level resulting from the increase and decrease of glaciations. *Fennia* 52, no. 5.
- RANKAMA, K. and SAHAMA, T. G. *Geochemistry*. University Chicago Press, Chicago 37, Illinois.
- RAVENSTEIN, P. R. (1886). *Proc. Roy. Soc.* 21.
- RAYLEIGH, LORD (1916). Convection currents in a horizontal layer of fluid when the higher temperature is on the under side. *Phil. Mag.* 32, 529.
- REICHEL, E. (1949). Zum Dampfgehalt- und Wasserkreislauf der Atmosphäre. *Meteor. Rundsch.* 2, 206.
- REICHEL, E. (1952). Der Stand des Verdunstungsproblems. *Ber. dtsh. Wetterdienst, Bad Kissingen* 35, 155.
- REVELLE, R. and MAXWELL, A. E. (1952). Heat flow through the floor of the eastern North Pacific Ocean. *Nature, Lond.* 70.
- RIEL VAN, P. M. (1932). Einige ozeanogr. Beobachtungen im Roten Meer, Golf von Aden und Indischen Ozean. *Ann. Hydr. Mar. Met.* p. 401.
- RIEL VAN, P. M. (1934). The Bottom Configuration in Relation to the Flow of the Bottom Water. "*Snellius*" *Exp. in the Eastern Part of the Netherlands East Indies* 1929-1930. Vol. 2, *Oceanogr. Res.* pt. 2, chap. 2. Utrecht.
- RIEMANN-WEBER (1901). Die partiellen Differentialgleichungen der math. Physik. 4. Aufl., Braunschweig, p. 91.
- RIIS CARSTENSEN, E. (1929). Nogle bemaerkninger vedrørende "Godthaab"-Exp. 1928. *Geogr. Tidsskr.* 32. Copenhagen.

- RIIS CARSTENSEN, E. (1936). The hydrographical work and material of "Godthaab" Exp. 1928. *Medd. om Grönland* 78, no. 3. Copenhagen.
- RINGER, W. E. (1906). Über die Veränderungen in der Zusammensetzung des Meerwassersalzes beim Ausfrüeren. *Verh. uit het Rjiks inst. voor het Onderzoek der Zee, den Helder* 1906.
- ROSSBY, C. G. (1936). Dynamics of steady ocean currents in the light of experimental fluid mechanics. *Pap. Phys. Oceanogr. Met.* 5, no. 1. p. 43.
- ROYEN, N. (1922). *Istryck vid temperatur högnigar Hyllningsskrift tillägnad Vilh. Hansen.*
- RUDEN, P. (1933). Turbulente Ausbreitungsvorgänge im Freistrah. *Naturwissenschaften* 21. Berlin.
- RUPPIN, E. (1906). Umkippthermometer als Tiefenmesser. *Wiss. Meeresuntersuchungen, Kiel*, N.F. 9, no. 5, s. 182.
- RUPPIN, E. (1912). Die hydrographischen und chemischen Methoden. *Wiss. Meeresuntersuchungen, Kiel*, N.F. 14, no. 2.
- SAUBERER, F. and RUTTNER, F. (1941). Die Strahlungsverhältnisse der Binnengewässer. *Probl. kosmischen Phys.* 21, Leipzig.
- SCHMIDT, W. (1908). Asorption der Sonnenstrahlung im Wasser. *S.B. Akad. Wiss. Wien.* 117.
- SCHMIDT, W. (1908). Über die Reflexion der Sonnenstrahlung an Wasserflächen. *S.B. Akad. Wiss. Wien.* 62.
- SCHMIDT, W. (1915). Strahlung und Verdunstung an freien Wasserflächen; ein Beitrag zum Wärmehaushalt des Weltmeeres und zum Wasserhaushalt der Erde. *Ann. Hydr. Mar. Met.* Bd. 43, p. 111.
- SCHMIDT, W. (1916). Das Ausstrahlungs- und Reflexionsvermögen des Wassers. *Met. Z.* pp. 111, 257.
- SCHMIDT, W. (1917). Der Massenaustausch bei ungeordneten Strömungen in freier Luft und seine Folgen. *S.B. Akad. Wiss. Wien. (Math.-Naturw. Kl.)* 126.
- SCHMIDT, W. (1917a). Die Wirkungen der ungeordneten Bewegungen im Wasser der Meere und Seen. *Ann. Hydr. Mar. Met.* p. 367.
- SCHMIDT, W. (1925). Der Massenaustausch in freier Luft und verwandte Erscheinungen. *Probl. Kosm. Phys.* 7. Hamburg.
- SCHOKALSKI, J. M. (1924). Océanographie de la Mer Noire. *Int. Géogr. Varsovie. Scient. Publ.* Leningrad.
- SCHOTT, G. (1904). Die grosse Eistrift bei der Neufundlandbank und die Wärmeverhältnisse des Meerwassers im Jahre 1903. *Ann. Hydr. Mar. Met.* p. 277.
- SCHOTT, G. (1914). Adiabatische Temperaturänderungen in grossen Meerestiefen. *Ann. Hydr. Mar. Met.* p. 321.
- SCHOTT, G. (1928). Die Verteilung des Salzgehaltes im Oberflächenwasser der Ozeane. *Ann. Hydr. Mar. Met.* p. 145.
- SCHOTT, G. (1928). Die Wasserbewegungen im Gebiete der Gibraltarstrasse. *J. Cons.* 3, no. 2. Copenhagen.
- SCHOTT, G. (1929). Über die Wasserbewegungen im Bab el Mandeb. *Ann. Hydr. Mar. Met.* p. 10.
- SCHOTT, G. (1934). Die Verteilung des Salzgehaltes im Oberflächenwasser der Ozeane. *J. Johnstone Mem.* p. 235. Liverpool.
- SCHOTT, G. (1935). *Geographie des Indischen und Stillen Ozean.* Hamburg.
- SCHOTT, G. (1942). *Geographie des Atlantischen Ozeans.* 3. Aufl. Hamburg.
- SCHUBERT, v. O. (1931). Zur Frage der Stabilität in grossen Meerestiefen bei Temperaturumkehr. *Gerl. Beitr. Geophys.* 31.
- SCHUBERT, v. O. (1935). Die Stabilitätsverhältnisse im Atlantischen Ozean "Meteor" *Wcrk* 6, no. 2. Berlin.
- SCHULZ, B. (1911). Strom und Temperatur des nördlichen Stillen Ozeans nördl. 40° N. *Ann. Hydr. Mar. Met.* pp. 177, 242.
- SCHULZ, B. (1917). Die Beurteilung des vertikalen Gleichgewichtes im Meer. *Ann. Hydr. Mar. Met.* p. 93.
- SCHULZ, B. (1921). Methoden und Ergebnisse der Untersuchungen des Kohlensäuregehaltes im Meerwasser. *Ann. Hydr. Mar. Met.* p. 273.
- SCHULZ, B. (1923). Hydrogr. Untersuchungen bes. über den Durchlüftungszustand in der Ostsee im Jahre 1922. *Arch. dtsch. Seewarte* 41. Hamburg.
- SCHULZ, B. (1924). Die Durchlüftung der Nord- und Ostsee. *Naturwissenschaften* 12.
- SCHULZ, B. and WULF, A. (1929). Hydrographie und Oberflächenplankton des westlichen Barentsmeeres im Sommer 1927. *Ber. dtsch. Komm. Meeresforsch.* N.F. 4, no. 5. Berlin.
- SCHUMACHER, A. (1922). Graphische Ermittlung von σ_t aus t (°C.) und $S(\text{‰})$. *Ann. Hydr. Mar. Met.* p. 305.
- SCHUMACHER, A. (1923). Neue Hilfstafeln für die Umkippthermometer nach Richter und Beiträge zur thermometrischen Tiefenmessung. *Ann. Hydr. Mar. Met.* p. 273.

- SCHUMACHER, A. (1933). Eine neue Berichtigungsformel für des Tiefsee-Umkipptthermometer. *Ann. Hydr. Mar. Met.* p. 74.
- SCHUMACHER, A. (1937). Der Oberflächenschöpfer von O. Sund in weiterentwickelter Form. *Ann. Hydr. Mar. Met.* p. 351.
- SCHUMACHER, A. (1938). Der Oberflächenschöpfer von O. Sund. *Ann. Hydr. Mar. Met.* p. 590.
- SEIWELL, H. R. (1937). Consumption of oxygen in seawater under controlled laboratory conditions. *Nature, Lond.* **140**, 506.
- SEIWELL, H. R. (1938). Application of the distribution of oxygen to the phys. oceanogr. of the Caribbean region. *Pap. Phys. Oceanogr. Met.* **6**, 60.
- SEIWELL, H. H. and SEIWELL, G. E. (1938). The sinking of decomposing plankton in seawater and its relationship to oxygen consumption and phosphorus liberation. *Proc. Amer. Phil. Soc.* **78**.
- SHEPARD, F. P. (1933). Submarine valleys. *Geogr. Rev.* p. 77.
- SHEPARD, F. P. (1948). Evidence of world-wide submergence. *J. Mar. Res.* **7**, 3, 1948; or *Contr. Scripps Inst. Oceanogr.*, N.S. no. 387. La Jolla.
- SHEPARD, F. P. and BEARD, CH. N. (1938). Submarine canyons: distribution and longitudinal profiles. *Geogr. Rev.* p. 439.
- SHOULEJKIN, W. (1928). The evaporation of seawater u.s.w. *Gerl. Beitr. Geophys.* Bd. 20.
- SIGEMATU, R. (1933). A brief note on the depths of the sea in the vicinity of the Mariana Islands. *Rec. of ocean. Works in Japan* **5**, no. 2, p. 100.
- SKOGSBERG, TAGE (1936). Hydrography of Monterey Bay, California. Thermal conditions 1929-33. *Amer. Phil. Soc. Trans.* N.S. **29**, 1-152.
- SMED, J. (1943). Annual and seasonal variations in the salinity of the North Atlantic surface water. *Rapp. Cons. Explor. Mer.* **112**.
- SMITH, E. H. (1927-6). Internal ice observations and ice patrol service in the North Atlantic Ocean. Season 1926. *U.S. Coast Grad. Bulletin* no. 15. Washington.
- SMITH, E. H. (1931). Arctic ice with especial reference to its distribution to the North Atlantic Ocean. The "Marion" Exp. 1928. *Sci. Res. Pt. 3*. Washington.
- SMITH, P. A. (1937). The submarine topography of Bogoslof. *Geogr. Rev.* **27**.
- SMITH, P. A. (1939). Atlantic submarine valley of the United States. With a chart: North-eastern U.S. showing relation of land and submarine topography. 1:1 Mill. *Geogr. Rev.* p. 648.
- SORET, J. and SARASIN, E. (1889). *C.R. Acad. Sci., Paris* **108**, 1248. Paris.
- SPEERSCHNEIDER, C. J. H. (1931). The state of ice in Davis-Strait. *Publ. fradet Danske Met. Inst. Medd.* no. 8. Copenhagen.
- SPILHAUS, A. F. (1938). A bathythermograph. *J. Mar. Res.* **1**, p. 95.
- SPILHAUS, A. F. (1940). A detailed study of the surface of the ocean in the neighborhood of the Gulf Stream with the aid of rapid measuring hydrog. instruments. *J. Mar. Res.* **3**, 51.
- SPRING, W. (1883, 1886, 1896). *Bull. Acad. Belg.* **5**, **12**, **13**.
- SPRING, W. (1898). *Arch. Soc. Phys.* **5**.
- STAHLBERG, W. (1920). Die Ermittlung der Meerestiefe. *Samml. "Meereskunde". Inst. Meereskunde, Berl.*, 13. Jahrgang, Heft. 10/11.
- STEFAN, J. (1890). *S.B. Akad. Wiss. Wien. Wien* **98**, no. 695. Wien.
- STENIUS, S. (1904). *Ofversigt Fin. Vet. Soc. Förh.* **46**, 6. Helsingfors.
- STETSON, H. C. (1937). Currents-measurements in the Georges Bank Canyons. *Trans. Amer. Geophys. Un.*, p. 216.
- STOCKMAN, W. (1936). The exchange of turbulency in the region of Agrachansky island in the Caspian sea. *J. Geophys.* **6**, Moscow.
- STOCKS, TH. (1935). Erkundung über Art und Schichtung des Meeresbodens mit Hilfe von Hochfrequenz-Echoloten. *Naturwissenschaften* p. 383.
- STOCKS, TH. (1936). Die Fortschritte der Erforschung des Atlantischen Ozeans 1854-1934. *Geogr. Z.*, p. 161.
- STOCKS, TH. (1937). Grundkarte der ozeanischen Lotungen. "Meteor" *Werk* **3**, no. 1, 4. Lfg. Berlin.
- STOCKS, TH. (1938). Morphologie des Atlantischen Ozeans. "Meteor" *Werk* **3**, no. 1. Berlin.
- STOCKS, TH. (1944). Zur Bodengestaltung des nordwestlichen Indischen Ozeans. *Z. Ges. Erdkunde, Berl.* p. 115.
- STOCKS, TH. and WÜST, G. (1935). Die Tiefenverhältnisse des offenen Atlantischen Ozeans. "Meteo" *Werk*, **3**, no. 1. p. 16 ff. Berlin.
- STOMMEL, H. (1947). A summary of the theory of convection cells. *Ann. N.Y. Acad. Sci.*, pp. 715-26, also in *Woods Hole Ocean. Inst. Coll. Repr.* no. 371.
- STOMMEL, H. (1950). Determination of the lateral diffusivity in the climatological mean Gulf Stream. *Contr. Woods Hole Oceanogr. Inst.* no. 552.

- SUDA, K. (1936). On the dissipation of energy in the density current (2. paper). *Geophys. Mag.* **10**, 131. Tokyo.
- Suess, E. (1888). *Das Antlitz der Erde*. **2**, 680. Berlin.
- SUND, O. (1929). An oceanographic sliderule. *J. Cons.* **4**, no. 1. Copenhagen.
- SUND, O. (1931). A new speed surface sampler. *J. Cons.* **6**.
- SVERDRUP, H. U. (1925). The north polar cover of cold air. *Monthly Weather Rev.* p. 53. Washington 1926.
- SVERDRUP, H. U. (1926). Dynamic of tides on the North Siberian Shelf. Res. from the "Maud" Exp. 1918-25. *Geofys. Publ.* **4**, 75, Oslo.
- SVERDRUP, H. U. (1929). The waters on the north-siberian shelf. North Pol. Exp. "Maud" 1918-25. *Sci. Res.* **4**, no. 2, Bergen.
- SVERDRUP, H. U. (1931). Origin of deep water of Pacific ocean. *Gerl. Beitr. Geophys.* **29**. Leipzig.
- SVERDRUP, H. U. (1933). Vereinfachtes Verfahren zur Berechnung der Druck-und Massenverteilung im Meer. *Geofys. Publ.* **10**, no. 1. Oslo.
- SVERDRUP, H. U. (1933). Narrative and oceanography of the "Nautilus" Exp. 1931. *Pap. Phys. Oceanogr. Met.* **2**, 63.
- SVERDRUP, H. U. (1936). Das maritime Verdunstungsproblem. *Ann. Hydr. Mar. Met.* Bd. 64.
- SVERDRUP, H. U. (1937-38). On the evaporation from the oceans. *J. Mar. Res.* **1**, no. 1. New Haven, Conn.
- SVERDRUP, H. U. (1938). Oceanic circulation. *Proc. 5. Int. Congr. Appl. Mechanic, Washington*.
- SVERDRUP, H. U. (1939). On the explanation of the oxygen minima and maxima in the oceans. *J. Con.* **13**, no. 2. Copenhagen 1938.
- SVERDRUP, H. U. (1940). Lateral mixing in the deep water of the South Atlantic Ocean. *J. Mar. Res.* **2**, no. 3.
- SVERDRUP, H. U. (1940). On the annual and diurnal variation of the evaporation from the oceans. *J. Mar. Res.* **3**, 93-104.
- SVERDRUP, H. U. and FLEMING, R. N. (1941). The waters of the coast of southern California (March to July 1937). *Bull. Scripps Inst. Oceanogr. Univ. Calif.* **4**, no. 10, 261.
- SVERDRUP, H. U. and Staff (1942). Oceanographic observations on the E.W. Scripps cruises of 1938. *Scripps Inst. Oceanogr. Rec. of Obs.* **1**, 63.
- SVERDRUP, H. U. and Colleagues (1942). *The Oceans, their Physics, Chemistry and General Biology*. New York; Prentice-Hall Inc.
- SVERDRUP, H. U. (1945). *Oceanography for Meteorologists*. London, 1945 resp. 1952.
- SVERDRUP, H. U. (1951). Evaporation from the oceans. *Comp. Meteor. Amer. Meteor. Soc.* pp. 1071-81. Boston, Mass.
- TAYLOR, G. J. (1915). Eddy motion in the atmosphere. *Phil. Trans. A*, **215**.
- TAYLOR, G. J. (1918). Phenomena connected with turbulence in the lower atmosphere. *Proc. Roy. Soc. A*, **94**.
- TAYLOR, G. J. (1922). Diffusion by continuous movements. *Proc. Math. Soc. Lond.*, Ser. **2**, **20**.
- THOMPSON, T. G. (1932). The physical properties of sea water. *Physics of the Earth*. Vol. 5, *Oceanography* pp. 63-4. Nar. Res. Coun. Bull. no. 85.
- THORADE, H. (1913-14). Die Geschwindigkeit der Triftströmungen. *Wiss. Beilage, Realschule zu Eilbeck*.
- THORADE, H. (1914). Die Geschwindigkeit von Triftströmungen und die Ekman'sche Theorie. *Ann. Hydr. Mar. Met.* p. 379.
- THORADE, H. (1931). Strömung und zungenförmige Ausbreitung des Wassers. *Gerl. Beitr. Geophys.* **34**.
- THORADE, H. and KALLE, K. (1940). Tabellen für die Dichte des Meerwassers. *Archiv. dtsh. Seewarte* **60**, no. 2. Hamburg.
- THOULET, M. J. and CHEVALLIER (1889) *C.R. Acad. Sci., Paris*. **108**, 794. 1889.
- THURAS, A. L. (1918). *J. Acad. Wash.* 1918, **8** and 1921, **11**.
- TOLLMEIN, W. (1926). Berechnung turbulenter Ausbreitungsvorgänge. *Z. ang. Math. Mech.* **6**.
- TRANSCHÉ, N. A. (1928). The ice cover of the arctic sea, with a genetic classification of the sea ice. Problems of polar research. *Spec. Publ. Amer. Geogr. Soc.* **7**. New York.
- UTTERBACK, C. L. (1936). Spectral bands of submarine solar radiation in the North Pacific and adjacent inshore waters. *Rapp. Cons. Explor. Mer.* **101/2**, no. 4. Copenhagen.
- VEATCH, A. C. and SMITH, P. A. (1939). Atlantic submarine valleys of the United States and the Congo submarine valley. *Spec. Pap. Geol. Soc. Amer.* no. **7**, 101 pp.
- VENING-MEINESZ, F. A. (1932). Gravity expeditions at sea 1923-30. 1. The Expeditions, the computations and the results. *Publ. Netherl. geod. Com.* Delft 1932.

- VENING-MEINESZ, F. A. (1934). Ergebnisse der Schwerekräftbeobachtungen auf dem Meere in den Jahren 1923–1932. *Erg. Kosm. Phys.* 2, Leipzig.
- VENING-MEINESZ, F. A. (1940). The earth crust deformation in the East Indies. *Proc. Kgl. Akad. wet. Amst.* 43, no. 3.
- VISSER, S. W. (1928). Surface observations (temp., sal., dens.). *The "Snellius" Exp.* 2, *Oceanogr. Res.* Pt. 4, Leiden.
- WATTENBERG, H. (1930). Über die Bestimmung der Alkalinität des Meerwassers. *Ann. Hydr. Mar. Met.* p. 277.
- WATTENBERG, H. (1931). Über den Kalgehalt des Ozeanwassers. *Ann. Hydr. Mar. Met.* p. 273.
- WATTENBERG, H. (1933). "Meteor" *Werk* 8, Berlin.
- WATTENBERG, H. (1935). Kalkauflösung und Wasserbewegung am Meeresboden. *Ann. Hydr. Mar. Met.* p. 387.
- WATTENBERG, H. (1936). Kohlensäure und Kalziumkarbonate im Meer. *Fortsch. Min., Krist. Petrogr.* 20, Berlin.
- WATTENBERG, H. (1939). Zur Chemie des Meerwassers. Über die in Spuren vorkommenden Elemente. *Z. anorg. Chem.*, 23.
- WATTENBERG, H. (1938). Die Verteilung des Sauerstoffs im Atlantischen Ozean. "Meteor" *Werk* 9, Berlin.
- WATTENBERG, H. (1941). Über die Grenzen zwischen Nord- und Ostseewasser. *Ann. Hydr. Mar. Met.* p. 265.
- WEGEMANN, G. (1920). Der tägliche Gang der Temperatur auf dem Meere u.s.w. *Wiss. Meeresuntersuchungen*, N.F. 19, Kiel.
- WEGENER, A. (1912). *Medd. om Grönland* 46, no. 1, p. 7, Copenhagen.
- WEGENER, A. (1924). Luftdruck und Mittelwasser am Danmark-Havn. *Ann. Hydr. Mar. Met.* p. 22.
- WEIBULL, W. (1947). The thickness of ocean sediments measured by a reflexion method. With a foreword by H. Pettersson. *Medd. Oceanogr. Inst.* no. 12, Göteborg.
- WEICKMANN, L. (1942). Die Erwärmung der Arktis. *Veröff. dtsch. Wiss. Inst. Kopenhagen*, Reihe Arktis, no. 1, Copenhagen.
- WEINBERG, B. (1907). *Ann. Phys.*
- WENNER, F. (1930). *J. Res. Bur. Stand., Wash.* 5, 720.
- WESTPHAL, A. (1900). Das Mittelwasser der Ostsee u.s.w. *Veröff. preuss. Geod. Inst.*, N.F., no. 2, Berlin.
- WEYPRECHT, K. (1879). *Osterreichisch-Ungarische Arktische Expedition 1872–1874*, Wien.
- WHEELER, A. S. (1910). *J. Amer. Chem. Soc.* 32, 646.
- WHITNEY, L. V. (1938). Cont. solar radiation measured in Wisconsin Lakes. *Trans. Wisc. Acad.* 31, 175.
- WIESE, W. (1922). Die Einwirkungen des Polareises im Grönländischen Meere auf die nordatl. zyklonale Tätigkeit. *Ann. Hydr. Mar. Met.* p. 271.
- WIESE, W. (1924). Polareis und atmosphärische Schwankungen. *Geogr. Ann.* 6, Stockholm.
- WIESE, W. (1930). Zur Kenntnis der Salze des Meereises. *Ann. Hydr. Mar. Met.* p. 282.
- WITTING, R. (1908). *Untersuchungen zur Kenntnis der Wasserumsetzungen in den Finnland umgebenden Meeren*, 1. *Fiml. hydr. biol. Unters.* no. 2, Helsingfors.
- WITTING, R. (1933). Zur Bestimmung der Mischung im Meer. *Soc. Sci. Fenn. Comm. phys.-math.* 7, no. 2, Helsinki.
- WÜST, G. (1921). Die Verdunstung auf dem Meere. *Veröff. Inst. Meereskunde, Berl.*, N.F. Reihe A, Heft 6, 1920. See also Schmidt's Referat darüber. *Ann. Hydr. Mar. Met.* Bd. 49, 1921, p. 190.
- WÜST, G. (1922). Verdunstung und Niederschlag auf der Erde. *Z. ges. Erdkunde*, p. 35, Berlin.
- WÜST, G. (1928). Der Ursprung der Atl. Tiefenwässer. *Z. Ges. Erdkunde*, May, 1928, Sonderband.
- WÜST, G. (1929). Schichtung und Tiefenzirkulation des Pazifischen Ozeans auf Grund zweier Längsschnitte. *Veröff. Inst. Meereskunde, Berl.* N.F., Reihe A, Heft. 20, Berlin.
- WÜST, G. (1932). "Meteor" *Werk* 4, no. 1, Berlin. (Ozeanographische Instrumente und Methoden. Absch. A: Methoden der Serienmessungen, Thermometrische Tiefenstimmung.)
- WÜST, G. (1934). Anzeichen von Beziehungen zwischen Bodenstrom und Relief in der Tiefsee des Indischen Ozeans. *Naturwissenschaften* 22.
- WÜST, G. (1934). Salzgehalt und Wasserbewegung im Suezkanal. *Naturwissenschaften* 22.
- WÜST, G. (1935). Fortschreitende Salzgehaltsabnahme im Suez-Kanal. *Ann. Hydr. Mar. Met.* 63.
- WÜST, G. (1936). Oberflächensalzgehalt, Verdunstung und Niederschlag auf dem Weltmeer. *Länderkundl. Forschung, Festschrift N. Krebs*. Stuttgart.
- WÜST, G. (1936). Das Bodenwasser und die Gliederung der Atl. Tiefsee. "Meteor" *Werk* 6, no. 1, Berlin.

- WÜST, G. (1936). Schwankungen der ozeanogr. Faktoren in der Stratosphäre. "Meteor" *Werk* 6, no. 1, 194. Berlin.
- WÜST, G. (1937). Bodentemperaturen und Bodenstrom in der Pazifischen Tiefsee. *Veröff. Inst. Meereskunde, Berl.*, N.F., Reihe A, Heft. 35, 1937.
- WÜST, G. (1938). Bodentemperatur und Bodenstrom in der Atl., Ind. u. Paz. Tiefsee. *Gerl. Beitr. Geophys.* 54.
- WÜST, G. (1939). Die Grenzen der Ozeane und ihrer Nebenmeere. *Ann. Hydr. Mar. Met. Beih.* 1939. Hamburg.
- WÜST, G. (1941). Relief und Bodenwasser im Nordpolarbecken. *Z. Ges. Erkunde.* p. 163 Berlin.
- WÜST, G. (1942). Die morpholog. und ozean. Verhältnisse der Nordpolarbeckens. *Veröff. dtsh. Wiss. Inst. Kopenhagen*, Reihe I, no. 6.
- WÜST, G. (1943). Der subarktische Bodenstrom in der westlichen Mulde *Ann. Hydr. Mar. Met.* 71, 249. (Conradheft).
- WÜST, G. (1948). Die Temperaturinversion im Tiefenwasser des Südatl. Ozeans. *Dtsch. Hydrogr. Z.*, p. 109.
- WÜST, G. (1954). Gesetzmässige Wechselbeziehungen zwischen Ozean und Atmosphäre, in der zonalen Verteilung von Oberflächensalzgehalt, Verdunstung und Niederschlag. *Arch. Meteor. Geophys. Bioklim. A*, 7, 305-28. Wien. (Defant Festschrift.)
- WÜST, G., BROGMUS, W. and NOODT, E. (1954). Die zonale Verteilung von Salzgehalt, Niederschlag, Verdunstung, Temperatur und Dichte an der Oberfläche der Ozeane. *Kieler Meeresforsch* 10.
- WYRTKI, K. (1950). Über die Beziehungen zwischen Trübung und ozeanographischem Aufbau. *Kieler Meeresforsch.* 7, no. 2, Kiel.
- ZUBOV, N. N. (1938). Morskic vody i l'dy (Marine water and ice). *Moskava: Gidrometeorologicheskoe Izdatel' stvo*, 451 p.
- ZUKRIEGEL, J. (1935). Cryologia maris. *Trav. geogr. Tcheques*, no. 15, Praha.

PART 2

DYNAMICAL OCEANOGRAPHY

Introduction

DYNAMICAL oceanography is concerned with the movements of the water masses of the oceans. In addition to the framework of the vertical and horizontal structure, in the sea, of the oceanographic factors such as temperature, salinity and density dealt with in detail in Vol. I, Pt. I, we have now to consider the forces present that cause displacements of the water masses. These displacements are termed *ocean currents*; they are phenomena that an observer will be directly aware of only occasionally, near land or in narrow straits. In the open sea they are shown only by calculations carried out for quite different purposes and only give a clear picture of the movement of the water masses when taken together over a larger area of the sea. The system of currents in the ocean, like that in the atmosphere around the Earth, is among the most striking phenomena in geophysics. The oceanic circulation involves the whole ocean and the conditions are aptly described by Heraclitus' expression $\pi\acute{\alpha}\nu\tau\alpha \rho\acute{\epsilon}\tilde{\iota}$ (it all moves).

In principle, dynamical oceanography can be subdivided into two main parts. One concerns *ocean currents* in the more restricted sense of the word as applied to the steady continuous transport of water in definite direction. In these currents movements in a horizontal plane predominate overwhelmingly, but there are also phenomena where a vertical component becomes important. The second part of dynamical oceanography concerns the phenomena associated with periodic water movements in which the whole process is repeated after a certain time. These are the *waves and tides*. Separate treatment of ocean currents (in the more restricted sense) on the one hand and of the waves and tides on the other considerably simplifies their presentation, although these phenomena are not separated in nature to the extent that might superficially be easily assumed.

Part II of this volume is therefore devoted mainly to ocean currents (in the narrower sense) while Volume II deals with the dynamics of the periodic phenomena (Waves and Tides).

An explanation of the movements of water masses in the ocean requires in the first place a study of the interplay between the oceanographic factors and of the effect of external forces on the water masses. It is self evident that *hydrodynamics* must play a major role in dealing with these questions, especially if the problems arising are treated more from a geophysical standpoint. Thus, in addition to a more statistical-geographical description of observed oceanic phenomena, hydrodynamic considerations have to be used and finally one attempts to explain them on a physical-mathematical basis.

Ordinary *classical* hydrodynamics develops the theory of movement in a liquid on the assumption that it is homogeneous and incompressible. As a first approximation the results of pure hydrodynamics are applicable within wide limits to the water

movements in the sea and allow a deeper insight into the basic causes of the phenomena observed. This is not entirely sufficient, however, because water masses of the ocean show quite large deviations from ideal homogeneity and their density depends strongly on the temperature and salinity. It is therefore necessary to take into account the stratification and compressibility of the water masses. Classical hydrodynamics is thus replaced by *physical hydrodynamics*, for which at the present time only for some of the more important parts a precise theoretical basis has been developed. (BJERKNES and co-workers, 1932 or GODSKE, BERGERON, BJERKNES and BUNDGAARD, 1957).

Chapter IX

The Geophysical Structure of the Sea

1. Introduction

SINCE the ocean currents are displacements of water masses the distribution of mass in the sea becomes of particular importance in all hydrodynamic investigations. It is specified by the distribution of the density or of the specific volume, which are both determined by the thermo-haline structure of the ocean. In addition to the distribution of mass there is an internal field of force due to the distribution of pressure of the water masses in both vertical and horizontal direction. The atmospheric pressure which exerts a varying force on the surface of the sea must be also considered a source for disturbances. In addition to these forces the only external conservative force, the gravity, must also be taken into account, since it intervenes in an essential way in all phenomena involving the movement and equilibrium of the water masses of the oceans. Thus the *fields of gravity, of pressure and of mass* in the ocean play an important part in all hydrodynamic investigations. For a quantitative description of a phenomenon the magnitude of the units used is essential. At the present time the absolute units of the CGS system [cm, g, sec] are preferably used, but in many cases according to the magnitude of the numerical values there are practical advantages in the use of larger units, usually obtained by multiplication by a suitable power of 10. The metre (10^2 cm) is a suitable unit of length in dynamic oceanography, but the nautical mile, which is the length of an arc of one minute at the equator (1852 m), is also used. The metric ton, the mass of a cubic metre of water with a density of 1 (10^6 g) is frequently used as mass unit together with the second, the minute and the hour as units of time. The velocity may be defined in absolute units (cm sec^{-1}) but is also frequently given in nautical miles per hour (= 1 knot = 51.4 cm sec^{-1}) (MAURER, 1938).

2. The Distribution of Gravity and Gravity Potential

Gravity is the result of the force of attraction of earthly masses and of the centrifugal force of Earth rotation. Its distribution at the surface of the Earth can be found by pendulum measurements, for which it is sufficient to use its normal values. At the present time the most frequently used formula for a calculation of gravity is that of HEISKANEN and CASSINI; LAMBERT, 1931:

$$g_0 = 978.049 (1 + 0.0052884 \sin^2 \phi - 0.0000059 \sin^2 2\phi) [\text{cm sec}^{-2}]. \quad (\text{IX.1})$$

Calculations of the gravitational acceleration within the sea must take into account the density of the water mass and also the result of the potential theory that the outer shell of a sphere exerts no attraction on a point in the interior of the sphere. If κ is the gravitational constant, M the mass of the Earth and R the radius of the Earth

then, as a first approximation, the gravitational acceleration at sea-level is given by

$$g_0 = \kappa \frac{M}{R^2}$$

while at a certain depth h where m is the mass of the Earth shell ($R - h$) it reduces to

$$g = \kappa \frac{M - m}{(R - h)^2},$$

so that in a first approximation

$$g = g_0 + 2g_0 \frac{h}{R} \left[1 - \frac{m}{2M} \frac{R}{h} \right].$$

If the mean density of the Earth ρ_m is 5.5 and ρ is the density of the shell $\{M = 3(4\pi^2 R^3)\rho_m$ and $m = 4\pi R^2 h \rho\}$, then the expression in brackets becomes

$$\frac{3}{2} \frac{\rho}{\rho_m}, \quad \rho \sim 1.05 \quad \text{and} \quad \frac{2g_0}{R} = 3.086 \times 10^{-5}.$$

In that way one obtains for the change in gravity within the sea the relation

$$g = g_0 + 2.303 \times 10^{-6}z, \tag{IX.2}$$

where z is the depth of the point under consideration.

Equations IX. 1 and 2 give the intensity of gravity, and its direction is fixed by the direction of the plumb-line. A surface which is always at right angles to the direction of gravity is termed a *level surface* (Niveau-Fläche). Considering only the gravitational force, no work will be expended in the displacement of a body along such a surface. The most important gravitational level surface is the free surface of the sea, the *ideal sea-level* (see p. 6), which forms a part of the geoid. Every other level surface is uniquely fixed by the amount of work that must be expended in moving a particle from the ideal sea-level to any point on the surface under consideration. For a surface at a depth h this work measured along the plumb-line direction is given by the product gh . The level surfaces are thus also surfaces of *equal gravitational potential* with the ideal sea-level as principal potential surface with zero potential. In this way the entire oceanic space can be regarded as intersected by a finite number of equipotential surfaces each of which is separated from the next one by a unit potential layer. The thickness of this layer varies as g alters from point to point but the product gh must always remain constant. The level surfaces must carefully be distinguished from surfaces of equal depth below the sea surface. The two sets of surfaces will intersect, and where a surface of equal depth is not at right angles to the vertical there will be a gravitational component in the direction of this surface. If the two surfaces were solid and smooth, a ball on a level surface would remain at rest, but on a surface of equal depth it would begin to roll away from the equator towards the pole under the influence of the gravitational component directed towards the poles.

A point within the sea may be fixed by taking three co-ordinates, either (1) ϕ the geographical latitude, λ the geographical longitude of the projection of the point under consideration on the surface of the sea along the plumb-line and h , the geometric depth of the point itself or, (2) the co-ordinates ϕ and λ as in (1) and as third

co-ordinate the potential value gh at the point under consideration (as a positive quantity). In the first case, all points with the same third co-ordinate will lie on surfaces of equal geometric depth and in the second case the points of equal third co-ordinate gh will lie on a level surface. The second system of co-ordinates is much more suitable for problems of the statics and dynamics of the ocean, since at every point in such a co-ordinate system the total force of gravity acts in the third direction: there is no component of gravity acting along the other two. As g is approximately 10 m sec^{-2} the potential gh will change by one unit if the unit mass is lowered by about $1/10 \text{ m}$. that means when the depth is reduced about by $1/10 \text{ m}$. BJERKNES (1910, 1912) has denoted this unit potential the dynamic decimeter (1 dyn.dm). Multiples and fractions of it are the dynamical metre (1 dyn.m) or the dynamical centimetre (1 dyn. cm), respectively. By the introduction of this potential quantity as the third co-ordinate the level surfaces become *surfaces of equal dynamic depth*.

The dynamic depth has the dimensions $[\text{g cm}^2 \text{ sec}^{-2}]$. The most practical unit of the dynamic depth is the dynamic metre. If h is expressed in metres then the dynamic depth D in dynamic metres is

$$D = \frac{gh}{10}, \quad (\text{IX.3})$$

and at this point there is a geopotential

$$\Phi = -10D. \quad (\text{IX.4})$$

Since the gravitational acceleration g changes with depth according to (IX. 2) the difference between two dynamic depths in the ocean is given by the relation

$$D_2 - D_1 = \frac{1}{10} \int_{h_1}^{h_2} g \, dh. \quad (\text{IX.5})$$

As a first approximation (IX. 3) thus gives

$$D = 0.98h \quad \text{and} \quad h = 1.02D. \quad (\text{IX.6})$$

The numerical difference between a dynamic metre and a geometrical metre is thus about 2%. Tables for converting one unit into the other according to more accurate formulae have been given by BJERKNES and co-workers (1912, 1913).

3. The Field of Mass

The mass field is given by the distribution of the density ρ or its reciprocal, the specific volume α . In the sea it can be represented in a suitable way by surfaces of equal density (*isopycnic surfaces*) or by surfaces of equal specific volume (*isosteric surfaces*). The latter are used preferably in oceanography. The field of specific volume $\alpha_{s,t,p}$ can be regarded as made up of two separate fields. The first of these $\alpha_{35, 0, p}$ represents the mass field of a homogeneous sea at 0°C and 35‰ S (standard ocean); it is in this way completely defined and invariable. The second is the field of the specific volume anomaly δ and this set of surfaces of equal anomaly δ is quite sufficient for the characterization of the mass field in the total oceanic space.

In a vertical section of the mass distribution the isosteres and the isopycnals appear as curved or wave-form lines deviating only slightly from the horizontal. A large

exaggeration of the vertical scale is required to show the slope of the lines in a better way. The geometrical depth, the dynamic depth or the pressure can all be used as the vertical co-ordinate. Such graphic representations are termed dynamical vertical cross-sections, in short *dynamic sections*.

4. The Pressure Field and its Relationship to the Mass Field. Solenoids

The internal stress in a liquid such as the ocean is characterized by the *pressure* per unit area. In a liquid in equilibrium, due to the absence of any resistance to deformation, this pressure acts perpendicular to any arbitrarily oriented surface through the liquid and is equal for any point and in all directions. This state is denoted as *hydrostatic stress state*. The water masses in an ocean at rest is subject to the influence of gravity and the static pressure p at a depth h is defined as that force produced by the weight of a water column of unit cross-section extending from this depth to the surface of the sea. This does not take into account the atmospheric pressure at the surface of the water so that p is defined solely as the water pressure. Thus

$$p = \rho_m gh,$$

where ρ_m is the mean density of the water column h . The dimensions of p is $[g \text{ cm}^{-1} \text{ sec}^{-2}]$. According to (IX. 3) the dynamic depth D can be substituted in place of the geometric depth h so that

$$p = \rho_m D. \quad (\text{IX.7})$$

The pressure of a column of pure water ($\rho_m = 1$) of a height of 1 dyn. m is defined as 1 *decibar*. This is a tenth part of a bar which is defined as 10^6 dyn/cm^2 and is the pressure of a column of pure water of 10 dyn.m. The practical pressure unit "one atmosphere", is only about 1% greater than one bar. Fractions of the bar in addition to the decibar are the centibar and the millibar. The latter corresponds to a water pressure of one dynamical cm of pure water and is equivalent to a pressure of 0.75 mm of mercury.

For an ocean of pure incompressible water the following rule applies: The numerical value of "sea pressure" expressed in decibars is the same as that of the depth in dynamic metres at which this pressure is exerted. Since ρ_m in the sea is not very different from 1 this rule also applies in very close approximation for sea-water. From equation (IX. 7) is obtained

$$D = \alpha_m p, \quad (\text{IX.8})$$

where α_m is the mean specific volume of the water column. If ρ or α vary, equations (IX. 7 and 8) will be replaced by the integral forms

$$p = \int \rho dD \quad \text{and} \quad D = \int \alpha dp, \quad (\text{IX.9})$$

where the integrals must be extended over the whole water column h . For numerical calculations the integral is split up into sums for the thinnest possible layers with approximately constant density or specific volume (see later).

The relationships between pressure, geometrical and dynamic depth and the vertical distribution of specific volume and of density are shown in Table 110 for a homogeneous sea at 0°C and 35‰ salinity (standard ocean).

Table 110. Vertical stratification of a homogeneous ocean at 0°C and 35‰ salinity (standard ocean)

Pressure (dbar)	Geom. depth (m)	Dynamic depth (dyn.m)	Spec. volume (10 ⁵ α)	Density (σ _t)	Dynamic depth (dyn.m)	Pressure (dbar)
0	0	0	97264	28.23	0	0
100	99.24	97.242	97219	28.61	100	102.837
200	198.45	194.438	97174	29.12	200	205.724
300	297.60	291.590	97129	29.64	300	308.659
400	396.71	388.696	97084	30.03	400	411.643
500	495.78	485.758	97040	30.50	500	514.677
600	594.80	582.776	96995	31.02	600	617.758
700	693.77	679.749	96951	31.45	700	720.889
800	792.69	776.678	96901	31.92	800	824.068
900	890.57	873.564	96863	32.41	900	927.296
1000	984.41	970.404	96819	32.85	1000	1030.572
1500	1482.97	1453.955	96602	35.17	1500	1547.696
2000	1975.43	1936.429	96388	37.47	2000	2065.967
2500	2465.96	2417.836	96177	39.75	2500	2585.445
3000	2956.20	2898.204	95970	41.99	3000	3106.094
3500	3445.55	3377.544	95766	44.21	3500	3627.903
4000	3932.89	3855.873	95566	46.40	4000	4150.862
5000	4904.57	4809.556	95173	50.72	5000	5200.185
6000	5873.38	5759.368	94791	54.95	6000	6253.981
7000	6836.43	6705.421	94421	59.08	7000	7312.174
8000	7796.89	7647.817	94060	63.15	8000	8374.688

The difference between the numerical values of the pressure in decibars and the geometrical depth in metres is of the order of 1% and remains the same also for other thermo-haline vertical stratifications. It is thus permissible, as a first approximation, to ignore this difference: at a depth of n geometrical metres there will be a pressure of n decibars. On the other hand, the difference between dynamic and geometric depth in metres is about 2%, and between dynamic metres and the pressures in decibars is almost 3%. For hydrographic purposes these differences are too large to be ignored. For rough calculations it is perhaps permissible and practical to approximate the values of Table 110 by the following formulae:

$$10^5\alpha = 97264 - 0.44p,$$

$$10^5\rho = 102823 - 0.46p.$$

The values calculated from these are accurate to some units in the fifth decimal place.

The pressure field can be represented by surfaces of equal pressure (*isobaric surfaces*). If these are drawn for each decibar then the entire volume of the sea is divided into layers of 1 decibar pressure difference. The *pressure gradient* G at any point on an isobaric surface is given by the decrease in the pressure p along the normal n to this surface

$$G = -\frac{dp}{dn}. \quad (\text{IX.10})$$

In general, the isobaric surfaces and the surfaces of equal dynamic depth (level surfaces) intersect. These lines of intersection are termed *dynamic isobaths* and are usually plotted at 5 dyn.mm intervals. In this way the *topography of the pressure surface* is obtained. On the other hand, the lines of intersection of the pressure surfaces with a level surface are denoted as *isobars* or lines of equal pressure. These give a chart of the pressure distribution at a given level. In oceanography it is more customary to represent the pressure field by charts of the dynamic topography of especially selected isobaric surfaces.

It should be emphasized that for a representation of the pressure distribution in the ocean only the actual *water or sea pressure* is used without taking the air pressure into account. If the total pressure is required the sea-level pressure of the atmosphere which on a crude average is about 10 decibars must be added. Furthermore, it should also be remembered that dynamic topographies are referred to the *physical sea-level* from which the measurements are made and not to the ideal sea level (the geoid) which is defined as the surface of zero gravitational potential (dynamic depth zero). The topography of the physical sea-level is unknown, so that in practice these topographies are always represented only as *relative topographies*, i.e., relative to the unknown topography of the physical sea-level. Expressed in another way, they are dynamic topographies relative to a physical sea-level assumed as "plane" (plane in a geodetic sense). In order to obtain the *absolute dynamic topography*, the absolute dynamic topography of the physical sea-level would have to be known, and for this a determination of the dynamic depth of the pressure values would have to be carried out starting from the physical sea-level.

A convenient and practical representation of the mass distribution is obtained by use of dynamic sections—or to be more specific, vertical sections—of pressure surfaces and the isosteric surfaces. Both of these sets of surfaces vary only slightly from the horizontal, and the vertical scale must be considerably exaggerated in order to obtain visible gradients. Usually, however, the inclination of the isobaric curves as compared with that of the isosteric ones is so slight that horizontal lines in the coordinate system can be taken as isobars. The specific volume anomaly is usually used instead of the specific volume itself and the mass field is therefore represented by lines of equal anomaly.

The two sets of curves (the isobars and the isosteres) divide the vertical surface into a number of parallelograms formed by wavy lines; they are the cross-sections of tubes formed by the intersection of (invariably) two isobaric surfaces and two isosteric surfaces. These differently-shaped parallelepipeds were denoted isobaric-isosteric tubes by BJERKNES (1900); they are denoted as unit tubes or *solenoids* if areas of units in pressure and specific volume are drawn on vertical sections.

The terminology "solenoid" is also used when the sets of curves are drawn at intervals of several units. If the mass field is given by lines of equal anomaly δ at unit intervals of a (in the CGS system: 10^{-5}), and the pressure field by isobars at intervals of 1 db (in the CGS system: 10^5 dyn. cm^{-2}), then a parallelogram formed by intersection of two isosteres and two isobars will enclose one solenoid of the CGS system. In practice, isosteres are usually drawn for every 20 of these units so that a surface element of the isobaric-isosteric tube contains 400 CGS solenoids. The solenoid is assigned a positive or negative sign depending on whether, on rotation in a positive

sense (anticlockwise) on the isostere with the *higher* value for the specific volume, the *higher* pressure comes before or after the lower. The solenoids have the same properties as the isobaric-isosteric tubes; they must be either fully enclosed or must terminate against a boundary surface. In the case of hydrostatic equilibrium the two sets of surfaces will not intersect and there will thus be no solenoids. On the other hand, as the inclination of the two sets of surfaces relative to each other increases, the number of solenoids will also increase, so that their number can be taken as a measure of the deviation of this state from hydrostatic equilibrium. Since the isobars in *practice* appear in the dynamic section as horizontal lines, the number of solenoids in a section enclosed by a closed curve is determined primarily by the degree of concentration of the isosteres and their slope. The number N of solenoids within a closed curve s is given by the equation

$$N = - \oint_s \alpha dp, \tag{IX.11}$$

where the integral is taken along the curve s in a positive sense of rotation. This is easily understood if the oblique-angled co-ordinate system of the p - and α -lines is transformed into rectangular co-ordinates, with the p -values as abscissa and the α -values as ordinate.

Of particular interest is the case of a curve s formed by two vertical lines and two isobars. The first two correspond to lump-lines at two oceanographic stations a and b , the latter two represent the intersection of the two dynamic topographies of certain pressure surfaces. The pressure at the upper isobaric line at sea-level will be p_0 , the pressure at the lower one p_1 , and will occur at station a at the dynamic depth D_a and at station b at the dynamic depth D_b (see Fig. 132). Since along the two iso-

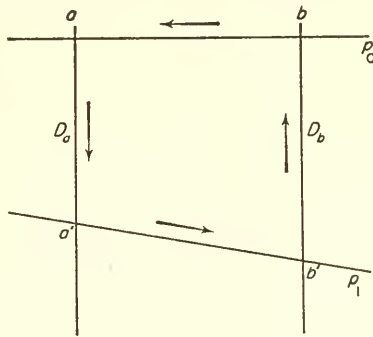


FIG. 132. To the computation of the number of solenoids enclosed by the curve $aa'bb'$.

baric lines $dp = 0$ these two parts of the curve s will not contribute to the integral in (IX. 11), so that

$$- \oint_s \alpha dp = \left[\int_{p_1}^{p_0} \alpha dp \right]_b + \left[\int_{p_0}^{p_1} \alpha dp \right]_a.$$

However, from the definition of equation (IX. 9)

$$D_a = \left[\int_{p_0}^{p_1} \alpha dp \right]_a \quad \text{and} \quad D_b = \left[\int_{p_0}^{p_1} \alpha dp \right]_b,$$

so that (IX. 12) becomes

$$N = D_a - D_b,$$

i.e. the difference in the dynamic depth of an isobaric surface at two oceanographic stations gives the number of solenoids in the cross-section between the two stations from the surface of the sea to the depth of the isobaric surface.

If the sets of surfaces of two properties of sea water L_1 and L_2 coincide, there must be a functional relationship $F(L_1, L_2) = 0$ between them; this represents only a purely geometrical connection between the two scalar quantities L_1 and L_2 and reveals nothing of the physical relationship which probably exists between them. Examples of such quantities are p , α , ρ and also the potential Φ or the dynamic depth D . All these sets of surfaces coincide only when there is internal equilibrium in the water mass (see p. 302). The field of the second scalar quantity L_2 was denoted by BJERKNES and co-workers (1933) in the case where $L_1 = p = \text{const.}$ (isobaric surfaces) *barotropic*, that means adjusted to the pressure field; in the case where $L_1 = t = \text{const.}$ (isothermal surfaces) *thermotropic*, where it is adjusted to the temperature field and in the case where $L_1 = S = \text{const.}$ (isohaline surfaces) *halotropic*, where it is adjusted to the salinity. There will then be a set of relationships

$$F(p, L_2) = 0, \quad F(t, L_2) = 0, \quad F(S, L_2) = 0.$$

In general, these relationships are denoted "conditions of homotropy". If no such functional relationships exist, then the field of the scalar quantity L_2 is *baroclinic*, *thermoclinic* or *haloclinic*, i.e. it is "inclined" relative to the pressure field, the temperature field, or the salinity field; only in these cases do solenoids exist.

If x is a definite point in a field and $x + dx$ is a neighbouring point, and if the geometrical changes on transition from one point to the other are $\Delta N_2 = \Delta p, \Delta t, \Delta S$ then the quantities

$$\Gamma_{N_2}^r = \frac{\Delta N_2}{\Delta p} = - \frac{\partial F / \partial p}{\partial F / \partial N_2}, \quad \Gamma_{N_2}^t = \frac{\Delta N_2}{\Delta t} = - \frac{\partial F / \partial t}{\partial F / \partial N_2}, \quad \Gamma_{N_2}^s = \frac{\Delta N_2}{\Delta S} = - \frac{\partial F / \partial S}{\partial F / \partial N_2}$$

are termed *homotropic coefficients* of N_2 , and specifically each as the barotropic, thermotropic and halotropic coefficients. These coefficients are entirely geometric in character, since they depend on the differences of the factors at two different spatial points. The behaviour of an *individual* small particle—e.g. on changes in pressure—is on the other hand a purely physical property of the field; for example, the density is given by the *piezotropic coefficient* of density

$$\gamma_\rho = \frac{d\rho}{dp} = - \frac{1}{\alpha^2} \frac{d\alpha}{dp},$$

the changes in ρ and α on displacement of a small particle depending on the change in pressure dp . The difference between the two coefficients is clearly shown by the following example: $\Gamma_\rho^p = (\Delta\rho/\Delta p) = 0$ indicates homogeneity of the mass field, while $\gamma_\rho = 0$ indicates the incompressibility of the medium. BJERKNES termed the special case $\Gamma_\rho^p = \gamma_\rho$ "autobarotropy", i.e., after exchange of any two small particles the mass field remains unaltered.

5. The Dynamical Method of Preparation of Oceanographic Data

The oceanographic measurements made at a station give the thermo-haline structure of the sea at this place in terms of temperature and salinity at definite depths. The dynamic evaluation of this data includes the determination of the density and the specific volume *in situ* at definite standard depths, and, in addition, the calculation of the pressure for given depths and the dynamic depths at given pressures, respectively. The starting point for this is the integrals of the two equations (IX. 9) which for practical calculation are expanded into sums of small intervals

$$p = \frac{\rho_0 + \rho_1}{2} \Delta D_1 + \frac{\rho_1 + \rho_2}{2} \Delta D_2 + \dots$$

and $D = \frac{\alpha_0 + \alpha_1}{2} \Delta p_1 + \frac{\alpha_1 + \alpha_2}{2} \Delta p_2 + \dots$ (IX.13)

For this it can be assumed as a first approximation that the dynamic depths and the pressures are expressed by the same values as valid for the geometric depths. This first approximation already gives sufficient accuracy in most cases. The most detailed tables for the calculation of these values are those given by BJERKNES and co-workers (1910). In these tables it is assumed

$$\rho_{s, t, D} = \rho_{35, 0, D} + \epsilon_s + \epsilon_t + \epsilon_{s, t} + \epsilon_{s, D} + \epsilon_{t, D}$$

and in addition to the basic values for the homogeneous oceans (Table 110) six tables are also given for the numerical determination of the six terms on the right-hand side. One term, $\epsilon_{s, t, D}$, is usually so small that it does not have to be taken into consideration. HESSELBERG and SVERDRUP (1914-15) have simplified the calculation of the density *in situ* by introducing the value of σ_t , which is known from

$$\rho_{s, t, \sigma} = 1 + 10^{-3} \sigma_t.$$

Putting

$$\rho_{35, 0, D} = \rho_{35, 0, 0} + \epsilon_D$$

gives

$$\rho_{s, t, 0} = 1 + 10^{-3} \sigma_{t, D},$$
 (IX. 14)

where

$$\sigma_{t, D} 10^{-3} = \sigma_t 10^{-3} + \epsilon_D + \epsilon_{s, D} + \epsilon_{t, D}.$$

If σ_t is known then only three tables are required instead of six for the calculation of the density *in situ*.

The calculation of the specific volume and especially the specific volume anomaly can be simplified in the same way (SVERDRUP, 1933b):

$$a_{s, t, p} = a_{35, 0, p} + \delta, \quad \text{where} \quad \delta = \delta_s + \delta_t + \delta_{s, t} + \delta_{\epsilon, p} + \delta_{t, p}$$

Putting

$$\delta_s + \delta_t + \delta_{s, t} = \Delta_{s, t}$$

gives

$$\delta = \Delta_{s, t} + \delta_{s, p} + \delta_{t, p}.$$
 (IX.15)

The first term can be readily found from σ_t and then

$$a_{s, t, 0} = a_{35, 0, 0} + \Delta_{s, t} = 1 - \frac{\sigma_t \times 10^{-3}}{1 + \sigma_t \times 10^{-3}}$$

The numerical value of $\alpha_{35,0,0}$, is 0.97264 so that

$$\Delta_{s,t} = 0.02736 - \frac{\sigma_t \times 10^{-3}}{1 + \sigma_t \times 10^{-3}}.$$

The specific volume anomaly δ can then be determined quickly and easily using three small tables.

The pressure p at a dynamic depth D is by definition

$$p = \int_0^D \rho_{s,t,D} dD.$$

Table 111. Example of the dynamic evaluation of oceanographic observations of a single station

("Meteor" St. 267, 18.II.27; $\varphi = 13.7^\circ$ N., $\lambda = 19.8^\circ$ W., 4206 m)

Depth (m)	Pressure (dbar)	Temp. ($^\circ$ C)	Salinity (‰)	Density (σ_t)	$10^5 \Delta_{s,t}$	$10^5 \delta_{s,p}$	$10^5 \delta_{t,p}$	$10^5 \delta$	ΔD	ΔD (dyn.m)
0	0	21.20	35.23 ₅	24.64	331.3	—	—	331		0.0
↓	25	21.12	35.21 ₅	24.64 ₅	330.8	—	1.0	332	0.0827	0.0827
	50	16.23	35.57	26.15	187.6	0.1	1.6	189	0.0651	0.1478
	75	16.25	35.42 ₅	26.48	156.3	0.1	2.0	158	0.0434	0.1912
	100	13.52	35.35 ₅	25.58	146.8	0.1	2.7	150	0.0350	0.2262
	150	12.58	35.25 ₅	26.69	136.4	0.1	3.8	140	0.0725	0.2987
	200	11.78	35.16	26.77	128.8	0.1	4.8	134	0.0650	0.3637
	300	10.62	35.06	26.93	113.6	0.0	6.8	120	0.1270	0.4907
	400	10.22	35.14	27.04	103.2	0.1	8.7	112	0.1160	0.6067
	500	9.06	35.02	27.14	93.7	0.0	9.9	104	0.1080	0.7147
	600	8.32	34.98	27.23	85.2	-0.1	11.2	96	0.1000	0.8147
	700	7.23	34.89	27.32	76.6	-0.1	11.5	88	0.0920	0.9067
	800	6.68	34.88	27.39	70.0	-0.1	12.2	82	0.0850	0.9917
	900	5.92	34.83	27.45	64.3	-0.2	12.7	77	0.0795	1.0712
	1000	5.51	34.85	27.52	57.7	-0.2	13.0	71	0.0740	1.1452
	1200	4.99	34.92	27.63	47.3	-0.1	14.0	61	0.1320	1.2772
	1400	4.68	34.97 ₅	27.71	39.7	-0.1	15.5	55	0.1160	1.3932
	1600	4.14	34.97 ₅	27.77	34.0	-0.1	15.8	50	0.1050	1.4982
	1800	3.74	34.97	27.81	30.2	-0.1	16.2	46	0.0960	1.5942
	2000	3.44	34.96 ₅	27.84	27.4	-0.1	16.6	44	0.0900	1.6842
	2250	3.21	34.95 ₅	27.85	26.4	-0.1	17.4	44	0.1100	1.7942
	2500	3.02	34.94 ₅	27.86	25.5	-0.2	18.2	44	0.1100	1.9042
	3000	2.73	34.93	27.87 ₅	24.1	-0.4	19.4	43	0.2175	2.1217
	3500	2.51	34.90	27.87	24.6	-0.5	20.4	44	0.2175	2.3392
	4000	2.37	34.89	27.87	24.6	-0.6	21.6	46	0.2250	2.5642

Replacing $\rho_{s, t, 0}$ by the relation (IX. 14) gives

$$p = D + 10^{-3} \int_0^D \sigma_{t, D} dD. \quad (\text{IX.16})$$

Here only the last term requires numerical integration and has to be summed only to the depth at which the pressure is required. The anomaly in dynamic depth ΔD for given pressures is also obtained in the same way. Since

$$D = D_{35, 0, p} + \Delta D, \\ \Delta D = \int_0^p \delta dp. \quad (\text{IX.17})$$

If δ is known it can also be found by numerical integration. Using the tables given by SVERDRUP (1933*b*) the complete dynamic calculation of the values for an oceanographic station down to 5000 m can with a little practice be done in less than half an hour since the numbers in the tables are always small.

The absolute values for the specific volume and of the dynamic depth can be obtained by adding the anomalies to the standard values for the standard ocean at 0°C and 35‰; they are given in Table 110. If σ_t is known accurately to the second decimal place, then the table will give the density *in situ* $\sigma_{s, t, D}$ correct to the second decimal place, and the pressure for a given dynamic depth correct to the third decimal place. The specific volume anomaly and that of the dynamic depth at given pressures can be found accurately to the fifth and fourth decimal places, respectively, but the last two places in the anomaly of the dynamic depth have only computational significance.

Table 111 shows as an example the complete dynamic evaluation for the "Meteor" station 267 (18.II.1927; $\phi = 13.7^\circ \text{ N.}$, $\lambda = 19.8^\circ \text{ W.}$, 4206 m), and also the calculation of the specific volume anomaly and that of the dynamic depth at given pressures in decibars according to the simplified method of Sverdrup.

Chapter X

Forces and their Relationship to the Structure of the Ocean

1. External, Internal and Secondary Forces

(a) Of the *external forces* that give rise to or maintain the ocean currents, the most important are the air currents, the changes in atmospheric pressure at the surface of the sea, and the periodic tide-generating astronomic forces. These forces can also initiate water movements in a homogeneous sea. The changes in atmospheric pressure are transmitted through the entire mass of water down to the sea bottom and thus give rise to horizontal pressure differences and the formation of gradient currents. The effect of air currents is twofold: First, the tangential force of the wind on the surface of the sea (wind stress) produces a surface current which is transmitted by the effect of viscosity (turbulence) to the water layers beneath the surface. Secondly, the wind produces waves at the surface of the sea and the pressure exerted by the wind on the windward side of these waves also initiates water movements in the direction of the wind (wind drift). These currents produced by the wind and by the changes in atmospheric pressure are considerably modified by the deflecting force of Earth rotation and by the boundary surfaces of the sea (coasts, continental slopes and sea bottom). The piling up of the water by coasts (Anstau) is by far the most important effect of the external forces and is responsible for the formation and the maintenance of an oceanic circulation in the deeper layers of the ocean.

In a sea of homogeneous structure the external forces can produce no change in the physical stratification of the water mass. In a non-homogeneous sea, however, the water movements displace different types of water relative to each other, and thus either directly or due to the boundary conditions produce changes in the thermo-haline structure of the ocean. This upsets the system of internal pressures forces and give rise to ocean currents.

(b) The *internal forces* arise from the vertical and horizontal distribution of mass within the ocean. These differences in the mass distribution (in horizontal and vertical direction) are the consequence of changes in the heat content (temperature) and in the salinity. If at first the water masses are in an internal equilibrium state, this equilibrium can be disturbed by changes of this type, thereby initiating ocean currents which in turn tend to restore the system to a new equilibrium. The principal sources for disturbances in the mass distribution can be found at the surface of the sea, where solar and atmospheric radiation and outgoing radiation first influence the ocean, and where evaporation also takes place. At the other boundary surface of the sea (the sea bottom) the intensity of the disturbances is small and usually of no importance in changing

the distribution of mass. Within the sea, the turbulence in the moving water masses may presumably also produce changes in the physical-chemical structure of multi-stratified water bodies. All these disturbances are, however, small compared with the changes in mass distribution due to atmospheric influences effective at the sea surface.

The only internal force dependent on the mass distribution is the *gradient force*. This force per unit volume is given by the *pressure gradient* G (see equation (IX. 10)). The pressure force per unit mass can be obtained by multiplication with the specific volume so that

$${}_aG = -\alpha \frac{dp}{dn} = -\frac{1}{\rho} \frac{dp}{dn}. \quad (\text{X. 1})$$

The pressure field also determines the field of force per unit mass, since the normal to the isobaric surface gives the direction, and the thickness of the isobaric unit layers gives the intensity of the pressure gradient at any point in oceanic space.

BJERKNES (1900) by analogy with the pressure gradient introduced a "mobility vector" B which gives the variations in specific volume in the direction n of *increasing* specific volume perpendicular to the isosteric surface.

$$B = \frac{d\alpha}{dn}. \quad (\text{X. 2})$$

The degree of concentration of the dynamic isobaths on an isobaric surface is of course also a measure of the gradient force, and is at the same time also a measure of the potential energy stored in the mass distribution. Figure 133 presents a section through an ocean and two oceanographic stations are indicated by A and B (L km apart). As a first approximation the pressure surface can be regarded as horizontal and coincident with the surfaces of equal geometric depth. The surfaces of equal geopotential (equal dynamic depth) are inclined relative to these so that the same pressure p_n at dynamic depth D_a at station A is found at the greater dynamic depth D_b at station B . $D_b - D_a$ is then the difference in potential energy between A' and B' . This potential difference can be regarded as a force along L which, if present alone, would set the water masses in motion. The force per unit mass resulting from the internal pressure difference is then

$$K = \frac{D_b - D_a}{L}. \quad (\text{X. 3})$$

According to (IX. 12), $D_b - D_a$ is the number of solenoids enclosed within the cross-section between the two stations A and B from sea-level to the depth in question. This number per unit length is thus a measure of the internal force resulting from the mass distribution.

(c) Among the *secondary* forces are included all those apparent forces that in themselves do not give rise to a current but which, when motion is present, are of decisive importance in determining the final form of the water displacement. These include the *deflecting force* arising from the rotation of the Earth (the *Coriolis* force) which affects solely the direction of the water movement, the *viscosity* (boundary friction and turbulence) which affects more the velocity of a current, and finally the *centrifugal force*, which for motion along a curved path (velocity V , radius of

ture R) gives a force V^2/R away from the centre of curvature; since for an angular velocity Ω , $V = \Omega R$ the centrifugal force for unit mass will be $\Omega^2 R$.

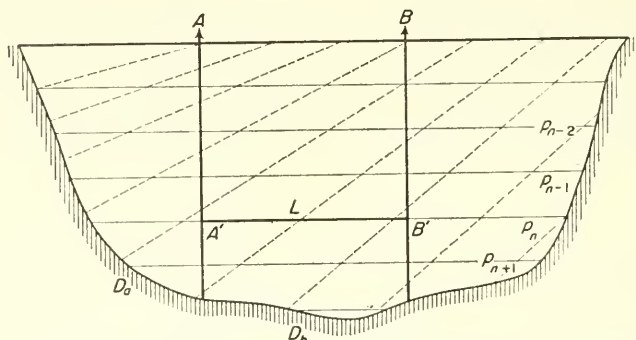


FIG. 133. Cross-section through an ocean. A and B are two oceanographic stations. Full lines: isobaric surfaces ($p = \text{const.}$); Dashed lines: surfaces of equal dynamic depth ($D = \text{const.}$); The pressure surface p_n appears in station A at the dynamic depth D_a , in station B at the dynamic depth D_b ; L denotes the horizontal distance of both stations (schematically).

(a) All observations on the rotating Earth are usually made with reference to a coordinate system rigidly connected with the Earth and therefore rotating with the Earth, although in the classical mechanical sense this is not a permissible reference system. Such a system should not follow the rotation of the Earth, but would for example have to be assumed at rest relative to the fixstars (absolute system). If the basic principles of Galileo–Newton mechanics are used and applied to the rotating Earth, deviations will appear which are due solely to the movement of the reference system imposed by the rotating Earth—a fact which we simply have to accept. These deviations have the character of two apparent forces which are additional to those forces present in the absolute system.

One of these forces depends only on the geographical location; this is the ordinary centrifugal force due to the rotation of the Earth $\omega^2 r$ (ω is the angular velocity of rotation of the Earth—one total revolution per one sidereal day $= (2\pi)/(86,164 \text{ sec}) = 7.29 \times 10^{-5} \text{ sec}^{-1}$, r is the distance from the axis of rotation of the particle under consideration). Since this additional force acts both on a stationary or on a moving mass particle it can be combined with the gravitational force and becomes in this way part of the force of gravity.

The second force, however, depends both on the geographical location and on the velocity of the mass particle set in motion on the Earth. This is denoted to *Coriolis force* and as a vector acting on unit mass has the form

$$\mathfrak{C} = 2[\mathfrak{v} \mathfrak{\omega}]. \quad (\text{X. 4})$$

Its absolute value is

$$C = |\mathfrak{C}| = 2V\omega \sin(\mathfrak{v} \mathfrak{\omega})$$

and it is directed at right angles to the direction of the velocity vector \mathfrak{v} and to the angular vector of the Earth's rotation $\mathfrak{\omega}$, which is in the direction of the Earth's axis, so that $|\mathfrak{\omega}| = \omega$. It therefore acts at right angles to the tangent to the path of movement

as well as in the direction of the equatorial plane. A complete derivation for the Coriolis force, unobjectionable in every respect, has been given by BJERKNES and co-workers (1933). If at any point on the surface of the Earth a co-ordinate system is chosen with the (xy) -plane coinciding with the tangential plane to the Earth (x -positive to the east, y -positive to the north, z -positive towards the Earth's interior), the components of the Coriolis force acting on a material particle on the Earth moving in any direction with a total velocity $V(u, v, w)$ can readily be calculated using equation (X. 4). This gives the components in the three co-ordinate-directions

$$C_x = 2\omega w \sin \phi - 2\omega v w \cos \phi, \quad C_y = -2\omega u \sin \phi, \quad C_z = -2\omega u \cos \phi. \quad (\text{X. 5})$$

From these it can be shown that every movement in the tangential plane to the surface of the Earth will be deflected by the Coriolis force to the *right* in the Northern Hemisphere and to the *left* in the Southern Hemisphere. The terms *cum sole* and *contra solem* suggested by Ekman can be used respectively for rotation in the direction of the azimuthal movement of the sun, i.e., to the right in the Northern Hemisphere and to the left in the Southern Hemisphere (*cum sole*), and for rotations in the opposite direction to the azimuthal movement of the sun, i.e. to the left in the Northern Hemisphere and to the right in the Southern Hemisphere (*contra solem*).† *Thus every movement in a horizontal direction is deflected cum sole by the Coriolis force.* It also follows from equation (X. 5) that there is a *vertical* component of the deflecting force only for zonal movements (x -component u) and not for meridional movements. The importance of the vertical component for the dynamics of moving masses is quite small since it acts in the same direction as gravity relative to which it is vanishingly small.‡

The *horizontal component* is very important, however; at the poles ($\phi = 90^\circ$) it amounts to $1.46 \times 10^{-4} \text{ cm sec}^{-2}$ for $u = 1 \text{ cm sec}^{-1}$ and is thus of the same magnitude as other forces acting in the same direction (gradient forces, tidal forces); it is zero at the equator and reaches the above maximum at the poles. Since it acts at right angles to the direction of movement it is unable to produce changes in velocity and is incapable of doing work; it can only produce changes in the *direction* of movement, but these changes are of decisive importance for the finally established patterns of motion. Due to the effect of the Coriolis force a mass particle moving freely in a horizontal plane with a velocity V will follow a curved track. Since the deflecting force acts at right angles to the velocity (apart from the effect of change in latitude) and its absolute value is constant, this path will describe a circle which is known as the *circle of inertia*. The

† Another terminology uniform for both hemispheres is that customary in meteorology: cyclonic = *contra solem* and anticyclonic = *cum sole*.

‡ The usual statement, that the vertical component of the Coriolis force need not be taken into consideration, since it is small by comparison with the gravitational acceleration is not entirely correct. In the static equilibrium state of the sea, gravity and the vertical pressure gradient neutralize each other. However, under quasi-static conditions the difference between gravity and vertical pressure gradient is so small that it may be of the same order of magnitude as the vertical component of the Coriolis force. Nonetheless, it is customary to neglect the latter in calculations; it can be regarded as an increase or decrease of gravity so that the acceleration towards the centre of the Earth is now $g + 2\omega u \cos \phi$. It can also be regarded as causing a small change in density in the ratio $(g + 2\omega u \cos \phi) : g$.

At the equator, when $u = 30 \text{ cm sec}^{-1}$ it may amount to 5 units in the sixth decimal place in ρ or 5 units in the third decimal place in σ_t , which can be disregarded.

radius of this circle follows from the condition that the forces acting on the moving mass particle must balance each other (centrifugal force = Coriolis force).

$$\frac{V^2}{R} = 2\omega V \sin \phi, \tag{X. 6}$$

so that

$$R = \frac{V}{2\omega \sin \phi}.$$

The term "circle of inertia" has been chosen to indicate that relative to the movement of the rotating Earth this circular movement in a certain sense replaces the linear inertia of absolute motion. The radius of the circle of inertia is a function of the latitude and the velocity. Table 112 gives values for this functional relationship.

Table 112. Radius of inertia circle as a function of V and φ
(V in mm sec⁻¹, cm sec⁻¹, m sec⁻¹; R in m, 10m, km units)

φ . .	5°	10°	20°	30°	40°	50°	60°	70°	80°	Poles
V = 1	79	40	20	14	10	9	8	7	7	7
2	157	79	40	27	21	18	16	15	14	14
3	236	118	60	41	32	27	24	22	21	21
4	315	158	80	55	43	36	32	29	28	27
5	393	198	100	69	53	45	40	36	35	34
6	472	237	120	82	64	54	48	44	42	41
7	551	277	140	96	74	63	55	51	49	48
8	629	316	160	110	85	72	63	58	56	55
9	708	356	180	124	96	81	71	66	62	62
10	786	395	201	137	106	90	79	73	70	69

The time required for one complete rotation on the circle of inertia (*inertia period*) is given by

$$T = \frac{2\pi R}{V} = \frac{\pi}{\omega \sin \phi} = \frac{12 \text{ sidereal hours}}{\sin \phi}. \tag{X.7}$$

If the period of rotation of the plane of oscillation of a Foucault pendulum is a pendulum day = (2π)/(ω sin φ), the period of rotation of the circle of inertia will be a *half pendulum day* whatever the value of the velocity V. Table 112a shows the time required for one revolution on the inertia circle (the inertia period) at different latitudes (from 5 to 5 degrees).

Table 112a. The period of rotation of the inertia circle (inertia period).

φ	0°	5°	10°	15°	20°	30°	40°	50°	60°	70°	80°	Poles
Hours (½ pendulum day)	∞	138	69	46	35	24	18.7	15.7	13.9	12.8	12.2	12.0

In lower latitudes the period may be several days, in middle latitudes 24 h and at high latitudes half a day; here, since it has a similar period as the daily and half-daily

components of the tide-generating forces, it is of particular importance in the dynamics of periodic phenomena.†

(β) In addition, *friction* is also of considerable importance in all oceanic movements. Like all liquids, sea-water has a *viscosity* which for deformation manifests itself as an internal friction. The friction of water over a solid and rough sea bottom is primarily an *external boundary surface friction*. This type of friction represents a retardation of the flow of the current but only in relatively shallow water can be taken as a measure of it; the most simple assumption describing the frictional mechanism is that the gliding flow of the water over the solid bottom meets a tangential resistance which is assumed proportional to the velocity of the current V . The frictional force in this case would correspond to a vector with a direction opposite to that of the velocity vector and has the absolute magnitude $k\rho V$. The quantity k is termed the *coefficient of gliding friction*. Hydraulic investigations on the dissipation of the kinetic energy of a river due to friction on the river bed have shown that the frictional force per cm^2 of the bottom surface is proportional not to the first power but rather to the square of the flow velocity. It can be expected that the dependence of the boundary surface friction on the velocity will also be of the same kind for shallow ocean currents. TAYLOR (1920) attempted to apply the conditions found in natural channels to coastal oceanic currents in shelf areas. In the friction formula the coefficient k for a normal sea bottom has the value 0.0026 for depths of about 50–100 m so that

$$R = -2.6 \times 10^{-3} \rho V^2. \quad (\text{X.9})$$

At more shallow depths with an especially irregular sea-bottom topography k may increase considerably (100 times the above value or even more). These frictional assumptions refer always to the mean tangential resistance exerted over the whole of a column of unit cross-section from the bottom to the sea surface due to the effect of boundary friction at the bottom. However, these assumptions do not specify the nature of the friction in the interior of the total water column above the sea bottom. The *internal friction* appears as a tangential shearing stress τ between individual layers of water gliding one above the other with different velocities. This stress per unit area is proportional to the velocity gradient perpendicular to the direction of the flow dV/dn , so that

$$\tau = \mu \frac{dV}{dn}. \quad \text{X.10}$$

The quantity μ is the coefficient of *dynamic viscosity* and has the dimensions $[\text{g cm}^{-1} \text{sec}^{-1}]$.‡

† The inertia movement has the form of a circle only if the Coriolis force is constant (mostly assumed as the mean value for the meridional width of the inertia circle). A general derivation for varying latitude has been given by WIPPLE (1917) but this was confined, however, to movements near the equator, since $\sin \phi$ was replaced by the arc ϕ of latitude and $\cos \phi$ by 1. Inertia movements superimposed on horizontal and zonal currents play a large part in the dynamics of ocean currents especially the occurrence of long waves and in vortical disturbances. (See in this connection DEFANT (1956) and Vol. I, Pt. II, Chap. XIII, 6.)

‡ The origin of viscosity can be sought in the continuous equalization of velocity between superimposed layers of water gliding over each other in a moving water mass. This equalization is due to the interchange of individual molecules and the consequent transfer of velocity from one layer to the next. This viewpoint is, however not entirely correct since the molecules in a liquid are so closely packed that usually they can only oscillate within the small intermolecular spaces present and therefore only

For this assumption concerning the inner friction, the effect of the solid, stationary sea bed appears as a corresponding boundary condition. If n is the direction of the normal to the sea bottom ($z = 0$) then

- (1) for *completely frictionless movement* of the water over the sea bed ($z = 0$): $dV/dn = 0$;
- (2) if the water is stationary at the bottom ($z = 0$): $V = 0$;
- (3) for *part-time gliding at the sea bottom*, that is for a discontinuity of the velocity at $z = 0$: $dV/dt = f(V)$, where $f(V)$ is a certain function of V , for example, $k\rho V^2$.

(X. 11)

In a volume element $\delta x \delta y \delta z$ (see Fig. 134) in a current in which the velocity V in a direction perpendicular to the vertical direction z is very much stronger, there will be a shearing stress $\tau\delta x\delta y$ on the lower surface $\delta x\delta y$ and a corresponding

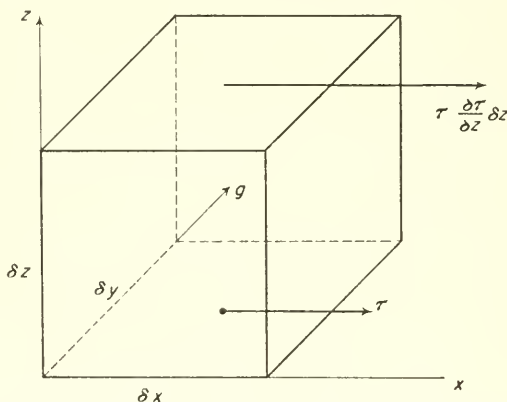


FIG. 134. Computation of the frictional force from the shearing stresses.

$\{\tau + (\partial\tau/\partial z)\delta z\}\delta x\delta y$ on the upper surface at a distance δz from the lower. On the entire volume element there acts thus a frictional force $(\partial\tau/\partial z)\delta x\delta y\delta z$ so that according to (X. 10) the frictional force per unit mass in the direction of the x -co-ordinate will be given by

$$R_x = \frac{\mu}{\rho} \frac{\partial^2 V}{\partial z^2}. \tag{X.12}$$

Where μ can be regarded as a constant.

From the general theory of friction in liquids it follows that for an *incompressible* fluid (and thus also with sufficient accuracy for sea-water) the components of the frictional force per unit mass in a viscous liquid are given by the three expressions:

$$R_x = \frac{\mu}{\rho} \Delta u, \quad R_y = \frac{\mu}{\rho} \Delta v, \quad R_z = \frac{\mu}{\rho} \Delta w, \tag{X.13}$$

Footnote continued from p. 317

seldom change position. These occasional changes in position are facilitated by the action of a tangential shearing stress especially in the direction of the stress itself and this alone permits the individual layers to glide over each other. The more frequent the changes in position of the molecules, the lower is the internal friction (viscosity) characteristic of the liquid.

where u, v, w are the velocity components in the direction of the three co-ordinate axes and Δ is the Laplace operator $\partial^2/\partial x^2 + \partial^2/\partial y^2 + \partial^2/\partial z^2$. The quantity $\nu = \mu/\rho$ is called the *kinematic viscosity coefficient* and has the dimensions $[\text{cm}^2 \text{sec}^{-1}]$. For numerical values of μ and ν for pure water and for sea-water see Vol. I, Pt. I, p. 104.

The actual movement of water masses in the oceans does not correspond to a simple ordered gliding of the individual superimposed layers relative to each other, but is rather a random disorganized movement that takes place in vortices and rolls similar to those which can be seen in a smoke plume. The first type of motion is called layered or *laminar* and the second *turbulent*. In turbulent flow there is a transfer of the flow momentum from one layer to another, not by the interchange of molecules as in physical internal friction but by the exchange of large elements of water (eddies) which move rather irregularly back and forth between the different layers and thus bring about a reduction in the velocity in the direction of the basic current; this is then referred to as *virtual internal viscosity* or *eddy viscosity*, which in an analogous way to the molecular viscosity can be characterized by a special *eddy viscosity coefficient*. It is easily seen that the eddy viscosity, by its nature, will be more effective than the molecular viscosity and is also understood by the numerically much larger viscosity coefficients. However, apart from this, the turbulent coefficient is no longer an invariable quantity like the molecular viscosity at constant temperature, but depends on the nature and the intensity of the turbulence itself. Further, the components of the frictional force of turbulent viscosity can be expressed in exactly the same way as those in equations (X. 12 and 13) if μ is replaced by the turbulent viscosity coefficient η . If this is not constant then, for example, equation (X. 12) is replaced by the expression

$$R = \frac{1}{\rho} \frac{\partial}{\partial z} \left(\eta \frac{\partial V}{\partial z} \right) \tag{X.14}$$

and the same applies for the other expressions in (X. 13).

To a very large extent ocean currents are movements along quasi-horizontal planes so that the turbulent viscosity for small oceanic spaces is limited to that appearing in connection with layered gliding motion of the water masses. Within the moving water mass turbulence creates a definite vertical velocity profile and tends to maintain it. If there is no viscosity this profile must be linear (see Fig. 135, I). The velocity of the

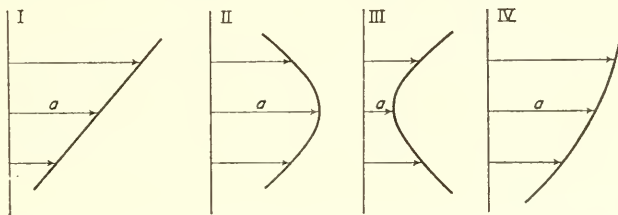


FIG. 135. Main types of vertical velocity distributions: (I) in the case of no friction; (II) in the case when friction retards the mean current filament; (III) in the case when friction accelerates the mean current filament; (IV) for a constant frictional force.

filament (a) in the middle of the current is then the mean of the velocities of the adjacent upper and lower masses. The accelerating influence of the upper layer will be exactly compensated by the retardation at one of the lower. In case II, where the

velocity of this middle layer is greater, the adjacent layers will exert, due to the transfer of their flow momenta, a retardation on the current maximum in the middle and will eventually eliminate it. The middle layer in case III will be accelerated by the equalization of velocity in the turbulent flow. Equation (X. 12) also shows that for a *constant* internal friction the vertical profile must take the form of a parabola.

2. The Basic Hydrodynamic Equations

For a complete description of the water movement in ocean currents, it is necessary to know on the one hand the *path* of each small element of water in it, and on the other hand the *position* of such a small element along this path at any time; i.e. it is necessary to know the co-ordinates of a small element of water as a function of time. The basic hydrodynamic equations of motion in their most general form are the mathematical-physical tool for dealing with and for a theoretical understanding of the different successive states of a water mass.

The motion can be looked at from two different view-points. The different mass elements may be followed as they pass a *fixed point* in space and particular attention may be paid to the changes in the state of motion of the water mass which occur at this point. Alternatively, the changes of state of individual small elements moving along their track may be followed, and thereby a description of the conditions in the current *in the course of their displacement* can be obtained. The first approach gives the Eulerian basic hydrodynamic equations of motion (EULER, 1755) and the second leads to the equations of motion of Lagrange (LAGRANGE, 1781); both of these concepts are applied in oceanography according to the type of problem to be solved.

For a small element of water in the point x, y, z the components of the velocity are denoted u, v, w in the directions of the co-ordinate-axes of a left-hand system (xy -plane horizontal, x -axis positive to the east, y -axis positive to the north, z -axis positive towards the centre of the Earth). They will be functions of x, y, z and of the time t . First of all the basic Newtonian relationship of mechanics is applied:

$$\text{Mass} \times \text{acceleration} = \text{sum of all forces.}$$

The individual accelerations $du/dt, dv/dt$ and dw/dt are made up of two parts. The first part arises from changes in the state of motion at the point; it is given by $\partial u/\partial t, \partial v/\partial t$ and $\partial w/\partial t$ (local change). The second arises since after a small time dt the water elements under consideration are no longer found at the initial point (x, y, z) but are displaced by $u dt, v dt$ and $w dt$, respectively (advective change). Thus to the local part must be added an advective part, so that the total *individual* acceleration in the x -direction of the small elements of the liquid under consideration will be

$$\frac{du}{dt} = \frac{\partial u}{\partial t} + u \frac{\partial u}{\partial x} + v \frac{\partial u}{\partial y} + w \frac{\partial u}{\partial z}. \quad (\text{X.15})$$

Similar equations apply for dv/dt and dw/dt . It may be emphasized here that the partial derivative $\partial/\partial t$ always represents the change in the quantity under consideration at a *fixed point*, while the total derivative d/dt represents the *individual* change in a quantity for one and the same element (which changes its position with time).

Taking the mass of unit volume as ρ , and considering that since the only external

conservative force is gravity acting in the positive direction of the z -axis (downward), the pressure gradient forces will be given by

$$-\frac{1}{\rho} \frac{\partial p}{\partial x}, \quad -\frac{1}{\rho} \frac{\partial p}{\partial y}, \quad -\frac{1}{\rho} \frac{\partial p}{\partial z},$$

respectively, and introducing the Coriolis force according to (X. 5) and the frictional forces according to (X. 13), then the basic hydrodynamic equations of motion will take the complete form

$$\left. \begin{aligned} \frac{du}{dt} &= \frac{\partial u}{\partial t} + u \frac{\partial u}{\partial x} + v \frac{\partial u}{\partial y} + w \frac{\partial u}{\partial z} = +2\omega v \sin \phi - \frac{1}{\rho} \frac{\partial p}{\partial x} + \frac{\mu}{\rho} \Delta u, \\ \frac{dv}{dt} &= \frac{\partial v}{\partial t} + u \frac{\partial v}{\partial x} + v \frac{\partial v}{\partial y} + w \frac{\partial v}{\partial z} = -2\omega u \sin \phi - \frac{1}{\rho} \frac{\partial p}{\partial y} + \frac{\mu}{\rho} \Delta v, \\ \frac{dw}{dt} &= \frac{\partial w}{\partial t} + u \frac{\partial w}{\partial x} + v \frac{\partial w}{\partial y} + w \frac{\partial w}{\partial z} = g - 2\omega u \cos \phi - \frac{1}{\rho} \frac{\partial p}{\partial z} + \frac{\mu}{\rho} \Delta w \end{aligned} \right\} \quad (\text{X.16})$$

The third equation in the z -direction can be considerably simplified, which shall be done at once. Since the movements of the water in the ocean occur very largely in a horizontal plane and w , dw/dt and the frictional term in this direction can always be assumed to be small, and further, since the vertical component of the Coriolis force can be neglected, the third equation in (X. 16) reduces to

$$0 = g - \frac{1}{\rho} \frac{\partial p}{\partial z} \quad (\text{X.17})$$

which corresponds to the basic hydrostatic equation (see p. 337).

For problems involving the whole or an extended part of the rotating Earth it is convenient to use polar co-ordinates. The reference surface selected is the free sea surface in a state of equilibrium (usually it is sufficiently accurate to take a spherical surface with the mean radius R of the Earth) and as co-ordinates can be taken the pole distance $\vartheta = 90 - \phi$, the longitude λ and the distance z from this surface (along the radius of sphere R , positive outwards). The velocities relative to the Earth along the three axes are then

$$u = (R + z) \frac{d\vartheta}{dt}, \quad v = R \sin \vartheta \frac{d\lambda}{dt} \quad \text{and} \quad w = \frac{dz}{dt}. \quad (\text{X. 18})$$

If the external forces have a potential Ω † and if the frictional terms are omitted, the equations of motion take the following form

$$\left. \begin{aligned} \frac{du}{dt} - 2\omega v \cos \vartheta &= -\frac{1}{R+z} \frac{\partial}{\partial \vartheta} \left(\frac{p}{\rho} + \Omega \right), \\ \frac{dv}{dt} + 2\omega u \cos \vartheta + 2\omega w \sin \vartheta &= -\frac{1}{R \sin \vartheta} \frac{\partial}{\partial \lambda} \left(\frac{p}{\rho} + \Omega \right), \\ \frac{dw}{dt} - 2\omega v \sin \vartheta &= -\frac{\partial}{\partial z} \left(\frac{p}{\rho} + \Omega \right). \end{aligned} \right\} \quad (\text{X.19})$$

† The forces X, Y, Z have a potential Ω when they can be represented by

$$X = -\frac{\partial \Omega}{\partial x}, \quad Y = -\frac{\partial \Omega}{\partial y}, \quad Z = -\frac{\partial \Omega}{\partial z}.$$

Since the depth of the sea is always very small as compared with the dimensions of the Earth, the term $(R + z)$ in the first equation of (X. 18) can be replaced in good approximation by R .

In the Lagrange equations of motion the co-ordinates x, y, z of a small mass element of the liquid are viewed as functions of the independent variables a, b, c and of the time t ; a, b, c are the initial co-ordinates of the particle under consideration, i.e., values of x, y, z at the time $t = 0$. These functions

$$x = f_1(a, b, c, t), \quad y = f_2(a, b, c, t), \quad z = f_3(a, b, c, t),$$

thus describe the history of each small element of the liquid within the current. If only the time t is altered, they give the path of the element under consideration; if on the other hand t is constant and only a, b, c are allowed to change, this gives the positions of the different elements at one and the same instant of time. Since the accelerations of the element a, b, c at the time t are given by

$$\frac{du}{dt} = \frac{d^2x}{dt^2}, \quad \frac{dv}{dt} = \frac{d^2y}{dt^2}, \quad \frac{dw}{dt} = \frac{d^2z}{dt^2}$$

the equation (X.15) can also be written in another form

$$\frac{d^2x}{dt^2} - X = -\frac{1}{\rho} \frac{\partial p}{\partial x}, \quad \frac{d^2y}{dt^2} - Y = -\frac{1}{\rho} \frac{\partial p}{\partial y}, \quad \frac{d^2z}{dt^2} - Z = -\frac{1}{\rho} \frac{\partial p}{\partial z}.$$

To eliminate at the right-hand sides the derivatives with respect to x, y, z these equations can be multiplied at first with

$$\frac{\partial x}{\partial a}, \quad \frac{\partial y}{\partial a}, \quad \frac{\partial z}{\partial a},$$

then with

$$\frac{\partial x}{\partial b}, \quad \frac{\partial y}{\partial b}, \quad \frac{\partial z}{\partial b} \quad \text{and} \quad \frac{\partial x}{\partial c}, \quad \frac{\partial y}{\partial c}, \quad \frac{\partial z}{\partial c},$$

respectively, and finally can be added. If the forces have a potential Ω , the Lagrange form of the equations of motion is obtained

$$\begin{aligned} \left(\frac{d^2x}{dt^2} - X\right) \frac{\partial x}{\partial a} + \left(\frac{d^2y}{dt^2} - Y\right) \frac{\partial y}{\partial a} + \left(\frac{d^2z}{dt^2} - Z\right) \frac{\partial z}{\partial a} + \frac{1}{\rho} \frac{\partial p}{\partial a} &= 0, \\ \left(\frac{d^2x}{dt^2} - X\right) \frac{\partial x}{\partial b} + \left(\frac{d^2y}{dt^2} - Y\right) \frac{\partial y}{\partial b} + \left(\frac{d^2z}{dt^2} - Z\right) \frac{\partial z}{\partial b} + \frac{1}{\rho} \frac{\partial p}{\partial b} &= 0, \\ \left(\frac{d^2x}{dt^2} - X\right) \frac{\partial x}{\partial c} + \left(\frac{d^2y}{dt^2} - Y\right) \frac{\partial y}{\partial c} + \left(\frac{d^2z}{dt^2} - Z\right) \frac{\partial z}{\partial c} + \frac{1}{\rho} \frac{\partial p}{\partial c} &= 0, \end{aligned}$$

The hydrodynamic equations of motion form a very complex set of equations. They have to be solved in order to obtain a complete description of the state of motion but only in very rare and in the most simple cases it is possible to arrive at a final and definite solution. In most cases it is considered sufficient to determine, if possible, the state of motion at each place and at each time without paying any attention to the further history of the individual water elements. There is a considerable simplification possible when dealing with so-called *stationary currents*. These are currents in which the state of motion at each point does not change with time and is thus completely fixed by specifying its direction and velocity. The condition for a steady state in the current is thus

$$\frac{\partial u}{\partial t} = \frac{\partial v}{\partial t} = \frac{\partial w}{\partial t} = 0. \quad (\text{X.20})$$

Some *kinematic* properties of the motion should perhaps be referred to here. The path of a small water element is obtained from the three simultaneous equations:

$$dx = udt, \quad dy = vdt, \quad dz = wdt. \quad (\text{X.21})$$

The integration constants for $t = 0$ are then the three initial co-ordinates a, b, c of the water element under consideration.

The *instantaneous* state of motion in a water mass is given by the *stream lines* (see Chap. XII) which everywhere indicate the direction of a current by the tangent at the point under consideration. Their differential equations are

$$\frac{dx}{u} = \frac{dy}{v} = \frac{dz}{w}. \quad (\text{X.22})$$

Since the state of motion in a steady current does not change with time it is understandable that the stream lines in this case coincide with the trajectories of the water elements. Steady currents are not without accelerations since only the local part of the acceleration disappears; the advective part, for example, $u(\partial u/\partial x) + v(\partial u/\partial y) + w(\partial u/\partial z)$ requires that the moving water element reaches any point with a velocity equal to that prescribed for that point.

3. The Continuity Equation and the Boundary-surface Conditions

To the equations of motion must be added, as a special condition, the continuity equation which is based on the law of the conservation of mass. This states that in any volume element specified in the interior of a liquid the mass entering it at a given time must be equal to that leaving it at the same time. Any excess in one or the other direction must appear as a corresponding change in the density if the liquid will permit such a change. Taking a volume element $\delta x\delta y\delta z$, investigation of the extent by which, as a consequence of flow through the boundaries the amount of liquid enclosed in it varies, shows that for a conservation of mass the continuity condition is given by the equation

$$\frac{\partial \rho}{\partial t} + \frac{\partial \rho u}{\partial x} + \frac{\partial \rho v}{\partial y} + \frac{\partial \rho w}{\partial z} = 0. \quad (\text{X.23})$$

Using the relationship equation (X. 15) this can be given the following form

$$-\frac{1}{\rho} \frac{d\rho}{dt} = +\frac{1}{a} \frac{da}{dt} = \frac{\partial u}{\partial x} + \frac{\partial v}{\partial y} + \frac{\partial w}{\partial z}. \quad (\text{X.24})$$

In an *incompressible* liquid $d\rho/dt = 0$ the continuity equation reduces to

$$\frac{\partial u}{\partial x} + \frac{\partial v}{\partial y} + \frac{\partial w}{\partial z} = 0 \quad (\text{X.25})$$

This does not assume that the liquid has the same density everywhere (homogeneous medium). The expression $\partial u/\partial x + \partial v/\partial y + \partial w/\partial z$ indicates the volume increase in unit time per unit volume of the element and is usually termed the three-dimensional or total *divergence* of the vector (u, v, w) . The continuity equation for an incompressible medium is then

$$\text{div } (u, v, w) = 0. \quad (\text{X.26})$$

Since the rotation of the Earth does not affect the conservation of the mass, the continuity equation does not contain the angular velocity of the Earth's rotation when a *polar co-ordinate system* is used for the rotating Earth (co-ordinates: pole distance $\vartheta = 90^\circ - \phi$, longitude λ and z along the Earth's radius R). However, there are changes in the cross-section of a current for meridional motion due to the convergence of the meridians and for vertical displacements of mass due to the divergence of the Earth's radii. Thus in the continuity equation for polar co-ordinates, in addition to the previous terms derived from flow through the volume element, there will be two further terms considering these further circumstances in this special co-ordinate system. These give the following equation:

$$\frac{\partial \rho}{\partial t} + \frac{1}{R \sin \vartheta} \left[\frac{\partial \rho u \sin \vartheta}{\partial \vartheta} + \frac{\partial \rho v}{\partial \lambda} \right] + \frac{\partial \rho w}{\partial z} + \frac{2\rho w}{R} = 0. \tag{X.27}$$

The effect of the convergence of the meridians is expressed in the term $(\rho u/R) \cot \vartheta$ which is obtained by differentiation of the first expression in the brackets and the effect of the divergence of the Earth's radii is contained in the term $2\rho w/R$. Since for vertical displacements of mass in the sea, which is shallow relative to the Earth's radius, the vertical velocities appearing are very small, this last term is not too important and can safely be neglected. For small oceanic spaces the convergence of the meridians can also be disregarded in first approximation, though not for large-scale ocean currents (see Chap. XXI).†

If the liquid has boundary surfaces either at a solid body (the sea bottom) or when it is surrounded by differently stratified liquids (other water bodies) the continuity equation will take special forms and must be replaced or supplemented by *special boundary conditions*. At a *solid* boundary, in order to secure a reasonable state of motion with no empty spaces, the component of the velocity perpendicular to the surface must be zero. If l, m, n are the direction-cosines of the normal to the surface then a necessary condition is

$$lu + mv + nv = 0. \tag{X.28}$$

† The continuity equation which corresponds to the Lagrange equations of motion is more difficult to derive and reference should be made to text-books of hydrodynamics. Taking the functional determinant

$$\begin{vmatrix} \frac{\partial x}{\partial a} & \frac{\partial y}{\partial a} & \frac{\partial z}{\partial a} \\ \frac{\partial x}{\partial b} & \frac{\partial y}{\partial b} & \frac{\partial z}{\partial b} \\ \frac{\partial x}{\partial c} & \frac{\partial y}{\partial c} & \frac{\partial z}{\partial c} \end{vmatrix} = \frac{\partial(x, y, z)}{\partial(a, b, c)},$$

the condition of constancy of mass in a volume element $\delta a \delta b \delta c$ will be

$$\rho \frac{\partial(x, y, z)}{\partial(a, b, c)} = \rho_0,$$

where ρ_0 is the initial density at the point (a, b, c) . For incompressible liquids $\rho = \rho_0$ the continuity equation takes the form

$$\frac{\partial(x, y, z)}{\partial(a, b, c)} = 1.$$

At all inner boundary surfaces, on the other hand, the velocity component perpendicular to the boundary surface must be the same on both sides of the surface. If the values for the quantities on both sides of the boundary are specified by separate indices, then this *kinematic boundary condition* can be represented as a special case of equation (X. 28)

$$l(u_1 - u_2) + m(v_1 - v_2) + n(w_1 - w_2) = 0. \quad (\text{X.29})$$

From the point of view of continuity it is allowed to make a free choice about the velocity component parallel to the inner boundary surface and solid surface, respectively.

If the liquid has a *free* upper surface this will be subject to the condition that all the small fluid elements which belong to it will always remain in the liquid. If $f(x, y, z, t) = 0$ is the equation for the free upper surface the foregoing condition requires that

$$\frac{df(x, y, z, t)}{dt} = 0. \quad (\text{X.30})$$

In addition to the kinematic, there is also a *dynamic boundary-surface condition* that must be satisfied at inner boundary surfaces as well as at a free surface. This requires that at the discontinuity surface where the individual quantities are subject to sudden changes, the pressure must be the same on both sides of the boundary. If $f(x, y, z, t) = 0$ is the equation for the discontinuity surface, which may be either moving or stationary, and if p_1 and p_2 give the pressures in the medium on both sides of the surface as functions of x_1, y_1, z_1 and x_2, y_2, z_2 , respectively, then the dynamic boundary condition will require that values of x, y, z and t , in order to satisfy $f(x, y, z, t) = 0$, must also satisfy the equation

$$p_1(x_1, y_1, z_1, t) - p_2(x_2, y_2, z_2, t) = 0. \quad (\text{X.31})$$

4. Potential Flow, the Bernoulli Equation, Impulse and the Impulse Form of the Hydrodynamic Equations

In very many cases the velocity components u, v, w can be expressed by a function φ , so that

$$u = -\frac{\partial\varphi}{\partial x}, \quad v = -\frac{\partial\varphi}{\partial y}, \quad w = -\frac{\partial\varphi}{\partial z}. \quad (\text{X.32})$$

This function then is called the *velocity potential*, and movement for which a function of this type is valid has been termed a *potential flow*. By this kind of definition it is shown that if such a potential is present:

- (1) The stream lines will be everywhere perpendicular to the surfaces $\varphi = \text{const.}$ (equi-potential surfaces of velocity). This follows from (X. 22) when combined with (X. 32).
- (2) The following combinatory relationships:

$$\frac{\partial u}{\partial y} = \frac{\partial v}{\partial x}, \quad \frac{\partial v}{\partial z} = \frac{\partial w}{\partial y}, \quad \frac{\partial w}{\partial x} = \frac{\partial u}{\partial z}$$

will apply; these state that the current in the presence of a velocity potential is *irrotational* (free of vorticity).

(3) The continuity equation for an incompressible medium will take the form

$$\frac{\partial^2 \varphi}{\partial x^2} + \frac{\partial^2 \varphi}{\partial y^2} + \frac{\partial^2 \varphi}{\partial z^2} = \Delta \varphi = 0.$$

Neglecting the Coriolis force and the frictional forces, the three Eulerian equations of motion equation (X. 16), on multiplication by dx , dy and dz , respectively, and taking further into account the identity

$$\frac{du}{dt} = \frac{\partial u}{\partial t} + \frac{1}{2} \frac{\partial}{\partial x} (u^2 + v^2 + w^2) \quad (\text{X.33})$$

and by subsequent addition, can be compressed into the single equation

$$\frac{\partial \varphi}{\partial t} + \frac{u^2 + v^2 + w^2}{2} + \frac{p}{\rho} + \Omega = F(t), \quad (\text{X.34})$$

where $F(t)$ is an arbitrary function of t alone and Ω is the potential of the external forces. For a steady current

$$\left(\frac{\partial u}{\partial t} = \frac{\partial v}{\partial t} = \frac{\partial w}{\partial t} = 0 \right)$$

in which the stream lines coincide with the trajectories of the fluid elements

$$\frac{u^2 + v^2 + w^2}{2} + \frac{p}{\rho} + \Omega = C, \quad (\text{X.35})$$

where the quantity C is constant along each stream line but changes on passing from one stream line to another. The equation (X. 35) is called the *Bernoulli theorem* (equation). It shows that for steady motions the pressure at points along a stream line is greatest where the velocity is smallest and *vice versa*. Considering that a fluid particle on transfer from higher to lower pressure is subject to an acceleration (increase in velocity) the above statement is readily understood. This is another way of expressing the conservation of energy, since for unit mass the first term is the kinetic energy of motion, the second is the work done against pressure and the third is the potential energy; in a steady flow the sum of these energies along a stream line must be constant. If the water movement is solely influenced by the gravity force, then since $\Omega = gz$, the Bernoulli pressure equation will have the form

$$\frac{c^2}{2} + \frac{p}{\rho} + gz = \text{const.}, \quad \text{with } u^2 + v^2 + w^2 = c^2. \quad (\text{X.36})$$

For a two-dimensional *potential flow* it is convenient to introduce a *stream function* ψ defined by the relations

$$u = - \frac{\partial \psi}{\partial y}, \quad v = + \frac{\partial \psi}{\partial x} \quad (\text{X.37})$$

and therefore from (X. 32)

$$\frac{\partial \varphi}{\partial x} = \frac{\partial \psi}{\partial y}, \quad \frac{\partial \varphi}{\partial y} = - \frac{\partial \psi}{\partial x}.$$

In addition, the differential equation $\Delta\psi = 0$ must also be satisfied by ψ . Since the curves $\psi = \text{const.}$ are perpendicular to the curves $\varphi = \text{const.}$

$$\left(\frac{\partial\varphi}{\partial x} \frac{\partial\psi}{\partial y} + \frac{\partial\varphi}{\partial y} \frac{\partial\psi}{\partial x} = 0 \right).$$

They represent stream lines (hence, the name stream function).

It can easily be shown that every analytical function of the complex variable $z = x + iy$ satisfies the continuity equation $\Delta\varphi = 0$, i.e. represents a solution for the equations of motion. If this function is given by

$$F(z) = F(x + iy),$$

then its real part is the velocity potential φ and the imaginary part is the stream function ψ or *vice versa*. This important consequence allows simpler current systems to be completely worked out kinematically. Use will be made of this later (see Chap. XII, 3).

In a few important cases the use of the *impulse theorems* for *steady* currents in a water mass has considerable advantages. The product of mass and velocity is termed the impulse or momentum; as a vector, like velocity, it has three components. The impulse theorem states that for any arbitrarily limited water mass (the outer boundary surfaces all together are usually termed "control surface") the change with time of the impulse in it is equal to the sum of the external forces acting on the mass. The internal forces in the system balance each other according to the principle of action and reaction. The change in momentum can be divided into two parts. The first gives the change with time of the impulse in the volume under consideration enclosed by the control surface; for a steady current this term vanishes. The second is the momentum entering or leaving it in unit time through all the boundaries (total control surface). For a steady current the vector sum of all pressures acting on the control surface must be equal to the transport of impulse through it.

As an example, the following two cases will be considered here. Fig. 136a shows a straight current tube formed by stream lines; we consider the part between 1 and 2. At the cross-section 1 (surface F_1) the current enters with a velocity V_1 . The water

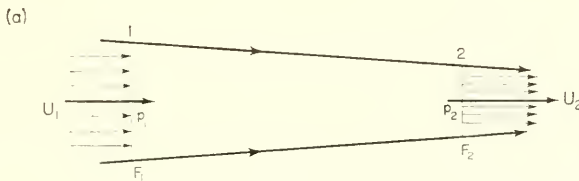


Fig. 136a

mass transported in unit time is $\rho V_1 F_1$, the impulse transport (momentum flux) through F_1 into the volume under consideration is $\rho V_1^2 F_1$; similarly, at cross-section 2 (surface F_2) an impulse amount $\rho V_2^2 F_2$ leaves the enclosed space; as a "counter action" it has to be taken with a negative sign. The impulse amount remaining in the space is thus $\rho(V_1^2 F_1 - V_2^2 F_2)$. In a steady current, in order to secure an equilibrium state,

it has to be balanced by the vectorial sum of all the surface pressures, that is, by $F_1 p_1 - F_2 p_2$. This gives for the current tube the equilibrium equation

$$\left(V_1^2 + \frac{p_1}{\rho_1} \right) F_1 = \left(V_2^2 + \frac{p_2}{\rho_2} \right) F_2$$

which corresponds to the Bernoulli pressure equation.

If the current tube is curved (Fig. 136b) the forces at both places 1 and 2 will have different directions and the resultant R of the two forces (indicated at point A) shows the effect of the pressure exerted by the curved flow on the adjacent water masses.

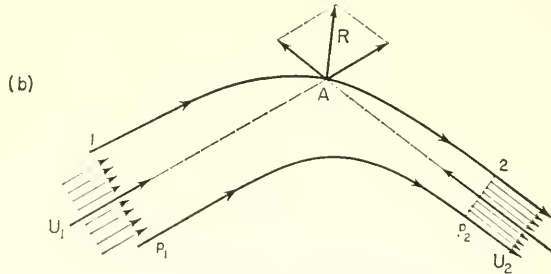


Fig. 136b

By the introduction of the continuity equation, the equations of motion can be put in a form which expresses changes in impulse more clearly (*impulse form of the equation of motion*). Multiplying the continuity equation (X. 23) by u, v, w and adding these expressions respectively to the first, second and third of the equations of motion (without Coriolis force and friction terms, X, Y, Z are the external forces), then

$$\left. \begin{aligned} \frac{\partial \rho u}{\partial t} + \frac{\partial \rho u u}{\partial x} + \frac{\partial \rho u v}{\partial y} + \frac{\partial \rho u w}{\partial z} &= \rho X - \frac{\partial p}{\partial x}, \\ \frac{\partial \rho v}{\partial t} + \frac{\partial \rho v u}{\partial x} + \frac{\partial \rho v v}{\partial y} + \frac{\partial \rho v w}{\partial z} &= \rho Y - \frac{\partial p}{\partial y}, \\ \frac{\partial \rho w}{\partial t} + \frac{\partial \rho w u}{\partial x} + \frac{\partial \rho w v}{\partial y} + \frac{\partial \rho w w}{\partial z} &= \rho Z - \frac{\partial p}{\partial z}. \end{aligned} \right\} \quad (X.38)$$

These show that the changes in the momentum within a volume element can be regarded either as the result of forces acting on the mass contained within the volume element, or as the result of the mass flux passing through the boundary surfaces carrying its own momentum with it.

The impulse-form of the equations of motion (X. 38) can be used with advantage in considerations concerning the internal structure of *turbulent* currents (REYNOLDS, 1894). At any point of a turbulent flow there will be more or less strong variations in the flow velocity. These variations will, however, balance each other completely if on the average the current is steady, and if a sufficiently long period is considered. The velocity components at a given point can then be represented by

$$u = \bar{u} + u', \quad v = \bar{v} + v', \quad w = \bar{w} + w', \quad (X.40)$$

where \bar{u} , \bar{v} , \bar{w} are the mean values of these components and u' , v' , w' are the components of the superimposed turbulent motion for which by definition

$$\bar{u}' = 0, \quad \bar{v}' = 0, \quad \bar{w}' = 0. \quad (\text{X.40})$$

The bar over these symbols indicates mean values considered over a sufficiently long time. It should further be noted that the mean values of the squares and products of u' , v' , w' of course must not necessarily vanish.

If the impulse equations (X. 36) are applied to such a turbulent flow it is not sufficient to consider the equations for the *mean steady flow* alone, since also the turbulent parts of the velocity changes are involved in the relationship between the mean steady current and the forces acting on the masses. This can be derived directly from the impulse theorem. Considering, for example, a part of the "control surface" that is at one time vertical to the x -axis and at another time vertical to the y -axis, then in the first case a mass ρu will pass through a unit area in unit time; the impulse transport due to the x -component u of the velocity is then ρuu and its mean value over a longer period $\rho \overline{uu}$. Now

$$uu = (\bar{u} + u')^2 = \bar{u}^2 + 2\bar{u}u' + u'^2.$$

In deriving the mean value \overline{uu} it should be noted that \bar{u} is already a mean value of u and $\bar{u}' = 0$, so that

$$\rho uu = \overline{\rho u^2} = \rho \overline{u'^2}.$$

To the impulse of the steady mean current a turbulence contribution is added in form of the square of the turbulent variation in velocity, which when inserted in equation (X. 38) has the effect on the mean motion of an *additional pressure*.

Similarly, a mass ρv will pass through unit area of the control surface perpendicular to the y -axis in unit time. The x -component of the impulse transferred through the surface is thus, in this case, ρuv and taking an average gives $\rho \overline{uv}$ per unit time. With

$$\overline{uv} = \overline{u\bar{v}} + \overline{u'v'} + \overline{\bar{u}v'} + \overline{u'\bar{v}'},$$

$$\rho \overline{uv} = \rho \overline{u\bar{v}} + \rho \overline{u'v'}.$$

In addition to the impulse of the steady mean current $\rho \overline{uv}$ must be added a turbulence contribution which in general does not vanish; because positive values of u' are mostly correlated with positive values of v' and *vice versa*, so that the products are preferably positive. In the opposite case the products are mostly negative.

If this turbulent contribution of the impulse transport is transferred to the right-hand side of equations (X. 36) it can be taken as a force acting along the x -axis, which in all cases will be perpendicular to the y -axis. It can therefore also be considered an *apparent shearing stress*

$$\tau = -\rho \overline{u'v'} \quad (\text{X.41})$$

arising from the turbulence of the current and was previously regarded (see pp. 317-319) as an apparent *internal friction*. Equation (X. 41) mediates between this viewpoint and the equation (X. 10) which defines the turbulent viscosity coefficient η .

5. Circulation and Vorticity

The Bjerknæs theorem concerning the formation of vortices and circulation acceleration (1898, 1900, 1901) has been found very useful in the theoretical treatment of

problems arising with oceanic currents. This applies to the dynamics of moving "non-homogeneous" media in which the effects of friction are considered unimportant. This method of treating problems of oceanic movements has the particular advantage that it takes into account the *total effect* of the mass field on the water movements including all their smaller details. It can only be used in its simpler form by neglecting friction; in general, however, at a distance from the boundary surfaces the friction does not change to any large extent the nature of the currents set up by the internal forces.

(a) *Circulation for an Earth at Rest and for a Rotating Earth*

In the presence of (p, α) solenoids, motions are always initiated the nature of which is that of a circulation, i.e., motions following in the most simple case a closed path. In a moving fluid a continuous chain of material elements may lie in a closed curve s . The velocity component of one of these small elements tangential to the curve s shall be V_t . The sum of all these components along the curve s is defined as the *circulation* C of the curve s

$$C = \oint_s V_t ds, \quad (\text{X.42})$$

where ds is a linear element of the curve s . An expression for the change of C in time is easily obtained from the equations of motion (X. 16) (stationary Earth, frictionless motion).

$$\frac{dC}{dt} = \oint_s \left(\frac{du}{dt} dx + \frac{dv}{dt} dy + \frac{dw}{dt} dz \right) = \oint_s \left(X dx + Y dy + Z dz - \oint_s \alpha dp \right). \quad (\text{X.43})$$

Since normally the external forces (gravity) have a potential, the first integral vanishes and the equation becomes

$$\frac{dC}{dt} = - \oint_s \alpha dp = N, \quad (\text{X.44})$$

where N is the number of isobaric-isosteric unit solenoids, enclosed by the curve s (see p. 307 equation (IX. 11)). Assuming that the curve s lies in a plane, then:

- (1) The circulation is constant with time ($dC/dt = 0$) if α is constant over the whole of the space under consideration (homogeneous sea) or if it is a function of pressure. The isobaric and the isosteric surfaces then coincide and the mass distribution is *barotropic*.
- (2) A circulation acceleration will be present if the specific volume is dependent not only on the pressure but also on other properties of the water (temperature, salinity). The mass field is then *baroclinic*. From equation (IX. 12) for a curve s in a dynamic section formed by two vertical lines, the physical sea-level ($p = 0$) and an isobaric line at depth p_1 , the number of solenoids enclosed will be given by the difference in dynamic depths of the isobar p_1 at the two stations. This gives

$$\frac{dC}{dt} = N = D_a - D_b. \quad (\text{X.45})$$

In the two-dimensional case (x, z)

$$\oint \alpha dp = \oint \left(\alpha \frac{\partial p}{\partial x} dx + \alpha \frac{\partial p}{\partial z} dz \right) \tag{X.46}$$

and from Stokes's law it follows that

$$\oint \alpha dp = \iint \left(\frac{\partial \alpha}{\partial x} \frac{\partial p}{\partial z} - \frac{\partial \alpha}{\partial z} \frac{\partial p}{\partial x} \right) dx dz. \tag{X.47}$$

If now ϵ and β are the angles of the ascendent of the pressure $\partial p/\partial n$ and the ascendent of the specific volume $\partial \alpha/\partial n$, respectively, with the x -axis, then

$$\frac{\partial \alpha}{\partial x} = \frac{\partial \alpha}{\partial n} \cos \beta, \quad \frac{\partial \alpha}{\partial z} = \frac{\partial \alpha}{\partial n} \sin \beta,$$

$$\frac{\partial p}{\partial x} = \frac{\partial p}{\partial n} \cos \epsilon, \quad \frac{\partial p}{\partial z} = \frac{\partial p}{\partial n} \sin \epsilon$$

and from equation (X. 47)

$$\oint \alpha dp = \iint \frac{\partial \alpha}{\partial n} \frac{\partial p}{\partial n} \sin (\epsilon - \beta) dx dz \tag{X.48}$$

and

$$\frac{dC}{dt} = - \iint \frac{\partial \alpha}{\partial n} \frac{\partial p}{\partial n} \sin (\epsilon - \beta) dx dz. \tag{X.49}$$

The two possible cases are shown graphically in Fig. 136c. If $\epsilon > \beta$ then the circulation acceleration $dC/dt < 0$ and produces an anticyclonic circulation. If, on the other hand,

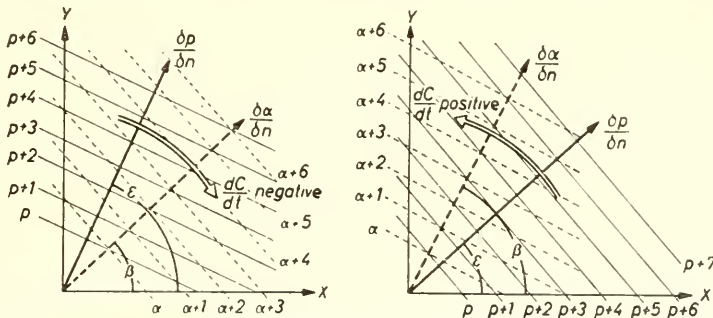


FIG. 136c. Cyclonic and anticyclonic circulation movements for different pressure gradients and specific volumes.

$\epsilon < \beta$ then $dC/dt > 0$ and the resultant movement is cyclonic. In the two cases (see Fig. 136c) the circulation proceeds from the ascendent of pressure to the ascendent of specific volume. In oceanography, as a first approximation, the isobaric surfaces are horizontal, i.e. $\epsilon = 90^\circ$, and thus

$$\frac{dC}{dt} = - \int \frac{g}{\alpha} \frac{\partial \alpha}{\partial n} \cos \beta dz \tag{X.50}$$

A cyclonic circulation is present when $\beta > 90^\circ$ and thus the isosteres decline towards

the left relative to the isobars and an anticyclonic circulation will be present when $\beta < 90^\circ$ and so the isosteres decline to the right.

The circulation theorem gives the change in *absolute* circulation C , i.e. the circulation referred to a co-ordinate system at rest. For oceanographic problems, however, it is the change in the circulation relative to the Earth which is of interest. The absolute velocity V_a referred to a fictitious Earth at rest can always be represented as the sum of the relative velocity V_r relative to the rotating Earth and the velocity V_e of Earth rotation. Thus in the direction of the tangent t to the curve s

$$V_{a,t} = V_{r,t} + V_{e,t}$$

and thus

$$C_a = C_r + C_e. \quad (\text{X.51})$$

The circulation C_e can be calculated. If the curve s lies in the equatorial plane then the velocity V_e for each point on the curve will be ωr where r is its distance from the Earth centre. The component of it coinciding with the direction of the tangent t to the curve s will be given by

$$V_{e,t} = r\omega \cos \beta,$$

where β is the angle between the tangents to the circle r and to the curve s . Thus

$$C_{e,t} = \omega \int_s r \cos \beta ds = 2\omega \int_s \frac{r}{2} \cos \beta ds = 2\omega F, \quad (\text{X.52})$$

where F is the area enclosed by the curve s . If the curve s does not lie in the equatorial plane it can be resolved into its projections on the equatorial plane and on the meridional plane. Since the velocity V_e is perpendicular to the meridional plane it will have no component in the direction of the tangent to the projection of the curve on the meridional plane and its contribution to $C_{e,t}$ will therefore be zero. The contribution of the projection of the curve on the equatorial plane is identical with equation (X.52); F is now the area within the projection of the curve s on the equatorial plane. Thus for the relative circulation acceleration is obtained

$$\frac{dC_r}{dt} = N - 2\omega \frac{dF}{dt}. \quad (\text{X.53})$$

As a first approximation, if the area is not too large, the latitude ϕ is assumed constant and F can be put equal to $F_m \sin \phi$,† where F_m is the area within the projection of the curve s on the sea surface. Thus

$$\frac{dC_r}{dt} = N - 2\omega \sin \phi \frac{dF_m}{dt}. \quad (\text{X.54})$$

The acceleration is made up of two terms; the first is the number N of solenoids enclosed by the curve and acts always in the direction from the ascendent $\partial a / \partial n$ to the

† More exactly

$$\frac{dF}{dt} = \frac{dF_m}{dt} \sin \phi + F_m \cos \phi \frac{d\phi}{dt} = \frac{dF_m}{dt} \sin \phi + F_m \cos \phi \frac{v}{R}.$$

Here v is the south-north velocity; in middle and higher latitudes the second term is insignificant but towards the equator the first vanishes and the second becomes important.

pressure gradient $\partial p/\partial n$ (Fig. 136c); the second represents the product of the Coriolis parameter with the change in time of the projection on the sea surface of the area enclosed by the curve. This term gives rise to a cyclonic circulation for a decrease in the area.

If the vertical stratification of the sea is auto-barotropic (see p. 308) then $N = 0$ and a change of the circulation with time can only be caused by the effect of the Earth's rotation. If a small horizontal layer of water (area F) moves polewards, its projection on the equatorial plane F_m will increase. If $N = 0$ there will be an acceleration in anti-cyclonic circulation according to equation (X. 54). If, on the other hand, it moves towards the equator it will be subject to a cyclonic circulation acceleration. The Bjerknes circulation theorem shows clearly the importance of the baroclinic stratification of the sea for the dynamics of ocean currents. For application see Chap. XV, 5.

(b) *Vorticity for an Earth at Rest and for a Rotating Earth*

A further important quantity in the dynamics of ocean currents is the vorticity. The horizontal area F enclosed by the curve s can be divided by two arbitrary sets of curves into a large number of very small surface elements δF . It can readily be seen that the sum of all the circulations δC , in the same direction along the boundaries of these surface elements δF , is equal to the circulation along the outer boundary s around the entire area F .

Thus

$$C = \int_F \delta C.$$

The limiting value of the ratio $\delta C/\delta F$ is termed the vorticity and is denoted by ζ . It is thus given by

$$\zeta = \lim \frac{\delta C}{\delta F}. \quad (\text{X.55})$$

The vorticity is thus the circulation around a horizontal surface unit and therefore

$$C = \oint (u \, dx + v \, dy) = \iint \zeta \, dx \, dy = \int_F \zeta \, \delta F. \quad (\text{X.56})$$

The circulation around a closed curve s is equal to the integral of the vorticity over the surface F enclosed by the curve s (Stokes's law). This is the two-dimensional case and ζ is thus only the *vertical* component of the total three-dimensional vorticity vector ($\text{curl } \mathbf{V}$).

For a horizontal surface element $\delta_x \delta_y$ (see Fig. 136d), along the boundary (in a positive sense of rotation) of a horizontal surface element

$$\delta C = u \, dx + \left(v + \frac{\partial v}{\partial x} \delta x \right) - \left(u + \frac{\partial u}{\partial y} \delta y \right) - v \, dy = \left(\frac{\partial v}{\partial x} - \frac{\partial u}{\partial y} \right) \delta x \, \delta y \quad (\text{X.57})$$

and from (X. 55)

$$\zeta = \left(\frac{\partial v}{\partial x} - \frac{\partial u}{\partial y} \right) = \text{curl}_z \mathbf{v} = \text{rot}_z \mathbf{v}. \quad (\text{X.58})$$

In the three-dimensional case analogously

$$\xi = \frac{\partial w}{\partial y} - \frac{\partial v}{\partial z}, \quad \eta = \frac{\partial u}{\partial z} - \frac{\partial w}{\partial x}, \quad \zeta = \frac{\partial v}{\partial x} - \frac{\partial u}{\partial y}. \quad (\text{X.59})$$

If the velocity has a potential (see p. 325) the vorticity will vanish and the movement is irrotational (vorticity-free potential current).

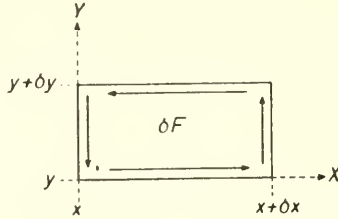


FIG. 136d. Rectangular surface element for the derivation of vorticity.

The vorticity for polar co-ordinates can be derived in a similar way and it can be assumed that the Earth and the co-ordinate system which is rigidly connected with it rotate with constant angular velocity ω . The vorticity is then made up of the vorticity of the rotating Earth and the *relative* vorticity of the water moving relative to the Earth. To derive the vertical component ζ_a of the absolute vorticity it is necessary to consider further a surface element δF formed by the intersection of two latitude circles and two meridians. If the latitudinal difference is $d\phi$ and the longitudinal $d\lambda$, then the total area δF is

$$\delta F = R^2 \cos \phi \, \delta\phi \, \delta\lambda.$$

The zonal velocity along a latitude circle ϕ is $u = R\Omega \cos \phi$, where $\Omega = \omega + d\lambda/dt$. However, along a meridian λ the meridional velocity is $v = R(\partial\phi/\partial t)$ and some simple calculations give for the vertical component of the absolute vorticity

$$\zeta_a = \frac{\delta C}{\delta F} = \frac{1}{\cos \phi} \frac{\delta^2 \phi}{\partial \lambda \partial t} - \frac{1}{\cos \phi} \frac{\partial}{\partial \phi} [\Omega \cos^2 \phi]. \quad (\text{X.57a})$$

For a small water column at rest relative to the Earth $\partial\lambda/\partial t = \partial\phi/\partial t = 0$, $\Omega = \omega$ and the vertical component the vorticity ζ_E of the rotating Earth can be derived from ζ_a as

$$\zeta_E = 2\omega \sin \phi = f, \quad (\text{X.58a})$$

thus equal to the Coriolis parameter.

The relative vorticity ζ of the water movement relative to the Earth (u zonal, positive towards the east; v meridional, positive towards the north) is then

$$\zeta = \zeta_a - f = \frac{1}{R \cos \phi} \frac{\partial v}{\partial \lambda} - \frac{1}{R \cos \phi} \frac{\partial}{\partial \phi} (u \cos \phi). \quad (\text{X.59a})$$

For small oceanic areas in which the latitude can be regarded as approximately constant, equation (X. 59a) reduces to

$$\zeta_a = f + \left(\frac{\partial v}{\partial x} - \frac{\partial u}{\partial y} \right) = f + \zeta. \quad (\text{X.60})$$

The vertical component of the absolute vorticity is thus always equal to the sum of the relative vorticity (vertical component) and the Coriolis parameter.

(c) *Vorticity and the Equations of Motion; Potential Vorticity*

Starting from the horizontal equations of motion (without frictional effects), equation (X. 16) gives

$$\left. \begin{aligned} \frac{du}{dt} - fv &= -\frac{1}{\rho} \frac{\partial p}{\partial x}, \\ \frac{\partial v}{\partial t} + fu &= -\frac{1}{\rho} \frac{\partial p}{\partial y}. \end{aligned} \right\} \quad (\text{X.61})$$

Taking as a first approximation that ρ is independent of x and y or assuming barotropic conditions so that $\rho = \rho(p)$ (a function of pressure only) then, by cross-wise differentiation of these equations and subtraction and simple calculation considering $\partial f/\partial t = 0$ gives

$$\frac{d(\zeta + f)}{dt} + (\zeta + f) \operatorname{div}_H v = 0; \quad \zeta_a = \zeta + f. \quad (\text{X.62})$$

This is the relative vorticity theorem of ROSSBY (1939); it is used for the analysis of stream fields in steady currents and for the analysis of moving oceanic waves.

The total change in the Coriolis parameter with time is

$$\frac{df}{dt} = 2\omega \cos \phi \frac{d\phi}{dt} \quad \text{and since} \quad v = \frac{1}{R} \frac{d\phi}{dt}. \quad (\text{X.63})$$

The theorem of relative vorticity then takes the form

$$\frac{df}{dt} = \frac{2\omega \cos \phi}{R} v = \beta v \quad \text{with} \quad \beta = \frac{2\omega \cos \phi}{R}. \quad (\text{X.64})$$

If the horizontal current (u, v) is non-divergent then equation (X. 62) reduces to

$$\frac{d\zeta}{dt} = -\beta v. \quad (\text{X.65})$$

The quantity $\beta = \partial f/\partial y$ is called the “Rossby parameter” and represents the meridional change in the Coriolis parameter (change with latitude). It is positive in both hemispheres so that the relative vorticity always increases when small elements move southward and decreases when they move northward.

The value of β at different latitudes is shown in the following Table 113.

Table 113.

	90°	75°	60°	45°	30°	15°	0°
$10^{13} \beta \text{ [cm}^{-1} \text{ sec}^{-1}] =$	0.0	0.593	1.145	1.619	1.983	2.212	2.290

In theoretical practice β is usually taken as a constant, that is, as independent of y . This approximation is more or less justified near the equator where β is a maximum

and its change with latitude amounts to only a few per cent. In higher latitudes, however, taking β as constant is only a rough assumption since between 45° and 60° the increase in β is about 29%.

If the current is *non-divergent* then from equation (X. 62) it follows that

$$\frac{d}{dt}(\zeta + f) = 0, \quad \zeta_a = \zeta + f = \text{const.} \quad (\text{X.66})$$

In a non-divergent, barotropic current the vertical component of the *absolute* vorticity is constant and the change in the *relative* vorticity must be compensated by a corresponding displacement in latitude.

To use the vorticity equation for a water mass of thickness h which is variable with both time and space, it is necessary to take the continuity equation for the water layer h into account in addition to (X. 62). For a horizontal current (u, v) it is easy to show that the continuity equation must have the form

$$\frac{\partial h}{\partial t} + \frac{\partial hu}{\partial x} + \frac{\partial hv}{\partial y} = 0 \quad \text{or} \quad \frac{dh}{dt} - h \text{div}_H v = 0. \quad (\text{X.67})$$

Combined with (X. 62) this gives

$$\frac{d}{dt} \left(\frac{\zeta + f}{h} \right) = 0 \quad \text{or} \quad \frac{\zeta + f}{h} = \text{const.} \quad (\text{X.68})$$

It is obvious that the relative vorticity now is variable not only with latitude, but also with the thickness of the water layer under consideration. The value $(\zeta + f)/h$ is thus invariable for a given water mass; it is termed the *potential vorticity*.

Chapter XI

The Ocean at Rest (Statics of the Ocean)

1. The Basic Static Equation and the Conditions for Static Equilibrium

If a water mass in the sea is at rest relative to the Earth, the only external force acting on it will be the conservative force of gravity. In the stationary state its effect is balanced exactly by the resistance of the masses underneath. The elastic force of the substratum is thus opposed by the weight of the water masses and any vertical displacement is extinguished, when both effects are equal (i.e. when the weight of the water masses above any surface is equal to the pressure exerted upwards by the water masses underneath this surface). The condition for internal equilibrium thus requires that no resultant of the gravity and the pressure force should act in the direction of the gravitational level surfaces. A horizontal cross-section through a water column enclosed between two vertical walls will carry a greater weight of water the deeper it is placed. At a depth z it shall be p_1 . At a small distance dz below this there will be a pressure

$$p_2 = p_1 + \frac{\partial p}{\partial z} dz.$$

The increase in pressure $p_2 - p_1$ will be identical with the weight of the water masses per unit area between the two surfaces:

$$p_2 - p_1 = \rho g dz.$$

From these two equations the "basic static equation" is obtained

$$g - \frac{1}{\rho} \frac{\partial p}{\partial z} = 0. \quad (\text{XI.1})$$

Since the negative derivative of the potential Φ with respect to z is equal to the gravitational acceleration, equation (XI. 1) can also be written in the form

$$d\Phi = - \alpha dp. \quad (\text{XI.2})$$

It contains the simplest statement about the three-dimensional fields of potential, mass and pressure in hydrostatic equilibrium. The gradient of the potential is perpendicular to the level surfaces and the pressure gradient is vertical to the isobaric surfaces. Since they have opposite directions the equi-potential surfaces and the isobaric surfaces must coincide if there is hydrostatic equilibrium. The equation (XI. 2) states further that at any point the ratio of the thickness of a thin potential sheet $d\Phi$ to the thickness of a thin isobaric sheet dp will be constant and taken with a negative sign must be numerically identical with the *mean* specific volume in this layer. From this it follows that in the case of static equilibrium the isosteric surfaces must

also coincide with the isobaric surfaces and with the surfaces of equal dynamic depth. If the three-dimensional fields are represented by unit layers then *each isobaric unit layer* is then composed of *several equi-potential unit layers*.

As shown on p. 308 this can also be expressed as follows: In the case of static equilibrium there exists at the same time a state of homotropy between the three-dimensional fields of mass, pressure and potential; the mass field is thus barotropic. Since the specific volume is lawful dependent on the temperature and the salinity the state of a basic equilibrium will also include thermotropy and halotropy.

2. Quasi-static Equilibrium and its Importance in the Dynamic Evaluation of Oceanographic Observations

Hydrostatic equilibrium in the sea occurs only when the water masses are at complete rest. If currents are present the homotropy of the three-dimensional mass, pressure and potential fields will be disturbed and equation (XI. 1) is no more exactly satisfied, since the vertical acceleration has to be taken into account in the third equation of motion (see p. 321). However, the water movements present in the sea are in most cases so weak and are, moreover, almost entirely horizontal, that deviations from static equilibrium will be extremely small. This means that to a close approximation equation (XI. 1) can be regarded as valid, and it has indeed been used to calculate the pressure field (see p. 304) from the mass field given by observation. This fact is of very great importance in oceanography, since it permits the determination of the geophysical oceanic structure along any vertical *without a knowledge of the currents present*.

Over small areas of the sea (a few km²) the deviations from hydrostatic equilibrium can hardly be detected. However, for larger areas of the ocean when the distance between oceanographic stations is greater, the inclination of the surfaces of equal specific volume relative to that of the isobaric surfaces and the inclination of the isobaric surfaces relative to that of equal dynamic depth are clearly evident; the oceanic structure is usually *baroclinic*. In practice, therefore, hydrostatic equilibrium can be assumed for each station as representative of a very small oceanic area and the pressure field can be calculated from the mass field according to the methods already described; however, this apparent static equilibrium changes step-wise in vertical direction from station to station (quasi-stationary state) and the inclination of the equi-scalar surfaces relative to each other manifests itself in this way (Fig. 137).

Rapid estimation of the relative inclinations of the isobaric surfaces in a mass field can be made in a simple way using the equations of equi-scalar fields and the basic hydrostatic equation (SVERDRUP and co-workers, 1946). The isobars and isopycnals in a dynamic section are defined by the equations

$$\frac{\partial p}{\partial x} dx + \frac{\partial p}{\partial y} dy = 0 \quad \text{and} \quad \frac{\partial \rho}{\partial x} dx + \frac{\partial \rho}{\partial y} dy = 0. \quad (\text{XI.3})$$

The inclination of these surfaces is thus

$$i_p = -\frac{\partial p / \partial x}{\partial p / \partial z} \quad \text{and} \quad i_\rho = -\frac{\partial \rho / \partial x}{\partial \rho / \partial z}.$$

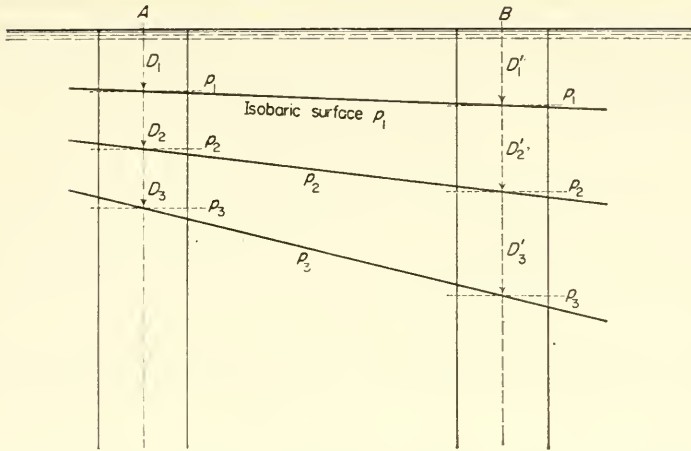


FIG. 137. Quasi-static equilibrium in the ocean, *A* and *B*: two oceanographic stations. At station *A* the pressures p_1, p_2, p_3 , etc., under the assumption of static equilibrium are found at the dynamic depths D_1, D_2, D_3 , etc., on the contrary at station *B* at the dynamic depths D'_1, D'_2, D'_3 etc. From this the inclination of the isobaric surfaces relative to that of the equi-potential surfaces can be deduced for the oceanic space between *A* and *B*.

Taking the hydrostatic equation (XI. 1) gives after some rearrangements

$$\frac{\partial}{\partial z} (\rho i_p) = i_p \frac{\partial \rho}{\partial z}$$

and from this

$$(\rho i_p)_2 - (\rho i_p)_1 = \int_1^2 i_p \frac{\partial \rho}{\partial z} dz.$$

For a dynamic section the integral can be directly evaluated giving

$$(\rho i_p)_2 - (\rho i_p)_1 = \bar{i}_p (\rho_2 - \rho_1), \tag{XI.4}$$

where \bar{i}_p indicates the *mean* inclination of the isopycnals. Introducing a mean value of the density ρ in the thin layer under consideration the inclination of the upper isobaric surface relative to that of the lower ones is obtained

$$i_{p_1} - i_{p_2} = -\bar{i}_p \frac{\rho_2 - \rho_1}{\rho} = \text{approx. } -\bar{i}_\delta (\delta_1 - \delta_2) \tag{XI.5}$$

if the densities are replaced by corresponding anomalies of specific volume. This equation permits the relative inclination of the isobaric surfaces to be readily determined from the distribution of the specific volume anomaly in a dynamic section. It also allows a determination of how closely isobaric and isosteric profiles fit together in dynamic profiles that have been obtained and plotted from oceanographic data.

3. Disturbances and Re-establishment of Static Equilibrium

According to the principle of Archimedes, a stationary water mass will remain floating and at rest within a more extended water mass if its weight is equal to the weight of the displaced water. If it is heavier than the surrounding water it will sink

under influence of a downward force. If it is lighter the corresponding upward force will cause it to rise. The forces initiating vertical displacements can be easily found from the third equation of motion in equation (X. 16). Neglecting Coriolis forces and friction they are given by

$$\frac{dw}{dt} = g - \alpha \frac{\partial p}{\partial z}.$$

If the surrounding water masses are in hydrostatic equilibrium and have a specific volume α' then

$$g - \alpha' \frac{\partial p}{\partial z} = 0.$$

From these two equations it follows that the enclosed water mass will be subject to an acceleration given by

$$\frac{dw}{dt} = g \frac{\alpha' - \alpha}{\alpha'}. \quad (\text{XI.6})$$

The upward or downward forces (buoyance force of Archimedes) is thus proportional to the difference between the specific volumes of the surrounding and the enclosed water masses; for water masses of either the same salinity and with a temperature difference of 10°C or of equal temperature and with 1‰ difference in salinity, the magnitude of this acceleration is about 1 cm sec^{-2} or about one-thousandth of the gravitational acceleration.

The nature of the equilibrium in a water column is dependent on the oceanographic structure and is shown by the acceleration acting on a small quantum after vertical displacement. The vertical equilibrium conditions that may occur in the ocean and the calculation of the vertical stability that characterize these states have been discussed in detail in Pt. I, particularly in Chap. V, 5. p. 196. It seems sufficient to refer here only to the previous statements.

In a system where there are no forces acting other than gravitational acceleration and the internal forces, a dynamic vertical section showing isobars and isosteres allows an immediate estimation of the direction of the water currents produced by the resultant forces due to density differences. Part of such a section is given in Fig. 138; the isobars can be regarded as horizontal and the inclination of the isosteres

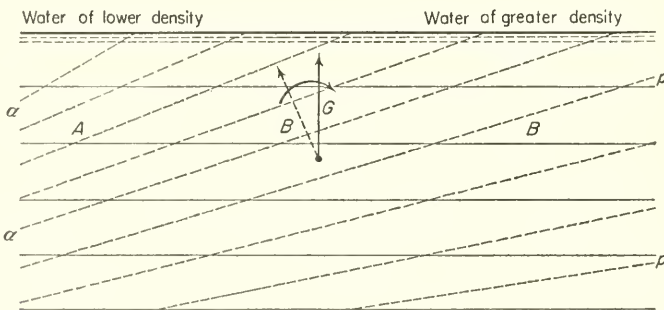


FIG. 138. Dynamic vertical cross-section: p , isobaric; α , isosteric surfaces. Disturbed equilibrium and return to equilibrium state.

relative to them show that the system is not in static equilibrium (disturbed equilibrium). The water at A is lighter than that at B in the same isobaric level, so that to establish hydrostatic equilibrium the water mass at A must rise and that at B must sink. The forces indicated by the mass distribution (solenoids) show a *rotational movement* (circulation) which tends to adjust the mass distribution closer to that of static equilibrium. In the final state the isobars must run parallel to the isosteres; a barotropic mass field is then established out from a baroclinic one. The direction of the circulation set up is given by the rule that it always proceeds along the *shortest path* from the mobility vector $B(\partial a/\partial n)$ to the pressure gradient $G(\partial p/\partial n)$ (Fig. 138). The strength of the forces and the intensity of the resultant circulation have been discussed in II/5; see Fig. 136c. A more convenient method of characterizing the nature of the equilibrium is by comparison of the piezotropy coefficient of the density γ_ρ with the barotropy coefficient Γ_ρ (see p. 308). The first determines the behaviour of an *individual* small element on changes in pressure (depth), while the second characterizes the state of a water mass in vertical direction. If $\Gamma_\rho = \gamma_\rho$ then the mass field is not affected by an interchange of any two small elements. In autobarotropism the equilibrium condition is thus indifferent (neutral), for $\Gamma_\rho > \gamma_\rho$ it will be stable and for $\Gamma_\rho < \gamma_\rho$ it will be unstable. Since in the first case the density differences set up by vertical displacements will tend to return the displaced elements to their initial positions, while in the second, on the other hand, they will tend to displace them further and further from it. Rhythmic (periodic) circulatory movements may be set up in this way, but in the sea, according to their nature, they can hardly persist for very long since the energy of these movements will soon be dissipated by turbulence (Inertia oscillations, see Chap. XIII, 6.

Chapter XII

The Representation of Oceanic Movements and Kinematics

1. Methods of Observation and Measurement of Oceanographic Currents

Two different methods can be used to determine the nature of the currents in the sea. One follows the Lagrange approach and investigates the track which a small element of water follows in time. This gives the *trajectory* of the water movement from the sequence of points in space through which the water element passes. The other method using an approach closer to that of Euler considers the current from a fixed point, and shows the nature of the current at a fixed point at any particular moment in terms of the current vector, which is variable with time. Graphic representation of the distribution of velocity in space by lines of equal intensity (*isotachs*, *velocity field*), or by representing the directional field by means of *stream lines* (see p. 326). The stream lines and the velocity field fix the *current* field at any particular instant.

The trajectories and stream lines must be carefully distinguished; they will coincide only in the case of a steady current and here the stream line will also be the same as the trajectory taken by a small water element.

(a) *Drift Bottles and Drifting Objects*

A more or less accurate indication of the direction and velocity of water currents can be obtained by following the drift of objects of all sorts which may temporarily or permanently be floating in the water, whether through chance or through having been placed there deliberately by man (KRÜMMEL, 1908). It is essential that these drifting bodies should project as little as possible out of the water so as to minimize the important influence of wind and waves on their displacements.

The course followed by drifting bodies of this sort, which are subject only to the effect of the currents, gives the trajectories of the water movement. Floating bodies put into the sea especially for this purpose may also be used (*drift bottle*, *bottle post*). On account of their cheapness and simple handling drift bottles have been frequently used, and with systematic and methodical work can give useful results. Since the path followed by a drift bottle depends to a considerable extent on chance, unambiguous results are given only by systematic work and by the use and recovery of a large number of such bottles. Large-scale experiments of this type have been made by Prince ALBERT I OF MONACO (1889) in the eastern North Atlantic, by FULTON (1897) in the North Sea and more recently, with particular success, by CARRUTHERS (1954) in the southern part of the North Sea and the English Channel.

The ordinary drift bottles usually give only the starting position and the place of

recovery of the bottle; an approximate mean value for the velocity of the current can be calculated from the path which the bottle is presumed to have taken and the interval between the two times. Large errors may occur in both these numerical values. These circumstances have brought the method into disrepute, but as shown by the results of CARRUTHERS and TAIT (1930) with the use of care and frequent repetition it may still give a good idea about the system of currents over small areas of the sea. See THORADE (1933*a*) for further details.

More accurate knowledge of the course of the currents can be obtained by following the course of the drifting body directly by means of continuous triangular measurement from three fixed points. KRÜGER (1911) and SCHULZ (1925) have used this method for the investigation of the currents in the Jade near Wangeroog and off the Flemish coast and have obtained valuable results.

(b) *Calculated Displacement*

The method of determining the course of the currents at the surface of the ocean most used in practice depends on the comparison of an astronomical position with a position given "by dead reckoning". The first gives the *true position of the ship* found by astronomical observations and the latter gives the position of the ship as calculated from the course steered by the ship and its speed, taking the wind-drift of the vessel into account, and the distance covered according to the log (the position by dead reckoning). Usually this does not coincide with the astronomical position of the ship, since it has been calculated from the apparent speed of the ship in the water. The difference between the two positions is called the ship's displacement and is considered to be due to currents in the time interval between successive positions (usually determined at noon). For example, a ship with a noon position $52^{\circ} 25' N., 42^{\circ} 16' W.$ (Fig. 139, point *A*) has travelled 225 nautical miles in the water in the direction $S. 35^{\circ} W.$ by the following noon. The triangle AA_2C gives the difference in latitude between *A* and the position by dead reckoning $A_2 = AC = 184$ nautical miles = 184 minutes of latitude. The difference in longitude A_2C is 129 nautical miles. Division by the cosine of the mean latitude gives the difference in longitude in arc minutes as $3^{\circ} 24'$, while the difference in latitude is $3^{\circ} 4'$. The position by dead reckoning at point A_2 is thus: $49^{\circ} 21' N., 45^{\circ} 40' W.$ Astronomical observation, however, gave $49^{\circ} 44' N., 46^{\circ} 22' W.$ Thus

$$\phi_1 = 49^{\circ} 44', \quad \phi_2 = 49^{\circ} 21', \quad \Delta\phi = 23', \quad A_1B = 23 \text{ nautical miles};$$

$$\lambda_1 = 46^{\circ} 22', \quad \lambda_2 = 45^{\circ} 40', \quad \Delta\lambda = 42', \quad A_2B = 42' \cos 49^{\circ} 32' = 27 \text{ nautical miles.}$$

From these values the drift A_1A_2 is 35.6 nautical miles and $\gamma = 49^{\circ} 47'$; it is thus $N. 50^{\circ} W., 36$ nautical miles. The calculation can be considerably shortened by the use of numerical or graphical tables.

Usually the ship displacement is regarded as the effect of an ocean current, so that *displacement = current*. This is not entirely correct, since the drift includes all the errors which have been made during the calculation of the position by dead reckoning and during the astronomical determination of the position (see MEYER, 1923). It can fairly safely be assumed that all the errors in both determinations are due mainly to chance; thus the mean of a sufficiently large number of displacement values at

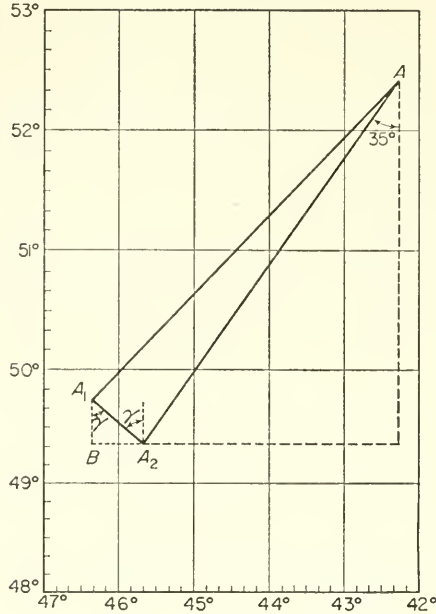


FIG. 139. Drift method for the determination of surface currents by the difference between the astronomical position and the position according to dead reckoning. Ship's displacement: A , position at noon of the previous day; A_1 , astronomical position; A_2 , position according to dead reckoning; A_2A_1 , ship's displacement; BA_1 , difference in latitude; BA_2 , difference in longitude.

any point will therefore give the *true mean current* at that point. However, this of course will only apply when the current is more or less a steady one.

(c) Current Measurements

Ship displacements give only the mean values of the currents over 24 h. If the instantaneous value of the current or a *continuous* record at one position is required then current measurements will be necessary. These will give the direction and strength of the current, both at the surface and also in layers beneath it. For measurements of this type at any point a *fixed reference-position* is needed. It is thus necessary to anchor the vessel from which the observations are to be made. In shallow waters this offers no difficulty but at great depths the difficulties increase considerably and a special technique and anchoring equipment are required.

If the vessel is firmly anchored and the anchor holds it is not necessarily a fixed reference-point from which current measurements can be made directly without more ado. Any ship anchored with a long cable will be subject to movements due to the changes in the wind and the current, and these movements can have considerable effect on the current measurements made from the vessel. Three types of ships' movements can be distinguished (DEFANT, 1932, p. 7). The first two types, *swinging round* (Schwoien) and *swinging* (Schwingen) are shown by changes in the heading of the ship with time and can be determined by continual readings of the ship's compass.

“Swinging round” is the oscillation of the ship with the cable about a certain point which in the extreme case will coincide with the fixed end position of the cable at the sea bottom. Between one position of the vessel at A to another at B there will be a change in angle γ corresponding to a change in the course of the vessel from β to α or *vice versa*. If the twisting forces of the wind and the current acting on the ship are in equilibrium the position of the vessel will be stationary for a constant heading. If, however, there is a change in these forces the position of the ship will alter and it will tend towards a new equilibrium position. Thus, for example, if the wind conditions are constant a periodic tidal current will move the vessel from a position A to B and back again in about 6 moon hours. If the combined length of the cable and the length of the vessel until the suspension point of the cable and the length of the vessel to the suspension of the current meter is projected on the sea surface, then the length of this projection is denoted by r . Since

$$\overline{AB} = r\gamma \frac{\pi}{180^\circ},$$

for r 500, 1000, 2000 m and $\gamma = 20^\circ$ the velocity v of the vessel will be $v = 0.8, 1.6, 3.2$ cm/sec. These speeds are thus rather small provided the swinging round period is sufficiently long and will scarcely cause errors of any importance in the current measurement. The current meter is displaced from A to B during such a movement and will thus simulate a current from B to A which will be superimposed on the actual current in current measurements. “Swinging” (Schwingen) can be regarded as an extreme case of swinging round. The centre of the swing is shifted to the point where the anchor cable is attached to the bow of the vessel. These oscillations will be recognizable from the occurrence of a cable azimuth. In swinging movements with a period of about an hour, the simulated current velocity will remain small also for large values of γ due to the small distance r ($\gamma = 60^\circ, r = 60$ m, $v = 1.7$ cm/sec), but when the period becomes short errors will increase so strongly that the current measurements will be unusable ($\gamma = 60^\circ, r = 60$ m, period = 10 min, $v = 10.5$ cm/sec). However, an instrument suspended at a certain depth (such as a very long and strongly damped pendulum) will react to the movement of the vessel and it is improbable that it will behave very differently from the vessel. If the period of the current meter plus the suspension wire and the swinging period of the ship are very different then the current recorder at a deeper level will be unable to follow the movements of the vessel and the measurements will give good results. If, however, the period of the entire system is of the same order of magnitude as the swinging period there may be rather large displacements of the current meter and the measurements will be erroneous. (Examples are given by DEFANT, 1932; DEFANT and SCHUBERT, 1934.)

The third type of ship movement is *yawing* (Gieren). The pull of the cable and the forces acting on the vessel (wind and current) keep the ship in an equilibrium position. If there is a change in the wind or the current the vessel will be displaced into a new equilibrium position whereupon the cable will either tighten or slacken. Thereby, the heading of the vessel will not change, but the angle between the cable at the bow of the vessel and the vertical will be altered. However, at a deep anchorage the change in this angle will be small, since the upper part of the cable will almost always be approximately vertical. The displacements of the vessel due to yawing may be considerable

and may be unpleasantly noticeable in the current recordings, even when the yawing movements are unnoticed in the open ocean. Only careful determination of the position will allow a decision to be made regarding the extent to which the movement of the vessel due to yawing has affected the recordings.

An excellent example of yawing movements was obtained at the "Meteor" anchor station 228 in the strong North Equatorial Current and the intensive north-east trade-wind. Figure 140 shows that there was a "freedom in the yawing movement" of 2473 m and the mean position of the ship was at a distance of 2760 m from the anchor point when projected on the sea surface. Since while the vessel was anchored, the direction of the wind was hardly varied and since there was a strong basic current (22 cm/sec), and a wind force of 5-6 Beaufort, the weak tidal currents could hardly move the vessel from its main position and the movement of the vessel must have been due to yawing. Actually as shown in Fig. 141 which gives the positions of the vessel determined astronomically while at anchor, there were almost only yawing movements. It can be seen that all factors (heading of the vessel, position, etc.) fit excellently to give a very plausible representation of the movements of the vessel while anchored (see also DEFANT, 1940a).

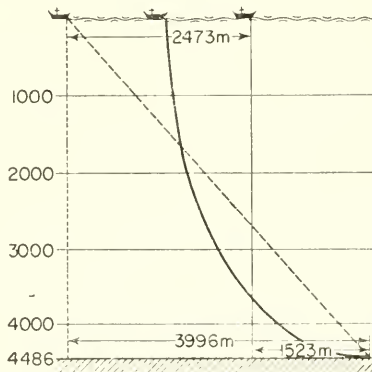


FIG. 140. Anchor station 288 of the "Meteor": water depth 4486 m, length of cable 6003 m, freedom for yawing 2473 m, anchor position—mean position of the ship 2760 m.

Since a really fixed point is scarcely obtainable in the open ocean at great depths, methods have been devised for the elimination of errors that occur for this reason in current measurements. WITTING (1930); THORADE (1933a) have reviewed the three methods so far used to replace the absolute method using a fixed point.

The *correction method* consists essentially of a careful observation of changes in the position of the ship relative to that of a buoy anchored by the shortest possible cable and in the correction of the current recordings by use of these observations. WITTING (1905) has given a procedure for calculation using numerical and graphical methods, but due to the complexity of the observations and the difficulty of evaluation of the measurements it has seldom been used. In the *difference method* the vessel is not anchored to the bottom but is kept stationary with a driving anchor; the current recorder then gives only the movements of the water relative to the ship. To find the true current it is necessary to know the absolute current at one of the depths investigated. NANSEN (1915) and later HELLAND-HANSEN (1926), for want of other possibilities, used a second current recorder close to the sea bottom, or as deep as possible, and assumed that the water here would be almost motionless. For current measurements in the ice drift off the North Siberian Shelf SVERDRUP (1929) on the "Maud"

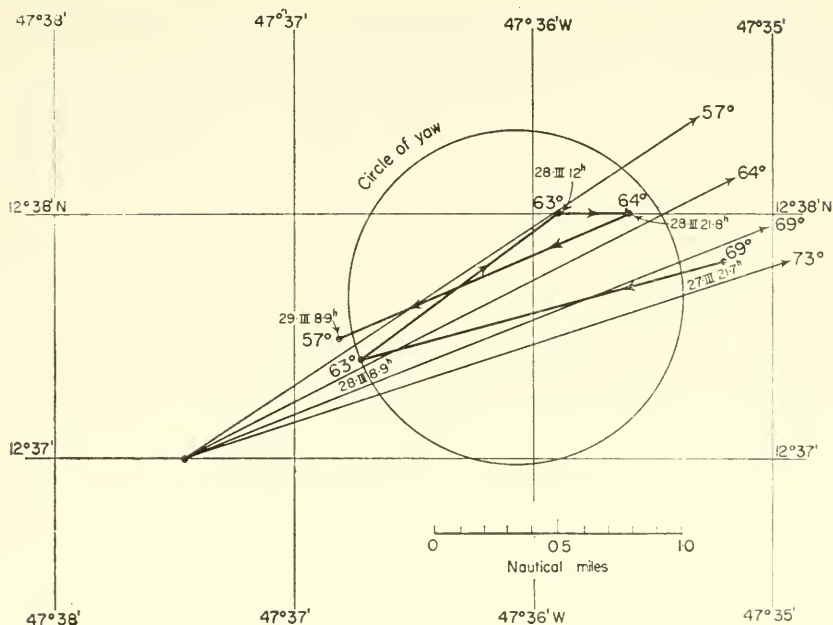


FIG. 141. Successive positions of the ship, ship's course and circle of yaw at the anchor station 288 of the "Meteor", 27-29 March 1927.

Ship's positions:

27.iii.	21.45 MGZ:	12° 37·8' N.;	47° 35·2' W.
28.iii.	08.54 MGZ:	12° 37·4' N.;	47° (36·7' W.)†
28.iii.	12.00 MGZ:	12° 38·0' N.;	47° 35·9' W.
28.iii.	21.47 MGZ:	12° 38·0' N.;	47° 35·6' W.
29.iii.	08.55 MGZ:	12° 37·5' N.;	47° 36·8' W.

† The computed longitude of 47° 37·7' W. is very probably an error; 36·7' W. should be the correct value.

modified the method by using a sounding line to obtain a fixed point at the sea bottom, but this can only be used in very shallow waters.

According to Witting, the best, fastest and also the most frequently used method is the "smoothing method". The current measurements are made from an anchored vessel at the shortest possible intervals and values for a time interval over which the different movements of the ship almost cancel out are combined to give a *mean value*. An interval of about 15-30 min seems to be sufficient to eliminate the variations due to the movements of the ship and irregular changes in the current direction and speed.

(d) The Scientific Use of Current Measurements

The technical refinements of the operative mechanism of the amazingly large number of current recorders used in oceanography need not be discussed here; reference can be made to THORADE (1938a), SVERDRUP and co-workers (1946) and particularly to *Oceanographic Instrumentation* ISAACS and ISELIN, 1952). However, the important subject of the scientific use of current measurements will be dealt with here in greater detail.

The individual values obtained from current measurements as discussed above will contain errors due to the simultaneous movement of the vessel, and correction to the true current can only be made if the movement of the ship is known with some accuracy. Since for current measurements in the open ocean only one current meter records on board ship, the correction method of determining the true current cannot usually be used. If the average true current changes only slowly, the *smoothing method* of eliminating short period movements of the vessel must be applied. How strongly the observations have to be smoothed has been shown by THORADE (1934) with observations made by the research vessel "Poseidon" in the Kattegat (August, 1931). The Rauschelbach current meter was used here to give continuous records of the current every 10 sec over a long period. Plotting all these current vectors starting from a single zero point of an appropriate co-ordinate system gives a current diagram of the type shown in Fig. 142. The individual current vectors are strongly scattering and

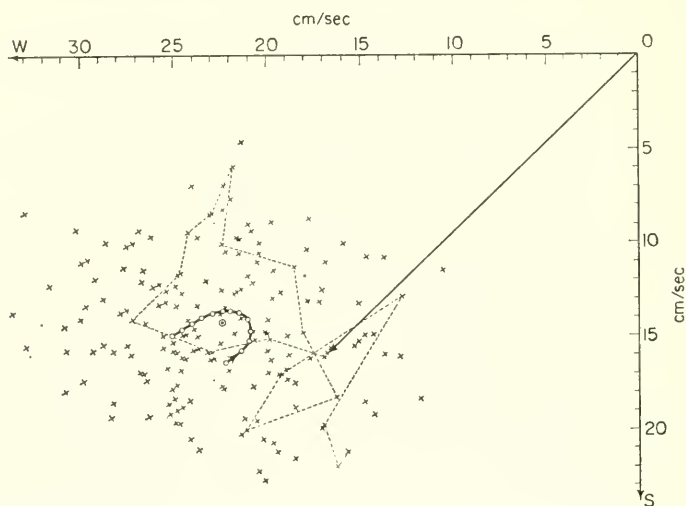


FIG. 142. Recordings of the Rauschelbach current meter at the anchor station of the "Poseidon" in the southern Kattegat during $\frac{1}{2}$ h for each 10 sec. (10 August 1931; 18.30–19.30 h). The current arrows must be drawn from the point O towards the crosses. The indicated arrow refers to the start of the observations. The dotted line shows the movement of the arrowhead during the following 3 min. The dashed-dotted line indicates the position of the arrowhead after smoothing, the point \odot shows the mean position during the $\frac{1}{2}$ h.

their end-points form a point cloud covering a relatively large area. It can hardly be assumed by the values given in the diagram that the true current has altered significantly within the half-hour observational time. The dashed line joins the end-points of the vectors for the first three minutes. Even for this short interval the vectors cover almost the entire area of the point cloud. This shows that single *current measurements made from an anchored vessel differing widely in the observation time are more or less worthless*. It is rather different, however, if for short observation intervals mean values are taken for more or less long intervals in time. Fig. 143 shows that for the same values as in Fig. 142 the individual means for each minute are rather scattered, but the means for intervals of 5 min, on the other hand, show only small variations during the half

hour. These findings by Thorade indicate that the effect of the movements of the vessel from which the measurements are made and other chance factors can be eliminated by such a smoothing procedure. Instead of using continuous recordings of the current followed by calculation of the mean over a long interval such equipment is used in practice which gives directly mean values for the direction and velocity over

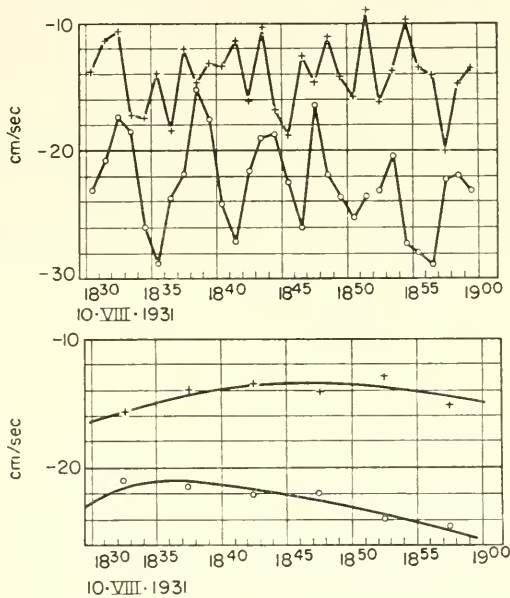


FIG. 143. Upper picture: mean for each minute; lower picture: mean for each 5 min of the north (— + — + —) and the east component (—○—○—) of the current measured from the "Poseidon" (see Fig. 142).

a longer interval (10 min or more). In deriving the means it should be remembered that they are vectors and in order to reduce them to mean values they must be resolved into north and east components. The mean obtained in this way is denoted the *vectorial mean*. Instead of this mean, which is mathematically accurate but inconvenient to calculate, the mean of all the velocities regardless of the direction is often used instead. This is termed a *scalar mean* of the velocity, and it represents the average velocity of the water displacement. The corresponding simple arithmetic mean of the angle of the flow direction is of no importance especially when the variations in the direction are large.

In the characterization of extensive current measurements a further quantity is used to give a numerical value for the *variations* in direction and speed of the current. The quotient of the vectorial velocity mean and the scalar mean is used for this and is termed the *constancy* (stability) of the current (*Kgl. Ned. Med. Inst. DE BILT, 1904, 1908*). From the definition of the two kinds of averages it follows that the stability is always a proper fraction. It has the value 1 if the directions of the individual vectors are always the same size, since the vectorial mean is then the same as the scalar. The *current constancy* is usually expressed as a percentage.

The magnitude of the current constancy is only affected to any large extent by variations in the direction of the flow, variations in the velocity have little influence. WAGNER (1932) has found, for example, that if the velocity was assumed to be the same for the individual values and the directions were scattered within an angle of 90° , then the stability was 90–100%, while if the directions were scattered within 180° the current stability was still 60–90%; individual values with greater velocities could, however, affect these stability values strongly in either direction.

A more accurate description of the distribution of a larger number of observations requires the use of statistical theory (THORADE, 1936). If the measured velocities of the current are $w_1, w_2, w_3, \dots, w_n$ for n -observations and $\alpha_1, \alpha_2, \alpha_3, \dots, \alpha_n$ are the corresponding directions (taken clockwise from north from 0° to 360°) then the corresponding E -components will be $u_i = w_i \sin \alpha_i$ and the N -components will be $v_i = w_i \cos \alpha_i$, where $i = 1, 2, \dots, n$. The arithmetic mean of the E -components will be \bar{u} , and that of the N -components \bar{v} ; then the vectorial velocity is

$$w_v^2 = \bar{u}^2 + \bar{v}^2$$

and the vectorial mean direction will be

$$\tan \alpha_v = \frac{\bar{u}}{\bar{v}}.$$

The deviations of the individual values from the vectorial mean are

$$\epsilon_i = u_i - \bar{u} \quad \text{and} \quad \eta_i = v_i - \bar{v}.$$

Comparison of the frequency distribution with a Gaussian distribution will then allow us to judge whether the deviations are generally random, so that statistical laws are applicable.

The mean scatter of the u_i - and v_i -values is then given by the mean error (standard deviation)

$$m_u^2 = \overline{\epsilon^2} \quad \text{and} \quad m_v^2 = \overline{\eta^2}.$$

For a case similar to that of Fig. 142 (150 observations over an interval of 10 sec) Thorade found a point distribution given in Fig. 144 for the frequencies of the deviations for intervals of 1 cm/sec; the curves show a Gaussian distribution indicating the completely random nature of the deviations, and show that in spite of the small number of observations the deviations approximate very closely to a random distribution. In this way, the direction varies between 270° and 318° and the velocities between 7.4 cm/sec and 21.8 cm/sec. The vectorial mean gave a current N. 66° W., 14.5 cm/sec, the scalar mean was 14.7 cm/sec, and the current constancy (stability) was therefore 98.6%; in spite of the rather large variations in direction and speed of the current this is a surprisingly high current stability value. The mean scatter gave a considerably better idea of these variations: $m_u = \pm 2.68$, $m_v = \pm 2.64$ cm/sec, which indicates that for a random distribution of the deviations about 68% of all the deviations ϵ_i of the E -component lie between $+2.68$ cm/sec and -2.68 cm/sec; analogous conditions apply for the η_i for the N -component.

According to statistical theory of scattering, the direction and velocity can be characterized most accurately by the "mean error ellipse" which must include half of all the individual values. Considerable numerical work is required for calculating this

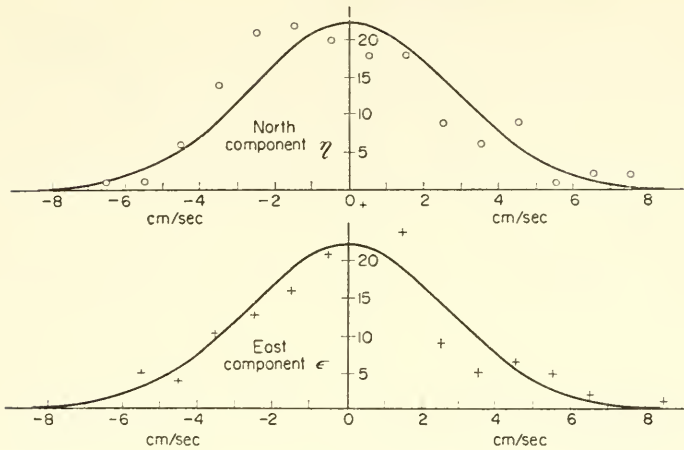


FIG. 144. Frequency distribution of scattering of the north and east component ϵ and η for the point cloud of the current measurements of Fig. 142 (the full lines indicate the Gaussian frequency distribution).

ellipse. In place of it Thorade used the *scatter circle* the radius of which is given simply by $\rho^2 = m_u^2 + m_v^2$. This circle is quite sufficient for the characterization of the scatter of a point cloud of current values. The probability that an observation will fall within the scatter circle is with sufficient accuracy about $2/3$, that is, about $2/3$ of all observed values will fall within the scatter circle. In the case previously mentioned (see Fig. 143). $\rho = 3.76$ cm/sec; the actual number falling within the scatter circle is 103 of the 150 values, which is about $2/3$.

Elimination of periodic components. The variations in speed and direction of ocean currents often include periodic components superimposed on the mean current (*the basic current*). The basic current because it is often obtained by elimination of the periodic components is therefore sometimes rather unsuitably called “residual current”.

The basic current need usually not to be constant either in direction or velocity, but these changes are mostly *aperiodic* and of long duration and therefore differ considerably from the periodic components. The presence of these components is shown particularly well by graphical representation of the individual vectors in a progressive vector diagram. A constant basic current plotted in this way will give a straight line, while a wavy or spiral trajectory indicates the presence of periodic components. Figure 145 shows a case of this type. Generally a water transport occurs directed towards west-south-west, but it is not uniform and shows wavy fluctuations to the north and the south (period of these oscillations about 14–15 h).

The periodic components can be eliminated by taking a mean over the periods present; the periodic components then cancel out giving the average basic current. Thus, the case of Fig. 145 gives a mean displacement over the entire period of 2.0 nautical miles towards the south and 7.5 nautical miles to the west in 24 h or a basic current of W. 15° S., 16.7 cm/sec.

The calculation process for such a separation of observed current values, taken over a long interval into the basic current, and the periodic components can be illustrated

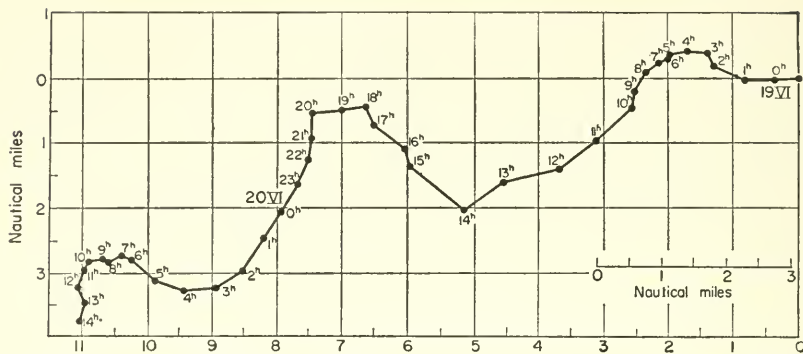


FIG. 145. Anchor station of the "Altair": path of a water particle from 19 June 1938 00.00 to 20 June 1938 14.14 MGZ. (Represented by a successive plotting of the observed current values† as a mean between the depth 5 and 15 m). Mean basic current from 19.00 to 20.00 MGZ: north component: -4.5 ; east component: $-16.1 = W. 15^{\circ} S., 16.7$ cm/sec.

† In order to simplify the numbers indicated at each individual point are values rounded off to total hours. Therefore n h is always $(n - 1)$ h 48 m, for example, 3 h = 2 h 48 m.

by an example. The method given below is mostly used but each case requires individual treatment. At the "Meteor" anchor station, 16–20 June 1938 ($44^{\circ} 33' N., 35^{\circ} 58' W.$, mean depth about 1400 m) the current values were measured for a single interval of 10 min in each hour at eight depths (DEFANT, 1940*b*). Figure 146 contains unsmoothed values for the N - and E -components at 5 and 15 m depth for the period from 17 June, 04.00 h to 19 June, 18.00 h (MGZ).

This gave a rather irregular, jagged curve, partly because of chance disturbances and partly because of errors in the measurement. Since the tidal currents were expected to be rather strong these were then eliminated by taking continuous means over 24 lunar hours (from one moon culmination to the next). The smoothing showed

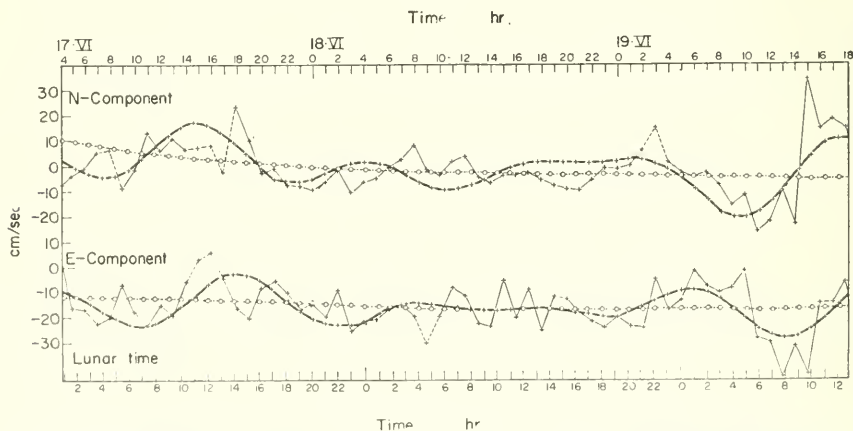


FIG. 146. Current components at the anchor station of the "Altair" June 1938 ($\phi = 44^{\circ} 33' N., \lambda = 33^{\circ} 58' W.$). —|—|—|—|—, N . and E . components according to the observation; -- o -- o --, basic current after elimination of the periodic parts (tidal current and inertia current); -- + -- + --, basic current + tidal current of the diurnal and semi-diurnal wave + current of the inertia wave (according to the values of the harmonic analysis).

in the present case that the remaining current was indeed very regular but still included a weak periodic disturbance of about 17 h. Since it was not improbable that a wave of this type could occur in such current measurements (inertia oscillation) this wave was also eliminated by taking means again over a 17 h period.* Finally, the basic current remains. It has been plotted in Fig. 146 for both components. It changes only slightly with time; the *N*-component gradually decreases from 10 to about -4 cm/sec and then remains almost constant, the *E*-component changes from -12 to -17 cm/sec.

A more detailed analysis of the periodic components can be made by ordinary *harmonic analysis* and gives the following equations (*t* in hours):

$$N\text{-component: } +6.6 \cos \frac{2\pi}{24}(t - 17.6 \text{ h}) + 4.6 \cos \frac{2\pi}{12}(t - 2.3 \text{ h}) \\ + 6.0 \cos \frac{2\pi}{17}(t - 12.6 \text{ h}).$$

$$S\text{-component: } +2.7 \cos \frac{2\pi}{24}(t - 20.4 \text{ h}) + 3.8 \cos \frac{2\pi}{12}(t - 5.2 \text{ h}) \\ + 5.3 \cos \frac{2\pi}{17}(t - 0.0 \text{ h}).$$

The time $t = 0$ corresponds thereby rather accurately to 3 moon hours before the moon passes the meridian at Greenwich (17 June, 1938). The amplitudes are given in cm/sec. All three waves show almost the same amplitude; the inertia wave also is quite pronounced and, as can be expected from this, can become quite visible in the current. Calculations of the current from both components obtained by the harmonic analysis, and in addition the basic current of the curves presented in Fig. 146, follow the observed values very satisfactorily. However, the differences between the smoothed curves and the observations show that the current measurement is subject to manifold disturbances which are very largely random (or observational errors).

From the smoothed mean values for a full period of the single waves *current diagrams* can be constructed and can be compared with the current ellipses which were calculated from the harmonic values. The left-hand side of Fig. 147 shows this comparison for the semidiurnal tide and on the right-hand side for the 17 h inertia wave. The smoothing of the subsequent values by harmonic analysis is rather obvious

* For a curve *y* formed by the superposition of two harmonic waves of different periods T_1 and T_2 which has the form

$$y = a \cos \frac{2\pi}{T_1}(t - \epsilon_1) + b \cos \frac{2\pi}{T_2}(t - \epsilon_2)$$

if a continuous mean is taken over the period T_2 the T_2 -wave will disappear completely and there will be left

$$y^1 = \frac{1}{T_2} \int_{t - \frac{1}{2}T_2}^{t + \frac{1}{2}T_2} y \, dt = a \frac{T_1}{\pi T_2} \sin \frac{2\pi T_2}{T_1} \cos \frac{2\pi}{T_1}(t - \epsilon_1).$$

The amplitude is changed, but not the period and the phase of the T_1 wave. If T_1 is 17 h and T_2 is 24 h then the amplitude of the 17 h wave which was previously *a* will now be $-0.22a$, that is, the T_1 -wave is now inverse to the original wave and its amplitude is almost five times less than before.

in both cases. Reference should be made to Vol. II for further discussion of these current diagrams. It may be mentioned here that the components, phases and amplitudes of the inertia waves correspond closely to those given by the theory of oscillations (see Chap. XIII, 6). Since the current diagram deviates only slightly from a circle (the fine dashed circle in Fig. 147); for this the amplitudes of both components must be

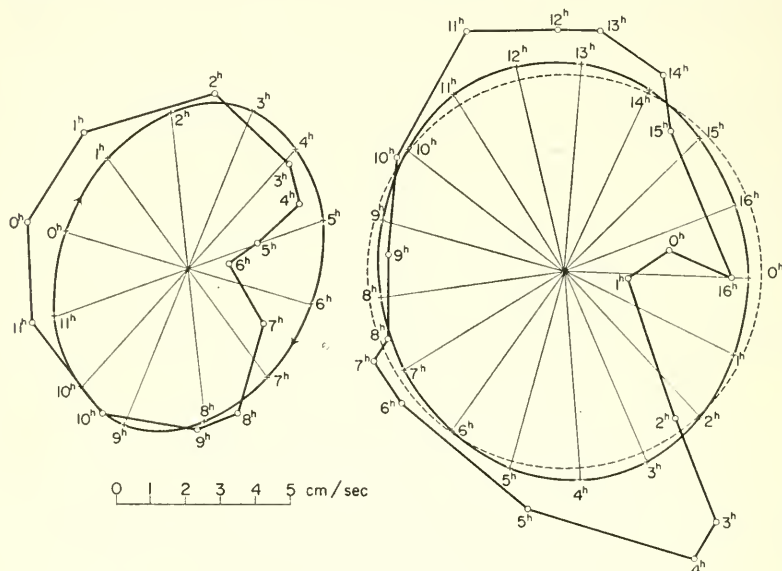


FIG. 147. Current measurements at the anchor station of the "Altair", 16-20 June 1938. Left side: current card of the semi-diurnal tide according to the smoothed values of the individual hours and the current ellipse according to the values of the harmonic analysis. Right side: the same for the 17-hourly inertia wave (the dashed circle indicates the theoretical inertia circle).

the same, and furthermore, the phase of the *E*-component must lag one-quarter of a period behind that of the *N*-component. The observations give an amplitude ratio of 1.14 and $12.6 \text{ h} + 4.25 \text{ h} = 16.85 \text{ h}$ as compared with 17.0 h which is a difference of only 0.15 h . These properties of the 17 h wave confirm that it is a pure inertia wave.

Decomposition of current data by means of other methods. After the elimination of the periodic components there still remain other more *aperiodic* effects superimposed on the basic current, which is almost constant in time. These deviations may be due to various causes such as piling up of water at shores (Anstau) or variable wind stress. The wind especially is liable to give rise to drift currents in the surface layers, the direction and strength of which depend on that of the wind and change with it. The observed current in these cases can be looked upon as the resultant of the drift current and the basic current. If the latter alone is required the two must be separated by a special procedure. NANSEN (1902) gave a suitable method for this which was used in the evaluation of the ice-drift observations of the "Fram". If intervals of time, for which the wind resultant is zero, are taken together and the effect of the wind on the water therefore considered very small, then the resultant current for the total interval will be due to the basic current alone. In that way he found by analysis of six rather

typical cases that the permanent current of the deep North Polar Basin flows first at 1.0 cm/sec N. 64° W. and later at 2.1 cm/sec S. 12° W. BRENNER (1921) and SVERDRUP (1928, 1931*b*) later used the same method to show from the ice-drift observations of the "Deutschland" and the "Maud" that there is no permanent surface current in either the Weddel Sea or off the North Siberian Shelf.

Later, Sverdrup developed another method that makes use of all the available wind and current observations. The vectorial resultant of the current is calculated for wind groups concerning certain directions (for example, four groups with the wind for each quadrant centred on N., E., S. and W.) and divided by the wind strength of each group to give the "relative" resultant current (for 1 m/sec wind). If a pure drift current is present then the resultant of the current vectors of all the wind groups must vanish, since they will be symmetrically grouped around the zero point. If, however, the observed current is made up of wind drift + basic current, the resultant of all the groups will not be zero but will represent the basic current. If a coastline impedes the development of the wind drift equally in all directions and favours a current parallel to the coast, then the circle connecting the ends of all the current vectors will be replaced by an *ellipse* (WITTING, 1909).

Table 114. "Fram" Expedition: 27 May 1895 - 27 June 1896. Ice drift grouped according to the directions of wind resultants

Wind quadrant centred at	Total drift				Wind drift (without basic current)	
	Wind speed v (m/sec)	Current intensity w (cm/sec)	Relative current w/v	Deflection angle	Relative current	Deflection angle
N.	3.30	4.16	1.26	9.5°	1.69	36.0°
E.	2.86	3.16	1.10	53.5°	1.65	27.5°
S.	2.48	5.54	2.23	42.0°	1.68	24.5°
W.	2.56	5.92	2.31	20.0°	1.65	34.0°
Mean	2.80	—	—	—	1.67	30.5°

Table 114 contains the ice-drift observations of the "Fram" for the period from 27 May, 1895 to 27 June, 1896 (Fig. 148) according to Sverdrup. The diagram on the left of Fig. 148 shows that the end-points of the vectors lie on a circle, but that the centre of the circle is not at the zero point but is displaced in the direction S. 82° W. Vectorial subtraction of the basic current (0.79 cm/sec, bearing 262°) results in the diagram given on the right of Fig. 148. The velocity 0.79 cm/sec refers to a wind speed of 1 m/sec. During the year, however, the mean wind speed was 2.80 m/sec, so that for the period under consideration there was a permanent surface current of 2.0 cm/sec along a bearing of 262° (direction relative to the 75° E. meridian). Nansen obtained by his method 2.0 cm/sec on a bearing of 256° which is in satisfactory agreement. The table shows that the relative wind drift is practically independent on the direction of the wind; the mean of the four groups shows that a wind with a strength of 1 m/sec gives rise to a surface drift of 1.67 cm/sec deflected 30.5° to the right of

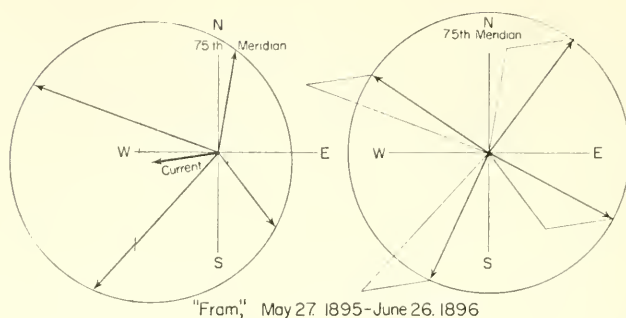


FIG. 148. Dependence of the ice drift on the wind direction according to the observations of the "Fram" expedition, 27 May 1895 to 27 June 1896. Left side: the observed total ice drift. Right side: the pure wind drift after subtraction of the effect of the permanent basic current (according to Sverdrup).

the wind direction. Also in this case almost identical values were obtained by Nansen's method.

PALMÉN (1930*b*) has studied these methods in his work on the currents of the Gulf of Bothnia and the Gulf of Finland more deeply and has used them with success, especially for the observations on wind and currents made at the light ship "Finngrundet" from 1923 to 1927.

2. The Current Field and its Representation

(a) Representation of Mean Current Conditions by Means of Compass Cards

To get an idea of the currents in any particular area of the sea the most practical procedure is to tabulate all the available data for the direction and strength of the currents for small areas over which uniform conditions can be expected. These small areas are usually chosen to cover a few degree squares (one, two or more degree squares). The question is thus to count out a large number of observations which can then be presented on a compass card. The prevalence of each direction is then shown by longer or shorter rays from the centre point, and the mean velocity in any direction is shown either by the thickness of this line or by the feathering on these rays. Such a current chart is actually only a graphical tabulation and is very largely free of subjective influences. A personal factor becomes involved only in the interpretation of the picture shown by such compass cards.

The representation of current conditions by compass cards best satisfies the requirements of a current chart for navigation, since it gives at a single glance the frequency and strength of currents in each direction and the possibility of representing large variations in the direction and strength of the current. The usefulness of charts containing compass cards for scientific investigation of the sea is, however, very limited, because sufficient observations are available only along shipping routes and there are larger areas of the sea for which cards cannot be constructed due to missing data.

The use of compass cards to show average current conditions was previously preferred, and by this a uniform evaluation of the enormous amount of ships reckoning displacements was made. One of the most recent representations using compass cards is that of the Netherlands Atlas for East Asian waters (*Kgl. Ned. Met. Inst.*

DE BILT, 1935-6). From this atlas the part contained in Fig. 149 was taken; for an explanation of this picture see the legend underneath.

A picture of current conditions easier to interpret can be obtained if only a selection of the particularly typical vectors are given as, for example, in the *Deutsche Seewarte Atlas* containing twelve monthly charts; however, in these the subjective viewpoint of the investigator has a large effect. A different type of representation has been used in the British Admiralty charts. The ship reckoning displacement is not shown by a straight arrow, but by a wave-like arrow with the mean velocity in nautical miles per day indicated by a number underneath. Where there is no displacement the chart is left blank but along the usual shipping routes they accumulate. In practice this method has the advantage that it shows the variations and the uncertainty in the occurrence of the ocean currents and the greater or lesser prevalence of current free regions or only of weak currents.

(b) *Representation of Average Current Conditions by Means of Stream Lines*

Instead of giving statistics of individual ship displacements in form of compass cards, these statistics can also be used to give the mean value of the currents in the degree squares. This has been done by the Netherlands Meteorological Institute (1908, 1915, 1919). A vectorial mean for one or two degree squares is taken of ship displacements, and calculations are also made of the *scalar* means and the stability. The results have been published in tables and charts. This observational material has then formed the basis for a whole series of investigations on ocean currents. Attempts to derive a comprehensive picture of the currents from these mean current vectors are of two types (SCHUMACHER, 1922); one of these represents the current by stream lines broken up into arrows with the feathering or the thickness of the arrows indicating the velocity. The other gives the direction of the current by *continuous* stream lines and the velocity by isolines (isotachs). To the first group belong the investigations of MICHAELIS (1923) and WILLIMZIK (1927) on the Indian Ocean, of MEYER (1923) on the Atlantic, a study by MERZ (1929) on the Pacific Ocean, and by WILLIMZIK (1929) on the Antarctic surface current and others. The second method was first used in oceanography by BJERKNES and co-workers (1913) for the currents in the Gulf of Mexico. During a renewal of the monthly current charts for the North Atlantic SCHUMACHER (1940) later used another method of representation. The arrows here were drawn to represent not the *mean* direction and velocity but the *most frequent*, which is more valuable both for the practical user and in most cases also for scientific purposes. All the available data on observed ship displacement were evaluated on this most frequent value (mode) principle. The quadrant containing the largest number of observations was found for each point; the enormous amount of work required was handled by a punched-card system (Hollerith). The direction separating this quadrant into two halves was then taken as the *prevailing* direction of the current. The velocity was taken as that usually found in the prevailing direction, that is, the *scalar mean* of the ship displacements falling within the selected quadrant.

Also, the stability was determined as before and was characterized by the probability of a displacement in the selected quadrant, i.e. by the numerical ratio of the number of observations falling within the quadrant to the total number of observations. Four different grades of stability were distinguished. If at least one-third of all observations

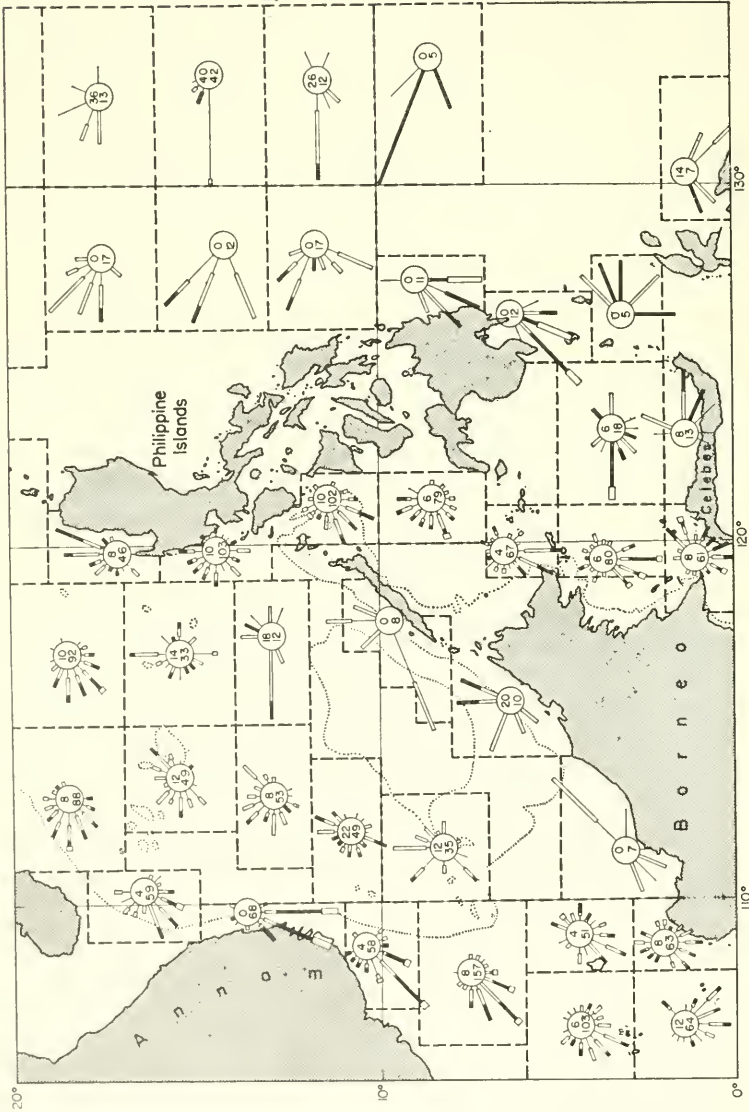
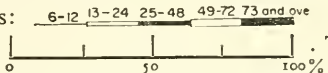


Fig. 149. Part of the January chart of the *Ocean. en Met. Waarnemingen in de Chinesesche Zeeën*, etc., Vol. I, published by Kgl. Nederl. Meteor. Inst. No. 115, DE BILT, 1935.

For explanation see next page.

EXPLANATION (to Fig. 149)

The current roses are drawn from observations within the areas shown by the pecked lines. Arrows indicate direction of current; north arrow current *towards N*. Velocity of current in *nautical miles per day* is represented as follows: . Length of arrows represents frequency, 1 mm 3.7%. The lower figure within the circle gives the total number of observations, the upper figure the percentage frequency of currents less than 6 miles per day.

falls within a quadrant this will be already predominant and its middle line can be regarded as the direction of the prevailing current. If the percentage of the ship displacements falling within the quadrant is between 33% and 66% then the prevailing current is termed "*variable*". The next grade "*rather steady*" is reached when at least 33% of all observations fall not only within one quadrant but within one octant. If more than 67% of observations fall within a quadrant and between 33% and 66% within an octant within the quadrant then the prevailing current is denoted "*steady*"; if both quadrant and octant contain more than 67% of all observations the current is "*very steady*". This characterization of stability is undoubtedly more illustrative than the ratio of the vectorial and scalar sums of the velocities.

An example of this type of representation is given in Fig. 150 which shows the chart for August of the surface currents in the North Atlantic as given by Schumacher. The length of the arrows indicating the prevailing direction has no significance here. The velocity is given by feathering or for large values by barbs at the arrow-heads; for the grade of the stability see the explanation on the chart.

A similar evaluation of ship displacements has also been given by SCHUMACHER (1943) for the South Atlantic so that modern monthly charts are now available for the whole of the Atlantic Ocean.

(c) Current Patterns and their Interpretation

Certain definite properties of the current field must be borne in mind in plotting stream lines on the basis of the current vectors. In the first place it should be noted that except at singular points and lines:

- (1) the individual stream lines are not allowed to intersect;
- (2) the stream lines are curves that neither start nor finish in the current field;
- (3) the stream lines are always continuously curved lines.

The stream lines are drawn mostly by vectorial interpolation by the eye. Such a graphical interpolation usually offers little difficulty if the current vectors cover the whole chart uniformly. However, this is usually not the case and the lines must sometimes be drawn with a minimum of observational values. For this it is necessary to have some idea of the *singularities* in the current field (BJERKNES and co-workers 1912, 1913). Because the position of these singularities fixes the general outline of the field and to complete the pattern then offers little difficulty.

The simplest singularities and their relationship to the structure of the water masses in the oceans will be described in the following section.

Lines of convergence and divergence. Figure 151 shows convergence and divergence from only one and from both sides of the stream lines. In case (a) and (b) there is an infinitely rapid convergence and divergence; cases which are rarely found in this extreme form. An infinite number of stream lines leaves or enters asymptotically

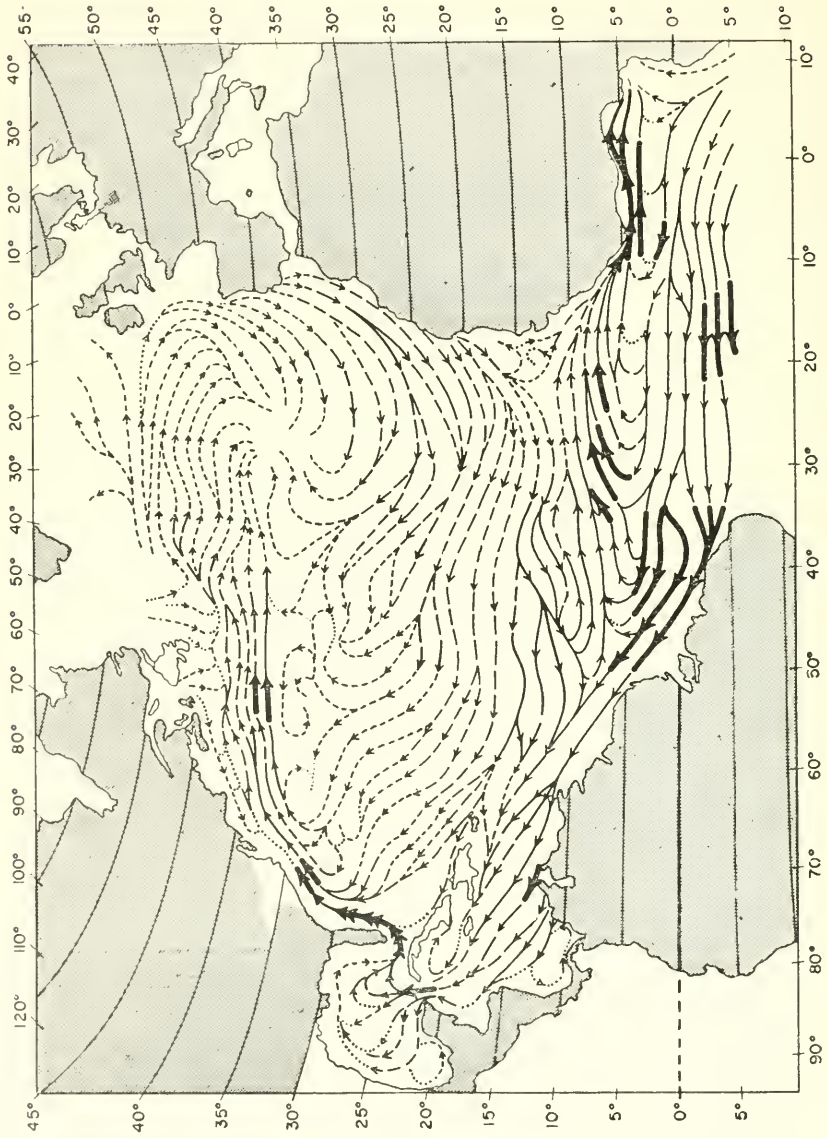


Fig. 150. For explanation see next page.

← FIG. 150. Chart of surface currents for August in the North Atlantic Ocean (according to Schumacher). (Stereographic azimuthal projection accurate at the equator, scale at 0° N., 30° W. 1: 10⁸.)

Velocity		Steadiness	
3.0-8.9 sm/Etm.	($\frac{1}{4}$ knots) — / ———	Very steady	—————
9.0-14.9	„ ($\frac{1}{2}$ knots) — < ———	Steady	-----
15.0-20.9	„ ($\frac{3}{4}$ knots) — ≤ ———	Rather steady	- - - - -
21.0-29.9	„ (1 knots) — ◀ ———	Variable	- · - · -
30.0-41.9	„ ($1\frac{1}{2}$ knots) — ◀◀ ———	} Dead reckoning or taken from other represent- ations	-----
42.0-53.9	„ (2 knots) — ◀◀◀ ———		-----
54.0-65.9	„ ($2\frac{1}{2}$ knots) — ◀◀◀◀ ———		-----
66.0-77.9	„ (3 knots) — ◀◀◀◀◀ ———		-----

Numerical limits for steadiness: from all ship displacements known in a certain area fall inside the quadrant which is cut by the current direction into two halves (quadrant and octant, respectively)

	quadrant (%) (up to 45° to the right and left)	octant (%) (at the most 22½° to the right and left)
Very steady	More than 67	More than 67
Steady	More than 67	33-66
Rather steady	33-66	33-66
Variable	More than 33	Less than 33

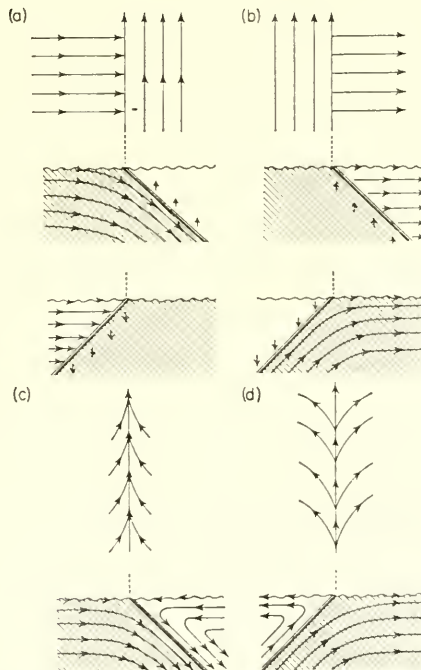


FIG. 151. Singularities in the current field: (a) one-sided convergence, (b) one-sided divergence, (c) and (d) double-sided convergence and divergence; for explanation see vertical cross-section.

from both sides the lines of divergence and convergence (case (c) and (d)). Lines of convergence and divergence in most cases represent the boundaries between different water types moving relative to each other. They are generated when heavy water meets lighter water or when lighter water spreads out over heavier water that is sinking. Fig. 151 gives a vertical section showing current conditions on both sides of an inclined gliding surface separating two different water masses. Similar vertical displacements can also be expected for divergence and convergence lines from both sides. In all these cases where there is a velocity component at right angles to the boundary surface the inclined gliding boundary surface cannot be expected to remain stationary.

The occurrence of divergence and convergence lines in oceanic current systems is a general phenomenon closely connected with the oceanic circulation. They represent the framework of the circulation and indicate the connecting places between the surface currents and the three-dimensional vertical circulation. Some examples will be given later.

RAUSCHELBACH (1931) while making current measurements in the Ost-Friesland Gatje (below Emden) took the opportunity to make measurements with a bifilar current meter at a convergence line running through the observation point (an anchored vessel). The convergence line, which was visible as a foam line, ran parallel to a dredging line; it moved the Ems upstream driving with the flood tide, while at the same time it was displaced from the middle of the channel towards the east. It passed the current meter at 17 h 3 min 30 sec. Figure 152 gives the velocity and direction of the current as measured by the current meter before and after the passage of the convergence line; Fig. 153 shows the distribution of the surface current around it. The course of the boundary surface in the lower layers was not that simple and according to current measurements at a depth of 1–2 m was disturbed by internal waves.

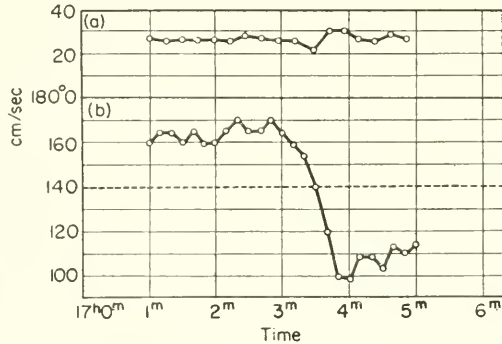


FIG. 152. Evaluation of a convergence line in the Ostfriesland Gatje (downstream of Emden) according to Rauschelbach: (a) current velocities, (b) current directions (clockwise from 0° to 360°).

Convergence lines are frequently indicated at the sea surface by more or less strong agitation of the water and are then recorded in ships' logs as *rips*. Closer attention has only been paid to them in more recent times. (RÖMER, 1935, 1936; SCHUMACHER, 1935; THIEL, 1937; UDA, 1936, 1938). It seems to be definitely established that rips in the open ocean are formed at the boundaries between converging and diverging water masses. Sometimes when lighter and heavier water are separated by either a convergence or a divergence line, the wind forces the lighter one to move above the heavier, as is often observed. Off the continental shelf and around island platforms there may

also be disturbances of the water movement due to the bottom configuration; the direction of the rips then usually corresponds with the main course of the shelf or of the irregularity in the bottom. In many cases a connection has been shown with the behaviour of the tidal currents in neighbouring oceanic regions. Particularly well known to seamen are the rips in the Straits of Gibraltar and in the Straits of Messina,

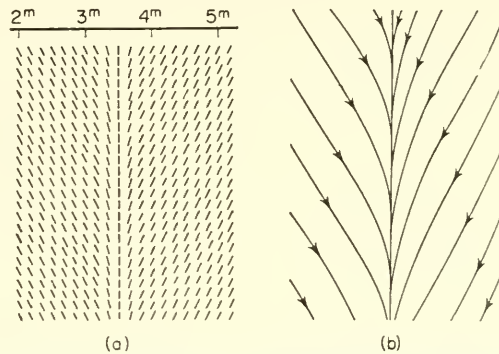


FIG. 153. Current directions and stream lines during the passage through the convergence line in the Ostfriesland Gatje (see Fig. 152).

where they are definitely connected with tidal currents carrying different water types and those off the eastern coast of North America in the area of the Gulf Stream, along the west coast of Mexico and in West African waters where they are related to upwelling phenomena.

Points of convergence and divergence (Fig. 154a, b). These points represent the intersection of an infinite number of stream lines. For continuity reasons, movements such as these must always be connected with movements perpendicular to the surface of the sea; thus a divergence point in a water layer near to the surface indicates upwelling and a convergence point indicates a sinking movement. This need not, however, be the case at greater distances from the surface. The divergence then merely indicates that due to the vertical movement more flows in at one side than leaves from the other; the reverse applies for convergence. The formation of curved stream lines near to the centre point (cyclonic and anti-cyclonic vortices) as shown in Fig. 154 depends largely on the effect of the Earth rotation.

If there are different types of water masses in the near vicinity of the vortex they will be drawn into it and *combined singularities* then occur. Cases of this type are shown in Fig. 154c, d; c represents a *cyclonic vortex* in the region between a lighter and a heavier water mass. Since the equilibrium state is upset at the boundary between the two water masses the lighter water tends to spread out over the heavier while the heavier sinks underneath the lighter. For such an inward spiraling motion a convergence line forms at the boundary surface; thereby one part of it will be an up-gliding *surface* where the lighter water moves over the heavier and the other will be a down-gliding *surface* where the heavier water sinks underneath the lighter. The lighter water will gradually extend completely over the heavier and will finally give a cyclonic vortex (in the top layer) with a simple convergence point of the form a.

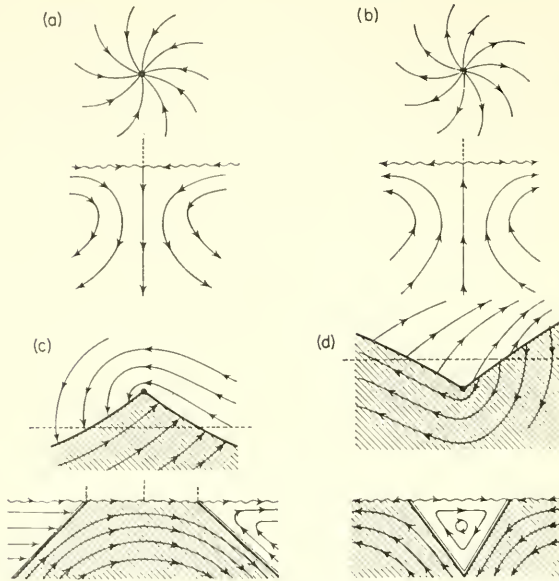


FIG. 154. Singularities of the current field: (a) and (b) convergence and divergence point; (c) and (d) superposition of singularities with convergence and divergence lines; (c) cyclonic, (d) anticyclonic vortex at the boundary between two water masses.

The form *d* represents an *anticyclonic vortex* in the region between the two water masses. Here the boundary surface splits up into two divergence lines. In this case the anticyclonic vortex causes a concentration of the lighter water in the central part of the vortex. The dynamics of such cyclonic and anticyclonic vortices will be discussed later (see Chap. XIV, 4).

Neutral points (Fig. 155*a, b*) occur when currents flowing in opposite direction meet each other and separate again without showing stronger vertical motion. Two asymptotes to the stream lines then intersect at the neutral point situated in the centre. Singular points of higher order are also possible. The current field is then very complicated, see, for instance, Fig. 155*a*. In place of the second water mass there may be a solid boundary at a coast line where the current divides into two parts. The neutral point then lies on the shore line. In the presence of a *wave motion* the stream lines take on a special pattern. During the propagation of a wave the individual water elements usually describe elliptical orbital motions in a vertical plane perpendicular to the wave front. The longer axis of the ellipse is horizontal and the smaller is vertical. For such a periodic wave motion it is of course only sensible to plot a stream-line pattern for a particular phase of the wave motion. Fig. 155*c* shows that for a propagation of a wave to the right the water masses will converge in front of the wave and will diverge in its rear. At the sea surface this gives rise to a convergence line in front of the wave and a divergence line behind it. Both the singular lines move with the wave at right angles to the wave front. Thus in a wave motion two types of strips occur, so that strips with a movement from left to right alternate with strips moving from right to left. If the wave is propagated to the right the first type of strips will correspond to the wave crests

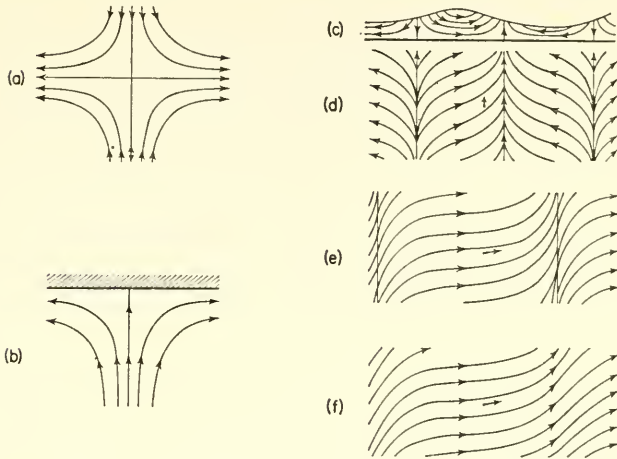


FIG. 155. Singularities in the current field: (a) neutral point, (b) one-sided neutral point, (c), (d), (e) and (f) singularities in wave motions: (c) stream lines in a vertical cross-section, (d) stream lines at the surface with a small translation parallel to the wave crests, (e) and (f) the same with a somewhat stronger or a very strong translation oblique to the wave crests (according to V. Bjerknes).

and the second to the wave troughs. If in addition to the wave motion there is also a more or less strong translatory motion in the water mass, then the two current fields will be superimposed on each other, and the resulting current field will consist of a system of convergence and divergence lines moving parallel to each other with the wave. Some fields of this type are illustrated in Fig. 155.

The singularities are closely connected with the velocity field. Where stream lines intersect the velocity must be zero; the points of convergence and divergence and the neutral points must therefore be points of zero velocity (places of no motion). The isolines of velocity must be closed around these points. When approaching singular lines there will always be more and more curvature in the lines of equal velocity. This curvature becomes stronger the more the stream lines converge towards the singular line. For weaker convergences this curvature is usually hardly noticeable in the observations.

Constructing stream lines usually offers little difficulty, especially if the position of the singularities is fixed first. Usually some of the stream lines running out from the singularities can be drawn in with some certainty and these fix the current field with almost sufficient accuracy. Attention should also be paid, of course, to the velocity field and to relationships with the dynamic phenomena expressed in the distribution of other oceanographic factors (temperature, salinity, etc.). SANDSTRÖM (1909) has given a method for the accurate construction of stream lines. Auxiliary lines termed *isogons* were drawn in first. An isogon is defined as a line along which the direction of the current is constant, and for each direction there exists only one isogonal curve. If the observed directions are expressed by numbers (usually 16 directions with the numbers 2 to 32) then numbers can be entered on the chart in place of the arrows indicating the direction of the current; the isolines of equal direction are then easily constructed. These are covered with rather short dashes pointing in the direction of

azimuth of each isogen so that the chart is covered complete with short dashes. It is then easy to draw in the curves tangential to these short dashes and these curves are the stream lines. WERENSKJOLD (1922) has pointed out that it is possible to draw in a number of isogons rather quickly by simply using two charts of the eastern and northern components of the current u and v . If α is the azimuth of the current then

$$\tan \alpha = \frac{v}{u} = k.$$

Each isogen is fixed by $k = \text{const.}$ Two isogons can thus be drawn in immediately: for $k = 0$ and $k = \infty$; they correspond to lines $v = 0$ and $u = 0$. Their intersections give the singular points through which all isogons must pass. Since the relation

$$v - ku = 0$$

is satisfied only at points where $u = v = 0$ for all values of k . Further isogons are easily found; they can be limited to the eight isogons where $k = 0, \pm\frac{1}{2}, \pm 1$ and ± 2 ; corresponding to these are the azimuths $0^\circ, 26\frac{1}{2}^\circ, 45^\circ, 63\frac{1}{2}^\circ, 90^\circ$ and so on. These usually fix the current field with sufficient accuracy.

The stream lines are given by integrations of the differential equation

$$\frac{dy}{dx} = k = \frac{v}{u}$$

(see equation (X. 22) on p. 323). If v and u are given as analytical functions of the coordinates x and y , then in many cases an accurate integration of the equation, and therefore also a representation, of the current field is possible. Werenskjold has given a large number of cases of this type and has discussed them in detail. Reference is made to these. Of particular interest are those cases where complex singularities occur; to draw these complicated patterns is usually rather tiresome, but mathematically they are no more difficult than the simple ones. An example will illustrate this. If u and v are given by

$$\begin{aligned} -u &= x^2 + (y + a)^2 - r^2, \\ v &= x^2 + (y - a)^2 + r^2, \end{aligned}$$

where $r^2 > a^2$, then the integration of the differential equation above gives the stream lines represented in Fig. 155a; the isogons $u = 0$ and $v = 0$ are circles which are shown by dotted lines in the figure. Their points of intersection give the singular points, one of which is a neutral point and the other is a convergence point; they are connected by a line of convergence. Such connections of the singularities are relatively frequent in stream-line patterns of ocean currents.

(d) *Examples of Current Charts*

Current charts based on these principles have been prepared for many parts of the ocean, usually for *mean* conditions since there are almost no synoptic data available. They show only surface currents. Various types of presentation have been used. An accurate representation based on strict hydrodynamic principles has been introduced by Bjerknæs. Analysis of the current fields and their resolution along the extended lines of convergence and divergence, with more or numerous complex singularities, has shown that the previous conception of large horizontal circulating systems in the

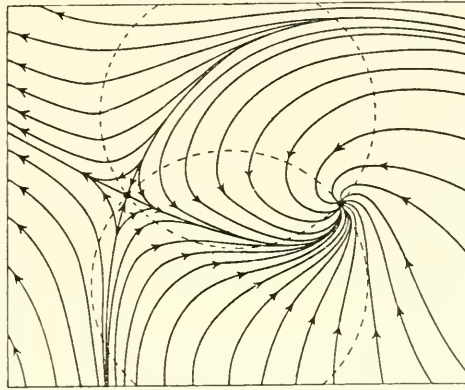


FIG. 155a. Example for a special current field according to Werenskjöld (integral curves of $dy/dx = v/u = k$; circles are curves $u = 0$ (below) and $v = 0$ (above)).

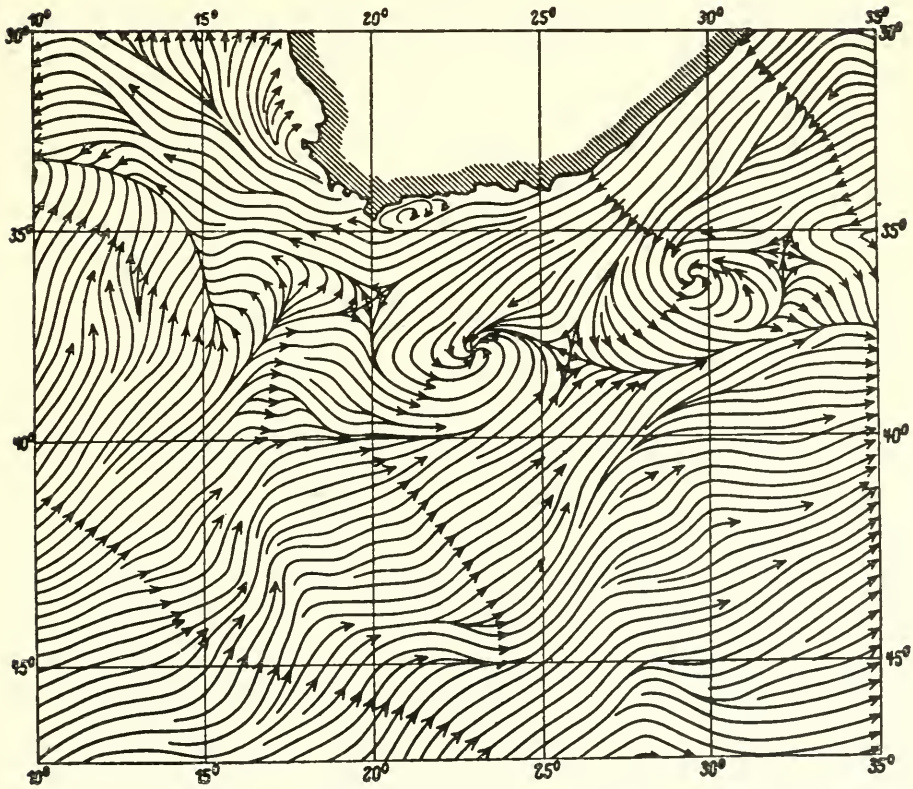


FIG. 156. Stream lines south of Africa for May (according to Merz).

currents of the surface layers is untenable, and that the deeper water layers are also involved in the surface current systems. An example of this type of representation is given in Fig. 156 which shows the surface currents to the south of Africa during May according to MERZ (1925). A line of convergence runs right across it separating the steady broad west wind drift in the south from the Agulhas Current south of Africa. Charts of this type do not indicate the velocity of the current, its prevalence or the amount of data on which it is based; velocity is mostly indicated by thin dotted lines (nautical miles per day). Because of gaps in the available data current charts such as these, constructed according to strictly hydrodynamic principles, are naturally not certain in all details, but the individual stream lines and singularities support each other by means of their course and position and thus offer the clearest possible picture of the water movement.

Another representation of essentially the same type was chosen by HELLAND-HANSEN and NANSEN (1909, p. 9) in which the stream lines are represented by a series of short arrows of more or less equal length (Fig. 157). Also here the velocity

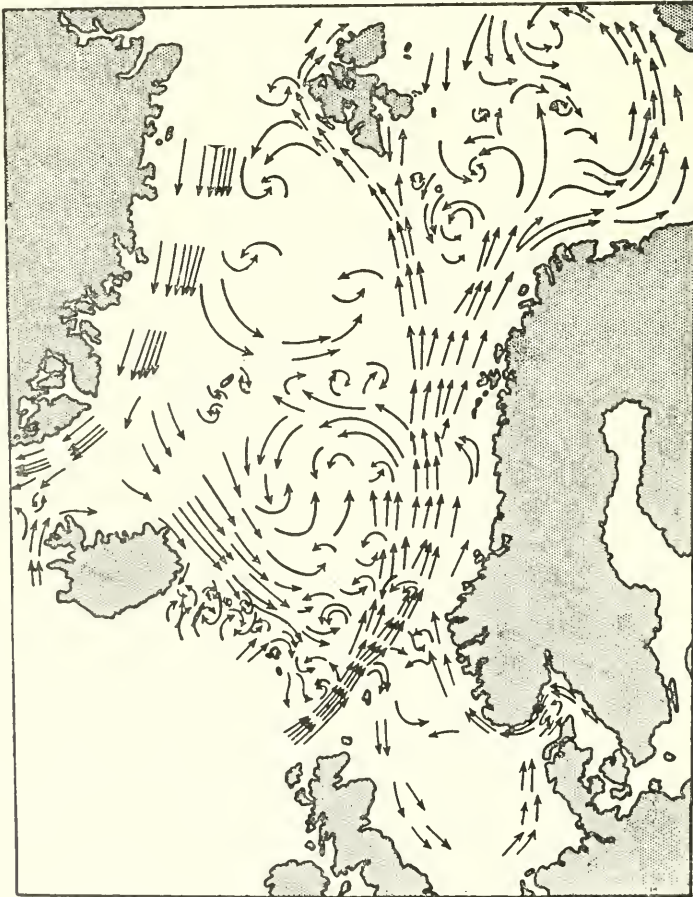


FIG. 157. Mean currents at the sea surface of the European North Sea (according to Helland-Hansen and Nansen).

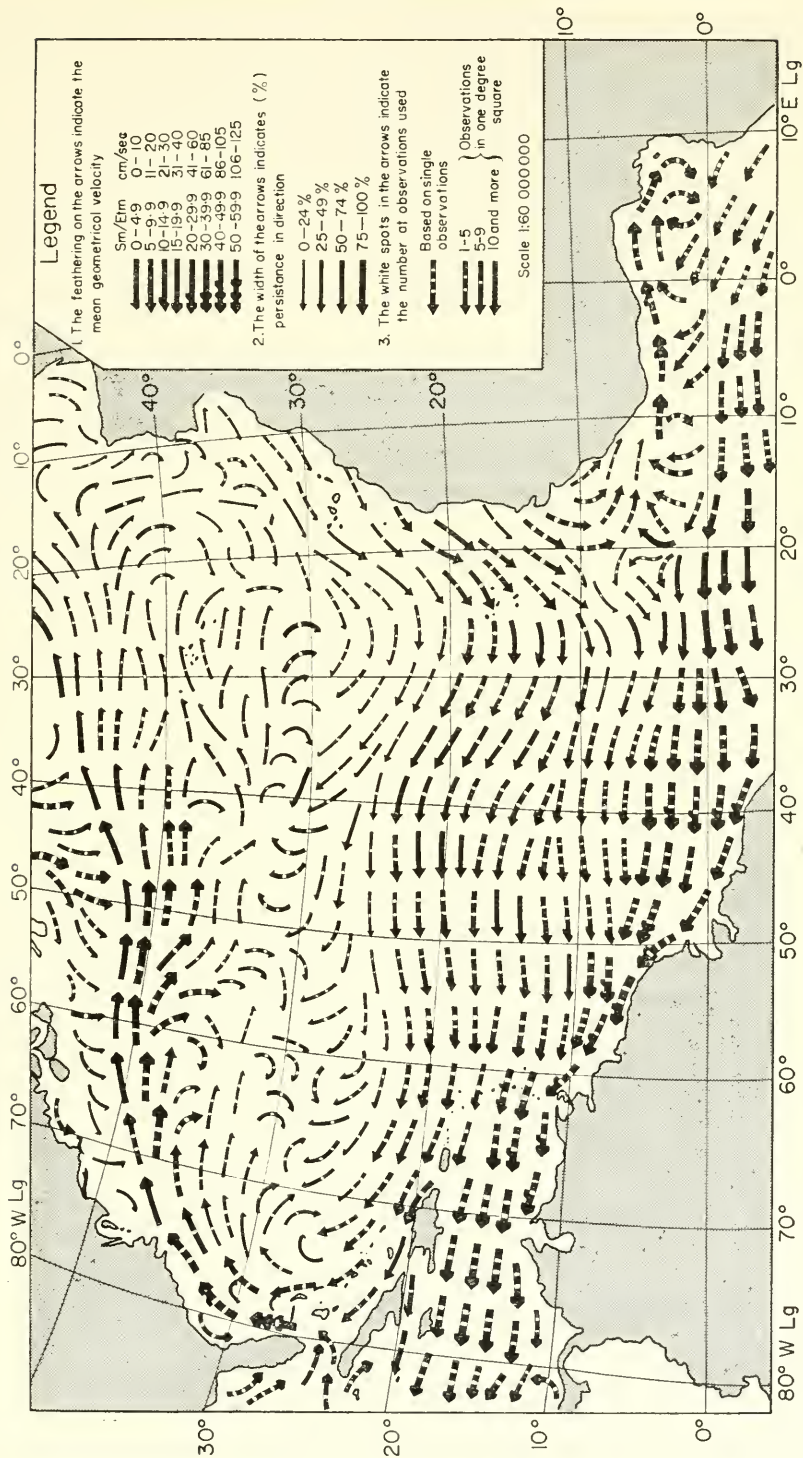


FIG. 158. Part of the sea surface chart of the ocean currents in the Atlantic Ocean for February (according to Meyer).

and the stability are omitted from these charts. This type of representation is usually chosen for current charts which are based less on direct current measurements and more on a qualitative assessment of the horizontal distribution of the temperature, salinity and other factors which the system of currents at the sea surface must reflect.

A more comprehensive representation of the currents in an ocean has been used by MEYER (1923) for an evaluation of Dutch observations on the currents in the Atlantic during February. Figure 158 shows a part of this chart. Here also the stream lines were broken up into a series of arrows of equal length but their thickness was used as a measure of the current constancy (stability), the feathering as a measure of the velocity and the amount of data available was indicated inside the breaks in the shaft of the arrow. The singularities in the current field are not shown so clearly by this type of representation and are therefore indicated by special signs, particularly in the case of the more important lines of convergence and divergence. These charts already permit a deeper insight into the nature of the water movements at the sea surface of the ocean under consideration and also allow an estimate of the reliability of the chart at any particular area of the oceanic region. Similar but somewhat modified representations have been chosen by SCHOTT (1926, 1935) and SCHUMACHER (1940, 1943).

In assessing the value of a chart and in its use, it is necessary to keep in mind the relatively large uncertainties which still remain attached to them. The number of observations on which the charts are based in the individual degree squares varies considerably and is often so small in some of the squares that chance can be rather important. These difficulties, however, may decrease with time since the number of observations collected by hydrographic institutes increases from year to year and mechanical evaluation of these data by computing machines is much faster than was previously possible.

3. Special Cases of Current Fields Near Land and at the Boundaries of Water Masses (Compensation Currents)

The boundaries of the sea, fixed either by coast lines or by the topography of the sea bottom, exert a considerable influence on the pattern of the ocean currents and especially on the form of the current field. For each steady current (potential flow) the water in the immediate vicinity of a solid boundary surface (coast or sea bottom) tends to approach the boundary as closely as possible. The effect of such disturbances is thus shown rather far from the source of disturbance in the current field and also in the distribution of the oceanographic factors (temperature, salinity, etc.). The most simple cases, which occur also in nature again and again can be expressed mathematically by the method given on p. 327; a few of these can be briefly treated here.

(1) Plane flow around a cylindrical obstacle (island) is given by a function $F = U(z + (a^2/z))$. Introducing in $z = x + iy$ polar co-ordinates, then

$$z = r(\cos \phi + i \sin \phi) = re^{i\phi}$$

and the velocity potential Φ and the stream function Ψ will thus be given by the expressions

$$\Phi = U \left(r + \frac{a^2}{r} \right) \cos \phi \quad \text{and} \quad \Psi = U \left(r - \frac{a^2}{r} \right) \sin \phi.$$

One stream line is the x -axis for which $\sin \phi = 0$, another one is the circumference

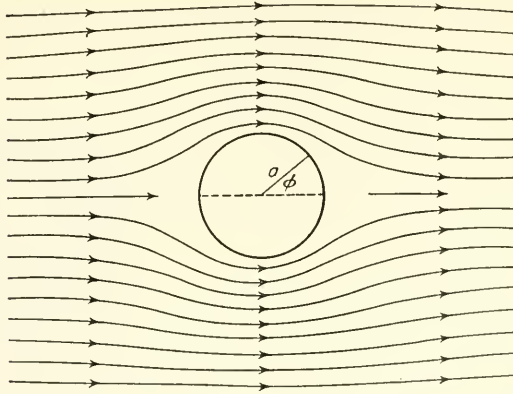


FIG. 159. Stream lines around a cylindrical obstacle (island).

of the obstacle where $r - a^2/r$ vanishes. The stream lines of the potential flow are given in Fig. 159.

(2) Choosing $F = (a/2)z^2$ then

$$\Phi = (a/2)(x^2 - y^2) \quad \text{and} \quad \Psi = axy.$$

The x -axis and the y -axis are stream lines ($\Psi = 0$) and one obtains in that way the flow towards a straight and vertical coast at which the flow divides into two branches (see Fig. 155 (b)).

(3) The function $F = Az^n$ leads to current cards for bays or around projecting land masses where as a first approximation the boundaries can be taken as straight. Introducing again polar co-ordinates we obtain

$$\Phi = Ar^n \cos n\phi \quad \text{and} \quad \Psi = Ar^n \sin n\phi.$$

Parts of the curves $\Psi = 0$ can be taken as solid boundaries; this leads to $\sin n\phi = 0$ or to the lines $\phi = 0$ and $\phi = \pi/n$. Putting $n = \pi/\alpha$, then $\phi = 0$ and $\phi = \alpha, 2\alpha, \dots$ can be taken one after the other as the solid boundary. This gives the irrotational flow (vorticity free) between or off two straight coasts which meet each other at an angle α . Fig. 160 shows some cases which are of interest.

The configuration of coast lines and outer boundaries of ocean basins are considerably more complex than in the simple cases which are susceptible to mathematical analysis. The simple character of currents that carry water masses from a distance into coastal areas will be disturbed and changed by the coast lines. An important role is

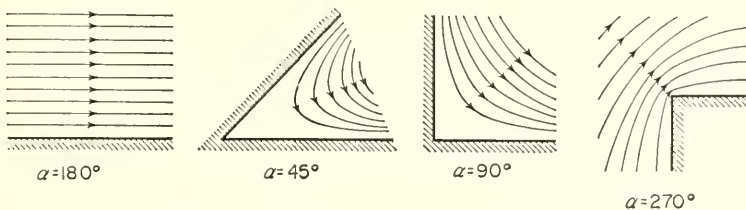


FIG. 160. Stream lines off a coast as shown on the picture (triangular shape).

played here by the *compensation requirement* which is a result of the continuity law. Since water is almost completely incompressible it cannot accommodate a widening or contracting of the stream lines by contraction or expansion and movements normal to the flow direction or even counter currents are set up to a much greater extent than in air movements in order to avoid the formation of empty space. The nature of these counter movements can only be fully explored empirically by observations in nature or by special suitable experiments. Experiments of this sort have been made extensively by KRÜMMEL (1911, p. 470) and have been used for a clarification of many phenomena exhibited by the pattern of the ocean currents. The results of that shown in Fig. 161 are particularly instructive. The resemblance of the experimental current system to that in the Central Atlantic can readily be seen; this system consists of the two wind

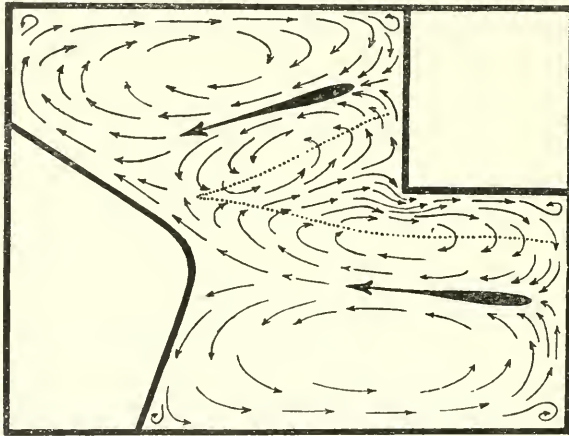


FIG. 161. Experimentally produced current patterns (simulation of the current system in the central part of the Atlantic Ocean) (according to Krümmel).

drifts induced at the sea surface by air currents, and the corresponding circulations to the north and the south as well as the (equatorial) counter current between them. At the projecting peak on the left-hand side of the experimental tank representing land (Cape San Roque) the current intensity was surprisingly large (corresponding to the Guayana Current).

Standing vortices are formed at coastal bays, in which the flow always shows such a sense of rotation that the current on the seaward side follows the main current while that on the landward side is opposed to it. Hydrodynamically such a vortex can be stationary, but it will always have the same water mass circulating within it and there will be no water transfer from the main current to the vortex. In nature this is usually not the case. Pulsations in the main current will always affect the intensity and the extent of the stationary vortex and will thereby lead to a renewal of the water circulating in it. Such replacement currents in bays and small gulfs are termed "neer currents" and are always present at any reasonably irregular coast consisting of small bays and projecting land. An example is shown in Fig. 162.

The compensation requirement need not always to be satisfied by horizontal transports, but vertical movements are also sometimes involved and give rise to very characteristic oceanographic phenomena (upwelling).

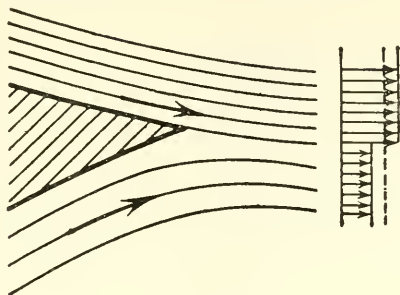


FIG. 162a. Two streams of water flowing together.

Conspicuous phenomena also occur where currents carrying two different water masses flow together and these deserve special attention. If two water masses of different type meet at a sharp land projection or at a motionless water mass there will usually be an appreciable transverse velocity jump at the boundary surface (Fig. 162a). It cannot be expected that separating surfaces of this type will keep for any length of time their simple form, since the state under consideration is highly unstable. Every boundary surface of this sort has a tendency to develop waves and all chance irregularities will thereby grow rapidly and the discontinuity surface will finally dissolve into a number of irregular vortices. These processes are particularly characteristic for the transition from waves to vortices and have been described in detail by BJERKNES (1933) and PRANDTL (1942). A boundary surface at which a temporary disturbance of the current field has given rise to a slight bulge is shown in Fig. 162b. This wave-form disturbance will move along the boundary surface with the average of the speeds of the two currents; relative to this wave one of the water masses will move to the right and the other to the left, and with reference to this kind of co-ordinate system the ridges and troughs of the waves will remain in the same place. According to the Bernoulli theory the disturbance in the course of the stream lines will be accompanied by a corresponding transverse pressure disturbance. For a steady state of motion the transverse pressure rise $1/\rho(\partial p/\partial s)$ must be balanced by the centrifugal acceleration c^2/r (c denotes the horizontal velocity, r the radius of curvature of the stream lines, s the direction of the normal to the stream lines). It becomes obvious that there will be a pressure surplus (+) in the ridges of the waves and a reduced pressure (-) in the troughs of the wave. This implies that the wave disturbance cannot be stationary but that the water begins to move from the surplus pressure areas to the adjacent areas of reduced pressure; that is, as the wave disturbance becomes stronger it will form current fields similar to those in Fig. 162c, in which the boundary surface will finally be rolled up into vortices, lying one behind the other and all rotating in the same sense. The same phenomenon occurs here in the *horizontal* plane between two water masses with different velocities as in the case of unstable waves at the boundary surface between water masses flowing one above the other (see Vol. II, Chap. XVI, p. 517 Internal waves). Examples of cases such as this are the vortex formations at the boundary between the East Greenland Current and the Atlantic Current in the Irminger Sea, or the vortex-formations at the boundary between the Gulf Stream and the Labrador Current south of the Newfoundland Banks (see p. 471).

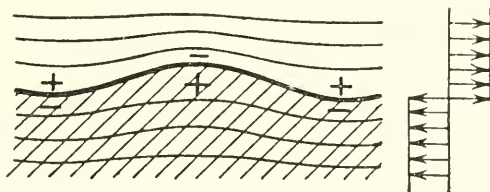


FIG. 162b. Disturbances in the pressure field due to wave-like deformations of a boundary surface between two currents.

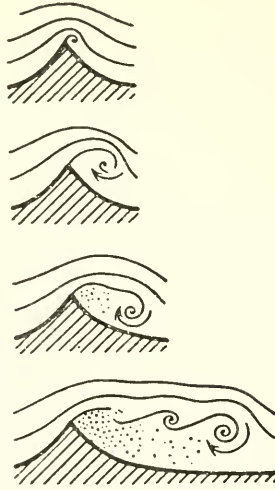


FIG. 162c. Formation of eddies behind a sharp edge and their growth.

4. Divergence of the Current Field and the Continuity Equation

The current field for a horizontal movement can give information about the place where vertical water movements must occur within the field. Since, on the one hand, in an incompressible medium, divergent and convergent stream lines must be associated with vertical displacements and on the other hand for parallel stream lines, velocity changes will lead to water accumulations (piling up of water; “Wasserstauungen”) which will also cause vertical movements. Quantitative relationships can be derived from the following considerations.

If AA' and BB' in Fig. 163 denote two adjacent stream lines, ds and ds' are elements of these, c and c' are two lines of equal velocity in the current field and δn as well as $\delta n'$ are the parts of these lines between the stream lines, then it is possible to calculate the amount of water flowing through the small area $ABA'B' = ds \delta n$ in unit time. This outflow per unit area is termed the *divergence of the current field* and is indicated by $\text{div } c$. It is a measure of the divergence and convergence of the stream lines and also of the velocity. One therefore obtains

$$\text{div } c = \frac{1}{ds \delta n} [c' \delta n' - c \delta n] = \frac{\partial c}{\partial s} + \frac{c}{\delta n} \frac{\partial \delta n}{\partial s} = \frac{1}{\delta n} \frac{\partial}{\partial s} (c \delta n). \quad (\text{XII.1})$$

If the velocity along the stream lines is constant ($c = \text{const.}$) and the small angle between the tangents to the two adjacent stream lines is denoted by $\delta \alpha$ then the *curve divergence* is given by

$$\text{div } c = \frac{c}{\delta n} \frac{\partial \delta n}{\partial s} = c \frac{\delta \alpha}{\delta n}. \quad (\text{XII.2})$$

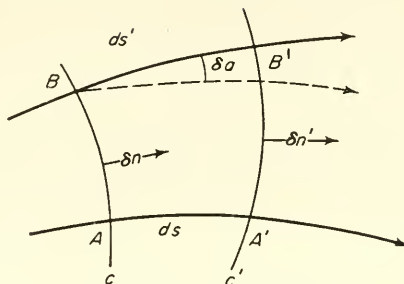


FIG. 163. Divergence of the current field.

The divergence is positive if the stream lines move apart and negative if they contract. If the stream lines are parallel ($\delta n = \text{const.}$) then

$$\text{div } c = \frac{\partial c}{\partial s}. \tag{XII.3}$$

The divergence here is a consequence of the change in velocity in the direction of the stream lines; a decrease indicates piling up (“Stauung”) and an increase indicates a suction of the water masses.

For a given current field the divergence field can be calculated numerically or graphically and can be represented on charts; special methods for this have been given by BJERKNES and co-workers (1912, 1913).

The general continuity equation (X. 22) can be written in the form

$$\frac{d\rho}{dt} + \rho \text{ div } c = 0 \tag{XII.4}$$

for an incompressible water mass this gives

$$\text{div } c = 0. \tag{XII.5}$$

If allowances are made for changes in density due to changes in temperature and salinity, then equation (X. 21) applies and for *stationary* conditions one obtains:

$$\frac{\partial \rho u}{\partial x} + \frac{\partial \rho v}{\partial y} + \frac{\partial \rho w}{\partial z} = \text{div } c = 0. \tag{XII.6}$$

The total horizontal water transport (“current amount”) in a water column from the surface ($z = 0$) to the bottom of the sea ($z = h$) is then

$$M = \int_0^h \rho c \, dz \tag{XII.7}$$

and its components along the x - and y -axes are given by

$$M_x = \int_0^h \rho u \, dz \quad \text{and} \quad M_y = \int_0^h \rho v \, dz. \tag{XII.8}$$

Multiplying equation (XII. 6) by dz and integrating from the surface to the bottom it follows that

$$\frac{\partial M_x}{\partial x} + \frac{\partial M_y}{\partial y} + (\rho w)_h - (\rho w)_0 = 0. \quad (\text{XII.9})$$

At the sea bottom w_h equals 0 and further if the vertical elevation of the sea surface above the equilibrium level (positive upwards) is denoted by ζ then $w_0 = -(\partial\zeta/\partial t)$ and from (XII. 9) follows

$$\frac{\partial \zeta}{\partial t} = -\frac{1}{\rho_0} \operatorname{div} M \quad (\text{XII.10})$$

The divergence of the current amount is thus always associated with vertical displacements of the sea surface and these can be readily calculated from (XII. 10) if the current amount is known. For a stationary state of the sea surface ($\zeta = \text{const.}$) it follows necessarily

$$\operatorname{div} M = 0, \quad (\text{XII.11})$$

that is, *at stationary sea surfaces the total current amount must be divergence free.* This need not be the case in every layer but in the entire water column an excess inflow in some of the individual layers must be balanced by a deficit in the other layers, if no effect on the sea-level should appear.

Under stationary conditions in the sea there must be in any volume element a constant amount of all the dissolved substances in the water besides the constancy in density (see DEFANT, 1941*d*). If the salinity for example is denoted by s and exchange processes are for the moment disregarded, this requires

$$\frac{ds}{dt} = \frac{\partial s}{\partial t} + u \frac{\partial s}{\partial x} + v \frac{\partial s}{\partial y} + w \frac{\partial s}{\partial z} = 0. \quad (\text{XII.12})$$

Multiplying this equation by ρ and then adding the continuity equation (X. 31) multiplied by s , it follows that

$$\frac{\partial \rho s}{\partial t} + \frac{\partial u \rho s}{\partial x} + \frac{\partial v \rho s}{\partial y} + \frac{\partial w \rho s}{\partial z} = 0. \quad (\text{XII.13})$$

For stationary conditions the first term on the left-hand side is zero and the condition of a constant salinity will be given by the remaining equation integrated over the total volume under consideration. Introducing a space vector S with horizontal components S_x and S_y which is given by the equation

$$S = \int_0^h \rho s c \, dz \quad (\text{XII.14})$$

allows the equation (XII. 13) for stationary conditions to be rewritten in the form

$$\operatorname{div} S = 0 \quad (\text{XII.14a})$$

S can be termed the *salinity amount* and the equation states that under stationary conditions the vector indicating the amount of salt flow must also be divergence-free.

The constancy of the water mass in a given space and the constancy of the characteristic water properties existing under stationary conditions has often been used in the derivation of the current

amount in the considered space. For example, the silicate content is q at three oceanographic stations a , b and c , where the vertical salinity distribution is s . For a prism taken by these stations down to a definite level, there will be current amounts M_1 , M_2 , M_3 passing through each side in unit time and a current flow M_u through the bottom surface. If it is then assumed that no water enters or leaves through the upper sea surface (zero precipitation and evaporation) then the constancy of the water volume requires that

$$M_1 + M_2 + M_3 + M_u = 0.$$

If further the corresponding mean amounts of salt and silicate passing through the three surfaces of the prism are indicated by s_1 , s_2 , s_3 and q_1 , q_2 , q_3 , respectively, and the amounts of salt and silicate in the prism are taken as constant, then

$$s_1 M_1 + s_2 M_2 + s_3 M_3 + s_u M_u = 0$$

and

$$q_1 M_1 + q_2 M_2 + q_3 M_3 + q_u M_u = 0.$$

If the current amount or the current at one of the lateral surfaces of the prism are known the three equations are sufficient for a calculation of the other three unknown currents.

OKADA (1934) has used these methods to study the oceanographic conditions in the Sagami Bay; and they have been used in a more extended form by HIDAOKA (1940*a*, *b*) to reduce the relative velocity distribution calculated from the oceanographic structure at different stations to the absolute values. Unfortunately, however, these methods cannot be used in most cases just for numerical reasons, since the coefficients of the equations differ numerically by so little that the determination of the unknowns becomes illusory. In the second and third of the above equations the mean salinity and silicate values at the three surfaces of the prism differ very little, so that the equations are only insignificantly different from the first. Small errors in the determination of the values of s and q and other random effects such as inaccuracies in the positions of the stations thus play such an important part in the solution that no reliance can be put on it.

In using the continuity equation for the determination of the current amount it should be borne in mind that the distribution of the characteristic water properties is largely controlled by exchange processes, so that these cannot be neglected since the magnitude of these effects is the same as that of the simple transport terms. To be strictly correct the equation (XII. 12) should also take into account the effects of mixing processes. This leads then to an equation which has already been used in Pt. I (see p. 120) in the explanation of the phenomena occurring during the spreading of a water mass into surrounding waters. For stationary conditions it takes the form

$$\frac{\partial \rho u s}{\partial x} + \frac{\partial \rho v s}{\partial y} + \frac{\partial \rho w s}{\partial z} = \frac{\partial}{\partial x} \left(A_x \frac{\partial s}{\partial x} \right) + \frac{\partial}{\partial y} \left(A_y \frac{\partial s}{\partial y} \right) + \frac{\partial}{\partial z} \left(A_z \frac{\partial s}{\partial z} \right). \quad (\text{XII.15})$$

Integrating this equation from the sea surface down to the sea bottom the last term on the right-hand side gives

$$\left(A_z \frac{\partial s}{\partial z} \right)_h - \left(A_z \frac{\partial s}{\partial z} \right)_0.$$

The first term of this expression is zero since A_z vanishes at the sea bottom. The second represents the difference between evaporation and precipitation per unit area at the surface of a water prism.

Neglecting the effect of the vertical component of velocity on the left-hand side of equation (XII.15) on account of its smallness and retaining on the right-hand side only the term for the vertical exchange, then for $\rho \neq 1$ and $A_z = \text{const.}$ an approximately correct equation is obtained

$$u \frac{\partial s}{\partial x} + v \frac{\partial s}{\partial y} = A_z \frac{\partial^2 s}{\partial z^2}$$

which has been used by OKADA, 1935; THORADE, 1935, in a graphical procedure for the investigation of currents. Integrating it from $z = 0$ to a depth $z = h$ and replacing in a first approximation the integral on the left-hand side by the mean value of the individual quantities (indicated by a bar over the symbol) then the following expression results

$$\bar{u} \frac{\partial \bar{s}}{\partial x} + v \frac{\partial \bar{s}}{\partial y} = \frac{A_z}{h} \left[\left(\frac{\partial s}{\partial z} \right)_h - \left(\frac{\partial s}{\partial z} \right)_0 \right].$$

Taking the x -axis in the direction tangential to an isoline so that $\frac{\partial s}{\partial x} = 0$ then, since $\frac{\partial s}{\partial y}$ is inversely proportional to the distance D between two isolines, the current component v perpendicular to the isoline will be given by

$$\frac{\bar{h}v}{A_z} = D \left[\left(\frac{\partial s}{\partial z} \right)_h - \left(\frac{\partial s}{\partial z} \right)_0 \right].$$

The expression in brackets on the right-hand side can be determined from observations and the velocity component can therefore be obtained. Lines of equal silicate content will in the same way give a second velocity component across these lines and finally afford an estimate of the *total* mean velocity, provided A is known by other means. Accurate determination of the isolines is, however, an essential presumption in the use of this method.

For a *homogeneous* sea with a homogeneous current structure the relationship (XII. 10) (u and v independent of z) takes the simple form

$$\frac{\partial \zeta}{\partial t} = h \left(\frac{\partial u}{\partial x} + \frac{\partial v}{\partial z} \right). \quad (\text{XII.16})$$

It can also be readily derived from the continuity equation. It can be used to judge the accuracy with which the vertical mass transport can be deduced from the distribution of the current flow vector. Thereby it shows immediately that for its evaluation the deeper the sea the more accurately the horizontal distribution of u and v must be known. The use of this relationship is thus limited to shallow shelf seas. Here, particularly in representations of tidal currents, it allows the corresponding vertical tide to be deduced (DEFANT, 1925). If c is the velocity of the tidal current

$$c = c_0 \cos(\sigma t + \epsilon),$$

$$\zeta = \zeta_0 \sin(\sigma t + \epsilon),$$

then using (XII. 1) the relation (XII. 16) can be given the form

$$\frac{\partial \zeta}{\partial t} = - \frac{h}{\delta n} \frac{\partial}{\partial s} (c \delta n). \quad (\text{XII.17})$$

Insertion of values for c and ζ gives the equation

$$\zeta_0 = - \frac{h}{\sigma \delta n} \frac{\partial}{\partial s} (c_0 \delta n) \quad (\text{XII.18})$$

which is independent of the time. Now the following cases may occur (see Fig. 163)

(1) *Parallel* stream lines

$$\delta n = \text{const.} \quad \text{and} \quad \zeta_0 = - \frac{h}{\sigma} \frac{\partial c_0}{\partial s}.$$

Assuming $\zeta_0 = 100$ cm, for the distance δs between two stations 50 km and for $h = 50$ m, then one obtains for the semidiurnal tide ($\sigma = 2\pi/12 \cdot 3$ h) the necessary

$\delta c_0 = -14 \text{ cm/sec} = -0.25 \text{ nautical miles per hour}$. This horizontal change in the maximum velocity component is well within the accuracy of measurement.

(2) *Divergent stream lines* for a constant velocity ($c_0 = \text{const.}$):

$$\zeta_0 = - \frac{hc_0}{\sigma} \frac{\delta\alpha}{\delta n}$$

For identical σ , ζ_0 and h and taking again the distance between two stream lines, $\delta n = 50 \text{ km}$ and c_0 as 50 cm/sec one obtains $-\delta\alpha = 0.284$ angle units or about 16 degrees of arc. This divergence is usually easily readable from charts of tidal currents. The method thus gives results of sufficient accuracy provided the ocean depth is not too great; for example, it has been applied successfully to the evaluation of the tidal conditions of the North Sea (see Vol. II).

Where the structure of the sea has two or more layers a relationship of the form of (XII. 16) can be derived for each boundary surface between two successive superimposed layers. These relations fix the time changes in the inclination and position of the boundary surfaces as a function of the divergence of the currents in the individual layers.

5. The Knudsen Relations

The relations for the current amount (XII. 11) and for the salinity amount (XII. 14) allow an insight into the current conditions in more or less exactly limited oceanic regions such as sea straits and river mouths and others. KNUDSEN (1900) derived some simple laws of this type which are based fundamentally on these relations and just because of their simplicity and clearness lead directly to valuable conclusions about the general current conditions in such areas.

In straits, river mouths and also in the open ocean lighter (low saline) water often spreads out over heavier (more saline); in such cases the currents in the two layers are mostly of opposite direction. In Fig. 164 *A* and *B* are two vertical cross-sections

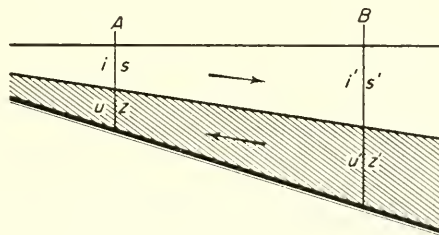


FIG. 164. Water and salt transport through sea straits.

through such an oceanic region (for instance a strait). If the *mean* salinities are s and s' at *A* and *B* in the upper current and z and z' in the lower current and the current amounts are i and i' in the upper current and u and u' in the lower, then, under steady conditions the constancy of water and salt transport in each current will give the equations

$$i - i' = u - u'; \quad is = uz; \quad i's' = u'z'$$

If the mean salinities are known these relationships give the Knudsen relations in the form

$$i' = i \frac{z' z - s}{z z' - s'}; \quad u = i \frac{s}{z}; \quad u' = i \frac{s' z - s}{z z' - s'}. \quad (\text{XII.19})$$

If the upper current is known at one point and the distribution of salinity is known at two, these relations allow an evaluation of the mean water transports at different cross-sections in the strait; if no current amount is known they give at least the inflow and outflow conditions which in itself is valuable.

If section *A* is taken so far inland within the river mouth that only fresh water is present ($s = 0$, as well as z and $u = 0$), then it is the mean water amount carried by the river seawards per second and from (XII. 19)

$$i' = i \frac{z'}{z' - s'} \quad \text{and} \quad u' = i \frac{s'}{z' - s'}. \quad (\text{XII.20})$$

A longitudinal section given by F. L. Ekman for the Götaelf showed $s = 18$, $z' = 22\%$ so that $i' = 5.5 i$ and $u' = 4.5 i$ that is $i' : u' = 11 : 9$. The thickness of the upper current was 3 m, that of the lower current was 9 m and thus in one second there was a flow of 11 volume units per unit area seawards in the upper current compared with a flow of 3 units upstream in the lower current.

Another example given by Knudsen refers to the Baltic. Cross-section *B*: cross-section through the outlets of the Baltic (the Öresund and a section from Gedser to Darsserort); cross-section *A*: the entire surface of the Baltic and sections through all the river mouths. Here i in (XII. 21) was the entire amount of water entering the Baltic per sec due to precipitation, evaporation and run off by rivers. From the salinity distribution is obtained $s' = 8.7$ and $z' = 17.4\%$ from which it follows that $i' = 2i$ and $u' = i$. Thus the upper current carries twice as much water out through all the outlets of the Baltic as is carried into the Baltic by the *lower* current and the amount of water flowing in with the *lower current* is equal to the actual inflow from other sources (precipitation, evaporation and river water). Since $i' = i + u'$ only half the outflow is derived from fresh-water gain, the other half is balanced by the inflow in the lower current from the sea.

In a third example Knudsen placed the cross-section *A* through the Öresund and the Kadet-channel and cross-section *B* through the Kattegat from Fornäs to the Skalle Riff. At *A*, $s = 8.7$ and $z = 17.4\%$; however, at *B*, $s' = 20$ and $z' = 33\%$. With these values the relationships XII, 20 give $i' = 1.27i$, $u' = 0.77 i$ so that $i' : u' = 1.65$.

The amount of water flowing out through the Kattegat section is about 5/4 times greater than that flowing in from the actual Baltic Sea through the Öresund and the Kadet-channel, that is, it is about 2.5 times larger than the total gain of the Baltic in fresh water. It is also found that the amount of salt water flowing in into the Kattegat from the south is about 1.5 times larger than the amount of salt water flowing in into the Baltic. This amount of water is the same as half the entire inflow into the Baltic and indeed penetrates into the western part of the Baltic but mixes with the upper current and is carried out again.

A further example is given by the oceanographic conditions in the Bosphorus. At a cross-section at the south-west end salinity measurements (September–October 1917 and May 1918; MÖLLER, 1928) gave $z = 37.65$ and $s = 17.47\%$ with the boundary surface at a depth of 23 m; however, a cross-section at the north-east end gave $z' = 35.79$ and $s' = 17.23\%$, the boundary surface depth being 44 m. From (XII. 19)

these values gave the relationships (calculated) $i' = 1.03 i$, $u = 0.465 i$, $u' = 0.449 i$ and $u' = 1.07 u$. Current measurements gave the relations (observed) $i' = 1.06 i$, $u = 0.55 i$, $u' = 0.449 i$ and $u' = 1.22 u$.

Considering that the observational values were obtained from only a few individual measurements and that meteorological factors have an appreciable influence on water transport through the Bosphorus the agreement is very satisfactory.

A generalization of the Knudsen relations has been given by WITTING (1906) in his study of the Gulf of Bothnia; here an attempt was made to consider in the calculation changes in salinity during the observational period, although one is mostly forced by the observations to be satisfied with the simpler equations (XII. 19). The investigations of GEHRKE (1907) on the current conditions west of Ireland and the British Isles, where the Atlantic current flows north-east were also based on these relationships; they are an example of how similar ideas can be applied to corresponding problems concerning the oceanic circulation, even then, when no upper and lower current flowing in opposite directions are present.

All these investigations are based entirely on the continuity equation for the water and salt contents and of course yield information only on *mean* conditions; they do not give any information about the internal structure of the currents or on the causative connections between them.

Chapter XIII

General Theory of Ocean Currents in a Homogeneous Sea

1. Introduction

A THEORY covering all the phenomena of ocean currents and taking into account all the effects of the internal and external forces must essentially be rather complex and would not allow an immediate insight. The theory must thus, as in other fields of natural sciences, take another path as soon as it can be based on well-founded geophysical principles, and must use simplifying assumptions taking only the effect of *one* single current-generating factor into account at a time. All these individual *current constituents* can then be combined to give some picture of all the factors involved in the generation and maintenance of the ocean currents. This, of course, is the aim of any theory; because of the complexity of the phenomena involved, little could be deduced from the dynamics of the ocean currents developed in their most general form that would assist in the elucidation of the nature of the oceanic circulation. The history of the theory of ocean currents is long and goes back a long way and would require considerable space; a more or less detailed account of the older parts has been given by KRÜMMEL (1911, pp. 442–449). The first simplification is the elimination of the internal forces; this is identical with the assumption of a *homogeneous sea*. In this case only external forces would be able to produce water movements. EKMAN (see especially 1927) was the first to develop the problems of the dynamics of the ocean currents of a homogeneous sea in a classically elegant form and went far towards successful solutions for these. There are two immediately apparent problems:

In a homogeneous sea, movements of the water may arise besides from the effect of the wind on the sea surface also from the pressure of a sea surface slope. This gives rise to a horizontal pressure gradient which is transmitted through the entire water mass down to the bottom. The first main problem is then the calculation of the velocity components at each level for a given wind force and a given gradient of the sea surface. The hydrodynamic equations of motion provide the basis for this and can be solved, as has been shown by Ekman, if the frictional coefficient is given. The current system produced by the action of these external forces at all points along a vertical was termed by Ekman the “*elementary*” current.

The constituents of the elementary current can be derived without taking the continuity equation into account. Due to differences from place to place in the wind distribution or the sea surface slope or due to local differences in the depth of the sea the continuity requirement cannot be satisfied by horizontal movements *alone*. The divergence of the currents caused in this way gives rise to changes in the sea-level which in turn affect again the elementary current (feed-back). The second main problem

consists only in following these changes in the elementary current or in determining under *stationary conditions* the elementary current that satisfies the continuity equation, and then in evaluating the associated time-independent sea-surface slope for all points of the oceanic region under consideration. Only then can the problem be considered as completely solved. This second problem is the more difficult one since the boundary conditions at coastlines must also be satisfied. It does, however, help to produce the total picture of the currents for a certain preassumed ocean basin.

The starting equations for the development of the dynamics of the ocean currents are the hydrodynamic equations of motion in their most general form (see equation X.16). The fact that its individual terms are of quite different significance led JEFFREYS (1922) to put forward a terminology for air currents which could also with advantage be applied to ocean currents. According to whether the horizontal pressure gradient is *balanced* principally by the acceleration or by the Coriolis force or by friction, it is possible to distinguish between (equations for the x -axis only, those for the y -axis being analogous):

$$\text{Euler current: } \frac{du}{dt} = -\frac{1}{\rho} \frac{\partial p}{\partial x};$$

$$\text{geostrophic current: } 0 = -\frac{1}{\rho} \frac{\partial p}{\partial x} + 2\omega \sin \phi v;$$

$$\text{antitriptic current: } 0 = -\frac{1}{\rho} \frac{\partial p}{\partial x} + \frac{\partial}{\partial z} \left(\mu \frac{\partial u}{\partial x} \right).$$

The Euler current will appear for rapid changes in the sea level (storm surges, etc.); this is also the relationship on which is based the simple theory of waves, where the water displacements in general have the character of a Euler current. The geostrophic current corresponds to another current constituent of the "elementary" current, namely to the gradient current (deep current), while, during the formation of the wind drift and the bottom current, besides the Coriolis force to a considerable extent friction is also involved. An antitriptic current can be expected in local circulations of small extent, for example, in equalization currents in sea straits where the narrow width prevents an effect of the Coriolis force.

2. Steady Currents in a Homogeneous Sea Without Friction

(a) General Equations

For a horizontal frictionless water movement, the equations of motion (X.16) for a homogeneous sea ($\rho = \text{const.}$) (Coriolis parameter $f = 2\omega \sin \phi$) will take the form:

$$\frac{du}{dt} = fv - \frac{1}{\rho} \frac{\partial p}{\partial x}; \quad \frac{dv}{dt} = -fu - \frac{1}{\rho} \frac{\partial p}{\partial y}. \tag{XIII.1}$$

In a homogeneous sea the pressure p at a depth z (counted as positive downwards from the undisturbed sea level $z = 0$) is given by

$$p = g\rho(z + \zeta), \tag{XIII.2}$$

where ζ is the elevation of the sea surface above the undisturbed level (counted positive upwards). Equations (XIII.1 and 2) then give

$$\frac{du}{dt} = fv - g \frac{\partial \zeta}{\partial x}; \quad \frac{dv}{dt} = -fu - g \frac{\partial \zeta}{\partial y} \tag{XIII.3}$$

and the condition for non-accelerated (stationary) current is then

$$fv = g \frac{\partial \zeta}{\partial x}; \quad fu = -g \frac{\partial \zeta}{\partial y}, \tag{XIII.4}$$

or if the total velocity $V = \sqrt{(u^2 + v^2)}$ and $\partial \zeta / \partial n$ is the total pressure gradient (n normal to the lines of equal water level)

$$V = -\frac{g}{f} \frac{\partial \zeta}{\partial n}. \tag{XIII.5}$$

For a steady current pressure force and Coriolis force will be in equilibrium. Fig. 165 shows diagrams of the forces acting on such currents for both the Northern and the Southern Hemisphere. The currents follow the lines of equal water level which are at the same time isobars on the level surfaces ("Niveau-Flächen") and it follows the proposition: *In the Northern Hemisphere when facing downstream for a steady frictionless water movement the higher water level will lie on the right-hand side of the current direction and the lower water level will be on the left-hand side*; the slope of the sea surface is a measure of the current intensity. Such a current is termed a geostrophic current.

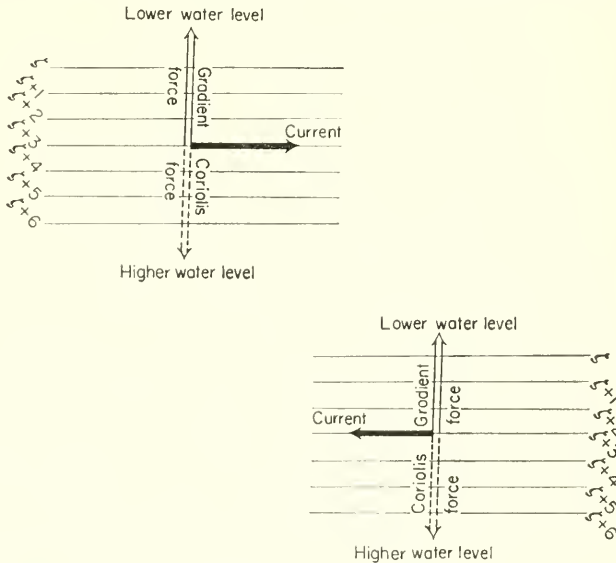


FIG. 165. Schematic distribution of the forces for a stationary current in a homogeneous ocean without friction (left side: Northern Hemisphere; right side: Southern Hemisphere).

Equation (XIII.3) permits integration if the topography of the sea-level is constant in time or unchanged by the current. Multiplying the first equation by u and the second by v , and adding, gives the relation

$$\frac{1}{2}dV^2 = -g d\zeta.$$

If a small water particle moves along a level surface from a point where the sea level

is ξ_0 above the equilibrium level, to another point where this deviation is ξ_1 , it will acquire a final velocity V_1 given by the relation

$$V_1^2 = 2g(\zeta_0 - \zeta_1) \tag{XIII.6}$$

if it was at rest at the starting point ($V_0 = 0$). Corresponding values of V_1 and $\zeta_0 - \zeta_1$ are given in Table 115.

Table 115

$\xi_0 - \xi_1$ (mm) . .	1	2	5	10	50	100	150
$p_0 - p_1$ (centibars)	0.01	0.02	0.05	0.10	0.50	1.00	1.50
V_1 (cm/sec)	14	20	31	44	98	139	312

If a water element glides downwards without friction along an oblique pressure surface through a short vertical distance, it will immediately acquire a very large velocity. If the water masses were not forced by the Coriolis action to move along the lines of equal water level under stationary conditions, even a very small slope would be able to cause enormously intense ocean currents. Equation (XIII.5) shows that the forces producing the movement (gradient force) do not, in the stationary case, determine the acceleration of the water movement, but solely, due to the Coriolis force, its velocity.

(b) The Effect of Changing Depth and the Spherical Shape of the Earth

Equations (XIII.4 and 5) show that the entire water column down to the sea bottom will have the same velocity; it will move like a solid body with a velocity V in the appropriate direction. This current can only satisfy the continuity equation if the sea bottom is plane. Under stationary conditions ($\partial\zeta/\partial t = 0$) according to equation (XII.16) the continuity equation takes the form

$$\frac{\partial u}{\partial x} + \frac{\partial v}{\partial y} = 0. \tag{XIII.7}$$

It will be satisfied by the values of u and v given by (XIII.4). At constant depth there will thus be no limitation to a geostrophic current. If there are boundaries to the sea in the form of vertical coasts then the boundary condition will require a constant ζ along them; the current will then flow only along the coast and there will be no flow perpendicular to the coast.

If the ocean depth is variable, conditions will be more complicated. In Fig. 166 is shown the case where a given uniform slope of the sea surface (Northern Hemisphere)

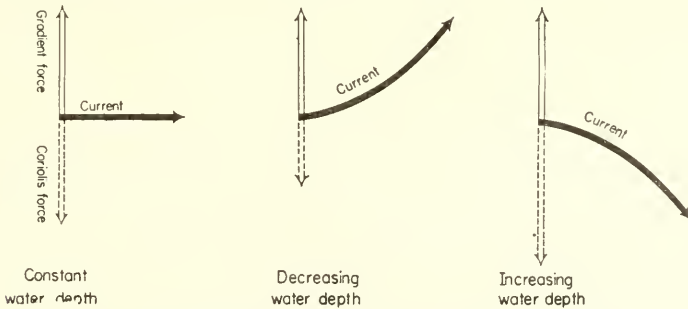


FIG. 166. Deviation of ocean currents for a variable bottom depth.

from the surface of the figure backwards gives rise to a uniform current from left to right; at first there will be an equilibrium in it between the gradient and Coriolis forces. If the depth of the sea increases in the current direction (bottom slopes downward) then for a constant flow amount, since the current cross-section becomes larger, there must be a decrease in velocity. The equilibrium between the two forces will be disturbed, the lower velocity attained will correspond to a smaller Coriolis force and the current will be deflected *contra solem*. However, if the depth decreases (i.e. the bottom rises) the velocity must increase; this will give an increase in the Coriolis force and a deflection of the current *cum sole*. The equilibrium state of equation (XIII.4) will continue for each stream line only when the current follows the depth lines of the bottom.

If the depth is variable, (XII.16) will be replaced by the continuity equation

$$\frac{\partial \zeta}{\partial t} = - \left(\frac{\partial hu}{\partial x} + \frac{\partial hv}{\partial y} \right). \quad (\text{XIII.8})$$

Under stationary conditions the equations of motion (XIII.4) will then give the condition

$$\frac{\partial h}{\partial y} \frac{\partial \zeta}{\partial x} - \frac{\partial h}{\partial x} \frac{\partial \zeta}{\partial y} = 0. \quad (\text{XIII.9})$$

This relation states that if the depth varies then steady frictionless currents are only possible if *the topography of the sea surface on a relative scale accords with that of the sea bottom*. The currents must thus run parallel to the bathymetric curves; the strength of the current is, however, free and depends only on the absolute gradient of the ζ -values. If there are coastal limits, the boundary condition requires that the depth should be constant along the outer boundary (the coast).

Since the continuity equation for currents in an ocean partly or completely covering the spherical Earth has a different form (equation (X.27)), the conditions for steady currents will also be different. The equations of motion for the meridional and zonal velocity components will now be (R = Earth radius, $\vartheta = 90^\circ - \phi$ = zenith distance):

$$u = - \frac{g}{fR \sin \vartheta} \frac{\partial \zeta}{\partial \lambda} \quad \text{and} \quad v = \frac{g \partial \zeta}{fR \partial \vartheta}. \quad (\text{XIII.10})$$

For a variable depth h and taking into account that h is always small compared with R , the continuity equation will have the form

$$\frac{\partial \zeta}{\partial t} = - \frac{1}{R \sin \vartheta} \left(\frac{\partial h \sin \vartheta}{\partial \vartheta} \frac{\partial u}{\partial \lambda} + \frac{\partial hv}{\partial \lambda} \right). \quad (\text{XIII.11})$$

The condition for a frictionless steady current is then under these conditions

$$\frac{\partial h}{\partial \lambda} \frac{\partial \zeta}{\partial \vartheta} - \frac{\partial h}{\partial \vartheta} \frac{\partial \zeta}{\partial \lambda} - h \tan \vartheta \frac{\partial \zeta}{\partial \lambda} = 0. \quad (\text{XIII.12})$$

The first two terms are identical with the condition for planar co-ordinates (equation XIII.9); they thus include only the effects of variable depth. The third term $h \tan \vartheta (\partial \zeta / \partial \lambda)$ takes into account the effect of the spherical shape of the Earth; it is largest in the equatorial regions (ϑ close to 90°) and vanishes at the poles ($\vartheta = 0^\circ$). Some special cases can be selected to illustrate the two effects.

(1) If the depth of the sea is constant, the conditional equation is satisfied only if $\partial \zeta / \partial \lambda = 0$, i.e., only if *zonal* currents are possible (along latitude circles).

(2) The depth shall be a function of the latitude only. Then $\partial h/\partial \lambda = 0$ and the topography of the sea bottom will be symmetrical about the poles. In that case, according to (XIII.12), there must be either $\partial \zeta/\partial \lambda = 0$ or $\partial h/\partial \vartheta + h \tan g \vartheta = 0$. The first condition leads again to zonal currents; the second gives on integration $h = H \cos \vartheta$ where H is the depth of the sea at the poles ($\vartheta = 0^\circ$).

In these cases both $\partial \zeta/\partial \vartheta$ and $\partial \zeta/\partial \lambda$ are free, that is, ζ is also free. For a meridional depth distribution of this type (decreasing gradually from a depth H at the poles to a depth zero at the equator) steady currents would be possible in any direction also in an ocean on the spherical Earth; conditions here are then the same as in a sea of constant depth with planar co-ordinates. For this depth distribution both effects balance exactly. It can therefore be deduced that in higher latitudes small changes in depth will be able to compensate the effect of the curvature of the Earth, this effect will therefore be small there. On the other hand, in lower latitudes larger changes in depth will be required to balance this effect and therefore almost only zonal currents will be possible. *The critical vertical gradient* in meridional direction which will be able to balance the effect of the spherical shape of the Earth is given by $(h/R) \tan \vartheta$. Table 116a gives these critical values for different latitudes and for depths of 3000 and 5000 m.

Table 116a

Polar distance . . .	20°	30°	40°	50°	60°	70°	80°
Latitude	70°	60°	50°	40°	30°	20°	10°
Critical bottom gradient for							
$h = 3000$ m	1:5810	1:3670	1:2540	1:1780	1:1220	1:773	13:73
$h = 5000$ m	1:3500	1:2190	1:1520	1:1070	1:735	1:464	1:224

The discussion of the above equation (DEFANT, 1929a, p. 61) leads to an estimate of the two effects on steady currents. Following EKMAN (1923), these can be summarized as follows: Up to 3–4° latitude—and when the changes in depth are small, even farther away from the equator—the effect of the bottom relief is rather unimportant for the tendency of the current to flow in zonal direction. Between 10° and 20° of latitude the two effects are equal and in higher latitudes (> 40°) the effect of the bottom topography gains in importance and the currents tend to follow definitely the isobaths of the sea bottom. The observed fact that in reality ocean currents do preferably follow a zonal direction in lower latitudes and their direction in higher latitudes is presumably more affected by the bottom topography, appears to be reasonably well explained by the theoretical results presented above.

3. Eddy Viscosity (Turbulent Friction) in Ocean Currents

(a) Mixing Length and Eddy Viscosity (Turbulent Frictional) Coefficient

The movement of the water masses in ocean currents is mostly disordered and turbulent and part of the strong variations in speed and direction of the flow which are observed in quick-response recordings (see p. 347) can be attributed reasonably to this internal turbulence. More or less large elements of water (water quanta) are continuously being carried by these internal turbulent motions into the layers above, below or

to the side and there is thus an equalization of the momentum (current impulse) in the direction of the strongest velocity gradient. There is also an associated equalization of all the characteristic substances and of the water properties. This equalization process has already been discussed in detail in Pt. I, Chapter II (see p. 105). For the property-pair momentum-velocity under conditions of immediate and complete equalization of the flow momentum a general expression for the *apparent shearing stress* of a turbulent flow has been derived having the form

$$\tau = \eta \frac{\partial \bar{u}}{\partial z}, \quad (\text{XIII.13})$$

where \bar{u} is the mean velocity along the x -axis, z is perpendicular to it, η is the exchange coefficient for momentum (eddy coefficient or turbulent frictional coefficient).

In Chapter II (see p. 329) another expression was derived for the apparent shearing stress occurring in turbulent flow from the analysis of the current variations in it. This was given as

$$\tau = -\rho \overline{u'v'}. \quad (\text{XIII.14})$$

The variations in velocity u' and v' are of course connected with the distribution of the *mean* velocity which varies across the stream lines. To give a practical form to equation (XIII.14) PRANDTL (see especially 1942) introduced the *mixing length* l , defined as the length which can be regarded as the diameter of the water quanta moving with the turbulent flow or as that distance that such a quantum travels before losing its identity due to mixing with the surroundings. A water element with a mean velocity $\bar{u}(z)$ at a point z (see Fig. 167) will have a mean velocity $\bar{u}(z+l) = \bar{u}(z) + l(\partial\bar{u}/\partial z)$ at a distance

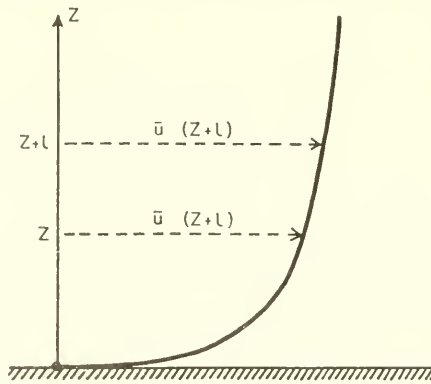


FIG. 167.

l across the current. If a water element is moved from one layer to another then the magnitude of u' is given by

$$u' = \bar{u}(z+l) - \bar{u}(z) = l(\partial\bar{u}/\partial z).$$

The variations in velocity v' arise from the movements of the water elements entering the place under consideration from different sides, moving one behind the other and approaching or receding from each other with a velocity difference of $2l(\partial\bar{u}/\partial z)$ and thus give rise to transverse movements. Thus v' will also have the order of magnitude $l(\partial\bar{u}/\partial z)$. Between u' and v' there must, however, be a *negative* correlation. The water

elements entering from below will have too small a velocity, those entering from above will have correspondingly too large a velocity as compared with the velocity at the point under consideration; positive v' will thus occur together with negative u' and *vice versa*. The product $u'v'$ is then always negative. The apparent shearing stress is thus always positive and of the order of magnitude $\rho\{l(\partial\bar{u}/\partial z)^2\}$. The proportionality factor is here arbitrarily taken as 1; this means only a slight change in the meaning of l . To express in this relation that positive $\partial\bar{u}/\partial z$ will accompany a positive shearing stress and negative $\partial\bar{u}/\partial z$ corresponds to a negative shearing stress, the eddy stress must be re-written in the form

$$\tau = \rho l^2 \left| \frac{\partial\bar{u}}{\partial z} \right| \frac{\partial\bar{u}}{\partial z}. \tag{XIII.15}$$

These turbulent shearing stresses change proportional to the square of the velocity and this has been shown experimentally in investigations in hydraulics. The mixing length l is not a constant here, but depends on the conditions in the current and will vary from place to place. At a solid boundary it is zero and increases with distance from the boundary.

Comparison of the two equations (XIII.13 and 15) leads to

$$\eta = \rho l^2 \left| \frac{\partial\bar{u}}{\partial z} \right|. \tag{XIII.16}$$

The eddy viscosity coefficient depends not only on the mixing length l but also on the velocity and density and is thus less susceptible to clarity than the concept of mixing length. However, oceanic turbulence problems can only be handled numerically using the quantity η , the eddy viscosity coefficient, especially for a freely developed turbulence remote from solid boundaries (coasts and sea bottom). In the layers near the bottom, however, there are considerable advantages in the introduction of the mean mixing length as a characteristic number giving the degree of the turbulence as a function of the distance from the bottom and of its roughness.

From relation (XIII.15) it can be seen that the quantity

$$\sqrt{\frac{\tau}{\rho}} = l \frac{\partial\bar{u}}{\partial z} \tag{XIII.17}$$

has the dimension of a velocity. It is termed the *friction velocity* (shearing stress velocity) u_* , so that $\tau = \rho u_*^2$ which as mentioned above gives the flow resistance as a quadratic function of the velocity.

The behaviour of a turbulent flow above a rough surface can be judged upon using equation (XIII.17), making an assumption about the mixing length l (PRANDTL, 1942, p. 108). Since l increases with the distance from the underlying surface ($z = 0$), it can be put equal to κz and if u_* is constant, (XIII.17) gives the solution

$$u = u_* \left(\frac{1}{\kappa} \ln z + C \right). \tag{XIII.18}$$

As has been shown in numerous investigations, the observed profiles are rather well approximated by such logarithmic velocity profiles; for the number κ the universal value 0.40 was obtained. If ordinary decadic logarithms are used instead of natural ones, equation (XIII.18) becomes

$$u = 5.75 u_* \log \frac{z}{c_0}. \tag{XIII.19}$$

This represents a rather simple connection between the friction velocity and the actual velocity distribution above the bottom. The integration constant c_0 can be related to a *roughness length* or parameter k . It has been found that for small bottom irregularities such as occur on a flat bottom, sand or snow surfaces or surfaces with not too large plants c_0 can be given the value $c_0 = (k/7.35)$, where k is the average roughness parameter corresponding to the irregularities. If the bottom irregularities are very large, it is difficult to determine the position of the point where $z = 0$ for which the mixing length should vanish. It is then best to shift the zero point upwards by a distance z_0 and to use $z + z_0$ in place of z in equation (XIII.19). This will then mean that in the space within the major irregularities the mean height of which is z_0 the turbulent mixing length falls very rapidly to zero.

The turbulent eddy viscosity coefficient η can be obtained from equations (XIII.16 and 17)

$$\eta = \rho h u_* = \rho u_* \kappa z. \quad (\text{XIII.20})$$

In the lowest bottom layers it will at first increase linearly with distance from the bottom; but above a certain height it is generally assumed to remain a constant.

There are very few oceanic observations with which it would be possible to test this logarithmic law for ocean currents above the sea bottom. This would require measurements at close intervals from just above the bottom to a considerable height above it. The measurements made by Merz (MÖLLER, 1928) in the southern entrance to the Dardanelles, which is sufficiently wide for the current to be unaffected by the lateral boundaries, are probably suitable for this. Only the layers just above the bottom need to be considered. Here the rather strongly scattered individual values of the three series of measurements gave the following distribution:

Height above the bottom (m)	. . .	2	7	12	17	22	27
u (cm/sec)	0.3	2.8	4.6	5.5	6.5	7.2

These values follow a logarithmic law rather well and lead to the equation

$$\frac{u}{u_*} = 5.75 \log \frac{z}{1.32}.$$

The representation of the observations by this equation is entirely satisfactory. It is of interest that in spite of the certainly rather pronounced unevenness of the bottom (hence a large value for c_0) the quantity z_0 introduced above is apparently zero. This may be because the heights z above the bottom are already heights above a "mean" sea bottom and in actual fact already represent $z + z_0$. This dependence of velocity on height appears to apply only up to 25 m above the bottom. As shown by observation the behaviour of u is then higher up completely different.

Current measurements near the sea bottom have been made by Mosby (1947) in order to study turbulence and friction in the bottom layers. Using a special apparatus he has measured the direction and intensity of the current in the Aavaerstrømmen (near Bergen, Norway) up to 2 m from the bottom over a period of $3\frac{1}{2}$ h; this gave the following mean vertical distribution of the horizontal velocity:

z (cm above the bottom)	. . .	25	50	75	100	125	150	200
u (cm sec ⁻¹)	16	23	27	29	31	31.7	32.5

These values can be represented rather well by the equation

$$\frac{u}{u_*} = 5.75 \log \frac{z}{0.473}.$$

It does not seem to be necessary to consider z_0 in the formula. Later measurements (1949) did not show such simple conditions; in the bottom layer (just above the sea bed) the velocity fell off very rapidly to small values. The changes in the u -values with time at different heights above the bottom show clearly the turbulence of the current; it appears to decrease only very slowly towards the bottom.

(b) Dissipation of Energy by Turbulence

The turbulent process mixes neighbouring water quanta; part of the energy is deviated from the direction of the mean basic current, the water masses are flattened out by vortices into thin layers and part of the energy is used up in this, which would otherwise remain in the basic current. The magnitude of the energy dissipation by turbulence can be calculated from the size of the shearing stress (XIII.13). This shearing force acts horizontally; the relative movement of two water sheets one above the other is $\partial\bar{u}/\partial z$. From this the work done by the turbulence (energy consumption by the apparent friction "Scheinreibung") will be $R = \eta(\partial\bar{u}/\partial z)^2$. This is that work which must be done in unit volume and unit time to maintain the turbulence against the velocity gradient. (SCHMIDT, 1919).

In the example described above, in the Dardanelles, the velocity decreased from 27 m down to 2 m above the bottom by 6.9 cm/sec. The mean velocity gradient was thus $(du/dz) = (1/362)$. The dissipation of energy per day amounted to 0.66η ergs per cm^3 . This appears rather small but over a longer period has an appreciable effect. If $\eta = 100 \text{ cm}^{-1} \text{ g sec}^{-1}$ then the kinetic energy of a current of 20 cm/sec will be 200 erg/cm^3 and this would be entirely absorbed by the turbulence in about 3 days if not continuously renewed by other forces.

(c) Turbulence and Stratification

That the turbulence is dependent on the stratification in the medium is apparent from the following considerations (EKMAN, 1906; SCHMIDT, 1917; PETERSSON, 1930, 1935). In the presence of stable stratification the mixing process is affected by the double work required to lift the lower heavier water masses against gravity and to lower the upper lighter ones against buoyancy forces. This hinders mixing and if the density differences become large enough the stability of the water stratification reaches so high a value that turbulence cannot act against it and may cease entirely. In subtropical oceanic regions cases occur in the tropospheric deeper currents in which a thin layer of highly saline water embedded between two layers of low-saline water can spread over thousands of miles without being absorbed in the layers above and below by mixing. The strong stability of the vertical stratification of the water masses completely prevents mixing. An example of this behaviour of the subtropical intrusions of highly saline water has been given in Pt. I, p. 169, Fig. 73 and the reader is referred to the discussion at that place.

The conditions under which the work expended in the vertical displacement of water elements by turbulence becomes so large that the turbulence is completely suppressed can be found by comparison of the energy dissipation by turbulence and the lifting work done against gravity by mixing. The buoyancy force per unit time and unit mass for a density gradient $\partial\rho/\partial z$ is given by $g(l/\rho)(\delta\rho/\partial z)$.* The vertical disturbance velocity w' according to the previous discussion can also be put proportional to $l(\partial\bar{u}/\partial z)$. From (XIII.16) and taking into account that for an equilization of the density differences (temperature and salinity), η must be replaced by the exchange coefficients for the material properties of the water A_z (pt. I, p. 103), it follows that the work done against gravity in unit volume and unit time is $g(A_z/\rho)(\delta\rho/\partial z)$. The work

* The symbol δ should indicate the necessary consideration of the changes in density due to adiabatic temperature changes.

done by the turbulent motion in unit volume is, however, $\eta(\partial\bar{u}/\partial z)^2$. The condition for the decrease of the turbulence in the disordered flow and its transformation into an ordered flow is thus that the dimensionless stratification quantity

$$\frac{(g/\rho)(\delta\rho/\partial z)}{(\partial u/\partial z)^2} > \frac{\eta}{A_z}. \quad (\text{XIII.21})$$

In earlier investigations it has mostly been assumed that η and A are numerically equal, i.e. that the mechanism of mixing of a material property is identical with that of the impulse or momentum transport. Then η would be equal to A , and since the stability of the stratification would be given by $(1/\rho)(\delta\rho/\partial z) = E$ (pt. I, p. 196), the condition for the suppression of the turbulence would be

$$\frac{gE}{(\partial u/\partial z)^2} > 1. \quad (\text{XIII.22})$$

The expression on the left-hand side has been denoted the *Richardson number* Ri . The upper limit at which all turbulent motion is extinguished is thus given by $Ri = 1$; however, in reality smaller values are sufficient. Referring to the latter statement, theoretical and experimental investigations of TAYLOR (1931) and Goldstein on small oscillations in a stratified flow with a linear decrease in velocity have shown that the limit can be expected at $Ri = 0.25$ or $\frac{1}{4}$.

In oceanography it has usually been found (see pt. I, p. 104) that the ratio $\eta:A$ is of the order of 5 to 20. In the equatorial regions of the Atlantic Ocean in the density transition layer (thermocline) $\partial\rho/\partial z$ is of the order of 3 to 9×10^{-4} for a 20 m height interval. The decrease in velocity $\partial u/\partial z$ should be between 5 and 10 cm/sec for every 20 m, so that Ri must be between 6 and 69 (DEFANT, 1936c, p. 296 and 363). It is clear that these figures are sufficiently high to prevent the occurrence of turbulence in the tropospheric deeper currents, as has been found by observation.

Observations at two stations in the Baltic for which there was almost no turbulence to be observed in the transition layer gave according to GUSTAFSON and KULLENBERG (1936) Ri -numbers of 0.59 and 0.95 which are in accord with the limiting values given by Taylor. Detailed measurements have been made by JACOBSEN (1913, 1918) at Schultz's Grund (Kattegat) and in the Randersfjord, which are very suitable for answering the question under consideration. Table 117 give as summary of all the values derived from these measurements.

Table 117. Turbulence and Ri -numbers at Schultz's Grund (according to Jacobsen)

Depth (m)	du/dz (cm sec ⁻¹ cm ⁻¹)	Salinity gradient per cm	$\frac{1}{\rho} \frac{d\rho}{dz}$	(g cm ⁻¹ sec ⁻¹)		Ri	$\frac{\eta}{A}$
				η	A		
2.5	10×10^{-3}	10×10^{-4}	7.5×10^{-7}	3.1	0.3	7.1	11.1
5.0	17	15	11.2	3.1	0.4	3.8	7.7
7.5	22	38	28.5	2.7	0.18	5.9	14.9
10.0	24	80	60.0	2.2	0.05	10.2	43.5
12.5	19	140	105.0	1.9	0.04	28.6	47.6
15.0	8	111	82.5	3.8	0.2	125.0	20.0

At all depths η has about 10 times the magnitude of the exchange coefficient A determined from salinity measurements made at the same time. The quotient η/A is almost always larger than the Ri-number and therefore according to the above condition is not compatible with turbulence. The Ri-numbers, which vary between 2.6 and 125, are so high that also according to this criterion a turbulent flow can hardly be present. However, the measurements indicated still a small, though very weak, turbulence with a frictional coefficient between 1.9 and $3.8 \text{ g cm}^{-1} \text{ sec}^{-1}$. According to these investigations, other factors seem also to be involved in the appearance and maintenance of turbulence (close distance to a solid boundary or the presence of an intermediate layer between the otherwise almost homogeneous water masses above and below).

(d) *Turbulence and Mixing in the Sea; Statistical Theory of Turbulence*

The modern hydrodynamic approach to ocean currents has led increasingly to the view that the turbulence of the ocean currents, which finds its visible expression in the oceanic mixing processes, is the basic cause of a number of oceanic phenomena. Oceanography has mostly been concerned solely with the *effects* of turbulence and mixing on oceanic phenomena; only recently has interest been directed also towards the *nature* of oceanic turbulence and one has asked the important question: of what kind is this nature? In laminar flow the velocity can be represented by a simple function of position and time. In turbulent flow the mean velocity, which again can be represented by a simple function of this sort, is superimposed on an additional, irregularly varying turbulent velocity component that changes with both time and space. The sharp distinction between the two types of flow is shown by experimental investigations which indicate that a discontinuous transition from laminar to turbulent flow occurs when a dimensionless quantity, the Reynolds number, exceeds a critical value, the magnitude of which is about 1000. The form of the Reynolds number indicates the cause of this basically different behaviour of the two types of flow. The Reynolds number is given by $R = \rho UL/\eta$, where ρ is the density, U and L are values for the velocity and the linear dimension which are characteristic for the structure of the particular current under consideration; η is the eddy viscosity coefficient (frictional coefficient). It is clear that the current will be turbulent when the momentum (impulse) of the flow ρU or the distance L passed through are large; it will be laminar if the viscosity is large. The viscosity is a force carrying neighbouring elements of the medium along the same path. Therefore, it is obvious that large viscosities will have a tendency to smooth the course of the flow. The empirical fact that the current tends to change to turbulent flow even with very small disturbances—i.e. that the laminar flow is unstable—shows that the turbulent flow has in a certain sense to be regarded as the natural form of motion of media with low viscosity. The Helmholtz vortex-laws of classical hydrodynamics show that a vorticity-free current cannot develop vortices spontaneously. Thus no turbulence can occur in it by itself. It can only be produced inside the fluid by friction at solid surfaces, or by similar processes through the formation of vortices at the boundary of the liquid. Once formed it will spread out in the fluid. This is, however, not the case which we meet in the open sea remote from the sea bottom and from the coasts. The ocean currents here usually have a considerable vortex-intensity from the beginning, i.e. from their formation; it is their further distribution

on vortices of smaller dimensions that has to be regarded as the turbulence of the current. The origin of the oceanic turbulence must thus be traced back to the conditions of formation of the ocean current, and this can definitely be considered to have been done, since the conditions which prevail initially during the formation of the current are certainly scarcely of the type that could be described by simple functions of the velocity distribution. On the contrary, everything indicates that during the formation of a current due to the complicated distribution of the shearing stresses of the winds, the ocean current looks right from the beginning rather confused in vertical and horizontal direction, so that *a priori* there is a very large probability that in the future the resulting current will attain a form which will fall within the general concept of turbulence.

Turbulence is not a form of motion that can maintain itself indefinitely. The kinetic energy of the current is continuously converted by the molecular viscosity into heat. If the current is not continuously supplied with fresh energy, it must in time die away. In the ocean, the currents are continually supplied with energy by the tangential shearing forces of the winds so that here *steady turbulent currents* are possible. This is of particular importance to the nature of ocean currents which are recognized as essentially *quasi-stationary* phenomena by observations.

Turbulence and mixing in *vertical* direction and also *lateral* turbulence of the ocean currents were already discussed in § III *d* and *e* of Pt. I of this volume. Lateral mixing is on a much larger scale than the vertical; the turbulence elements are of considerably larger dimension, so that the eddy viscosity and eddy diffusion coefficients are very large. The ratio of vertical to lateral mixing coefficients is of the order of 10^5 to 10^7 . It can be shown both experimentally and by observation that there is a "continuous spectrum" of mixing and turbulence coefficients extending from the molecular viscosity coefficients to values for the eddy conductivity of 10^{12} (one billion) or more (RICHARDSON, 1926).

In a turbulent current where u is the velocity at a certain point and varies with time, the basic velocity is defined as (time interval T):

$$U = \frac{1}{T} \int_0^T u(t) dt$$

and further the supplementary turbulent velocity as $u' = u(t) - U$, whereby

$$\frac{1}{T} \int_0^T u'(t) dt = 0,$$

the intensity of the turbulence is given by $J = 1/\sqrt{\{(\bar{u}')^2\}}$ and its kinetic energy by $E = \frac{1}{2} \rho (\bar{u}')^2$.* These quantities characterizing the turbulence of the flow depend of course on the length of the time-interval T , and in fact a sufficiently large value for T has to be selected or these quantities lose their meaning altogether. In laboratory experiments in wind tunnels this requirement can always be closely approached, but whether this is also the case for oceanic water masses is difficult to judge. If T is less than a few hours then the $u'(t)$ -values will include terms for the small-scale turbulence such as local mixing, while the basic velocity U will include the long-periodic variations

* The bar above a quantity indicates its mean value taken over the time-interval T .

in the velocity such as the tidal currents and the annual changes in u' . If T is selected with a value of about a month the tidal currents will also be included in the value of $u'(t)$. If T is chosen for 10 years or more, the seasonal changes will also be included in u' and only the secular changes will remain in U . From this it can be understood that, in nature, motions in water masses as they appear in the ocean will be much more complicated than, for example, in an experimentally controlled wind tunnel or a water channel. Every size and all different velocities of the turbulent vortices can be expected to occur in oceanic turbulence, and it is not easy to distinguish between the basic velocity and the additional turbulent velocity. These difficulties occurring with turbulent phenomena of the ocean and atmosphere seem to be fundamentally connected with the nature of turbulence.

In dealing with mixing processes in the ocean, the simple relationship

$$\frac{\partial S}{\partial t} = K \frac{\partial^2 S}{\partial z^2}$$

has usually been used, where $S(z, t)$ is the concentration of the diffusing substance and K denotes the mixing coefficient (eddy diffusivity, eddy conductivity), [$\text{cm}^2 \text{sec}^{-1}$]. This is termed the "Fickian diffusion equation" (see Pt. I, pp. 95 and 104). It is derived by analogy with molecular processes for the larger-scale processes in turbulent currents using simplifying assumptions on the internal nature of turbulence; it does not accord fully with more recent data, and especially not with the fact that the larger the mixing coefficient becomes, the larger the scale of the phenomena under consideration, i.e. with the existence of a continuous spectrum of the diffusion coefficient.

With molecular diffusion, as described by the Fickian equation, the movement of each molecule is independent of that of a neighbouring one. In contrast to this, however, in a *turbulent* current, adjacent elements have increasingly similar turbulent velocities, and in fact the more there are the smaller the distance from each other. The reason for this is easily understood when the behaviour and the effect of the turbulent vortices of all sizes are studied altogether in detail. The distance between two initially adjacent elements is altered only by the smallest vortices; the effects of the larger vortices cause no significant change in distance, since they give rise only to a simple transport of these elements. If, however, the distance between two elements becomes larger, the effect of the larger vortices is added to that of the smaller ones so that as the distance between them increases the diffusion effect due to the larger-size vortices becomes more and more involved.

The most important independent variable cannot be, as in molecular diffusion processes, the position of an element, but the *distance from its neighbouring element*. This requires that the concentration of a diffusing substance is only a function of the mutual separation of the particles inside this substance and not a function of the position only.

RICHARDSON first showed this difference as compared with molecular diffusion and further investigations have then been carried out to account for this circumstance (WITTING, 1933; SVERDRUP, 1946; PROUDMAN, 1948). The theory that the concentration of a diffusing substance is not a function of the position of the element which it occupies, but rather of its distance l from the adjacent element leads to the conclusion

that the diffusion coefficient F is a function of the neighbour-distance l and is given by the equation

$$F(l) = \frac{(l_1 - l_2)^2}{2t}, \tag{XIII.24}$$

where l_0 is the distance between the elements which are at the same distance in the turbulent current at time $t = 0$, while l is the distance at time t . F can be determined from experimental series-measurements from the values for l and this allows a decision as to whether the Fick or the Richardson concept of the internal nature of the turbulence fits the observed data; since according to the Fickian theory F must be independent on l (see also, ICHVE, 1950). All the observations made (RICHARDSON, 1926; WITTING, 1933; STOMMEL, 1949; HANZAWA, 1953; INOUE, 1952) show that F is in fact strongly dependent on l and that there exists a definite relationship between them of the special form

$$F(l) = \epsilon l^{4/3}. \tag{XIII.25}$$

Figure 167a shows a summary of observed data and it is easily seen that the assumption of a 4/3 power seems to be fully justified.

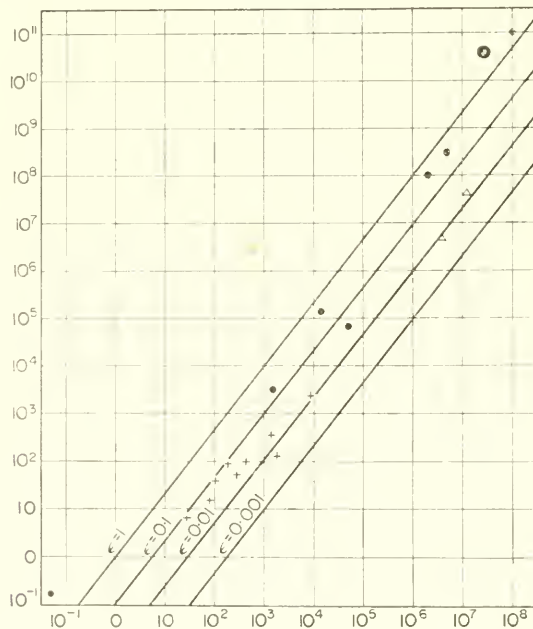


FIG. 167a. The relation $F(l) = \epsilon l^{4/3}$ according to observations (logarithmic scale): points, values of Richardson from the atmosphere; crosses, values of Stommel (Blaimore, Bermuda and Woods Hole); triangles, values of Hanzawa.

Equation (XIII.25) which has been found inductively has been given a sound theoretical basis by closer study of the rate of the energy decrease due to turbulent mixing of the large-scale motion. This method of investigation was first introduced by KOLMOGOROFF (1941) and after some intermediate work WEISZÄCKER (1948) and HEISENBERG (1948) have brought this statistical theory of turbulence to a certain degree of

completion. This theory leads to the same 4/3-power law for the turbulent exchange coefficient which was previously derived from observations. With some modifications this theory can be applied to large-scale processes occurring with oceanic currents, and offers the possibility of obtaining a picture of the spectral distribution of energy in oceanic turbulence. It is thus of a considerable interest for oceanography.

The semi-permanent wind systems such as the trade winds, the prevailing westerlies of temperate latitudes, and furthermore, the aperiodic air currents of the extra tropical pressure disturbances, give rise to large-scale movements in the surface layers of the ocean due to the shearing stresses acting on the sea surface. Thereby, these shearing stresses tend to increase the kinetic energy of the currents produced. However the mean kinetic energy of the ocean currents remains largely constant (quasi-stationary conditions) so that finally as much energy is dissipated in heat as is gained by the work done by the shearing stress of the wind. Ocean currents which initially show large-scale turbulence tend to break up into vortices which subsequently degenerate into smaller and smallest vortices. This proceeds until finally the smallest vortices are formed, which are so small that their energy is converted in irreversible processes by molecular viscosity into heat energy. An exact dynamic explanation of the reasons why the large ocean currents break up into turbulent currents, with more or less large vortices of widely varying size, has not yet been given. However, the empirical facts of their existence have been shown by synoptic surveys, for instance, in the more recent Gulf Stream investigations.

A complete *spectrum of vortex sizes* certainly exists. This spectrum is necessary for the dispersion of the kinetic energy of the ocean currents continuously supplied by the shearing forces of the wind. In practical oceanography it has long been recognized that the concept of the mean velocity of the oceanic currents is rather dependent on the length of the time interval over which its value was determined. The same applies for space-means of the current intensity. This leads to the expectation that the magnitude of the turbulent coefficients also depends fully on what kind of evaluation of the mean has been used. The concept of a turbulence coefficient is absolutely meaningless if the way in which the mean was found is not specified. This can be seen already from the greater magnitude of the turbulence coefficients the greater the dimensions of the movements under consideration; a fact which could not be explained in earlier work.

The Weiszäcker–Heisenberg statistical theory provides information on the frequency distribution of the energy in different size-intervals of turbulent vortices, on the way in which the *mean* velocity depends on the type of mean taken, and lastly on the dependence of the turbulence coefficients on the type of mean taken.

If L_n is the side of a square over which the n th mean is taken then according to Weiszäcker the spectral law is, for the turbulent velocity distribution:

$$\bar{u}_n \text{ proportional to } L_n^{1/3},$$

for the turbulence coefficient:

$$\eta_n \text{ proportional to } L_n^{4/3}$$

and for the turbulent energy distribution:

$$E_n \text{ proportional to } L_n^{2/3}.$$

Weiszäcker took a discrete velocity spectrum as the basis of his theory, Heisenberg chose a continuous velocity distribution and provided an elegant mathematical proof (in this connection see also ICHVE, 1951).

The principal result of the theory, as far as it concerns the exchange coefficients of turbulent motion, is in complete agreement with the $4/3$ power law derived from observed data. The more recent statistical theory of turbulence can give a better description of actual conditions in nature than the classical Fickian theory. In particular, the theory gives an explanation for the large differences in size between the turbulence coefficients for small- and large-scale motion, for which there was no explanation in earlier time. For small-scale oceanic phenomena the values found for the diffusion coefficient η are on the average about $50\text{--}100\text{ cm}^2\text{ sec}^{-1}$. For large-scale ocean currents, on the other hand, the values were between 10^8 and $10^7\text{ cm}^2\text{ sec}^{-1}$. The ratio between these is about 5×10^5 to 10^6 . For small-scale processes L can be taken as about 50 m and for large-scale currents as about 1000 km. The ratio of the L -values is 2×10^4 and for the η -values should be according to the theory about 5.4×10^5 . The agreement with the values derived from observations is rather good.

The question could also be raised, how far the assumptions made by the theory are justified in oceanic conditions. STOMMEL (1949) has closely examined this question. Not all the sources for turbulence in the ocean are due to air currents, a part is certainly due to the thermo-haline structure of the ocean currents the dependence of which, of course, on solar radiation and evaporation is known. The assumption of a continuous series of vortex sizes with horizontal isotropy can hardly be valid for the large oceanic vortices; it can be postulated as a first approximation only when they are of smaller dimensions, i.e. for the genuine turbulent vortices of oceanic currents. The changes which should be introduced for oceanic conditions involve the dividing of the vortex sizes into two parts: an anisotropic one, including all the kinematically dissimilar, large-scale horizontal movements, and an isotropic part, including all the kinematically, similar-to-each-other, turbulent vortices. The latter part only appears after a certain n th averaging process. The first part is thus essentially concerned with the advection of different water types. The exchange is only involved in the second, and the statistical theory of turbulence should be fully applicable here. However, in spite of these changes in many of the assumptions the basic idea of the theory remains and offers a solid basis for the study of dynamic conditions of the ocean currents.

4. Steady Currents in a Homogeneous Ocean under the Action of External Forces

(a) Introduction

The first ideas about the effect of friction on the movement of water masses were based on the assumption that it arose from the roughness of the bottom surface (gliding friction). The frictional force was thus given, as already shown on p. 317, by

$$R = -\kappa\rho V.$$

GULDBERG and MOHN (1876) using this principle for atmospheric flow presented a diagram of the forces necessary for a steady motion. It can also be applied to water movements in shallow ocean currents for which the frictional effects of the bottom act throughout the entire water column. In that case the resultant of Coriolis force and frictional force must balance the gradient force. The direction of the current is

now no longer parallel to the isobars but is deflected at an angle proportional to κ . On the right-hand side of the equations of motion (XIII.1) the components for the frictional force $-\kappa u$ and $-\kappa v$ have to be added. Multiplying the first equation by u and the second by v and adding, gives

$$\frac{1}{2} \frac{d^2 V}{dt^2} + \kappa V = -\frac{1}{\rho} \frac{dp}{dt}.$$

For the movement of a water element along an isobar ($dp/dt = 0$) this equation gives

$$V = V_0 e^{-\kappa t}.$$

The velocity of the current which is acted upon by Coriolis force and friction, usually decreases until it vanishes. The value $1/\kappa$ gives the time needed by the bottom friction to reduce the velocity by a factor of 2.72. For currents in shallow waters κ is of the order of 10^{-6} to 10^{-7} sec $^{-1}$, so that the velocity of the water movement will fall to a tenth between 2 and 25 days.

The Guldberg-Mohn frictional principle makes no allowance for the fact that a turbulent flow is affected also *from above* by mass exchange with the layers above it, in addition to the effect of the bottom surface which affects the flow *from below*. SANDSTRÖM (1910) has taken this circumstance into account by assuming that the frictional force does not exactly oppose the current, but its vector deviates by a small angle to the left of the current direction (or the force acts backwards and to the right of the current).

Also this frictional principle can only be considered as a makeshift and gives acceptable results only for currents in very shallow waters. If all the factors involved in the formation and maintenance of the ocean currents are to be taken into account it is necessary to return to the hydrodynamic equations of motion in the form given in (X.16). Besides friction, there must also be taken into account the effect of the Coriolis force and as current producing factors, especially the tangential pressure of the wind on the sea surface, the pressure gradient and gravity. For *horizontal* water transports, i.e. along the gravitational level surfaces, gravity is less important as an impelling force. If only the wind stress, the Coriolis force and friction are acting, the current will be a *pure drift current*; if, however, gradient force, Coriolis force and friction are the decisive factors, it will be a *pure gradient current*. The following section is concerned with these two *basic forms* of water movement.

The fundamental work in this direction is due almost entirely to EKMAN (1905, 1906, 1922) who first gave a strict mathematical form to the effects of the Coriolis force and friction in the theory of the ocean currents in a homogeneous sea. The great significance of these two forces for the generation of drift currents had already been recognized and demonstrated by means of observational data by NANSEN (1902, 1905). These investigations opened a first way to the development of a complete theory of ocean currents.

(b) Pure Drift Currents

A pure drift current is a result of the wind stress acting on the surface of the sea. This stress is produced either by friction of the air passing over the water, or by the pressure effect of the wind on waves which transfers part of the momentum of the

wind to the water. Both effects usually act in the same direction and can be combined as a single *tangential force*. If there is no pressure gradient within the water mass the surface of the sea must be level $\{(\partial p/\partial x) = (\partial p/\partial y) = 0\}$. With this the condition of an infinite extent of the ocean is basically connected, since otherwise the currents produced will give rise to a piling up of water at the coast lines which will tend to form gradient currents. Such currents will, however, for the moment be disregarded here. In the case of a steady acceleration-free horizontal current $\{(du/dt = (dv/dt) = 0 \text{ and } w = 0\}$ and for constant frictional coefficients the equations of motion (X.16) will take the form ($f = 2\omega \sin \phi$, z positive downwards):

$$\rho f v + \eta \frac{\partial^2 u}{\partial z^2} = 0 \quad \text{and} \quad -\rho f u + \eta \frac{\partial^2 v}{\partial z^2} = 0. \quad (\text{XIII.23})$$

Multiplying the second equation by $i = \sqrt{-1}$ and adding to the first gives

$$\frac{\partial^2}{\partial z^2} (u + iv) = \frac{i\rho f}{\eta} (u + iv). \quad (\text{XIII.23a})$$

For practically unlimited ocean depths the general solution can be taken in the form

$$u + iv = A e^{-(1+i)(\pi z/D)}, \quad (\text{XIII.24})$$

where

$$D = \pi \sqrt{\left(\frac{2\eta}{f\rho}\right)} = \pi \sqrt{\left(\frac{\eta}{\rho\omega \sin \phi}\right)}.$$

The boundary condition that the velocity of the drift current vanishes for large depths ($z = \infty$) is already satisfied by (XIII.24). At the surface of the sea ($z = 0$), a wind in the direction of the positive y -axis will give rise to a shearing stress T , which can be represented by the relation

$$\eta \frac{\partial(u + iv)}{\partial z} = -iT,$$

for $z = 0$. The solution then takes the form

$$u + iv = (1 + i) \frac{TD}{2\pi\eta} e^{-(1+i)\pi'z/D}. \quad (\text{XIII.25})$$

From this the two velocity components of the drift current are then obtained

$$u = V_0 e^{-\pi z/D} \cos\left(45^\circ - \frac{\pi}{D}z\right) \quad \text{and} \quad v = V_0 e^{-\pi z/D} \sin\left(45^\circ - \frac{\pi}{D}z\right) \quad (\text{XIII.26})$$

with

$$V_0 = \frac{\pi T}{\sqrt{2}D\rho\omega \sin \phi} \quad \text{and} \quad D = \pi \sqrt{\left(\frac{\eta}{\rho\omega \sin \phi}\right)}.$$

At the sea surface the water in a pure drift current moves with a velocity V_0 in a direction 45° *cum sole* from the wind direction. At increasing depth the angle of deflection increases while at the same time the velocity of the current rapidly decreases. At a depth D the deflection will amount to a full 180° and the velocity will have fallen

to $e^{-\pi} = 1/23$ of the surface value. This velocity is already so small that by comparison with the surface value it can usually be neglected. The depth D can therefore be taken as a measure of the depth of penetration into the sea of a wind-generated ocean current on the rotating Earth. It can in general also be taken as a measure of how far downwards the effect of a steadily flowing horizontal layer penetrates into the adjacent water masses. It was termed by Ekman the “frictional depth”; for drift currents the additional word “upper” is used in order to indicate that here solely conditions in the top-layer of the ocean are dealt with.

According to equation (XIII.26) D can also be taken as a measure of the internal turbulent friction. It should be noted that the shearing stress T is not involved in the equation relating D and η ; this could be interpreted to mean that the vertical thickness of the drift current should be independent of the wind intensity producing it and maintaining it against friction. This apparent contradiction is clarified by considering that the frictional coefficient increases with increasing wind strength as does also the frictional depth D .

Figure 168, according to Ekman, shows the vertical structure of a pure drift current; the arrows projecting from the central column which are also shown in a projection

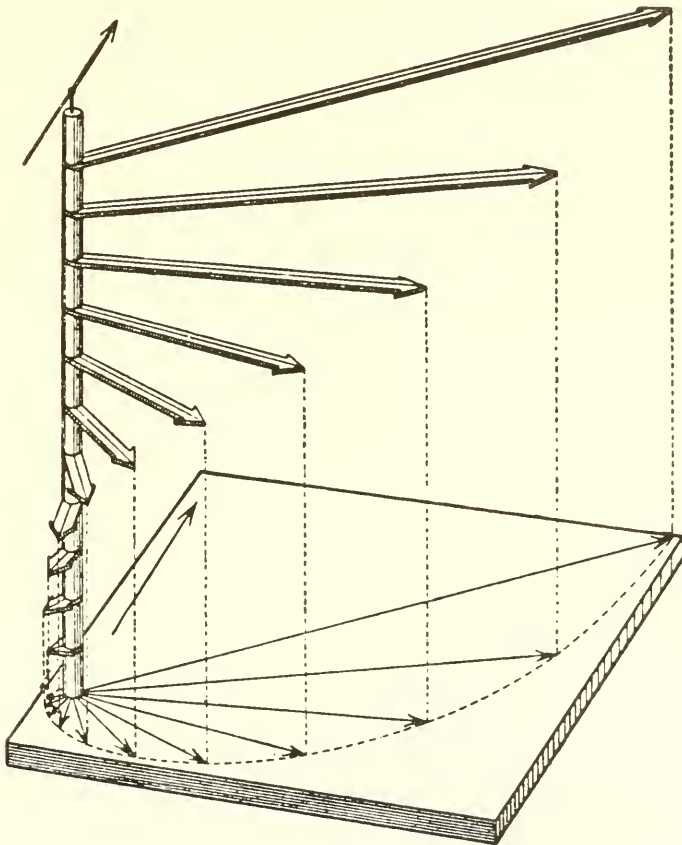


FIG. 168. Vertical structure of a pure drift current (according to Ekman).

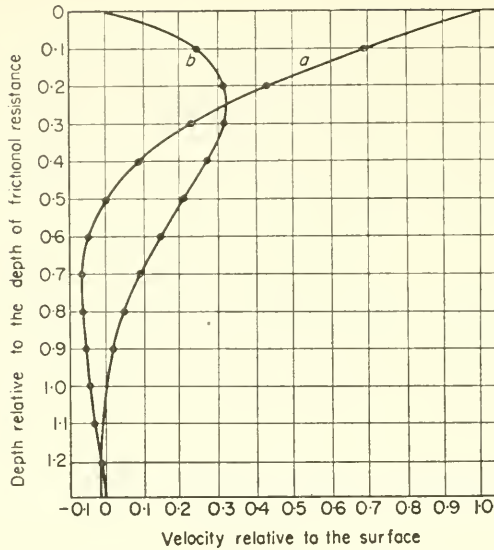


FIG. 169. Vertical current distribution in a pure drift current: (a) in the direction of the surface current; (b) normal to the direction of the surface current.

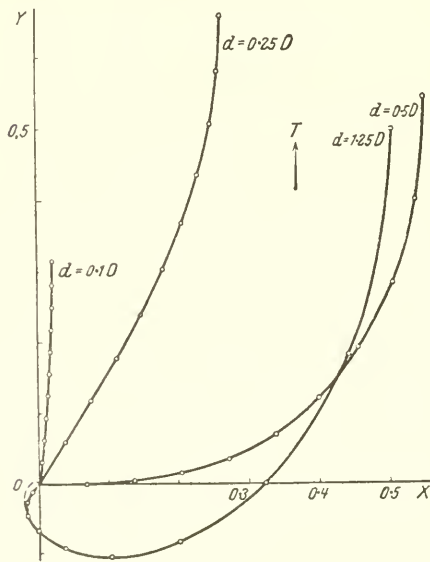


FIG. 170. Vertical structure in drift currents for an ocean depth d nearly equal or smaller than the upper frictional depth D (10 small circles indicate on each curve the end-points of the velocity vectors for the depth $0.0, 0.1, 0.2 d$ and so on until $0.9 d$). The dashed curve at $1.25 D$ refers to $d = 2.5 D$, the remaining part coincides with the curve for $1.25 D$).

on a horizontal plane, give a representation of the direction and strength of the current at the surface and at equidistant levels $0.1D$, $0.2D$, etc. The arrow at the peak of the vertical line represents the direction of the wind. The arrow-heads lie on a doubly curved spiral and the end-points of the vectors on the horizontal plane lie on a logarithmic spiral (*Ekman spiral*). Referring the current components to the direction of the current at the surface and at right angles to it the diagram pictured in Fig. 169 is obtained, which allows one immediately to judge whether the observed vertical distribution of the current carries the character of a drift current.

Equation (XIII.26) shows further that the sea surface velocity increases in proportion to the shearing stress T but in inverse proportion to the frictional depth D . This is reasonable since, for equal T the more water that is set in motion, the smaller must the velocity of the drift current be, i.e. the greater the depth D . The total drift current transport per unit area of the sea surface is given by

$$M = \int_{\infty}^0 (u + iv) dz = \frac{T}{f},$$

that is

$$M_x = (T/f) \quad \text{and} \quad M_y = 0.$$

The total water transport due to a drift current occurs *perpendicular cum sole* to the direction of the shearing stress of the wind producing it and since η is not involved it is independent of the assumption concerning the effects of eddy viscosity. For an arbitrarily chosen co-ordinate system with shearing stresses T_x and T_y in the x - and y -directions, the water transports in these directions will be

$$M_x = \frac{T_y}{f} \quad \text{and} \quad M_y = -\frac{T_x}{f}. \tag{XIII.27}$$

Finite water depth. When the depth of the water is about of the same order as D it has a noticeable effect on the drift current. For a depth d the e -functions in the solution will be replaced by hyperbolic functions. At the sea bottom ($z = d$) $u = 0$ and $v = 0$ are assumed as boundary conditions indicating “adhering” (“Haften”) of the water on the underlying surface. It is apparent from this solution and follows also from Fig. 168 that as long as the depth of water is greater than the frictional depth D the vertical distribution of the drift current will be unaffected, since the water layers below the frictional depth have an insignificant share in the drift current. When, however, the water depth d becomes smaller than D , the effect of the bottom will be of more influence the shallower the sea. Figure 170 shows the vertical current structure for depths $d = 1.25D$, $0.50D$, $0.25D$ and $0.1D$. The thin dotted curve near the origin of the co-ordinate system for the curve $d = 1.25D$ shows the deviation towards the curve for an infinitely large depth; thus in practice there is no significant difference between them. The angle of deflection decreases rapidly with the depth of the water and at very small depths, approximately from about $d < 0.1D$, the movement shows almost no effect of the Earth rotation.

Other frictional assumptions. In addition, Ekman has given a solution for the case where the frictional coefficient is proportional, not to the difference in velocity between two adjacent layers, but rather to its square. This gives essentially the same results as for a constant η ; the angle of deflection of the sea surface current is now

49.1° and the current dies away at the finite depth of $1.25D$. It should be pointed out that the relationship between T , D and V_0 are somewhat different. The total transport for the quadratic frictional law is, however, also given by (XIII.27) and is thus independent of the frictional assumption. This can also be shown by strict mathematical treatment. For a variable η the expression

$$\eta \frac{\partial^2(u, v)}{\partial z^2}$$

in equation (XIII.23) is replaced by

$$\frac{\partial}{\partial z} \left(\eta \frac{\partial(u, v)}{\partial z} \right);$$

see p. 319. Integrating this equation from $z = 0$ to $z = \infty$ or respectively down to a depth at which the drift current can no longer be detected, and considering that the shearing stress is present only at the sea surface, then with the help of equation (XIII.13) relationships are obtained which are identical with (XIII.27). These, however, were derived for a constant η . It could possibly be expected that during the transfer of the turbulent wind momentum to the water masses at the sea surface the two horizontal components of the shearing stress (in the direction of the wind and at right angles to it) would be governed by different turbulent coefficients. An extension of the Ekman theory along such lines has been given by ERTEL (1937). It leads to deflection angles different from 45° while the vertical current structure becomes a deformed spiral.

Another principle applicable both to the wind stress at the sea surface and to the friction at the bottom has been developed by JEFFREYS (1923). In conformity with turbulence theory he assumed that at both the sea surface and at the bottom, "gliding" of the water masses occurs in which the friction is assumed proportional to the square of the velocity differences. The boundary condition at the sea bottom is taken as

$$-\eta \frac{\partial(u, v)}{\partial z} = \kappa \rho(u^2, v^2)$$

and at the sea surface as

$$\eta \frac{\partial(u, v)}{\partial z} = -\kappa \rho'(u'^2, v'^2),$$

where ρ' is the density of the air and u' and v' are the velocity components of the wind relative to the water movement at the sea surface (see p. 317, equation (X.9).)

The more recent results of research in turbulence also show that in the vicinity of boundary surfaces the assumption of a constant frictional coefficient leads to current distributions which do not accord with the observed facts. This makes it necessary to introduce turbulent coefficients, which vary with the distance from the solid boundary. That such a method leads to results satisfactorily explaining the observed features has been shown by an investigation of FJELSTAD (1929) using observations made by Sverdrup on a drift current over the North Siberian Shelf, where there was a strong increase of the frictional coefficient from the bottom to the surface. He succeeded in deriving a functional relationship for these coefficients of the form

$$\eta = \eta_0 \left(\frac{z + \epsilon}{h + \epsilon} \right)^{3/4}$$

and was then able to obtain a solution for the corresponding equations of motion Fig. 171 presents the vertical distribution of the frictional coefficient as well as of the theoretical current structure, both for a constant frictional coefficient and for a coefficient varying with depth, according to a summary made by THORADE (1931). The observed current values are indicated by crosses. There remains no doubt that agreement with the observed data is obtainable only by using coefficients variable with depth.

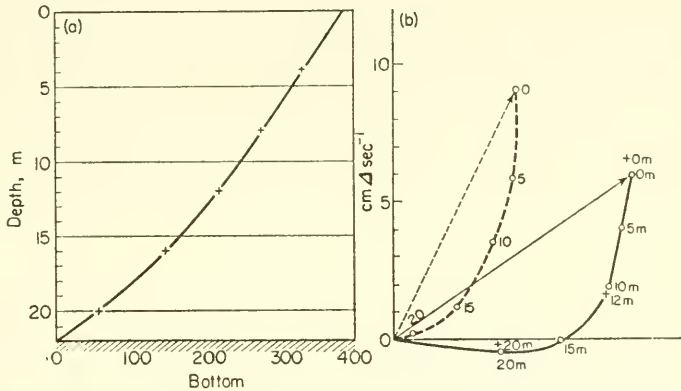


FIG. 171. (a) Vertical distribution of the turbulent coefficient at a station of the North Siberian shelf. (b) Current diagrams: -- o -- o --, theoretical distribution for a constant frictional coefficient; — o — o —, theoretical distribution for a frictional coefficient as in (a); + + + + +, the observed values according to Sverdrup.

The application of the modern theory for a turbulent flow to drift currents will be discussed later together with its application to gradient currents (see p. 311).

Effect of stratification. Assuming a horizontal and stratified sea with a normal density increase with depth, then only minor deviations occur as compared with the case for a homogeneous sea (DEFANT, 1927). However, essentially different conditions appear for sudden vertical density changes (boundary surfaces between different water masses). Here the stratification affects especially the frictional coefficient, which inside the flow of each more or less homogeneous water mass may remain approximately constant and relatively large but may fall almost to zero inside the density transition layer (thermocline). The effect of the wind is thus confined essentially to the top layer and the drift current in this is transmitted only very slowly to the lower water mass across the transition layer. As a boundary condition at the side beneath the top layer it must be assumed, since the water here meets almost no resistance, that there is perfect “gliding” and the drift current in the top layer will thus be different from that over a solid surface. If d is the thickness of the top layer ($z=d$) this boundary condition is given by

$$\frac{\partial (u+iv)}{\partial z} = 0 \quad \text{for } (z = d).$$

Solutions of this sort have been discussed in greater detail by NOMITSU (1933). The shallower the layer of water in motion the stronger is the current produced by the wind and the larger the angle of deflection; a result which is exactly opposite to that

of the previous case of "adhering" ("Haften") at the sea bottom. For a small thickness an almost geostrophic current is obtained. As the thickness of the layer increases, the structure of the current will of course approach that of the Ekman spiral.

(c) *Pure Gradient Currents*

Drift currents in normal form are seldom found to occur in the sea, since the water transport connected with such currents will give rise to piling up of water at coast lines ("Anstau") leading to inclination of the sea surface. In a homogeneous sea the pressure differences produced in this way would extend their influence down to the sea bottom; if there were no frictional effects a geostrophic current would be generated from the sea surface down to the sea bottom. However, friction at the bottom gives rise to disturbances which are of considerable importance for oceanic currents.

The equation of motion (X.16) for a steady current will be of the form

$$fv - \frac{1}{\rho} \frac{\partial p}{\partial x} + \frac{\eta}{\rho} \frac{\partial^2 u}{\partial z^2} = 0 \quad \text{and} \quad -fu - \frac{1}{\rho} \frac{\partial p}{\partial y} + \frac{\eta}{\rho} \frac{\partial^2 v}{\partial z^2} = 0. \quad (\text{XIII.28})$$

Replacing the pressure gradient by the slope ζ of the sea surface (equation (XIII.2), p. 383) and assuming that there is a pressure gradient only along the y -axis ($\partial p / \partial x = 0$), then, according to (XIII.5), the geostrophic current will flow in the direction of the positive x -axis and its velocity will be

$$U = -\frac{g}{f} \frac{\partial \zeta}{\partial y}. \quad (\text{XIII.29})$$

Considering this in the equations (XIII.28) they can be compressed in the same way as for a drift current into

$$\frac{\eta}{\rho} \frac{\partial^2}{\partial z^2} (u + iv) - if(u + iv) + ifU = 0. \quad (\text{XIII.30})$$

To this equation add the following boundary conditions:

(1) no wind at the sea surface, that is

$$\text{for } z = 0: \quad \frac{\partial u}{\partial z} = \frac{\partial v}{\partial z} = 0$$

and

(2) at the sea bottom "adhering" occurs ("Haften")

$$\text{for } z = d: \quad u = v = 0.$$

The solution given by Ekman for (XIII.30) is

$$u + iv = U \left[1 - \frac{\cosh(1-i)(\pi/D)z}{\cosh(1+i)(\pi/D)z} \right] = U(1 - \phi + i\psi),$$

whereby

$$\phi = \frac{\cosh(\pi/D)(d+z) \cos(\pi/D)(d+z) + \cosh(\pi/D)(d-z) \cos(\pi/D)(d-z)}{\cosh 2\pi(d/D) + \cos 2\pi(d/D)} \quad (\text{XIII.31})$$

for ψ the functions \cosh and \cos are replaced in the numerator by the complementary functions \sinh and \sin . Thus

$$u = (1 - \phi)U \quad \text{and} \quad v = \psi U, \tag{XIII.32}$$

D denotes again the frictional depth to which now, since it refers to the sea bottom, is supplemented the additional word "lower". The functions ϕ and ψ determine the vertical velocity distribution of the gradient current. For $z = d$ one obtains $\phi = 1$ and $\psi = 0$ as required by the boundary conditions. Its further course is best shown by evaluating the equations for different values of d/D . Figure 172 presents as an example

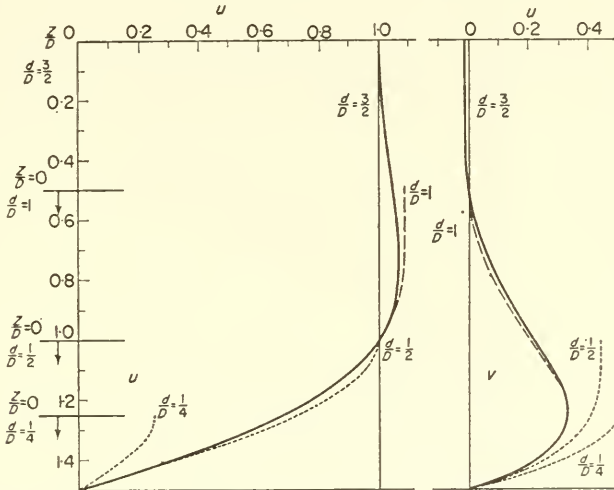


FIG. 172. Vertical distribution of the velocity components u and v for different values of h/D (for values $h/D = \frac{3}{2}$ the course of the u -component coincides with the straight line 1.0; the v -component approaches rapidly the straight line 0.0).

the vertical distribution of the two components for the $d/D = 1.5, 0.5$ and 0.25 . In the curves for depths somewhat greater than the frictional depth the course of both components is the same. Until a depth above the bottom is reached corresponding to the frictional depth u increases rapidly and reaches here the value of the geostrophic current U . The u -component increases a little further but then reverts to the U -value and remains then almost constant. The v -component (in the direction of the pressure gradient) rapidly reaches a maximum not far above the bottom, then falls almost to zero and oscillates with decreasing amplitude around the zero value. For depths $d > 1.5 D$ the structure of the pure gradient current has the form shown in Fig. 173; this is drawn in the same way as Fig. 168. At distances from the bottom greater than D there is a practically uniform velocity at right angles *cum sole* to the pressure gradient. This is the uniform *deep current*; it corresponds to the frictionless geostrophic current. The bottom layer is governed by the *bottom current*, the velocity of which decreases according to a logarithmic spiral down to the sea bottom. For greater depths of the sea the only change in this structure is in the vertical thickness of the deep current; the bottom current always corresponds to the frictional depth D .

Since the deep current runs parallel to the topographic lines ("Niveaulinien") of

the sea surface it cannot contribute to the equalization of the sea surface slope. This can only be accomplished by the bottom current which always has a component in the direction of the pressure gradient, i.e. a transport of water from a higher to a lower level. This component does the work required to overcome bottom friction.

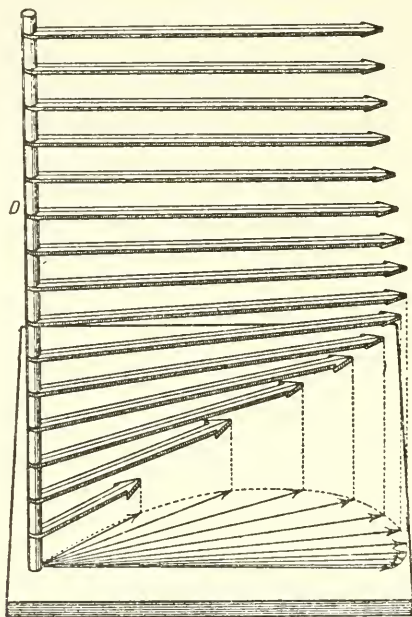


FIG. 173. Vertical structure in a pure gradient current (according to Ekman).

The transports (current amounts) M_x and M_y of a gradient current can be calculated by integration between 0 and d of equation (XIII.32), after its multiplication by ρ . In case of no bottom current the current component M_x would be $U\rho d$ and it becomes smaller due to the velocity decrease at the bottom. One obtains

$$M_x = U\rho d - U \frac{D\rho}{2\pi} ; \quad M_y = \frac{D\rho}{2\pi} U.$$

For depths less than D the effect of bottom friction is noticeable throughout the entire water layer, and the more so the smaller the ratio d/D . The curves in Fig. 174 illustrate the gradient current at depths $1.25 D$, $0.5 D$ and $0.25 D$. The angle of deflection

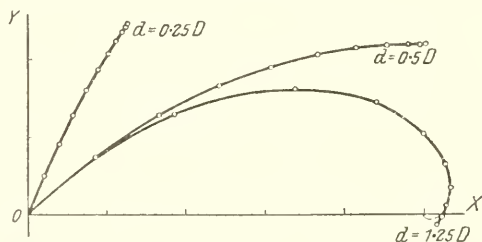


FIG. 174. Vertical structure of gradient currents for ocean depths d nearly equal or smaller than the lower frictional depth D (for more detail see Fig. 172).

between the current and the gradient direction becomes smaller and smaller as the sea becomes shallower; the effect of the Earth's rotation then becomes less important than that of friction.

Other assumptions about friction. The Ekman theory assumes a constant frictional coefficient. It has been used in this form in meteorology and provides an unobjectionable explanation of the deflection of the wind direction to the right with increasing height. However, it was found that the lowermost layers of the wind structure follow different laws. These deviations can be attributed mainly to the assumption of a constant frictional coefficient in the bottom layers being no longer valid. This fact EKMAN (1928) has taken into account by assuming in agreement with the observations a current structure made up of a straight section OA , at A changing into a logarithmic spiral over AB (Fig. 175). Thereby OB is thus the geostrophic wind in higher altitude. The same conditions as for the surface wind must also apply to the oceanic bottom

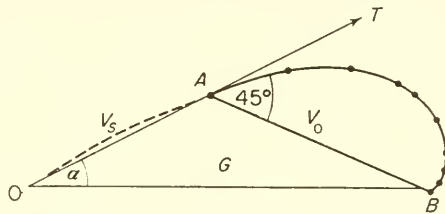


FIG. 175. Vertical structure in a bottom current with a boundary layer above the bottom (according to Ekman).

current, and it is already known from current measurements in moving waters and from laboratory experiments that the vertical structure in these, apart from the deviation due to the Coriolis force, is somewhat different from that of the Ekman spiral. The velocity curve of Fig. 175 can therefore only be given a physical meaning by assuming the presence of a *boundary layer* just above the bottom in which the velocity changes approximately linearly, and without change in direction from zero at the bottom to the value $OA = V_s$ at its upper limit. The water mass present above this lower boundary layer flows as though *gliding* over the bottom; it is retarded only by the slowly moving boundary layer. Ekman assumed a constant frictional coefficient in each of the two layers and investigated the thickness of the boundary layer, the decrease in velocity in it and the angle of deflection which would be able to prove the validity of such a concept.

This concept can more or less accommodate the fact that the lowermost layer just above the bottom has a special status, and that in practice the assumption of a constant turbulent coefficient in the water masses above is quite justified. Modern hydrodynamic fluid research approaches the whole problem from the point of view that the variation of the frictional coefficient with distance from the solid underlying surface changes with its roughness, whereby the entire current structure takes on a different form. The Prandtl theory (see especially 1942, p. 318) starts with the components of the shearing stress T_x and T_y at the bottom. Taking z -positive upwards, furthermore a variable η , a pressure gradient in the direction of the positive y -axis and taking into account equation (XIII.13), then equations (XIII.28) can be transformed into

$$T_x = f \int_0^h \rho v dz \quad \text{and} \quad T_y = f \int_0^h \rho(U - u) dz. \quad (\text{XIII.33})$$

Here h denotes the lower frictional depth at which the deviations $U - u$ and v from the geostrophic current vanish. It can further be assumed that T at the bottom has the same direction as the velocity at the bottom, so that

$$\frac{T_y}{T_x} = \left(\frac{v}{u} \right)_{z=0} = \tan \alpha, \quad (\text{XIII.34})$$

where α is the angle between the direction of the resulting T and that of the uniform deep current. These relationships form the basis of the vertical current structure of the bottom current, but further extension of the calculation fails due to the still imperfect knowledge of the laws of turbulent flow. However, by use of the above presented basics for turbulent friction a rather good estimate of the vertical velocity profiles to be expected can be obtained.

As a first approximation it can be assumed that in the vicinity of the bottom u varies with the n th root of z

$$u = U \left(\frac{z}{h_1} \right)^{1/n}.$$

Further, near the bottom $v = u \tan \alpha$; in order that v vanishes at a height $z = h_1$ one has to assume

$$v = u \left(1 - \frac{z}{h_1} \right) \tan \alpha.$$

h_1 is smaller than h and must be chosen so that the current structure near the bottom is in accordance with that shown by turbulence research (equation XIII.19). The equation (XIII.33) then gives

$$\operatorname{tg} \alpha = \frac{\sqrt{(2n+1)}}{n} \quad \text{and} \quad T_x = \frac{n}{(n+1)\sqrt{(2n+1)}} \rho f h_1 U. \quad (\text{XIII.35})$$

For an indifferent mass structure the equation (XIII.19) gives

$$u = 5.75 \sqrt{\left(\frac{T_x}{\rho} \right) \log \frac{z}{c_0}} \quad (\text{XIII.36})$$

for the velocity distribution above a rough surface. In $c_0 = (k/7.35)$ the quantity k is a measure of the roughness height of the bottom. Since for $z = h_1$, u must be equal to U the ratio T_x/ρ can be expressed in terms of U

$$T_x = \frac{\rho U^2}{\{5.75 \log (h_1/c_0)\}^2} \quad (\text{XIII.37})$$

and from (XIII.36)

$$u = U \frac{\log (z/c_0)}{\log (h_1/c_0)}. \quad (\text{XIII.38})$$

This gives a second equation for u and both must give a curve of the same shape. The most suitable assumption is that both give the same values for the transport

(current amount) which will lead to the same value for $\int_0^h (U - u) dz$. From this a relationship between h_1 and n is obtained having the form

$$\log \frac{h_1}{c_0} = (n+1) \log e. \tag{XIII.39}$$

Putting the expressions for T_x equal in (XIII.35 and 37) gives a further relationship between h_1 and U

$$h_1 = 0.160 \frac{\sqrt{(2n + 1)} U}{n(n + 1) f}. \tag{XIII.40}$$

This relation shows that h_1 is directly proportional to U as was to be expected. With this all the unknowns are determined.

Numerical values can be obtained in the following way: for a given value of n , which according to equation (XIII.35) fixes the angle α , and for given latitudes ϕ and velocities U , the equation (XIII.40) allows to compute the related h_1 and (XIII.39) gives the value for c_0 . From c_0 the roughness height k can be found quite simply and finally (XIII.37) gives the value of T_x . This then fixes the current structure completely.

Table 118 presents corresponding values for different roughness values of the sea bottom as they could be expected to occur in reality. These values are valid for $\phi=50^\circ$

Table 118. Basic values for the structure of the bottom current (according to the Prandtl theory); $\phi=50^\circ$, $U=100$ cm/sec

n	5	7	9
α	$33\frac{1}{2}^\circ$	29°	26°
Angle of deflection	$56\frac{1}{2}^\circ$	61°	64°
Frictional depth h	174	94	76
c_0	0.43	0.031	0.0034
Roughness height k	3.1	0.23	0.125
Friction velocity u^* (cm/sec)	6.7	5.0	4.0

($f=1.016 \times 10^{-4} \text{ sec}^{-1}$) and for $U=100$ cm/sec. The three roughness values correspond to average conditions. The frictional depths are obtained in a row as 174, 94 and 76 m which are plausible values. The vertical velocity distribution of u and v is shown in Fig. 176 for the first case ($n=5$, $h=174$ m) together with a vectorial representation (uv); for comparison with the values given by the Ekman theory the corresponding curves are shown by the dotted lines. The greatest differences, as would be expected, appear in the immediate vicinity of the bottom; up to about 5 m from the bottom the velocity increases linearly with distance from the bottom as was assumed by Ekman to be the case inside his boundary layer.

Similar considerations also apply for the drift current caused by the wind. Here U must be zero in equation (XIII.37) and in addition the boundary condition at the surface ($z=h$) must be

$$T_y : T_x = \left(\frac{\partial v}{\partial z} \right)_{z=h} : \left(\frac{\partial u}{\partial z} \right)_{z=h} = \operatorname{tg} \beta.$$

Thereby β was presumed to be the direction of the wind stress. At the same time it should be noted that under the influence of the turbulence of the wind the frictional coefficient is largest at the sea surface and decreases with depth. In order to satisfy

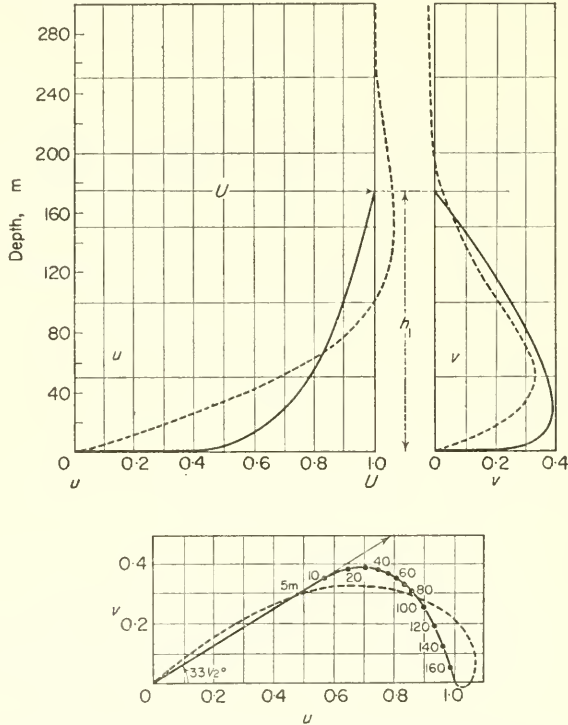


FIG. 176. Turbulent bottom current according to Prandtl (full lines: $n = 5$, $h_1 = 174$ m; dotted lines: bottom current according to Ekman (see Fig. 172).

these conditions the vertical current structure in the drift current will differ from that in the bottom current where the frictional coefficient converges to zero at the bottom; it will have a similar form as compared with that shown in Fig. 172.

A theory of drift and gradient currents based on similar principles was put forward by ROSSBY (1932) and later extended by ROSSBY and MONTGOMERY (1935). This was based on the principles of the newer turbulent flow theories and introduces in place of the earlier used frictional coefficient the Prandtl mixing length. In drift currents this is largest in the surface layers where the intensity of movement is greatest and decreases with depth to vanish at the frictional depth. The theoretical treatment of this assumption is very complicated and the results can only be shown by means of tables. Also here the deflection angle of the wind drift comes out to be dependent on both the wind speed and latitude, while according to the Ekman theory it should have a constant value of 45° . The ratio of the velocity of the surface current to the wind speed (wind factor, p. 418) results as equally dependent in a rather complicated way on the same

quantities. Table 119 gives some values for these relationships. A comparison of these results with those of the Ekman theory and with observational data is given later on (see p. 418). The introduction of a mixing length decreasing with depth and vanishing at the frictional depth should give a correct representation of actual conditions only if the turbulence arises *solely* from the wind drift and not from other currents which may be present (for instance, tidal currents, gradient currents). If such influences exist, it is necessary to introduce in the theory of wind-drift currents the vertical distribution of the turbulent coefficients which corresponds to the *total* current. This, however, modifies in turn the results. At present the Ekman theory appears to be a perfectly satisfactory approximation to actual conditions, as long as our knowledge about the vertical distribution of turbulence is not increased.

Table 119. Deflection angle and wind factor as a function of latitude and wind speed according to the theory of Rossby and Montgomery (1935)

Wind speed w m/sec.		Deflection angle in degrees				Wind factor V_0/w			
		5	10	15	20	5	10	15	20
ϕ :	15°	35.0	38.7	41.1	43.0	0.0317	0.0291	0.0276	0.0266
	30°	38.6	42.8	45.7	48.0	0.0292	0.0268	0.0254	0.0245
	45°	40.6	45.4	48.4	50.9	0.0280	0.0256	0.0243	0.0234
	60°	42.0	46.8	50.2	52.7	0.0273	0.0249	0.0237	0.0228

(d) The “Elementar” Current

In a homogeneous ocean no currents are possible other than drift and gradient currents; at every point the steady current is made up of a pure wind drift and a pure gradient current. These can be superimposed without mutual interference since each component is entirely independent of the other. If the depth of the sea d is larger than the upper and lower frictional depths D' and D'' , the resulting current system can be separated into *three current layers* (see Fig. 177, left-hand side).

- (1) The *bottom current* from the sea bottom to a height D'' (lower frictional depth).
- (2) The *deep current* from the level D' (the upper frictional depth) to the level D'' (the lower frictional depth).
- (3) The *surface current* which is the resultant of the uniform deep current and the pure drift current generated by the wind.

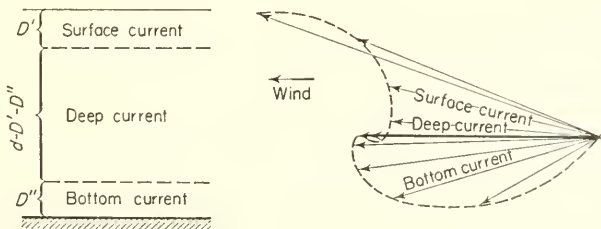


FIG. 177. Vertical structure of the “elementar” current (according to Ekman).

This vertical current stratification was termed by Ekman the “*elementar*” current. In limited seas the condition of continuity must also be satisfied. For stationary conditions where everything remains invariable with time the inflow and outflow must balance for a given oceanic space. The drift current is determined by the wind, thus the slope of the sea surface and hence the gradient current must be such as to maintain the constancy of the current system in time. The continuity equation and the boundary conditions in this way determine the structure of the “*elementar*” current. A simple case can be taken to illustrate these conditions (Fig. 177, right-hand side). A wind parallel to a long straight coast will produce a drift current through which a total water transport away from the coast down to the upper frictional depth is initiated. This causes the surface of the sea to lower along the entire coast and will thus produce a gradient current. The uniform deep current extending downwards from the surface to the lower frictional depth D'' will run parallel to the coast and thus cannot compensate the removal of water away from the coast accomplished by the wind current. This compensation must be provided for by the bottom current which carries water towards the coast in the direction of the pressure gradient. The slope of the sea surface will thus increase continuously, until the removal of water from the coast, due to the drift current, is exactly balanced by the bottom current. The current in the top layer will then be a vector composition of drift and deep current. The angle of deflection at the surface will thus decrease from 45° to 18° . The current vectors are shown in Fig. 177 for depth intervals of $0.2D$, with the same for the bottom current (at $D' = D''$). The uniform deep current occupying the deepest water layer between surface current and bottom current is shown by the thick arrow; it is non-divergent and because of its thickness is the decisive current component for the water transport in the oceans. Further interesting cases of “*elementar*” currents in oceanic regions of special shapes will be discussed in the following section.

It is of some interest to deal in some detail with the *diagrams of forces* for the three layers of “*elementar*” currents. Since the vectors of Coriolis force and gradient force are fixed by the current vector at the point under consideration, and by the sea surface slope the primary task is to fix the frictional vector. This can be done in the following way. If the current vector is denoted by \mathfrak{v} (components u and v), the vector of the deep current by \mathfrak{B} (U, V) and the difference vector by \mathfrak{w} (w_x, w_y) = $(\mathfrak{w} - \mathfrak{B})$. ($u - U, v - V$), then the equations of motion will have the form

$$-fv = -g \frac{\partial \zeta}{\partial x} + R_x \quad \text{and} \quad fu = -g \frac{\partial \zeta}{\partial y} + R_y,$$

whereby $\mathcal{R}(R_x, R_y)$ is the frictional vector.

However, for the uniform deep current

$$-fV = -g \frac{\partial \zeta}{\partial x} \quad \text{and} \quad fU = -g \frac{\partial \zeta}{\partial y}.$$

Subtraction gives

$$-fw_y = R_x \quad \text{and} \quad fw_x = R_y$$

so that $w_x R_x + w_y R_y = 0$.

This, however, is the necessary condition for the vector of the frictional force $\mathcal{R}(R_x, R_y)$ to be at right angles to the direction of the difference vector \mathfrak{w} . Thus the direction of the vectors of all three forces involved are known and therefore a diagram

of forces for each layer of the “elementar” current can be constructed. Figure 178 shows these force diagrams for always one level of the three current layers. In the surface current the frictional vector is directed to the side of the gradient vector pointing in the direction of the water movement, and rotates in a clockwise direction with decreasing intensity when going downwards and vanishes at the frictional depth. In the deep

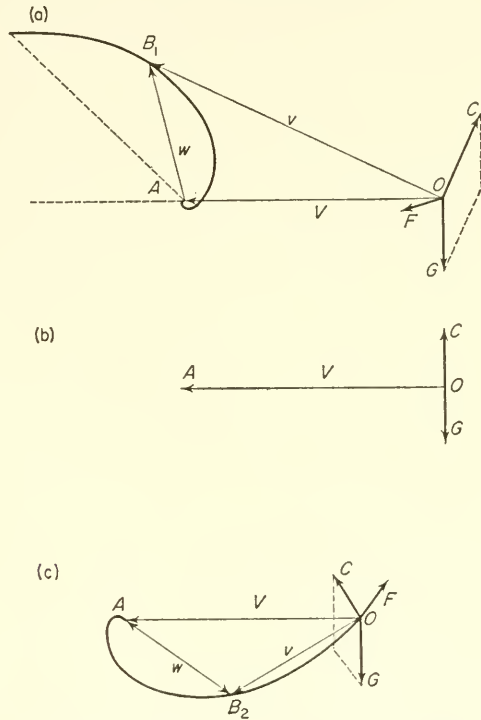


FIG. 178. Schematic diagram of forces for three levels of the “elementar” current (Northern Hemisphere): (a) surface current, (b) deep current, (c) bottom current. OG , OC and OF vectors of pressure gradient, of Coriolis force and of frictional force; v = velocity vector in the level under consideration; V = velocity vector of the deep current; w = vector of the velocity difference: $v - V$.

current, gradient and Coriolis force balance each other without any frictional effect. In the bottom current the frictional vector is directed to the side of the Coriolis force pointing more or less in the opposite direction to that of the velocity and rotates anticlockwise while approaching the bottom. From this distribution it can be realized that in the surface current the frictional vector corresponds to a driving shear stress which takes its strength at the sea surface from the energy of the wind, while in the bottom current it indicates the retarding effect of the underlying bottom topography (break on the motion).

(e) *Drift and Gradient Currents according to Observations; Piling up of Water by Wind (“Windstau”)*

The two parts of the “elementar” current are never developed in the ocean in pure form and it is to be expected that pure drift currents in the ocean will always be somewhat masked by the effects of superimposed gradient currents. It will therefore not be

easy to test the properties required by the theory. Three consequences of the theory are possibly most suitable for such a test:

- (1) the deflection of about 45° *cum sole* from the direction of the wind which is almost independent of latitude (except near to the equator);
- (2) the restriction of penetration of the drift current by the frictional depth D ;
- (3) the dependence of the sea surface velocity of the drift current on the shearing stress of the wind.

Angle of deflection. By special selection of oceanic areas, where it would be expected that the wind alone would be decisive in determining the currents, GALLE (1910) showed that the deflection required by theory was actually present. For this he used the large amount of data available for the Indian Ocean for all November months from 1858 to 1904 between 20° N. and 50° S. and 10° E. and 130° E. Taking together two degree zones in each ten-degree field, the theoretical deflection to the right was obtained in 77% of all cases in the Northern Hemisphere and in 69% in the Southern Hemisphere. Three areas were examined with particular care: the sea between Socotra and the Maldives, the South Equatorial Current and the west wind drift of higher southern latitudes. Table 120 shows average values for larger areas. The mean of all values is about 46° and in fact there seems to be no dependence on the latitude; both these circumstances are in accordance with the theory for a constant frictional viscosity coefficient. FORCH (1909) used the survey on wind and current conditions in the Eastern Mediterranean published by the "Deutsche Seewarte" to obtain an estimate of the

Table 120. Mean angle of deflection in the Indian Ocean (*cum sole*) in all cases

5°-20° N.	50°-60° E.	62°	40°-50° S. {	10°-20° E.	55°
	60°-70° E.	44°		20°-30° E.	41°
10°-20° S.	70°-80° E.	47°		30°-40° E.	42°
	80°-90° E.	51°		70°-80° E.	41°
				80°-90° E.	43°

Table 121. Mean angle of deflection in the Eastern Mediterranean (*cum sole*) in all cases

Area	36°-38° N. 15°-20° E.	34°-36° N. 15°-20° E.	34°-36° N. 20°-25° E.	32°-34° N. 25°-30° E.				
Annual mean	38.2°	33.1°	52.4°	43.0°				
Mean for the four fields	Jan./Feb. 44½°	Mar./Apr. 45°	May 86°	June/July 47°	Aug./Sept. 23°	Oct./Nov. 23°	Dec. 45°	Mean 41.1°

deflection of the current from the wind direction. The differences between wind and current azimuth for the four larger areas are given in Table 121 as annual average values derived from the monthly means. The mean of these rather scattered values is around 42° *cum sole*. In the annual variation the angle is nearly 45° from December to April, reaches a very high value in May and then during the warmer part of the year from August to November is about 20° . It is possible that the strong surface

density gradient during the summer gives rise to a strong differentiation in the magnitude of the frictional coefficients in a vertical direction whereby the angle of deflection is reduced.

Even more penetrating investigations have been made of the deflection angle in shallow seas (lightship observations). These values have, however, mostly been made in coastal areas or over large banks where disturbances can be expected but these can be eliminated by special grouping of the data. According to the Ekman theory there will be no strong deep currents in any largely enclosed sea (see p. 428). A comparison between theory and observation can then be made in such a case. For a shallow sea (depth d) the theory requires the deflection to be smaller the smaller the ratio $d:D$. On the other hand, the thickness D of the drift current will increase with increasing wind strength. It can thus be expected that *in a shallow enclosed sea, the angle of deflection will become smaller as the wind increases*. From data on currents recorded by Finnish light-ships, WITTING (1909) found that the angle of deflection was always *cum sole* and that it could be expressed by the relation

$$a = 34^\circ - 7.5^\circ \sqrt{w},$$

where w is the strength of the wind in m/sec. The strong ellipticity of the current ellipses at the different lightships indicates a preferred current direction caused along the longer axis of the sea which certainly affects the results. Qualitatively, however, it corresponds fully to the requirements of the theory. Also DINKLAGE (1888) obtained similar results from observations made at the Adlergrund light-ship (Baltic).

The question of testing the Ekman theory has been discussed in detail by PALMÉN (1930 b, 1931) in connection with an evaluation of the currents in the northern part of the Baltic. This was based principally on observations made at the rather openly situated Swedish lightship "Finngrundet" (60.0° N. 18.5° E. at the southern end of the Gulf of Bothnia) for the period 1923–27. Tables 122 and 123 show clearly the relationship between wind and current on the one hand for different wind strengths and on the other hand for different wind directions. These correspond rather well to the requirements of the theory. Especially the confirmation of the turn of the current direction with increasing depth deserves our attention because only few observations of that kind are available. After elimination of non-significant disturbances the following corrected values are obtained for wind strengths of 4–5 Beaufort:

$$V_0 = 9.2 \text{ cm/sec}, \quad a_0 = 35^\circ, \quad V_{20}:V_0 = 0.76;$$

$$V_{20} = 7.0 \text{ cm/sec}, \quad a_{20} = 54^\circ, \quad \Delta a = 19^\circ.$$

Table 122. Currents at different wind strengths at the lightship "Finngrundet" (Gulf of Bothnia, 1923–27) (according to Palmén)

Wind strength (Beaufort)	1.0	2.0	2.9	3.9	4.9	5.9	6.8	7.8	9.0	9.9
V_0 (cm sec)	2.0	3.1	5.8	8.4	11.3	12.3	14.7	19.2	22.9	27.3
V_{20} (cm/sec)	1.6	2.2	4.5	6.2	9.6	10.2	13.0	18.3	19.7	24.1
$V_{20}:V_0$	0.87	0.71	0.78	0.74	0.85	0.83	0.88	0.95	0.86	0.88
Deflection a_0	26°	41°	38°	33°	34°	35°	32°	25°	36°	8°
a_{20}	32°	50°	48°	42°	41°	45°	52°	38°	40°	11°
$a_{20} - a_0$	6°	9°	10°	9°	7°	10°	20°	13°	4°	3°

Table 123. Currents for different wind directions at the lightship "Finngrundet" (mean value at 2-7 Beaufort)

Wind direction	N.	N.E.	E.	S.E.	S.	S.W.	W.	N.W.	Mean
V_0 (cm/sec)	8.6	11.2	12.1	8.7	7.5	9.2	7.4	8.2	9.2
V_{20} (cm/sec)	6.8	9.6	11.5	6.8	5.5	7.9	5.7	7.0	7.6
$V_{20}:V_0$	0.79	0.86	0.95	0.70	0.73	0.86	0.77	0.85	0.81
α_0	30°	35°	41°	41°	40°	38°	22°	34°	35°
α_{20}	39°	46°	47°	46°	55°	50°	41°	47°	46°
$\alpha_{20} - \alpha_0$	9°	11°	6°	5°	15°	12°	19°	13°	11°

The directional turn between 0 and 20 m depth is 19° *cum sole* and at the same time the velocity falls by about a quarter of the surface value. This turn of the current is in good agreement with the theory; the decrease in velocity is, however, much too small to be explained by a constant frictional coefficient; for a water depth of 23 m and for a η about 200-300, it must be about 0.12 instead of 0.81. Only an assumption of a variable η with depth approximately in the sense of the discussion given on p. 405 could explain such a small decrease.

The relationship of wind strength to current strength. According to the theory the surface velocity V_0 is given by the relation

$$V_0 = \frac{T}{\sqrt{(2\eta\rho w \sin \phi)}} \quad (\text{XIII.41})$$

From this it follows that for constant η and ρ the surface velocity V_0 is proportional to the wind velocity w and is inversely proportional to the square root of $\sin \phi$:

$$V_0 = \frac{\lambda}{\sqrt{(\sin \phi)}} w \quad (\text{XIII.42})$$

λ is a universal constant. The quantity V_0/w is denoted as the "wind factor". Numerous investigations have been made of this relationship (see especially THORADE, 1914); the following values have been found for λ , when V_0 and w are expressed in cm/sec:

Mohn	Dinklage	Witting	Thorade	Palmén
0.0103	0.0127	0.0100	0.0126	0.0114
	Nansen	Sverdrup	Brennecke	
	0.0190	0.0177	0.0269	

The first of these values are in good agreement. For the ice drift, on the other hand, considerably higher values were obtained (NANSEN, 1902; SVERDRUP, 1928; BRENNCKE, 1921). See p. 437 concerning these. Usually an almost linear relationship has been found between the wind velocity and the velocity of the surface current. Witting and Thorade, however, arrived at a different result: for a wind force of up to 3 Beaufort a better fit to the observations was obtained by a quadratic relation. Palmén believed, however, that this was due to the uncertainty of the conversion of wind strength from the Beaufort scale into m/sec. For the magnitude of η it seems to be also of importance, on what height the wind measurements are based; a better agreement could probably be obtained if also this was taken into account (EXNER, 1912; DURST, 1924).

The shearing stress of the wind and piling up of water caused by the wind. There are two ways in which the wind stress can be determined. The first is afforded by equation (XIII.41). This requires a knowledge of the frictional coefficient η , but its dependence on the wind strength is not well-enough known. Ekman has indicated a second possibility using the piling up of the water ("Wasserstau") by the wind and using the current produced by the wind over a *confined* sea. If the effect of the Earth's rotation is disregarded ($f = 0$), and if $\partial p / \partial x$ is replaced by the slope i of the sea surface, then the first of the equations (XIII.28) for a variable η gives the equation

$$\frac{\partial}{\partial z} \left(\eta \frac{\partial u}{\partial z} \right) + g \rho i = 0,$$

This can be integrated considering the boundary conditions

$$\left(\eta \frac{\partial u}{\partial z} \right)_{z=0} = -T \quad \text{and} \quad (u)_{z=d} = 0$$

and taking into account the continuity equation

$$\int_0^d u \, dz = 0.$$

The frictional coefficient η increases strongly with distance from the sea bottom. Using the relationship introduced by FJELSTAD (see p. 405)

$$\eta = \eta_0 \left(1 - \frac{z}{d + \epsilon} \right)^n,$$

where n is a positive number smaller than 1 and ϵ is a very small and positive number as compared with d , then the integration, neglecting small terms, gives an approximately valid relation (PALMÉN, 1932, 1933)

$$i = - \frac{3 - n}{2} \frac{T}{g \rho d}. \tag{XIII.43}$$

For a constant frictional coefficient ($n = 0$) it transforms to

$$i = - \frac{3}{2} \frac{T}{g \rho d}. \tag{XIII.44}$$

This equation applies for stationary conditions and a constant density. In the ocean the water is stratified and the wind itself gives rise to changes in the oceanic structure. Thereby solenoid fields are generated and the use of the formulac under these real conditions must necessarily lead to difficulties. To avoid these, EKMAN and PALMÉN (1936) therefore reformulated the equation (XIII.44)

$$i = - \frac{\epsilon T}{g \rho d}, \tag{XIII.45}$$

where ϵ is always smaller than 3/2. Assuming that there is no bottom friction (gliding), then $\epsilon = 1$; when the depth is large (greater than D) this is only approximately true. If there is adhering ("Haften") of the water at the bottom, then $\epsilon = 3/2$. It is not possible to determine ϵ in each case; if $\epsilon = 1$, then T is somewhat too large at shallow

depths. Since, however, due to the dependence of the frictional coefficient η on the depth, the stress T is somewhat too small it is of no great importance if ϵ is put equal to 1, especially for more intense winds.

Most important, therefore, is the determination of i . This slope is made up of three components: the first depends on the direct piling up of water by the wind, the second is the static effect of the atmospheric pressure distribution, and the third is due to the deep current produced in the enclosed basins by the wind (current effect). The atmospheric pressure effect can be eliminated quite simply (pt. I, p. 7); the current effect depends in the first place on the boundaries of the basin and on the stratification of the water in it. In elongated seas with strong stratification (such as the Gulf of Finland) it is rather large and acts at *right angles to the main direction of the current*. In an oceanic area without any particular major axis the greatest piling up occurs exactly in the direction of the wind (for example, in the Gulf of Bothnia).

The equations (XIII.43-45) were first applied by EKMAN (1905) for the case of a storm in the southern Baltic (COLDING, 1881) and gave $T = 3.2 \times 10^{-6}w^2$ (w in cm/sec). Inserting the density of the air, $\rho' = 1.25 \times 10^{-3}$ gives

$$T = 2.6 \times 10^{-3} \rho' w^2.$$

This relation applies for wind speeds of up to 20 m/sec. The magnitude of piling up by the wind is given in Table 124. In more recent investigations Palmén has determined the dependence of the piling up by the wind on the strength of the wind and the depth of the water for the Gulf of Bothnia from observations of the water level. He found that, for the water depths in the area under investigation, the "Windstau" was directly proportional to the wind intensity for lighter winds, while for strong winds was rather proportional to the second power of the wind strength. Furthermore, the tangential pressure of the wind according to equation (XIII.45) could usually be expressed by the formula

$$T = 0.14 \times 10^{-2}w + 0.022 \times 10^{-4}w^2.$$

Table. 124. Piling up of water "Wasserstau" by the wind for a depth of 50 m (according to Palmén)

Wind in m/sec	1	3	5	10	15	20	25	30
Piling up of water (cm/100 km) . . .	0.07	0.59	1.65	6.6	14.9	26.4	41.3	59.4

In a later investigation PALMÉN and LAURILA (1938) found

$$id = 3.15 \times 10^{-9}w^2$$

for rather intense winds during a storm in October 1936, which leads for a mean water depth of 50 m and $\rho' = 1.3 \times 10^{-3}$ to

$$T = 2.4 \times 10^{-3} \rho' w^2.$$

The values for the constant k agree well with this (see equation X.9). A more recent determination in a similar way was made by HELA (1948), who found $k = 1.9 \times 10^{-3}$ [$g \text{ cm}^{-1} \text{ sec}^{-2}$].

According to recent hydrodynamic theory (see for instance, PRANDTL, 1942, p. 108) the investigations of flow over smooth and rough surfaces have shown that the shearing stress of the wind follows the relations:

$$\text{for a smooth surface: } \frac{w}{\sqrt{(\tau/\rho')}} = 5.5 + 5.75 \log \frac{z\rho'}{\eta} \sqrt{(\tau/\rho')} \quad (\text{XIII.46})$$

and

$$\text{for a rough surface: } w = 5.75 \sqrt{(\tau/\rho')} \log \frac{z + z_0}{z_0}. \quad (\text{XIII.47})$$

To decide whether a water surface is considered "smooth" or "rough" for different wind conditions it is necessary to investigate the vertical wind distribution over it. This has been done by WÜST (1920) and by ROSSBY and MONTGOMERY (1935), who have discussed the results and have concluded that for winds of more than 6–8 m/sec (measured 15 m above the surface, Beaufort 4) the water surface must be considered as "rough". As a result it was ascertained that for moderate and strong winds the roughness length z_0 was independent of the wind strength and had a constant value of 0.6 cm. The formula (XIII.47) then gives

$$T = 2.9 \times 10^{-3} \rho' w_{10}^2, \quad (\text{XIII.48})$$

where w_{10} is the wind speed at 10 m above the surface. This formula, however, no longer applies when $w_{10} < \text{Beaufort 4}$ or 6–8 m/sec and the surface has to be considered as "smooth". In this case the formula (XIII.46) will be valid. The values of T calculated in this way are about a third less than those computed from (XIII.48). As a reasonable first approximation they satisfy the relation

$$T = 0.9 \times 10^{-3} \rho' w_{10}^2. \quad (\text{XIII.49})$$

This shows that there is a *laminar boundary layer* of small vertical extent in wind profiles above the water surface, which reduces friction considerably (ROSSBY, 1936 b). Further analyses of measurements of the tangential wind stress and the roughness of the sea surface have been made by NEUMANN (1948) who showed that the frictional factor at the surface decreases with increasing wind speed and that in general at the surface of the sea

$$T = 0.9 \times 10^{-3} \rho' v^{3/2}.$$

Neumann attempted to explain this striking behaviour of the hydrodynamic roughness at the sea surface by changes in the nature of the sea-way dependent on the wind strength. The waves move with the wind and the surface of the sea will very likely tend towards a profile, offering the least possible resistance to the wind over it (MODEL, 1942); see MUNK (1955) for a more detailed discussion. Further measurements of the wind stress over water have been made by VAN DORN (1952).

Another method for the determination of the wind stress on the water given by SHEPARD and OMI (1952) making use of the geostrophic deflection of the wind at the sea surface and upwards to a height of some hundred metres above it. The geostrophic wind can be calculated with sufficient accuracy and the deviation of the observed wind from this depends only on the friction. This method gives resistance coefficients about 1×10^{-3} .

A summary of all values of the resistance coefficient shows that the stress can be represented by a formula of the form

$$\tau = \kappa \rho' w_{10}^n,$$

where n may differ somewhat from 2 or κ itself is a function of w . For wind speeds of up to 10 m/sec the values of κ are very scattered and it is not easy to decide whether this scattering is due to errors in measurement or due to effects which have not been taken into account (such as the vertical stability of the air mass over the water or deviations from the steady state or stratification of the water and others). The discontinuity imagined by Munk at 6–8 m/sec has not yet been confirmed and no definitive relationship between the stress and the wind can be obtained at the present time.

Frictional depth and frictional coefficient. According to equations (XIII.26) the frictional depth depends on the wind stress T and on the surface velocity V_0 . For T a dependence of the form (XIII.48) can be taken with an average coefficient of 2.9×10^{-3} $\rho' = 3.5 \times 10^{-6}$; V_0 is related to the wind speed w by (XIII.42) (λ approx. 0.0114). T and V_0 can be eliminated in this way from the formula

$$D = \frac{\pi T}{\sqrt{2} \cdot V_0 \rho \omega \sin \phi}$$

giving

$$D = \frac{7.61w}{\sqrt{(\sin \phi)}}, \quad (\text{XIII.50})$$

where w is given in m/sec and D in m. If V_0 is retained, a very simple formula results which was already derived by Ekman

$$D = 670V_0 \quad (\text{XIII.51})$$

which is very useful for the estimation of D . This states that the frictional depth is approximately equal to the distance travelled by the surface water in a pure drift current in about 600 sec or 10 min. It should be noted that equation (XIII.51) does not involve the latitude. THORADE (1914) derived the equation

$$D = \frac{3.67\sqrt{w^3}}{\sqrt{(\sin \phi)}}$$

for wind speeds less than Beaufort 3 (about 6 m/sec). All these formulae are of course only approximations, since at the present time systematic current measurements from which accurate values could be derived are not available.

Observations on the thickness of drift currents are usually in general agreement concerning magnitude with the values given by formula (XIII.50). The oceanic structure in the region of the North and South Equatorial Currents in the Atlantic Ocean indicates that the wind current here has a depth of about 150 to, at the most, 200 m and thus that the frictional depth in these latitudes only barely reaches these values. Towards higher latitudes it decreases. BRENNECKE (1921) found a frictional depth of about 50 m during the ice drift of the "Deutschland" in the Weddell Sea and SVERDRUP (1928) has shown from Brennecke's values that there is an increase with increasing wind speed as is shown by the following values:

Drift velocity (cm/sec) :	5.52	9.81	14.85	24.60
Frictional depth D (m) :	45.6	56.2	(39.1)	69.1.

Using the equations previously derived to calculate η gives

$$\eta = 1.03 w^3 \text{ for } w < 6 \text{ m/sec,}$$

and

$$\eta = 4.3 w^2 \text{ for } w > 6 \text{ m/sec.}$$

The values calculated from these formulae are also to be regarded as only approximate average values; the few directly determined values are widely scattering and indicate a large dependence on the vertical stratification of the water masses. SCHMIDT (1917) has presented some values:

Wind speed (m/sec)	1	3	5	7	10	20
η (cm ⁻¹ g sec ⁻¹)	(1)	28	110	220	430	1720.

The high values for strong winds apply of course only for the especially intense turbulence produced by the wind in the uppermost water layer; below this layer the coefficient decreases rapidly with depth. An average value for the top layer of the ocean will be between 50 and 100. Its magnitude in the deep layers will be about 1-10.

Diagrams of forces for a wind-driven, stratified ocean. With a complete knowledge of the total current and pressure structure of the ocean diagrams of forces for any layer can be derived in the following way (DEFANT, 1941 b). Denoting the sea surface slopes (of the isobaric surfaces in the deeper layers) in the positive x -direction (towards east) with i_x and in the y -direction (towards north) with i_y , then the equations of motion for a variable η are of the form

$$f\rho v + g\rho i_x + \frac{\partial}{\partial z} \left(\eta \frac{\partial u}{\partial z} \right) = 0; \quad -f\rho u + g\rho i_y + \frac{\partial}{\partial z} \left(\eta \frac{\partial v}{\partial z} \right) = 0. \quad (\text{XIII.52})$$

Integrating these equations from the surface to the depth D with the assumption that the current falls to zero at a depth d and taking furthermore into account that for $z = 0$ the components of the wind stress are given by

$$T_x = -\eta \frac{\partial u}{\partial z} \quad \text{and} \quad T_y = -\eta \frac{\partial v}{\partial z}$$

and vanish when $z = d$, the following equations are obtained:

$$\overline{f\rho v} + \overline{g\rho i_x} + T_x = 0 \quad \text{and} \quad \overline{-f\rho u} + \overline{g\rho i_y} + T_y = 0, \quad (\text{XIII.53})$$

where the integrals (sums) down to the depth d are indicated by a bar. This states merely that for a steady current the Coriolis force must be in equilibrium with the sum of the total pressure force and the total wind stress exerted on the entire layer.

The equations (XIII.53) can be evaluated numerically from the absolute topography of the pressure surfaces and of the physical sea-level, as well as from the rather reliable vertical current distribution as measured at two anchor stations in the region of the South Equatorial Current in the Atlantic. Table 125 contains all the necessary numerical values and Fig. 179 shows the vertical changes in current- and pressure-gradient quantities for calculation of the integrals. It can be seen that the E -component of the velocity decreases regularly with depth, while the N -component changes already in the uppermost layers from small positive values to negative values and then falls back to zero at 100 m. This distribution leads to a turn of the current vector *cum sole* which must be the case in drift currents. Below this there is only a gradient current

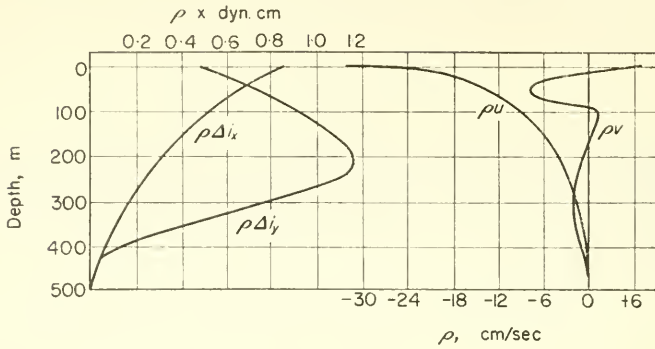


FIG. 179. Vertical changes in the pressure gradients and of the velocity components in the central part of the South Equatorial Current in the Atlantic Ocean.

which, however, also disappears at 500 m depth since there the isobaric surfaces become almost horizontal.

Table 126 gives integral values for the equations (XIII.53) and the corresponding resultant values of the wind stress; Fig. 180 presents the diagram of forces for this central part of the South Equatorial Current. The average direction of the south-east trade wind during the observational period was S. 40° to 45° E. and the mean wind force

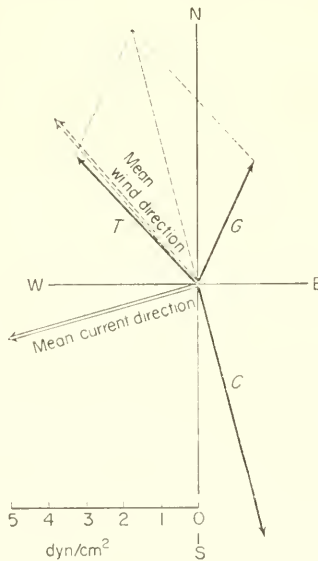


FIG. 180. Schematic diagram of the forces in the South Equatorial Current in the South Atlantic Ocean.

about 12 m/sec. This wind direction is in excellent agreement with the direction of the wind stress. The wind stress can be calculated from the meteorological data using equation (XIII.48) or from the oceanographic data using equation (XIII.37). In the first case wind stress and wind speed lead to a constant value for k of 2.5×10^{-3} which is

Table 125. South Equatorial Current in the Atlantic Ocean
(approx. 14° S., 20° W. to 8° S., 15° W.)

p (dbars) depth (m)	Pressure gradient		dyn cm/100 km		Vertical current distribution				σ_t <i>in situ</i>
	Direction	Δp , 100 km (dyr. cm)	ρi_x	ρi_y	u	v	ρu	ρv	
0	N. 60° E.	0.97	0.86	0.49	-32	+7	-32.9	+7.2	24.3
50	—	—	—	—	-14	-8	-14.3	-8.2	24.7
100	N. 30° E.	1.00	0.51	0.89	+9	+1	-9.2	+1.0	25.9
200	N. 20° E.	1.20	0.42	1.16	-4	-1	-4.1	-1.0	27.7
500	0	0.00	0.00	0.00	0	(+1)	0.0	+1.0	29.4

Table 126. Diagram of forces in the South Equatorial Current of the Atlantic Ocean
(Forces in dyn/cm²)

Coriolis force	Pressure force	Wind stress
$-f\bar{p}v = +1.77$	$g\bar{\rho}i_x = +1.49$	$T_x = -3.26$
$+f\bar{\rho}u = -6.73$	$g\bar{\rho}i_y = +3.28$	$T_y = +3.45$
S 15° E 6.95	N 24° E 3.51	N 43° W 4.74

in good agreement with the known values. Alternatively, taking h_1 (the frictional depth of the drift current) as about 200 m, the roughness parameter c_0 as 0.3 and the surface velocity U as 35 cm/sec, equation (XIII.37) gives exactly the required value of 4.74. These calculations show in any case that the oceanic current conditions are in good agreement with hydrodynamic concepts about the driving forces.

The dissipation of the current energy in the ocean. It is probably of some interest to calculate the amounts of energy dissipated in a drift current due to the apparent friction. The energy consumption is of course largest in the uppermost layer and decreases rapidly with increasing depth. If only the *total* energy consumption is required this can be calculated rapidly in the following way. The total work done in the interior of the water must be supplied from the wind at the sea surface. This is, however, given by force \times distance. The force is the wind-stress component in the direction of the surface current; the component at right angles does not enter into the calculation. This component is $T \cos 45^\circ$ and the distance travelled in unit time is V_0 . The energy consumption per second in a vertical water column of 1 cm² cross-section can then be obtained using equation (XIII.26) (SCHMIDT, 1919) and is given by

$$W = V_0 \sqrt{(\eta \rho \omega \sin \phi)}.$$

The values of η given by THORADE give the energy values shown in Table 127. In a vertical water column the total work expended should lie between 2 and 40 erg/sec. There is a considerable increase in these amounts with increasing wind speed and the latitude also has an appreciable effect.

Table 127. Energy Dissipation in Ocean Currents
(according to Schmidt)
(Values in erg cm⁻² sec⁻¹)

Wind speed w (cm/sec)		4	6	8	10	15	20
Latitude	10°	4.5	15	35	69	230	550
	40°	2.3	7.7	18	36	120	290
	70°	1.9	6.3	15	29	100	240

(f) The Effects of Coasts on the "Elementar" Current

The vertical structure of the "elementar" current depends essentially on the direction of the wind relative to the general outline of the coast, since this has a large effect on the equation expressing the condition that for stationary conditions the transport component at right angles to the coast must be zero. EKMAN (1923) has presented a solution in two simple and very instructive cases. The first case assumes an extended oceanic region off a long straight coast over which blows a wind of constant force and direction. The water depth d is assumed to be constant and greater than $2D$. The sea-level will fall uniformly from the coast towards the open sea and the pressure gradient produced by the piling up of water by the wind ("Windstau") will be at right angles to the coast. With an arbitrary orientation of the co-ordinate system the transport components M'_x and M'_y will be given by equation (XIII.27). The transport components of the gradient current are given by

$$M''_x = bU_x - BU_y \quad \text{and} \quad M''_y = BU_x + bU_y, \quad (\text{XIII.54})$$

whereby U_x and U_y are the components of the uniform deep current and

$$B = \frac{\rho}{2\pi} \quad \text{and} \quad b = \left(\rho d - \frac{\rho D}{2\pi} \right).$$

If the x -axis is oriented along the coast, then $U_y = 0$ and from continuity equation $M'_y \times M''_y = 0$ is obtained

$$U_x = \frac{T_x}{Bf} = \frac{\pi}{\rho\omega D \sin \phi} T_x.$$

For a given T and a given angle between wind and coast the drift current and the gradient current is fully determined. Ekman has given a simple graphical method for the construction of the total current structure in this case. Figure 181 shows this current structure in some special cases. The current arrows have to be visualized as drawn from the point \odot to the points on the curve and the small points refer to heights of 0.1, 0.2 D etc., above the sea bottom and to depths of 0, 0.1 D , 0.2 D etc., below the sea surface. The wind direction is indicated by the arrow. The cases correspond to angles of $\beta = 0, +45^\circ$ and -45° .*

There is a considerable difference between conditions when the water flow is unhindered in all directions or when it is adhered due to any kind of influence. In the

* $\beta = 0$ indicates a wind direction parallel to the coast; the increase in β is positive to the right and negative to the left.

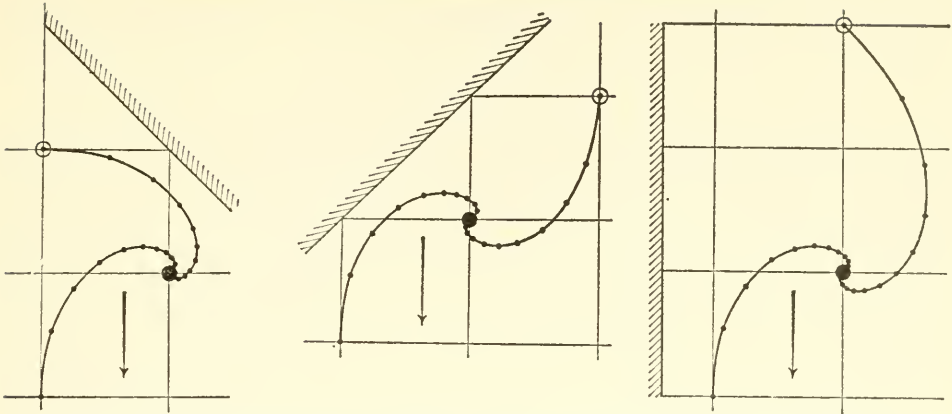


FIG. 181. Vertical structure of the "elementar" current for different orientations of the coast relative to the wind (according to Ekman) (the arrow indicates the wind direction).

first case only a pure drift current is formed and the effect of the wind is restricted to a relatively thin top layer. At coasts, however, the effect of the current-producing wind extends almost down to the sea bottom due to the generation of deep currents. Their velocity is not insignificant and may be as much as half of that of the surface current. The second case is that of a sea enclosed by land, with a wind of constant direction and constant speed blowing over its entire surface. Here the continuity condition requires that the transport in all directions should be zero, that is, that the total gradient current transport must be the same as that of the drift current and directed oppositely. The boundary condition equations are now

$$M'_x + M''_x = 0 \quad \text{and} \quad M'_y + M''_y = 0.$$

Taking the positive y -axis along the direction of the wind stress, then $T_x = 0$ and $T_y = T$. This gives

$$T/f + bU_x - BU_y = 0 \quad \text{and} \quad BU_x + bU_y = 0$$

from which it follows that

$$U_x = -\frac{bT}{f(b^2 + B^2)} \quad \text{and} \quad U_y = \frac{BT}{f(b^2 + B^2)}.$$

If the angle (*cum sole*) between the gradient current transport and the pressure gradient is denoted by β and if $U_y = 0$, then

$$\frac{M''_x}{M''_y} = \frac{b}{B} \quad \text{and} \quad \beta = \tan^{-1} \frac{b}{B}.$$

This angle is almost 90° , if the depth of the sea is not too small (for $d/D = 1, 2, 10$, β is approx. $79^\circ, 85^\circ$ and 89° , respectively). However

$$\frac{U_x}{U_y} = -\frac{b}{B} = \tan \alpha,$$

where α is the angle between the direction of the deep current and that of the wind, or $\alpha - \frac{1}{2}\pi$ is the angle between the directions of pressure gradient and wind. Since

$\alpha = \pi - \beta$, this angle will be $\frac{1}{2}\pi - \beta$ (*cum sole*). The velocity of the deep current is then

$$U = \frac{T}{bf} \sin \beta = \frac{2\pi T}{\rho f D} \cos \beta.$$

The gradient current now extends almost throughout the entire water mass, so that even a low velocity of this current is sufficient to compensate the drift current transport. The greater the depth of the water, therefore, the lower will be the velocity of the gradient current, and the less will be the effect of the coasts on the surface current given by the resultant drift and gradient current. As shown by the above equation, containing $\cos \beta$ and the frictional depth D in the denominator, the deep current U is very weak. Ekman has calculated numerically three special cases ($d = 0.5 D$, $d = 1.25 D$ and $2.5 D$). Figure 182 shows the vertical current structure in the usual way

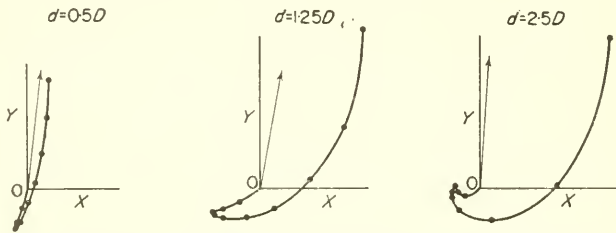


FIG. 182. Vertical structure of the "elementar" current in a water basin with everywhere closed (according to Ekman) (the arrow indicates the direction of the water "stau" (direction in which the water is piled up by the wind)).

The uniform deep current can be realized at greater depths, however, it is very weak and at still greater depths vanishes almost entirely. The water is piled up nearly in the wind direction in all cases and is therefore only slightly affected by the Earth's rotation. This may be the reason for the late recognition of the effect of the Earth's rotation on ocean currents.

(g) Effect of Bottom Topography

The results so far presented of the theory of steady currents in a homogeneous ocean, of which the most important one is the derivation of the "elementar" current, permit a considerable insight into ocean currents produced by the wind in a homogeneous sea; however, they can only be applied to smaller oceanic areas over which the effects of latitude variation, as well as that of local variations in depth and wind can still be disregarded. The further development of the theory by EKMAN (1923, 1928 *a*, 1932 and THORADE, 1933 *b*) was devoted primarily to the uniform deep current, and an investigation was made to determine the kind of change which occurs in the deep current when the water masses transported enter

- (1) into areas with non-uniform winds,
- (2) into areas with varying depth, and
- (3) into widely differing latitude regions.

Thereby conditions become rather complicated, especially with the additional assumption that the upper and lower frictional depth vary, not only from place to

place but also with the velocity of the deep current. In that way the theory becomes very complete indeed, but then in most cases the results do not allow a clear insight. It is therefore necessary to investigate the effect of each factor separately.

The condition for a constant sea-level is that the total transport M , which is made up of M' and M'' , the transport for the drift and the gradient current should satisfy the equation:

$$\operatorname{div} M' + \operatorname{div} M'' = 0. \tag{XIII.55}$$

To this must be added the boundary condition along the coast (vertical coast down to the sea bottom at depth d)

$$M'_n + M''_n = 0, \tag{XIII.56}$$

where the index n indicates the transport components at right angles to the coast. Disregarding differences in latitude and in the two frictional depths, then the equations (XIII.55, 56 and 57) after some calculation give the differential equation

$$\frac{\partial^2 \zeta}{\partial x^2} + \frac{\partial^2 \zeta}{\partial y^2} + \frac{g}{B} \left(\frac{\partial d}{\partial x} \frac{\partial \zeta}{\partial y} + \frac{\partial d}{\partial y} \frac{\partial \zeta}{\partial x} \right) = \frac{1}{gB} \left(\frac{\partial T_y}{\partial x} - \frac{\partial T_x}{\partial y} \right) \tag{XIII.57}$$

The effect of the difference in depth can be investigated more closely using this equation in special cases. A simple case is shown in Fig. 183 which represents a vertical section in the sea directed along the x -axis and parallel to the coast. The sea bottom slopes downwards in the direction of the coast by D over a distance l , so that the gradient is $\partial d / \partial x = D/l$. It is necessary to investigate whether a deep current parallel to the coast is at all possible. If the wind is assumed to be constant over the area ($\partial T_y / \partial x = \partial T_x / \partial y = 0$), then since $\partial \zeta / \partial x = 0$ and since for $\rho = 1$, $D/B = 2\pi$, (XIII.57) gives the differential equation

$$\frac{\partial^2 \zeta}{\partial y^2} + \frac{2\pi}{l} \frac{\partial \zeta}{\partial y} = 0 \tag{XIII.58}$$

the solution of which is given by

$$\frac{\partial \zeta}{\partial y} = i_0 e^{-(2\pi/l)y} \quad \text{and} \quad U = U_0 e^{-(2\pi/l)y}, \tag{XIII.59}$$

where i_0 is the slope of the sea surface and U_0 is the velocity of the deep current at the coast. The latter decreases rapidly with distance from the coast, so that at a distance $\frac{1}{2}l$ U_0 has fallen to $\frac{1}{23} U_0$. The deep current is limited to a narrow strip off the coast, the individual current filaments perform a shearing motion relative to each other and an observer on the sea would notice a vortex motion *contra solem*. Figure 183 shows the assumed wind direction off the coast. The thin dotted line shows the decrease in velocity for a frictional depth proportional to the velocity of the deep current.

For constant D and for a locally constant wind it is also easy to investigate how the deep current is transformed when flowing over a sea bottom shaped like *corrugated sheet-iron*. The outline of the coast and the wind direction are assumed to be at right angles to the ridges of the bottom waves. The depth of the sea is then a function only of x and with $-\partial \zeta / \partial y = i_0 = \text{const.}$ and if the sea depth $d = d_0 + \delta \cos(2\pi/l)x$, one obtains from (XIII.57)

$$\frac{\partial \zeta}{\partial x} = -\frac{2\pi\delta}{D} i_0 \cos \frac{2\pi}{l} x.$$

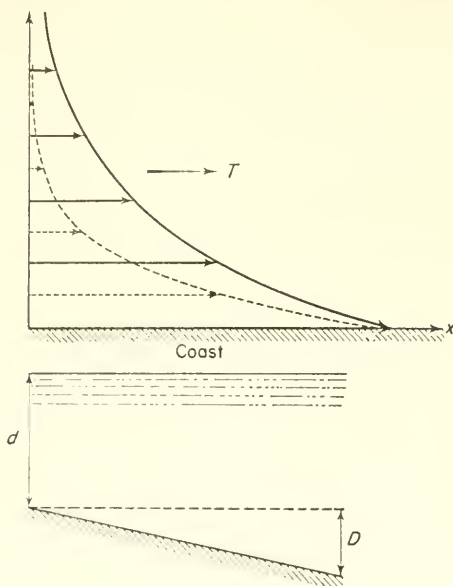


FIG. 183. *Upper picture*: vertical cross-section parallel to the coast through an ocean with increasing depth. *Lower picture*: horizontal section through the field of the deep current (full line and arrows are valid for a constant frictional depth; dotted curve and arrows are valid for a variable frictional depth. The arrow at T indicates the assumed direction of the wind stress.

From this it follows easily that

$$U_x = \frac{g}{f} i_0 \quad \text{and} \quad U_y = \frac{2\pi}{f} \frac{g\delta}{D} \cos \frac{2\pi}{l} x$$

and the stream lines are given by the equation

$$y = \frac{\delta l}{D} \sin \frac{2\pi}{l} x + \text{const.}$$

At a sufficient distance from the coast the current field shows sine waves (Fig. 184) the amplitude of which depends on the *absolute* size of the bottom waves. The depth of the sea plays no role here; thus the velocity in the direction of the coast is constant, but the total velocity is smaller than in a sea with a constant depth. At the same time the stream lines deviate more and more from a straight course and take on a curvature *cum sole* as the current passes over decreasing depth and the reverse (*contra solem*, increasing depth).

The effect of varying latitude is shown principally by the fact that the deep current is no longer exactly divergence-free. However, this divergence only becomes important in lower latitudes, and in middle and higher latitudes it is always very small. Since in lower latitudes the direction of surface currents is predominantly zonal, this should also apply to deep currents and also here the effect of $\text{div } U$ then remains small.

If all three of the factors influencing the deep current (wind field, bottom topography and the Earth curvature) are considered at the same time the treatment becomes

more difficult. Instead of determining curl U , EKMAN in his older theory (1923) investigated a quantity W , termed the "quasi-vortex". It is strictly not identical with curl U but in most cases agrees with it in sign and magnitude. This quantity W is the sum of three terms

$$W = W_T + W_a + W_\phi. \tag{XIII.59 a}$$

The first term depends only on the wind and is directly proportional to the vorticity of the wind (*anemogenic* vortex effect), W_a depends on the slope of the bottom topography but not on the total depth (*topographic* vortex effect), W_ϕ depends only on the curvature of the Earth (*planetary* vortex effect). The two latter effects are the most important; their mode of action has been illustrated in the examples previously discussed. When a current flows across the isobaths of the sea bottom, even quite small

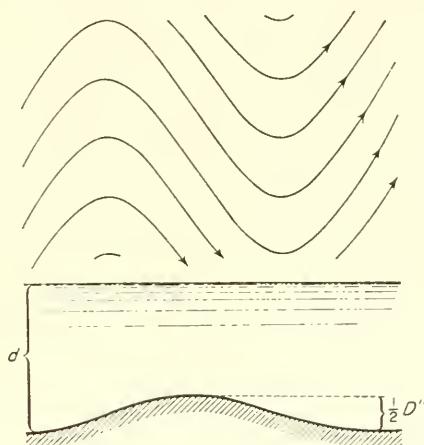


FIG. 184. Deep current influenced by a wave-form sea bottom profile. Lower picture: vertical cross-section parallel to the coast. Upper picture: horizontal section through the current field.

slopes can affect the deep current and usually give it quite a different appearance. On the other hand, the curvature of the Earth so strongly resists forced meridional water movements that in the lower latitudes almost only zonal currents are possible. For the combined topographic and planetary vortex effect Ekman obtained the same results as were derived earlier for frictionless gradient currents (see p. 386). This suggests that the simplifications introduced for their calculation eliminate the frictional effect to such a degree that only the part for frictionless currents remains.

In a new theory EKMAN (1932) extended his investigations, in which he still deals only with *steady* currents. But previously these currents were also subject to the condition of no acceleration $du/dt = dv/dt = 0$, while for a steady current only the condition $\partial u/\partial t = \partial v/\partial t = 0$ is required. Accelerations are thus possible due to the circumstance that water elements are subjected to velocity change when changing their position. These accelerations give rise to changes in the form of the current which may be quite large. For example, the case discussed previously of a current over a wave-shaped sea bottom (Fig. 184) would show two types of change: First, the amplitude

of the stream lines would be reduced, and secondly, the entire wave form would be displaced so that the bottom waves would coincide more with that of the stream lines. Both changes depend on the depth of the water, as well as on the current velocity and wave length of the bottom waves. As long as the expression $\pi d/D\tau$ is only a small fraction the deviations from the previous state remain small, but they become considerable when it approaches or even exceeds 1. Therein τ is the time in pendulum hours (see p. 316) in which the deep current requires to move through the wave length of a single bottom wave. The values found for this expression from observed data are relatively large, so that it is probable that bottom waves and stream lines are therefore closely in phase.

In general, the effects of the three factors are of the same type as before but they are no longer independent of each other; the topographical and the planetary vortex effects especially are interrelated in a complex way and disturb each other in extended oceanic areas during the generation of a uniform deep current. In general, an irregular bottom topography seems to have a tendency to reduce the velocity of the deep currents. Deep currents do not then play the dominant role ascribed to them earlier. This is probably the reason why many results of the earlier theory based on the most simple assumptions were in good agreement with the observed data, although these assumptions were only approximately satisfied in nature. If the topography of the sea bottom is very irregular the topographical and planetary vortex effects will disturb and sometimes destroy the deep currents, so that essentially there will remain only pure steady drift currents.

The investigation of the *effects of the bottom topography* on ocean currents has a direct connection with the discussion on p. 386, where it was stated that a deflection of a current *cum sole* would occur on top of a rising sea bottom and a deflection *contra solem* on top of a bottom fall. Without taking friction into account a quantitative estimate of this vortex effect can be made. For an extended bottom wave with a triangular shape (Fig. 185 ; x -axis at right angles to its crest, y -axis along its crest), and assuming a uniform current U in front of the ridge extending throughout the total water mass (depth of water H) and flowing towards the crest, equation (XIII.29) gives:

$$-g \frac{\partial \zeta}{\partial y} = fU \quad \text{and} \quad \frac{\partial \zeta}{\partial x} = 0; \quad V = 0.$$

Over this bottom ridge under stationary conditions ($\partial u/\partial t = \partial v/\partial t = 0$) the equations of motion will be

$$u \frac{\partial v}{\partial x} = -g \frac{\partial \zeta}{\partial y} - fu = f(U - u).$$

If the origin of the co-ordinate system is placed at O vertically underneath the highest point of the ridge, the half-width of which ($OA = AB$) is l , and height of which at O is h , then the depth of water will be

$$d = d_0 \mp (h/l)x,$$

where the upper sign applies for the forefront side and the lower sign for the rear of the bottom ridge. The equation of continuity requires the same transport through every cross-section, that is

$$UH = u\{d \mp (h/l)x\}.$$

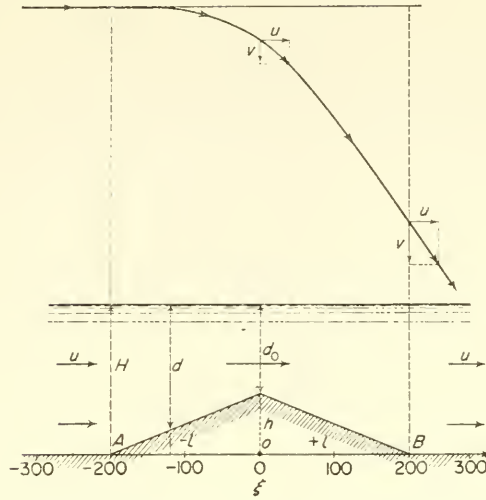


FIG. 185. Topographic influence of a submarine bottom ridge on a current flowing normal to the longer axis of the obstacle. *Lower picture*: vertical profile through the bottom ridge (width, 400 km; height, 200 m; water depth, 4 km; $\rho = 30^\circ \text{ N.}$). *Upper picture*: stream lines of the main current ($U = 50 \text{ cm/sec.}$).

This gives

$$\frac{\partial v}{\partial x} = -\frac{fh}{Hl} (\pm x + l).$$

Over the rise the flow thus is subjected to an acceleration acting along the longer axis of the ridge with a maximum value of $-fh/H$ above its highest point. This acceleration gives rise to a curvature of the stream lines *cum sole*. To the velocity u is added a transverse velocity v which at a point $x = \xi - l$ (ξ is the distance of the point under consideration from point A) is given by

$$v = -\frac{fh}{2Hl} \xi^2 = -\frac{f}{H} F,$$

whereby F denotes the cross-section of the bottom surface for the distance from A to ξ . The deflection of the current from the initial x -direction will be v/u , and for a small bottom slope is given with sufficient accuracy by v/U .

The deflection on passing over a bottom ridge is the larger, the smoother the sea, the higher the ridge and the smaller the velocity U . Since in the ocean U is relatively small, it can be expected that the bottom topography will have a stronger effect on the currents. Fig. 185 presents a numerical evaluation of a single case: width of bottom ridge 400 km, its height 200 m, ocean depth 4000 m and $\phi = 30^\circ \text{ N.}$ while U is taken as 50 cm/sec (somewhat high because of the absence of friction in the current). At the crest of the ridge the deflection will be -37° and in the rear of the rise at its end -55° . The deflection is of course associated with a corresponding change in the sea-level; to the normal slope directed along the crest is now added a slope directed normal to the ridge crest and a corresponding lowering of the sea-level along the x -direction. If instead of a single ridge the bottom has a series of ridges and troughs

the vortex formation is repeated periodically corresponding to these bottom waves. Figure 186a shows this case for the Northern Hemisphere; there is a current curvature *cum sole* above the ridges and *contra solem* above the troughs. If the sea surface has an overall slope so that already at a larger distance from the ridge a current at right angles to the ridge is produced then a current field will be formed similar to that shown in

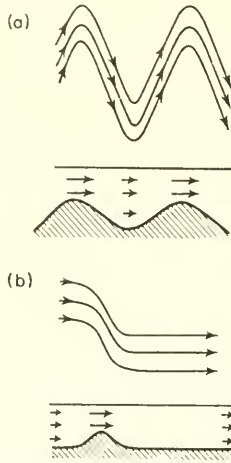


FIG. 186. Stream line pattern: (a) for currents crossing a wave-form bottom configuration; (b) for the crossing of a single bottom ridge (Northern Hemisphere, according to V. Bjerknes and co-workers).

Fig. 186b. The stream lines approach the ridge directly at right angles and pass over it bending *cum sole* on the forefront side and *contra solem* in its rear and then finally return to their original direction. This latter curvature in the rear can, however, only occur if there is a convergence on the lee side which is stronger than the divergence on the forefront side.

Recently, GÖRTLER (1941) has gone into this problem more carefully taking into consideration the *frictional effects* also. The mathematical formulation is different as compared with the previous one and shows an improvement in so far as it leads to simpler basic equations which are more likely to be solved quantitatively. The results otherwise agree with those obtained previously. Görtler dealt mainly with a case similar to that above. The bottom ridge was assumed to have a vertical profile $h = \frac{1}{2}h_0\{1 + \cos(2\pi/l)x\}$ with $|x| < \frac{1}{2}l$ and $h = 0$ outside this region. A horizontal projection of the stream lines of the main current is shown in Fig. 187 in the same way as in Fig. 185, but here friction has been considered. For an insight into the frictional effect the dimensionless quantity h_r/H is decisive where h_r depends on the frictional depth and H is the depth of the sea. This quantity usually appears in the expression $G = (R/l)/(h_r/H)$, where $R = U/f$ gives the radius of inertia associated with the current velocity U (equation XIII.26), with which the flow approaches the obstacle. The different curves in Fig. 187 show for a fixed value of R/l the effect on the course of the stream lines of the disturbance in the equilibrium between gradient and Coriolis force above the ridge due to the generation of a "secondary" current. When G is 3

or greater there is no essential difference as compared with the frictionless case ($h_r = 0, G = \infty$). For reasonable values of H and l Görtler estimated the magnitude of G as between 3 and 80, depending on the intensity of U , the latitude and the roughness of the bottom. This shows that for actual conditions in nature everything is the same as in the case of no frictional influence. This is important for the practical use of the above results. The effect of the topography of the sea bottom on the course of the ocean currents has been clearly demonstrated for many oceanic regions. Ekman

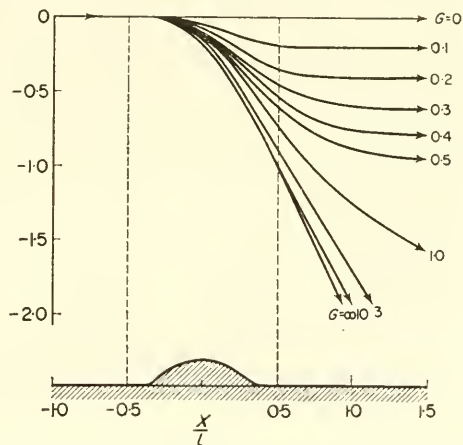


FIG. 187. *Upper picture*: stream line pattern for a crossing of a bottom ridge depending on friction. *Lower picture*: vertical cross-section through the bottom ridge.

by using these principles was the first to offer an explanation for the striking bending of the current trajectories, of the dynamic isobaths south of the Newfoundland Banks (HELLAND-HANSEN, 1912) which was not understood by simple reasoning. The course of the stream lines is in good qualitative agreement with that given by theory for the changes in depth actually present even if a closer qualitative examination of the phenomenon was not possible.

The dynamic evaluation of the observational data made by the "Meteor" expedition in the South Atlantic has afforded a good example of these effects of the bottom topography (DEFANT, 1941 b). This example makes it very probable that the large irregularities in the east-west course of the dynamic isobaths that were found in the western part of the convergence zone between about 25° and 50° S. have a fixed position and can be attributed primarily to the morphology of the sea bottom. If the lines of convergence and divergence for this disturbance are traced on transparent paper and laid over a depth chart the relationship between the two phenomena shows unmistakably. These conditions are illustrated by a diagram in Fig. 188. The lower part of the figure shows two depth profiles at 30° and at 35° S. extending from the South American continent to 0° W.; they indicate the course of the bottom irregularities running in a meridional direction as far as the mid-Atlantic Ridge in this part of the South Atlantic. In the upper part are shown the stream lines plotted according to the dynamic isobaths over the area from 30° to 45° S. Every "wave trough" in the bottom corresponds to a bend *contra solem* in the stream lines (here the reverse of the conditions as shown in

Fig. 186, since this is in the Southern Hemisphere). The extremes do not always coincide in position but particularly in the eastern part are in excellent agreement.

SCHUMACHER (1940, 1943) has indicated further examples. Over the mid-Atlantic Ridge especially, there is often a corresponding bending of the current to observe. The large stationary *cum sole* vortex off the eastern side of the Azores plateau must also

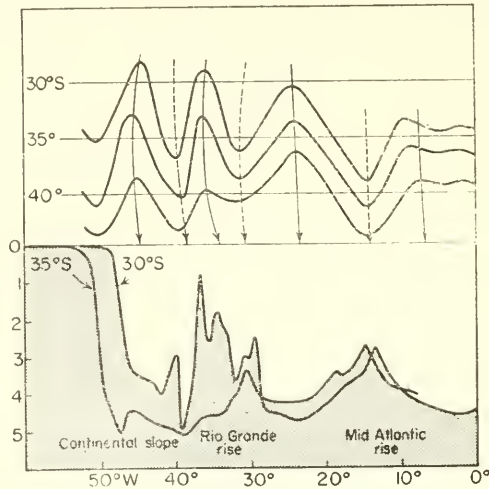


FIG. 188. *Upper picture*: bottom topography and stream lines for the gradient current in the disturbance region of the subtropical convergence zone in the South Atlantic Ocean (30°–45° S., 50°–0° W.). *Lower picture*: vertical bottom profiles at 30° and 35° S. according to the depth chart of the Atlantic Ocean.

be favoured by the bottom topography. In the Equatorial Counter Current the presence of the Atlantic Ridge shows this very typical effect. If the water masses are stratified, there will be corresponding displacements in the isosteres inside the region of influence of the bottom irregularity (see p. 558). If an isolated submarine ridge lies in the path of a current a *cyclonic vortex* will be formed above it. An example of a vortex of this type is given in the description of oceanic conditions around the “Altair” submarine volcano in the North Atlantic (NEUMANN, 1940) (see also, SCHOTT, 1939).

In discussing the effect of the bottom topography on ocean currents it has always been assumed that the current is more or less uniform from the sea surface down to the sea bottom. In almost all cases, however, the velocity of the current falls off rapidly with depth and in addition there are changes in the direction of the current. In these circumstances it is not so easy to accept a direct effect of the bottom topography on the current in the upper layers of the sea, since these are often separated from the bottom currents by very thick motionless water layers or layers with quite a different type of current. Attention should be drawn to these considerations in any discussion of the effect of the bottom topography on the currents.

5. Ice Drift

The wind drift of the ice in the polar regions (see pt. I, Chap. VIII, p. 243), like the ordinary wind-driven ocean currents, is dependent on three forces: wind stress, internal turbulent friction and Coriolis force; in addition to these it is also affected by

a resisting force arising from the random movement of the ice which is proportional to the drift velocity and acts in the opposite direction. This ice resistance is the reason why the Ekman theory for the ice drift is inadequate. Nansen had already shown in 1902 from the "Fram" data that the ice resistance cannot be neglected and indicated that one of its effects must be the small deflection angle observed for the ice drift. BRENNCKE (1921) and SVERDRUP (1928) have made important contributions to the clarification of the interrelated forces acting and that of Sverdrup can be regarded as a complete theory of the ice drift (see also, ROSSBY and MONTGOMERY, 1935). However, the observations of the "Fram" are not suitable for testing this theory, since the ice drift here includes a component due to the permanent surface current (see p. 358), but over the North Siberian Shelf ("Maud" observations) and in the Weddell Sea ("Deutschland" observations) the ice drift is free from a basic current and is suitable for this purpose. There is, however, one fundamental difference between these two drifts, due to the very different hydrographic conditions under which these drifts occur, and this has a considerable effect on the nature of the *pure* drift current (without ice).

Over the Siberian Continental Shelf the oceanic structure consists of essentially two layers: a top layer of lighter water and a heavier bottom layer separated by a sharp density transition layer (thermocline). In the surface layer the vertical equilibrium state is indifferent (neutral) throughout almost all the year and the turbulence in it is intense. In the discontinuity layer it falls nearly to zero and this therefore has the character of a gliding layer. The entire water mass of the top layer is thus drawn along with the surface current and this, together with the ice masses floating in it, behaves like an elastic sheet. The resistance against the movement thus arises from the effect of varying winds driving this sheet together. In the deep Weddell Sea the oceanographic conditions are different; here there exists no transition layer near to the sea surface and the density increases continuously with depth. A drift current thus develops in the normal way, and also the expected decrease in the velocity of the current and its turn in direction could be observed. In the Weddell Sea it appears necessary to take into account the effect of turbulent friction besides that of the ice resistance. These circumstances require to deal with each of the cases separately.

A shallow sea with a density transition layer (thermocline). The wind stress is taken as proportional to the wind velocity w and thus as equal to cw (c is termed the wind effect); the resisting force (ice resistance) as proportional to the velocity of the ice drift and in opposite direction of it is denoted by $-ku$ (with components $-ku_x$ and $-ku_y$ along the co-ordinate axes). Then as shown by Sverdrup for the case of the North Siberian Shelf, for non-accelerated motions (wind along the positive y -axis)

$$ku_x - fu_y = 0 \quad \text{and} \quad ku_y + fu_x = cw.$$

This gives

$$u_x = \frac{cfw}{k^2 + f^2} \quad \text{and} \quad u_y = \frac{ckw}{k^2 + f^2}, \quad (\text{XIII.60})$$

where

$$\tan \alpha = \frac{u_x}{u_y} = \frac{f}{k} \quad \text{and} \quad r = \frac{u}{w} = \frac{c}{f} \sin \sigma.$$

Here α is the angle of deflection of the ice drift from the wind direction and r is the wind factor (relative drift velocity, p. 418). Both the angle of deflection and the wind factor increase with decreasing ice resistance if the wind effect is constant.

It can easily be shown that the end-points of the vectors of the wind factors must lie on a circle with its centre on a straight line at right angles *cum sole* to the wind direction. Its radius is $R = c/2f$. In Fig. 189 the vectors shown represent the drifts for values $k = 5f, 3f$ and f .

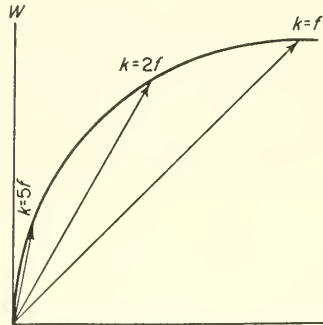


FIG. 189. Relation between wind and ice drift for stationary wind conditions and for different ice resistance (according to Sverdrup)

A deep sea with a continuous vertical density increase. Here the equations of motion are the same as for a pure drift current (XIII.23). The boundary conditions are, however, the following (wind along the positive y -axis):

$$\text{for } z = 0: \quad \frac{\eta}{\rho} \frac{\partial u_x}{\partial z} = f(u)u_x \quad \text{and} \quad \frac{\eta}{\rho} \frac{\partial u_y}{\partial z} = -F(w)w + f(u)u_y$$

$$\text{for } z = \infty: \quad u_x = u_y = 0.$$

The functions $f(u)$ and $F(w)$ are for the moment unknown. $F(w)w$ is equal to the wind stress T . With these boundary conditions a solution for the equations is thus

$$\tan \alpha = \frac{D\omega \sin \phi}{D\omega \sin \phi + \pi f(u)} \quad \text{and} \quad r = \frac{u}{w} = \frac{\pi}{D\omega \sin \phi} F(w) \sin \alpha. \quad (\text{XIII.61})$$

Also in this case the wind factor decreases with increasing ice resistance for otherwise equal conditions, since the angle of deflection α decreases with increasing resistance. As in the previous case, the end-points of the relative drift vectors drawn from the starting point of the wind vector lie on a similar circle as before. The radius is, however, $R = \{\pi F(w)\} / (2D\omega \sin \phi)$. The functions introduced here are not identical with the coefficients k and c used in the previous case, but are in a way similar to them. The function $f(u)$ depends on the state of the ice while $F(w)$ is related to the turbulence state of the wind blowing over the ice.

The observations made during the ice drift allow the determination of both α and r in both cases, and from these the coefficients k and c in the first case and the functions $f(u)$ and $F(w)$ in the second can be determined. For a test of the relations only those periods can be used, of course, in which a quasi-stationary state prevails. These factors are grouped according to increasing wind factor and increasing deflection angle and presented in Table 128; Fig. 190 shows these mean values in a graphical presentation

for a comparison with those required by theory (see Fig. 189). The theoretical relation is satisfied reasonably well, indeed, but the individual values are strongly scattered—which in view of the possible sources of error is not surprising. With the wind direction almost constant the coefficient of the ice resistance k computed from the “Maud” values decreases from 5.75 to 1.21. In the “Deutschland” values the resistance function

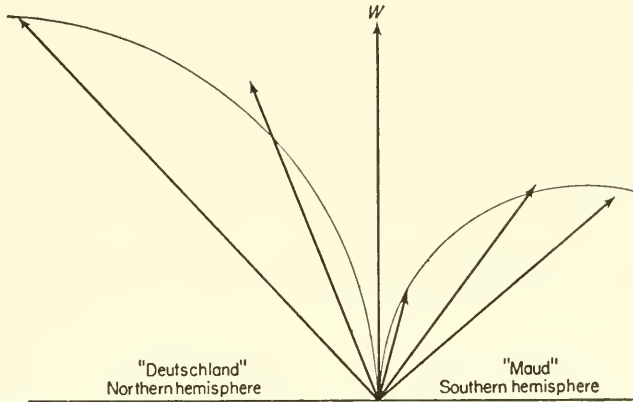


FIG. 190. Observed relation between wind and ice drift for a constant wind influence, but for an increasing ice resistance.

$f(u)$ increases with increasing wind and drift velocities and in fact so, that a linear function is obtained for $f(u)$. For the ice resistance this gives

$$f(u)u = au^2.$$

It is thus approximately proportional to the square of the drift velocity.

For the ice drift over the North Siberian Shelf Sverdrup found that the ice resistance was directly proportional to the drift velocity. This difference can be explained by the different nature of the ice cover in the two cases. Over the Siberian Shelf the sea is covered throughout the year by a solid connected ice layer, about 3 m thick (Pt. I, p. 273). In the Weddell Sea, on the other hand, the ice cover forms only throughout the winter and also then is not nearly as thick as the Arctic drift ice. Furthermore, in the Weddell Sea even in the winter there are frequent long open spaces in the ice cover (“Wacken”) so that even at low wind speeds the ice has a much greater freedom for movement.

Table 130. Relationship between wind and ice drift under quasi-stationary conditions (mean values)

	“Maud”				“Deutschland”	
	< 1.50	1.51–2.00	> 2.00		< 2.8	> 2.8
Group $10^2 \times r$	< 30°	31°–40°	> 40°	$10^2 \times r$	< 29°	> 29°
a				a		
$10^2 \times r$	0.77	1.75	2.07	$10^2 \times r$	2.32	3.39
a	13.8°	36.5°	49.3°	a	21.8°	42.8°
$10^4 \times k$	5.75	1.90	1.21	$10^3 a$	15.0	0.7
$10^6 \times c$	4.56	4.15	3.86	$10^4 b$	3.4	3.1

According to the observational data the wind function $F(w)$ can be approximately given the form

$$F(w) = b\sqrt{w},$$

so that the wind stress $T = bw^{3/2}$. By this the results of Palmén are brought in mind because they are in a way similar. The coefficients a and b thus like k and c characterize the strength of the ice resistance and the effect of the wind.

The seasonal changes in the relationship between wind and ice drift fit in well with the above considerations. Table 129 shows these changes, together with the calculated variations in the resistance coefficient and in the wind effect. Over the North Siberian Shelf both the relative drift velocity and the angle of deflection show a pronounced minimum in spring and a maximum in summer. This is partly due to the change in the resistance coefficient k and partly due to the wind-effect c .

The value of k increases gradually from a summer minimum until the first half of the winter and then rises rapidly to a maximum at the end of the winter in order to fall off again just as rapidly to the summer minimum. These variations can very well be explained by the state of the ice cover during the year. In summer the ice resistance is small due to the numerous open spots ("Wacken") and consequently greater freedom of movements for the ice. In autumn and at the beginning of winter these open

Table 129. Seasonal changes in wind factor, angle of deflection, resistance coefficient and the wind-effect on the ice drift

		Jan.-Feb.	Mar.-Apr.	May-June	July-Aug.	Sept.-Oct.	Nov.-Dec.
"Maud"	$10^2 \times k$	1.67	1.43*	1.67	2.20	2.30†	1.79
	a°	29.4	17.9*	23.0	40.8†	39.4	30.8
	$10^4 \times k$	2.51	4.66†	3.46	1.63*	1.72	2.37
	$10^6 c$	4.82	6.97†	6.12	4.76*	5.12	5.00
"Deutschland"	$10^2 \times r$	—	3.21	2.23	2.90	2.85	(3.00)
	a°	—	4.18	3.00	3.33	2.48	(2.71)
	$10^3 \times a$	—	2.6	7.8	6.9	9.5	(11.2)
	$10^4 \times b$	—	3.2	2.7	3.2	3.9	(4.0)

* Minimum; † Maximum.

stretches are covered with fresh ice, and the ice pressure increases the resistance until a maximum resistance is reached at the end of the winter when the ice-cover is strongest and most solid. The annual variation of the wind effect c is more complex. Sverdrup was, however, able to show that it was in full agreement with the turbulent state of the air movement over the ice. In the Weddell Sea also the seasonal changes in a and b are completely analogous. The ice resistance shows, in general, an increase during winter and spring, but the changes from month to month are more pronounced and irregular because of the stronger changes in ice conditions of this broken cover. The coefficient of the wind effect b follows a regular course with the lowest values around the middle of winter and with an almost steady increase towards the end of winter.

This also was shown as at least partly dependent on the turbulent state of the air above the ice.

The ice drift thus to a large extent follows regular laws; it is dependent on three forces: the effect of the wind on the ice, the frictional resistance between different ice masses and the deflecting force of the Earth rotation. The much greater wind factor over the Weddell Sea than over the open ocean (see p. 449) is due to the fact that the exposed surface of the ice is more favourable to the action of the wind than that of the freely moving open sea. Over the Siberian Shelf, on the other hand, the wind factor observed was smaller than over the Weddell Sea; this may be due to the thickness and compactness of the Arctic ice cover which must offer a much greater resistance to movement than the ice of the Weddell Sea.

6. Inertia Currents

In the preceding sections ocean currents in a homogeneous sea have everywhere been considered as stationary phenomena. Observations show that in most cases this assumption corresponds more or less closely with actual conditions. However, it can hardly be assumed that the forces involved will always be in equilibrium. Any disturbance of the equilibrium must, however, alter the state of motion of the water masses and in this the inertia of the water will play a major role. It is only in more recent times that one has started to draw attention to such phenomena.

(a) Inertia Currents as Disturbances of a Steady Current

A water mass moving frictionless in a horizontal direction under the action of a gradient force will, speaking completely in general, be subject to the equations of motion (X.16). If the x -axis is taken in the direction of the pressure gradient ($\partial p / \partial y = 0$), and this pressure gradient corresponds to a steady current (geostrophic current), then

$$V_0 = \frac{1}{f\rho} \frac{\partial p}{\partial x} \quad \text{and} \quad U_0 = 0$$

and one obtains (disregarding frictional forces)

$$\frac{du}{dt} = f(v - V_0) \quad \text{and} \quad \frac{dv}{dt} = -fu.$$

A periodic solution for an observer moving with current is

$$\begin{aligned} u &= v_0 \sin ft + u_0 \cos ft, \\ v &= v_0 \cos ft + u_0 \sin ft + V_0, \end{aligned}$$

or

$$\begin{aligned} u &= c_0 \sin (ft + \psi), \\ v &= c_0 \cos (ft + \psi) + V_0, \end{aligned}$$

where

$$c_0 = \sqrt{(u_0^2 + v_0^2)} \quad \text{and} \quad \tan \psi = \frac{u_0}{v_0}$$

c_0 is the impulse of disturbance imparted to the steady current V_0 at the time $t = 0$. If this disturbance is *only* applied in the direction of the steady current and if at the time $t = 0$ the total velocity is denoted by V , then

$$u = (V - V_0) \sin ft \quad \text{and} \quad v = V_0 + (V - V_0) \cos ft. \quad (\text{XIII.62})$$

If the permanent equilibrium of a steady current is disturbed, the difference between the disturbance vector and the steady gradient current is transformed into an inertia movement with a corresponding circle of inertia. The period of the circular movement is

$$T = \frac{2\pi}{f} = \frac{\pi}{\omega \sin \phi} = \frac{1}{2} \text{ pendulum day.}$$

The amplitude of the two velocity components is the same, and the phase of the y -component precedes that in the x -component by one-quarter of a period. These are the characteristic features of a pure inertia movement. It is superimposed on the uniform gradient current and thus gives an *oscillating flow*, the period of which depends on the Coriolis force. This period is identical with the period of one revolution around the circle of inertia; numerical values for it are given in Table 112a (see p. 316) for different latitudes. Inertia oscillations are not associated with any large transverse displacements of the water masses, since the disturbance velocity $c = V - V_0$ usually remains small. The magnitude of these can be taken from Table 2 for different latitudes and velocities. In the open ocean these transverse displacements are usually of little importance but they are still characteristic phenomena which are quite noticeable in current measurements.

If pressure forces are present in a homogeneous sea due to a slope in the sea surface ($\partial\zeta/\partial x = i_x$; $\partial\zeta/\partial y = i_y$) the equation of motion (XIII.3) will apply. A steady motion (geostrophic current) is associated with a corresponding slope of the sea surface given by \bar{i}_x and \bar{i}_y so that

$$\bar{i}_x = \frac{f}{g} V \quad \text{and} \quad \bar{i}_y = -\frac{f}{g} U.$$

If, further at the time $t = 0$, there are current components u_0 and v_0 and slopes $i_{x,0}$ and $i_{y,0}$ which do not correspond to the condition for a steady state, then the above equations have the following general solution (FR. DEFANT, 1940):

$$\left. \begin{aligned} u &= U + (u_0 - U) \cos ft + [v_0 - (g/f)i_{x,0}] \sin ft, \\ v &= V + (v_0 - V) \cos ft - [u_0 - (g/f)i_{x,0}] \sin ft, \\ i_x &= \bar{i}_x + [i_{x,0} - \bar{i}_x] \cos ft - [i_{y,0} - \bar{i}_y] \sin ft, \\ i_y &= \bar{i}_y + [i_{y,0} - \bar{i}_y] \cos ft + [i_{x,0} - \bar{i}_x] \sin ft. \end{aligned} \right\} \quad (\text{XIII.63})$$

This set of equations shows that for a completely free initial state, both the current field and the sea surface will perform inertia oscillations around their equilibrium position which, however, will not correspond in all points to the conditions for *pure* inertia waves. In the current field the amplitudes of the corresponding velocity components will be equal only when the sea surface slope corresponds initially to the steady state. But according to the second pair of equations the sea surface does not

perform any inertia oscillations at all but will rather remain from the beginning in the stationary position. Thus in the general case the amplitudes of corresponding terms are no longer equal and the motion is then elliptical instead of circular. However, the amplitudes of corresponding terms in the sea surface oscillations are always equal and these are therefore always pure inertia movements. It has been found that currents flowing into a wide area uninfluenced by coastal effects usually follow a wave-form course rather than a straight course. A current with an oscillatory streamline seems to be a more stable type of motion than one with a linear course. Once a bulge is formed in any direction, the centrifugal force draws the water further and further out and the bulge produced by such disturbances will grow steadily; consequently, progressive waves and vortices will be formed in which the current will *oscillate about a mean direction*. In dealing with problems concerning these oscillating currents it is of course necessary to take the Coriolis force into account (EXNER, 1919). It surpasses the scope of this section to penetrate more deeply into the dynamics of progressive waves of this type in an infinitely extended medium; it rather belongs to and will also be discussed when dealing with the theory of progressive tidal waves (Vol. II); for an account of progressive waves with inertia period see FR. DEFANT (1940) and EKMAN (1941).

(b) *Inertia Movements Associated with Drift and Gradient Currents*

In the formation of steady drift and gradient currents the state of motion changes from the first motionless initial equilibrium state into a second state in which there is an equilibrium between all the forces acting. It can be expected that this transfer will give rise to inertia oscillations which will gradually be damped by friction until the new stationary equilibrium state is reached. EKMAN (1905) examined in some detail the case of a suddenly starting wind over a deep, extended ocean. A comprehensive treatment of all questions arising has been given by FJELDSTAD (1930). The equations of motion (X.16) which stand in question can be combined introducing $u + iv = w$ ($i = \sqrt{-1}$) in order to obtain a single equation

$$\frac{\partial w}{\partial t} + ifw = \frac{\eta}{\rho} \frac{\partial^2 w}{\partial z^2}. \tag{XIII.64}$$

The boundary conditions to be satisfied are

$$\text{for } t = 0: w = 0$$

and

$$\text{for all } t: \begin{cases} \text{for } z = 0: & -\eta \frac{\partial w}{\partial z} = T(t) \\ \text{for } z = h: & w = 0. \end{cases}$$

If the wind arises suddenly at a time $t = 0$ with a tangential pressure T in the direction of the positive y -axis, then the velocity components u and v are given by

$$u = \frac{2\pi T}{\rho Df} \int_0^\tau \frac{\sin 2\pi\xi}{\sqrt{\xi}} \exp\left(-\frac{\pi z^2}{4D^2\xi}\right) d\xi \tag{XIII.65}$$

and

$$v = \frac{2\pi T}{\rho Df} \int_0^\tau \frac{\cos 2\pi\xi}{\sqrt{\xi}} \exp\left(-\frac{\pi z^2}{4D^2\xi}\right) d\xi.$$

D is the frictional depth and $\tau = (ft/2\pi)$ is the time expressed in units of 12 pendulum hours. The gradual formation of the drift current can be illustrated by plotting the time-variable velocity vector at different depths in the form of the hodograph curves given by Ekman (Fig. 191). For a suddenly starting wind this curve at the surface will have the form of a damped circular oscillation with a period of 12 pendulum hours which is superimposed on the final stationary state of motion. In the deeper layers the oscillation will at first grow somewhat and then regularly decrease again. The velocity

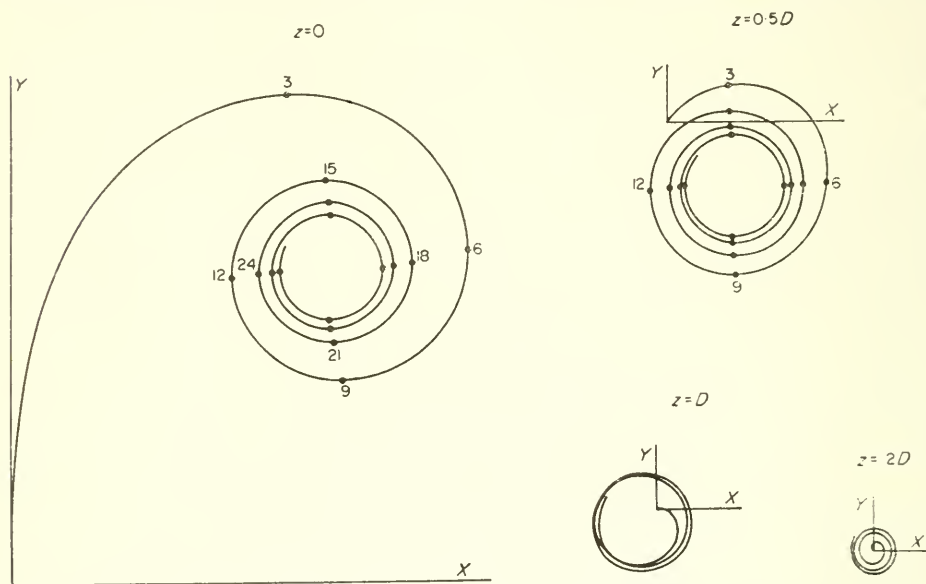


FIG. 191. Hodograph curves for different depths of the pure drift current which develops due to a wind beginning suddenly (ocean depth unlimited).

components can also be plotted separately along the time axis thereby obtaining the curves shown in Fig. 192. Each component shows a damped oscillation around a stationary final state and both together show very clearly the characteristics of inertia oscillations. At different depths the oscillations have *exactly the same phase* but with a decreasing amplitude. If the water depth is less than the frictional depth the close distance from the bottom becomes apparent in the curves, but the oscillation is strongly damped only in the immediate vicinity of the bottom; for $h/D = 0.25$ the current approaches almost aperiodic the steady state. Solutions can also be found for the case in which the effect of the wind is not applied suddenly but only gradually, and also for the case where the wind maintaining a wind drift current either suddenly or gradually ceases. For more detail see HIDAKA (1933), NOMITSU (1933), Fr. DEFANT (1940).

The sudden formation of a sea surface slope in a similar way as in the case of a drift current must also give rise for a gradient current to inertia oscillations. Ekman has given the theoretical basis also for this case and has pointed out that for an ocean of greater depth, due to the small frictional effect in the geostrophic current, these inertia oscillations will die away very slowly so that a longer duration of these must

be assumed. If the pressure gradient, due to a suddenly imposed sea surface slope, acts along the positive y -axis there will be an extra term $+fU$ (to be added on the right-hand side) in the equation of motion (XIII.64), where U is the velocity of the steady gradient current (geostrophic current) corresponding to the sea surface slope. This equation must be solved assuming the boundary conditions that for $z = 0: \partial w/\partial z = 0$ and for $z = h: w = 0$ and for $t = 0: w = 0$ and for $t = \infty: w = U$ (stationary state);

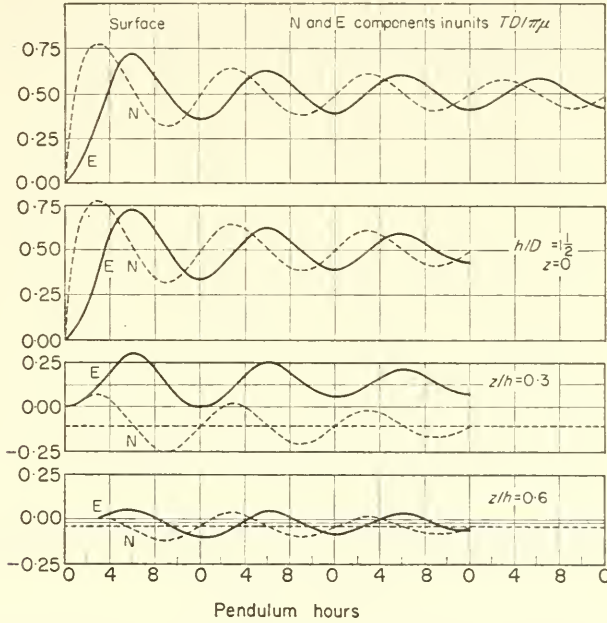


FIG. 192. Upper pair of curves: drift current of an ocean of infinite depth for $z = 0$ (surface). Lower pair of curves: drift current for $h/D = 1\frac{1}{2}$ and in fact for $z = 0$ (surface), $z/h = 0.3$ and $z/h = 0.6$ (north and east components always in units $TD/\pi\mu$ according to Fr. Defant).

the velocity components of the steady gradient current are denoted by u_{st} and v_{st} . Introducing again $u + iv = w$, then the equations of motion reduce to the single relation

$$\frac{\partial w}{\partial t} + ifw = \frac{\eta}{\rho} \frac{\partial^2 w}{\partial z^2} + ifU.$$

For stationary conditions ($\partial w/\partial t = 0$, equation XIII.30) the solution is given by equation (XIII.31). Under non-stationary conditions a solution is obtained most easily by assuming

$$w = w_{st} - w_{st} F(t)$$

with the condition

$$F(\infty) = 0 \quad \text{for } t = \infty.$$

This can only be given as a series which, however, converges rapidly. As in the case of developing gradient current, oscillations about the final stationary state with inertia periods and decreasing amplitude are produced in both components.

For the upper layers when the depth of the sea is great, one obtains in close approximation

$$u = U - U \cos ft \quad \text{and} \quad v = U \sin ft, \quad (\text{XIII.66})$$

which indicates a simple harmonic inertia motion with an amplitude U . In reality of course a decrease always occurs in a spiral form but when the depth is large this decrease is extremely small. These oscillations can be found by observation as far down as near to the sea bottom. Figure 193 shows the course in the velocity components at the surface, for a middle depth and for a layer near to the bottom in the case where

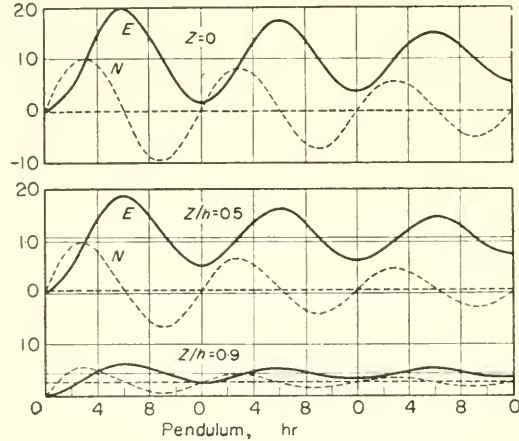


FIG. 193. Gradient current in the ocean for an ocean depth $h/D = \frac{3}{2}$, and in fact for $z = 0$ (surface), $z/h = 0.5$ and 0.9 . (Values for the north and east components for u/U and v/U , according to Fr. Defant).

$h/D = \frac{3}{2}$. It can be seen that due to small damping the amplitude of the inertia oscillation is still quite large in the mid-depth. Calculations can also be made for the case of a gradually developing sea surface slope; the amplitude of the inertia oscillation produced depends on the rate at which this slope develops but the character of the oscillation is still kept.

(c) Inertia Currents in Ocean Currents

The preceding discussion leads to the expectation that inertia currents will be of frequent occurrence in ocean currents, but a considerable time passed before their existence was actually proved. This was due to the circumstance that in order to prove the presence of *cum sole*, turning current variations of this type corresponding to their period, current measurements from an anchored ship over an interval of several days were needed. Measurements of this type are only seldom made and are associated with considerable difficulties which have been overcome only in recent times. The first current measurements in which the presence of inertia currents was suspected, was the long series of measurements made by HELLAND-HANSEN and EKMAN (1931) in the trade wind region of the Eastern North Atlantic. At the anchor station with the longest observational period (141 h, 30.2° N., 14.0° W.) there were, besides oscillations with tidal periods and also others with inertial oscillation, periods with 23.844 mean

hours. This period is only 13 min shorter than the diurnal moon period K_1 of 23·94 h which presumably was also present. This difference is, however, sufficiently large to decide out of six wave trains which of the waves is present. Figure 194 shows the diurnal regular oscillation after elimination of the semi-diurnal tide. While during the first three days there was a regular damping of the waves, at the end of the series there

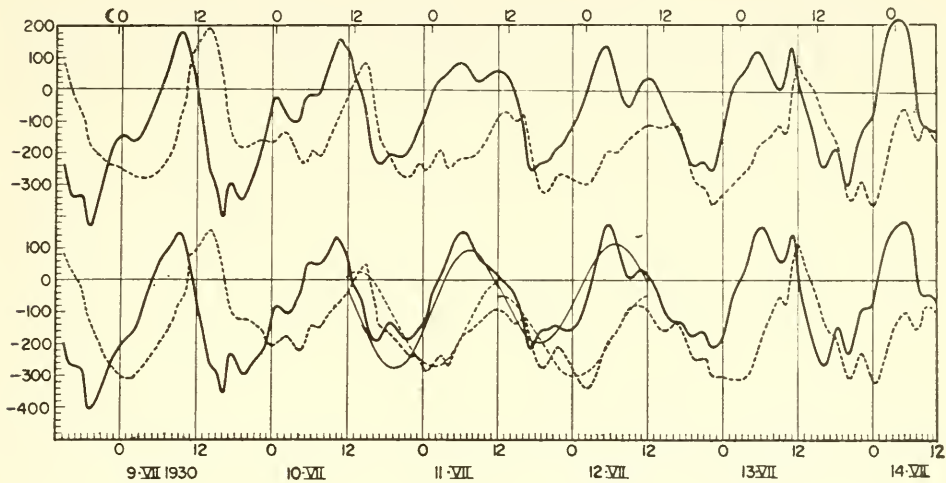


FIG. 194. North Atlantic Ocean: anchor station of the "Armauer Hansen" 30° 13' N., 13° 57' W. Current measurements in 5 m depth after elimination of the semi-diurnal tide. Full line, north component; dashed line, east component; velocity scale in mm/sec. At the upper rim moon hours. The distance between two vertical lines is very nearly 6 pendulum hours (according to Helland-Hansen and Ekman).

appeared to be a phase shift in the meridional component due to a new disturbance; the oscillations then lose rapidly in regularity. Harmonic analysis for the first three and then for the following three days gave (cm/sec, t in pendulum hours):

$$\begin{aligned}
 N &= 1.88 \cos(2\pi/12 \cdot t - 112^\circ) & \text{and} & & N &= 1.58 \cos(2\pi/12 \cdot t - 102^\circ) \\
 E &= 1.51 \sin(2\pi/12 \cdot t - 115^\circ) & \text{and} & & E &= 1.29 \sin(2\pi/12 \cdot t - 97^\circ)
 \end{aligned}$$

These oscillations are pictured by the full and dotted sine curves in Fig. 194. The good agreement led Helland-Hansen and Ekman to interpret these waves as inertia movements. The phase difference between the two components was 12 min more for the first days and for the second three days 20 min less than the theoretical required value of 6 h. The average ratio of the amplitudes was 1·23 as compared with a theoretical value of 1. The oscillations were thus of the elliptic type with a ratio of 5:4. Considering that besides the inertia oscillations presumably the diurnal tide was also present, the results obtained are very satisfactory.

An unambiguous proof of the occurrence of inertia oscillations was provided by the current measurements organized by H. Pettersson in the Baltic. As an adjacent sea without any significant tides this is particularly suitable for such an investigation. GUSTAFSON and OTTERSTEDT (1932) and GUSTAFSON and KULLENBERG (1933, 1936) have made a detailed analysis of the suitable current measurements in the Baltic; in many

cases there was no doubt of the presence of pure inertia movements. The best example is that contained in the measurements of 17–24 August. The recordings were made between Gotland and the mainland (57.8° N. 17.8° E., depth 100 m) at a depth of 14 m over a period of 162 h. The structure of the sea showed a well-developed density transition layer (thermocline) at 25 m and an almost homogeneous top layer. The variations in direction and strength of the current can be given in the form of a progressive vector diagram which shows the track of a single small water element. On the current directed towards the NNW there is superimposed an oscillation rotating to the right, at first increasing and then decreasing (Fig. 195). The changes

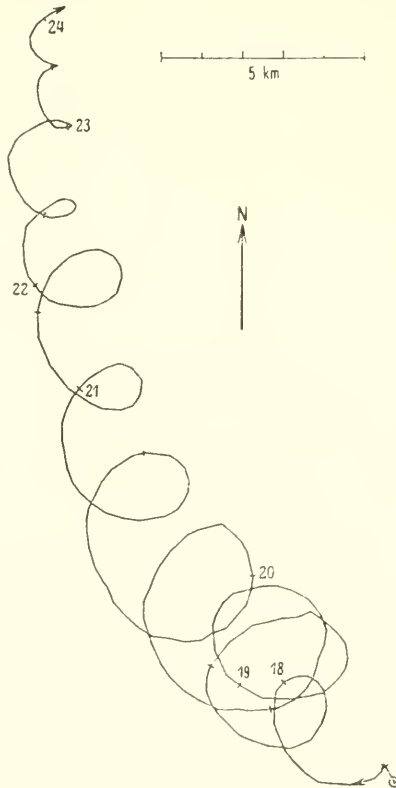


FIG. 195. Inertia oscillations in the Baltic in hodograph representation (according to Gustafson and Kullenberg).

with time in the two velocity components are shown in Fig. 196. This diagram is particularly reminiscent of the theoretically derived oscillation due to a suddenly starting wind or to a suddenly imposed pressure gradient (Figs. 192, 193). If the first waves of the excitation period are omitted the period of the oscillations is 14.0 h as compared with 14.14 h for the inertia oscillation. The phase difference is almost exactly a quarter of a period and the amplitudes are very nearly equal.

The meteorological observations taken at the same time do not permit any deductions about the origin of this inertia wave. The question concerning the horizontal

extent of this type of inertia oscillation was examined in later current measurements in the Baltic. Recordings from four anchored oceanographic research vessels between the Latvian coast and Öland (along the 56° 20' parallel) in the Baltic all, except for the vessel next to the Latvian coast, showed regular inertia oscillations at 15 m depth (density transition layer) with amplitudes of up to 20 cm/sec. The inertia oscillations (period 14.42 h = ½ pendulum day) had almost the same phase value but decreased very rapidly towards the coast. The water masses along the parallel investigated thus took part as a whole in the inertia oscillations (KULLENBERG and HELA, 1942).

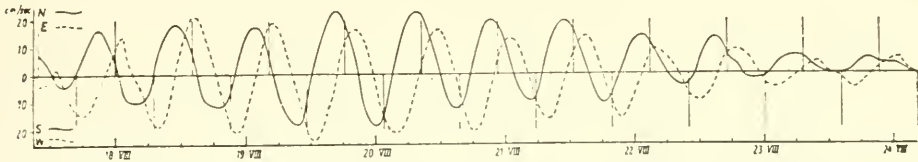


FIG. 196. Velocity components of the currents pictured in Fig. 195 (according to Ekman).

Specific inertia oscillations were found at the “Altair” anchor station in the area of the Gulf Stream north of the Azores (44.6° N. 34.0° W., 16–20 June 1938). Analysis of current measurements made at this station down to great depths (DEFANT, 1940 b) showed that besides the semi-diurnal tide there was also a 17 h oscillation; this had a large amplitude at all depths but the phases changed with depth. These phase changes which are related to the oceanographic structure at this station indicate that these inertia oscillations were coupled with *internal waves* which are the expression of a whole system of inertia oscillations of the surrounding water masses (see Vol. II). The combination of the 17 h wave with the semi-diurnal tide gives rise to beat phenomena with a period of 14.3 h and a beat interval of 1.86 days. This shows in a typical way the current values at all depths so that there can be no doubt that besides the tides, inertia oscillations were present here. Harmonic analysis gave besides the tidal wave also the value for the 17 h wave presented in Table 130. Division into different layers follows from the similarity in the phase which between 15 and 30 m and between 500 and 800 m shows an abrupt change of about half a period. The 17 h wave shows

Table 130. Inertia oscillations at the “Altair” station (16–20 June 1938; 44.6° N., 34.0° W.). Period 17 h

Depth of layer (m)	Current				Ratio of ampl. N.:E.	Phase N. + 4.25 h	Difference towards E.
	N-component		E-component				
	Ampl. (cm sec)	Phase (h)	Ampl. (cm sec)	Phase (h)			
5–10	8.75	14.45	8.25	1.85	1.06	1.70	+0.15
30–100	10.0	7.33	10.0	12.27	1.00	11.58	+0.69
300–500	5.0	9.0	5.0	14.85	1.00	13.25	+1.60
800	8.0	2.0	8.0	8.0	1.00	6.25	+1.75

all the characteristics of inertia oscillations. At $\phi = 44^\circ 33'$ the theoretical period is 17.1 h. The amplitudes of the components are almost identical and also the requirement that the *E*-component should follow the *N*-component by a quarter of a period (4.24 h) is fully justified. The deviations in the deeper layers must be a consequence of internal waves. Figure 197 shows the course of the *N*- and *E*-components for the layer

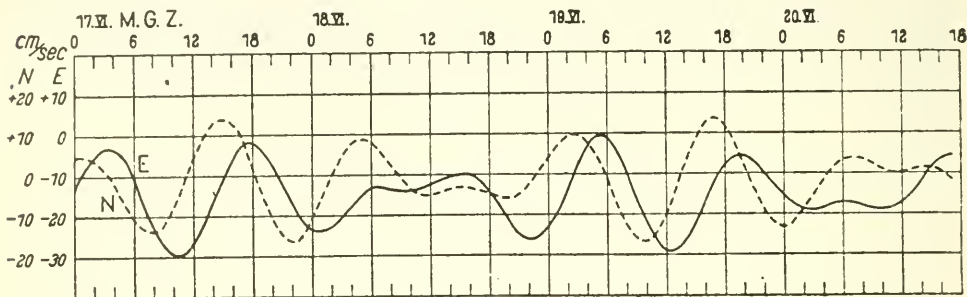


FIG. 197. North and east component of the current at the "Altair" anchor station according to the values of the harmonic analysis for the depth interval 5-15 m (basic current + 17 h period + 12.3 h period).

between 5 and 15 m as given by the values obtained by harmonic analysis. The beats stand out clearly, as does the retardation of the *E*-component behind the *N*-component characteristic of inertia oscillations.

The inertia oscillations at the "Altair" anchor station are of considerable interest in so far as they show that the entire current system, together with the oceanic structure of the surrounding waters, seems to take part in these oscillations following the rhythm of the inertia period. These oscillations which may be initiated by any external disturbance impulses stand out particularly well in stratified waters, since coupled with these oscillations of the flow are corresponding oscillations of the density transition layer and of the system of isosteres which are thus reflected in all layers (see Vol II).

Chapter XIV

Water Bodies and Stationary Current Conditions at Boundary Surfaces

1. Water Bodies and the Boundary Surface Between Them

THE theory of ocean currents in a homogeneous sea gives results which allow in many cases its application to actual conditions, although the sea itself is far from being homogeneous. In changing from a homogeneous to a stratified ocean it is necessary to consider two homogeneous water masses (water bodies) situated side by side and separated by a *discontinuity surface* (boundary surface). On passing through this, changes in physical and chemical properties occur and also in the state of motion of water masses. This is, of course, also only a schematic model, since in reality the individual water bodies are not quite homogeneous and the transition from one to the other is seldom abrupt. Usually in Nature there is a rapid "transition layer" between the more or less homogeneous water bodies inside which a steady, rapid change of the properties occurs, while passing through it.

The genesis of boundary surfaces of this type is due to the circumstance that in certain oceanic regions specific water types are continuously formed and carried away by the ocean currents together with their characteristic properties. In this way two different water bodies are brought into close contact at singularities in the current field and a boundary surface between them is formed at convergence lines. The principal changes in the horizontal distribution of a property (such as temperature or salinity and others) occur always in connection with so-called deformation fields of the motion (BJERKNES and co-workers, 1933). The most simple case of a horizontal deformation field is the current field at a neutral point (see p. 365, Fig. 155 *a*) with hyperbolic stream lines in each of the sectors formed by intersection of the two stream lines in the neutral point (Fig. 198). These straight lines are the principal axes of deformation of the field; one of them is an *axis of dilatation* and the other at right angles to it is an *axis of contraction*. This deformation field when superimposed on the field of one of the water properties will have a marked effect on the latter. The two full lines in Fig. 198 represent two isolines of a property, such as for example, the temperature. The current field will produce displacements in the position of these lines: all isolines which initially are parallel to the axis of contraction will move away from it and isolines parallel to the dilatation axis will move towards it. It can also be shown that two isolines through the current will always tend towards a direction parallel to the dilatation axis, so that they will first move away from each other to a maximum distance, and then after reaching a certain angle to the dilatation axis will move towards it again. In the case of a temperature distribution the effect of the deformation

field is thus a concentration of the isotherms parallel to the dilatation axis and the horizontal temperature gradient will increase very strongly (according to theory indefinitely). This, therefore, leads to the formation of discontinuity surfaces the intersections of which with the sea surface show as *discontinuity lines* or *fronts*.

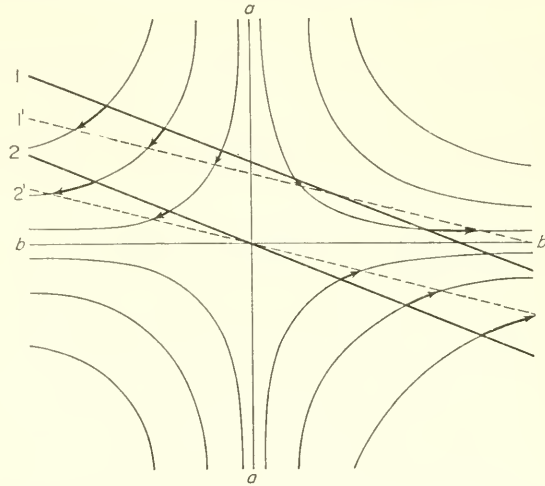


FIG. 198. Deformation field and the change of a field of a characteristic water property. *a—**a*, shrinking axis; *b—**b*, axis of dilatation; 1—2, isolines of the property in the beginning; 1'—2', isolines of the property at the end of deformation.

The formation of strong horizontal gradients in the boundary regions of water bodies actually occurs most often in association with stationary oceanic deformation fields. However, other circumstances are involved in their maintenance. These are coupled with the effect of the deformation field and may lead to *stationary fronts* which are particularly characteristic for the horizontal distribution of the oceanographic factors. For an initially meridional temperature gradient and a steady meridional ocean current v the conditions will develop along the following lines (see Pt. I, p. 111): the temperature ϑ at a fixed point will change according to the relation (positive y -axis directed polewards)

$$\frac{\partial \vartheta}{\partial t} = \frac{1}{c_p} Q - v \frac{\partial \vartheta}{\partial y}.$$

If v is directed towards the pole, the temperature at a fixed point will increase since $\partial \vartheta / \partial y$ is negative (temperature increase by advection), that is, the isotherms will be displaced towards the pole provided that Q is small. However, due finally to the increase of temperature the first term on the right-hand side will also be increased and as a result all the factors affecting the temperature will maintain an equilibrium state. Although the ocean current is directed towards the pole the temperature distribution will remain stationary. Similar reasoning will also apply to the horizontal distribution of other oceanographic factors. Besides stationary fronts of this type there are also frontal formations due to aperiodic occurring processes. However, due to the lack of synoptic observations the course of these usually cannot be traced. An interesting case has been given in Pt. I, p. 182 in the discussion

on mixing processes in the transitional area between the North Sea and the Baltic. These are real, progressing hydrographic fronts that are associated with the interchange of water between the two seas.

The parts of the ocean where more or less stationary fronts are found are actually closely connected with the occurrence of quasi-stationary deformation fields with an axis of dilatation in the current system of the oceans deviating as little as possible from the east–west direction. The position of these can be found directly from a chart of ocean currents. In the Northern Hemisphere the most important are:

(1) The *North Atlantic Polar Front* which is present with its main part to the south of Newfoundland and there forms the boundary between the Gulf Stream water and the Arctic water of the Labrador Current; its continuation separates the cold low-saline water of the East—and in part also of the West—Greenland Current from the Atlantic water masses. Other parts lie south of Spitzbergen and in the Barents Sea.

(2) The *North Pacific Polar Front* with its main part between the Kuroshio and the Oyashio which can be traced to about the middle of the ocean. These fronts are a consequence of quasi-stationary deformation fields in the current system in this part of the ocean.

(3) This is also the case, though less clearly, in the *Southern Hemisphere Polar Front* which runs right around the Earth. It lies between the West Wind Drift and the Antarctic Current. In the parts where it is particularly well developed (for instance, south of South America and between the Falkland Islands and South Georgia) the connection with the local deformation field is clearly shown.

2. Stable Discontinuity Surfaces

If two motionless water bodies are present together in the ocean for a stable equilibrium, the heavier water type must lie underneath of the lighter and the discontinuity surface between them must coincide with a level surface. Two water bodies at rest, situated side by side, will never be in equilibrium, even if each water body by itself has a stable vertical stratification. Since, due to their different densities, the pressure in each water mass will increase with depth at different rates, pressure differences are created; the resultant water movements will overturn the water bodies and they will only cease when the water bodies are again situated one above the other, separated by a horizontal boundary surface. However, two water bodies side by side can be in stable equilibrium *if they are in motion*. The form and position of the resulting discontinuity surface was first given by MARGULES (1906) following up an investigation by HELMHOLTZ (1888); a more general representation was given later by J. BJERKNES (1921) and later an application to the analogous conditions in oceanic water bodies has been given by DEFANT (1929 *b*).

A stationary state of the boundary surface is possible only for a certain definite state of motion in the two water bodies; thereby the boundary surfaces will lie at an angle to the level surfaces, so that the denser water always spreads out in a wedge-form underneath the lighter water. It will be a discontinuity surface for density (temperature, salinity or both) but not for pressure, since otherwise movements would immediately start directed towards the boundary surface. This, however, would interfere with the condition of stationary state. On the contrary, the boundary surface will be a discontinuity surface for the *pressure gradient*. According to the

Hadamard classification (1903)[†] it is thus a discontinuity surface of zero order for the density and of the first order for the pressure. The horizontal movements in each water body must thus be parallel to the boundary surface since otherwise the surface could not remain at rest.

There are kinematic and dynamic boundary conditions that must be satisfied at the discontinuity surface (see p. 324). The *kinematic condition* (equation X.29) requires that

$$(u_1 - u_2) \cos (nx) + (v_1 - v_2) \cos (ny) + (w_1 - w_2) \cos (nz) = 0, \quad (\text{XIV.1})$$

where n is the direction of the normal to the boundary surface; u_1, v_1, w_1 are the velocity components of the lighter and u_2, v_2, w_2 are those for the heavier water type. The *dynamic condition* (equation X.29) requires that the pressure should be the same on both sides of the boundary surface (pressure equal counter pressure)

$$p_1 - p_2 = 0. \quad (\text{XIV.2})$$

If $\dot{u}, \dot{v}, \dot{w}$ are the total acceleration components and X, Y, Z are the components of the forces, the equation of motion for the lighter water body 1 can then be written in the form:

$$dp_1 = \rho_1 [(X_1 - \dot{u}_1) dx + (Y_1 - \dot{v}_1) dy + (Z_1 - \dot{w}_1)] dz. \quad (\text{XIV.3})$$

An analogous equation will apply for the heavier water body 2. The equations

$$dp_1 = 0 \quad \text{and} \quad dp_2 = 0$$

will then give the equations for the *isobaric surfaces* according to the motion in each water body while the dynamic condition (XIV.2) will give the equation of the boundary surface

$$[(\rho_1 X_1 - \rho_2 X_2) - (\rho_1 \dot{u}_1 - \rho_2 \dot{u}_2)] dx + [(\rho_1 Y_1 - \rho_2 Y_2) - (\rho_1 \dot{v}_1 - \rho_2 \dot{v}_2)] dy + [(\rho_1 Z_1 - \rho_2 Z_2) - (\rho_1 \dot{w}_1 - \rho_2 \dot{w}_2)] dz = 0. \quad (\text{XIV.5})$$

In the most general form these are the equations for the slope of the isobaric surfaces in each of the water bodies and for the inclination of the boundary surface.

If the water bodies, each in itself, are both homogeneous (ρ_1 and $\rho_2 = \text{const.}$), the motion is non-accelerated ($\dot{u} = \dot{v} = \dot{w} = 0$) and is directed *straight along the y-axis* ($u_1 = u_2 = 0$ and $w_1 = w_2 = 0$), then there will be a *static equilibrium* in each water body and

$$X_1 = f v_1, \quad Z_1 = g \quad \text{and} \quad X_2 = f v_2, \quad Z_2 = g.$$

Further, if the slope of the isobaric surfaces in the (xz) -plane is denoted by $dz/dx = \tan \beta$ and that of the boundary surface by $dz/dy = \tan \gamma$, then the above equations will give

$$\tan \beta_1 = -\frac{f}{g} v_1; \quad \tan \beta_2 = -\frac{f}{g} v_2, \quad (\text{XIV.6})$$

[†] According to the classification of such surfaces introduced by HADAMARD (1903), a discontinuity surface at which the velocity and the density (temperature and salinity) change abruptly by a finite amount from one to the other side, is termed a *discontinuity surface of zero order*. It is defined to be of the *first order* when the characteristic properties of the water bodies at the surface change continuously but their derivatives normal to the surface are subject to abrupt changes.

and

$$\tan \gamma = - \frac{f}{g} \frac{\rho_2 v_2 - \rho_1 v_1}{\rho_2 - \rho_1} \tag{XIV.7}$$

In each water body there will be a gradient current (geostrophic current). The angles β_1 and β_2 will determine the slope of the planar isobaric surfaces and that of the physical sea level.

The slope of the boundary surface is of quite a different order of magnitude. Taking $\phi = 45^\circ \text{ N.}$; $\sigma_1 = 28.13$; $\sigma_2 = 27.33$ (density at 0°C and 35‰, as well as at 0°C and 34‰) and in addition if the water body 2 is at rest ($v_2 = 0$), while for water body 1 $v_1 = 100 \text{ cm/sec}$, then one obtains $\gamma = 0^\circ 46' 13''$. The boundary surface is only little inclined to the level surfaces and rises only 13.5 m/km. In the water body at rest the isobaric surfaces are horizontal; in the upper, moving water body they rise very slightly to the right of the current direction because $\beta_1 = 0^\circ 0' 2.2''$, which means a rise of 1 cm in 1 km (Fig. 199; the slopes, in order to make them visible at all, are shown with a considerable vertical exaggeration). The slope of the boundary surface

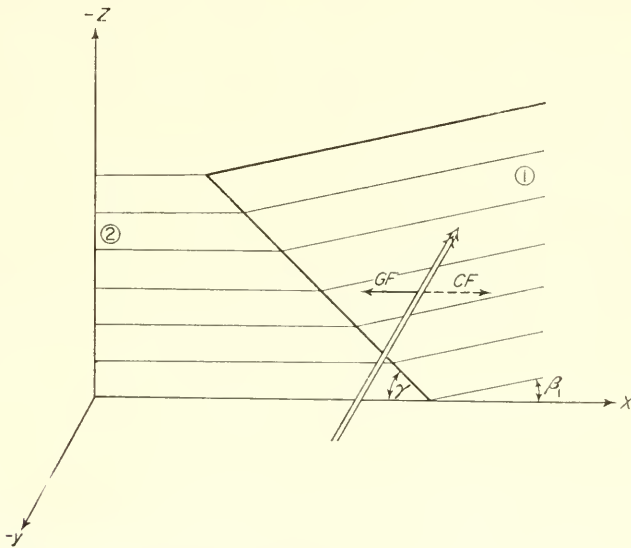


FIG. 199. Stationary current system of two water masses situated side by side (position of the boundary surface, isobaric surfaces and the physical sea surface); GF gradient force; CF Coriolis force.

is about 1000 times greater by magnitude than that of the isobaric surfaces and that of the physical sea level, in the moving water body. Table 131 gives the slopes when $\rho_1 = 1.027$; $\rho_2 = 1.028$; $v_2 = 0$, for different values of v_1 at 45°N . The lighter water mass always glides as a pointed wedge on top of the heavier and superimposes the heavier near the boundary surface as a quite shallow layer.

Equation (XIV.7) can be simplified if the slope of the isobaric surfaces is neglected by comparison with the much greater slope of the boundary surface. This gives

$$\tan \gamma = - \frac{f}{g} \frac{\rho_1}{\rho_2 - \rho_1} (v_2 - v_1) \tag{XIV.8}$$

When $v_2 = 0$ it follows

$$\tan \gamma = - \frac{\rho_1}{\rho_2 - \rho_1} \tan \beta_1$$

and since $\rho_2 - \rho_1$ is of the order of 10^{-3} , the slope of the boundary surface will be about 1000 times greater than that of the isobaric surfaces; it has, moreover, the *reverse* inclination as compared with that of the isobaric surfaces in the upper water body; the physical sea level has thus the opposite inclination in comparison to that of the boundary surface underneath.

Table 131. *Slope of the boundary surface and the isobaric surfaces for moving water masses. $\phi = 45^\circ$ N. $\rho_1 = 1.027$, $\rho_2 = 1.028$; $v_2 = 0$, $\beta_2 = 0$*

v (cm/sec)	10	20	30	40	50
γ	$0^\circ 3' 42''$	$7' 26''$	$11' 8''$	$14' 51''$	$18' 33''$
$\tan \gamma$	1:926	1:463	1:309	1:232	1:185
Rise (m) {					
over 10 km	10.8	21.6	32.4	43.2	54.0
over 50 nautical miles	100	200	300	400	500
β_1	$-0^\circ 0' 0.3''$	$-0' 0.4''$	$-0' 0.7''$	$-0' 0.9''$	$-0' 1.1''$
$\tan \beta_1 \cdot 10^{-6} \times$	1.05	2.10	3.15	4.20	5.25
Rise (cm) {					
over 10 km	1.05	2.10	3.15	4.20	5.25
over 50 nautical miles	10	20	29	39	49

The slope of the Margules boundary surface can also be derived quite readily from the equations of motion. This will be given here since it will be required later. We consider two water bodies 1 and 2, one above the other, the upper limit of the lower being the boundary surface and the upper limit of the lighter above it being the physical sea level; furthermore, we allow only slopes along the x -axis. The position of the two boundary surfaces can be defined by the deviations ζ_1 and ζ_2 from their equilibrium position at rest (level surfaces). The pressures at an arbitrary point A in the water body 1 and at a similar point B in the water body 2 will then be:

$$p_1 = (h_1 + h_2 - z)\rho_1 g - \rho_1 g \zeta_1$$

and

$$p_2 = - \rho_1 g \zeta_1 + (h_1 + \zeta_2)\rho_1 g + (h_2 - \zeta_2 - z)\rho_2 g.$$

Then for *stationary* state the equations of motion will take the form

$$1 \quad f v_1 + g \frac{\partial \zeta_1}{\partial x} = 0; \quad 2 \quad f v_2 + \frac{\rho_1}{\rho_2} g \frac{\partial \zeta_1}{\partial x} + \frac{\rho_2 - \rho_1}{\rho_2} g \frac{\partial \zeta_2}{\partial x} = 0.$$

The first equation gives immediately the slope of the physical sea level

$$\tan \beta_1 = \frac{\partial \zeta_1}{\partial x} = - \frac{f}{g} v_1.$$

Elimination of $\partial \zeta_1 / \partial x$ from the second gives the slope of the boundary surface

$$\tan \gamma = \frac{\partial \zeta_2}{\partial x} = - \frac{f}{g} \frac{\rho_2 v_2 - \rho_1 v_1}{\rho_2 - \rho_1}$$

which are the same equations as before.

It might be mentioned here that equation (XIV.7) can also be written

$$\tan \gamma = \frac{\rho_2 \tan \beta_2 - \rho_1 \tan \beta_1}{\rho_2 - \rho_1}$$

which gives the slope of the boundary surface directly from the slopes of the isobaric surfaces. Further the equations of motion give a relationship between the horizontal pressure gradients on either side of the surface

$$\frac{\partial p_2}{\partial x} - \frac{\partial p_1}{\partial x} = - g(\rho_2 - \rho_1) \tan \gamma.$$

According to equation (XIV.7), stable boundary surfaces on the rotating earth are usually inclined and are horizontal only when the specific momentum ρv (velocity impulse) is the same in both water bodies. When $f = 0$, that is at the equator, discontinuity surfaces are of course always horizontal. The following rule can be deduced governing the inclination of the boundary surface and of the physical sea level for steady frictionless currents in the Northern Hemisphere: In every water body there will be a geostrophic current; looking in the direction of the current (downstream) the isobaric surfaces and the physical sea level will rise from left to right. The lighter water body will be situated on top of the heavier as a very sharp wedge and will move to the right relative to the heavier when looking from the the heavier towards the lighter. In the Southern Hemisphere this will, of course, be reversed (it is simply necessary to replace "right" by "left").

A good example of steady current conditions in the simplest form is found inside the current system of the East Greenland Current. Here a cold low-saline water mass flows along the coast towards the south; on its left-hand side it borders against the almost stationary Atlantic Water in the middle part of the European North Sea. The main core of the East Greenland Current keeps to the west along the shelf of the east coast of Greenland. Figure 200 shows a density section across the current according to the observations of the "Belgica" expedition (Amundsen). In the vicinity of the current the isopycnals rise with a mean gradient of 1:300 towards ESE. The water of this cold low-saline current is strongly stratified and especially at the surface there is a strongly heated, very light top layer. The isopycnal, $\sigma = 28.0$, indicates the boundary

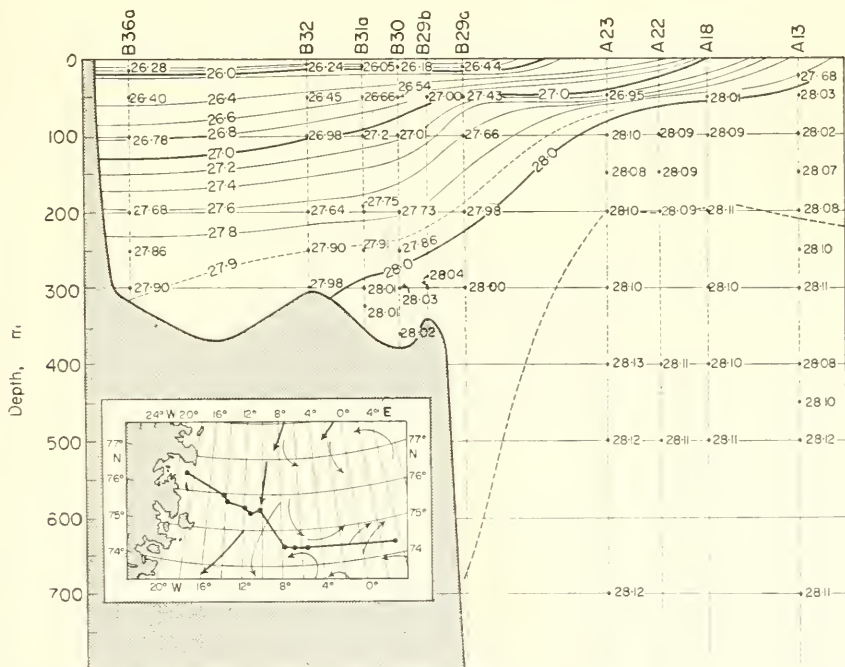


FIG. 200. Density cross-section normal to the East Greenland current according to the observations of the "Belgica" expedition and the observations of Amundsen. (The small map contains the position of the cross-section and the stations used.)

between the Greenland Current water and the almost homogeneous Atlantic Water ($\sigma = 28.1$). The wedge-shaped spreading of lighter polar water over the heavier Atlantic Water to the east stands clearly out. Taking $\sigma_1 = 27.1$ for the polar water and a velocity v_1 of about -25 cm/sec (towards the south) and $\sigma_2 = 28.1$, $v_2 = -5$ cm/sec (towards the south) for the Atlantic Water, then equations (XIV.6 and 7) give the boundary surface slope as $\gamma = 0^\circ 10' 2''$ which corresponds to 1:343 rising towards the east and for the slope of the physical sea level and that of the isobaric surfaces in the Greenland Current one obtains $\beta_1 = 0^\circ 0' 0.7''$ which is about 35 cm in 100 km towards the west. The slope calculated for the boundary surface is in good agreement with that actually found. The rise of the physical sea level towards the coast is rather remarkable and even these simplified assumptions lead to the conclusion that the sea level along the east coast of Greenland will be on the average about 20–30 cm higher than in the central parts of the Norwegian Sea.

3. Stable Stratification of Water Masses

Water bodies are frequently found in the ocean, situated in a remarkable way side by side, which are apparently in stable equilibrium. This can only occur if certain definite current conditions are present in each water mass. The resulting upwelling and sinking water movements in these water masses must be counter balanced by the current system present. These conditions take a simple form, if one considers at first water bodies *arranged in strips* which are motionless and are embedded in moving adjacent water masses of a different type (DEFANT, 1929 b).

(a) A Motionless Heavy Water Body Embedded into Moving Light Water Masses

The conditions required for stationary equilibrium are shown schematically in Fig. 201 (Northern Hemisphere; reversed current directions in the Southern Hemisphere). This is readily understood on the basis of the rule given above. In the heavier

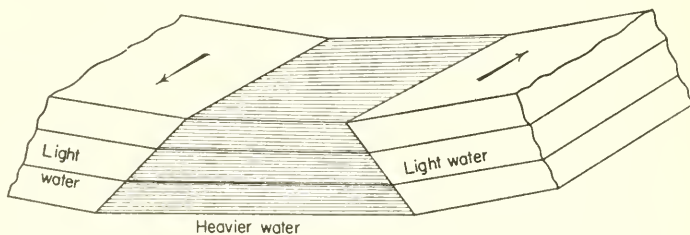


FIG. 201. Motionless heavy water mass embedded in moving lighter water (Northern Hemisphere).

water body the pressure at the same level must be lower than in the surrounding water and correspondingly the physical sea level will be lower than on either side. An elongated depression of it will thus indicate on the sea surface the position of the heavier water body which extends in wedge-form in the deeper layers underneath the moving water masses to either side. If the water body in the middle between the moving water masses is not motionless then this movement must be added vectorially to the currents of the surrounding water masses on both sides in order to conserve a stable

equilibrium state, i.e. a uniform gradient current with the corresponding slopes of the isobaric surfaces and of the sea level must be superimposed on the entire system shown in Fig. 201. This will change somewhat the position of the isobaric surfaces and that of the physical sea level. This circumstance should always be kept in mind in dealing with the phenomena described in this section.

The oceanic structure in the boundary area between the Labrador Current and the Gulf Stream to the south of the Newfoundland Banks is usually chosen as an example for the oceanic structure presented in Fig. 201. Figure 202 shows a section through the

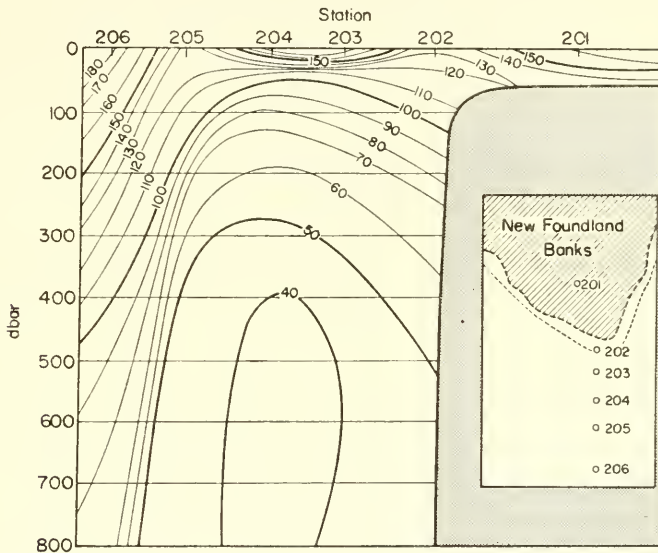


FIG. 202. Distribution of the specific volume anomalies in a meridional cross-section south of the Great Banks of Newfoundland (according to Smith). Horizontal scale, 1:2 million; vertical scale, 1:5000.

currents and the distribution of specific volume anomaly (SMITH, 1926); the currents here are approximately zonal ones (directed almost east-west). Disregarding the thin top layer about 50 m thick, there is a heavier water body found in the middle flanked to the north and south by water masses of greater specific volume. On the southern side (Sts. 205 and 206) the lighter Gulf Stream water flows to the east (out of the plane of the diagram), while on the northern side the water masses of the Labrador Current flow towards the west in the area just to the south of the Newfoundland Banks (Sts. 202 and 203). Figure 203 presents the topography, calculated from the mass distribution, of some isobaric surfaces and of the physical sea level. As required by theory, the presence of the heavier water body in the middle is shown by a low pressure trough and at the surface by an elongated depression of the water level.

(b) Motionless Light Water Body Embedded into Moving Heavier Water Masses

The oceanic structure is also given here in the same way as for case (a) by the rules for the stationary stratification of adjacent water bodies (Fig. 204). Here also the sea level is lowest over the lighter water body, but this deep pressure trough diminishes

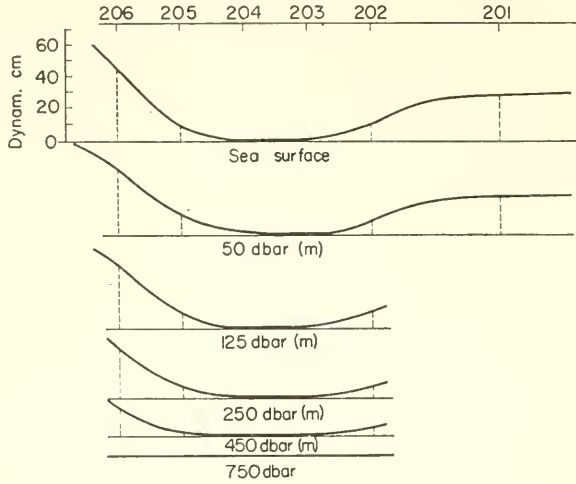


FIG. 203. Distribution of the specific volume anomaly. Form of the physical sea surface and of the isobaric surfaces in a meridional cross-section south of the Great Banks of Newfoundland.

in the deeper layers due to the wedge-shaped spreading of the adjacent heavier waters underneath, which in the absence of the effect of Earth rotation would press upwards the lighter water in the middle. The equilibrium of all the forces prevents this upward movement and maintains the structure in a stationary state.

This simplest arrangement of water bodies is not readily found in ocean currents. DIETRICH (1935) in an investigation of the Agulhas Current found a mass distribution which was similar to that pictured in Fig. 204, although with the current directions exactly opposite that in Fig. 204. The pressure distribution as well as the topography of the physical sea level would then be different. Dietrich assumed rising isobaric surfaces towards the central lighter water body and no motion in the lighter body (planar sea level and isobaric surfaces). The gradient currents in the adjacent heavier water masses then correspond to the pressure field, but the current system as a whole does not correspond to the rule of a stable position of the boundary surface. The schematic representation given by Dietrich is in error.

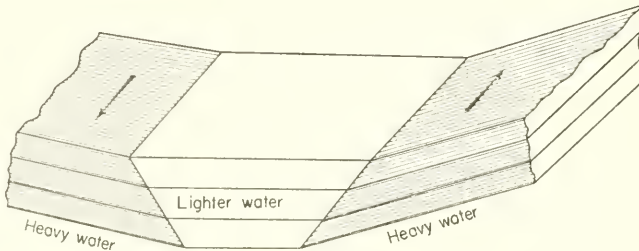


FIG. 204. Motionless lighter water mass embedded in moving heavier water (Northern Hemisphere).

Figure 205 presents a dynamic section from Capetown towards the south-west based on the "Meteor" observations (profile 1 a, 8–12 July 1925). The distribution of the specific volume anomaly gives the structure shown schematically in Fig. 204. With this stratification it can be expected theoretically (for the Southern Hemisphere) that there will be a current flowing WNW to ESE just south of Africa (St. 20) and further

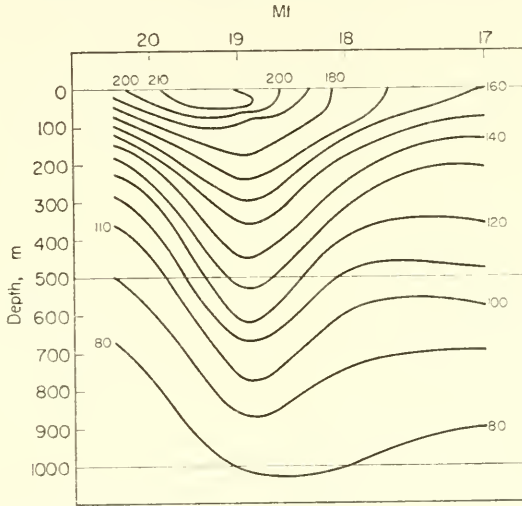


FIG. 205. Specific volume anomaly in a cross-section south-west of Capetown ("Meteor" profile 8–12 July 1925, 34° 49' S., 17° 48' E. to 41° 12' S., 11° 31' E.).

south (St. 18) there should be a current from ESE to WNW, if there is no motion in the central region of the lighter water body. The observations show, however, that this is not the case. According to dynamic calculations of the pressure field (Fig. 206) there is a high-pressure ridge in the region of the central lighter water sloping downwards to the WNW in the northern part and to the ESE in the southern part. The system of forces in the simple case of Fig. 204 is thus superseded by another pressure system, which modifies conditions. It must be sufficiently strong to be able to reverse the effect of the weaker opposite pressure gradient. These conditions can be represented in a schematic way as shown in Fig. 207. Everywhere over the whole area the isobaric surfaces and the physical sea level decline outwards though this is less so in the heavier water masses than in the lighter central water. The current velocity in the heavier water masses is thus less than in the lighter one in the middle. On the total northern side there is a current from the east (the Agulhas Current), and on the entire southern side is a current from the west (the West Wind Drift). The rule for a boundary surface slope is now fulfilled; since always when looking from the heavier towards the lighter water the first moves towards the left relative to the latter (Southern Hemisphere).

Of particular interest is the application of the rule for the position of the boundary surface between water bodies in subtropical and tropical seas, where the upper part of the troposphere is to a large extent separated into two layers. The tropospheric discontinuity layer separates an almost homogeneous top layer from the subtropospheric water masses of only slightly different density. Here, in places, the transition

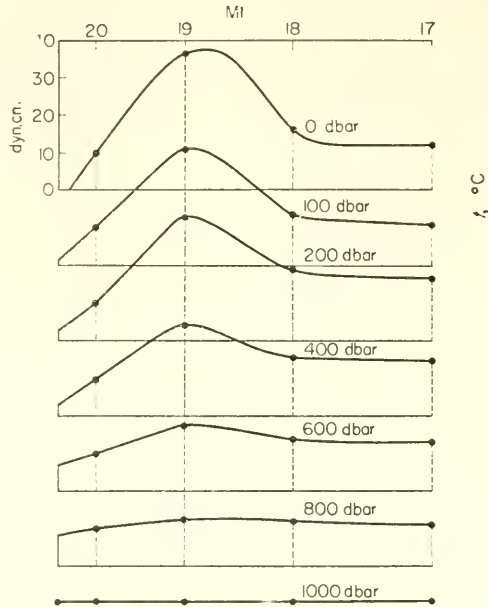


FIG. 206. Position of the physical sea surface and of the isobaric surfaces in a cross-section south-west of Capetown through the Agulhas Current and the West Wind Drift.

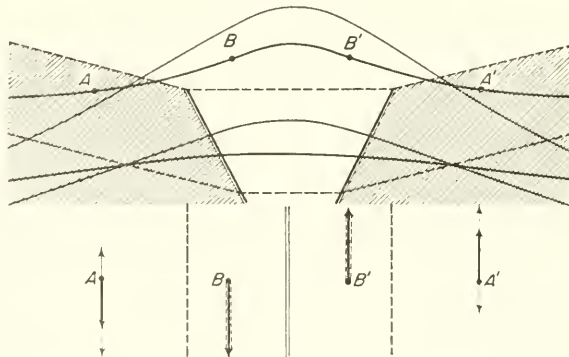


FIG. 207. Schematic representation of the oceanic structure in a cross-section normal to the Agulhas Current and the West Wind Drift south of Africa. *Shaded*, heavier water masses; *non-shaded*, lighter water masses; *dashed lines*, isobaric surfaces of this system; *thin full arrows in A and A'*, corresponding currents, in A from west towards east, in A' from east towards west. Superimposed the pressure field of a water-"stau" in the central region; *thin full lines in the cross-section*: isobaric surfaces, *dashed in A, B and A', B'*: corresponding currents, in A and B from east towards west, in A' and B' from west towards east. *Thick full lines in the section*: resulting pressure field of the final current system. *Thick full arrows underneath*: direction and speed of the resulting currents; in A and B from east towards west, in A' and B' from west towards east.

layer carries the character of a real discontinuity surface and its position depends principally on the currents in the top layer, since the cold water masses beneath are almost motionless. Since the equatorial currents in both hemispheres flow from east to west (North and South Equatorial Current) the dynamic equilibrium requires an accumulation of the heavy water of the lower layer on the left side in the Northern Hemisphere and on the right side in the Southern Hemisphere. The discontinuity layer thus arches upwards in the equatorial regions and this must be associated with a depression in the physical sea level at the equator. The vertical stratification of the water bodies, the position of the isobaric surfaces and of the physical sea level is presented schematically in Fig. 208a (SVERDRUP, 1932, 1934a, DEFANT, 1936c,

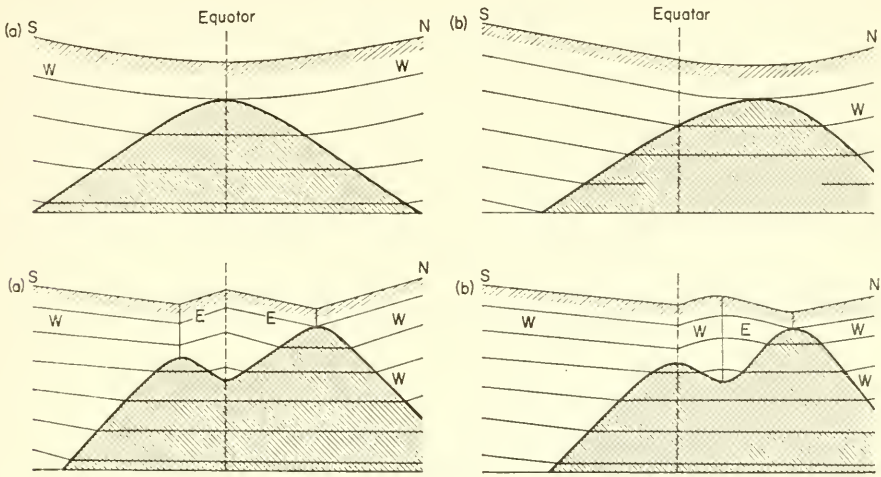


FIG. 208. Different positions of the thermocline and of the physical sea surface in the tropics and subtropics and the corresponding current systems (according to Sverdrup). *W*, current towards west; *E*, current towards east.

p. 315). When the currents are symmetrical about the equator, this stratification will also be symmetrical. However, neither of these conditions actually occur in the Atlantic nor in the Pacific and very probably also not in the Indian Ocean. The thermal equator is at times found north of the geographical equator so that the equatorial currents are *not symmetrical* about the equator. In the Indian Ocean the thermal equator lies to the south of the equator during the southern summer. This complicates the adjustments of the boundary surfaces, since the Coriolis force, the effect of which is *symmetrical* about the equator, acts as a counter force to the non-symmetrical pressure field. An accumulation of the subtropical water masses, asymmetric to the equator, more or less as in case *b* in Fig. 208 with the position of the physical sea level and of the isobaric surfaces indicated there, *cannot be stable*. This is because, for stable stationary conditions, the topography of the sea level and of the isobaric surfaces at the equator must always show either a maximum or a minimum. In case *b* there will be a current from the west on the southern side of the equator and a current towards the east on its northern side, and at the equator itself the velocities will be infinite

(disregarding friction). The current system can only be stabilized by distributions pictured in cases *c* and *d*. In both cases a *counter current flowing eastward* must be introduced between the westward flowing equatorial currents of the Northern and Southern Hemisphere. In case *c* it lies entirely within the Northern Hemisphere, together with parts of the South Equatorial Current which extends across the equator; in case *d* the counter current is broader and extends somewhat across the equator into the Southern Hemisphere. This kind of adjustment position of the pressure surfaces and of the boundary surface, thus satisfies the requirements of a boundary surface slope for moving water bodies.

These theoretical considerations can be tested by using the available observational data. Figure 209 presents for a meridional profile, along the strongest inclination of the surfaces, the topography of the pressure surfaces and of the physical sea level of the

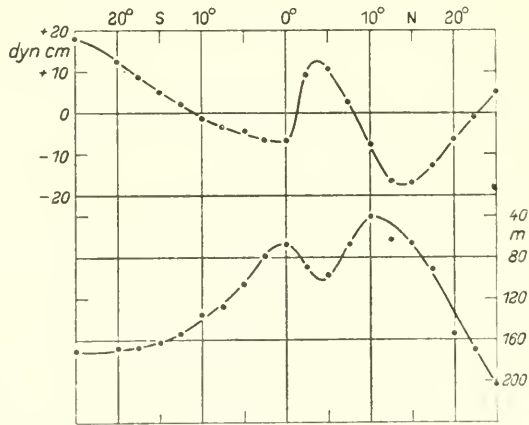


FIG. 209. Meridional cross-section through the Atlantic Ocean (25° N. to 25° S., 20° W. to 30° W.). *Upper picture*: physical sea surface (relative to the lower current 400:1 exaggerated). *Lower picture*: depth of the thermocline (tropospheric discontinuity layer).

Atlantic Ocean. The structure shown corresponds entirely to that given in Fig. 207*c*. There is no doubt that the adjustment of the tropospheric discontinuity layer is dynamically controlled and to a large extent imposed by the arrangement of the ocean currents in the top layer; there seems to exist a very close mutual adjustment between them. The observed slope agrees not only quantitatively but also qualitatively with that required by theory (Table 132). If the slope of the boundary surface, given in metres per 3 degrees of latitude, is denoted by i and that of the physical sea level by i_1 , then taking a mean value for ρ_1 of 1.024 and putting $f = l \times 10^{-5}$ the formula (XIV.8) gives

$$i = 3.46 \frac{l}{\sigma_2 - \sigma_1} v_1 \quad \text{and} \quad i_1 = -9.77 \times 10^{-4} m.$$

The value for v_1 is taken as the approximate average over the entire top layer. The observed and calculated values are nearly equal.

Table 132. Slope of the tropospheric transition layer and the physical sea level in the North and South Equatorial Current in the Atlantic Ocean.

	5° S.	17.5° N.
σ_1	24.0	24.6
σ_2	26.5	26.5
$\sigma_2 - \sigma_1$	2.5	1.9
v_1 (cm/sec)	15	6.5

Theoretical value: $m = 26.4$ m; $m_1 = -2.58$ cm; $m = 52.0$ m; $m_1 = -5.1$ cm
 Observed value: $m = 26.4$ m; $m_1 = -2.4$ cm; $m = 52.5$ m; $m_1 = -5.0$ cm

(c) Stationary Vortices in a Two-Layered Ocean

When the water masses in a two-layered ocean are in rotation they will be subject to a centrifugal force in addition to the gradient and Coriolis forces. Under stationary conditions these three forces must balance. Such systems of rotating water masses have been examined in detail by EXNER (1917) and especially by BJERKNES (1921). When the motion is symmetrical around the rotation axis, the vortices are termed "circular vortices". In cylindrical co-ordinates r is the distance at right angles from the axis of rotation z (positive downwards) and c is the rotational velocity (at right angles to r , positive for cyclonic and negative for anticyclonic motion). For a non-accelerated current ($\dot{c} = 0$) the following quantities can be introduced in the boundary surface equation (XIV.5):

$$X_1 = fc_1 + \frac{c_1^2}{r}; \quad Z_1 = g; \quad X_2 = fc_2 + \frac{c_2^2}{r}; \quad Z_2 = g,$$

c^2/r is the centrifugal force, which must be taken into account for curved trajectories. The slopes of the pressure surfaces, of the physical sea level for the lighter and the heavier water and of the boundary surface can be determined, and it is obtained

$$\tan \beta_1 = -\frac{f}{g} c_1 - \frac{c_1^2}{rg}; \quad \tan \beta_2 = -\frac{f}{g} c_2 - \frac{c_2^2}{rg} \tag{XVI.9}$$

and

$$\tan \gamma = -\frac{f}{g} \frac{\rho_2 c_2 - \rho_1 c_1}{\rho_2 - \rho_1} - \frac{1}{rg} \frac{\rho_2 c_2^2 - \rho_1 c_1^2}{\rho_2 - \rho_1}.$$

The third equation can be somewhat simplified. With sufficient accuracy, when $\Delta c = c_2 - c_1$

$$\tan \gamma = -\frac{f}{g} \frac{\rho_1 \Delta c}{\rho_2 - \rho_1} \left(1 - \frac{c_1 + c_2}{fr} \right). \tag{XVI.10}$$

On comparison with formula (XIV.8) it can be seen that the effect of the centrifugal force is contained in the expression in brackets. The difference between the slope of the boundary surface in a rotating flow from that in a straight current remains small; assuming $f = 1 \times 10^{-4}$ (about 45° latitude), $r = 100$ km and $c_1 + c_2 = 40$ cm/sec, then the expression in brackets gives 1.04, that is, an increase of about 5% can scarcely

be expected for extensive vortices. For small vortex sizes, however, it may be as large as 30–40%. A difference from the case for straight flow exists in so far as the slope of the boundary surface depends on the distance from the axis of rotation. In general, when the area immediately around the axis of rotation is disregarded, the oceanic structure of a circular vortex of this type can be readily derived from the rule given above. Four cases can be distinguished (Fig. 210, Northern Hemisphere).

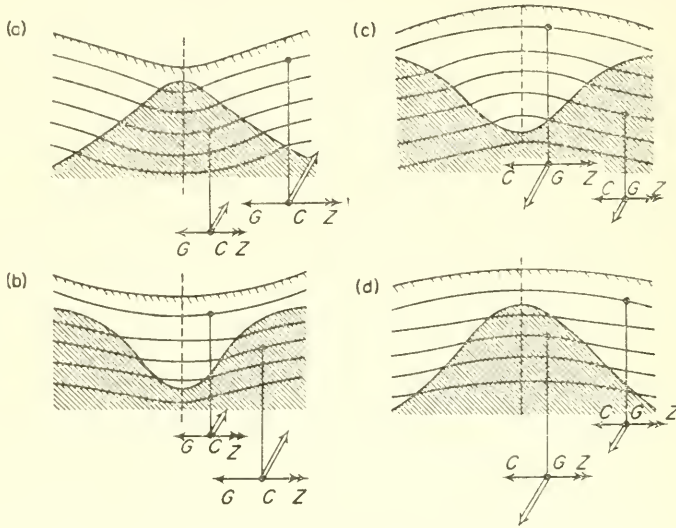


FIG. 210. Rotational symmetric stationary vortex in a two-layered ocean (position of the boundary surface and form of the isobaric surfaces, physical sea surface, respectively). *a and c*, cyclonic and anticyclonic rotation in case of a faster rotation of the upper layer. *b and d*, cyclonic and anticyclonic rotation in case of a faster rotation of the lower layer (underneath the sections diagram of forces for only one point of the lighter and heavier water mass. *G*, gradient force; *C*, Coriolis force; *Z*, centrifugal force).

Case a: $\Delta c < 0$, for cyclonic rotation $c_2 < c_1$: $\tan \gamma > 0$. The boundary surface rises towards the centre, in fact more rapidly near the vortex axis and less further out; $\tan \beta$, on the other hand, is negative in both layers, that is, the pressure surfaces and the physical sea level rise outwards, more so in the upper than in the lower layer. This is the case of a *cyclonic vortex with the upper layer rotating more rapidly*. Due to the rotational effect the heavier water accumulates around the axis of rotation while the lighter top layer is forced to the outside. In the central area there is a depression in the physical sea level and the isobaric surfaces.

Case b: $\Delta c > 0$, for a cyclonic rotation $c_2 > c_1$: $\tan \gamma < 0$. $\tan \beta$ is negative in both layers and the boundary surface, the pressure surfaces and the physical sea level rise towards the outside; *cyclonic vortex with the lower layer rotating more rapidly*. The lighter water masses accumulate around the vortex axis and there, as in the previous case, the physical sea level and the pressure surfaces show a depression. In these cyclonic cases the sum of Coriolis force and the centrifugal force act towards the outside and a larger gradient force is required to balance this combined action. The boundary surface slope must therefore be greater than for water bodies arranged in strips.

Case *c*: $\Delta c > 0$, for anticyclonic rotation $|c_1| > |c_2|$. As long as the term in brackets in (XIV.10) remains positive, which is always true except in extreme cases, then $\tan \gamma < 0$ and the boundary surface rises towards the outside. $\tan \beta$ is positive in both layers and the slope of the pressure surfaces is less in the heavier water body than in the lighter: *anticyclonic vortex with the top layer rotating more rapidly* and a central dome-like uplift of the pressure surfaces and of the physical sea level. The rotation gives rise to an accumulation of the lighter water masses around the rotational axis.

Case *d*: Finally, it is possible in an anticyclonic rotation to have $\Delta c < 0$ and then $|c_2| > |c_1|$. The slope of the boundary surface rises towards the centre since $\tan \gamma$ is positive (with the same restriction as in case *c*). The pressure surfaces also rise towards the centre but in this case more strongly in the heavier than in the lighter water layer: *anticyclonic vortex with the lower layer rotating more rapidly* and a central dome-like uplift of the sea level and the isobaric surfaces. Here the lower heavier water accumulates around the vortex axis. Since in the sea the current velocity almost always decreases with depth, cases *a* and *c* will predominate. In a cyclonic vortex the deep water is lifted close to the surface and if the vertical velocity gradient is sufficiently large the boundary layer may reach the surface. Then the vortex centre will be filled with deep water. In an anticyclonic vortex, on the other hand, there is an accumulation of the lighter upper water around the vortex axis that may extend downwards to considerable depth.

The actual stratification in the sea seldom consists of only two layers; the same laws apply, however, also to a continuously stratified ocean (see Chap. XV). The boundary surface slope is then replaced by the slope of the isosteres and in place of sharp kinks there appears a steady curvature in the isobars. Also here, due to the low velocities and the large radii of curvature of the current trajectories, the centrifugal force is of little importance compared with the Coriolis force for an estimate of the mass field adjustment. Figure 211 shows dynamic sections through such cyclonic and anticyclonic

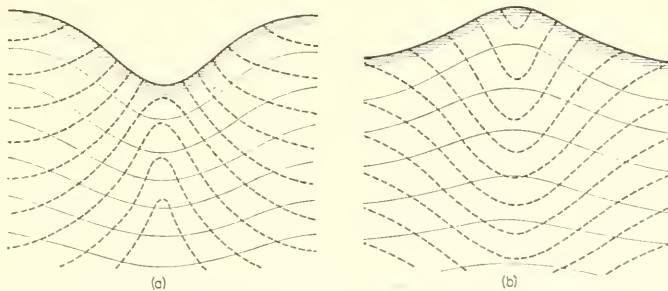


FIG. 211. Mass and pressure distribution in rotationally symmetric layered vortices with a decreasing rotational velocity with depth. (a) Cyclonic; (b) anticyclonic rotation.

circular vortices in a stratified ocean; in both cases *it is assumed that the velocity of the current decreases with depth*; for a two-layered ocean they correspond to the cases *a* and *c* of Fig. 210.

Charts of ocean currents often show more or less extensive vortices in the top layers. They are found mostly in those areas where the wind field also indicates

rotational (cyclonic or anticyclonic) motion. The anticyclonic winds around the subtropical high-pressure centres thus give rise in both hemispheres to anticyclonic large-scale vortices between the oceanic West Wind Drift and the Equatorial Currents. These are elongated corresponding to the shape of the high-pressure cells and take the form of a broad *convergence zone*. In the central parts of these anticyclonic vortices there is always a mass distribution corresponding to that in Fig. 211 *b*; that is, with an accumulation of lighter water in the central part of the convergence area. Conditions of this type are particularly well developed in the North Atlantic, where there is an accumulation of warmer water with a corresponding depression of the isosteres to 600–800 m; the isobaric surfaces and the physical sea level show a corresponding uplift.

Large-scale vortices with cyclonic sense of rotation are found in the intermediate region between the oceanic West Wind Drifts and the Polar Currents; that in the North Atlantic between the Polar and the Atlantic Current. Here the actual oceanic structure will be very nearly that pictured in Fig. 211 *a*, which shows that the isosteres arch upwards. Such cases will be referred to again when discussing the current conditions in particular oceanic regions.

A very typical case of a smaller-size cyclonic vortex was observed in the Gulf Stream just north of the Azores above the “Altair” cone during the International Gulf Stream Survey, 1938 (DEFANT, 1940 *b*). The centre of the vortex was found in upper layers a little south of the greatest submarine elevation; in deeper layers it appeared directly above the cone. All the vertical oceanographic sections show this vortical disturbance and its vertical structure. Figure 212 presents a somewhat smoothed

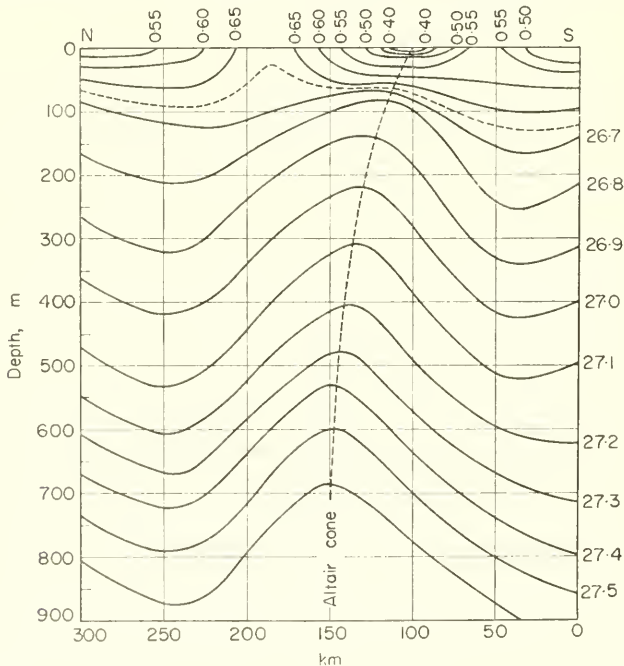


FIG. 212. Meridional density section through the cyclonic vortex above the “Altair” submarine volcano in the Atlantic Ocean (somewhat smoothed).

density section. Although the axis of the vortex is somewhat inclined towards south, current measurements and the mass distribution suggest a subdivision of the total vortex into *two parts or systems*.

(1) *The upper system* down to 100–150 m depth includes a discontinuity layer at about 25 m. The velocity of the basic current in the top layer is about 15 cm/sec and in the denser lower layer, however, 20 cm/sec. This is thus a *strongly stratified cyclonic vortex with a speed of rotation increasing with depth*. Under steady conditions the isosteres must therefore dip downwards in the lighter water masses which are concentrated around the vortex axis. This is shown very clearly by the section given in Fig. 212.

(2) *The lower system* extends through the layers below 150 m, where there is a normal increase in density with depth and a steady decrease in the velocity from about 20 cm/sec at 200 m to about 6 cm/sec at 800 m. This is therefore a *weakly stratified cyclonic vortex with decreasing rotational velocity with depth*. The required uplift of the isosteres (accumulation of lower denser water around the vortex axis) is again obvious from Fig. 212.

Also quantitatively the observed slopes are in a good agreement with that required by theory (equation XIV.10). Since $\phi = 44^\circ 33' \text{ N.}$ and therefore $f = 1.023 \times 10^{-4} \text{ sec}^{-1}$ equation (XIV.10) gives for the upper system: $\sigma_1 = 26.30$, $c_1 = 15 \text{ cm/sec}$, $\sigma_2 = 26.65$, $c_2 = 25 \text{ cm/sec}$; the isosteres slope downwards towards the centre by 92 m in 60 km; observed 70–90 m. For the lower system: $\sigma_1 = 26.8$, $c_1 = 20 \text{ cm/sec}$, $\sigma_2 = 27.5$, $c_2 = 6 \text{ cm/sec}$; the isosteres slope upwards towards the centre by 214 m in 100 km; observed 230–290 m.

The cyclonic vortex performed pulsations, as was indicated by the observations made at the anchor stations. The period of these pulsations corresponded to the period of inertia oscillations (see p. 472).

SANDSTRÖM (1914, 1918), has carried out laboratory experiments to test the effects of cyclonic and anticyclonic air currents on stratified water masses underneath. Reference is made to these in this connection.

4. Up- and Down-gliding Surfaces: Pulsations of Stationary Vortices

In systems of moving water bodies for a stationary position of the boundary surfaces there will be no vertical motions according to equation (XIV.7). If the equilibrium conditions are not satisfied, accelerations will occur and as a consequence vertical motions are generated which will lead to changes in the position of the discontinuity surfaces. If the slope angle of the boundary surface is denoted by ϵ and differs from that for its stationary equilibrium γ , then ϵ will tend towards its equilibrium slope γ . If the boundary surface is steeper inclined than in the equilibrium state ($\epsilon > \gamma$), in order to reduce ϵ the upper lighter water must spread out over the lower heavier water and the lower one will intrude underneath the lighter. Above the boundary surface there will be an up-gliding and below it a down-gliding (*up-gliding surface*).

If, on the other hand, for $\epsilon < \gamma$ the reverse will apply. In the lighter water type there will be down-gliding and in the heavier up-gliding (*down-gliding surface*). The processes occurring at the boundary surface can be decisively influenced by the initiated vertical motions. EXNER (1924) and J. BJERKNES (1924) have investigated the processes that may

occur at arbitrarily inclined discontinuity surfaces. Taking horizontal accelerations into account but neglecting the very small vertical accelerations ($\dot{w}_1 = \dot{w}_2 = 0$) and if the boundary surface is parallel to the y -axis having an inclination $\tan \gamma$ then equation (XIV.5) gives the relations (z -positive upwards):

$$(\rho_1 \dot{u}_1 - \rho_2 \dot{u}_2) = f(\rho_1 v_1 - \rho_2 v_2) - g(\rho_1 - \rho_2) \tan \epsilon \quad \text{and} \quad \rho_1 \dot{v}_1 - \rho_2 \dot{v}_2 = f(\rho_1 u_1 - \rho_2 u_2) \tag{XIV.11}$$

Near the boundary surface the velocity in each of the water bodies will be tangential to it: $w_1 = u_1 \tan \epsilon$ and $w_2 = u_2 \tan \epsilon$, so that

$$\rho_1 \dot{w}_1 - \rho_2 \dot{w}_2 = (\rho_1 \dot{u}_1 - \rho_2 \dot{u}_2) \tan \epsilon. \tag{XIV.12}$$

These equations form the basis of the dynamics of up- and down-gliding surfaces. If in the first of these equations $\epsilon = \gamma$ (stationary boundary surface condition), then $\rho_2 \dot{u}_2 - \rho_1 \dot{u}_1 = 0$ and from (XIV.12) it follows that $\rho_1 \dot{w}_1 = \rho_2 \dot{w}_2$. On the other hand, according to the second part of the equation (XIV.11)

$$\rho_1 \dot{v}_1 - \rho_2 \dot{v}_2 \neq 0.$$

This implies that: *up- and down-gliding can also occur at stationary boundary surfaces if the currents are accelerated also in the direction parallel to the gliding plane.* If the mutual adjustment between current velocities and stable position of the boundary layer gets disturbed by changes in the velocities, then up- and down-gliding motions must occur along the boundary surface in order to preserve a stationary state of its inclination. Thus when

$$(1) \quad \rho_1 \dot{v}_1 - \rho_2 \dot{v}_2 < 0: \quad \rho_1 u_1 - \rho_2 u_2 > 0 \quad \text{and} \quad \rho_1 w_1 - \rho_2 w_2 > 0$$

and when

$$(2) \quad \rho_1 \dot{v}_1 - \rho_2 \dot{v}_2 < 0: \quad \rho_1 u_1 - \rho_2 u_2 < 0 \quad \text{and} \quad \rho_1 w_1 - \rho_2 w_2 < 0.$$

In the first case where there is a stronger acceleration in the lower water mass along the positive y -axis than in the upper, an *up-gliding surface* is to be expected. In the second case, however, where there is a stronger relative acceleration along the positive y -axis in the upper water mass, there will be a down-gliding surface. These two cases are illustrated in Fig. 213; they apply for the Northern Hemisphere. In the Southern

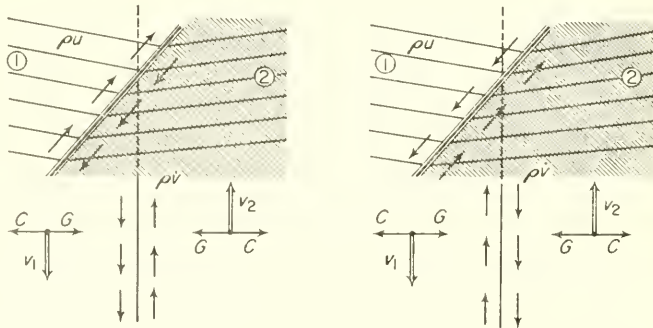


FIG. 213. Stationary up-gliding (to the left) and down-gliding surfaces (to the right) (Northern Hemisphere).

Hemisphere the arrow-directions indicating the velocities and the accelerations parallel to the boundary surface have to be reversed.

So far the discussion applies only for infinitely extended boundary surfaces. If they intersect the sea surface (fronts) or the sea bottom the up- and down-gliding motions will give rise to horizontal water currents in its vicinity and consequently to changes in the position of the boundary surface.

Cases of this type can be found at the oceanic polar fronts. Figure 214 shows the polar front between the East Greenland Current and the Atlantic water to the south of the Denmark Strait. The mass distribution requires larger velocities in the polar current towards the south and smaller ones in the Atlantic water as is found by observation.

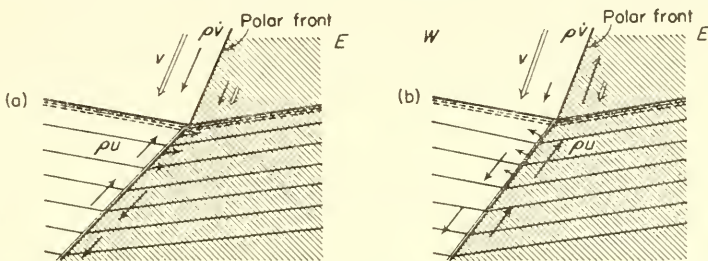


FIG. 214. Oceanic vertical stratification and currents at the East Greenland oceanic polar front. *Picture to the left:* up-gliding of the polar water and down-gliding of the Atlantic water for an accelerated East Greenland Current: boundary surface progresses towards east. *Picture to the right:* down-gliding of the polar water and up-gliding of the Atlantic water for an accelerated Atlantic current: boundary surface progresses towards west.

In general, there exists a stable equilibrium in the current system between the mass structure and the currents with a stable boundary surface position. If, however, an easterly wind piles up polar water (“Anstau”) along the east coast of Greenland, or if other conditions in the North Polar Sea cause an increase in the strength of the East Greenland Current, then the water masses of the current will be accelerated towards the south and the boundary surface will become an up-gliding surface (Fig. 214 a). This up-gliding along the boundary surface in the lighter polar water mass must come to an end at the sea surface; here it gives rise to a reduction in the inclination of the boundary surface, that is, the extent of the East Greenland Current at the surface will increase and will force the Atlantic water masses seaward.

In the opposite case (Fig. 214 b) if the Atlantic water is accelerated towards the north, the boundary surface becomes a down-gliding surface. It thus becomes steeper and the extension of Atlantic water is increased. Pulsations in the basic currents will be associated with variations in the mass distribution. The large-scale aperiodic atmospheric disturbances of these regions must be accompanied by corresponding large changes in the oceanic structure and the ideas outlined above are of major importance in the coupling of these two phenomena.

Similar conditions must apply for the much longer polar front in the Southern Hemisphere. Here the temperature is the decisive factor for the mass structure and the boundary surface between the West Wind Drift and the South Polar Current slopes downward towards the north (towards the equator). In order to secure stationary

conditions, the West Wind Drift must have a greater velocity towards the east than the South Polar Current to the south of it, which is also directed east. Since here also disturbed meteorological conditions are frequent in this region, the varying influence of the action of the atmospheric flow will sometimes accelerate the oceanic West Wind Drift and sometimes the South Polar Current, and therefore the polar boundary surface will change from an up-gliding to a down-gliding surface and back again and there will be corresponding *displacements of the polar front in meridional direction*. These processes seem to continue nearly all the time and may be associated with the observed sinking process of large water quanta of sub-Antarctic waters. This process is most probably of a pulsatory character and is definitely the source of the sub-Antarctic intermediate water penetrating far to the north.

Variations of the boundary surface can also arise in circular vortices if there are changes in the vertical current structure. If (see in Fig. 215) for example, the boundary

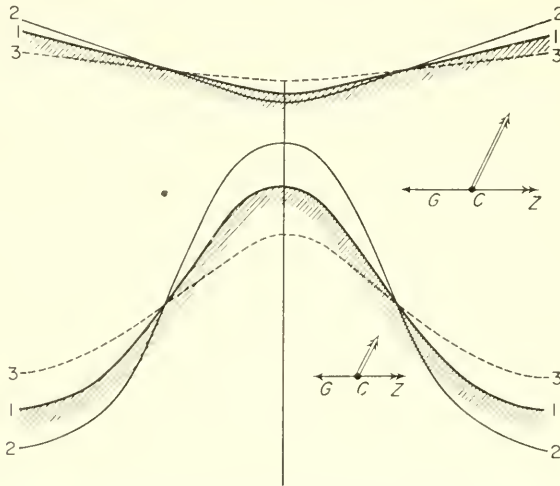


FIG. 215. Pulsations of a circular vortex in cyclonic rotation.

surface and the physical sea level lie in the position 1-1 under average conditions, then, if the velocity between the upper and lower water bodies increases, there will be greater accumulation of the lower water type around the axis of the vortex and the inclination of the boundary surface will increase (position 2-2). If, on the other hand, this difference becomes less, then the accumulation of lower water will be dispersed and the inclination will decrease. Periodic variations in the mass structure will thus occur in the vortex; the boundary surface and the physical sea level will oscillate around a mean position and these oscillations will have the character of standing waves (see Vol. II).

In the cyclonic vortex over the "Altair" submarine cone in the Gulf Stream north of the Azores (see p. 454) periodic variations of this type were present both in the oceanic structure and in the vertical current distribution. They were very well developed in the upper system and of a period corresponding to the inertia period (17 n). Since the periodic variations in the current amounted to as much as half of the velocity of the

basic current, the changes in time of the distribution of the isosteres must have been quite considerable. Figure 216 shows these changes in the vertical current structure in the two layers of the upper system: 5–15 m and 30–100 m. In the lower part of the vortex the velocity is greatest between 2 and 3 h and at the same time least in the upper part. During this time-interval there is thus an increase with depth of the velocity of rotation. In the interval between 9 and 16 h conditions are reversed; at 10 h the

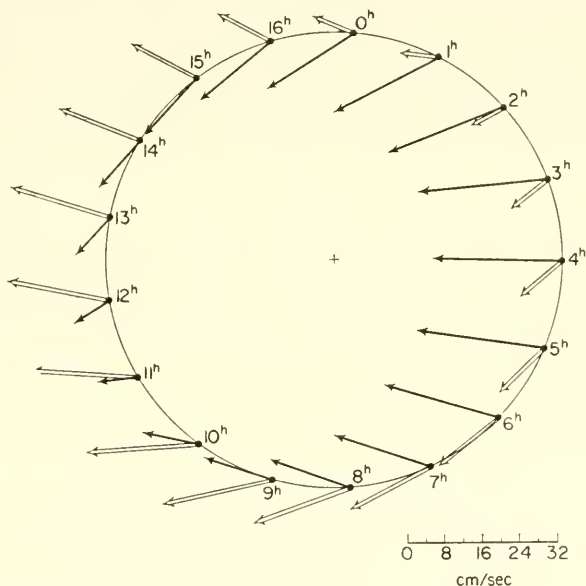


FIG. 216. Changes in the vertical structure of the current of the upper system in the cyclonic vortex above the "Altair" submarine volcano. \leftarrow , current in the layer between 5 and 15 m depth; \leftarrow —, current in the layer between 30 and 300 m depth.

top layer has the greatest velocity and there is thus at this time a decrease in the rotational velocity with depth. This feed-back of these oscillations of the current field on the mass distribution in the vortex must be extremely strong to give a complete reversal of the current structure. At 10 h there must be an increase of the up-lift of the isosteres and at 2 h an increased depression. These oscillations of the isosteric surface about nodal lines at a certain distance from the vortex centre have been demonstrated by observations of the anchor station. The isotherms and isohalines oscillate around a mean position with an inertia period of 17 h, so that the anchor station must be somewhat displaced towards the outer edge of the vortex, because the isosteres are always lowered at 10.5 h and always lifted at 2 h.

The oscillations in a circular two-layered vortex can be accounted for theoretically (DEFANT, 1940 *b*) and an estimate can be made of the period of the *free* oscillations of such a system. If the effect of centrifugal force is neglected (it is always small) then the mean position of the boundary surface in such a vortex will correspond to the following relation (z positive upwards; centre of the vortex at $x = 0$; horizontal extent of the vortex = $2l$):

$$z = h_2 + \delta \cos(\pi/l)x, \quad (\text{XIV.13})$$

where

$$\delta = -\frac{f}{g} \frac{(\rho_2 u_2 - \rho_1 u_1)}{\rho_2 - \rho_1}$$

(Margules boundary surface slope).

If small periodic variations (disturbance values) are imposed on this equilibrium system in the currents u_1 and u_2 , then the boundary surface will oscillate about its steady-state position. As a consequence in the most simple case these oscillations will give rise to upward and downward movements in the central part of the vortex with a phase exactly opposite to that of the outer vortex portions. To the equation (XIV.13) will thus be added an additional periodic term of the form

$$z = A \cos \frac{n\pi}{l} \cos \sigma_n t, \quad (\text{XIV.14})$$

whereby σ_n is the frequency of the free ("Eigen") oscillation (period $T = 2\pi/\sigma_n$; $n = 1, 2, 3, \dots$, gives the number of node-points in the oscillating system).

When corresponding boundary conditions are taken into account the equations of motion give an equation for the determination of the frequency σ_n of the "Eigen" oscillations of the oscillating vortex as a function of the dimensions of the system. The following equation is obtained

$$\sigma_n = \sqrt{\left(f^2 + \frac{n^2 \pi^2 g}{l} \frac{\rho_2 - \rho_1}{\rho_1/h_1 + \rho_2/h_2}\right)}, \quad (\text{XIV.15})$$

where h_1 and h_2 are the thicknesses of the two layers and $2l$ is the total horizontal extent of the vortex. These "Eigen" frequencies depend in a characteristic way on the angular velocity of the Earth. If the Earth were not rotating ($f = 0$) then the period of the free oscillation would be given by

$$T_r = \frac{2\pi}{\sigma_r} = \frac{2l}{n} \sqrt{\left(\frac{\rho_1/h_1 + \rho_2/h_2}{g(\rho_2 - \rho_1)}\right)}. \quad (\text{XIV.16})$$

This is a period for an internal standing wave in a two-layered water mass of an extent l (see Vol. II).

If for large dimensions of the oscillating system the period T_r for a *non-rotating Earth* is large, then the second term in the equation (XIV.15) will be so small as compared with f^2 that it can be neglected and the longest "Eigen" period of the system will be equal to the *inertia period*.

$$T_i = \frac{1}{2} \text{ a pendulum day} = \frac{\pi}{\omega \sin \phi}. \quad (\text{XIV.17})$$

If the second expression accompanying f^2 in the equation (XIV.15) cannot be neglected, then it is obtained with sufficient accuracy

$$T = T_i \left[1 - \frac{1}{2} \left(\frac{T_i}{T_r} \right)^2 \right] \quad \text{when } (T_r \gg T_i),$$

however,

$$T = T_r \left[1 - \left(\frac{T_r}{T_i} \right)^2 \right] \quad \text{when } (T_r \ll T_i).$$

In most cases in the ocean $T_r \ll T_i$, so that the "Eigen" period of such an oscillating system will always be close to the inertia period. In the vortex over the "Altair" cone $2l = 120$ km; the mean densities of the upper and lower layer ρ_1 and ρ_2 are 1.0263 and 1.0283 and $f = 1.023 \times 10^{-4} \text{ sec}^{-1}$, then for $h_1 = 30$ m and $h_2 = 1000$ m it is found that $T_i = 17.1$ h and the "Eigen" period of the system according to equation (XIV.15) is $T = 16.76$ h. Thus the "Eigen" period of the vortex over the "Altair" cone approaches closely the period of an inertia oscillation, as was found by observation; inertia oscillations are merely the free oscillations of an enclosed sea the equilibrium state of which has been disturbed. They are probably set up by external causes especially by meteorological conditions (like storms and similar phenomena). In this particular case a storm occurring just before the anchoring of the "Altair" seems to be the cause for the pulsation of the otherwise stationary vortex above the "Altair" submarine volcano.

Chapter XV

Ocean Currents in a Non-homogeneous Ocean

1. Introduction

If all the external forces that may act on the sea are excluded, ocean currents can still be produced by *internal forces*. Differences in the mass structure will represent an internal system of forces that will act until the resultant mass displacements lead to the establishment of a mass distribution corresponding to that of a static equilibrium. It is customary to denote ocean currents generated by such internal forces as "convection currents" although they have nothing to do with oceanic convection phenomena. In order to avoid this unsuitable notation it seems to be advisable to call them "density currents", since they depend solely on the three-dimensional difference in the density field. Treatment of these density currents involves greater difficulties than that of drift and gradient currents, in particular, since the external forces (wind and atmospheric pressure) can be regarded as independent from the currents themselves, while the density currents and the density differences producing them influence each other. Furthermore, the density anomalies, being internal forces, are distributed three-dimensionally in space, while wind and atmospheric pressure at the sea surface act only in two dimensions.

The beginnings of a theory of density currents goes back to MOHN (1885, 1887) whose work can without doubt be described as "the beginning of a new era in physical oceanography" (HELLAND-HANSEN and NANSEN, 1909, Vol. II, 2, p. 390). However, this theory, the aim of which was rather wide-spanned, was incapable of influencing the further development of theoretical oceanography, since it was running far ahead of the development of oceanography, which at that time made its progress mainly along geographical lines and because the defects in it were difficult to eliminate. It was soon forgotten (THORADE, 1925). The foundation for a firmly founded theory of density currents was provided by the application of the Bjerknes theorems of vortex formation and circulation acceleration to oceanographic problems. Thereby it was necessary to leave aside classical hydrodynamics, dealing only with homogeneous media, and to make use of physical hydrodynamics where the media had a full physical reality. Some of the results were later derived directly from the hydrodynamic equations of motion. These derivations are, in part, clearer and more comprehensible, and it therefore seems advisable to discuss the simpler problems first.

2. Relationships Between Current and Density Fields in a Horizontal plane. The law of Parallel Fields

A general relationship between density and current fields can be derived quite simply (DEFANT, 1931). In general, the vertical component of the velocity, that is,

the vertical slope of the stream lines is so small that the current field can be regarded as horizontal. Under stationary conditions the stream lines follow the stream function $\psi(x,y) = c_1$; the horizontal density distribution shall be given by $\rho(x,y) = c_2$. The angle between the two sets of curves may be γ . If the stream lines are at an angle α to the positive x -axis and correspondingly the isopycnals at an angle β , then

$$\tan \alpha = - \frac{\partial \psi / \partial x}{\partial \psi / \partial y} \quad \text{and} \quad \tan \beta = - \frac{\partial \rho / \partial x}{\partial \rho / \partial y}.$$

From this it follows that

$$\tan \gamma = \frac{\frac{\partial \psi}{\partial x} \frac{\partial \rho}{\partial y} - \frac{\partial \psi}{\partial y} \frac{\partial \rho}{\partial x}}{\frac{\partial \psi}{\partial x} \frac{\partial \rho}{\partial x} + \frac{\partial \psi}{\partial y} \frac{\partial \rho}{\partial y}}. \tag{XV.1}$$

If the stream lines are parallel to the density lines ($\gamma = 0$), then consequently

$$\frac{\partial \psi}{\partial x} \frac{\partial \rho}{\partial y} - \frac{\partial \psi}{\partial y} \frac{\partial \rho}{\partial x} = 0. \tag{XV.2}$$

Disregarding for the moment the effects of friction (turbulence), and if there are no physical changes in the water masses due to external circumstances then, for stationary conditions $du/dt = dv/dt = 0$, the equations of motion (XIII.1) will also apply for a non-homogeneous sea. Eliminating the pressure p and taking into account the continuity equation and introducing a stream function (equation X.35), equation (XV.2) is obtained. In a non-homogeneous sea stationary conditions require that the *stream lines and the isopycnals (isosteres) are parallel*. This result is self-evident since otherwise these surfaces would be displaced and this would contradict the condition of a stationary state. The same also applies to isothermal and isohaline surfaces. On the other hand, the following equation can be derived from the equation of motion and the hydrostatic equation (ERTEL, 1933)

$$f^2 \left(\rho v \frac{\partial \rho u}{\partial z} - \rho u \frac{\partial \rho v}{\partial z} \right) = - \frac{\partial^2 p}{\partial y \partial z} \frac{\partial p}{\partial x} + \frac{\partial^2 p}{\partial x \partial z} \frac{\partial p}{\partial y}.$$

By means of the hydrostatic equation

$$\frac{\partial p}{\partial z} = g \rho$$

this equation can also be written in the form

$$f^2 \rho^2 v^2 \frac{\partial}{\partial z} \left(\frac{u}{v} \right) = g \left(\frac{\partial \rho}{\partial x} \frac{\partial p}{\partial y} - \frac{\partial \rho}{\partial y} \frac{\partial p}{\partial x} \right).$$

If the total velocity V is at an angle χ to the y -axis so that $u = V \sin \chi$ and $v = V \cos \chi$ then

$$(f \rho V^2) \frac{\partial \chi}{\partial z} = g \left(\frac{\partial \rho}{\partial x} \frac{\partial p}{\partial y} - \frac{\partial \rho}{\partial y} \frac{\partial p}{\partial x} \right) = gD. \tag{XV.3}$$

If the isobars and isopycnals are parallel in a horizontal plane, then the expression in brackets, D , is zero. The mass field is therefore barotropic and $\partial \chi / \partial z = 0$, that is, the

current does not turn with depth, or *the current directions at all depths will lie in one and the same vertical plane*. Since for frictionless motion the current follows the isobars and these coincide with the stream lines, D will be identical with equation (XV.2). Except at special disturbance locations (discontinuity surfaces, discontinuity layers and fronts) the stream lines therefore will also coincide with the isolines at all depths.

If turbulent friction should also be taken into account, it is necessary to go back to the general equations of motion and elimination of p leads to the equation

$$\frac{\partial \psi}{\partial x} \frac{\partial \rho}{\partial y} - \frac{\partial \psi}{\partial y} \frac{\partial \rho}{\partial x} = \frac{\eta}{f} \frac{\partial^2}{\partial z^2} (\Delta \psi). \quad (\text{XV.4})$$

For a simple potential flow $\Delta \psi = 0$ and the condition of parallelism of stream lines and density lines still applies. If, however, a vortical motion has to be dealt with, this parallelism will be lost.

The angle at which they intersect will depend on the turbulence and on the water depth. It can be shown that now

$$\tan \gamma = \frac{\eta(\partial^2 \zeta / \partial z^2)}{f \rho \zeta - \Delta p},$$

where $\zeta = \partial v / \partial x - \partial u / \partial y$ denotes the vertical vorticity component. If the co-ordinate system is placed in the direction of the average current, then $v = 0$. At the sea surface assuming a linear pressure gradient ($\Delta p = 0$) and a decrease of velocity with depth $u = \frac{1}{2} a z^2$ (sea bottom $z = 0$) as well as a depth of water h , is obtained

$$\tan \gamma = \frac{2\eta}{f \rho h^2}.$$

For $\eta/\rho = 200 \text{ cm}^2/\text{sec}$ and $f = 10^{-4} \text{ sec}^{-1}$ (at about 45° N .)

$$\tan \gamma = \left(\frac{20}{H} \right)^2$$

if the depth of water H is measured in metres. For a large water depth γ will be almost zero; if the water is shallow (shelf seas) it may reach values of 10 – 20° .

Summarizing, it may be stated that for steady frictionless currents in a non-homogeneous sea the isolines of the different oceanographic factors and the stream lines must coincide, but in the presence of strong turbulence especially in shallow seas this parallelism is lost.

Attempts have very often been made in oceanography to deduce the current field from the distribution of the temperature and the salinity and other factors. In general, such deductions are permissible and the method gives results corresponding reasonably with reality, but deductions from isoline charts should not be taken as more than indications of the rough course of the currents. However, exactly at the point where the current field is of particular interest (near discontinuity surfaces and fronts) the method fails completely (CASTENS, 1931).

These arguments are connected with the "law of parallel fields" (HELLAND-HANSEN and EKMAN, EKMAN, 1923). Comparison of the distribution of the oceanographic factors at different depths shows the striking phenomenon that the isolines at any particular depth are parallel to each other, and moreover that they are parallel also

with those in deeper layers. This agreement in the course of these lines also extends to the dynamic isobaths at any depth. It must therefore be concluded that the current vectors are also tangential to all these sets of curves and that there is complete equality between all these lines. This law allows deduction according to the *Ekman theory* of the direction of the deep current outside the upper and lower frictional depth which represents the layers in which the drift current and the bottom current are found. All modern cartographic representations of the horizontal distribution of these factors at different depths confirm the general validity of this law (see, for example, the "*Meteor*" Reports, Vol. VI, Atlas).

The basic prerequisites for the validity of this law are the same as in the rules derived above for the relationships between the oceanographic factors and the current field in any horizontal plane. These are satisfied for the deep currents except in those areas where they are disturbed by discontinuity layers, or where due to mixing processes there cannot be any stationary spatial density distribution.

3. Horizontal Steady Currents in a Stratified Ocean

The dependence of the vertical velocity distribution in a current on the stratification of the water masses in the pressure field is already shown by the behaviour of two adjacent water bodies. In steady state continuous changes in density require also a definite mutual adjustment between the mass and pressure field. If the flow is directed along the positive y -axis, then for a steady frictionless motion

$$fv = a \frac{\partial p}{\partial x}.$$

Inserting the hydrostatic equation $g = a(\partial p/\partial z)$ (z counted positive downwards), elimination of p leads to the relation

$$\frac{\partial v}{\partial z} = v \frac{\partial \log a}{\partial z} - \frac{g}{f} \frac{\partial \log a}{\partial x}. \tag{XV.5}$$

This states that for a given vertical and horizontal mass distribution there will always be a vertical velocity distribution given by (XV.5). Introducing the slope of the isobaric surfaces $\tan \beta = -(f/g)v$ and that of the isosteric surfaces $\tan \gamma = -(\partial \rho/\partial x)/(\partial \rho/\partial z)$ the equation takes the form

$$\frac{\partial v}{\partial z} = \frac{g}{f} (\tan \gamma - \tan \beta) \frac{\partial \log a}{\partial z}. \tag{XV.6}$$

Since $\partial \log a/\partial z$ is always negative, the expression in parenthesis decides about increase or decrease in the velocity with depth. In other words, this increase or decrease in velocity depends on the difference in the slope of the two intersecting sets of surfaces or lines in a dynamic section. Figure 136c (page 331) shows the two possible cases (v is always positive); in that shown on the left-hand side the expression in brackets is always positive, and therefore $\partial v/\partial z < 0$, or there will be a decrease in velocity with depth. In the case on the right-hand side $\partial v/\partial z > 0$, and there will be an increase in velocity with depth. When $\gamma = \beta$ then $\partial v/\partial z = 0$ which is the barotropic case with a constant velocity at all depths. These results can be expressed by the following rule:

If the isosteres slope downwards (upwards) from left to right when facing downstream, then a steady current will show a decrease (increase) in velocity with depth (Northern Hemisphere).

It can be seen that equation (XV.6) allows a determination only of the vertical velocity differences and it does not give the velocity itself and thus affords only *relative velocity difference distributions* in vertical direction. This state of affairs recurs in all similar cases and is a consequence of the indeterminate nature of the problem. Equation (XV.6) has been derived from the equations of motion *alone*; to determine the entire state of motion completely requires the continuity equation. Only then are the conditions uniquely defined.

Equation (XV.5) can be written also in another form:

$$\alpha \frac{\partial v}{\partial z} = v \frac{\partial \alpha}{\partial z} - \frac{g}{f} \frac{\partial \alpha}{\partial x}.$$

This can be used for a step-wise calculation of the vertical velocity distribution from layer to layer (DEFANT, 1929 *b*).

If at two stations separated by a distance L at a depth $z = 0$ the specific volumes are α_0 and α'_0 and at a depth $z = h$ α_1 and α'_1 , the following formula can be used for a numerical determination of the velocity difference $v_0 - v_1$

$$(\alpha_1 + \alpha'_1)v_0 - (\alpha_0 + \alpha'_0)v_1 = \frac{gh}{fL} (\alpha_0 - \alpha'_0 + \alpha_1 - \alpha'_1). \quad (\text{XV.7})$$

Table 133 contains the specific volumes at six depths down to 750 m for the stations 205 and 206 on the section through the Gulf Stream and the Labrador Current south of the Newfoundland Banks (Fig. 202). For $\phi = 40^\circ 10'$ and $L = 59$ km the equation (XV.7) gives the vertical velocity on the assumption of no motion at a depth of 750 m.

Table 135. Calculation of the vertical velocity in the Gulf Stream south of the Newfoundland Banks

Depth (m)	St. 205 α	St. 206 α'	$L = 59$ km $\alpha' - \alpha$	h (m)	$(\alpha_0 - \alpha'_0) + (\alpha_1 - \alpha'_1)$	v (cm/sec)
0	0.97393	0.97449	$56 (\times 10^{-5})$	50	$107 (\times 10^{-6})$	64.7
50	363	414	51	75	102	59.7
125	312	363	51	125	112	52.5
250	217	278	61	200	101	39.3
450	119	159	40	300	72	20.3
750	0.96973	005	32			0.0

WERENSKJÖLD (1935, 1937) has developed a simple and practical method for the same objective. Neglecting in equation (XV.6) $\tan \beta$ in comparison with $\tan \gamma = i$,

which is always permissible and integrating it between level $z_0(\rho_0, v_0)$ and the level $z_1(\rho_1, v_1)$ gives

$$v_0 - v_1 = \frac{g}{\rho_m f} \int_{\rho_0}^{\rho_1} i d\rho, \tag{XV.8}$$

whereby ρ_m is a mean density for the layer $z_1 - z_0$. Denoting the tangents of the slope angles of the isopycnals or isosteres drawn in a dynamic section with intervals $\Delta\rho$ and $\Delta\alpha$, respectively, by J , then equation (XV.8) can be transformed into the simple relation

$$v_0 - v_1 = \frac{g}{nf} \frac{\Delta\rho}{\rho_m} \Sigma J = \frac{g}{nf} \frac{\Delta\alpha}{\alpha_m} \Sigma J. \tag{XV.9}$$

The summation has to be taken over all the isopycnals or isosteres which cut a given vertical line between levels z_0 and z_1 and n is the vertical exaggeration of the section. Values of J can be read directly from the section using a transparent scale (Fig. 217). If the isopycnals in a vertical section are plotted at intervals of 10^{-4} and the isosteres at intervals of 5×10^{-5} and if the vertical scale of the section is 1:2500 and the horizontal

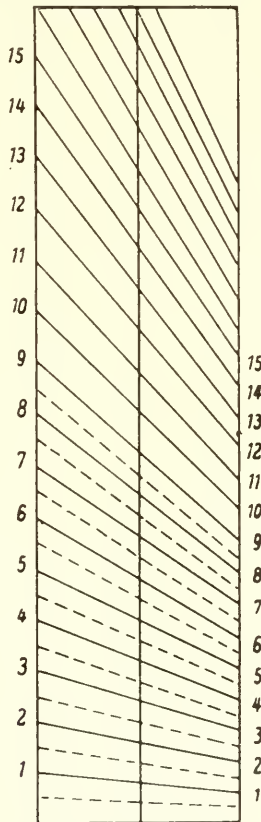


FIG. 217. Tangent scale for the determination of the inclination (according to Werenskjöld).

scale 1:500,000, then the vertical exaggeration n is 200 and one obtains for isopycnals

$$v_0 - v_1 = \frac{3.77}{\sin \phi} \Sigma J$$

and for isosteres

$$v_0 - v_1 = \frac{1.885}{\sin \phi} \Sigma J \text{ (cm/sec).}$$

4. Ekman's Theory of Density Currents Including Friction

Consideration of frictional effects in a stratified ocean is more difficult than in a homogeneous sea for two reasons.

First, the mathematical difficulties increase considerably, and secondly, the dependence of the frictional coefficients on the stratification is very incompletely known. In a stratified ocean friction should be less than in a homogeneous sea and the introduction of a *constant* frictional coefficient, which must be made, does not fit so well under these conditions as in the case of homogeneous water.

Nevertheless, the results obtained on this basis afford some insight into the effect of friction on the formation of density currents. EKMAN (1905, 1906) has also dealt with this in his theory of ocean currents and has made important contributions to clarify this problem. A general solution, however, cannot be given. By means of some typical cases only can conclusions be reached, from which the effects of friction can be deduced by comparison with the frictionless cases.

A simple case is that where the specific volume decreases *uniformly* with depth and the isobaric surfaces are thus inclined planes. If, as a consequence of this assumption, there is no pressure gradient at a particular depth d (horizontal isobaric surface), then taking

$$-\frac{1}{\rho} \frac{\partial p}{\partial x} = -fV \quad \text{and} \quad -\frac{1}{\rho} \frac{\partial p}{\partial y} = +fU$$

(U , V are the components of the geostrophic current) the equations of motion (XIII.28) give

$$\frac{D^2}{2\pi} \frac{\partial^2 u}{\partial z^2} + v = V \quad \text{and} \quad \frac{D^2}{2\pi} \frac{\partial^2 v}{\partial z^2} - u = -U. \quad (\text{XV.10})$$

Therein D is the frictional depth (equation XIII.26). For a co-ordinate system with the x -axis parallel to the isobaric surfaces ($V = 0$) and taking as before $U = b(d - z)$ a solution can be given for (XV.10). The velocity profile can be calculated for different values of d/D (Fig. 218) from the very complicated equation obtained. The velocity is given in the diagram in units of $U/5$; they can also be considered as given in cm/sec if the total layer from the sea surface down to the layer of no motion d , of the dynamic section oriented in the direction of the gradient, contains in each 1 km layer a total of $10^6 \omega \sin \phi$ solenoids (for 45° there are 51.6 solenoids). The difference from the velocity profiles presented in Figs. 173 and 174 for a homogeneous mass structure is considerable. Wherever the depth of no motion d may be, the motion there occurs nearly *in a plane*. The friction affects principally the direction of this plane. Table 136 gives the largest (α_{\max}) and the smallest (α_{\min}) angle of deflection from the gradient

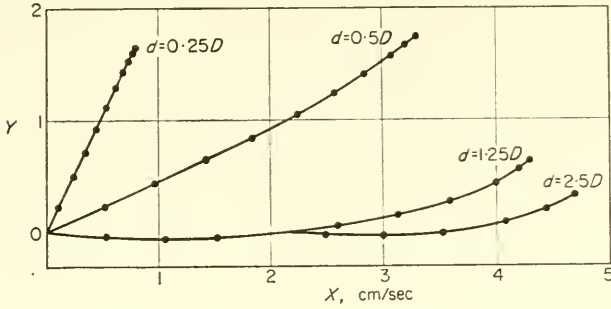


FIG. 218. Velocity profiles in density currents for shallow ocean depths (according to Ekman). The unit of the velocity scale is $U/5$.

Table 134. Frictional influence on density currents in different depth of the ocean

d, D	0.25	0.50	1.25	2.50	∞
α_{max}	26°	67°	93°	91°	90°
α_{min}	26°	62°	82°	86°	90°
$\frac{u_{surface}}{U} \%$	37	74	86	94	100

direction and in addition the velocity of the surface current as a percentage of the geostrophic current U . The vertical velocity decrease is at first very slow and then becomes almost linear. By this it is shown that the law of parallel fields also applies to a close approximation when frictional effects are present.

Simple mass distributions such as these rarely occur in nature. In addition EKMAN has also investigated cases in which the effect of a homogeneous solenoid field is superimposed on a gradient current. A lighter stratified top layer spreads out over a homogeneous deep water. The lighter water body may, for instance, be coastal water lying in a wedge-form off a long coast and can be regarded as a mixed layer of fresh water from the land and of deep water. External forces are not taken into account; at the boundary surface between the top and the deep layer the water movement of the upper density current exerts a shearing force on the deep water which gives rise to an "internal drift current". A closer examination of the case of a boundary layer at a depth d , parallel to a straight coast between a homogeneous upper and lower layer, gives the velocity profiles for different values of d/D presented in Fig. 219. The points on each curve refer again to the depths $0.0, 0.1 D, 0.2 D \dots$, below the sea surface. The part of the curve referring to the top layer is shown by a thick line; the points on the thin part of the curve (deep water) have been omitted for clarity. The unit of velocity is the same as in Fig. 218. If the depth of the top layer is small as compared with D , there will be a strong deflection of the upper current away from the coast. The effect of the deep water lying just underneath the top layer varies according to variations in the depth of the top layer. If $d < \frac{1}{2}D$ the deep water will in part be dragged out to sea by the water of the top layer so that underneath this there will be a current directed away from the coast and

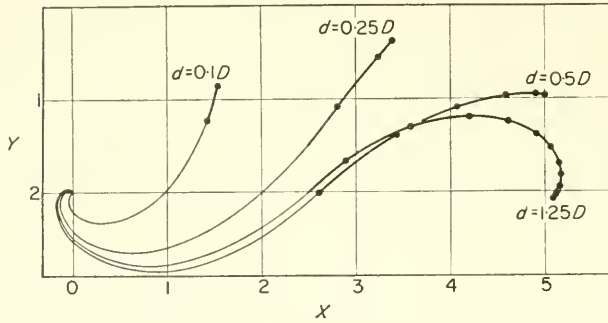


FIG. 219. Vertical structure in a convection current off a long straight shore (x -direction) for a homogeneous top layer of the vertical extent d and homogeneous deep water (D , frictional depth; unit of the velocity as in Fig. 218, according to Ekman).

only below this, the current is directed towards the coast. If, on the other hand, $d > D$, then there will be a normal gradient spiral in the top layer and a corresponding inverse one in the deep water. If the water of the top layer is stratified, the general current structure will be significantly changed (Fig. 220). Now the deep water will be carried along, only to a lesser extent. The deeper the surface layer, the closer will the flow parallel the coast and the lesser will be the effect on the layer beneath. As in the case of Fig. 218 the current is limited to the stratified top layer and its intensity falls near the boundary layer almost to zero.

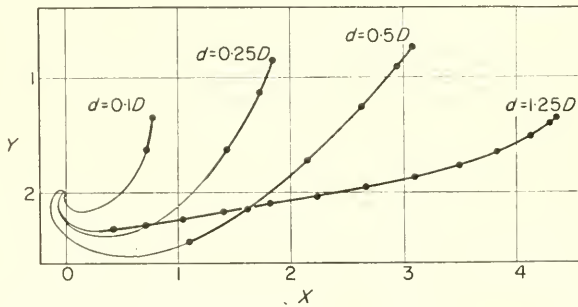


FIG. 220. The same as in Fig. 219 for a stratified top layer (according to Ekman).

EKMAN (1928 *b*) summarized these results and arranged them in a clear manner in Fig. 221. Three alternative assumptions have been made on the thickness (in metres) of the top layer d_s :

- (1) the top layer is divided into two homogeneous halves with a discontinuity surface in the middle (— \times — \times —);
- (2) the top layer is stratified so that in it a density current is generated with a velocity distribution following a cosine-function (— \bullet — \bullet —);
- (3) in the top layer the velocity decreases linearly with depth and there is a discontinuity layer (— \circ — \circ —).

Velocity profiles for the currents produced are shown on the right-hand side of Fig. 221; in the upper picture for a top layer the thickness of which is assumed equal

to the frictional depth and in the lower layer is assumed as equal to double the frictional depth. The thin lines refer to the lower layer and the thick lines to the top layer. The two arrow-heads at the right-hand edge connected with the + sign represent the vector of the surface current in the case of frictionless motion. For sharper discontinuity surfaces and a greater thickness of the top layer the velocity profile, as before, is made up of two Ekman spirals. If the top layer is stratified there is in both cases a

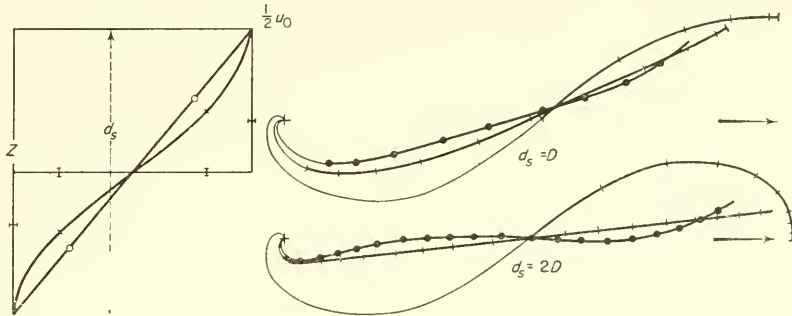


FIG. 221. Density currents in a top layer considering friction and for motionless deep water (according to Ekman).

current of almost uniform direction and the current velocity will decrease almost linearly with depth. Due to the stratification of the current, intensity in the lower layer (internal drift current) will be strongly reduced, and for a deeper top layer this current will disappear almost entirely. The transport in the deep current will then be insignificant. This leads to the important conclusion that: *the sea surface under the influence of external disturbances will adjust itself in such a way that the pressure gradient arising from density differences in the top layer has a maximum value at the sea surface, decreases with depth and will largely or entirely vanish at the lower boundary of the top layer; the deep water will remain practically motionless.*

The “elementar” current in a vertically complicated stratified ocean consisting of a stratified top layer and an almost homogeneous deep water will thus, according to Ekman, have the following *three current constituents*.

(1) The physical sea level and the isobaric surfaces of the top layer will be turned in such a way that the pressure gradient has the same direction everywhere and will be proportional at every level to the density; in the homogeneous deep water, however, this pressure gradient will remain constant. The current produced by this mass structure will be a simple *gradient current*.

(2) If the physical sea level and the isosteric surfaces are brought back to the initial position, then an additional current resulting from this mass displacement adds to the gradient current described above. This is called the *density current*.

(3) In addition, the effect of the wind on the sea surface generates a pure *drift current*. This current will differ only slightly from that in a homogeneous sea if the top layer is sufficiently thick. However, the density current will not be confined to the top layer alone, but when this is reasonably thick, the influence on the homogeneous deep water from above remains small.

Laboratory experiments with stratified water have been made by SANDSTRÖM (1908, 1918) in order to demonstrate experimentally the effect of stratification on wind-generated currents. In the experiment, an air flow over the surface of a multiple-stratified water mass in a narrow rectangular basin immediately produces a current in the direction of the wind. The piling up of water at the windward end of the basin gives rise to a counter current in the lower part of the uppermost layer; there is a closed circulation in this layer. Friction then produces a somewhat weaker circulation with an opposite sense of rotation in the layer immediately beneath the uppermost one. Further circulations are formed in successive layers beneath this, each with the opposite (direct or indirect) rotational sense to that above it. Sandström's experimental results for a narrow basin cannot be applied directly to actual conditions in the ocean. In the laboratory experiment, in the first place, boundary conditions at the outer rim of the *narrow* basin will play a decisive role, and secondly, the deflecting force of earth rotation will have no effect and thus it is precisely that factor which most decisively influences ocean currents in nature that is left out of consideration. The laboratory experiment is thus applicable in nature only to narrow confined sea basins and to lakes.

5. Oceanographic Applications of Bjerknes's Circulation Theorem

The theory of ocean currents in a non-homogeneous sea received a very strong stimulus from the circulation theorem of Bjerknes, since it opened the road for studying in a quantitative way and for the first time the effects of baroclinic mass fields. There are manifold possibilities to apply this theorem in oceanography some of which will be discussed here in more detail.

(a) The Steady State of Motion

The most important use of the equation (X.54) is for the steady state in which the circulation accelerations vanish. In this case

$$N = f \frac{dF_m}{dt} \tag{XV.11}$$

(here again N = number of solenoids, f = Coriolis Parameter, F_m = area of the projection of curves on the sea surface). The curve s is now made up of the two station verticals AC and BD and of two isobars AB and CD (Fig. 222). The water

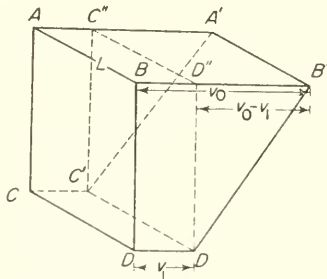


FIG. 222.

masses at the upper level move with an average velocity v_0 and those at the lower level with an average velocity v_1 at right angles to the section. After unit time the water elements, initially at AB , will lie at the line $A'B'$ and those from the isobaric interval CD at $C'D'$. The total surface $ABCD$ transforms into $A'B'C'D'$. The change of the projection of the surface $ABCD$ on the sea surface thus becomes $A'B'C''D''$, so that $dF_m/dt = (v_0 - v_1)L$, where L is the distance between the two stations A and B . Equation (XV.11) combined with (X.45) gives

$$(v_0 = v_1) = \frac{D_a - D_b}{fL}. \tag{XV.12}$$

This equation, which was first derived by HELLAND-HANSEN (1905), forms the fundamental equation of dynamic oceanography. From the difference in dynamic depth of the isobaric surfaces $D_a - D_b$ a simple calculation gives the increase in velocity from one surface to the next. Analogous treatment to that on p. 466, however, affords only velocity differences and only the component at right angles to the selected section is obtained. Equation (XV.12) contains fundamentally the same as equation (XV.7) derived directly from the equations of motion. In the practical application of (XV.12) it should be noted that $D_a - D_b$ has to be expressed in units of the potential, that is, in dynamic decimetres when the metre is taken as the length unit. The difference in dynamic depth anomaly, $\epsilon_a - \epsilon_b$, can, of course, be used instead of the difference $D_a - D_b$.

The section to the south of the Newfoundland Banks between stations 205 and 206 can be used again as an example (see Fig. 202). Table 135 contains the dynamic depths, their anomalies and values of $\epsilon_a - \epsilon_b$ for selected pressure surfaces down to 750 decibars. In equation (XV.12) $\phi = 41^\circ 10' N.$; $f = 9.60 \times 10^{-5}$; $L = 59$ km and the denominator is 5.664. The anomaly differences are multiplied by 10 in order to obtain dynamic dm ; this gives then v in m/sec. The last column gives velocities on the assumption that there is no motion at 750 m (see Table 133). If calculations of this type are available for a sufficient number of station pairs it is possible to obtain a complete velocity field at right angles to the cross-section. A comparison of the velocities calculated in this way from the mass field with the observed velocities was first given by WÜST (1924) for a cross-section through the Gulf Stream in the Florida Strait. The

Table 135. Computation of the velocity profile south of the Great Banks of Newfoundland.

Pressure (dbar)	St. 205		St. 206		$D_a - D_b$	$v_0 - v_1$ (cm/sec ²)	v (cm/sec)
	Depth (dyn. m)	Anomaly ϵ	Depth (dyn. m)	Anomaly ϵ			
0	0—	0—	0—	0—	0—	0.0	64
50	48.6887 ₅	0.0622 ₅	48.7175 ₀	0.0910 ₀	0.0287 ₅	5.1	59
125	121.6918 ₈	0.1467 ₆	121.7571 ₃	0.2120 ₁	0.0652 ₅	11.5	53
250	243.2725 ₀	0.2525 ₁	243.4077 ₆	0.3877 ₇	0.1352 ₆	23.9	40
450	437.5985 ₀	0.3650 ₁	437.8427 ₆	0.6092 ₇	0.2442 ₆	43.1	21
750	728.7215 ₀	0.5020 ₁	729.0847 ₆	0.8652 ₇	0.3632 ₄	64.1	0

agreement was very satisfactory; later this kind of comparison has often been repeated confirming the results.

If, instead of as in Fig. 222, the vertical section is placed in the direction of the relative velocity $V_0 - V_1$, then there will be no component at right angles to the surface, that is, in (XV.12) $v_0 - v_1 = 0$ as well as $D_a - D_b = 0$ and the dyn. depths in the cross-section must be the same at C and D . If one of these verticals is kept fixed, then the other will move away at the relative velocity $V_0 - V_1$ and for every point along its track always applies $D_a - D_b = 0$. This implies that: *curves of equal dyn. depth, which then give the dyn. topography of an isobaric surface relative to another, represent at the same time stream lines of the relative velocity (velocity of one surface relative to that of the other).*

This theorem is of great importance in the discussion and interpretation of the relative topographies of individual pressure surfaces in the ocean. An example is presented in Fig. 223 which shows the relative topography of the isobaric surface at 750 decibars for the same area containing the section shown in Fig. 202. The indication arrows show the direction and the intensity (nautical miles per hour) of the (relative) velocity of the layer at 750 m depth relative to that of the surface. If the water in this depth is motionless, then they represent the sea surface current. The dyn. isobaths are stream lines for the whole system.

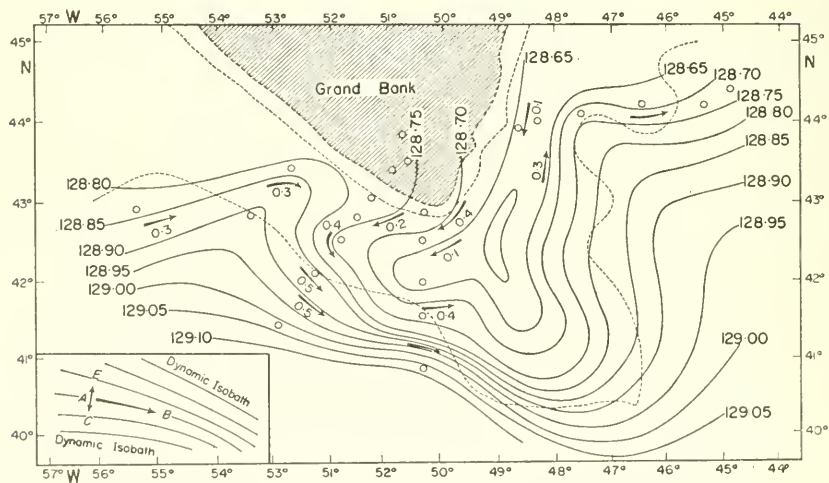


FIG. 223. Dynamic topography of the 750-decibar surface south of the Great Banks of Newfoundland according to the observations from 5 to 7 May 1922 (according to Smith). The arrows indicate the computed relative current in nautical miles per hour.

Both applications of the circulation theorem have made use of curves in vertical planes, which contain a large number of solenoids. The theorem may also be applied to *horizontal curves*, which include little or no solenoids. For curves of this type the first term on the right-hand side of equation (X.54) vanishes and there remains only the term expressing the effect of the Coriolis force. On integration it gives

$$-C_0 = -f(F_{m-1} - F_{m-2}). \quad (\text{XV.13})$$

A horizontal circulation free-curve ($C_0 = 0$) will acquire by contraction a cyclonic circulation and by expansion an anticyclonic circulation.*

If curves extending as parallel circles all around the Earth and containing an ocean covering the entire Earth are carried towards the equator by the general oceanic circulation, then their projection on the equatorial plane will expand and they will thus acquire a zonal anticyclonic circulation, that is, from east to west. On the other hand, if they are displaced towards the poles there will be a shrinking of the areas enclosed within the parallels and thus there will be a zonal cyclonic movement from west to east. Considerable changes can also occur in the area enclosed by horizontal curves flowing over a submarine ridge thereby causing the formation of cyclonic or anticyclonic circulations. These will be superimposed on the basic current and will give rise to a wave-form character of the current structure (see p. 431).

(b) *The Sandström Theorem*

In the ocean there exist closed circulations of greater or smaller extent, which are maintained by the continuous supply of heat at certain fixed places and the continuous withdrawal of heat at others. These sources of heat and cold maintain the differences in specific volume. Thus circulation velocity in a frictionless medium will continuously increase, since the circulation acceleration in equation (X.44) has a positive value. In reality, however, all circulations are affected by frictional forces. Another term R must therefore be added to equation (X.44) containing all the frictional effects. There will be a steady state only when

$$-\int_s a \, dp + R = 0 \tag{XV.14}$$

that is, in a *steady state* (disregarding the rotation of the Earth) the work done by the pressure forces (i.e. $-\int_s a \, dp$) is used exclusively in overcoming the frictional forces. This can only be the case when

$$-\int_s a \, dp < 0. \tag{XV.15}$$

From this controlling equation it is easy to draw conclusions as to how the sources of heat and cold should be located in space inside the circulation in order to allow for a stationary state. The concept of sources of heat and cold must be given in the ocean a

* It follows from equation (X.54) $dC/dt = f \, dF_m/dt$ that for an increase in the area $dF_m/dt > 0$ there will be an anticyclonic deflection and correspondingly for a decrease a cyclonic deflection. This can, of course, also be derived directly from the equations of motion. For a geostrophic frictionless current these are

$$-fv = -\frac{1}{\rho} \frac{\partial p}{\partial x} \quad \text{and} \quad +fu = -\frac{1}{\rho} \frac{\partial p}{\partial y}.$$

By cross-wise differentiation and rearrangement

$$f \operatorname{div} v_H + \beta v = 0, \quad \text{whereby} \quad \beta = \frac{df}{dy}.$$

If the current is divergent ($\operatorname{div} v_H < 0$) v must be positive; this indicates that the deflection will be anticyclonic or to the right in the Northern Hemisphere; for a convergence ($\operatorname{div} v_H > 0$) v is negative with a corresponding cyclonic turn.

somewhat wider sense. In the real ocean differences in specific volume are produced not only by heat gain or heat loss, that means *thermally*, but also by changes in salinity. Evaporation will increase salinity and precipitation, ice melting and the inflow of fresh water (run-off) will reduce it. An increase in salinity has the same effect as a cold source and a decrease in salinity will be equivalent to a heat source. In the following the sources of heat and cold will be taken as including always the combined effects of both factors.

In a Carnot cycle one single and complete revolution shall now be considered on an $[a, p]$ -diagram (Fig. 224) consisting of two isobars ($dp = 0$) and of two adiabatic curves along which there is no addition or removal of heat and changes will occur only due to expansion or contraction. There are two possible cases:

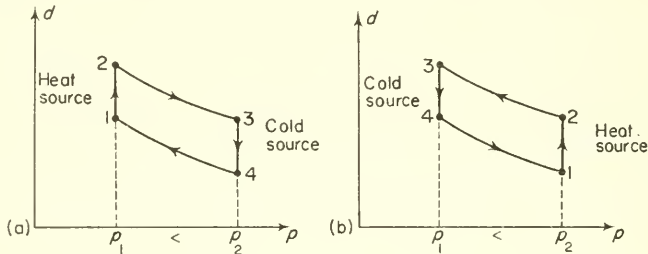


FIG. 224. Carnot's cycle. Case *a*: heat source at lower pressure (small ocean depth) than cold source. Case *b*: heat source at higher pressure (great ocean depth) than cold source. A stationary circulation is only possible in case *b*, not in case *a*.

(*a*) *Clockwise cyclic process.* From 1 to 2 at a constant, but *lower pressure* ($p_1 < p_2$, in the upper part of the sea) there will be a heat input (heat source), from 2 to 3 there will be an adiabatic compression followed from 3 to 4 by a heat removal (cold source) at higher pressure (in the lower part of the sea). Finally, an adiabatic expansion occurs from 4 to 1. Evaluation of the integral (XV.15) gives, since the isobaric sections of the cycle make no contribution

$$\int_s a dp = \int_{p_1}^{p_2} (a_{2,3} - a_{4,1}) dp > 0,$$

since both $(a_{2,3} - a_{4,1})$ as well as dp are greater than zero. The pressure forces are incapable to do work. Any existing circulation will in time be destroyed by frictional effects.

(*b*) *Counter-clockwise cyclic process.* The heat source works at *high pressure* $p_1 < p_2$, in the lower part of the sea).

In this case

$$\int_s a dp = \int_{p_1}^{p_2} (a_{4,1} - a_{2,3}) dp < 0.$$

The pressure forces are capable to do work. If this is so large as to overcome all the frictional forces there will be a steady circulation.

If there were no friction, this would be a reversible process and the degree of efficiency of this thermodynamic machine would be given by $W = (Q_1 - Q_2)/Q_1$, where Q_1 is the amount of heat absorbed by the medium from its surroundings at the

heat source, and on the other hand Q_2 is that lost to the surroundings at the cold source. If frictional effects are present, then the process will be irreversible. The machine will give off a quantity of heat Q_2 during the course of this process which is greater than in the reversible case ($Q'_2 > Q_2$). The degree of efficiency of such a circulation is less than W and is given by $(Q_1 - Q'_2)/Q_1$. In a circulation for which the work done by the pressure forces is exactly sufficient to balance the loss of energy by friction the degree of thermodynamic efficiency will be exactly zero. The Sandström theorem thus states: *a closed steady circulation can only be maintained in the ocean if the heat source is situated at a lower level than the cold source.* SANDSTRÖM (1908) in order to elucidate the content of his theorem has performed a number of very instructive laboratory experiments. Later on BJERKNES (1936) has presented a detailed analysis of all the questions raised when dealing with thermodynamic machines of this type. The two most important of the Sandström experiments are:

(a) *Heat source at a higher level than cold source.* Here a single water type is contained in a narrow basin but there are two sources (Fig. 225, upper picture). The heat source ("warm") lies at a higher level than the cold source ("cold"). At the beginning

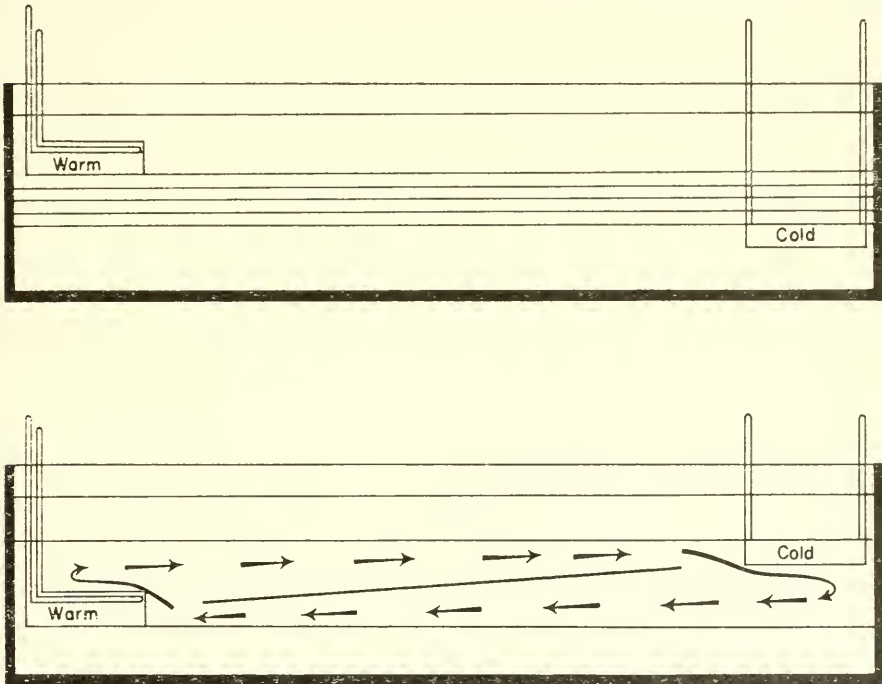


FIG. 225. *Upper picture:* heat source situated above cold source; no circulation and vertically stable stratified water layers. *Lower picture:* heat source situated below cold source; generation of a stationary circulation in the layer between the levels of the heat and cold source.

of the experiment motions will be set up because the heated water will rise in the layers *above* the level of the heat source and cooled water will sink in the water layers *below* the cold source. However, when the upper water reaches the temperature of the heat source and the lower water that of the cold source, these water movements will

cease and there will be a *stable stratification* with the temperature decreasing with depth. A state of no motion is created since the circulations previously present will be halted rapidly by friction.

(b) *Heat source at a lower level than cold source.* This is the same experiment as in (a) except that the position of the two sources is inverted. Convectional currents will be set up in this case also, but soon there will form a steady circulation confined to the layers between the levels of the two sources (Fig. 225, lower picture). Above there will be a water movement from warm to cold and below from cold to warm; the most heated water will be above the level of the heat source and the coldest below the cold source. But these layers will not take part in the circulation which is solely confined to the intermediate layers.

Later on, Sandström modified the experiment in several ways, especially to show more clearly its application to oceanographic conditions; basically, however, these do not give any new results. JEFFREYS (1925) has questioned the general validity of Sandström's conclusions but Sandström's deductions from the circulation principle are undoubtedly correct. The circulations produced by thermo-haline differences are the more intense the greater the vertical distance between the level of the warm and that of the cold source. However, conditions existing in nature in the ocean are not particularly favourable to the formation of any more intense circulations of this type, since the principal heat supply in the ocean is primarily due to the combination of solar radiation and back-radiation from the atmosphere and the loss of heat primarily due to outgoing radiation. These processes operate to a very large extent at the boundary between the ocean and the atmosphere (almost horizontal sea level and evaporation and precipitation also act here. The vertical distance between the location of the heat and cold sources is thus very small. Probably the heat source in equatorial areas lies somewhat deeper than in higher latitudes, but nevertheless the thermo-haline circulation must be limited to a very shallow top layer. Observations provide complete confirmation of the consequences deduced from the circulation principle (see p. 576).

6. The "Reference-level" for the Conversion of the Relative Topography of the Pressure Surfaces into the Absolute One

The relative topography of the isobaric surfaces (relative to the sea level) assumed as plane) can be determined by the methods described on p. 309 and the following pages. Using equation (XV.12) this also gives the *relative* velocity differences from layer to layer. In order to obtain a complete quantitative knowledge of the water movements it is necessary to convert these relative topographies into *absolute* topographies. This can be done if the relative topography can be referred to a known *topography of any isobaric surface*. This determination of the absolute topography would be easy if it were possible to determine from current measurements such a depth level at which the velocity of the current is zero, since at this "depth of no motion" the isobaric surface must coincide with a level surface ("Niveaufläche").

In this way, for example, Wüst used the current measurements made by Pillsbury in the Florida Strait in order to determine the current profile of the Gulf Stream from the mass field. The number of current measurements available for the open ocean is, however, insufficient to fix with some accuracy the position of such a "zero level"

("Nullfläche"), quite apart from the fact that short series of current measurements are almost always strongly disturbed by the tides. Thus the essential data needed to decide about the position of the "zero level" is largely lacking. The effort to utilize the observations as fully as possible and to determine the pressure differences as good as possible, at least in the upper layers, has led to place the zero surface as deep as possible. This choice was also suggested by the generally rapid decrease in the velocity of the currents with depth.

Over the entire area under consideration most investigators have thus usually placed the zero level at a constant dynamic depth and as deep as possible (as far as the water depth and the observations available allowed), and from this have derived the absolute topography of the pressure surfaces and that of the physical sea level from the relative topographies. Table 136 presents a summary of all the depths selected for the zero level by different investigators. The differences of more than 1000 m indicate that these are pure assumptions for which there is no firm basis. However, all investigators have been aware of the inadequacy of this procedure and have regarded the selection made purely as a make-shift. The assumption of a zero level at a constant large depth will, of course, conceal all currents in the layers just above and below this depth, and these

Table 136. Depth of the "zero level" (Nullfläche) in the Atlantic Ocean according to the assumption of different investigators

Investigator	Year	depth (m)	Investigator	Year	depth (m)
Bouquet de la Grye	1882	4000	Helland-Hansen and Nansen	1926	2000
Mohn	1885	550	Jacobsen	1929	1000
Zöppritz	1887	2000	Iselin	1930	1200
Wegemann	1899	1000	Helland-Hansen	1930	1000
Schott	1903	500	Iselin	1936	1800
Castens	1905	650			

are thus falsified if by chance the zero level selected does not correspond with the actual position of such a level. On the other hand, the deeper the zero level is placed, the less will it disturb the pressure conditions at the sea surface.

To obtain a correct idea of the deep current, it is not sufficient to assume a constant depth for the zero level. Such an assumption, moreover, does not correspond to the dynamics of the ocean currents in nature and, as has been stressed by EKMAN (1939) takes no account of the topography of the sea bottom. These problems of dynamic oceanography have been dealt with by DIETRICH (1937 a, c), who has thrown light on a number of aspects of them. The zero level, more suitably could be called "reference-surface" and has to be placed at such a depth where the velocity component at right angles to the dynamic section under consideration is zero. It must, of course, closely adapt to the mass structure of the entire oceanic area, since this is in fact a consequence of the currents and is closely connected with them. In these circumstances it is to be expected, especially when larger areas of the sea are taken into consideration, that the reference-level for the reduction of relative into absolute topography must be

a surface of locally varying depth. The determination of its form and the different factors that must be considered for fixing its position in oceanic space is not an easy task. It should be stressed that the choice of such a surface is always more or less subjective, and such an assumption can only be made plausible by giving proper weight to all the different view points which are in question.

(a) *Determination of the Topography of the Reference-Level*

A first attempt was made by Dietrich in an investigation of the dynamics of the Gulf Stream to introduce a reference-level of variable depth by investigating characteristic features in the distribution of oxygen in order to fix the reference-level. He thus accepted the widely held view that the layers showing the intermediate oxygen minima (see Pt. I, p. 66 and following pages) are at the same time also layers of very weak motion or of no motion at all, and could thus be regarded as motionless boundary layers between individual components of the deep-sea circulation. However, ROSSBY (1936 *a*), ISELIN (1936) and especially WATTENBERG (1938) and SVERDRUP (1938 *b*) have questioned this assumption and have expressed doubts about the suitability of these oxygen minima as reference-levels. In the upper layers of the ocean the oxygen distribution can be regarded, on the one hand, as a consequence of thermal and biochemical oxygen consumption, and on the other hand, of the renewal of the water masses by horizontal advection. The intermediate minima are thus regions of particularly strong oxygen consumption and can hardly be regarded as completely motionless layers. The results obtained by Dietrich for the currents in the Gulf Stream on the basis of this assumption are not such as to give confidence in reference-levels derived from the oxygen minimum. Even the customary division of the water masses of an ocean, pictured by major longitudinal and transverse sections and allowing for the characterization of the different water bodies, is scarcely suitable for the determination of the topography of the reference-level. Even though they may be practical and useful in giving a general qualitative picture of the meridional and zonal velocity components of the ocean currents.

DEFANT (1941 *b*) has gone a quite different way in order to determine the dynamic reference-level in the Atlantic, which avoids the use of any particular boundary layer between the individual water types and makes use only of dynamic evaluations of observational data, which must be closely connected with the structure of the water masses of the particular area. The differences in dynamic depth of the pressure values between two neighbouring stations give, by means of equation (XV.12), a relative measure of the velocity difference perpendicular to the cross-section between the sea surface and the corresponding depth. When these differences are plotted in an appropriate co-ordinate system (ordinate: pressures; abscissa: difference in dynamic depth) they give a *relative* vertical velocity profile at right angles to the section between the two stations (Fig. 226). This profile cannot be converted to an absolute velocity profile without knowing the zero point on the abscissa. By comparison of a large number of difference-curves for neighbouring pairs of stations it shows in most cases that in each profile there is a layer of considerable vertical thickness in which the differences in dynamic depth are constant or almost constant. If the zero point of the abscissa scale is placed outside of this layer then the entire layer must have a *constant* velocity,

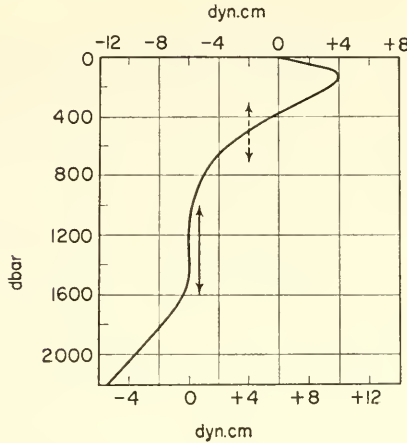


FIG. 226. Schematic example for fixing the reference-level by means of the vertical distribution of the dynamic depth of the standard pressures of two neighbouring stations. (The lower "displaced" scale of the abscissa only has its correct position, if the reference-level is assumed in the layer denoted by the vertical arrow; a position of the reference-level at the dashed arrow, for example, would be quite improbable.)

while the dynamic structure of the other layers will be divided up in a rather unintelligible way. It is more plausible to suppose that this more prominent layer should be motionless, or almost motionless, so that the reference-level should lie within it. Such a layer with obviously low velocities is apparently characteristic not only for the pair of stations under consideration, but is to some extent depending on the pressure field of the entire oceanic region under consideration. The reliability of this method is increased if the individual reference depths, determined from a large number of station pairs, can be combined to give a closed system representing a definite topography of the reference-level.

To illustrate the method the difference-curves for the dynamic depths are shown in Fig. 227 for a meridionally distributed set of stations in the Atlantic; for each curve the vertical extent for which a layer of no motion or only weak motion is most probable,

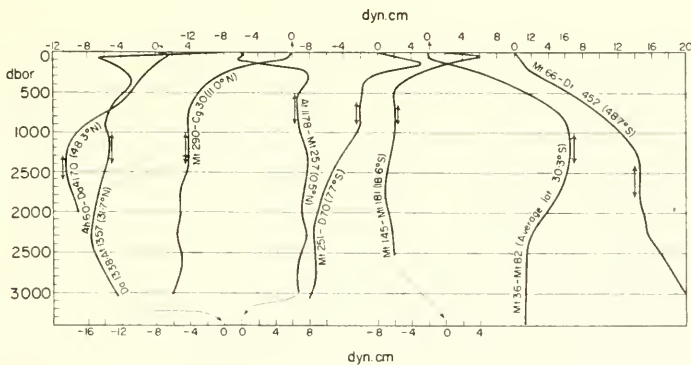


FIG. 227. Fixing of the dynamic reference-level for a series of meridionally distributed stations in the Atlantic Ocean.

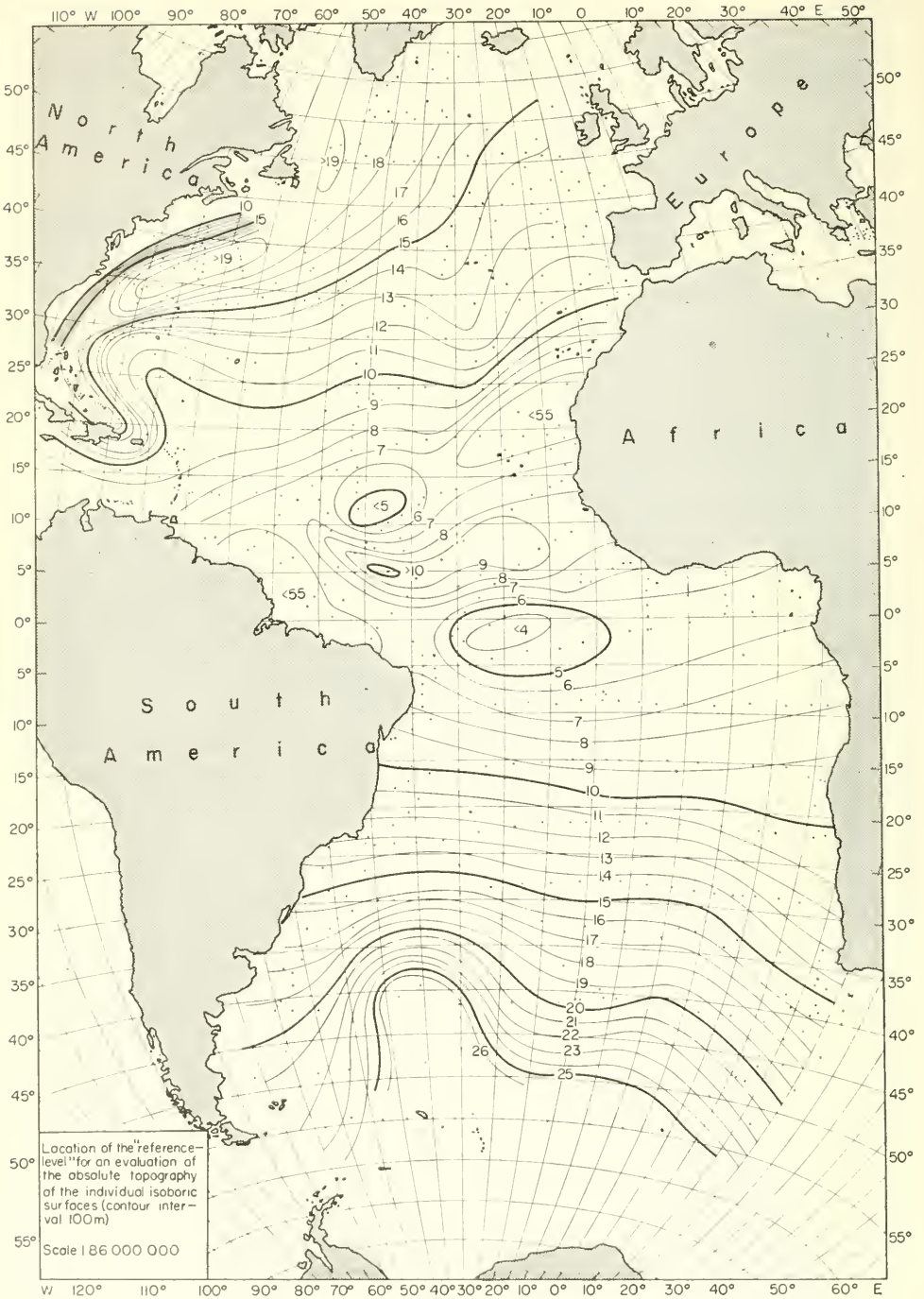


FIG. 228. Position of the reference-level for transforming relative topographies into absolute depth (numbers in 100 m units).

is marked with a vertical double arrow. The reference-level for conversion of relative into absolute topography must lie within this layer. Already these station pairs show roughly the meridional distribution of the depth of the reference-level in the Atlantic: lower depth in high latitudes (approx. 1500 m or deeper), rising up to 500 m at the equator. The topography of the reference-level can thus be derived for the whole of the Atlantic from a large number of such diagrams. Figure 228 presents the topography determined by this method. The lines are drawn at 100 m intervals (or decibars); for a reduction of the relative into absolute pressure values it is sufficient to know the position of the reference-level to the nearest 50 decibars. It is clearly shown that the assumption of a reference-level of constant depth can never do justice to the dynamic structure of the water masses of the Atlantic Ocean; even over smaller oceanic areas there are appreciable variations in its position. Along each meridian the depth of the reference-level is least near the equator (up to 400 m), in the Southern Hemisphere it sinks uniformly to great depths in high latitudes. But in the Northern Hemisphere conditions are more complex. From the equator it sinks at first to a secondary minimum between 5° and 10° N. (about 900 m), then rises again to another maximum between 10–20° N. and from there begins the lowering towards the north-west to greater depths. The irregularity in the northern subtropics has the same form as the asymmetry in the position of the subtropical and tropical thermocline (see Pt. I, p. 120). There is undoubtedly a causal connection between the two phenomena. In the Gulf Stream region there are considerable deviations from normal. Near to the current core (intense flow) the reference level rises steeply upwards to a depth of 1000 m or less. This phenomenon, which belongs to the characteristic features of this area, must be connected causatively with the inclination of the isosteres in a stratified ocean with intense motion (see p. 331).

From the chart shown in Fig. 228, NEUMANN (1954, 1955) has computed zonal averages of the depth of no meridional motion D (zero level) for the North Atlantic and has plotted them against the latitude (Fig. 228 *a*). Individual values along the 20°W-meridian were used for the South Atlantic, since the variation in D in the east-west direction is small as compared with the variation of D in a meridional direction. In Fig. 228 *a* the values of D are marked by circles and the full drawn curves represent the function

$$D = -K \sin \phi = -K \cos \vartheta. \tag{XV.16}$$

The constant K is different in the Northern and Southern Hemisphere but the increase of D with latitude follows this function closely except in the equatorial regions, where apparently another physical law applies (see Pt. I, p. 120).

Excluding the equatorial regions, the relative variation of D with latitude is given by

$$\frac{1}{D} \frac{\partial D}{\partial \vartheta} = -\tan \vartheta. \tag{XV.17}$$

Then, it follows from the Coriolis parameter, $f = 2 \omega \cos \vartheta$ that

$$\frac{1}{f} \frac{\partial f}{\partial \vartheta} = -\tan \vartheta. \tag{XV.18}$$

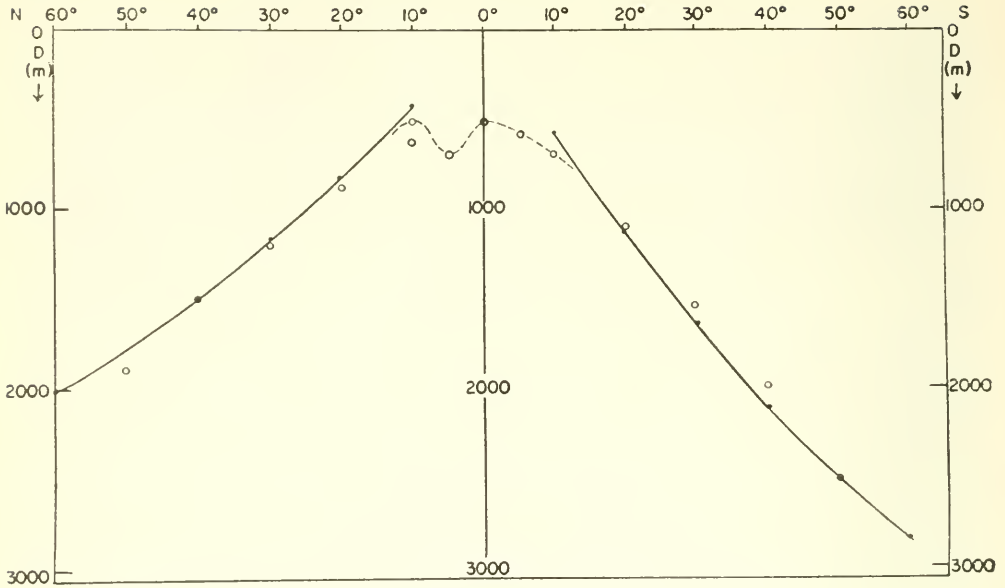


FIG. 228a. Average depth of the reference-level (layer of no motion) in the Atlantic Ocean (according to Neumann).

Thus for the large scale major oceanic circulations the fundamental relation

$$\frac{\partial f}{\partial \vartheta} = \frac{f}{D} \frac{\partial D}{\partial \vartheta} \tag{XV.19}$$

is obtained. An investigation of the reference level (layer of no motion) similar to that made by Defant was also carried out by NEUMANN (1942, 1943) in an evaluation of observational data for the Black Sea. For the strong vertical stratification of this adjacent sea the topography of the reference level is more closely connected with the position of the boundary layers characterizing this vertical structure. Figure 229 shows the position of the different boundary surfaces in a longitudinal section near 43° N. It is almost the same everywhere: the lower plankton limit, the maximum density

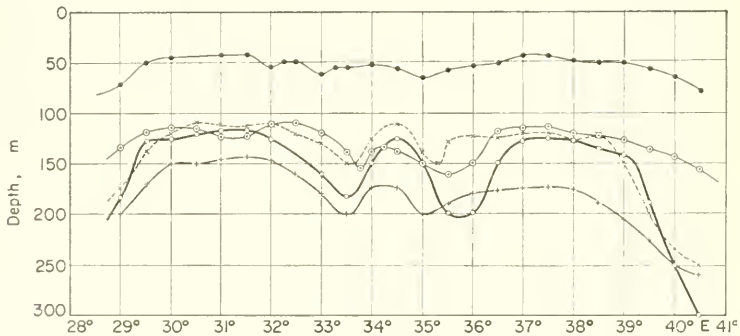


FIG. 229. Depth of different characteristic boundary layers in a longitudinal cross-section through the Black Sea in 43° N. (according to Neumann).

gradient, the upper limit of the H_2S -layer and the reference level are all more or less coincident (except near the coastal areas in the eastern part). All these surfaces join here, forming a single closed system, an almost motionless boundary layer.

If in an adjacent sea a density discontinuity layer is found everywhere, the determination of the position of a dynamic reference level is considerably simplified, since the lower limit of the top layer is then usually also the lower limit of the upper flow and the discontinuity layer coincides with a layer of no motion. These methods have already been used by WITTING (1918) in his investigations on the continental rise around the Baltic. This simple method can, of course, only be used when the thickness of the top layer is not too great; it is also possible to apply this method with success to shelf areas, having a sharp subdivision in the vertical into two layers.

A new method for the determination of the depth of no meridional motion has been presented by STOMMEL (1956). It is of interest in so far as it permits a determination of this depth directly from the observed vertical distribution of the oceanographic factors, and because it also shows that there is in actual fact no depth of no motion in the ocean but rather the depth of no meridional motion always coincides with the layer of maximum vertical velocity. From the general equations for a wind driven motion and the continuity equation cross differentiation leads to the following three relations:

$$\left. \begin{aligned} \frac{\partial}{\partial z} (\rho v) &= -\frac{g}{f} \frac{\partial \rho}{\partial x} - \frac{1}{f} \frac{\partial^2 T_x}{\partial z^2}, \\ -\frac{\partial}{\partial z} (\rho u) &= -\frac{g}{f} \frac{\partial \rho}{\partial y} - \frac{1}{f} \frac{\partial^2 T_y}{\partial z^2}, \\ \frac{\partial}{\partial z} (\rho w) &= \frac{\beta}{f} \rho v - \frac{1}{f} \frac{\partial}{\partial z} \left[\frac{\partial T_y}{\partial x} - \frac{\partial T_x}{\partial y} \right]. \end{aligned} \right\} \quad (\text{XV.20})$$

The quantity ρv in the third equation can be eliminated by means of the first equation, giving

$$\frac{\partial^2 (\rho w)}{\partial z^2} = \frac{\beta g}{f^2} \frac{\partial \rho}{\partial x} - \frac{\partial^2}{\partial z^2} F(z), \quad (\text{XV.21})$$

where

$$F(z) = \frac{\partial}{\partial x} \left(\frac{T_y}{f} \right) - \frac{\partial}{\partial y} \left(\frac{T_x}{f} \right).$$

This function $F(z)$ is more or less indeterminate, but according to Ekman differs from zero only in a thin upper layer extending from $z = 0$ to the depth of frictional influence. $F(0)$ is known in terms of the distribution of the wind stress on the sea surface. If the sea bottom is at $-d$, then the first integral of equation (XV.21) can now be obtained:

$$\frac{\partial}{\partial z} (\rho w) = \frac{\beta}{f} \left[\Phi(z) + C \right] - \frac{\partial F}{\partial z} \Big|_{-d}^z, \quad (\text{XV.22})$$

whereby $\Phi(z)$ is defined

$$-\frac{g}{f} \int_{-d}^z \frac{\partial \rho}{\partial x} dz$$

and where C is an integration constant. The meaning of the function $\Phi(z)$ is easily understood, since for a purely geostrophic flow (from the first equation in XV.20) it follows

$$\rho v = \Phi(z) + C.$$

The constant C is the indeterminate reference velocity and the determination of C can be readily seen to be equivalent to the determination of the depth of no meridional motion, that is, the depth at which ρv vanishes. Since for deeper layers $F = 0$, it follows from (XV.22)

$$\frac{\partial}{\partial z} (\rho w) = 0.$$

By this it is shown that the level of no meridional motion coincides with the level of maximum vertical motion. Since the bottom currents are rather weak, the hypothesis

$$\left. \frac{dF}{dz} \right|_{-d} = \frac{dF}{dz}$$

allows the integration of equation (XV.22) between z and $-d$. Taking $F(-d) = 0$ and $\rho w(-d) = 0$, the following expression for ρw is obtained

$$\rho w = \frac{\beta}{f} \left[\int_{-d}^z \Phi(z) dz + C \cdot (z + d) \right] - F(z). \quad (\text{XV.23})$$

At the surface, $z = 0$, ρw vanishes; the quantity $F(0)$, according to (XIII.27) is the net convergence of the wind-driven layer and (XV.23) gives

$$C = \frac{1}{d} \left[\int_{-d}^0 F(0) - \int_{-d}^0 \Phi(z) dz \right].$$

The depth at which $\Phi(z) + C$ vanishes, is the depth of no meridional motion.

In physical terms the method, given in formal terms above, can be loosely described in the following way. At any geographical position in the ocean the distribution of the winds produces a net convergence (or divergence) of the surface waters. In the steady state the only outlet (or inlet) for this water is downwards (upwards) through the bottom of the frictional layer. In the deep frictionless (by hypothesis) geostrophic flow, water elements will stretch (or shrink) vertically as they move towards the poles (equator). The cumulative effect of this expansion or contraction added up over the entire vertical column from the ocean bottom to the bottom of the frictional layer leads to a vertical component of velocity which, by the conservation of mass, must be equal to that induced at the bottom of the frictional layer by the winds. This balance will only hold for a specific choice of the reference-level which thereby fixes this level (Stommel).

Stommel has given a numerical example for two "Atlantis" stations situated at about 32° N., 50° and 63° W., respectively. Here the depth of no meridional motion is found to be at about 1500 m; the maximum vertical velocity 24×10^{-5} cm sec $^{-1}$, also occurs at this depth. This depth agrees well with that inferred by Defant from his method.

(b) Conversion of Relative to Absolute Topographies Using a Reference-level of Varying Depth

For a reference-level of constant depth there is little difficulty in the conversion from relative to absolute topography (see p. 211). The differences in dynamic depth represent at the same time also differences in the physical sea level and in the level of individual isobaric surfaces, respectively. If the depth of the dynamic reference level varies from place to place this simple procedure can no longer be used; the individual differences of dynamic depths above or below the reference level must be coupled or interconnected one to the next in a suitable way in order to construct step wise the surfaces of equal pressure (DIETRICH, 1937 a). To determine the absolute topography of a pressure surface p_0 above the reference level, three oceanographic stations A, B, C were chosen and p_a, p_b, p_c are the pressures at the points on the reference level at which by necessity the pressure surfaces parallel the level surfaces (Fig. 230).

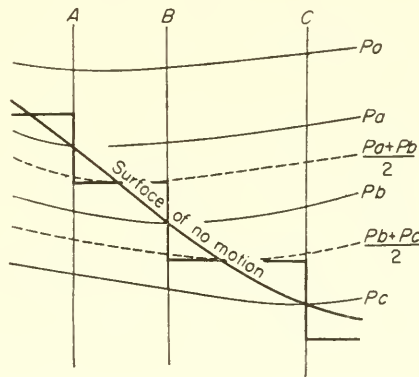


FIG. 230. To the method of transforming relative into absolute dynamic topographies.

If the stations are sufficiently close to each other, the dynamic reference level can as an approximation be broken up into a step wise course. Along the section from A to B the mean pressure will be given by

$$p_{a, b} = \frac{1}{2}(p_a + p_b)$$

and that between C and D by

$$p_{b, c} = \frac{1}{2}(p_b + p_c).$$

The dynamic height differences δ_a and δ_b of the isobaric surface p_0 over the mean reference level can be determined in the usual way for stations A and B , as well as the differences in dynamic height δ'_b and δ_c of the isobaric surface p_0 above the reference-level between B and C . Then $\delta_a + \delta_b$ and $\delta_a + \delta'_b + \delta_c$ are the vertical deviations of the isobar p_0 from the level surface, running through the point A . The conversion can thus be made quite simply for dynamic sections. If the stations are distributed over a larger oceanic region, then the condition has to be satisfied that the absolute values calculated along different paths (sections) must lead to the same value. DEFANT (1941 b) has developed a triangle method which has been found very useful in the determination of the absolute topography of the Atlantic Ocean from a large network

of stations. However, it requires laborious calculations since the errors occurring with each triangle computation, although not large, must be eliminated by a smoothing technique from triangle to triangle. Neumann has in some way modified this method for practical use by taking all stations with the same reference level depth together, thus obtaining a series of pairs of stations with constant reference level depth. For these, however, the previous simple procedure is applicable. To connect one series of station pairs to the next requires only one station triangle, and this can be selected in the most favourable position where the triangle errors are small. In this way each station series can rapidly be connected to the next with minimum error thus overcoming the difficulties otherwise occurring for a varying depth of the reference level.

(c) *Consideration of Stations in Shallow Waters*

In shallow parts of the sea the reference-level is usually found below the sea bottom and the method described above can no more be used. It is, however, desirable to know the absolute topography of the pressure surfaces in these shallow waters also, especially as the most intense currents are often found here. JACOBSEN and JENSEN (1926), as well as HELLAND HANSEN (1934), have devised methods for calculation in this case. It is necessary to preassume for these that the internal friction can be left out of consideration, and the velocities as well as the horizontal pressure gradients at the sea bottom should be zero. The method proposed by Helland-Hansen is based on the following reasoning:

Figure 231 shows a dynamic section starting at a coastal point *E* across a shelf containing station *D*, *C*, *B* and ending at station *A* out in deep water. The thin lines are

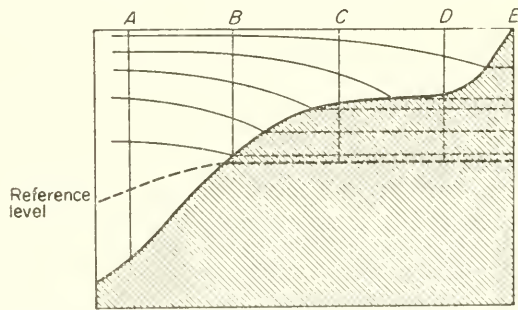


FIG. 231. To the method of fitting shelf stations together with deep-sea stations.

isosteres. In the sea between *A* and *B* the dynamic reference-level runs along the thick dashed line. In the shelf area *BCD* the depth of the sea is less than the depth of the reference-level in the deep water. In order to obtain the deviations of the dynamic topographies of the isobaric surfaces we can imagine for the shallow part a fictive vertical section from *B* to *D* below the level of the sea bottom, assuming the velocities to be zero at the sea bottom. The isosteres in this imaginary section are horizontal and therefore there is no motion in this part. The actual movements in the real section and that in its imaginary extension will thus be the same. The latter can, however, be used to extend the topography of the pressure surfaces above the shelf as far as the coast.

In the method presented by Jacobsen and Jensen, further assumptions are added to those used before which simplify matters even more. A and B (Fig. 232) are two stations at which observations are available down to the bottom. The depth at B is greater than at A and the difference in the physical sea level between A and B has to be found. A_0 and B_0 are the points on the sea bottom at the stations A and B and

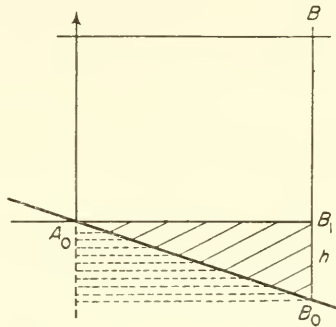


FIG. 232.

A_0B_1 shall be a level line ("Niveaulinie"). The dynamic height difference B_0B_1 is denoted by h and the specific volumes at A_0 and B_1 by $\alpha_{A,0}$ and $\alpha_{B,1}$. Provided that:

- (1) the sea bottom A_0B_0 is linear in the vertical section and
- (2) within the triangular section $A_0B_0B_1$ the mass field is linear and the isosteres are therefore straight, equidistant and parallel lines and
- (3) the pressure gradient vanishes at the bottom.

Then a simple integration method enables the required level difference to be calculated by first calculating the difference in sea level between A and B , on the assumption that the pressures at A_0 and B_1 are the same, and then adding the correction term $\frac{1}{2}h(\alpha_{B,1} - \alpha_{A,0})$. EKMAN (1939) has shown that the method of Helland-Hansen leads to exactly the same correction term. Both methods require that not only the current velocity but also the horizontal pressure gradient should vanish at the sea bottom. The first condition is satisfied because of the bottom friction, but the second is in many cases a rather doubtful assumption, since considerable density differences sometimes appear in both vertical and horizontal directions, at the shelf bottom. Before applying the method it is thus first necessary to ascertain whether the presumptions are approximately satisfied or not. The method of Jacobsen and Jensen is simpler for use and less time consuming than that of Helland-Hansen and requires also less complete data.

A third method has been suggested by SVERDRUP and co-workers (1942, p. 451). They postulate below the sea bottom an imaginary water body in which the specific volume α (or its anomaly δ) and the slope of the isosteres is given at each depth by the corresponding value on the continental slope. It is easily shown that the slope of an isobaric surface p_1 relative to that of p_2 can be computed approximately from the simple equation $i_p = -\bar{i}_\delta(\delta_1 - \delta_2)$, where \bar{i}_δ is the mean slope of the δ -lines between p_1 and p_2 ; δ_1 and δ_2 are the specific volume anomalies at points 1 and 2. The mass distribution in the imaginary water body then gives the pressure distribution, and the

method thus avoids the difficulty that the horizontal pressure gradient should vanish at the bottom. GROEN (1948) has somewhat modified this method by assuming that *only* the slope of the isosteres in the imaginary water body is identical at each depth with that at the bottom slope. The values of the anomaly at the bottom slope and the distribution of the slopes over the entire space completely determine, however, the entire distribution of the specific volume. No special assumption about the distribution of δ is required. The difference from the previous assumption cannot be very large but the method is more correct. Therefore, all the methods described here give results which essentially do not differ from each other.

7. Remarks About the Observational Material Necessary for a Dynamic Computation and Critical Discussion of the Procedure

In order to understand the importance of the absolute topographies of the isobaric surfaces it must be realized that a knowledge of these allows a complete evaluation of the field of motion at individual depths. The current vectors parallel in this field the isohypses of the pressure surfaces, and the velocities are inversely proportional to the distances between them as well as to the sine of the latitude. In the Northern Hemisphere for an observer looking downwards along the slope of the pressure surfaces (Fig. 233) the current will flow to the right. A practical formula for the numerical evaluation of topographies is

$$v = \frac{10}{2\omega \sin \phi} \frac{\Delta D}{\Delta n} \quad (\text{XV.26})$$

from which v is obtained in m/sec if ΔD is entered in dynamic metres and Δn in ordinary metres.

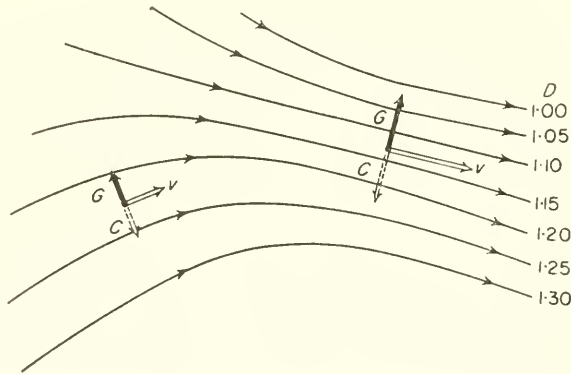


FIG. 233. Schematic representation of an absolute dynamic topography with the corresponding velocities and diagrams of forces (G , gradient force; C , Coriolis force).

The following prerequisites for the use of this formula should be borne in mind:

- (1) the topographical charts must approximate the actual state within the particular oceanic area at a definite time as accurately as possible,
- (2) the currents must be steady,
- (3) it must be possible to disregard the effect of friction.

At the present time this dynamic method of computation is used extensively everywhere. It is used particularly for the dynamic evaluation of widely varying vertical profiles and gives information on the water displacements at right angles to the profile. The scientific treatment of observational data cannot be considered complete if it does not include dynamic methods. Few complete evaluations exist at present of the relative and absolute topographies of the isobaric surfaces for larger oceanic regions. The available data is in most cases insufficient for this, since it requires a reasonably uniform network of stations over a rather extensive area. Of surveys of this type which have been made may be mentioned: the regular series observations of the International Ice Patrol Service near the Newfoundland Banks; those made by the "Marion" and "General Green" expeditions in Davis Strait and the Labrador Sea by Smith, Soule and Mosby; in the eastern North Atlantic by Helland-Hansen and Nansen; in the Caribbean Sea and the Cayman Sea by Parr; in the Antarctic Ocean by Deacon; in the Gulf Stream area by Iselin and Dietrich; in the area off the Californian coast by the Scripps Oceanographic Institution La Jolla and in the area east of Japan. A complete dynamic evaluation of the observational material accumulated for the whole of the Atlantic is given in the "Meteor" report. The results of these surveys will be discussed later in connection with the flow conditions in individual oceans.

The observational data for investigations of this type must satisfy certain demands. In the first place they must be as *homogeneous* as possible and this can only be achieved by a collection of the data according to uniform principles, and by a critical dynamic evaluation using standard methods. Strictly speaking, the data should be collected synoptically, but this cannot be done by expeditions using only a single vessel. For larger oceanic areas it is customary, if there are no pronounced seasonal variations in the current conditions, to combine all the available series observations and consciously abandon the ideal of simultaneous observations. It lies in the nature of such a procedure that a representation of the phenomena in this way cannot, of course, show individual details and the resulting charts only contain the main features. Repetition of such surveys in the same area shows to what extent the topography remains stationary. More importance will certainly be attached in the future to the need for simultaneous synoptic observations. This, however, will require a greater number of oceanographic vessels doing survey work in groups at the same time, or simultaneous recording instruments put out into the open ocean to form a synoptic network to be collected later.

Observational data, as well as being homogeneous and synoptic should satisfy a further requirement which is equally not easy to fulfil. This is the *density in the station network* necessary for each oceanographic survey. If only the major features of the phenomena are required, then the interval between stations customary for oceanographic expeditions (50–150 nautical miles) seems to be sufficient. Data collected on this basis will not give refined details—neither in the distribution of the oceanographic factors nor in topographic charts. It also will give no idea of differences between small oceanic areas. It is, however, difficult to specify just how dense the network of stations should be in order to obtain a *representative picture* of oceanographic conditions. These questions are closely connected with changes in the oceanographic factors with time and it is obvious that these variations cannot be studied by a *single* oceanographic vessel alone. These essential questions of oceanography were dealt with in detail by

HELLAND-HANSEN (1939) and others. The surveys made in the southern part of the Norwegian Sea during June/July 1935 (station interval 20 nautical miles) and June/July 1936 (station interval 10 nautical miles) have shown strikingly large changes in the appearance of different water types which must be due to both, to changes in time and to local variations over short distances. In most cases they could be most probably related to stationary, and in some cases also to progressive vortices. Such disturbances are apparently characteristic of many more intense ocean currents in which there may be waves and vortices of larger dimensions.

As in the Norwegian Sea, large and regular local variations, as well as variations in time of the different oceanic factors, will also be present in the open ocean, especially in the upper layers, and for larger distances between the stations these can introduce an unpleasant degree of uncertainty for the dynamic preparation of the data. Only by this can it be understood why discrepancies between the results of different investigators for a particular area occur and why representations of the same oceanic region often deviate widely from each other. Helland-Hansen has presented an instructive schematic example showing how difficult conditions may be.

Figure 234 shows two neighbouring profiles *I* and *II* through a strong current taken at two different times *A* and *B*. The vertical lines represent the position of the stations on

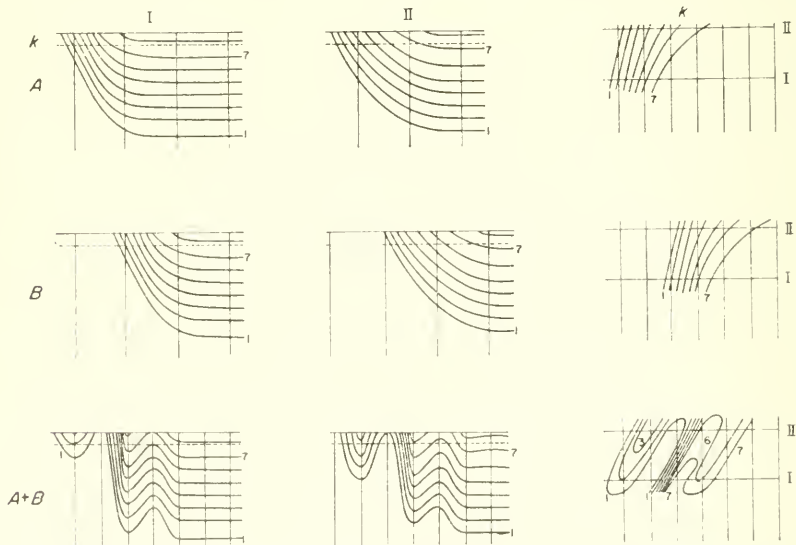


FIG. 234. To the critical discussion of a joint scientific use of observational data, which are gained in a non-synoptical way.

which the profiles are based, which were different in both cases. In the first survey (*A*) the horizontal section at a level *k* was obtained directly from the vertical profiles. The curves represent isotherms, isosteres or similar curves. Below this are shown the conditions of the second survey (*B*). Thus it is assumed that the current was the same during both surveys, but that at the time of the second survey it had been displaced relative to the first survey somewhat to the right. In an oceanographic survey in the

open sea it is either entirely impossible, or possible only with great loss of time, to place a station in exactly the same position as in a previous survey. The assumption in the figure, that the stations of survey *B* are halfway between those of survey *A*, is probably exaggerating matters a little. Since the conditions have apparently not essentially changed, it seems to be justifiable in spite of the rather wide distance between the stations to combine the data from both surveys as has been done below. However, the conclusions drawn from this section are obviously erroneous. For a large station network conditions may be the same, even in the absence of variations in time, when dealing with a single oceanic area where large local differences are present (stationary vortices, strong deflections of the current and others). In such cases (macro-turbulence of the flow) only a dense network of more or less synoptic character would then result in a correct picture of the oceanographic conditions.

There are an additional number of sources for errors in the calculation of topographies that should be mentioned here. In the usual calculation of dynamic depths at fixed standard pressures one proceeds according to equation (IX.9), so that the values of the specific volume α found at certain depths (given in metres) were actually found at depth (given in decibars). At the same time the integral values of p are put equal to the depths given in ordinary metres. The integral expressions for the dynamic depths D will thus be about 1% (or at the most 2%) too small. A further error results from the uncertainty in the α -values, especially in the upper layers, due to errors in depth in series measurements when there is a large vertical gradient in α . Proof can be given that an error ϵ_n in α at a depth h_n will give rise to an error δ_n in D which can be calculated from the equation

$$\delta_n = \epsilon_n \frac{h_{n+1} - h_{n-1}}{2},$$

where h_{n+1} and h_{n-1} are the observed depths immediately above and below h_n ; if the error at all depths is equal to ϵ then the total error in D will be $\delta_n = \epsilon h$, where h is the total depth of D . In general, these errors are not large, and they can be avoided by calculation of a second approximation but this is rarely done. PARR (1936, 1938 *b*) has given an emphatic warning against uncritical use of the dynamic methods and has pointed out that no more can be expected of these than their simple assumptions permit. The calculations are seldom so accurate that the stream lines obtained can be regarded as actual trajectories as should be the case for steady currents. The stream lines determined by the dynamic method are connected only with a single isobaric surface and this may also give rise to erroneous conclusions. In reality they are not subject to this constraint. Vertical displacements are also possible. This plays probably a role in areas of upwelling water.

Another circumstance is of much greater importance. The oceanic structure at stations where there are strong vertical density gradients depends on the occurrence of *internal waves*. With these the water masses in a water column are displaced in a periodic way and these periodic variations in oceanic structure will show in the dynamic evaluations made for that station. The magnitude of such effects can be judged upon at anchor stations, where repetitions of series observations at short intervals are made. Dietrich has calculated an example of this type (Table 137, "Meteor" anchor station no. 197, series 9). During the period of the measurements the physical

Table 137. Extreme positions of the isobaric surfaces at the "Meteor" St. 197 (8.7° S., 16.6° W.); for comparison "Meteor" St. 198 (9.0° S., 19.8° W.) (reference-level at 3000 decibars)

Pressure (dbar)	Anchor St. "Meteor" 197		Difference (dyn. cm)	"Meteor" St. 198 (dyn. cm)
	Maximum position (dyn. cm)	Minimum position (dyn. cm)		
0	226	216	10	224
50	209	199	10	206
100	193	184	9	190
150	182	174	8	179
200	174	167	7	171
300	161	155	6	159
500	139	135	5	138
1000	97	94	3	97
1000	44	42	2	44
2500	21	21	0	22
3000	0	0	0	0

sea level showed displacements of about 10 dynamic cm and even at 1000 m the variation was still about 3.2 dynamic cm. Similar calculations have been made by SEIWELL (1932) for an "Atlantis" station to the north-west of Bermuda. These show a displacement not only of the absolute position of the pressure surfaces but also the horizontal pressure gradient is influenced. Comparison with the neighbouring "Meteor" St. 198 shows the magnitude of such variations in the pressure gradient due to the passage of internal waves, unless these are only simulated. It is therefore not surprising that the dynamic topographies remote from strong currents can be very confused and only can be looked upon with utmost caution and criticism.

8. The Determination of Water Transport in Density Currents

The methods of topographical cartography of the isobaric surfaces allows an insight, with the limitations discussed in the previous section, into the structure of a density current, and when the pure drift and gradient currents are added, a complete picture is obtained of the *Ekman "elementar" current* at any particular place. In many cases it will scarcely be possible to give accurate details about each of the constituents of the "elementar" current and the complete current structure will be so complicated that it can only be shown graphically or by means of numerical tables. Even a less detailed knowledge of the current conditions would be of considerable value. EKMAN (1929), by calculation of the *current transport of a convection current*, first showed the possibility of obtaining information on the *total mass of water carried by a current* in a relatively simple way without investigating the individual layers. He was thereby able to show that this method of calculating the mass transport is entirely independent of any arbitrary assumptions about friction, which seems to be

particularly valuable since this is not the case of the individual constituents of the "elementar" current.

(a) *Volume and Mass Transport*

If the action of the wind at the sea surface producing a drift current almost independent on the mass structure is disregarded, then the "elementar" current according to Ekman (see p. 413) is made up of a pure *gradient current* and a *density current*. The gradient current depends only on the slope of the physical sea level and, if the bottom layer is disregarded, represents a flow in geostrophic balance independent on the depth (equation X.4), while the density current depends only on the distribution of mass in the interior of the ocean. This mass distribution allows to evaluate the *relative* vertical velocity distribution in the density current (equations XV.7 and 12). The *total* vertical pressure distribution in the ocean equally is composed of two parts. The first one originates from the slope of the physical sea level and is independent on the depth. If the deviation of the sea level from its equilibrium position (level surface) is denoted by ζ (positive upwards), then the resultant pressure disturbance will be $\Delta p = g\rho\zeta$. The second part p_i originates from the mass distribution in the interior of the sea so that $p = p_i + \Delta p$.

For a steady frictionless state the equations of motion will be

$$u = -\frac{\alpha}{f} \frac{\partial p_i}{\partial y} + U \quad \text{and} \quad v = \frac{\alpha}{f} \frac{\partial p_i}{\partial x} + V, \quad (\text{XV.16})$$

where U and V are the components of the geostrophic current (equation XIII.4). The first term on the right-hand side in these equations gives the density current which will have velocity components

$$u_i = -\frac{\alpha}{f} \frac{\partial p_i}{\partial y} \quad \text{and} \quad v_i = \frac{\alpha}{f} \frac{\partial p_i}{\partial x}. \quad (\text{XV.17})$$

Introducing instead of pressure the dynamic depth of the isobaric surfaces D , according to (IX.8), and taking into consideration that the unit of the potential is $-10 D$ (equation IX.4), then one obtains from

$$u_i = \frac{10}{f} \frac{\partial D}{\partial y} \quad \text{and} \quad v_i = -\frac{10}{f} \frac{\partial D}{\partial x}, \quad (\text{XV.18})$$

whereby D can also be replaced by the anomaly of the dynamic depth. The volume transport in a horizontal flow is given by

$$S_x = \int_0^d u \, dz \quad \text{and} \quad S_y = \int_0^d v \, dz \quad (\text{XV.19})$$

and the mass transport by the components

$$M_x = \int_0^d \rho u \, dz \quad \text{and} \quad M_y = \int_0^d \rho v \, dz, \quad (\text{XV.20})$$

where d is the depth of the sea. The corresponding quantities for the pure gradient current can be written down immediately since it is independent on the depth. The

volume transport of the density current can be determined from (XV.18), if the vertical mass distribution is known. One obtains

$$S_x = \frac{10}{f} \int_0^d \frac{\partial \Delta D}{\partial y} dz \quad \text{and} \quad S_y = -\frac{10}{f} \int_0^d \frac{\partial \Delta D}{\partial x} dz \quad (\text{XV.21})$$

Using the equation defining D (equation IX.9) a quantity

$$Q = \int_0^d \int_0^p \delta dp dz \quad (\text{XV.22})$$

can be introduced in equations (XV.21) giving

$$S_x = \frac{10}{f} \frac{\partial Q}{\partial y} \quad \text{and} \quad S_y = -\frac{10}{f} \frac{\partial Q}{\partial x}. \quad (\text{XV.23})$$

Since the anomalies of the dynamic depths of the isobaric surfaces are always calculated when evaluating observational data, it is always possible to obtain the volume transport of the density current without difficulty.

A determination of the mass transport of the density current is considerably more difficult. The first theoretical calculations of this type were made by EKMAN (1929) who has given later (1939) a detailed and extensive account of this and of the related problems. He obtained also formulae similar to (XV.22) but rather more difficult to evaluate; it involves the pressures at given dynamic depths which are usually not calculated during the dynamic preparation of observational data. Since the mass transport can be obtained with sufficient accuracy from the volume transport by multiplication with the mean density, it is not necessary to calculate it independently. Calculations of the volume transport and the introduction of the quantity Q have been done by JAKHELIN (1936). For the practical application of the equations (XV.21 and 22), p has to be taken in decibars and the depth d in metres which both can be expressed approximately in the usual way by the same figures. This inaccuracy leads to values of Q which, as was shown by Jakhelin, are systematically about 1% too low. Although the errors are small, it is nevertheless desirable to apply a correction for this to the calculated values. The volume transport between two stations A and B (B to the right of A at a distance L) is thus finally

$$S = L \int_0^d v dz = \frac{10}{f} \int_0^d (\Delta D_A - \Delta D_B) dz. \quad (\text{XV.24})$$

It depends only on the dynamic depth anomaly at the two stations and is independent of the distance between them. In this way it is also independent of the mass distribution within this space. Lines of equal Q can be drawn for any larger area. Their direction gives the direction of the volume transport and their spacing at any point is proportional to the volume transport. This proportionality factor, however, depends on the latitude. The same "current amount" does not flow everywhere between each pair of Q -lines; for a current towards the north and south the transport in the flow direction will decrease and increase respectively.

For more extensive oceanic areas this dependence on the latitude cannot be neglected. Attempts to show the changes in transport with latitude directly on a transport chart,

by drawing isolines of the quantity $Q/(\sin \phi)$ instead of the Q -lines, are based on incorrect reasoning because lines obtained in this way are then no longer stream lines; they will be intersected by the flow and thus lose their meaning. It is therefore better to retain the Q -lines (THORADE, 1937 *b*). Volume transport charts over more extended oceanic areas have not yet been prepared, although the complete dynamical evaluation of the observational data for such an undertaking would be available.

(b) Water Transport in Coastal Currents

WERENSKIOLD (1935, 1937) has presented a very convenient method for the calculation of the volume transport in coastal currents, for which, in a cross-section at right angles to the coast, a lighter water is spreading out in a wedge-form on top of a heavier slowly moving and almost homogeneous water. Figure 235 shows a vertical section across a current between two stations A and B . The x -axis is placed in the sea surface in the

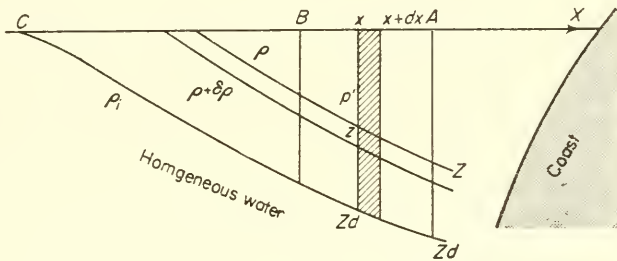


FIG. 235. To the computation of the water transport in a coastal current (according to Werenskjold).

direction $A \rightarrow B$ and the water depth is denoted by z . In the section there are drawn two isopycnals ρ and $\rho + \delta\rho$ and two plumb-lines x and $x + dx$. The boundary surface of the wedge-shaped top layer forms the isopycnal ρ_i reaching the surface at C . The top-layer has a depth z_a at point x , however, the depth Z_a at the station A . At an arbitrary point M on one of the plumb-lines (density ρ) the component of the velocity of the density current at right angles to the section will given by the equation (VII.8):

$$v_i = \frac{g}{f\rho_m} \int_{\rho}^{\rho_i} j \, d\rho.$$

Thereby j is the slope of the isopycnal which is dependent on x and z . Denoting $g/f\rho_m$ by b , then one obtains from the relation above

$$\frac{dv_i}{d\rho} = -bj = -b \frac{dz}{dx}, \tag{XV.25}$$

where the derivative dz/dx has to be taken along an isopycnal, that is, for a constant ρ . The volume transport at a plumb-line can then be obtained by integration from 0 to z_a . By partial integration one obtains

$$S = \int_0^{z_a} v_i \, dz = \left(v_i z \right)_0^{z_a} - \int_0^{z_a} z \, dv_i.$$

The first expression on the right-hand side is zero, since $v_i = 0$ for z_d and thus using (XV.25) one obtains

$$S = b \int_{\rho_0}^{\rho_i} z \frac{dz}{dx} d\rho = \frac{b}{2} \int_{\rho_0}^{\rho_i} \frac{dz^2}{dx} d\rho.$$

ρ_0 is the density at the sea surface. The total volume transport through the entire top layer from C to station A is thus finally obtained by integration from x_c to x_A

$$S_t = \int_{x_c}^{x_A} S dx = \frac{b}{2} \int_{x_c}^{x_A} \int_{\rho_0}^{\rho_i} \frac{dz^2}{dx} d\rho.$$

The integral of $(dz^2/dx) dx$ is equal to Z^2 where Z is the depth of the isopycnal at the station A . Finally, on repeating the partial integration, since Z is zero at the sea surface, we have

$$S_t = \frac{g}{2f} \int_0^{Z_d^2} \frac{\rho_i - \rho}{\rho_m} dZ^2. \quad (\text{XV.26})$$

If the transport between two arbitrary verticals A and B is required, then the expressions (XV.26) are evaluated at both places and the difference is taken. The water transports obtained in this way are subject to the same limitations for the quantity Q . It is noticeable that a knowledge of the mass structure at the two stations is sufficient for the determination of the transport through the vertical section between them, without having a knowledge of the distance between the two stations. Werenskiold offered an explanation for this fact by pointing out that the flux in horizontal direction through the section is unaffected by stretching or shrinking of part of this section, because the pressure gradient and therefore also the current intensity are changed inversely proportional to the current width, and the distance between the two stations is eliminated. It seems, therefore, that only the mass distribution of a *single* station is required in order to calculate the transport through a vertical section by means of equations (XV.26). However, this is not true at all since a knowledge of the stratification at two stations C and A is required and, furthermore, the water at C is homogeneous and has the same density as the deep water at A .

Since the integration of equation (XV.26) is performed using ordinary metres, the correction required previously for Q is not needed here.

Chapter XVI

Currents in a Strait

1. Water Stratification and Water Movements in Sea Straits

SEA straits connect the open ocean with mediterranean and adjacent seas. By means of the water flux through the connecting straits directed towards the open ocean a mediterranean sea can often produce considerable effects on the oceanographic conditions in the open ocean. This influence is sometimes so powerful as to involve entire parts of an ocean, changing drastically the oceanic conditions in these parts. Present knowledge of oceanographic conditions in sea straits is only partly satisfactory. The main outlines and the typical features are known but much remains to be explained especially in the details, that will require systematically arranged observations and measurements.

The continuous interchange of water between mediterranean and adjacent seas which are completely surrounded by land and the open ocean is controlled very largely by two factors:

- (1) by the proportion between fresh-water inflow (precipitation and run off (river water and other water)) and evaporation in the mediterranean sea, and
- (2) by the depth and width of the passage to the open ocean, that is, the morphology of the sea strait.

The currents in a sea strait are a consequence of the difference in vertical thermo-haline stratification between the water masses in the adjacent sea and that of the open ocean off the entrance to the strait.

Sea straits can be divided on the basis of the currents flowing in them into two groups:

(1) Those in which the adjacent sea is surrounded by *arid* land masses. Here evaporation exceeds precipitation ($E - P > 0$). The loss of water due to this excess must be replaced from the open ocean through the strait.

(2) If the entire oceanic area lies in a humid climate ($E - P < 0$), then the excess of precipitation over run-off will flow out into the ocean through the connecting strait.

To the first group belong—inside the area of the Eastern Hemisphere rich in evaporation and with little precipitation—the *Strait of Gibraltar*, connecting the Atlantic with the high-salinity European Mediterranean; the *Strait of Bab el Mandeb*, connecting the Indian Ocean (Gulf of Aden) with the highly saline Red Sea and the *Strait of Hormuz* between the Arabian Sea (Gulf of Oman) and the Persian Gulf.

To the second group belong—in the northern humid region—the weakly saline Baltic Sea which is connected by way of *narrow belts and Sounds* through the *Kattegat* and the shelf-like North Sea with the open ocean; the predominantly humid Black Sea connected with the arid Mediterranean through the *Bosporus* and the *Dardanelles*;

the White Sea and the Barents Sea with the so-called *Gorlo* and the Gulf of St Lawrence connected with the Atlantic by the *Cabot Strait* and others.

The interchange currents in all these sea straits occur characteristically on *two different levels*; there are always two currents in the strait, one above the other. The upper layer always flows toward the sea having greater density, the lower layer in the opposite direction, and between them there is usually a well-developed discontinuity layer in the density field (see Pt. I, pp. 133 and 182–184 (Figs. 56, 83–85) on the general distribution of temperature and salinity in sea straits). Thus in straits of moderate width there are always two water bodies one above the other with a boundary layer between them sloping down from the sea with the greater density towards that with the lesser. *The wedge-form of these superimposed water layers along the strait* is a characteristic feature of the structure of the water masses in a sea strait. Table 138 gives a summary of mean density in the upper and lower water layer and of the slope of the boundary layer for some sea straits in different climatic regions (VERCELLI, 1929; MÖLLER, 1931). The greater the slope the smaller the density difference, i.e., the slower the interchange movements. In addition to this effect of the density differences other circumstances also control the slope of the boundary layer, particularly the bottom topography of the sea strait, because it affects the continuity requirement of a complete balance between the mass transport in the upper and lower current under stationary conditions. For example, in the Bosphorus, the slope of the boundary layer is strongly dependent on the bottom inclination and because of this the wedge-form character of the lower water is lost there.

Table 138. Mean slopes of the boundary layer and mean densities of the upper and lower water in several sea straits

Sea strait	Mean width (km)	Mean length (km)	Minimum depth (m)	Boundary layer slope (m/km)	Mean density		Difference
					Upper water	Lower water	
Danish sounds (Belts)	ca. 20	ca. 100	6.9	0.12	13.5	23.5	10.0
Dardanelles	4.5	60	57	0.20	18.0	28.8	10.8
Bosphorus	0.7	30	37	1.13	13.5	27.5	14.0
Gibraltar	20	60	333	4.2	26.8	28.8	2.0
Bab el Mandeb	—	134	185	3.0	25.9	27.4	1.5

Besides this longitudinal slope there should also be a *transverse slope* of the boundary layer due to the effect of the Coriolis force. The faster the currents and the wider the strait the greater will this slope be. If the upper homogeneous water mass in the strait has a velocity u_1 and the lower one a velocity u_2 , and if the transverse inclination of the sea surface is given by $\partial\zeta_1/\partial y$ and that of the boundary surface between the upper and the lower current by $\partial\zeta_2/\partial y$, then, under stationary conditions the equations

$$g \frac{\partial\zeta_1}{\partial y} = -fu_1 \quad \text{and} \quad g \frac{\partial\zeta_2}{\partial y} = -f \frac{\rho_2 u_2 - \rho_1 u_1}{\rho_2 - \rho_1} \quad (\text{XVI.1})$$

will be valid where ($f = 2\omega \sin \phi$).

In Fig. 236 which shows a cross-section through the strait, u_1 (upper current) is positive and u_2 (lower current) is negative, and as a consequence the sea surface rises to the right while the boundary surface between the two water types slopes downward to the right. This latter inclination is considerably steeper than the first. For a certain definite velocity u_1 the water mass of the upper current may be too small to cover,

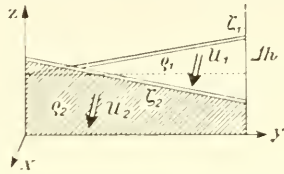


FIG. 236. A model in order to study the thermo-haline circulation in sea straits.

during its displacement to the right, the whole of the lower water mass. Choosing in equation (XVI.1)

$$\frac{\partial \zeta_2}{\partial y} = \frac{\Delta h}{L} = -\frac{f}{g} u_1, \tag{XVI.2}$$

$f = 10^{-4}$, $g = 1000$ and $u_1 = 100$ cm/sec, then $\Delta h = 10^{-5} \times L$, where Δh is the elevation of the water level for a given width L of the strait. For the Dardanelles $L = 5$ km and therefore Δh is 5 cm; in the Strait of Gibraltar $L = 20$ km and Δh is 20 cm. The latter value is already quite large. For quite a large width of the strait the inclination may be so steep that in a narrow strip along the coast the opposite moving heavier water may rise to the surface, so that in the strait at the sea surface there will be a front with currents flowing in opposite directions on either side. In narrower straits transverse slopes of this sort will be barely detectable.

The internal structure of both water bodies is usually stratified; however, this stratification is only slight in salinity, but at time it may be pronounced in the temperature. In all cases in low-salinity seas where the access depth to the strait is deeper than the discontinuity layer, due to increased radiation in summer, a *temperature inversion* will be formed within the upper current with a minimum above the boundary surface; below this in the lower water a secondary maximum appears and then the temperature will decrease again to the bottom value. Figure 237 shows two vertical temperature and salinity curves of this type for the northern parts of the Bosphorus. The temperature minima always decrease in the direction of the surface current due to the effect of mixing.

The discontinuity layer in the salinity remains fairly sharp along the total length of the strait, though in each of the water bodies the absolute values will change somewhat due to mixing: in the upper water body the salinity will therefore usually increase and in the lower it will decrease. The changes in the Bosphorus and the Dardanelles are thus over 300 km about 10‰. Similar values have been found in the Danish sounds (Belts). The greatest changes are, of course, usually found where there are large irregularities in the bottom topography where eddies and vortices are generated.

As a further characteristic phenomenon found in sea straits the boundary layer between the water bodies often does not coincide with the level of reversal of the

current direction (level of no-horizontal motion). The latter surface can be found either above or below the boundary layer between the two water bodies, but the height-difference is never large. This phenomenon has been observed in the Bosphorus, the Dardanelles and in the Strait of Gibraltar. As has been shown theoretically (NOMITSU, 1927) the two layers can coincide only when the water bodies are completely homogeneous. Deviations from such a state are due to mixing processes occurring at the boundary surface between the two oppositely moving currents.

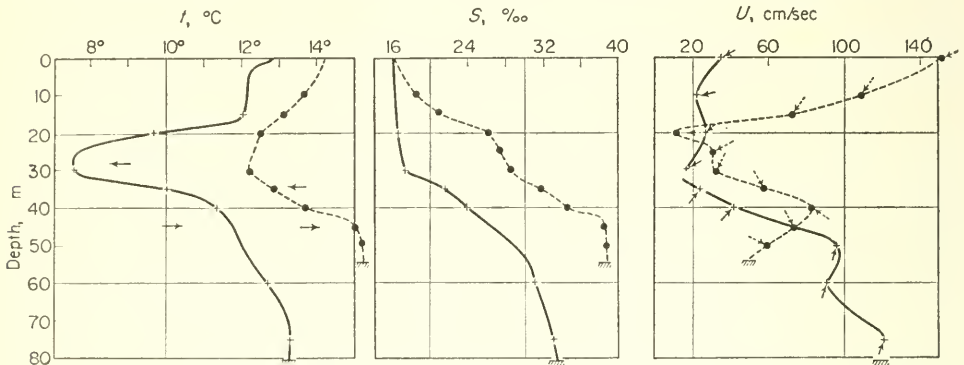


FIG. 237. Vertical curves of temperature, of salinity and of the current for always a single station in the northern and southern Bosphorus. *Full lines*: station 110 in the section Karibdian Burnu–Porias Burnu, 12 May 1918. *Dashed lines*: station 123 in the section Orta Köi–Istawros, 23 May 1918. At the current curves the arrows in the current are situated such that: west, towards left; east, towards right.

The currents within a strait are completely known only in the Bosphorus and in the Dardanelles where accurate *current profiles* have been obtained by Merz (MÖLLER, 1928). For other sea straits current measurements have been made for short time intervals only and at few stations. In general, the greatest velocity in the upper current is found close to the sea surface. In a cross-section the current distribution corresponds to that of a river in which the lines of equal velocity (isotachs) follow approximately the river bed. Due to the wedge-form of the upper water body the velocity increases in the direction of the current (in the Bosphorus and in the Dardanelles from 50 to 150 cm/sec). The transition from the upper to the lower current does not occur discontinuously but increases in sharpness as the density jump becomes greater. This phenomenon is also due to the turbulence of the current, which is strongly suppressed when there is a large density discontinuity in the vertical. When the depth of the water is not too great the lower current follows the bottom topography of the sea strait, and therefore the cores of the upper and the lower current need not lie exactly above each other. The vertical current distribution in the lower current shows a maximum in its central core situated about half way between the current reversal layer and the bottom. For continuity reasons a decrease in velocity occurs in the lower current if the depth increases along the strait; however, if the depth decreases there will be a corresponding increase in velocity. At the bottom the velocity may be so intense that it causes considerable erosion. The occurrence of rolls in a depression of the sea bottom (Kolke, deep hole) may simulate a decrease of the velocity to zero near the bottom (see p. 390).

A special phenomenon found in the current systems in irregular shaped straits is the occurrence of *stationary vortices* with vertical axes. They are used with considerable advantage in navigation. In the Bosphorus and in the Dardanelles they are well developed in both surface and bottom currents (Fig. 261). In some cases two stationary vortices are formed side by side with an opposite sense of rotation so that side branches ("neer" currents) develop returning later into the direction of the main current.

Table 142 gives an idea of the very large amounts of water passing through major sea straits. In broad and deep straits, such as the Straits of Gibraltar and Bab el Mandeb, the transport may be 5 to 20 times greater than in narrow shallow straits. Expressing the amount of inflow or outflow by means of water-level change (in mm) of the total Mediterranean, a particularly clear idea of the great difference between the humid and the arid, semi-arid areas, respectively, is obtained.

2. Theory of Currents in Sea Straits

The dynamic cause of currents in sea straits lies in the density difference between the open ocean and the enclosed sea, or more exactly, in the density difference at the level of the bottom of the strait between the entrance to the strait and its outlet. The thermodynamic mechanism inherent in this circulation can be demonstrated by a simple model (DEFANT, 1955) (Fig. 238). In a strait with a depth h limited at ad and

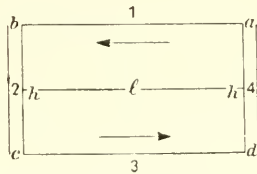


FIG. 238. Cross-section through a rectangular sea strait and its current system.

bc at either end by two water columns belonging respectively to the ocean and the enclosed sea, the system will be made up of horizontal layers of water 1 and 3 between ab and cd , respectively, and vertical columns 2 and 4 between bc and ad , respectively. We assume a stationary state and neglect—because of the narrow strait—the effect of the Coriolis force. The currents which adjust under stationary conditions must be

Table 139. Water transport through sea straits (according to Möller)
(+, current from the adjacent sea; -, current into the adjacent sea)

Sea strait	Upper current (km ³ /year)	Lower current (km ³ /year)	Outflow amount (km ³ /year)	Outflow height (mm)	Adjacent sea	Area (10 ³ km ²)
Danish sounds (Belts)	+304	-152	+152	} +488	Baltic Sea	397
Bosphorus . . .	+398	-193	+205		Black Sea	420
Dardanelles . . .	+591	-386	+205			
Gibraltar . . .	-55198	+51886	-3312	-1330	Europ. Medit.	2496
Bab el Mandeb . . .	-16450	+12800	-3650	-7980	Red Sea	458

solely antitryptic, that is, the pressure and the frictional forces will be in equilibrium (see p. 323). The system will be subject to the equations

$$-\frac{1}{\rho} \frac{\partial p}{\partial x} - R_i = 0 \quad (i = 1 \text{ and } 3) \text{ along } 1 \text{ and } 3 \quad (\text{XVI.3})$$

and

$$g - \frac{1}{\rho} \frac{\partial p}{\partial z} - R_i = 0 \quad (i = 2 \text{ and } 4) \text{ along } 2 \text{ and } 4,$$

where R_i is the effect of friction along each of the sections. Multiplying the equations (XVI.3) by ρ and integrating along the individual sections one obtains, after adding, the relations:

$$g \left(\int_b^c \rho dz + \int_d^a \rho dz - \oint_{abcd} \rho R_i ds \right) = 0, \quad (\text{XVI.4})$$

$$g(\rho_2 - \rho_4)h = \oint_{abcd} \rho R_i ds. \quad (\text{XVI.5})$$

Here ρ_2 and ρ_4 are the *mean* densities in the vertical water columns 2 and 4. All the quantities R_i are positive and depend on the current velocity. From (XVI.5) it follows then that the left-hand side must also be positive. That is, the mean density in bc must be greater than in ab or $\rho_2 > \rho_4$. This relation thus fixes the direction of the current in the strait and also give the dependence of the current velocity on the density distribution in the water masses. This can be used to find an approximate value for the current velocity maintained by the thermodynamic forces acting inside the system. According to the circulation theorem, when $\alpha = 1/\rho$

$$-\oint_{abcd} \alpha dp = \oint_{abcd} R_i ds \quad (\text{XVI.6})$$

and since

$$D_i = \left[\int_0^p \alpha dp \right]_i$$

gives the dynamic depth of the pressure surface p in the water column i , we obtain from (XVI.6)

$$D_4 - D_2 = (R_1 + R_3)l + (R_2 + R_4)h. \quad (\text{XVI.7})$$

The integral $-\int \alpha dp$ is the work done by the pressure forces in the system; if it is positive, this work can thus be balanced by the work required by the friction. The relation (XVI.6) states that, in the thermodynamic machine the expansion takes place at a higher pressure than the contraction. Since an expansion is associated with an input of heat and a contraction is associated with a heat loss, the heat gain must therefore occur at a higher pressure than the heat loss. Actually, in the model of the sea strait in point there will be a higher pressure and a higher temperature, the latter due to a greater heat gain. Such a sea strait system is thus a true thermodynamic machine in action.

The current intensities in a strait can be calculated approximately by means of the above equation (XVI.5). For a channel of length l , if friction is neglected in the vertical part of the circulation, the equation will take the form

$$2\rho Rl = g(\rho_2 - \rho_4)h. \quad (\text{XVI.8})$$

In addition, it is necessary to make an assumption about the dependence of the friction on the current velocity. For a shallow current it is possible to put R equal to $\kappa \rho \bar{u}^2$ dyn/cm² (see equation X.9). However, for each horizontal branch

$$\bar{u} = \frac{\int u \, dz}{\frac{1}{2}h}$$

and the friction per unit mass of this branch is

$$\frac{\kappa \bar{u}^2 \rho}{\rho \frac{1}{2}h} = \frac{2\kappa \bar{u}^2}{h} \tag{XVI.9}$$

The total friction is therefore given by

$$R = \frac{\kappa(2\bar{u})^2}{h}$$

and the equation (XVI.8) thus gives an equation for the determination of the mean velocity in one water body

$$\bar{u}^2 = \frac{1}{8} \frac{gh^2}{\kappa l} \frac{\rho_2 - \rho_1}{\rho} \tag{XVI.10}$$

If the dimensions of the strait are known, \bar{u} can be calculated. Only the value of the Taylor frictional constant requires a little further comment. For a smooth channel κ has been found experimentally to be 0.0025. It cannot be expected that the value of κ will be as small as this because of the irregular configuration of the sea bottom and sides of an actual sea strait. In rivers, for example, κ may be as much as 10 times this value or about 0.03. Considerably higher values of the boundary friction are therefore to be expected due to the roughness of the bottom in a somewhat wider strait. A proof of this is the frequently observed sharp decrease in velocity in the layer next to the bottom.

Choosing mean values for the dimension of a sea strait, for example, $l = 50$ km, $h = 100$ m and the difference in density $\Delta\rho = 10 \times 10^{-3}$, according to Table 140, then putting $\kappa = 0.03$ the equation gives $\bar{u} = 28$ cm/sec which accords with the average velocities found by observation. In the Danish sounds (Belts) the velocity of the current is about 10 cm/sec, in the Dardanelles about 25 cm/sec, in the Bosphorus 30 cm/sec, in the Strait of Gibraltar 30–35 cm/sec and in the Strait of Bab el Mandeb about 40 cm/sec. The calculated value fits thus very well in this series of observed values.

For a detailed theory of currents in sea straits it is necessary in the treatment of the stationary state to return to the antitriptic equations of motion in which the gradient force and all the frictional forces are always in equilibrium (DEFANT, 1930). A suitable model is a rectangular channel, depth h_2 and length L , connecting two seas with different thermo-haline structures. Both water types are homogeneous (upper water density ρ_1 , thickness in the middle of the channel h_1 ; lower water density ρ_2 , thickness in the middle of the channel $h_2 - h_1$ over a plane bottom). The co-ordinate origin is placed in the middle of the channel at sea level with the positive z -axis directed upwards. The upper current flows in the direction of the negative x -axis (see Fig. 239) and the physical sea level must therefore also slope downwards in this direction (pure slope current). The static pressure in the upper layer [z from ζ_1 to $-(h_1 - \zeta_2)$] will be

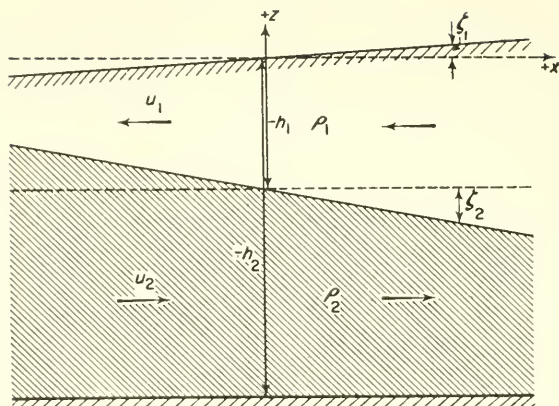


FIG. 239. To the theory of ocean currents in sea straits.

$p_1 = p_0 + g\rho_1(\zeta_1 - z)$, however, in the lower layer [z from $-(h_1 - \zeta_2) - h_2$] will be $p_2 = p_0 + g(\rho_2 - \rho_1)(\zeta_2 - h_1) + g\rho_1\zeta_1 - g\rho_2z$. p_0 is the atmospheric pressure at the sea surface. Putting $p_0 = -g\rho_1\zeta$ then ζ is the displacement of the sea surface produced by an atmospheric pressure p_0 . The equations of motion in the stationary state, disregarding the Coriolis force and friction on the sides of the channel are then

$$-g \frac{\partial}{\partial x} (\zeta_1 - \zeta) + \frac{\eta}{\rho} \frac{\partial^2 u_1}{\partial z^2} = 0, \quad (\text{XVI.11})$$

$$-g \frac{\rho_1}{\rho_2} \frac{\partial}{\partial x} (\zeta_1 - \zeta) - g \frac{\rho_2 - \rho_1}{\rho_2} \frac{\partial \zeta_2}{\partial x} + \frac{\eta}{\rho} \frac{\partial^2 u_2}{\partial z^2} = 0.$$

If ζ_1 and ζ_2 are small compared with the depth of the strait then, for a linear slope of the physical sea level, u_1 and u_2 will be independent of x and the continuity equation will take the simple form

$$\int_0^{-h_1} u_1 dz + \int_{-h_1}^{-h_2} u_2 dz = 0. \quad (\text{XVI.12})$$

The volume transport of the upper current must be equal to that of the lower current. The boundary conditions are as follows:

(1) If there is no wind, $\partial u_1 / \partial z = 0$ when $z = 0$. The effect of a wind along the channel can be taken into account by the assumption

$$\eta \frac{\partial u_1}{\partial z} = \kappa_1 \rho_a w^2,$$

where ρ_a is the density of the air, κ_1 is the Taylor constant (equation X.9) and w is the wind velocity relative to that of the water. Taking $\partial u_1 / \partial z = M$ for $z = 0$ allows the effect of the wind to be taken into account.

(2) At the boundary surface there will be a reversal of the current direction, that is, when $z = -h_1$, then $u_1 = u_2 = 0$ (no horizontal motion).

(3) At the bottom ($z = -h_2$) three different cases of boundary friction can be

considered: adhesion to the bottom $u_2 = 0$, gliding $\partial u_2 / \partial z = 0$ and average frictional influence $\eta(\partial u_2 / \partial z) = \kappa \rho_2 u_2^2$. If the roughness of the sea bottom is slight the factor κ is of the same magnitude as κ_1 ; for a rough bottom it has been found in hydraulics to be about 10 times greater.

Solutions of equation (XVI.11) can be given for all three cases. For the extreme cases of adhering (haften) and gliding (gleiten) and with uniform atmospheric pressure ($\xi = 0$) one obtains

$$\left. \begin{aligned}
 \text{Slope of the physical sea level: } i_1 &= \frac{2\eta}{g\rho_1} a. \\
 \text{Slope of the boundary layer: } i_2 &= -\frac{2\eta}{g\rho_1} \gamma. \\
 \text{Velocity of the upper layer: } u_1 &= a(z^2 - h_1^2) + M(z + h_1). \\
 \text{Velocity of the lower layer:} \\
 \text{adhering: } u_2 &= A(z + h_1)(z + h_2) \quad \text{with } A = -m \left(\frac{h_2}{h_1} - 1\right)^{-3}, \\
 \text{gliding } u_2 &= A[(z^2 - h_1^2) + 2h_2(z + h_1)] \quad \text{with } A = -\frac{m}{4} \left(\frac{h_2}{h_1} - 1\right)^{-3},
 \end{aligned} \right\} \text{(XVI.13)}$$

where

$$\gamma = \frac{\rho_1}{\rho_2 - \rho_1} a \left[1 - \frac{\rho_2}{\rho_1} A \right] \quad \text{and} \quad m = 4a - \frac{3M}{h_1}.$$

Because A is always negative, the slope of the internal boundary surface will always be opposite to that of the sea surface; however, because of the density difference ($\rho_2 - \rho_1$) in the denominator it is always considerably larger. The slope of the boundary surface found by observation is a function of the water interchange between the two seas. The currents in the two water bodies always flow in opposite directions. The current profile in both water bodies is of a parabolic form. In the upper current the maximum occurs at the sea surface; if the wind is in the direction of the upper current it will decrease rapidly with depth, but if the wind is against the upper current the decrease will be small. The upper water in this case will be piled up against the current. If there is a very strong wind at the surface against the upper current, the current maximum may be somewhat below the sea surface. All these theoretical conclusions are in complete agreement with observation. In the lower current the velocity maximum will adjust in variable depth below the boundary surface according to the variable friction at the sea bottom. If there is adhesion it will appear in the middle part of the lower layer, if there is gliding at the bottom it will occur at the bottom itself and for moderate friction it will be situated between the discontinuity surface and sea bottom.

Numerical values corresponding roughly to those for the Bosphorus may be taken as an example: length of the strait = 30 km, depth = 70 m; upper layer $\rho_1 = 1.013$ down to 40 m; lower layer $\rho_2 = 1.027$, $\rho_2 - \rho_1 = 14 \times 10^{-3}$; slope of the physical sea level 6 cm in 30 km, $\eta/\rho = 250 \text{ cm}^2/\text{sec}$, which is about the same as the frictional coefficients for tidal currents; wind = 5 m/sec along the strait. For the slope of the boundary surface (metres in 30 km) the equation gives the values contained in Table 142.

Table 140. Slope of the boundary layer (given in m/30 km)

	For adhering	For gliding	Moderate friction
Wind <i>with</i> the upper current	44	14	33
Wind <i>against</i> the upper current	53	17	37

The magnitude of these values is similar to those actually found in the Bosphorus which average about 34 m. In the case of a south-west wind the slope is steeper than for a north-east wind, which agrees with the theoretical result. Figure 240 shows the

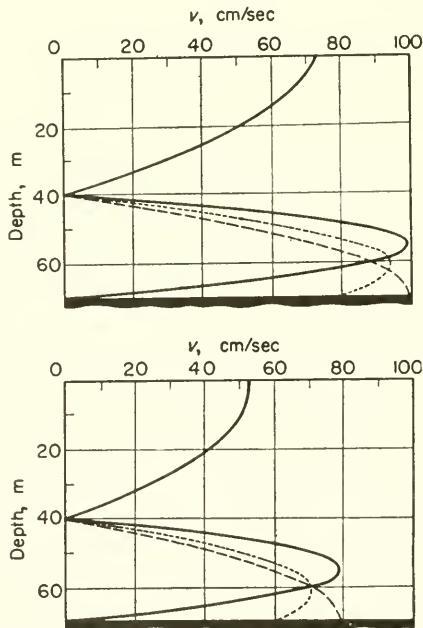


FIG. 240. Vertical current distribution in the upper and lower current for a certain wind direction at the sea surface of the sea strait (in the lower current: ———, in the case of clinging to (Haften); - - - -, in the case of gliding (Gleiten); ·····, for a medium friction of the water at the sea bottom).

current profile in the upper and lower current (omitting signs). These values are also in agreement in all cases with those observed in the Bosphorus and the wind effect was also of a similar kind.

The theory is based on two water bodies that are homogeneous over a cross-section at right angles to the strait. In nature they will be stratified and the cross-sectional area can vary considerably along the length of the strait. Furthermore, mixing at the internal boundary surface will tend to spread the discontinuity surface into a density transition layer. The current boundary surface will then no longer coincide with the lower limit of the upper water since there is no longer any sharp boundary. Then conditions become so complex that they can no longer be handled mathematically.

However, the stratification does not appear to be of decisive importance to the principal phenomena of the water interchange and therefore the simple case of two homogeneous water types gives the essential outlines.

3. Ocean Currents in Individual Sea Straits

(a) *Bosphorus and Dardanelles*

Due to the investigations of MERZ and MÖLLER (1921, 1938, with Atlas) these are the straits in which conditions are best known. Systematic surveys along cross-sections and longitudinal sections have given a good understanding of the three-dimensional thermo-haline structure of the water masses and the corresponding currents in both straits and some insight into the detailed mechanism of the processes involved. Over the whole area of water interchange between the Aegean and the Black Sea there is a characteristic stratification with a sharp density transition layer. From a depth of 200–150 m in the Black Sea it rises at the entrance into the Bosphorus to less than 150 m and in the narrow part it rises rapidly to 20–15 m at Istanbul. It remains at this depth throughout the Marmara Sea until it rises again in the Dardanelles, at first very slowly, then more rapidly in the straits between Nagara and Tschanak to 10 m. At the southern entrance to the Dardanelles it reaches almost to the surface. Figure 241 presents the density distribution in two longitudinal sections along both straits.

The wedge-form of the upper water shows clearly in both straits; in the lower water it is present only in the Dardanelles, since the sea bed in the Bosphorus slopes downwards towards north as much as the internal boundary surface. At the entrance to the Bosphorus the salinity of the upper water is 16–18‰ and at the outlet from the Dardanelles into the Aegean it is 26–28‰. Of this increase 2‰ occurs in the Bosphorus, 5‰ in the Sea of Marmara and 3‰ in the Dardanelles. Mixing in the straits thus cannot be very effective; this is also shown by the maintenance of the *temperature inversion* which is still partly present in the Dardanelles (see Fig. 237).

The *upper current* runs through the channels as a narrow band within limits set by the projections of the coast. In several coastal bays on both sides of the straits numerous standing vortices occur. The current profile shows that the velocity is greatest at the sea surface and decreases rapidly with depth. Due to the wedge-form of the current it increases from north to south; under average conditions it is 40–50 cm/sec at the entrance to the straits and 150 cm/sec or more at the other end.

The *lower current* follows the windings of the channel more closely than the upper current and the stream lines of the two currents are therefore not always superimposed. The lower current is strongest in the central parts of the lower water (in the Bosphorus about 16 m and in the Dardanelles about 45 m above the bottom). The velocity is 100–150 cm/sec in the Bosphorus and decreases from 25 to 10 cm/sec in the Dardanelles.

In the straits the boundary surfaces between different currents and between different water types do not coincide; the first rises from north to south more slowly than the thermo-haline transition layer and they intersect at the narrowest part of the straits. Thus in the northern part of both straits upper water flows with the lower current and in the southern parts lower water returns with the upper current. The changes in the currents due to variations in wind and atmospheric pressure are pronounced. During strong north-east wind the surface current is accelerated, the current core thereby

Currents in a Strait

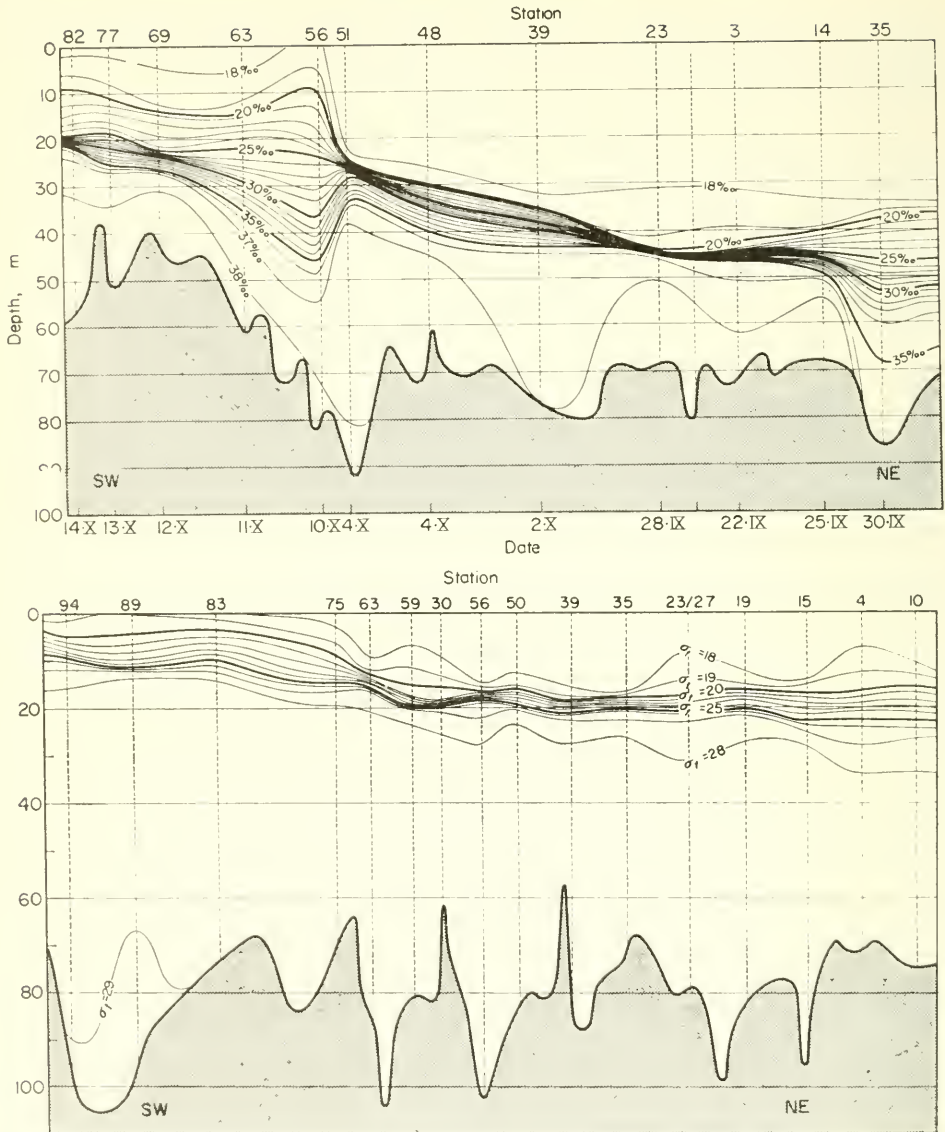


FIG. 241. Longitudinal section of the density σ_t . *Upper picture:* through the Bosphorus in Sept/Oct. 1917. *Lower picture:* through the Dardanelles June/July 1918 (according to Möller).

narrows and the standing vortices increase in extent. During south-west winds the surface current becomes weaker and broader and the lower current is accelerated. Figure 242 gives a longitudinal section through both straits showing the currents during a period with stronger north-east winds with a large pressure gradient towards the south-west. This wind influence produces a strong asymmetry in the current structure. For a period with a south-west wind the current conditions are affected in the opposite way. These flow conditions, however, no longer represent a stationary state.

A comparison with the theory presented above can only be achieved by means of current profiles in which the varying effects of changes in pressure and wind are eliminated. A computation of average profiles out of three typical ones for each strait allows a qualitative comparison. Figure 243 shows that excellent agreement can be obtained by suitable choice of the frictional coefficients. A numerical evaluation of equations (XVI.13) is given in Table 142. The average decline of the physical sea level along the Bosphorus is about 6 cm in 30 km and is greater at the northern end, less at the southern end. Along the 65 km Dardanelles it is only 7 cm; the value of 12 cm in

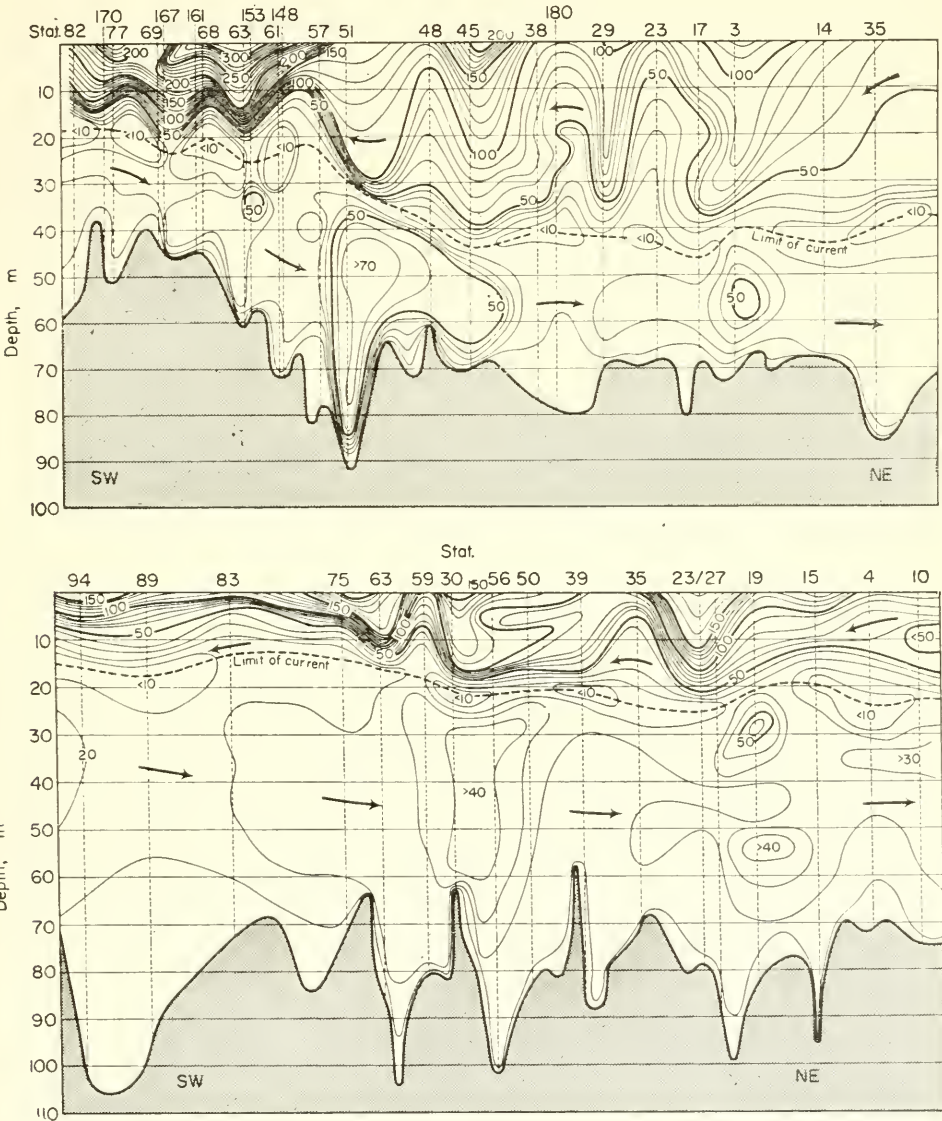


FIG. 242. Longitudinal section of the current velocities (cm/sec). Upper picture: Bosphorus for N.E. 5 and $\Delta p = 4.5$ mm. Lower picture: Dardanelles for N.E. to E. 3-4 and $\Delta p = 3$ mm.

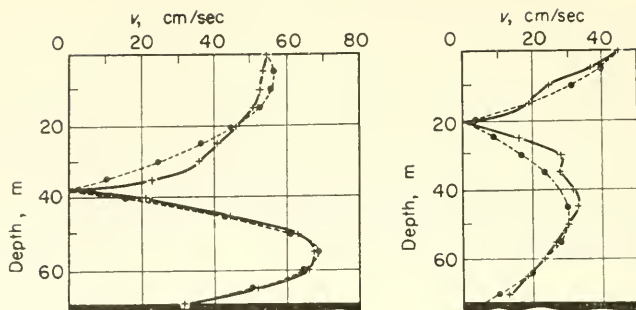


FIG. 243. Vertical current distribution in the northern part of Bosphorus (to the left) and of the Dardanelles (to the right); + — + — + —, according to the observations;, according to the theory.

the middle of the strait must be due to piling-up of water in the narrowest part of the strait.

Table 141. Sea surface and slope of the internal boundary surface, as well as frictional coefficients in the Bosphorus and the Dardanelles, calculated from current profiles

	Bosphorus			Dardanelles		
	Northern part	Middle part	Southern part	Northern part	Middle part	Southern part
Wind conditions	NE-SW	NE. ₂	NE and SSW	NE. ₃₋₄	SW	NE. ₃₋₄
Slope of { Sea surface boundary surface	10.1	5.6	2.4 cm/30 km	7.6	12.2	7.2 cm/65 km
	36	36	36 m/30 km	10	12	19 m/65 km
Turbulent coefficient (cm ² /sec)	298	371	485	82	28	420
Bottom friction κ	0.017	0.155	0.015	0.109	0.038	0.388

The turbulent coefficient is of the same order of magnitude as in tidal currents. The coefficient of bottom friction has a mean value of 0.12 which is very large. The individual values are strongly scattered but are around 50 times larger than the values found for natural channels and about 5 times larger than those found for rivers. The rolls with horizontal axis produced by the very irregular bottom and which cannot be observed by means of current measurements may simulate a bottom friction larger than actually present.

(b) Water Interchange Between North Sea and Baltic

This takes place in the area between the Kattegat in the north and the Darsser and Drogden ridges in the south. These give access to the Baltic at depths of 18 and 7 m, respectively. The annual inflow of fresh water into the Baltic averages about 500 km³ of which 467 km³ is the inflow from rivers and 206 — 182 = 24 km³ is the excess of

precipitation over evaporation (WITTING, 1918). This inflow of fresh water disturbs the equilibrium between the North Sea and the Baltic and gives rise to a water interchange with an upper current flowing towards the North Sea and a lower current flowing into the Baltic. KNUDSEN's relations (see Chap. XII. 5) afford an estimate of the water interchange balance. It appears from this that the inflow due to the lower current over the rise on the west side of the Arkona basin is equal to the inflow of fresh water into the Baltic and that the outflow in the upper current is twice as great. Detailed data indicate that the decrease in the water amount being carried by the lower current between the Skagerrak and the Baltic is opposed by a corresponding increase in water amount carried by the upper current. Therefore important mixing processes must always act within the sea straits.

Calculation of the proportion of water with a salinity of 33‰ in the lower current (see Table above) shows that until the Fornäs section, not less than 67% of the water entering the Kattegat has mixed the water of the upper current and that almost 80% of the remainder mixes with the upper water before reaching the Arkona basin. Thus only 7% of the water of 33‰ salinity entering the Kattegat in the lower current finally enters the Baltic. The remaining 93% mix with the upper water and return to the Skagerrak. In the same way a large part of the upper water mixes with the lower current and is carried again towards the Baltic. About a third of the water leaving the Baltic in the upper current west of the Arkona basin returns to the Baltic and not less than two-thirds of the water in the under current flowing into the Baltic over the rises has come from the Baltic itself, and only one-third is the water with a salinity of 33‰ that flows into the Kattegat in the lower current (SCHULZ, 1930).

This applies only for the annual means. For the investigation of the water interchange in individual months the assumption of a constant water amount in the Baltic is no longer valid, since the water level shows an annual variation and other shorter oscillations. In some months the outflow from the Baltic is stronger and in others less. Investigations by Witting for the period 1898 to 1912 indicate that there are pronounced maxima in fresh-water outflow from February to June, as well as in September. A detailed treatment of the data on currents in the Öresund and the Belts recorded between 1910 and 1916 by Danish and Swedish light-ships has been made by JACOBSEN (1925), who found for the period in question good agreement with the annual variation in water outflow from the Baltic found by Witting.

In water interchange processes *two* phenomena must be distinguished. The first is the orderly steady water interchange that takes place in a strait connecting two seas of different thermo-haline structure. This interchange is associated with the two currents which are essentially antitryptic flowing along an inclined boundary surface. In addition to this continuous steady water interchange there is a second phenomenon, the *total displacement* in both directions of the entire water mass of the strait by the wind or due to differences in atmospheric pressure. In the Bosphorus and the Dardanelles these meteorological influences are of minor importance in comparison with the regular thermo-haline water equalization, but in the connecting straits between the Baltic and the North Sea conditions are reversed. Here the piling up of water by the wind ("Windstau") and by atmospheric pressure differences is so strong that the regular steady interchange currents are almost completely masked. The main phenomenon is thus an irregularly occurring, occasional transport of the whole water mass in its total vertical extent more or less in the same direction in spite of its pronounced vertical stratification. The regular steady interchange can only be obtained by elimination of these irregular movements which can be achieved by taking mean values over long periods. Strong tidal effects are also present and must be eliminated by a harmonic analysis. Mean values have been calculated by JACOBSEN (1909, 1912, 1913), and the mean structure at four different stations is shown in Table 144.

Table 142. Mean currents in the Öresund and in the Great Belt (cm/sec)

(+, directed towards the North Sea; -, directed towards the Baltic Sea)

Depth (m)	Lightship			
	Lappegrunden	Drogden	Schultz's Grund	Southern Great Belt
0	—	—	—	+37
2.5	+47.1	+12.6	+2.4	—
5	+31.4	+11.0	+0.4	+30
10	-7.5	+8.8 (7 m)	-9.4	+12
15	-11.4	—	-18.2	-2
20	-7.6	—	-19.0	-15
25	-4.0 (23 m)	—	-15.0	-13
30	—	—	—	-13
35	—	—	—	-9

The lightship "Lappegrunden" lies in the most northern part of the sound, the lightship "Drogden" lies in the central part and the Schultz Grund lightship lies in the southern part of the Kattegat at the entrance to the Great Belt. For larger depth the mean upper current is directed towards the North Sea and the lower current towards the Baltic. The current profile corresponds rather well to that deduced theoretically. In the shallow waters of the Öresund ("Drogden") the entire current from the surface down to the bottom is directed towards the North Sea. As shown by Jacobsen, the internal field of force is very weak here and the great width of the channel permits cross-circulations to play an important part.

This steady water interchange produced by the internal field of force is [superimposed on the strong currents] almost always present in this area; which are produced by differences in level between the Kattegat and the southern part of the Baltic due to the piling up of water by the wind and due to differences in atmospheric pressure. These are also antitriptic slope currents and give rise to displacements of the internal front between the water bodies which here are situated side by side (Skagerrak and Baltic water) (see Pt. I, p. 182, Fig. 85). WATTENBERG (1941) has made a detailed investigation dynamics of the displacement of these fronts and of the duration of the movements, and has given a basis for the estimation of mixing in the Belts and of the flow of North Sea water into the Baltic. There is a close correlation between the flow through the Great Belt (computed by means of lightship current measurements) and the changes in salinity. A rather close connection exists also with the meridional pressure gradient. The duration of inflow and outflow periods changes, of course, according to the variability in the all-over weather situation over wide limits; the long-period variations are well shown by cyclic variations in the salinity, since the inertia of the water masses weakens or even completely suppresses the smaller shorter-period disturbances. Extreme positions of the internal fronts are due to prolonged inflow and outflow periods (Fig. 244). In the north the front may reach out from the Belt Sea as far as into the middle of the Kattegat. Towards the south under reversed conditions the front may in extreme cases reach the Darsser and the Drogden rises separating the Baltic from the Danish sounds. This difference in behaviour to the north and to the

south is due to the following facts. During outflow the upper water is not subject to any resistance and may therefore spread out arbitrarily at the surface, while during inflow the more saline water advances towards lighter water in front of it, and in this case the bottom topography exerts great influence. On passing the rises in the south the denser water sinks down to the bottom and the position of the front at the surface remains fixed near the rise. In this way large amounts of highly saline water flow into the basin of the Baltic thus renewing the stagnating deep and bottom water. Such processes are necessarily connected with long periods of weather favourable for inflow, which cause the front to remain in extreme southern position.

More recently, KNUDSEN (JACOBSEN, 1936) has organized detailed hydrographic investigations in the area to the south of Denmark. This work has been devoted mainly to the collection of accurate records for the sections between Gedser and Dars and across the Fehmarn Belt, thus providing continuous surveillance of the water interchange between the Baltic and the Kattegat.

(c) *The Straits of Gibraltar and Bab el Mandeb*

In the strait of Gibraltar, instead of a single bottom rise there are three, all west of Cape Tarifa. The first one extends in an arc from the Cabezos reef to Punta al Boassa (maximum depth 320 m), the second one runs from Cape Trafalgar over "The Ridge" (in places only 55 m deep) to Cape Spartel (maximum depth 366 m) and the third one lies about 10–20 km west of the second with a maximum depth of over 300 m. The water interchange between the Atlantic and the Mediterranean takes place in the two channels, one to the north and one to the south of "The Ridge" and follows exactly the same principles as those outlined above. Complete scientific use has been made of the available observational data by SCHOTT (1928 *b*). Longitudinal temperature and salinity sections are presented in Pt. I, p. 182, Fig. 83 for the transitional period between spring and summer during which more or less mean current conditions prevail. Seasonal variations in the velocity and extent of the upper current towards the east and in the lower current towards the west are quite large. In the winter months (including April) the thickness of the upper current is small, while that of the lower current is rather large. During the summer months (to the end of October) the thickness of the upper current increases by 80–100 m and that of the lower current is decreased correspondingly. During this part of the year the upper current must make up the evaporation deficit in the Mediterranean. From the limiting position of the boundary layer between the two water types it can be concluded that its annual variation west of the rise is of the order of 70–80 m, while east of the rise correspondingly 100 m or little more. The current boundaries also vary by similar amounts. The water boundaries and the boundary between the currents do not coincide, but mixed Mediterranean water is carried back with the upper current over almost the whole of the area. Figure 245 gives a schematic representation of this. According to DE BUEN (1926), Mediterranean water does not pass westward over the Gibraltar rise in the deep layers, but is piled up on the eastern side and is carried backwards into the Mediterranean by the upper Atlantic current with an upward motion. Analysis of the oceanographic series observations leaves no doubt of the incorrectness of this view of de Buen.

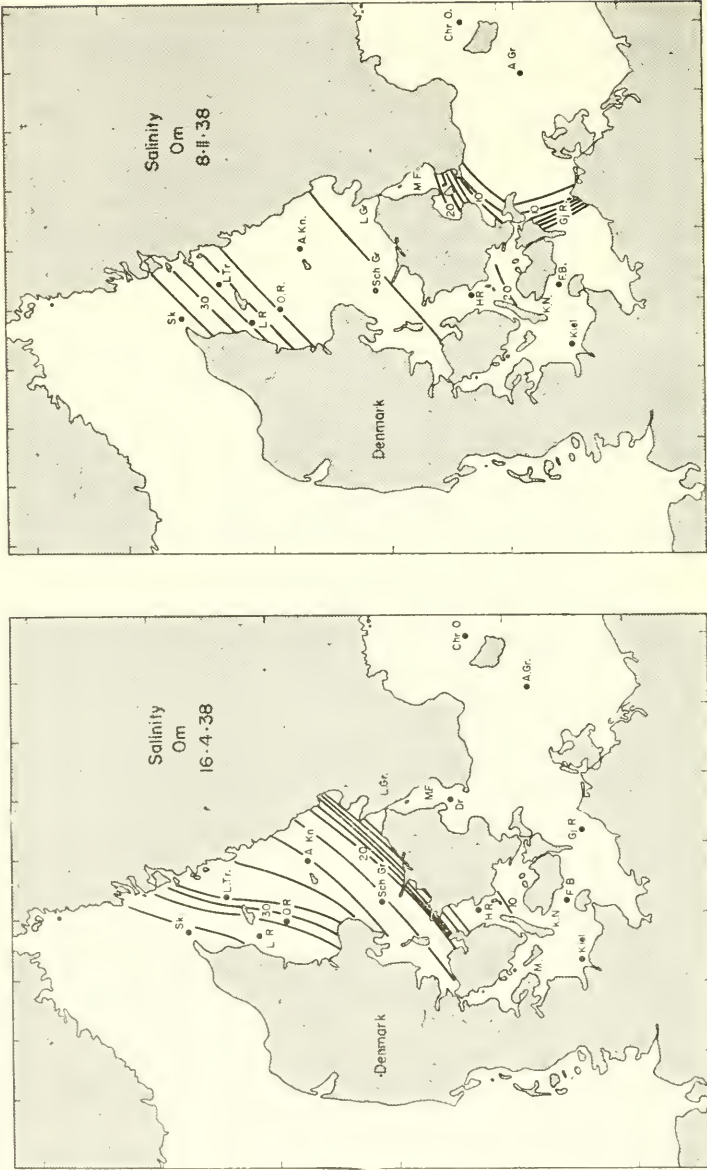


Fig. 244. Extreme position of the front after long periods of outward directed current (to the left) and periods of inward directed current (to the right) (according to Wattenberg).

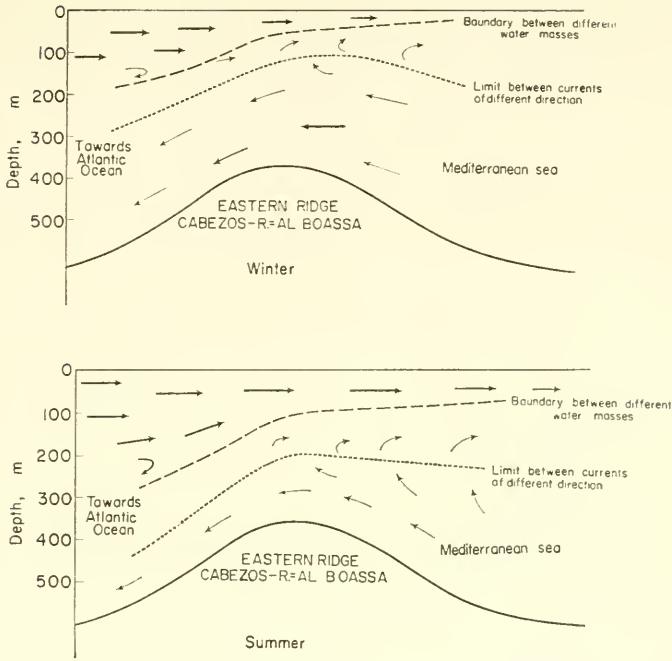


FIG. 245. Schematic representation of the water type and of the current limit in the inner region of the Strait of Gibraltar (according to Schott).

The few sporadic current measurements that have been made in the Strait of Gibraltar are in good agreement with the currents deduced from the longitudinal sections. The upper current towards the east is particularly strong in the middle of the strait and on its southern side. In the bays on both sides of the strait there are large vortical movements ("neer" currents). The main current is considerably affected by wind and tides and persistent easterly winds may even stop at times the inflow into the Mediterranean. The mean velocity of the upper current core according to NARES (1872) is 34 cm/sec; ebb and flood superimpose the mean velocity and this results in a velocity of ± 57 cm/sec giving an eastward flood current of 91 cm/sec and a westward ebb current of 23 cm/sec. The currents are strongest along the southern edge of the deeper southern channel and may reach as much as 210 cm/sec. The preference for the southern side, due to the Earth's rotation, can also be seen by means of the thermo-haline cross-sections which show the Atlantic water of low salinity deflected to the right along the African side.

Measurements made by the "Michael Sars" expedition (MURRAY and HJORT, 1912, p. 290) give the vertical current profile shown in Fig. 246. The current boundary lies at a depth of 142 m. Equation (XVI.13) allows a computation of the average down slope of the physical sea level from the Atlantic Ocean to the Mediterranean and one obtains as an average value 0.6 cm in 100 km, while the current boundary surface rises by about 15 m in 100 km. In spite of the simplifying assumptions in the theory there is satisfactory agreement between observations and theory. Direct current

measurements have been made by IDRAC (1928) on the vessel "Pourquoi-pas" in March 1927 to the south of Tarifa. These gave the following values (depth 600 m).

Depth (m)	0	100	200	300	400	500
Current towards	NE 1/4 E	NE 1/4 E	W 1/4 N	W 1/4 N	W 1/4 N	W 1/4 N
Velocity (cm sec ⁻¹)	72	41	56	62	47	25

The current boundary surface very probably lies at 150 m which is about the same depth as that found above. This can be compared with more recent investigations by MENÉNDEZ (1956).

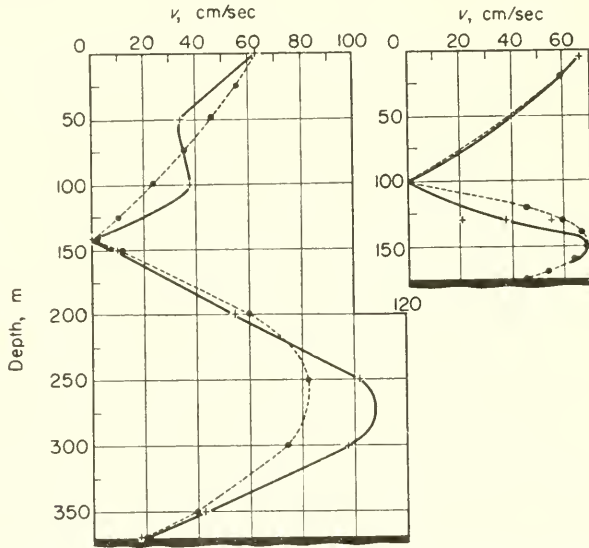


FIG. 246. Vertical current distribution in the Straits of Gibraltar and Bab el Mandeb; + — + — + —, according to the observations; · — · — · —, according to the theory.

Conditions in the *Strait of Bab el Mandeb* are essentially similar. The temperature and salinity distribution are given in Pt. I, p. 182, Fig. 84. Rather early current measurements have been made by GEDGE (1898) in the Perim Strait at the surface and at 192 m, and they indicate a strong inflow with a velocity of at least 2–2.75 nautical miles per hour at the surface. The current intensity decreased rapidly with depth and showed a reversal in direction at 130–140 m; the speed of the lower current was variable between 1 and 3 nautical miles per hour. The research vessel "Arimondi" in 1924 made a 15-day measurement at almost the same place and a harmonic analysis of this data was made by VERCELLI (1925). The results for the basic current are given in Table 143.

Table 143. Velocities of the basic current in the Strait of Bab el Mandeb (March 1924) sea bottom at 175 m; depth of boundary surface at 100 m (+, inflow from the Gulf of Aden; —, outflow from the Red Sea)

Depth (m)	5	20	50	100	130	150
Velocity (cm/sec)	+66	+59	+40	+1	–30	–68

This also gives a good fit between observed values and the theoretical current profile (Fig. 246); the low value at 130 m depth is apparently due to the uncertain elimination of the tides. From the Gulf of Aden to the Red Sea the sea level falls 1.1 cm in 100 km and the internal current boundary surface rises about 40 m. Since the sea bottom from the sill out into the Gulf of Aden falls almost steadily from 150 to

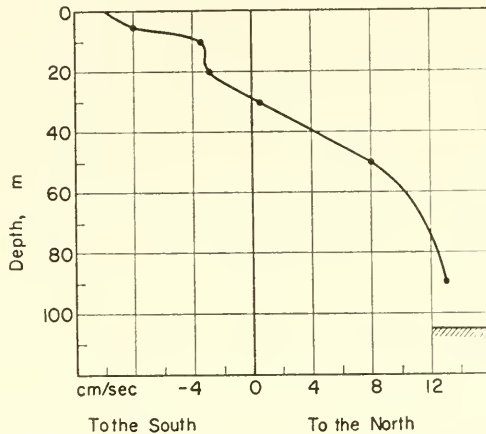


FIG. 247. Vertical stratification of the basic current in the Strait of Messina (according to the observations of the anchor station of the R.N. "Marsigli", 16-30 August 1922).

about 350 m, the internal boundary surface will also decline in the same direction, so that the value given above is merely the deviation from the bottom slope. Because of changes in the direction of the wind from the winter monsoon (east to south-east) to the summer monsoon (north-west to west) the currents in the Strait of Bab el Mandeb are subjected to oscillations with a semi-annual period. In the winter the inflow into the Red Sea is a wind-drift current of strong permanence in speed and direction but larger variations are to be expected during the summer monsoon.

(d) Strait of Messina

The smallest cross-section in this strait between the Ionian and the Tyrrhenian Sea is at the northern end of the strait. Here it has a cross-sectional area of only $\frac{1}{3}$ km² with a mean depth of about 80 m and a maximum one of about 120 m. From this sill the sea bottom slopes downward, uniformly and rather rapidly in valley form on either side. At the northern outlet the mean depth is 140 m and towards the south it is already about 900 m at about 30 km south of the sill. Since the water of the Ionian Sea is heavier, the current flows from the Tyrrhenian Sea into the Ionian Sea in the upper layer and in the opposite direction in the lower layer. Current measurements over a 15-day interval by the research vessel "Marsigli", at different depths down to 90 m at a section in the narrowest part of the strait, have been analysed harmonically by VERCELLI (1926). Figure 247 shows the vertical current profile. Down to a depth of 30 m the current flows to the south, below this, down to the sea bottom, to the north. The velocities are small, in accordance with the low density differences, with on the average about 4.3 in the upper current and about 9.3 cm/sec in the lower current. Strong tidal currents are superimposed on the basic current and there are also strong

disturbances due to atmospheric pressure and wind variations (velocities of up to 50 cm/sec). The current transport in the strait can be estimated from the KNUDSEN relations (see Chap. XII. 5). For cross-sections at the narrowest point (Punta Pezzo-Ganzirri) and at the rise of Punta Pellaro to the south of this, the mean salinities are:

$$s = 37.9, \quad z = 38.4 \quad \text{and} \quad s' = 38.5, \quad z' = 38.75\text{‰}.$$

The equations (XIII.19) then give as an approximation $i = u$ and $i' = u' = 2i$. Under stationary conditions the transports will be the same in upper and lower currents, but the transport through the southern cross-section is twice as large as that over the rise. Thus only about half of the water of the lower current entering the southern part of the channel flows over the sill to the north, the other half is carried back in the upper current mixed with Tyrrhenian water. A corresponding calculation for a cross-section to the north of the sill shows that part of the Tyrrhenian water entering the strait from the north mixes with the lower current and is carried back into the Tyrrhenian Sea. There must therefore be large turbulent mixing processes within the strait (see Vol. II).

4. External Influences (Bottom Topography, Tides) on the Oceanographic Conditions in Sea Straits

The normal steady current conditions in sea straits may be modified by external circumstances. It has already been mentioned that the atmospheric pressure and winds have considerable influence. Some idea about these influences can be obtained by simple numerical calculations. Besides these there are also other effects, especially that of the bottom topography of the strait and also those of tides, which penetrate from both sides from the open ocean into the sea strait and give rise to special current phenomena there. These latter phenomena will be discussed later in Vol. II, but it seems to be of advantage to mention these processes in connection with the fundamental phenomenon of water interchange between two seas already here.

(a) Disturbances Due to the Sea Bottom Configuration

The influence of a wave-form bottom topography on a horizontally flowing current can be understood quite easily by means of theoretical computation, provided the bottom relief can be expressed in the simple form

$$y = -h + \gamma \cos \kappa x, \tag{XVI.14}$$

where $\kappa = 2\pi/L$ is determined by the known wavelength of the bottom waves. The current with a velocity c over such a bottom will also take a wave-form, i.e. all layers from the bottom to the surface will follow the bottom topography but with an amplitude decreasing with distance from the bottom. The sea surface itself will be a stream line and its profile is determined from

$$y = \frac{\gamma}{\cosh \kappa h (1 - (g/\kappa c^2) \tanh \kappa h)}. \tag{XVI.15}$$

The denominator will be positive or negative according to whether

$$c \gtrless \{(g/\kappa) \tanh \kappa h\}^{1/2}.$$

This expression is, however, the velocity of propagation of a wave in *motionless water* of constant depth h . If the dimensions of the bottom waves are large compared with

the depth, which is usually the case, then this critical velocity of propagation reduces to the value \sqrt{gh} . The stationary current waves in moving water will have exactly the same form throughout the entire water layer as the bottom wave if $c > \sqrt{gh}$; if, however, $c < \sqrt{gh}$ then above a certain height it will be inverted, that is, above a rise in the bottom there will be a depression of the water level and above a depression in the bottom there will be a lift of the water level. If the velocity c is exactly the velocity of free waves then *resonance* will occur and in this case the frictional forces will be decisive. In all cases occurring in nature \sqrt{gh} is always several times larger than c and the stream lines show the wave-form of the bottom with decreasing amplitude and only up to a certain height; above this level of no horizontal motion the wave is inverted, but the amplitude is so small that these waves will scarcely be noticeable. It cannot be excluded that many of the vertical displacements in isotherms and isohalines, which are always found at the same place, may be due to effects of this type produced by bottom disturbances.

In stratified water conditions are different, especially when there are well-developed transition layers. Under certain conditions the disturbance by the bottom relief may be shown in amplified form at a boundary layer; it may even be larger than the disturbance causing it, while the surface of the water remains almost entirely unaffected. Theoretical treatment is also possible in this case (DEFANT, 1923). If the thickness of the upper layer is h_1 and that of the lower layer h_2 , resonance (enlarged amplitude of the stream-line waves) will occur at *two* values of the current velocity. If the total depth of water $h_1 + h_2$ is small as compared with the wavelength of the bottom disturbance these values are given by the equations

$$c_1 = \sqrt{\{g(h_1 + h_2)\}} \quad \text{and} \quad c_2 = \sqrt{\left\{ \left(1 - \frac{\rho_1}{\rho_2} \right) g \frac{h_1 h_2}{h_1 + h_2} \right\}}. \quad (\text{XVI.16})$$

The first value c_1 already for small depth is many times larger than any values found in nature. c_2 is the velocity of propagation of *internal waves* at the internal boundary surface (see Vol. II) and may be so small that it can be quite close to the observed current velocities. At these values the boundary surface will show the greatest variations while the sea surface remains almost undisturbed. For example, choosing $\rho_2 - \rho_1 = 10^{-3}$, $\rho_2 = 1.028$ then for larger h_2 and $h_1 = 50$ m c_2 will be 0.7 m/sec. Values of this order are frequently found in sea straits and it can be expected that at corresponding current velocities there will be large stationary vertical displacements in the density transition layer.

The currents in the two water masses in sea straits usually have different velocity values and are of opposite directions. This case can also be treated theoretically. If the thickness of the upper and lower layer is small compared with the wavelength of the bottom wave and their velocities are c_u and c_l , then the conditions for large stationary boundary waves is given with sufficient accuracy by

$$c_l^2 h_1^2 + c_u^2 h_2^2 = \left(1 - \frac{\rho_1}{\rho_2} \right) g h_1 h_2. \quad (\text{XVI.17})$$

A good example of this case is shown in the longitudinal density section through the Bosphorus in Fig. 241. The isopycnals clearly follow the outline of the bottom.

The disturbances are obviously due to this since the equation (XVI.17) is approximately satisfied. Putting $\rho_2 = 1.028$, $\rho_2 - \rho_1$ as approximately 15×10^{-3} , $h_1 = 25$ m and $h_2 = 45$ m, and since by observation $c_u : c_l = 2$ then equation (XVI.17) gives the critical velocity of the upper current as $c_u = 1.77$ m/sec, while the observed values lie between 1 and 2 m/sec.

The upward bulging of the boundary layer in the Strait of Gibraltar and the Strait of Bab el Mandeb is undoubtedly due to the passage of the current over the rise in the middle of the strait. Bulges such as these do not occur in a plane channel.

(b) Tidal Effects

Since tidal currents entering a sea strait affect the whole water mass from the sea surface down to the bottom, the ebb and flood currents will be superimposed on both, upper and lower currents, either reducing or accentuating them.

Since these currents flow in opposite directions the current profile will show rapid changes over a tidal period. An example can be taken of a strait 300 m deep with current reversal at 200 m in which the upper current flows east and the lower current flows west; the upper current is assumed with a surface velocity of 100 cm/sec decreasing parabolically with depth, while the lower current is supposed to increase below the boundary surface. The amplitude of the tidal current may be 86 cm/sec and the phase 3 moon hours (ebb towards the east at 3 h and flood towards the west at 9 h). The current structure over a total tidal period is then shown schematically in Fig. 248. At 3 h there is a current directed to the east through the entire water mass with a maximum at the surface; 6 h later conditions are almost reversed and the current is directed towards west with a maximum at the bottom.

In addition to this direct influence there is also a second one affecting the boundary surface. This will perform periodic internal vertical displacements initiated by the tidal

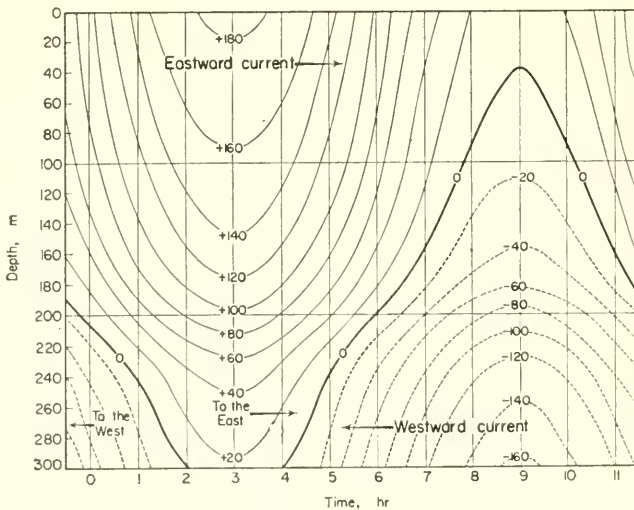


FIG. 248. Isopleths of the current velocity (cm/sec) in a water column during a total moon period with a superposition of the basic and tidal current. (Type of currents in the Gibraltar Strait.)

rhythm which will also give rise to variations in the oceanographic factors. It can be shown that the small periodic variations in the slope of the sea surface, produced by the passage of the tidal wave, will be accompanied by waves at the internal boundary layer of corresponding form, but of increased amplitude which will affect the normal water interchange between the two seas.

A disturbance of the internal boundary surface in a sea strait due to a periodic displacement of the sea surface (tide) can be treated theoretically in a simple way. The equations of motion for both layers can be obtained from equation (XVI.11), taking the local accelerations $\partial u_1/\partial t$ and $\partial u_2/\partial t$, respectively, into account. A periodic displacement of the sea surface can be given the form

$$\zeta_1 = \frac{\eta}{h_1^2 g} a \cos \lambda x \exp \left(i \frac{\eta}{h_1^2} \sigma t \right), \tag{XVI.18}$$

where the variation in the surface gradient has a wavelength λ , a period σ and amplitude a . These periodic vertical displacements of the sea surface give rise to corresponding variations in the upper and lower currents of the form

$$u_1 = v(z)a \sin \lambda x \exp \{i(\eta/h_1)\sigma t\} \quad \text{and} \quad u_2 = \Phi(z)\gamma \sin \lambda x \exp \{i(\eta/h^2)\sigma t\} \tag{XVI.19}$$

and these will be associated with a period vertical displacement of the boundary surface

$$\zeta_2 = \frac{\eta}{h_1^2 g} \gamma \cos \lambda x \exp \left(i \frac{\eta}{h_1^2} \sigma t \right) \tag{XVI.20}$$

$v(z)$ and $\Phi(z)$ fix the vertical velocity distributions in the upper and lower currents, respectively, and follow from the differential equations of motion mentioned above and the corresponding boundary conditions. γ in equation (XVI.20) is the magnitude of the variations of the internal boundary surface; its value is given by

$$\gamma = - \frac{\rho_1}{\rho_2 - \rho_1} a \left[1 - \frac{\rho_2}{\rho_1} M \right]. \tag{XVI.21}$$

Since M (see p. 520) is always negative, it is clear that the variations of the boundary surface will always be the reverse of those at the sea surface, and since γ is inversely proportional to the difference in density between the two water types they will be many times (of the order of about 1000) greater than the latter.

Variations of this type appear in all extensive series of observations. SCHOTT (1928) has investigated the observations made by the "Dana" expedition in the eastern part of the Strait of Gibraltar and obtained the results shown in Fig. 249. Values for the layer from 100 to 200 m were combined to eliminate the irregularities in individual values and to accentuate the connection with the tidal period. The isotherms and isohalines rise and fall in time with the sea surface tide at Gibraltar; here the oscillations of the internal boundary reach the large value of 70–80 m. Similar results were obtained at the "Dana" station for 14–15 July 1928 by JACOBSEN and THOMSEN (1934) where the 37‰ isohaline had an average amplitude of 66 m, at neap tides 42 m, and at spring tides 90 m.

Similar vertical oscillations in the density transition layer were found at the 15-day anchor station in the Strait of Bab el Mandeb; they follow the rhythm of the tidal currents and have amplitudes of up to 100 m. In this case there is a phase shift of 3 h between the current curve and the thermo-haline curve. This is shown in a particularly clear manner by taking the mean of 5 semi-diurnal periods. (Table 144.) The extreme values of temperature and salinity occur at the times of current reversal. Here, as in the Strait of Gibraltar, the main cause of the variations in the density transition layer is the passage of tidal waves. These quite large displacements of the boundary layer can also be explained quantitatively by the theory. Assuming the amplitude of the

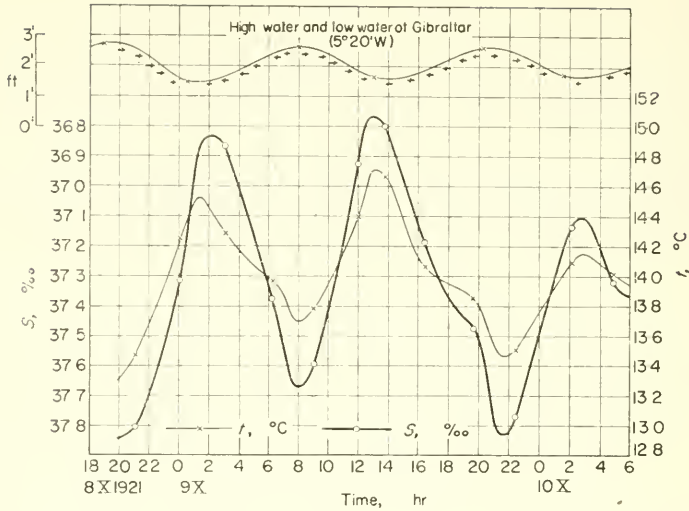


FIG. 249. Strait of Gibraltar: periodic oscillations in the mean salinity and mean temperature of the layer 100–200 m according to the observations of the “Dana” St. 1138 ($5^{\circ} 30' W.$) (according to Schott).

Table 144. Tidal current and periodic variations in temperature and salinity in the Strait of Bab el Mandeb at 100 m depth (Five semi-diurnal moon periods)

Moon hours	0	1	2	3	4	5	6	7	8	9	10	11
10^2 nautical miles per hour	+89	+87	+67	-7	-61	-112	-102	-71	-36	+36	+100	+105
	Flood current			Ebb current						Flood current		
Salinity 36 ‰	0.84	0.91	0.96	0.99†	0.99†	0.89	0.78	0.69	0.59	0.52*	0.60	0.66
Temperature 25 °C	0.28	0.21*	0.24	0.25	0.23	0.25	0.51	0.69†	0.69†	0.55	0.46	0.39

* minimum; † maximum.

oscillation in the sea surface slope as 10 cm in a model of the Strait of Gibraltar between Tarifa and Gibraltar, gave an internal boundary oscillation with tidal period and amplitude of 110 m which is in agreement with the order of magnitude of the observed values. Strong well-developed internal tide waves were also found at the 15-day anchor station in the Strait of Messina. This case is of particular interest because the wave here reaches the limits of stability characteristic for such waves and at times even exceeds it (see Vol. II).

5. Processes in Estuaries (River Mouths)

River water flowing into the sea gives rise to *compensation currents* along the river bed, which show similarities to current processes in sea straits. EKMAN (1876) in an

investigation of Swedish rivers found that the outflow of river water in the estuary was accompanied by an inflow of sea water in the lower layers. Thus, at the mouth of the Götaelf into the Elfsborgsfjord, there was a strong compensation requirement for the outflowing surface water which could not be satisfied by inflow from the sides. It therefore gave rise to upwelling motions *from below*. The consequent reverse deep current was clearly shown by the salinity distribution at different depths and could also be shown experimentally by drift buoys. The rising water was both more saline and more transparent than the sewage-laden river water. Figure 250 shows the salinity distribution along a longitudinal section; the upstream directed lower current is demonstrated clearly by the 20‰ isohaline.

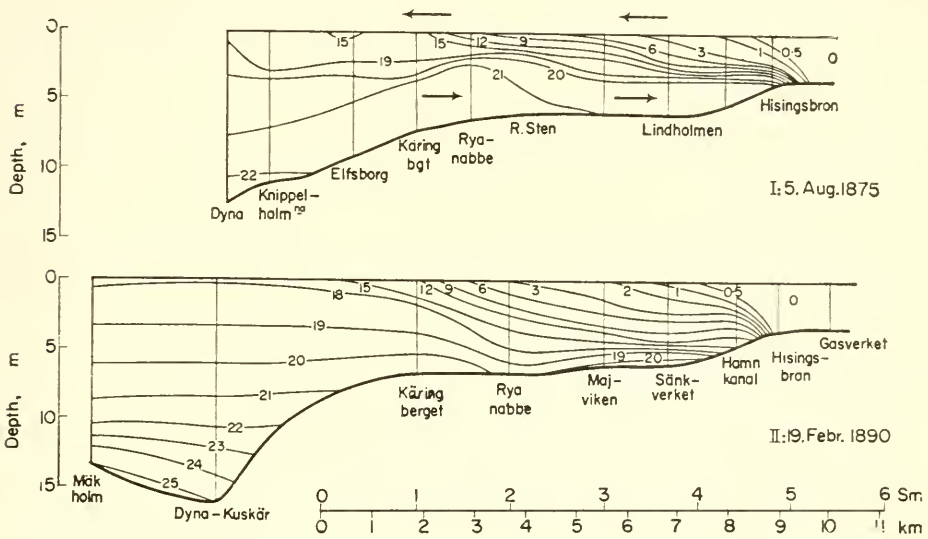


FIG. 250. Vertical distribution of salinity in the river mouth of the Götaelf. (I) 5 August 1875; (II) 19 February 1890.

A theoretical investigation of the occurrence of lower currents of this type in river mouths (estuaries) was made by EKMAN (1899) using principles similar to those used in the theory of currents in sea straits. He found that under normal conditions there were no currents carrying sea water upstream, but that such a current was formed immediately if there was a *tangential force* acting on the sea surface. The shallower the water, the greater must be the tangential pressure in comparison with the surface (river) velocity in order to allow for the generation of a compensation current in the deep water. River water entering an estuary flows on top of the sea water partly because of its inertial momentum and partly because of its lower density. It thus exerts the tangential pressure on the lower layer which favours the compensation current.

The momentum and the density are apparently, however, of less importance than the density difference between the upper and lower layers and turbulent mixing of the two water types.

This compensation-current phenomenon probably occurs at the mouths of most rivers, especially those carrying large quantities of water but no accurate systematic investigation has been made of these processes.

The situation is different for processes *in the sea* remote from the mouth of a river. These are easily handled theoretically (TAKANO, 1954, 1955) and the stratification in the sea, the vertical and lateral mixing and the turbulence of the current can be taken into account.

Taking a vertical coast as the y -axis and at this coast a river mouth where $-l < y < l$ from which the river water with a constant velocity u_0 flows into the open sea at right angles to the coast, then, neglecting inertial terms and any tidal effects present, the equations of motion and the continuity equation will be

$$\left. \begin{aligned} -\rho f v &= -\frac{\partial p}{\partial x} + A_h \nabla_u^2 + \frac{\partial}{\partial z} \left(A_z \frac{\partial u}{\partial z} \right), \\ \rho f u &= -\frac{\partial p}{\partial y} + A_h \nabla_v^2 + \frac{\partial}{\partial z} \left(A_z \frac{\partial v}{\partial z} \right), \\ \frac{\partial \rho u}{\partial x} + \frac{\partial \rho v}{\partial y} &= 0. \end{aligned} \right\} \quad (\text{XVI.22})$$

A_h and A_z are the lateral and vertical eddy viscosities and f is the Coriolis parameter which can be assumed constant.

Assuming that the stress both at the surface ($z = -\zeta$) and at the bottom ($z = d$) vanishes and introducing the volume transport ($\rho \sim 1$) one obtains

$$M_x = \int_{-\zeta}^d \rho u \, dz \quad \text{and} \quad M_y = \int_{-\zeta}^d \rho v \, dz \quad (\text{XVI.23})$$

and putting $P = \int_{-\zeta}^d p \, dz$ gives from equation (XVI.22)

$$\left. \begin{aligned} A_h \nabla^2 M_x + f M_y &= \frac{\partial P}{\partial x}, \\ A_h \nabla^2 M_y - f M_x &= \frac{\partial P}{\partial y}, \\ \frac{\partial M_x}{\partial x} + \frac{\partial M_y}{\partial y} &= 0. \end{aligned} \right\} \quad (\text{XVI.24})$$

If the stream function is taken as usual

$$M_x = -\frac{\partial \psi}{\partial y} \quad \text{and} \quad M_y = +\frac{\partial \psi}{\partial x}, \quad (\text{XVI.25})$$

then from (XVI.24)

$$\nabla^4 \psi = 0, \quad (\text{XVI.26})$$

whereby

$$\nabla^4 = \frac{\partial^4}{\partial x^4} + 2 \frac{\partial^4}{\partial x^2 \partial y^2} + \frac{\partial^4}{\partial y^4}$$

is the biharmonic operator. With the boundary conditions

$$\left. \begin{aligned} &\text{at } x = 0 \text{ and } -l < y < l: M_x = M_0 \\ &\text{at } x = 0 \text{ and } -l > y > l: M_x = 0, \end{aligned} \right\} \quad (\text{XVI.27})$$

where M_0 is the volume transport of the river flow at the mouth (which is assumed to be uniform), the solution of (XVI.26) will be given by

$$\psi = \frac{M_0}{\pi} \left\{ (y + l) \tan^{-1} \frac{y + l}{x} - (y - l) \tan^{-1} \frac{y - l}{x} \right\}. \quad (\text{XV.28})$$

Equation (XVI.24) thus gives

$$P = \frac{M_0}{\pi} \left\{ -f \left\{ (y + l) \tan^{-1} \frac{y + l}{x} - (y - l) \tan^{-1} \frac{y - l}{x} \right\} + 2A_h \left\{ \frac{y + l}{x^2 + (y + l)^2} - \frac{y - l}{x^2 + (y - l)^2} \right\} \right\} \quad (\text{XVI.29})$$

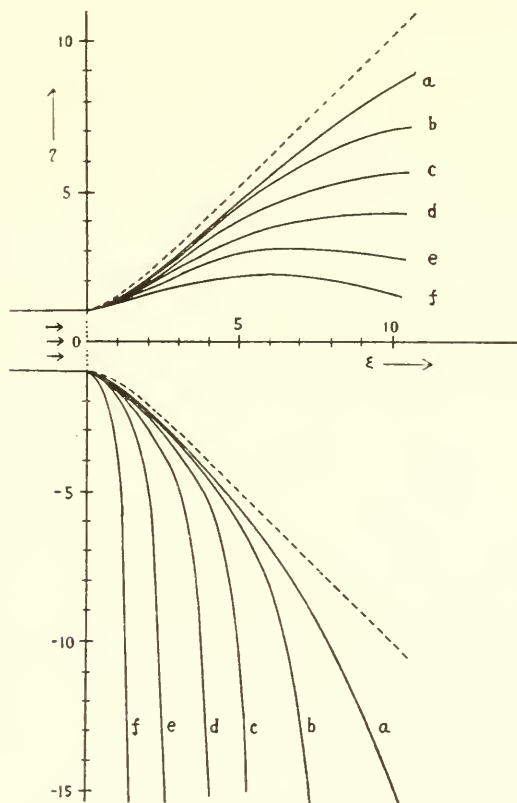


FIG. 251. Spreading of light river water off the mouth in the ocean for different values of the horizontal exchange. (a) $R = 1/500$; (b) $R = 2/500$; (c) $R = 4/500$; (d) $R = 8/500$; (e) $R = 16/500$; (f) $R = 32/500$. Dashed curves: $f = 0$ (zero Coriolis parameter, non-rotating system) (according to Takano, 1955).

The vertical density distribution is assumed to correspond to that of the REID model (1948)

$$\rho = \rho_0; \quad -\zeta \leq z \leq h; \quad \rho = \rho_a - \Delta\rho e^{1-z/h} \quad (h \leq z \leq d) \quad (\text{XVI.30})$$

where

$$\Delta\rho = \rho_a - \rho_0 \quad \text{and} \quad \rho = \rho_a \quad (d \leq z).$$

This corresponds to a *homogeneous* top layer of thickness h with a lower layer in which the density increases to ρ_a . Then as a first approximation

$$\frac{\partial\zeta}{\partial x} \sim \frac{2\Delta\rho}{\rho_0} \frac{\partial h}{\partial x} \quad \text{and} \quad \frac{\partial P}{\partial x} \sim \frac{5g\Delta\rho}{2} \frac{\partial h^2}{\partial x}. \quad (\text{XVI.31})$$

Analogous equations will apply for y and furthermore

$$h^2 = \frac{2}{5g\Delta\rho} P. \quad (\text{XIV.32})$$

The integrated pressure P can be taken to represent the thickness of the upper homogeneous layer. Putting $f = 0$ in equation (XVI.29), that is, neglecting the Coriolis force gives

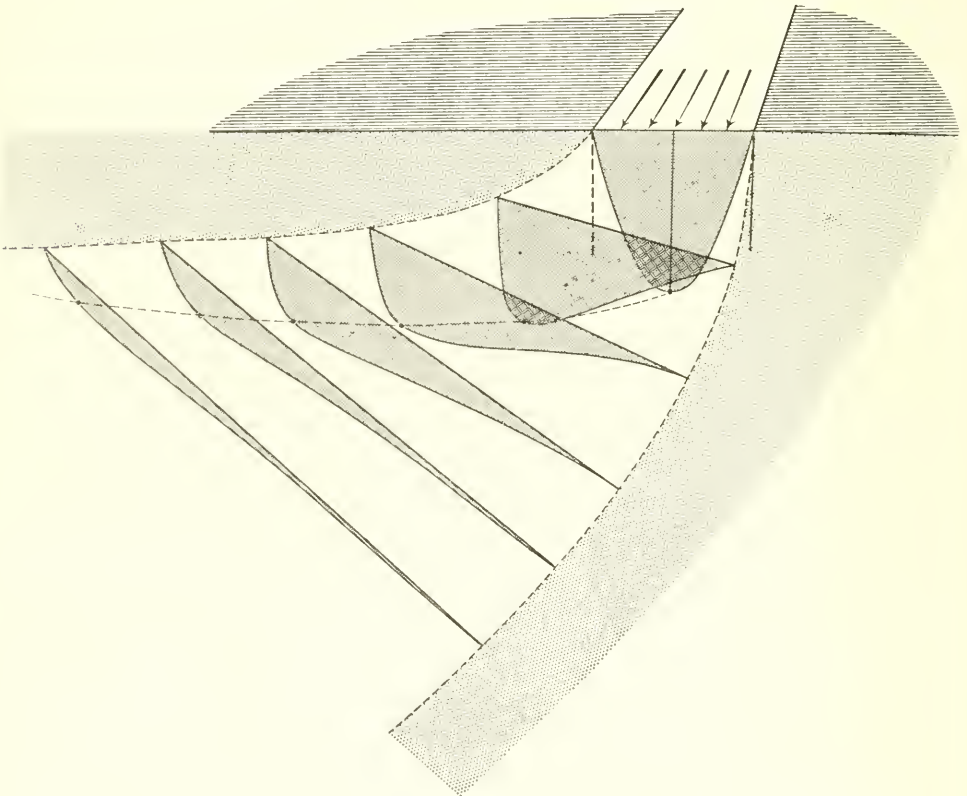


FIG. 251a. Schematic representation of the spreading of river water in the ocean off the river mouth.

$$\begin{aligned}
 P_{f=0} &= \frac{2A_h M_0}{\pi} \left\{ \frac{y+l}{x^2+(y+l)^2} - \frac{y-l}{x^2+(y-l)^2} \right\} \\
 &= \frac{4A_h M_0 l}{\pi} \left\{ \frac{x^2 - y^2 + l^2}{[x^2+(y+l)^2][x^2+(y-l)^2]} \right\}.
 \end{aligned}
 \tag{XVI.33}$$

If $y^2 - x^2 = l^2$ then h vanishes, that is, the lighter river water fills only the volume between the hyperbolic branches $y^2 - x^2 = l^2$ and $x = 0$. The river water flows as an upper layer over the lower layer, spreading out laterally between these hyperbolic branches. The first term in (XVI.29) modifies this simple symmetrical spreading of the river water on top of the lower water. This is purely an effect of the lateral and vertical mixing process; it causes the homogeneous layer to be deeper on the right-hand side and shallower on the left-hand side. The inflow is thus directed to the right in the Northern Hemisphere. Figure 251 shows the limits of the river water for the different cases

$$R = \frac{fl^2}{A_h} = \frac{1}{500}; \quad \frac{2}{500}; \quad \frac{4}{500}; \quad \frac{8}{500}; \quad \frac{16}{500} \quad \text{and} \quad \frac{32}{500},$$

where the dashed curve is for $f = 0$ (non-rotating system).

Table 145

$2l$ in m :	a	b	c	d	e	f
200	5.0×10^6	2.0×10^6	1.25×10^6	6.2×10^5	3.1×10^5	1.6×10^5
600	4.5×10^7	2.2×10^7	1.1×10^7	5.7×10^6	2.8×10^6	1.4×10^6
1000	1.26×10^8	6.2×10^7	3.1×10^7	1.6×10^7	7.8×10^6	3.9×10^6
2000	5.0×10^8	2.0×10^8	1.25×10^8	6.2×10^7	3.1×10^7	5.6×10^7

Exchange coefficients for the cases shown in Fig. 257 are contained in the following Table 145 for a corresponding river mouth width $2l$ and for $f = 10^{-4} \text{ sec}^{-1}$. The Coriolis force deflects the seaward flow towards the right and gives rise at the mouth of a river in the Northern Hemisphere to a water level sloping from the right bank down to the left bank. For the lateral exchange coefficients found in practice, 10^6 to 10^8 , and for a river mouth width between about 300 m and 1 km there will be quite a sharp deflection to the right (approximately as in curves d to f). The flow of river water into the sea at the mouth of a river is shown schematically in Fig. 251*a* and conditions actually found in nature will probably correspond reasonably well to this.

Chapter XVII

Effect of Wind on the Mass Field and on the Density Current

UNDER stationary conditions all the forces acting must be in equilibrium and the mass distribution must be adapted to this equilibrium if it is to be maintained. In this case it is not possible to distinguish between cause and effect; there is usually a *mutual adjustment between the internal field of force and the current present*. If there is a change in the field of force then there must also be a subsequent change in the current; conversely if there is a change in the current there must be a rearrangement of the field of force until equilibrium is again restored. These circumstances should be kept in mind for an understanding of the way in which wind influences density currents.

1. A Limited and Stratified sea

Conditions in a limited trough-like sea shall be considered first. Work in this direction has been done by PALMÉN (1926, 1930 *a, b* and with LAURILA as co-worker, 1938) for the Gulf of Finland and the Gulf of Bothnia, principally in particular cases which are only able to give some insight into the mechanism of the processes which occur. The influence on the water stratification occurs as follows:

We assume at first no wind at all over a barotropic sea; the isosteric surfaces and especially the transition layer between the top layer and the deep water will then follow level surfaces (Niveauflächen). If a wind starts, the surface waters are forced to move first in the direction of the wind, but the Coriolis force will soon produce a deflection to the right (Northern Hemisphere) and a piling-up of the water along the sea coasts. In an elongated ocean bay the final result will be a current predominantly occurring along its longer axis. In addition to the wind-generated current in the top layer a gradient (Stau) current is then added in the deeper layers due to the piling up of water which will flow approximately in the opposite direction. Thus a *vertical circulation in a longitudinal direction* is set up and an equilibrium state is present in which the transport due to the surface current is exactly balanced by that of the deep current. This quasi-stationary state of the current is fixed at each level by an equilibrium between the gradient force, the Coriolis force and the frictional force. Since a stronger current is only possible along the longitudinal axis of the bay it follows that the direction of the gradient force usually does not coincide with the direction of the current itself but the deviation will not be great. In addition to the principal gradient in a longitudinal direction in the layers above and below the level of current reversal (layer of no motion) there will also occur smaller components of the pressure force acting at right angles to the direction of the current. These will be largest at the surface and

will decrease with depth-changing sign at the layer of no motion. This will modify the mass field which then can no longer remain barotropic. The isosteric surfaces must slope transversally; the *mass field becomes baroclinic*. The structure of the associated density current can be computed by means of ordinary methods from this mass field. The primary factor will now no longer be the water stratification but rather the current, while the water stratification can be regarded as a consequence of this current.

Palmén investigated data for the Gulf of Finland for steady westerly and steady easterly winds and distinguished between a west type and an east type. He deduced mean mass fields over a cross-section for these two cases from the large amount of data available. In the east type the lighter surface water lies in a wedge-form at the Finnish coast with the isosteres sloping downwards from south to north, while in case of the west type conditions are reversed. Figure 252 shows the distribution of density for the two opposite types. The interpretation is simple: the west wind produces a drift current in which the transport is directed towards the Estonian coast where the lighter surface water will pile up. For an east wind the opposite occurs. Palmén has demonstrated the reality of these changes in sea level between the northern and southern sides out of observations of water level in Hangö, Reval and Helsinki. For the east

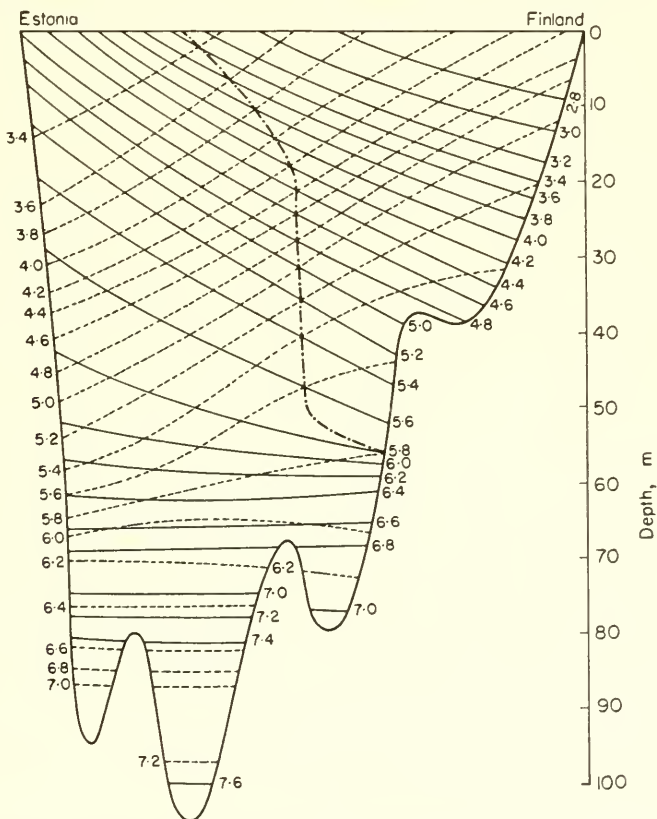


FIG. 252. Normal density distribution in the cross-section Åransgrund-Kokskär (Fennic Bay, 25° E.); σ_t , values. —, east type; ---, west type (according to Palmén).

type the difference in water level was 4.4 cm and for the west type this difference is 3.4 cm. The absolute velocity of the wind-generated surface current will thus be for the east type 6.9 cm/sec towards the west and for the west type 5.3 cm/sec towards the east. Current measurements give 7.5 and 6.0 cm/sec, which is in good agreement. The relative changes in velocity with depth can be calculated by ordinary methods (equation XV.20) from the mass field and can then be converted to absolute velocities using the surface velocities given above. Table 148 containing these values shows clearly the division of the current structure into two layers; at the middle of the Gulf of Finland the current reversal is at a depth of approximately 27 m. It changes in a corresponding way towards the Finnish and Estonian coasts. The calculated values are a little too large, since friction has been neglected, but otherwise are in satisfactory agreement with observed values. In some special cases for a strong wind and steeper inclination of the isosteres in the transverse section, the velocities are much greater (for instance, 7 October 1936; surface velocity 23.5 cm/sec) and the layer of no motion occurs at greater depth (about 35 m) in full agreement with the observed values.

Table 146. Current stratification for different wind directions in the Gulf of Finland (according to Palmén) (positive sign towards west; negative sign towards east)

Depth (m)	0	10	20	30	40	50	60	70
Velocity (cm/sec)								
For east type	+7.3	+5.1	+1.8	-0.9	-3.3	-4.3	-5.3	-5.3
For west type	-5.3	-3.7	-1.1	+1.3	+3.7	+4.6	+5.0	+5.3

When the wind is in a direction other than directly east or west only the eastern or western component will have any effect. The inclination of the isosteres in the transverse section will therefore be correspondingly less and the number of solenoids will thus be reduced and must therefore show a dependence on the wind direction.

The rearrangement of stratification caused by the wind in an elongated oceanic region will thus proceed in the following way:

(1) A steady wind with a component along the longitudinal axis of the sea will originate a vertical circulation; this will be made up of a drift current in the top layer and a corresponding gradient current in the deep water.

(2) This current system will produce a vertical transverse circulation which in turn will give rise to an inclination of the density transition layer and of the isosteric surfaces, that is, the longitudinal circulation produced by wind will give rise to a solenoid field at right angles to this circulation. The strength of this field will be a function of the wind influence. When an equilibrium state is reached this cross circulation will vanish.

(3) A transverse slope in the physical sea level will develop at the same time and its intensity will also be dependent on the wind.

(4) From the solenoid field and the transverse slope of the sea surface the current structure in a transverse section can be calculated. In a steady equilibrium state the slope of the internal boundary surface in a two-layered sea will be greater than that

of the physical sea level in the ratio $\rho_1:(\rho_2 - \rho_1)$. It is easily shown that this slope is given by

$$i = - \frac{T}{g(\rho_2 - \rho_1)h_1},$$

where ρ_1 and ρ_2 are the densities of the top and lower layers, respectively, h_1 is the thickness of the top layer when the system is at rest and T is the shearing stress of the wind. The deep water is assumed to be motionless. This relationship has the same form as the equation (XIII.45) which gives the piling up of water by the wind (Windstau) in a homogeneous sea except that ρ is replaced by the density difference $(\rho_2 - \rho_1)$. HELLSTRÖM (1941) showed that in a stratified sea with two layers the piling up of water by the wind differs markedly from that in homogeneous water and that the effect of the wind is larger. The wind stress calculated from equation (XIII.45) (p. 419) is much too large, and the less the depth of the discontinuity layer the greater is the error. Palmén's investigations, however, showed that the changes in water level in the Baltic due to the effect of the wind are almost independent of the water stratification. This contradiction was resolved by PALMÉN (1941) by estimation of the time required to establish an equilibrium state. This time required is very large, of the order of several days, while only a few hours are needed to produce a piling up of the water similar to that for homogeneous water. Usually, the wind direction does not remain invariable for a longer time to allow the slopes of the discontinuity layer and the sea surface to reach a steady state. Initially, the piling up of water by the wind in a stratified sea is approximately the same as in a homogeneous sea. However, the longer the duration of the wind the closer is the approach to the Hellström values. The equation (XIII.45) can thus be used in almost all cases for the calculation of the wind pressure, although strictly it is valid only for homogeneous water.

FJELSTAD (1946) has made a thorough theoretical examination of steady currents in a stratified water contained in a wide channel and has obtained results in complete agreement with the observations.

The transverse circulation is usually connected with another important phenomenon. In a sea of sufficient width a strong wind may produce an inclination of the density transition layer sufficient to bring the deep water to the sea surface. A rapid fall in temperature will then occur and an increase in salinity in a long band along the coast to the left of the current (Northern Hemisphere). The phenomenon of "cold upwelling water" along an extended coastline has previously been regarded largely as a direct result of an offshore wind (land wind) (SANDSTRÖM, 1922; KRÜMMEL, 1911, p. 536 and following), forcing the deep water upwards to the surface at the lee coast while the surface water is forced downwards to deeper layers at the windward coast (luv-coast). Besides this direct effect, the effect of earth rotation in the above senses, seem however, of more importance. In the Gulf of Finland and in the Baltic (MÄE, 1928) the upwelling of cold water found during strong persistent longitudinal winds gives support to the importance of the indirect wind effect.

2. General Conditions in the Open Ocean

These are essentially the same as in channel-form elongated oceanic regions. The effect of the wind is mostly restricted to a more or less broad band of the sea surface, and outside this area the water is either motionless or subject to the effect of a wind

from another direction. Thus, for example, in a broad band of an oceanic region with vertical increase of density and forming a channel around the earth in the Northern Hemisphere, conditions will be more or less as follows.

If there is a persistent wind in the direction of the channel the immediate effect of the drift current (westerly wind) is to transport lighter surface water to the right (south) side of the channel. In the top layers the isosteric surfaces can no longer be horizontal and will adjust with an inclination from north to south in order to correspond with the accumulation of lighter water on the right-hand side of the wind. A solenoid field of this type will, however, produce a density current in the direction of the wind in which the velocity will decrease with depth corresponding to a similar decrease in the slope of the isosteres. At the same time, water will be piled up on the right-hand (south) side of the channel and this will give rise to a gradient (Stau) current in the direction of the wind. Its velocity will remain constant down to the lower frictional depth. In this way the stratification will lead to a considerable complication of the conditions and even more so if changes due to other factors (heating, cooling, evaporation and others) must, too, be taken into consideration.

It is doubtful whether a gradient (Stau) current will be generated in such a current system. The displacement of the water masses in the top layer, where the solenoids are numerous and which is superimposed on deep water where the solenoids are few, may proceed so that the isobaric surfaces in the deep water remain horizontal (see discussion on p. 483 and following pages). If the effect of the water accumulation (rise in physical sea level) occurring on the right-hand side of the wind direction (Northern Hemisphere) on the pressure field of the deeper water is compensated exactly by the baroclinic mass distribution of the top layer there will be no gradient (Stau) current. In actual practice, the relationship between the topography of the physical sea level and the mass structure of the upper layers is usually satisfied so that any deep reaching slope current is improbable.

A complete theoretical treatment of the problem of currents in a baroclinic ocean offers considerable mathematical difficulties, since it must take into account vertical frictional effects, lateral mixing processes and boundary-surface conditions. In connection with an investigation on the circulation of the antarctic circumpolar waters, SVERDRUP (1933) has discussed the possibility of formation of a *steady* drift current in the presence of a baroclinic stratification of the water masses. He showed, in agreement with the results of Ekman, that steady vertical circulations can hardly develop in the ocean if only the effect of wind is taken into account. Due to the non-uniformity of the wind field (divergences and convergences), and due to the boundaries between different water bodies and the coasts, vertical circulations will be formed and will produce changes in the mass field. However, since the density distribution in the sea is usually a stationary one and apparently steady circulations still occur, it follows that the effect of the vertical circulations produced by wind must be compensated by other factors which affect the density. This gives emphasis to the great importance of these factors for the development and maintenance of the oceanic circulation. Heating, cooling, evaporation, precipitation and other factors thus take part indirectly in the formation of the oceanic circulation. The convective sinking of cold waters in higher latitudes plays an especially important part for the maintenance of vertical oceanic circulations.

EKMAN (1931) has drawn attention to a special effect of the wind on a given solenoid field. In a top layer (the place where density currents occur) the isosteric surfaces are assumed to rise from south to north (Northern Hemisphere; approximately the conditions found in the Atlantic between 40° to 50° N. and 30° to 40° W.). In the absence of wind there will be a density current directed towards the east. If now a steady persistent wind gives rise to a drift current, thus altering the mass field, then, for a northerly wind the total transport of the drift current will be directed to the west and for a southerly wind to the east. The basic current therefore will be either retarded or accelerated. An east wind blowing against the current will produce a transport of the upper water to the north and will thus tend to even out meridional density differences, and in this way to decrease the velocity of the density current. If the wind blows towards the west (as in the Atlantic over the Gulf Stream), then the upper layer will be driven towards the south and the slope of the isosteric surfaces will increase. As long as only the total system of surfaces without internal change is displaced towards the south the strength of the density current, which is largely fixed by the horizontal distances between the isosteres, will remain unchanged; however, under certain conditions changes in inclination of these surfaces will also occur and the density current will increase its strength. This is especially the case when the upper lighter water is displaced by the wind, while the lower one remains unaffected. The wind blowing in the direction of the density current, in addition to the generation of a drift current, also has the effect of localizing the density current and may transform an otherwise broad and slow current into a narrow rapid one, still with the same transport. Ekman saw in this process an explanation for the narrowness to which the Gulf Stream is confined in this part of the Atlantic. This peculiar phenomenon of a "river in the sea" is in any case an argument in favour of such wind effects.

Another example of wind effect on the mass field is the boundary surface found throughout the interior of the entire Antarctic Ocean which appears at the sea surface of the ocean as the *Antarctic Convergence Line* (Southern Hemisphere Polar Front). This boundary surface separates the heavier, colder, Antarctic water to the south from the lighter but more saline water of the oceanic troposphere to the north. The boundary surface has a slope corresponding to the density and current conditions. It behaves like a solid wall (continental slope) and makes an Antarctic vertical circulation possible. Figure 253 (SVERDRUP, 1933*a*) shows a meridional density section at 30° W. derived from the observations of the "Discovery" expedition. The boundary surface meets the sea surface at 50° S. in the Antarctic convergence line. The topography of the physical sea level and the 1000 decibars surface (both relative to the 3000 decibars surface) are shown in the diagram above. These isobaric surfaces slope downwards from north to south corresponding to the current flowing eastward in both water bodies; this current must be stronger on the northern side than in the Antarctic water to the south.

The cause of the formation of a discontinuity surface is not immediately apparent, since the current flows exactly towards east in all latitudes and meridional current components are required in order to produce and to maintain it.

Two factors favour the occurrence of a northward component in the Antarctic water.

(1) The prevailing westerly winds, and

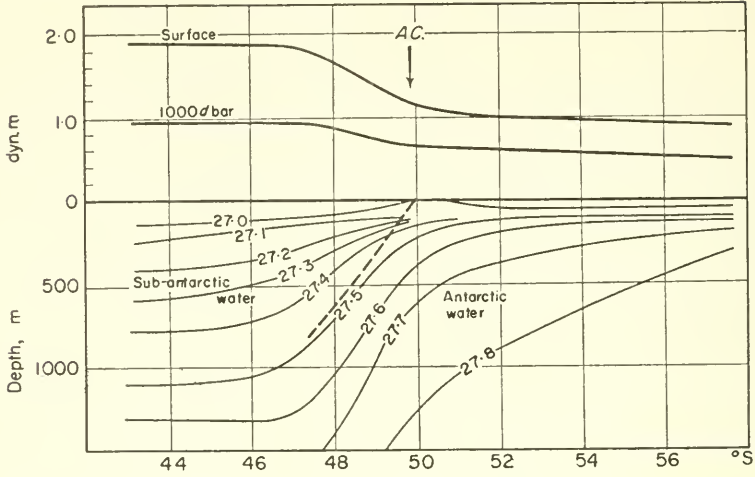


FIG. 253. Vertical section of density (σ_t) in the Atlantic Ocean along 30° W. between 24° and 58° S. Above: topography of the physical sea level and of the 1000-decibar surface (relative to the 3000-decibar surface assumed as plane). A.C., Antarctic convergence (oceanic polar front).

(2) the continuous supply of water with low salinity which is produced by melting of the northward drifting pack-ice.

This second factor requires the presence of a thermo-haline circulation directed at the surface from an area with high specific volume to another one with a low specific volume. A circulation of this type is certainly present but the wind conditions are probably the main cause (DEACON, 1934; SVERDRUP, 1934*b*). In latitudes between 40° to 65° S. the prevailing wind is always westerly and gives rise to a drift current and a consequent surface water transport to the north. According to meteorological observations the strongest surface wind in higher latitudes occurs between 50° and 60° S. The water transport to the north is thus greatest between 60° and 50° S. and north of 50° S. is comparatively smaller. This gives rise to the formation of a convergence line and a discontinuity layer in the mass field. The wind and its differentiation in a meridional direction may also be considered the main reason for the intensification and concentration within a narrow strip of the density current which would otherwise spread out over a wider area.

3. General Relationships Between Wind and Currents

The investigation of steady currents produced by wind in a baroclinic top layer is easily handled, since the deep water can be regarded as essentially motionless and the wind field as quasi-permanent showing no changes with time or position. This allows the effects of both the vertical and horizontal eddy viscosities to be taken into account. The equations of motion (XIII.52) must then include terms for the horizontal eddy viscosity, denoted briefly by h_x and h_y . Integration of these equations over the entire depth d and introduction of

$$H_x = \int_0^d h_x dz, \quad H_y = \int_0^d h_y dz \quad \text{and} \quad P = \int_0^d p dz \quad (\text{XVII.2})$$

gives

$$\left. \begin{aligned} -\frac{\partial P}{\partial x} + fM_y + T_x + H_x &= 0, \\ \frac{\partial P}{\partial y} - fM_x + T_y + H_y &= 0. \end{aligned} \right\} \quad (\text{XVII.3})$$

Therein M is the vector of the mass transport (equation XII. 8, p. 376). To these must be added the continuity equation for an incompressible fluid.

$$\frac{\partial M_x}{\partial x} + \frac{\partial M_y}{\partial y} = 0. \quad (\text{XVII.4})$$

For a given value of T and ignoring the effects of the horizontal components of the eddy viscosity the three equations (XVII.3 and 4) can be regarded as equations with three unknowns P , M_x and M_y . Thus, in such a baroclinic current the total pressure P and the mass transport M can be represented as functions of the wind stress.

Elimination of P by cross-differentiation, taking into account equation (XVII.4) and putting $\beta = df/dy$ gives

$$\left(\frac{\partial T_x}{\partial y} - \frac{\partial T_y}{\partial x} \right) + \beta M_y + \left(\frac{\partial H_x}{\partial y} - \frac{\partial H_y}{\partial x} \right) = 0. \quad (\text{XVII.5})$$

According to this *vorticity equation* the wind-stress vorticity must be balanced at every locality by the vorticity of lateral mixing and by the term βM_y , which is the effect of the change of the Coriolis parameter with latitude. This equation is reminiscent of the equation (XIII.59a) derived by Ekman who designated the term βM_y the *planetary vorticity*.

SVERDRUP (1947) and REID (1948) have applied this equation to the equatorial currents of the eastern Pacific Ocean which correspond closely to the above conditions.

The x -axis is taken pointing eastward and the y -axis pointing northward. For the trade wind belt it is possible to put $\partial T_y/\partial x = 0$ so that neglecting lateral mixing, (XVII.5) gives

$$\beta M_y = -\frac{\partial T_x}{\partial y} \quad (\text{XVII.6})$$

and with (XVII.4)

$$M_x = \frac{\Delta x}{2\omega \cos \phi} \left(\frac{\partial \overline{T_x}}{\partial y} \tan \phi + R \frac{\partial^2 \overline{T_x}}{\partial y^2} \right) \quad (\text{XVII.7})$$

and

$$\frac{\partial P}{\partial x} = \overline{T_x} - \frac{\partial \overline{T_x}}{\partial y} R \tan \phi$$

and

$$\frac{\partial P}{\partial y} = -\Delta x R \frac{\partial^2 \overline{T_x}}{\partial y^2} \tan \phi + T_y.$$

Thus for $x = 0$, (at the north-south vertical boundary), $M_x = 0$ (integration limits 0 to Δx). The bars denote average values of the stress derivatives. The mass transports M_x and M_y can be found directly from (XVII.3) if $\partial P/\partial x$ and $\partial P/\partial y$ are known.

These equations have been tested by the "Carnegie" and "Bushnell" observations of corresponding areas (approximately between 160° to 80° W. and 10° S. to 20° N.) and showed good agreement with the values derived from the observations. The theoretical values were calculated from the distribution of wind stress obtained from the wind field given in oceanic climatological charts; thereby use has been made of formulae (XIII.48 and 49). Figure 254 shows the excellent agreement between the observed and theoretical meridional distributions of $\Delta P/\Delta x$ and M_x . It should be kept in

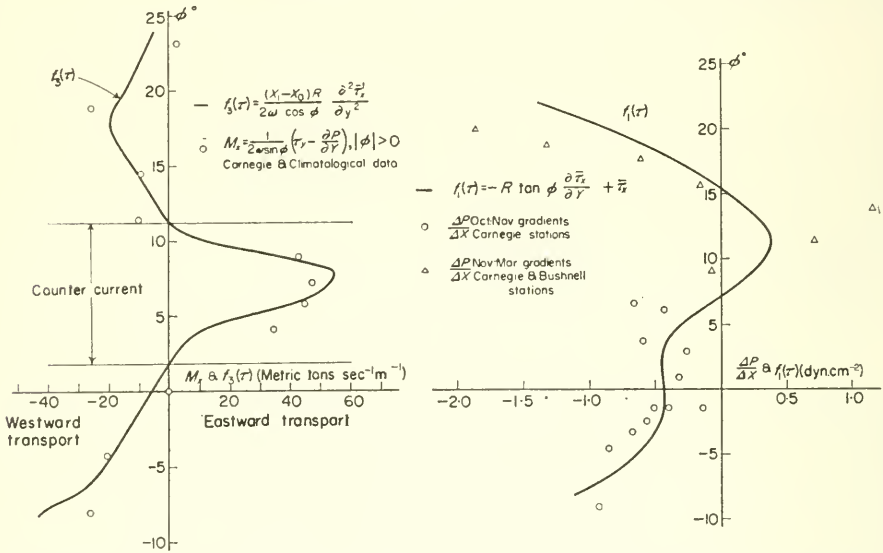


FIG. 254. Picture to the left: theoretical and observed values $\Delta P/\Delta x$ in two sections of "Carnegie" and "Bushnell" stations. Picture to the right: Latitude dependence of the longitudinal mass transport computed by two independent methods. (M_x = eastward mass transport in tons per sec through a column of 1000 m depth and 1 m width).

mind that the theoretical values are derived from *mean* wind conditions while the observed values are based on some oceanographic stations made at different times of the year. From these results it can be concluded that mass structure and mass transport of the currents in the eastern equatorial areas of the Pacific can be regarded as a consequence of the average shearing stress of the air currents on the surface of the sea. This conclusion should also be valid for the equatorial currents in other oceans.

4. Velocity Computations of Oceanic Surface Currents in the Equatorial Regions from Wind Data

The currents in the equatorial regions can, as a first approximation, also be regarded as the result of a drift current and a gradient current of the type described by Ekman. However, at the equator itself the two components are indeterminate and the geostrophic approximation gives infinitely large values. In dynamic calculation these areas must therefore be excluded. The question of how to calculate the currents in the immediate vicinity of the equator from oceanographic data has been dealt with by WEENINK and GROEN (1952), which gave an exact solution to the problem and by

TSUCHIVA (1955*a, b*) who made a second approximation to the geostrophic current equation for $f = 0$. For the surface velocity of a drift current and a frictionless gradient current the equations (XIII.26 and 31) give

$$\left. \begin{aligned} v_{x,0} &= \frac{T \cos(\psi - \pi/4)}{\sqrt{(f\rho_0\eta)}} - \frac{1}{f\rho_0} \left(\frac{\partial p}{\partial y} \right)_0, \\ v_{y,0} &= \frac{T \sin(\psi - \pi/4)}{\sqrt{(f\rho_0\eta)}} + \frac{1}{f\rho_0} \left(\frac{\partial p}{\partial x} \right)_0, \end{aligned} \right\} \quad (\text{XVII.6})$$

where ψ is the angle between the wind stress and the direction of the E -current; the subscript zero refers to the sea surface. Indeterminate solutions are obtained from (XVII.6) for the equator. If an exact solution is required the eddy viscosity cannot be taken as insignificant by comparison with the pressure gradient and the Coriolis force. Only in this way there is an equilibrium between the wind stress, the pressure force and the vertical friction in the equatorial belt. The simple equation of motion (corresponding to (XIII.23*a*) and (XIII.30)) is now

$$\frac{\partial p}{\partial x} + i \frac{\partial p}{\partial y} = -i\rho_0 f v + \eta \frac{\partial^2 v}{\partial z^2}, \quad (\text{XVII.7})$$

where

$$v = v_x + i v_y \quad \text{and} \quad \rho \sim \rho_0.$$

The boundary conditions are

$$\left(\eta \frac{\partial v}{\partial z} \right)_0 = -T = -(T_x + i T_y) \quad \text{and} \quad v(z = \infty) = 0 \quad (\text{XVII.8})$$

(XVII.7) is identical with

$$\frac{\partial^2 v}{\partial z^2} - av = b, \quad (\text{XVII.9})$$

where

$$a = \frac{if\rho_0}{\eta} \quad \text{and} \quad b = \frac{1}{\eta} \left(\frac{\partial p}{\partial x} + i \frac{\partial p}{\partial y} \right).$$

If $b(z)$ is known from observations then, taking equation (XVII.8) into account and since a is independent of z this can be solved. To determine $b(z)$ WEENINK and GROEN used the REID model (1948) which gives a good approximation for the equatorial regions. This postulates a homogeneous layer of thickness h below which the density of the water increases with depth according to an exponential function (see XVI.30). For this model (as in XVI.31) one obtains

$$\left(\frac{\partial p}{\partial x} \right)_0 = 2g\rho_0 \frac{\Delta\rho}{\rho_1} \frac{\partial h}{\partial x}; \quad \left(\frac{\partial p}{\partial y} \right)_0 = 2g\rho_0 \frac{\Delta\rho}{\rho_1} \frac{\partial h}{\partial y}$$

and the solution of (XVII.9) at the surface ($z = 0$) will be

$$v_0 = \frac{T}{\eta\sqrt{a}} - \frac{b_0}{a} \left(1 - \frac{1 + \frac{1}{2}h\sqrt{a}}{1 + h\sqrt{a}} e^{-h\sqrt{a}} \right). \quad (\text{XVII.10})$$

When the value of $h\sqrt{a}$ or of f is large the expression in brackets will equal 1 and (XVII.10) will be nearly equal to (XVII.6). It is thus apparent that at a latitude of 2° to

3° the value of $h\sqrt{a}$ is already large enough to allow equation (XVII.6) to be used instead of (XVII.10).

For a sufficiently narrow belt on both sides of the equator expansion into a power series with respect to $h\sqrt{a}$ gives, neglecting higher order terms

$$v_0 = \frac{1}{\sqrt{a}} \left(\frac{T}{\eta} - \frac{5}{2} b_0 h \right) + 4b_0 h^2 + \dots \quad (\text{XVII.11})$$

If lateral mixing is neglected ($H = 0$) the equations (XVII.3) become

$$T = \Delta P + ifM \quad (\text{XVII.12})$$

and (XVII.11) with (XVI.31) becomes

$$v_0 = 4b_0 h^2 + \frac{M\sqrt{a}}{\rho_0} + \dots \quad (\text{XVII.13})$$

Since M remains finite at the equator this gives finally by means of (XVI.31) and (XVII.12)

$$v_0 = \frac{8Th}{5\eta}. \quad (\text{XVII.14})$$

The behaviour of v_0 can be illustrated in the following way. If the first term on the right-hand side of (XVII.10) is the drift current and the remainder of v_0 is taken as the slope current, then both components tend to infinity on approaching the equator, but due to the coupling between these two components they behave in such a way that their sum remains finite and approaches the vector (XVII.14) as a limit of zero latitude. The surface current, the wind stress and the surface pressure gradient all have the same direction at the equator. Figure 255 illustrates their behaviour near the equator.

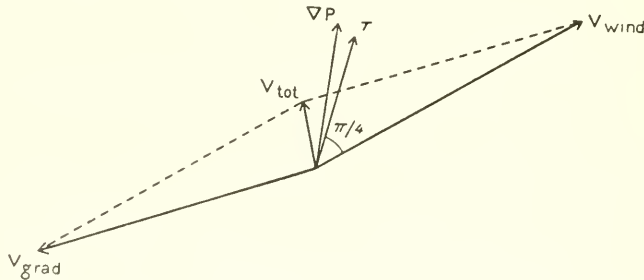


FIG. 255. The two components (v_{wind} and v_{grad}) of the current velocity (v_{tot}) somewhere near the equator. Exactly at the equator the vectors of the current velocity, the pressure gradient Δp and the wind stress T fall all in the same direction.

More recently YOSHIDA (1955) has shown that the model used by Weenink and Groen apparently leads to a solution involving a discontinuity in the vicinity of the equator. This singularity originates in the assumptions of the model. A modification of the model which seems more realistic in the light of recent observations appears to give a reasonable solution.

The method of Tsuchiva is simpler. The equations of motion of the geostrophic current are

$$fu = -\frac{\partial D}{\partial x} \quad \text{and} \quad fv = \frac{\partial D}{\partial x}, \quad (\text{XVII.15})$$

where D is the geodynamic depth. All the quantities in these equations can now be expanded into the Taylor series with respect to y and equation of terms of the same power of y gives, putting $\beta = df/dy$,

$$\left(\frac{\partial D}{\partial y}\right)_0 = 0; \quad \beta_0 u_0 = -\left(\frac{\partial^2 D}{\partial y^2}\right)_0 \quad \text{and} \quad \left(\frac{\partial D}{\partial x}\right)_0 = 0; \quad v_0 = 0. \quad (\text{XVII.16})$$

The distribution of D is easily found from oceanographic data. The east-west component u_0 of the current velocity at the equator can therefore be obtained from the second equation (XVII.16) and the north-south component v_0 is zero. At the same time $(\partial D/\partial x)_0$ and $(\partial D/\partial y)_0$ must be zero. The oceanographic data show that these conditions are fairly well satisfied in most cases. Values of u and v near the equator can be obtained by substitution of higher-order derivatives of u and v into expansions of these quantities. In a later paper Tsuchiva has also dealt with the effects of the inertia and frictional terms but these do not seem to alter the previous results. In the immediate vicinity of the equator the east-west velocity component of the current is determined by the curvature of the isobaric surface in the meridional vertical section and not by the slope. The geostrophic approximation for the ocean currents can be used much closer to the equator than has so far been done. The method used by Tsuchiva is purely mathematical and not founded on any physical basis.

Chapter XVIII

Basic Principles of the General Oceanic Circulation

1. Introduction

THE ultimate cause of all movements in the sea is the supply of energy by solar radiation. The meridional variations in the energy supplied lead to regional differences in the structure of the oceans. The oceanic circulation modifies, however, the distribution of temperature and salinity, which are basically determined by the climate, and also affects the distribution of dissolved gases in the sea; it therefore has an indirect influence on the distribution and accumulation of marine life. The general oceanic circulation is therefore the fundamental problem of oceanography.

The transformation of solar radiation into heat in atmosphere and sea takes place mainly in the layers close to the interface between air and land, between air and water, respectively. Other important influences from the hydrosphere on the atmosphere and the reverse are also localized at the sea surface and in this way the sea surface becomes one of the most important interfaces of the earth; it is the starting point of both the atmospheric and the oceanic circulation. The principal factors involved in these, such as the solar and sky radiation, outgoing radiation, evaporation, precipitation, melting of ice and the wind stress on the water exert their major effects here. In comparing the atmospheric and oceanic circulation the special circumstance should be kept in mind that the interface (sea surface) which is decisive for the initiation of vertical motions is situated *below* the atmosphere but *above* the sea. Therefore, in order to start a vertical circulation in the atmosphere air must be lighter than the surrounding air masses (rising motion), while in the ocean water as compared with the surrounding waters must be denser (sinking motion). The variable position of this interface, from which the vertical circulations originate, causes corresponding differences of the circulation system (DEFANT, 1929).

According to the general causes, mentioned above, of steady water movements in the sea, two fundamental factors stand in question:

- (1) the internal field of force of the mass structure, and
- (2) the external field of force due to the winds.

Other less important external forces such as the supply of water by precipitation or its removal by evaporation are less effective than the wind forces (see p. 572).

These two basic factors act quite differently on the water movements and an understanding of the general circulation can only be based on the *resultant* of the two effects. Most investigations have been limited to the components of motion of the

circulation in a meridional plane with only supplementary extensions to three-dimensional space. This has no doubt been unavoidable in the past due to the lack of sufficient observations, but a complete understanding of the oceanic circulation can be obtained only in terms of *spatial phenomena*. The magnitude and the complexity of the problems makes it understandable that a solution in full detail has not yet been obtained and probably will not in the near future, but the accumulation of further data and the advance of theoretical knowledge will lead closer to a comprehensive elucidation of the mechanism of the general oceanic circulation which is the aim of oceanography.

The permanent oceanic currents can be divided into three groups according to their genetic origin:

- (1) currents produced by thermo-haline convection, mainly due to cooling of surface water in higher latitudes;
- (2) currents produced and maintained by the transfer of wind energy to the sea surface;
- (3) currents maintained by the excess of precipitation over evaporation, or vice versa occurring in special oceanic regions.

Each of these types of flow shows a different physical behaviour and acquires on the rotating earth an individual form, which is also strongly influenced by continental slopes acting as barriers for the oceanic movements.

2. Oceanic Sea Surface Currents

(a) Charts of Sea Surface Currents

It has taken quite a long time until data on sea surface currents were that numerous as to allow a reliable representation of the currents over the entire ocean surface. Charts of currents presented in ordinary atlases are seldomly based on critically tested observations and are often constructed making hypothetical assumptions. As amount and density of the observational material (current measurements) increased, charts of current conditions over smaller oceanic areas could gradually be extended until finally world maps of ocean currents could be constructed. At the suggestion of NEUMAYERS (1898), Schott prepared a world chart of ocean currents. A new edition of this was published in 1942 incorporating in an excellent manner the oceanographic progress of the last 40 years. This chart (SCHOTT, 1942), *Deutsche Admiralitätskarte* no. 1947, 2 sheets, 1942) shows the total earth for the Northern Hemisphere winter and an inset map for 30° N. to 20° S. shows seasonal variations for the tropics during the Northern Hemisphere summer. North of 50° N. the chart represents more summer conditions for which the data are more numerous. This current chart is reproduced in Plate 8 on an equal area projection. The use of current arrows has been simplified in places: velocities are indicated at $\frac{1}{2}$ knot intervals with a lower limit of 12 nautical miles in 24 h and an upper limit of 36 nautical miles in 24 h. Differences in velocity are indicated by the thickness of the arrows and the constancy of the current by the length; the last factor was expressed in four degrees: variable, fairly steady, steady and very steady corresponding roughly to 25, 25–50, 50–75 and 75% flow displacement in the direction of the arrow. Naturally in such large-scale charts only a somewhat general representation of the currents can be given and some subjective interpretation is always possible. Details in the infrequently navigated parts of the ocean are, of course,

highly deficient and must be supported by theoretical deductions. For details in particular areas of the ocean, reference must be made to special charts; the literature sources will be indicated below.

As is apparent from the current charts in Plate 8, the more schematic distribution of oceanic currents known from earlier work is really present to a large extent in all oceans. Northern and southern equatorial currents characterize everywhere the tropical surface circulation and are usually separated by an equatorial counter current flowing in the opposite direction, while the surface circulation of higher latitudes is composed principally by the West Wind Drift and the Polar Current. Separation of these current regions gives convergence and divergence lines which are specially indicated in the current chart. They are rarely clear-cut lines; instead they are usually rather wide areas intruding between individual currents. It is often difficult to determine their position accurately since they move backward and forward periodically in time. The connection of this surface current system with the currents of the deeper layers lies in these singularity areas, and they are thus of great importance.

In the following sections a brief description will be given of the surface-current conditions in the individual oceans and of their seasonal variations. The dynamics of single currents will be dealt with later.

(b) The Surface Currents of the Atlantic Ocean

The backbone of the system of currents present in the Atlantic is formed by the two equatorial currents; that in the Southern Hemisphere is the stronger one and is more constant and of greater extent. During the whole of the year this current crosses the equator from west of the island of St Thomé until the South American coast. The meridional distribution of the current intensity shows a double current core for nearly all months; one of the two just north of the equator at about 1° to 2° N. and the other one at about 4° to 5° S. (especially between 20° to 30° W.). Between them along the equator is the equatorial region of divergence which belongs to the tropospheric deep sea circulation (p. 595). This divergence coincides with the tongues or island of cooler water that are shown in temperature charts, particularly in the period from June to August and indicate the upwelling of deep water accompanying the divergence. In the central part (8° to 40° S.) the South Equatorial Current is most intense from June to July and hardly drops below 20 nautical miles in 24 h. The southern current core divides into two parts at Cape San Roque—one turning south and becoming the *Brazil Current*, and the other joining the northern current core in the latitude of the Amazon estuary to form the strong *Guiana Current* flowing along the South American coast.

The Northern Equatorial Current is less constant in extent and strength. Its northern boundaries fluctuate, but from about 20° N. its intensity decreases and it passes into an extensive region of weak and variable currents with frequent motionless areas. South of 20° N. its average intensity is about 15–17 nautical miles in 24 h. SCHUMACHER's monthly charts (1940) which give greater detail show the effect of the bottom topography on the current system where it passes over the mid-Atlantic Ridge (see p. 435).

During the winter months when the equatorial counter current is very weak the North and South Equatorial Currents flow together along a convergence line from about 20° W., 4° N. to approximately 50° W., 11° N. but during the summer months

when the counter current is more strongly developed this only occurs between 50° W., 10° N. and 60° W., 14° N. From here a combined current runs in a westerly direction towards the West Indies throughout the whole year; this is the source for the surface currents in the West Indies and therefore also for the Gulf Stream (DIETRICH, 1937 b; 1939), which is in agreement with the results of Brooks (1930, see also, SHAW and HEPWORTH, 1910) showing that the fluctuations in the south-east trade winds are more closely connected with water and air temperatures in Western Europe than are those of the north-east trade winds.

The *Equatorial Counter Current* lies between the two equatorial currents. Table 147 presents its position in different seasons. During almost the whole of the year it is divided into two parts; the "western" counter current weak and not very broad, found particularly during the first winter months and the "eastern" counter current which is present all the year round. Only in the summer months do they join, thereby forming a mighty counter current. The origin of this lies west of 50° W., near the American coast, its width covers the area between 10° and 3° N. showing considerable speed and constancy. During the period of its greatest extent the central area of the current is characterized by a convergence region towards which water flows from both sides. An attempt has been made by SCHUMACHER (1940) to show a connection between the temporary interruptions in the counter current above the mid-Atlantic Ridge and the topography of the rise.

Table 147. *Extent of the Equatorial Counter Current in the Atlantic Ocean*
(according to Schumacher)

	Western Counter Current				Eastern Counter Current		Region with no currents (deg. lat.)
January	53° W.,	10° N.	until	37° W.,	6° N.	26° W., 7° N.	11
February	49°	9°	until	41°	6°	19° 5°	22
March	53°	10°	until	47°	7°	20° 4°	27
April	52°	9°	until	37°	0°	24° 4°	13
May	47°	6°	until	33°	0° **	28° 5°	5
June	51°	9°	until	38°	3° **	36° 5°	2
July	51°	9°				—	0
August	56°	10° *				—	0
September	52°	10° *				—	0
October	53°	10° *				—	0
November	54°	10° *	until	32°	8°	31° 7°	1
December	51°	9°	until	30°	6°	29° 6°	1

* Starts presumably farther north-west,** with interruptions.

Northern Hemisphere. The combined equatorial currents enter the Caribbean Sea between the Antilles and spread over almost its entire width as the *Caribbean Current*; this flows almost due west with its greatest velocities in the southern part. In some months large vortices are formed off the coast of Costa Rica, Panama and Colombia.

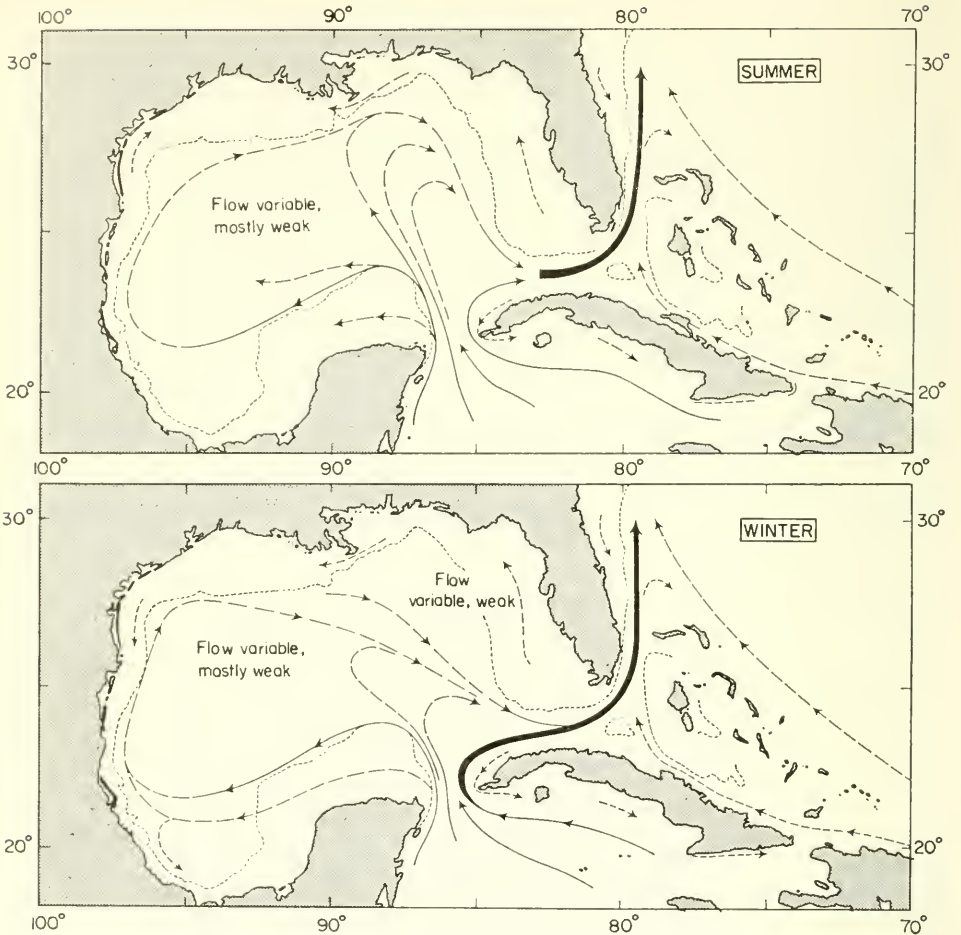


FIG. 256. Schematic picture of the sea surface currents in the Gulf of Mexico (according to Schumacher).

The current then enters the Gulf of Mexico through the Yucatan Channel with velocities of up to 3.7 knots at the current core. The currents of this mediterranean sea are shown in Fig. 256 (SCHUMACHER, 1940). The major part of the stream lines leaving the Yucatan Strait tend to circle or cross the Gulf clockwise following the shelf line. The branch that flows directly to the Florida Straits is stronger and is steady only during the winter months.

The eastern branch of the Yucatan Current forms the *Florida Current* the water transport of which is the main source of the Gulf Stream. No other ocean current has been so intensively investigated as this. An enormous amount of literature has been accumulated on the subject that is impossible to cite here in detail. The water piled up in the Gulf of Mexico flows out through the Florida Straits towards the north as a gradient current (*Florida Current*) against the prevailing winds. This current becomes stronger where the channel narrows off Bimini and may have a velocity of over 60

nautical miles in 24 h with up to 80–100 nautical miles in the current core. These values correspond to about 1.5–2.5 m/sec which is hardly reached even in the downstream parts of big rivers. According to KRÜMMEL (1911, p. 576), the axis of the stream under steady conditions is:

- 35 nautical miles in the Yucatan Channel (east of Contoy Island),
- 25 nautical miles north of Havana (85° W.),
- 11 nautical miles east of Fowey Rocks (Florida 25.7° N.),
- 19 nautical miles east of the Jupiter light tower (Florida 27° N.),
- 38 nautical miles south-east of Cape Hatteras.

At the edges, particularly on the western side, the current shows often variations in direction and strength. Not infrequently there is a counter current flowing in a south-westerly or westerly direction along the Florida Keys into the Gulf of Mexico and is well separated from the basic Gulf Stream. It is connected with the counter current always found further north off the east coast of America. In the most narrow parts of the channel the current has a width of about 30 nautical miles, off Cape Canaveral (28.5° N.) about 60 and off Charleston a width of as much as 120 to 150 nautical miles. In general, the western border of the blue coloured warm water of the current follows the continental slope. To the west of it on the shelf the cold green water of the "cold wall" is usually travelling slowly to the south; (see Pt. I, p. 144, Fig. 60). The Florida Current is joined here by the important *Antilles Current* flowing north-west to the north of the Bahamas. Before the junction (27° N.) it is narrowed in the convergence region of the Sargasso Sea, whereby it becomes of some importance (see NIELSEN, 1925; WÜST, 1924). North of Cape Hatteras the Gulf Stream turns farther and farther away from the continental slope, possibly due to offshore winds, Coriolis influence and the increasingly strong cold coastal current of low salinity. This is the beginning of the *second part of the Gulf Stream*. Its left-hand boundary remains sharply separated from the coastal waters but the right-hand edge is extremely blurred. Here, due to the deflection of the stream lines a counter current is formed which, although narrow, weak and variable is a characteristic phenomenon of the eastern flank of the main current, but because of its narrowness it can rarely be detected by means of ship displacements; however, the farther to the north-east the stronger and more frequent this current appears. Only mean positions of the current can be deduced by evaluation of the average physical conditions at the sea surface. Better results can be obtained by systematic recordings of the sea-surface temperature at short time intervals; these then give a more accurate indication of the mean position of the warm Gulf Stream core and also of its northern and southern limit (see Pt. I, p. 144, also FUGLISTER, 1947). Determinations of the Gulf Stream position obtained by different methods can be combined to give an average picture (NEUMANN and SCHUMACHER, 1944) but it should always be borne in mind that the boundaries of the warm-water belt cannot necessarily be regarded as identical with the boundaries of the current.

From about 55° W. the left side of the Gulf Stream is flanked by the cold and weakly saline water of the *Labrador Current*. At this polar front the cold water masses sink below those of the Gulf Stream and thereby numerous vortices are formed. To the south of the Newfoundland Banks the Gulf Stream turns sharply towards the south (p. 421) and again back towards north and from here gradually widens and splits into

current branches of varying strength and of varying temperature. From Cape Hatteras to the Irish coast its direction remains mainly eastwards or north-eastwards; the average velocity falls from 15 to 5 nautical miles in 24 h and its constancy from 70 to 30%. The almost synoptic surveys of the International Gulf Stream Expedition of 1938 showed that the Gulf Stream to the north of the Azores is no longer a single current, but is broken up into several branches flowing to the north-east as warm and highly saline intrusions between cold, weakly saline water masses moving slowly in the opposite direction. NEUMANN (1940) has shown that this finger-like interaction of

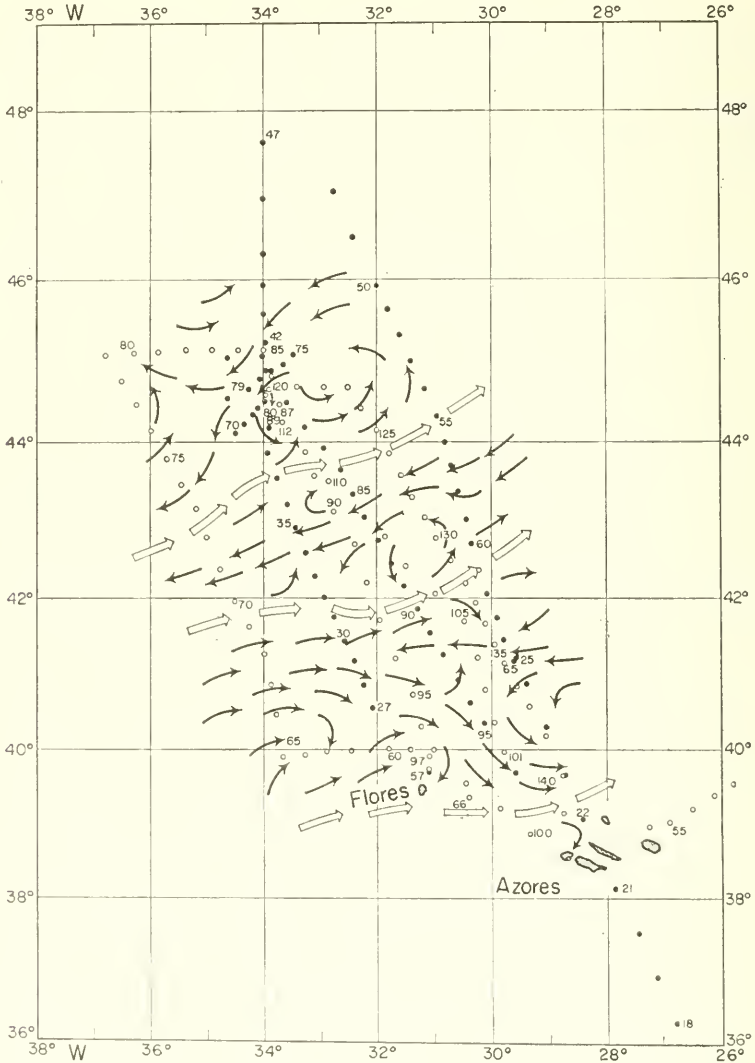


FIG. 257. Most probable course of the Gulf Stream north of the Azores in June 1938. (The open arrows indicate the assumed position of the cores of individual branches of Gulf Stream.)

different water types was no chance phenomenon present in June 1938 but is a permanent feature of the current in these regions (see Fig. 257).

In the eastern half of the ocean the *Atlantic Current* divides into two main branches at about 20° W.; one of these flows north-east past Ireland and with a reduced strength and moderate constance through the Faeroes—Shetland Channel into the Norwegian Sea and along the Norwegian coast. It is still noticeable in the Arctic Ocean. The weak and variable second branch turns east-south-east towards the French and Spanish coasts (the Portugal Current). The stronger and also more steady *Canaries* current in the south-eastern North Atlantic cannot be regarded as a continuation of the Gulf Stream (THORADE, 1928). It seems to be advisable to refer to the whole current from the Florida Straits to the Norwegian coast as the *Gulf Stream System* but to distinguish six separate parts of this system (ISELIN, 1938); the most important are:

- (1) the Gulf Stream close to the coast or the Florida Current (from the Gulf of Mexico to Cape Hatteras);
- (2) the Gulf Stream in the open ocean (from Cape Hatteras until north of the Azores);
- (3) the Irish Current (from the splitting point until the Faeroes—Shetland sill);
- (4) the Atlantic (or Norwegian) Current (along the Norwegian coast).

A side branch of the Irish Current flowing from the south of Iceland to its convergence with the East Greenland Current is called the *Irminger Current*. HELLAND-HANSEN and NANSEN (1909) deduced the sea surface currents of the Norwegian Sea from an analysis of temperature and salinity in charts and vertical sections (Fig. 157, p. 368). North of the Lofoten the Atlantic current divides into a branch flowing towards north and north-west (towards Spitzbergen) and another one flowing north-east into the Barents Sea (SCHULZ, 1929). Towards Greenland the East Greenland Current is still wide and strong north of the Denmark Strait. In the central part of the Norwegian Sea there is an extensive area of extended vortices apparently connected with the topography of the sea bottom.

Southern Hemisphere. The *Brazil Current* is a continuation of the South Equatorial Current from Cape San Roque southward. Between 15° S. and 20° S. it is still inside the region of the south trade winds. Off Cape Sao Thomé and Cape Frio the main current flowing south-westwards shows a contraction from its eastern (left) side during most months; from here it follows the continental shelf line fairly close, probably due to the influence of the Coriolis force. Over the shelf a counter current exists which can be regarded as a branch of the current along the Patagonian shelf (Falkland Current). Off the La Plata estuary the eastern part of the Brazil current turns south-eastwards working into each other in a finger-like fashion with the *Falkland Current* flowing from the south-west. Near the coast the Falkland Current intrudes to the north and north-east as far as 35° S., deflecting the Brazil Current to the east. Between the two opposing currents there is thus a sharp convergence line formed which is clearly shown by the distribution of the oceanographic factors. This gives rise to vortices found in this part of the ocean. The interaction between Falkland and Brazil Current form a southern hemisphere counterpart to the Labrador Gulf Stream system in the Northern Hemisphere, but the first ones are less well developed and of less intensity.

The area of the *West Wind Drift* includes the whole of the southern part of the South Atlantic Ocean between about 35° and 63° S. It belongs to the large circumpolar

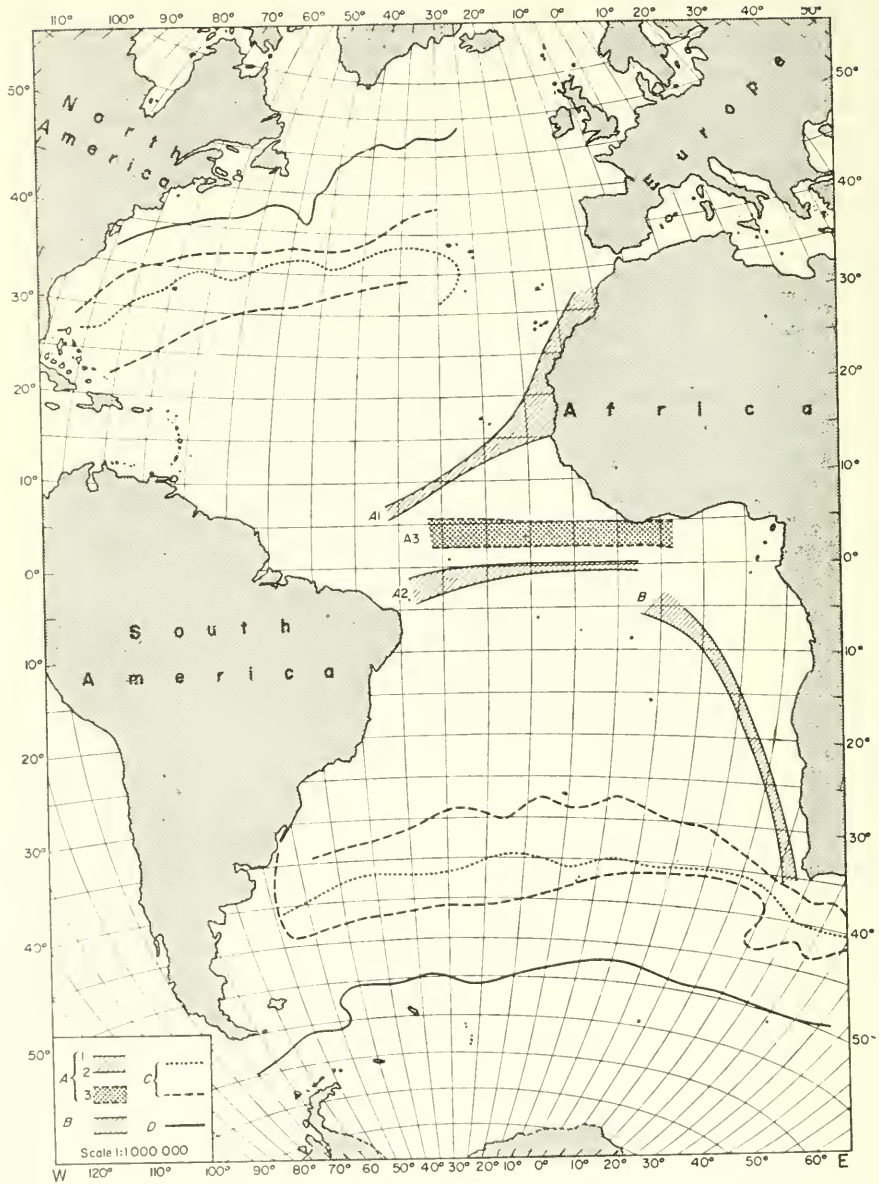


FIG. 258. Singular lines in the current field of the sea surface in the Atlantic Ocean. (A) in the system of the tropospheric circulation: (1) the divergence region in the area of the Cap Verde Islands (7° to 15° N.); (2) the equatorial divergence region; (3) the convergence region in the Equatorial Counter Current. In the region of the tropical thermocline these singular lines correspond to inverse ones. (B) the divergence region of the Benguela Current. (C) ·····, subtropical convergence; -----, polar and equatorial limits of the subtropical convergence regions. (D) ———, the oceanic polar front (Arctic and Antarctic convergence).

current which keeps the water masses constantly in motion around the earth from west to east. It is of much greater strength and constancy than the corresponding West Wind Drift in the North Atlantic. South of 35° S. and east of 20° W. it flows mainly in a north-easterly direction. There are widely differing opinions about the position of its northern boundary in the area of the subtropical convergence; the southern boundary is found at about 63° S. but is not sharply defined either. At the core of the West Wind Drift lies the boundary between two quite different water types, the *subantarctic water* of middle latitudes and the *Antarctic polar water*. In the Atlantic this latter water type has its origin almost entirely in the Weddell Sea. A small part only comes from the Pacific through the Drake passage. The boundary between the two water bodies is denoted the South Polar Front (*Antarctic Convergence*) on both sides of which the currents flow between east and east-north-east but the velocity is greater on the northern side. For the dynamics of this front see p. 549.

The Polar Current in the Southern Hemisphere flows in the coastal regions of the Antarctic carrying cold polar water westward until the Weddell Sea where it turns in a great arc around a central almost motionless region and flows towards north or north-east to become the southern part of the West Wind Drift. East of 10° W. the course of this Antarctic polar current coincides almost entirely with the mean pack-ice limit of the southern summer.

The framework of the circulation system of the sea surface formed by singular lines and regions inside the current field is shown in Fig. 258. In the tropical and subtropical circulation the divergence lines stand out clearly in the eastern parts of the North and South Equatorial Currents. In almost all months there is a narrow area of divergence off the West African coast in particular between the Canaries and the Cape Verde Islands that extends towards the south-west beyond 35° W. as a two-sided divergence line and forms the southern boundary of the North Equatorial Current. This is connected with the upwelling of cold water off the West African coast. Its counterpart in the Southern Hemisphere is the extended divergence line in the area of the *Benquela Current* off the coast of South West Africa; the upwelling of cold water also occurs here (DEFANT, 1936a). Reference has already been made to the divergence line along the equator between the northern and southern branches of the Equatorial Current (p. 559) and also to the convergence line in the Equatorial Counter Current. The Cape Verde divergence line, the equatorial divergence line and the convergence line that lies between them are all part of the tropospheric circulation system and are associated with contrary singularities in the lower layers of the troposphere (p. 595).

The oceanic regions between the Equatorial Currents and the West Wind Drifts in both hemispheres contain weak and variable currents. Stream lines deflected to the right from the Atlantic Current and from the North Equatorial Current together form the region of *subtropic convergence*. This extends across the Atlantic from 75° to 20° W. but is not a continuous uniform convergence line. Vortex formations are the characteristic type of motion with the existing slight density differences. In these vortices warm water sinks to become part of the warm-water mass of the troposphere in this region. This convergence is always indistinct and shows everywhere large seasonal variations (FELBER, 1934) and is therefore more appropriately called a subtropical convergence region than a convergence line. In this convergence region the interaction

between highly saline and warm water from lower latitudes with weakly saline and colder water from higher latitudes lead to vortical movements of large extent. Similar conditions are found in the subtropical convergence region of the South Atlantic. There are rather different opinions about the question how far the West Wind Drift reaches equatorward depending on whether the subtropical convergence is fixed according to ship displacements or if it is derived by means of the distribution of oceanographic factors. The position given by DEACON (1937), deduced mainly from the temperature distribution, is always about 6° to 10° further south than that obtained from current measurements. According to BÖHNECKE (1938, p. 201) the "subtropical convergence" (of the currents) should be carefully distinguished from the "subtropical boundary" (deduced from temperature and salinity). The former in a rather characteristic way coincides with the tropic boundary and the latter with the polar boundary of that large disturbance region which extends between the southern limit of the Equatorial Current and the West Wind Drift (p. 564) as is found during the dynamic preparation of serial observations. Also here it seems more appropriate to speak of a convergence "region" between the two bordering water types being the place for subtropical vortex formations.

The Southern Hemisphere Polar Front (Antarctic convergence line) has been discussed on p. 549. The Northern Hemisphere Polar Front is sharply developed between the Labrador Current and the Gulf Stream near the Newfoundland Banks but gradually fades towards the north-east, reappearing again as a frontal zone between the East Greenland Current and the Irminger Current. Larger and smaller vortex formations with corresponding vertical movements are also found along this convergence line.

(c) Sea Surface Currents in the Indian Ocean

Ships displacements available for other oceans are much less numerous than in most parts of the Atlantic and current charts are therefore correspondingly more uncertain. Reference to analogous conditions as in the Atlantic will usually permit briefer description here, but the Indian Ocean has a single particular peculiarity in its northern part where the wind system changes character completely every six months, correspondingly causing similar changes of the ocean currents. This is the best possible proof that the winds are decisive for the generation and maintenance of ocean currents. A full cartographic description of the currents here requires monthly charts (British Admiralty 1895; Deutsche Seewarte 1908; DALLAS and WALKER, 1908; MÖLLER, 1929) but charts for the summer monsoon and for winter are usually considered sufficient.

The currents during the time of the north-east monsoon (north-east trades) correspond best to the general system of ocean currents. They resemble those of the Atlantic and the Pacific except that the Equatorial Counter Current lies between about 2° S. and 8° S., that the Northern Equatorial Current moves partially into the Southern Hemisphere; during this part of the year the thermal equator is always south of the equator. In the north the North Equatorial Current (monsoon drift) runs almost due west. It is strongest to the south and south-west of Ceylon where the cross-section through the current is narrow. In the Bay of Bengal there is an anticyclonic vortex. The strong north-west to north-east winds over the Arabian Sea produce a

drift current towards west-south-west or west. Thereby a current boundary is formed beginning north-west of Cape Comorin and can be followed along about 10° N. westwards until 60° E. It carries the character of a convergence line between water from the Arabian Sea and water masses of the main current flowing from the east. SCHOTT (1928a) has mentioned the great contrasts in surface salinity here. Part of this water transport into this region enters as a very strong current into the Gulf of Aden and continues through the Strait of Bab el Mandeb into the Red Sea. The other part forms a strong south-west current flowing along the Somali coast to about 7° S., where the Equatorial Counter Current starts rather abruptly having a direction towards east.

South of the counter current flows the broad South Equatorial Current and shows large seasonal variations in velocity and constancy caused by the annual variation of the south-east trade winds. The current core lies near the northern boundary of the current at about 10° S. to 15° S. in both summer and winter (MICHAELIS, 1923). The irregularities in the South Equatorial Current due to Madagascar have been investigated by PAECH (1926). In the Southern Hemisphere summer a "Stau" current flows as a southward current along the African coast starting at 10° S., the *Mozambique Current*, with a tributary current from the east coast of Madagascar. Both form the source for the *Agulhas Current* at about 30° S., which continues closely to the continental shelf until it swings out from the shelf around the Agulhas Bank at the southern tip of Africa. The northern part of the core, however, still keeps to a very large extent over the continental shelf. From the southern end of the Agulhas Bank part of the current then flows north-west as the *Benguela Current* and part turns back into the Indian Ocean forming a series of large vortices. The complicated nature of the currents in this part of the convergence zone between the Agulhas Current and the west wind drift is clearly shown in an analysis of the current field which has been prepared by MERZ (1925).

The atmospheric pressure and wind distribution over the Indian Ocean north of the equator changes drastically during April. Almost immediately the sea surface currents react to this change in the wind direction and at the same time there is a redistribution of the water piled up at the coasts. The South Equatorial Current still remains in the Southern Hemisphere (south of 5° S.) but is considerably intensified. The counter current disappears and over the entire northern part of the ocean except the coastal zones a fairly constant eastward current appears, the *South-west Monsoon Current*. The convergence line between the South Equatorial Current and this monsoon current is well developed along the total width of the ocean and broken only in the extreme west where a strong branch turns northwards from the South Equatorial Current between 5° S. and 0° and flows along the coast into the Arabian Gulf as the *Somali Current*. It follows closely the steep pressure gradient off the coast between the region of piled up water ("Anstau"-Gebiet) between 5° and 10° S. and the area from which water has been removed by the monsoon current between 5° N. and 10° N. This is accompanied by upwelling just off the African and Arabian coasts (PUFF, 1890). The Somali Current possesses mostly an extreme intensity, so that speeds here are greater than in the Florida Current (often more than 100 nautical miles in 24 h) (Fig. 259). The formation of anticyclonic vortices to the south-east of Ras Hafun and the marked concentration of the current core into a narrow coastal belt is characteristic and accords with the increase of the Coriolis force towards north.

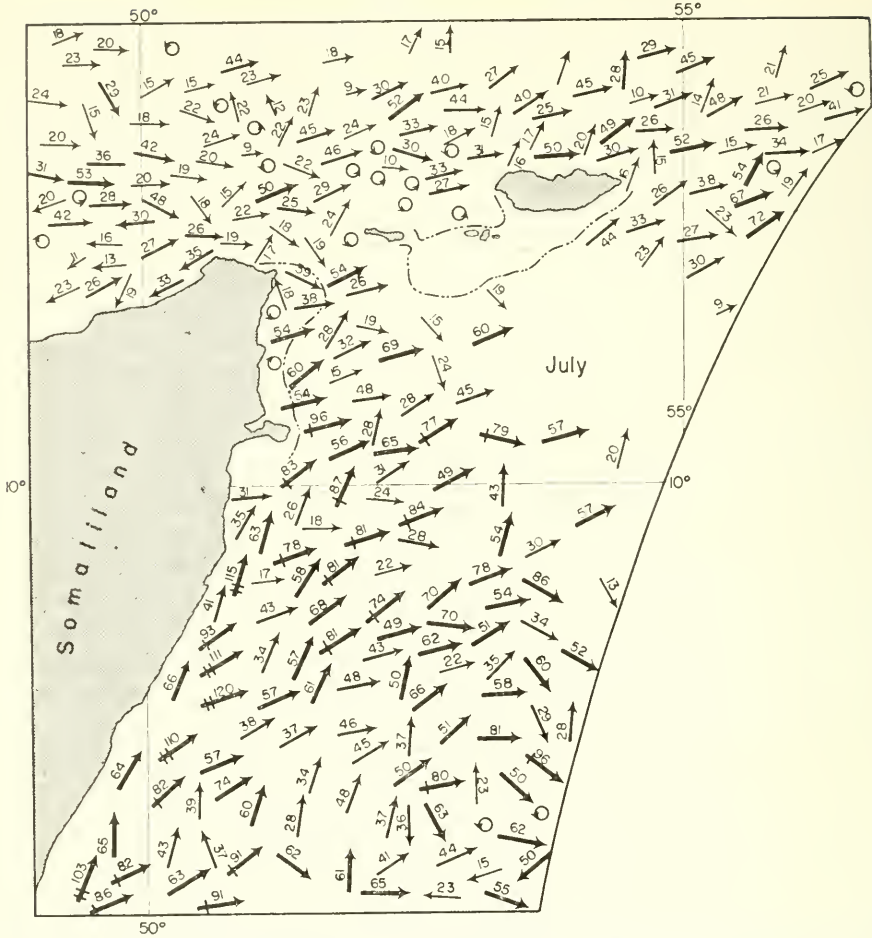


FIG. 259. Current displacements in the Somali Current at the time of south-west monsoon.

The southern boundary between the current branches of the South Equatorial Current and the West Wind Drift is again a long convergence line at about 40° S. For its position see WILLIMZIK (1929) and the alternative interpretation by SCHOTT (1925, p. 163). South of the convergence region and especially in higher latitudes the West Wind Drift has a very low constancy corresponding to the variable winds of this region. The non-uniform character in the current is already shown by the rapid decrease in constancy as the number of observations increases. The *Antarctic Convergence* runs right across this broad current gradually receding from 48° S. in the west to about 54° S. In this area the West Wind Drift flowing east-south-east meets the cold coastal Antarctic water flowing west-north-west and north-west (WILLIMZIK, 1927).

(d) Sea Surface Currents in the Pacific Ocean

The principal currents of the Pacific are again the North and South Equatorial Current. Because of the great width of the Pacific they are almost purely east-west

currents. Since the thermal equator remains in the Northern Hemisphere throughout the whole year these currents are not symmetrical about the geographical equator. The southern boundary of the North Equatorial Current lies between 6° N. and 7° N. in winter and between about 9° N and 11° N. in summer. It is much stronger in winter. At its southern boundary the current at each location has a purely zonal direction and constant speed, while its velocity increases steadily towards the west. Off the Philippines (north of Mindanao) the strong current divides: one branch flowing northward to become the Kuroshio and the other turning sharply southward into the Equatorial Counter Current. Off the east coast of Mindanao it flows southwards with a 100% constancy (SCHOTT, 1939, see also PULS, 1895).

The South Equatorial Current covers the wide south-east trade wind belt between about 5° N. and 40° S. The greatest velocities and constancy again lie along the northern border between 5° N. and 5° S. and, as in the Atlantic, a double current core is occasionally present. By this a long and narrow tongue of extremely low temperature is caused in the thermal field in the eastern part of the Pacific west of the Galapagos Islands. These areas of cold water are associated with the occurrence of eastward ship's displacements within the South Equatorial Current. Similar ship's displacements are occasionally observed in the Atlantic. West of New Guinea and the Solomons the South Equatorial Current during the northern summer is a torrent current extending almost as far as Halmahera; it supplies the main water mass of the counter current. Off the east coast of Australia the South Equatorial Current bends and is called from thereon *the East Australian Current* which corresponds to the Agulhas Current in the Indian Ocean.

All the year long a well-developed *counter current* is inserted between the two Equatorial Currents. During the northern winter it is weak and narrow, except in its starting area in the west, but during the northern summer especially during August and September it flows with great constance from Mindanao–Palau–Halmahera to Panama (almost 8000 nautical miles) with a width of about 300 miles between 5° N. and 10° N. It is separated from the Equatorial Currents by well-defined boundaries especially on the northern side.

The *Kuroshio* is a continuation of the North Equatorial Current and in many respects an important phenomenon for Eastern Asia. A review of what is known of this current and a comparison with the Gulf Stream system with numerous references has been given by WÜST (1936a, see also, UDA and OKAMOTO 1930, 1931; UDA, 1933). In summer it starts flowing northward east of Formosa with a velocity of 24–36 nautical miles in 24 h and a width of about 300 nautical miles. Then it runs west of the Ryukyu Islands between the Ryukyu Ridge and the East China shelf with decreasing width and correspondingly increasing speed (36–48 nautical miles in 24 h) until it branches south of Japan; one branch, the *Tsusima current* enters the Sea of Japan and flows north-north-west, the other, the proper Kuroshio, flows with a reduced width along the south-eastern coast of Japan. Between 31° and 35° N. it is only about 150 km wide but its velocity rises to 48–56 nautical miles per day. Its left-hand boundary is sharply defined but the right-hand one (oceanic side) is blurred. Here, like the Gulf Stream, it has a weak counter current. It turns abruptly eastwards towards the open ocean at 36° N. off the Boso Peninsula with an almost invariable width but with gradually decreasing velocity (48–24 nautical miles per day). This deflection of the

current has been regarded by HIDAHA (1927–28) from experimental evidence as due to the change in direction of the north-east coast of Japan, but Wüst believed that topographical factors south of the Boso Peninsula were responsible. The Kuroshio extends out into the open ocean as a relatively strong current along 34–36° N. as far as 175° E. a distance of about 1,600 miles. Only for a short distance along the coast the current keeps the north-east direction. Figure 260 shows a schematic representation of the main current cores of the Kuroshio system during the summer as given by Wüst. Table 148 gives a comparison with the Gulf Stream system.

Table 148. Comparison between Kuroshio and Gulf Stream
(Mean values for summer, according to Wüst)

Current section	Width (km)	Direction	Speed (cm/sec)	Nautical miles/24 h	Temp. (°C)	Salinity ‰
Kuroshio						
23°–24° N. .	300	N. to E.	51–77	24–36	} 22–28	34·8–34·9
27°–28° N. .	230	N.E.	77–103	36–48		
31°–33° N. .	150*	N.E.	100–120	48–56		
About 36° N. † .	150	E.	51–100	24–48		
Gulf Stream						
23°–24° N. .	110	E.	100–120	48–66	} 22–28	36·0–36·4
27°–28° N. .	140	N.	140–160	66–75		
31°–33° N. .	180‡	N.E. to N.	About 120	About 56		
About 36° N. .	180	N.E.	About 100	About 48		

* After separation of the Tsushima Current.

† 400 km east of the Japanese Coast.

‡ After confluence with the Antilles Current.

The Oyashio flows south-west to south-south-west in the dead angle between the north-west coast of Japan and the north-western branch of the Kuroshio as far as 37° N. It is a relatively cold current with a very low salinity (33·5‰). It does not reach as far south in summer as in winter. According to Uda the boundary between the Kuroshio and the Oyashio as a convergence region consists of numerous vortices similar as at the boundary between Labrador Current and Gulf Stream. Differences in temperature and salinity across this convergence line in winter will be at least as large as those off the Newfoundland Banks. Driven by the strong northerly and northwesterly winds the Oyashio takes its cold water supply from the Sea of Okhotsk near the Kuriles and in part also from the Bering Sea.

The water is mostly in slow motion between the cold boundary which runs eastwards a little north of 40° N. and gradually fades away and the subtropical convergence which begins in the west at 20° N. and turns northward, at first only slowly, to reach 35° N., remaining in this latitude until about 138° W. This continuation of Kuroshio is termed the *North Pacific Current*. Its main part turns southward between 150° and 135° W., part joining the California Current and part mixing with the water from the North Equatorial Current along the subtropical convergence.

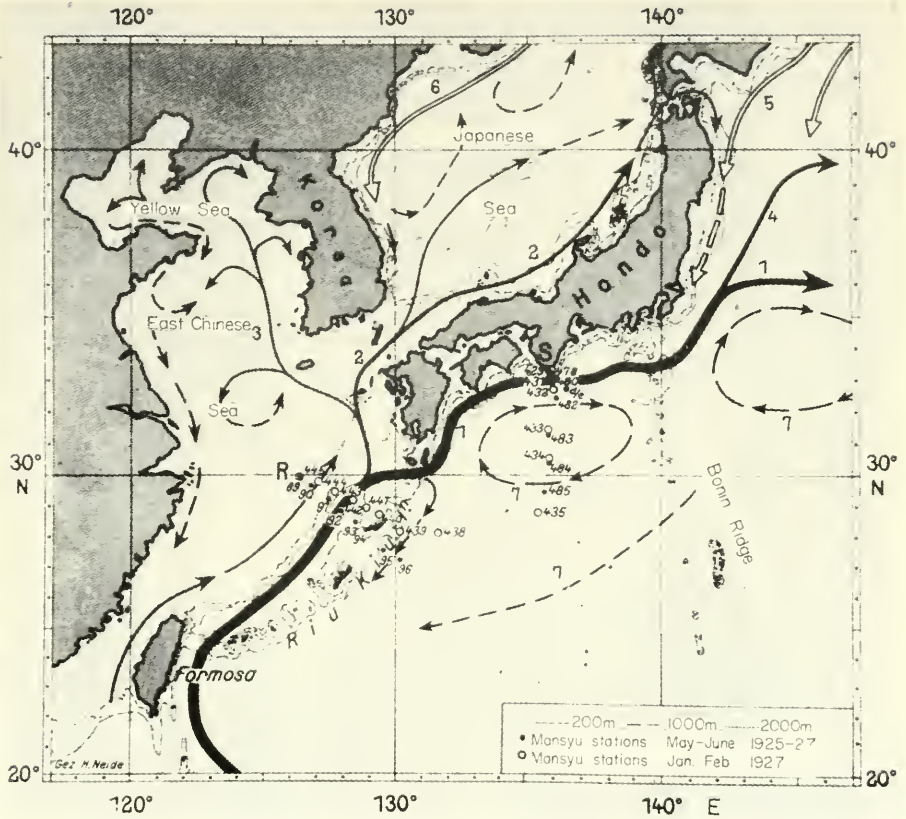


FIG. 260. Main current branches of the Kuroshio system (according to Wüst). (1) Kuroshio (main current); (2) Tsushima Current; (3) Korean side-branch; (4) northern branch of Kuroshio; (5) Oyashio; (6) Liman Current; (7) Counter currents of the Kuroshio. At R position of the Riu-Kiu section, at S position of the Shiono-Misaki section.

The northern part of the North Pacific Current turns northward and flows in an anticlockwise direction around the Gulf of Alaska; it is a well-developed current and is fairly constant, particularly near to the coast. This *Alaska Current* flows along the Aleutians and extends into the southern Bering Sea through all the passages between the islands. In the eastern part of the Pacific the southward movement off the California coast is denoted the *Californian Current* (THORADE, 1909; WARMER, 1926). It replaces the water which is carried westward by the north-east trade winds. The north-east to south-west direction of the current indicates the presence of an off-shore movement, giving rise to the upwelling of cold water along the greater part of the Californian coast. This upwelling occurs mainly during the warm part of the year.

The northward to north-westward movement of water along the entire western coast of South America is called the *Humboldt Current* after its early investigator. Where it runs close to the Chilean and Peruvian coasts it is called the *Peru Current* and this current and its variations have been described in a detailed monograph by SCHOTT (1931). A later evaluation of the available data has been given by GUNTHER (1936, 1936a). Figure 261 shows the probable field of motion according to Schott for the two seasonal extremes. During the period of intensified trade winds in the Southern Hemisphere winter (Chart *a*, Aug.–Sept.) the Humboldt drift current and its continuation, the South Equatorial Current, intensify considerably. The strength of the current rises from 0.5 to 0.7 knots along the coast of northern Chile and Peru and increases to 1 and occasionally 2 knots where it flows north-westwards in a wide region around the Galapagos Islands. Further out to sea it turns westwards. The

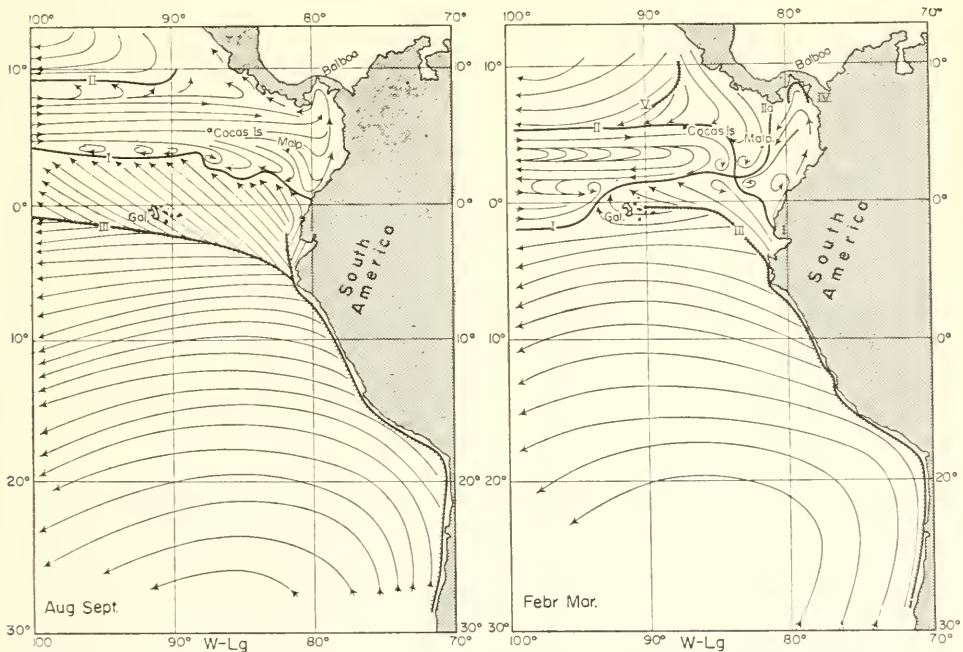


FIG. 261. Most probable current pattern in the region of the Humboldt Current and north of it (according to Schott): (a) for the Southern Hemisphere winter (August/September); (b) for the Southern Hemisphere summer (February/March).

coast as far as 5° S. is thus a one-sided *convergence line* and as a consequence upwelling occurs along its entire length. The other extreme of seasonal variation is at the end of the Southern Hemisphere summer (Chart *b*; Feb.–Mar.). Conditions in the equatorial region at this period are very complex and unstable and are subject to the influence the more or less pronounced development of the Equatorial Counter Current and the North Equatorial Current. The Humboldt Current is now weaker and about 4° C warmer at the coast. The unstable character of the current is due to simultaneous instability in *meteorological conditions* in the entire area between the Cocos Islands, the Galapagos and the coast of Ecuador and Peru. In many years the thermal equator and the associated zone of minimum atmospheric pressure are displaced into the Southern Hemisphere, so that the south-eastern trades along the Peruvian coast are then disturbed and rainy north and north-west winds occur in northern Peru. These disturbances of atmospheric and oceanic conditions are, however, usually not too powerful, but in general conditions are so unstable in northern Peru that abnormal developments frequently occur. The warm weakly saline water of the Equatorial County Current can then easily advance into the area of the Humboldt Current. This warm water is then carried southward by the northern and north-western winds (most often at Christmas time). This current in contrast to the Peru Current is regarded as a “counter current”; it is called “El Nino”. Normally the changes are not very great but occasionally when the disturbances are particularly well developed there may be torrential rains followed by flood catastrophes in coastal areas of northern Peru which are adapted to a dry climate. The simultaneous change in the character of the water masses off the coast in addition has disastrous consequences for the guano birds which are suddenly deprived of food. Detailed descriptions have been given for years when these disturbances have been particularly well marked, for 1925 by ZORELL (1928); MURPHY (1926) and SCHOTT and for 1891 by SCHOTT (1931).

The wide area of the Pacific covered by the essentially eastwards flowing West Wind Drift extends south of the subtropical convergence which is more a “convergence region” than a line. The available data on this current, especially in the thirties and forties, is rather uncertain. Near 40° S., off the South American coast there exists a zone of remarkably low salinity (34‰) apparently originating from western Patagonia (SCHOTT, 1934). Corresponding to this distribution the West Wind Drift must swing sharply north to north-westward, that is, to the left. The Antarctic Convergence runs through the West Wind Drift at about 55° S. It was encountered in every profile recorded by the “Discovery” Expedition and is the only convergence line circling the entire earth in the Antarctic region.

3. Currents Caused by Excess of Precipitation and Run-off Over Evaporation

The possibility of the direct formation of ocean currents due to the flow of excess water from the precipitation areas and those with run-off from rivers into evaporation regions, was first investigated in detail by EKMAN (1926) using his classical theory of deep and bottom currents. For a circular oceanic region he obtained after considerable simplifications a final equation of the form

$$\text{curl } V = - \frac{2\pi}{\rho D} (P - E), \quad (\text{XVIII.1})$$

where V is the velocity of the deep current produced, ρ is the average density of the bottom current layer D and $(P - E)$ is the difference between precipitation and evaporation in the area under consideration. Estimation of the velocity in some actual oceanic regions gave *maximum* velocities of the "evaporation currents" of not more than 1–2 cm sec⁻¹, but probably only fractions of this value are reached.

This is valid for open sea surfaces. For partly enclosed basins the quantity $(P - E)$ may be of exceeding consequence; the current processes occurring with water interchange in sea straits have been already discussed before (Chap. XVI, p. 513). Besides the water transport through the sea straits also the salt transport stand in question. If the inward water transport is M_i , the outward water transport M_o and the corresponding salt transports are S_i and S_o , then under stationary conditions the two equations

$$M_i S_i = M_o S_o \quad \text{and} \quad M_i = M_o - (P - E) \quad (\text{XVIII.2})$$

are valid, and thus

$$M_i = (P - E) \frac{S_o}{S_i - S_o}. \quad (\text{XVIII.3})$$

This formula is identical with the simple Knudsen relations (p. 379). For example, when the inflow through the Straits of Gibraltar is about 1.75×10^6 tons sec⁻¹, the average salinity of the inflowing water about 36.25‰ and of the outflowing water 37.75‰, then for the Mediterranean Sea according to the formula (XVIII.3) the quantity $E - P$ results to 0.07×10^6 tons sec⁻¹, which is in good agreement with other estimates.

More recently, GOLDSBROUGH (1933) has dealt with ocean currents produced by the given distribution of precipitation and evaporation. Already before that HOUGH (1897) in his famous theoretical study of tides on a rotating globe has dealt with this problem of currents produced by a zonal distribution of precipitation and evaporation. Since he ignored frictional effects, he found a uniformly accelerated system of purely east-west geostrophic currents as a consequence of these distributions. From the impossibility of finding a steady state solution he concluded that precipitation and evaporation cannot be a significant cause of ocean currents. Hough did not accept any meridional boundaries in the ocean. Goldbrough took instead a model with precipitation predominating in one hemisphere, evaporation in the other and assumed meridional boundaries in the ocean. This model gave a steady current field, provided that the integral of the precipitation-evaporation function taken along each parallel of latitude between the two boundaries, vanishes. This is a very severe restriction which no natural distribution of precipitation-evaporation necessarily fulfils. Figure 262 shows the current system produced in this case for one hemisphere; the other hemisphere will be the mirror image of this. The field of pressure, the elevation of the free surface and the flow will be steady. The horizontal velocity components will thus be entirely geostrophic, and the current will flow along the isobars. The vertical component will be zero at the bottom and will increase linearly from the bottom up to the sea surface where it will equal the precipitation-evaporation rate. At the eastern edge of the precipitation hemisphere there will be two low-pressure cells, and at the western edge two high-pressure cells. At the poles the flow is directed from the region of evaporation into the region of precipitation; however, in the opposite direction in

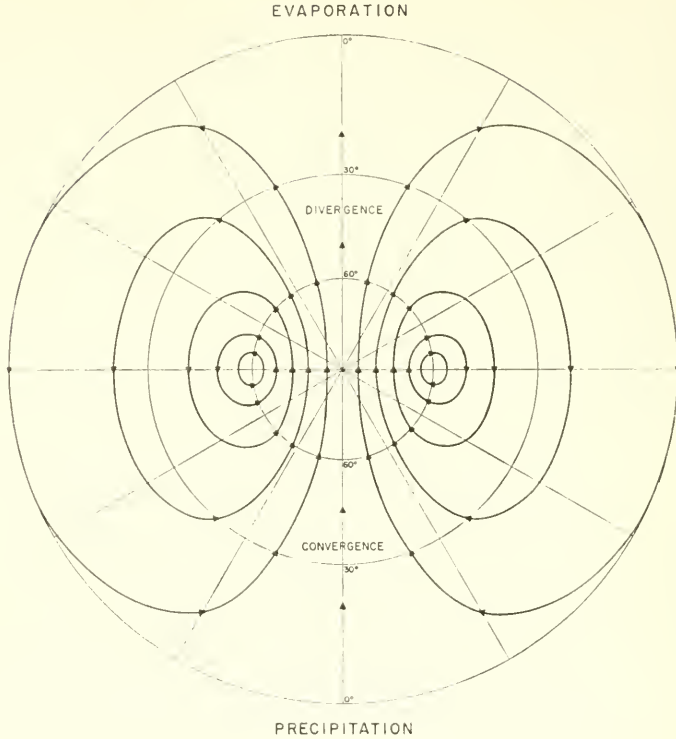


FIG. 262. The steady circulation of Goldsbrough type driven by precipitation over one-half of a hemisphere and evaporation over the other half. Only one hemisphere has been pictured, for the other hemisphere applies the reflected image. The curved lines with attached arrows are isobars. The centres of high- and low-pressure cells are to the right resp. To the left of the middle line.

subtropical and tropical regions. The geostrophic current will everywhere be directed towards the equator in the precipitation hemisphere and towards the poles in the evaporation hemisphere. The current towards the equator will require a horizontal divergence, that towards the poles will require horizontal convergence. This divergence (or convergence) distribution must be sufficient everywhere to absorb (or supply) the water locally precipitated (or evaporated).

The solution in Fig. 262 is valid for an entire hemisphere but it is evident that a coastal barrier could be placed along any complete isobar without affecting the solution. Thus, meridional barriers can be placed through the centres of the precipitation and evaporation hemispheres, and also the equator itself can be selected as such a barrier.

This schematic representation of Goldsbrough's results has been discussed here in some detail, since Stommel has used it as a basis for a discussion of the fundamental principles of ocean circulation (see Chap. XXI).

4. The Thermo-haline Circulation

The general atmospheric circulation is produced solely by heat differences in meridional direction, ultimately caused by the sun radiation. By analogy to the

atmospheric conditions it was assumed at an early date that there would be a simple water circulation in a vertical plane between the equatorial zone and the polar oceans. This opinion was first expressed by HUMBOLDT (1814, 1845, p. 322) who also offered a more detailed reason for it. He pointed out that the very low temperatures in the deeper water layers at low latitudes could only be regarded as a consequence for the cold water transport in the deeper layers from the poles towards the equator, which would also imply a surface water transport towards the poles. The entire mass of the oceans between the equator and the poles including the water at very great depths would thus be in constant motion. Humboldt considered the differences in density between equatorial and polar water masses as the cause for this closed circulation system. Since the circulation is in accordance with the given temperature distribution, he concluded that the distribution of salinity was not such as to disturb the thermally produced circulation. Humboldt's ideas were adopted by many investigators and for three-quarters of a century formed the basis of a generally accepted view on ocean circulation. LENZ (1847) found that already for small depths, temperatures in the equatorial regions are much lower than in the subtropics, and he concluded that the almost horizontally flowing deep current coming from higher latitudes must assume an upward directed component near the equator. He deduced from this that, symmetric to the equator, there must therefore be two major vortices in a vertical plane, one on either side of the equator with the cold deep currents rising and merging in the equatorial region; cold deep water would thus be found nearer the sea surface here than further north or south. He found support for his conclusion in the salinity minimum of the equatorial zone.

FERREL (1856) took the Coriolis force into account and proposed a modified form of Lenz's vortices limited not in the polar regions, but only in middle latitudes, but followed by another vortex in the polar regions of each hemisphere with a rising movement near the poles. The analogy between the atmospheric and the oceanic circulation is particularly evident in Ferrel's model; he completely ignores the difference due to heating of the ocean from above, and of the atmosphere from below, and also disregarded the effects of the salinity distribution and winds.

The wide adoption of the thermal circulation theory is due to the circumstance that it has been included in an important oceanographic work of that period by MAURY, *The Physical Geography of the Sea* (1st edition, New York, 1856). CROLL (1870-71, 1875) refused it, but took another extreme viewpoint, since he regarded each vertical circulation as produced by the wind. Also CARPENTER (1870-77) tried to conclude from the "Challenger" observations that a thermal circulation was present. Both agree on the existence of a major vertical circulation and differ only on its cause.

Detailed analysis by BUCHANAN (1885) and BUCHAN (1895) of data from the "Challenger" expedition showed that the actual spatial distribution of temperature and salinity is incompatible with a vertical circulation of the type suggested by Lenz. In all oceans there are alternating layers of different temperature and salinity underneath a relatively shallow top layer. This excludes the possibility of a single closed circulation system with two vortices symmetrically placed on either side of the equator. According to Sandström's proposition (p. 491) a thermo-haline circulation is substantially promoted and intensified if the heat source is at a lower level than the cold source, particularly when the effects of heat conductivity and turbulence are of

minor importance as is the case in the ocean. It was mentioned that in the ocean these heat and cold sources are at approximately the same level and that therefore conditions are not favourable for the development of powerful circulation systems. In any case they can be only of small vertical extent and they will be entirely incapable of filling the whole of the oceanic space from the poles to the equator. Conditions along a meridian will be more or less the following:

Latitude 60° 50° 40°	30° 20°	10° 0°
Predominance of heat loss due to outgoing radiation	Heat gain due to incoming radiation	
Predominance of salinity decrease ($P-E > 0$, melting of ice)	Salinity increase ($P-E < 0$, predominance of evaporation)	Salinity decrease through precipitation and run-off

Since a salinity increase is equivalent to a heat loss and a salinity decrease to a heat gain, the thermal and haline circulation will act in the same direction in the region between the equator and in the Ross latitudes (0° until 30° N. and 30° S.). North and south of the subtropical regions, however, they will counteract each other. A powerful thermo-haline circulation can thus be expected only in the tropics and subtropics. The water transport occurs towards the poles in the uppermost layer and toward the equator underneath with an upward motion in the equatorial regions and a descending one in the subtropics. This circulation can, however, develop only in a thin top layer and the Lenz schematic circulation is restricted to this kind of shallow circulatory water movement. The circulation of this tropical and subtropical top layer is dealt with in Chapter XIX.

5. Wind Effects and the Current System in a Hydrographic Circular Vortex

That the wind system of the atmosphere is also involved in the development of the ocean circulation was not excluded by many investigators, but no agreement was reached about the importance of its effects as long as the properties of wind drifts were still unknown. The significance of atmospheric currents as a cause of the ocean circulation was considerably clarified by Ekman's investigations. Probably the most important result was to show that the wind affects directly only a top layer of not more than 100–150 m thickness. The piling up of water at a coast by the wind will, however, give rise to a slope in the physical sea level and to gradient currents reaching downwards to greater depths. In stratified water, mass compensation between upper and lower levels (pp. 485 and 548) seems to prevent the development of deep-reaching gradient currents. This remarkable compensation principle is readily illustrated by a two-layered oceanic model. If in such a water mass (upper layer: ρ_1, h_1 ; lower layer: ρ_2 and $h_2 - h_1$; Fig. 263) a current V is generated along AB in the upper layer, then the physical sea level along AB will adjust itself to give a state of equilibrium between the gradient and the Coriolis force. The deviation of the physical sea level from a level surface ("Geoid") is denoted by ζ_1 . Displacements of mass in the upper layer will also disturb the equilibrium in the lower layer with a resultant mass transport in the direction from D towards C , the internal boundary surface will decline ($C'D'$), but

in a direction exactly opposite to that of the sea level. This displacement of the internal boundary surface will automatically reduce the pressure gradient imposed on the lower layer from above. In the final equilibrium state of the lower layer there will be no pressure gradient and therefore no motion. If ζ_2 is the deviation of the internal boundary surface from a level surface, the condition for this new state of equilibrium is given by

$$\zeta_2 = - \frac{\rho_1}{\rho_2 - \rho_1} \zeta_1. \quad (\text{XVIII.4})$$

This simple relationship will always be present if sufficient time is available. Conditions at the outer boundaries of the current at AC and BD will be considered later (p. 622 *et seq.*).

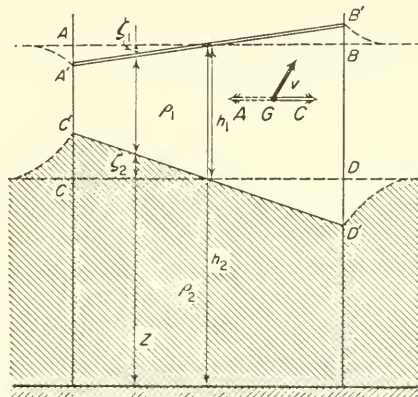


FIG. 263. Position of the physical sea surface and of the internal boundary surface of a two-layered ocean for a forced movement of the upper layer in the interval $AC-BD$.

The total effect of air currents on the ocean surface can be suitably illustrated by the simple case of an ocean uniformly covering the entire earth (no continents). This ocean can be assumed to have two layers, an upper troposphere and a lower stratosphere, separated by a clearly defined density transition layer. To correspond to actual conditions in the tropics and subtropics it can be assumed further on that the troposphere in these regions is subdivided by a transition layer at about 100 m depth separating the top layer from the subtropospheric water masses beneath. Only zonal (east-west) currents will be present in this hydrosphere covering the total earth and it can be regarded as a circular vortex as described by BJERKNES (1921), centred around the axis of the earth. The movement of the water masses in this vortex will be east-west, and the adjacent stream lines will not influence each others. The hydrosphere will be affected only by the atmospheric currents at the sea surface, that is, by the trade winds between the equator and the Ross latitudes (30° N. and S.), by the west winds in middle latitudes between 30° and 60° N. and S., and by polar east winds polarwards 60° N. and S. The oceanic movements in the individual zones of the circular vortex and the position of the boundary surface will then be a consequence of these effects. Since conditions are symmetrical around the rotational axis it is only required to consider a meridional section through such a wind-generated circulation. Fig. 264

gives a schematic representation of the water movements expected according to these theoretical considerations.

Between 30° N. and 30° S. the north-east and south-east trade winds give rise to the broad North Equatorial and South Equatorial Current of the Northern and Southern Hemisphere, respectively. The maximum intensity is reached in the regions where the

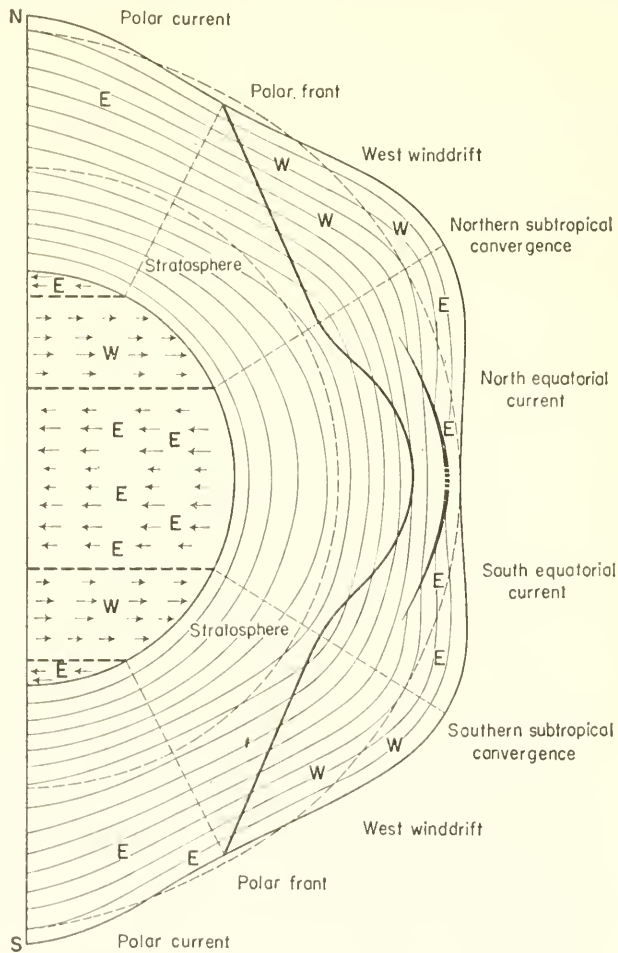


FIG. 264. Schematic representation of the hydrosphere as a circular vortex. Current zones and position of the main boundary surface and of the isobaric surfaces (with a strong exaggeration of the vertical scale). (*W*, current towards west; *E*, current towards east).

trade winds are most strongly developed; their intensity decreases toward the regions of high atmospheric pressure in the subtropics and also towards the equator. They are deflected 45° *cum sole* from the wind direction and must be associated with a water transport towards the poles. Water will therefore be piled up at their polar boundaries (in about 30° latitude) and therefore a pressure gradient will be generated in the troposphere towards the equator. Sea level and the isobaric surfaces will be depressed at the equator and will rise from here towards the poles. If there is no motion

in the water masses of the stratosphere the boundary separating it from the troposphere will slope in the opposite direction in accordance with the compensation principle mentioned above. At this internal surface there is a stratospheric ridge at the equator and a trough in Ross latitudes. Thus in the Atlantic the boundary is at 300 m depth at the equator and at 700 m depth in Ross latitudes: $\zeta_2 = 400$ m at 30° latitude. With the observed values $\rho_1 = 1.0260$, $\rho_2 = 1.0275$, equation (XVIII.1) gives the rise in physical sea level from the equator to 30° latitude as approximately 58 cm; an order of magnitude which agrees with the dynamic computations of the absolute topography of isobaric surfaces. At 20° latitude where the physical sea level has a rise of 35 cm and $\rho_2 - \rho_1 = 25 \times 10^{-3}$, the decline of the tropospheric transition layer is 140 m, also in good agreement with observation. In this circular vortex there is no circumstance which would give rise to an equatorial counter current.

Winds in the atmospheric West Wind Drift are of rather variable character; but only in the general average westerly winds predominate. In the top layer they produce an oceanic West Wind Drift and a consequent piling up of water *cum sole* towards the subtropics, which counteracts the accumulation of water associated with the equatorial currents. There is thus an accumulation of water from both sides in a belt around the earth. On the equatorial side of this belt water flows westward, on the polar side eastward. This is the *subtropical convergence region*, one of the most important boundary lines of the oceanic circulation. Corresponding to the downward slope of the physical sea level towards the poles there is an upward slope in the internal boundary surface between the troposphere and the stratosphere from its deepest position in the subtropics to the surface of the ocean at the polar front (*polar convergence*). This is the 60° N. and S. it must rise 700 m over 30 degrees of latitude. When $\rho_1 = 1.0265$ and $\rho_2 = 1.0275$ the physical sea level will have a slope of 68 cm according to equation (XVIII.1). If the physical sea level at the equator is taken as zero, it will have an elevation of 58 cm in the subtropics and a depression of 10 cm at the polar front. The prevailing easterly winds around the polar caps produce a westward drift current (polar currents) and there is a corresponding rise in the sea level from its lowest position at the polar front.

Although the circulation system shown in Fig. 262 is only schematic, it shows the main features of the surface circulation system clearly, particularly as in the Pacific and in the circumpolar Antarctic waters where it is not strongly disturbed by the presence of continents. With a circular vortex of this type under stationary conditions no vertical movements are to be expected. A deep-sea circulation will therefore not develop and the three horizontal current zones (the Equatorial Currents, the West Wind Drifts and the Polar Currents) can be explained as solely caused by winds. The topography of the physical sea level, of the internal boundary surface between the troposphere and the stratosphere and of the tropospheric transition layer of the tropics and subtropics are coupled with these zones.

6. The Influence of Meridionally Oriented Coasts on the Oceanic Circulation

The oceans are bounded everywhere on their western and eastern sides by continents which act as meridional barriers to the oceanic circulation and prevent the formation of a simple circular vortex around the earth. At the meridional barriers the equation of continuity must be satisfied, and in order to allow the conservation of

mass, meridional currents must develop that will determine the nature of the circulation. It appears that these boundary conditions are more easily fulfilled for a sea with a meridionally oriented eastern coast than for one with a meridionally oriented western coast.

(a) Conditions West of a Meridionally Oriented Coast

SVERDRUP (1947) has shown that a steady state solution can be found for a density-layered ocean by starting at a meridional boundary and working westwards even when frictional effects are neglected. In the vorticity equation (XVII.5) the wind stress vorticity must be balanced by the planetary vorticity alone and, as shown already in XVII.3 second of the major boundaries of the oceanic circulation. To reach the surface at the boundary conditions and the equation of continuity (XVII.4) determine the currents westward from the meridional boundary (east coast). For a purely zonal wind ($T_y = 0$), the mass transports (omitting the first term of (XVII.7); lower latitudes) will be given by

$$M_y = -\frac{1}{\beta} \frac{\partial T_x}{\partial y} \quad \text{and} \quad M_x = \frac{\Delta x}{\beta} \frac{\partial^2 T_x}{\partial y^2}. \tag{XVIII.5}$$

Assuming in a schematic way according to actual conditions in the ocean (equator to 30°: easterly winds; 30° to 60°: westerly winds)

$$T_x = -a \sin \frac{2\pi}{l} y, \tag{XVIII.6}$$

where l is the distance from the equator until 60°, then

$$\frac{\partial^2 T_x}{\partial y^2} = \frac{4\pi^2 a}{l^2} \sin \frac{2\pi}{l} y.$$

From this it is easy to derive the following table of signs of the different quantities for an eastern or western meridional barrier.

Barrier to the east					Barrier to the west				
y	$0 - \frac{1}{4}l$	$\frac{1}{4}l - \frac{1}{2}l$	$\frac{3}{4}l - \frac{3}{4}l$		$0 - \frac{1}{4}l$	$\frac{1}{4}l - \frac{1}{2}l$	$\frac{3}{4}l - \frac{3}{4}l$		
T_x	-	-	+	+	-	-	+	+	
Δx	-	-	-	-	0	+	+	+	+
$\partial^2 T_x / \partial y^2$	+	+	-	-	0	+	+	-	-
M_x	-	-	+	+	0	+	+	-	-
Possible case					Impossible case				

West of the barrier, T_x and M_x are, according to (XVIII.5), both positive or both negative. However, east of the barrier they are of opposite signs, which is impossible. The equations (XVIII.5 and 6) give a steady state solution only for a sea area to the west of the boundary. The following example can be taken as an illustration of such a solution.

Selecting $T_x = -0.4 \sin 6\phi$ dyn cm⁻², gives

$$M_y = \frac{2.4}{2\omega \cos \phi} \cos 6\phi; \quad M_x = \frac{14.4 \Delta x}{2R\omega \cos \phi} \sin 6\phi \quad \text{and} \quad \psi = -\frac{2.4 \Delta x}{2\omega \cos \phi} \cos 6\phi.$$

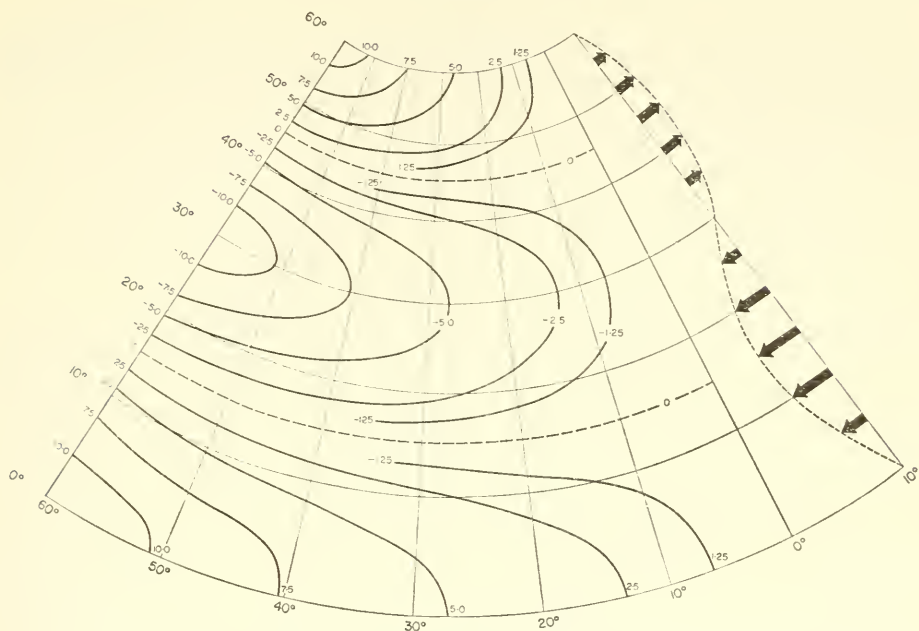


FIG. 265. Stream lines of the flow representing the field of mass transport; differences of the values of the stream function between two stream lines represent the net mass transport in 10^6 metric tons per second flowing between these stream lines (from the surface down to a depth of no motion).

Figure 265 shows stream lines of flow representing the field of mass transport. The principal troughs and ridges are accounted for by the wind stress function. Off the coast in the east the currents are weak and the meridional component is directed southwards in middle latitudes.

The integrated equations give no information on the distribution of vertical motions in the deep oceanic layers. A better comprehension of these currents can be gained by accurate calculations for the very simple model of Sverdrup. STOMMEL (1957) has recently given a very instructive description of such a case, in which zonal wind stress was assumed to act on a homogeneous ocean surface with an eastern coast line. Figure 266 shows the solution. At the surface there is a zonal wind stress with a similar distribution as that shown in Fig. 265. The stream lines will therefore also be similar to those in the diagram. The transport in the thin Ekman layer, indicated by the upper arrows, will produce a vertical downward velocity in the central part of the diagram. Outside the zonal belt of westerly winds the vertical velocity will be directed upwards. These vertical components from the bottom of the Ekman layer to the bottom of the ocean decrease linearly to zero. The divergence and convergence system of the meridional components of geostrophic velocity are coupled with this vertical velocity field. At the latitude of maximum westerly wind, where there is no impressed vertical velocity, the geostrophic flow will be entirely zonal and will decrease linearly towards the eastern coast. The topography of the physical sea surface, which determines the pressure field associated with the geostrophic flow, is also shown in Fig. 265.

If in addition bottom friction of the type described by Ekman is taken into account, the current field will be slightly altered; now the bottom current must also contribute in order to satisfy the convergences and divergences appearing in the current field of the Ekman top layer.

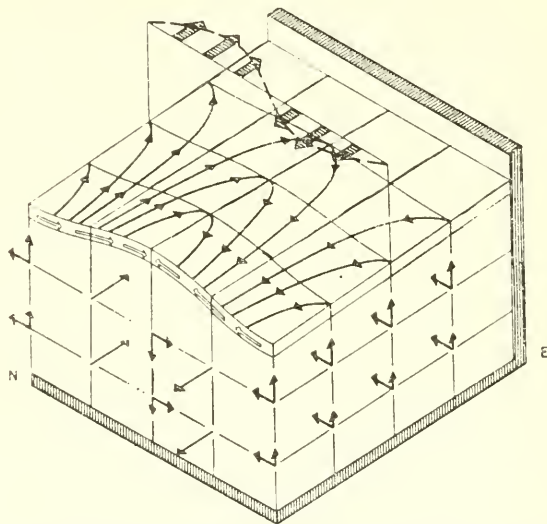


FIG. 266. Sverdrup-type solution in a homogeneous ocean of uniform depth, bounded by a meridional coastal wall on its eastern side. The wind system with sinusoidal pattern is indicated by shaded arrows hovering above the surface. The curved lines with arrows are isobars and give the direction of the geostrophic horizontal flow (independent of the depth). At a number of subsurface depths the velocity components are shown by solid arrows (according to Stommel 1957).

Considerably more complicated models of this type can, of course, be developed, but they will all show that the boundary conditions at any coast to the west cannot be satisfied except by taking into account processes involving the dissipation of energy.

(b) Conditions East of a Meridionally Oriented Coast

In the western part of the oceans, and particularly along the western boundary, the vorticity related to lateral friction must also be taken into account with an additional term in order to satisfy mass conservation and space continuity conditions in the vorticity equation (XVII.5). With this equation STOMMEL (1949, 1951) was the first to give an explanation of the westward intensification of ocean currents. He took the case of a symmetrical anticyclonic wind circulation over a closed rectangular oceanic area in the Northern Hemisphere. The wind stress vorticity is thus negative over the entire ocean. The effect of the wind stress can be expected to cause an anticyclonic circulation in the sea. The horizontal eddy viscosity will tend to counteract the effect of wind stress. In the western parts of this ocean the anticyclonic flow will transport water northward, in the eastern parts southward; in equation (XVII.5) the planetary vorticity effect is therefore negative at the western side of the ocean and positive at the eastern side. This is a consequence of the conservation of angular momentum or, what amounts to the same, of the variation of Coriolis parameter with latitude.

If the absolute numerical values of the three vorticity terms in (XVII.5) are denoted by a , b and c , then for a symmetrical wind system, (a) would be negative and would have the same numerical value in both east and west. For an equal velocity, a symmetrical oceanic circulation would require an equally great frictional vorticity; (b) would thus be positive and have the same numerical value in the east as in the west. The planetary vorticities in the west and in the east would also have the same numerical value but are of opposite signs. Thus

Off the western boundary

$$-a + b - c = 0$$

Off the eastern boundary

$$-a + b + c = 0$$

These requirements are satisfied only when $c = 0$, that is, when there is no meridional transport, and are therefore incompatible with the conservation of mass. This is a qualitative explanation

- (1) of the impossibility of a symmetrical circulation in association with a symmetrical wind field,
- (2) of the impossibility, mentioned above, of deriving a suitable circulation off the western coast of an ocean without accounting for frictional influences.

As shown by Stommel, an anticyclonic circulation is possible in the case just discussed only when the water transport off the western boundary is substantially intensified and the lateral shearing stresses consequently, of course, increased correspondingly. To illustrate this, Stommel gives some arbitrary values for the vorticity terms in an asymmetric circulation. These are shown in the following Table 149.

Table 149. *Vorticity tendencies in an asymmetric circulation*

	Strong northward flowing currents in the western edge	Southward flowing current over the rest of the ocean
Wind stress (a) .	- 1.0	-1.0
Frictional (b) .	+ 10.0	+0.1
Planetary (c) .	- 9.0	+0.9
Total . . .	0.0	0.0

Among the interesting consequences of this theory are:

- (1) the fact that although energy is added to the oceans by work done by the wind over the entire surface, it is dissipated primarily in the strong western currents;
- (2) that a good representation of the circulation in the zonal currents of westward or eastward direction can be obtained independently of friction from a knowledge of the wind stress field alone.

MUNK (1950) was able to evolve a comprehensive theory of a wind-driven ocean circulation by combining three new concepts:

- (a) the introduction of lateral stresses associated with the horizontal exchange in large eddies (DEFANT, 1926; ROSSBY, 1936a),
- (b) the possibility of computing currents in baroclinic oceans from the known wind stresses (SVERDRUP, 1947), and

- (c) the consideration of the variability of Coriolis parameter with latitude (STOMMEL, 1948) which makes it possible to explain the westward intensification of a wind-generated ocean circulation.

This theory accounts for many of the major features and some of the details of the general ocean circulation on the basis of known mean annual winds. Briefly the fundamentals of this new theory are:

The vorticity equation (XVII.5) can be put into a practical form by the introduction of expressions for the lateral frictional forces. According to (XI.13 and 14) these frictional forces have the form

$$H_x = A \left(\frac{\partial^2 u}{\partial x^2} + \frac{\partial^2 u}{\partial y^2} \right) \quad \text{and} \quad H_y = A \left(\frac{\partial^2 v}{\partial x^2} + \frac{\partial^2 v}{\partial y^2} \right). \quad (\text{XVIII.7})$$

A is the lateral eddy viscosity pertaining to horizontal shear which is presumed to be constant and horizontally isotropic, neglecting variations due to differences between zonal and meridional motion of large horizontal vortices on a rotating earth. Introduction of these expressions into (XVII.5) with the stream function according to (XVI.25), gives the differential equation for mass transport

$$\left(A \nabla^4 - \beta \frac{\partial}{\partial x} \right) \psi = - \text{curl}_z T, \quad (\text{XVIII.8})$$

where ∇^4 is the biharmonic operator (see XVI.26) and $\text{curl}_z T$ is the vertical vorticity component of the wind stress. It can be shown, in accordance with the relationship

$$\left. \begin{array}{l} \underbrace{\text{lateral stress curl} + \text{planetary vorticity}}_{\text{western solution}} + \underbrace{\text{wind stress curl}}_{\text{central solution}} = 0 \end{array} \right\} \quad (\text{XVIII.9})$$

that in the central and eastern oceanic areas the planetary vorticity and the wind-stress curl have opposite signs, resulting in balance in which the lateral stress plays a negligible part. Along the western boundary the planetary and the wind-stress curl have the same sign, and the lateral-stress curl balances both, planetary vorticity and wind-stress curl. It can be verified that in this region the wind-stress curl is numerically unimportant although it is, of course, the primary cause of the circulation.

To equation (XVIII.7) must be added the boundary conditions

$$\psi = 0; \quad \left(\frac{\partial \psi}{\partial \nu} \right)_{\text{boundary}} = 0, \quad (\text{XVIII.10})$$

where ν is normal to the boundary. The first equation states that the boundary itself is a stream line, the second that no slippage occurs against the boundary.

Munk assumed:

(1) a rectangular ocean extending from $x = 0$ to $x = r$ and from $y = -s$ to $y = +s$. The boundary conditions will then be

$$\left. \begin{array}{l} \psi = \partial \psi / \partial x = 0 \quad \text{for } x = 0 \quad \text{and} \quad x = r \\ \psi = \partial \psi / \partial y = 0 \quad \text{for } y = -s \quad \text{and} \quad y = +s \end{array} \right\} \quad (\text{XVIII.11})$$

(2) a zonal wind circulation ($T_y = 0$); for this the stress on the ocean surface in the interval $-s < y < +s$ can be given as a Fourier series, a general term of which is

$$T_{x,n} = c + a \cos ny + b \sin ny \quad \text{with} \quad n = j \frac{\pi}{s}; \quad (j = 1, 2, \dots) \quad (\text{XVIII.12})$$

The solution of (XVIII.8) which satisfies the boundary conditions is $\psi = -rX\beta^{-1} \text{curl}_z T$ whereby

$$X = \underbrace{\left(1 - \frac{1}{kr}\right) \left[-\frac{2}{\sqrt{3}} e^{-\frac{1}{2}kx} \cos\left(\frac{\sqrt{3}}{2}kx - \frac{\pi}{6}\right) + 1\right]}_{\text{west}} \underbrace{- \frac{1}{kr} \left[kx - e^{-k(r-x)}\right]}_{\substack{\text{central} \\ \text{east}}} \quad (\text{XVIII.13})$$

Here k is the ‘‘Coriolis friction’’ wave-number which has the value $\sqrt[3]{(\beta/A)}$ and is assumed to be constant. The solution is valid as a first approximation when $\gamma = (n/k)^4 \ll 1$ and $e^{-kr} \ll 1$. When $k = 0.016 \text{ km}^{-1}$ and $r = 6000 \text{ km}$ the value of the stream function ψ will be accurate within 10%, if $\gamma < 0.25$, corresponding to a minimum zonal wavelength, $2\pi/n$, of about 1500 km. Since for the mean annual stress distribution the shortest wave length of the important north-south variations, the distance between the northern and southern trade winds amount to 4000 km, the approximation leading up to (XVIII.13) therefore appears to be valid for a study of the general ocean circulation in relationship to the general atmospheric circulation.

A knowledge of the wind distribution over an ocean thus permits a direct quantitative calculation of the current field in the ocean. It was calculated by Munk for the North Pacific, first as an approximation for a rectangular ocean, and later for a triangular ocean (MUNK and CARRIER, 1950), which gives a better representation of actual conditions.

The solution (XVIII.13) shows in the first place that the zonal wind system divides the ocean circulation into a number of gyres. The dividing lines between them lie in the latitude of maximum west wind, in the northerly and southerly trade winds and in the doldrums. The latitudinal axis of each gyre may be defined by $d^2T_x/dy^2 = 0$. The Atlantic Sargasso Sea is associated with the inflection point in the mean wind stress curve between the westerly winds and the north-easterly trades. The inflection points between the doldrums and the northern and southern trades determine the boundary of the equatorial counter current.

When X is computed from (XVIII.13), it is found that the equations fall naturally into three parts, each of which dominates in a given sector. At the western edge of the ocean $x \ll r$, and becomes

$$X_{\text{west}} = \frac{2}{\sqrt{3}} e^{-\frac{1}{2}kx} \cos\left(\frac{\sqrt{3}}{2}kx - \frac{\pi}{6}\right) + 1 \quad (\text{XVIII.14})$$

representing slightly ‘‘underdamped’’ oscillations with a wavelength given by

$$L_{\text{west}} = \frac{4\pi}{\sqrt{3}k} = \frac{4\pi}{\sqrt{3} \sqrt[3]{\beta}} A^{\frac{1}{3}}. \quad (\text{XVIII.15})$$

A remarkable feature is a *counter current* east of the main current, with a magnitude of 17% of that of the main one. There can be little doubt that such counter currents exist, although this fact has been obscured in some instances by the smoothing of data. This theoretical result has in fact been shown to be in agreement with observations (see p. 536 *et seq.*).

The *total* transport of the western current and counter current is found by putting numerical values of X into X.14) giving

$$\psi_{\text{west}} = -1.17 r\beta^{-1} \text{curl}_z T. \quad (\text{XVIII.16})$$

The resulting expressions are *independent* of A and the transport can be computed with a relatively high degree of accuracy; the uncertainty is of the same order as that in the calculation of wind stress. Table 150 gives a comparison between the transport values of some western currents determined from oceanographic observations, and those computed from the zonal wind stress using equation (XVIII.14). The two sets of values are of the same order of magnitude, but the calculated transport values differ from the observed values by a factor of as much as two; the discrepancy is not surprising when it is considered that amongst other uncertainties the wind and current data are not for the same year, nor necessarily for the same time of the year. Another source of error may be due to possible underestimation of the wind stresses at low wind speeds. It can be assumed, in accordance with views held at the present time, that the dependence of wind stress on the wind velocity is given by $\kappa = 0.0026$ at high wind speeds and $\kappa \sim 0.008$ at low speeds, with the discontinuity at Beaufort 4 (see p. 421 and especially MUNK, 1947). This assumption, however, does not appear to be absolutely certain and further investigations are required.

Table 150. The mass transport of some western currents determined from the wind stress and from oceanographic observations

Current	Lat.	$10^{13} \beta$ ($\text{cm}^{-1} \text{sec}^{-1}$)	r (km)	$10^{10} (\partial T_x / \partial y)$ (g cm^{-2})	$10^{12} \psi$ by wind stress (g sec^{-1})	Ocean. obs. (g sec^{-1})
Gulf Stream .	35° N.	1.9	6500	70	36	74* (55)†
Kuroshio .	35° N.	1.9	10000	50	39	65*
Oyashio C. .	50° N.	1.5	5500	-15	-6.5	-7‡
Brazil C. .	20° S.	2.2	5500	-20	-5.8	-5 to -10*

* Sverdrup *et al.* (1942), pp. 605, 761.

† Adjusted for a supposed southward motion of 19×10^{12} g of slopewater.

‡ For August (Uda, 1938).

Away from both boundaries the stream-line function X reduces to

$$X_{\text{central}} = 1 - \frac{x}{r} \quad (\text{XVIII.17})$$

which gives the central oceanic drift; this is a broad *constant* drift that compensates for the swift shallow western currents. Equation (XVIII.17) also gives

$$M_y = \frac{\partial \psi}{\partial x} = \frac{1}{\beta} \text{curl}_z T \quad (\text{XVIII.18})$$

which agrees with the relationship derived by Sverdrup (see p. 580, equation XVIII.5).

In the eastern part of the ocean, the eastern solution is valid in the form

$$X_{\text{east}} = 1 - \frac{x}{r} - \frac{1}{kr} \left[1 - e^{-k(r-x)} \right]. \tag{XVIII.19}$$

It represents an exponential slippage zone with a width of approximately π/k . If $A = 5 \times 10^7 \text{ cm}^2 \text{ sec}^{-1}$, the width will be about 200 km.

The complete circulation of an ocean shows pronounced east-west asymmetry. The westward intensification of ocean currents is an effect of the planetary vorticity. The asymmetry may be expressed by either of the ratios:

$$\frac{M_y \text{ (west. cur.)}}{M_y \text{ (cent. cur.)}} = -0.55kr \quad \text{or} \quad \frac{r}{x \text{ (west. cur. axis)}} = \frac{\sqrt{3}}{2} kr \tag{XVIII.20}$$

that is, by either the ratio of the maximum western current to the central drift, or by the ratio of the width of the ocean to that of the western current. The asymmetry increases with r , decreases with A and ϕ ; for the Atlantic $kr \approx 100$.

Along the western coasts of the continents there are relatively strong seasonal ocean currents (California Current, Benguela Current, Peru Current), which cannot be explained by the simple assumption of zonal winds. To cover these currents which are also essentially dependent on winds, the theory must be expanded by the introduction of corresponding meridional wind stresses. This solution also has been given by Munk together with a general solution in which is introduced a general field of wind stress associated with the large-scale atmospheric circulation.

To demonstrate the ability of this theory of the general ocean circulation to express the actual mean current conditions in an ocean, a theoretical solution for the Pacific as an approximation for a triangular ocean is given for comparison with a recent representation of currents based on observations in Figs. 267 and 268 (cf. MUNK and CARRIER, 1950).

It can be clearly seen that all the essential features of the current patterns are covered by the theory.

There is no doubt that the Stommel-Munk theory of ocean circulation explains the large-scale geographic picture of the horizontal ocean currents in all oceans as a direct effect of the permanent wind system over these oceans. There is very good qualitative agreement between the water transport computed from wind distribution and that

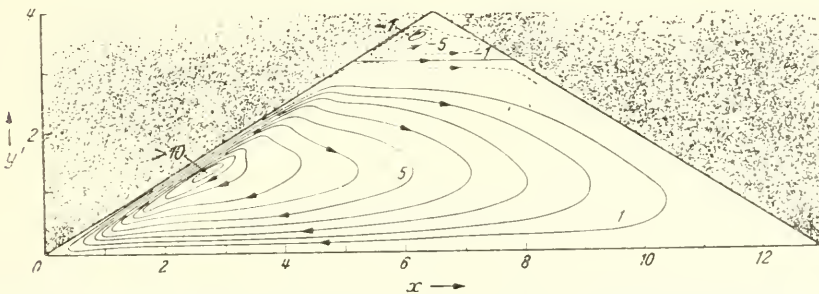


FIG. 267. The computed mass transport in an ocean of triangular form represented by stream lines. Between two neighbouring stream lines 6 million tons of water flow in the direction of the arrows per second.

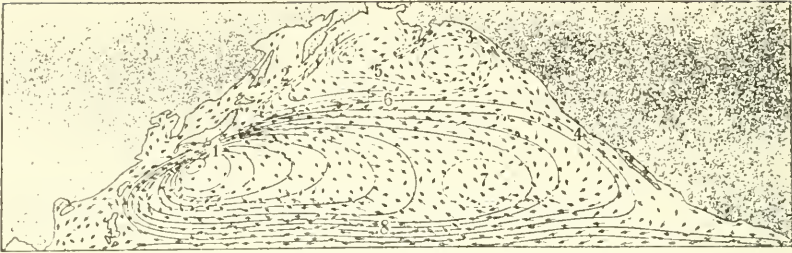


FIG. 268. The oceanic mass transport of the North Pacific Ocean, derived from data available. Between two neighbouring stream lines 6 million tons of water flow per second. (1) Kuroshio; (2) Oyashio; (3) Alaska Current; (4) California Current; (5) Sub-Antarctic Current; (6) North Pacific Current; (7) East Pacific Vortex; (8) North Equatorial Current.

deduced from oceanographic observations, and this agreement is confirmed by all investigations that have been carried out along the lines of Munk's computations. HIDAOKA (1950, *a, b, c*, 1951) has dealt in particular with the wind-generated ocean circulation of the Pacific and has obtained an overall climatological oceanic circulation, that fits admirably with that deduced from ship's displacements. His mathematical treatment of the problem differs from that used by Munk only in taking higher order terms into consideration and in using infinite series for the solution of the differential equation, in some instances with spherical co-ordinates, while Munk and his collaborators have used planar co-ordinates. More recently, HIDAOKA (1955) has presented a detailed numerical theory of the general circulation of the Pacific which he regards as a purely wind-generated phenomenon. He uses the assumption that the vertical velocity vanishes *exactly* at all points. Further, he gives the horizontal distribution of the stream lines for different subsurface levels. These circulation patterns are all similar to the sea surface circulation. The only noticeable difference is a general reduction in intensity of the movement with depth. It may be already as little as half the surface intensity in 250 m depth. His numerical results are, however, difficult to interpret on a physical basis, and appear insufficient for an explanation of the vertical mass transports necessary for continuity.

HANSEN (1951, 1954) treated the circulation problem as a boundary value problem ("Eigen" value problem). His method is equally suitable for finding the volume transport and the form of the sea surface in an enclosed part of the ocean from the known wind field. Hansen calculated the volume transport and the sea surface topography for the equatorial part of the Atlantic from the average August wind field, and obtained a satisfactory agreement with results based on observations of ship's displacements and of the density distribution.

While for all methods the agreement is very good qualitatively, this is not always so quantitatively. Munk, for instance, obtained transport values for the Atlantic and the Pacific which were only half as great as those computed from observational data (36 and 39×10^6 m³/sec for maximum transport by the Gulf Stream and the Kuroshio, respectively, against observed mean values of 55 to 74 and 65×10^6 m³/sec, respectively). It is not improbable that the discrepancy arises from the fundamentals of the theory, possibly from the use of the *mean* wind stress based on climatological wind

charts without taking into account the deviations. It might also be due to the imperfections in the present knowledge of the relationships between wind velocity and wind stress (see pp. 421 and 586) or due to the use of plane co-ordinates instead of spherical ones for the calculation of conditions on the curved surface of the earth. It is noteworthy that Hidaka has obtained good numerical agreement for transport in the Kuroshio Current using spherical co-ordinates. The most probable reason however is that the actual dynamics of the strong western boundary currents (such as the Gulf Stream and the Kuroshio) are left essentially unexplained by the Stommel–Munk theory. In order to explain the narrowness of these boundary currents it is necessary to take an eddy viscosity so large that the eddy sizes would be comparable to the width of the current. This can never be the case. Pressure inertia and the variations of Coriolis parameter with latitude all seem to play an important part in the dynamics of these boundary currents (see p. 550). It is striking that there is no indication of a “westward intensification” of ocean currents in the Southern Hemisphere; the Brazil Current and the East Australian Current for instance are not so strongly developed along the east coast of the continents as the Gulf Stream and the Kuroshio. It would be expected that if the planetary vorticity were the only cause of the westward intensification in the oceans of the Northern Hemisphere it would show the same effect in the South Atlantic and South Pacific. It appears however that the vertical structure of the ocean also plays a role in the theory since the depth d is correlated with the oceanic structure and the magnitude of d cannot be chosen arbitrarily. d denotes the depth over which an integration has to be performed in order to eliminate the effect of the vertical oceanic stratification and of internal vertical friction. Usually the depth of no motion has been taken as d and only the horizontal velocity of the water movement has been taken into consideration; the vertical velocity is presumed to be zero or so small that it can be neglected. This assumption is certainly incorrect and may lead to an entirely false picture of the horizontal circulation. STOMMEL (1956) has given a detailed discussion showing that the existence of a level of no motion in the ocean where all the three velocity components vanish cannot be substantiated; in fact the maximum vertical velocity occurs at the depth of no meridional velocity (see p. 499). A paper by NEUMANN (1955) is of interest here. He has re-examined the theory for a horizontal wind-driven ocean current taking into account the spherical shape of the earth the average vertical density stratification and the variable depth of the lower boundary of the circulation system. The latter assumption is the same as the assumption that the depth d is the depth of the layer of no meridional motion. Integration of the usual equations of motion for the geostrophic wind taken over the depth z between $+\zeta$ and $-d$ and with $\rho = \rho(x, y, z)$ gives the equations of transport

$$\left. \begin{aligned} -fM_x &= \frac{\partial P}{\partial y} - \rho(\xi) \frac{\partial \zeta}{\partial y} - p(-d) \frac{\partial d}{\partial y} \\ fM_y &= \frac{\partial P}{\partial x} - \rho(\xi) \frac{\partial \zeta}{\partial x} - p(-d) \frac{\partial d}{\partial x} \end{aligned} \right\} \quad \text{(XVIII.21)}$$

Introducing

$$\bar{\rho} = \frac{1}{\zeta + d} \int_{-d}^{\zeta} \rho(z) dz; \quad P(-d) = g\bar{\rho}(\zeta + d) \quad \text{and} \quad P = \int_{-d}^{\zeta} p dz = \frac{g\bar{\rho}}{2} (\zeta + d)^2$$

and taking into account that the divergence of the total mass transport is zero and $\zeta \ll d$, one obtains

$$-\beta M_x = gd \left(\frac{\partial x}{\partial d} \frac{\partial \bar{\rho}}{\partial y} - \frac{\partial d}{\partial y} \frac{\partial \bar{\rho}}{\partial x} \right) + g\bar{\rho} \left(\frac{\partial x}{\partial d} \frac{\partial \zeta}{\partial y} - \frac{\partial d}{\partial y} \frac{\partial \zeta}{\partial x} \right) \quad (\text{XVIII.22})$$

and from the second equation

$$fM_x = \frac{1}{2}gd^2 \frac{\partial \bar{\rho}}{\partial \zeta} + g\bar{\rho} d \frac{\partial \zeta}{\partial x} \quad (\text{XVIII.23})$$

Equating M_x in (XVIII.22) and (XVIII.23) gives

$$\left(\frac{\beta}{f} - \frac{1}{d} \frac{\partial d}{\partial y} \right) \frac{\partial \zeta}{\partial x} + \left(\frac{\beta d}{f} - \frac{\partial d}{\partial y} \right) \frac{1}{\bar{\rho}} \frac{\partial \bar{\rho}}{\partial x} + \left(\frac{1}{d} \frac{\partial \zeta}{\partial y} + \frac{1}{\bar{\rho}} \frac{\partial \bar{\rho}}{\partial y} \right) \frac{\partial d}{\partial x} = 0. \quad (\text{XVIII.24})$$

In the case of a *homogeneous* ocean ($\bar{\rho} = \text{const.}$), equation (XVIII.24) reduces to

$$\left(\frac{\beta}{f} - \frac{1}{d} \frac{\partial d}{\partial y} \right) \frac{\partial \zeta}{\partial x} + \frac{1}{d} \frac{\partial \zeta}{\partial y} \frac{\partial d}{\partial x} = 0. \quad (\text{XVIII.25})$$

This equation states that in the case of a constant depth d only zonal steady currents are possible, because the first term will vanish only when $\partial \zeta / \partial x = 0$. When the depth d is variable, all current directions are possible, if d satisfies certain conditions according to (XVIII.24). If the depth d is a function only of y (the latitude), then, provided that $\partial d / \partial y \neq 0$

$$\frac{\beta}{f} = \frac{1}{d} \frac{\partial d}{\partial y}. \quad (\text{XVIII.26})$$

This equation is identical with (XVI.19) and states that for stationary currents the decline of the lower depth d of the current system towards the poles must follow a law $d = K \sin \phi$. In a *stratified* ocean ($\bar{\rho} = \bar{\rho}(x, y, z)$) the interrelationship is more complicated. Equation (XVIII.24) shows, however, that for a constant depth d of no horizontal motion, there can be no meridional mass transport due to frictionless currents, since when $d = \text{const.}$, the equation reduces to

$$\frac{\partial \zeta}{\partial x} = - \frac{d}{2\bar{\rho}} \frac{\partial \bar{\rho}}{\partial x}. \quad (\text{XVIII.27})$$

On substitution in equation (XVIII.23) it is found that $M_x = 0$.

It has been shown above (p. 497) that in the Atlantic Ocean the zonal mean of the depth of no meridional motion follows the above equation. This can be interpreted to mean that the planetary vorticity (βM_y) is compensated by a corresponding balanced topography of the lower boundary of the current system. This is frequently the case in the South Atlantic, and here the westward intensification, which of course is a consequence of the planetary vorticity effect, is only weakly developed.

In criticism of Neumann's arguments, Stommel has questioned the assumption that the depth d is a depth of no motion, and has pointed out that on the contrary, the greatest vertical velocities occur at this depth. Neumann's equations can also be derived from the basic assumption that the potential vorticity in the large-scale

oceanic circulation is constant (see p. 336); that is, $d/dt(\zeta + f)/d\zeta = 0$, where ζ is here the relative vorticity. Since generally $\zeta \ll f$, this equation reduces to

$$\frac{\partial}{\partial y} \left(\frac{\zeta + f}{d} \right) = 0$$

for stationary predominantly zonal currents. From this it follows, since $\zeta \ll f$, that

$$\frac{f}{d} \sim \text{const.} \quad \text{or} \quad \frac{1}{d} \frac{\partial d}{\partial y} = \frac{1}{f} \frac{\partial f}{\partial y} = \frac{\beta}{f} \quad (\text{XVIII.28})$$

which is equation (XVIII.26). However, the assumption of constant potential vorticity is valid only for horizontal geostrophic currents, but does not hold when vertical velocity components are also present. Stommel's objection seems then to be justified and Neumann's equations are valid as a first approximation only when the vertical velocities are small compared with the horizontal ones.

Chapter XIX

The Tropospheric Circulation

1. The Position and Structure of the Oceanic Troposphere

THE important subdivision of the oceanic space into troposphere and stratosphere is due primarily to the *climatic* influence of the atmosphere on the water masses of the uppermost ocean layers. More or less constant conditions in weather and radiation at the ocean surface give rise to the development and maintenance of water types of different character in different climatic zones. Broadly speaking there are two principal water types which are constantly being formed in large quantity and with a rather constant internal structure; they correspond to the two great zones of contrasting climate, the tropical and subtropical regions, and the polar regions. These two water types are:

(1) the tropical-subtropical water type which is warm due to the excess of incoming radiation and has a high salinity due to evaporation, and

(2) the cold weakly saline water type of the subpolar and polar zones.

The former is lighter, the latter heavier, and this difference is the cause of continuous large-scale movements. These movements follow the fundamental principle that *each water type tends to flow by the shortest route, by vertical or horizontal displacement to the depth in the ocean at which it will be in a stable equilibrium corresponding to its density*; here it will spread out as a layer. The heavier subpolar water type therefore sinks to greater depths, and spreads more or less horizontally to fill in this way the deep lower layers of all the oceans. The lighter tropical and subtropical water type, on the other hand, remains in the upper layers of its original zone as the lightest water type. The subdivision in the structure of the oceans is thus a consequence of circulation. It is to be expected already from the history of formation of the two main oceanic subspaces, that they will have essentially separate circulations; these will be called *tropospheric* and *stratospheric*. This does not imply that there is no connection between the two circulations; on the contrary, at certain places interactions occur and the water masses of both type undergo transformation by turbulent mixing and manifold atmospheric influences so that tropospheric water becomes stratospheric and vice versa.

The thermo-haline structure of the troposphere has been explained in pt. I, Chapter III, §4, p. 117 *et seq.* and IV §3, p. 165 *et seq.* The most important phenomenon is the *layer of discontinuity* in the vertical distribution of temperature and density which is always sharply defined in the tropics and subtropics and is associated with a characteristic salinity distribution. An example is shown in Fig. 70 of pt. I. Beneath the discontinuity layer which acts as a barrier to upward and downward movement, is the subtroposphere which is occupied by little differentiated and nearly motionless waters.

It is usually difficult to fix a definite boundary between the troposphere and the stratosphere. In the vertical density profile it appears as a slight intensification of the vertical gradients; but often it is quite indistinct because of the very great distance between observation levels at these depths. It should probably be referred to only as a boundary layer. An approximate boundary can be obtained using the oxygen content as a criterion (WÜST, 1936*b*, see pt. I, p. 66 *et seq.*); it is then defined by the intermediate oxygen minima. The method is based on the assumption that these minima indicate layers where the air supply is least, that is, those localities where the renewal of the water masses is particularly slow and where horizontal movement of the water is entirely missing. It has frequently been pointed out (p. 494) that in the uppermost layers the position of the oxygen minima is affected by biological processes. However, oxygen minima can be used at greater depths to specify approximately the different circulations. In the Atlantic the oxygen minimum extends across the 110 degrees of latitude (from 45° S. to 55° N.) between the oceanic polar fronts of both hemispheres; its mean depth along a meridional section is given in Table 151.

From the Southern Hemisphere polar front the lower limit of the oceanic troposphere sinks rapidly down to 600 m in the southern convergence region (between 35° and 25° S.), and rises again to about 300 m in the tropics. Just north of the equator, it is at first somewhat irregular and then sinks gradually down to about 950 m in the northern convergence region (30° to 40° N.).

Reasonably accurate data are available for the tropospheric circulation which extends throughout the space between the sea surface and the lower boundary of the troposphere. DEFANT'S (1936*c*) representation of conditions in the Atlantic also includes subsurface data over the whole area. For the other oceans the series observations are sufficient for interpretation only along single meridional or zonal sections. No major differences between the oceans in the principal features of circulation are to be expected.

Table 151. Lower limit of the troposphere in the Atlantic Ocean
(Determined from the position of the oxygen minimum. Depth in metres.)

Section	50°	45°	40°	35°	30°	25°	20°	15°	10°	5°	Equator	
Western section	N	—	—	(1000)	850	830	820	770	550	280*	350	400
	S	—	—	400	500	550	600†	580	450	300	280*	
Central section	N	450	790	770	830	880†	870	680	470	380	330*	400
	S	—	(100)	320	500	600†	580	550	420	300*	400	
Eastern section	N	(900)	(900)	(900)	(900)†	(250)	820	680	(550)	520	400	350*
	S	—	300	470	530†	510	450	380	300*	390	400	

N. Northern Hemisphere; S. Southern Hemisphere

* Minimum values; † Maximum values.

2. The Tropospheric Circulation of the Tropical and Subtropical Oceans

The tropical and subtropical circulation of the oceanic troposphere is dominated by the enormous water transports of the North and South Equatorial Currents. They determine dynamically the position of the tropical and subtropical discontinuity layer. Its depth in the Atlantic between 25° N. and 25° S. is shown in Fig. 269. From a depth of more than 200–300 m in western Ross-latitudes of both hemispheres

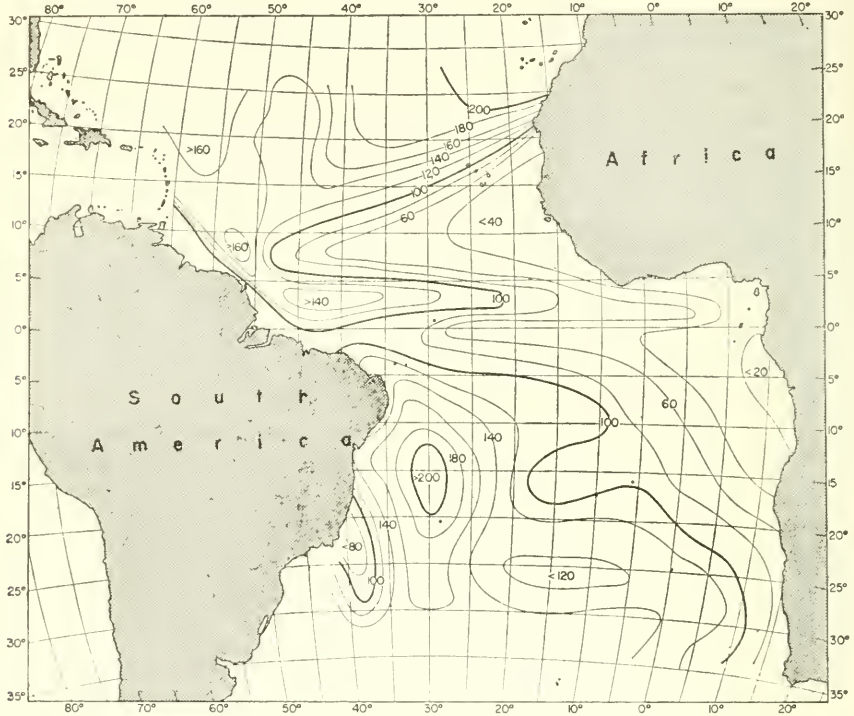


FIG. 269. Depth (m) of the tropospheric discontinuity (thermocline) in the Atlantic Ocean between 25° N. and 25° S.

the discontinuity layer rises towards the southeast to a depth of 40 m in the Northern Hemisphere and towards the north-east to a depth of 20 m in the Southern Hemisphere. Between the equator and about 6°–10° N. these rising slopes are separated by an east–west depression extending into the Gulf of Guinea. This striking arrangement of the topography of the discontinuity surface is a direct consequence of the equatorial currents on either side of the equator; because of dynamic reasoning these currents also determine the rise of the discontinuity layer towards the equator. Up to about 6° to 10° N., the depth of the density transition layer is associated with the Equatorial Counter Current and its further extension (the Guinea Current). For a connection between the state of motion of the water masses above and below the discontinuity and the topography of the discontinuity layer see p. 463 *et seq.* Further information on the conditions of motion in the individual layers of the oceanic troposphere can be gained by investigation of the striking salinity maxima near the discontinuity layer,

that intervenes between the homo-haline and weakly saline top layer and the deeper lower salinity layers with an equally low salinity. Study of the position of these maxima and their development showed that they intrude under the less saline top layer from the extensive subtropical accumulations of highly saline water to the north and south. These intrusions spread along preferred paths, the location of which throws some light on movements within the middle and lower layers of the troposphere. This spreading and its dynamics have been discussed in pt. I, Chapter IV, p. 166. There Fig. 72 (p. 168) shows that the salinity maxima are present everywhere except in two narrow bands in both hemispheres where the density transition layer comes closest to the sea surface. Evidently, the horizontal extension of the highly saline intermediate layer is cut short in this region, and here the water masses must be deflected upward. The region between the two bands without salinity maxima lies in the Equatorial Counter Current. Here the supply of water that forms the salinity maxima comes from the west, from regions which are not reached by the bands free from the salinity maxima and are fed here from north and south. From these facts it is possible to derive a three-dimensional system of currents in the oceanic troposphere of the tropics and subtropics, that is illustrated schematically by the meridional section in Fig. 270.

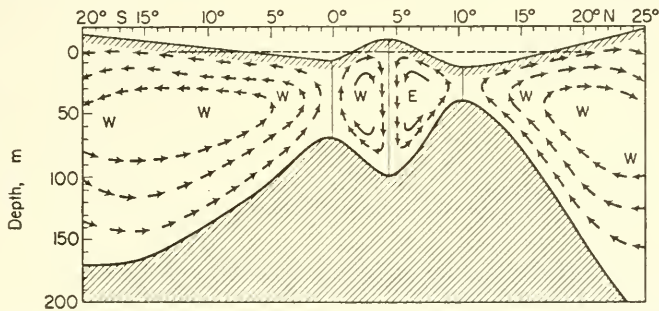


FIG. 270. Schematic representation of the zonal and meridional velocity components of the tropospheric circulation in the Atlantic Ocean (the topography of the thermocline is exaggerated in the vertical scale by about 1:1 million; that of the physical sea surface even more); *W*, current towards west; *E*, current towards east.

Where the stream lines are divergent in the top layer they are convergent in the discontinuity layer; the two bands with a low salinity are thus regions of upwelling water.

The zonal components of motion do not appear in the meridional section and it should not be forgotten that these are considerably more important. Compared with these the transverse circulation is rather weak. This transverse circulation is primarily a thermo-haline circulation and is the consequence of the internal forces of the mass distribution (p. 575). It involves only the top layer down to the density transition layer and in the strong zonal motions of the wind-driven equatorial currents it can hardly be detected. It is, however, responsible for the pronounced vertical and horizontal salinity distribution that is characteristic for the uppermost layers of the tropical oceans.

The water masses beneath the density transition layer (in the *subtroposphere*) are very uniform and colourless and the water movements here must therefore be very weak. Since they lie beneath the barrier, they can be only slightly affected by turbulence

and convection and they have an extremely low concentration of oxygen which is largely due to the almost total stagnation and also due to biological causes.

The internal forces, providing the motive force for the entire current system of the tropics and the subtropics, are produced, on the one hand, by the wind system present in these zones and on the other hand, by the internal pressure field set up by the thermodynamic conditions. Figure 271 shows the absolute topography of the physical sea level in the Atlantic Ocean pictured by isobaths drawn at intervals of 5 dyn/cm between 35° N. and 35° S. and at intervals of 10 dyn/cm outside this area (DEFANT, 1941*d*). The direction of this stationary gradient current, which corresponds to this pressure field is indicated by arrow-heads on the dynamic isobaths. Comparison of this topography in the tropical and subtropical area with that of the tropospheric density transition layer (Fig. 269) shows that they are almost mirror images; in deeper layers the

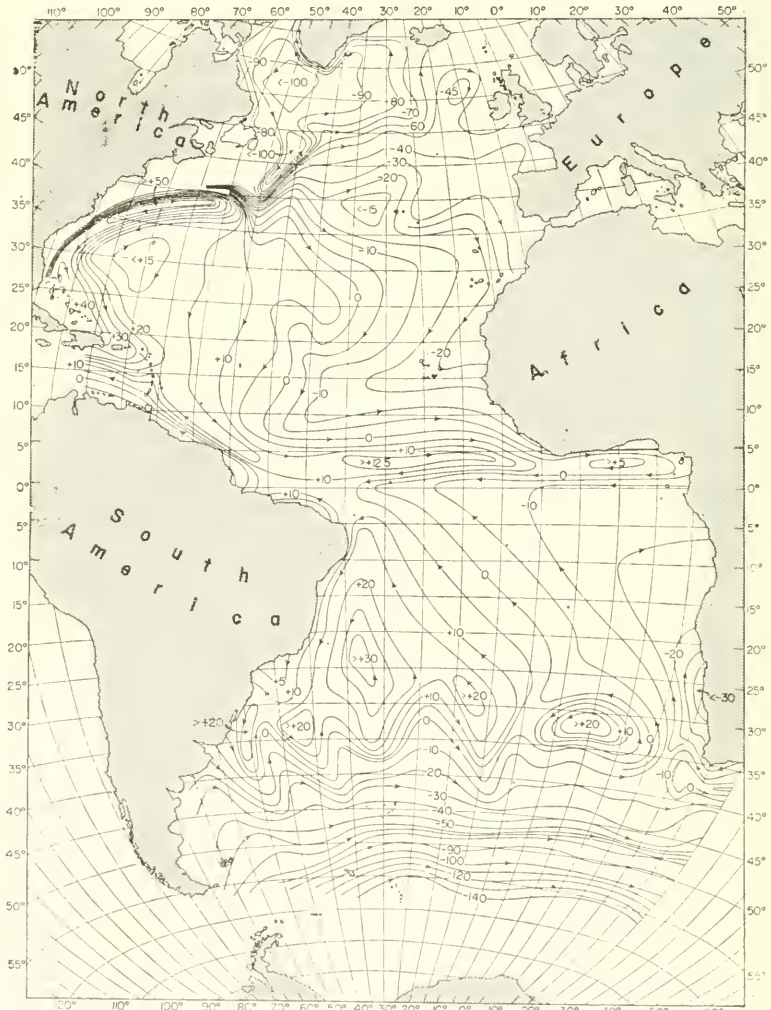


FIG. 271. Absolute topography of the physical sea surface (dynamic isobaths drawn from 5 to 5 dyn cm, 10 to 10 respectively).

pressure surfaces are of the same form as the sea surface but the pressure gradient decreases rapidly with depth (Fig. 272). The lower limit of the tropical and subtropical circulation must lie at the 500 decibar surface where the pressure gradient is almost zero; already at 200–300 m depth the velocity of the currents is very slight and the Equatorial Counter current does not reach nearly as deep as this (approx. down to 150 m). A comparison of the topography of the physical sea level and the gradient

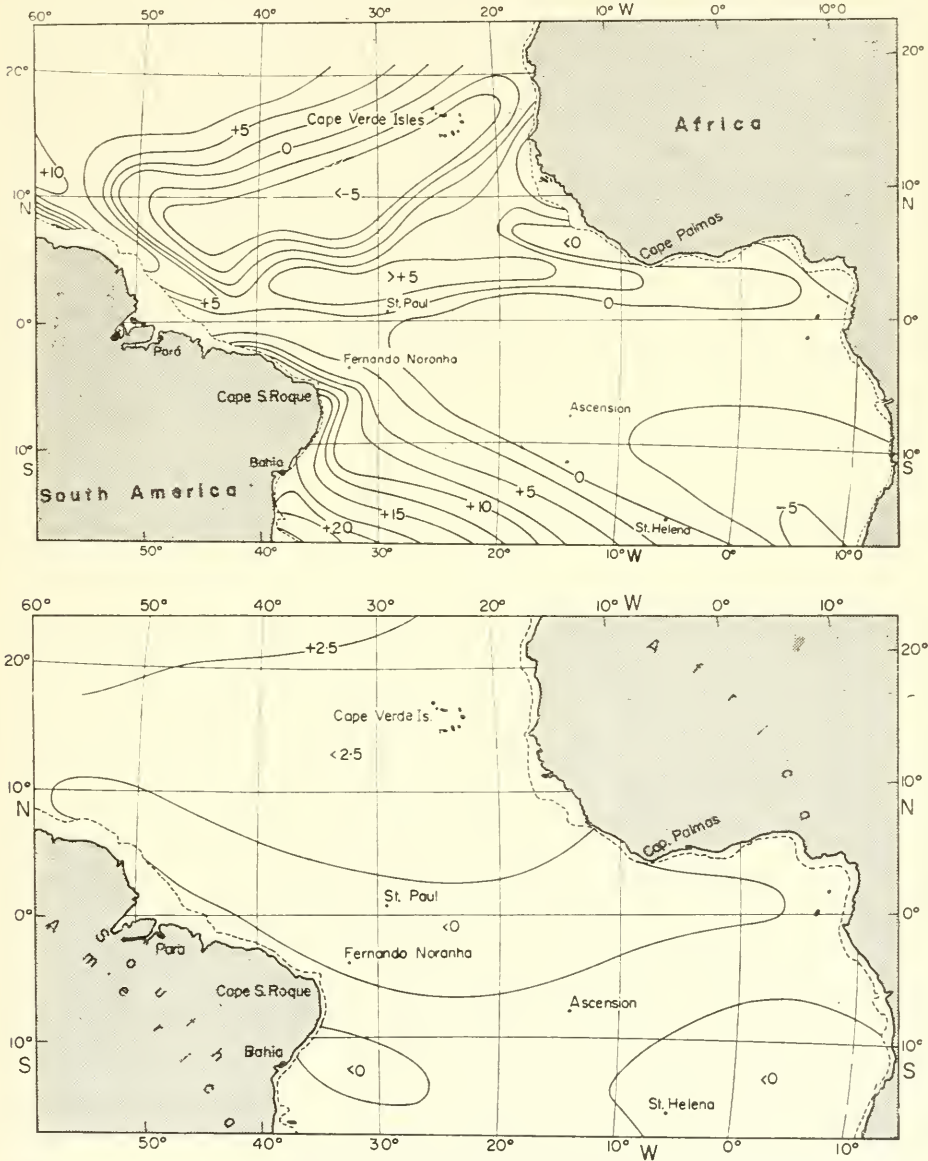


FIG. 272. Absolute topography of the 100-decibar (upper picture) and 500-decibar surface (lower picture) of the subtropical and tropical region of the Atlantic Ocean (dynamic isobaths are drawn from 2.5 to 2.5 dyn cm).

currents at the sea surface derived from it (see "*Meteor*" Report VI §2, supplement 22) with current charts derived from observations shows that the trade winds are the main cause of the currents in the uppermost layer of the sea. These give rise to a total water transport at right angles *cum sole* of the wind direction. In the Northern Hemisphere the water flows towards west-north-west and in the Southern Hemisphere towards west-south-west. Along the east coasts of continents and also at the eastern boundary of the strong water displacements, which are directed from north to south along the coast lines, water is accumulated and *piled up* and thus a pressure gradient is created to the south-east in the Northern Hemisphere and to the north-east in the Southern Hemisphere. This is shown clearly by the topographies of the pressure surfaces and of the sea surface, respectively. In the trade-wind region the resultant ocean current is then no longer solely due to the effect of the permanent air currents characteristic for these latitudes, but is also affected decisively by the mass distributions in the uppermost layers. A diagram of forces for the central part of the South Equatorial Current according to the "*Meteor*" observations, has already been discussed (Fig. 180, p. 424). It allows an estimate to be made of the effect of the individual forces in the formation of this major current. It is of particular interest that the water masses in the equatorial currents *flow against the slope of the physical sea level and the pressure surfaces, that is to say, uphill*. Part of the force transferred to the water by the winds is used in overcoming this gradient, so that the velocities of the water displacement are correspondingly somewhat reduced.

The pressure field associated with the Equatorial Counter Current is clearly shown in the topography of the physical sea level (Fig. 271) and in the topography of the isobaric surfaces (Fig. 272). This current is undoubtedly an essential feature necessary for the stability of the tropical current system. Its asymmetry about the equator is a consequence of the displacement of the thermal equator into the Northern Hemisphere and of the accompanying asymmetry of the atmospheric circulation (see p.463). The main contributions to the theoretical explanation of the mode of formation of an Equatorial Counter Current have been primarily due to SVERDRUP (1932); DEFANT (1935, 1941); THORADE (1941) and PALMÉN and MONTGOMERY (1940). For an atmospheric circulation assumed symmetrically about the equator, the Equatorial Counter Current can be readily explained as a *compensation current* produced by the disturbances of the pressure field by a meridional continent opposing the wind drifts corresponding to the North and South Equatorial Currents. It flows eastwards as a gradient current in the direction of downward sloping sea level and is retarded only by friction at the lower boundary surface and at both sides of the current. STOCKMAN (1946a-d) has attempted to consider also the baroclinic mass field, though without taking into account the dependence of the Coriolis parameter on latitude. According to this explanation the accumulation of water carried westwards and piled up by the equatorial currents is the most important factor in the formation of the counter current. The asymmetry of the counter current about the equator would then be due to the asymmetry of the atmospheric circulation. Presumably for the Atlantic this explanation of the counter current can be considered as an adequate one, but for the considerably more extended Pacific it is doubtful whether the effect of the water accumulation piled up in the west is sufficient in order to give rise to a counter current as a very narrow band over such a great distance.

Evidence against this conception of the equatorial counter current as a pure gradient current has been accumulated by SVERDRUP (1947) and REID (1948), who showed that the main features of the baroclinic mass distribution in the tropical and subtropical Eastern Pacific are due *entirely* to the effects of the mean wind stress distribution in these regions. A method for the determination of the mass field and the mass transport of the currents from the given wind field has already been described on p. 550 and following pages. By means of Fig. 254 it has been demonstrated that the mass structure and the currents of the equatorial region of the Eastern Pacific are only effects of the wind stresses. In these investigations full account was taken of the dependence of the Coriolis parameter on the latitude, but the influence of lateral friction and of thermodynamic effects such as radiation and evaporation and others was neglected. The good agreement between theory and observations is an indication that the latter effects are of secondary importance in the dynamics of the equatorial counter current. Figure 273 presents diagrams of forces for the equatorial currents and

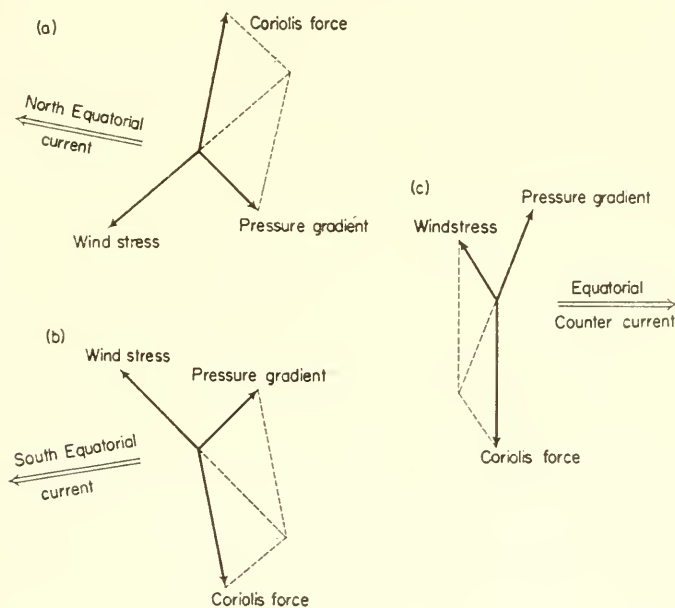


FIG. 273. Diagrams of forces: (a) for the North Equatorial Current; (b) for the South Equatorial Current; (c) for the Equatorial Counter Current.

for the counter current. Basically there is no difference between them; since they are each produced and maintained primarily by the wind in a sea with a baroclinic mass structure.

A comprehensive representation of the oceanic structure and circulation in a section along the middle axis of the Atlantic is contained schematically in Fig. 274. It is self-evident that this picture is of a schematic nature only, however, an attempt has been made to include all the characteristic features of the tropospheric oceanic structure as well as the corresponding three-dimensional circulatory movements. This circulation in its zonal extent is largely a consequence of the air currents over the sea surface. The

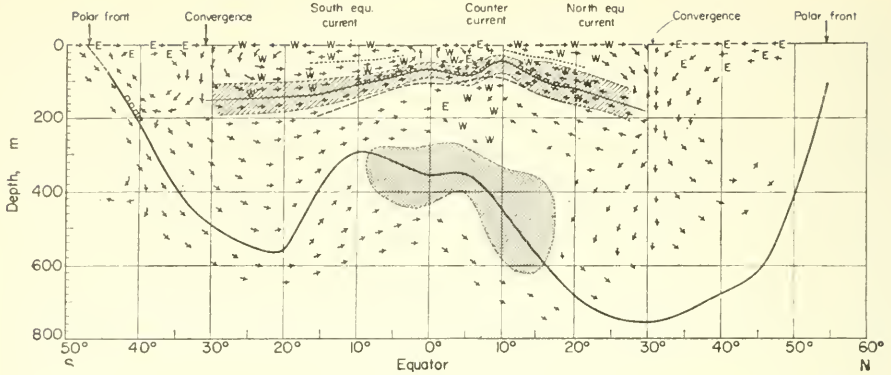


FIG. 274. Schematic picture of structure and circulation in the troposphere of Atlantic Ocean in meridional direction.

- Limit between the tropo- and stratosphere.
- Position of maximal density gradients.
- Tropical-subtropical thermocline.
- Layers of extremely low oxygen contents ($< 1.5 \text{ cm}^3/1$).
- Position of tropical-subtropical salinity-maxima.
- W, E Zonal velocity component (W towards west, E towards east).

meridional components of motion, on the other hand, are a consequence of meridional variations in radiation and evaporation-precipitation difference and are therefore only weak.

The lower currents stand clearly out in salinity sections of the Pacific and of the Indian Ocean as tongues of high salinity. They originate and spread out again from the subtropical accumulations of highly saline water. A meridional salinity section through the central part of the Pacific Ocean (Pt. I, p. 172, Fig. 76) shows that the intrusion of this water from the South Pacific is the stronger one reaching as far as 12° N . in a depth of 150–250 m. The northern branch, however, is present only between 22° and 25° N . In the east these intrusions seem to be still weaker (see the vertical section in the Eastern Pacific given by SCHOTT, 1935, p. 182); contrary in the west Pacific region they are stronger. The southern undercurrent shows as a spectacular phenomenon (see Fig. 275, Wüst, 1929) though again, the northern branch is only weakly developed.

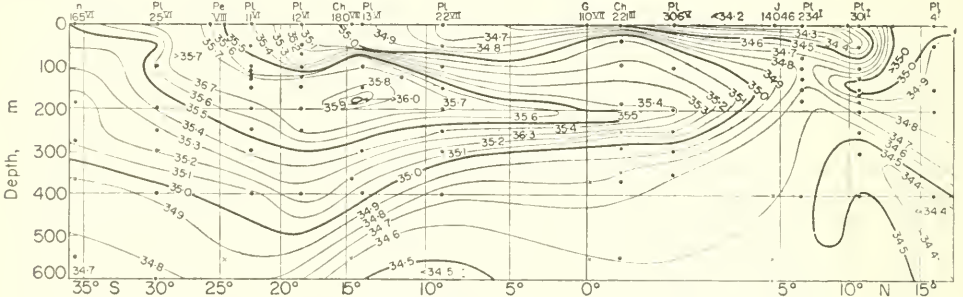


FIG. 275. Longitudinal section of salinity through the subtropical deep current in the West Pacific Ocean (according to Wüst).

The equatorial currents are particularly well developed in the Pacific. As in the Atlantic the counter current lies in the Northern Hemisphere throughout the whole year and especially far from the equator during the northern summer. The surface velocities reach values of more than 2 knots. The structure of the water masses was first pictured in a "Carnegie" section (at about 140° W.) in October 1929 (SVERDRUP *et al.* 1942., p. 709). Figure 276 shows the temperature and salinity distributions between

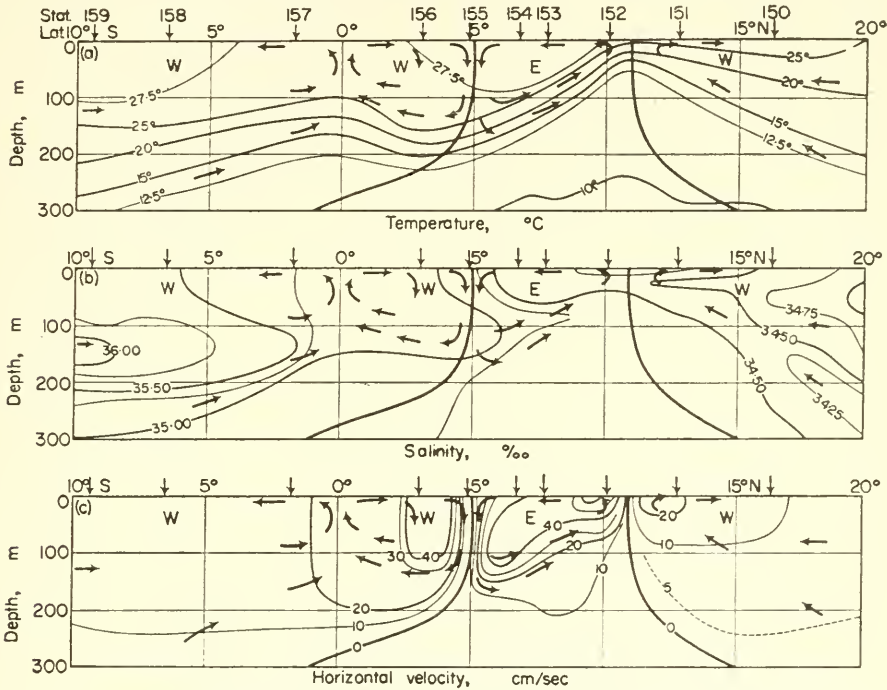


FIG. 276. Temperature, salinity and computed velocity in a vertical section in the Pacific Ocean between 10° S. and 20° N. (according to the "Carnegie" observations; arrows indicate direction of the north-south flow; *E.* and *W.* indicate flow towards east and west respectively) (according to Sverdrup, 1942).

the sea surface and 300 m as well as the velocity distribution calculated on the assumption of no motion at the 700-decibar surface. The equatorial counter current lies between 5° and 10° N., and in correspondence with the sea surface slope flows downwards in the calm belt between the trade winds. The maximum velocity at the surface is a little over 50 cm sec^{-1} , in good agreement with observed values. The "Carnegie" section gives an eastward transport by the equatorial counter current of approximately $25 \text{ million m}^3 \text{ sec}^{-1}$. The character of the transverse circulation is evident from the distribution of salinity, oxygen, phosphate and also silicate and is quite similar to that shown in Fig. 269 derived from observations in the Atlantic.

A detailed theoretical treatment of the circulation in the top layer of the equatorial parts of the oceans has been given by YOSHIDA, MAO and HOOVER (1953). They start out with the steady-state equations involving the Coriolis force, the pressure gradient and horizontal as well as vertical mixing. For the mean wind-stress distribution and

the mean density distribution they took REID'S model (1948) which is generally applicable in equatorial regions. The wind drift and gradient current were superimposed correspondingly considering the boundary conditions, and finally the vertical velocity in the upper mixed layer was calculated using the continuity equation.

Figure 277 shows the dependence on the latitude of the horizontal velocity components u and v at the sea surface and the horizontal wind stress T_x , acting only in zonal direction. It is evident that a strong equatorial counter current is formed between

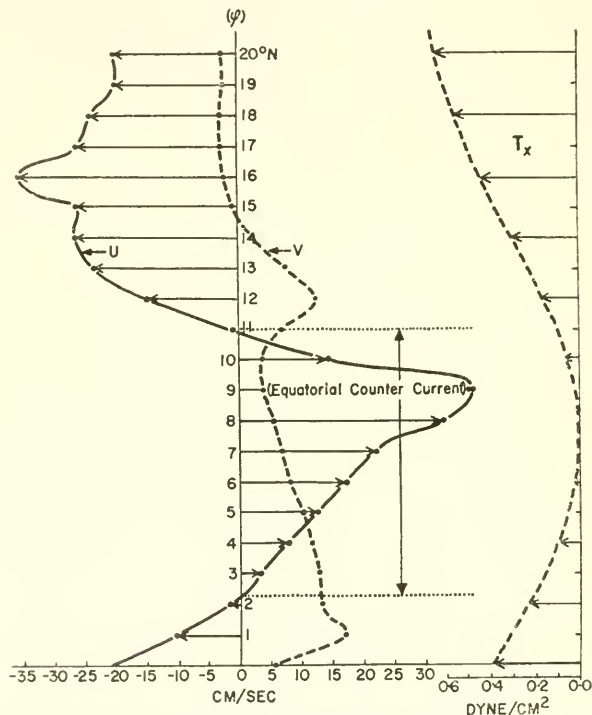


FIG. 277. Latitude dependence of the horizontal velocity components u and v at the sea surface and the horizontal wind stress T_x acting only in zonal direction on the ocean surface.

2.5° and 11° N. in the area of weak westward wind stress between the strong north-east and north-west trade winds. All the velocity components decrease somewhat with depth down to the lowermost boundary of the upper mixed layer, the u -component of the equatorial counter current decreases least so that almost uniform values are found throughout the entire top layer. The vertical velocity resulting from the continuity equation is shown in Fig. 278. Its distribution is rather noteworthy. It shows:

- (1) very strong upwelling at or near the equator, this is the equatorial divergence;
- (2) strong sinking at the southern boundary of the counter current; and
- (3) fairly strong upwelling at the northern boundary of the counter current.

The vertical velocity is of the order of 10^{-4} and 10^{-3} cm sec⁻¹. Farther to the north the velocities are small and irregularly distributed. Considering that the REID model is only a crude approximation of true conditions and especially that the wind-stress distribution with *zonal* components *only* can hardly correspond to actual conditions,

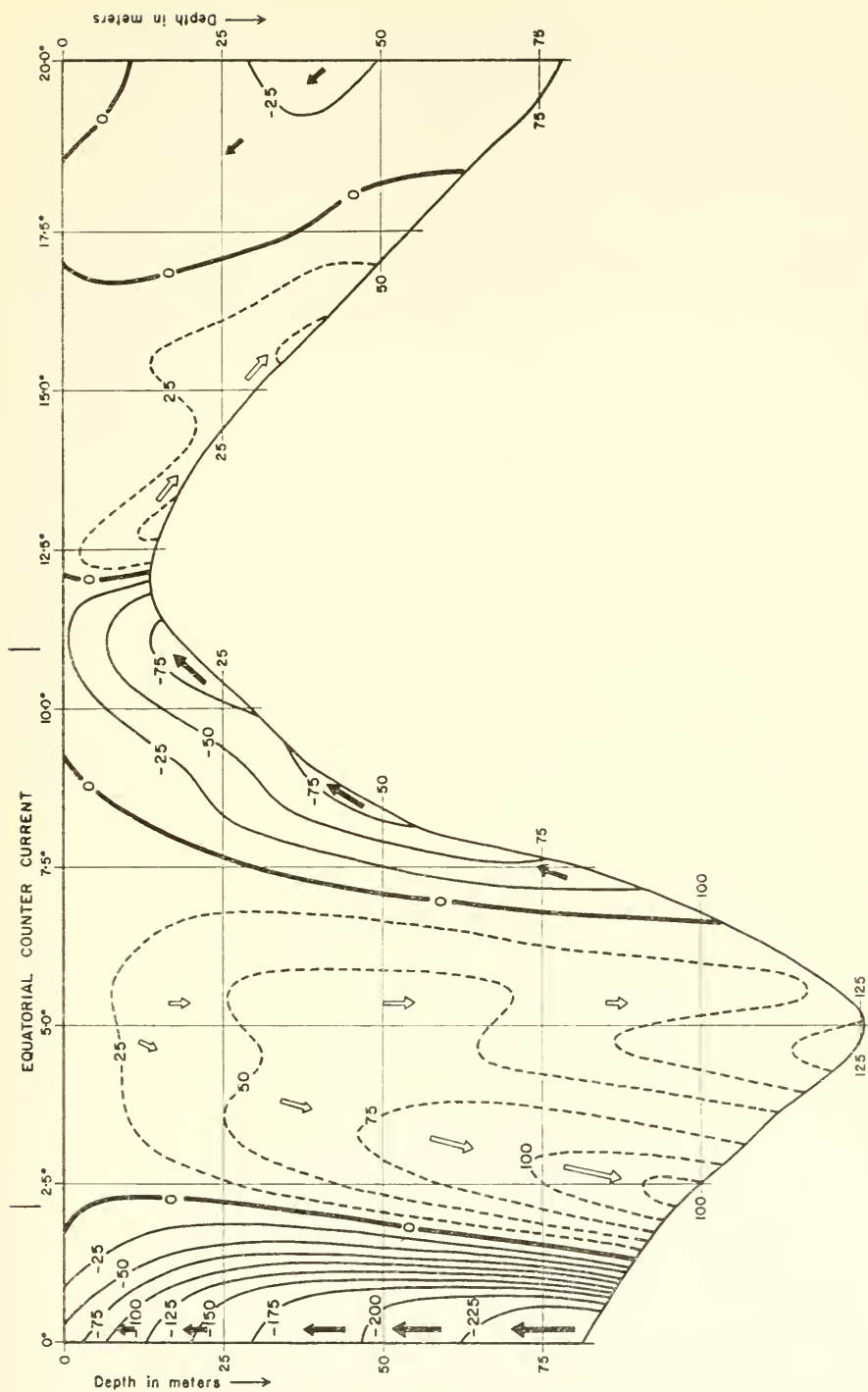


FIG. 278. Distribution of the vertical component of the current velocity in the equatorial North Pacific Ocean (given in 10^{-5} cm/sec).

the similarity with the vertical velocity field shown in Fig. 269 is remarkable. It should be noted that the vertical velocity component does not vanish at the lower boundary of the upper mixed layer. The current does not follow the inclined surface of this boundary unless the divergence of mass transport in the upper mixed layer is zero. This does therefore never correspond to the conditions shown in Fig. 269.

Also in the Indian Ocean conditions are similar with the same much weaker development of the phenomenon in its eastern parts (see Pt. I, p. 172, Fig. 75). Since the thermal equator remains here always south of the equator the tropospheric circulation is again rather asymmetrical and, as in the Pacific, the southern hemispheric branch is the stronger one. However, while the conditions in this branch are almost unchanged throughout the total year, complications must appear in the Northern Hemisphere due to the seasonal changes in the current system of the sea surface. During the summer months the strong south-west monsoon current extends down to the lower layers of the troposphere and the subtropical undercurrents are suppressed. The available sections do not show the nature of this change. Probably the highly saline water masses of the southern hemispheric lower currents extend into the Northern Hemisphere and partly enter the influence region of the wind drifts of the south-west monsoon.

The Equatorial Undercurrent. CROMWELL, MONTGOMERY and STROUP (1954) discovered an Equatorial Undercurrent in the Central Pacific in a zone between the equator and latitude 1° N. and at a depth of 50–150 m. It is found as a narrow eastward current both in the lower part of the top layer at the equator and in the upper part of the thermocline in this zone, where the South Equatorial Current extends into the Northern Hemisphere. Its position in the vertical and horizontal circulation of this area is sketched in Fig. 279. FOFONOFF and MONTGOMERY (1955) have shown that the Equatorial Undercurrent agrees with a simple application of the vorticity equation

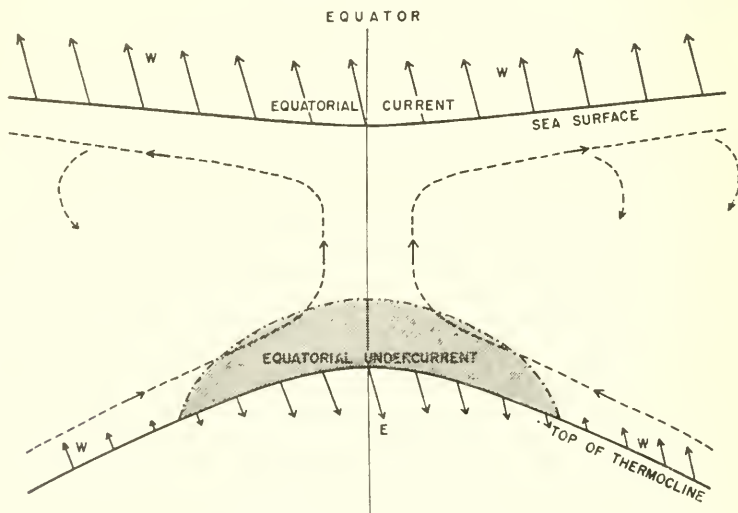


FIG. 279. Meridional section showing idealized currents in the surface layer (about 100 m deep within about 3° of equator, reader looking west). The flux components in the plane of the section are indicated by broken arrows. Zonal components of velocity at the top and the bottom of the layer are indicated by diagonal arrows drawn in perspective.

(X.68). In a cross-section through the meridional circulation the water flows towards the equator in the part of the top layer beneath the drift current and rises at the equator. The zonal component of the surface current can be taken as uniform and the relative vorticity f_0 being zero. If a water layer moves without friction from an initial state ζ_0, f_0, h_0 to a new state the vorticity equation gives the relationship

$$\frac{f + \zeta}{h} = \frac{f_0 + \zeta_0}{h_0} \quad (\text{XIX.1})$$

For water sinking from the surface $\zeta_0 = 0$, and if the thickness is assumed to remain constant during the displacement, and if all the water is assumed to have started from the same initial state, the distribution of the zonal velocity component can be found by integration of

$$f + \zeta = f_0. \quad (\text{XIX.2})$$

For a predominantly zonal current

$$\zeta \sim - \frac{\partial u}{\partial y} = - \frac{1}{R} \frac{\partial u}{\partial \phi}$$

and for low latitudes the solution can be written in the simpler approximate form

$$u - u_0 = R\omega(\phi - \phi_0)^2. \quad (\text{XIX.3})$$

If, in the South Equatorial Current, the surface water has a velocity of 0.5 knots with no lateral shear and sinks from latitude $\phi_0 = 2.7^\circ$ and flows without friction or changes in thickness to the equator, it will reach the equator as the east undercurrent with a velocity of 2 knots.

The component of the velocity directed towards the equator in waters moving from latitude 3° to the equator can also be calculated. The zonal velocity component is given by the equation

$$\frac{du}{dt} = fv - gi_{x,\phi} \quad (\text{XIX.4})$$

where $i_{x,\phi}$ is the longitudinal slope of the sea surface at latitude ϕ . Its existence is made possible by the presence of the continental barriers. Since

$$fv - \frac{du}{dt} = fv - v \frac{\partial u}{\partial y} = (f + \zeta)v = f_0v$$

(XIX.4) can be written in the form

$$v = \frac{g}{f_0} i_{x,\phi} \sim \frac{g}{2\omega\phi_0} i_{x,\phi}. \quad (\text{XIX.5})$$

If $\phi_0 = 3^\circ$; $f_0 = 7.6 \times 10^{-6} \text{ sec}^{-1}$ and $i_{x,\phi} = -3 \times 10^{-8}$ (see MONTGOMERY and PALMÉN (1940) and JERLOV (1953)), the velocity component v towards the equator is -4 cm/sec or 2 nautical miles a day.

The Equatorial Undercurrent is consistent with the flow towards the equator in the lower part of the top layer close to the equator, if this flow is approximately frictionless so that absolute cyclonic vorticity is conserved. Continental barriers which permit a longitudinal component of the pressure gradient, are essential for any extensive development of the undercurrent.

3. Other Currents of the Oceanic Troposphere

(a) *The Guiana Current and the Current Conditions of the American Mediterranean*

The stream lines of the tropospheric undercurrents of the Southern Hemisphere converge from the whole of the South Atlantic towards the area off Cape San Roque on the east coast of South America and the water of the South Equatorial Current flows into the Northern Hemisphere at this point. The subtropical salinity maximum of 36.7‰ at about 120 m depth can be followed far to the north (as far as the West Antilles and beyond) in a salinity section following the course of the Guiana Current north-westwards along the South American coast. The character of this water remains almost unchanged from the area of South Equatorial Current in the Southern Hemisphere to the Antilles. For the most part the current axis remains over the broad shelf off the mouths of the Amazon and the Orinoco. The corresponding pressure gradient could be determined so far only from very few stations. The direction of the pressure gradient in a gradient current must be reversed on passing from the Southern to the Northern Hemisphere. This can be seen in the sea level topography given in Fig. 271. South of the equator the higher pressure occurs at the coast with the lower pressure farther out; north of the equator this is reversed and here the Guiana Current is accompanied along its right-hand edge by a narrow ridge of high water level with a down slope towards the coast which in accord with the great strength of the current is quite considerable. The Guiana Current, together with the southern part of the North Equatorial Current, flows into the Caribbean through the passages between the Lesser Antilles (sill depth less than 1000 m). The observational data for this sea has been evaluated principally by PARR (1935, 1937*a*, 1938*a*); see also SEIWELL (1938) and RAKESTRAW and SMITH (1937) on chemical aspects and a review of these conditions by DIETRICH (1939). The tropospheric currents between 100 and 200 m are very clearly shown by the salinity maxima of the undercurrents which are a continuation of those of the North and South Equatorial Currents. Figure 280 shows a chart of surface

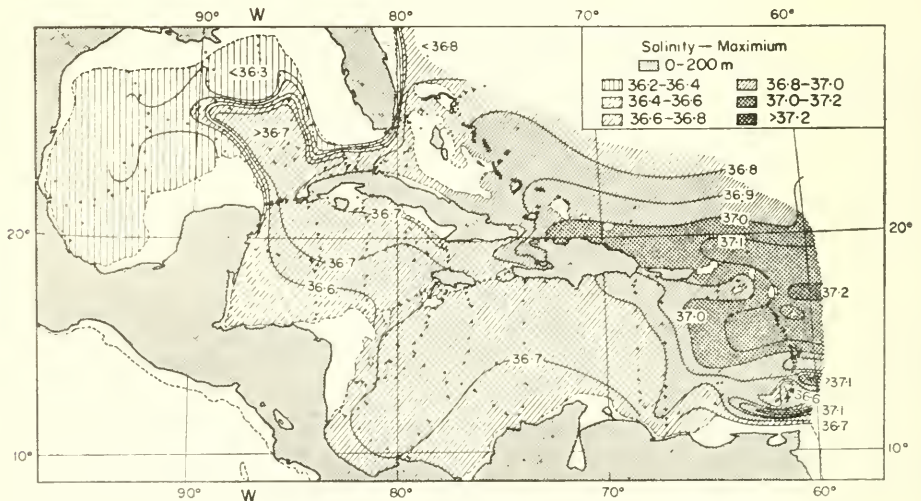


FIG. 280. Distribution of salinity in the core of the subtropical salinity maximum in the American Mediterranean (according to Dietrich).

currents during the spring. The large salinity differences which appear where the undercurrents of the Equatorial Current join off the Antilles soon disappear in the eastern Caribbean. There is a striking uniformity in the Caribbean and in the Yucatan Channel due to lateral mixing. The weak inflow through the Windward Passage (sill depth about 1600 m) makes little change. The differences in the Gulf of Mexico are larger. The extended areas with vortices in the north-eastern and the western parts of the Gulf which are very pronounced in the surface currents remain outside the circulation of the tropospheric layers. Investigation of $[T,S]$ -curves in the water masses of the South Equatorial Current, the Sargasso Sea and the Yucatan Channel allows to estimate how much of the inflow water through the Antilles takes part in the water passing through the Yucatan Channel. ISELIN (1936) found that of a total transport of about 26 million m^3/sec through the Yucatan channel approximately 6 million originates in the South Atlantic. For the deeper layers the effects of the inflow through the Windward Passage and the Virgin Passage are of greater importance (see Pt. I, p. 133). The uniformity of the distribution of the oceanographic factors over the area shows the effect of the mixing processes which are stronger here than the pure transport processes. Dynamic evaluation of the data for the latter should give greater information (PARR 1937*b*). Figure 281 gives the dynamic topography of the physical sea level relative to that of the 1200-decibar surface for the Caribbean and for the Cayman Sea. The mean current core running from the Antilles through the Yucatan Strait to the Florida Strait is clearly marked. The course of the dynamic isobaths shows that the water flows uphill to reach the Yucatan Channel (see also SVERDRUP, 1939). Similarly as in both the Equatorial Currents, the water transport here is also largely due to the air currents (prevailing wind to the east-north-east with a mean velocity of 10 m/sec). Thus to a very large extent these currents are also gradient currents in a baroclinic sea though they are subject to significant modification by the wind.

(b) The Gulf Stream and its Internal Structure

Although the Gulf Stream is the largest and the most important current of the Northern Hemisphere a more dynamic investigation of its course has only recently been started. The first current measurements in it were made by PILLSBURY in 1885-9 from the "Blake" which was anchored in very deep water. Further investigations were begun in 1914 by the oceanographic survey vessel "Bache" (BIGELOW, 1917, four transverse profiles through the Florida Current and the Antilles Current). More recently a systematic survey has been started by the oceanographic survey vessel "Atlantis" (Woods Hole Oceanographic Institution).

The first dynamical evaluation of some transverse profiles in the Florida Current was given by WÜST (1924) using the "Blake" measurements. This and subsequent work have afforded a more or less complete description of the vertical structure of this current from the Florida Strait to the Newfoundland Banks. Special mention should be made of the work of JACOBSEN (1929) on the Sargasso Sea using "Dana" observations and that of ISELIN (1936) giving a detailed review of the comprehensive results collected by "Atlantis". DIETRICH (1937*b*, see also WÜST, 1930*a*) has given a detailed analysis of numerous sections to show the process of formation and the dynamics of the Gulf Stream. The thermo-haline structure of the Gulf Stream is immediately apparent from the set of six success profiles given by WÜST (Figs. 282, 283). Profile I



FIG. 281. Dynamic topography of the physical sea surface (relative to that of the 1200 decibar surface) for the Caribbean Sea and the Cayman Sea. (Lines of equal dynamic anomaly drawn with an interval of 0.05 dyn m.)

is in the Yucatan Channel, profile II north of Cuba, profile XII at the narrowest part of the Florida Strait, profile IV at the exit from the Florida Strait just before the junction with the Antilles Current, profile V at Cape Hatteras and profile VI from the Newfoundland Banks in southward direction. The temperature profiles show that the Gulf Stream is by no means a deep-reaching current of high temperature. It differs only little in the thermal structure from the neighbouring Sargasso Sea. The steep oblique slope of the isothermals and isohalines is characteristic and the narrower the section the more rises the lower, cold and weakly saline water at the left-hand boundary. This baroclinic mass distribution is connected with the current velocity and direction and is more pronounced the stronger the flow. It is thus more prominent in the narrow sections to the south. Profile V shows the Gulf Stream beyond the junction of the Florida Current and the Antilles Current where it has its greatest vertical thickness, about 1000 m, and has the considerable core width of about 50–70 km. Its left-hand

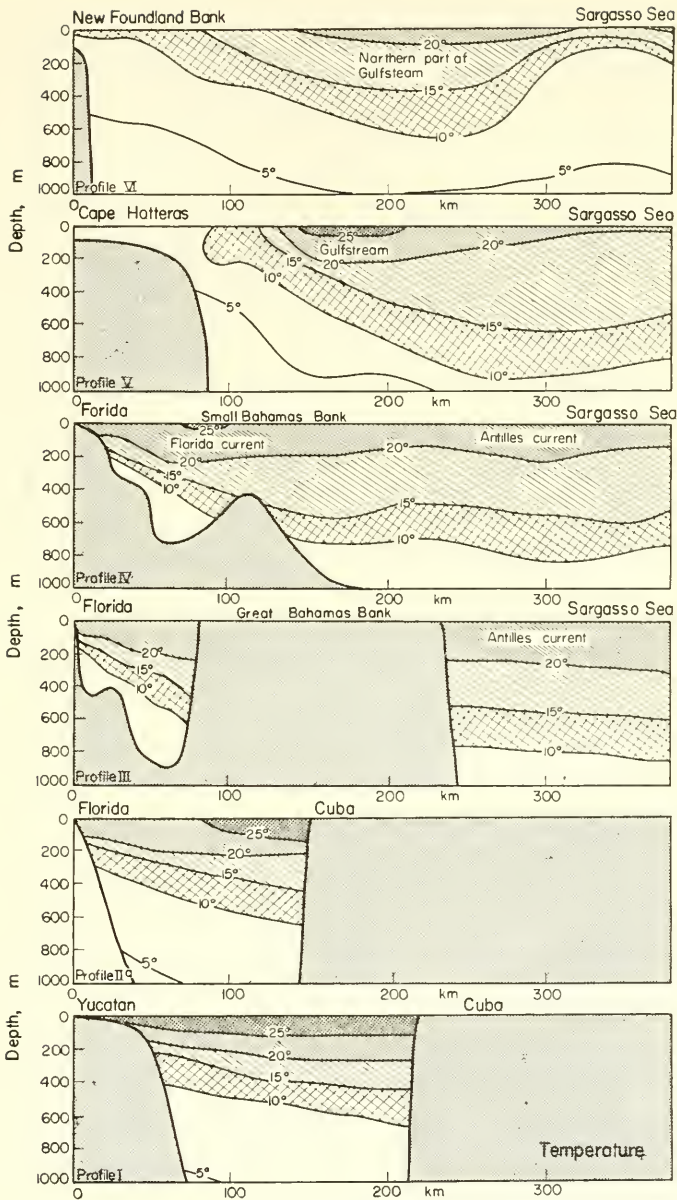


FIG. 282. Cross-section of temperature through the Gulf Stream (profiles I, IIa and V according to Jacobsen; profile VI according to Helland-Hansen; profile II and IV according to Wüst).

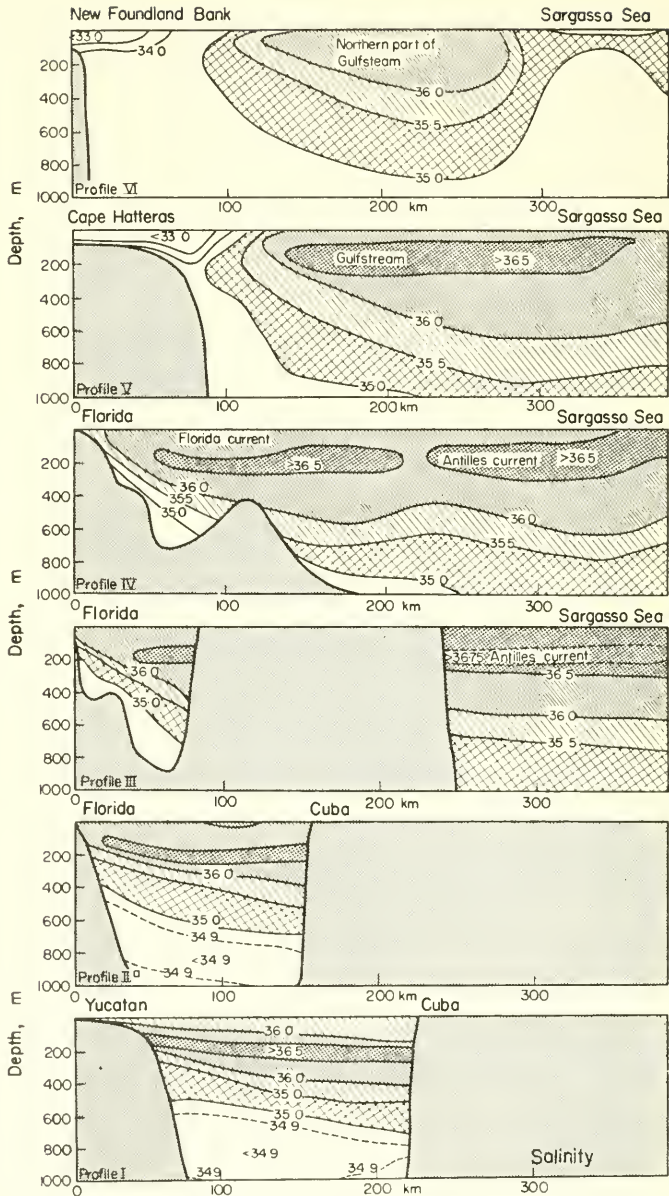


FIG. 283. Cross-section of salinity through the Gulf Stream (see remarks below Fig. 282).

edge is sharply defined and keeps about 100 km off the coast. The right-hand edge is diffuse and differs little from the water farther to the east. Where it swings eastward the current spreads out and loses thermal and haline thickness by mixing with colder surrounding waters. To the south of the Newfoundland Banks it begins to break up into a number of branches; profile VI shows only the northern branch which borders on the Labrador Current. The further branching of the current in the east has been discussed on p. 562, Fig. 257.

The Gulf Stream is only slightly more saline than the Sargasso Sea and in the deep layers there is no difference. The salinity maximum lies in the subtropical undercurrents which enter through the Antilles as part of the North and South Equatorial Currents into the American Mediterranean and from there across the Gulf of Mexico into the Florida Strait. It is thus a long-range effect of the tropospheric circulation of the tropical and subtropical Atlantic. The Antilles Current also shows this highly saline intermediate layer; but here it is in direct connection with the highly saline top layer of the Sargasso Sea. Further along the course of the Gulf Stream this salinity maximum comes at times up to the surface, but in the North Atlantic Current it dips beneath the weakly saline surface layers. It can be traced well into the Norwegian Sea (see pt. I, p. 171, Fig. 74). The salinity profile also shows another long-range effect of the Atlantic circulation: this is the last traces of the weakly saline subantarctic intermediate water which can still be seen at a depth of between 700 and 1000 m ($S < 34.9\text{‰}$) as far north as 25° N. in the Florida Strait; in the Sargasso Sea, however, it reaches only to 10° N.

The dynamics and the water transport of the Gulf Stream are derived primarily from velocity profiles. Several such profiles are available at the present time; they are based partly on direct-current measurements and partly on dynamic calculations from the mass field. The cross-section is not everywhere completely occupied by the current; particularly where the current flows out of the Florida Strait into the open ocean. The current flows as a jet through the narrow part of the strait and follows the direction imposed on it for a considerable distance. The velocity distribution in the cross-section is related to the mass field and the agreement between the calculated and observed current profiles is generally good. Beyond the junction of the Florida Current and the Antilles Current the weak counter current between them disappears completely, but the counter current on the right-hand side of the main one is retained. In the cross-section off Chesapeake Bay shown in Fig. 284 it lies just outside the profile.

A deeper insight into the dynamics of the current can be obtained from the absolute topography of the isobaric surfaces and of the physical sea level. These are particularly dependent on the choice of the reference-level. In the narrows of the Florida Strait this lies near the bottom where the velocity decreases almost to zero. Further north it lies in the Sargasso Sea at about 1900 m depth (corresponding to Fig. 272) and rises steeply from the right-hand side of the Gulf Stream to 1000 m depth or even less. Over the current core the physical sea level rises steeply from left to right and at Cape Hatteras this rise amounts to about 100 dyn cm. It remains more or less of the same order up to the Newfoundland Banks, but gradually spreads out horizontally so that the actual gradient falls to about a third. The right-hand side of the Gulf Stream is associated with a high-pressure ridge which can be traced from the Bahamas to the

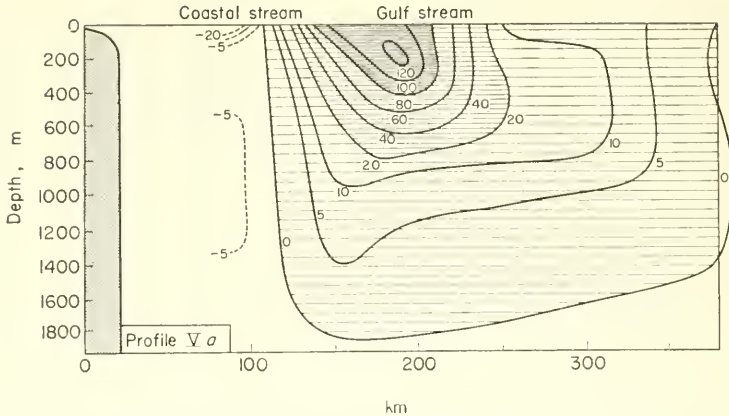


FIG. 284. Velocity profile (cm/sec) across the Gulf Stream off Chesapeake Bay, 20-22 April 1932.

south-west of the Newfoundland Banks. Eastwards from here there is a *counter current* steadily broadening to the south. The absolute topography of the 500 decibar surface still shows clearly the same pressure gradient as at the sea surface but it is rather weakened. The 800 decibar surface shows a rise across the current of at the most 20 dyn cm; and the pressure gradient has fallen to about a quarter. The 1400 decibar surface is almost plane and the lower limit of the current system must therefore lie between 1000 and 1200 m.

A detailed analysis of the origin and the transformations of the Gulf Stream water as it flows from the Florida Strait to the Newfoundland Banks were investigated by DIETRICH (1937) with the aid of distribution of oxygen content in numerous profiles. He was able to show that the water masses of the Florida Strait and of the Antilles Current to the north of the Lesser Antilles were made up partly of tropical South Atlantic water and partly of subtropical water from the western North Atlantic. The Gulf Stream water reaching Cape Hatteras has, however, undergone changes making it almost completely identical in its properties with the water of the western North Atlantic. This transformation was attributed by Dietrich to the transverse circulation and to mixing. From the distribution of the oceanographic factors such a transverse circulation seems not unlikely, but it is not possible to determine it from the pressure field because of the low velocity and probably also because of its variability.

The amounts of water and heat carried by the Gulf Stream are enormous. The Florida section shown in Fig. 284 gives a water transport of about 25 million m^3/sec . It can be assumed that this will also be the transport in the currents through the Caribbean and the Yucatan Channel, since the precipitation and the inflow of river water (run-off) are small compared with this very large quantity. Some idea of the enormous quantity of water involved is given by the estimate that it is twenty-two times as much as is carried by all the rivers of the earth together. The amount of water carried by the Gulf Stream further north is much larger than this and the transverse profile off Chesapeake Bay gives a transport three times greater (82 million m^3/sec). It can be assumed as a first approximation that the amount of water carried by the North

Equatorial Current, together with that carried by the Guiana Current and passing between the Lesser Antilles will be about the same as the total transport of the Gulf Stream through a cross-section off Cape Hatteras. From this it follows that the part of the Gulf Stream that passes through the Florida Strait makes up only about a third of the total transport. According to Wüst the Antilles Current carries 12 million m^3/sec and the Florida Current about 37 million m^3/sec . From here the current enters regions with larger depth and there occurs a rapid increase in the water transport because the current absorbs water masses with a temperature of less than $8^\circ C$ from the lower layers of the south-western Sargasso Sea. Further along to the north and north-east the Gulf Stream is subject to a velocity decrease and an increase in width, but the water transport remains nearly constant. However, it becomes more and more difficult to distinguish its limits from the surrounding sea. Iselin has attempted to divide up the Gulf Stream velocity profile at Chesapeake Bay (Fig. 284) into individual inflow components (Fig. 285). The area *A* contains water warmer than $20^\circ C$ and the

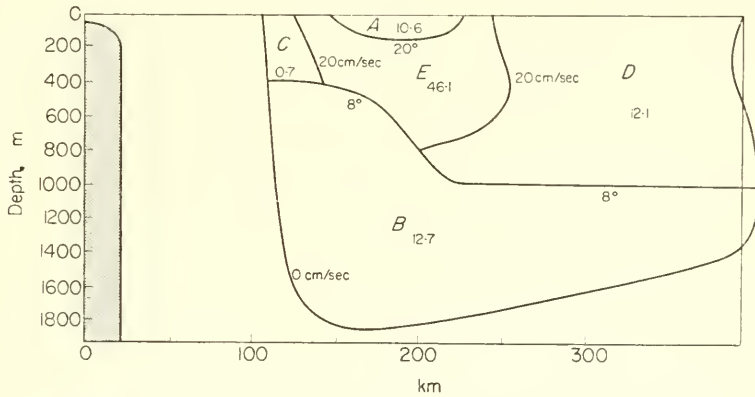


FIG. 285. Subdivisions of the velocity profile across the Gulf Stream off Chesapeake Bay, 20-22 April 1932. The figures give the transport (in mill. $m^3 sec^{-1}$) for the different parts of the current (according to Iselin).

velocity of this gives a transport of 10.6 million m^3/sec . The same layer in the Florida current according to the Wüst profile corresponds to 13.1 million m^3/sec and in the Antilles Current to 4 million m^3/sec . The sum of these two is greater but no more so than could be due to differences in the homogeneity of the material. The area *B* contains only water colder than $8^\circ C$, most of which was absorbed by the Gulf Stream in the section with a larger depth. According to the velocity profile this area corresponds to 12.7 million m^3/sec and only a very small part of it can possibly be assumed to have its origin in the Florida Strait. Water is also drawn into the main current along both edges by friction and mixing. If these areas in the profile are limited by the isoline of 20 cm/sec, these areas *C* and *D* will correspond to a transport of 0.7 and 12.1 million m^3/sec respectively. These figures indicate that water is drawn into the current on the right-hand side much more strongly than along the more sharply defined left-hand boundary. The remaining area *E* corresponds to 46.1 million m^3/sec . In the Wüst profile for the Florida Current and the Antilles Current this area corresponds to

about 26.4 million m^3/sec . The transport in the current core has thus grown to twice its magnitude in a distance of about 600 nautical miles. This very large increase from 26 to 83 million m^3/sec , where the current passes into a region with larger depth, can be attributed to three principal sources. The smallest of these is due to the Antilles Current which brings the total transport up to 37.1 million m^3/sec leaving 45 million to be accounted for from the other sources. This is supplied, on the one hand, by water drawn in from the south-western part of the Sargasso Sea and on the other hand, by water fed by the counter current coming from the area of the Newfoundland Banks and mixed with the Gulf Stream by means of numerous vortices. In this way Iselin derived the schematic outline of the main sources and of the course of the Gulf Stream shown in Fig. 286. Each line represents a water transport of about 12 million m^3/sec . This may seem somewhat schematic, however, it gives an instructive idea about the origin and composition of the water masses transported by the Gulf Stream.

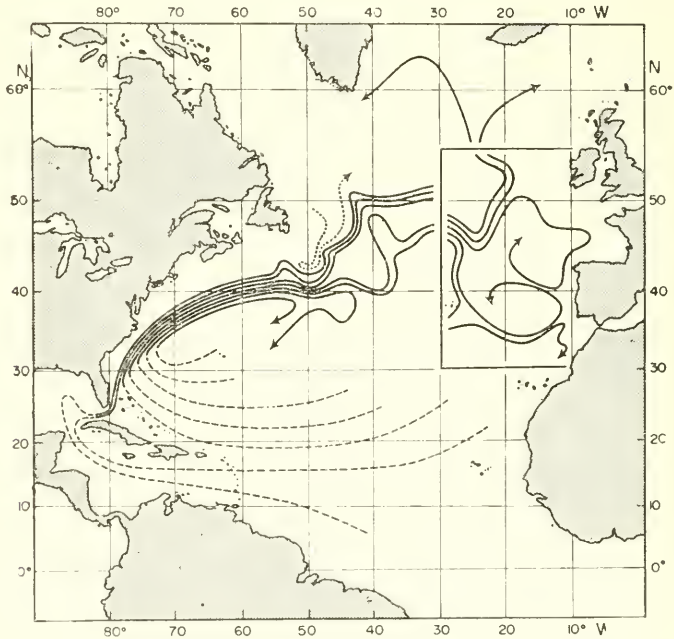


FIG. 286. Schematic representation of the main sources of the Gulf Stream waters (broken lines) and the pattern of the Gulf Stream system (continuous lines). In the western half of the ocean each stream line represents a water transport of approximately $12 \times 10^6 \text{ m}^3 \text{ sec}^{-1}$ (according to Iselin, 1935).

The systematic survey of the Gulf Stream between Montauk Point and the Bermudas carried out by the "Atlantis" from June 1937 (ISELIN, 1940) showed that the mass transport of the Gulf Stream varied between 93 and 76 million m^3/sec . There was a definite annual variation with two maxima in early summer and in winter and two minima in October–November and April–May. The differences in the sea-level across the current are closely related to these variations and can be deduced from them. This annual variation is probably due to variations in the intensity of the atmospheric

circulation over the southern part of the North Atlantic. In winter the strong anti-cyclonic circulation over the ocean increases the inflow into the Gulf Stream and in the summer there are more frequent southerly winds and a greater part of the water masses of the North Equatorial Current is blown directly into the Gulf Stream without passing through the Caribbean and the Florida Strait. Both of these effects intensify the Gulf Stream. It is not improbable that the aperiodic variations from year to year will provide an extremely good indicator of the variations in the intensity of the atmospheric circulation over the Atlantic.

The most recent investigations of the Gulf Stream have the main goal to obtain accurate detailed surveys of the current at short successive intervals, that is, to obtain *quasi-synoptic* surveys of an extended part of the current. Such methods of investigation need in the first place the rapid gain of the structure of the water masses down to great depths, while the survey vessel is under way whereby the position of each station has to be fixed with accuracy. Both of these conditions can be satisfied by the more recent methods used on board of the oceanographic survey vessels. Quasi-synoptic surveys of this type have been made for the Gulf Stream down to 275 m depth between Cape Hatteras and the Newfoundland Banks but at the present time only few of them exist. They give a very clear picture of the complicated course of the current and show particularly the very considerable local variations in form of meandering wave patterns of large amplitude at both sides of the current. Occasionally a water mass in one of the amplified troughs and ridges is cut off from the main current to form finally a large vortex which will be cyclonic on the southern side and anticyclonic on the northern side. These vortices are different from the smaller size eddies in the shearing zones of a turbulent current that also occur in the Gulf Stream (SPILHAUS, 1940). Furthermore, the synoptic surveys have shown that the current velocity in the core may be intensified up to about 4–5 knots over a relatively narrow band (about 10–15 miles wide) a little inside the left-hand boundary of the current; in the counter current the velocity reaches 3–4 knots. It is not surprising that the approximate and mean values obtained by the previous methods of investigation gave only low velocities.

The first multiple ship survey of the Gulf Stream area between Cape Hatteras and the Newfoundland Banks was made during 6–23 June 1950. Six oceanographic survey vessels took part in this “Operation Cabot” and they obtained an almost synoptic survey of the Gulf Stream down to 275 m which gave a clear picture of the complicated nature of the current. Figure 287 presents the course of the current as characterized by the mean temperature of the upper 200 m layer. According to this survey the Gulf Stream is a remarkably narrow band about 40–60 km wide and sharply separated at the edges from the surrounding water masses. The early view of Franklin of the Gulf Stream structure was confirmed, and certainly in the sector between Cape Hatteras and the Newfoundland Banks the Gulf Stream resembles a “river in the ocean” rather than a broad diffuse ocean current. The current does not, however, follow a straight line, but instead flows in *long waves* which are usually of small amplitude but take occasionally quite a large amplitude. Successive surveys have shown that these long lateral waves move slowly eastwards with increasing amplitude. Figure 288 shows the position of the Gulf Stream at the beginning (8 June) and the end of the operation (21 and 22 June). The current core therefore tends towards a *meandering* behaviour of a pronounced character. The amplitude of these meanders may increase so much

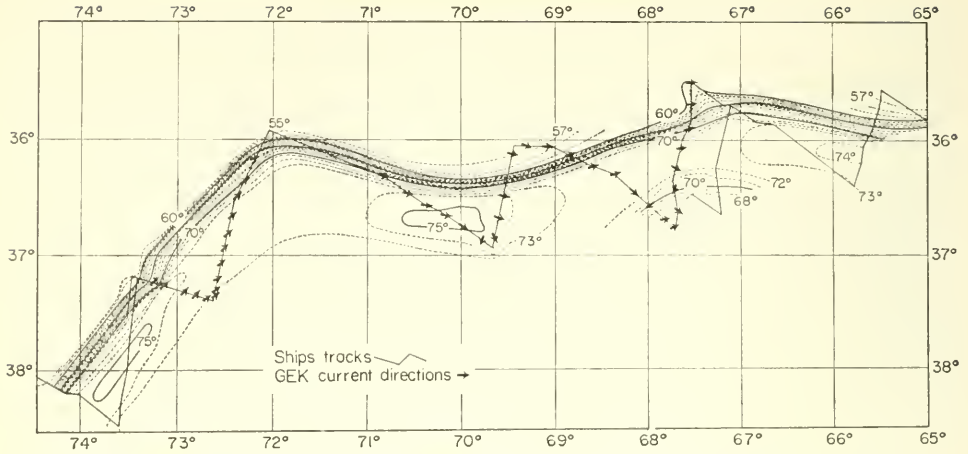


FIG. 287. Mean temperature ($^{\circ}$ F) in the upper 200 m layer of the Gulf Stream, 8 June 1950.

while moving eastwards that large sections of the current can be cut off. This process results in the ejection of a water mass from the current and the formation of large cyclonic vortices on the southern side of the main current. This cut-off process is similar to processes involved in polar jet phenomena in the upper atmosphere which are of major importance in the dynamics of these air currents. The process can be followed clearly in successive charts from 16 June to 21 June. On 17 June this process reaches its maximum stage (Fig. 289). The cyclonic vortex clearly stands out in the band of temperature concentration and in direct current recordings. It was at first a strong vortex but gradually weakened during the following days and finally vanished.

A further characteristic phenomenon is the break-up of the Gulf Stream into several separate branches. Usually there are three, sometimes separated by counter currents. Figure 290 shows the current velocity and temperature distribution usually found at the sea surface.

Consideration of these recent results shows that there are three principal questions on the internal dynamics of the Gulf Stream that require an answer.

(1) Why is the current asymmetrically developed and why is the current core displaced to the left-hand side (looking downstream)?

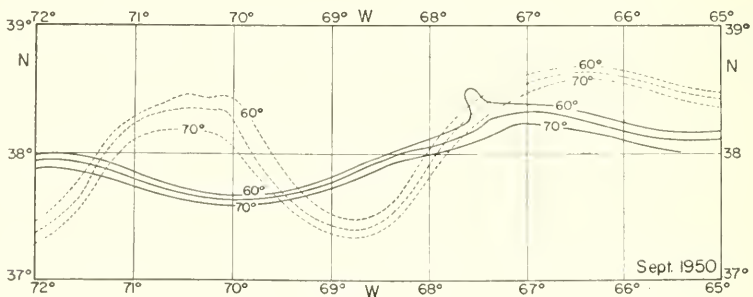


FIG. 288. Position of the Gulf Stream. Mean temperature ($^{\circ}$ F) of the upper 200 m layer for 8 June (full lines) and for 21 and 22 June 1950 (dashed lines).

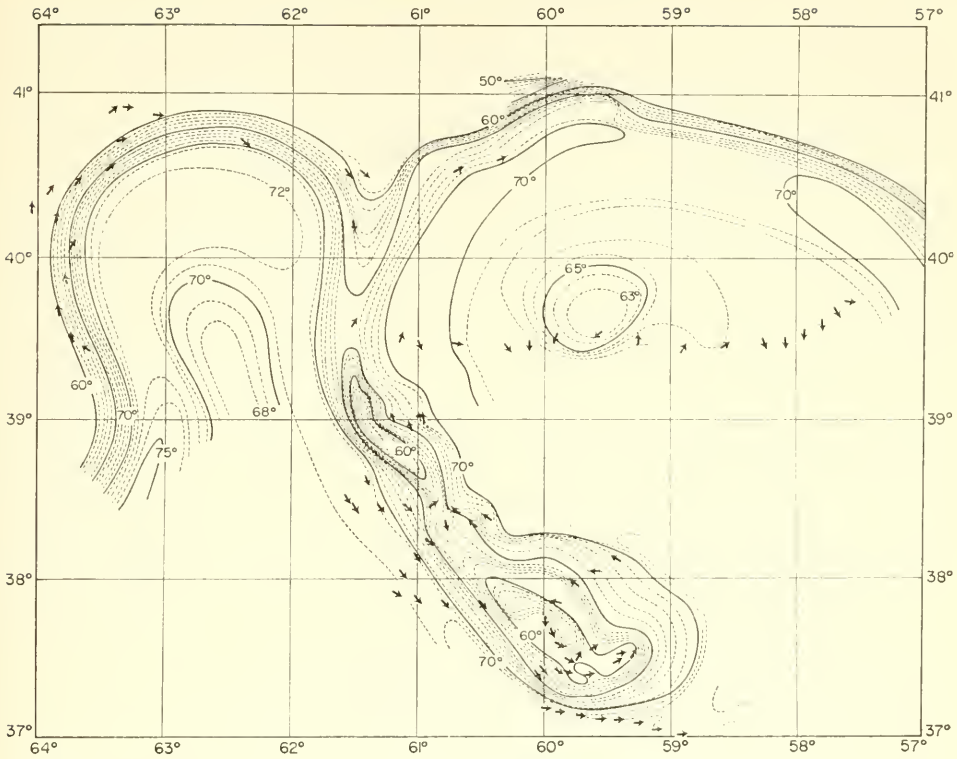


FIG. 289. Mean temperature ($^{\circ}\text{F}$) in the upper 200 m layer on 17 June 1950. Current direction from geomagnetic electrokinetograph (GEK) (according to Arx, 1950).

(2) Why does the Gulf Stream keep such a concentrated narrow form over a long distance sometimes taking on a meandering character? Why does it break up into several smaller branches separated by motionless bands or weak counter currents?

(3) Why is the total energy of the current concentrated in a relatively thin top layer and why does the current not penetrate down to the deeper layers when it flows out over regions with larger depth?

Research on these questions is in progress but more fundamental results have been obtained only for some individual questions. It appears that these strong oceanic boundary currents are analogous in many respects to the "jet streams" of the strong westerlies in the upper atmosphere and are especially characteristic for the dynamics of free jets.

(c) *To the Dynamics of the Gulf Stream*

ROSSBY (1936, 1937, 1938) in a series of papers has advanced some new ideas on the theory of ocean currents which are of some interest. These arguments have been applied primarily to the Gulf Stream System between the Florida Strait and the area south of Newfoundland. But their use is not limited to these currents and in many respects they can also be applied to all boundary currents flowing parallel to a coast

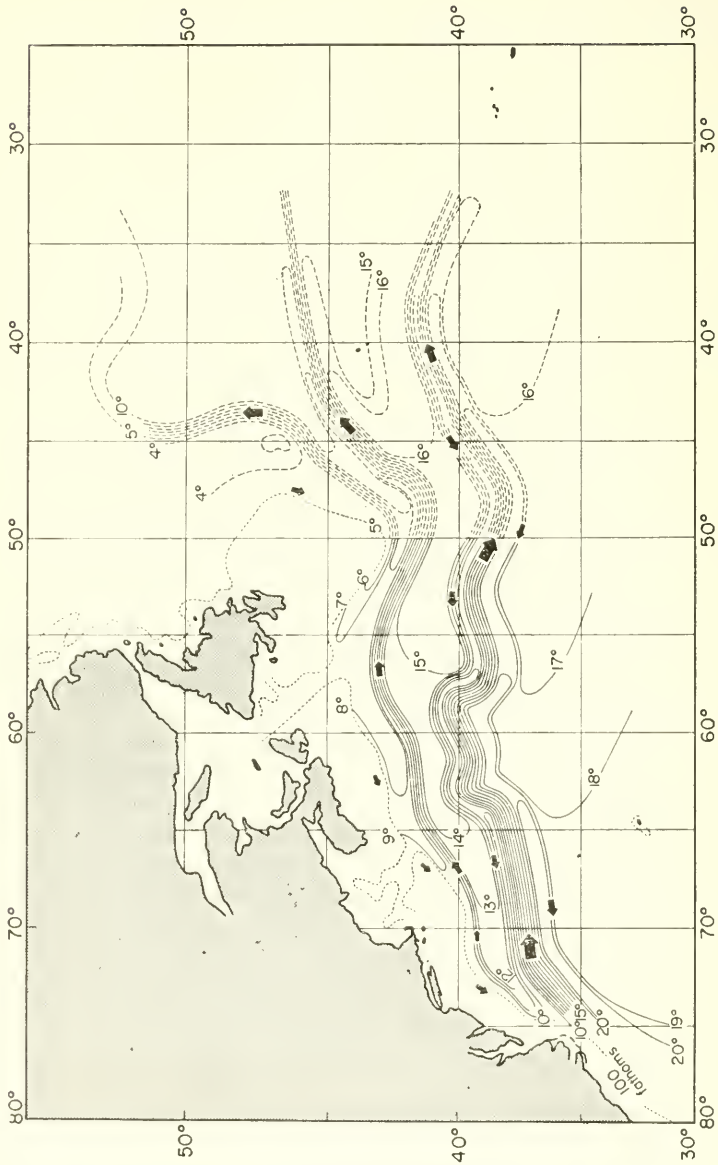


FIG. 290. Schematic chart of temperature ($^{\circ}\text{C}$) at a depth of 200 m in the Gulf Stream region.

(Kuroshio, Peru Current) and others. ROSSBY'S theoretical investigations are put forward mainly along two lines. The first deals besides the vertical also with the lateral frictional effect which is of influence on the horizontal velocity profile in currents. The second deals with currents of constant momentum (impulse) transport and in particular applies the theory of free jets to ocean currents. Since the exchange coefficients of lateral mixing are of considerably greater magnitude than those for vertical exchange (see Pt. I, p. 103 *et seq.*) Rossby considered it absolutely necessary to account for frictional forces due to lateral mixing and put strong emphasis on these forces. The usual equilibrium conditions in a geostrophic current for mass elements along a vertical line primarily determine—as always—the vertical velocity distribution. By introduction of the lateral shearing forces this condition will not be changed in any great extent, but the lateral shear imposes a definite transverse velocity profile to which little attention has been paid in the past.

A linear current in the positive y -direction with a mean velocity \bar{v} will be fixed by the geostrophic equilibrium between the pressure gradient $-(1/\rho)(\partial p/\partial x)$ and the Coriolis term $-fv$. As a result of the horizontal turbulence, however, the individual mass elements will have a movement at right angles to the mean direction of the current and the equations of motion (XIII.1), will apply for its horizontal components u and v . If the deviations of u and v from the mean velocities $\bar{u} = 0$ and \bar{v} are denoted by u' and v' then:

$$\frac{dv'}{dt} = -fu' \quad \text{and} \quad \frac{du'}{dt} = fv' \quad \text{with} \quad -\frac{1}{\rho} \frac{\partial p}{\partial x} - f\bar{v} = 0. \quad (\text{XIX.6})$$

From (X.39) the lateral shearing stress is

$$\tau = -\rho \overline{u'v'}. \quad (\text{XIX.7})$$

Introducing the Prandtl mixing length l of lateral mixing (p. 388) allows (XIX.7) to be rewritten as

$$\tau = \rho l \bar{u}' \left(f + \frac{\partial \bar{v}}{\partial x} \right). \quad (\text{XIX.8})$$

For a uniform horizontal current the lateral shearing stress will not approximate to zero except when

$$\frac{\partial v}{\partial x} = -f. \quad (\text{XIX.9})$$

Under stationary conditions the lateral mixing imposes a definite horizontal velocity profile, and indeed there must be a velocity decrease towards the right-hand edge of the current (Northern Hemisphere). This is quite large and in middle latitudes (43°) amounts to 1 cm/sec in 100 m.*

Since such large transverse variations in velocity are hard to observe it must be presumed that the right-hand edge of the current always tends to accelerate the left-hand side even when the right-hand side has a lower velocity. This effect ceases only when the condition (XIX.9) is satisfied.

* Against this conclusion the objection has been raised by PRIESCH (1943), that besides the lateral turbulence across the gradient current, also that in the direction of the current should be taken into account. If this is done, it is found that the effect of the earth's rotation mentioned above no longer exists. On the average the effects in the two directions balance exactly.

The second part of Rossby's arguments concerns the problem of a straight accelerated turbulent current. In such a current the horizontal pressure gradient will not be equal to that corresponding to the *mean* basic current and not balance completely the Coriolis force in stationary equilibrium. This gradient of the stationary current was termed the *Coriolis pressure gradient* by Rossby and for this the following relations apply

$$-\frac{\partial p_c}{\partial x} = -\rho f v \quad \text{and} \quad -\frac{\partial p_c}{\partial y} = +\rho f u. \quad (\text{XIX.10})$$

A numerical value can always be found for given u and v . The turbulent accelerated motion, however, will be subject to other equations:

$$\rho \frac{du}{dt} = \rho f v - \frac{\partial p}{\partial x} + \frac{\partial \tau_{xy}}{\partial y} \quad (\text{XIX.11})$$

and

$$\rho \frac{dv}{dt} = -\rho f u - \frac{\partial p}{\partial y} + \frac{\partial \tau_{yx}}{\partial x},$$

where τ_{xy} and τ_{yx} are the x - and y -components of the lateral shearing stress. Introducing $p = p_c + p_r$ then by means of (XIX.10)

$$\rho \frac{du}{dt} = -\frac{\partial p_r}{\partial x} + \frac{\partial \tau_{xy}}{\partial y} \quad (\text{XIX.12})$$

and

$$\rho \frac{dv}{dt} = -\frac{\partial p_r}{\partial y} + \frac{\partial \tau_{yx}}{\partial x}.$$

The movements which correspond to these equations occur under influence of "residual pressure gradients" p_r as though the earth was not rotating. The continuity equation

$$\frac{\partial u}{\partial x} + \frac{\partial v}{\partial y} = 0 \quad (\text{XIX.13})$$

fixes the current field u, v , while (XIX.10) gives the Coriolis pressure gradient and the corresponding mass field. Since p_c is usually considerably greater than p_r it is clear that the general pressure distribution is of secondary importance in considering accelerated currents. The mass field which is determined by the mean steady current field gives no information on the cause of the currents. However, according to Rossby p_r should, dynamically, be more important than p_c .

Against these considerations DEFANT (1937) and EKMAN (1939) have raised doubts affecting more particularly the practical usefulness of the above equations. But nothing can be said generally against the main lines of the basic argument if one remains in agreement with actual conditions.

For an application of the above equations to Gulf Stream problems Rossby took into account the phenomena that occur when the flow of a medium takes the form of a jet. The theory of *free jets* (PRANDTL, 1926) has been further developed by TOLLIEN, 1926; FORTHMAN, 1934; RUDEN, 1933. For a steady state ($\partial u/\partial t = 0$) in a laterally restricted current the first of the equations (XIX.12) together with the continuity equation (XIX.13) gives

$$\int \rho u^2 dy = \text{constant}, \quad (\text{XIX.14})$$

that is, in a current of this type the *momentum (impulse) transport through a current cross-section is constant*. Neglecting $\partial p_r / \partial x$ (which is permissible) and introducing the shearing given by

$$\tau_{xy} = \rho l^2 \left(\frac{\partial u}{\partial y} \right)^2$$

according to equation (XII.15), then for a mixing length $l = cx$ (proportional to the distance travelled) a complete solution can be found that fixes the horizontal current profile in the free jet. The very good agreement between theory and experimental results for the current profile in a free jet, is a consequence of the assumption made for the mixing length which is completely valid only for limited dimensions. Whether it is also applicable for the very large dimensions of ocean currents is questionable.

One consequence of the assumption is also that in a free jet with constant momentum transport the mass transport increases *downstream*, and is in fact proportional to the square root of the distance travelled. Due to the incorporation of surrounding water the current cross-section will increase downstream while the mean velocity will decrease. Since the energy remains the same, the mass transport will increase. Conditions are somewhat different if the inflow through the initial cross-section does not start from a point source but has a finite width. The velocity profile in Fig. 291 is

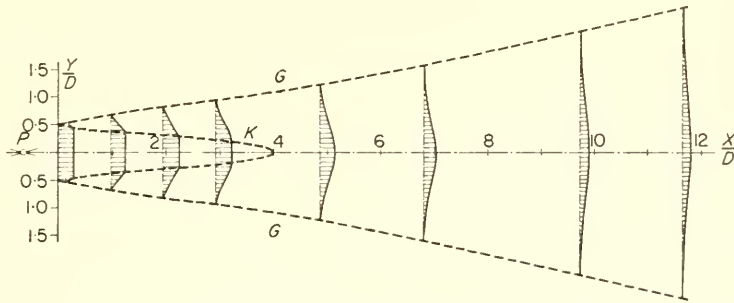


FIG. 291. Velocity distributions in a jet (Freistrahle, according to Ruden). D , nozzle diameter, all lengths are given as multiples of D .

based on experimental values for the velocity at different distances from the outlet of a nozzle through which there is a constant inflow. In a free jet there is a core in which the initial velocity and the other properties of the medium remain unchanged for a relatively long distance from the nozzle. The formation of a core region and a surrounding one of mixing are characteristic of the phenomena occurring in the ocean under similar conditions.

These results apply in the absence of rotation. According to Rossby, the principal effect of earth rotation is the formation of a different mass distribution (according to (XIX.10)) corresponding to the Coriolis pressure force; the velocity profile, however, will not be disturbed further by it. The stationary properties of the current, that is that the stream lines, isobars and contours of the physical sea level coincide, remain more or less unchanged. The deviations from a geostrophic current occurring in the interior of the free jet that are produced by the shearing stress, will be accentuated by the deviations due to inertia. There will thus be an overall dynamic equilibrium. According

to this concept it is the residual pressure field even though it is weak that provides the driving forces. This is the basic idea of the Rossby theory. It is undoubtedly attractive but whether it actually corresponds to reality is impossible to say. In any case it deserves considerable attention.

The further phenomena that occur when the medium in which the free jet is formed, is stratified, can be fairly readily dealt with. If there are two layers in the medium the velocity of the upper layer will affect the sea surface slope and also the position of the internal boundary surface between the two water masses. The sea surface slope and the internal boundary slope are given by equations (XIV.6 and 7) (p. 455). If the lower layer is assumed to be motionless then the velocity of the free jet gives the mass distribution in a transverse section. This is shown schematically in Fig. 292. In the current the

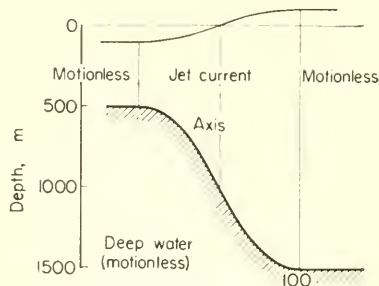


FIG. 292. Cross-section through a jet (Freistrah) current in a two-layered ocean.

boundary surface will slope downwards, in the Northern Hemisphere from left to right, and the thickness of the free jet will therefore vary across the current. The total mass transport through a cross section will be

$$M = \int \rho u (D_0 + \zeta_1 + \zeta_2) dy, \quad (\text{XIX.15})$$

where D_0 is the mean thickness of the top layer and ζ_1 and ζ_2 are the deviations of the physical sea level and the boundary surface from their positions when the system is at rest. Evaluation of this integral gives the result that the difference, $D_{\text{right}} - D_{\text{left}}$ between the two sides of the current must increase *downstream* as long as the mass transport increases. This has several effects on the course of the current. The inflow of water from the surroundings into the free jet will be asymmetric because of the asymmetry of the system. On the left there will be only a shallow water layer available, but on the right the water can be drawn in from greater depths. Under steady conditions the transverse velocity must therefore be greater on the left-hand side than on the right.

The surrounding water masses can be assumed to be stationary, but this state can hardly be expected to persist under the given conditions. At some distance from the current boundary the thickness of the layer D in the motionless water will be somewhat greater than D_{left} and D_{right} at the left- and right-hand edges. On the way from motionless water towards the boundary and into the interior of the free jet the water columns drawn into the current will undergo deformations, which will be associated with *hydrodynamic vortex formation* at the current boundary. The theoretical form for a cross-section through a free jet of this type is that shown in Fig. 293. This requires

a counter current at the left-hand edge of the free jet and a current in the direction of the main current at the right-hand edge. Due to the increased sea level difference between the right- and left-hand sides, the counter current on the left-hand side will increase in strength downstream, while on the contrary the other current will become weaker on the right-hand side until it finally vanishes. The effect of the free jet and the counter current must thus increase steadily downstream and therefore tend towards impossible unstable conditions. The effect of the vortex formation will give rise to a water movement through the main body of the current from right to left, and since the left-hand

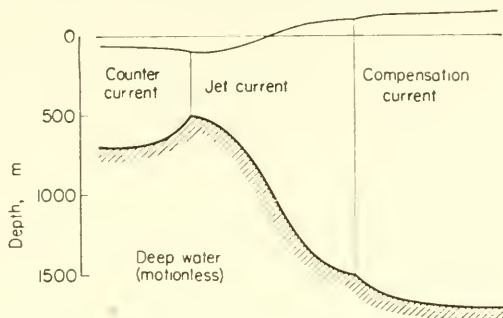


FIG. 293. Cross-section through a jet (Freistrah) current in a two-layered ocean with a full development of a counter current and compensation current in the adjacent water masses (according to Rossby).

edge and the counter current are shallow there must also be a transverse current in the lower part of the top layer in the opposite direction in order to compensate the upper transport. This gives a *cross-circulation* as was assumed by Dietrich. In addition to his earlier work, the processes occurring at the edges of a jet-form current penetrating a motionless water body have been discussed in two later papers by Rossby (1937, 1938). Thereby, he assumed that the initiation of the current from a state of rest was due to a wind field whose action was restricted to a band-like oceanic region. Particular attention was paid on the one hand to processes at the edges of the current, on the other hand to oscillatory processes which occur while the current tends towards a steady state. In such cases *counter currents* are formed on both sides of the basic current; in homogeneous water they are broad and slow, but in a two-layered sea narrow and intense. The zones between the basic current and the counter current are dynamically unstable and show a tendency to break up into large horizontal vortices. The depth to which a surface disturbance may penetrate into the lower layer down to the sea bottom, and the time required for the restoration of stationary conditions, are of particular interest and are especially important in dynamic oceanography (see Chap. XXI. 4).

Without question the theory has applications to the Gulf Stream between the Florida Strait and the Newfoundland Banks, and several theoretical consequences are undoubtedly realized in the actual behaviour of the Gulf Stream. The criticism on this theory expressed by Ekman is concerned not so much with the theoretical fundamentals, but more with the question of the extent to which the Gulf Stream actually keeps the character of a free jet and contains the energy (momentum of motion) required by the

theory. By means of approximate calculations he was able to demonstrate that the current leaving the Florida Strait will probably have a kinetic energy, so that already half of this energy would be able to carry the water against frictional resistances of various types exactly as far as a wind of 3 to 4 Beaufort could do blowing from the Florida Strait until Cape Hatteras in the current direction. Over this section of the current the theory should be able to make the most important characteristics of the Gulf Stream understandable. However, for the section of the current from 60° to 20° W conditions appear to be rather different, and in this section the initial velocity of the water seems to be only of minor significance. Ekman therefore came to the conclusion that for most of the ocean currents the theory is of limited usefulness only and can be applied solely to very fast currents (such as the Florida Current and its immediate continuation, see also, THORADE, 1938). The Rossby theory, due to its consequent and careful style, had a very stimulating effect and has led to a better understanding of a number of phenomena displayed by the Gulf Stream between Cape Hatteras and the Newfoundland Banks.

A satisfactory theory of the Gulf Stream must take into account a further important fact that has already been referred to by DIETRICH (1937*a*). Determination of the mean sea level along the North American coast from Florida in the south to Nova Scotia in the north by means of precise trigonometric measurements has shown that the sea level rises along this total route to the north with a mean slope of 13 cm in 1000 km. The strongest slope occurs just north of Cape Hatteras (see Table 152 according to ANVERS, 1927 and RAPPLEYE, 1932).

The Gulf Stream thus shows an *upward* motion along this section like the Caribbean Current where according to Parr and Sverdrup (p. 607) there is a slope of about the same magnitude. However, as it was shown by Dietrich, that the Gulf Stream in contrast to the Caribbean Current does not show this slope when the physical sea level

Table 152. Average Mean Water Along the North American East Coast.

(Zero point relative to Florida-Georgia)

Location	Mean water			Distance along the coast (km)	Rise in cm per 1000 km
	Anvers	Rappleye	Average		
St Augustine, Fla. Fernandina, Fla. Brunswick, Ga. }	0	0	0	0	6
Norfolk, Va.	4	7	6	1000	
Cape May, N.J. Atlantic City, N.J. Fort Hamilton, N.J. }	16	24	20	1400	35 13
Boston, Mass. Portland, Me. }	25	30	28	2000	12
Halifax, Nova Scotia	—	35	35	2600	

topography is calculated from the mass distribution along the continental slope. Dietrich took the oxygen minimum layer as reference-level but recalculation for a

deeper reference level changes the results very little. There is thus a contradiction between the "geodetic" and the "oceanographic" levelling which requires explanation. A plausible explanation was indicated by SVERDRUP (and co-workers 1946, p. 578) based on the following assumptions.

(1) That the geodetically determined gradient of the sea level is actually present in the coastal waters just off the coast and that corresponding to this there is a coastal current flowing southwards.

(2) That in the neighbouring waters the physical sea level slopes down seawards until the left-hand edge of the Gulf Stream which causes a current to flow southward due to the piling up of water. This gradient current would be one part of the large *elongated vortex* on the left-hand side of the Gulf Stream while the second part flows along the left-hand edge of the main current and in the same direction.

(3) Corresponding to this current and the adjoining Gulf Stream, the physical sea level rises steeply seaward from the coast (p. 607). The depression showing the deepest water level thus would follow the continental slope rather closely so that the southward flowing branch of the vortex lies over the shelf. The topography in a transverse section across the Gulf Stream thus has some similarity with that shown in Fig. 203

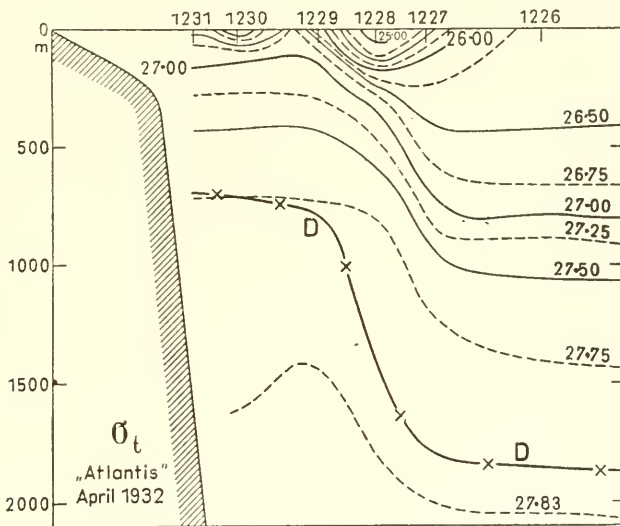


FIG. 294. Density distribution (σ_t) and position of the lower limit d of the current system in a cross-section through the Gulf Stream. "Atlantis", April 1932 (Chesapeake Bay, Bermuda).

(p. 460) south of the Newfoundland Banks where on the other side of the depression in sea level the Labrador Current flows eastward. According to the Rossby theory the elongated vortex between the Gulf Stream and the continental slope is a dynamic necessity. The Gulf Stream now would flow downhill in accordance with its mass structure and the surface slope would be directed southwards only at the coast. This piling up of water over the continental shelf was regarded by Sverdrup as due to the prevailing wind over the North Atlantic. The south-west wind over the northern part of this ocean maintains a high water level along its northern borders and maintains

in this way a decline of the physical sea level along the eastern and western sides. This would be the geodetically determined rise between Florida and Nova Scotia.

All cross-sections through the Gulf Stream show a strong stratification in the upper layers but beneath this where the current is weak it is less pronounced. It is to be expected that there will be a layer of no motion just beneath this layer. Figure 294 given by NEUMANN (1956) shows the position of the zero level d in an "Atlantic" cross-section through the Gulf Stream. The latter one indicates clearly the form given in Fig. 292 with shallow depth along the left-hand edge of the current, a strong downward slope below the maximum transverse density change and uniform larger values at the right-hand edge. This distribution is characteristic of all sections through free jet currents in the ocean. Neumann has also shown that over the whole of the moving layer from the surface down to the depth of no motion d there are only slight changes in the mean density distribution. There exists thus in a first approximation no transverse density gradient. This means that the entire current system is an equivalent to that of a two-layered model in which there are two water bodies, one on top of the other with an internal boundary surface between. Thus as a first approximation the Gulf Stream can be regarded as an equivalent-barotropic system in which the boundary layer slopes downward from the left-hand to the right-hand edge. Figure 295 shows the

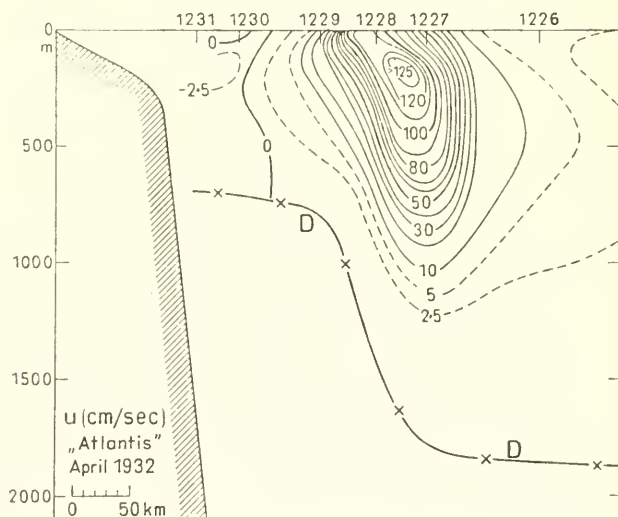


FIG. 295. Velocity distribution in the "Atlantis", section Chesapeake Bay-Bermuda, April 1932 (d , lower limit of the current system).

velocity distribution calculated from the mass field (Fig. 295) for a cross-section at the lower limit of the current system d . For the vertical shear under equivalent-barotropic conditions as a first approximation one obtains

$$\frac{\partial v}{\partial z} = - \frac{g}{f \bar{\rho}} \frac{\partial \rho}{\partial x}, \quad (\text{XIX.16})$$

where $\bar{\rho}$ is the mean density of the current layer. If as on p. 608 ζ denotes the surface

of the physical sea level and $-d$ and ρ_{-d} are the depth and the corresponding density of the layer of no motion, then from (XIX.16) when $u_{-d} = 0$ and

$$\bar{\rho} = \frac{1}{\zeta + d} \int_{-d}^{\zeta} \rho \, dz$$

it follows

$$v_{\zeta} = -\frac{g}{f} \left[\frac{\bar{\rho} - \rho_{-d}}{\bar{\rho}} \frac{\partial d}{\partial x} + \frac{d}{\bar{\rho}} \frac{\partial \bar{\rho}}{\partial x} \right]. \tag{XIX.17}$$

If $\partial \bar{\rho} / \partial x$ is exactly zero then

$$v_{\zeta} = -\frac{g}{f} \frac{\bar{\rho} - \rho_{-d}}{\bar{\rho}} \frac{\partial d}{\partial x} \tag{XIX.18}$$

which corresponds to a strictly equivalent-barotropic field where the boundary surface lies at a depth $-d$ and the current layer has a density $\bar{\rho}$ while the motionless layer beneath has a density ρ_{-d} . Since in the transverse section through the Gulf Stream $\partial \bar{\rho} / \partial x$ is very small, the effect of the first term in (XIX.17) will predominate and the actual distribution will approximate closely that of an equivalent-barotropic model.

A model of this type has been worked out by CHARNEY (1955). Earlier investigations by STOMMEL (1953) and CHARNEY (1955) have clarified the question how a boundary current possibly might be influenced by a consideration of the inertial terms in the total equations of motion and by stratification of the water masses.

This model assumes the y -axis along the edge of the continental shelf with the x -axis at right angles; with a slight approximation it can be assumed that the y -axis points northward and the x -axis eastward. Ignoring the unimportant kinematic effects of the earth's curvature it follows from the theorem of the constance of potential vorticity (p. 336) that for a steady current in a water layer h above a motionless lower layer

$$u \frac{\partial}{\partial x} \left(\frac{\zeta + f}{h} \right) + v \frac{\partial}{\partial y} \left(\frac{\zeta + f}{h} \right) = 0 \tag{XIX.19}$$

Introducing from the equation of continuity the volume transport stream function ψ which is defined by

$$hu = -\frac{\partial \psi}{\partial y}, \quad hv = \frac{\partial \psi}{\partial x} \tag{XIX.20}$$

allows (XIX.19) to be rewritten in the form

$$\frac{1}{h} \left[\frac{\partial}{\partial x} \left(\frac{1}{h} \frac{\partial \psi}{\partial x} \right) + \frac{\partial}{\partial y} \left(\frac{1}{h} \frac{\partial \psi}{\partial y} \right) + f \right] = F(\psi) \tag{XIX.21}$$

where F is a function of ψ to be determined. A second equation relating ψ and h is the Bernoulli-equation. This gives

$$\frac{1}{2} \left[\left(\frac{1}{h} \frac{\partial \psi}{\partial x} \right)^2 + \left(\frac{1}{h} \frac{\partial \psi}{\partial y} \right)^2 \right] + g^* h = G(\psi), \tag{XIX.22}$$

where $g^* = (\rho_h - \rho) / \rho_h \cdot g$ and ρ_h is the density of the lower motionless layer and ρ is the density of the upper moving layer. $G(\psi)$ is another function of ψ , which has to be determined.

Taking into account the magnitude of the different terms in the equations (XIX.21) and (XIX.22) these can be written simply as

$$\frac{1}{\bar{h}} \left(\frac{\partial v}{\partial x} + f \right) = F(\psi), \quad (\text{XIX.23})$$

$$\frac{v^2}{2} + g^*h + G(\psi), \quad (\text{XIX.24})$$

where v is given by the second equation of (XIX.20). The determination of the functions F and G is laborious and requires the use of the outer (seaward) boundary condition. Denoting quantities at this boundary by a bar, it follows from (XIX.23) and (XIX.24), since at the boundary ($x = \infty$) both v and $\partial v / \partial \rho$ are zero, that

$$f / \bar{h} = F(\bar{\psi}) \quad \text{and} \quad g^* \bar{h} = G(\bar{\psi}). \quad (\text{XIX.25})$$

For $x = \infty$, $\bar{\psi}$ and \bar{h} are functions of y and also \bar{h} is a function of $\bar{\psi}$, that is, F and G are then also functions of $\bar{\psi}$ and y .

Since F and G are in principle to determinate for $x = \infty$ they must also be determinable at every point in the interior region connected with the outer boundary by a stream line. It is therefore possible to determine $F(\psi)$ and $G(\psi)$ at all interior points. The function $\bar{\psi}$ is taken as a parabolic function of y which is made plausible by the observations at the eastern edge of the Gulf Stream.

$$\bar{\psi} = \bar{\psi}_0 - \gamma(y - y_0)^2. \quad (\text{XIX.26})$$

With sufficient accuracy f can be taken as a linear function of y

$$f = f_0 + \beta(y - y_0) \quad (\text{XIX.27})$$

which gives finally after some calculation

$$\left. \begin{aligned} G'(\psi) &= g^* \left[\bar{h}_0^2 - \frac{2f}{g^*} (\bar{\psi}_0 - \psi) + \frac{4\beta}{3g^* \sqrt{\gamma}} (\bar{\psi}_0 - \psi)^{3/2} \right]^{1/2} \\ \text{and} \quad \frac{dG}{d\psi} &= F \end{aligned} \right\} (\text{XIX.28})$$

which is valid for all values of y and ψ .

The equation (XIX.23) and (XIX.24) then give the final equation

$$\frac{\partial \psi}{\partial h} - \frac{f}{g^* h} - \frac{1}{g^*} \left(\frac{\partial G}{\partial \psi} - F \right) = 0. \quad (\text{XIX.29})$$

Its solution, subject to the boundary conditions $h = \bar{h}(y)$ and $\psi = \bar{\psi}(y)$ is

$$h^2 = \bar{h}^2 + \frac{2f}{g^*} (\psi - \bar{\psi}). \quad (\text{XIX.30})$$

The velocity v is obtained as a function of ψ and y from the equation (XIX.24) and the values of x corresponding to ψ and y are given by the equation

$$dx = \frac{d\psi}{hv} \quad (\text{XIX.31})$$

which only requires a numerical quadrature; the boundary condition here is $\psi = 0$ at $x = 0$.

The application of this theory put forward by Charney starts with the determination of the two constants in equation (XIX.26). Taking $\psi = 0$ at the coast, then $\bar{\psi}$ is the volume transport of the current. The zero point for y is midway between the Florida Strait and Cape Hatteras ($y = y_0$), that is, 700 km from both sides. The calculated geostrophic transport in the Florida Strait is approximately $30 \times 10^6 \text{ m}^3 \text{ sec}^{-1}$ and the increase from here to Cape Hatteras is approximately $50 \times 10^6 \text{ m}^3 \text{ sec}^{-1}$.

Hence $\bar{\psi}_0 = 80 \times 10^6 \text{ m}^3 \text{ sec}^{-1}$ and γ has the value $2.55 \times 10^{-5} \text{ msec}^{-1}$. Furthermore, in (XIX.27), $f_0 = 0.84 \times 10^{-6} \text{ sec}^{-1}$ and $\beta = 1.8 \times 10^{-11} \text{ m}^{-1} \text{ sec}^{-1}$.

If we postulate that $h = 0$ when $x = 0$, $y = y_0$ and $\psi = 0$, then substituting these values in equation (XIX.30) gives

$$\bar{h}_0 = \left(\frac{2f}{g^*} \bar{\psi}_0 \right)^{1/2} = 820 \text{ m} \tag{XIX.32}$$

which compares well with the observed mean value of 900 m given by ISELIN (1936).

The results of the integrations are shown in Fig. 296. This gives in perspective the calculated position of the boundary surface h by contours of h (full lines) at 100 m intervals and on this surface the stream lines (broken lines) of the volume transport for each 10 million $\text{m}^3 \text{ sec}^{-1}$. On top are given calculated velocity profiles for several cross-sections through the Gulf Stream. Comparison of the position of the internal boundary surface with the observed mean depth of the 10° C isotherm, which gives approximately the lower limit of the Gulf Stream, shows that they are in excellent agreement. The characteristic way in which the current swings away from the coast in the northern part of the region considered can also be seen. This takes place away from any projection of the coast line and is found both in the Gulf Stream and in the Kuroshio. The current profile shows towards higher latitudes an increasing concentration of the current energy towards the left-hand edge (westward intensification). The velocities along the left-hand edge are probably too high in the north but would be reasonable since boundary friction was neglected.

The theory takes a simple form if a quasi-geostrophic approximation is made, that is, when both u and v are assumed to be geostrophic and when \bar{h} varies linearly with y , then

$$h = \bar{h}_0 + \mu(y - y_0).$$

With the condition $h = h_c$ at $x = 0$ (at the coast) the solution is

$$h = \bar{h}(y) - (\bar{h} - h_c)e^{-x/\lambda}. \tag{XIX.33}$$

The width of the current is given approximately by

$$\lambda = \sqrt{\left(\frac{g^* \mu}{f\beta} \right)}.$$

Since at the right-hand edge the lateral velocity at the outer boundary is $|\bar{u}| = (g^*/f)\mu$, one obtains

$$\lambda = \sqrt{(\bar{u}/\beta)}. \tag{XIX.34}$$

It is apparent that the Gulf Stream is a phenomenon that depends essentially on the variation of the Coriolis parameter with latitude. Observed values of \bar{u} and β give a value for λ of about 50 km. v decreases laterally to a quarter at a distance of about 70 km which is in accordance with the down-slope to the right shown in Fig. 294. The geostrophic approximation predicts roughly the character of the current but does not predict all the details.

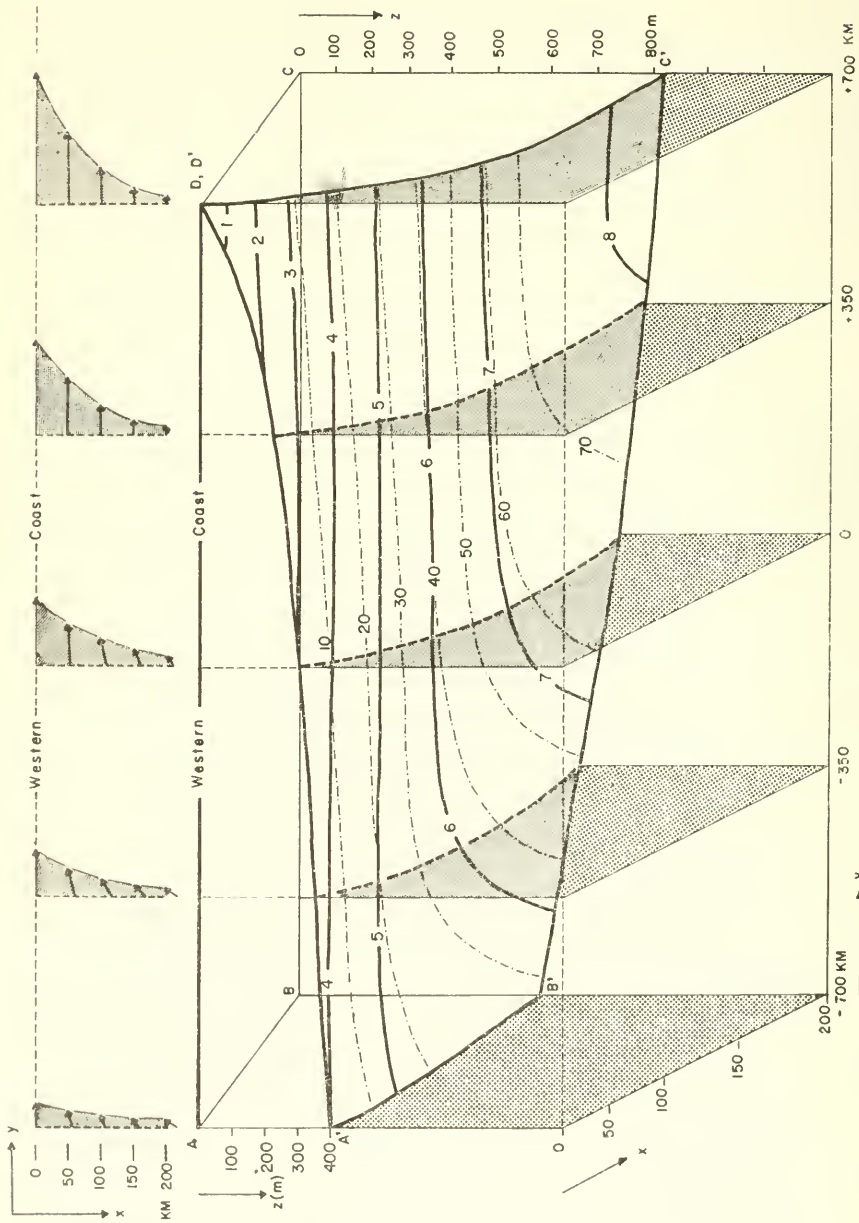


FIG. 296. Schematic perspective representation of the computed position of the thermo-cline h shown by contours of h (drawn for each 100 m). Broken lines are stream lines of the volume transport for each 10 million m^3 sec. On top of the picture the calculated velocity profiles across the Gulf Stream are given for a number of cross-sections (according to the computations of Charney).

The theory of the Gulf Stream and similar boundary currents requires further development. The double-layered model must be replaced by one with continuously stratified water and the effects of friction in both vertical and horizontal directions must be taken into account. Lateral friction against the coast should give a reduction in the velocity of the current at the left-hand side as is shown by observations.

The boundary current theory attributes the ocean boundary currents of the general oceanic circulation, in so far as they have the character of a free jet, to the effects of pressure and inertia and to the variation of the Coriolis parameter with latitude. It has been pointed out above (p. 580) that the Sverdrup solution starting from an eastern continental boundary and working westwards is unable to satisfy the boundary conditions at the west coast of the ocean. Only by including the effects of a strong lateral friction (mixing) Stommel and Munk have been able to satisfy the boundary conditions at a western boundary and to give a general theory of a wind-driven ocean circulation. However, along the eastern side of a continent (western side of oceans) the currents apparently do not correspond to this theory. They are narrower and more intense than would be expected from the general theory. The Charney theory gives the explanation for this and yields in this way a western continuation to the Sverdrup solution, without the addition of strong frictional effects but taking into account the effects of inertial terms and the variation of the Coriolis parameter with latitude. The density stratification of the water and the lateral inflow into a meridionally directed jet current have been found to be of particular importance in the formation of these boundary currents. These provide the connection with the western transport of the zonal wind currents of lower latitudes.

(d) Further Aspects of the Dynamics of the Gulf Stream

Associated with the questions raised on p. 617 another one stands out concerning the total current energy in a relatively thin top layer. This energy concentration in a narrow current band occurring in the very upper layers persists for more than 2000 km, from Cape Hatteras to the region east of the Newfoundland Banks while beneath this top layer the velocities remain small. This remarkable phenomenon is probably explicable by an association between momentum losses in the lower portion of the current and the upper energy concentration. It should be stressed that the zonal width and the high speed of the upper Gulf Stream layers rather definitely exclude an interpretation of the current in this part of the Atlantic as the result of momentum added locally by the prevailing winds. ROSSBY (1951) has attempted to find out what kind of vertically velocity profile would be formed in an immiscible stratified current subject to momentum losses through contact with the underlying surface or at lateral boundaries. It would be of particular value to know the nature of the special velocity profile corresponding to a minimum value of the momentum transfer in unit time across a vertical plane normal to the current axis. It is reasonable to assume that this profile represents a limiting state which would be gradually approached by any stratified current subject to momentum losses but unable to escape to the sides.

In a straight aparallel current of this type in which the water is considered to be incompressible and the density varies with depth, the momentum transfer across a vertical strip normal to the current axis is given by

$$MT = \int_0^D (\rho u^2 + p) dz, \quad (\text{XIX.35})$$

where z is counted upward from the bottom and where p is the water hydrostatic pressure. Assuming that the mass transport in every infinitesimal isopycnic layer remains constant during the variation process, then

$$\rho u \dot{z} d\sigma = \rho u_0 \dot{z}_0 d\sigma = v(\sigma) d\sigma, \quad (\text{XIX.36})$$

where the subscript 0 indicates initial conditions. Here σ is a new independent variable which determines the vertical density distribution and $\dot{z} = dz/d\sigma$. With these quantities (XIX.35) gives

$$MT = \int_0^1 \left(\frac{v^2}{\rho \dot{z}} + p \dot{z} \right) d\sigma. \quad (\text{XIX.37})$$

With the fundamental hydrostatic equation

$$\dot{p} = \frac{dp}{d\sigma} = -g\rho \dot{z} \quad (\text{XIX.38})$$

one obtains finally

$$MT = - \int_0^1 \left(\frac{gv^2}{\dot{p}} + \frac{p\dot{p}}{g\rho} \right) d\sigma. \quad (\text{XIX.39})$$

The variation problem is the determination of the particular function p of σ which reduces MT to a minimum value for the given distribution of v with σ . The variation of p vanishes at the sea surface and it can be assumed that it also vanishes at great depths. Under these circumstances the minimum value of MT is then given by

$$\delta(MT) = \int_0^1 \left[\left(\frac{gv^2}{\dot{p}^2} - \frac{p}{g\rho} \right) \delta\dot{p} - \frac{\dot{p}}{g\rho} \delta p \right] d\sigma = 0. \quad (\text{XIX.40})$$

This is true for arbitrary values of δp provided the function p satisfies Euler's equation

$$\frac{\dot{p}}{g\rho} + \frac{d}{d\sigma} \left[\frac{gv^2}{\dot{p}^2} - \frac{\dot{p}}{g\rho} \right] = 0 \quad (\text{XIX.41})$$

which on substitution reduces to

$$du^2 = p da, \quad (\text{XIX.42})$$

where a is the specific volume.

To determine the final velocity distribution from the initial mass transport distribution it is necessary to combine (XIX.42) with (XIX.36) or

$$\rho u dz = v(\sigma) d\sigma. \quad (\text{XIX.43})$$

Rossby has discussed several models with special density distributions according to this principle; only those more or less directly concerned with the Gulf Stream will be considered here.

For a uniformly stratified current with speed u_0 and depth D_0 that is flowing on top of a homogeneous bottom layer of density ρ_b , in which the volume transport is zero and that is allowed to readjust itself to a minimum momentum transfer current

profile, a determination of the density and velocity distribution in the final state can be made by taking

$$\rho = \rho_s(1 + 2\kappa\sigma) \quad \text{and} \quad \rho_b = \rho_s(1 + 2\kappa), \quad (\text{XIX.44})$$

where ρ_s is the surface density and ρ_b is the deep water density. For a uniform initial stratification (subscript 0) it follows that

$$\sigma = \frac{z}{D_0} \quad \text{and} \quad \left(\frac{dz}{d\sigma}\right)_0 = D_0. \quad (\text{XIX.45})$$

With the continuity requirement, the basic equation gives as a good approximation

$$u = \frac{\kappa g}{2u_0 D_0} (D^2 - z^2) \quad \text{and} \quad \sigma = \frac{\kappa g}{2u_0 D_0^2} \left(D^2 z - \frac{z^3}{3} \right). \quad (\text{XIX.46})$$

Further when $\sigma_{z=D} = 1$ one obtains

$$\frac{D}{D_0} = \left(\frac{3u_0^2}{\kappa g D_0} \right)^{1/3} \quad \text{and} \quad \frac{u_s}{u_0} = \frac{3}{2} \left(\frac{D_0}{D} \right). \quad (\text{XIX.47})$$

It follows that the current must become shallower and the bottom layer will increase in thickness whenever u_0 falls below the critical value, $u_{0,\text{crit}}$ defined by

$$u_0 < u_{0,\text{crit}} = \sqrt{\left(\frac{\kappa g D_0}{3} \right)}. \quad (\text{XIX.48})$$

The end of the adjustment process can be illustrated by means of a numerical example. Initially the upper moving layer extends down to 600 m ($D_0 = 600$) and $u_0 = 0.75$ m sec⁻¹. In the Gulf Stream region an adequate value of the total range in σ_t is 4.5 so that to a close approximation $2\kappa = 4.5$.

Thus D results to 300 m and for u_s one obtains 2.25 m sec⁻¹. Figure 297 shows a graphical representation of this case.

It is clear that the dimensionless quantity F defined by

$$F = \frac{u_0^2}{\{(\rho_b - \rho_s)/\rho_b\}gD_0} \quad (\text{XIX.49})$$

has the form of a Froude number in which the gravitational acceleration is reduced in proportion to the total percentage density range of the fluid. It can be seen that this new number determines the nature of the baroclinic movements of a current subject to momentum losses due to frictional influence. If the "internal Froude number" is less than a certain critical value (in the above case $\frac{1}{6}$) the current will be concentrated in the lighter top layers.

Apparently, oceanic currents usually have subcritical values of F . They then have a tendency to develop a strong shearing motion with increasing velocity and increasing stability near the sea surface and decreasing velocity and stability lower down.

In the Straits of Florida and in the Gulf Stream region as far as Cape Hatteras the range in σ_t is smaller than it is further downstream and there is no homogeneous deep water to facilitate a separation of the current from the bottom. After the current leaves Cape Hatteras, however, the momentum it gains due to direct action of the wind on the narrow strip exposed at the atmosphere is presumably incapable of balancing the losses

which result from interaction with the deeper water masses or are due to lateral mixing. The current thus tends to become more and more superficial; this process maintains the high surface velocities.

The cause for the horizontal meander-like oscillations of the narrow current band of the Gulf Stream after leaving the continental shelf is not entirely clear. These meanders occasionally become unstable and then complete cut-off vortices are formed;

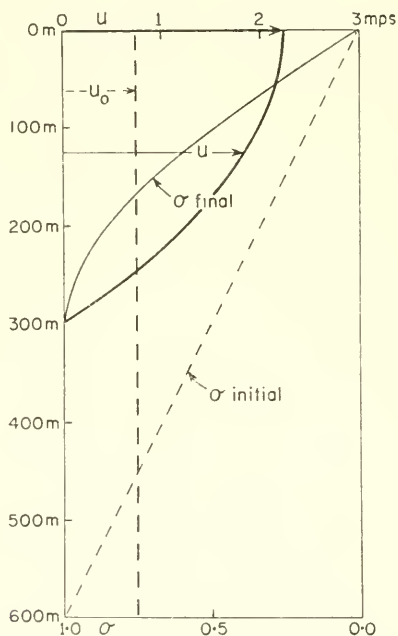


FIG. 297. Transformation of a uniform current with a constant vertical density gradient into a flow characterized by a minimum value of the momentum transfer. The initial uniform velocity distribution is given by the heavy broken line, the final velocity distribution by the heavy full line. The density distributions before and after adjustment are given by lines marked by $\sigma_{(initial)}$ and $\sigma_{(final)}$. Note that the depth of the final current is one half of the initial depth. The total percentage density range has the value 0.0045.

this has been discussed already on p. 616. Recent investigations on the vertical stratification in the Gulf Stream (ARX, BUMPUS and RICHARDSON, 1954) using stations with little distance from each other have shown that the narrow current band has a filamentary structure. It is composed of thin layers of high velocity alternating with layers of lower velocity. This extraordinary stratification is possibly connected with gliding processes imposed by external circumstances on the individual water layers of the Gulf Stream and can be assumed to be a consequence of turbulence processes, which are imposed from outside.

The meandering of the narrow current band of the Gulf Stream appears to be a common phenomenon. These meanders show wavelengths of about 200 km and their speed of propagation is about 11 nautical miles a day, which is about a tenth of the speed of the current itself. STOMMEL (1953) has given a simple meander theory for a

wide current in a stratified ocean in which he showed that the stability of the waves depends on whether

$$U^2 \gtrless g \frac{\Delta\rho}{\rho} D. \tag{XIX.50}$$

Here U is the velocity of the basic current, D is the thickness of the upper moving layer and $\Delta\rho$ is the density difference between the lower, homogeneous and motionless layer and the homogeneous upper layer. The upper inequality sign results only in stable waves and the lower one only in unstable waves. For $U^2 = g(\Delta\rho/\rho)D$ there is a single "just unstable" wave, the wave-number of which is given by $\kappa = f/(U\sqrt{2})$. This wave always remains stationary.

Choosing a surface layer 200 m thick moving at 200 cm sec⁻¹ and having a density ratio $\Delta\rho/\rho = 2 \times 10^{-3}$ the wavelength of the "just unstable" perturbation is 180 km. All other wavelengths are stable and do not grow. It is remarkable that this wavelength corresponds closely to that observed. Some objections can be raised against the application of the Stommel perturbation theory to the meanders actually observed in the Gulf Stream and it would be desirable to test the Stommel model somewhat more closely and to specialize some of his assumptions.

In order to handle the problem of the meandering behaviour of the Gulf Stream in a more comprehensive way, the problem may be looked upon as intimately connected with the way in which the stability of a narrow geostrophic current is changed when this flow is subjected to external perturbations. In a deeply penetrating way the latter question has been dealt with by VAN MIEGHEM (1951) for atmospheric currents. He assumed a straight geostrophic flow in hydrodynamic equilibrium in any direction on the rotating earth allowing for horizontal (transversal) and vertical wind shear. On this current he imposed a disturbance acting in lateral (transverse) as well as vertical direction and attempted to find the conditions under which the disturbance decreased in time (stable state) or increased in time (unstable state). In the stable case the chance disturbances vanish with time; in the unstable case they grow into meanders and may even degenerate into independent vortices. If the positive x -axis is chosen in eastward direction, the y -axis normal to it (to the north) and the z -axis positive towards the zenith and if the geostrophic current flows along the y -axis ($u_x = 0$, $u_y = u(x,z)$, $u_z = 0$), then the equilibrium values of the pressure $P = P(x,z)$ and the specific volume $\alpha = \alpha(x,z)$ are only functions of x and z and the equation of motion as well as the quasihydrostatic equation leads to the Margules equilibrium condition of the geostrophic current:

$$2\omega_z \frac{\partial u}{\partial z} + 2\omega_x \frac{\partial u}{\partial x} = \frac{\partial P}{\partial x} \frac{\partial \alpha}{\partial z} - \frac{\partial P}{\partial z} \frac{\partial \alpha}{\partial x} \equiv N, \tag{XIX.51}$$

where ω_x and ω_y are the horizontal and vertical components of earth rotation vector ($\omega_x = \omega_y = \omega \cos \phi$ and $\omega_z = \omega \sin \phi$) and N is the number of solenoids in the cross-section (x,z) (baroclinicity). For a small fluid particle in the interior of the water mass which is at the co-ordinate origin at time t_0 and at that instant is subject to a transverse impulse, its velocity components relative to the earth at the same instant will then be

$$V_x = u + v_x, \quad V_y = v_y, \quad V_z = v_z. \tag{XIX.52}$$

Assuming that the specific volume α_0 of the disturbed particles is conserved, then the equations of motion for the displaced particles will take the form:

$$\left. \begin{aligned} \frac{dv_x}{dt} + 2\omega_y v_z &= \psi_x, \\ \frac{dv_z}{dt} - 2\omega_y v_x &= \psi_y, \end{aligned} \right\} \quad (\text{XIX.53})$$

where

$$\left. \begin{aligned} \psi_x &= -a_{xx}x - a_{xz}z, \\ \psi_y &= -a_{zx}x - a_{zz}z, \end{aligned} \right\} \quad (\text{XIX.54})$$

x and z are the displacements of the small particles in the x - and z -directions and may be positive or negative. The coefficients a_{xx} , a_{xz} and a_{zz} are given by

$$\left. \begin{aligned} a_{xx} &= +f \left(f + \frac{\partial u}{\partial x} \right) - \frac{\partial P}{\partial x} \frac{\partial \alpha}{\partial x}, \\ a_{xz} &= -f \left(f^* - \frac{\partial u}{\partial z} \right) - \frac{\partial P}{\partial x} \frac{\partial \alpha}{\partial z}, \\ a_{zz} &= +f^* \left(f^* - \frac{\partial u}{\partial z} \right) - \frac{\partial P}{\partial z} \frac{\partial \alpha}{\partial z} \end{aligned} \right\} \quad (\text{XIX.55})$$

with $a_{xz} = a_{zx}$ and $f^* = 2\omega \cos \phi$.

It can then be shown that at a point in a geostrophic current at which there acts a transverse disturbance, conditions will be stable, neutral or unstable according to whether the quadratic form (Kleinschmidt):

$$Q = a_{xx} \cdot x^2 + 2a_{xz} \cdot xz + a_{zz} z^2 \geq 0. \quad (\text{XIX.56})$$

The sign of Q is determined firstly by that of the discriminant

$$a = a_{xz}^2 - a_{xx} a_{zz} \quad (\text{XIX.57})$$

and secondly by the sign of one of the coefficients of the quadratic terms in Q (for instance a_{zz}). The condition (XIX.56) thus becomes

$$a \gtrless 0 \quad \text{or} \quad \left(\frac{\partial u}{\partial x} - \frac{\partial \alpha / \partial x}{\partial \alpha / \partial z} \cdot \frac{\partial u}{\partial z} \right) + f \gtrless 0. \quad (\text{XIX.58})$$

The last equation can be re-written with the help of (XIX.55) and by neglecting terms of lower order one obtains

$$\left(f \frac{\partial u}{\partial z} \right)^2 \gtrless f \left(f + \frac{\partial u}{\partial x} \right) \frac{g}{\alpha} \frac{\partial \alpha}{\partial z} \quad (\text{XIX.59})$$

The expression $\frac{g}{\alpha} \frac{\partial \alpha}{\partial z} = -\frac{g}{\rho} \frac{\partial \rho}{\partial z}$ is the static stability (z -positive upwards; p. 196) and

$f(f + \partial u / \partial x)$ is the expression for the inertial stability. The equation (XIX.59) gives a hydrodynamic measure in as far as the geostrophic equilibrium in the current under consideration is hydrodynamically stable or unstable when subject to external impulses acting normal to the direction of the flow (in transverse or vertical direction).

The application of these equilibrium conditions to the Gulf Stream requires an estimate of the order of magnitude of the individual terms. These can be obtained approximately from the "Atlantis" sections for concentrated boundaries of the current and one obtains the following values given in the [cm g sec]-system:

$$\left| \begin{array}{cc|c} u \dots 10^2 & \frac{\partial \alpha}{\partial x} \dots 10^{-10} & f \dots 10^{-4} \\ \frac{\partial u}{\partial x} \dots 10^{-4} & \frac{\partial \alpha}{\partial z} \dots 10^{-7} \text{ to } 10^{-8} & \left(f \frac{\partial u}{\partial z} \right)^2 \dots 10^{-14} \\ \frac{\partial u}{\partial z} \dots 10^{-3} & \frac{g}{a} \frac{\partial \alpha}{\partial z} \dots 10^{-5} & f \left(f + \frac{\partial u}{\partial x} \right) \dots 10^{-8} \end{array} \right|$$

Introducing these values in equation (XIX.59) shows that in the Gulf Stream, in spite of always secured static stability and in spite of the almost always secured inertia instability, hydrodynamic instability may still occur provided the vertical shear in the flow reaches excessive values.

This can be illustrated by an example taken from the "Atlantis" section shown in Fig. 294. (Chesapeake Bay-Bermuda, April 1932). Along the left-hand side of the Gulf Stream in the region of largest vertical and horizontal shear (depth 220 m) one obtains

$$\frac{\partial u}{\partial z} = 0.47 \times 10^{-2} \text{ sec}^{-1}; \quad \frac{\partial u}{\partial x} = 0.33 \times 10^{-4} \text{ sec}^{-1} \quad \text{and} \quad \frac{\partial \rho}{\partial z} = 0.33 \times 10^{-6}.$$

With these values and with $f = 0.85 \times 10^{-4}$

$$\left(f \frac{\partial u}{\partial z} \right)^2 = 0.16 \times 10^{-12},$$

while

$$f \left(f + \frac{\partial u}{\partial x} \right) \frac{g}{a} \frac{\partial \alpha}{\partial z} = 3.31 \times 10^{-12}.$$

The current and density stratification is thus, of course, hydrodynamically stable as could be expected since at this part of the Gulf Stream the current shows no tendency to meander. Hydrodynamic instability would only occur if the vertical shear in the flow would reach values four times larger. Further to the north, in the section between Cape Hatteras and the Newfoundland Banks, conditions might be different and may readily be so that the current system becomes hydrodynamically unstable; these small horizontal wave formations will soon grow into large meanders and finally lead to the formation of vortices. Strong vertical current shear and low static stability are required for this. It can be understood that a strong acceleration of the flow in the top layers of the Gulf Stream caused by the direct action of a strong westerly wind acting on the sea surface will provide the necessary vertical current shear to give rise to hydrodynamic instability in the current system and to lead to the formation of meanders.

HAURWITZ and PANOFSKY (1950) in a study of the stability and meandering behaviour of the Gulf Stream have attempted to show that especially favourable conditions for the development of unstable waves occur when the Gulf Stream is not too

close to the continental shelf. The tendency towards a formation of meanders appears only after the Gulf Stream leaves the continental shelf, but probably there are other factors that will decide about the development of meandering motion than the distance from the continental shelf.

As yet no fully satisfactory explanation has been given for the observed split of the Gulf Stream into a number of branches. HANSEN (1952) has demonstrated that under certain conditions a northwards flowing current while turning towards the east can break up into several branches; but his solution is of more formal character and no actual reasons can be offered for this phenomenon.

(e) *The Kuroshio*

The three-dimensional structure and the dynamics of this current have been investigated by UDA (1930), SIGEMATSU (1933) and KISINDO (1934) on the basis of series observations made by the hydrological department of the Japanese Marine and the Imperial Fisheries Experimental Station in Tokyo (since 1925) and also by the oceanographic survey vessel "Mansyu". A number of transverse profiles have been prepared and critically worked with by WÜST (1936*a*) in a comparative study of the Kuroshio and the Gulf Stream and further valuable work has been performed by KOENUMA (1939). Wüst has dealt with a cross-section at right angles to the chain of islands, the Ryu-kyu, from 27° to 29° N., just before the Tsushima current splits into branches and with another cross-section farther north (little to the south of Shiono at Misaki, the south cape of the projecting Kii peninsular at about 30° to 34° N.). See Fig. 261 for the position of these sections.

The inclination of the isolines of the oceanographic factors forced by the water movement appears clearly in all cross-sections through this strong current. A comparison with conditions in the Gulf Stream shows that there is an almost identical thermal structure but considerable differences occur in the salinity distribution; the Kuroshio has a low salinity 34.32 to 34.98‰ and a very weak vertical salinity stratification, while the Gulf Stream possesses considerably higher salinity (34.97–36.65‰) and a pronounced stratification. The Kuroshio region also shows an intermediate salinity minimum at 500–800 m depth resulting from an intrusion of the weakly saline sub-Arctic intermediate water flowing in from the north (p. 172).

Figures 298 and 299 show the temperature and salinity distributions in the Ryu-kyu section (Feb. 1927) and in the Shiono-Misaki section (Jan. 1927). Disregarding the top layers, the sections for the summer months show entirely similar conditions. These sections have also certain similarities with those through the Gulf Stream (see Figs. 282, 283).

The Ryu-kyu section corresponds closely to that through the Florida Strait, the Shiono-Misaka section to the Chesapeake Bay transverse section. It is also apparent from these sections that the Kuroshio is throughout the entire vertical extent a weakly saline current as compared with the Florida Current; the highly saline core layer can again be explained as a distant effect of the tropospheric circulation of the subtropics and tropics. The velocity distribution calculated from the mass field of the Ryu-kyu winter section shows maximum intensities of 61 cm/sec below the sea surface at 150 m depth. In summer highest values of about 90 cm/sec occur at the sea surface. The weakening and downward displacement of the current maximum in winter is in

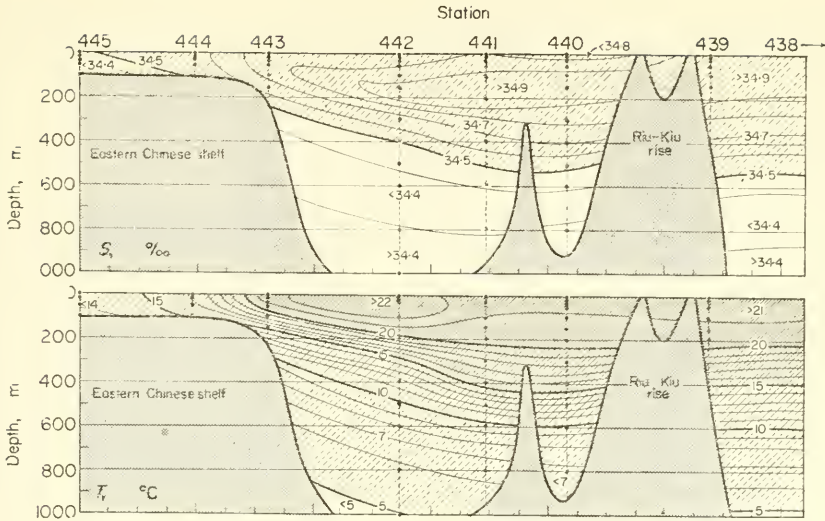


FIG. 298. Cross-sections of temperature through the Kurochio (*R*, Riu-Kiu section at 28° to 29° N., “Mansyū” stations; *S*, Shiono-Misaki section at 34° to 30° N., “Mansyū” stations, January 1927) (according to Wüst).

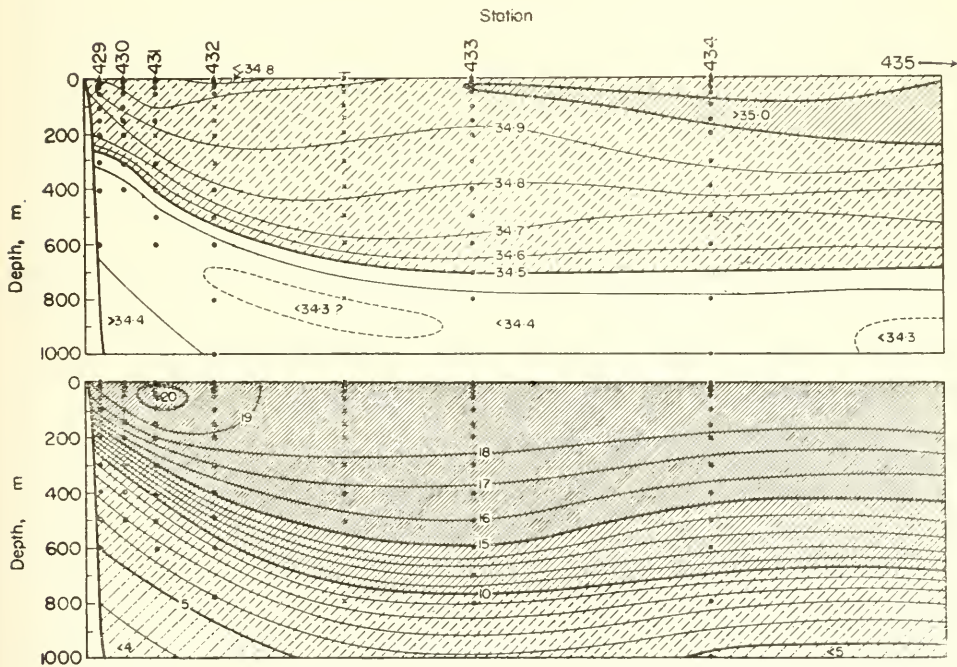


FIG. 299. Cross sections of salinity through the Kurochio, section *S* (Shiono-Misaki) (see remarks below the Fig. 298).

correspondence to the piling-up effect (“Aufstau-Effekt”) of the winterly north-west monsoon. These values are in good agreement with direct current measurements at a station in the current core. The total amount of water transported through this section amounts to 21 million m^3/sec in winter and about 23 million m^3/sec in summer. The Kuroshio and the Florida Current thus carry about the same amount of water.

The Shiono-Misaki section has been evaluated both by Wüst and by Koenuma. Wüst thereby placed the reference-level at the upper limit of the weakly saline intermediate water, at about the depth of the 10° isotherm; Koenuma on the other hand, bases his calculations on velocities of 16 cm/sec of the intermediate water observed in coastal areas moving there to the north-east and for larger distances from the coast he assumed that the intermediate water was transported to the south-west at 5 cm/sec. The two vertical velocity profiles independently found by both methods thus do not agree. The velocity distribution obtained by Koenuma is in good agreement with actual current measurements while the values obtained by Wüst are somewhat too low. The Kuroshio here keeps closely to the coast with velocities of 160–180 cm/sec and extends seawards for 140 km. As is true for the Gulf Stream, there is a counter current to observe towards the south-west on the right-hand side with maximum velocities of up to 20 cm/sec. Here also a downstream increase in the water transport can be noticed, but the counter current on its right-hand side with its higher velocities compensates the outflow towards the east to a considerable extent. There is so far no proof whether there are any seasonal changes in the amount of water transported (see also, in this connection the works of ICHIVA, 1953–54).

The Kuroshio does not show such pronounced characteristic properties as to be termed without more ado as a free jet current in the sense of the Rossby theory. It lacks especially the jet-like outflow from a narrow sea strait; it is formed instead by the gradual deflection of the stream lines out from the North Equatorial Current and only at a later stage forces its way into the relatively narrow channel-like region between the shelf and the submarine ridge of the Ryu-kyu Islands. By the further weakening due to the separation of the Tsushima branch its quasi-jet character is entirely lost.

The continuation of the Kuroshio out into the Pacific from about 35° N. onwards (see p. 570), according to vertical sections (UDA, 1935), possesses the character of a relatively narrow current which, however, like the Gulf Stream in the central parts of the Atlantic, has a tendency to break up into single-current branches intermittently separated by vortices and counter currents. The one branch turning north from the Kuroshio meets the cold water masses of the Oyashio, and there in dynamic respect similar conditions occur as are present when the Gulf Stream meets the Labrador Current off the Newfoundland Banks.

Table 153 finally presents a survey about mean water, heat and salt transports according to Wüst for the Gulf Stream and the Kuroshio. About 22 times as much water passes through the Kuroshio section and even about 33 times through the Gulf Stream as is carried by the water transports of all the rivers and glaciers on the earth (run-off from the continents on the average about 1.2 million m^3/sec). Even more spectacular are the enormous amounts of salt carried through these cross-sections, corresponding roughly to loads of 79,000 and 121,000 rail-road goods wagons respectively, each of which takes 10 tons. The question thus arises, why the climatic effect of the Kuroshio on the eastern Pacific and on the neighbouring continent

Table 153. Mean water, heat and salt transports of the Gulf Stream and of the Kuroshio between 27° N and 37° N.

	Gulf Stream (Florida and Champspeake section)	Kuroshio (Ryu Kyu section)	Ratio between (Kuroshio : Gulfstream)
Water amount 10^6 m ³ /sec	32.50	22.20	1 : 1.46
Heat amount 10^{10} kg cal/sec	54.60	38.00	1 : 1.44
Salt amount 10^6 tons/sec	1.21	0.79	1 : 1.54

is so much weaker than the corresponding effect of the Gulf Stream on the Eastern Atlantic and on Europe, although the heat transport is not appreciably less. This difference must be governed by topographical conditions (DALL, 1881, KÖPPEN, 1911). After leaving the Japanese coast at 35° N. until it diverges northwards and southwards on the eastern side of the ocean the Kuroshio water travels about 8000 km, while the Gulf Stream water after leaving the American west coast travels only about 5000 km. Beneath the Kuroshio waters there is weakly saline, cold sub-Antarctic water, but beneath the Gulf Stream the water is warmer and more saline and continuously renewed by the outflow of the highly saline European Mediterranean waters (see p. 529, Fig. 245). The Gulf Stream water is thus protected from considerable heat and salinity losses downwards. The greater efficiency of the Gulf Stream must be attributed to the much longer conservation of its properties over the considerably shorter distance it travels and to the favourable conformation of the European coasts.

(f) The Agulhas Current

This current is due to the outflow of the water piled up by the South Equatorial Current of the Indian Ocean along the coast of South Africa and Madagascar and as such is a typical gradient current. A detailed dynamic evaluation of the observational data available from the different expeditions has been carried out by DIETRICH (1935). For the surface currents see p. 567; for the structure and dynamic of it see p. 470, Figs. 205–7. As subtropical and Antarctic water masses are situated side by side the three-dimensional mass distribution is a rather complex one. Everywhere along the African continental slope as far as the latitude of Capetown there is a steep rise of heavier water (cold, but weakly saline) towards the coast. Towards the Agulhas Bank the slope is flattened out and on the shelf itself is occasionally superimposed by lighter water brought in from the south and south-east by the wind. To the south of this heavy water mass there is found a relatively lighter (warmer, but more saline) water mass of subtropical origin in a trough-like fashion bordering on the denser sub-Antarctic water which moves eastwards in the south. Figure 205 shows the distribution of the specific volume anomaly in a cross-section oriented from Capetown in south-westerly direction. All cross-sections through the current are of similar nature as this one. The depth of the trough-like confined mass of the lighter water body (corresponding to the schematic picture of Fig. 204) is about 1000 m. Underneath this, weakly saline sub-Antarctic intermediate water spreads out everywhere, in which the salinity minimum weakly follows the trough-form and the rise towards the coast.

Since the sub-Antarctic water forms an almost zonal boundary to the lighter water mass in the south, the trough of lighter water is narrowed towards west by the African continent, until it finally takes almost a wedge-form at the southern peak of the Agulhas Bank. In the further course this wedge then splits into three separate branches with simultaneously occurring vortex formations; the southernmost of these intrude into the heavier sub-Antarctic water and the northernmost intrude into the subtropical water of the South Atlantic. The lighter water thereby decreases considerably in thickness.

A dynamic interpretation of the above-mentioned section running south-west of Capetown has been attempted in Fig. 206; similar scientific evaluation of the other sections gave results in agreement with this. The nature of the current is shown more clearly by the dynamic topography of the isobaric surfaces. Figure 300 shows the dynamic depth anomaly for the 200 decibar-surface relative to that of the 1000 decibar-surface; the first one can be taken as an approximation to the absolute topography of the 200 decibar-surface. According to this the Agulhas Current at the 200 m depth flows with intense velocities along the continental coast as far as the southern tip of Africa. However, it thereby diminishes rapidly its mass and velocity and finally loses its current character forming three large quasi-stationary vortices, the cores of which are identical with the three branches of lighter water mentioned before. According to Dietrich about three-quarters of the water masses of the Agulhas Current, transported at the southern tip of Africa into the South Atlantic, is drawn into these vortices and after mixing with the current of the higher latitudes returns to the Indian Ocean.

Analysis of the pressure distribution in the current interior shows it to be the resultant of two components. The first is an effect of the internal pressure determined by the mass distribution, and corresponds to the normal pressure distribution in a system in which a lighter motionless water mass is embedded between two denser moving water bodies. The second component corresponds to a ridge of high pressure occurring in the boundary region between the two currents flowing in opposite direction and is due to the piling up of water. Since the Agulhas Current in the northern part of the current system as well as the broad oceanic West Wind Drift in its south both give a total water transport towards left. In the boundary region between them water accumulates giving rise to the second pressure component. In combination with the first a total pressure distribution is generated which is characteristic for that found in the Agulhas Current. Especially typical is the circumstance that the two adjacent currents of opposite direction face each other with their faster moving parts. The large lateral shearing forces thus formed give rise to large vortical movements (p. 570) in which most of the flow energy is dissipated.

DIETRICH, 1936 has given a comparative discussion about the structure and movement of the Gulf Stream and of the Agulhas Current and reference is made to this investigation here.

4. Upwelling Phenomena

A characteristic phenomenon occurring in the narrow oceanic strips off the western coast of the continents in middle latitudes is the observed cold coastal water, which due to its influence on the atmosphere is of considerable climatological importance. Until recently the investigation of these phenomena had to be based on surface data only,

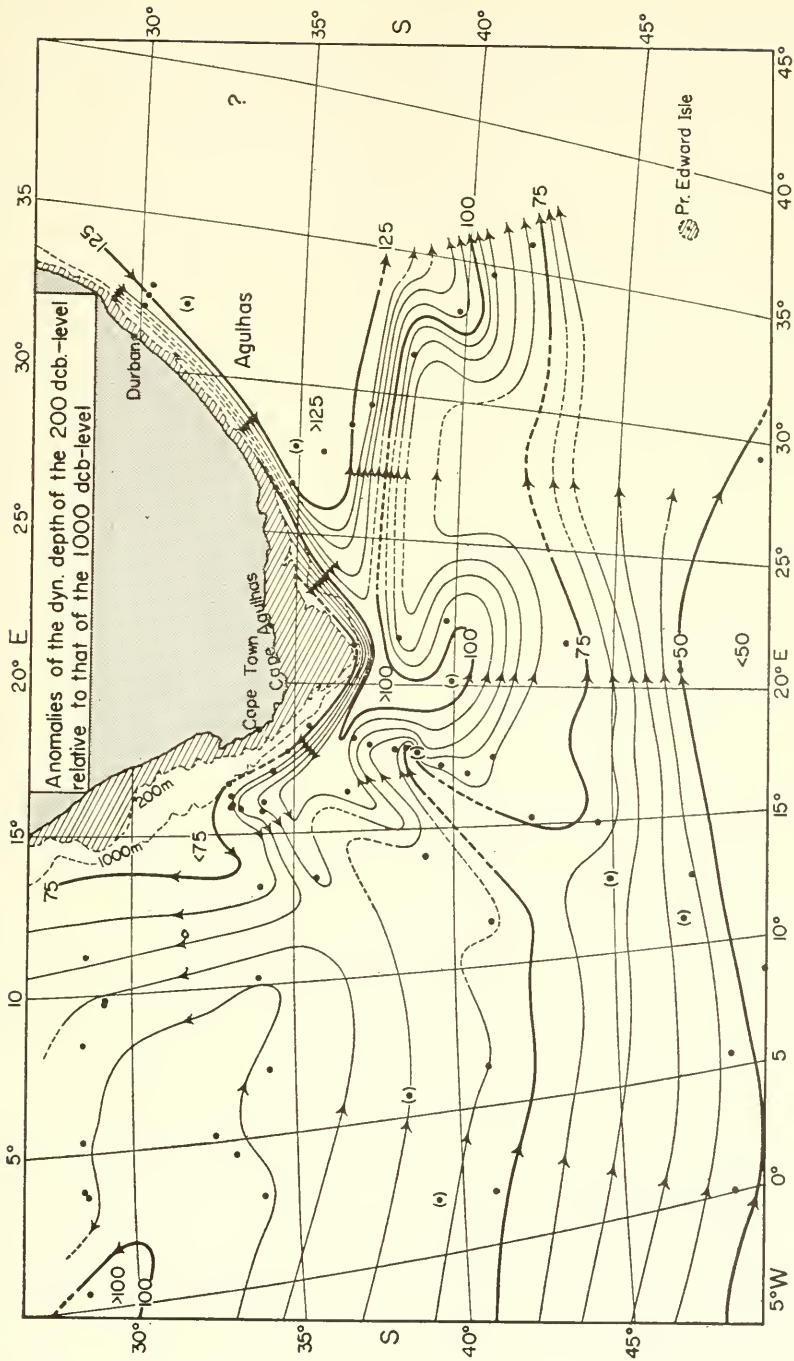


FIG. 300. Topography of the 200-decibar surface relative to that of the 1000-decibar surface (isolines are drawn from 5 to 5 dyn cm; according to Dietrich).

which was not enough to afford any insight into the inner mechanism of this phenomenon. Some data for the area off Chile and Peru have been obtained by the last "Carnegie" cruise (SVERDRUP, 1930) and the "Meteor" expedition during the spring of 1937 made six profiles at right angles to the coast with the objective to study the upwelling water phenomenon off the north-west coast of Africa (DEFANT, 1936a). Detailed systematic investigations of the strong upwelling phenomena off the Californian coast have been made since 1937 by the Scripps Institution of Oceanography (SVERDRUP, 1938a, SVERDRUP and FLEMING, 1941). These cover the development of upwelling phenomena in successive surveys and have provided some understanding of the dynamics of the upwelling process. Some comments might be made here on individual regions with upwelling. A summary for the oceanic regions off south-west Africa has been given by DEFANT (1936a), see also, BOBZIN, 1922). The surface temperature conditions are given in the charts of the "Meteor" Report, vol. v, Atlas. In all months the low temperatures occupy the total width of the shelf (about 100 nautical miles), at the continental slope occurs the rapid rise to the higher temperatures in the west. During every month the temperature anomaly is highest at the coast with maximum values of -8°C to -10°C . The area of maximum anomaly moved in a meridional direction during the course of the year: in the summer (January) it occupies its southernmost position and is strongest between Table Bay and Luderitz Bay (32°S to 23°S .); in winter it moves furthest to the north (between the Luderitz Bay and Walvis Bay, 27° to 14°S .). During the entire year the current system of the sea surface shows a particularly characteristic *one-sided divergence line* which extends along the coast from about 30° to 20°S . or even more. In the south its distance from the coast amounts to about 160 nautical miles; in the north, however, 300 to 360 nautical miles. The region to the east of this divergence line is the region of cold upwelling. Where the unilateral divergence is most strongly developed, also the temperature anomaly is greatest. The anomaly at the coast vanishes north of 20°S ., where the divergence with a decreasing intensity turns westwards and gradually fades away. The uniform rise of the isopycnals from west to east (towards the coast) is a particularly marked feature of the thermo-haline structure of the upwelling region. Off the coast especially in the north there is a well-developed transition layer, and all the isolines immediately beneath this transition layer off the coast show a surprisingly sharp downward deflection to a depth of 350 m. This is only explicable as an effect of piling up of water at the continental slope whereby in the depths lower than 30 or 40 m the water masses are pressed downwards.

Similar conditions apply also to regions with cold water upwelling off the north-west coast of Africa. From January to May especially this region can be visualized by a tongue of cold water extending from higher latitudes southwards along the coast. Figure 301 shows this temperature anomaly for April; it occupies the entire area between the Canaries and Cape Verde in which the anomaly already on the average is increased to almost -7°C just off the coast and for individual cases reaches values of -10°C or more (see SCHUMACHER, 1933). Here also a sharp density transition layer can be found extending along the edge of the shelf until just off the coast.

Particularly well-developed upwelling phenomena occur in the region off the western coast of North America between about 46°N and 25°N ., especially off California with extreme conditions at Cape Mendocina (north of San Francisco). An

analysis of the thermal conditions in this oceanic region has been carried out by THORADE (1909) and MCEWEN (1912, 1934). The onset of upwelling phenomena usually occurs in March and reaches its maximum during the summer months (July to August). The culmination coincides with the maximum frequency of the north-west winds. It is absent during the autumn and winter although off-shore south-easterly winds are not

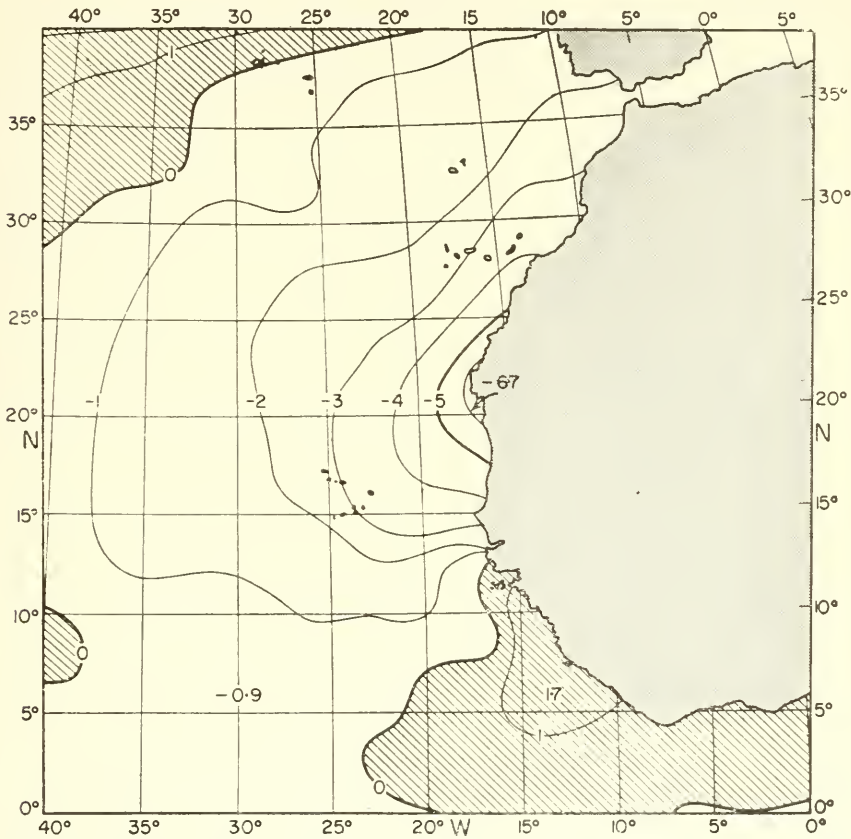


FIG. 301. Mean anomaly of the sea surface temperature off the north-west coast of Africa for April (drawn from means of two degree squares of the Atlantic Ocean).

uncommon. The cold upwelling water off the South American coast has been dealt with by GUNTHER (1936) (see p. 571). The west coast of Australia is not entirely free of cold coastal water as has been shown by SCHOTT (1933) and rising water sometimes occurs off the north-western coast. Occasional observations of cold upwelling water have also been made along many other coasts, for instance, off the Somali coast during the summer months during off-shore winds and at the southern tip of Ceylon and others.

In considering the dynamics of the phenomenon it should particularly be remembered that for a current in stratified water the mass field adjusts baroclinic, so that

under stationary conditions the lower and cold as well as nearly always weakly saline waters are lifted on the right-hand side of the current core in the Northern Hemisphere and on the left-hand side in the Southern Hemisphere. If there is a parallel coast along this special side of the current the water off the coast already for this reason alone will be colder and will have a lower salinity than further out. This state does not represent an upwelling phenomenon, but rather a state of long duration dependent on the nature of the vertical water stratification and on the current strength. Most of the anomalies appearing off the coasts are due to such a simple effect on the mass field produced by the currents. Upwelling of cold deep water occurs only if in a wind-driven current with a flow component parallel to the coast a water transport away from the coast sets in. The continuity condition then requires a rising water movement at the coast.

In a first attempt in order to explain this phenomenon THORADE, 1909 used this theory, and later on particular interest has been devoted to the determination of the vertical velocity profiles in the rising water (MCEWEN, 1912) and to the determination of the depths in which the upwelling phenomenon starts out (SVERDRUP, 1930). It was soon found out from the thermo-haline structure in the upwelling region, that these depths could not be large and that due to the inclination of the isothermal layers off the coast an upward water movement of only a few hundred metres would be sufficient to explain the observed sea surface anomaly. The formation of a one-sided divergence line running more or less parallel to the coast is the characteristic feature of the current field. The occurrence of rising movements at divergence lines in the case of non-stationary discontinuity surfaces and vortices is, of course, understood theoretically (p. 469) and water movements of this type are shown definitely by numerous observations of the vertical and horizontal distribution of the oceanographic factors (for example, equatorial cold tongues in the Atlantic and Pacific (pp. 558 and 569); boundary regions at the oceanic polar fronts, p. 471).

In the upwelling regions off the west coasts of continents all upwelling phenomena are of a similar type as discussed above. From the analysis of the mean oceanic state off the coast of South West Africa DEFANT (1936*a*) has derived the schematic diagram shown in Fig. 302 of the structure and the water movements in a cross-section at right angles to the coast. Essentially the cross-sectional movement consists of an elongated vortical motion around a horizontal axis which is superimposed on a much stronger and uniform current parallel to the coast. The water beneath the axis of the transverse vortical motion flows in the lower part of the top layer, in the density transition layer and beneath it towards the coast and gradually rises just off the coast. The upwelling phenomenon is very largely confined to the narrow strip between the divergence line and the coast. It rises up to the sea surface from a depth of only 100–200 m and as a consequence of the current field the temperature distribution, observed *in vertical* direction remote from the coast, is twisted around and changes its position into a horizontal one; so to say is projected on the horizontal sea surface.

A necessary consequence of this circulation is the destruction of the density transition layer in the upwelling region off the coast. This is clearly shown by the “Meteor” cross-section (1937) over the shelf off the north-west African shelf. The gradual break down of the transition layer, which at times is also strongly developed in the area

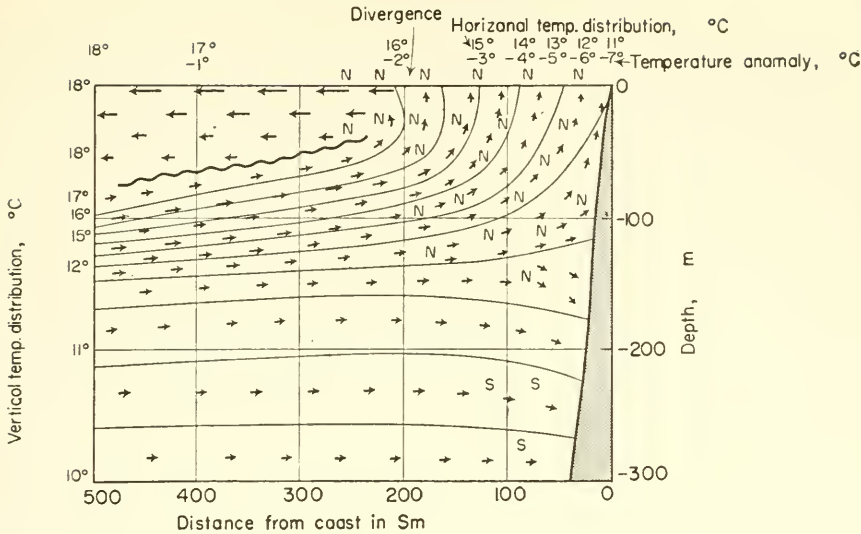


FIG. 302. Schematic cross-section normal to the coast of south-west Africa. *Full lines*, isopycnals; *arrows*, zonal and vertical velocity components (the length of the arrows can be taken approximately as a measure of the speed); *letters*, meridional velocity components and in special; *N*, parallel to the coast towards north; *S*, parallel to the coast towards south (the size of the letters can be taken approximately as a measure of the speed); *wavy lines*, axis of the vertical current vortex (vertical exaggeration 1:2300).

nearest the coast, is a consequence of internal tidal waves which gradually become unstable as is definitely shown by the series of observations. This is thus a precondition for the upwelling of deep water (see vol. II, p. 581).

SVERDRUP (1938a) in the evaluation of the almost synoptic surveys made by the Scripps Institution of Oceanography, La Jolla, from March to June 1937 along a transverse section off and at right angles to the Californian coast from Port San Luis (35.2° N., 120.7° W.) has obtained good insight into the dynamics of the upwelling processes. Figure 303 presents two topographies of the physical sea level as well as the 100 and 200 decibar-surfaces relative to that of the 500 decibar-surface. In the time between the two surveys typical mass displacements have occurred. The changes in the profile occurring down to the 200 decibar-surface can only be interpreted by a water transport away from the coast and by the piling up of the lighter surface water near Sts. 4 and 5. These movements can be looked upon as a consequence of the winds which blow with little variation for long periods, on the average from N. 23° W. at about 6.7 m/sec, almost parallel to the coast. According to the Ekman-theory under these conditions a transport directed away from the coast can be expected. This transport can be derived from the change in the course of the density lines between the two surveys. These surface waters are carried outwards and piled up about 100 km off the coast.

From the analysis of all the fields Sverdrup has derived the mean current field shown in Fig. 304 during the period between the surveys. The calculated maximum transverse velocity seawards thereby amounts to 11 cm/sec, in good agreement with the velocity of the wind drift. Between the coast and the water piled up further out

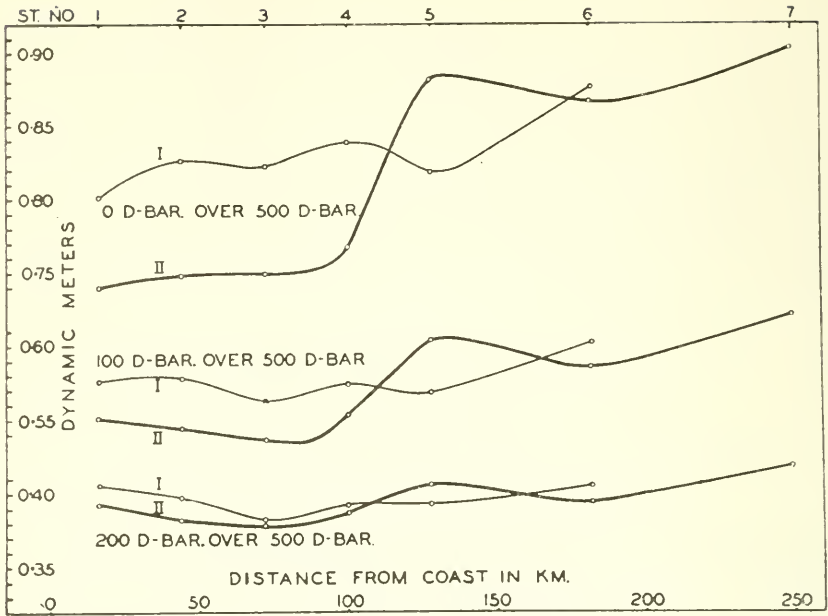


FIG. 303. Topography of the physical sea surface and of the isobaric surfaces (relative to the 500-decibar surface) for the oceanographic surveys. I, 25-26 March 1937, and II, 5-6 May 1937, of the profiles through the Californian region of upwelling water (according to Sverdrup).

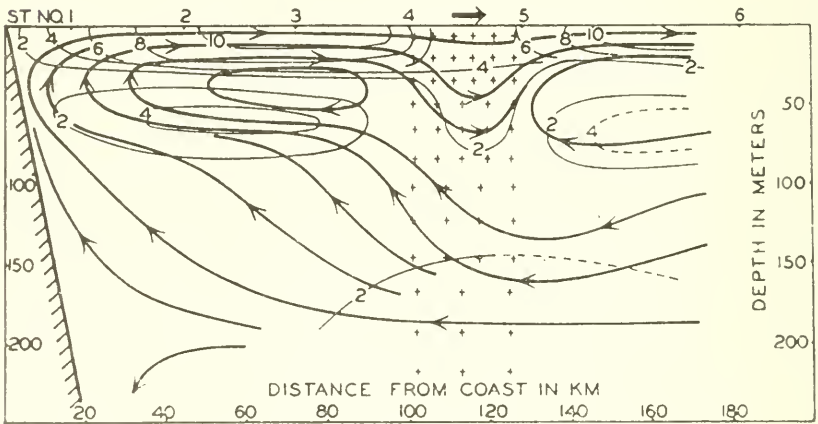


FIG. 304. Computed mean vertical circulation for both profiles I and II in the cross-section through the Californian region of upwelling water (according to Sverdrup). The direction of the motions is indicated by the thick lines with feathers; the horizontal velocities are given by the thin lines. The region indicated by + + + + + shows a zone with stronger flow parallel to the coast and directed into the picture.

there is a partly closed circulation down to a depth of 80 m. In the upper half of this circulation the water flows away from the coast, in the lower half towards the coast. Near to the coast the water rises and in the region remote from the coast it sinks along a boundary layer. This outer boundary layer itself moves away from the coast and as a compensation a replacement has to be made from below (from depths of not more than 200 m). In other cases dealt with by Sverdrup conditions are somewhat more complicated but the essential characteristics are retained.

In a study of the large amount of observational data, on the Californian upwelling region, collected by the Scripps Institution of Oceanography in La Jolla, DEFANT (1950, 1951) it has been shown that the piling up and upwelling processes are associated with characteristic displacements of the sea surface and of the internal boundary layer which gradually develop under wind influence and adjust with simultaneously formed and normal to the coast occurring circulations. They finally tend towards a stationary state. These condition can be illustrated by two opposite cases. During the first cruises (28 February to 15 March 1949) it was found that the wind component *towards* the coast predominated over the entire region with a maximum of 5 m/sec and caused considerable piling up of water along the coast. During the second cruise (27 April to 15 May 1949), in contrast to the first case, the water was driven *away* from the coast where as a consequence upwelling occurred.

Cruise 1 thus is a typical example for a water accumulation along the coast, while cruise 2 is typical for coastal upwelling. Figure 305 shows the dynamic topography of the ocean surface represented by lines of equal positive and negative deviation from the basic distribution produced by the Californian Current flowing south. This basic distribution has been obtained by elimination of the disturbances caused by tide waves and internal waves (DEFANT, 1950). The two cases show completely opposite trends. First of all it may be noticed that the channels of positive and negative deviation (shown by the contours) are more or less parallel to the coast following the wave-like form of the disturbance, thereby forming a marked regular pattern. In cruise 1 the coastal strip shows a pronounced positive deviation—with maximum values at the coast. Outside this there is a strip of negative deviation, then farther out a strip of positive deviation, and finally a second negative strip forms the western border of the region. Cruise 2 gave the same pattern with the signs reversed.

In cruise 1 there is undoubtedly a piling up of water at the coast; it was fully developed at the beginning, but during the remainder of the cruise (about two weeks) it could be maintained to this extent only if the tangential wind stress towards the coast exactly balances the pressure gradient of the sloping physical sea surface. The water masses piled up on the continental shelf are drawn from the oceanic strip just off the continental slope; there the sea level consequently lies somewhat deeper (trough-like form). This disturbance then develops wave-like oscillations farther westwards and generates the adjoining disorders. Exactly the same applies to cruise 2 but instead of piling up of water a depression in water level occurs. Consequently, to these primary disturbances the adjacent displacements in the sea level thus take place in the reversed order.

The dynamics of the processes of upwelling and removal of water as a surface drift requires that the rise and fall of the physical sea surface should be accompanied by a corresponding fall and rise in the density transition layer. In these processes (close to a

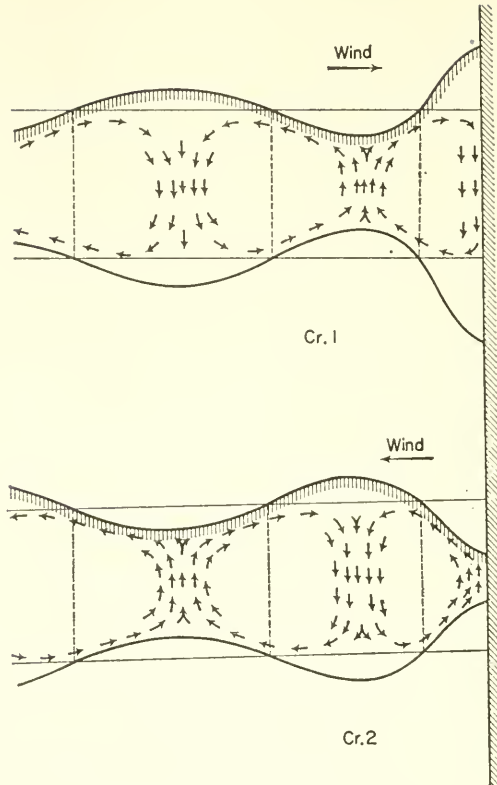


FIG. 305. Position of the physical sea surface and of the internal thermohaline boundary surface and the corresponding circulation cells of the upper layer during the cruises 1 and 2. In the first case: "Anstau" at the coast (piling up of water); in the second case: upwelling off the coast. The inclinations of both boundary surfaces are strongly exaggerated, that of the physical sea surface by far more than that of the thermocline.

stationary equilibrium) in a sea composed of two layers, the displacement of the physical sea surface is always inverse to that of the internal discontinuity surface. However, the fluctuations of the internal discontinuity surface is many times greater (inversely proportional to the difference in density of the two water masses). Figure 306 shows a schematic cross-section for cruises 1 and 2. The effect of the wind on the sea surface gradually builds up to such a stage where the wind effect is exactly in balance with the developing pressure gradients. While approaching this stage *circulations* have developed mainly in the mixed layer, and must take the form shown in Fig. 306. On cruise 1 the water accumulation at the coast causes a downward circulation here and a sinking of the density transition layer. Upwelling occurs in the trough forming outside this region of accumulation.

In contrast to these conditions, during cruise 2 the water is driven away from the coast, where upwelling thus takes place and the water masses sink down in the accumulation region away from the coast. These primary circulations at the coast are followed further out by successive secondary circulations of diminishing intensity.

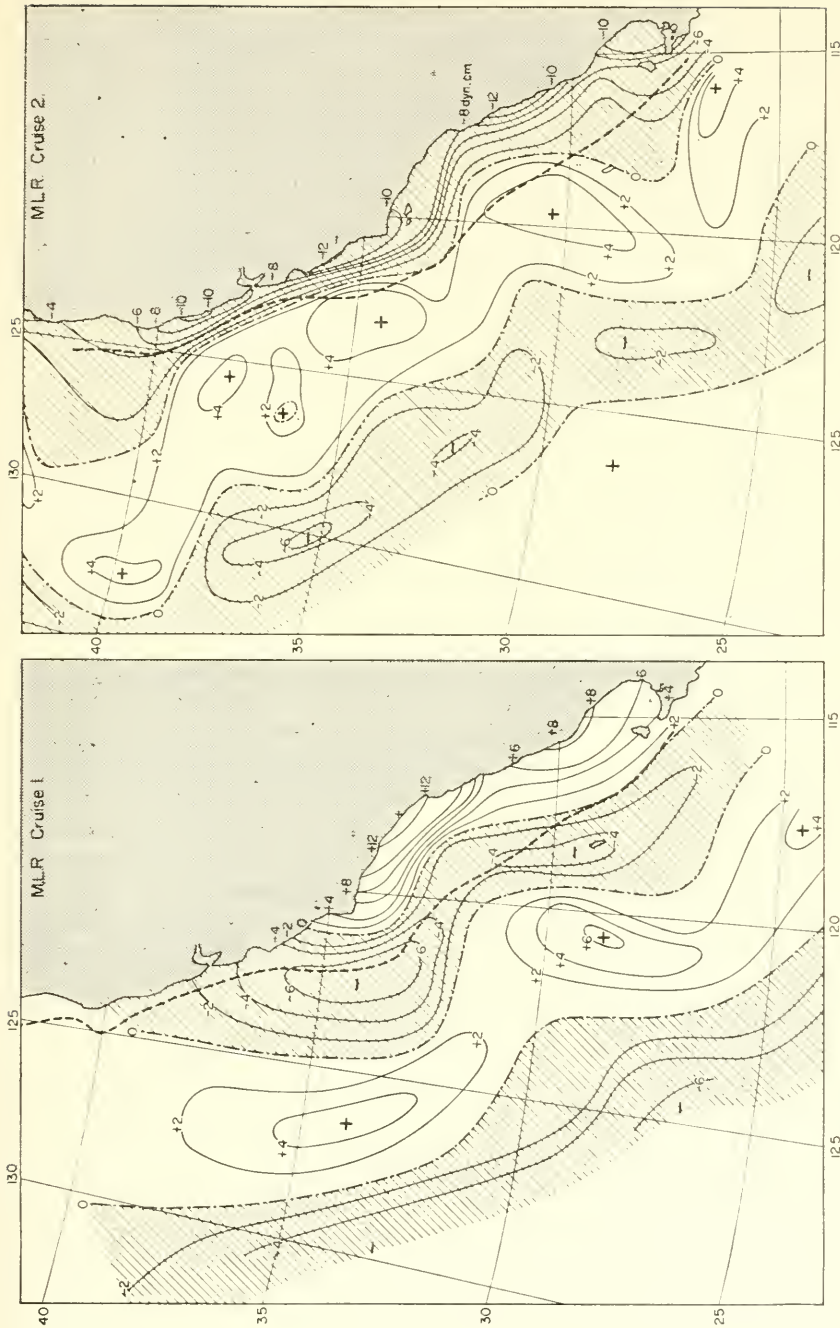


FIG. 306. Dynamic topography of the sea surface given by lines of equal positive and negative deviation from the basic distribution (drawn with intervals of 2 dyn cm). *Picture to the left*: cruise 1 (28 February to 15 March 1949). Piling up of water at the coast, "Anstau"; *Picture to the right*: cruise 2 (28 April to 14 May 1949). Upwelling of water at the coast.

To the Dynamics of Upwelling

There are a number of causes for the vertical water movements in the ocean. For continuity reasons these vertical motions are closely connected with the divergence and convergence of the surface waters, and there is no doubt that the upwelling and sinking of oceanic waters is primarily connected with convergence and divergence regions occurring at the sea surface. The cause of these divergences and convergences in most cases lies in the distribution of wind stress exerted by the prevailing wind on the sea surface. A totally satisfying explanation of upwelling at continental coasts has not yet been given, and is probably not possible at all since the total process is composed of a number of substages each of which is always controlled by other factors. Coastal upwelling is confined to a narrow strip close to the coast (less than 100 km) and must therefore be regarded as a boundary phenomenon.

It is a known fact that winds blowing at a suitable angle to a coast will carry light surface waters away from it and the water mass transported away must be replaced near the coast by heavier subsurface water. DEFANT (1952) gave a theoretical explanation on the assumption of a sea composed of two layers with different density; previous to this a more general investigation was made by Jeffreys on the effect of a steady wind on the surface of a homogeneous ocean near the coast. The application of a theoretical model as simple as this showed that the stationary wave disturbances at right angles to the coast take their origin from the piling-up region or the upwelling region ("Anstau oder Auftriebsgebiet") near the coast (see Fig. 306) and gave results in good agreement with those obtained by observation.

A theory of the upwelling produced by a wind parallel to a coast has been given by HIDAHA (1954) whereby the effect of the earth's rotation and the frictional forces due to both vertical and lateral mixing have been taken into account. He deals only with a case of a steady state. The equations of motion, together with the equation of continuity and the boundary conditions which must be satisfied at the sea surface and along the coast, give a rather complicated solution to the problem. Calculation of the magnitude of the off-shore currents and the upwelling velocity for a numerical example allows the results to be compared with values estimated correctly from observations. Figure 307 gives the solution in the form of stream lines in a vertical plane perpendicular to the coast. Upwelling develops close to the coast and there is no off-shore movement of the water in the upper layers of the sea directly beneath the surface swept by the wind. The upwelling is confined to the strip until $0.5D_v$ from the coast and the sinking process occurs outside the wind zone. If the vertical mixing coefficient A_v is chosen with a value of about 1000 then the vertical Ekman frictional depth D_v will be 162 m at 30° N. For a horizontal mixing coefficient $A_h = 10^9$ the horizontal frictional depth will be about 162 km. Estimation gives the width of the coastal upwelling region as $2D_h = 339$ km. From this the average velocity between the surface and the layer $0.2D_v$ can be calculated as 3.35 cm/sec (off-shore the maximum upwelling is 2.7 m/day upward or approximately 80 m/month). SVERDRUP (1938) obtained a similar large value for the upwelling velocity off southern California. The depth at which the upwelled water originates is about 200 m which is also in fair agreement with observed values off the southern Californian coast. Hidaka has also investigated the cases arising when the wind is at certain angles to the coast. If the wind is at right angles to the coast, then the induced circulation has a rather complicated

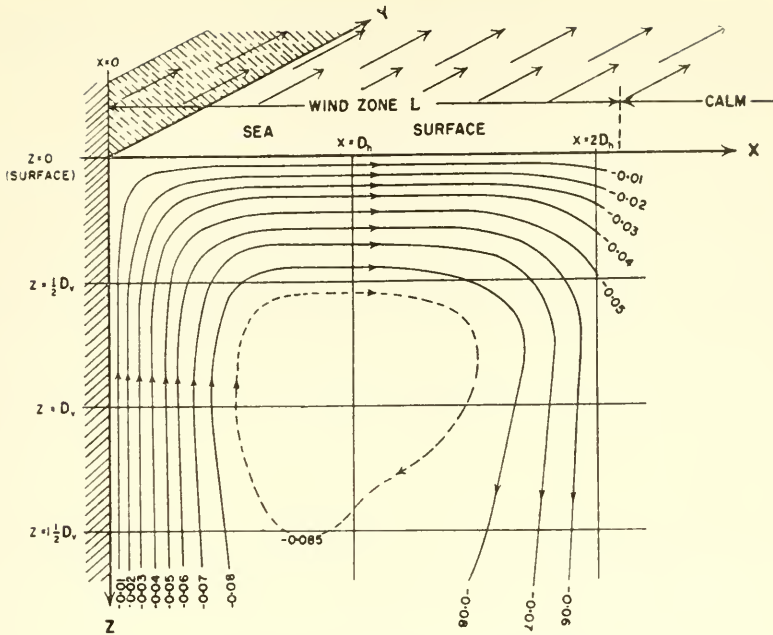


FIG. 307. Upwelling as induced by a wind parallel to the coast illustrated by the stream lines in the vertical plane perpendicular to the coast. In the numerical example $D_v = 162$ m and $D_h = 162$ km; the width of the coastal wind belt is about 340 km.

structure with two vortices in the upper layers, one of which is situated close to the coast and the other near the outer boundary of the wind belt. The upwelling due to a longshore wind (Fig. 307) is far more effective in lowering the temperature of the coastal region than that induced by an off-shore wind, since the former one brings a larger amount of colder water to the surface from deeper levels than the latter. This theory put forward by Hidaka deals only with the stationary case; no attention is paid to the water stratification which as shown by observations plays a decisive role for the processes involved before a steady state is reached.

The process of upwelling is shown by observations to be variable with time. If the duration of the wind is as short as a few hours, the off-shore component of surface water transport will not be very large since drift currents will not fully develop. If the winds are more or less steady for several hours up to as much as a day, the drift currents may develop but they will not be followed by considerable upwelling because of oscillations of the thermocline. However, the process will be different if the wind continues for several days up to a week. If the wind continues for a longer time-interval than about a week, the surface currents will reach a steady state with an intermediate stage for a wind lasting a few days up to a week during which the geostrophic equilibrium is approached. This latter section of the process has been dealt with theoretically by YOSHIDA (1955) using the conditions in Californian waters as a guide. In his model the x -axis is directed eastwards, the y -axis directed northwards and represents the coast line. The z -axis is chosen positive downwards with $z = 0$ being placed along a mean sea level. The conditions were taken as constant in a north-south

direction. In addition at this stage only small-scale processes, i.e., processes extending over a period of several days to a week and over a distance of up to 10 km, were considered of interest. The equations of motion are then

$$-fv = -\frac{\partial p}{\partial x} \quad (\text{XIX.60})$$

$$\frac{\partial v}{\partial t} + fu = \frac{\partial}{\partial z} \left(A \frac{\partial v}{\partial z} \right) \sim \frac{T_y}{H} \quad (\text{XIX.61})$$

A is the eddy viscosity, T_y is the northward component of wind stress, T and H is the average thickness of the mixed layer. The corresponding vorticity and divergence equations are

$$\frac{\partial \zeta}{\partial t} - \frac{fw_h}{H} \sim \frac{\text{curl}_z T}{H}, \quad (\text{XIX.62})$$

$$f\zeta \sim \frac{\partial^2 p}{\partial x^2}, \quad (\text{XIX.63})$$

where w_h is the vertical velocity at $z = h$ (depth of the thermocline). The equation of continuity and a condition for the quasi-isostatic adjustment with $g^* = g(\Delta\rho/\rho)$ give

$$w_h \sim \frac{1}{g^*} \frac{\partial p}{\partial x}. \quad (\text{XIX.64})$$

The mutual adjustment between the pressure and the current seems to be completed within a period of one to two days, so that the above equation is reasonable for up to about a week after this first stage of adjustment is over. From the equations (XIX.62-64) is obtained

$$\frac{\partial^2 w}{\partial x^2} - k^2 w = \frac{k^2}{f} \frac{\partial T_y}{\partial x}, \quad (\text{XIX.65})$$

where $k = f/\sqrt{(g^*H)}$. The boundary condition along the coast ($u = 0$) will require

$$\left(\frac{\partial w}{\partial x} \right)_0 = \frac{k^2}{f} (T_y)_0.$$

with the condition $w = 0$ when $x = -\infty$ the solution of (XIX.65) will be

$$w = \frac{k^2}{f} \left[\int_0^h T_y e^{k(x-\xi)} d\xi + \int_{-\infty}^x T_y e^{-k(x-\xi)} d\xi + e^{kx} \int_{-\infty}^0 T_y e^{k\xi} d\xi \right]. \quad (\text{XIX.66})$$

It can be shown that

$$w = -\frac{1}{f} \frac{\partial T_y}{\partial x}$$

for values $|kx| \gg 1$ and along the coastline we have

$$w_0 = \frac{k^2}{f} \int_{-\infty}^0 T_y e^{kx} dx. \quad (\text{XIX.67})$$

A uniform northerly wind over off-shore water will give rise to a coastal upwelling given by

$$w_0 = \frac{T_{y,0}}{\sqrt{(g^*H)}}. \quad (\text{XIX.68})$$

The upwelling velocity will be proportional to the intensity of the northerly wind but is not directly dependent on the latitude. When $g^* = g(\Delta\rho/\rho) = 2.5$, $H = 40 \text{ m} = 4 \times 10^3 \text{ cm}$ and $T_{v,0} = -0.5$ then

$$w_{x=0} = -5 \times 10^{-3} \text{ cm sec}^{-1}.$$

In five days this upwelling will give an upward displacement of the thermocline of 22 m. This upward movement of the thermocline off the coast will continue until an equilibrium is reached in about a week and according to observations seems then to be maintained for about one or two months. The region where this coastal upwelling occurs is confined almost entirely within a narrow strip close to the coast. With the numerical values introduced above, k will result to $\sim 0.7 \times 10^{-6} \text{ cm}^{-2}$; at a distance of 40 km, w will be reduced to 6% of that at the coast and to only 3% of the coastal w -value at 50 km. The process is practically limited to a distance of 40–50 km from the coast. The effective width of coastal upwelling is given by a characteristic length

$$L = \frac{\pi}{k} = \frac{\pi\sqrt{(g^*H)}}{f}.$$

Yoshida also investigated the changes in surface conditions which were derived from the above model of a transient state of upwelling. He found that the variations in surface characteristics were largely confined within the narrow coastal regions. The coastal upwelling is associated with considerable changes in surface conditions within the coastal waters of width L , while upwelling or sinking outside this strip will not give rise to such significant changes during a period of only a week or two. In the succeeding stage of the upwelling process, in which now the isostatic adjustment can be considered a complete one, the lateral mixing process in the inshore regions stands out as the most important factor. The dynamic equations are now

$$-fv = -\frac{\partial p}{\partial x}, \tag{XIX.69}$$

$$fu = \frac{T_v}{H} + A_h \frac{\partial^2 v}{\partial x^2}, \tag{XIX.70}$$

where A_h is the coefficient of lateral mixing. The upward movement of the thermocline, due to the ascending motions, will produce a sharp horizontal density gradient and when conditions are variable in an oscillatory way, as is usually the case, internal waves will originate and cause intense mixing *across the thermocline*. The equation for the conservation of mass will now become

$$w \frac{\partial \rho}{\partial z} = A_h \frac{\partial^2 \rho}{\partial x^2}$$

or, approximately

$$w = -A_h \frac{\partial^2 h}{\partial x^2}.$$

The boundary condition at the coast gives $v_0 = 0$ so that finally

$$w_h = -\frac{f}{g^*} \frac{\partial v}{\partial x}. \tag{XIX.71}$$

The equation for w will become the same as in the earlier state and the vertical velocity distribution will therefore remain unchanged throughout the whole period of upwelling process as long as the wind is kept steady. During this period the ascending water movement will be subject to mixing with the surrounding waters and the thermocline will not be raised to any large extent. From equation (XIX.71) it follows that at this stage the vorticity in the surface layer will be proportional to the vertical velocity. Upwelling will thus be associated with cyclonic vorticity in contrast to the initial inshore increase in negative vorticity produced by the coastal upwelling. This approach developed by Yoshida undoubtedly appears to give a deeper insight into the dynamics of the upwelling process, but a more specific representation in detail of these processes would be desirable.

5. Processes at the Polar Boundary of the Subtropical Convergence Region

The subtropical convergence regions are oceanic areas where the oceanographic factors show large local and time variations (p. 575). They can be interpreted as consequences of vortex formations between the two somewhat different types of water on the polar and the equatorial sides of the convergence region. On the one hand, there are intrusions of warm highly saline water from lower towards higher latitudes, and on the other hand, intrusions of cold and weakly saline water occur in the opposite direction. All the isolines of the oceanographic factors and the isolines of the dynamic topography of the pressure surfaces thus show a wave-like structure. Whether all the deviations from a smooth curved pattern are of an aperiodic nature propagated in one direction along the boundary region between the two water types and in time dying out, cannot be decided without a rapid succession of synoptic surveys. Since series-observations, made in the convergence region at quite different times, can all be combined without excluding any large number of individual values into closed comprehensive representations; it may be safely concluded that the disturbances are often *quasi-stationary* vortical disturbances whose position and extent are probably determined by external factors.

These wave-form disturbances are particularly well developed in the convergence region of the South Atlantic. The topography of the physical sea level between 25° and 50° S. (Fig. 308) shows the irregular wave-like patterns in the course of the dynamic isobaths. This starts suddenly off the broad Patagonian–Argentinian shelf and extends across the total width of the Atlantic to the region south of Africa. According to the topographies of the deeper levels these wave-form disturbances reach down to considerable depth but their intensity decreases rapidly with depth. They can hardly be detected in the topography of the 1400-decibar surface. Their greatest intensity is always found in the top layers where they must originate and therefore the reason for their formation must be looked for here. The entire oceanic structure is shifted towards the poles and the equator, respectively, by the interacting intrusions of different water masses in a strip-like manner, and thereby differently stratified oceanic spaces oppose each other side by side that would normally be found arranged in a zonal fashion. Then inside the resultant vortical formations of both water types, heavier water sinks down at the boundary surface extending to more southern latitudes, while the lighter water at the same time is lifted and extends further towards the poles. The sinking process of the heavier waters apparently does not take place everywhere along the

extended more or less zonal boundary surface, but rather in form of *individual* mass intrusions (*quantum-like*) at different places whereby as a consequence mixing is considerably increased. The nature of the processes involved can be illustrated by putting side by side successive stages of the oceanic state in a meridional section (DEFANT, 1941*b*), and one obtains thereby all the characteristics of the disturbances which occur. The bottom topography in this part of the South Atlantic was earlier assumed (p. 435) to be the cause of the wave-form current pattern appearing in the region of the subtropical convergence (Fig. 187). It should be emphasized, on the other hand, however, that the vortical disturbances originate on the shelf of the South American continent between 45° and 35° S. far in the west, and from here extend as a continuous chain of regular vortices throughout the entire area as far as the southern tip of Africa. This source region or birth place, is the region where the denser water of the Falkland Current meets the lighter water of the Brazil Current and where the tendency for a vortex formation is extremely large. Here a strong solenoidal field is continuously regenerated, which can be considered as the necessary condition out of which vortices are formed and the disturbance field then stretches far out into the Atlantic.

A probable explanation of these wave-form disturbances can be derived by means of the arguments put forward by ROSSBY and co-workers (1939) in a discussion of the sinusoidal disturbances in zonal atmospheric air currents. In a wave-like disturbance, which is superimposed on a pressure field that decreases to the south (Fig. 309,

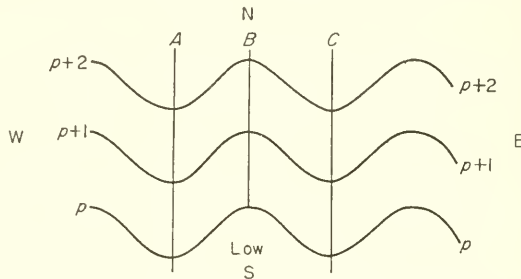


FIG. 309. Wave flow for a uniform towards south decreasing pressure field.

Southern Hemisphere) the water transport through the cross-sections *A* and *C* where there is an anticyclonic curvature of the isobars will be greater because of the occurring centrifugal force than that through section *B* where there is a cyclonic curvature. There will therefore be a horizontal divergence and pressure fall between sections *B* and *C* and a horizontal convergence and pressure rise between *A* and *B*. The wave disturbance will thus move eastwards and since the centrifugal force is larger when the curvature is greater the shorter waves will travel eastwards faster than the longer ones. In addition to this effect, there will be a pure latitude effect which originates from the relation of the geostrophic flow to the pressure gradient. Due to the Coriolis force the mass transport across the section *B* in a lower latitude will be greater than that across sections *A* and *C* in higher latitudes. This gives rise to convergence and pressure rise between *A* and *B*. This latitude effect which is independent from the wavelength causes a westward movement of the wave. Both effects are of the same order of magnitude and it is easily understood that for a particular wavelength the wave disturbance will be

stationary. The mathematical basis extended by HAURWITZ (1940) affords a relation between the wavelength L , the latitudinal extent D of the stationary disturbance and the velocity of the basic current, U , in the form

$$U = \frac{\beta}{4\pi^2} L^2 \frac{1}{1 + L^2/D^2},$$

whereby $\beta = \partial f/R\partial\phi = (2\omega \cos \phi)/R$ is the change of the Coriolis parameter f with latitude and R the earth radius.

Analysis of wave disturbances in the South Atlantic convergence region gives an average disturbance length at latitude circle 38° S. of $10\cdot0^\circ$ or 880 km. The latitudinal extent averages 15° or 1650 km. With these values the velocity of the basic current U is obtained as between 26 and 28 cm/sec. This means that the wave disturbance within the zonal basic current (oceanic West Wind Drift) can be *stationary* only if such a mean velocity towards East is present. Current charts show an average surface velocity of 25–30 cm/sec. It is thus very probable that the stability of the stationary wave system in the convergence region is due to an equilibrium state between the action of the latitudinal dependence of the Coriolis force and the effect of the curvature of the current trajectories on the horizontal mass transport. The strong solenoidal fields at the boundary between the Brazil and the Falkland Currents may be responsible for the formation of the eastward following series of vortical disturbances inside the general oceanic West Wind Drift. If this is so then the topographical effect of the bottom configuration will be only a supplementary effect which may intensify and probably modify these disturbances.

Similar phenomena may also develop in the North Atlantic. In the oceanic strip of the North Atlantic Current to the north of the subtropical convergence region there are marked pulsations that also stand out clearly in the charts of the dynamic topography of the individual isobaric surfaces and in that of the physical sea level. The results of the International Gulf Stream Survey (1938) to the north of the Azores enabled a study to be made of the oscillations in the current system in this particular region. The oceanographic work of the "Armauer Hansen" in 1909, 1925 and 1935–6 in the Norwegian Sea off the coast of Norway (HELLAND-HANSEN, 1934, 1939) showed that vortices with vertical axes probably played an important role in the interior of the Atlantic Current. They are also associated with considerable variations in mass transport. It is rather obvious that such variations at fairly long intervals cause reactions in the oceanic phenomena in the Arctic and take influence on climatic conditions in the Scandinavian countries. At present, however, the investigation of these phenomena is only at the very beginning and systematic and synoptic surveys are required in order to obtain a deeper insight into the mechanisms involved. An unusual theory of the variations of the surface circulation in the North Atlantic, especially of the current branches off the coast of Europe, has been given by LE DANOIS (1934) in his *Atlantic Transgressions*. He distinguished between three water types in the Atlantic: the tropical, the polar and the continental. The latter has an extremely variable salinity and remains at shallow depths in a relatively narrow band along the coasts. His "transgressions" are periodic movements of variable amplitude carrying Atlantic water of tropical origin, in temporary intrusions into water masses of polar and especially continental origin. The water of the transgressive masses always has a

salinity greater than 35‰. From a large number of individual cases Le Danois has attempted to derive definite rules according to which these transgressions move to the north-east. These intrusions of Atlantic water into north-west European waters are discernible only in their effects on the "continental" water masses over the shelf. Here the warm transgressions at the surface over the continental plateau always are preceded by highly saline transgressions in the deeper layers. The transgressions appeared nearly always to follow the course of the valleys of the submarine relief. The direction of spread is mainly to the north-north-east, so that the speed of this spread of the intrusions is the less the more it deviates from this direction. By following these phenomena in the sea off the coast of France for a large number of years Le Danois has found certain periodicities in the occurrence of the transgressions, which superimpose each other in the same manner as waves.

However, it appears difficult to follow the Le Danois theory of these transgressions, since he uses several arguments quite contradictory to the established fundamentals of dynamic oceanography (SCHUBERT, 1935).

Chapter XX

The Stratospheric Circulation

1. Introduction

BEYOND the polar convergence (oceanic polar front) towards the poles the oceanic stratosphere reaches upward to the sea surface and is here subject to the full influences of the atmosphere (radiation, evaporation, precipitation, freezing processes and others). The water types continually formed by the climatic conditions here are heavier, due to their low temperature and in spite of their low salinity, than the waters of the adjacent convergence regions of the oceanic troposphere. Thus, in relation to these latter water types they tend to sink, intruding beneath the oceanic troposphere, until they reach a depth corresponding to their density. The sinking, strongly favoured by the thermo-haline structure, reaches down to great depths. After sinking, the almost horizontal spread of the water underneath of the troposphere causes a layered leaf-like structure in the oceanic stratosphere. When this structure is sufficiently well developed it is therefore possible to tell from it something about the path of spread of the water masses and gain thereby an insight into the stratospheric circulation. This is the method that has been used up to the present time in the study of the water movements inside the stratosphere. In the absence of sufficient direct current measurements, however, the results of such investigations were largely only of a qualitative nature. Preparation of the observational data according to dynamic methods can provide further insight into the nature of the stratospheric oceanic flow, but at the present time only a few investigations of this type have been made. All these methods, of course, give *mean* conditions only. Over large parts of the ocean, however, especially for the deeper layers the basic prerequisite of stationary movements will be satisfied. But aperiodic disturbances of shorter or longer duration and of greater intensity undoubtedly occur. By means of the observations available at present, and also due to the manner in which they have been gained, it seems hardly possible to draw any conclusions about the nature of these disturbances.

The surface layers of the oceanic stratosphere poleward (the polar fronts) are, of course, subject to wind influence, so that also in the polar and subpolar seas wind-driven ocean currents are generated. The complicated orographic configuration of the continents in the Northern Hemisphere affects the nature of these surface currents and exerts strong influence during their transformation into gradient currents. In this way, piling up (Stau) phenomena play the principal role, and meridionally oriented coasts in higher latitudes form excellent guiding channels for southward outbreaks of the cold polar water masses. The zonal polar circulation obtains in that way meridional components, so that on the eastern sides of polar land mass water flows south, while on the western sides mainly water of subtropical origin flows north.

2. Polar Currents of the Northern Hemisphere

Phenomena similar to those found in the subtropical convergence region can be expected also to occur at the polar convergences. These will be even more intensive there, since a much sharper density difference exists between the adjacent water masses. External factors will, at many places, cause the formation of vortices between the warmer highly saline waters of subtropical origin and the cold weakly saline polar waters. These travel along the boundary zone, continually forming and disappearing and thus giving rise to a continuous mixing of the two water bodies. For these reasons, in the Northern Hemisphere, the left-hand border of the polar currents is not sharply developed and here polar waters and water masses of subtropical origin work into each other. This is shown to be true for all currents, especially for the East Greenland Current along its boundary region against the Irminger Current to the south of Iceland and for the Labrador Current where it encounters the Gulf Stream.

Some insight into the processes involved in the vortex formation in the region of interaction between two adjacent water masses, especially as found in this part of the ocean, has been obtained from the almost synoptic surveys made by U.S. Coast Guard vessels (see the bulletins of the U.S. Coast Guard, International Ice Patrol, Washington).

The sea around Greenland (Greenland Sea, Labrador Sea, Davis Strait and Baffin Bay) has been well surveyed oceanographically by numerous expeditions, and from the entire data available it is possible to obtain an idea about extent and course of all the currents. This is especially true of the *East Greenland Current* which can be followed along its entire course from the Denmark Strait to Cape Farewell and from thereon as the West Greenland Current until it finally disappears (see DEFANT, 1936*b* for references). Little information is available on the East Greenland Current from its origin near the Spitzbergen Rise to the Denmark Strait but there are appreciably more data to the south of this strait. All cross-sections show a similar structure. The polar water layer always has a cold core in which the temperature is almost at freezing point. Figures 310 and 311 show two cross-sections through the East Greenland Current in the Denmark Strait and off Cape Farewell. The analysis of 37 sections of this type through the East and West Greenland Currents has enabled the course of the polar water flowing around Greenland to be followed in detail. In Fig. 312 an attempt has been made to show the boundary separating polar water from Atlantic water; in addition, the average minimum temperature in the core layer of the polar water is indicated in this figure which is usually at a depth of 80 m. The minimum temperature in the core layer gradually rises from -1.7°C in the Denmark Strait to about -1.0°C at Cape Farewell. Past the southern tip of Greenland, where the current turns sharply around, the core layer rises towards the surface; its temperature increases rapidly and from about 61°N . on is usually no longer negative. The East Greenland Current from the Denmark Strait southwards where the width of it is more than two-thirds of the width of the strait remains entirely over the shelf; where the shelf is broad the current is also wide and where the shelf is narrow (for instance between 62° to 63°N .) its width is very small and does not exceed 25 to 30 nautical miles. The lens of cold water forming the current core at first extends well to the east, but becomes smaller towards south and shrinks from the Denmark Strait to Cape Farewell under the impact of the warm water of the Irminger Current. It is, however, still present and shows that the polar

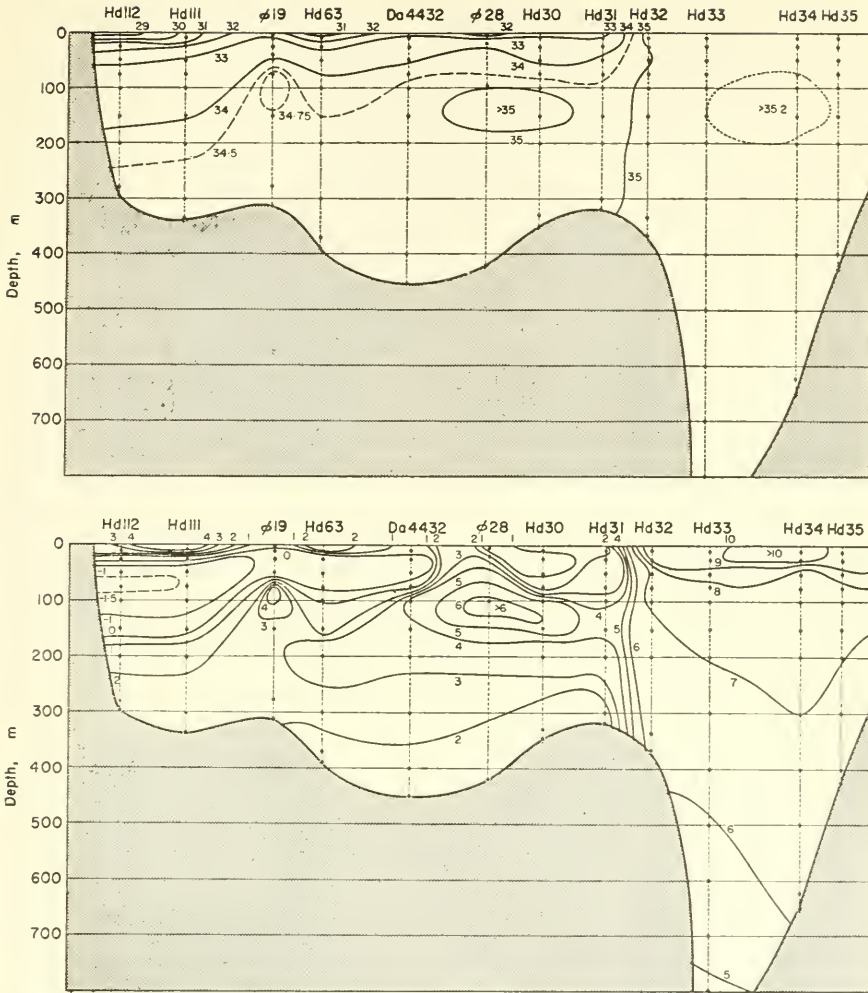


FIG. 310. Vertical cross-section through the East Greenland Current for the region of the Denmark Strait at about 67° to 65° N.; below, temperature; above, salinity.

water is an uncustomary water type in the oceanic space under consideration and is maintained only by continuous renewal. The intrusions of the Atlantic water occurs in the form of vertical vortices which break through the polar front, broaden and deepen and if the inflow weakens soon disappear. (DEFANT, 1930a; BÖHNECKE, HENTSCHEL and WATTENBERG, 1930-32). From Cape Farewell the current bends northwards still keeping also here over the shelf. At first the cold core layer is still present but its temperature rises rapidly indicating stronger mixing with the Atlantic Water penetrating northwards along the continental slope. From about 64° N. the current weakens more and more and near the Davis Strait (about 66.5° N.) there are only traces of the cold core layer found off the Greenland coast. In this region, in all

profiles, another core layer at about 80 m depth shows, which must clearly be fed from the north-west by cold polar water that flows in through the Davis Strait with the southward along Baffin Land directed current and finally joins the Labrador Current.

As yet no dynamic preparation has been made of all the available data for the East Greenland Current. Topographies of the physical sea level and the isobaric surfaces in this region are also contained in Fig. 271 (see also Fig. 200). The downward slope of the isobaric surfaces from the Greenland coast towards the open sea is quite large and shows clearly the entire system of the East and West Greenland Currents. This current system can no longer be seen in the 800 decibar surface; the stronger current intensity is thus confined to the top layers.

The main cause for the development for the East Greenland Current must lie in the wind- and atmospheric-pressure conditions over the North Polar Basin. At all times of the year due to wind and atmospheric pressure the water is driven eastwards and water laden with pack-ice and drift-ice is carried towards the coast of north-east Greenland. Here they find, supported by the wind turn towards south, a guiding channel in the form of the Greenland coast. The pressure due to the piled up water in combination with the action of the deflecting force of the earth's rotation produces a southward gradient current. It could be expected that these cold weakly saline waters on penetration into the warm but highly saline Atlantic water masses would soon be dispersed by mixing. This is not the case and they still show, only slightly weakened, as far as the southern tip of Greenland. They are maintained only by the continuous advection of polar water from the north and by the climatic régime which maintains the inland ice in Greenland. The polar climate generated by the inland ice, together

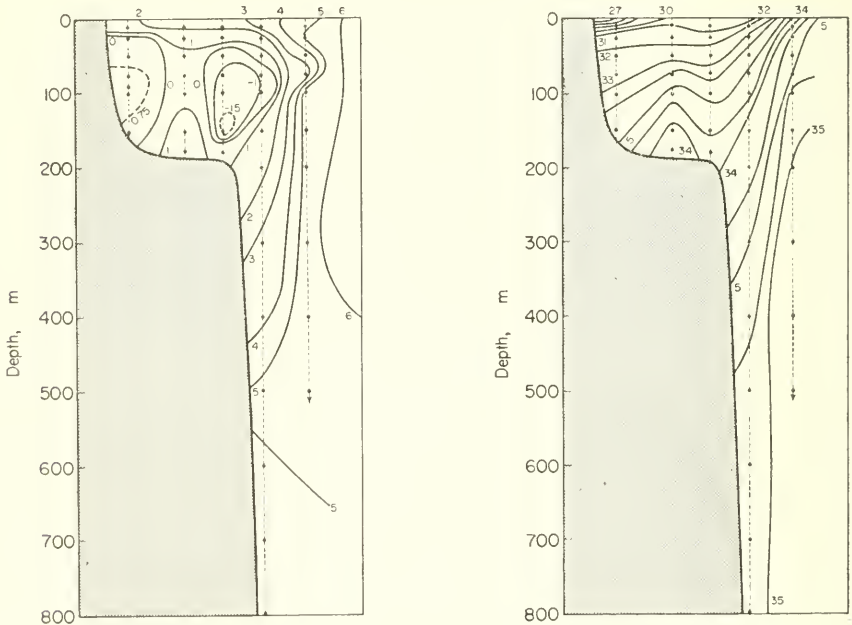


FIG. 311. Vertical cross-section through the East Greenland Current somewhat north of Cape Farvel (about 60° N.); left-hand side, temperature; right-hand side, salinity.

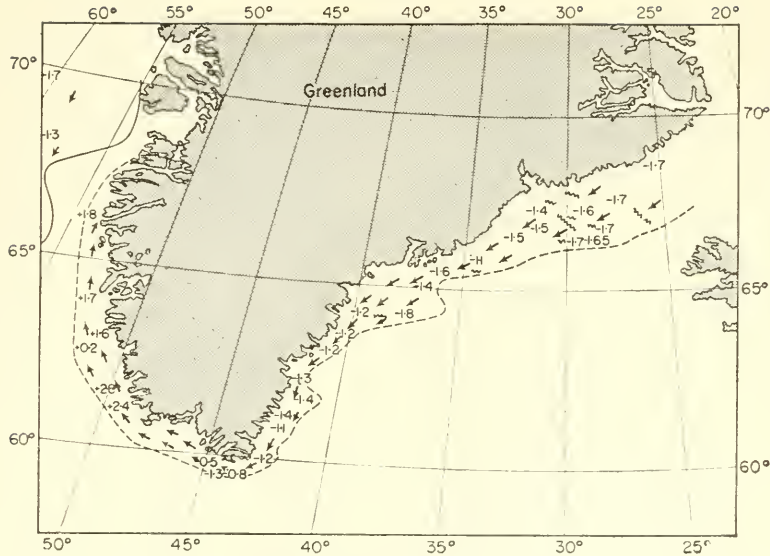


FIG. 312. Spreading of water masses of the East and West Greenland Currents derived from 35 oceanographic cross-sections. — — — — —, limit between the east and west respectively of Greenland Current and the Atlantic water. — — — — —, limit of the core layer of the Baffin water -1.8°C : minimum temperature in the core layer of the polar water.

with the continuous transport of cold inland air which spreads well out over the sea, produces a belt around Greenland in which the temperature is lowered so much that also there a polar climate prevails. Within this belt the East Greenland Current maintains itself as a polar current as far south as 60°N .

An excellent monograph on the water masses of the oceanic region between Greenland and North America with numerous temperature and salinity sections and velocity profiles calculated on the basis of these sections is that by SMITH, SOULE and MOSBY (1937). For a general understanding of conditions here any of the cross-sections can be selected from each current section since the main features are very similar in all of them. Figure 313 shows these conditions in a cross-section through the Davis Strait. The different water types moving through the strait are clearly shown, in particular by the temperature distribution. Water with a temperature of less than -1°C keeps well towards the Baffin Land side and forms the core of the Baffin Land Current; its centre is found at about 100 m depth and here as shown by the velocity profile the current direction points towards south. On the western side of the strait there is a warm weakly saline top layer flowing northwards with a small velocity that represents the last branching remnants of the West Greenland Current. There is a core of warm and highly saline water at about 400 m depth; this is Atlantic water that moves northwards within the lower layers of the West Greenland Current along the continental slope. Along the 600 nautical miles that this water travels in about 3 months from Cape Farewell its temperature falls by 4°C and the salinity by 0.50‰ due to mixing. The Labrador Current, after reinforcement by the inflow through Hudson Strait, also keeps close to the continental coast and as in the case of the East Greenland

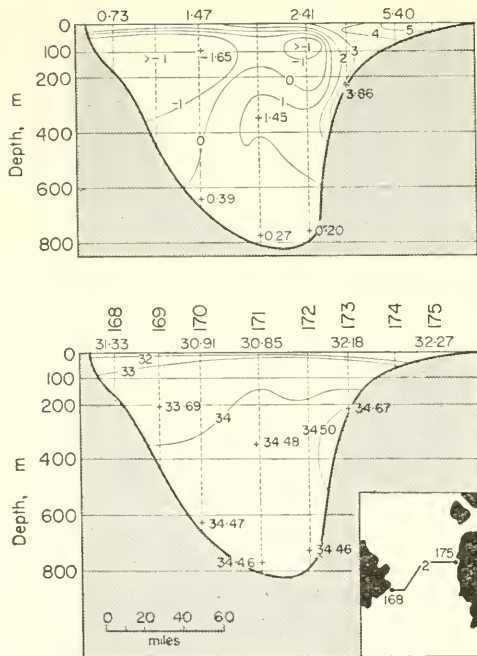


FIG. 313. Cross-section of temperature (above) and of salinity (below) through the Davis Strait ("Godthaab" stations 168-175, 17-19 September 1928).

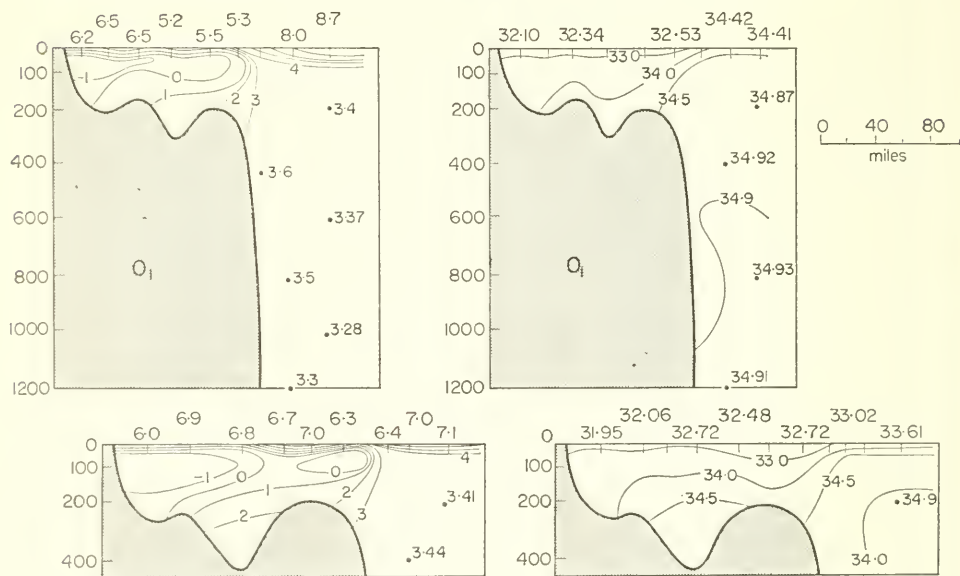


FIG. 314. Above: cross-section O₁ of temperature (to the left) and of salinity (to the right) through the Labrador Current near the Belle Isle Strait ("General Green" stations 1333-1341, 7-8 August 1931). Below: Cross-section P₁ of temperature (to the left) and salinity (to the right) through the Labrador Current near White Bay ("General Green" stations 1229-1238, 6-7 July 1931).

Current the shelf forms the main path of the southward-flowing cold, weakly saline water. Figure 314 shows this in a marked way and is characteristic of all the cross-sections from Davis Strait to the Newfoundland banks.

A calculated dynamic topography of the sea surface relative to that of the 1500-decibar surface based on a dynamic evaluation of all the observational data (1928-35) is shown in Fig. 315. This gives some idea of the current conditions in the very upper layers, since it should correspond rather well to the absolute topography. The trough-like depression of the water level between Greenland and Labrador stands out particularly well in this figure, with an even narrower continuation reaching southward as far as the southern end of the Newfoundland Banks. The strong concentration of the dynamic isobaths and a high coastal water level off south-west Greenland indicates the West Greenland Current and off the north-east coast of America the Labrador Current, while the strong rise from the southern peak of the Newfoundland Banks towards the north-east is due to the Gulf Stream. According to the topographies of the 600- and 1000-decibar surfaces, the strength of the currents decreases very rapidly with depth. In the region of the Labrador Current there are differences in water level of about 30 dyn. cm at the sea surface while over the same distance the difference in sea level at 600 decibars is only 3 cm and at 1000 decibars is not more than 1 dyn cm. These currents are thus typical density currents and are confined to the top layers.

Volume transports calculated from the velocity profiles for several different cross-sections are given in Table 154 which also gives a rough budget for the water and heat exchange amounts in the Labrador Sea. The pure gain in water is about 7.5 million m³/sec while the outflow along the Labrador Coast amounts to about 5.6 million m³/sec. Both values refer to a transport down to 1500 m depth. This gives a difference of 1.9 million m³/sec from which the authors assume that it is the water of the West Greenland Current that sinks down to depths below 1500 m and very probably flows out of the Labrador Sea in the deepest layers. Figures for different seasons and for different years vary considerably; for instance the transport of the Labrador Current was 1.31 million m³/sec in 1930 and 7.60 in 1933. From this it must thus be concluded that

Table 154. Exchange of water and heat in the Labrador Sea
(after Smith, Soule and Mosby)

	Exchange of	
	Water × 10 ⁶ m ³ sec ⁻¹	Heat × 10 ⁹ kg cal
Inflow		
West Greenland Current (average at Cape Farewell)	5.0	17.5
Baffin Land Current	2.0	-1.2
Hudson Bay discharge	0.5	0.5
Total	7.5	16.8
Outflow		
West Greenland Current to Baffin Bay	1.0	0.5
Labrador Current (average South Wolf Island)	4.6	14.6
Total	5.6	15.1

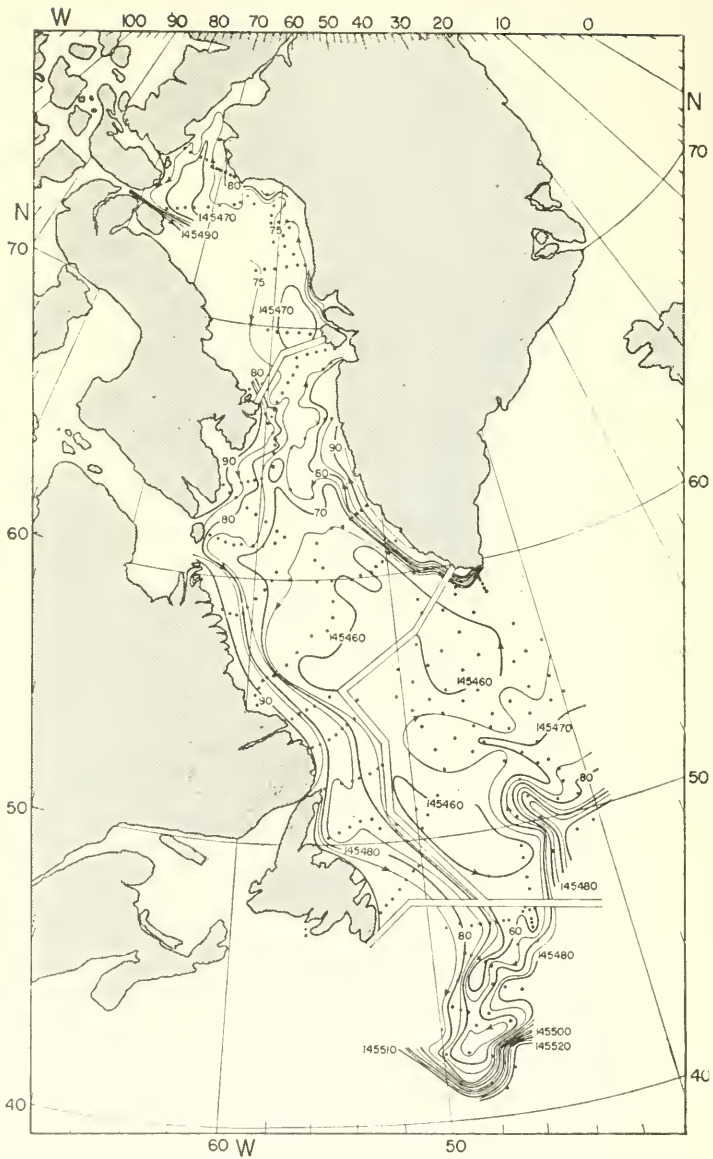


FIG. 315. Dynamic topography of the physical sea surface in the region of the Davis Strait and the Labrador Sea, relative to that of the 1500-decibar surface (Mean for the period 1928-35, according to Smith, Soule and Mosby).

the out-flow from the Labrador Sea is subject to large variations dependent on a number of different phenomena occurring at the sea surface of the polar regions (see also KILLERICH, 1939).

Table 156 also contains a heat budget for the Labrador Sea. The heat gain amounts to 1.7×10^9 kg cal/sec. If the mean temperature of the waters which sink below 1500 m is taken as 3.2°C then the heat flux with the outflow mentioned above will be about 6.1×10^9 kg cal. This then gives for the Labrador Sea a heat deficit of 4.4×10^9 kg cal. It is not improbable that this heat deficit according to its magnitude is totally compensated by the heat absorption of solar radiation in the water during the summer. It can be calculated that of the total radiation from sun and atmosphere about 20×10^9 kg cal reach the sea surface of the Labrador Sea. Of this then more than 40% (8×10^9) is lost by reflection; the remaining 12×10^9 kg cal goes to radiation, evaporation and absorption. Since the radiation is probably not very effective, about two-thirds of this goes to evaporation and one third or about 4×10^9 kg cal to absorption. This quantity is of the same order of magnitude as the quantity given above, but due to the uncertainty of the calculation this result should only be accepted with reservations.

3. The Processes which occur at the Antarctic Convergence Zone

The causes for the formation of an Antarctic convergence within the broad oceanic West Wind Drift of higher latitudes in the Southern Hemisphere were discussed on p. 549. This discontinuity layer in the thermo-haline structure of the upper water masses appears in the pressure field as a discontinuous step in the meridional slope of the isobaric surfaces and the physical sea level (Fig. 253). This can also clearly be seen in representations of the dynamic topography of the isobaric surfaces constructed by DEACON (1937) according to the data obtained by the "Discovery" for the broad ring of water surrounding the Antarctic continent. Figure 316 shows the dynamic topography of the physical sea level (relative to that of the 3000-decibar level) for this oceanic region. The downward slope of the pressure surfaces towards south at all meridians is not uniform and a discontinuity extends all around the earth that makes the meridional gradient much stronger in a belt coinciding with the Antarctic polar front. This frontal zone is also shown to exist in the topographies of the isobaric surfaces for larger depths; but corresponding to the much smaller gradient it is less strongly developed in the deep sea.

From the analysis of a series of vertical sections between Antarctica and South America (partly in the Drake Strait) as well as at 30° W. in the South Atlantic between 36° and 50° S. based on the observations of the "Discovery" SVERDRUP (1933a) has deduced the vertical circulation in the Antarctic Convergence Zone. Since conditions around the Antarctic continent are very uniform, the results should be typical for the whole of the circumpolar region. The essential details can be seen in the temperature, salinity and oxygen sections at 30° W. shown in Fig. 317. According to all such meridional sections and also according to those for the other oceans the water masses of the upper layers south of the Antarctic Convergence sink down along the boundary layer. In the salinity distribution this is clearly shown by a tongue of weakly saline water. At the polar front at first the water sinks immediately down to 400 m and then spreads almost horizontally to the latitude of the subtropical convergence region where

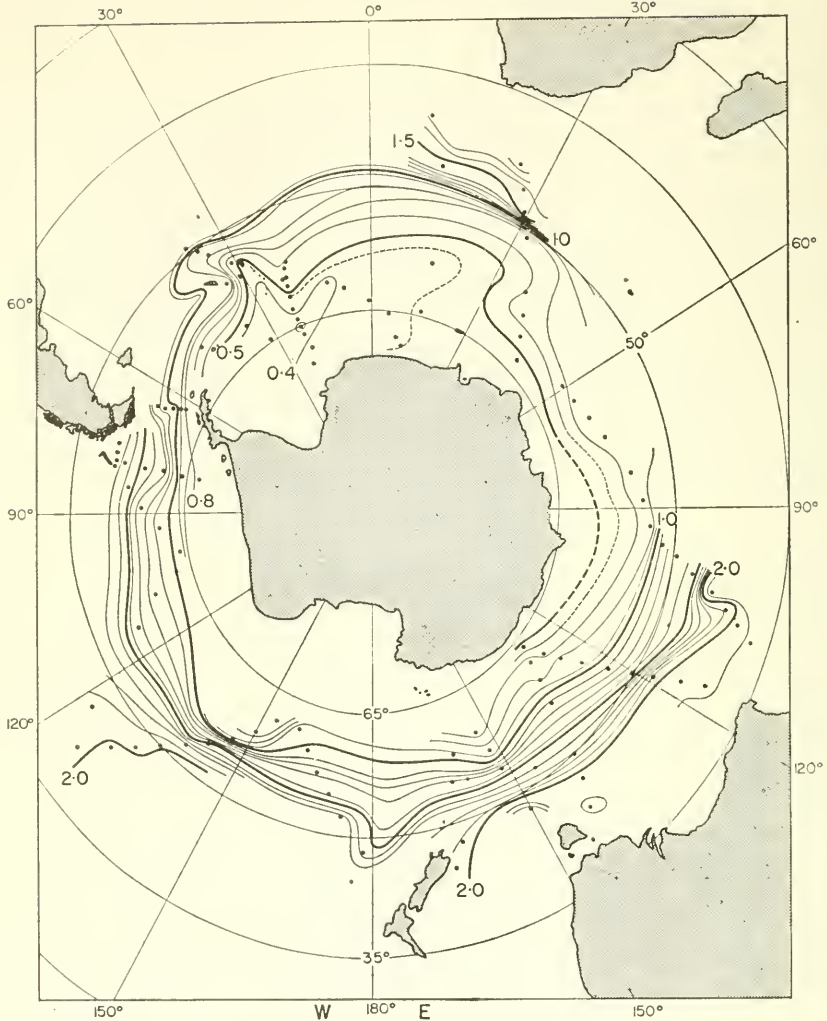


FIG. 316. Dynamic topography of the physical sea surface relative to that of the 3000-decibar surface (according to Deacon). The figures are anomalies of the dynamic depths referred to a homogeneous ocean of 0°C and a density σ_t of 28.00.

it sinks again rapidly to 800 m or more. The temperature sections show a tongue of relatively warm water beneath the Antarctic water of the uppermost layers that forms an intermediate layer between 400 and 800 m and must be interpreted as a returning current flowing back towards south. Since this warm intermediate layer is found everywhere it seems to be a general phenomenon. Above it, in all sections (in summer), a tongue with a lower temperature is found directed *northwards* at a depth of between 80 and 200 m. This stratification is no effect of a northward water transport but is rather a remainder of the cooling which has been effective during the previous winter (see Pt. I, p. 137).

In the deep layers the salinity distribution indicates a deep flow from north to south between 1800 and 3200 m and, beyond 40° S, gradually rising to 1000 m, while in the far south just off the Antarctic continent the cold Antarctic water sinks to the bottom layers of the ocean. The following sections of this chapter are devoted to these processes.

Inside the water masses south of the convergence there is thus found in the upper layers a vertical circulation that extends down to about 1000 m which occurs in an anticlockwise sense when looking towards east. The uppermost layers are carried northwards by the wind, sink down at the Antarctic convergence and form the main constituent of the subantarctic intermediate current. Part of this water mass, however, mixes with deep water and returns southwards in the Antarctic circumpolar ocean as a warmer intermediate current. The top layers of sub-Antarctic water are rich in plant

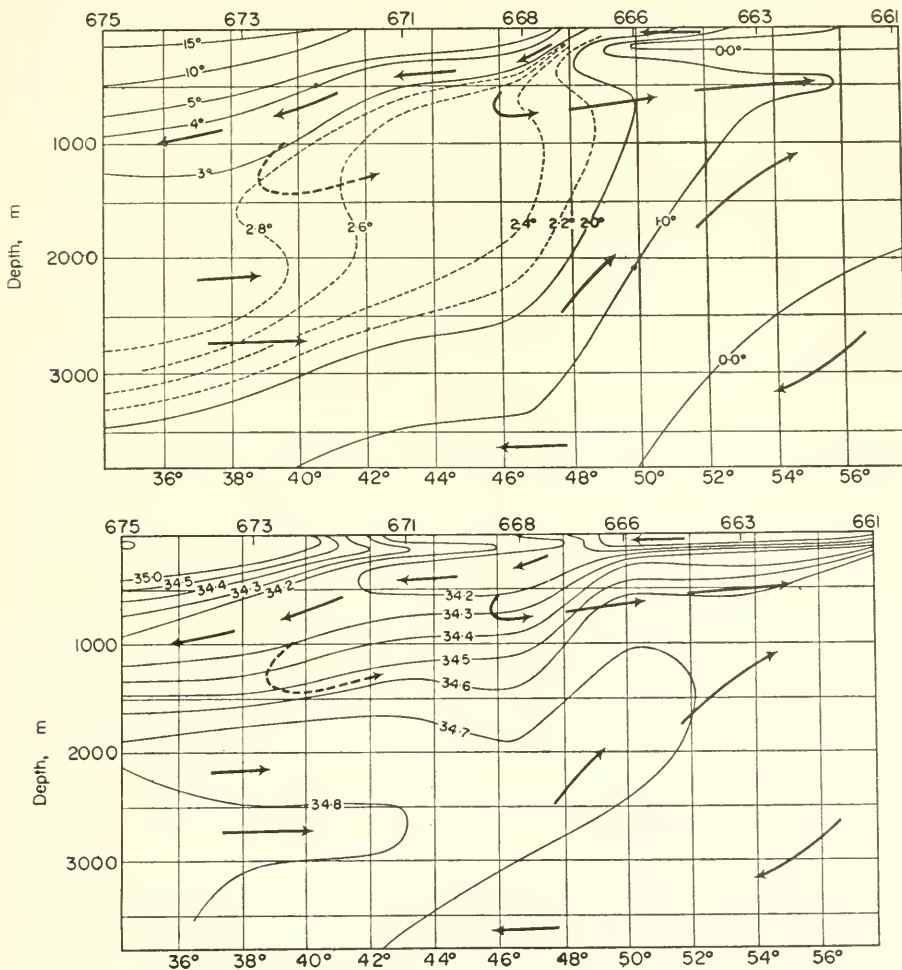


FIG. 317. Distribution of temperature (upper picture) and of salinity (lower picture) in a vertical section at 30° W. from 34° S. to 58° S. in the South Atlantic Ocean (series measurements of the "Discovery II", end of April 1931, according to Sverdrup).

and animal organisms. Dead organisms sink downwards and decompose and therefore the water of the returning intermediate current is also rich in phosphate. The lower oxygen content in and just beneath the returning current indicates strong oxidation of organic matter. Since only a part of the water transported in the uppermost layers returns to the south there must be a compensating poleward component in the deep layers in order to replace the cold polar waters sinking down in the very southern latitudes along the Antarctic continental slope. Beneath the vertical circulation of the upper layers there should therefore be a somewhat weaker one which rotates in a clockwise sense looking east. These vertical circulations are superimposed on a general basic movement towards the east so that the resultant motion occurs in form of elongated spirals. In these circulatory motions of the water the water properties are altered in the upper layers by influences from the atmosphere above while in the lower layers changes occur due to mixing. The water of the higher southern latitudes is thus made up partly of water of the returning intermediate current and partly of deep water from lower latitudes. The schematic block diagram presented by Sverdrup that is shown in Fig. 318a shows the meridional components of motion in the Antarctic Circumpolar Ocean.

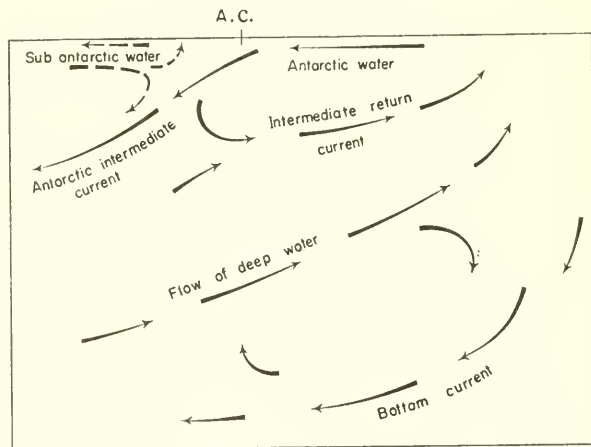


FIG. 318a. Schematic representation of the meridional circulation inside the Antarctic Circumpolar Current (according to Sverdrup).

This concept of the circulation character occurring in these higher latitudes of the Southern Hemisphere differs somewhat from the ideas expressed in elder investigations. MERZ and WÜST (1928), for instance, interpreted the warm and highly saline water of the intermediate layer of the higher southern latitudes only as the last traces of Atlantic Deep Water reaching the sea surface in this region. According to CLOWES (1933), this water should be of Pacific origin and should reach the Atlantic only by way of the zonal circulation. Both suppositions are only partly tenable. Sverdrup attempted to estimate also the magnitude of the meridional velocity components, on the one hand, from the shearing stresses of the wind leading to an estimate of the resultant total water transport, and on the other hand, from the steady-state condition in the temperature field of the returning intermediate current. For the upper layers a mean value was about

2.5 cm/sec. The time required to perform a single complete cycle in the upper vortex with a horizontal axis in the area of Drake Strait thus amounts to at least a year when the above mean velocity value is used. This transverse circulation is, however, undoubtedly stronger here than elsewhere in the Antarctic Circumpolar Ocean.

South of the oceanic West Wind Drift the physical sea level and the isobaric surfaces rise again towards the Antarctic continent. An indication of this rise in the Atlantic Ocean can be seen also in Fig. 316. Near the continent easterly winds prevail, and the currents flow towards west. In this flow along the continent there will thus occur a vertical circulation similar to that appearing in the oceanic West Wind Drift except that it performs a clockwise rotation when looking east. There are indications of such a circulation found in the observations of many Antarctic expeditions. In this connection, Sverdrup also drew attention to the transport of lighter water by the wind towards the Antarctic shelf where it is strongly cooled. The wind thus has a tendency to pile up the lighter surface water against the shelf and produces stronger and stronger solenoidal fields, which are of no consequence, however, since the water simultaneously is cooled there. Both effects thus work in opposite sense and prevent the development of strong solenoid fields and also of stronger currents which would otherwise be formed solely by the action of the wind.

4. Dynamics of the Antarctic Circumpolar Current

It is of interest to investigate the extent, in a broad current which encircles the whole earth, to which the wind stresses acting on the sea surface are balanced by frictional stresses against the outer boundaries of the ocean basins. For most oceanic currents the computed transports differ as was shown by MUNK (1950), by a factor of not more than 2 from the observed transports. MUNK and PALMÉN (1951) have made a similar calculation for the Antarctic Circumpolar Current. They considered the Antarctic Circumpolar Current as an eastward flow on a plane tangential to the earth at the south pole. The flow is induced by the constant eastward winds and depends only on the distance r of this plane from the pole. The balance between the wind stress T and the lateral friction is expressed by the relation

$$T + A_h \frac{d}{dr} \left(\frac{dM}{dr} + \frac{M}{r} \right) = 0, \quad (\text{XIX.1})$$

where A_h is the lateral kinematic viscosity and M is the eastward mass transport across a normal vertical plane of unit width extending from the sea surface to the sea bottom. For a solution in which M vanishes at the Antarctic continent ($r = r_0$), and at some other latitude ($r = r_1$) the total mass transport of the flow will be

$$\bar{M} = \int_{r_0}^{r_1} M dr = \frac{T}{18A_h} \left(r_1^3 - r_0^3 - \frac{6r_1^2 r_0^2}{r_1 + r_0} \ln \frac{r_1}{r_0} \right). \quad (\text{XIX.2})$$

Putting $T = 2 \text{ dyn cm}^{-2}$, $A_h = 10^8 \text{ cm}^2 \text{ sec}^{-1}$ and $r_0 = 70^\circ \text{ S.}$, $r_1 = 45^\circ \text{ S.}$ one obtains $\bar{M} = 5 \times 10^{16} \text{ g sec}^{-1}$ while the observed transport is at least $1.5 \times 10^{14} \text{ g sec}^{-1}$. This discrepancy is not materially altered on taking spherical co-ordinates or allowing for the variation of the wind with latitude. The transport \bar{M} is inversely proportional to A_h and only values of 10^{10} or more can give an agreement with the observed facts.

Values of A_h as large as this are, however, improbable. Munk and Palmén attempted to reconcile the two values by taking into account the friction at the bottom especially

there where the major submarine ridges lie as transverse obstacles in the path of the current. If the wind stress should be completely balanced by the frictional stresses along the sea bottom, then the Antarctic Circumpolar Current must extend deep enough to reach the sea bottom. It is certain from the vertical oceanic stratification in these latitudes that the current reaches down to very large depths; this is clearly indicated by the dynamic topographies of the individual isobaric surfaces. However, the velocities decrease very rapidly with depth and at depths of more than 4000 m the flow intensity of the Antarctic Circumpolar Current is extremely small. Correspondingly, the frictional stresses at the sea bottom will also remain rather small. By making the most favourable assumptions Munk and Palmén showed that the retarding pressure of the submarine ridges against the deep current might still be able to balance the wind stress on the surface.

HIDAKA and TSUCHIYA (1953) have recently taken up the problem again and attempted to find a hydrodynamic solution. From the equations of motion and the continuity equation with the corresponding boundary conditions they derived for planar co-ordinates, a complete solution in the form of infinite series giving the total mass transport, the surface slope and the vertical velocity distribution. Their calculations using some arbitrary numerical values of the lateral and vertical eddy viscosity (A_h and A_v) give the same results as those of Munk and Palmén. For $A_v = 2 \times 10^3$ and $A_h = 10^{10} \text{ cm}^{-1} \text{ g sec}^{-1}$ they found a total mass transport of $9.3 \times 10^{14} \text{ g sec}^{-1}$, a surface slope of 3 m per 25° lat. and directions and strength of the currents in good agreement with those observed. But also in this case choosing values of A_h less than 10^{11} would give impossible conditions. In a more recent treatment of this problem TAKANO (1955) introduces a special vertical and meridional density distribution corresponding approximately to the observed ones. The rather complicated mathematical solution led to the following conclusions: if the Ekman frictional layer is disregarded then the geostrophic approximation can be safely applied for the small velocities near the sea bottom. However, in order to obtain agreement with the observed values of the surface velocity, of the surface slope, of the density differences at the sea surface and of the mass transport, it is necessary to take $A_h = 1.1 \times 10^{10}$. This is again the same large value that was found to be a necessity in the investigations mentioned before.

There must thus be yet another source of energy dissipation in order to have a complete balance in the sense put forward by Munk and Palmén between wind stress and frictional stress. This can probably be obtained by taking into account the effect of the boundary friction, not only at the sea bottom but rather along the extended continental slope of the Antarctic continent which was previously neglected. An essentially different explanation of the dynamics of the Antarctic Circumpolar Current has been given recently by STOMMEL (1957). While Munk and Palmén and all others who have treated the problem regarded the Antarctic Ocean as an example of an ocean without meridional barriers for which a Sverdrup type solution could not be constructed, Stommel believed that while the circumpolar ocean was indeed a continuous ring of water around the earth, it was so strongly narrowed at Drake's Passage between Grahamland and the southern tip of South America that a pure zonal flow could hardly develop in this section. On this basis the Antarctic Circumpolar Current is amenable to treatment by the Sverdrup theory and is essentially frictionless except

in a short section after its passage through Drake's Passage. The entire energy dissipation and all the other disturbances occur at this point; in all the other sections of the current course it is a simple frictionless geostrophic current.

Stommel developed a simple model (Fig. 318*b*,*a*) consisting of a homogeneous ocean of uniform depth surrounding a schematic Antarctic continent and only at one place (indicated by the heavy radial line) a barrier closes Drake's Passage completely. The zonal wind system assumed is also shown in Fig. 318*b*,*a*) with trade winds from the equator to 30° S., westerlies from 30° S. to a little over 60° S. and further south a narrow zone of easterlies. The Ekman drift current transport is northwards in the westerlies and southwards in the easterlies. Therefore a divergence zone exists between about 55° and 50° S. and a convergence zone further north. Since there is a complete barrier it is not difficult to maintain a wind-driven circulation. The meridional components of this circulation are indicated by arrows in Fig. 318*b*,*a*) and the entire circulation is shown in Fig. 318*b*,*b*). At the western coast of the ocean (the eastern side of the barrier) an intense western boundary current will be set up and this simple circulation will be characterized by two immense gyres around the earth parallel to the latitude circles. Stommel calculated that the transport in the southern gyre would be somewhat more than $100 \times 10^6 \text{ m}^3 \text{ sec}^{-1}$, and somewhat less in the northern gyre.

In fact, however, the northern gyre is broken up by the African and by the Australian–New Zealand land mass. If now the barrier between South America and the Antarctic is broken in the manner indicated in Fig. 318*b*,*c*) then the transport lines will run through this opening and a circulation to the east will develop at the southern rim of the barrier. The flow through the passage still remains unexplained but without doubt models can be devised in order to describe it. Stommel's explanation of the dynamics of the Circumpolar Current is quite different from the previous explanations. He also attempted to make this explanation more plausible by embedding this current system under consideration into the system of the sub-Antarctic–Antarctic circulation.

5. The Sub-Antarctic Intermediate Current

The most important facts concerning the spread of the subpolar Antarctic intermediate water as far as they can be deduced from the distribution of the oceanographic factors have been described already in Pt. I, p. 173. This water type forms the uppermost part of the oceanic stratosphere. The sinking at the polar convergence is shown by all meridional salinity sections (see Pt. I; Fig. 62 for the Atlantic, p. 147, Fig. 75 for the Indian Ocean and Fig. 76 for the Pacific, p. 172). The fact that this process at the Antarctic convergence (see p. 669) occurs with about the same intensity all round the earth indicates that at all places the sinking and the subsequent spread of this water type are caused by the same factors.

In the Northern Hemisphere the morphological configuration of the continents interferes with the formation of an Arctic intermediate current and traces of it are found only along the western side of the Atlantic. The weakly saline intermediate current in the Atlantic is consequently *not symmetrical about the equator* and we may only speak of a sub-Antarctic intermediate current here. In the Pacific the northern current branch is almost as strong as the southern one and therefore in the region of the thermal equator (6° to 8° N.) very similar water types come in contact with each other. In the Atlantic the Antarctic branch is, however, so strongly

developed that it extends past the equator and can be traced almost as far as 20° N. It is noteworthy that the thickness of the intermediate water at first is about 1000 m and later on diminishes in wedge-form, and that it is found *across the entire width of all cross-sections* through the ocean (see Pt. I, Fig. 77 p. 174).

A detailed analysis of the sub-Antarctic intermediate current in the Atlantic—which is the only ocean for which this is possible at the present time—using the core layer method and the [TS]-relationship has been given by WÜST (1936*b*). By a determination of the percentage with which the original water type can be found south of the Polar Front at each place in the entire space, and how much of it has been lost due

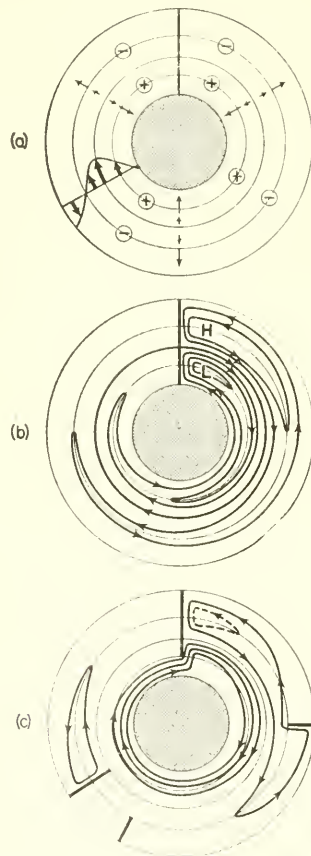


FIG. 318*b*. (a) The schematic southern ocean. Antarctica is the full black circle. The meridional barrier projecting out from Antarctica is represented by the full heavy black line. The schematic wind system (purely zonal) is depicted by the heavy arrows on the lower left. Latitudes of Ekman convergence and sinking at the surface are indicated by \ominus , latitudes of divergence and upwelling are indicated by \oplus . The direction of the required meridional geostrophic flow is indicated by thin radial arrows.

(b) Transport lines of the solution for the model depicted in Fig. 318*b*,(a) The western boundary currents are to be interpreted schematically.

(c) Hypothetical form of the solution, that results from rupturing the American–Antarctic barrier in such a way as to permit water to flow throughout, to obstruct all latitude circles (according to Stommel 1957).



FIG. 319. Absolute topography of the 800-decibar surface (smoothed representation). (Dynamic isobaths north of the subtropical convergence region drawn from 1 to 1 dyn cm, otherwise from 5 to 5 dyn cm.)

to mixing, one obtains a rather good insight into the mixing process going on in the total space of spreading (with reference to these conditions see Pt. I, p. 212 and following pages and particularly the Figs. 100–102). In general, the diagrams indicate a uniform spread towards the north taking place over the whole cross-section almost immediately after the sinking at the polar convergence, but further north there is a preference for the western half of the ocean which must be due to the effect of the Coriolis force. Here close to the South American continent the spread possesses current character. The entire width of the layer across the total ocean gets its supply, then from the western side by *lateral turbulence* and by occasional occurring large intrusions but the salinity distribution shows only the final stage after lateral mixing has been effective and does not give information about the nature and way with which the lateral mixing process operates.

Since a current is formed on the western side along the South American continent these processes can be regarded as a case of free turbulence (DEFANT, 1936c) and the ratio [exchange:velocity] can be determined along the entire spread of this water type. This then gives some idea about the *current character of the spread* of the Antarctic intermediate water. In order to find the pressure forces that give rise to this water transport it is necessary to determine the dynamic topographies of the isobaric surfaces at these depths. The absolute topography of the 800-decibar surface which corresponds north of 40° S. closest to the core layer of the sub-Antarctic intermediate water is shown in Fig. 319 for the region of 20° N. South of 40° S. the zonal course of the dynamic isobaths indicate the downward extension of the large Antarctic Circumpolar Current flowing eastward; but at this depth the meridional pressure gradient is only half of that observed at the sea surface. Also, the broad high-pressure ridge in the subtropical convergence region is present only with a somewhat diminished intensity and in the convergence regions still vortical disturbances appear extending down to these depths.

North of the high pressure ridge the isobaths run also from east-north-east to west-north-west, but beyond 25° W. they turn towards the north and finally run along the South American continent as far as Cape San Roque. The pressure gradient here is thus directed towards the east but this gradient does not extend very far out from the coast; the broad area from about 20° S. to 20° N. as far as the African coast shows almost no gradient. Already downward from 500 m the water movements in this large region must be extremely weak and there is no indication whatsoever of a circulation. The water displacement corresponding to the absolute topography (see Fig. 320) on the northern side of the subtropical disturbance zone in the Southern Hemisphere is directed first to the west-north-west and then to the north-west and finally extends *in a narrow band* along the South American coast as far as the West Indies and continues into the Gulf Stream region. The velocities everywhere remain small, between 6 and 12 cm/sec in the core layer, falling *rapidly* to weak intensities towards the eastern edge.

An analysis of the salinity distribution in the Intermediate Current gives values for the ratio [exchange:velocity] of 0.8 to 2–3 at the upper and lower edges, respectively. This leads to exchange coefficients of about (5–10 g cm⁻¹sec⁻¹) which is in good agreement with the order of magnitude found by other methods at such depths.

6. The Polar Bottom Current

The second water type originating at the sea surface of the Antarctic ocean is the *Antarctic Bottom Water*. It is formed all along the Antarctic continental shelf and especially in the area of the Weddel Sea which is the place of formation for this coldest and thus heaviest water type; it sinks along the continental slope down to the greatest depths and extends northward following the bottom topography of the ocean as an Antarctic Bottom Current. As it spreads it is subject to continuous mixing with the water masses above. Its spread is hindered by transverse ridges which the current must pass and limits are set to spread by meridionally oriented rises; the deep passages through these zonally and meridionally oriented ridges thus form important guiding channels for the bottom currents. The extension of antarctic bottom water in the individual oceans as deduced from the thermo-haline structure has been described in detail during the discussion of the temperature distribution in the bottom layers of the ocean, so that the reader is only referred to this here (see Pt. I, p. 149). The spread of the bottom water is shown in Plate 4 by lines of equal potential temperature and from these the course of the bottom currents can be readily followed.

The generation of bottom water in the Antarctic is so enormous that the same process in the Arctic is by comparison quite insignificant. In the Atlantic one can hardly speak of any proper Arctic bottom current, since the high upward extending ridges between North America, Greenland, Spitzbergen and further to the south between Greenland, Iceland, the Faeroes and Scotland almost completely block the outflow of bottom water from the Arctic Basin. Bottom water with a characteristic potential temperature of between -0.2° and -1.5°C passes over the above mentioned submarine rises into the open ocean in only very small amounts.

Recent investigations of the flow near the bottom across the Iceland–Faeroes Ridge have been made by DIETRICH (1956, 1957). All the five cross-sections over these rises have shown that the warm North Atlantic Water and the cold sub-Arctic water are in contact over the ridge forming a narrow frontal zone. The heavy sub-Arctic water lying underneath the lighter north-east Atlantic water always covers a large part of the summit plateau of the Iceland–Faeroes Ridge, and sinks down immediately on its western side because of its higher density keeping thereby close to the slope. In spite of mixing with warmer water of smaller density its density remains still higher than that of the surroundings, and consequently it sinks to form the bottom water in the north-east Atlantic at depths below 3000 m. The velocity of this downward directed bottom current on the western side of this ridge can be determined using a formula given by DEFANT (1955) and results to about 35 cm sec^{-1} . For a thickness of the sinking water of 50 m and with a total width of the passage of 150 nautical miles the water transport will amount to about $50 \times 10^6\text{ m}^3\text{ sec}^{-1}$. Like a waterfall these waters flow out in individual bursts and may be observed at any time of the year at the Iceland–Faeroes Ridge. Oceanographically they have a greater importance than the sinking movements caused by winter cooling over the shelf of the Bay of Biscay and elsewhere along the continental shelf and slope which can occasionally be observed (see COOPER and VAUX, 1949 and COOPER, 1952).

The main mass of North Atlantic Bottom Water thus originates outside the Arctic. WÜST (1943) termed this water type with a potential temperature of between 1° and 2°C as the *sub-Arctic bottom water* and the current fed by it the “*sub-Arctic*

bottom current." This sub-arctic bottom water comes mainly from two source regions:

- (1) from the north-western Labrador Basin where the colder bottom water with a temperature of less than 1.2°C is formed (WATTENBERG, 1938; SMITH, SOULE and MOSBY, 1937) and
- (2) from a region of formation extending all along the 3000 m depth of the south-east Greenland continental slope into the inner angle of a bay; this source was already referred to by NANSEN (1912).

From these two main centres the sub-Arctic bottom water spreads out towards more southern regions. Influenced by the bottom topography, this spread, however, keeps close to the western side along the foot of the continental shelf off the Labrador coast as far as 50°N . A Labrador submarine rise here prevents its further southward spread. The second centre of formation in the Irminger Sea is obviously less productive; since already in about 55°N this water type has mixed with warmer waters and has lost its characteristic cold temperature.

A small Arctic bottom current also occurs in the Pacific; cold bottom water in moderate amounts penetrates over the boundary rises of the Okhotsk Sea into the open ocean. However, this is likewise only of sub-Arctic origin and its productiveness remains small.

The ratio [exchange:velocity] can also be derived from the analysis of meridionally oriented temperature and salinity sections (see Pt. I, p. 153) and stream lines of the water transport can be constructed in order to obtain a representation of the current course in its core (Fig. 321). The stream lines follow closely the bottom topography. Over the crests of the ridges values of the above ratio lie between 2 and 3, in the depression between 5 and 6. For the same values of exchange the current intensity shows a proportion of about 2.5:1. WATTENBERG (1935) by keeping track of chemical processes at the sea bottom and in the layers just above it found an exchange of about $4\text{ cm}^{-1}\text{ g sec}^{-1}$. With this value, the velocity of the bottom current on the western side

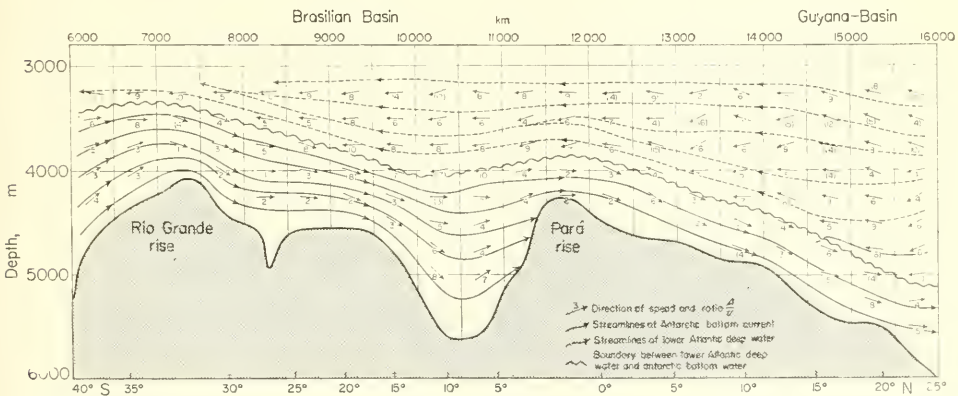


FIG. 321. Stream lines and values of the ratio between exchange and velocity in the core of the Antarctic Bottom Current in the Atlantic Ocean (evaluated from the temperature and salinity distribution in a longitudinal section of the Western Atlantic Trough).

of the Atlantic should be of the order of 0.5–2 cm/sec. In order to flow through the distance from 50° S. to the equator, Antarctic waters would thus require about 10–30 years and would have lost 40% of its characteristic water properties on reaching the equator. Variations in these properties occurring at a certain moment in the area of formation of the water types could only be noticed in the bottom layers at the equator after appreciably long time and with a considerably diminished intensity.

WÜST (1957) has recently made a dynamic investigation of the “Meteor” profiles and has thereby extended the determination of the absolute topography of the physical sea level and the isobaric surfaces made by DEFANT to the layers between 2500 m and the deep-sea bottom. He based his computations on the topography given by Defant for the dynamic reference surface (p. 496) and continued the calculations from this surface to the sea bottom. These topographies were used to determine the velocity components at right angles to the profiles. Figure 322 shows the resultant chart of the

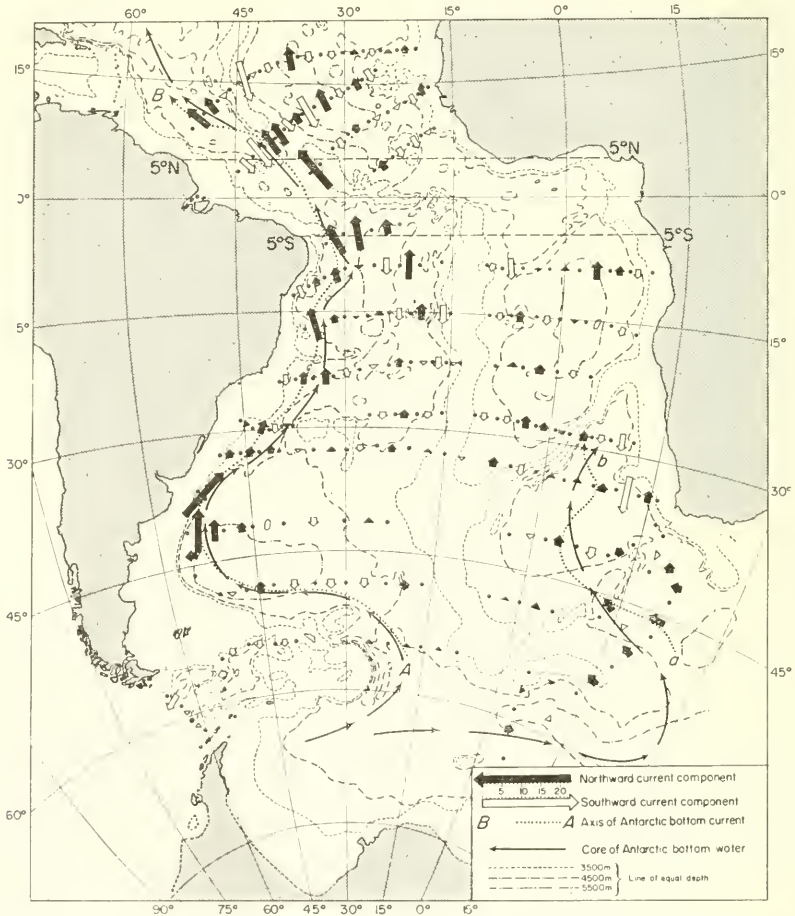


FIG. 322. Current distribution in the Antarctic Bottom Water of the Atlantic Deep Sea (in a depth of more than 3500 m) computed from the mass distribution taking as a basis the reference level of Defant (according to WÜST, 1957).

bottom currents. The Antarctic bottom current in the Southern Hemisphere shows measurable velocities ($>3 \text{ cm sec}^{-1}$) only close to the western side of the West Trough, that is, at the foot of the continental slope and about 1000 m above the level of the proper deep-sea bottom. With few exceptions only very weak velocity components were found in the east. These results derived from dynamical computations agree well with the above described ones. With these new velocity values the water masses of the bottom would need about 5.5 years in order to travel from the southern rim of the Argentine Basin (48° S.) to the northern rim of the Brazilian Basin (5° S.).

7. The Deep Currents in the Middle Part of the Oceanic Stratosphere of Individual Oceans

In a *fully symmetrical* ocean there would be in each hemisphere a subpolar intermediate current in the uppermost part of the oceanic stratosphere and a polar bottom current in the lowermost part of it. These water transports directed towards the equator for reasons of a compensation require an additional poleward water transport in the middle part of the stratosphere. These compensation movements are called the "deep currents" of the oceans.

In this way the scheme of the meridional components of the stratospheric circulation (Fig. 323) thus consists of *two* closed circulations in each hemisphere; one circulation in the upper part of the oceanic stratosphere containing the intermediate current and the upper half of the deep current and moving in a clockwise sense when looking east in the Northern Hemisphere, and a second circulation in the lower part of the oceanic stratosphere that includes the polar bottom current and the lower half of the deep current and moves in an anticlockwise sense. It should be borne in mind in looking at Fig. 323 that only the meridional flow components of the two circulations are shown which are always weaker than the zonal ones.

The rather varying character of the polar components in the actual oceans gives

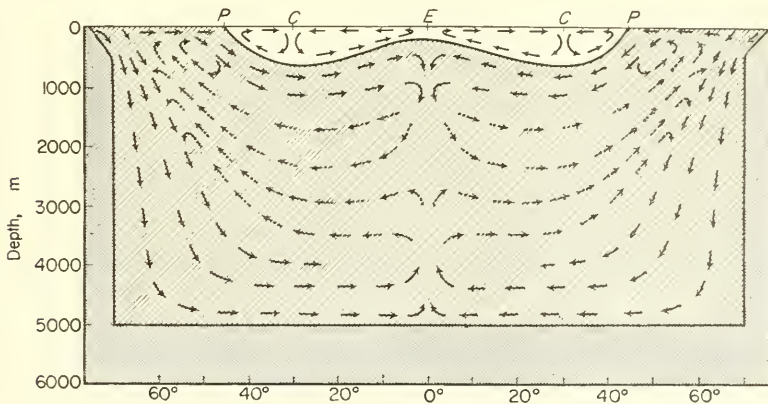


FIG. 323. Schematic representation of the meridional components of the oceanic circulation in a symmetrical ocean. $\leftarrow\leftarrow\leftarrow$, circulation of the troposphere; $\leftarrow\leftarrow\leftarrow$, subpolar intermediate currents; $\leftarrow\leftarrow\leftarrow$, polar bottom currents of the stratosphere; $\leftarrow\leftarrow\leftarrow$, mean deep currents of the stratosphere; $\leftarrow\leftarrow\leftarrow$, limit between oceanic tropo- and stratosphere; P , polar front (polar convergence); C , subtropical convergence; E , equatorial counter current.

rise, of course, to large differences in the development of the deep currents. The closest approach to the ideal case pictured in Fig. 323 is found in the Pacific. The meridionally oriented sections, although they are based on insufficient data and often do not reach right to the bottom show the approximately symmetrical arrangement of the subpolar intermediate currents about the equator. Warm water sinks in the convergence region of both these currents as it is required in Fig. 323; such downwards motions are indeed indicated by a downward bulging of the isothermal layers in the meridional temperature sections. At greater depths the deep layers of the Pacific are almost uniform and there is no special differentiation to indicate any particular motion (WÜST, 1929, 1930*b*). This is supported also by the absence of any temperature inversions which are very characteristic of the Atlantic and the Indian Ocean.

The *marked asymmetry* of the polar components in the Atlantic Ocean due to the almost complete absence of the Arctic current branches gives rise to a strong development of the southward directed North Atlantic Deep Current. This provides the only compensation here for the Antarctic water carried north by the intermediate and bottom current. Disregarding at the moment the water layers from about 1000 to 1500 m between 50° N and 20° N. (particularly on the eastern side) the oceanic spaces underneath are filled with relatively salinity- and oxygen-rich waters. The structure of these waters indicate by their vertical structure a sub-Arctic origin. Its principal characteristic is the *oxygen content* of the core layer and the distribution of this shows clearly its origin from the area east and south-east of Greenland and from the boundary zone between the East Greenland Current and the Irminger Current south-west of Iceland as well as from regions in the north of the Labrador Sea. These are the same regions that form the source of the sub-Arctic bottom water (p. 680). WÜST termed this sub-Arctic bottom water as the "Lower North Atlantic Deep Waters" as opposed to the "Middle Deep Water" occurring above. In these regions mentioned above the almost homogeneous structure of the sea during autumn and winter allows the surface waters to sink to great depths forming there the source of the more or less horizontal southward water transport between 1500 and 2500 m depth.

In the "Meteor" cruise made in late winter 1935 the kind of conditions were found along a profile south of Greenland which are required to allow the autumn and winter convection to proceed to great depths. The oxygen distribution along this profile (Fig. 324) clearly shows this downwards tendency of the surface layers (WATTENBERG, 1938). Below 1000 m the source for the middle North Atlantic Deep Water is formed here. When this water moves further to the south the transport obviously keeps *closely to the western side of the ocean* due to the influence of the Coriolis force, but even after crossing the equator it still prefers the western side and the effect of the Middle Atlantic Ridge is clearly noticeable. The upper layers of this southward water movement show the effect of mixing with Mediterranean water (see later) since the [TS]-relationship for the core layer at 35° N. shows a definite reversal point (see Fig. 325); apart from this the curve as far as 50° S. is almost a straight line and indicates gradual mixing with the water types above and below. Beyond 30° S. these waters enter the deep-reaching circumpolar flow of the very southern latitudes and under the influence of this are deflected to the east. The pressure conditions in the core layer of the North Atlantic Deep Water are best indicated by the topography of the 2000-decibar surface. Figure 326 shows immediately that the main course of the isobaths is in

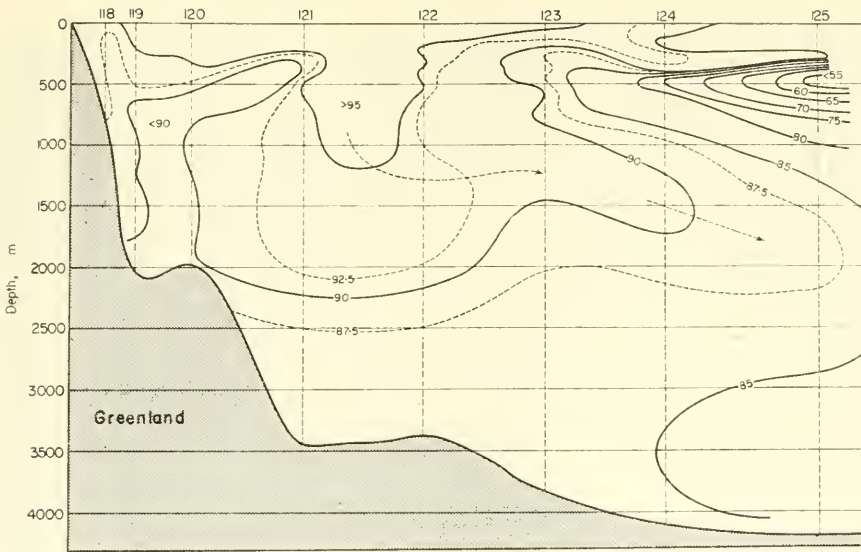


FIG. 324. Distribution of oxygen (in percentage) in a section from the southern tip of Greenland to the Great Banks of Newfoundland (according to Wattenberg).

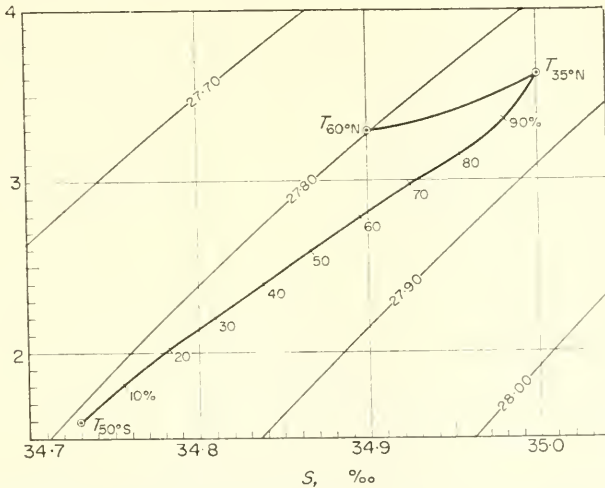


FIG. 325. Standard curve of the [TS]-relation in the core-layer of the mean North Atlantic Deep Water.

its main features in agreement with the spread of this water type deduced from the thermo-haline structure.

The source of this water transport is in the north-west of the Atlantic and from here it flows southwards principally in three branches (see Fig. 327). The western branch keeps close to the North American continental slope, passes through the North American Basin and enters into the Southern Hemisphere to the east of the Antilles. The middle branch follows the eastern slope of the middle Atlantic Ridge as far as 5° N.

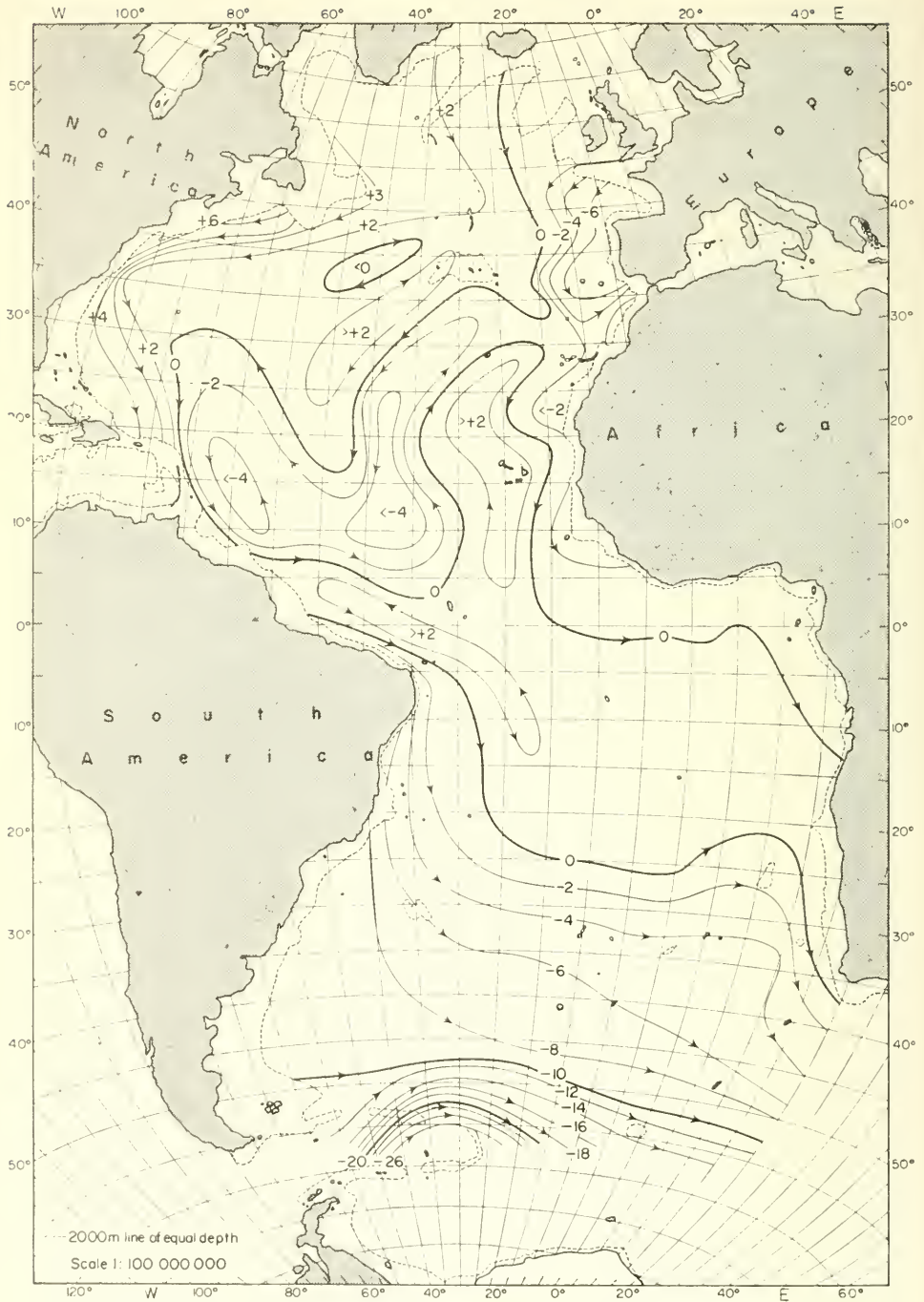


FIG. 326. Absolute topography of the 2000-decibar surface in a somewhat smoothed representation (dynamic isobaths are drawn from 2 to 2 dyn cm).

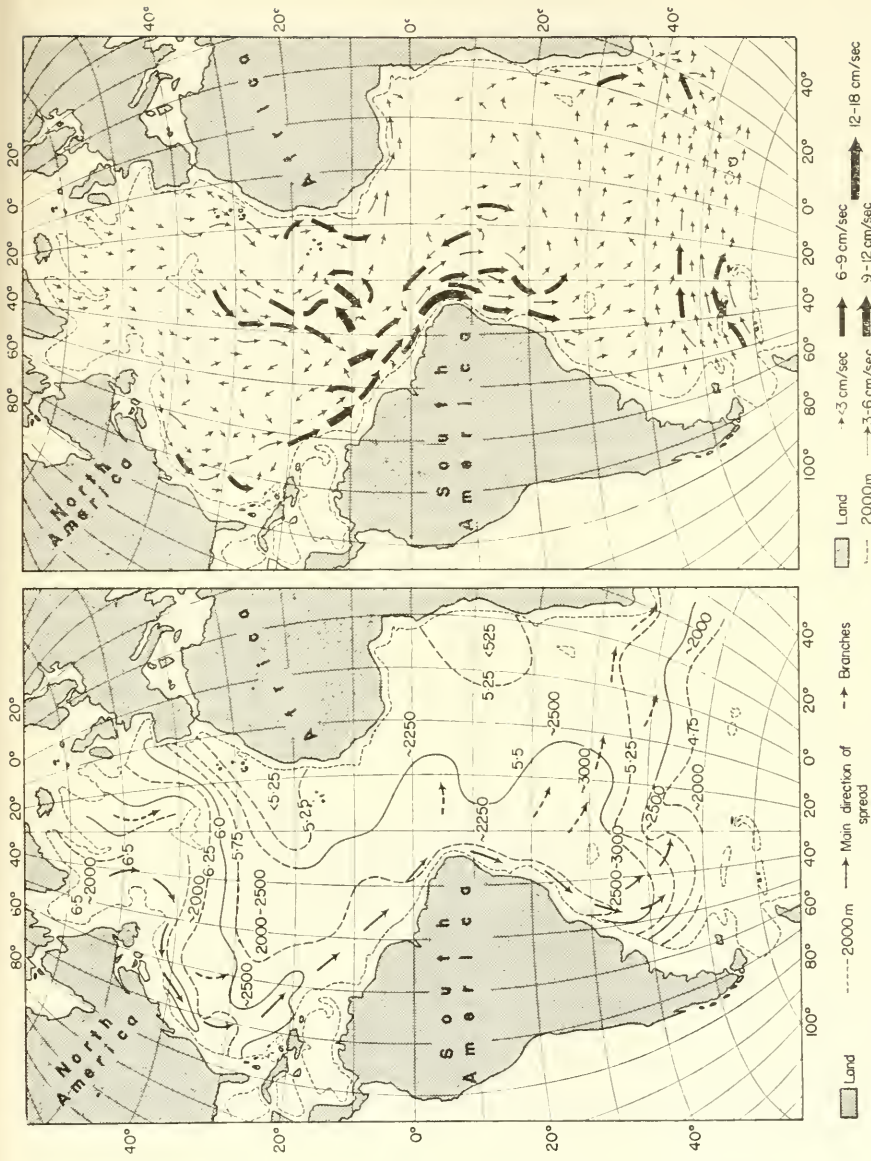


FIG. 327. *Picture to the left:* spreading of the core masses of the mean North Atlantic Deep Water (O₂ content in the layer of the intermediate oxygen maximum in a depth of about 2000-3000 m; the figures more than 100 indicate the depth of this maximum (according to Wüst, 1936). *Picture to the right:* current field in a depth of 2000 m (computed from the absolute topography of the 2000-decibar surface (according to Defant, 1941)).

and then breaks up into vortices. The third much weaker branch meanders along the East Atlantic Trough past Madeira to the Canaries and the Cap Verde Islands and a side branch of it seems to enter the Guinea Bight. The course of the first two branches under the influence of the Coriolis force used apparently the bottom morphology as guiding limits for their spread. The westernmost and most important branch keeps also in the Southern Hemisphere at first close to the continental slope until about 25° S. and then bends towards east-south-east and fills from here as a broad water transport the total oceanic space between 25° S. and 40° S. Finally, it passes south of Africa into the Indian Ocean. The velocities in the Northern Hemisphere branches of the current are seldom more than 2 cm/sec. Where the current concentrates along the South American continental slope it reaches about 3–4 cm/sec until 15° S. and at Cap San Roque it reaches maximum speeds of 8–12 cm/sec before falling off to 0.5–1.5 cm/sec further south.

The spread of middle North Atlantic Deep Water as deduced from the oxygen content of its core layer is shown in the left-hand chart of Fig. 327; the arrows in this figure indicate the principal branches of spread determined from the dynamic topography of the pressure surfaces. The agreement between the results of the two methods is remarkable. SVERDRUP (1930) has given a diagram showing the deep currents in the southern part of the South Atlantic based on the "Carnegie" observations that fits well in the topography of the 2000-decibar surface.

WÜST (1957) has calculated the corresponding velocities at right angles to the "Meteor profiles" for the current course of the Atlantic Deep Water in the area between 10° N. and 30° S. The distribution of these velocity components is presented in Fig. 328 and shows obviously good agreement with the distribution in the right-hand diagram of Fig. 326. In the core the velocity (reduced to the "true" direction) is now 9.2 cm sec⁻¹ with individual values varying between 2.1 and 17.4 cm sec⁻¹. It should especially be noticed that also here the flow is concentrated towards the west just off the American continent while the eastern parts of the oceans are completely inactive.

In the Indian Ocean a deep current stands out between 2000 and 3000 m marked by a highly saline deep layer and a pronounced temperature inversion. Its strong development is due primarily to the large density differences between the equatorial and polar water masses which are continuously renewed by the supply of salt from the Red Sea and the Persian Gulf (Pt. I, pp. 183 and 529). A deeply penetrating detailed analysis of some oceanographic series observations in the Indian and Pacific Oceans has been made by HELGE THOMSEN (1933, 1935). From the [TS]-diagrams it appears rather doubtful whether there is actually a deep current in the Indian Ocean between 2000 and 3000 m similar to that in the Atlantic. On the other hand, the Intermediate Current and the Bottom Current are well developed as well as the effects from the Red Sea are easily followed far to the south.

8. A Survey of the Water Transports in the Individual Layers of the Atlantic Ocean

The total amounts of the water transport in meridional direction in the South Atlantic total space (between 5° S. and 35° S.) which Wüst has derived from mean velocity values calculated from the individual profiles of the "Meteor" expedition are of great interest. The most important results are summarized in Table 157. The figures

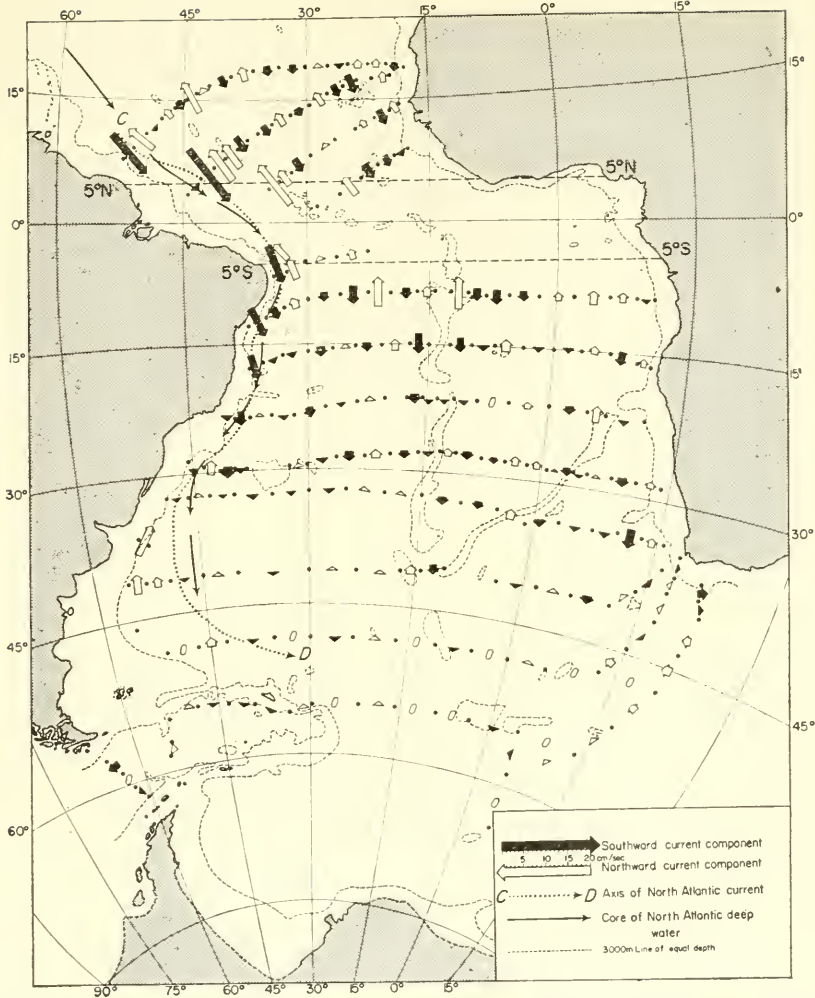


FIG. 328. Current distribution in the lower Atlantic Deep Current (3000 m depth) computed from the mass distribution taking as a basis the reference level of Defant (according to Wüst, 1957).

given in this Table show considerable scattering due to random errors and inaccuracies in the basic data. Nevertheless, they give a rather good idea of the budget of the water transports in the South Atlantic space which is valuable in many respects. The final budget of the meridional transports (current amounts) is practically perfect with a discrepancy of only 0.1 million $m^3 \text{ sec}^{-1}$. A complete balance between northward and southward transports in each of the two troughs cannot be expected. In the Western Trough the North Atlantic Deep Current with 27.5 million $m^3 \text{ sec}^{-1}$ towards the south is the main circulation component; this is very largely confined to the narrow strip along the South American coast. The transport in the uppermost part and with the Bottom Current together is only 9.0 million $m^3 \text{ sec}^{-1}$. In the Eastern Trough the transport towards the north in the bottom and deep currents is exceedingly small.

There is no current here which can be continuously followed through carrying water in large quantities to the south. Probably only very weak spreading and mixing processes operate here in variable direction. The deep sea circulation of the Western Trough is thus dominant and sets the basic pattern for the whole of the South Atlantic oceanic space.

Table 155. Mean values of the meridional water transport in the total space of the South Atlantic Ocean (between 5° S. and 35° S.) given in units $10^6 \text{ m}^3 \text{ sec}^{-1}$.

Current constituents	Water transports throughout entire width of the ocean		Through the Western Trough towards		Through the Eastern Trough towards	
	Towards the north	Towards the south	north	south	north	south
Sea surface current	22.7	—	7.0	—	15.8	—
Deeper currents						
Intermediate current						
Deep current	—	25.6	—	27.5	4.8	—
Bottom current	3.0	—	2.0	—		

9. The Effects of the Subtropical Adjacent Seas on the Deep Sea Circulation.

Analysis of series measurements in mid-latitudes of the eastern North Atlantic led already at an early stage to the recognition of a warm highly saline water type with little oxygen content, the principal characteristics of which point towards the Straits of Gibraltar which can therefore be considered as effects on the waters of the Atlantic, of the water flowing out of the European Mediterranean. The significance of "Mediterranean water" in the Atlantic deep-sea circulation was first pointed out by JACOBSEN (1929).

A detailed investigation and review of the phenomenon was then given by WÜST (1936) in the "Meteor" Report; he termed this water type "upper North Atlantic Deep Water". It is characterized by its high salinity which is in sharp contrast to the Antarctic intermediate water above it. Off Spain the core layer can be found at about 1000–1250 m and lowers down towards the equator reaching a depth of 2000 m between 10° S. and 20° S. From the salinity distribution in the core layer it is immediately obvious (see Fig. 329) that the spread takes its origin from the waters off Spain, and that it obtains its high salinity content of 36.4‰ or more by way of the Mediterranean water flowing out through the Straits of Gibraltar in the lower layers (p. 529 *et seq.*, see also, pt. I. p. 182). This water sinks to about 1000 m where it finds a corresponding density and then spreads out in a *fan-like* fashion under the action of turbulence and Coriolis force. Figure 330 impressively shows the great distances to which still an effect of the Mediterranean Water can be traced. It extends northwards past 50° N. and it reaches particularly pronounced directly across the entire Atlantic as far as the American coast. Towards the south the last traces can be followed even to the higher latitudes of the Southern Hemisphere. The percentage of Mediterranean water present at any point can be determined from a standard curve for the [TS]-relationship in the



FIG. 329. Spreading and depth of the upper North Atlantic Deep Water (Mediterranean Water). The thin dashed lines indicate the depth of the core layer in metres (according to Wüst).

core layer of this upper North Atlantic Deep Water (Fig. 330). In the western part of the North Atlantic there is still a content of 25–30%, at the equator 20–18% in the South Atlantic the Mediterranean content gradually falls to below 2%. The form of the $[TS]$ -relationship which is nearly a straight line indicates that the changes in the core layer are due essentially to a simple mixing process.

The great effect of the water flowing out from the Straits of Gibraltar on the composition of the water masses in the Atlantic is at first sight astonishing. A rough calculation shows, however, that it is of the right order. According to SCHOTT (1939), about

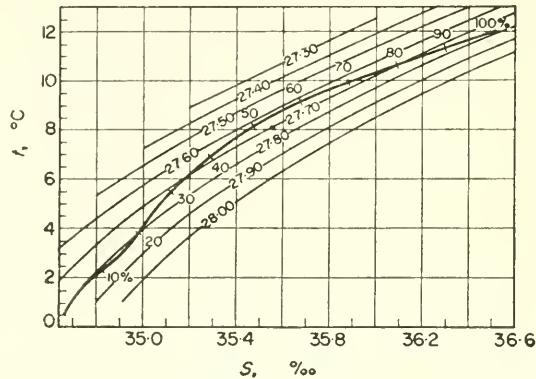


FIG. 330. Standard curve of the $[TS]$ -relationship in the core layer of the upper North Atlantic Deep Water (Mediterranean Water).

52·000 km³ of water a year flows out from the Mediterranean into the Atlantic. For a mean velocity of spread of about 2 cm/sec it would require about 6 years to spread over the area between 45°N to 15° N. During this time the Straits of Gibraltar will supply 312·000 km³ of Mediterranean Water, which, distributed *evenly* over a layer of 500 m thickness from 45° N to 15° N., would mean a contribution of about 3·4%. The layers inside the Spanish bay will, of course, show a considerably higher percentage.*

ISELIN (1936) has not quite agreed with the idea of an extension of Mediterranean Water to the higher latitudes of the Southern Hemisphere. On the basis of "Atlantis" observations he investigated the deviations of individual values from the standard value for the whole region using the Helland-Hansen anomaly method (see Pt. I, p. 114). A positive anomaly is present at 1200 m depth only as far as about 20° N. (until the North Equatorial Current), while farther south deficits appear due to the effect of mixing with Antarctic intermediate water. According to Iselin the effect thus extends no further than 20° N. This difference in viewpoint can be explained by differences in the definition of the "Mediterranean Water"; the fact at least remains that *traces* of Mediterranean Water can be followed far into the South Atlantic.

The process of spread of Mediterranean Water through the Straits of Gibraltar and out into the Atlantic is certainly of a twofold nature. During the first part of the outflow and sinking of the heavier Mediterranean Water, until it reaches the shelf and the continental slope and until it finds the depth of equal density inside the Atlantic,

* These percentages refer to the water present between 600 and 700 m depth west of the Straits of Gibraltar which has a temperature of 11·9° C and a salinity of 36·5‰ and was termed "Mediterranean Water" by Wüst. If absolute values are required of the proportion of Mediterranean Water from east of the Straits of Gibraltar then the given values must be reduced by half.

the Mediterranean waters flow with considerable velocity and due to the influence of the Coriolis force keep especially in the Spanish Bay to the northern side. Finally, they pass around Cape San Vincent while steadily sinking and still keeping close to the Portuguese coast past Cape Finisterre as far as the Bay of Biscay. Observations show that this is the first stage of spreading; and the whole process of spread behaves exactly in the way described on p. 524 *et seq.* and in Fig. 251a. The second stage of spreading starts from this tongue of Mediterranean Water off the Portuguese coast. Due to the much lower velocities the Coriolis force is no longer effective and the influence of lateral and vertical mixing becomes dominant. The picture presented in Fig. 330 is thus an effect of mixing processes and DEFANT (1957) has shown that a lateral eddy viscosity coefficient of about $5.5 \times 10^7 \text{ cm}^2 \text{ sec}^{-1}$ is quite sufficient to explain the lateral spread. A precise account of the whole process, however, requires systematic series observations and current measurements along suitable sections.

The Indian Ocean also shows in all meridional salinity sections, starting from the Gulf of Aden in the north-west, an unmistakable effect of the highly saline waters spreading out from the Red Sea through the Gulf of Aden into the Indian Ocean. In this case also the effect of this outflow is of decisive importance for the stratospheric circulation.

It is only to be expected that there will be seasonal variations in the extent of the spread of the water from the subtropical adjacent seas, since the outflow in itself is known to be subject to rather strong variations of this period (p. 503). The observational data available at the present time do not allow to show the influence of such seasonal fluctuations in the open ocean.

Investigations of the extent of spread of the Mediterranean Water show the great importance of the subtropical adjacent seas for the deep-sea circulation. Due to the high density of the water masses flowing with the deeper currents into the open ocean the layers of the stratosphere will have a sinking tendency and form a source for the onset of large-scale circulations. This source is at least as important as the convection acting from the sea surface downward in polar and subpolar seas. These inflows are also important because of another reason. Mixing of the water masses transported by these currents with tropospheric water masses above causes an interaction between the oceanic troposphere and stratosphere, and direct exchange between the two main layers of the ocean is probably restricted to these places. While the Atlantic and Indian Oceans are affected by subtropical adjacent seas, the outflow from which considerably intensifies the circulation in the uppermost part of the oceanic stratosphere, there are no adjacent seas of this type connected with the Pacific. Consequently, the Pacific lacks the large meridional contrast in salinity of the deeper layers which provides the driving force for a stronger circulation.

Chapter XXI

The Main Features of the General Oceanic Circulation and Their Physical Exploration

1. The Oceanic Circulation in the Atlantic

THE results obtained by numerous expeditions in the Atlantic allow a complete and, in itself, closed picture to be built up of the tropospheric and stratospheric oceanic circulations. Knowledge of the circulation systems in the other oceans is not so precise, but the conditions in them should not be so very different as is confirmed clearly by the available observations. An attempt has been made in Fig. 331 to picture the entire circulation system of the Atlantic in a somewhat schematic meridional section in order to summarize its main characteristics. This representation applies mainly to the *western side*. It can be seen that the main water movements are confined to an extremely thin layer. The circular representation shows especially the enormous horizontal extent of the oceanic troposphere. Its vertical thickness is, however, small so that in spite of the large vertical exaggeration in scale it is difficult to picture the internal circulation properly in the figure. All the main currents and singular points of the current system of the sea surface are indicated at the edge of the figure. It should be remembered that all extensive ocean currents are mainly surface currents and belong essentially to the oceanic troposphere; they extend down to the water masses of the oceanic stratosphere in only a few places and to a limited extent. This is especially so in the tropics and the subtropics.

As compared with the large horizontal extent of the oceanic troposphere the source regions for the stratospheric water types appear small, nevertheless they remain the regions of origin for the water movements inside the extended space of the oceanic stratosphere. In these regions also the forces must be contained for a renewal of the stratospheric waters and their movements. The effect of the European Mediterranean which can be regarded as a *lateral* intrusion from the east appears of no less importance. The small arrows in the diagram indicate the direction of spread of the individual water types; the current-like spread is thereby mostly indicated by full arrows while convectional spread is shown by wavy arrows. The figure shows only the *meridional* components of the water movement and deals only with mean conditions. The zonal components surpass by far the meridional ones especially in the southern part of the South Atlantic and in middle latitudes in the North Atlantic. The characteristic asymmetry of the Atlantic circulation and the great importance of the Antarctic for the stratification and movement of the water masses throughout the entire Atlantic

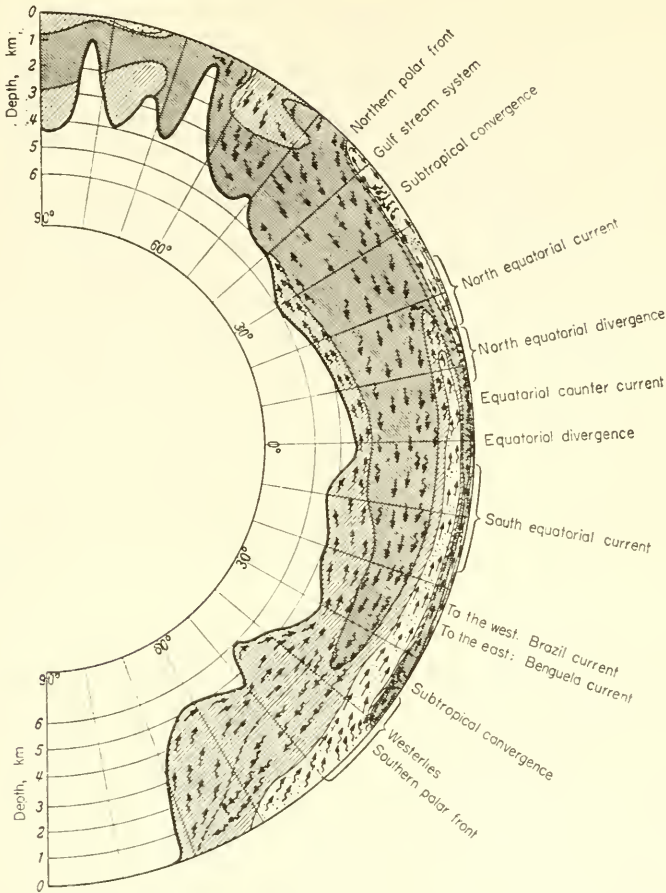
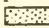
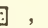
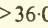
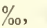


FIG. 331. Meridional vertical cross-section from pole to pole through the Atlantic Ocean. Schematic representation of the tropospheric and stratospheric oceanic circulation. ———— ocean bottom, - - - - - , boundary layer between tropo- and stratosphere from Northern polar front to Southern polar front. Salinity distribution:  , $>36.0\text{‰}$,  , $36.0\text{--}34.9\text{‰}$,  , $34.9\text{--}34.6\text{‰}$,  , $<34.6\text{‰}$, \rightarrow , current-form spreading, \sim , convection-like spreading and convection-like sinking, exaggeration about 1:400.

stand out particularly in this diagram. In the north the effects are more sub-arctic due to the bottom topography, but their influence on the stratospheric water movements is still extremely important.

If we ask for the driving forces of the stratospheric oceanic circulation it must be stated that only *differences in the thermo-haline structure of the water masses* can be the cause for these circulations, and these contrasts can only be maintained by atmospheric influences affecting the regions north of the oceanic polar fronts and are so regenerated again and again. Thermodynamic machines of this type can only do work when the compressions of the medium set into motion occur at a lower pressure than the expansions (see p. 489 and following pages). The water in the upper circulation branch is set in motion from a region of smaller to a region of greater density, and in

the opposite direction in the lower branch. The meridional density sections show that this condition is satisfied and the dynamic evaluation of the observational data has given proof of the internal forces acting in the pressure field and resulting from the three-dimensional mass structure.

In the troposphere the thermo-haline circulation in a meridional direction is less important as compared with the effects of the wind. The air currents therefore set the characteristic pattern for the circulation here and determine its more zonal direction. The western and eastern boundaries set by the continents to the oceans, due to the surface accumulation of water (piling up; Anstau), give rise to gradient currents which besides the wind drift determine the character of the tropospheric oceanic circulation.

Wüst chose a different type of representation to show the oceanic circulation. The surface currents and the deep-sea circulation of the Atlantic were shown in form of a block-diagram in order to arrive at a three-dimensional representation and to elucidate thereby the internal completeness of the circulations (Fig. 332). This survey of the oceanic circulation teaches that the basic causes of the entire oceanic circulation lie in the atmosphere. They are due partly to the *wind* which transfers energy to the water, and partly due to *climatic effects* on the water masses, especially in polar and subpolar oceanic regions. These then give rise in the first place to the water movements in the deep layers.

2. Summary of Present Individual Theories and the Prospects of a Comprehensive Theory of the General Circulation Including the Deep Layers

The existing theory of the wind-driven circulation in closed oceanic basins has been found applicable to individual parts of the ocean, but a comprehensive theory of the wind-driven circulation covering all oceanic parts is so far still missing. It has already been pointed out (p. 583 *et seq.*) that the highest advanced theory of MUNK and CARRIER (1950, led at least qualitatively to very reasonable results. Criticism has been expressed primarily on account of the high value of the coefficient of lateral eddy viscosity required in order to explain the intense currents along western coasts. MORGAN (1956) in attempts to overcome this drawback has examined the necessity of the inclusion of the lateral eddy viscosity for balancing the wind torque on the water surface.

The ocean can be represented on a different model from those used previously. In this it is divided into a northern and a southern part, and attention is paid only to the southern one which in itself is subdivided into an interior region and a boundary region adjacent to the western shore. Figure 333 shows these three oceanic subdivisions and the boundaries between them. The figure contains a typical stream line of the circulation, most of which or perhaps all of the stream lines can be expected to pass through all three regions. The equations of motion given for spherical co-ordinates are formally integrated over the depth both for a homogeneous ocean and for a two-layered ocean. From these the approximate equations are derived applicable to the interior region I_i of the currents, that is, to a region sufficiently remote from any coast. They show that all terms which are non-linear in the velocity components as well as the terms giving the contributions of the lateral eddy viscosity are negligibly small there. This is the same result as obtained from the Sverdrup solution. Wind and Coriolis forces are the principal forces in this region. For the boundary region I_b

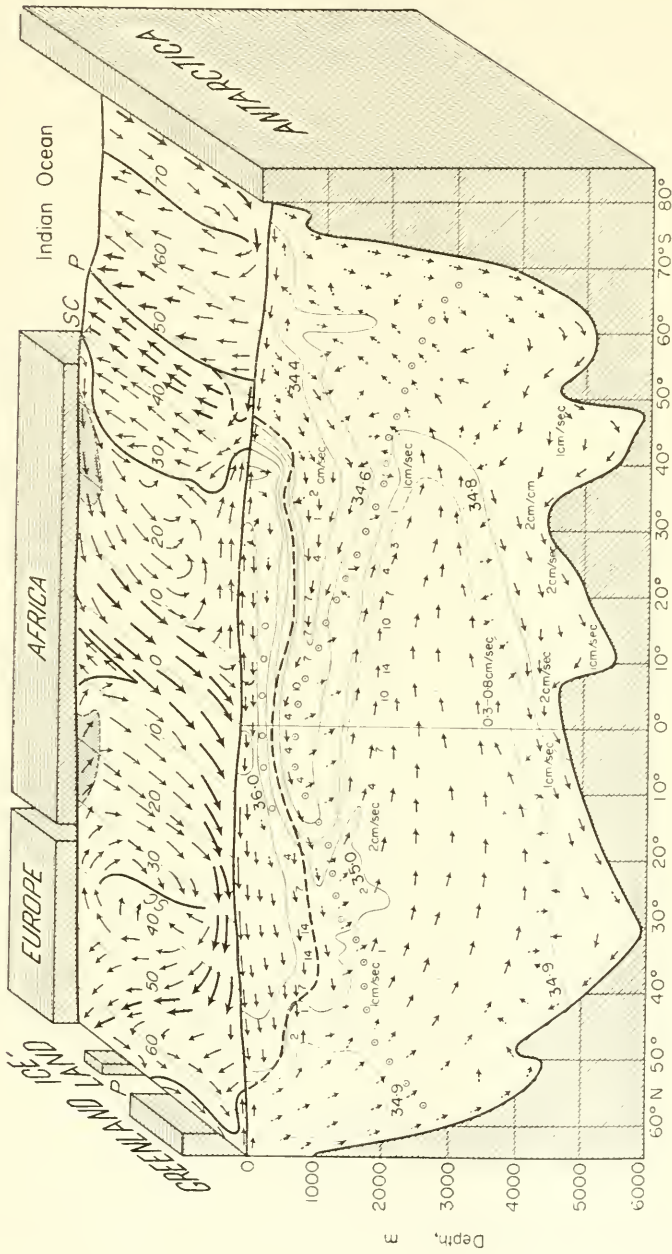


FIG. 332. Schematic block-diagram of the surface currents and of the deep sea circulation of the Atlantic Ocean (according to Wüst).

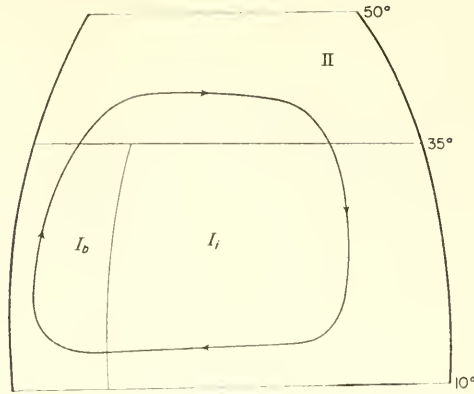


FIG. 333. The three regions of an ocean model according to Morgan, 1956, I_i , interior region; I_b , frictionless stream region; II, northern region, non-steady, and lateral friction effects possibly in an important way.

an investigation was required to show whether a lateral eddy viscosity is needed to explain the intense current in the region close to the western shore.

A general discussion based on the momentum balance alone shows that if the frictional torque is essential to the torque balance it is certainly not the only contribution to it. On the contrary, a boundary layer analysis, together with an accurate estimate of the order of magnitude of the separate terms, shows the predominance in this region of the pressure terms, the non-linear inertia terms and the terms arising from the variation of the Coriolis parameter with latitude. This is in complete agreement with the theoretical results of CHARNEY (1955) for the Gulf Stream (p. 627) but not with the result of Munk which presumes here a large lateral friction. In region II, the non-linear terms, the lateral eddy viscosity and non-stationary effects become of the greatest importance. Transitions from one region to the other must, of course, be considered more closely, but it appears that this leads to no further difficulties, so that it seems possible to obtain a comprehensive picture of the entire ocean circulation.

Very recently STOMMEL (1957), in an extremely interesting and instructive survey article, has compared the different theories of ocean currents and discussed their basic physical ideas. Avoiding mathematical ballast he tried to represent the three-dimensional oceanic movements by means of schematic block-diagrams, which are, however, based on strict theoretical principles. It seems not possible to describe all the details here but only the most essential points in connection with the upper wind-driven circulation and the deep-sea circulation shall be dealt with. Figure 334 shows a rudimentary simplified model of the Atlantic Ocean with meridional boundaries 60° apart in which a certain zonal wind-stress distribution (indicated on the left) generates a wind-driven circulation. Westerlies prevail between 30° lat. and the poles and the trade winds extend across the equator from 30° S. to 30° N. The lines shown are isobars parallelling the geostrophic flow. A certain contribution of the Ekman wind-driven transport in the surface layers has been omitted in order to retain clarity in the picture. Obviously, a system of gyres and western currents is obtained as in previous theoretical investigations. The boundaries between the gyres correspond to the latitudes

of no Ekman layer convergence (see p. 581, Fig. 265); the regions of maximum geostrophic meridional flow in each gyre correspond to the latitudes of maximum convergence (meridional flow towards the equator) or of maximum divergence (meridional flow towards the poles) of the Ekman wind-driven layer. Western boundary currents corresponding to continuity requirements have been introduced along the western boundary region.

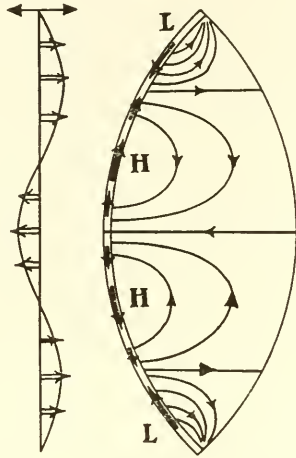


FIG. 334. The steady circulation produced in an ocean of uniform depth bounded by meridional coasts 60° apart, acted upon by a distribution of zonal winds, which are indicated on the left. The western boundary current is shown schematically by the double line at the western coast and its transport is indicated by heavy arrows (according to Stommel, 1957).

This simple circulation, derived from the application of previously described mathematical principles to a homogeneous or a vertically integrated ocean, can now be interrelated with the internal oceanic circulation of the deep layers which corresponds to a thermo-haline circulation. For this purpose Stommel subdivided the total ocean into two layers by means of a *level surface* half way to the bottom, for instance, at 1500–2000 m. Across this level surface there is a vertical mass transport which is specified geographically. The geostrophic flow of the wind-driven circulation superimposes on the water transports of the internal circulation and the continuity conditions require that the vertically integrated transport over both layers together should vanish. Figure 336 shows this model given by Stommel, a similar kind of presentation as used for the previous model. A level surface *L* divides the ocean into an upper and a lower layer. The thermo-haline convection processes allow a sinking of the water masses across the level surface in sub-Arctic latitudes (p. 684) and a corresponding rise across the level surface in sub-Antarctic latitudes (p. 675).

These convection processes are indicated by vertical transport lines drawn through the level surface in Fig. 335. The remainder of the thermo-haline circulation is completely determined by continuity and dynamic reasoning; the transport of water between the two hemispheres takes place in a narrow western boundary current according to the dynamic principles frequently mentioned above that are effective on the rotating earth. The field of motion in this circulation is entirely internal; its

vertically integrated transport vanishes at all points. This internal thermo-haline circulation postulated by Stommel is in full accord with the deep-sea currents deduced from the observations of the "Meteor expedition. The sinking of sub-Arctic water masses in the Iceland–Greenland region (p. 684), the concentration of the North Atlantic Deep Current close along the western side (p. 672), the rise in the sub-Antarctic region of the water masses carried southwards (p. 687) and the sub-Antarctic intermediate current flowing north (p. 679) are the principal constituents of this internal thermo-haline circulation which derives its driving force from the density differences between the sub-Arctic and the sub-Antarctic oceanic regions. The deficiency of the Stommel representation of this internal circulation is that in the Atlantic as in the other oceans, the *Antarctic Bottom Current* in which the Antarctic water after sinking at the continental shelf into the deepest troughs flows northwards beneath the sub-Arctic branch of the thermo-haline internal circulation (lower Atlantic Deep Current), penetrates further into the North American Basin and after mixing with the upper waters is carried south again in this current (see Figs. 323 and 331).

In Fig. 335*b*, Stommel now shows separately a wind-driven circulation in the upper layer corresponding to Fig. 334, except for the additional gyre just north of the equator caused by the presence of an area of doldrums in the wind field there (p. 601). Both

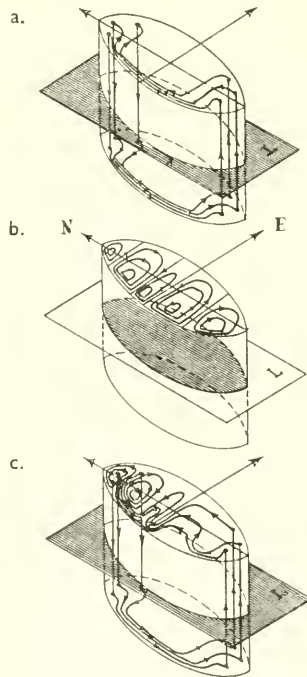


FIG. 335. A schematic interpretation of the circulation in the Atlantic Ocean constructed by a superposition of an internal thermo-haline mode associated with a flow across a level surface *L* at mid-depth (*a*) and a purely wind-driven circulation in the surface layers (*b*).

The sum of these two is shown in Fig. (*c*). According to Stommel, 1957.

Dashed arrows indicate portions of flow not given by elementary theory but evidently required by continuity and sketched in.

these circulations are now superimposed on each other in Fig. 335c. Particularly noticeable is the absence of the Brazil Current and the intensity of the Gulf Stream, even though the vertical integrated transport is the same for both currents; but according to the interpretation suggested by Stommel the current in the deep layers opposes the Gulf Stream but flows in the same direction as the Brazil Current. The Gulf Stream is reinforced by the thermo-haline component but the Brazil Current is so weakened that it almost disappears. This picture of the circulation of the Atlantic Ocean is undoubtedly interesting and instructive and will stimulate further thinking and conclusions which, however, must be supplemented by corresponding further oceanographic surveys and current measurements in the deeper layers of the oceans.

3. Model Experiments on Stationary Planetary Flow Patterns

Thoughts about the physical fundamentals of the oceanic circulation lead to an analysis of simple flow patterns in a homogeneous fluid layer: (1) of uniform depth on a rotating sphere and bounded by meridional barriers; (2) of uniform depth on a β -plane (plane with $\beta=2\omega \sin \phi = \text{const}$, see p. 556) and bounded by barriers running north-south; (3) of radially non-uniform depth on a rotating plane and bounded by radial barriers. Analyses of this type and associated model experiments have been made recently in a very instructive form by STOMMEL, ARONS and FALLER (1958). Although these investigations cannot be regarded as concluded they, nevertheless, throw some light on the physical processes operating in the oceanic circulation, so that it seems appropriate to present the main contents of these investigations here. The essential elements which define the simplified régime described above are:

- (a) the flow in the whole layer is steady and geostrophic except and only;
- (b) at the western boundary where a narrow intense western boundary current is permitted to depart markedly from geostrophic conditions, and moreover;
- (c) this system which would otherwise be at rest is driven by a distribution of fluid sources and sinks representing various different driving agents such as the wind. This is no real restriction.

Some of these analyses and thoughts were tested by experiments in a pie-shaped sector of a fluid basin rotating counter-clockwise. The free surface was a paraboloid cylinder with vertical axis, concave upwards. The undisturbed depth varied radially from a minimum at the centre to a maximum at the outer rim. The top was covered with a sheet of glass in order to prevent the air in the room exerting any stress on the surface. After rotation for some time the fluid is completely at rest relative to the basin. There will be a component of flow radially outward (or inward) in the interior of the fluid only if there is a local fluid source (or sink). Components of geostrophic flow along circles of constant radius are permissible without divergence except where blocked by radial barriers. Figure 336 shows possible variations in the relative distribution of sources and sinks and the currents that would be expected in each case. The point source \oplus and sink \ominus of equal intensity were placed:

- (a) near to the eastern boundary of the sector at the end of radii of different length;
- (b) as an isolated source only at the apex of the sector. Since no point sink is provided the free surface will rise uniformly;
- (c) as an isolated source at the western edge of the rim.

The current flows along the shortest path to the western boundary of the sector.

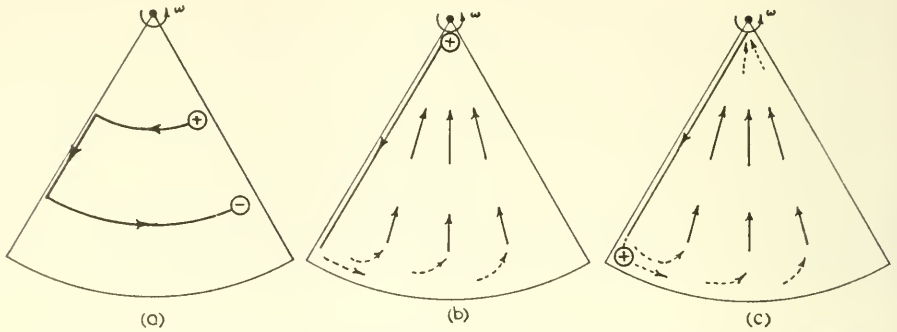


FIG. 336. (a) Diagram of circulation induced in a rotating sector by a source \oplus and a sink \ominus positioned as shown. (b) Sketch of flow pattern expected with source \oplus at apex of sector, surface of fluid rising uniformly. (c) Sketch of flow pattern expected with source \oplus at western edge of rim, surface of fluid rising uniformly (according to Stommel, Arons and Faller, 1958).

There a narrow intense western boundary current develops always, and in (a) after reaching the outer rim the water returns in another zonal geostrophic current to the sink \ominus . In (b) there develops a narrow intense western boundary current and in a surprising way the basin fills up from the rim although water is added at the apex. Even more surprising is case (c). The sector is allowed to fill up from the isolated source at the western edge of the rim. The interior geostrophic flow is again directed towards the centre, but the interior radial transport is so large that it feeds at the apex a narrow western boundary current which flows back *towards* the source \oplus .

The theory of these processes explains convincingly the nature of the water transports and explains the formation of the western boundary current which governs the process, though without, however, giving any detailed dynamic explanation. To check and to illustrate the principles of the theory and quantitative ideas concerning the flow in the rotating sector, Stommel, Arons and Faller have made rotational experiments in a tank with the form of a truncated sector of 60° width. In Fig. 337 are shown the experiments corresponding to those of Figures 336a and c; these confirm clearly the qualitative and theoretical argument.

The application of the results of such experiments to phenomena which can be observed in the ocean, is readily understood and their further development with the guidance of carefully chosen theoretical models should contribute much to an understanding of the phenomena occurring in ocean currents.

4. The Transient Response of an Ocean to a Variable Wind Stress

In all theoretical investigations of the ocean circulation induced by zonal winds it has been assumed that the effect of the wind does not change with time (is constant with time). It is known, however, that this is true only for a first approximation and attempts have occasionally been made to study the effect of a wind that changes with time on vertical structure and circulation of an ocean. A study of the time-dependent wind-driven circulation in a homogeneous, rectangular ocean has been given by VERONIS and MORGAN (1955). Already somewhat earlier the problem has also been considered by ICHYE (1951). They start essentially from the same equations of motion

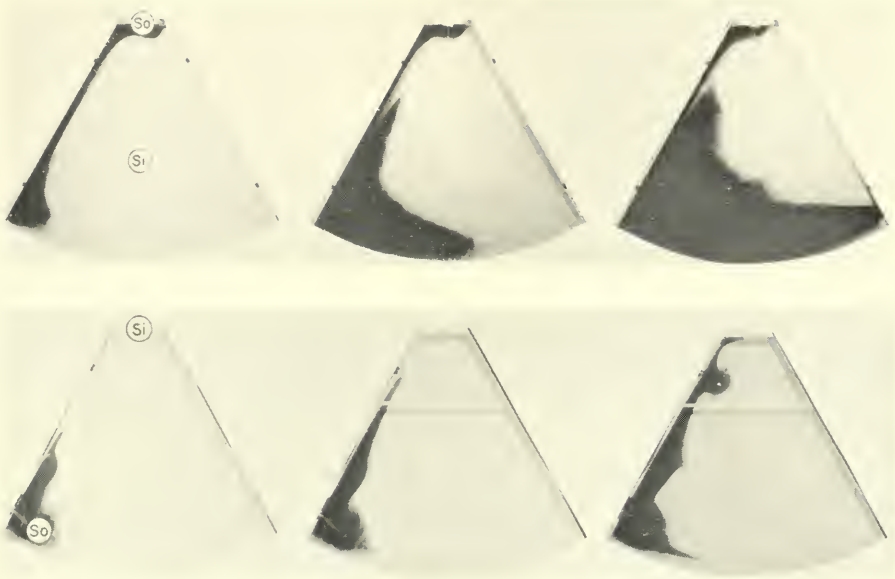


FIG. 337. (a) a photograph at 20, 80 and 220 min after the introduction of dye. The source was at the apex and there was no external sink (corresponding Fig. 336*b*). (b) Photographs at 5, 10 and 20 min. The dyed fluid was injected through a vertical glass tube in the south-west corner of the tank and the sink was at the apex (corresponding Fig. 336*c*). (According to Stommel, Arons and Faller, 1958.)

as used by MUNK (1950) and HIDAKA (1950) taking into account the lateral eddy viscosity and obtain, for a zonal wind stress whose amplitude varies harmonically with time, the variations in the strength of the currents and the phase lag behind the wind in the individual circulation gyres. The results seem to be somewhat outdated by the more recent developments in the theory of the general oceanic circulation.

A new and rather important contribution to the effect of a time-dependent wind on a stratified ocean has been made by VERONIS and STOMMEL (1956). Now one deals with *non-stationary* conditions, which stand in question and which can in general be regarded as aperiodic disturbances across the given current field; these disturbances of rather different dimensions may therefore vary with both time and position. A model was used in which the ocean was taken as horizontally unlimited—coastal effects were thus disregarded—and it consists of two layers (an upper and a lower layer separated by a boundary surface). The wind system introduced, however, is of a finite size. In agreement with the theoretical work on the dynamics of ocean currents in the central parts of the oceans (SVERDRUP, 1947 and REID, 1948) the lateral eddy viscosity was disregarded. The theoretical investigation tends towards an understanding of the way in which a two-layered ocean would react to changes in the wind field acting on it. The main questions were as follows:

(a) will the wind-generated current restrict itself to the top layers so that the horizontal pressure gradients and the velocities in the deep layers could be neglected, and how will the boundary surface and the physical sea level behave under these conditions?; and

(b) will the wind-driven current extend down to both layers, and is the horizontal pressure gradient in both layers down to the sea bottom of the same order of magnitude?; or

(c) will the wind influence cause combination of (a) and (b)?

Movements of type (a) are called internal or *baroclinic*, those of type (b) external or *barotropic*. This is illustrated by the scheme given in Fig. 338. It has often been

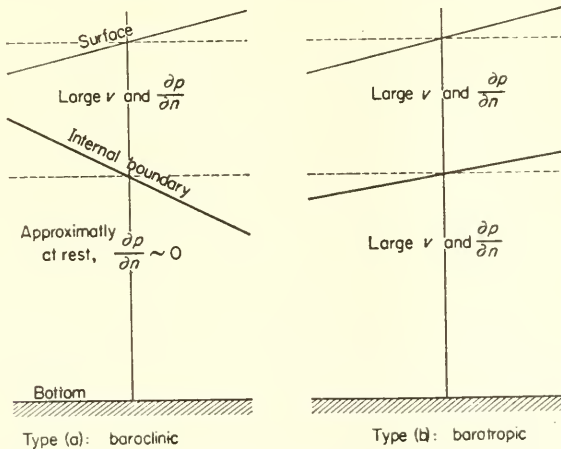


FIG. 338. The type of motion in a two-layered ocean. (a) baroclinic or internal type, with a motion in the upper layer and a nearly motionless lower layer. (b) barotropic or external type. Horizontal pressure gradient nearly equal in both layers.

pointed out in previous work that for a time-variable wind effect the three-dimensional structure of the sea tends to be baroclinic, which is in fact fairly readily understood. If the physical sea level inclines due to a wind influence the correspondingly generated horizontal pressure gradient at first extends down to the bottom also in the case of a two-layered ocean. In addition to the flow in the uppermost layers, more or less in the direction of the wind producing it a flow in the lower layers will thus also occur, only in the opposite direction (see Fig. 339). This latter current will increase in intensity until the slope of the internal boundary surface (opposite to that of the sea surface) causes the horizontal pressure gradient to disappear in the lower layers, so that the

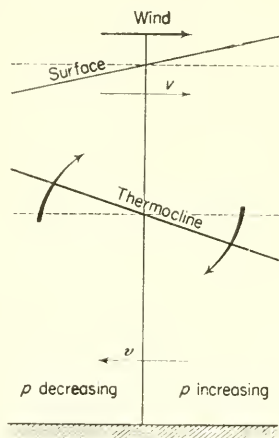


FIG. 339. Transition from a barotropic type in the first phase of wind influence to the final baroclinic type.

lower part of the ocean will finally be at rest. In the upper layer there will then be a drift current and underneath a geostrophic flow, while in the lower layers the ocean is at rest. It is therefore to be expected that the mass field of the sea and the wind-generated currents of the upper layers act and react on one another and this interrelation is such as to restrict the wind-driven currents to the upper layers of the ocean.

This striking *compensation principle between the upper and lower layers* is confirmed by experience and is one of the most important experimental facts of oceanography. If this were not the case it would not be possible to build up a picture of oceanographic conditions in the deep layers and their mass displacements on the basis of wide-spaced oceanographic observations; that is, it would be impossible from observations at widely differing times to form a picture of the average conditions of stratification and field of flow in the deep layers. This supports the theoretical results, since if these were somewhat different there would undoubtedly be a contradiction with experience and the model chosen would be unsuitable for such a purpose. This problem was first discussed by ROSSBY (1938), but his results were unsatisfactory since they gave more or less barotropic flow systems which is impossible. A barotropic state can only persist for a short time and finally a baroclinic state must predominantly prevail. After other attempts Veronis and Stommel⁽¹⁹⁵⁵⁾ have re-examined the problem and attempted its solution by means of a large mathematical apparatus.

In the two-layered oceanic model there are as usual two equations of motion for each layer, one for the u -component and the other for the v -component of the velocity, and the continuity equation. The equations of motion for the upper layer therefore take into account the wind stress acting on the sea surface. This then gives three pairs (2 times 3) of differential equations. By cross-wise differentiation, and taking into account the variation of the Coriolis parameter with latitude, one obtains for each layer a vorticity equation. As a first assumption the movements are taken as independent of the y -direction. As a consequence, the problem is thus one-dimensional and the equations are considerably simplified. This gives two equations which permit a study of the reponse of the physical sea level and the internal boundary surface to the variable shearing stress of the wind. It is interesting from the mathematical point of view that these equations can be combined to give an equation with a single variable without raising the order. It is of the fourth order and has the form

$$\lambda^2 k R_{xxxxt} - \frac{1}{f^2} R_{xttt} - R_{xt} + \beta \lambda^2 k R_{xx} - \frac{\beta}{f^2} R_{tt} = \frac{T_{xx}}{f}. \quad (\text{XXI.1})$$

R has a fixed numerical relationship to the displacement of the sea surface and the internal boundary surface and can have two values, R_1 and R_2 . In the same way k has the numerical values k_1 and k_2 corresponding to the values R_1 and R_2 . Moreover, $\lambda^2 (= gD_2/f^2)$ where D_2 is the equilibrium thickness of the lower layer and λ is a quantity termed by Rossby the "deformation radius". The solution of the differential equation (XXI.1) gives the "normal values of motion" (equation of normal modes) and makes it possible to determine all the desired quantities of the model such as the displacement of the boundary surfaces and the velocity in the different layers.

This equation can be used to derive the *free waves* of the system and their dependence on the dimensions of the system, when the wind stress is omitted in the equation. A knowledge of the *free waves* is of considerable value because of its great importance, since in view of resonance phenomena they may have considerable influence on the forced waves which are generated by the action of the wind. Assuming a normal mode of the form

$$R_i = S_i \sin (lx + \omega_i t) \quad (i = 1, 2); \quad (\text{XXI.2})$$

that is, in form of a wave progressing in the negative x -direction with a frequency ω_i , then the equation (XXI.1) transforms into

$$\left(\frac{\omega_i}{f}\right)^3 - \frac{\beta}{fl} \left(\frac{\omega_i}{f}\right)^2 + (1 + \mu_i^2) \frac{\omega_i}{f} + \frac{\beta \mu_i^2}{fl} = 0 \quad (\text{XXI.3})$$

with

$$\mu_i^2 = k_i l^2 \lambda^2.$$

The solution of this algebraic equation (three positive roots) gives the frequency ω_i as a function of the wave-number $2\pi/l$ or of the wavelength L . The roots are $\omega_{i,1}$; $\omega_{i,2}$; $\omega_{i,3}$ and correspondingly there exist in total six possible modes of wave motion. Figure 341 gives frequencies and periods of the waves for $D_1 = 500$ km, $D_2 = 3500$ km, $f = 10^{-4}$ sec $^{-1}$, $\beta = 2 \times 10^{-11}$ m $^{-1}$ sec $^{-1}$ and for wavelengths $10 \leq L \leq 12,000$ km covering the entire region under consideration.

Two of the waves have large periods and in these the flow is in geostrophic equilibrium; they are the barotropic and baroclinic Rossby waves. The other four waves, two of which are barotropic and the other two baroclinic, are inertial-gravitational waves resulting from an imperfect balance between the pressure and the Coriolis force. In general, the barotropic waves are pure gravitational waves with a velocity of propagation $\sqrt{g(D_1 + D_2)}$ the baroclinic waves are pure inertial waves with a period of a

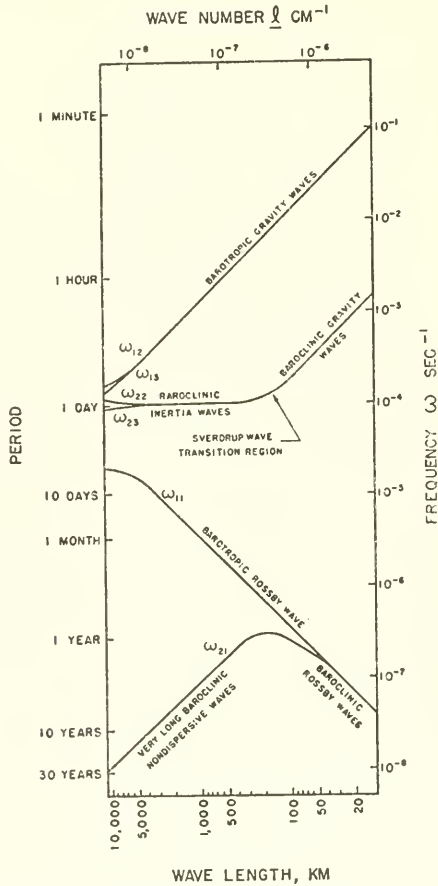


FIG. 340. The velocity and frequency of all the various free waves, which may occur in a two-layered ocean (according to Veronis and Stommel, 1956).

half a pendulum day $2\pi/f$; at the short branch in their connection on the right (see Fig. 340) are ordinary internal waves at the boundary surface with periods of between 1 h and 1 day.

This derivation of all possible wave types from a single equation is extremely interesting and instructive. Two types of disturbances in time will be taken for a study of wind-driven motions. In the first case they are forced waves generated by a moving wave-wind system. This wind system as to the order of magnitude shall be comparable with atmospheric disturbances as are shown in 5-day average charts. This corresponds

to a period of about 2 weeks and a wavelength of about 6000 km. The force producing them thus has the form $W \sin (lx + vt)$, where W is about $1 \text{ cm}^2 \text{ sec}^{-1}$; for an eastwards movement of the disturbance v is negative. For periods of 1–7 weeks—values which are comparable with the periods of barotropic Rossby waves—the ocean reacts largely as a *homogeneous* water body. As the period increases the baroclinic effects become also larger and for longer periods (more than a year) the motion is only partly barotropic and the baroclinic effects will be more important. For very long wind-periods (at least about 100 years) the motion is entirely baroclinic. The flow is geostrophic and in full accord with a stationary state.

The second type of wind-driven ocean currents is that produced by a *stationary* wind field imposed suddenly at a given time. In this case all the possible free waves of the system may develop and an investigation can be made of the relative importance of inertial-gravitational waves and of geostrophically balanced motions.

If the action of the wind lasts for a period comparable with that of an ordinary storm then the geostrophically balanced motion will be partly barotropic and partly baroclinic. The internal boundary surface also reacts on the wind influence and this effect can definitely be found (10–20 m), if the wind continues for 3 or more days. The deep currents, however, remain weak and are probably no stronger than the thermo-haline currents such as those produced by Antarctic cooling. The effect of storms can thus make little contribution to the large-scale lateral mixing inside the oceanic stratosphere.

Other movements of inertia and gravitational character which may be generated are stronger but are not accompanied by measurable displacements of the boundary surface; they are pure horizontal inertia oscillations without any horizontal pressure gradients and depend largely on the earth rotation.

These investigations of Veronis and Stommel are undoubtedly of great importance for a knowledge of the dynamics of the ocean currents. They are, of course, so far incomplete; they do not, for instance, provide an explanation for the effects of barriers (coasts and the sea bottom) as well as for the effects of friction. At the present time, however, it is sufficient to gain some insight into the time-variable action of the wind. This is all the more important because of the extreme difficulty of gaining an insight into such rapidly changing phenomena solely by means of oceanographic observations.

Bibliography

- ALBERT, I. VON MONACO, FÜRST, (1889). Experiences de flottage sur les courants superficiels del' Atlantique Nord. *Congr. Intern. Scie. Geogr. en 1889*. Paris 1889.
- ANVERS, H. G. (1927). A study of the variation of mean sea-level from a level surface. *Amer. Geophys. Union Trans., Nat. Res. Coun. Bull.* No. 61, p. 56. Washington 1927.
- ARAKAWA, H. (1935). On the general secondary circulations of the ocean. *Mem. Imp. Mar. Obs., Kobe.* 6, No. 1.
- ARAKAWA, H. and OOMA, S. (1935). On the general circulation of the Ocean. *Geophys. Mag., Tokyo.* 9, No. 1.
- ARAKAWA, H., OOMA, S. and NAGAOKA, W. (1935). On the secondary circulation of ocean produced by winds. *Proc. Phys.-Math. Soc. Japan.* Ser. 3, 17, No. 10.
- ARX VON, W. S. (1950). An Elektromagnetic method for measuring the velocities of ocean current from a ship under way. *Phys. Oceanogr. Met.* 11, 1-62. Woods Hole 1950.
- ARX VON, W. S., BUMPUS, D. F. and RICHARDSON, W. S. (1955). On the fine-structure of the Gulf Stream front. *Deep. Sea Res.* 3, 46-65.
- BIGELOW, B. (1917). Explorations of the U.S. Coast and Geod. Surv. Steamer *Bache* in the western Atlantic, Jan.-March 1914. *Oceanogr. Rep. of the Comm. of Fish.* 1915. App. 5. Washington 1917.
- BJERKNES, J. (1924). Diagnostic and prognostic application of mountain observations. *Geofys. Publ.* 3, No. 6. Oslo 1924.
- BJERKNES, V. (1898). Über einen hydrodynamischen Fundamentalsatz und seine Anwendung bes. auf die Mechanik der Atmosphäre und des Weltmeeres. *K. Svenska Vetensk. Akad. Handl.* 31, No. 4 Stockholm 1898.
- BJERKNES, V. (1900). Das dynamische Prinzip der Zirkulationsbewegung in der Atmosphäre. *Met. Z.* p. 97.
- BJERKNES, V. (1901). Circulation relativ zur Erde. *Öfers. K. Vetensk. Akad. Förhandl.* No. 10. Stockholm 1901.
- BJERKNES, V. (1921). On the dynamics of the circular vortex with applications to the atmosphere and atmospheric vortex and wave motions. *Geofys. Publ.* 2/4. Oslo 1921.
- BJERKNES, V. (1929). Über die hydrodyn. Gleichungen in Lagrange'scher und Euler'scher Form und ihre Linearisierung für das Studium kleiner Störungen. *Geofys. Publ.* 5, No. 11. Oslo 1929.
- BJERKNES, V. (1936). Über thermodynamische Maschinen, die unter der Mitwirkung der Schwerkraft arbeiten. *Abh. sächs. Akad. Wiss.* 35, No. 1. Leipzig 1936.
- BJERKNES, V. *et al.* (1910). *Dynamic Meteorology and Hydrography.* Pt. I, Statics. *Carnegie Inst. Wash., Publ.* No. 88.
- BJERKNES, V. und MITARB. (1912). *Dynamische Meteorologie und Hydrographie.* 1. Teil, Vieweg & Sohn, Braunschweig 1921.
- BJERKNES, V. (1913). *Dynamische Meteorologie und Hydrographie,* 2. Teil, Vieweg & Sohn, Braunschweig 1913, p. 169.
- BJERKNES, V. *et al.* (1933). *Physikalische Hydrodynamik.* Mit Anwendungen auf die dyn. *Meteorologie.* 3. Springer, Berlin. 1933.
- BOBZIN, E. (1922). Vergleichende Betrachtungen des Klimas und der kalten Auftriebsströmungen an der südwestafrikanischen und südarabischen Küste. *Dtsch. Übers. Met. Beob.* Hft. 23. Hamburg 1922.
- BÖHNECKE, G., HENTSCHEL, E. u. WATTENBERG, H. (1930). *Ann. Hydr. Mar. Met.* 1930, 1931 und 1932.
- BRENNECKE, W. (1921). Die ozeanogr. Arbeiten der Deut. Antarktischen Exp. 1911/12. *Arch. Deut. Seewarte,* 39/1. Hamburg 1921.
- BROOKS, C. E. P. (1930). The role of the oceans. *Quart. J. Roy. Met. Soc., Lond.* 56.
- BUEN DE R. (1926). Résultats des investigations espagnoles dans le détroit de Gibraltar. *Rapp. et Proc. Verb.* 44. Kopenhagen 1927.
- CARRUTHERS, J. N. (1930). Further investigations upon the water movements in the English Channel. *J. Mar. Biol. Ass.* 7, No. 1.
- CARRUTHERS, J. N. (1954). Some inter-relationships of oceanography and fisheries. *Arch. Met. Wien. Serie B.* 6, 167-189 (Festschrift Defant).

- CASTENS, G. (1931). Strömung und Isolinienform. *Ann. Hydr. Mar. Met.* 41.
- CHARNEY, I. G. (1955). The generation of ocean currents by wind. *J. Mar. Res.* 14/4, 477–498.
- CHARNEY, I. G. (1955). The Gulf Stream as an inertial boundary layer. *Proc. Acad. Sci.* 41/10, 731–740. Washington 1955.
- CLOWES, A. J. (1933). Influence of the Pacific on the circulation in the Southwest Atl. Ocean. *Nature, Lond.* 81.
- COLDING, A. (1881). *Danska vid. Selsk. Skr.* 1, No. 4.
- COOPER, L. H. N. and VAUX, D. (1949). Cascading over the continental slope of water from the Celtic Sea. *J. Mar. Biol. Ass.* 28, 719.
- COOPER, L. H. N. (1952). Water movements over the continental slope in relation to fisheries hydrography. *Rapp. et P.V. Cons. Int. Explorat. Mer.* 131, 44.
- CROLL, J. (1870/71 and 1875). In several treatises in *Phil. Mag.* 40 u. 42, in *Climate and time*, Kap. 6–10. London 1875.
- CROWELL, T., MONTGOMERY, R. B. and STROUP, E. D. (1954). Equatorial Undercurrent in Pacific revealed by new methods. *Science* 119, 648–9.
- DALL, W. (1881). Hydrologie des Bering-Meeress und der benachbarten Gewässer. *Petermanns Geogr. Mitt.* 1881, p. 361.
- DALLAS, W. L. and WALKER, G. T. (1908). *Meteorolog. Atlas of the Indian seas and the North Indian ocean*. Simla 1908.
- DEACON, G. E. R. (1934). Die Nordgrenzen antarktischen und subantarktischen Wassers im Weltmeer. *Ann. Hydr. Mar. Met.* 1934, p. 129. See also *Nochmals: Wei entsteht die antarktische Konvergenz?* p. 475.
- DEACON, G. E. R. (1937). The hydrology of the southern ocean. *Discovery-Rep.* 15. Cambridge 1937.
- DEFANT, A. (1923). Theoretische Überlegungen und experimentelle Untersuchungen zum Aufbau höherer Zyklogen und Antizyklogen. *SB. Akad. Wiss., Wien. Abt. II a*, 132, 83. Wien 1923.
- DEFANT, A. (1925). *Ann. Hydr. Mar. Met.* p. 231.
- DEFANT, A. (1923). Triftströme in geschichteten Wasser. *Z. Geophys.* p. 310.
- DEFANT, A. (1929a). Dynamische Ozeanographie. *Einführung in die Geophysik*, 3. J. Springer, Berlin 1929.
- DEFANT, A. (1929b). Stabile Lagerung ozeanischer Wasserkörper und dazugehörige Stromsysteme. *Veröff. Inst. Meeresk. Univ. Berl. A*, Hft. 19. Berlin 1929.
- DEFANT, A. (1929c). *Die ozeanische Zirkulation*. I. Intern. Ozeanogr. Kongr. Sevilla, Mai 1929.
- DEFANT, A. (1930a). Bericht über die ozeanogr. Untersuchungen im der Dänemarkstrasse und in der Irmingersee. I. *S.B. Preuss. Akad. Wiss. Phys. Math. Kl.* p. 7. Berlin 1930.
- DEFANT, A. (1930b). Die Bewegungen und der thermo-haline Aufbau der Wassermassen in Meeresstrassen. *S.B. Preuss. Akad. Wiss. Phys.-Math. Kl.* 14. Berlin 1930.
- DEFANT, A. (1931). Bericht über die ozeanogr. Untersuchungen des "Meteor" in der Dänemarkstrasse und Irmingersee. II. *Ber. Sitzber. Preuss. Akad. Wiss. Phys.-Math. Kl.* 19. Berlin 1931.
- DEFANT, A. (1932). Die Gezeiten und inneren Gezeitenwellen des Atl. Ozeans. "*Meteor*" *Werk* 7/1, 7. Berlin 1932.
- DEFANT, A. (1933). Der Abfluss schwerer Luftmassen auf geneigtem Boden, nebst einigen Bemerkungen zu der Theorie stationärer Luftströme. *S.B. Preuss. Akad. Wiss.* 18, 624–635.
- DEFANT, A. (1935). Der Äquatoriale Gegenstrom. *Sitzber. Preuss. Akad. Wiss. Phys.-Math. Kl.* 28. Berlin 1935.
- DEFANT, A. (1936a). *Das Kaltwasserauftriebsgebiet vor der Küste Südwestafrikas*. Länderkundliche Studien (Festschrift W. Krebs). Stuttgart 1936.
- DEFANT, A. (1936b). Bericht über die ozeanogr. Untersuchungen des "Metears" in der Dänemarkstrasse und in der Irmingersee. III. *Ber. S.B. Preuss. Akad. Wiss. Phys.-Math. Kl.* p. 232. Berlin 1936.
- DEFANT, A. (1936c). Schichtung und Zirkulation des Atlantischen Ozeans. "*Meteor*" *Werk* 6/1. Berlin 1936.
- DEFANT, A. (1936). Die Austauschgrösse der atmosphärischen und ozeanischen Zirkulation. *Ann. Hydr. Mar. Met.* p. 12.
- DEFANT, A. (1937). C. G. Rossby, Dynamik stationärer ozeanischer Ströme im Lichte der experim. Stromlehre. Nebst einigen Bemerkungen. *Ann. Hydr. Mar. Met.* p. 58.
- DEFANT, A. (1938). Aufbau und Zirkulation des Atlantischen Ozeans. *S.B. Preuss. Akad. Wiss. Phys.-Math. Kl.* Berlin 1938.
- DEFANT, A. (1940a). Die Lage des Forschungsschiffes "Altair" auf der Ankerstation 16–20 Juni 1938 usw. Aus den *Wiss. Erg. der Intern. Golfstrom-Unternehmung 1938*, 3. Lief. *Ann. Hydr. Mar. Met.*

- DEFANT, A. (1940b). Die ozeanogr. Verhältnisse während der Ankerstation des "Altair" am Nordrand des Hauptstromstriches des Golfstromes nördlich der Azoren. Aus den Wiss. Erg. der Intern. Golfstrom-Unternehmen 1938. *Ann. Hydr. Mar. Met.* Beih. Nov. 1940.
- DEFANT, A. (1940). Scylla und Charibdis und die Gezeitenströmungen in der Strasse von Messina. *Ann. Hydr. Mar. Meteor.* 68, 1451–57.
- DEFANT, A. (1941a). Die relative Topographie einzelner Druckflächen im Atl. Ozean. "Meteor" *Werk.* 6/2. Berlin 1941.
- DEFANT, A. (1941b). Die absolute Topographie des phys. Meeresniveaus und der Druckflächen, sowie die Wasserbewegungen im Atl. Ozean. "Meteor" *Werk.* 6/2. 5. Lief. Berlin.
- DEFANT, A. (1941c). Zur Dynamik des äquatorialen Gegenstromes. *Ann. Hydr. Mar. Met.* p. 249.
- DEFANT, A. (1941d). Die absolute Berechnung ozeanischer Ströme nach dem dynamischen Verfahren. *Ann. Hydr. Mar. Met.* p. 169.
- DEFANT, A. (1941e). Die phys. Meeresniveau des Atl. Ozeans. *Z. Ges. Erdkunde zu Berlin* p. 145.
- DEFANT, A. (1950). Reality and illusion in oceanographic survey. *J. Mar. Res.* 9/2, 120–138.
- DEFANT, A. (1950). Memorandum concerning the work of the Marine Life Research Program. *Scripps Inst. Oceanogr.* La Jolla, Univ. of California.
- DEFANT, A. (1951). Windstau und Auftrieb an ozeanischen Küsten. *Arch. Met. Wien.* 4, Serie A. 206–308.
- DEFANT, A. (1952). Theoretische Überlegungen zum Phänomen des Windstaus und des Auftriebs an ozeanischen Küsten. *Dtsch. Hydrogr. Z.* 5/2–3, 69–80.
- DEFANT, A. (1955). Die Strömungen in Meeresstrassen. *Dtsch. Hydrogr. Z.* 8/1.
- DEFANT, A. (1956). Atmosphärische und ozeanische lange Wellen und Wirbelstörungen und ihre Ähnlichkeit mit Trägheitsbewegungen. *Dtsch. Hydrogr. Z.* 9/2, 49–55.
- DEFANT, A. und SCHUBERT, V. O. (1934). Strommessungen und ozeanographische Serienbeobachtungen der 4-Länder-Untersuchung im Kattegat 10.–17. Aug. 1931. *Veröff. Inst. Meeresk. Univ. Berl. A.* Hft. 25. Berlin 1934.
- DEFANT, F. (1940). Trägheitsschwingungen im Ozean und in der Atmosphäre. *Veröff. Met. Inst. Univ. Berl.* 4, No. 2.
- DIETRICH, G. (1935). Aufbau und Dynamik des südlichen Agulhasstromgebietes. *Veröff. Inst. Meeresk. Univ. Berl. A.* Hft. 27. Berlin 1935.
- DIETRICH, G. (1936). *Die Naturwissenschaften*, p. 225.
- DIETRICH, G. (1937a). Die Lage der Meeresoberfläche im Druckfeld von Ozean und Atmosphäre. *Veröff. Inst. Meeresk. Univ. Berl. A.* Hft. 33. Berlin 1937.
- DIETRICH, G. (1937b). Bewegung und Herkunft des Golfstromwassers. *Veröff. Inst. Meeresk. Univ. Berl. A.* Hft. 33. Berlin 1937.
- DIETRICH, G. (1937c). "Die dynamische Bezugsfläche", ein Gegenwartsproblem der dyn. Ozeanographie. *Ann. Hydr. Mar. Met.* p. 506.
- DIETRICH, G. (1939). Das Amerikanische Mittelmeer. Ein meereskundlicher Überblick. *Z. Ges. Erdkunde zu Berlin*, p. 108.
- DIETRICH, G. (1956). Schichtung und Zirkulation in der Irmiger-See im Juni 1955. *Ber. Dtsch. Wiss. Komm. Meeresforsch.* 14/4, 255–312.
- DIETRICH, G. (1956). Überströmung des Island-Färöer-Rückens in Bodennähe nach Beobachtungen mit dem Forschungsschiff "Anton Dohrn", 1955/56. *Dtsch. Hydrograph. Z.* 9/2, 78–89.
- DINKLAGE, L. E. (1888). Die Oberflächenströmungen im südwestlichen Teil der Ostsee und ihre Abhängigkeit vom Winde. *Ann. Hydr. Mar. Met.* p. 1.
- DORN, VAN, W. G. (1952). Wind stress over water. *Scripps Inst. Oceanogr. A.F. Tech. Rep.* No. 1, Nov. 1952.
- DUDEN, P. (1933). Turbulente Ausbreitungsvorgänge im Freistrahle. *Die Naturwissenschaften* 1933, p. 375.
- DURST, C. S. (1924). The relationship between current and wind. *Quart. J. Roy. Met. Soc. Lond.* 50.
- EKMANN, F. L. (1875). *Nova Acta Reg. Soc. Upsala* 1876, or *Ofers. Vet. Akad. Handl. Stockh.* No. 7.
- EKMANN, V. W. (1899). Ein Beitrag zur Erklärung und Berechnung des Stromverlaufes in Flussmündungen. *Ofers. Kgl. Vet. Akad. Handl. Stockh.* No. 5, p. 469.
- EKMANN, V. W. (1905). On the influence of the earth rotation on ocean currents. *Ark. Math. Astr. och Fys.* 2, No. 11. Stockholm 1905.
- EKMANN, V. W. (1906). Beiträge zur Theorie der Meeresströmungen. *Ann. Hydr. Mar. Met.* p. 428.
- EKMANN, V. W. (1922). *Dynamische Gesetze der Meeresströmungen*. Vorträge aus dem Gebiet der Hydro- u. Aerodynamik. Innsbruck 1922.
- EKMANN, V. W. (1923). Über die Horizontalzirkulation winderzeugter Meeresströmungen. *Ark. Math., Astr. och Fys.* 17, No. 26. Stockholm 1923.

- EKMAN, V. W. (1926). Können Verdunstung und Niederschlag im Meere merkliche Kompensationsströme verursachen? *Ann. Hydr. Mar. Met.* **54**, 261–270.
- EKMAN, V. W. (1927). Meeresströmungen. *Handb. Phys. Techn. Mechanik.* **5**, p. 196. Hrg. von Auerbach u. Hort. Leipzig 1927.
- EKMAN, V. W. (1928a). Note on the theoretical causes of ocean-currents. *J. Cons. Intern.* **3**, No. 1. Kopenhagen 1928.
- EKMAN, V. W. (1928b). A survey of some theoretical investigations on ocean-current. *J. Cons. Intern.* **3**, No. 3. Kopenhagen 1928.
- EKMAN, V. W. (1928c). Eddy viscosity and skin-friction in the dynamics of winds and ocean-currents. *Mem. Roy. Soc. Lond.* **2**, No. 20.
- EKMAN, V. W. (1929). Über die Strömmenge der Konvektionsströme im Meere. *Lund Univ. Arsskr.* N.F. Afd. 2, **25**, No. 6. Lund and Leipzig 1929.
- EKMAN, V. W. (1931). Zum Problem des Golfstromes. *Gerl. Beitr. Geophys.* **32**, Köppenbd. II, p. 353.
- EKMAN, V. W. (1932). Studien zur Dynamik der Meeresströmungen. *Gerl. Beitr. Geophys.*, **36**, 385.
- EKMAN, V. W. (1939). Neuere Ergebnisse und Probleme zur Theorie der Konvektionsströme im Meer. *Ergebn. Kosm. Phys.* **4**. Leipzig 1939.
- EKMAN, V. W. (1941). Trägheitsschwingungen und Trägheitsperiode im Meer. *Ann. Hydr. Mar. Met.* p. 238.
- EKMAN, V. W. and HELLAND-HANSEN, B. (1931). Measurements of ocean-currents (Experiments in the North Atl.). *Kgl. Fysiogr. Sällsk. Lund.* **1**, No. 1.
- ERTEL, H. (1933). Verallgemeinerung eines Satzes von A. DEFANT u.s.w. *Sitzber. Preuss. Akad. Wiss. Math.-Phys. Kl.* p. 751.
- ERTEL, H. (1937). Eine Erweiterung der V. W. EKMAN'schen Theorie stationärer Driftströme. *Gerl. Beitr. Geophys.* **49**, 368.
- EULER, LEONHARD (1755). *Historie de l'Academie Royale de Berlin.*
- McEWEN, G. F. (1912). The distribution of ocean temperatures along the west coast of North America deduced from Ekman's theory of upwelling of cold water from adjacent ocean depth. *Intern. Rev. ges. Hydrobiol. Hydrogr.*
- McEWEN, G. F. (1934). Rate of upwelling in the region of San Diego computed from serial temperatures. *Proc. Fifth Pacific Sci. Congr.* 1933, **3**, Univ. Toronto 1934.
- EXNER, F. (1912). Zur Kenntnis der unteren Winde über Land und Wasser und die durch sie erzeugten Meeresströmungen. *Ann. Hydr. Mar. Met.* p. 22.
- EXNER, F. (1917). *Dynamische Meteorologie.* J. Springer, Berlin, 1917, p. 159.
- EXNER, F. (1919). Über oscillierende Strömungen im Wasser und Luft. *Ann. Hydr. Mar. Met.* p. 155.
- EXNER, F. (1924). Über die Auslösung der Kälte- und Wärmeeinbrüche in der Atmosphäre. *S.B. Wien Akad. Wiss. Math.-Naturw. Kl.* p. 133. Wien 1924.
- FELBER, O. H. (1934). Oberflächenströmungen des Nordatl. Ozeans zwischen 15° und 50° N. *Br. Arch. Deut. Seewarte* **53**, No. 1. Hamburg 1934.
- FERREL, W. (1861). An essay on the wind and currents of the ocean. *Nasville Jour. of Med. and Surv.* **9**, Nos. 4–5, 1856. See also *Amer. J. Sci.* **31**.
- FJELDSTAD, J. E. (1929). Ein Beitrag zur Theorie der winderzeugten Meeresströmungen. *Gerl. Beitr. Geophys.* **23**, 237.
- FJELDSTAD, J. E. (1930). Ein Problem der Windstromtheorie. *Z. Angew. Math. Mech.* **10**, 121.
- FJELDSTAD, J. E. (1940). Stationary current in heterogeneous water. *Arch. Math. Naturvid.* **48**, No. 6. Oslo 1946.
- FÖRTHMAN, E. (1934). Über turbulente Strahlausbreitung. *Ing. Arch.* **5**, 42.
- FORNOFF, N. P. and MONTGOMERY, R. B. (1955). The Equatorial Undercurrent in the light of vorticity equation. *Tellus* **7/4**, 518–21.
- FORCH, C. (1909). Über die Beziehungen zwischen Wind und Strom im Europäischen Mittelmeer. *Ann. Hydr. Mar. Met.* p. 435.
- FUGLISTER, F. C. (1947). Average monthly sea surface temperatures of the western North Atlantic Ocean. Pap. in *Phys. Oceanogr. and Met.* **10**, No. 2. Cambridge (Mass.) 1947.
- FULTON, T. W. (1897). The surface currents of the North Sea. *Scott. Geogr. Mag.* **13**. Edinburgh 1897.
- GALLE, P. H. (1910). Zur Kenntnis der Meeresströmungen. *Med. Verh. Kon. Ned. Met. Inst. Utrecht*, No. 102.
- GEDGE, H. J. (1898). Report on the undercurrents in the straits of Bab el Mandeb. London 1898. Extract in *Ann. Hydr. Mar. Met.* p. 519.
- GEHRKE, J. (1907). Mean velocity of the atlantic currents running north of Scotland and through the English Channel. Publ. de Circ. No. 40. Kopenhagen 1907.
- GODSKE, C. L., BERGERON, T., BJERKNES, J. and BUNDGAARD, R. C. (1957). Dynamic Meteorology and Weather Forecasting. *Amer. Met. Soc.*

- GORTLER, H. (1941). Einfluss der Bodentopographie auf Strömungen über der rotierenden Erde. *Z. Angew. Math. Mech.* **21**, 279. See also: Neuere Beiträge zur Dynamik atmosphärischer und ozeanischer Strömungen. *Naturwissenschaften* p. 473.
- GOLDSBROUGH, G. R. (1933). Ocean currents produced by evaporation and precipitation. *Proc. Roy. Soc. Ser. A*, **141**, 512-17.
- GROEN, P. (1948). Methods for estimating dynamic slopes and currents in shallow water. *J. Mar. Res.* **7**, No. 3 (Sverdrup Sixth. Anniv.).
- GULDBERG, et MOHN (1876). *Etudes sur les mouvements de l'atmosphère*. Christiania 1876.
- GUNTHER, E. R. (1936). Report on oceanogr. Investigations in the Peru coastal current. *Discovery Rep.* **13**. Cambridge 1936.
- GUNTHER, E. R. (1936a). Variations in intensity of the Peru coastal current. *Geogr. J.* **88**. London 1936.
- GUSTAFSON, T. and OTTERSTEDT, B. (1932). Observations de courants dans la Baltique 1931. *Sven. Hydr.-Biol. Komm. Skr. Ny Ser.: Hydr.* **9**. Lund 1932.
- GUSTAFSON, T. and KULLENBERG, B. (1933). Trägheitsströmungen in der Ostsee. *Medd. Göteborgs Oceanogr. Inst.* No. 5. Göteborg 1933.
- GUSTAFSON, T. and KULLENBERG, B. (1936). Untersuchungen von Trägheitsströmungen in der Ostsee. *Sven. Hydr.-Biol. Komm. Skr. Ny Ser.: Hydr.* No. 13. Lund 1936.
- HADAMARD, J. (1903). *Lecons sur la propagation des ondes et les équations de l'hydrodynamique*. Paris 1903.
- HANSEN, W. (1951). Winderzeugte Strömungen im Ozean. *Dtsch. Hydrogr. Z.* **4**, 161-72.
- HANSEN, W. (1952). Einige Bemerkungen zum Golfstromproblem. *Dtsch. Hydrogr. Z.* **5/23**, 80-94.
- HANSEN, W. (1954). Neuere Untersuchungen über Meeresströmungen. *Naturwissenschaften* **41/9**, 202-5.
- HANZAWA, M. (1953). On the eddy diffusion of pumices ejected from Myojin reef in the southern sea of Japan. *Recent oceanogr. works in Japan*, N.S. **1**, No. 1.
- HAURWITZ, B. (1940). The motion of atmospheric disturbances. *J. Mar. Res.* **3**, No. 1.
- HAURWITZ, B. and PANOFKY, H. A. (1950). Stability and meandering of the Gulf Stream. *Trans. Amer. Geophys. Un.* **31/5**, 723-31.
- HELA, J. (1948). On the stress of the wind on the water surface. *Geophysica* No. 3, Geophys. Soc. Finland, Helsinki 1948, pp. 146-61.
- HELLAND-HANSEN, B. (1905). *Report on Fishery and Hydrogr. Invest. in the Faroer-Shedland Channel and the northern part of the North Sea* in 1902. London 1905.
- HELLAND-HANSEN, B. (1912). In MURRAY and HJORT, *The depths of the ocean*. London 1912, Kap. 5, p. 267.
- HELLAND-HANSEN, B. (1934). The sognefjord section. Oceanogr. Obs. in the northernmost part of the North Sea and the southern part of the Norwegian Sea. *J. Johnstone Mem. Vol.* p. 257. Liverpool 1934.
- HELLAND-HANSEN, B. (1939). Untersuchungen über örtliche und zeitliche Schwankungen des "Golfstromes" im Norwegischen Meer usw. *Norsk. Geogr. Tidsskr.* **7**, Nos. 5-8, Oslo 1939.
- HELLAND-HANSEN, B. and NANSEN, FR. (1909). *The Norwegian Sea*, Rep. *Norw. Fish. Mar. Invest.* Christiania 1909.
- HELLAND-HANSEN, B. and NANSEN, FR. (1926). *The eastern North Atlantic*. *Geofys. Publ.* **4**, No. 2. Oslo 1926.
- HELLSTRÖM, B. (1941). Wind effect on lakes and rivers. *Ing. Vet. Akad. Handl.* No. 158. Stockholm 1941.
- HELMHOLTZ, H. v. (1888). Über atmosphärische Bewegungen. *S.B. Preuss. Akad. Wiss. Berl., Math.-Phys. Kl.*
- HESELBERG, TH. und SVERDRUP, H. U. (1914/15). Beitrag zur Berechnung der Druck- und Massenverteilung im Meer. *Bergens Museums Aarbok*. No. 14. Bergen 1915.
- HIDAKA, K. (1927/28). Experm. studies on the North Pacific ocean currents near Japan. *Geophys. Mag. Tokyo*, **1**, No. 3 and 4.
- HIDAKA, K. (1933). Non stationary ocean-currents. Part I. *Mem. Imp. Mar. Obs. Kobe* **5**, No. 3.
- HIDAKA, K. (1940a). Absolute evaluation of oceanic currents in dyn. calculations. *Proc. Imp. Acad. Tokyo* **15**, No. 8.
- HIDAKA, K. (1940b). Practical evaluation of ocean currents. *Proc. Imp. Acad. Tokyo* **16**, No. 16.
- HIDAKA, K. (1950a). Circulation in a zonal ocean induced by a planetary wind system. *Geophys. Notes* **3**, No. 10.
- HIDAKA, K. (1950b). Wind-driven currents and surface contours in an enclosed ocean and the lateral mixing. *Geophys. Notes* **3**, No. 12.
- HIDAKA, K. (1950c). Drift currents in an enclosed ocean. Part I and II *Geophys. Notes* **3**, Nos. 23 and 38 (1950), Part III, **4** No. 3 (1951).

- HIDAKA, K. (1954). A contribution to the theory of upwelling on coastal currents. *Trans. Amer. Geophys. Un.* 35/3, 431-44.
- HIDAKA, K. (1955). A theoretical study on the general circulation of the Pacific Ocean. Contribut. from Dep. of Oceanogr. of the Agricul. and Mech. Coll. Texas, *Oceanogr. Ser. No. 42, Pacific Science* 9/2, 183/220.
- HIDAKA, K. and TSUCHIYA, M. (1953). On the Antarctic Circumpolar Current. *J. Mar. Res.* 12/2, 214-22.
- HOUGH, G. G. (1897). On the applications of harmonic analysis to the dynamical theory of the tides. Part I: On Laplace's oscillations of the first species and on the dynamics of ocean currents. *Phil. Trans. Ser. A*, 189 (IX), 201-58.
- HUMBOLDT, A. v. (1814). *Reisen in die Aquatorial-Gegenden des neuen Kontinents*. Originalausgabe 1814, AUSGABE, v. H. HAUFF, Stuttgart 1861, 1, p. 22; also "Kosmos" Stuttgart 1845, 1, p. 322.
- ICHIYE, T. (1950). Some remarks on Richardson's neighbour diffusion equation. *Oceanogr. Mag.* 2, No. 3, 101-4.
- ICHIYE, T. (1951). Theory of oceanic turbulence. *Oceanogr. Mag.* 3, No. 3.
- ICHIYE, T. (1953 and 1954). On the variations of oceanic circulation V, VI. *Geophys. Mag.* 25. Centr. Met. Obs. Tokyo 1953 and 1954, VI: *Oceanogr. Mag.* 6/1.
- IDRAC, P. (1928). Enregistrement des courants sous-marins du détroit de Gibraltar. *C.R. Acad. Sci. Paris* 186, No. 16, 1058.
- INODE, E. (1952). On the structure of wind near the ground. *Bull. Nat. Inst. Agr. Sci. Ser. A/2*.
- ISAACS, J. D. and ISELIN, C. O'D. (1952). Oceanographic Instrumentation. *Conf. Rancho Santa Fe, Cal.* 21-23 June 1952. Off. of Naval Research.
- ISELIN, C. O'D. (1936). A study of the circulation of the western North Atlantic. Pap. in *Phys. Oceanogr. Met.* 4, No. 4. Cambridge (Mass.) 1936.
- ISELIN, C. O'D. (1938). The development of our conceptions of the Gulf Stream system. *Trans. Nat. Res. Com. Wash.* June, 1938.
- ISELIN, C. O'D. (1940). Preliminary report on long-period variations in the transport of the Gulf Stream system. Pap. in *Phys. Oceanogr. Met.* 8, No. 1. Cambridge (Mass.) 1940.
- ISELIN, C. O'D. and FUGLISTER, F. C. (1948). Some recent developments in the study of the Gulf Stream. *J. Mar. Res.* 7, No. 3. (Sverdrup Sixt. Anniv.) 1948.
- JACOBSEN, J. P. (1909). Gezeitenströme und resultierende Ströme im Gr. Belt in verschiedenen Tiefen im Monat Juni 1909. *Medd. Komm. Havundersog.* (Ser. Hydr.) 1, No. 14. Kopenhagen 1910.
- JACOBSEN, J. P. (1912). *Strommessungen in der Tiefe der dänischen Gewässer in den Jahren 1909-11. Ibid.* 2, No. 3.
- JACOBSEN, J. P. (1913 u. 1918). Beiträge zur Hydrographie der dänischen Gewässer. *Medd. Komm. Havundersog.* (Ser. Hydr.) 2, No. 2. Kopenhagen 1913. *Ibid.* No. 7. Kopenhagen 1918.
- JACOBSEN, J. P. (1925). Die Wasserumsetzung durch den Öresund, den Grossen Belt und den Kleinen Belt. *Medd. Komm. Havundersog* (Ser. Hydr.) 1/9. Kopenhagen 1925.
- JACOBSEN, J. P. (1929). Contribution to the hydrography of the North Atlantic. *The "Dana" Exp.* 1921-22. Kopenhagen 1929.
- JACOBSEN, J. P. (1936). Die Wasserbewegungen in den Verbindungsstrassen zwischen der Ostsee und dem Kattegat. *V. Hydr. Konf. d. baltischen Staaten*. Finnland, Juni 1936, Mittl. 9B.
- JACOBSEN, J. P. and JENSEN, A. J. C. (1926). Examination of hydr. measurements from the research vessels "Explorer" and "Dana" during the summer 1924. *Rapp. Cons. expl. Mer.* 39, 31. Kopenhagen 1936.
- JACOBSEN, J. P. and THOMSEN, H. (1934). Periodical variations in temperature and salinity in the straits of Gibraltar. *J. Johnstone Mem. Vol.* p. 275. Liverpool 1934.
- JAKHELIN, A. (1936). The water transport of gradient currents. *Geofys. Publ.* 2/11. Oslo 1936.
- JEFFREYS, H. (1922). On the dynamics of wind. *Quart. J. Roy. Met. Soc.* p. 29. London 1922.
- JEFFREYS, H. (1923). The effect of a steady wind on the sea-level near a straight shore. *Phil Mag.* 46, 115-25.
- JEFFREYS, H. (1925). On fluid motions produced by differences of temperature and humidity. *Quart. J. Roy. Met. Soc.* 51. London 1925.
- JERLOV, N. G. (1953). Studies of the Equatorial Currents in the Pacific. *Tellus* 5/3, 308-14.
- KILIERICH, ALF B. (1939). The Godthaab Exp. 1928. A theoretical treatment of the hydr. observation material. *Medd. Gronland.* 78, No. 5, 149.
- KISINDO, S. (1934). Methods of ocean current observations now used by Hydr. Depart. Tokyo and some results obtained to date. *Hydr. Rev.* 11, No. 1. Monaco 1934.
- KNUDSEN, M. (1900). Ein hydrographischer Lehrsatz. *Ann. Hydr. Mar. Met.* p. 310.
- KOENUMA, K. (1939). On the hydrography of south-western part of the North Pacific and the Kuroshio. *Imp. Mar. Obs. Mem.* 7, 41. Kobe 1939.

- KÖPPEN, W. (1911). Wodurch ist die hohe Wärme Europas und des Nordatl. Ozeans bedingt? *Ann. Hydr. Mar. Met.* p. 113.
- KRÜGER, W. (1911). Meer und Küste bei Wangeroog und die Kräfte, die auf ihre Gestaltung einwirken. *Z. Bauw.* 61. Berlin 1911.
- KRÜMMEL, O. (1911). *Handbuch der Ozeanographie* 2 Bd. Stuttgart 1911.
- KULLENBERG, B. und HELA, J. (1942). Om tröghetssvängningar i Ostersjön. *Sven. Hydr. Biolog. Kom. Skr. N.S. Hydrogr.* 16. Göteborg 1942.
- LAGRANGE, DE J. L. (1781). *Nouv. Mém Acad. Berlin.*
- LAMBERT, W. D. (1931). *Bull. Géodés.* p. 327 (with numerical tables).
- LE DANOIS, E. (1934). Les transgressions oceanique. *Rev. Trav. Off. Pêches Mar.* No. 4, p. 28. Paris 1934.
- LENZ, E. (1847). Bericht über die ozeanischen Temperaturen in verschiedenen Tiefen. *Bull. Class. hist.-phil. Acad. Sci. Petersburg.* 3, Suppl. p. 11.
- MÄE, H. (1928). Über die Temperaturesprünge in der Ostsee. *S.B. Akad. Wiss. Wien, Abt. II a*, 137. Wien 1928.
- MARGULES, M. (1906). Über Temperaturschichtung in stationär bewegter und ruhender Luft. *Met. Z.* p. 243.
- MAURER, H. (1938). Die Masseinheiten für Fahrt, Strom und Strömung. *Ann. Hydr. Mar. Met.* p. 355.
- MENÉNDEZ, N. (1955). El estrecho de Gibraltar clave de la oceanografía de sus mares adyacentes. *Las Comunicaciones Euro-Africanas* 2. Cons. super. de Inst. Cientif. 1955.
- MERZ, A. (1921). Die Strömungen von Bosporus und Dardanellen. *Verh. d.20. Dtsch. Geogr.-Tag, Juni 1921.*
- MERZ, A. (1925). Die Deutsche Atl. Expedition auf dem Vermessungs- und Forschungsschiff "Meteor". *S.B. Preuss. Akad. Wiss. Phys.-Math. Kl.* 31. Berlin 1925.
- MERZ, A. (1929). In Wüst. Schichtung und Tiefenzirkulation des Pazifischen Ozeans. *Veröff. Inst. Meeresk. Univ. Berl. A.* Hft. 20. Berlin 1929.
- MEYER, H. H. F. (1923). Die Oberflächenströmungen des Atl. Ozeans im Februar. *Veröff. Inst. Meeresk. Univ. Berl. A.* Hft. 11. Berlin 1923.
- MICHAELIS, G. (1923). Die Wasserbewegungen an der Oberfläche des Indischen Ozeans im Januar und Juli. *Veröff. Inst. Meeresk. Univ. Berl. A.* Hft. 8. Berlin 1923.
- MIEGEN, VAN J. M. (1951). Hydrodynamic instability. *Comp. Meteor. Amer. Met. Soc.* pp. 434-53.
- MODEL, F. (1942). Die Rauhhigkeit der Meeresoberfläche. *Beitr. Geophys.* 59, Hft. 2.
- MOHN, H. (1885). Die Strömungen des Europäischen Nordmeeres. *Petermanns Geogr. Mitt.* 17.
- MOHN, H. (1887). Nordhavets Dyber, Temp. og Ströminger. *Den Norske Nordhavs Exp.* 1876-78, 2, No. 2.
- MÖLLER, L. (1928). A. Merz, Hydrogr. Untersuchungen im Bosporus und Dardanellen. *Veröff. Inst. Meeresk. Univ. Berl. A.* Hft. 18. Berlin 1928.
- MÖLLER, L. (1929). Die Zirkulation des Indischen Ozeans. *Veröff. Inst. Meeresk. Univ. Berl. A.* Hft. 21. Berlin 1929.
- MÖLLER, L. (1931). Wasserschichtung und-bewegung in Meerengen. *Ann. Hydr. Mar. Met.* p. 7.
- MONTGOMERY, R. G. and PALMÉN, E. (1940). Contributions to the question of the equatorial counter current. *J. Mar. Res.* 3, 112.
- MORGAN, G. W. (1956). On the wind-driven ocean circulation. *Tellus.* 8/3, 301-20.
- MOSSBY, H. (1947). Experiments on turbulence and friction near the bottom of the sea. *Bergens Mus. Aarb.* 1946/47, Naturv. rek. no. 3. Bergen 1947.
- MOSSBY, H. (1949). *Experiments on bottom friction.* Univ. Aarb. Bergen 1949, Naturv. rek. no. 10. Bergen 1949.
- MUNK, W. (1947). A critical wind speed for air-sea boundary processes. *J. Mar. Res.* 6, No. 3.
- MUNK, W. H. (1950). On the wind-driven ocean circulation. *J. Met.* 7, 79-83.
- MUNK, W. H. (1955). Wind stress on water: an hypothesis. *Quart. J. Roy. Met. Soc.* 81, 320-32; or *Contr. Scripps Inst. Oceanogr.* N.S. no. 795.
- MUNK, W. H. and CARRIER, G. F. (1950). On the wind-driven circulation in ocean basins of various shapes. *Tellus.* 2, 158-67.
- MUNK, W. H. and PALMÉN, E. (1951). Note on dynamics of the Antarctic Circumpolar Current. *Tellus.* 3/1, 53-5.
- MURPHY, R. C. (1926). Oceanic phenomena along west coast of South America during 1925. *Geogr. Rev.* p. 26.
- MURRAY, J. and HJORT, J. (1912). *The depths of the ocean.* London 1912.
- NANSEN, FR. (1902). The oceanography of the North Polar Basin. The Norw. North Polar Exp. 1893-96. *Sci. Res.* 3, 357 Christiania 1902.

- NANSEN, FR. (1905). Die Ursache des Meeresströmungen *Petermanns. Geogr. Mitt.*
- NANSEN, FR. (1915). Spitzbergen waters. Oceanogr. Obs. during the cruises of the "Vesle möy" to Spitzbergen in 1912. *K. Vet. Selsk. Skr. Mat.-Nat. Kl. No. 2*. Kristiania 1915.
- NARES, G. N. (1872). Investigations of currents in the straits of Gibraltar. *Proc. Roy. Soc.* 20.
- NEUMANN, G. (1940). Doe ozeanogr. Verhältnisse an der Meeresoberfläche im Golfstromsektor nördlich und nordwestlich der Azoren. Aus den wiss. Erg. d. Intern. Golfstrom-Unternehmung 1938. *Ann. Hydr. Mar. Met.* Beih. Juni.
- NEUMANN, G. (1942). Die absolute Topographie des phys. Meeresniveaus und die Oberflächenströmungen des Schwarzen Meeres. *Ann. Hydr. Mar. Met.* p. 265.
- NEUMANN, G. (1943). Über den Aufbau und die Frage der Tiefenzirkulation des Schwarzen Meeres. *Ann. Hydr. Mar. Met.* p. 1.
- NEUMANN, G. (1948). Ueber den Tangentialdruck des Windes und die Rauigkeit der Meeresoberfläche. *Z. Met.* 2, 193-203.
- NEUMANN, G. (1948). *Z. Met.* 2, 193.
- NEUMANN, G. (1954). *Notes on the wind-driven ocean circulation*. New York University, College of Eng., Research Division.
- NEUMANN, G. (1955). *Dynamics of wind-driven ocean currents*. *Met. Pap.* 2/4. New York University, College of Eng., August 1955.
- NEUMANN, G. (1956). Zum Problem der "Dynamischen Bezugsfläche" insbesondere im Golfstromgebiet. *D. Hydr. Z.* 9/2, 66-78.
- NEUMANN, G. and SCHUMACHER, A. (1944). Strömungen und Dichte der Meeresoberfläche vor der Ostküste Nordamerikas. *Ann. Hydr. Mar. Met.* p. 277.
- NEUMAYER, G. V. (1898). *Ann. Hydr. Mar. Met.* p. 409. (Merkatorprojektion: äquatorialer Masstab 1: 28 Mill.).
- NIELSEN, N. (1925). Golfströmen. *Geogr. Tidsskr.* 28. Kopenhagen 1925.
- NOMITUSU, T. (1927). On the so-called "Grenzfläche" in the current due to the difference of density. *Mem. Coll. Sci. Kyoto*, Ser. A, 10, No. 3.
- NOMITSU, T. (1933). A theory of the rising stage of drift-currents in ocean I u. II. *Mem. Coll. Sci., Kyoto.* 16, No. 2, p. 4.
- OKADA, M. (1934). Estimation of the steady current, etc. *Bull. Jap. Soc. Sci. Fish.* 3/3.
- OKADA, M. (1935). A grafical method of determining ocean currents. *Bull. Jap. Soc. Sci. Fish.* 3/5, 231.
- PAECH, H. (1926). Die Oberflächenströmungen um Madagaskar in ihrem jährlichen Gang. *Veröff. Inst. Meeresk. Univ. Berl.* A, Hft. 16. Berlin 1926.
- PALMÉN, E. (1926). Über die Verteilung von Temperatur und Salzgehalt im Finnischen Meerbusen bei stationären Stromzustände. *J. Cons. Intern.* 1, No. 4. Kopenhagen 1926.
- PALMÉN, E. (1930a). Ein Beitrag zur Berechnung der Strömungen in einem begrenzten und geschichteten Meere. *Rapp. Proc. Verb.* 64. Kopenhagen 1930.
- PALMÉN, E. (1930b). Untersuchungen über die Strömungen in den Finnland umgebenden Meeren. *Soc. Sci. Fenn. Comm. Phys.-Math.* 5, No. 12. Helsingfors 1930.
- PALMÉN, E. (1931). Zur Bestimmung des Triftstromes aus Terminbeobachtungen. *J. Conseil Intern.* 6/3. Kopenhagen 1931.
- PALMÉN, E. (1932). Über die Einwirkung des Windes auf die Neigung der Meeresoberfläche. *Soc. Sci. Fenn. Comm. Phys.-Math.* 6, No. 4. Helsingfors 1932.
- PALMÉN, E. (1932). Versuch zur Bestimmung des Tangentialdruckes des Windes auf die Meeresoberfläche mittels Wasserstandbeobachtungen. *Ann. Hydr. Mar. Met.* p. 435 (Berichtigung 1933, p. 43).
- PALMÉN, E. (1936). Über die von einem stationären Wind verursachte Wasserstauung. V. Hydrol. Konf. d. baltischen Staaten. Finnland, Juni 1936, *Ber.* 15B.
- PALMÉN, E. (1941). Zur Frage des Windstaues in einem geschichteten Meer. *Comm. Phys.-Math. Soc. Sci. Fenn.* 7, No. 7. Helsinki 1941.
- PALMÉN, E. und LAURLA, E. (1938). Über die Einwirkung eines Sturmes auf das hydrogr. Zustand im nördlichen Ostseegebiet. *Soc. Sci. Fenn. Comm. Phys.-Math.* 10, No. 1. Helsingfors 1938.
- PARR, A. E. (1935). Rep. on hydr. obs. on the Gulf of Mexico . . . during the Exp. on the "Mabel Taylor" in 1932. *Bull. Bingham Oceanogr. Coll.* 5, No. 1. New Haven 1935.
- PARR, A. E. (1936). On the relationship between dynamic topography and direction of currents under the influence of external (climatic) factors. *J. Cons. Intern.* 11. Kopenhagen 1936.
- PARR, A. E. (1937a). A contribution to the hydrography of the Caribbean and Cayman seas. *Bull. Bingham Oceanogr. Coll.* 5, No. 4. New Haven 1937.
- PARR, A. E. (1937b). On the longitudinal variations in the dynamic elevations of the surface in the Caribbean sea. *Bull. Bingham Oceanogr. Coll.* 6, No. 2. New Haven 1937.

- PARR, A. E. (1938a). Further obs. on the hydrography on the eastern Caribbean and adjacent Atl. waters. *Bull. Bingham Oceanogr. Coll.* 6, No. 4. New Haven 1938.
- PARR, A. E. (1938b). On the validity of the dynamic topographic method for determination of ocean current trajectories. *J. Mar. Res.* 1, No. 2.
- PETTERSSON, H. (1930 u. 1935). Eddy-viscosity in stratified water; I and II. *Medd. Oceanogr. Inst. Göteborg* No. 8. and 11.
- PRANDTL, L. (1926). Über ausgebildete Turbulenz. *Verh. Intern. Kongr. techn. Mech.*, p. 62. Zürich 1926.
- PRANDTL, L. (1942). *Führer durch die Strömungslehre*. F. Vieweg & Sohn, Braunschweig 1942, p. 47; oder *Essentials of fluid dynamics*, Glasgow 1952, p. 51.
- PRIEBSCHE, J. (1943). Eine Bemerkung zur Dynamik turbulenter Strömungen unter Einfluss der Erdrotation. *Ann. Hydro. Mar. Met.* p. 169.
- PROUDMAN, J. (1948). On the mixing of sea water by turbulence. *Proc. Roy. Soc. (A)* 195. London 1948.
- PUFF, A. (1890). *Das kalte Auftriebswasser an der Ostseite des Nordatl. und an der Westseite des Nordindischen Ozeans*. Marburg 1890, p. 67.
- PULS, C. (1895). Oberflächentemperaturen und Strömungsverhältnisse des Äquatorialgürtels des Stillen Ozeans. *Arch. Dtsch. Seewarte*, 18. Hamburg 1895.
- RAPPEYE, H. S. (1932). The 1929 adjustment of the level net. *Milit. Engr. Wash.* 24, No. 138.
- RAKESTRAW, W. and SMITH, H. P. (1937). A contribution to the chemistry of the Caribbean and Cayman seas. *Bull. Bingham Oceanogr. Coll.* 6, No. 1. New Haven 1937.
- RAUSCHELBACH, H. (1931). Gezeitenbeobachtungen im Ostfriesischen Gatje 1927. *Ann. Hydr. Mar. Met.* p. 1.
- REID, R. O. (1948). A model of the vertical structure of mass in equatorial wind-driven current of a baroclinic ocean. *J. Mar. Res.* 7/3, 304–12.
- REID, R. O. (1948). The equatorial currents of the Pacific as maintained by the stress of the wind. *J. Mar. Res.* 7, No. 2.
- REYNOLDS, O. (1894). On the dynamical theory of incompressible viscous fluids, etc. *Phil. Trans. A*, 186. London 1894. (or Papers II, p. 535.)
- RICHARDSON, L. F. (1926). Atmospheric diffusion shown on a distance-neighbour graph. *Proc. Roy. Soc. (A)*, 110, 709.
- RICHARDSON, L. F. and STOMMEL, H. (1948). Note on eddy diffusion in the sea. *J. Met.* 5, 238.
- ROSSBY, C. G. (1932). A generalization of the theory of the mixing length with applications to atmospheric and oceanic turbulence. *Pap. Phys. Oceanogr. Met.* 1, No. 4. Cambridge (Mass.) 1932.
- ROSSBY, C. G. (1936a). Dynamics of steady ocean currents in the light of experimental fluid mechanics. *Pap. Phys. Oceanogr. Met.* 5, No. 1. Cambridge (Mass.) 1936.
- ROSSBY, C. G. (1936b). On the frictional force between air and water and on the occurrence of a laminar boundary layer next to the surface of the sea. *Pap. Phys. Oceanogr. Met.* 4, No. 3. Cambridge (Mass.) 1936.
- ROSSBY, C. G. (1937 and 1938). On the mutual adjustment of pressure and velocity distributions in certain simple currents systems. I and II. *J. Mar. Res.* 1, No. 1 and 1, No. 3.
- ROSSBY, C. G. (1939). Relation between variations in the intensity of the zonal circulation of the atmosphere and the displacement of the semi-permanent centers of action. *J. Mar. Res.* 2/1, 49.
- ROSSBY, C. G. (1951). On the vertical and horizontal concentration of momentum in air and ocean currents. I. *Tellus*, 3/1, 15–27.
- ROSSBY, C. G. *et al.* (1939). Relation between variations in the intensity of zonal circulation of the atmosphere and the displacement of the semi-permanent centers of actions. *J. Mar. Res.* 2, No. 1.
- ROSSBY, C. G. and MONTGOMERY, R. B. (1935). The layer of frictional in wind and ocean currents. *Pap. Phys. Oceanogr. Met.* 3, No. 3. Cambridge (Mass.) 1935.
- RÖMER, E. (1935). Anhäufungen stationärer Stromkabelungen in den nord-afrikanischen Gewässern. *Ann. Hydr. Mar. Met.* p. 10.
- RÖMER, E. (1936). Ortlich periodisch auftretende Kabelungen an der mexikanischen und mittel-amerikanischen Westküste. *Ann. Hydr. Mar. Met.* p. 55.
- SANDSTRÖM, J. W. (1908). Dynamische Versuche mit Meerwasser. *Ann. Hydr. Mar. Met.* p. 6.
- SANDSTRÖM, J. W. (1909). Über die Bewegung der Flüssigkeiten. *Ann. Hydr. Mar. Met.* p. 242.
- SANDSTRÖM, J. W. (1910). Über die Beziehungen zwischen Luftdruck und Wind. *K. Sven. Vet. Handl.* 45, No. 10. Stockholm 1910.
- SANDSTRÖM, J. W. (1914). Über die Anhäufung des warmen Meerwassers in den Rossbreiten. *Ark. Math. Astr. Fys.* 9, No. 32. Stockholm 1914.
- SANDSTRÖM, J. W. (1918). The hydrodynamics of Canadian waters. *Canad. Fish. Exp.* 1914/15, p. 241. Ottawa 1918.

- SANDSTRÖM, J. W. (1922). Deux théorèmes fondamentaux de la dynamique de la mer. *Sven. Hydr.-Biol. Komm. Skr.* 7.
- SCHMIDT, W. (1917). Wirkungen der ungeordneten Bewegungen im Wasser der Meere und Seen. *Ann. Hydr. Mar. Met.* p. 379.
- SCHMIDT, W. (1919). Der Verbrauch an Strömungsenergie im Meer. *Ann. Hydr. Mar. Met.* p. 11.
- SCHOTT, G. (1926). *Geographie des Atlantischen Ozeans*. 2. Aufl. Hamburg 1926.
- SCHOTT, G. (1928a). Die Verteilung des Salzgehaltes der Oberfläche der Ozeane. *Ann. Hydr. Mar. Met.* p. 153.
- SCHOTT, G. (1928b). Die Wasserbewegungen im Gebiete der Gibraltarstrasse. *J. Cons. Intern.* 3, No. 2, 139. Kopenhagen 1928.
- SCHOTT, G. (1931). Der Peru-Strom und seine nördlichen Nachbargebiete in normaler und anormaler Ausbildung. *Ann. Hydr. Mar. Met.* pp. 161, 200 and 240.
- SCHOTT, G. (1934). Verteilung des Salzgehaltes im Oberflächenwasser der Ozeane. *J. Johnstone Mem. Vol.* p. 235. Liverpool 1934.
- SCHOTT, G. (1935). *Geographie des Indischen und Stillen Ozeans*. Hamburg 1935.
- SCHOTT, G. (1939). Die äquatorialen Störungen des Westlichen Stillen Ozeans. *Ann. Hydr. Mar. Met.* p. 247.
- SCHOTT, G. (1942). Grundlagen einer Weltkarte der Meeresströmungen. *Ann. Hydr. Mar. Met.* p. 329.
- SCHUBERT, O. v. (1935). Die Theorie der Transgressionen von Le Danois und ihre Beziehungen zum Golfstrom-Problem. *Ann. Hydr. Mar. Met.* p. 140.
- SCHULZ, B. (1925). Beiträge zur Kenntnis der Gezeiten an der flandrischen Küste und auf der unteren Schelde. *Arch. Deut. Seewarte* 47, Hft. 2. Hamburg 1925.
- SCHULZ, B. (1929). Hydrographie des westl. Barentsmeeres. *Ber. Deut. Wiss. Komm. Meeresf.* N.F., v. 4, Nr. 5. Berlin 1929.
- SCHULZ, B. (1930). Der Wasseraustausch zwischen Nord- und Ostsee. *Petermanns Geogr. Mitt.* No. 209, 183. Gotha 1930.
- SCHUMACHER, A. (1922). Neuere Arbeiten zur Kartographie der Meeresströmungen. *Ann. Hydr. Mar. Met.* p. 455.
- SCHUMACHER, A. (1933). Zwei Oberflächenschnitte durch das Nordwestafrikanische Auftriebswasser. *Ann. Hydr. Mar. Met.* p. 333.
- SCHUMACHER, A. (1935a). Neuere Arbeiten über den Golfstrom im westl. Atl. Ozean. *Ann. Hydr. Mar. Met.* p. 53.
- SCHUMACHER, A. (1935b). Über Stromkabelungen besonders im Guineastrom und seiner Umgebung. *Ann. Hydr. Mar. Met.* p. 373.
- SCHUMACHER, A. (1940). Monatskarten der Oberflächenströmungen im Nordatlantischen Ozean (50°S bis 50°N). *Ann. Hydr. Mar. Met.* p. 109.
- SCHUMACHER, A. (1943). Monatskarten der Oberflächenströmungen im äquatorialen und südlichen Atl. Ozean. *Ann. Hydr. Mar. Met.* p. 209.
- SEIWELL, H. R. (1937). Short period vertical oscillations in the western basin of the North Atl. in *Phys. Oceanogr. Met.* 5, No. 2. Cambridge (Mass.) 1937.
- SEIWELL, H. R. (1938). Application of the distribution of oxygen to the phys. oceanography of the Caribbean sea region. Pap in *Phys. Oceanogr. Met.* 6, No. 2. Cambridge (Mass.) 1938.
- SHAW, W. N. and HEPVORTH, C. (1910). *The trade winds of the Atlantic ocean*. Met. Office. London 1910.
- SHEPARD, P. A. and OMAR, M. H. (1952). The wind stress over the ocean from observations in the Trades. *Quart. J. Roy. Met. Soc.* 78, 583.
- SIGEMATU, R. (1933). Some oceanogr. investigations of the results of oceanic survey, carried out by "Mansyu" from April 1925 to March 1928. *Bull. Hydr. Depart. Imp. Navy, Tokyo* 1933, p. 475.
- SMITH, E. (1926). A practical method for determining ocean currents. *Coast Guard Bull.* No. 14. Washington 1926.
- SPIILHAUS, A. F. (1940). A detailed study of the surface layers of the ocean in the neighbourhood of the Gulf Stream with the aid of rapid measuring hydrographic instruments. *J. Mar. Res.* 3, No. 1.
- STOCKMANN, W. B. (1946a). A theory of equatorial counter currents in the ocean. *C.R. Acad. Sci. U.R.S.S.* 52, 309.
- STOCKMANN, W. B. (1946b). A theoretical explanation of certain peculiarities of the meridian profile of the surface of the Pacific Ocean. *C.R. Acad. Sci. U.R.S.S.* 53, 323.
- STOCKMANN, W. B. (1946c). A tentative indirect determination of the velocities of the trade winds in the equatorial part of the Pacific. *C.R. Acad. Sci. U.R.S.S.* 53, 515.
- STOCKMANN, W. B. (1946d). Equations for a field of total flow induced by the wind in a non-homogeneous sea. *C.R. Acad. Sci. U.R.S.S.* 54, 403.

- STOMMEL, H. (1948). The westward intensification of wind-driven ocean currents. *Trans. Amer. Geophys. Un.* **29**, No. 2. Washington 1948.
- STOMMEL, H. (1949). Horizontal diffusion due to oceanic turbulence. *J. Mar. Res.* **8**, 199–225.
- STOMMEL, H. (1952). An elementary explanation of why ocean currents are strongest in the west. *Bull. Amer. Met. Soc.* **32**, 21; or Contr. No. 532 from Woods Hole Oceanogr. Inst.
- STOMMEL, H. (1953). Examples of the possible role of inertia and stratification in the dynamics of the Gulf Stream system. *J. Mar. Res.* **12/2**, 184–95.
- STOMMEL, H. (1956). On the determination of the depth of no meridional motion. *Deep Sea Res.* **3**, 273–8.
- STOMMEL, H. (1957). A survey of ocean current theory. *Deep Sea Res.* **4**, 149–84.
- STOMMEL, H., ARONS, A. B. and FALLER, A. J. (1958). Some examples of stationary flow patterns in bounded basins. *Tellus.* **10/2**.
- SVERDRUP, H. U. (1928). Die Eistrift im Weddelmeer. *Ann. Hydr. Mar. Met.* p. 265.
- SVERDRUP, H. U. (1929). The waters on the North Siberian Shelf. The Norw. North Polar Exp. "Maud" 1918–1925. *Sci. Res.* **4**, No. 2. Bergen 1929.
- SVERDRUP, H. U. (1930). Some oceanogr. results of the "Carnegie" work in the Pacific; the Peruvian currents. *Trans. Nat. Res. Coun.* p. 257. June 1930.
- SVERDRUP, H. U. (1931a). The origin of the deep water of the Pacific ocean indicated by the oceanographic work of the Carnegie. *Beitr. Geophys.* **29**, 95.
- SVERDRUP, H. U. (1931b). The wind-drift of the ice on the North-Siberian Shelf. North Polar Exp. "Maud" 1918–1925. *Sci. Res.* **6**, No. 1. Bergen 1931.
- SVERDRUP, H. U. (1932). Arbeider i luft-og havforskning Beretn. *Chr. Michelsens Inst. Vidensk.* **2**, No. 5. Bergen 1932.
- SVERDRUP, H. U. (1933a). On vertical circulation in the ocean due to the action of wind with application to conditions with the Antarctic circumpolar current. *Discovery Rep.* **7**. Cambridge 1933.
- SVERDRUP, H. U. (1933b). Vereinfachtes Verfahren zur Berechnung der Druck- und Massenverteilung im Meer. *Geophys. Publ.* **10**, No. 1. Oslo 1933.
- SVERDRUP, H. U. (1934a). The circulation on the Pacific. *Proc. Fifth Pacific Sci. Congr.* 1933. Toronto 1934.
- SVERDRUP, H. U. (1934b). Wie entsteht die antarktische Konvergenz? *Ann. Hydr. Mar. Met.* p. 315.
- SVERDRUP, H. U. (1938a). On the process of upwelling. *J. Mar. Res.* **1**, No. 2.
- SVERDRUP, H. U. (1938b). On the exploration of the oxygen minima and maxima in the ocean. *J. Coun. Intern.* **13**, No. 2, p. 163. Kopenhagen 1938.
- SVERDRUP, H. U. (1946). Speculations on horizontal diffusion in the ocean. *Coll. Rep. Scripps Inst. Oceanogr.* No. 1. La Jolla 1946.
- SVERDRUP, H. U. (1947). Wind-driven currents in a baroclinic ocean; with application to the equatorial currents of the Eastern Pacific. *Proc. Nat. Acad. Sci. Wash.* **33**, No. 11.
- SVERDRUP, H. U. and FLEMING, R. H. (1941). The waters of the coast of southern California, March to July 1937. *Scripps Inst. Oceanogr. Bull.* **4**, No. 10, 261.
- SVERDRUP, H. U. et al. (1946). *The Oceans, their Physics, Chemistry, and General Biology*. Prentice-Hall, Inc. New York 1946.
- TAIT, J. B. (1930). The water drift in the northern and middle area of the North Sea and in the Faroer-Shetland Channel. *Fish. Board of Scotland, Scie. Invest.* 1930, No. 4. Edinburgh 1930.
- TAKANO, K. (1954). On the salinity and the velocity distribution off the mouth of a river. *J. Oceanogr. Soc. Japan* **10/3**, 92–8.
- TAKANO, K. (1955). A complementary note of the diffusion of the seawater river flow off the month. *J. Oceanogr. Soc. Japan* **11/4**, 147–9.
- TAKANO, K. (1955). On the Antarctic Circumpolar Current. *Rec. Oceanogr. works in Japan* **2/1**, 71–75.
- TAYLOR, G. J. (1920). Tidal friction in the Irish sea. *Phil. Trans. Roy. Soc. A*, **220**, 1.
- TAYLOR, G. J. (1931). Internal waves and turbulence in a fluid of variable density. *Rapp. Proc. Verb.* **74**. Kopenhagen 1931.
- THIEL, G. (1937). Über Stromkonvergenzlinien und-kabelungen. *Ann. Hydr. Mar. Met.* p. 109.
- THOMSON, HELGE (1933). The iculation in the depth of the Indian Ocean. *J. Cons. Intern.* **8**, No. 1. Kopenhagen 1933.
- THOMSON, HELGE (1935). Entstehung und Verbreitung einiger charakteristischer Wassermassen in dem Indischen und südlichen Pazifischen Ozean. *Ann. Hydr. Mar. Met.* p. 293.
- THORADE, H. (1909). Die Kalifornischen Meeresströmungen. *Ann. Hydr. Mar. Met.* p. 17.
- THORADE, H. (1914). Die Geschwindigkeit von Triftströmungen und die Ekman'sche Theorie. *Ann. Hydr. Mar. Met.* p. 379.
- THORADE, H. (1925). Henrik Mohn und die Entwicklung der Meereskunde. *Ann. Hydr. Mar. Met.* p. 182.

- THORADE, H. (1928). Neuere Anschauungen über Oberflächenströmungen. Monatskarten des Südatlantischen Ozeans. *Deut. Seewarte*. Hamburg 1928.
- THORADE, H. (1931). Mischung, Turbulenz und Grenzfläche. *Rapp. Proc. Verb.* **74**, 44. Kopenhagen 1931.
- THORADE, H. (1933a). Methoden zum Studium der Meeresströmungen. *Aberhaldens Handbuch der biol. Arbeitsmethoden*, Abt. 11/3, Heft 3. Berlin 1933.
- THORADE, H. (1933b). Verfeinerung der Ekman'schen Theorie. *Ann. Hydr. Mar. Met.* p. 387.
- THORADE, H. (1934). Über Stromunruhe. Nach den Beobachtungen im Kattegat, Aug. 1931. *Ann. Hydr. Mar. Met.* p. 365.
- THORADE, H. (1935). Untersuchungen von Meeresströmungen mittels der Kontinuitätsgleichung. *Ann. Hydr. Mar. Met.* p. 316.
- THORADE, H. (1936). Beständigkeit und Streuung bei Strömen. *Ann. Hydr. Mar. Met.* p. 13.
- THORADE, H. (1937a). Die Stratosphäre und Troposphäre des Atl. Ozeans. *Ann. Hydr. Mar. Met.* p. 174.
- THORADE, H. (1937b). Die Strommenge der Konvektionsströme. *Ann. Hydr. Mar. Met.* p. 577.
- THORADE, H. (1938). Kann eine Meeresströmung sich als Freistrahle entwickeln? *Ann. Hydr. Mar. Met.* p. 308.
- TOLLMIEN, W. (1926). Berechnung turbulenter Ausbreitungsvorgänge. *Z. Angew. Math. Mech.* **6**, p. 468.
- TSUCHIYA, M. (1955a and b). On a simple method of estimating the current velocity at the equator. 1 and II. *J. Oceanogr. Soc., Japan* **11**/1, 1-4; *Rec. oceanogr. works in Japan* **2**/2.
- UDA, M. (1930). On some oceanogr. Researches of the sea-water of Korisowo. *Record of oceanogr. works in Japan* **2**, No. 2.
- UDA, M. (1933). Hydr. researches on the normal monthly conditions of Oyasiwo- and Kurosiwo-Area. *J. Imp. Fish. Exper. Stat. Tokyo* **1**, No. 3.
- UDA, M. (1935). The results of simultaneous oceanogr. investigations in the North Pacific Ocean adjacent to Japan made in Aug. 1933. *J. Imp. Fish. Exper. Stat. Japan* No. 6, 130.
- UDA, M. (1936). An experimental Study of "Siwome" or current rip as a train of horizontal vortices. *Bull. Jap. Soc. Sci. Fish.* **5**, No. 1.
- UDA, M. (1938). Researches on "Siwome" or current rip in the seas and oceans. *Geophys. Mag.* **11**, No. 4; Central Met. Obs. Tokyo, mars 1938.
- UDA, M. and OKAMOTO, G. (1930 and 1931). Of the monthly oceanogr. charts of the adjacent seas of Japan based on the averages for eleven (sixteen) years from 1918 to 1929 (1934), with description of the current-system inferred from the charts. Part I July to Dec., Part II Jan. to June. *J. Imp. Fish. Exper. Stat. Tokyo* **1**, No. 1.
- UDA, M. and OKAMOTO, G. (1938). Hydrographical fluctuation in the northeastern sea region adjacent to Japan of North Pacific Ocean. *J. Imp. Fish. Stat., Japan*, **9**, 64-85.
- VERCELLI, F. (1925). Campagna idogr. nel mar. Rosso; Ammiraglio Magnaghi 1923/24. *Ricerche di oceanogr. fisica*. Part I a; Correnti e maree. Genua 1925.
- VERCELLI, F. (1926). Il regime delle correnti e delle maree. Crociere per lo studio dei fenomeni nello stretto di Messina. R.N. "Marsigli" 1922/23. Com. intern. del Mediterraneo, Venezia 1926.
- VERCELLI, F. (1929). Lo studio degli stretti come vie di comunicazione fra i mari. *Intern. Congr. Oceanogr. Sevilla*, Mai 1929.
- VERONIS, G. and MORGAN, G. W. (1955). A study of the time-dependent wind-driven ocean circulation. *Tellus*, **7**/2, 232-47.
- VERONIS, G. and STOMMEL, H. (1956). The action of variable wind stresses on a stratified ocean. *J. Mar. Res.* **15**/1, 43-75.
- WAGNER, F. (1932). Was bedeutet der Ausdruck "Beständigkeit des Windes"? *Ann. Hydr. Mar. Met.* p. 36.
- WARMER, H. (1926). Coastal currents along the Pacific coast. U.S. Coast and Geod. Surv. Nr. 330. *Spec. Publ.* No. 121. Washington 1926.
- WERENSKKJOLD, W. (1922). Mean monthly air transport over the North Pacific Ocean. *Geofys. Publ.* **2**, No. 1. Oslo 1922.
- WERENSKKJOLD, W. (1935). Coastal currents. *Geofys. Publ.* **10**, No. 13. Oslo 1935.
- WERENSKKJOLD, W. (1937). Die Berechnung von Meeresströmungen. *Ann. Hydr. Mar. Met.* p. 68.
- WATTENBERG, H. (1935). Kalkauflösung und Wasserbewegung am Meeresboden. *Ann. Hydr. Mar. Met.* p. 387.
- WATTENBERG, H. (1938). Die Verteilung des Sauerstoffs im Atl. Ozean. "Meteor"-Werk. **9**/1. Berlin 1938.

- WATTENBERG, H. (1941). Über die Grenzen zwischen Nord- und Ostseewasser. *Ann. Hydr. Mar. Met.* p. 265.
- WEENINK, M. P. H. and GROEN, P. (1952). On the computation of ocean surface current velocities in the equatorial regions from wind data. *Proc. Kongl. Nederl. Akad. Wetens. Amsterdam*, Ser. B. 55/3, 239–46.
- WILLIMZIK, M. (1929). Die Strömungen im subtropischen Konvergenzgebiet des Indischen Ozean. *Veröff. Inst. Meeresk. Univ. Berl. A*, Hft. 14. Berlin 1929.
- WILLIMZIK, M. (1927). Die Antarktischen Oberflächenströmungen zwischen 50° und 110° O. *Veröff. Inst. Meeresk. Univ. Berl. A*, Hft. 17. Berlin 1927.
- WIPPLE, F. J. W. (1917). The motion of a particle on the surface of a smooth rotating globe. *Phil. Mag.* 33, No. 198.
- WITTING, R. (1905). Etliches über Strommessungen. *Publ. de Circ.* No. 31. Kopenhagen 1905.
- WITTING, R. (1906). Der Bottnische Meerbusen, eine hydrogr. Übersicht. *Ann. Hydr. Mar. Met.* p. 416.
- WITTING, R. (1909). Zur Kenntnis des vom Winde erzeugten Oberflächenstromes. *Ann. Hydr. Mar. Met.* p. 202.
- WITTING, R. (1918). Hafstan, Geodytan oer Landhöjningen utmed baltiska hafvet och vid nordsjön. Helsingfors 1918.
- WITTING, R. (1930). Determination of currents direct and indirect. *Rapp. et Proc. Verb.* 64. Kopenhagen 1930.
- WITTING, R. (1933). Zur Bestimmung der Mischung im Meere. *Comm. phys. math. Soc. Sci. Fenn.* 7, No. 2. Helsinki 1933.
- WÜST, G. 1920. Die Verdunstung auf dem Meere. *Veröff. Inst. Meeresk. Univ. Berl. A*, Hft. 6. Berlin 1920.
- WÜST, G. (1924). Florida- und Antillenstrom. *Veröff. Inst. Meeresk. Univ. Berl. A*, Hft. 12. Berlin 1924.
- WÜST, G. (1928). Der Ursprung der Atl. Tiefenwässer. *Sonderbd. Ges. Erdkunde Berl.*
- WÜST, G. (1929). Schichtung und Tiefenzirkulation des Pazifischen Ozean. *Veröff. Inst. Meeresk. Univ. Berl. A*, Hft. 20. Berlin 1929.
- WÜST, G. (1930a). Der Golfstrom. *Z. Ges. Erdkunde Berl.* p. 42.
- WÜST, G. (1930b). Meridionale Schichtung und Tiefenzirkulation in den Westhälften der drei Ozeane. *J. Cons. Intern.* 5, No. 1. Kopenhagen 1930.
- WÜST, G. (1936a). Kuroshio und Golfstrom. Eine vergleichende hydrodyn. Untersuchung. *Veröff. Inst. Meeresk. Univ. Berl. A*, Hft. 29. Berlin 1936.
- WÜST, G. (1936b). Die Tiefenzirkulation im Raum des Atlantischen Ozeans. *Naturwissenschaften*, p. 133.
- WÜST, G. (1936c). Schichtung und Zirkulation des Atl. Ozeans. *“Meteor” Werk.* 6/1. Berlin 1936.
- WÜST, G. (1943). Der subantarktische Bodenstrom der westatlantischen Mulde. *Ann. Hydr. Mar. Met.* p. 249.
- WÜST, G. (1950). Blockdiagramme der Atlantischen Zirkulation auf Grund der “Meteor”-Ergebnisse. *Kieler Meeresforsch.* 7/1, 24–34.
- WÜST, G. (1951). Über die Fernwirkung antarktischer und nordatlantischer Wassermassen in den Tiefen des Weltmeeres. *Naturw. Rdsch.* Heft 3, 91–108. Stuttgart 1951.
- WÜST, G. (1957). Stromgeschwindigkeiten und Strommengen in den Tiefen des Atlantischen Ozeans. *Wiss. Erg. Dtsch. Atl. Exp. “Meteor” 1925–1927*, 6, part 2, 261–420. Berlin 1957.
- See also: Stromgeschwindigkeiten im Tiefen- und Bodenwasser des Atlantischen Ozeans auf Grund dynamischer Berechnung der “Meteor”-profile der Dtsch. Atl. Exp. 1925–1927. *Pap. Mar. Biol. Oceanogr.* 373–97. London 1957.
- YOSHIDA, K. (1955). A note on dynamics near the equator, in view of recent observations in the eastern Equatorial Pacific. *Geophys. Notes* 8/2. Univ. Tokyo 1955.
- YOSHIDA, K. (1955). Coastal upwelling off the Californian coast. *Geophys. Notes* 8/2; or *Rec. Oceanogr. works, Japan* 2/2.
- YOSHIDA, K., MAO, HAN-OU and HOOVER, P. L. (1953). Circulation in the upper mixed layer of the equatorial North Pacific. *J. Mar. Res.* 12/1, 99–120.
- ZORELL, F. (1928). “El nino”-Strom im Jahre 1925. *Ann. Hydr. Mar. Met.* p. 167.

Author Index

- PRINCE ALBERT I OF MONACO, 342
 AITKINS, W. R. G., 55, 57
 ALBRECHT, F., 236
 ANDERSON, E. D., 116, 122
 ÅNGSTRÖM, A., 59, 91, 92, 224, 225
 ANVERS, H. G., 8, 624
 ARONS, 701, 702
 ARX, VON W. S., 617, 634
 ASCHKINAS, 51
- BEIN, W., 43, 57
 BÉNARD, H., 199
 BERGERON, T., 300
 BERGTEN, E., 8
 BERNOULLI, 325, 326, 328, 374
 BIGELOW, B., 593
 BJERKNES, J., 300, 453, 469
 BJERKNES, V., 42, 300, 303, 306, 308, 313, 315,
 329, 357, 359, 365, 366, 372, 375, 434, 451, 466,
 476, 486, 491, 577
 BÖHNECKE, G., 32, 35, 111, 112, 140, 141, 154,
 161, 186, 190, 566, 663
 BOWEN, J. S., 225
 BOWIE, W., 8
 BOZIN, E., 644
 BREITFUSS, L. L., 137
 BRENECKE, W., 12, 73, 74, 149, 341, 418, 422,
 437
 BROCKAMP, R., 256
 BROOKS, C. E. P., 264, 559
 BRUCH, H., 221
 BRÜCKNER, E., 232, 234
 BUCH, K., 71, 72, 74, 76, 77, 80, 83
 BUCHAN, A., 561
 BUCHANAN, J. Y., 43, 575
 BÜDEL, J., 257, 263
 BUEN DE, R., 182, 529
 BULLARD, G., 12, 89
 BUMPUS, D. F., 634
 BUNDGAARD, R. C., 300
- CARNOT, 490
 CARPENTER, 575
 CARRIER, G. F., 585, 587, 696
 CARRIT, 65
 CARRUTHERS, J. H., 17, 342, 343
 CASSINI, 287
 CASTENS, G., 478, 493
 CHARNEY, I. G., 627, 629, 630, 631, 698
 CHERUBIM, R., 222
 CHEVALIER, 48
 CHURCH, PH. E., 143, 144
 CLARKE, G. L., 55
 CLOWES, A. J., 148, 672
 COLDING, A., 420
 COLLINS, 51, 52
 COOPER, L. H. V., 22, 680
- CRARY, A. P., 12
 CROLL, J., 575
 CROMWELL, T., 604
- DALL, W., 641
 DALLAS, W. L., 666
 DALY, R. A., 22
 DEACON, G. E. R., 72, 144, 145, 148, 149, 173,
 505, 550, 666, 669, 670
 DEFANT, A., xv, 1, 11, 27, 28, 95, 98, 104, 105,
 106, 107, 109, 115, 121, 122, 136, 138, 144, 148,
 153, 160, 164, 166, 173, 204, 211, 232, 283, 317,
 344, 345, 346, 352, 376, 378, 387, 392, 305, 413,
 435, 449, 453, 458, 463, 468, 473, 476, 480, 494,
 498, 500, 501, 517, 519, 535, 556, 565, 583, 593,
 596, 598, 620, 644, 646, 649, 652, 660, 662,
 663, 678, 679, 680, 682, 687, 693
 DEFANT, FR., 442, 443, 444, 445, 446
 DIETRICH, G., 5, 8, 31, 42, 51, 56, 109, 116, 117,
 132, 133, 134, 236, 460, 493, 494, 501, 505, 507,
 559, 606, 607, 623, 624, 641, 642, 643, 680
 DINKLAGE, L. E., 417, 418
 DITTMAR, C., 37, 38, 74
 DORN, VAN W. G., 421
 DRYGALSKI, E. V., 244, 260, 261, 273, 274, 275
 DURST, C. SC., 418
- EKMAN, F. L., 380
 EKMAN, V. W., 34, 42, 49, 104, 125, 195, 315,
 387, 391, 399, 401, 403, 404, 406, 408, 409, 412,
 413, 414, 417, 420, 422, 426, 427, 428, 431, 443,
 444, 446, 447, 449, 480, 482, 484, 485, 493, 503,
 508, 509, 510, 540, 541, 548, 549, 552, 572, 576,
 581, 582, 620, 623, 624, 647, 699
 EMDEN, 95
 EMMEL, V. M., 65
 ERICSON, D. B., 22
 ERTEL, H., 103, 160, 232, 404, 477
 EUCH, 83
 EULER, L., 320, 383
 EWING, M., 12, 22, 256
 EXNER, F., 418, 443, 465, 469
- FALKENBERG, G., 60
 FALLER, 701, 702
 FELBER, O. H., 565
 FERREL, W., 575
 FISCHER, K., 232
 FJELDSTAD, J. E., 104, 115, 404, 443, 557
 FLEMING, R. H., 51, 105, 107, 644
 FÖRTHMAN, E., 620
 FORONOFF, N. P., 604
 FORCH, C., 416
 FOX, CH., 65
 FRITSCHÉ, E., 249

- FUGLISTER, F. C., 561
 FULTON, T. W., 342
- GALLE, P. H., 416
 GANS, R., 61
 GEDGE, H. D., 532
 GEHRKE, J., 101, 159, 381
 GEISSLER, H., 36
 GODSKE, C. L., 300
 GOERTLER, H., 434
 GOLDSBROUGH, G. R., 573, 574
 GOLDSCHMIDT, V. M., 81
 GOLDSTEIN, 392
 GRANQUIST, G., 159
 GRAY, 256
 GROEN, P., 504, 552, 553, 554
 GULDBERG 398, 399
 GUNTHER, E. R., 571, 645
 GUSTAFSON, T., 392,
- HABER, F., 40
 HADAMARD, J., 554
 HAHN, A., 8
 HAMBERG, A., 74, 248
 HANN, v. J., 117
 HANSEN, H. E., 267
 HANSEN, W., 588, 638
 HANZAWA, M., 396
 HARVEY, 65
 HAURWITZ, B., 637, 659
 HECSON, 22
 HEGEMANN, F., 266
 HEISKANEN, 301
 HEISSENBERG, TH., 396, 397, 398
 HELA, J., 420, 449
 HELLAND, A., 273
 HELLAND-HANSEN, BJ., xv., 41, 46, 114, 125, 189,
 199, 202, 346, 368, 435, 446, 447, 478, 486, 493,
 502, 503, 505, 506, 563, 659
 HELLSTRÖM, B., 547
 HELMHOLTZ, v. H., 453
 HENTSCHEL, E., 563
 HEPVORTH, C., 559
 HESS, H. H., 26
 HESSELBERG, TH., 42, 195, 309
 HESSEN, K., 7
 HIDAKA, K., 36, 377, 444, 470, 588, 652, 653, 673,
 703
 HILDEBRANDSSON, H. H., 283
 HJORT, J., 531
 HIRSEKORN, H. G., 43
 HOMEN, 109
 HOOVER, 601
 HUMBOLDT, v. A., 119, 575
 HUNTSMAN, A. G., 264, 265
- ICHIYE, T., 640, 702
 IDRAC, P., 532
- JACOBS, W. C., 225, 236, 242
 JACOBSEN, J. P., 101, 102, 104, 170, 207, 208, 210,
 211, 212, 214, 392, 502, 503, 527, 529, 537, 607
 JAENICKE, J., 40
 JAKHELIN, A., 510
 JEFFREYS, H., 200, 383, 404, 492
- JENSEN, 502
 JERLOV, N. G., 51, 56, 605
 JESSEN, O., 22
 JNOUE, 396
 JOSEPH, J., 54, 56
 INTERN. HYDROGRAPHIC BUREAU, MONACO, 4
 JSAACS, J. D., 333
 JSELIN, C. O'D., 333, 493, 494, 505, 563, 607, 613,
 614, 629, 692
- KAEHNE, K., 22
 KALLE, K., 36, 39, 41, 60, 61, 63, 64
 KILERIC, A. B., 669
 KISINDO, G., 638
 KLEINSCHMIDT, E., 224
 KNUDSEN, M., 34, 37, 39, 73, 379, 381, 527, 529,
 534
 KOENUMA, K., 115, 638, 640
 KOEPPEN, W., 641
 KOLMOGOROFF, 396
 KOSSINNA, E., 2, 3, 5, 14, 15, 17, 18, 21
 KOSSMAT, F., 24
 KREUSLER, 51, 52
 KRÜGER, W., 343
 KRÜMMEL, O., 8, 43, 50, 51, 141, 153, 261, 342,
 372, 382, 547
 KUENEN, PH. H., 22
 KUHLBRODT, E., 92, 110
 KULLENBERG, B., 22, 392, 447, 448, 449
- LAGRANGE, DE J. L., 320, 322, 324, 342
 LAMBERT, W. D., 301
 LANDOLT-BÖRNSTEIN, 5, 42
 LAURILA, E., 420, 544
 LAUSCHER, F., 59, 60, 61, 91
 LE DANOIS, E., 659, 660
 LENZ, E., 575, 576
 LETTAU, H., 81, 82, 236
 LEVERKINK, 8
 LÜTGENS, R., 222
 LUMBY, J. R., 34
- MC EWEN, G. F., 104, 645, 646
 MÄE, H., 533
 MAKAROFF, 247, 256
 MAKIN, C. J. S., 38
 MALMGREN, F., 117, 245, 246, 247, 248, 249, 250,
 251, 253, 254, 255
 MAO, 601
 MARGULES, M., 453, 456, 474, 635
 MARMER, H. A., 8
 MARVIN, C. F., 221
 MATTHEWS, D. J., 41
 MAUSTRAD, A., 244
 MAURER, H., 301
 MAURY, 575
 MAXWELL, A. E., 89
 MECKING, L., 264, 269, 275, 277
 MEINARDUS, W., 110, 144, 235, 264, 268
 MENÉNDEZ, N., 532
 MERCANTON, 273
 MERZ, A., 109, 122, 203, 357, 367, 368, 373, 390,
 516, 523, 567, 672
 MEYER, H. H. F., 32, 39, 357, 369, 370
 MICHAELIS, G., 357, 567
 MIEGHEM, VAN J. M., 635
 MODEL, F., 421

- MOHN, H., 220, 252, 398, 399, 418, 476, 493
MÖLLER, L., 43, 148, 172, 373, 380, 390, 514, 516
517, 523, 524, 564
MONTGOMERY, R. B., 170, 193, 195, 196, 222,
229, 231, 412, 413, 598, 604, 605
MORGAN, G. W., 696, 698, 702
MOSBY, H., 36, 91, 224, 225, 390, 505
MOSBY, O., 665, 667, 668, 681
MOSKATOV, 257
MOSSMANN, R., 234
MOTHES, H., 256
MUNK, W. H., 116, 122, 231, 421, 422, 583, 584,
585, 586, 587, 588, 589, 631, 673, 674, 696, 703
MURPHY, R. C., 572
MURRAY, J., 531
- NANSEN, FR., 43, 67, 97, 123, 189, 346, 354, 355,
368, 399, 418, 476, 493, 505, 563
NARES, G. N., 531
NERNST, E., 48, 243
NEUMANN, G., 68, 69, 116, 134, 156, 158, 159,
187, 200, 421, 426, 497, 498, 561, 562, 589, 590,
626
NEUMAYER, v. G., 557
NIKITIN, W. N., 68, 134
NOMITSU, T., 8, 405, 444, 516
NUSSER, F., 263
- OKADA, M., 377, 378
OKAMOTO, G., 8, 569
OMI, 421
OSTER, 55
OTTERSTEDT, B., 447
- PAECH, H., 567
PALMÉN, E., 356, 417, 418, 419, 420, 440, 544
545, 546, 547, 598, 605, 673, 674
PANOFSKY, 637
PARR, A. E., 105, 132, 192, 505, 507, 606, 607, 624
PENCK, A., 8, 20, 220
PERLEWITZ, 12
PERNTER, J. M., 54
PETTERSSON, H., 12, 40, 43, 54, 391
PETTERSON, O., 43, 97, 116, 247, 249, 250, 281
PILLSBURY, 607
POLLAK, M. J., 197
POOLE, H. H., 55, 57
PRANDTL, L., 175, 373, 388, 389, 411, 412, 421,
620
PRATJE, O., 11
PRIESCH, J., 619
PROUDMAN, J., 395
PUFF, A., 567
PULS, C., 569
- QUENNEL, W. A., 264
QUERVAIN, DE A., 273
- RAKESTRAW, N. W., 65, 606
RAMANATHAN, K. R., 61
RANKAMA, K., 82
RAPPLEYE, H. S., 624
RAUSCHELBACH, H., 348, 362
RAVENSTEIN, P. R., 9
- RAYLEIGH, LORD, 200
REICHEL, E., 236
REID, R. O., 542, 551, 553, 599, 601, 602, 603
REVELLE, R., 51, 89
REYNOLDS, O., 328, 393
RICHARDSON, L. F., 392, 394, 395, 396, 634
RIEL, VAN P. M., 127, 130, 131
RIETSCHEL, E., 8
RIIS CARSTENSEN, E., 275
RINGER, W. E., 247, 250
RÖMER, E., 362
ROSSBY, C. G., 335, 412, 413, 421, 494, 583, 617,
619, 620, 621, 622, 623, 624, 625, 631, 632, 640,
658, 704, 707
ROYEN, N., 256
RUDEN, P., 175, 620
RUPPIN, E., 12, 50
RUTHERFORD, H. M., 12
RUTTNER, F., 54
- SAHAMA, T. G., 82
SANDSTRÖM, J. W., 42, 365, 399, 469, 486, 489,
547
SARASIN, E., 56, 57
SAUBERER, F., 54
SAWYER, 51, 52
SCHMIDT, W., 53, 54, 59, 90, 102, 104, 110, 128
221, 223, 224, 391, 423, 425, 426
SCHOKALSKI, J. M., 68
SCHOTT, G., 60, 111, 127, 140, 148, 161, 170, 171,
181, 182, 188, 235, 269, 370, 436, 493, 529, 531,
537, 538, 557, 567, 569, 571, 572, 600, 645, 687
SCHUBERT, v. O., 127, 197, 198, 345, 660
SCHULZ, B., 70, 72, 74, 127, 136, 266, 343, 563
SCHUMACHER, A., 34, 36, 41, 357, 359, 362, 370,
436, 559, 560, 561, 644
SEIWELL, H. R., 67, 104, 508, 606
SHAW, W. N., 559
SHEPARD, F. P., 21, 22, 421
SHOULEIKIN, W., 222
SKORZOW, 134
SIGEMATU, R., 24, 638
SKOGSBERG, TAGE., 115
SIMPSON, 139
SMITH, E. H., 259, 270, 272, 274, 275, 276, 279,
281, 459, 488, 505, 606, 665, 667, 668, 681
SMITH, P. A., 21, 22, 27
SORET, J., 56
SOULE, F. M., 505, 665, 667, 668, 681
SPEERSCHNEIDER, C. J. H., 269
SPILHAUS, A. F., 36, 143, 601
STAFF, 104
STAHLBERG, W., 11
STEFAN, J., 252
STENIUS, S., 48
STOCKMAN, W. B., 104
STOCKS, TH., 12, 17, 19, 27, 30, 31
STOMMEL, H., 105, 200, 496, 499, 500, 581, 582,
583, 584, 587, 589, 591, 627, 631, 634, 635, 674,
676, 698, 699, 700, 701, 702, 703, 704, 706, 707
STROUP, E. D., 604
SUDA, K., 104
SUESS, E., 8
SUND, O., 34, 43
SVERDRUP, H. U., 42, 43, 67, 104, 105, 107, 108,
115, 123, 124, 148, 157, 179, 195, 227, 229, 236,
237, 242, 247, 254, 309, 311, 346, 347, 355, 356,
395, 405, 418, 422, 437, 438, 440, 563, 494, 503

- SVERDRUP, H. U.—*contd.*
 548, 549, 550, 551, 580, 581, 583, 584, 598, 599,
 601, 607, 624, 625, 631, 644, 646, 647, 648, 652,
 669, 671, 672, 684, 688, 703
- TAIT, J. B., 343
 TAKANO, K., 540, 541, 674
 TAYLOR, G. J., 102, 317, 392
 THIEL, G., 362
 THOMPSON, T. G., 48
 THOMSEN, HELGE, 547, 688
 THORADE, H., 41, 104, 107, 343, 346, 347, 348,
 349, 350, 378, 405, 418, 422, 428, 476, 511, 563,
 571, 598, 624, 645, 646
 THORNE, A. M., 256
 THOULET, M. J., 48
 THURAS, W., 43
 TIMONOFF, 184
 TOLLMEIN, W., 175, 620
 TRANSCHÉ, N. A., 260
 TSUCHIVA, M., 541, 673
- UDA, M., 362, 569, 592, 638, 640
 UTTERBACK, C. L., 55
- VAUX, D., 22, 680
 VENING-MEINESZ, F. A., 26
 VERCELLI, F., 514, 532, 533
 VERONIS, G., 702, 703, 704, 706, 707
 VINE, A., 12
 VISSER, S. W., 154, 157
- WAGNER, F., 350
 WALKER, G. T., 566
 WARMER, H., 573
- WATTENBERG, H., 39, 67, 71, 72, 73, 74, 76, 77, 78,
 80, 83, 84, 85, 86, 104, 182, 186, 494, 528, 530,
 663, 681, 684, 685
 WEENINK, M. P. H., 552, 553, 564
 WEGEMANN, G., 110, 493
 WEGENER, A., 7
 WEIBULL, W., 12
 WEICKMANN, L., 140, 270
 WEINBERG, B., 256
 WEISZÄCKER, 396, 397, 398
 WENNER, F., 43
 WERENSKJOLD, W., 366, 480, 481, 511, 512
 WESTPHAL, A., 8
 WEYPRECHT, K., 243
 WHEELER, A. S., 38
 WHITNEY, L. V., 59
 WIESE, W., 269
 WILLIMZIK, M., 357, 568
 WIPPLE, F. J. W., 317
 WITTING, R., 45, 105, 346, 347, 355, 381, 395, 396,
 417, 418, 499, 527
 WITTSTEIN, 61
 WÜST, G., 4, 12, 27, 29, 30, 32, 92, 122, 127, 136,
 140, 147, 148, 149, 150, 162, 163, 165, 172, 179,
 180, 189, 204, 212, 213, 215, 221, 222, 223, 224,
 225, 226, 230, 231, 235, 487, 492, 569, 570, 593,
 600, 607, 609, 613, 638, 639, 640, 672, 676, 679,
 680, 682, 684, 687, 688, 689, 691, 692, 697
 WULF, 136
 WYRTKI, K., 56
- YOSHIDA, K., 554, 601, 653, 654
- ZOEPFRITZ, K., 693
 ZORELL, F., 572
 ZUBOV (Subov), N. N., 104, 139
 ZUKRIEGEL, J., 244

Subject Index

- Absorption of radiation, *see* radiation
Adjacent seas, subtropical, effects on deep sea circulation 690-3
Agulhas current 641-2
Alcalinity 72
 distribution 73
 relation to calcium carbonate content 85
 and salinity 74
Antarctic circumpolar current, dynamic of 673-5
Antarctic convergence zone, process in 679-682
Austausch (turbulent exchange coefficient) 92
 102, 103
Axis, of contraction 451
 of dilatation 451
Baltic Sea, vertical structure of water masses 70
 see also North Sea
Barotropy coefficient 308, 341
Benquela current 565
Bénard convection cell 199-201
Bjerknes circulation theorem 332
 oceanographic applications 486-492
Black Sea, vertical structure of water masses 69
Boiling point of sea water 44
Bosphorus and Dardanelles, current in 513-526
Bottom polar current 680-3
Bottom water in the oceans 149
Boundary surface between water bodies 451-469
Calcium carbonate in the sea, as function of depth changes by chemical and biological causes 85-7
 saturation at surface of Atlantic Ocean 86
 solubility 83-5
 solution near bottom 86
Canyons 22-4
Carbon dioxide, annual budget on Earth surface 81
 dissociation constants 75-7
 distribution on surface on South Atlantic 73
 exchange with atmosphere 80
 in deep places of oceans 77-80
 in a section in subtropical part of South Atlantic 79
 partial pressure 71
 solubility 71
Chart datum 5, 9
Charts of sea surface currents 557-8
Circulation, oceanic
 basic principles 556-561
 influence of meridional coast 579 *et seq.*
 mean features in the Atlantic 694
 theorem of Bjerknes 330-3
 oceanographic applications 486-492
 thermo-haline 574-6
 tropospheric of tropical and subtropical oceans 594-604
 stratospheric 661-683
 theory, of Stommel and Munk 583-591
 summary of individual theories 696-8
 comprehensive theory 698-701
 oceanic and atmospheric-, effects of polar-ice conditions 279
Colour of the sea 60-4
Compensation currents 370
Computation of velocity of surface currents in equatorial regions from wind data 552-5
Conductivity, thermal 50, 92, 95, 103
Continuity equation and divergence of current field 374-9
Convergence, antarctic, process in 669-672
 internal structure 671
 process at the polar boundary of 656-660
 subtropical 144
 stream line 359
 point 363
 theory of disturbance and wave formation 658-9
Convection, autumn and winter, in polar regions 133-140
 Bénards cell 199-201
 dynamic 101
 heat exchange between ocean and atmosphere and 92
 horizontal 105
 thermo-haline 96-100
Continental slope 16
Conversion of relative in absolute topography of isobar surface 492-502
Critical discussion on dynamic computation of oceanographic data 504-8
Current from ships displacement 343
Current measurements,
 from a ship 344
 correction method 346
 difference method 346
 smoothing method 347
 scientific use of 345-7
 elimination of periodic components 351
Current, compensation 370
 inertia 441-450
 equatorial under 604-5
 oceanic, in a homogeneous sea; theory of 382-450
 steady, without friction 383
 drift 399-406
 gradient 406-13
 elementar 413-9
 effects of coast on 426-8
 oceanic effects, of bottom topography 428-430
 of friction 432-6
 of varying latitude 420-4
 in a non-homogeneous sea 474-512
 and density field in a horizontal plane 476-9

- Current—*contd.*
 caused by excess of precipitation and run-off over evaporation 562-4
 density, effect of wind on 544-555
 relationship between wind and 550-2
 surface density, computation of velocity in equatorial regions from wind data 552-5
 steady in a stratified ocean 479
 including friction 482
 stationary, and water bodies 451-469
 system in a hydrographic vortex 578-9
 and thermocline near the equator 463
 in sea straits 513-543
 theory of 517-523
 sea surface currents 557-572
 charts of sea surface currents 557
 in Atlantic Ocean 558-566
 in Indian Ocean 566-8
 in Pacific Ocean 568-572
 polar currents of the Northern Hemisphere 662-9
 antarctic circumpolar currents 673-9
 sub-antarctic intermediate 684-9
 in the middle part of the stratosphere 683-8
 polar bottom 680-3
 distributions in the lower Atlantic deep currents (3000 m) 689
- Deep-sea bottom 16
 data
 depressions and trenches 16, 24-7
 methods of recording 10
 indirect methods with unprotected thermometers 12
 large-scale features 27-31
 circulation, effects of subtropical adjacent seas on 690-3
- Density of sea water,
 dependence on temperature, salinity and pressure 41
 diurnal and annual variations at the surface 185-6
 distribution at surface of the oceans 187
 potential 192
 vertical distribution 191, 194
 current, effect on wind on 544-554
- Development of oceanography xiii
 Diffusion (*see* eddy diffusivity) 101
 Discontinuity surface, stable 453-9
 Divergence of stream lines 359
 points, 363
- Drift bottles and drifting objects 342
 current 399-406
 according observations 415
- East and West Greenland current 662-5
- Echo sounding 11
 profiles of 19
- Eddy
 conductivity 92
 lateral 93, 105
 numerical values 93, 415
 diffusivity 103
 importance of tongue-like distributions 101, 106
 numerical values 103
 viscosity 103
 numerical values 104
see also viscosity
- Effects of subtropical adjacent seas on deep-sea circulation 690-3
- Energy budget between ocean and atmosphere 235-242
- Equatorial counter current 559, 569, 599, 602
- Equilibrium, condition for static 337
 disturbance and re-establishment of static 339
 indifferent, stable, labile or unstable 126, 127, 195
 quasistatic 338
 vertical in the Oceans 195
 radiational in uppermost oceanic layers 94
- Estuaries (River mouths), current in 538-543
 theory of currents in 540-3
- Evaluation, dynamic, of oceanographic observations 338
- Evaporation, determination from energy considerations 222-5
 distribution 163, 221-5, 229
 measurement and computation of 219-21
 geophysical process of 225-31
- Expeditions, oceanographic xiv
- Experiments, model, on planetary flow patterns 687-8
- Freezing point of sea-water 44, 45
- Friction, Guldberg-Mohn 398
 turbulent, *see* eddy viscosity
 velocity 389
- Frictional depth and frictional coefficient 422
- Fronts, stationary 452
- Geoid 6
- Gibraltar and Bab el Mandeb, currents in 529-533
- Glaciation in the polar regions 271
- Glaciers calving into the sea 272
- Gliding, up and down-surface 469
- Gradient current 406-413
 according observations 415
- Guiana current 606
- Gulf Stream, dynamic of 617-638
 comparison with Kuroshio 634-5
 internal structure 607-617
 main sources of 614
 quasi synoptic investigations 615-7
- Gulf Stream, stability of 635-7
 Charney's theory 627-637
- Heat, budget for the ocean 88-90, 223
 annual 116
 conducted through ocean bottom 89, 128
 exchange 88, 92
 sources and losses 88, 89, 93
- Helland-Hansen's fundamental equation of dynamic oceanography 486
- Hydrogen-ion concentration 74
 role in carbon dioxide system 78
- Hypsographic curve of the Earth 15
- Ice, *see also* Sea-ice
 conditions in both polar caps 257

- Ice—*contd.*
 land, in the sea 271
 pack-ice limits in the Antarctic regions 267
 pack-ice distribution round of Newfoundland Banks 265
 limits in the Barents Sea for each month 262, 271
 limits along the eastern coast of Greenland, in Davis Strait and Baffin Bay 263
 limits in the north-western adjacent seas of Pacific Ocean 266
 character of ice-years around Iceland and in the Davis Strait 268, 269
 polar effect on the atmospheric and oceanic circulation 279–284
 formation in polar regions and autumn and winter convection 133, 137–140
- Iceberg, calving, size, shape and destruction 273–5
 drift 436–441
 in shallow sea 423
 in deep sea 424
 in the arctic and Antarctic 275–8
 productivity in the Arctic 273
 south of Newfoundland and of the Grand Banks 265
 seasonal and aperiodic variations in, frequency off Newfoundland 278
- Inertia currents 441–450
 in oceanic currents 446–450
 periods of oscillating vortex 474
- Interchange between sea-surface and atmosphere 235–242
- Intermediate subpolar water 173–8, 211–215
- Isentropic analysis 192
- Isostatic adjustment of the Earth crust 6, 9
- Kinematic of the ocean 342
- Knudsen's Relations 379
- Kuroshio, comparison with Gulf Stream 634–5
 internal structure 638–640
 surface currents in 569
- Labrador current, internal structure 665–9
 surface currents in 561
 Law of parallel fields 477
- Mass field, effect of wind on 544–555
 in a limit and stratified sea 544–7
 general conditions in the open sea 547–550
- Mediterranean, American, current conditions 606–7
- Messina, strait of, current 533–4
- Mixing length 387–391
 processes
 lateral 93, 105
 vertical 101
- Model experiments on planetary flow patterns 701–2
- Morphology of sea bottom 12–18
- Morphological structure of three oceans 18
- Motion of sea level (eustatic, nomic and juvenile) 8
- Neutral point of stream line 364
- Nitrogen dissolved, amount in sea-water 66
- North Sea and Baltic, water interchange between 526–9
- Norwegian Fjords, amount of H₂S 69
- Oceans, area, volume and mean depth of 17
 boundaries 1
 horizontal extent 1
 morphological structure of three oceans 18
 three-dimensional structure of 10, 13
- Osmotic pressure 44, 47
- Oxygen dissolved, solubility 66
 consumption 67
 vertical distribution 68
- Oyashio, surface currents in 569
- Peru current, surface 571
- Pilling up of water by wind (Windstau) 419
- Polar bottom current 680–3
- Polar currents of Northern Hemisphere 662–9
- Polar front, oceanic 144
- Productivity of glaciers calving 272
- Production of ice-bergs in the Arctic 273
- Radiation, absorption in pure water 52
 behaviour of sea-water for diffuse incoming and outgoing 59
 direct solar 90
 effective back, radiation in long-waves 59, 91, 93
 influence of sun's altitude on 90
 extinction coefficients 54–6
 refraction and reflection 56
- Radioactive elements 40
- Reference level 492–502
 by stations in shallow waters 502–4
 determination of 494–501
- Refractive index 57
- Response, transient, of ocean to variable wind stress 702–7
- River mouth (estuaries), current in 538–562
 theory 540–3
- Roughness length 390
- Salinity, determination 36
 periodic variations at surface 154
 annual variations 156
 variations caused by precipitation 159
 horizontal distribution at the surface 161
 mean meridional distribution 163
 vertical distribution 165–6
 of oceanic stratosphere 172–3
 of homo-haline top layer 166
 of subpolar intermediate water 173–8
 of the deep water below 1500 m 178
 of oceanic troposphere 166–172
 in particular depths 179–181
 in adjacent seas and sea straits 181–4
- Sandström's theorem 489–492
- Samples, oceanographic 32
- Sea bottom 12
 topography 18–27
 of individual oceans 27–31
 and land zones of 5° latitude 3
- Sea level 5
 mean physical 6, 7

- Seas adjacent, marginal or mediterranean 4, 30-32
- Sea-ice, density and porosity 247-9
 formation and terminology 243-5
 mechanical properties 255-7
 physical and chemical properties 245-257
 salinity 245-7
 seasonal and aperiodic variations in Arctic and Antarctic regions 257
 thermal properties and temperatures of 249-55
- Sea-water, its physical and chemical properties 32-87
 principal constituents 37
 trace elements in 40
 density 41-4
 boiling point 44
 freezing point 44
 optical properties 51
 osmotic pressure 44
 specific heat 48
 vapour pressure of 44
 viscosity 50
 chemistry of 64-87
 oxygen, nitrogen and hydrogen sulphide contents 65-70
 calcium carbonate 83-7
 carbon dioxide 41-83
- Section, dynamic 338
- Shelf, continental 16, 20
- Ships journals xiii
- Singularities in current field 359-366
- Singular lines in current field of Atlantic 564
- Specific heat of sea-water 48
- Structure, vertical of total Earth 1
- Surface tension of sea-water 51
- Stability in the oceans 195
 in the deep trenches 197
 distribution in Atlantic 198
- Static of the ocean 337
 equation 337
- Steady currents in a homogeneous sea
 without friction 383
 under the action of external forces 398-436
 effects of changing depth and spherical shape of the Earth 385
- Straits, sea, water stratification and movements in 513-7
 external influences on oceanographic conditions 534-8
- Stratification, stable, of water masses 458-469
- Stratosphere, oceanic 122
 circulation 661-673
 temperature in 123
 salinity in 172
- Stream line 342
 convergence and divergence lines 359
 convergence and divergence points 363
 neutral points 364
 singularities in 359-365
- Sub-antarctic intermediate current 675-9
- Subtropical convergence 144
- Temperature, measurements 34-6
 determination in ocean layers 34
 changes caused by radiation absorption 94
 diurnal variation at the surface 109
 in surface layers 110
 annual variation at the surface 110-14
 in surface layers 114
 theory 115
 distribution in horizontal and vertical sections 140-49
 vertical distribution 117-19
 in adjacent seas 129-33
 in adjacent seas at higher latitudes 133
 mean, for zonal oceanic zones 153
 of bottom in the three oceans 149
 adiabatic changes 123-6
 potential 123, 125
 and stability 126-7
- Temperature-salinity relationship 202-16
 practical significance 203
 illustrating water masses 210-14
 in Atlantic 202-16
 and mixing of water masses 203-10
- Thermocline (transition layer)
 with physical surface in tropics and subtropics 463
 in Atlantic 120
 theory 121-22
- Topography, absolute, of physical sea surface in Atlantic Ocean 596
 of 100 and 500 decibar isobar surface 517
 of 800 and 2000 decibar isobar surface 674, resp. 686
 in convergence region of South Atlantic 657
 in the Antarctic convergence zone 670
 in Davis Strait and Labrador Sea 668
- Trajectory of water movements 342
- Transgressions, Atlantic, of Le Danois 659
- Transient response of ocean to variable wind stresses 702-7
- Trenches, deep-sea 24-7
 and gravity profiles 26-7
- Troposphere, oceanic, position and structure 592-602
 salinity 166-72
 circulation 592-660
- Troughs, *see* Trenches
- Turbulence, dissipation of turbence energy 391
 and stratification 391
 and mixing in the sea 393
 statistical theory 393-8
- Turbulent friction, *see* eddy viscosity
- Undercurrent, equatorial 604-5
- Upwelling phenomena 643-66
 theory of Defant, Sverdrup, Hidaka 646-656
- Vapour pressure of sea-water 44
- Velocity, friction 389
- Velocity field 342, 356-370
 representation, by means of compass cards 356
 by means of stream lines 356
 near land 370
 divergence of 374-9
- Viscosity of sea-water 50
 eddy 104
 in sea currents 387-391
 coefficient 387
- Vortex, circular hydrographic, wind effects and current system 576-9
- Vortices, development of 373-4
 standing 372

- Vortices—*contd.*
stationary in a two layered ocean 465
pulsation of 469-475
Eigen-period of oscillating vortex 474
- Water bodies 451
stable stratification between 460-479
- Water budget of Earth 231-5
- Water interchange between North Sea and
Baltic 526-9
- Water masses of oceans 216-17
- Water transport in the individual layers of
Atlantic Ocean 688-690
in density current 508-511
in coastal current 511
- Wind, effects of, and the current system in a
hydrographic circular vortex 576-9
on mass field and density current 544-555
computation of velocity of equatorial currents
from, data 552-5
relationships between wind and currents
550-2
- Wind stress, variable, effect on oceanic currents
702-7
- Windstau (piling up of water by wind) 419



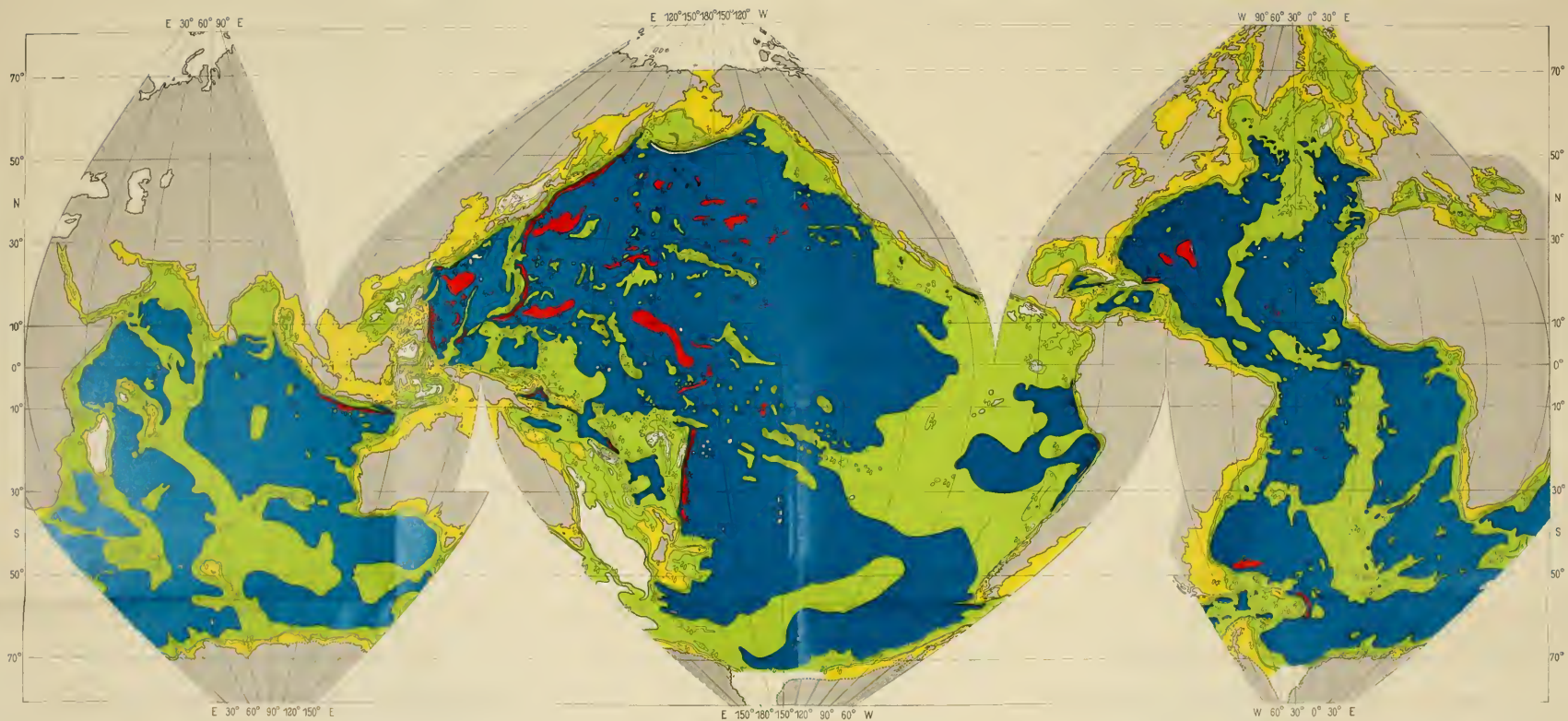


PLATE 1. World-map of ocean depth.

Isobaths for 1000 and 2000 m and from there on for each 2000 m-interval. The isobath are denoted on the maps by 100 m-units (for example 4000 m = 400).

Colouring 0 - 1000 m light yellow; 1000 - 4000 m light green; 4000 - 6000 m blue; 6000 m red.

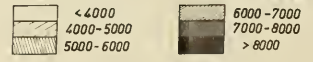
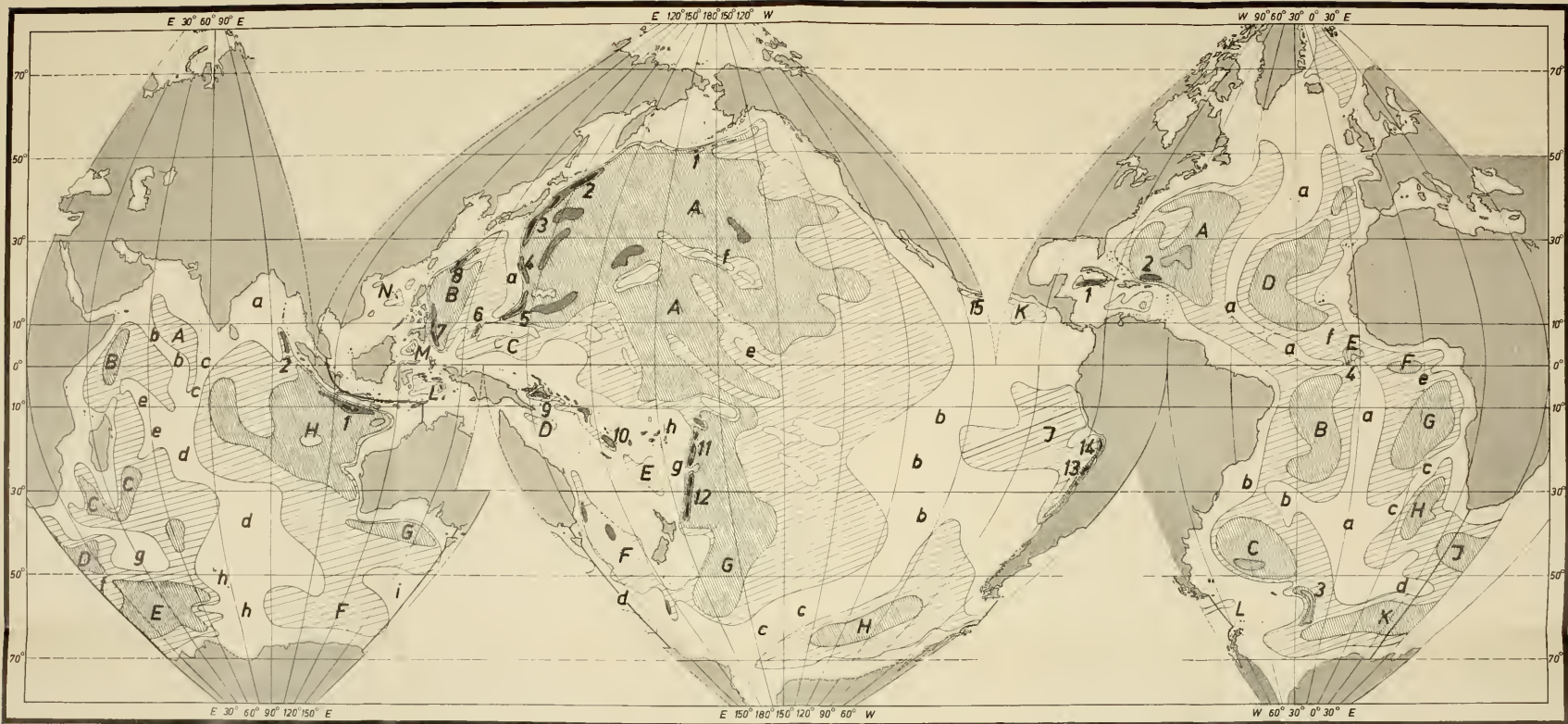


PLATE 2. Schematically simplified world-map of ocean depth. (Sci. Vol. I, Pt. 1, p. 13)

(The depth-intervals are specified underneath the map; the letters and numbers are referred to in the text; for Atlantic Ocean see p. 28, for Indian Ocean see pp. 29 and 30.)

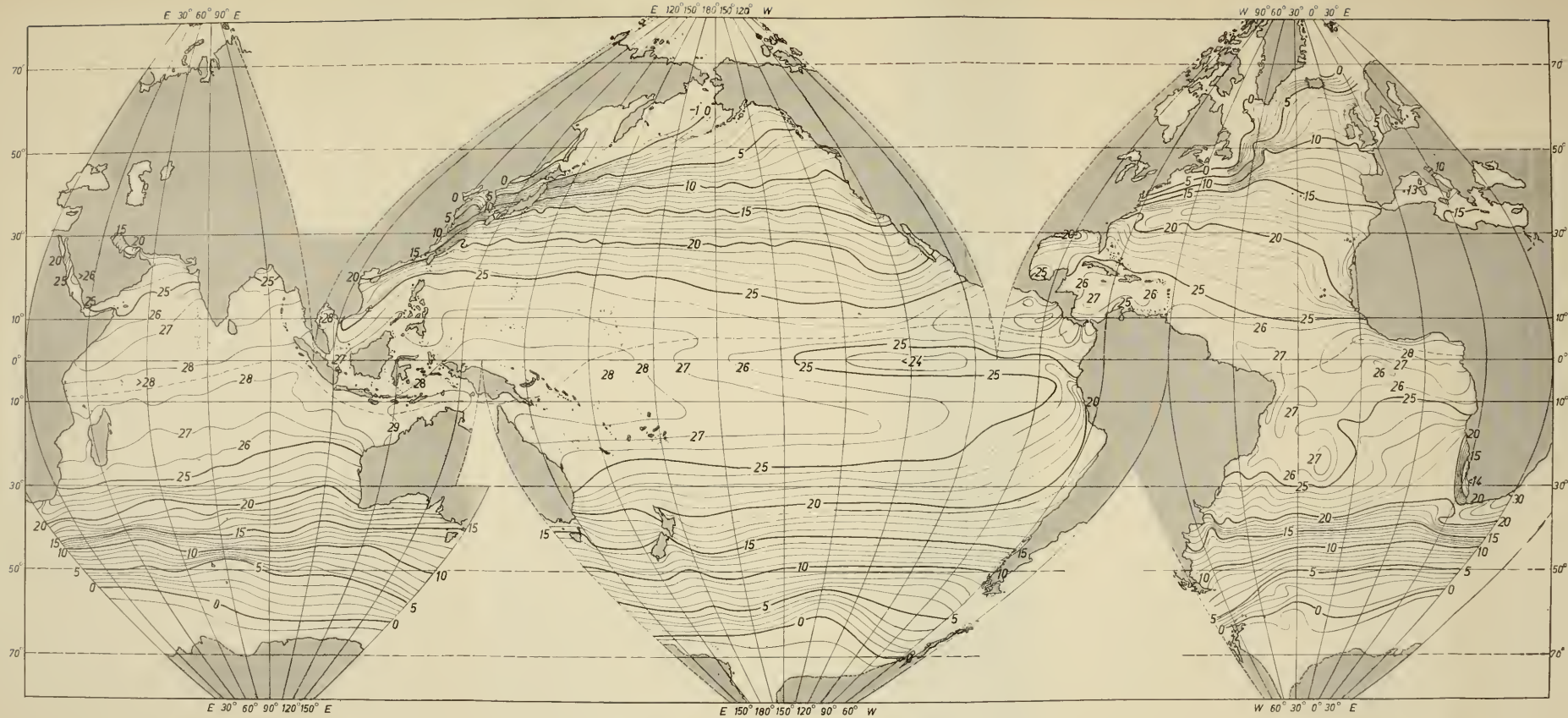


PLATE 3A. Surface-temperature (°C) of the world oceans for February.

(See Vol. I. Pl. I, p. 140 *et seq.*)

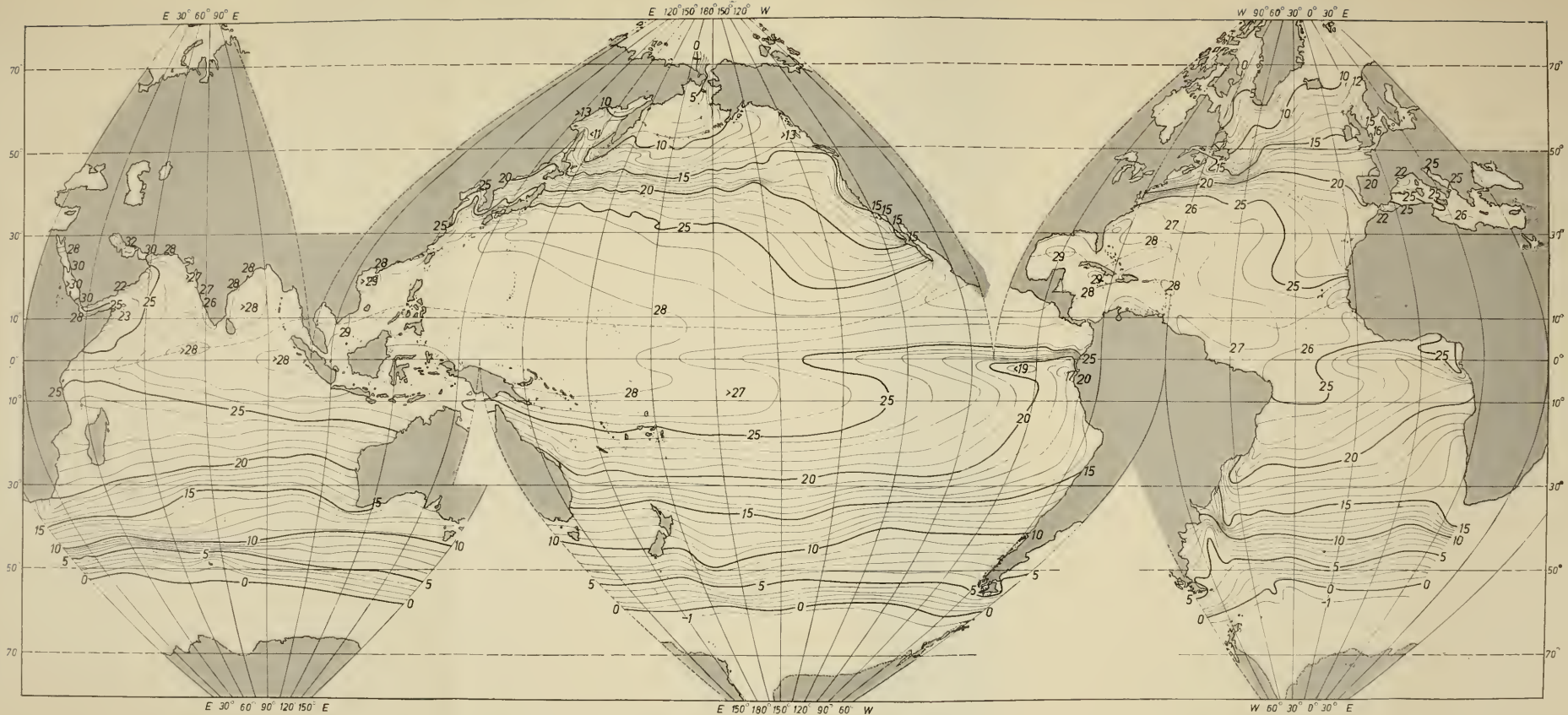


PLATE 3B. Surface-temperature ($^{\circ}$ C) of the world oceans for August.

(See Vol. I. Pt. I, p. 140 *et seq.*)



PLATE 4. Bottom-temperature (°C) of the world oceans.

(For temperature-intervals indicated by different shades, see specifications in the lower righthand side of the map.)

(See Vol. I. Pl. I, p. 149 et seq.)

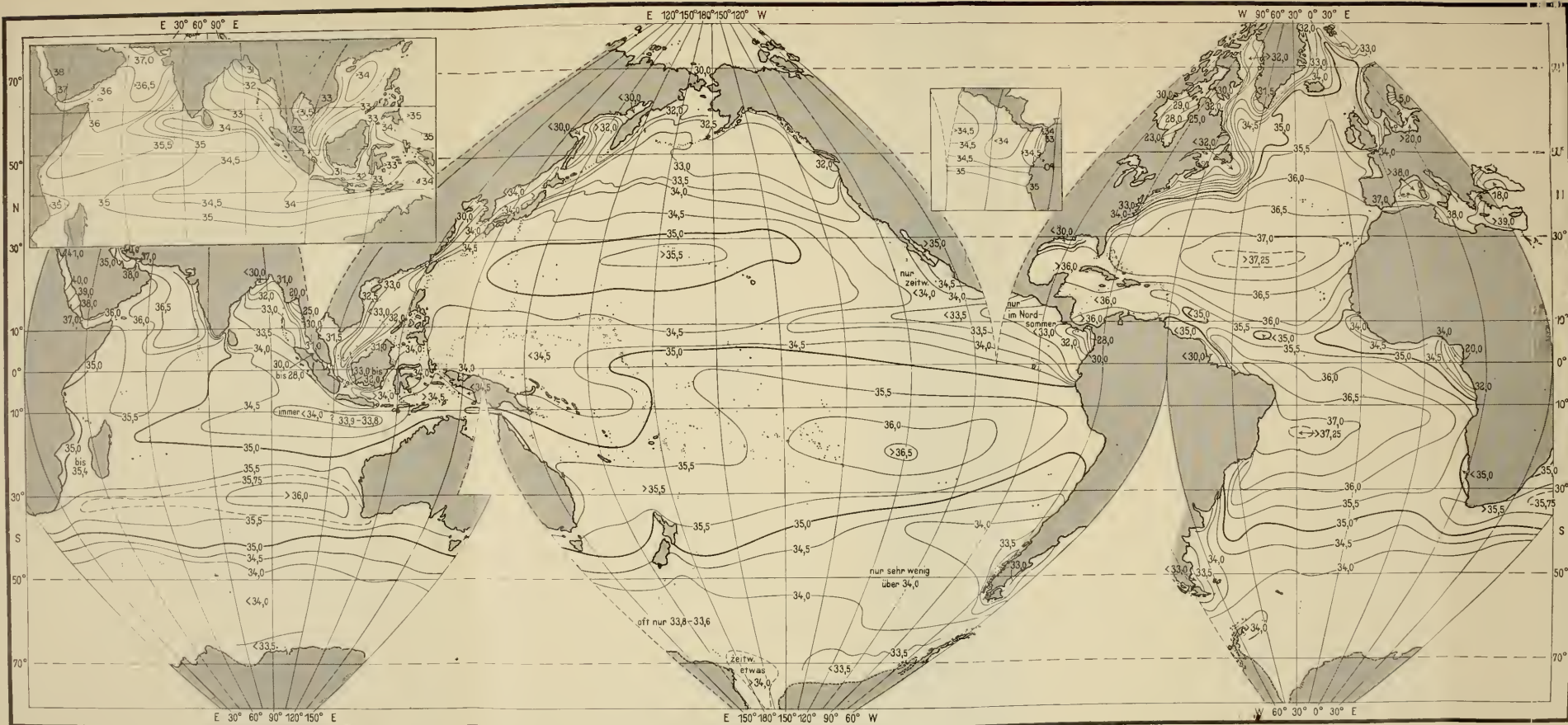


PLATE 5. Average sea-surface salinity (‰) of the world oceans.

(See Vol. I, Pt. I, p. 161 et seq.)

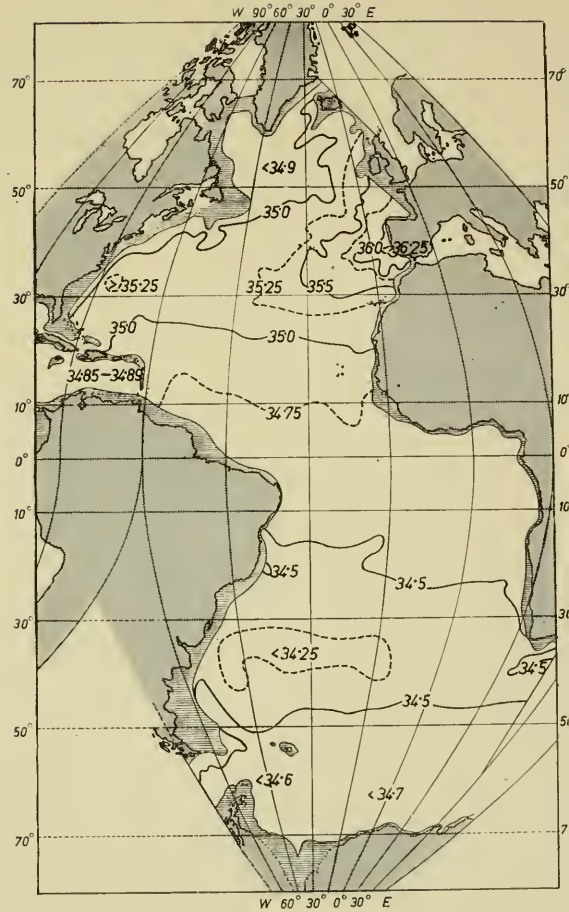


PLATE 6. Average salinity (‰) in the Atlantic Ocean.

(Picture to the left: in 400 m depth; picture to the right: in 1000 m depth.)

(See Vol. I, Pt. I, p. 179 *et seq.*)

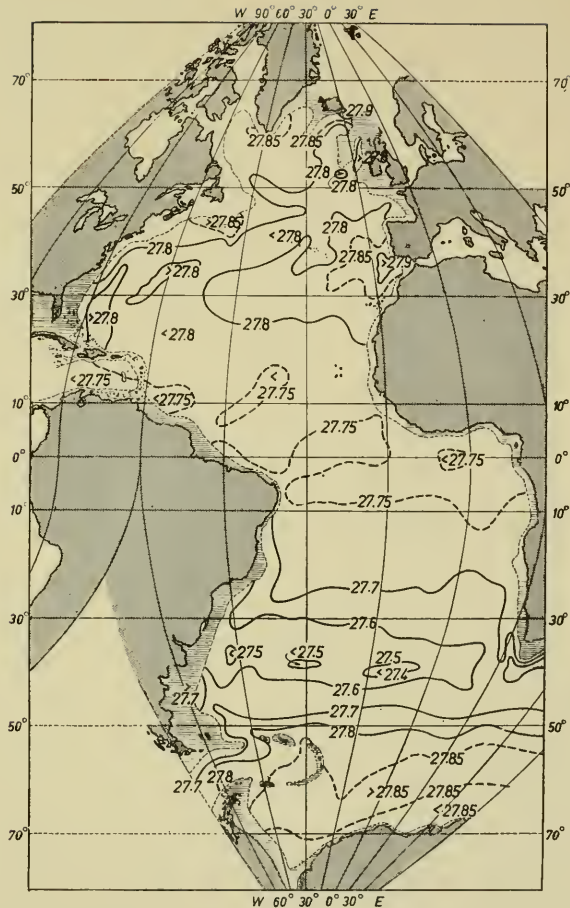
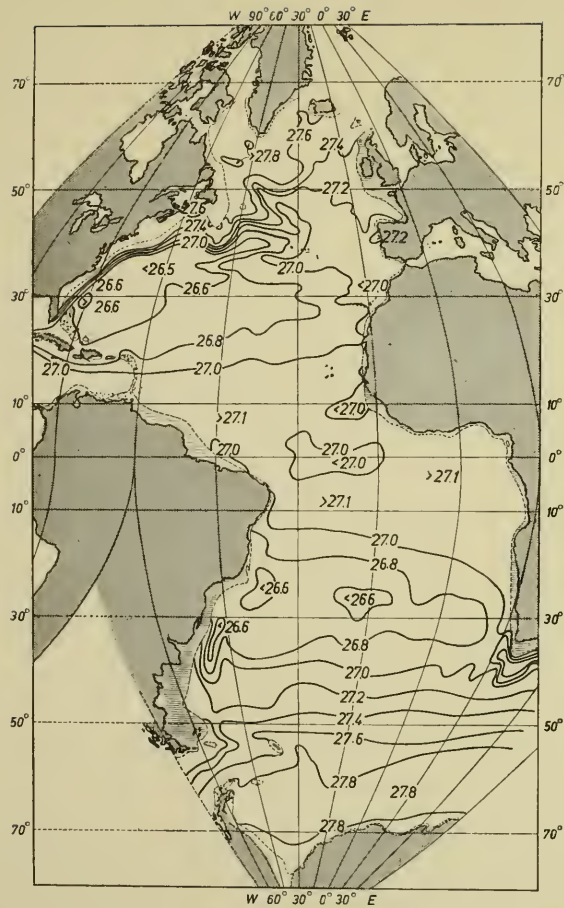


PLATE 7. Average density (σ_t) in the Atlantic Ocean.

(Picture to the left: in 400 m depth; picture to the right: in 1000 m depth.)

(For sea-surface see: Vol. I, Pt. I, Fig. 89, p. 191, for depth charts p. 192.)

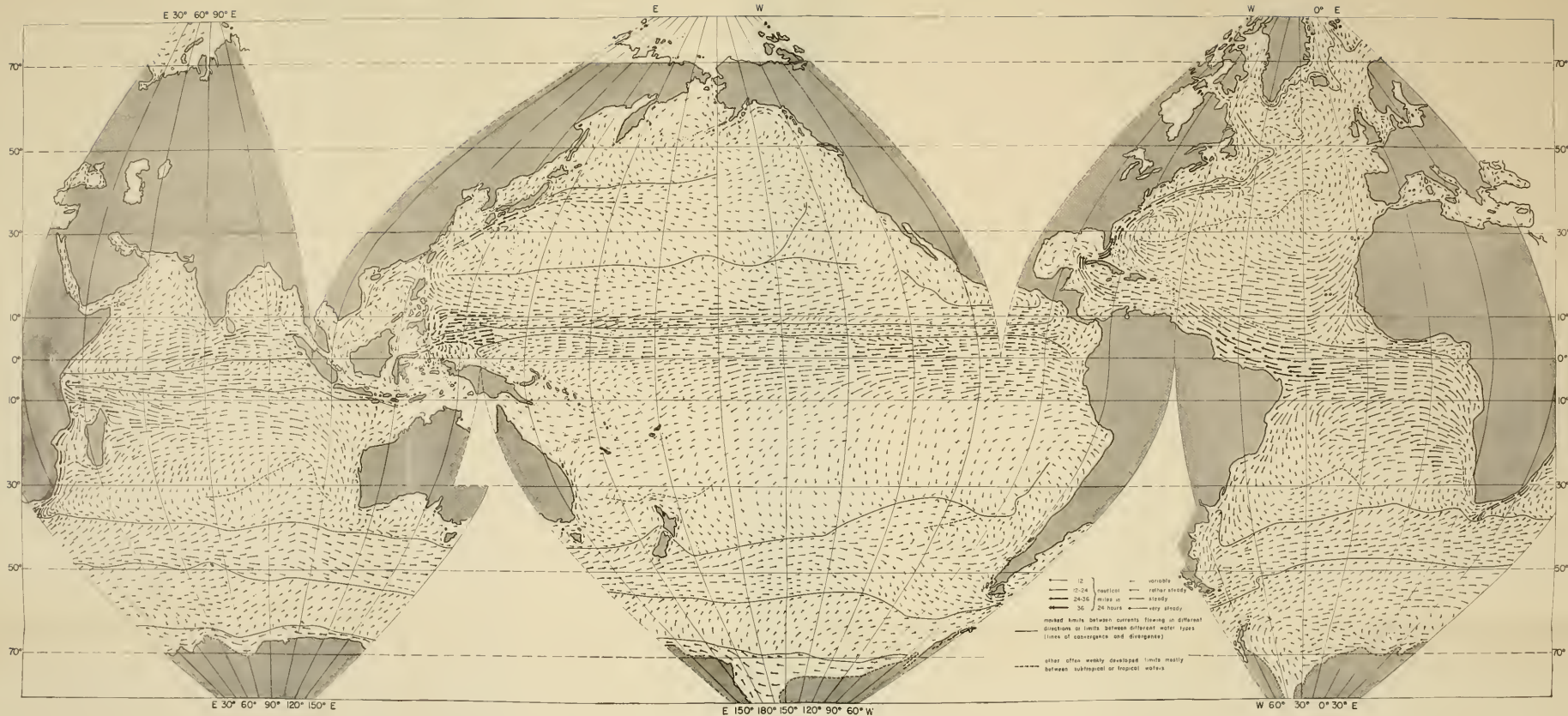


PLATE 8. World chart of oceanic sea-surface currents for the Northern Hemisphere winter. (See: Vol. I, Pt. II, p. 543.)

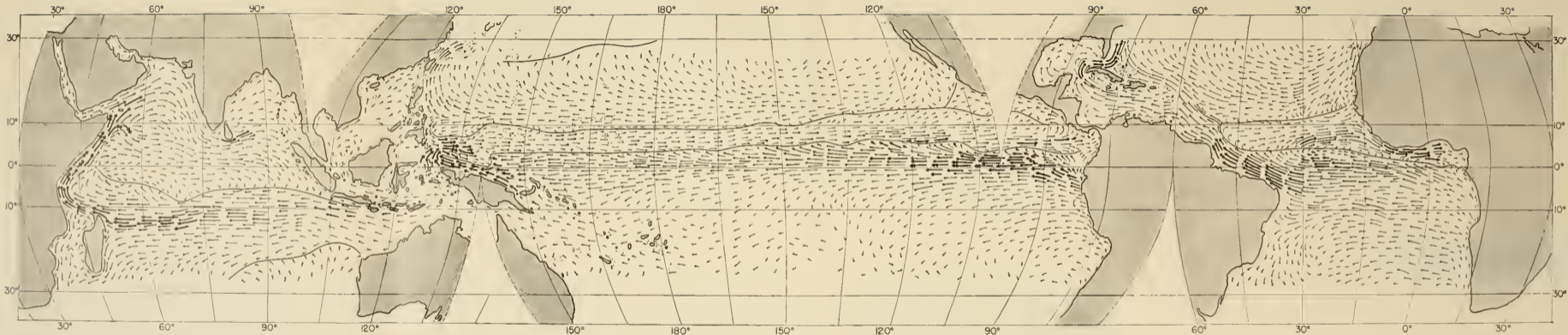


PLATE 8a. The Plate 8a shows for 30° N. and 20° S the seasonal variations of the oceanic sea-surface currents for the tropics during the Northern Hemisphere summer.

GEOGRAPHICAL REVIEW

EXCERPT FROM VOL. 52

NO. 4 1962 pp.624-625

PUBLISHED BY

THE AMERICAN GEOGRAPHICAL SOCIETY
OF NEW YORK

BROADWAY AT 156th ST., NEW YORK 32, N. Y.

Hudson Laboratories, Columbia University Contribution No. 161.

PHYSICAL OCEANOGRAPHY. By ALBERT DEFANT. Vol. 1, xvi and 729 pp.; Vol. 2, viii and 598 pp.; maps, diags., ills., bibliogr., indexes. Pergamon Press, New York, Oxford, London, Paris, 1961. \$35.00. 10 x 6 $\frac{3}{4}$ inches.

The oceans have been described in exciting dramas, which use the violence or desolateness of the sea to draw out human traits. Except for an occasional storm, tidal wave, or other such phenomenon, one tends to consider the oceans uninteresting in themselves. Nevertheless, by subtle movements resulting from small changes in the properties of water, these millions of square miles of liquid establish conditions that allow man to exist on earth. The mechanism behind this forms a part of the general description of oceanic movements in Defant's two-volume work on physical oceanography. Even marine life is excluded from this overdue tribute to the seas.

Oceanography has gained much from Professor Defant's past contributions, and it is fortunate that a man of his stature has written these volumes. His insight and his organization of material have resulted in a work that in other hands could have been a shambles instead of a badly needed coherent description of the state of physical oceanography. He has considered literature written up to May, 1957, and the vitality of the field is such that this study can now be regarded as a starting reference work.

The first pages of Volume 1 present a description of the oceans—their extent, the distribution of temperature, salinity, and density, their water budget and conversion into ice near the poles. The remainder of the volume reviews pertinent physical concepts and applies them to the general problem of water circulation in all parts of the oceans. Some welcome elaborations of hydrodynamic situations are also presented.

Waves and tides form the subject matter of the second volume. Again, basic physical ideas are clarified before the author goes into the extensive literature describing the periodic movements of the sea. The treatment is thorough enough to encompass, for example, the water transport associated with irrotational surface waves.

Professor Defant wrote this work in German over a period of years. Fortunately, the Office of Naval Research, United States Navy, was willing to sponsor its translation into English. This must have been a formidable undertaking, and the occasional clumsy sentence constructions are easily forgiven.—T. E. POCHAPSKY

